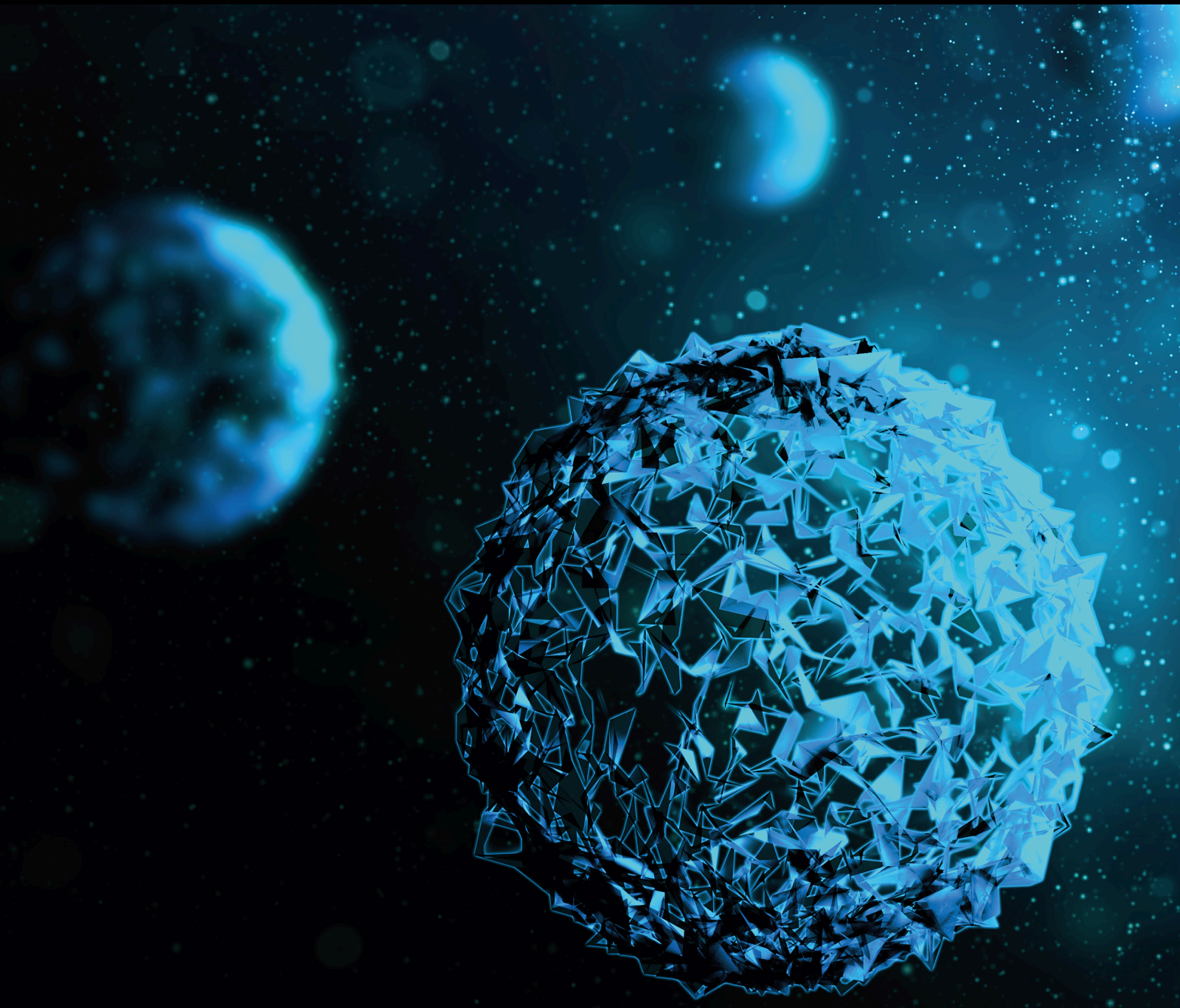


# Possible Biomarkers in Neurovascular Disorders

Lead Guest Editor: Yuzhen Xu

Guest Editors: Qian Wang, Zhenpeng Song, Juan Yang, and Yi Lu





---



# **Possible Biomarkers in Neurovascular Disorders**

BioMed Research International

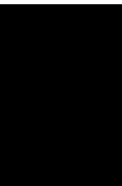
---

## **Possible Biomarkers in Neurovascular Disorders**

Lead Guest Editor: Yuzhen Xu

Guest Editors: Qian Wang, Zhenpeng Song, Juan Yang, and Yi Lu





Copyright © 2024 Hindawi Limited. All rights reserved.









This is a special issue published in "BioMed Research International." All articles are open access articles distributed under the Creative Commons Attribution License, which permits unrestricted use, distribution, and reproduction in any medium, provided the original work is properly cited.

## Section Editors



Penny A. Asbell, USA  
David Bernardo , Spain  
Gerald Brandacher, USA  
Kim Bridle , Australia  
Laura Chronopoulou , Italy  
Gerald A. Colvin , USA  
Aaron S. Dumont, USA  
Pierfrancesco Franco , Italy  
Raj P. Kandpal , USA  
Fabrizio Montecucco , Italy  
Mangesh S. Pednekar , India  
Letterio S. Politi , USA  
Jinsong Ren , China  
William B. Rodgers, USA  
Harry W. Schroeder , USA  
Andrea Scribante , Italy  
Germán Vicente-Rodriguez , Spain  
Momiao Xiong , USA  
Hui Zhang , China

## Academic Editors

### Vascular Medicine

Ken-ichi Aihara , Japan  
Zsuzsa Bagoly , Hungary  
Pedro Cabrales , USA  
Betti Giusti , Italy  
Silvia Lacchini , Brazil  
Giovanni Mariscalco , Italy  
Yasushi Matsumoto, Japan  
Shirley Moore, Australia  
Francesco Onorati, Italy  
Giuseppe M. Sangiorgi , Italy  
Monvadi Barbara Srichai, USA  
Dobrin Vassilev, Bulgaria  
Gelin Xu , China

### Neuroscience

Jafri Malin Abdullah , Malaysia  
Musaad Alshammari , Saudi Arabia

Adomas Bunevicius , USA  
Dong-Yuan Cao , China  
Sheng Chen , China  
Mark A. Cline , USA  
Luca Cucullo , USA  
Changmeng Cui , China  
Sulagna Das , USA  
Francesco Doglietto , Italy  
Giuseppe Donato, Italy  
Andrew Ducruet , USA  
Shaikh Anowarul Fattah , Bangladesh  
Shun Gong, China  
Hiroyuki Hioki , Japan  
Sushil K. Jha , India  
Jong Min Lee , Republic of Korea  
Cheng-Hsien Lu , Taiwan  
Mario Manto , Belgium  
Alessandro Martorana , Italy  
Gerard M. Moloney , Ireland  
Simon Ngamli Fewou , United Kingdom  
Mauro S. Oliveira , Brazil  
Bence Racz , Hungary  
Joaquim Radua , United Kingdom  
Milena Raffi , Italy  
Diane Ruge , United Kingdom  
Jessica Sala , Italy  
Arianna Scuteri , Italy  
Young Joon Seo , Republic of Korea  
Nicola Simola , Italy  
Yasir Ahmed Syed , United Kingdom  
Sung-Chun Tang , Taiwan  
Luigia Trabace , Italy  
Leyan Xu , USA  
Shi-Jie Zhang , China



## Contents

---

**Retracted: The Conditioned Medium of *Lactobacillus rhamnoides* GG Regulates Microglia/ Macrophage Polarization and Improves Functional Recovery after Spinal Cord Injury in Rats**  
BioMed Research International  
Retraction (1 page), Article ID 9895413, Volume 2024 (2024)

**Retracted: High-Throughput Screen of Natural Compounds and Biomarkers for NSCLC Treatment by Differential Expression and Weighted Gene Coexpression Network Analysis (WGCNA)**  
BioMed Research International  
Retraction (1 page), Article ID 9892473, Volume 2024 (2024)

**Retracted: A Predictive Model for the Risk of Cognitive Impairment in Patients with Gallstones**  
BioMed Research International  
Retraction (1 page), Article ID 9890654, Volume 2024 (2024)

**Retracted: Experimental Study of lncRNA RP11-815M8.1 Promoting Osteogenic Differentiation of Human Bone Marrow Mesenchymal Stem Cells**  
BioMed Research International  
Retraction (1 page), Article ID 9869571, Volume 2024 (2024)

**Retracted: Identification of the Potential Biomarkers Involved in the Human Oral Mucosal Wound Healing: A Bioinformatic Study**  
BioMed Research International  
Retraction (1 page), Article ID 9852192, Volume 2024 (2024)

**Retracted: Interfering with pak4 Protein Expression Affects Osteosarcoma Cell Proliferation and Migration**  
BioMed Research International  
Retraction (1 page), Article ID 9849782, Volume 2024 (2024)

**Retracted: Mechanism of *Radix Astragali* and *Radix Salviae Miltiorrhizae* Ameliorates Hypertensive Renal Damage**  
BioMed Research International  
Retraction (1 page), Article ID 9848535, Volume 2024 (2024)

**Retracted: Osmotic Demyelination Syndrome: Clinical, Neuroimaging Characteristics, and Outcomes in a Series of 18 Cases**  
BioMed Research International  
Retraction (1 page), Article ID 9847541, Volume 2024 (2024)

**Retracted: Genome Assembly and Analyses of the Macrofungus *Macrocybe gigantea***  
BioMed Research International  
Retraction (1 page), Article ID 9843427, Volume 2024 (2024)

**Retracted: Protective Effect of Triphala against Oxidative Stress-Induced Neurotoxicity**  
BioMed Research International  
Retraction (1 page), Article ID 9842820, Volume 2024 (2024)

**Retracted: The Relationship between the Mean Platelet Volume and Carotid Atherosclerosis and Prognosis in Patients with Acute Cerebral Infarction**

BioMed Research International

Retraction (1 page), Article ID 9837150, Volume 2024 (2024)

**Retracted: Applicability of High-Frequency Ultrasound to the Early Diagnosis of Diabetic Peripheral Neuropathy**

BioMed Research International

Retraction (1 page), Article ID 9835145, Volume 2024 (2024)

**Retracted: Constructing a Predictive Model of Depression in Chemotherapy Patients with Non-Hodgkin's Lymphoma to Improve Medical Staffs' Psychiatric Care**

BioMed Research International

Retraction (1 page), Article ID 9834359, Volume 2024 (2024)

**Retracted: Clinical Efficacy and Safety of "Three-Dimensional Balanced Manipulation" in the Treatment of Cervical Spondylotic Radiculopathy by Finite Element Analysis**

BioMed Research International

Retraction (1 page), Article ID 9828931, Volume 2024 (2024)

**Retracted: Flat Panel CT Scanning Is Helpful in Predicting Hemorrhagic Transformation in Acute Ischemic Stroke Patients Undergoing Endovascular Thrombectomy**

BioMed Research International

Retraction (1 page), Article ID 9823857, Volume 2024 (2024)

**Retracted: Effects of Ozone on Hippocampus BDNF and Fos Expressions in Rats with Chronic Compression of Dorsal Root Ganglia**

BioMed Research International

Retraction (1 page), Article ID 9821958, Volume 2024 (2024)

**Retracted: Facial Nerve Monitoring under Different Levels of Neuromuscular Blockade with Cisatracurium Besilate in Parotid Tumour Surgery**

BioMed Research International

Retraction (1 page), Article ID 9819172, Volume 2024 (2024)

**Retracted: Analysis of Age and Prevention Strategy on Outcome after Cerebral Venous Thrombosis**

BioMed Research International

Retraction (1 page), Article ID 9814716, Volume 2024 (2024)

**Retracted: The Impact of Study Setting on Clinical Characteristics in Older Chinese Adults with Subjective Cognitive Decline: Baseline Investigation of Convenience and Population-Based Samples**

BioMed Research International

Retraction (1 page), Article ID 9810529, Volume 2024 (2024)



# Contents

---

**Retracted: Agomelatine Softens Depressive-Like Behavior through the Regulation of Autophagy and Apoptosis**

BioMed Research International

Retraction (1 page), Article ID 9809082, Volume 2024 (2024)

**Retracted: A Prediction Model for Cognitive Impairment Risk in Colorectal Cancer after Chemotherapy Treatment**

BioMed Research International

Retraction (1 page), Article ID 9808217, Volume 2024 (2024)

**Retracted: Downregulation of LHPP Expression Associated with AFP Acts as a Good Prognostic Factor in Human Hepatocellular Carcinoma**

BioMed Research International

Retraction (1 page), Article ID 9808126, Volume 2024 (2024)

**Retracted: Effects of Carotid Artery Stent and Carotid Endarterectomy on Cognitive Function in Patients with Carotid Stenosis**

BioMed Research International

Retraction (1 page), Article ID 9806516, Volume 2024 (2024)

**Retracted: Effects of Omega-3 Polyunsaturated Fatty Acids on Cognitive Function after Splenectomy in Rats**

BioMed Research International

Retraction (1 page), Article ID 9802612, Volume 2024 (2024)

**Retracted: Pancancer Analysis of Neurovascular-Related NRP Family Genes as Potential Prognostic Biomarkers of Bladder Urothelial Carcinoma**

BioMed Research International

Retraction (1 page), Article ID 9802197, Volume 2024 (2024)

**Retracted: Measuring Subthalamic Nucleus Volume of Parkinson's Patients and Evaluating Its Relationship with Clinical Scales at Pre- and Postdeep Brain Stimulation Treatment: A Magnetic Resonance Imaging Study**

BioMed Research International

Retraction (1 page), Article ID 9802021, Volume 2024 (2024)

**Retracted: The Prognostic Value of Leucine-Rich  $\alpha 2$  Glycoprotein 1 in Pediatric Spinal Cord Injury**

BioMed Research International

Retraction (1 page), Article ID 9801452, Volume 2024 (2024)

**Retracted: Effects of Different Intervention Time Points of Early Rehabilitation on Patients with Acute Ischemic Stroke: A Single-Center, Randomized Control Study**

BioMed Research International

Retraction (1 page), Article ID 9801094, Volume 2024 (2024)

**Retracted: Safety and Efficacy of Early Carotid Endarterectomy in Patients with Symptomatic Carotid Artery Stenosis: A Meta-Analysis**

BioMed Research International

Retraction (1 page), Article ID 9797043, Volume 2024 (2024)

**Retracted: Predicting Decreased Activities of Daily Living in Patients with Moyamoya Disease after Revascularization: Development and Assessment of a New Predictive Nomogram**

BioMed Research International

Retraction (1 page), Article ID 9796412, Volume 2024 (2024)

**Retracted: Modified Prehospital Acute Stroke Severity (mPASS) Scale to Predict Emergent Large Arterial Occlusion**

BioMed Research International

Retraction (1 page), Article ID 9783823, Volume 2024 (2024)

**Retracted: A Network Pharmacology to Explore the Mechanism of *Calculus Bovis* in the Treatment of Ischemic Stroke**

BioMed Research International

Retraction (1 page), Article ID 9768532, Volume 2024 (2024)

**Retracted: Potential Factors for Psychological Symptoms at Three Months in Patients with Young Ischemic Stroke**

BioMed Research International

Retraction (1 page), Article ID 9764670, Volume 2024 (2024)

**Retracted: Celastrol Attenuates Learning and Memory Deficits in an Alzheimer's Disease Rat Model**

BioMed Research International




Retraction (1 page), Article ID 9758139, Volume 2024 (2024)

**[Retracted] Interfering with pak4 Protein Expression Affects Osteosarcoma Cell Proliferation and Migration**

Yuxin Fu, Lun Fang, Qipu Yin, Qi Wu, Wei Sui, Ying Sun, Xindi Zhao, Yadi Wu , and Lu Zhou 


Research Article (10 pages), Article ID 9977001, Volume 2021 (2021)

**[Retracted] Effects of Omega-3 Polyunsaturated Fatty Acids on Cognitive Function after Splenectomy in Rats**

Yong Guo , Feng Ping , Yongmei Cao, Jiawei Shang, Junfeng Zhang, Hong Jiang, and Shudong Fang 

Research Article (6 pages), Article ID 5513886, Volume 2021 (2021)

**[Retracted] Effects of Ozone on Hippocampus BDNF and Fos Expressions in Rats with Chronic Compression of Dorsal Root Ganglia**


Lingling Zhu, Yanxiu Wang, Xiaowen Lin, Xu Zhao, and Zhi jian Fu 

Research Article (10 pages), Article ID 5572915, Volume 2021 (2021)



## Contents

### **Crosstalk between Heart Failure and Cognitive Impairment via hsa-miR-933/RELB/CCL21 Pathway**

Wenxiao Feng, Jie Yang, Wenchao Song, and Yitao Xue 



Research Article (16 pages), Article ID 2291899, Volume 2021 (2021)

### **[Retracted] Effects of Different Intervention Time Points of Early Rehabilitation on Patients with Acute Ischemic Stroke: A Single-Center, Randomized Control Study**

LiLi Liu , YanQin Lu , QianQian Bi , Wang Fu , XiaoYu Zhou , and Jue Wang 





Research Article (7 pages), Article ID 1940549, Volume 2021 (2021)

### **[Retracted] Downregulation of LHPP Expression Associated with AFP Acts as a Good Prognostic Factor in Human Hepatocellular Carcinoma**

Xu Chao , Wei Zhang, Jieqiong Wu, Xuesong Feng, Hailong Shi, Luyan Zhao, Haiyu Shen, and Chao Jiang 

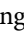

Research Article (9 pages), Article ID 1971048, Volume 2021 (2021)

### **[Retracted] High-Throughput Screen of Natural Compounds and Biomarkers for NSCLC Treatment by Differential Expression and Weighted Gene Coexpression Network Analysis (WGCNA)**

Ling Kui , Min Li, Xiaonan Yang, Ling Yang, Qinghua Kong, Yunbing Pan, Zetan Xu, Shouling Wang, Dandan Mo, Yang Dong , Yao Liu , and Jianhua Miao 



Research Article (20 pages), Article ID 5955343, Volume 2021 (2021)

### **A Potential ceRNA Network for Neurological Damage in Preterm Infants**

Jin Huang , Xuejing Liang, and Zhenyu Cai 


Research Article (15 pages), Article ID 2628824, Volume 2021 (2021)

### **[Retracted] Celastrol Attenuates Learning and Memory Deficits in an Alzheimer's Disease Rat Model**

Yao Xiao, Xifeng Wang, Siyi Wang, Jun Li, Xueyu Xu, Min Wang, Gang Li , and Wei Shen 



Research Article (11 pages), Article ID 5574207, Volume 2021 (2021)

### **A Potential miRNA-mRNA Network for Dementia and Hernia Crosstalk**

De-jian Chen and Da-peng Li 

Research Article (14 pages), Article ID 4324068, Volume 2021 (2021)

### **Single-Cell Transcriptomics-Based Study of Transcriptional Regulatory Features in the Mouse Brain Vasculature**

Wei-Wei Lin , Lin-Tao Xu, Yi-Sheng Chen, Ken Go, Chenyu Sun, and Yong-Jian Zhu 


Research Article (15 pages), Article ID 7643209, Volume 2021 (2021)

### **[Retracted] Modified Prehospital Acute Stroke Severity (mPASS) Scale to Predict Emergent Large Arterial Occlusion**


Xiaoli Si, Jie Ruan, Lingfei Li, Shan Lu, Huan Huang, Wenqing Xia, Keqin Liu, Tianwen Chen, Lin Jiang , and Congguo Yin 

Research Article (6 pages), Article ID 5568696, Volume 2021 (2021)

**[Retracted] Constructing a Predictive Model of Depression in Chemotherapy Patients with Non-Hodgkin's Lymphoma to Improve Medical Staffs' Psychiatric Care**

Cheng Hu, Qian Li , Ji Shou, Feng-xian Zhang, Xia Li, Min Wu, Meng-jing Xu, and Li Xu  
Research Article (12 pages), Article ID 9201235, Volume 2021 (2021)




**[Retracted] A Predictive Model for the Risk of Cognitive Impairment in Patients with Gallstones**

Zhaofang Liu  and Chuanyan Li  
Research Article (13 pages), Article ID 3792407, Volume 2021 (2021)

**[Retracted] Facial Nerve Monitoring under Different Levels of Neuromuscular Blockade with Cisatracurium Besilate in Parotid Tumour Surgery**

Huimin Huang, Hong Jiang , Jinxing Liu, Jie Chen , Lin Qiu, Jiayi Wang, Wenhui Liu, and Huan Chen  
Research Article (11 pages), Article ID 5655061, Volume 2021 (2021)




**[Retracted] The Conditioned Medium of Lactobacillus rhamnoides GG Regulates Microglia/Macrophage Polarization and Improves Functional Recovery after Spinal Cord Injury in Rats**

Fangqi Lin , Baokun Zhang, Qiang Shi, Jiaming Liang, Xin Wang, Xiaofeng Lian , and Jianguang Xu   
Research Article (13 pages), Article ID 3376496, Volume 2021 (2021)




**[Retracted] The Prognostic Value of Leucine-Rich  $\alpha 2$  Glycoprotein 1 in Pediatric Spinal Cord Injury**

Hong Ma, Fengshan Lu, Yueming Guo , Zhaoxiang Shen , and Yuanzhen Chen   
Research Article (5 pages), Article ID 7365204, Volume 2021 (2021)




**A Single-Center Clinical Study to Evaluate Shenxiong Glucose Injection Combined with Edaravone in the Treatment of Acute Large-Area Cerebral Infarction**

Zongqin Li , Xiaoxia Rong, Jun Luo, Tao Zeng, Pan Huang , and Xuejie Xu   
Research Article (6 pages), Article ID 9935752, Volume 2021 (2021)



**Relationship of Neutrophil-to-Lymphocyte Ratio with Carotid Plaque Vulnerability and Occurrence of Vulnerable Carotid Plaque in Patients with Acute Ischemic Stroke**

Xin Li , Jing Li , and Guode Wu   
Review Article (8 pages), Article ID 6894623, Volume 2021 (2021)







**C-Reactive Protein Levels and Clinical Prognosis in LAA-Type Stroke Patients: A Prospective Cohort Study**






Qingjia Zeng, Yaying Zeng, Mark Slevin, Baoqiang Guo, Zhipeng Shen , Binbin Deng , and Wenbo Zhang   
Research Article (8 pages), Article ID 6671043, Volume 2021 (2021)






**Corrigendum to "Potential Factors for Psychological Symptoms at Three Months in Patients with Young Ischemic Stroke"**






Dongjuan Xu , Xi Chu, Kun Wang, Lianyan Wei, Yunyun Xu, Xiaomin Huang, Jinna Li, Lina Xu, Lu Yin , Hong Liu, Xiaolei Liu, Haixia Leng, Qing Xue, Mao Peng, Longbin Jia, and Hongxing Wang  
Corrigendum (2 pages), Article ID 9863187, Volume 2021 (2021)



## Contents



**[Retracted] The Impact of Study Setting on Clinical Characteristics in Older Chinese Adults with Subjective Cognitive Decline: Baseline Investigation of Convenience and Population-Based Samples**  
Mingyan Zhao , Guanqun Chen , Taoran Li , Can Sheng , Yuxia Li , and Ying Han   
Research Article (9 pages), Article ID 5538323, Volume 2021 (2021)







**The Influence of Serum Uric Acid Level on Alzheimer's Disease: A Narrative Review**  
Mengyuan Qiao , Chongli Chen , Yuqing Liang , Yuxi Luo , and Wenbin Wu   
Review Article (8 pages), Article ID 5525710, Volume 2021 (2021)



**[Retracted] Osmotic Demyelination Syndrome: Clinical, Neuroimaging Characteristics, and Outcomes in a Series of 18 Cases**  
Xinhuang Lv , Qian Hong , Xiuxiu Lin , Weian Chen , and Yuan Tian   
Research Article (9 pages), Article ID 9944632, Volume 2021 (2021)



**Score for Predicting Active Cancer in Patients with Ischemic Stroke: A Retrospective Study**  
Jiwei Jiang , Xiuli Shang , Jinming Zhao, Meihui Cao, Jirui Wang, Runzhi Li , Yanli Wang , and Jun Xu   
Research Article (9 pages), Article ID 5585206, Volume 2021 (2021)

**Decreased Levels of Serum IL-34 Associated with Cognitive Impairment in Vascular Dementia**  
Yang Wang, Wei Lu, Wenjing Ning, Yan Chen , and Lingxing Li   
Research Article (6 pages), Article ID 6793860, Volume 2021 (2021)




**Repulsive Guidance Molecule-a and Central Nervous System Diseases**  
Jinhua Tang, Xiaopeng Zeng, Hang Li, Lu Ju, Jinzhou Feng , and Jun Yang   
Review Article (8 pages), Article ID 5532116, Volume 2021 (2021)

**[Retracted] Predicting Decreased Activities of Daily Living in Patients with Moyamoya Disease after Revascularization: Development and Assessment of a New Predictive Nomogram**  
Yani Zhao , Dongliang Yang , Gang Li , Peng Zhao , Xiaorong Luan , and Haiyan Li   
Research Article (8 pages), Article ID 6624245, Volume 2021 (2021)

**The Relationship of Large-Artery Atherothrombotic Stroke with Plasma Trimethylamine N-Oxide Level and Blood Lipid-Related Indices: A Cross-Sectional Comparative Study**  
Dongjuan Xu, Wenfeng Zhao, Juexian Song , Lu Yin, Kun Wang, Lianyan Wei, Yunyun Xu, Hongfei Li, Baoquan Min, Ning Tang, Xiaoyan Jiang, Hui Liu, Shuo Yan, Haixia Leng, Qing Xue, Mao Peng, and Hongxing Wang   
Research Article (7 pages), Article ID 5549796, Volume 2021 (2021)

**[Retracted] Mechanism of *Radix Astragali* and *Radix Salviae Miltiorrhizae* Ameliorates Hypertensive Renal Damage**  
Guangjian Hou, Yuehua Jiang, Yuekun Zheng, Meng Zhao, Yuanzhen Chen, Yonghao Ren, Congan Wang , and Wei Li   
Research Article (7 pages), Article ID 5598351, Volume 2021 (2021)

**Advances in the Development of Biomarkers for Poststroke Epilepsy**

Mengke Liang , Liren Zhang , and Zhi Geng 

Review Article (8 pages), Article ID 5567046, Volume 2021 (2021)

**[Retracted] Pancancer Analysis of Neurovascular-Related NRP Family Genes as Potential Prognostic Biomarkers of Bladder Urothelial Carcinoma**

Chao Deng, Hang Guo, Dongliang Yan , Tao Liang, Xuxiao Ye, and Zuowei Li




Research Article (31 pages), Article ID 5546612, Volume 2021 (2021)

**A Novel Clinical Nomogram to Predict Transient Symptomatic Associated with Infarction: The ABCD3-SLOPE Score**

YanQin Lu , QianQian Bi , Wang Fu , LiLi Liu , Yin Zhang , XiaoYu Zhou , and Jue Wang 







Research Article (8 pages), Article ID 5597155, Volume 2021 (2021)






**[Retracted] Flat Panel CT Scanning Is Helpful in Predicting Hemorrhagic Transformation in Acute Ischemic Stroke Patients Undergoing Endovascular Thrombectomy**

Liuwei Chen, Yi Xu, Rui Shen, Jiping Sun, Xiang Zhang , Quanbin Zhang , and Feng Wang 

Research Article (8 pages), Article ID 5527101, Volume 2021 (2021)

**[Retracted] Protective Effect of Triphala against Oxidative Stress-Induced Neurotoxicity**


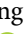















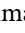



Wanchen Ning , Simin Li , Jokiyab Tsering , Yihong Ma , Honghong Li , Yuezhu Ma , Anthony

Chukwunonso Ogbuehi , Hongying Pan , Hanluo Li , Shaonan Hu , Xiangqiong Liu , Yupei

Deng , Jianlin Zhang , and Xianda Hu 




Research Article (11 pages), Article ID 6674988, Volume 2021 (2021)

**Shared Molecular Mechanisms between Alzheimer's Disease and Periodontitis Revealed by Transcriptomic Analysis**

Jieqi Jin , Mengkai Guang , Anthony Chukwunonso Ogbuehi , Simin Li , Kai Zhang , Yihong Ma , Aneesha Acharya , Bihan Guo , Zongwu Peng , Xiangqiong Liu , Yupei Deng , Zhaobi Fang , Xiongjie Zhu , Shiting Hua , Cong Li , Rainer Haak , Dirk Ziebolz , Gerhard Schmalz , Lei Liu , Baohua Xu , and Xiaofeng Huang 

Research Article (22 pages), Article ID 6633563, Volume 2021 (2021)

**[Retracted] Clinical Efficacy and Safety of "Three-Dimensional Balanced Manipulation" in the Treatment of Cervical Spondylotic Radiculopathy by Finite Element Analysis**

Shengnan Cao, Yuanzhen Chen, Feng Zhang, Shifei Sun, Congan Wang, Guangjian Hou, Dandan Wang , Guodong Sun , and Bin Shi 

Research Article (8 pages), Article ID 5563296, Volume 2021 (2021)




**[Retracted] Experimental Study of lncRNA RP11-815M8.1 Promoting Osteogenic Differentiation of Human Bone Marrow Mesenchymal Stem Cells**

Xiang Sun , Junchuan Cao , Jiusong Han , Bo Jia , Jing Wang , Junxiang Lian , Jianwei Gao , Shuguang Liu , and Hui Xiao 

Research Article (8 pages), Article ID 5512370, Volume 2021 (2021)


## Contents

### **Sirt-1 Regulates Physiological Process and Exerts Protective Effects against Oxidative Stress**

Lei Liu , Guangyuan Xia, Peifan Li, Yiming Wang , and Qian Zhao 

Research Article (12 pages), Article ID 5542545, Volume 2021 (2021)

### **Serum ICAM-1 as a Predictor of Prognosis in Patients with Acute Ischemic Stroke**

Lei Wang, Yan Chen, Depeng Feng, and Xiaoling Wang 




Research Article (6 pages), Article ID 5539304, Volume 2021 (2021)

### **[Retracted] Applicability of High-Frequency Ultrasound to the Early Diagnosis of Diabetic Peripheral Neuropathy**

Xishun Ma , Tongxia Li, Lizhen Du , Gang Liu, Ting Sun, and Tongliang Han 







Research Article (6 pages), Article ID 5529063, Volume 2021 (2021)

### **[Retracted] Agomelatine Softens Depressive-Like Behavior through the Regulation of Autophagy and Apoptosis**

Fengpei Chen, Shijia Chen , Jie Liu, Nashwa Amin, Weidong Jin , and Marong Fang 




Research Article (10 pages), Article ID 6664591, Volume 2021 (2021)

### **[Retracted] A Network Pharmacology to Explore the Mechanism of *Calculus Bovis* in the Treatment of Ischemic Stroke**

Fangchen Liu , Ling Li , Jian Chen , Ying Wu , Yongbing Cao , and Ping Zhong 

Research Article (20 pages), Article ID 6611018, Volume 2021 (2021)

### **Plasma Resolvin D2 to Leukotriene B<sub>4</sub> Ratio Is Reduced in Diabetic Patients with Ischemic Stroke and Related to Prognosis**

Zhijuan Miao , Xin Tang, Marianne Schultzberg, Yuwu Zhao , and Xiuzhe Wang 


Research Article (8 pages), Article ID 6657646, Volume 2021 (2021)

### **[Retracted] Measuring Subthalamic Nucleus Volume of Parkinson's Patients and Evaluating Its Relationship with Clinical Scales at Pre- and Postdeep Brain Stimulation Treatment: A Magnetic Resonance Imaging Study**

Li Lu, Kai Xu , Lin Shi, Weiqiang Dou, Kai Liu , Hong Ma, Lixiang Xie, Chao Zhang, and Cailuan Lu

Research Article (7 pages), Article ID 6646416, Volume 2021 (2021)

### **[Retracted] A Prediction Model for Cognitive Impairment Risk in Colorectal Cancer after Chemotherapy Treatment**

Shu-Ping Zhou, Su-Ding Fei , Hui-Hui Han, Jing-Jing Li, Shuang Yang, and Chun-Yang Zhao

Research Article (13 pages), Article ID 6666453, Volume 2021 (2021)




















### **The Relationship between Serum Amyloid A Level and Cognitive Dysfunction in Patients with Vascular Dementia: Preliminary Findings**

Min Xu , Xiao-ying He , and Pan Huang 

Research Article (6 pages), Article ID 6676144, Volume 2021 (2021)




**[Retracted] Identification of the Potential Biomarkers Involved in the Human Oral Mucosal Wound Healing: A Bioinformatic Study**

Wanchen Ning , Xiao Jiang , Zhengyang Sun , Anthony Chukwunonso Ogbuehi , Wenli Gu , Aneesha Acharya , Zhaobi Fang , Xiongjie Zhu , Qianhua Ou , Muhui Zeng , Cong Li , Shiting Hua , Prabhakar Mujagond , Xiangqiong Liu , Yupei Deng , Hongying Pan , Shaonan Hu , Xianda Hu , and Simin Li 





Research Article (16 pages), Article ID 6695245, Volume 2021 (2021)

**[Retracted] Potential Factors for Psychological Symptoms at Three Months in Patients with Young Ischemic Stroke**

Dongjuan Xu, Xi Chu, Kun Wang, Lianyan Wei, Yunyun Xu, Xiaomin Huang, Jinna Li, Lina Xu, Lu Yin, Hong Liu, Xiaolei Liu, Haixia Leng, Qing Xue, Mao Peng, Longbin Jia, and Hongxing Wang 

Research Article (7 pages), Article ID 5545078, Volume 2021 (2021)

**The Hsp90 Inhibitor 17-DMAG Attenuates Hyperglycemia-Enhanced Hemorrhagic Transformation in Experimental Stroke**

Jiaming Zhang , Kai Wang , Jia Qi, Xiaodong Cao , and Feng Wang 




Research Article (7 pages), Article ID 6668442, Volume 2021 (2021)

**Imaging Hyperreflective Foci as an Inflammatory Biomarker after Anti-VEGF Treatment in Neovascular Age-Related Macular Degeneration Patients with Optical Coherence Tomography Angiography**

Jing Wu , Chaoyang Zhang , Qian Yang , Hai Xie , Jingting Zhang , Qinghua Qiu , Kun Liu , Dawei Luo, Fang Liu , and Jingfa Zhang 

Research Article (7 pages), Article ID 6648191, Volume 2021 (2021)

**[Retracted] Genome Assembly and Analyses of the Macrofungus *Macrocybe gigantea***

Ling Kui , Zhe Zhang, Yangzi Wang, Yesheng Zhang, Shiming Li, Xiao Dong, Qiuju Xia, Jun Sheng , Jian Wang, and Yang Dong 


Research Article (14 pages), Article ID 6656365, Volume 2021 (2021)

**The Value of Combined Detection of D-dimer and CD62p in Judging the Severity of Acute Cerebral Infarction and Short-Term Prognosis**

Min Xu , Xiao-ying He , and Pan Huang 




Research Article (6 pages), Article ID 6620311, Volume 2021 (2021)

**[Retracted] Safety and Efficacy of Early Carotid Endarterectomy in Patients with Symptomatic Carotid Artery Stenosis: A Meta-Analysis**

Xiao Chen, Jing Su, Guojun Wang , Han Zhao, Shizhong Zhang, Tao Liu, Xindi Su, and Ning Zhou

Review Article (8 pages), Article ID 6623426, Volume 2021 (2021)

**[Retracted] The Relationship between the Mean Platelet Volume and Carotid Atherosclerosis and Prognosis in Patients with Acute Cerebral Infarction**




Min Xu , Xiao-ying He , and Pan Huang 

Research Article (6 pages), Article ID 6685740, Volume 2020 (2020)

## Contents



---

**[Retracted] Effects of Carotid Artery Stent and Carotid Endarterectomy on Cognitive Function in Patients with Carotid Stenosis**

Pan Huang , Xiao-ying He , and Min Xu 



Review Article (7 pages), Article ID 6634537, Volume 2020 (2020)

**[Retracted] Analysis of Age and Prevention Strategy on Outcome after Cerebral Venous Thrombosis**

Xiuli Chu, Jianlin Zhang, Bin Zhang , and Yuwu Zhao 



Research Article (6 pages), Article ID 6637692, Volume 2020 (2020)

**Association between Serum IL-37 and Spinal Cord Injury: A Prospective Observational Study**

Yuanzhen Chen, Dandan Wang, Shengnan Cao, Guangjian Hou, Hong Ma , and Bin Shi 




Research Article (5 pages), Article ID 6664313, Volume 2020 (2020)

**Serum CCL21 as a Potential Biomarker for Cognitive Impairment in Spinal Cord Injury**

Yuanzhen Chen, Liangke Liang, Shengnan Cao, Guangjian Hou, Qian Zhang, Hong Ma , and Bin Shi 

Research Article (5 pages), Article ID 6692802, Volume 2020 (2020)

**The Role of miRNA-146a and Proinflammatory Cytokines in Carotid Atherosclerosis**

Pan Huang , Xiao-ying He , and Min Xu 

Research Article (7 pages), Article ID 6657734, Volume 2020 (2020)

**Increased Levels of Serum Neuregulin 1 Associated with Cognitive Impairment in Vascular Dementia**

Xiaoling Wang, Fengyu Zhang, Weibin Ma , Depeng Feng, Jingjing Zhang, and Jialei Xu 

Research Article (5 pages), Article ID 6683747, Volume 2020 (2020)

## *Retraction*

# **Retracted: The Conditioned Medium of *Lactobacillus rhamnoides* GG Regulates Microglia/Macrophage Polarization and Improves Functional Recovery after Spinal Cord Injury in Rats**

### **BioMed Research International**

Received 12 March 2024; Accepted 12 March 2024; Published 20 March 2024

Copyright © 2024 BioMed Research International. This is an open access article distributed under the Creative Commons Attribution License, which permits unrestricted use, distribution, and reproduction in any medium, provided the original work is properly cited.

This article has been retracted by Hindawi following an investigation undertaken by the publisher [1]. This investigation has uncovered evidence of one or more of the following indicators of systematic manipulation of the publication process:

- (1) Discrepancies in scope
- (2) Discrepancies in the description of the research reported
- (3) Discrepancies between the availability of data and the research described
- (4) Inappropriate citations
- (5) Incoherent, meaningless and/or irrelevant content included in the article
- (6) Manipulated or compromised peer review

The presence of these indicators undermines our confidence in the integrity of the article's content and we cannot, therefore, vouch for its reliability. Please note that this notice is intended solely to alert readers that the content of this article is unreliable. We have not investigated whether authors were aware of or involved in the systematic manipulation of the publication process.

Wiley and Hindawi regrets that the usual quality checks did not identify these issues before publication and have since put additional measures in place to safeguard research integrity.

We wish to credit our own Research Integrity and Research Publishing teams and anonymous and named

external researchers and research integrity experts for contributing to this investigation.

The corresponding author, as the representative of all authors, has been given the opportunity to register their agreement or disagreement to this retraction. We have kept a record of any response received.

### **References**

- [1] F. Lin, B. Zhang, Q. Shi et al., "The Conditioned Medium of *Lactobacillus rhamnoides* GG Regulates Microglia/Macrophage Polarization and Improves Functional Recovery after Spinal Cord Injury in Rats," *BioMed Research International*, vol. 2021, Article ID 3376496, 13 pages, 2021.

## Retraction

# Retracted: High-Throughput Screen of Natural Compounds and Biomarkers for NSCLC Treatment by Differential Expression and Weighted Gene Coexpression Network Analysis (WGCNA)

### BioMed Research International

Received 12 March 2024; Accepted 12 March 2024; Published 20 March 2024

Copyright © 2024 BioMed Research International. This is an open access article distributed under the Creative Commons Attribution License, which permits unrestricted use, distribution, and reproduction in any medium, provided the original work is properly cited.

This article has been retracted by Hindawi following an investigation undertaken by the publisher [1]. This investigation has uncovered evidence of one or more of the following indicators of systematic manipulation of the publication process:

- (1) Discrepancies in scope
- (2) Discrepancies in the description of the research reported
- (3) Discrepancies between the availability of data and the research described
- (4) Inappropriate citations
- (5) Incoherent, meaningless and/or irrelevant content included in the article
- (6) Manipulated or compromised peer review

The presence of these indicators undermines our confidence in the integrity of the article's content and we cannot, therefore, vouch for its reliability. Please note that this notice is intended solely to alert readers that the content of this article is unreliable. We have not investigated whether authors were aware of or involved in the systematic manipulation of the publication process.

Wiley and Hindawi regrets that the usual quality checks did not identify these issues before publication and have since put additional measures in place to safeguard research integrity.

We wish to credit our own Research Integrity and Research Publishing teams and anonymous and named external researchers and research integrity experts for contributing to this investigation.

The corresponding author, as the representative of all authors, has been given the opportunity to register their agreement or disagreement to this retraction. We have kept a record of any response received.

### References

- [1] L. Kui, M. Li, X. Yang et al., "High-Throughput Screen of Natural Compounds and Biomarkers for NSCLC Treatment by Differential Expression and Weighted Gene Coexpression Network Analysis (WGCNA)," *BioMed Research International*, vol. 2021, Article ID 5955343, 20 pages, 2021.

## Retraction

# Retracted: A Predictive Model for the Risk of Cognitive Impairment in Patients with Gallstones

### BioMed Research International

Received 12 March 2024; Accepted 12 March 2024; Published 20 March 2024

Copyright © 2024 BioMed Research International. This is an open access article distributed under the Creative Commons Attribution License, which permits unrestricted use, distribution, and reproduction in any medium, provided the original work is properly cited.

This article has been retracted by Hindawi following an investigation undertaken by the publisher [1]. This investigation has uncovered evidence of one or more of the following indicators of systematic manipulation of the publication process:

- (1) Discrepancies in scope
- (2) Discrepancies in the description of the research reported
- (3) Discrepancies between the availability of data and the research described
- (4) Inappropriate citations
- (5) Incoherent, meaningless and/or irrelevant content included in the article
- (6) Manipulated or compromised peer review

The presence of these indicators undermines our confidence in the integrity of the article's content and we cannot, therefore, vouch for its reliability. Please note that this notice is intended solely to alert readers that the content of this article is unreliable. We have not investigated whether authors were aware of or involved in the systematic manipulation of the publication process.

Wiley and Hindawi regrets that the usual quality checks did not identify these issues before publication and have since put additional measures in place to safeguard research integrity.

We wish to credit our own Research Integrity and Research Publishing teams and anonymous and named external researchers and research integrity experts for contributing to this investigation.

The corresponding author, as the representative of all authors, has been given the opportunity to register their agreement or disagreement to this retraction. We have kept a record of any response received.

### References

- [1] Z. Liu and C. Li, "A Predictive Model for the Risk of Cognitive Impairment in Patients with Gallstones," *BioMed Research International*, vol. 2021, Article ID 3792407, 13 pages, 2021.

## *Retraction*

# **Retracted: Experimental Study of lncRNA RP11-815M8.1 Promoting Osteogenic Differentiation of Human Bone Marrow Mesenchymal Stem Cells**

### **BioMed Research International**

Received 12 March 2024; Accepted 12 March 2024; Published 20 March 2024

Copyright © 2024 BioMed Research International. This is an open access article distributed under the Creative Commons Attribution License, which permits unrestricted use, distribution, and reproduction in any medium, provided the original work is properly cited.

This article has been retracted by Hindawi following an investigation undertaken by the publisher [1]. This investigation has uncovered evidence of one or more of the following indicators of systematic manipulation of the publication process:

- (1) Discrepancies in scope
- (2) Discrepancies in the description of the research reported
- (3) Discrepancies between the availability of data and the research described
- (4) Inappropriate citations
- (5) Incoherent, meaningless and/or irrelevant content included in the article
- (6) Manipulated or compromised peer review

The presence of these indicators undermines our confidence in the integrity of the article's content and we cannot, therefore, vouch for its reliability. Please note that this notice is intended solely to alert readers that the content of this article is unreliable. We have not investigated whether authors were aware of or involved in the systematic manipulation of the publication process.

Wiley and Hindawi regrets that the usual quality checks did not identify these issues before publication and have since put additional measures in place to safeguard research integrity.

We wish to credit our own Research Integrity and Research Publishing teams and anonymous and named

external researchers and research integrity experts for contributing to this investigation.

The corresponding author, as the representative of all authors, has been given the opportunity to register their agreement or disagreement to this retraction. We have kept a record of any response received.

### **References**

- [1] X. Sun, J. Cao, J. Han et al., "Experimental Study of lncRNA RP11-815M8.1 Promoting Osteogenic Differentiation of Human Bone Marrow Mesenchymal Stem Cells," *BioMed Research International*, vol. 2021, Article ID 5512370, 8 pages, 2021.

## Retraction

# Retracted: Identification of the Potential Biomarkers Involved in the Human Oral Mucosal Wound Healing: A Bioinformatic Study

### BioMed Research International

Received 12 March 2024; Accepted 12 March 2024; Published 20 March 2024

Copyright © 2024 BioMed Research International. This is an open access article distributed under the Creative Commons Attribution License, which permits unrestricted use, distribution, and reproduction in any medium, provided the original work is properly cited.

This article has been retracted by Hindawi following an investigation undertaken by the publisher [1]. This investigation has uncovered evidence of one or more of the following indicators of systematic manipulation of the publication process:

- (1) Discrepancies in scope
- (2) Discrepancies in the description of the research reported
- (3) Discrepancies between the availability of data and the research described
- (4) Inappropriate citations
- (5) Incoherent, meaningless and/or irrelevant content included in the article
- (6) Manipulated or compromised peer review

The presence of these indicators undermines our confidence in the integrity of the article's content and we cannot, therefore, vouch for its reliability. Please note that this notice is intended solely to alert readers that the content of this article is unreliable. We have not investigated whether authors were aware of or involved in the systematic manipulation of the publication process.

Wiley and Hindawi regrets that the usual quality checks did not identify these issues before publication and have since put additional measures in place to safeguard research integrity.

We wish to credit our own Research Integrity and Research Publishing teams and anonymous and named external researchers and research integrity experts for contributing to this investigation.

The corresponding author, as the representative of all authors, has been given the opportunity to register their agreement or disagreement to this retraction. We have kept a record of any response received.

### References

- [1] W. Ning, X. Jiang, Z. Sun et al., "Identification of the Potential Biomarkers Involved in the Human Oral Mucosal Wound Healing: A Bioinformatic Study," *BioMed Research International*, vol. 2021, Article ID 6695245, 16 pages, 2021.

## Retraction

# Retracted: Interfering with pak4 Protein Expression Affects Osteosarcoma Cell Proliferation and Migration

### BioMed Research International

Received 12 March 2024; Accepted 12 March 2024; Published 20 March 2024

Copyright © 2024 BioMed Research International. This is an open access article distributed under the Creative Commons Attribution License, which permits unrestricted use, distribution, and reproduction in any medium, provided the original work is properly cited.

This article has been retracted by Hindawi following an investigation undertaken by the publisher [1]. This investigation has uncovered evidence of one or more of the following indicators of systematic manipulation of the publication process:

- (1) Discrepancies in scope
- (2) Discrepancies in the description of the research reported
- (3) Discrepancies between the availability of data and the research described
- (4) Inappropriate citations
- (5) Incoherent, meaningless and/or irrelevant content included in the article
- (6) Manipulated or compromised peer review

The presence of these indicators undermines our confidence in the integrity of the article's content and we cannot, therefore, vouch for its reliability. Please note that this notice is intended solely to alert readers that the content of this article is unreliable. We have not investigated whether authors were aware of or involved in the systematic manipulation of the publication process.

Wiley and Hindawi regrets that the usual quality checks did not identify these issues before publication and have since put additional measures in place to safeguard research integrity.

We wish to credit our own Research Integrity and Research Publishing teams and anonymous and named external researchers and research integrity experts for contributing to this investigation.

The corresponding author, as the representative of all authors, has been given the opportunity to register their agreement or disagreement to this retraction. We have kept a record of any response received.

### References

- [1] Y. Fu, L. Fang, Q. Yin et al., "Interfering with pak4 Protein Expression Affects Osteosarcoma Cell Proliferation and Migration," *BioMed Research International*, vol. 2021, Article ID 9977001, 10 pages, 2021.



## Retraction

# Retracted: Mechanism of *Radix Astragali* and *Radix Salviae Miltiorrhizae* Ameliorates Hypertensive Renal Damage

### BioMed Research International

Received 12 March 2024; Accepted 12 March 2024; Published 20 March 2024

Copyright © 2024 BioMed Research International. This is an open access article distributed under the Creative Commons Attribution License, which permits unrestricted use, distribution, and reproduction in any medium, provided the original work is properly cited.

This article has been retracted by Hindawi following an investigation undertaken by the publisher [1]. This investigation has uncovered evidence of one or more of the following indicators of systematic manipulation of the publication process:

- (1) Discrepancies in scope
- (2) Discrepancies in the description of the research reported
- (3) Discrepancies between the availability of data and the research described
- (4) Inappropriate citations
- (5) Incoherent, meaningless and/or irrelevant content included in the article
- (6) Manipulated or compromised peer review

The presence of these indicators undermines our confidence in the integrity of the article's content and we cannot, therefore, vouch for its reliability. Please note that this notice is intended solely to alert readers that the content of this article is unreliable. We have not investigated whether authors were aware of or involved in the systematic manipulation of the publication process.

Wiley and Hindawi regrets that the usual quality checks did not identify these issues before publication and have since put additional measures in place to safeguard research integrity.

We wish to credit our own Research Integrity and Research Publishing teams and anonymous and named external researchers and research integrity experts for contributing to this investigation.

The corresponding author, as the representative of all authors, has been given the opportunity to register their agreement or disagreement to this retraction. We have kept a record of any response received.

### References

- [1] G. Hou, Y. Jiang, Y. Zheng et al., "Mechanism of *Radix Astragali* and *Radix Salviae Miltiorrhizae* Ameliorates Hypertensive Renal Damage," *BioMed Research International*, vol. 2021, Article ID 5598351, 7 pages, 2021.

## Retraction

# Retracted: Osmotic Demyelination Syndrome: Clinical, Neuroimaging Characteristics, and Outcomes in a Series of 18 Cases

### BioMed Research International

Received 12 March 2024; Accepted 12 March 2024; Published 20 March 2024

Copyright © 2024 BioMed Research International. This is an open access article distributed under the Creative Commons Attribution License, which permits unrestricted use, distribution, and reproduction in any medium, provided the original work is properly cited.

This article has been retracted by Hindawi following an investigation undertaken by the publisher [1]. This investigation has uncovered evidence of one or more of the following indicators of systematic manipulation of the publication process:

- (1) Discrepancies in scope
- (2) Discrepancies in the description of the research reported
- (3) Discrepancies between the availability of data and the research described
- (4) Inappropriate citations
- (5) Incoherent, meaningless and/or irrelevant content included in the article
- (6) Manipulated or compromised peer review

The presence of these indicators undermines our confidence in the integrity of the article's content and we cannot, therefore, vouch for its reliability. Please note that this notice is intended solely to alert readers that the content of this article is unreliable. We have not investigated whether authors were aware of or involved in the systematic manipulation of the publication process.

Wiley and Hindawi regrets that the usual quality checks did not identify these issues before publication and have since put additional measures in place to safeguard research integrity.

We wish to credit our own Research Integrity and Research Publishing teams and anonymous and named

external researchers and research integrity experts for contributing to this investigation.

The corresponding author, as the representative of all authors, has been given the opportunity to register their agreement or disagreement to this retraction. We have kept a record of any response received.

### References

- [1] X. Lv, Q. Hong, X. Lin, W. Chen, and Y. Tian, "Osmotic Demyelination Syndrome: Clinical, Neuroimaging Characteristics, and Outcomes in a Series of 18 Cases," *BioMed Research International*, vol. 2021, Article ID 9944632, 9 pages, 2021.

## Retraction

# Retracted: Genome Assembly and Analyses of the Macrofungus *Macrocybe gigantea*

### BioMed Research International

Received 12 March 2024; Accepted 12 March 2024; Published 20 March 2024

Copyright © 2024 BioMed Research International. This is an open access article distributed under the Creative Commons Attribution License, which permits unrestricted use, distribution, and reproduction in any medium, provided the original work is properly cited.

This article has been retracted by Hindawi following an investigation undertaken by the publisher [1]. This investigation has uncovered evidence of one or more of the following indicators of systematic manipulation of the publication process:

- (1) Discrepancies in scope
- (2) Discrepancies in the description of the research reported
- (3) Discrepancies between the availability of data and the research described
- (4) Inappropriate citations
- (5) Incoherent, meaningless and/or irrelevant content included in the article
- (6) Manipulated or compromised peer review

The presence of these indicators undermines our confidence in the integrity of the article's content and we cannot, therefore, vouch for its reliability. Please note that this notice is intended solely to alert readers that the content of this article is unreliable. We have not investigated whether authors were aware of or involved in the systematic manipulation of the publication process.

Wiley and Hindawi regrets that the usual quality checks did not identify these issues before publication and have since put additional measures in place to safeguard research integrity.

We wish to credit our own Research Integrity and Research Publishing teams and anonymous and named external researchers and research integrity experts for contributing to this investigation.

The corresponding author, as the representative of all authors, has been given the opportunity to register their agreement or disagreement to this retraction. We have kept a record of any response received.

### References

- [1] L. Kui, Z. Zhang, Y. Wang et al., "Genome Assembly and Analyses of the Macrofungus *Macrocybe gigantea*," *BioMed Research International*, vol. 2021, Article ID 6656365, 14 pages, 2021.

## Retraction

# Retracted: Protective Effect of Triphala against Oxidative Stress-Induced Neurotoxicity

### BioMed Research International

Received 12 March 2024; Accepted 12 March 2024; Published 20 March 2024

Copyright © 2024 BioMed Research International. This is an open access article distributed under the Creative Commons Attribution License, which permits unrestricted use, distribution, and reproduction in any medium, provided the original work is properly cited.

This article has been retracted by Hindawi following an investigation undertaken by the publisher [1]. This investigation has uncovered evidence of one or more of the following indicators of systematic manipulation of the publication process:

- (1) Discrepancies in scope
- (2) Discrepancies in the description of the research reported
- (3) Discrepancies between the availability of data and the research described
- (4) Inappropriate citations
- (5) Incoherent, meaningless and/or irrelevant content included in the article
- (6) Manipulated or compromised peer review

The presence of these indicators undermines our confidence in the integrity of the article's content and we cannot, therefore, vouch for its reliability. Please note that this notice is intended solely to alert readers that the content of this article is unreliable. We have not investigated whether authors were aware of or involved in the systematic manipulation of the publication process.

Wiley and Hindawi regrets that the usual quality checks did not identify these issues before publication and have since put additional measures in place to safeguard research integrity.

We wish to credit our own Research Integrity and Research Publishing teams and anonymous and named external researchers and research integrity experts for contributing to this investigation.

The corresponding author, as the representative of all authors, has been given the opportunity to register their agreement or disagreement to this retraction. We have kept a record of any response received.

### References

- [1] W. Ning, S. Li, J. Tsering et al., "Protective Effect of Triphala against Oxidative Stress-Induced Neurotoxicity," *BioMed Research International*, vol. 2021, Article ID 6674988, 11 pages, 2021.

## Retraction

# Retracted: The Relationship between the Mean Platelet Volume and Carotid Atherosclerosis and Prognosis in Patients with Acute Cerebral Infarction

### BioMed Research International

Received 12 March 2024; Accepted 12 March 2024; Published 20 March 2024

Copyright © 2024 BioMed Research International. This is an open access article distributed under the Creative Commons Attribution License, which permits unrestricted use, distribution, and reproduction in any medium, provided the original work is properly cited.

This article has been retracted by Hindawi following an investigation undertaken by the publisher [1]. This investigation has uncovered evidence of one or more of the following indicators of systematic manipulation of the publication process:

- (1) Discrepancies in scope
- (2) Discrepancies in the description of the research reported
- (3) Discrepancies between the availability of data and the research described
- (4) Inappropriate citations
- (5) Incoherent, meaningless and/or irrelevant content included in the article
- (6) Manipulated or compromised peer review

The presence of these indicators undermines our confidence in the integrity of the article's content and we cannot, therefore, vouch for its reliability. Please note that this notice is intended solely to alert readers that the content of this article is unreliable. We have not investigated whether authors were aware of or involved in the systematic manipulation of the publication process.

Wiley and Hindawi regrets that the usual quality checks did not identify these issues before publication and have since put additional measures in place to safeguard research integrity.

We wish to credit our own Research Integrity and Research Publishing teams and anonymous and named external researchers and research integrity experts for contributing to this investigation.

The corresponding author, as the representative of all authors, has been given the opportunity to register their agreement or disagreement to this retraction. We have kept a record of any response received.

### References

- [1] M. Xu, X.-y. He, and P. Huang, "The Relationship between the Mean Platelet Volume and Carotid Atherosclerosis and Prognosis in Patients with Acute Cerebral Infarction," *BioMed Research International*, vol. 2020, Article ID 6685740, 6 pages, 2020.

## Retraction

# Retracted: Applicability of High-Frequency Ultrasound to the Early Diagnosis of Diabetic Peripheral Neuropathy

### BioMed Research International

Received 12 March 2024; Accepted 12 March 2024; Published 20 March 2024

Copyright © 2024 BioMed Research International. This is an open access article distributed under the Creative Commons Attribution License, which permits unrestricted use, distribution, and reproduction in any medium, provided the original work is properly cited.

This article has been retracted by Hindawi following an investigation undertaken by the publisher [1]. This investigation has uncovered evidence of one or more of the following indicators of systematic manipulation of the publication process:

- (1) Discrepancies in scope
- (2) Discrepancies in the description of the research reported
- (3) Discrepancies between the availability of data and the research described
- (4) Inappropriate citations
- (5) Incoherent, meaningless and/or irrelevant content included in the article
- (6) Manipulated or compromised peer review

The presence of these indicators undermines our confidence in the integrity of the article's content and we cannot, therefore, vouch for its reliability. Please note that this notice is intended solely to alert readers that the content of this article is unreliable. We have not investigated whether authors were aware of or involved in the systematic manipulation of the publication process.

Wiley and Hindawi regrets that the usual quality checks did not identify these issues before publication and have since put additional measures in place to safeguard research integrity.

We wish to credit our own Research Integrity and Research Publishing teams and anonymous and named external researchers and research integrity experts for contributing to this investigation.

The corresponding author, as the representative of all authors, has been given the opportunity to register their agreement or disagreement to this retraction. We have kept a record of any response received.

### References

- [1] X. Ma, T. Li, L. Du, G. Liu, T. Sun, and T. Han, "Applicability of High-Frequency Ultrasound to the Early Diagnosis of Diabetic Peripheral Neuropathy," *BioMed Research International*, vol. 2021, Article ID 5529063, 6 pages, 2021.

## *Retraction*

# **Retracted: Constructing a Predictive Model of Depression in Chemotherapy Patients with Non-Hodgkin's Lymphoma to Improve Medical Staffs' Psychiatric Care**

### **BioMed Research International**

Received 12 March 2024; Accepted 12 March 2024; Published 20 March 2024

Copyright © 2024 BioMed Research International. This is an open access article distributed under the Creative Commons Attribution License, which permits unrestricted use, distribution, and reproduction in any medium, provided the original work is properly cited.

This article has been retracted by Hindawi following an investigation undertaken by the publisher [1]. This investigation has uncovered evidence of one or more of the following indicators of systematic manipulation of the publication process:

- (1) Discrepancies in scope
- (2) Discrepancies in the description of the research reported
- (3) Discrepancies between the availability of data and the research described
- (4) Inappropriate citations
- (5) Incoherent, meaningless and/or irrelevant content included in the article
- (6) Manipulated or compromised peer review

The presence of these indicators undermines our confidence in the integrity of the article's content and we cannot, therefore, vouch for its reliability. Please note that this notice is intended solely to alert readers that the content of this article is unreliable. We have not investigated whether authors were aware of or involved in the systematic manipulation of the publication process.

Wiley and Hindawi regrets that the usual quality checks did not identify these issues before publication and have since put additional measures in place to safeguard research integrity.

We wish to credit our own Research Integrity and Research Publishing teams and anonymous and named external researchers and research integrity experts for contributing to this investigation.

The corresponding author, as the representative of all authors, has been given the opportunity to register their agreement or disagreement to this retraction. We have kept a record of any response received.

### **References**

- [1] C. Hu, Q. Li, J. Shou et al., "Constructing a Predictive Model of Depression in Chemotherapy Patients with Non-Hodgkin's Lymphoma to Improve Medical Staffs' Psychiatric Care," *BioMed Research International*, vol. 2021, Article ID 9201235, 12 pages, 2021.

## Retraction

# Retracted: Clinical Efficacy and Safety of “Three-Dimensional Balanced Manipulation” in the Treatment of Cervical Spondylotic Radiculopathy by Finite Element Analysis

### BioMed Research International

Received 12 March 2024; Accepted 12 March 2024; Published 20 March 2024

Copyright © 2024 BioMed Research International. This is an open access article distributed under the Creative Commons Attribution License, which permits unrestricted use, distribution, and reproduction in any medium, provided the original work is properly cited.

This article has been retracted by Hindawi following an investigation undertaken by the publisher [1]. This investigation has uncovered evidence of one or more of the following indicators of systematic manipulation of the publication process:

- (1) Discrepancies in scope
- (2) Discrepancies in the description of the research reported
- (3) Discrepancies between the availability of data and the research described
- (4) Inappropriate citations
- (5) Incoherent, meaningless and/or irrelevant content included in the article
- (6) Manipulated or compromised peer review

The presence of these indicators undermines our confidence in the integrity of the article’s content and we cannot, therefore, vouch for its reliability. Please note that this notice is intended solely to alert readers that the content of this article is unreliable. We have not investigated whether authors were aware of or involved in the systematic manipulation of the publication process.

Wiley and Hindawi regrets that the usual quality checks did not identify these issues before publication and have since put additional measures in place to safeguard research integrity.

We wish to credit our own Research Integrity and Research Publishing teams and anonymous and named

external researchers and research integrity experts for contributing to this investigation.

The corresponding author, as the representative of all authors, has been given the opportunity to register their agreement or disagreement to this retraction. We have kept a record of any response received.

### References

- [1] S. Cao, Y. Chen, F. Zhang et al., “Clinical Efficacy and Safety of “Three-Dimensional Balanced Manipulation” in the Treatment of Cervical Spondylotic Radiculopathy by Finite Element Analysis,” *BioMed Research International*, vol. 2021, Article ID 5563296, 8 pages, 2021.



## *Retraction*

# **Retracted: Flat Panel CT Scanning Is Helpful in Predicting Hemorrhagic Transformation in Acute Ischemic Stroke Patients Undergoing Endovascular Thrombectomy**

### **BioMed Research International**

Received 12 March 2024; Accepted 12 March 2024; Published 20 March 2024

Copyright © 2024 BioMed Research International. This is an open access article distributed under the Creative Commons Attribution License, which permits unrestricted use, distribution, and reproduction in any medium, provided the original work is properly cited.

This article has been retracted by Hindawi following an investigation undertaken by the publisher [1]. This investigation has uncovered evidence of one or more of the following indicators of systematic manipulation of the publication process:

- (1) Discrepancies in scope
- (2) Discrepancies in the description of the research reported
- (3) Discrepancies between the availability of data and the research described
- (4) Inappropriate citations
- (5) Incoherent, meaningless and/or irrelevant content included in the article
- (6) Manipulated or compromised peer review

The presence of these indicators undermines our confidence in the integrity of the article's content and we cannot, therefore, vouch for its reliability. Please note that this notice is intended solely to alert readers that the content of this article is unreliable. We have not investigated whether authors were aware of or involved in the systematic manipulation of the publication process.

Wiley and Hindawi regrets that the usual quality checks did not identify these issues before publication and have since put additional measures in place to safeguard research integrity.

We wish to credit our own Research Integrity and Research Publishing teams and anonymous and named

external researchers and research integrity experts for contributing to this investigation.

The corresponding author, as the representative of all authors, has been given the opportunity to register their agreement or disagreement to this retraction. We have kept a record of any response received.

### **References**

- [1] L. Chen, Y. Xu, R. Shen et al., "Flat Panel CT Scanning Is Helpful in Predicting Hemorrhagic Transformation in Acute Ischemic Stroke Patients Undergoing Endovascular Thrombectomy," *BioMed Research International*, vol. 2021, Article ID 5527101, 8 pages, 2021.

## *Retraction*

# **Retracted: Effects of Ozone on Hippocampus BDNF and Fos Expressions in Rats with Chronic Compression of Dorsal Root Ganglia**

### **BioMed Research International**

Received 12 March 2024; Accepted 12 March 2024; Published 20 March 2024

Copyright © 2024 BioMed Research International. This is an open access article distributed under the Creative Commons Attribution License, which permits unrestricted use, distribution, and reproduction in any medium, provided the original work is properly cited.

This article has been retracted by Hindawi following an investigation undertaken by the publisher [1]. This investigation has uncovered evidence of one or more of the following indicators of systematic manipulation of the publication process:

- (1) Discrepancies in scope
- (2) Discrepancies in the description of the research reported
- (3) Discrepancies between the availability of data and the research described
- (4) Inappropriate citations
- (5) Incoherent, meaningless and/or irrelevant content included in the article
- (6) Manipulated or compromised peer review

The presence of these indicators undermines our confidence in the integrity of the article's content and we cannot, therefore, vouch for its reliability. Please note that this notice is intended solely to alert readers that the content of this article is unreliable. We have not investigated whether authors were aware of or involved in the systematic manipulation of the publication process.

Wiley and Hindawi regrets that the usual quality checks did not identify these issues before publication and have since put additional measures in place to safeguard research integrity.

We wish to credit our own Research Integrity and Research Publishing teams and anonymous and named external researchers and research integrity experts for contributing to this investigation.

The corresponding author, as the representative of all authors, has been given the opportunity to register their agreement or disagreement to this retraction. We have kept a record of any response received.

### **References**

- [1] L. Zhu, Y. Wang, X. Lin, X. Zhao, and Z. j. Fu, "Effects of Ozone on Hippocampus BDNF and Fos Expressions in Rats with Chronic Compression of Dorsal Root Ganglia," *BioMed Research International*, vol. 2021, Article ID 5572915, 10 pages, 2021.

## *Retraction*

# **Retracted: Facial Nerve Monitoring under Different Levels of Neuromuscular Blockade with Cisatracurium Besilate in Parotid Tumour Surgery**

### **BioMed Research International**

Received 12 March 2024; Accepted 12 March 2024; Published 20 March 2024

Copyright © 2024 BioMed Research International. This is an open access article distributed under the Creative Commons Attribution License, which permits unrestricted use, distribution, and reproduction in any medium, provided the original work is properly cited.

This article has been retracted by Hindawi following an investigation undertaken by the publisher [1]. This investigation has uncovered evidence of one or more of the following indicators of systematic manipulation of the publication process:

- (1) Discrepancies in scope
- (2) Discrepancies in the description of the research reported
- (3) Discrepancies between the availability of data and the research described
- (4) Inappropriate citations
- (5) Incoherent, meaningless and/or irrelevant content included in the article
- (6) Manipulated or compromised peer review

The presence of these indicators undermines our confidence in the integrity of the article's content and we cannot, therefore, vouch for its reliability. Please note that this notice is intended solely to alert readers that the content of this article is unreliable. We have not investigated whether authors were aware of or involved in the systematic manipulation of the publication process.

Wiley and Hindawi regrets that the usual quality checks did not identify these issues before publication and have since put additional measures in place to safeguard research integrity.

We wish to credit our own Research Integrity and Research Publishing teams and anonymous and named external researchers and research integrity experts for contributing to this investigation.

The corresponding author, as the representative of all authors, has been given the opportunity to register their agreement or disagreement to this retraction. We have kept a record of any response received.

### **References**

- [1] H. Huang, H. Jiang, J. Liu et al., "Facial Nerve Monitoring under Different Levels of Neuromuscular Blockade with Cisatracurium Besilate in Parotid Tumour Surgery," *BioMed Research International*, vol. 2021, Article ID 5655061, 11 pages, 2021.

## Retraction

# Retracted: Analysis of Age and Prevention Strategy on Outcome after Cerebral Venous Thrombosis

### BioMed Research International

Received 12 March 2024; Accepted 12 March 2024; Published 20 March 2024

Copyright © 2024 BioMed Research International. This is an open access article distributed under the Creative Commons Attribution License, which permits unrestricted use, distribution, and reproduction in any medium, provided the original work is properly cited.

This article has been retracted by Hindawi following an investigation undertaken by the publisher [1]. This investigation has uncovered evidence of one or more of the following indicators of systematic manipulation of the publication process:

- (1) Discrepancies in scope
- (2) Discrepancies in the description of the research reported
- (3) Discrepancies between the availability of data and the research described
- (4) Inappropriate citations
- (5) Incoherent, meaningless and/or irrelevant content included in the article
- (6) Manipulated or compromised peer review

The presence of these indicators undermines our confidence in the integrity of the article's content and we cannot, therefore, vouch for its reliability. Please note that this notice is intended solely to alert readers that the content of this article is unreliable. We have not investigated whether authors were aware of or involved in the systematic manipulation of the publication process.

Wiley and Hindawi regrets that the usual quality checks did not identify these issues before publication and have since put additional measures in place to safeguard research integrity.

We wish to credit our own Research Integrity and Research Publishing teams and anonymous and named external researchers and research integrity experts for contributing to this investigation.

The corresponding author, as the representative of all authors, has been given the opportunity to register their agreement or disagreement to this retraction. We have kept a record of any response received.

### References

- [1] X. Chu, J. Zhang, B. Zhang, and Y. Zhao, "Analysis of Age and Prevention Strategy on Outcome after Cerebral Venous Thrombosis," *BioMed Research International*, vol. 2020, Article ID 6637692, 6 pages, 2020.

## *Retraction*

# **Retracted: The Impact of Study Setting on Clinical Characteristics in Older Chinese Adults with Subjective Cognitive Decline: Baseline Investigation of Convenience and Population-Based Samples**

### **BioMed Research International**

Received 12 March 2024; Accepted 12 March 2024; Published 20 March 2024

Copyright © 2024 BioMed Research International. This is an open access article distributed under the Creative Commons Attribution License, which permits unrestricted use, distribution, and reproduction in any medium, provided the original work is properly cited.

This article has been retracted by Hindawi following an investigation undertaken by the publisher [1]. This investigation has uncovered evidence of one or more of the following indicators of systematic manipulation of the publication process:

- (1) Discrepancies in scope
- (2) Discrepancies in the description of the research reported
- (3) Discrepancies between the availability of data and the research described
- (4) Inappropriate citations
- (5) Incoherent, meaningless and/or irrelevant content included in the article
- (6) Manipulated or compromised peer review

The presence of these indicators undermines our confidence in the integrity of the article's content and we cannot, therefore, vouch for its reliability. Please note that this notice is intended solely to alert readers that the content of this article is unreliable. We have not investigated whether authors were aware of or involved in the systematic manipulation of the publication process.

Wiley and Hindawi regrets that the usual quality checks did not identify these issues before publication and have since put additional measures in place to safeguard research integrity.

We wish to credit our own Research Integrity and Research Publishing teams and anonymous and named external researchers and research integrity experts for contributing to this investigation.

The corresponding author, as the representative of all authors, has been given the opportunity to register their agreement or disagreement to this retraction. We have kept a record of any response received.

### **References**

- [1] M. Zhao, G. Chen, T. Li, C. Sheng, Y. Li, and Y. Han, "The Impact of Study Setting on Clinical Characteristics in Older Chinese Adults with Subjective Cognitive Decline: Baseline Investigation of Convenience and Population-Based Samples," *BioMed Research International*, vol. 2021, Article ID 5538323, 9 pages, 2021.

## Retraction

# Retracted: Agomelatine Softens Depressive-Like Behavior through the Regulation of Autophagy and Apoptosis

### BioMed Research International

Received 12 March 2024; Accepted 12 March 2024; Published 20 March 2024

Copyright © 2024 BioMed Research International. This is an open access article distributed under the Creative Commons Attribution License, which permits unrestricted use, distribution, and reproduction in any medium, provided the original work is properly cited.

This article has been retracted by Hindawi following an investigation undertaken by the publisher [1]. This investigation has uncovered evidence of one or more of the following indicators of systematic manipulation of the publication process:

- (1) Discrepancies in scope
- (2) Discrepancies in the description of the research reported
- (3) Discrepancies between the availability of data and the research described
- (4) Inappropriate citations
- (5) Incoherent, meaningless and/or irrelevant content included in the article
- (6) Manipulated or compromised peer review

The presence of these indicators undermines our confidence in the integrity of the article's content and we cannot, therefore, vouch for its reliability. Please note that this notice is intended solely to alert readers that the content of this article is unreliable. We have not investigated whether authors were aware of or involved in the systematic manipulation of the publication process.

Wiley and Hindawi regrets that the usual quality checks did not identify these issues before publication and have since put additional measures in place to safeguard research integrity.

We wish to credit our own Research Integrity and Research Publishing teams and anonymous and named external researchers and research integrity experts for contributing to this investigation.

The corresponding author, as the representative of all authors, has been given the opportunity to register their agreement or disagreement to this retraction. We have kept a record of any response received.

### References

- [1] F. Chen, S. Chen, J. Liu, N. Amin, W. Jin, and M. Fang, "Agomelatine Softens Depressive-Like Behavior through the Regulation of Autophagy and Apoptosis," *BioMed Research International*, vol. 2021, Article ID 6664591, 10 pages, 2021.

## Retraction

# Retracted: A Prediction Model for Cognitive Impairment Risk in Colorectal Cancer after Chemotherapy Treatment

### BioMed Research International

Received 12 March 2024; Accepted 12 March 2024; Published 20 March 2024

Copyright © 2024 BioMed Research International. This is an open access article distributed under the Creative Commons Attribution License, which permits unrestricted use, distribution, and reproduction in any medium, provided the original work is properly cited.

This article has been retracted by Hindawi following an investigation undertaken by the publisher [1]. This investigation has uncovered evidence of one or more of the following indicators of systematic manipulation of the publication process:

- (1) Discrepancies in scope
- (2) Discrepancies in the description of the research reported
- (3) Discrepancies between the availability of data and the research described
- (4) Inappropriate citations
- (5) Incoherent, meaningless and/or irrelevant content included in the article
- (6) Manipulated or compromised peer review

The presence of these indicators undermines our confidence in the integrity of the article's content and we cannot, therefore, vouch for its reliability. Please note that this notice is intended solely to alert readers that the content of this article is unreliable. We have not investigated whether authors were aware of or involved in the systematic manipulation of the publication process.

Wiley and Hindawi regrets that the usual quality checks did not identify these issues before publication and have since put additional measures in place to safeguard research integrity.

We wish to credit our own Research Integrity and Research Publishing teams and anonymous and named external researchers and research integrity experts for contributing to this investigation.

The corresponding author, as the representative of all authors, has been given the opportunity to register their agreement or disagreement to this retraction. We have kept a record of any response received.

### References

- [1] S.-P. Zhou, S.-D. Fei, H.-H. Han, J.-J. Li, S. Yang, and C.-Y. Zhao, "A Prediction Model for Cognitive Impairment Risk in Colorectal Cancer after Chemotherapy Treatment," *BioMed Research International*, vol. 2021, Article ID 6666453, 13 pages, 2021.

## *Retraction*

# **Retracted: Downregulation of LHPP Expression Associated with AFP Acts as a Good Prognostic Factor in Human Hepatocellular Carcinoma**

### **BioMed Research International**

Received 12 March 2024; Accepted 12 March 2024; Published 20 March 2024

Copyright © 2024 BioMed Research International. This is an open access article distributed under the Creative Commons Attribution License, which permits unrestricted use, distribution, and reproduction in any medium, provided the original work is properly cited.

This article has been retracted by Hindawi following an investigation undertaken by the publisher [1]. This investigation has uncovered evidence of one or more of the following indicators of systematic manipulation of the publication process:

- (1) Discrepancies in scope
- (2) Discrepancies in the description of the research reported
- (3) Discrepancies between the availability of data and the research described
- (4) Inappropriate citations
- (5) Incoherent, meaningless and/or irrelevant content included in the article
- (6) Manipulated or compromised peer review

The presence of these indicators undermines our confidence in the integrity of the article's content and we cannot, therefore, vouch for its reliability. Please note that this notice is intended solely to alert readers that the content of this article is unreliable. We have not investigated whether authors were aware of or involved in the systematic manipulation of the publication process.

Wiley and Hindawi regrets that the usual quality checks did not identify these issues before publication and have since put additional measures in place to safeguard research integrity.

We wish to credit our own Research Integrity and Research Publishing teams and anonymous and named external researchers and research integrity experts for contributing to this investigation.

The corresponding author, as the representative of all authors, has been given the opportunity to register their agreement or disagreement to this retraction. We have kept a record of any response received.

### **References**

- [1] X. Chao, W. Zhang, J. Wu et al., "Downregulation of LHPP Expression Associated with AFP Acts as a Good Prognostic Factor in Human Hepatocellular Carcinoma," *BioMed Research International*, vol. 2021, Article ID 1971048, 9 pages, 2021.



## *Retraction*

# **Retracted: Effects of Carotid Artery Stent and Carotid Endarterectomy on Cognitive Function in Patients with Carotid Stenosis**

### **BioMed Research International**

Received 12 March 2024; Accepted 12 March 2024; Published 20 March 2024

Copyright © 2024 BioMed Research International. This is an open access article distributed under the Creative Commons Attribution License, which permits unrestricted use, distribution, and reproduction in any medium, provided the original work is properly cited.

This article has been retracted by Hindawi following an investigation undertaken by the publisher [1]. This investigation has uncovered evidence of one or more of the following indicators of systematic manipulation of the publication process:

- (1) Discrepancies in scope
- (2) Discrepancies in the description of the research reported
- (3) Discrepancies between the availability of data and the research described
- (4) Inappropriate citations
- (5) Incoherent, meaningless and/or irrelevant content included in the article
- (6) Manipulated or compromised peer review

The presence of these indicators undermines our confidence in the integrity of the article's content and we cannot, therefore, vouch for its reliability. Please note that this notice is intended solely to alert readers that the content of this article is unreliable. We have not investigated whether authors were aware of or involved in the systematic manipulation of the publication process.

Wiley and Hindawi regrets that the usual quality checks did not identify these issues before publication and have since put additional measures in place to safeguard research integrity.

We wish to credit our own Research Integrity and Research Publishing teams and anonymous and named external researchers and research integrity experts for contributing to this investigation.

The corresponding author, as the representative of all authors, has been given the opportunity to register their agreement or disagreement to this retraction. We have kept a record of any response received.

### **References**

- [1] P. Huang, X.-y. He, and M. Xu, "Effects of Carotid Artery Stent and Carotid Endarterectomy on Cognitive Function in Patients with Carotid Stenosis," *BioMed Research International*, vol. 2020, Article ID 6634537, 7 pages, 2020.

## Retraction

# Retracted: Effects of Omega-3 Polyunsaturated Fatty Acids on Cognitive Function after Splenectomy in Rats

### BioMed Research International

Received 12 March 2024; Accepted 12 March 2024; Published 20 March 2024

Copyright © 2024 BioMed Research International. This is an open access article distributed under the Creative Commons Attribution License, which permits unrestricted use, distribution, and reproduction in any medium, provided the original work is properly cited.

This article has been retracted by Hindawi following an investigation undertaken by the publisher [1]. This investigation has uncovered evidence of one or more of the following indicators of systematic manipulation of the publication process:

- (1) Discrepancies in scope
- (2) Discrepancies in the description of the research reported
- (3) Discrepancies between the availability of data and the research described
- (4) Inappropriate citations
- (5) Incoherent, meaningless and/or irrelevant content included in the article
- (6) Manipulated or compromised peer review

The presence of these indicators undermines our confidence in the integrity of the article's content and we cannot, therefore, vouch for its reliability. Please note that this notice is intended solely to alert readers that the content of this article is unreliable. We have not investigated whether authors were aware of or involved in the systematic manipulation of the publication process.

Wiley and Hindawi regrets that the usual quality checks did not identify these issues before publication and have since put additional measures in place to safeguard research integrity.

We wish to credit our own Research Integrity and Research Publishing teams and anonymous and named external researchers and research integrity experts for contributing to this investigation.

The corresponding author, as the representative of all authors, has been given the opportunity to register their agreement or disagreement to this retraction. We have kept a record of any response received.

### References

- [1] Y. Guo, F. Ping, Y. Cao et al., "Effects of Omega-3 Polyunsaturated Fatty Acids on Cognitive Function after Splenectomy in Rats," *BioMed Research International*, vol. 2021, Article ID 5513886, 6 pages, 2021.

## *Retraction*

# **Retracted: Pancancer Analysis of Neurovascular-Related NRP Family Genes as Potential Prognostic Biomarkers of Bladder Urothelial Carcinoma**

### **BioMed Research International**

Received 12 March 2024; Accepted 12 March 2024; Published 20 March 2024

Copyright © 2024 BioMed Research International. This is an open access article distributed under the Creative Commons Attribution License, which permits unrestricted use, distribution, and reproduction in any medium, provided the original work is properly cited.

This article has been retracted by Hindawi following an investigation undertaken by the publisher [1]. This investigation has uncovered evidence of one or more of the following indicators of systematic manipulation of the publication process:

- (1) Discrepancies in scope
- (2) Discrepancies in the description of the research reported
- (3) Discrepancies between the availability of data and the research described
- (4) Inappropriate citations
- (5) Incoherent, meaningless and/or irrelevant content included in the article
- (6) Manipulated or compromised peer review

The presence of these indicators undermines our confidence in the integrity of the article's content and we cannot, therefore, vouch for its reliability. Please note that this notice is intended solely to alert readers that the content of this article is unreliable. We have not investigated whether authors were aware of or involved in the systematic manipulation of the publication process.

Wiley and Hindawi regrets that the usual quality checks did not identify these issues before publication and have since put additional measures in place to safeguard research integrity.

We wish to credit our own Research Integrity and Research Publishing teams and anonymous and named external researchers and research integrity experts for contributing to this investigation.

The corresponding author, as the representative of all authors, has been given the opportunity to register their agreement or disagreement to this retraction. We have kept a record of any response received.

### **References**

- [1] C. Deng, H. Guo, D. Yan, T. Liang, X. Ye, and Z. Li, "Pancancer Analysis of Neurovascular-Related NRP Family Genes as Potential Prognostic Biomarkers of Bladder Urothelial Carcinoma," *BioMed Research International*, vol. 2021, Article ID 5546612, 31 pages, 2021.

## Retraction

# Retracted: Measuring Subthalamic Nucleus Volume of Parkinson's Patients and Evaluating Its Relationship with Clinical Scales at Pre- and Postdeep Brain Stimulation Treatment: A Magnetic Resonance Imaging Study

### BioMed Research International

Received 12 March 2024; Accepted 12 March 2024; Published 20 March 2024

Copyright © 2024 BioMed Research International. This is an open access article distributed under the Creative Commons Attribution License, which permits unrestricted use, distribution, and reproduction in any medium, provided the original work is properly cited.

This article has been retracted by Hindawi following an investigation undertaken by the publisher [1]. This investigation has uncovered evidence of one or more of the following indicators of systematic manipulation of the publication process:

- (1) Discrepancies in scope
- (2) Discrepancies in the description of the research reported
- (3) Discrepancies between the availability of data and the research described
- (4) Inappropriate citations
- (5) Incoherent, meaningless and/or irrelevant content included in the article
- (6) Manipulated or compromised peer review

The presence of these indicators undermines our confidence in the integrity of the article's content and we cannot, therefore, vouch for its reliability. Please note that this notice is intended solely to alert readers that the content of this article is unreliable. We have not investigated whether authors were aware of or involved in the systematic manipulation of the publication process.

Wiley and Hindawi regrets that the usual quality checks did not identify these issues before publication and have since put additional measures in place to safeguard research integrity.

We wish to credit our own Research Integrity and Research Publishing teams and anonymous and named external researchers and research integrity experts for contributing to this investigation.

The corresponding author, as the representative of all authors, has been given the opportunity to register their agreement or disagreement to this retraction. We have kept a record of any response received.

### References

- [1] L. Lu, K. Xu, L. Shi et al., "Measuring Subthalamic Nucleus Volume of Parkinson's Patients and Evaluating Its Relationship with Clinical Scales at Pre- and Postdeep Brain Stimulation Treatment: A Magnetic Resonance Imaging Study," *BioMed Research International*, vol. 2021, Article ID 6646416, 7 pages, 2021.

## Retraction

# Retracted: The Prognostic Value of Leucine-Rich $\alpha 2$ Glycoprotein 1 in Pediatric Spinal Cord Injury

### BioMed Research International

Received 12 March 2024; Accepted 12 March 2024; Published 20 March 2024

Copyright © 2024 BioMed Research International. This is an open access article distributed under the Creative Commons Attribution License, which permits unrestricted use, distribution, and reproduction in any medium, provided the original work is properly cited.

This article has been retracted by Hindawi following an investigation undertaken by the publisher [1]. This investigation has uncovered evidence of one or more of the following indicators of systematic manipulation of the publication process:

- (1) Discrepancies in scope
- (2) Discrepancies in the description of the research reported
- (3) Discrepancies between the availability of data and the research described
- (4) Inappropriate citations
- (5) Incoherent, meaningless and/or irrelevant content included in the article
- (6) Manipulated or compromised peer review

The presence of these indicators undermines our confidence in the integrity of the article's content and we cannot, therefore, vouch for its reliability. Please note that this notice is intended solely to alert readers that the content of this article is unreliable. We have not investigated whether authors were aware of or involved in the systematic manipulation of the publication process.

Wiley and Hindawi regrets that the usual quality checks did not identify these issues before publication and have since put additional measures in place to safeguard research integrity.

We wish to credit our own Research Integrity and Research Publishing teams and anonymous and named external researchers and research integrity experts for contributing to this investigation.

The corresponding author, as the representative of all authors, has been given the opportunity to register their agreement or disagreement to this retraction. We have kept a record of any response received.

### References

- [1] H. Ma, F. Lu, Y. Guo, Z. Shen, and Y. Chen, "The Prognostic Value of Leucine-Rich  $\alpha 2$  Glycoprotein 1 in Pediatric Spinal Cord Injury," *BioMed Research International*, vol. 2021, Article ID 7365204, 5 pages, 2021.

## Retraction

# Retracted: Effects of Different Intervention Time Points of Early Rehabilitation on Patients with Acute Ischemic Stroke: A Single-Center, Randomized Control Study

### BioMed Research International

Received 12 March 2024; Accepted 12 March 2024; Published 20 March 2024

Copyright © 2024 BioMed Research International. This is an open access article distributed under the Creative Commons Attribution License, which permits unrestricted use, distribution, and reproduction in any medium, provided the original work is properly cited.

This article has been retracted by Hindawi following an investigation undertaken by the publisher [1]. This investigation has uncovered evidence of one or more of the following indicators of systematic manipulation of the publication process:

- (1) Discrepancies in scope
- (2) Discrepancies in the description of the research reported
- (3) Discrepancies between the availability of data and the research described
- (4) Inappropriate citations
- (5) Incoherent, meaningless and/or irrelevant content included in the article
- (6) Manipulated or compromised peer review

The presence of these indicators undermines our confidence in the integrity of the article's content and we cannot, therefore, vouch for its reliability. Please note that this notice is intended solely to alert readers that the content of this article is unreliable. We have not investigated whether authors were aware of or involved in the systematic manipulation of the publication process.

Wiley and Hindawi regrets that the usual quality checks did not identify these issues before publication and have since put additional measures in place to safeguard research integrity.

We wish to credit our own Research Integrity and Research Publishing teams and anonymous and named external researchers and research integrity experts for contributing to this investigation.

The corresponding author, as the representative of all authors, has been given the opportunity to register their agreement or disagreement to this retraction. We have kept a record of any response received.

### References

- [1] L. L. Liu, Y. Q. Lu, Q. Q. Bi, W. Fu, X. Y. Zhou, and J. Wang, "Effects of Different Intervention Time Points of Early Rehabilitation on Patients with Acute Ischemic Stroke: A Single-Center, Randomized Control Study," *BioMed Research International*, vol. 2021, Article ID 1940549, 7 pages, 2021.

## *Retraction*

# **Retracted: Safety and Efficacy of Early Carotid Endarterectomy in Patients with Symptomatic Carotid Artery Stenosis: A Meta-Analysis**

### **BioMed Research International**

Received 12 March 2024; Accepted 12 March 2024; Published 20 March 2024

Copyright © 2024 BioMed Research International. This is an open access article distributed under the Creative Commons Attribution License, which permits unrestricted use, distribution, and reproduction in any medium, provided the original work is properly cited.

This article has been retracted by Hindawi following an investigation undertaken by the publisher [1]. This investigation has uncovered evidence of one or more of the following indicators of systematic manipulation of the publication process:

- (1) Discrepancies in scope
- (2) Discrepancies in the description of the research reported
- (3) Discrepancies between the availability of data and the research described
- (4) Inappropriate citations
- (5) Incoherent, meaningless and/or irrelevant content included in the article
- (6) Manipulated or compromised peer review

The presence of these indicators undermines our confidence in the integrity of the article's content and we cannot, therefore, vouch for its reliability. Please note that this notice is intended solely to alert readers that the content of this article is unreliable. We have not investigated whether authors were aware of or involved in the systematic manipulation of the publication process.

Wiley and Hindawi regrets that the usual quality checks did not identify these issues before publication and have since put additional measures in place to safeguard research integrity.

We wish to credit our own Research Integrity and Research Publishing teams and anonymous and named external researchers and research integrity experts for contributing to this investigation.

The corresponding author, as the representative of all authors, has been given the opportunity to register their agreement or disagreement to this retraction. We have kept a record of any response received.

### **References**

- [1] X. Chen, J. Su, G. Wang et al., "Safety and Efficacy of Early Carotid Endarterectomy in Patients with Symptomatic Carotid Artery Stenosis: A Meta-Analysis," *BioMed Research International*, vol. 2021, Article ID 6623426, 8 pages, 2021.

## *Retraction*

# **Retracted: Predicting Decreased Activities of Daily Living in Patients with Moyamoya Disease after Revascularization: Development and Assessment of a New Predictive Nomogram**

### **BioMed Research International**

Received 12 March 2024; Accepted 12 March 2024; Published 20 March 2024

Copyright © 2024 BioMed Research International. This is an open access article distributed under the Creative Commons Attribution License, which permits unrestricted use, distribution, and reproduction in any medium, provided the original work is properly cited.

This article has been retracted by Hindawi following an investigation undertaken by the publisher [1]. This investigation has uncovered evidence of one or more of the following indicators of systematic manipulation of the publication process:

- (1) Discrepancies in scope
- (2) Discrepancies in the description of the research reported
- (3) Discrepancies between the availability of data and the research described
- (4) Inappropriate citations
- (5) Incoherent, meaningless and/or irrelevant content included in the article
- (6) Manipulated or compromised peer review

The presence of these indicators undermines our confidence in the integrity of the article's content and we cannot, therefore, vouch for its reliability. Please note that this notice is intended solely to alert readers that the content of this article is unreliable. We have not investigated whether authors were aware of or involved in the systematic manipulation of the publication process.

Wiley and Hindawi regrets that the usual quality checks did not identify these issues before publication and have since put additional measures in place to safeguard research integrity.

We wish to credit our own Research Integrity and Research Publishing teams and anonymous and named external researchers and research integrity experts for contributing to this investigation.

The corresponding author, as the representative of all authors, has been given the opportunity to register their agreement or disagreement to this retraction. We have kept a record of any response received.

### **References**

- [1] Y. Zhao, D. Yang, G. Li, P. Zhao, X. Luan, and H. Li, "Predicting Decreased Activities of Daily Living in Patients with Moyamoya Disease after Revascularization: Development and Assessment of a New Predictive Nomogram," *BioMed Research International*, vol. 2021, Article ID 6624245, 8 pages, 2021.



## *Retraction*

# **Retracted: Modified Prehospital Acute Stroke Severity (mPASS) Scale to Predict Emergent Large Arterial Occlusion**

### **BioMed Research International**

Received 12 March 2024; Accepted 12 March 2024; Published 20 March 2024

Copyright © 2024 BioMed Research International. This is an open access article distributed under the Creative Commons Attribution License, which permits unrestricted use, distribution, and reproduction in any medium, provided the original work is properly cited.

This article has been retracted by Hindawi following an investigation undertaken by the publisher [1]. This investigation has uncovered evidence of one or more of the following indicators of systematic manipulation of the publication process:

- (1) Discrepancies in scope
- (2) Discrepancies in the description of the research reported
- (3) Discrepancies between the availability of data and the research described
- (4) Inappropriate citations
- (5) Incoherent, meaningless and/or irrelevant content included in the article
- (6) Manipulated or compromised peer review

The presence of these indicators undermines our confidence in the integrity of the article's content and we cannot, therefore, vouch for its reliability. Please note that this notice is intended solely to alert readers that the content of this article is unreliable. We have not investigated whether authors were aware of or involved in the systematic manipulation of the publication process.

Wiley and Hindawi regrets that the usual quality checks did not identify these issues before publication and have since put additional measures in place to safeguard research integrity.

We wish to credit our own Research Integrity and Research Publishing teams and anonymous and named external researchers and research integrity experts for contributing to this investigation.

The corresponding author, as the representative of all authors, has been given the opportunity to register their agreement or disagreement to this retraction. We have kept a record of any response received.

### **References**

- [1] X. Si, J. Ruan, L. Li et al., "Modified Prehospital Acute Stroke Severity (mPASS) Scale to Predict Emergent Large Arterial Occlusion," *BioMed Research International*, vol. 2021, Article ID 5568696, 6 pages, 2021.

## Retraction

# Retracted: A Network Pharmacology to Explore the Mechanism of *Calculus Bovis* in the Treatment of Ischemic Stroke

### BioMed Research International

Received 12 March 2024; Accepted 12 March 2024; Published 20 March 2024

Copyright © 2024 BioMed Research International. This is an open access article distributed under the Creative Commons Attribution License, which permits unrestricted use, distribution, and reproduction in any medium, provided the original work is properly cited.

This article has been retracted by Hindawi following an investigation undertaken by the publisher [1]. This investigation has uncovered evidence of one or more of the following indicators of systematic manipulation of the publication process:

- (1) Discrepancies in scope
- (2) Discrepancies in the description of the research reported
- (3) Discrepancies between the availability of data and the research described
- (4) Inappropriate citations
- (5) Incoherent, meaningless and/or irrelevant content included in the article
- (6) Manipulated or compromised peer review

The presence of these indicators undermines our confidence in the integrity of the article's content and we cannot, therefore, vouch for its reliability. Please note that this notice is intended solely to alert readers that the content of this article is unreliable. We have not investigated whether authors were aware of or involved in the systematic manipulation of the publication process.

Wiley and Hindawi regrets that the usual quality checks did not identify these issues before publication and have since put additional measures in place to safeguard research integrity.

We wish to credit our own Research Integrity and Research Publishing teams and anonymous and named external researchers and research integrity experts for contributing to this investigation.

The corresponding author, as the representative of all authors, has been given the opportunity to register their agreement or disagreement to this retraction. We have kept a record of any response received.

### References

- [1] F. Liu, L. Li, J. Chen, Y. Wu, Y. Cao, and P. Zhong, "A Network Pharmacology to Explore the Mechanism of *Calculus Bovis* in the Treatment of Ischemic Stroke," *BioMed Research International*, vol. 2021, Article ID 6611018, 20 pages, 2021.

## Retraction

# Retracted: Potential Factors for Psychological Symptoms at Three Months in Patients with Young Ischemic Stroke

### BioMed Research International

Received 12 March 2024; Accepted 12 March 2024; Published 20 March 2024

Copyright © 2024 BioMed Research International. This is an open access article distributed under the Creative Commons Attribution License, which permits unrestricted use, distribution, and reproduction in any medium, provided the original work is properly cited.

This article has been retracted by Hindawi following an investigation undertaken by the publisher [1]. This investigation has uncovered evidence of one or more of the following indicators of systematic manipulation of the publication process:

- (1) Discrepancies in scope
- (2) Discrepancies in the description of the research reported
- (3) Discrepancies between the availability of data and the research described
- (4) Inappropriate citations
- (5) Incoherent, meaningless and/or irrelevant content included in the article
- (6) Manipulated or compromised peer review

The presence of these indicators undermines our confidence in the integrity of the article's content and we cannot, therefore, vouch for its reliability. Please note that this notice is intended solely to alert readers that the content of this article is unreliable. We have not investigated whether authors were aware of or involved in the systematic manipulation of the publication process.

Wiley and Hindawi regrets that the usual quality checks did not identify these issues before publication and have since put additional measures in place to safeguard research integrity.

We wish to credit our own Research Integrity and Research Publishing teams and anonymous and named external researchers and research integrity experts for contributing to this investigation.

The corresponding author, as the representative of all authors, has been given the opportunity to register their agreement or disagreement to this retraction. We have kept a record of any response received.

### References

- [1] D. Xu, X. Chu, K. Wang et al., "Potential Factors for Psychological Symptoms at Three Months in Patients with Young Ischemic Stroke," *BioMed Research International*, vol. 2021, Article ID 5545078, 7 pages, 2021.

## Retraction

# Retracted: Celastrol Attenuates Learning and Memory Deficits in an Alzheimer's Disease Rat Model

### BioMed Research International

Received 12 March 2024; Accepted 12 March 2024; Published 20 March 2024

Copyright © 2024 BioMed Research International. This is an open access article distributed under the Creative Commons Attribution License, which permits unrestricted use, distribution, and reproduction in any medium, provided the original work is properly cited.

This article has been retracted by Hindawi following an investigation undertaken by the publisher [1]. This investigation has uncovered evidence of one or more of the following indicators of systematic manipulation of the publication process:

- (1) Discrepancies in scope
- (2) Discrepancies in the description of the research reported
- (3) Discrepancies between the availability of data and the research described
- (4) Inappropriate citations
- (5) Incoherent, meaningless and/or irrelevant content included in the article
- (6) Manipulated or compromised peer review

The presence of these indicators undermines our confidence in the integrity of the article's content and we cannot, therefore, vouch for its reliability. Please note that this notice is intended solely to alert readers that the content of this article is unreliable. We have not investigated whether authors were aware of or involved in the systematic manipulation of the publication process.

Wiley and Hindawi regrets that the usual quality checks did not identify these issues before publication and have since put additional measures in place to safeguard research integrity.

We wish to credit our own Research Integrity and Research Publishing teams and anonymous and named external researchers and research integrity experts for contributing to this investigation.

The corresponding author, as the representative of all authors, has been given the opportunity to register their agreement or disagreement to this retraction. We have kept a record of any response received.

### References

- [1] Y. Xiao, X. Wang, S. Wang et al., "Celastrol Attenuates Learning and Memory Deficits in an Alzheimer's Disease Rat Model," *BioMed Research International*, vol. 2021, Article ID 5574207, 11 pages, 2021.

## Retraction

# Retracted: Interfering with pak4 Protein Expression Affects Osteosarcoma Cell Proliferation and Migration

### BioMed Research International

Received 12 March 2024; Accepted 12 March 2024; Published 20 March 2024

Copyright © 2024 BioMed Research International. This is an open access article distributed under the Creative Commons Attribution License, which permits unrestricted use, distribution, and reproduction in any medium, provided the original work is properly cited.

This article has been retracted by Hindawi following an investigation undertaken by the publisher [1]. This investigation has uncovered evidence of one or more of the following indicators of systematic manipulation of the publication process:

- (1) Discrepancies in scope
- (2) Discrepancies in the description of the research reported
- (3) Discrepancies between the availability of data and the research described
- (4) Inappropriate citations
- (5) Incoherent, meaningless and/or irrelevant content included in the article
- (6) Manipulated or compromised peer review

The presence of these indicators undermines our confidence in the integrity of the article's content and we cannot, therefore, vouch for its reliability. Please note that this notice is intended solely to alert readers that the content of this article is unreliable. We have not investigated whether authors were aware of or involved in the systematic manipulation of the publication process.

Wiley and Hindawi regrets that the usual quality checks did not identify these issues before publication and have since put additional measures in place to safeguard research integrity.

We wish to credit our own Research Integrity and Research Publishing teams and anonymous and named external researchers and research integrity experts for contributing to this investigation.

The corresponding author, as the representative of all authors, has been given the opportunity to register their agreement or disagreement to this retraction. We have kept a record of any response received.

### References

- [1] Y. Fu, L. Fang, Q. Yin et al., "Interfering with pak4 Protein Expression Affects Osteosarcoma Cell Proliferation and Migration," *BioMed Research International*, vol. 2021, Article ID 9977001, 10 pages, 2021.

## Research Article

# Interfering with pak4 Protein Expression Affects Osteosarcoma Cell Proliferation and Migration

Yuxin Fu,<sup>1</sup> Lun Fang,<sup>1</sup> Qipu Yin,<sup>1</sup> Qi Wu,<sup>2</sup> Wei Sui,<sup>1</sup> Ying Sun,<sup>1</sup> Xindi Zhao,<sup>1</sup> Yadi Wu <sup>1,3</sup> and Lu Zhou <sup>1,3</sup>

<sup>1</sup>Institute of Sports Medicine, Shandong First Medical University & Shandong Academy Medical Sciences, 619 Changcheng Road, Taian, 271016 Shandong, China

<sup>2</sup>Taian Maternal and Child Health Hospital, 386 Longtan Road, Taian, 271000 Shandong, China

<sup>3</sup>Clinical Center for Sports Medicine and Rehabilitation, The Affiliated Hospital of Shandong First Medical University, 706 Taishan Great Street, Taian, 271000 Shandong, China

Correspondence should be addressed to Yadi Wu; 13854862627@163.com and Lu Zhou; coolzhoulu@163.com

Received 17 May 2021; Revised 8 October 2021; Accepted 12 November 2021; Published 30 December 2021

Academic Editor: Yuzhen Xu

Copyright © 2021 Yuxin Fu et al. This is an open access article distributed under the Creative Commons Attribution License, which permits unrestricted use, distribution, and reproduction in any medium, provided the original work is properly cited.

**Purpose.** A number of studies have discovered various roles of PAK4 in human tumors, including osteosarcoma. However, the exact role of PAK4 in osteosarcoma and its mechanism have yet to be determined. Therefore, this study focused on interrogating the PAK4 effect on the proliferation and migration ability of osteosarcoma and its underlying mechanisms. **Materials and Methods.** Western blot and QRT-PCR were utilized to quantify the PAK4 relative protein and mRNA levels. To measure cellular viability and mobility, the MTT and wound-healing assays were preferred. **Results.** With the adenovirus-mediated overexpression of PAK4, the proliferation and migration of U2-OS and MG-63 osteosarcoma cells were stimulated. Furthermore, a liposome-mediated knockout of PAK4 will inhibit osteosarcoma cells from proliferating. In terms of mechanism, we observed the positive correlation of PAK4 expression with expression of P21, CyclinD1, CyclinE1, CDK2, and CDK6, which drives G0/G1 to the G2/M phase transition. PAK4 can also activate Erk expression in OS cells and induce EMT. **Conclusion.** Interfering with PAK4 protein expression has been shown to affect osteosarcoma proliferation and migration.

## 1. Introduction

Osteosarcoma (OS), a primary malignant bone tumor, is characterized by triangular stromal cells originating from primitive intercellular cells and producing osteoid tissue [1]. It is most commonly seen in the adolescent metaphysis of the long bones of the extremities [2]. Owing to its high malignancy, rapid development, and poor prognosis, it accounts for a significant proportion of cancer-related deaths in young adults and children. Amputation was the only treatment option for osteosarcoma patients in the 1970s, with less than 20% of a 5-year survival rate. The advancement of chemotherapy has significantly increased the life expectancy of osteosarcoma patients and makes it possible to preserve them, with a 5-year survival rate of 70% [3]. Despite chemotherapy, 30 to 40% of patients expe-

rienced metastasis or tumor recurrence. Osteosarcoma has a high risk of lung metastasis, and patients suffering from lung metastasis showed poor prognosis, with a 20% of 5-year survival rate [4]. The lack of knowledge about the precise mechanisms of proliferation, metastasis, and apoptosis in osteosarcoma has hampered treatment development, resulting in a leveling of overall survival in osteosarcoma patients over the past few decades. Therefore, the discovery of new biomarkers linked to progression, and prognosis may improve the treatment and prognosis for patients with osteosarcoma.

The p-21-activated kinases (PAKs), which are members of the serine/threonine protein kinase family, are thought to be important downstream effector molecules of Rac1, Cdc42, and the key small Rho GTPase proteins. They are made up of six members who are divided into two groups

TABLE 1: Sequences and accession numbers for forward (FOR) and reverse (REV) primers for the QRT-PCR.

Gene	Sequences for primers	Accession no.
P21	FOR: TGCAACTACTACAGAACTGCTG REV: CAAAGTGGTCGGTAGCCACA	NM_181617
CyclinD1	FOR: GCTGCGAAGTGGAACCATC REV: CCTCCTTCTGCACACATTTGAA	NM_053056
CyclinE1	FOR: AAGGAGCGGGACACCATGA REV: ACGGTCACGTTTGCCTTCC	NM_001238
CDK6	FOR: GCTGACCAGCAGTACGAATG REV: GCACACATCAAACAACCTGACC	NM_001145306
CDK2	FOR: TGTTTAACGACTTTGGACCGC REV: CCATCTCCTCTATGACTGACAGC	NM_005851
Erk	FOR: CGGGGCATCTTCGAGATCG REV: CAGAACAACGCCGTTTCAGTT	NM_001030312
E-cadherin	FOR: CGAGAGCTACACGTTTCACGG REV: GGGTGTGCGAGGAAAAATAGG	NM_004360
N-cadherin	FOR: TTTGATGGAGGTCTCCTAACACC REV: ACGTTTAAACACGTTGAAATGTG	NM_004061

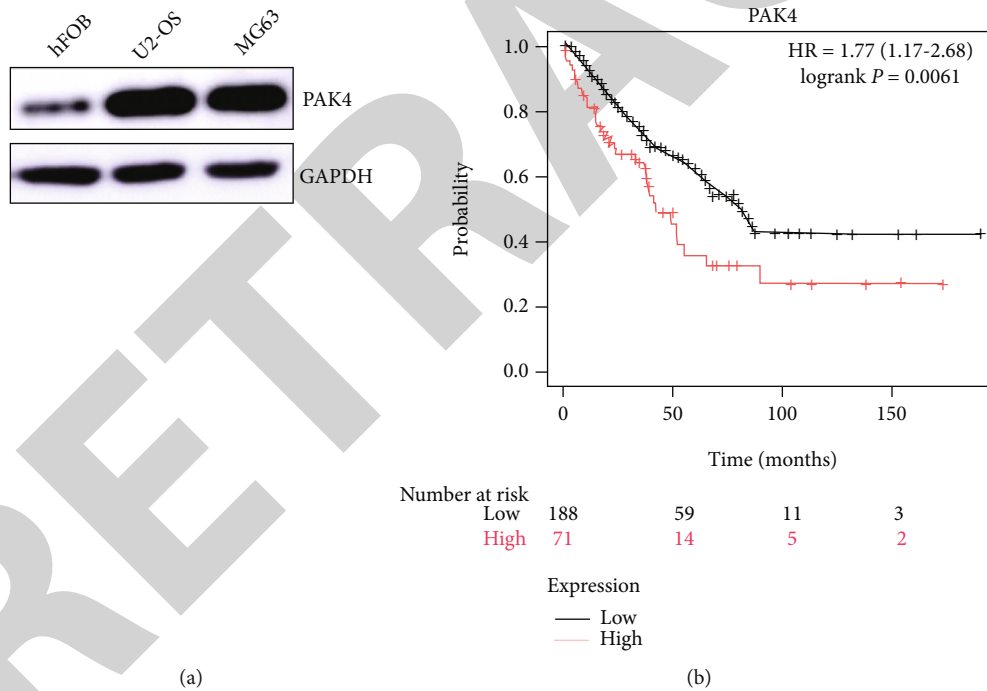


FIGURE 1: The Kaplan-Meier online database was used to study the relationship between differential expression of PAK4 and survival rate.

based on homology sequence: group I (PAK1-3) and group II (PAK4-6) [5]. PAK4 is a group II cancer-related factor that is found in subcellular domains of the cytoplasm and nucleus. Overexpression of PAK4 can be found in a wide range of tumors, including pancreatic cancer [6], gastric carcinoma [7], and ovarian cancer [8]. It can inhibit apoptosis of tumor cells, promote cell survival, cause uncontrolled growth, trigger cell morphology to lose its regulatory function, inhibit cell adhesion, and promote cell migration and

tumor formation. In addition, it is capable of regulating the independent growth of the cells by relying on independent kinase activity to stimulate the growth, invasion, and metastasis of tumor cells [9]. These outcomes discovered that PAK4 may serve a critical part in the occurrence and progression of osteosarcoma tumors. A recent study has found that inhibition of PAK4 can limit human osteosarcoma cell proliferation, invasion, and migration, but the specific regulatory mechanism, especially on cell proliferation



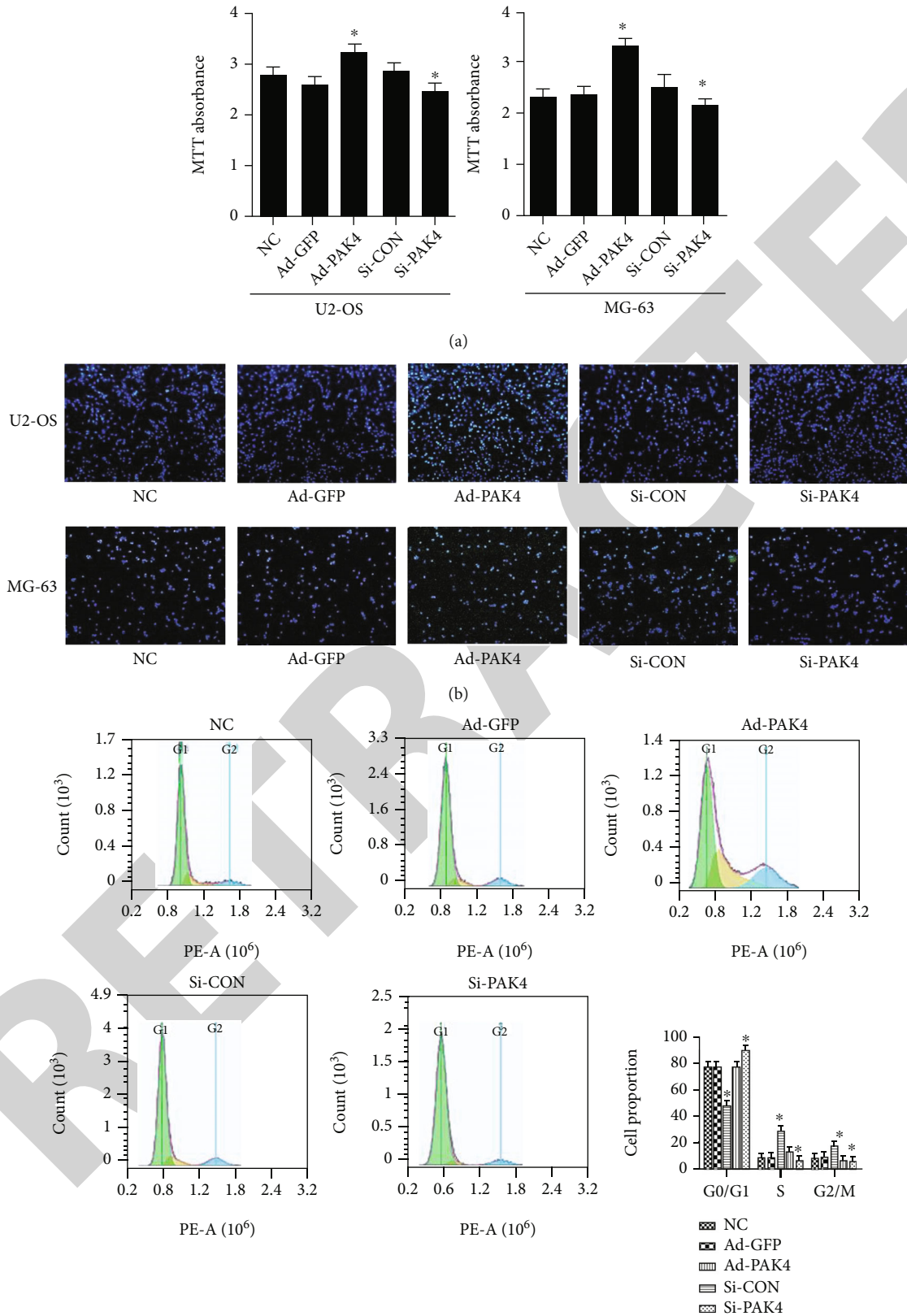


FIGURE 2: Effect of PAK4 on OS cell lines proliferation. (a) Cell viability was analyzed with MTT. (b) Detection of EdU-488 staining of PAK4 on proliferation of osteosarcoma cells. EdU-labeled proliferating cell nucleus fluoresce green and overlap with Hoechst 33342-stained blue nucleus. (c) Influence of PAK4 on cell cycle of osteosarcoma cells U2-OS by flow cytometry. Compared with the control group, \* $P < 0.05$ .



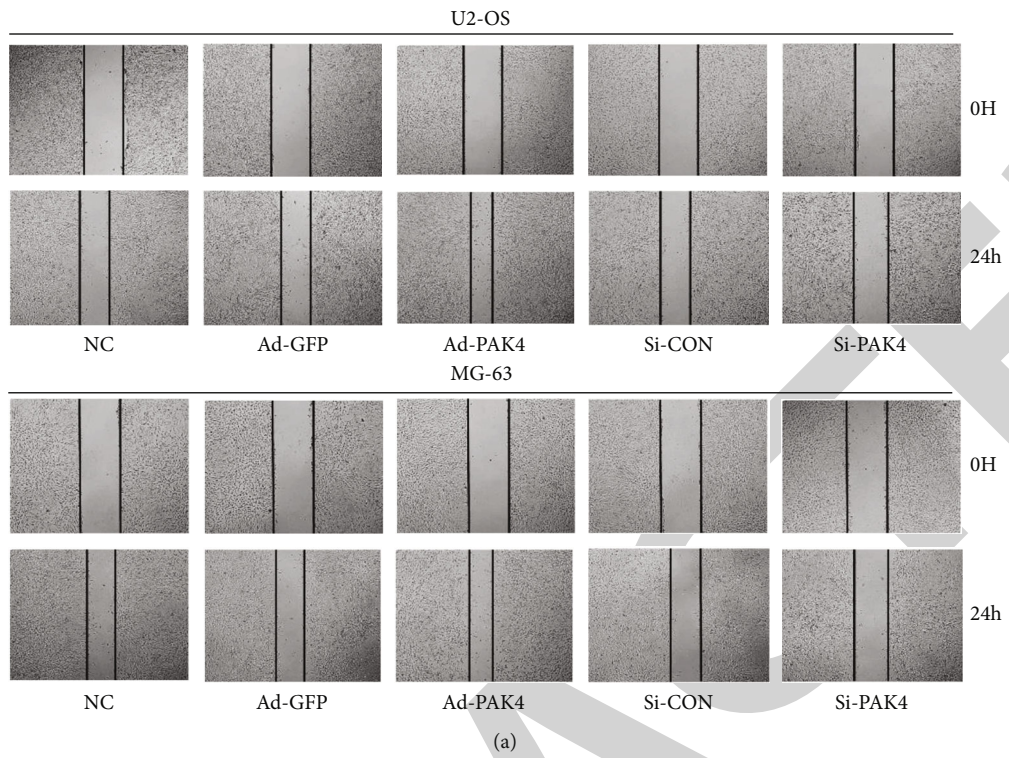


FIGURE 3: Continued.

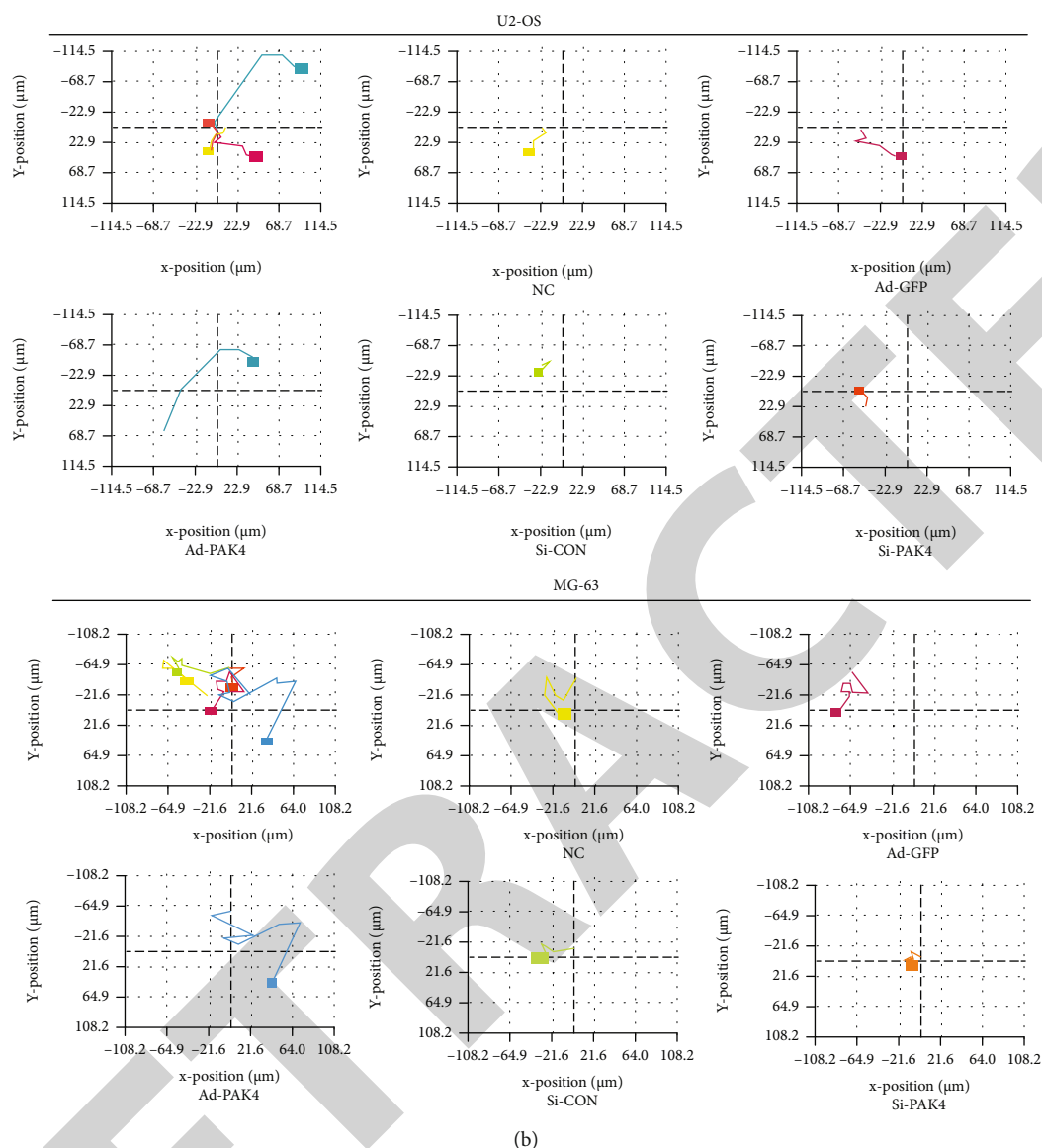


FIGURE 3: Effect of PAK4 on OS cell lines migration. (a) Migration ability was determined by applying a wound healing assay. (b) Each color represented the migration trajectory of different groups of cells. (a) Comprehensive comparison of migration distances of several different groups. (b-f) The migration distance of each group of cells was analyzed by holography microscopy.

ability, is still not clear [10]. Therefore, PAK4's function in controlling OS proliferation, invasion, and metastasis, as well as its basic mechanism, requires further investigation.

This study focuses on the examination of the expression and function of PAK4 in OS. The data indicate that PAK4 overexpression promotes osteosarcoma cell proliferation and migration. Moreover, mechanistic studies reveal that PAK4 induces epithelial-mesenchymal transition (EMT) by activating the Erk level in osteosarcoma cells. Therefore, these results provide evidence for a functional role in OS and suggest that it may be a new therapeutic target for the disease.

## 2. Materials and Methods

**2.1. Cell Culture.** In this analysis, the human osteosarcoma cell line U2-OS and MG-63 and human osteoblast cell line

(hFOB) were used and purchased from the Cell Bank of the Chinese Academy of Sciences (Shanghai, China) and were plated in 6-well plates at a density of  $1.5 \times 10^6$  cells/well in Dulbecco's Modified Eagle Medium (DMEM; Gibco; Lot. 8121218). These cells were grown at 37°C under a humidified 5% CO<sub>2</sub> atmosphere, supplemented with 10% fetal bovine serum (FBS; Biological Industries; Lot. 2033119), 10 units/ml penicillin, and 10 μg/ml streptomycin (Sigma-Aldrich, St. Louis, MO, USA).

**2.2. Cell Transfection.** For the PAK4 silencing experiment, transfection of osteosarcoma cells was performed by using small interference (si) RNA. PAK4-siRNA was purchased from GenePharma. Lipofectamine 2000 (Invitrogen; Thermo Fisher Scientific, Inc., Waltham, MA, USA) was used, according to the provided manual, for transient

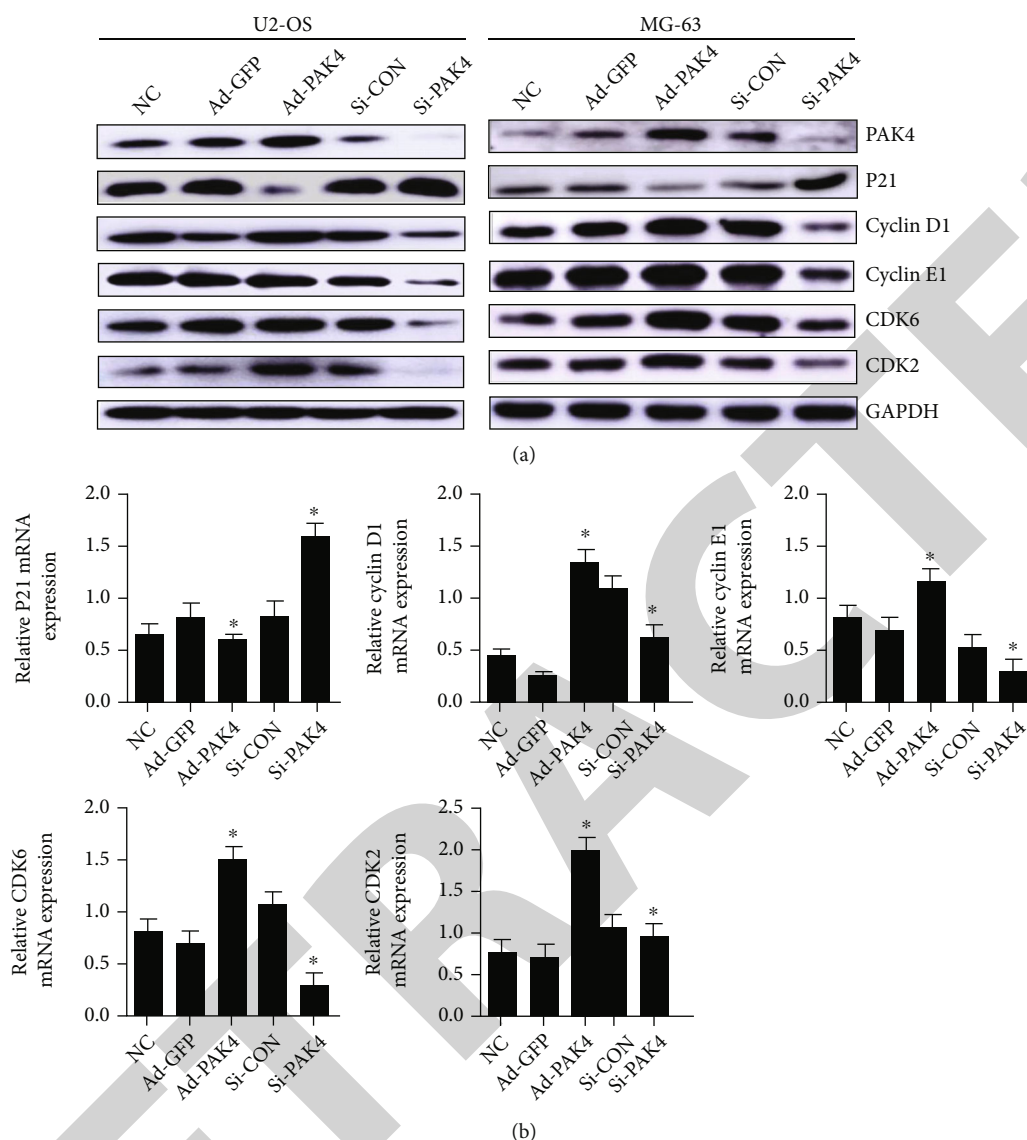


FIGURE 4: Interference effect of PAK4 on OS cell proliferation. P21, Cyclin D1, Cyclin E1, CDK2, and CDK6 protein levels detected in osteosarcoma cells with NC, ad-GFP, ad-PAK4, si-CON, and si-PAK4 treatment, respectively. (b) The expression of PAK4 is closely related to the relative gene about the cell cycle in human osteosarcoma cell lines. The relative expression of the target protein was measured with the expression of GAPDH. \* $P < 0.05$  as compared to the NC group.

transfection at 37°C for 6 h using a final concentration of siRNA of 5 nM. For the PAK4 overexpression experiment, osteosarcoma cells were transfected for 12 h at 37°C with  $1 \times 10^9$  particle forming units of PAK4 adenovirus, which was purchased from Vigene Biosciences. As a control, the ad-GFP was purchased from Abcam. To improve transfection quality, U2-OS and MG-63 cells were incubated in DMEM medium without antibiotics for 24 h before transfection.

**2.3. MTT Assay.** The viability of the cells was determined by using the MTT assay. In 96-well plates, cells were plated at a density of  $1 \times 10^4$  cells per well in 10% FBS and antibiotics supplemented DMEM medium. Incorporation of MTT solution (Biotopped) in plates was made at a concentration of 0.5 mg/ml for 3 h at 37°C. After removing the medium, the

prepared formazan crystals were dissolved in 100  $\mu$ l dimethyl sulfoxide. At 570 nm, the absorbance was detected with a spectrophotometer.

**2.4. EdU-488 Cell Proliferation Assay.** Cell proliferation was detected with BeyoClickEdU-488 Cell Proliferation Assay Kit (Beyotime Biotechnology, C0071S). Cells at a density of 5000 cells/ml were seeded into 24-well plates. After 24 h of cell culture, an equal volume of 20  $\mu$ mol/l EdU working solution was added to each well to continue incubation for 2 h. Then, 4% tissue cell fixative was fixed at room temperature for 20 min, and PBS permeabilizing solution containing 0.3% TritonX-100 was incubated at room temperature for 15 min. 500  $\mu$ l click reaction solution per well, prepared according to the instructions, was incubated at room temperature for 30 min in the dark for click reaction. Hoechst

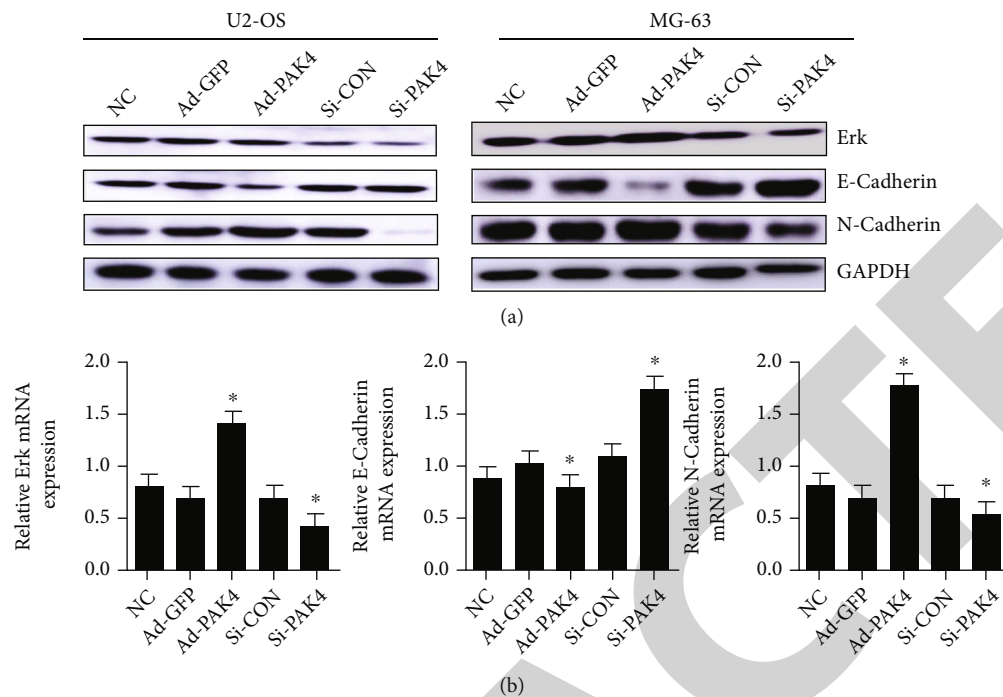


FIGURE 5: PAK4 promotes the cell migration of osteosarcoma by regulating the Erk protein expression to induce EMT. The expression level of Erk, N-Cadherin, and E-Cadherin was detected by using Western blot (a) and qRT-PCR (b). GAPDH expression was utilized to study the relative expression of the target protein. \* $P < 0.05$  versus the normal control group.

33342 solution was incubated at room temperature in the dark for 10 min. Ultimately, staining results were observed under a fluorescence microscope.

**2.5. Wound Healing Assay.** In the logarithmic growth phase, osteosarcoma cells were digested with trypsin (0.25%), and a density of  $5 \times 10^5$  cells/well was seeded into the 6-well plate and cultured at 37°C overnight in the presence of 5% CO<sub>2</sub>. The next day, the scratching was performed with a 200  $\mu$ l pipette tip followed by thrice washing with PBS to remove suspension cells before being applied to a serum-free medium. The migration of cells (each group) was detected using a microscope after 24 hours of incubation at 37°C in a 5% CO<sub>2</sub> incubator. With one optical microscope, pictures were obtained at 0 and 24h, separately.

**2.6. Digital Holographic Microscopy.** The Holomonitor™ M4 microscope (Phase Holographic Imaging AB, Lund, Sweden) was used for tracking and imaging the movement of U2-OS and MG-63 cells. There are various good advantages for this technique, such as quantitative and long-term cytokinetic analysis avoiding any marking. Moreover, to achieve parameter stability, we switched on the microscope component of the HoloMonitor M4 system and left it overnight in a CO<sub>2</sub> incubator. A total of 24 hours of observations were taken and separated by 10 minutes. Following a period of 24h, the M4 Studio tracking software version 2.6.2 was applied to analyze the data.

**2.7. Cell Cycle Analysis.** Cell ( $1-5 \times 10^5$ ) were incubated in 6-well plates for 48h with ad-PAK4 (100 MOI), ad-GFP

(100MOI), or PAK4 siRNA and control siRNA. Cells were trypsinized and collected, then performed PBS washing thrice and fixed overnight in ethanol (70%) at 4°C, and then, performed three times washing in PBS with 0.1% BSA. Incubation of cells was performed at 4°C for 90 minutes with 50 mg/ml PI and 5 mg/ml RNase A (DNase free). A FAC Star flow cytometer was used to observe the fractions of cells in various cell cycle stages.

**2.8. Western Blot.** In the lysis buffer, the cells were placed for 30 min and centrifuged for 30 min at 4°C at 13,200 x g. The resulting supernatant was kept at -80°C till use. Determination for the concentration of protein was performed to use the BCA (Vazyme). The lysate separation was performed with 10% SDS-PAGE followed by electroblotting to PVDF membranes (Millipore, Billerica, MA, USA) for 1h at 100 volts. After being locked with 5% skim milk, the resulting blot was then probed with primary antibodies for PAK4 (1:2000; cat.no. ab19007; Abcam.), CDK2 (1:2000; cat.no.2546; Cell Signaling Technology, Inc.), CDK6 (1:2000; cat.no.3136; Cell Signaling Technology, Inc.), Cyclin D1 (1:2000; cat.no.GB11079; Servicebio), Cyclin E1 (1:2000; cat.no.GB13305; Servicebio), P21 (1:2000; cat.no. ab86696; Abcam.), Erk (1:2000; cat.no. ab54230; Abcam.), E-Cadherin (1:2000; cat.no.14472; Cell Signaling Technology, Inc.), and N-Cadherin (1:2000; cat.no.14215; Cell Signaling Technology, Inc.).

**2.9. RNA Isolation and the Real-Time RT-PCR Analysis.** The TRIzol reagent (Invitrogen, Carlsbad, CA, USA) was used for the total RNA extraction from the cells. The random



primer (hexamer) included in the first-strand cDNA synthesis kit (Takara, Shiga, Japan) was used to generate first-strand cDNA. Primer Express software was used to design specific primers for each gene (Takara, Shiga, Japan). The ABI Prism 7900Ht Sequence Detection system (Applied Biosystems) was used to perform the PCR reaction. Specific primers for each gene (Table 1) were designed using Primer Express software (Applied Biosystems). All experiments were carried out in triplicate.

**2.10. Statistical Analysis.** The data was statistically analyzed using the Duncan's test and ANOVA. Differences with a  $P$  value  $< 0.05$  were considered statistically significant.

### 3. Results

**3.1. PAK4 Was Overexpressed in OS Cell Lines, and the Expression Level of PAK4 Affects the Survival Rate of Osteosarcoma Patients.** For ensuring the expression of PAK4 in OS, we detected the expression of PAK4 in OS cell lines; as Figure 1(a) shows, PAK4 was lower in OS cell lines U2-OS and MG-63 than in osteoblastic cell hFOB. And to examine the PAK4 impact on the occurrence and development of osteosarcoma and osteoblast, we analyzed the online database of OS high-throughput gene chip data through the Kaplan-Meier (<http://kmplot.com/analysis/>) and found significantly lower overall survival of patients in the PAK4 mRNA high transcript level group compared with the PAK4 low level group (Figure 1(b)). These findings suggested that PAK4 dysregulation could be a predictor of OS prognosis.

**3.2. PAK4 Induces Cell Proliferation in Human Osteosarcoma Cells.** After 48 h transfection of the ad-PAK4 or the PAK4 siRNA, we analyzed the cellular proliferation of U2-OS and MG-63 cells. The results of MTT analysis suggested that the Ad-PAK4 overexpression increased the proliferation. Meanwhile, the PAK4 siRNA reduced the cellular proliferation in the human osteosarcoma (Figure 2(a)). The results of EdU-488 staining showed that a large amount of green fluorescence was observed in the proliferating cells. The number of proliferating cells increased significantly in the Ad-PAK4 group compared with the NC group, while decreased in the Si-PAK4 group (Figure 2(b)). These findings demonstrated that PAK4 affected cell proliferation.

**3.3. PAK4 Promotes Osteosarcoma Cell Migration and Metastasis.** Wound healing was carried out to investigate the migration speed of OS cells following ad-PAK4 and si-PAK4. As illustrated in Figure 3(a), cell migration was increased remarkably in PAK4 adenovirus cells as compared to the NC group. Furthermore, digital holographic microscopy has produced consistent images of cell mobility. According to single-cell tracking analysis, the distance of migration and the motility of the ad-PAK4 group markedly increased than that of the control group (Figure 3(b)). Moreover, the assay results were congruent between U2-OS and MG-63 cell lines. Collectively, overexpression of PAK4 facilitates OS migration and metastasis.

**3.4. PAK4 Induces the Transition of the G0/G1 to the G2/M Phase in Human Osteosarcoma Cells.** Following a 48-hour transfection with PAK4 adenovirus or siRNA, FACS analysis was used to determine cell cycle distribution after PAK4 overexpression (Figure 2(c)). CDK6 has been shown to induce cell transformation from G0/G1 to G2/M, promoting cell proliferation and facilitating tumorigenesis. In the U2-OS cell line, a lower proportion of cells was observed in the G1 phase in the ad-PAK4 group than that of the control group. At the same time, the cellular proportion in the G2 phase and S phase in the experimental group also decreased to different degrees, indicating that PAK4 can induce the cell cycle progression of human osteosarcoma. To find out PAK4's effect on cell cycle transition, we observed the increased expression of CyclinD1, CyclinE1, and cyclin-dependent kinases (CDKs) CDK2 and CDK6 in PAK4 overexpression of OS cell line (Figure 4(a)). Meanwhile, the number of cells expressing the cell cycle inhibitor, p21, was reduced. However, ad-GFP was transfected with adenovirus, while si-CON was transfected with the plasmid, so the results of these two groups were different. Such observations suggested that PAK4 may exert a critical role in the U2-OS cell cycle transition of the G0/G1 to the G2/M phase.

**3.5. Real-Time RT-PCR Analysis of Oncogenes.** To explore the molecular mechanism through which PAK4 activated the proliferation of U2-OS cells, we studied the interaction of PAK4 with oncogenes on proliferation using RT-PCR. The RNA was isolated from PAK4 adenovirus or siRNA transfected cell. According to the result of Western blotting, the levels of expression of several related genes were investigated. P21 RNA levels were found to be inversely related to PAK4 expression. The RT-PCR data demonstrated that the RNA level of cyclin D1, CyclinE1, CDK2, and CDK6 were increased (Figure 4(b)). These results specify that the PAK4 overexpression may promote osteosarcoma proliferation through driving G0/G1 to the G2/M phase transition via regulation of expression level of cyclinD1, cyclinE1, CDK2, CDK6, and P21.

**3.6. Erk/EMT Is Involved in PAK4-Medicated Migration of Osteosarcoma Cells.** To determine whether PAK4 promotes osteosarcoma cell migration by regulating Erk levels, Western blotting was used to identify variations in the protein expression that are involved in the Erk/EMT signaling pathway. The results showed that in the PAK4-adenoviral group, expression of Erk and N-Cadherin was upregulated, while E-cadherin expression was downregulated. Meanwhile, it was further verified that PAK4-silenced resulted in Erk and N-Cadherin downregulation and E-Cadherin upregulation (Figure 5). These data suggest that PAK4 overexpression stimulates the migration of osteosarcoma cells by stimulating the EMT signaling pathway via regulation of Erk levels.

### 4. Discussion

In the current study, we focused on whether PAK4 plays a role in the growth and metastasis of OS. We demonstrated the increased level of PAK4 in osteosarcoma cell lines.

Unrestricted cell replication and invasive metastasis are two critical steps during tumor development. And our study found that the expression level of PAK4 was increased in osteosarcoma cell lines, and silencing PAK4 inhibited the proliferation and migration of osteosarcoma cells.

Previous researches have shown that PAK4 has important biological effects on tumor growth and migration, and it has become one of the hotspots in tumor biological signal transduction research [11–13]. Our results indicate that several proteins related to cell cycle, CDK2, CDK6, CyclinD1, and CyclinE1 expression levels were shown to be increased after PAK4 overexpression treatment, while the expression level of p21 was decreased. But the results were completely opposite after silencing PAK4. Nekrasova and Minden reported that PAK4-null fibroblasts arrested in G1 phase, which was associated with increased expression of p21 and decreased expression of cyclinD1, respectively [14]. As everyone knows, cell proliferation is a complex and ordered process that is rigorously regulated by a number of factors, including cyclin, cyclin-dependent protein kinase (CDK), and cyclin-dependent kinase inhibitor (CKI) [15]. The normal cell cycle requires balance and precise coordination between cyclin, a positive regulator of CDK, and CKI, a negative regulator. When this balance is upset, it leads to uncontrolled cell proliferation and, eventually, carcinogenesis. CyclinD1 and CyclinE1 exert a key role in the G1 phase regulation and G1/S phase transition [16]. CDK2 and CDK6 are important CDK family members, and activated CDK can promote the cell cycle to enter the S phase through the restriction point of G1/S, which controls the replication of DNA and centrosome, and can also promote the occurrence of mitosis during the G2/M transition [17]. Nevertheless, p21 has the potential to inhibit the activity of cyclin complex and proliferating cell nuclear antigen. Abnormal p21 (either decreased or disappeared expression) lost the normal regulation of the activity of cyclin-CDK complex, which leads to misreplication of cellular DNA, cellular dissimilation or carcinogenesis, and cell cycle arrest [18]. Meanwhile, EdU-488 staining visually reflected the effect of PAK4 on osteosarcoma cell proliferation. Moreover, the results of flow cytometry also revealed that PAK4 could push osteosarcoma cell cycle transition and promote cell proliferation. In addition, it has been confirmed that the proliferation of lung adenocarcinoma cells is restricted and the cell cycle is arrested in G1 phase after PAK4 inhibition [19].

Our study also found that PAK4 could promote the EMT process, and expressed ERK in osteosarcoma cell lines in vitro. PAK4 overexpression increased the expression level of N-Cadherin and decreased the expression level of E-Cadherin. Upregulation of N-Cadherin and downregulation of E-Cadherin induce EMT, loss of cell polarity, improve their migration ability, and significantly enhance their affinity to other stromal tissues, thereby metastasizing and spreading malignant cells [20]. Moreover, PAK4 can specifically bind and phosphorylate the EMT transcription factor Slug, which mediates PAK4-induced EMT and prostate cancer invasion [21]. In addition, Erk is a key factor in the induction of EMT. The elevated level of Erk was observed in various cancer types, including osteosarcoma.

MicroRNA-765 targeting MTUS1 has been reported to promote proliferation, migration, and invasion of osteosarcoma by mediating the ERK/EMT pathway [22]. Tan et al. also reported that type I collagen plays a crucial role in the morphology, proliferation, and invasiveness of U2-OS cells and the ERK signaling pathway in collagen-treated cells, while it can also induce the EMT process in U2-OS cells [23]. According to studies on the signaling pathways involved in the EMT process, we found that PAK4 silencing downregulated Erk expression and synchronously inhibited EMT, which attenuated cell invasion and metastasis.

## 5. Conclusion

The following conclusions can be drawn from the current study. PAK4 overexpression in OS cells can promote tumor proliferation, invasion, and metastasis. Additionally, it can promote the proliferation of osteosarcoma by inhibiting the expression of P21 and upregulate the level of Cyclin D1, CyclinE1, CDK2, and CDK6, which drives G0/G1 to the G2/M phase transition. By activating the Erk signaling pathway, PAK4 can trigger EMT in OS cells, which promotes tumor migration and invasion. Taken together, our findings provide an experimental basis for targeting PAK4 as a possible osteosarcoma therapeutic target. It is suggested that this point investigated in future studies.

## Data Availability

The data used to support the findings of this study are included within the article.

## Conflicts of Interest

The authors declare that there are no competing interests regarding the publication of this paper.

## Authors' Contributions

Yuxin Fu, Lun Fang, and Qipu Yin contributed equally to this work.

## Acknowledgments

This work was supported by the National College Students Innovation and Entrepreneurship Training Program (grant no. S202010439008), Shandong Provincial Natural Science Foundation of China (grant no. ZR2019MH120), and the Projects of Medical and Health Technology Development Program in Shandong Province (grant no. 2019WS397).

## References

- [1] J. Li, Z. Yang, Y. Li et al., "Cell apoptosis, autophagy and necroptosis in osteosarcoma treatment," *Oncotarget*, vol. 7, no. 28, pp. 44763–44778, 2016.
- [2] L. Mirabello, R. J. Troisi, and S. A. Savage, "International osteosarcoma incidence patterns in children and adolescents, middle ages and elderly persons," *International Journal of Cancer*, vol. 125, no. 1, pp. 229–234, 2009.

## Retraction

# Retracted: Effects of Omega-3 Polyunsaturated Fatty Acids on Cognitive Function after Splenectomy in Rats

### BioMed Research International

Received 12 March 2024; Accepted 12 March 2024; Published 20 March 2024

Copyright © 2024 BioMed Research International. This is an open access article distributed under the Creative Commons Attribution License, which permits unrestricted use, distribution, and reproduction in any medium, provided the original work is properly cited.

This article has been retracted by Hindawi following an investigation undertaken by the publisher [1]. This investigation has uncovered evidence of one or more of the following indicators of systematic manipulation of the publication process:

- (1) Discrepancies in scope
- (2) Discrepancies in the description of the research reported
- (3) Discrepancies between the availability of data and the research described
- (4) Inappropriate citations
- (5) Incoherent, meaningless and/or irrelevant content included in the article
- (6) Manipulated or compromised peer review

The presence of these indicators undermines our confidence in the integrity of the article's content and we cannot, therefore, vouch for its reliability. Please note that this notice is intended solely to alert readers that the content of this article is unreliable. We have not investigated whether authors were aware of or involved in the systematic manipulation of the publication process.

Wiley and Hindawi regrets that the usual quality checks did not identify these issues before publication and have since put additional measures in place to safeguard research integrity.

We wish to credit our own Research Integrity and Research Publishing teams and anonymous and named external researchers and research integrity experts for contributing to this investigation.

The corresponding author, as the representative of all authors, has been given the opportunity to register their agreement or disagreement to this retraction. We have kept a record of any response received.

### References

- [1] Y. Guo, F. Ping, Y. Cao et al., "Effects of Omega-3 Polyunsaturated Fatty Acids on Cognitive Function after Splenectomy in Rats," *BioMed Research International*, vol. 2021, Article ID 5513886, 6 pages, 2021.

## Research Article

# Effects of Omega-3 Polyunsaturated Fatty Acids on Cognitive Function after Splenectomy in Rats

Yong Guo<sup>1</sup>, Feng Ping<sup>1</sup>, Yongmei Cao<sup>1</sup>, Jiawei Shang<sup>1</sup>, Junfeng Zhang<sup>2</sup>, Hong Jiang<sup>3</sup>, and Shudong Fang<sup>3</sup>

<sup>1</sup>Department of Critical Care Medicine, Shanghai Jiao Tong University Affiliated Sixth People's Hospital, Shanghai 200233, China

<sup>2</sup>Department of Anesthesiology, Shanghai Jiao Tong University Affiliated Sixth People's Hospital, Shanghai 200233, China

<sup>3</sup>Department of Anesthesiology, Shanghai Ninth People's Hospital, Shanghai Jiao Tong University School of Medicine, Shanghai 200011, China

Correspondence should be addressed to Shudong Fang; [drfangshudong@163.com](mailto:drfangshudong@163.com)

Received 18 February 2021; Revised 9 October 2021; Accepted 7 December 2021; Published 26 December 2021

Academic Editor: Yuzhen Xu

Copyright © 2021 Yong Guo et al. This is an open access article distributed under the Creative Commons Attribution License, which permits unrestricted use, distribution, and reproduction in any medium, provided the original work is properly cited.

**Background.** Postoperative cognitive dysfunction (POCD) is a common complication after abdominal surgery. Several studies have reported that POCD is related to neuroinflammation caused by surgery. Omega-3 polyunsaturated fatty acids (PUFAs) can effectively inhibit the systematic inflammatory response. So, we use fish oil to study the effect of fish oil on inflammation, immunity, and cognitive behavior after splenectomy in rats. **Methods.** 60 SD (Sprague-Dawley) rats were randomly divided into control group (group C,  $n = 20$ ), surgery group (group S,  $n = 20$ ), and omega-3 (fish oil) intervention group (group F,  $n = 20$ ). Omega-3 PUFA was injected intraperitoneally from 3 days before operation to 7 days after operation in group F, and normal saline was injected simultaneously in group S. Rats in group S and group F received splenectomy under general anesthesia. Morris water maze behavioral evaluation was performed on the first, third, fifth, and seventh day after operation. The levels of IL-1 $\beta$  (interleukin-1 $\beta$ ), IL-6 (interleukin-6), TNF- $\alpha$  (tumor necrosis factor- $\alpha$ ), SOD (superoxide dismutase), and GSH-PX (glutathione peroxidase) were detected. **Results.** Serums IL-1 $\beta$ , IL-6, and TNF- $\alpha$  concentrations in group S and group F were higher than those in group C ( $P < 0.01$ ), while those inflammatory cytokines in group F were significantly lower than those in group S ( $P < 0.01$ ); serum GSH-PX levels in group F were higher than group S ( $P < 0.01$ ). The Morris water maze behavior test performance of group F was better than that of group S ( $P < 0.05$ ). **Conclusion.** Omega-3 PUFA can effectively improve postoperative inflammatory response, reduce the damage of antioxidant defense system, and improve postoperative cognitive function.

## 1. Introduction

Postoperative cognitive dysfunction (POCD) is a central nervous system (CNS) complication after anesthesia and surgery. Its clinical symptoms are memory loss, abstract thinking, and disorientation, accompanied by decreased social activities and fusion ability [1, 2]. POCD is common in surgical patients, which not only affects the quality of life of patients and increases the medical burden but also increases the incidence of postoperative complications and mortality of patients [3, 4]. Current studies suggest that the pathogenesis of POCD is not very clear. Low level of education, preoperative cognitive dysfunction, severe complica-

tions, long-term anesthesia, and secondary surgery are the key factors for POCD [5, 6]. At present, research on POCD mainly involves genes, surgery, trauma, stress, hypoxia, calcium homeostasis, inflammatory response, etc., and its pathogenesis mainly involves gene theory, epigenetic theory, neurotransmitter theory, brain injury theory, amyloid- $\beta$  ( $\alpha$ - $\beta$ ) theory, and neuroinflammation theory [7]. However, in recent years, a large number of studies have found that various mechanisms of POCD ultimately work through a common pathway—neuroinflammation. Some scholars believe that neuroinflammatory reaction is the central link in the occurrence and development of POCD and plays a key role in the occurrence and development of POCD [8].



Omega-3 polyunsaturated fatty acids (PUFA) (fish oil injection) can effectively inhibit the body's inflammatory response. The possible mechanism is that EPA (c20:5, omega-3) and DHA (c22:6, omega-3) in omega-3 polyunsaturated fatty acids family can replace arachidonic acid (AA, omega-6) in cell membrane phospholipids and compete for cyclooxygenase and lipoxygenase, thus reducing the inflammatory mediators from AA and reducing inflammation. So, we used PUFA to explore the effects of PUFA on postoperative inflammation, immunity, and cognitive behavior of rats.

## 2. Materials and Methods

**2.1. Animal Model Preparation and Grouping.** SPF (specific pathogen-free) male Sprague-Dawley (SD) rats weighing 200-250 g were purchased from Department of Experimental Animal Science, Shanghai Jiao Tong University (animal experiment ethics no: 2017-0268.). Sixty SD rats were randomly divided into the control group (group C,  $n = 20$ ), operation group (group S,  $n = 20$ ), and fish oil intervention group (group F,  $n = 20$ ). In group F, omega-3 fish oil fat emulsion was injected intraperitoneally from 3 days before operation to 7 days after operation. In group S, normal saline was injected at the same time. Splenectomy was performed in groups S and F under 3% inhaled sevoflurane anesthesia. Behavioral examination and biological samples were collected during perioperative period. All biosafety procedures were approved by the experimental animal ethics committee of Shanghai Jiao Tong University.

**2.2. Reagents and Instruments.** Omega-3 fish oil fat emulsion injection (Omegaven®) was purchased from Fresenius Kabi Austria GmbH (Wuxi, China). The ELISA (enzyme-linked immunosorbent assay) kits for IL-1 $\beta$  (interleukin-1 $\beta$ ), IL-6, and TNF- $\alpha$  (TNF- $\alpha$  (tumor necrosis factor- $\alpha$ )) were imported and repackaged (R&D Company, USA). Superoxide dismutase (SOD) and glutathione peroxidase (GSH-PX) kits were purchased from Nanjing Jiancheng Reagent Company.

**2.3. Medication, Surgical Treatments, and Behavioral Tests.** Group S and group F underwent open splenectomy. All the experimental rats were fasted on the day of surgery, and they started to feed normally 1 day after surgery. After 1-5 days after operation, group F was given intraperitoneal injection of fish oil (2 ml/kg) every day; group C and group S were given normal saline. The Morris water maze is used to detect and evaluate the learning and memory ability of rats, which is divided into two parts: (1) place navigation test (seconds) and (2) spatial probe test (frequency). Morris water maze behavioral tests were performed before surgery and on the first, third, fifth, and seventh day after surgery. At the same time, blood samples were collected.

The experimental rats were sacrificed 7 days after operation, and samples were taken for testing. The specific anesthesia surgery methods for splenectomy and perioperative behavioral tests refer to previous study [9].

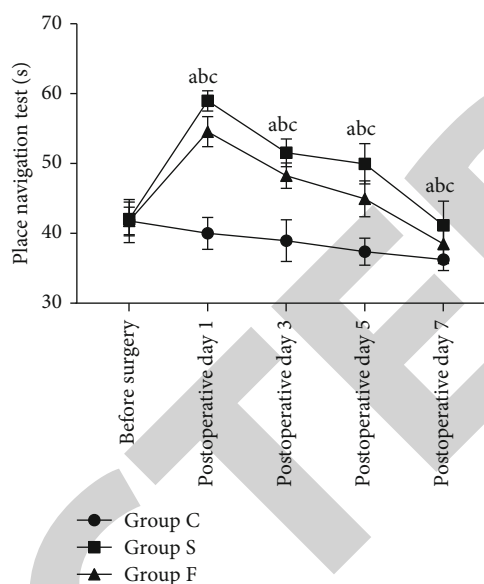


FIGURE 1: The results of place navigation test of three groups. The results of group F were better than those in group S ( $P < 0.01$ ). (a)  $P < 0.01$ , group S vs. C. (b)  $P < 0.01$ , group F vs. C. (c)  $P < 0.01$ , group F vs. S.

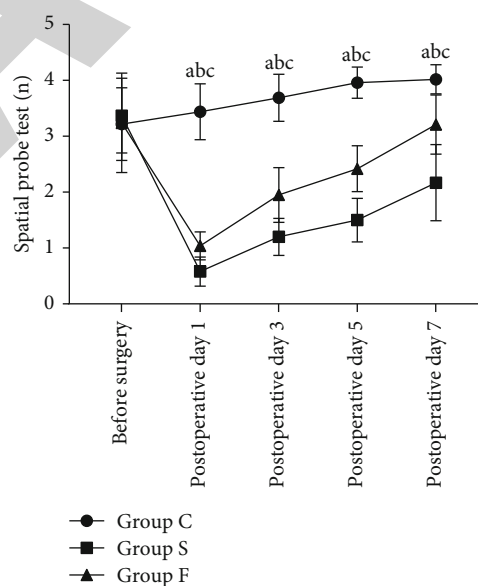


FIGURE 2: The results of spatial probe test of three groups. The results of group F were better than those in group S ( $P < 0.01$ ). (a)  $P < 0.01$ , group S vs. C. (b)  $P < 0.01$ , group F vs. C. (c)  $P < 0.01$ , group F vs. S.

### 2.4. Sample Preparation and Detection

- (1) Blood test: 2% sodium pentobarbital (0.35 ml/100 g) was injected subcutaneously into the abdomen. After anesthesia, the tail vein blood was collected, centrifuged at 3000 r/min, and IL-1B, IL-6, TNF- $\alpha$ , SOD, and GSH-PX were detected according to the kit instructions

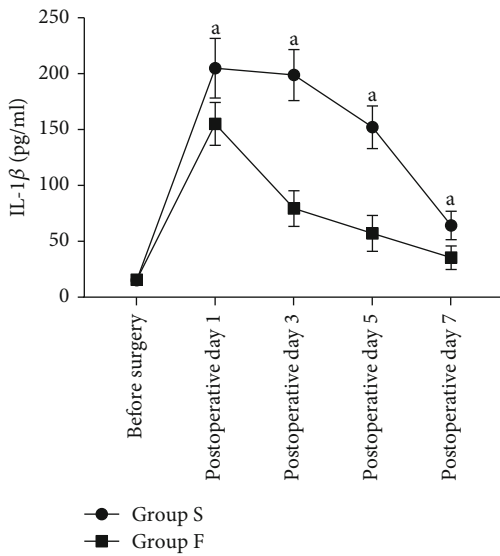


FIGURE 3: The kinetics of IL-1β during the perioperative period. (a)  $P < 0.01$ , group F vs. S.

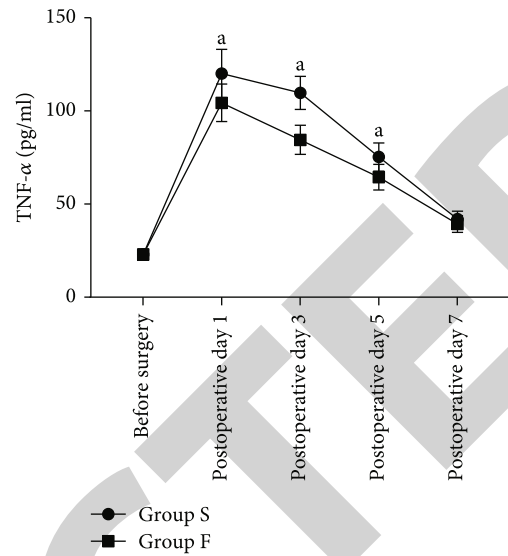


FIGURE 5: The kinetics of TNF-α during the perioperative period. (a)  $P < 0.01$ , group F vs. S.

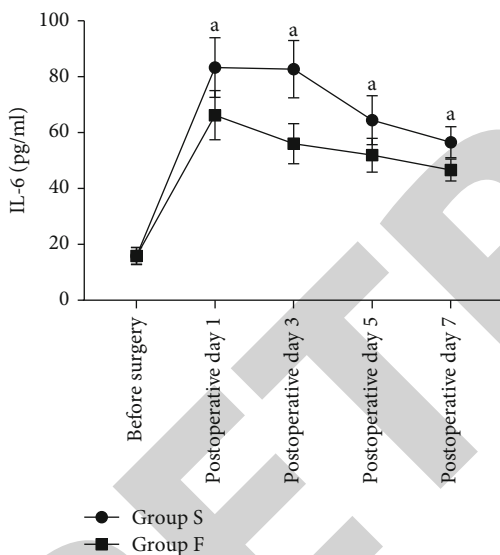


FIGURE 4: The kinetics of IL-6 during the perioperative period. (a)  $P < 0.01$ , group F vs. S.

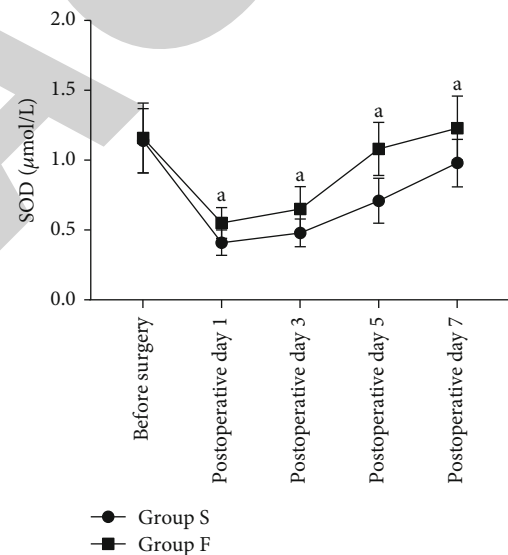


FIGURE 6: The kinetics of SOD during the perioperative period. (a)  $P < 0.01$ , group F vs. S.

(2) Histological observation: First perfuse the living heart, open the chest cavity, insert the needle into the left ventricle, and then clamp it with hemostatic forceps. Then, cut the right atrial appendage, inject about 300 ml of normal saline within 2-4 minutes to replace the circulating blood, and then inject about 150 ml of 4% paraformaldehyde solution within 1-2 minutes for in vivo fixation. All perfusion solutions are precooled at 4°C. Then, the head was decapitated, the skull was opened, and the whole brain was removed. The coronal slices containing the hippocampus and striatum were cut with the aid of a stereotaxic device, fixed with 4% paraformaldehyde, washed with water at 4°C overnight, dehydrated with gradient alcohol, transparent xylene, embedded in paraffin, and

sectioned. HE (hematoxylin-eosin) staining was used to observe the changes in cell morphology

2.5. *Statistical Methods.* SPSS 16.0 software was used to analyze the data. The data were expressed as mean ± standard deviation ( $\bar{x} \pm s$ ). LSD (least significant difference) and *S-N-K* tests were used for comparison among different groups, and paired *t*-test was used for comparison at different time points in the same group. A *P* value of less than 0.05 was considered statistically significant.

### 3. Results

3.1. *Morris Water Maze Test Results.* As shown in Figures 1 and 2, there was no difference in the results of place

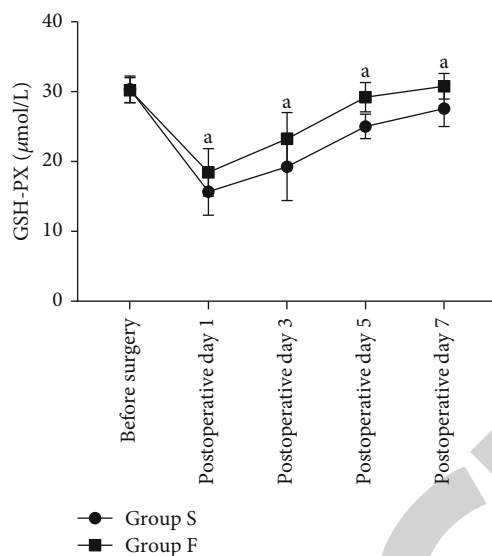


FIGURE 7: The kinetics of GSH-PX during the perioperative period. (a)  $P < 0.01$ , group F vs. S.

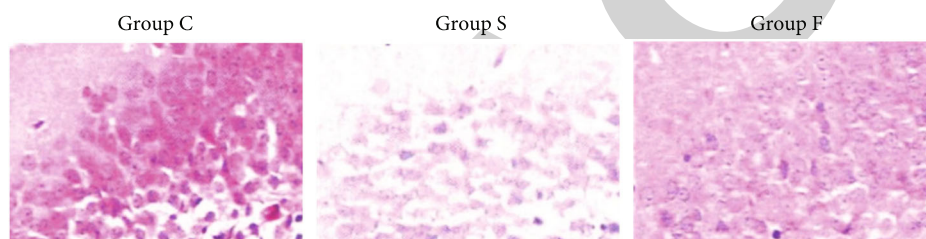


FIGURE 8: Pathological staining of the hippocampus (dentate gyrus) before and 7 days after operation (HE,  $\times 200$ ).

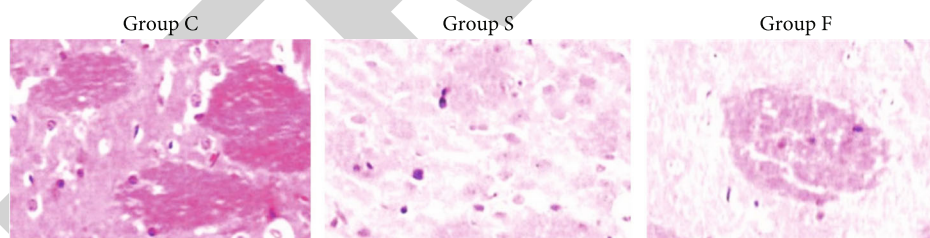


FIGURE 9: Pathological staining of the striatum before and 7 days after operation (HE,  $\times 200$ ).

navigation test and spatial probe test between groups before surgery ( $P > 0.05$ ). After surgery, the results of place navigation test and spatial probe test of group C were better than those of group F and group S. Besides, the results of water maze test performance between group F and group S after surgery were different. The group F performed better than the group S in the water maze test ( $P < 0.01$ ).

**3.2. Measurement of Serum Biochemistry Indicators.** As shown in Figures 3, 4, and 5, inflammatory factors IL- $1\beta$ , IL-6, and TNF- $\alpha$  increased after surgery. Serum IL- $1\beta$ , IL-6, and TNF- $\alpha$  concentrations in group S and group F were higher than those before surgery ( $P < 0.01$ ), while those inflammatory cytokines in group F were significantly lower than those in group S ( $P < 0.01$ ). As shown in Figures 6 and 7, the enzyme activity of SOD and levels of GSH-PX decreased after surgery. Serum enzyme activity of SOD and

levels of GSH-PX in group F were higher than those in group S ( $P < 0.01$ ).

**3.3. Pathological Examination of Rat Hippocampus.** As shown in Figures 8 and 9, the pathological HE staining of hippocampus and striatum showed that in group C, the neurons in the hippocampus and striatum were arranged compactly, with normal cell morphology and no obvious damage; in group S, the neurons were arranged sparsely, with normal cell morphology and visible cell contour, but the cytoplasmic staining became shallow, some cells had nucleolus shrinkage, and some cells had annular bands around them; in group F, the number of neurons in the hippocampus and striatum was higher than that in group S. There was a significant improvement. In addition, the striated cell bridge structure connecting putamen and caudate nucleus was clearly visible in group C and sparse and fuzzy

in group S, and the above situation in group F was significantly improved more than that in group S.

#### 4. Discussion

Our research results show that due to surgical trauma and stress, IL-1 $\beta$ , IL-6, and TNF- $\alpha$  are significantly increased after surgery, SOD and GSH-PX are significantly reduced after surgery, and behavioral tests in rat performance have also dropped significantly. By supplementing omega-3 PUFA during the perioperative period, the postoperative inflammation was alleviated and the behavioral performance of the rats was improved. In addition, through histopathological examination, it was found that supplementation of omega-3 PUFA during the perioperative period can protect the central neuron cells from stress damage caused by surgical trauma. Regarding the mechanism of action of omega-3 PUFA, we believe that, on the one hand, it can inhibit the expansion of the body's inflammatory response [10] and enhance the ability to resist oxidative stress; on the other hand, intraperitoneal injection may inhibit inflammatory signals locally.

POCD is a central nervous system complication after surgery, manifested as confusion, anxiety, personality changes, and memory impairment [1, 2]. The mechanism of POCD involves cerebrovascular disease, cerebral blood perfusion, preoperative cognitive impairment, genetic susceptibility, changes in neurotransmitter function, and central nervous system inflammation (with inflammatory mediators IL-1 $\beta$ , TNF- $\alpha$ , IL-6, and others) [6, 11, 12]. It is currently believed that POCD is induced by surgery and anesthesia on the basis of neurodegeneration and is the result of the synergistic effect of multiple factors. It may be related to the patient's own factors, such as age, mental factors, genetic factors, sleep disorders, combined underlying diseases, alcohol and smoking, and education level; perioperative factors such as type of surgery, anesthesia methods, anesthesia drugs and other drugs, depth of anesthesia, hypoxia, hypotension, postoperative infection, postoperative pain, secondary surgery, and many other factors are related [6, 13]. Multiple animal experiments have proved that the increase in proinflammatory cytokines caused by surgery is related to cognitive impairment and neurodegeneration [14–16]. Moreover, the stress response caused by surgery is related to POCD [17]. Our animal experiments found that the operation caused the increase of serum IL-1 $\beta$ , IL-6, and TNF- $\alpha$  and the decrease of SOD and GSH-PX. Histopathology found that the neuronal cells in the operation group were sparsely arranged, and the cell morphology was normal, but the cytoplasm was stained lightly, some cells shrank nucleoli, and some cells appeared ring-shaped bands around them. These changes suggest that surgery can cause systemic inflammation, damage the ability to resist oxidative stress, and cause histological changes in central neurons.

Metabolic disorders of polyunsaturated fatty acids (PUFAs) have been reported to be related to a variety of neurological diseases, such as depression, bipolar disorder, schizophrenia, attention deficit hyperactivity disorder, and Alzheimer's disease (AD) [18, 19]. Among them, omega-3

PUFAs (ALA, EPA, and DHA) play an important role in the process of neurogenesis, synaptic development, and synaptic plasticity [20, 21]. Dietary supplementation of polyunsaturated fatty acids (PUFAs), especially omega-3 PUFA, shows outstanding effects in antioxidant and immune regulation [22]. Studies have shown that long-chain omega-3 PUFAs can reduce the risky process of patients with high-risk schizophrenia [23]; large intake of omega-3 PUFAs is associated with low levels of  $\beta$ -amyloid 42 (A $\beta$ 42) in plasma [24]. The development of white matter hyperintensity was associated with a low serum EPA/AA ratio but was not related to a low serum DHA/AA ratio [25]. In the rat animal model of traumatic brain injury (TBI), intraperitoneal injection of omega-3 polyunsaturated fatty acids can reduce microglia-mediated nerves by inhibiting the HMGB1/TLR4/NF- $\kappa$ B pathway inflammation [26]. A study just published in cells reported that oral linoleic acid can rescue C57BL/6N mice (8 weeks old) from neuroinflammation and cognitive dysfunction induced by  $\beta$ -amyloid peptide (intraventricular injection) [27]. Omega-3 PUFA can activate blood vessel cells, restore elasticity of blood vessels, and repair damaged blood vessel walls; at the same time, they can effectively reduce blood viscosity, accelerate blood circulation, and quickly regulate High-density lipoprotein, Low-density lipoprotein, Glycerol triester and Cholesterol. Therefore, omega-3 PUFAs also have the potential to prevent POCD. Our animal experiments have found that supplementation of omega-3 PUFA during the perioperative period can reduce postoperative inflammation, enhance the ability to resist oxidative stress, protect the structure of central neurons, and improve neurobehavioral performance.

In summary, the development of POCD may be associated with postoperative excessive inflammation and oxidative stress. Supplementing experimental rats with omega-3 PUFA during the perioperative period may reduce systemic inflammation, antagonize early postoperative oxidative stress, and improve POCD.

#### Data Availability

The data used to support the findings of this study are available from the corresponding authors upon request.

#### Conflicts of Interest

There is no conflict of interest among authors.

#### Authors' Contributions

Experiments were designed by S.F., H.J., and J.Z. Experiments were performed by Y.G., F.P., Y.C., and J.S. The manuscript was written by Y.G. and edited by S.F.. Yong Guo and Feng Ping are equal contributors.

#### Acknowledgments

This work was supported by grants from the Shanghai Municipal Commission of Health and Family Planning Foundation for Key Developing Disciplines (2015ZB0103).

## *Retraction*

# **Retracted: Effects of Ozone on Hippocampus BDNF and Fos Expressions in Rats with Chronic Compression of Dorsal Root Ganglia**

### **BioMed Research International**

Received 12 March 2024; Accepted 12 March 2024; Published 20 March 2024

Copyright © 2024 BioMed Research International. This is an open access article distributed under the Creative Commons Attribution License, which permits unrestricted use, distribution, and reproduction in any medium, provided the original work is properly cited.

This article has been retracted by Hindawi following an investigation undertaken by the publisher [1]. This investigation has uncovered evidence of one or more of the following indicators of systematic manipulation of the publication process:

- (1) Discrepancies in scope
- (2) Discrepancies in the description of the research reported
- (3) Discrepancies between the availability of data and the research described
- (4) Inappropriate citations
- (5) Incoherent, meaningless and/or irrelevant content included in the article
- (6) Manipulated or compromised peer review

The presence of these indicators undermines our confidence in the integrity of the article's content and we cannot, therefore, vouch for its reliability. Please note that this notice is intended solely to alert readers that the content of this article is unreliable. We have not investigated whether authors were aware of or involved in the systematic manipulation of the publication process.

Wiley and Hindawi regrets that the usual quality checks did not identify these issues before publication and have since put additional measures in place to safeguard research integrity.

We wish to credit our own Research Integrity and Research Publishing teams and anonymous and named external researchers and research integrity experts for contributing to this investigation.

The corresponding author, as the representative of all authors, has been given the opportunity to register their agreement or disagreement to this retraction. We have kept a record of any response received.

### **References**

- [1] L. Zhu, Y. Wang, X. Lin, X. Zhao, and Z. j. Fu, "Effects of Ozone on Hippocampus BDNF and Fos Expressions in Rats with Chronic Compression of Dorsal Root Ganglia," *BioMed Research International*, vol. 2021, Article ID 5572915, 10 pages, 2021.



## Research Article

# Effects of Ozone on Hippocampus BDNF and Fos Expressions in Rats with Chronic Compression of Dorsal Root Ganglia

Lingling Zhu,<sup>1,2</sup> Yanxiu Wang,<sup>2</sup> Xiaowen Lin,<sup>1</sup> Xu Zhao,<sup>1</sup> and Zhi jian Fu<sup>1</sup> 

<sup>1</sup>Department of Pain Management, Provincial Hospital Affiliated to Shandong University, Shandong University, 324 Jingwu Road, Jinan, Shandong 250021, China

<sup>2</sup>Department of Pain Management, Taian City Central Hospital, 29 Longtan Road, Taian, Shandong 271001, China

Correspondence should be addressed to Zhi jian Fu; zhijian\_fu@163.com

Received 26 January 2021; Accepted 26 October 2021; Published 26 November 2021

Academic Editor: Yuzhen Xu

Copyright © 2021 Lingling Zhu et al. This is an open access article distributed under the Creative Commons Attribution License, which permits unrestricted use, distribution, and reproduction in any medium, provided the original work is properly cited.

The effects of ozone on hippocampal expression levels of brain-derived neurotrophic factor (BDNF) and c-fos protein (Fos) were evaluated in rats with chronic compression of dorsal root ganglia (CCD). Forty-eight adult female Sprague-Dawley rats were randomly divided into the following 4 groups ( $n = 12$ ): sham operation (sham group), CCD group, CCD with 20  $\mu\text{g/ml}$  of ozone (CCD +  $\text{AO}_3$  group), and CCD with 40  $\mu\text{g/ml}$  of ozone (CCD +  $\text{BO}_3$  group). Except the sham group, unilateral L5 dorsal root ganglion (DRG) compression was performed on all other groups. On days 1, 2, and 4 after the operation, the CCD +  $\text{AO}_3$  and CCD +  $\text{BO}_3$  groups were injected with 100  $\mu\text{l}$  of ozone with concentrations of 20 and 40  $\mu\text{g/ml}$ , respectively. Thermal withdrawal latencies (TWLs) and mechanical withdrawal thresholds (MWTs) were measured at various time points before and after the operation. BDNF and Fos expressions were examined in the extracted hippocampi using immunohistochemistry. The TWLs and MWTs of CCD model rats that received ozone were lower with decreased BDNF and increased Fos expression levels, on day 21 after the operation, compared to those of the sham group ( $P < 0.05$ ). The TWLs and MWTs of the CCD +  $\text{AO}_3$  and CCD +  $\text{BO}_3$  groups were higher with increased BDNF and decreased Fos expression levels, on day 21 after the operation, compared to those of the CCD group ( $P < 0.05$ ). The TWLs were longer and the MWTs were higher in the CCD +  $\text{BO}_3$  group at each time point with increased BDNF and decreased Fos expression levels, on day 21 after the operation, compared to those of the CCD +  $\text{AO}_3$  group ( $P < 0.05$ ). Our results revealed that ozone can relieve the neuropathic pain caused by the pathological neuralgia resulting from DRG compression in rats. The mechanism of action for ozone is likely associated with changes in BDNF and Fos expression levels in the hippocampus.

## 1. Introduction

Since its first use in 1988, ozone has been widely used to treat pain in many diseases. Lumbar and leg pain have been treated with epidural ozone injection in clinical studies; however, its specific mechanism is still unclear. As a classical model of neuropathic pain, chronic compression of dorsal root ganglia (CCD) simulates the lumbar and leg pain caused by clinical disc herniation and intervertebral foramen stenosis [1]. Previous studies have shown that the hippocampus is a crucial area affected by pain stimulation and involved in pain signal processing [2, 3].

Rat hippocampi usually comprise two regions, CA1 and CA3. The CA1 region is an especially sensitive region; cere-

bral ischemia has been reported to selectively damage hippocampal CA1 neurons, while keeping neurons in other subfields undamaged [4, 5]. The CA1 region has been shown to be closely associated with the occurrence and development of chronic pain. For instance, formalin-induced inflammatory pain stimulation has been shown to increase the probability and amplitude of long-term potentiation (LTP) induction in the DG and CA1 regions, which could be completely abolished by blocking nociceptive inputs at the peripheral injury site [6]. Microinjecting N-methyl-D-aspartic acid receptors (NMDARs) inhibitors into the CA1 region has been shown to significantly inhibit chronic pain.

Brain-derived neurotrophic factor brain-derived neurotrophic factor (BDNF) and c-fos protein (Fos) are expressed

abundantly in the hippocampus. BDNF is a polypeptide secreted by nerve cells and target tissues. Fos is a well-established marker of pain pathway activation. Under painful stimuli, a decreased BDNF level induces the autophosphorylation of tyrosine protein kinases, thereby activating ERK1/2 through a series of cascades into p-ERK1/2 and transporting it from the cytoplasm into the nucleus. The aforementioned processes promote the transcription and expression of certain genes including c-fos, which initiates cell proliferation and differentiation while playing an important role in cell growth, development, and proliferation. Acute or chronic pain has been shown to significantly reduce the levels of BDNF mRNA [7]. t-5224, an inhibitor of c-fos, has been found to alleviate spared nerve injury-(SNI-) induced pain responses in mice. Studies have also shown that spinal c-fos expression can be reduced by analgesic drug application [8, 9].

This study evaluated the effects of epidural ozone injection on pain threshold and hippocampus expressions of BDNF and Fos in a CCD rat model to elucidate the mechanism of ozone therapy in lumbar and leg neuralgia, thereby providing an experimental basis for clinical application.

## 2. Materials and Methods

**2.1. Animal Selection and Grouping.** In total, 48 healthy female 8-week-old rats weighing 250~280 g were procured from Beijing Huafukang Biotechnology Co., Ltd. and acclimatized at 20~25°C for 24 hours. These rats were randomly divided using digital tables into the 4 following groups ( $n = 12$ ): sham group, CCD group, CCD model with 20  $\mu\text{g/ml}$  ozone (CCD + AO<sub>3</sub>) group, and CCD model with 40  $\mu\text{g/ml}$  ozone (CCD + BO<sub>3</sub>) group.

**2.2. Model Preparation and Epidural Catheterization.** Apart from the sham group, the CCD model was induced in all other groups, as described by Song et al. [1]. Rats were anesthetized by intraperitoneally injecting sodium pentobarbital. Then, the lumbosacral region was routinely shaved and disinfected before a posterior median left lateral incision was made along the rat spinous process, and the skin was incised from the left border of the L4-L6 vertebrae, followed by blunt separation to the transverse process. Once the extraforaminal foramen at the root of the transverse process is exposed, cephalad insertion of a needle (bent at 90°) into the foramen was performed at angles of 30° and 10° to the median and the spinal horizontal lines, respectively. The needle was withdrawn once the nerve root palpation caused a slight tic in the ipsilateral hindlimb muscles. Subsequently, a stainless-steel column with a length of 6 mm and a diameter of 0.6 mm was inserted into the intervertebral foramen along the needle to ensure constant compression of the adjacent nerve roots. The muscles and low back fascia were then sutured sequentially. For rats in the sham group, no steel column compression was applied after identifying the intervertebral foramen position. The method described by Nishiyama [10] was used to place the outer tube of the hard film for each group. After determining the position of the T13/L1 gap and separating the interspinous and ligamentum

flavum from the intervertebral space, a 13 cm long PE catheter was inserted at one end 1.5 cm caudally and secured to the adjacent muscles using silk sutures. The neck skin was incised by 0.5 cm to create a subcutaneous tunnel; the PE catheter was secured to the neck with a transcutaneous tunnelled silk suture at the other end. After the operation, normal saline was used to flush the incision, before the back fascia and skin were sutured. Rats in each group received penicillin intraperitoneally to prevent infection. After remaining awake for 2 hours, rats from all groups were returned to single cage housing in the animal holding room. On days 1, 2, and 4 after surgery, the rats in the CCD + AO<sub>3</sub> and CCD + BO<sub>3</sub> groups were injected with 100  $\mu\text{l}$  each of ozone through the epidural catheter at concentrations of 20 and 40  $\mu\text{g/ml}$ , respectively.

**2.3. General Behavioural Observation.** Health statuses and activity levels of rats were continuously observed. Changes in skin, muscle tone, posture, and gait of the hind limbs on the operated side of rats were recorded daily. Rats with no ulceration, paralysis, and autophagic limbs were selected for subsequent tests.

**2.4. Determining Thermal Withdrawal Latency (TWL).** TWL was detected on the day before the operation as well as 1, 3, 5, 7, 14, and 21 days after the operation. According to the method described the Hargreaves [11], a BME-410C type thermal pain stimulator was used for testing, which was developed by Institute of Biomedical Engineering, Chinese Academy of Medical Sciences. Rats were placed over a 3 mm thick plexiglass plate with the thermal pain stimulator placed below. The light source was focused to illuminate the plantar skin corresponding to the 4<sup>th</sup> and 5<sup>th</sup> metatarsals on the postoperative rat hind limbs. The latency from the initiation of illumination up until the appearance of hindlimb withdrawal responses was determined as the sensitive observation indicator of heat-induced pain. Measurements were repeated 3 times at 5 min intervals; the mean for each rat was used for statistical analysis.

**2.5. Detection of Mechanical Withdrawal Threshold (MWT).** The mechanical withdrawal threshold (MWT) was measured on the day before the surgery as well as 1, 3, 5, 7, 14, and 21 days after the surgery. Four hours after the TW measurements, the mechanical pain threshold was measured using von Frey filaments (up-down method) [12]. Rats were placed inside a clear Plexiglas box for detection; the skin corresponding to the 4<sup>th</sup> and 5<sup>th</sup> metatarsal bones of the rat left hind foot was perpendicularly stimulated with von Frey cilia with different folding forces (in ascending order). The cilia were bent into a sigmoid shape and maintained for 6~8 s at 30 s intervals. Positive responses of the rats included rapid withdrawal of hind foot, flinching, and other phenomena. If a positive response was not observed in a rat after stimulation, then, ciliary restimulation with a higher force is applied. Ciliary stimulation was repeated 5 times for each force. The minimum intensity that elicited more than three positive responses was recorded. If no positive response was observed in rats upon application of the maximum cilia

force, then, this maximum force was used for subsequent calculations. The following specific formula was used to calculate MWT:  $(10^{[xf+\kappa\delta]})/10000$  where  $xf$  is the logarithmic value of the last used force;  $\kappa$  is the coefficient under different stimulation conditions, and  $\delta$  has a fixed value of 0.224.

**2.6. Nissl Staining.** Six rats were randomly selected from the CCD and CCD + BO<sub>3</sub> groups and abdominally anesthetized using 10% hydrochloraldehyde (0.38 mL/100 g). The heart was perfused with 50 ml of 4% paraformaldehyde/0.1 mol/L phosphate buffer, and the dorsal root ganglion (DRG) of L5 was removed and fixed with 4% paraformaldehyde for 24 h. After routine dehydration and paraffin embedding, serial sections were taken. Sections approximately 4  $\mu$ m thick were extracted until the entire hippocampus was removed. Sections were stained with cresyl violet (Nissl staining) for 50 s, dehydrated, diaphanized, and mounted for observation. Cell counting was performed in three adjacent DRG sections. Only cells with visible nuclei and nucleoli were counted. Five visual fields were randomly selected, and images were captured from each slice in the cerebral cortex area (400 power microscope). The number of living cells in each high-power microscope visual field was determined.

**2.7. Immunohistochemical Examinations.** The process of obtaining sections is the same as Nissl staining. Antibodies against BDNF (batch number: sc20981, Santa Cruz company, USA) and Fos (batch number: sc-271243, Santa Cruz company, USA) were diluted at 1:150. The cells were incubated overnight at 4°C in 50  $\mu$ l of the diluted antibody solutions. Cells were then incubated with the horseradish peroxidase-labelled secondary antibody for 30 min. PBS was used as the negative control instead of using primary antibody. Three sections were labelled by each antibody, and two nonoverlapping visual fields were randomly selected from each section in the target area. The average optical densities of BDNF and Fos in hippocampal tissues were measured using Image Pro Plus 6.0.

**2.8. Western Blot Test.** After the last pain threshold test, the rats were anesthetized with sodium pentobarbital. Six rats in each group were randomly selected and sacrificed with an intraperitoneal injection of 10% chloral hydrate (0.38 ml/100 g body weight). The hippocampal tissue on the operation side was extracted and stored in liquid nitrogen. Tissue samples were weighed, cleaned, and centrifuged. The ratio of protease inhibitor to the protein extraction reagent (precooling to 4°C) was 1:99. After 1  $\mu$ g of tissue was added to 10  $\mu$ l of tissue cell lysis solution, the tissue was homogenized, incubated on ice for 30 min, and then centrifuged at 12,000 rpm for 30 min at 4°C. The supernatant was collected, and the protein concentration was determined using the BCA method. The remaining protein supernatant was proportionally added to the loading buffer, mixed evenly, and denatured in 100°C metal bath for 10 min. Subsequently, it was cooled to room temperature and stored at -80°C. In total, 40  $\mu$ g of the protein samples was separated by 10% SDS-PAGE and transferred to PVDF membrane by wet electro-spinning. After sealing the membrane in 5%

skimmed milk powder for 1 h at room temperature, the membrane was washed three times with TBST (tris buffered saline tween) for 5 min each. BDNF (1:1 000), Fos (1:500), and  $\beta$ -actin (1:1000) antibodies were incubated with the membrane overnight at 4°C. The next day, the membrane was washed three times with TBST for 10 minutes each. The membrane was incubated with horseradish peroxidase-labelled secondary antibody (1:5000) at room temperature for 1 h. Subsequently, the membrane was washed 3 times with TBST for 15 min each. The ECL chemiluminescence method was used to image the protein bands. Image-Pro Plus 6.0 was used to quantitatively analyse the protein bands.

**2.9. Statistical Analysis.** The data were processed using the SPSS 22.0 statistical software, and the measured data were expressed as mean  $\pm$  standard deviation. Values between two groups were compared using independent *t*-tests. One-way ANOVA was also used to compare between groups, and the Student Newman Keuls test was used to compare the sample means.  $P < 0.05$  was considered statistically significant.

### 3. Results

**3.1. Successful Establishment of the CCD SD Rat Model.** Eight SD rats were preexperimental before formal experimentation, two died within 24 h and one within 72 h after surgery, so the mortality rate of rats was 0.75%. No further rat death occurred until the end of the formal experiment. After the formal experiment, we found that all CCD rats walked normally with no obvious gait alterations; no self-injurious behaviours were observed. All rats developed a frequent lifting action of the postoperative hind foot and licking. Therefore, the CCD model success rate was 100% in formal trials.

**3.2. Epidural Ozone Injection Increases TWL.** Compared to the preoperative values, there was no significant change in the TWL at each time point for the sham group ( $P > 0.05$ ). On day 1, compared with those of the sham group, TWL values of the remaining groups decreased significantly ( $P < 0.05$ ); however, there was no significant difference between the CCD model group and the groups that received ozone. Until the 5<sup>th</sup> postsurgery day, the TWLs of CCD + A O<sub>3</sub> group were not significantly different from those of the CCD group; however, the TWLs of CCD + BO<sub>3</sub> group (day 3, mean  $\pm$  SD = 6.96  $\pm$  1.91; day 5, mean  $\pm$  SD = 8.78  $\pm$  2.43) were higher than those of the CCD group (day 3, mean  $\pm$  SD = 4.91  $\pm$  1.16,  $P = 0.005$ ; day 5, mean  $\pm$  SD = 5.71  $\pm$  1.58,  $P = 0.002$ ) and higher than those of CCD + AO<sub>3</sub> group as well (day 3, mean  $\pm$  SD = 5.37  $\pm$  0.98,  $P = 0.013$ ; day 5, mean  $\pm$  SD = 6.18  $\pm$  2.11,  $P = 0.004$ ). This result suggested that a high concentration of ozone can significantly increase the thermal threshold from day 3 to day 5 after the operation. On the 7<sup>th</sup> day, TWL values of the CCD + AO<sub>3</sub> (8.67  $\pm$  0.99,  $P = 0.012$ ) and CCD + BO<sub>3</sub> groups (10.97  $\pm$  2.47,  $P < 0.001$ ) continued to increase and were significantly higher than that of the CCD group (6.35  $\pm$  1.89,  $P < 0.001$ ). After 14 and 21 days, the ozone intervention groups had significantly higher TWLs than that of the CCD group; TWLs for the CCD + B



O<sub>3</sub> group was also higher than those of the CCD + AO<sub>3</sub> group ( $P < 0.05$ ). These results showed the ozone significantly reduced the thermal pain threshold of rats with time. The effect of high concentration ozone on pain relief was higher than that of low concentration ozone. (Figure 1(a)).

**3.3. Epidural Ozone Injection Increases MWT.** Before surgery, there was no significant difference in MWT among all groups ( $P > 0.05$ ). On days 1 and 3 days after the operation, the MWT values of other groups decreased significantly compared to that of the sham group ( $P < 0.05$ ); however, there were no significant differences between model and intervention groups. On day 5 after operation, MWT of the CCD group ( $5.01 \pm 0.98$ ) had no significant change; however, the MWTs of the ozone intervention groups (CCD + AO<sub>3</sub>,  $6.30 \pm 1.53$ ,  $P = 0.046$ ; CCD + BO<sub>3</sub>,  $6.80 \pm 1.66$ ,  $P < 0.018$ ) were higher than that of CCD group. There were no significant differences between the CCD + AO<sub>3</sub> and CCD + BO<sub>3</sub> groups. On the 7<sup>th</sup> day after the operation, the MWT value of the ozone intervention groups (CCD + AO<sub>3</sub>,  $7.19 \pm 1.29$ ,  $P < 0.001$ ; CCD + BO<sub>3</sub>,  $8.78 \pm 1.31$ ,  $P < 0.001$ ) continued to increase, which was significantly higher than that of the CCD group ( $5.11 \pm 1.25$ ). The CCD + BO<sub>3</sub> group had a higher MWT than that of the CCD + AO<sub>3</sub> group on day 7 postsurgery ( $P < 0.01$ ). On days 14 and 21 after the operation, the MWTs for the ozone intervention groups were significantly higher than those of the CCD group; the MWT of the CCD + BO<sub>3</sub> group was higher than that of the CCD + AO<sub>3</sub> group ( $P < 0.01$ ). These results showed that ozone group significantly reduced the mechanical pain threshold of rats with time. Moreover, the effect of high ozone concentration was higher than that of low ozone concentration (Figure 1(b)).

**3.4. Ozone Improves the Morphology and Number of DRG Cells after CCD.** Under normal conditions, the DRG cells are morphologically regular and closely arranged. Nissl bodies of DRG neurons are dark blue dense granules. In the CCD group, DRG cells were shrunken with indistinct cytoplasm, loose arrangement, and faint staining (Figure 2(a)). After ozone intervention, not only did the number of DRG cells increase, but the Nissl staining also became darker compared to that in the CCD group (Figure 2(b)). Sensitive neuronal survival was investigated by counting the number of L5 DRG neurons. Ozone treatment also led to an obvious reduction in neuronal preservation. The number of DRG neurons in the CCD + BO<sub>3</sub> group ( $73.5 \pm 16.5$ ) was significantly higher than that in the CCD group ( $42.6 \pm 12.33$ ) ( $P < 0.01$ ) (Figure 2(c)). This result indicated that ozone improves the morphology and number of dorsal root ganglion cells after CCD.

### 3.5. Immunohistochemical Results

**3.5.1. Average Optical Density of BDNF Significantly Increases in Hippocampal Cells after Epidural Ozone Injection.** Visual naked-eye observation of the brown staining revealed that BDNF is mainly expressed in the cytoplasm and on the cell membrane of hippocampal cells in each group. Although it was lower than that of the sham group (Figure 3(a)), the

staining intensity was higher in the CCD + BO<sub>3</sub> group (Figure 3(d)) than in the CCD + AO<sub>3</sub> group (Figure 3(c)), which in turn was higher than that in the CCD group (light stain) (Figure 3(b)). The average optical density of BDNF in the CCD group ( $0.14 \pm 0.038$ ) was lower than that in the sham group ( $0.37 \pm 0.045$ ) ( $P < 0.001$ ), whereas those in the CCD + AO<sub>3</sub> ( $0.21 \pm 0.043$ ) and CCD + BO<sub>3</sub> groups ( $0.28 \pm 0.049$ ) were higher than that in the CCD group ( $P < 0.05$ ). The expression level of BDNF in the CCD + BO<sub>3</sub> group was notably higher than that in CCD + AO<sub>3</sub> group ( $P = 0.012$ ); however, it was still lower than that in the sham group ( $P = 0.002$ ) (Figure 3(e)).

**3.5.2. Average Optical Density of Fos Significantly Decreases in Hippocampal Cells after Epidural Ozone Injection.** Brown staining representing Fos was mainly concentrated in the nuclei. Although it was higher than that in the Sham group (Figure 4(a)), the degree of staining in the CCD + BO<sub>3</sub> group (Figure 4(d)) was lower than that in the CCD + AO<sub>3</sub> group (Figure 4(c)), which in turn was clearly lower than that in the CCD group (Figure 4(b)). The average optical density of Fos in CCD group ( $0.40 \pm 0.065$ ) was higher than that in the sham group ( $0.13 \pm 0.048$ ) ( $P < 0.001$ ). The average optical densities of Fos in the CCD + AO<sub>3</sub> ( $0.29 \pm 0.058$ ) and CCD + BO<sub>3</sub> groups were lower than that in the CCD group ( $P < 0.05$ ). The average optical density in the CCD + BO<sub>3</sub> group was also lower than that in CCD + AO<sub>3</sub> group ( $P = 0.043$ ); however, it was still higher than that in the sham group ( $P = 0.003$ ) (Figure 4(e)).

**3.6. Gray Values of BDNF and Fos Are Significantly Elevated in Hippocampal Cells after Ozone Intervention.** Analysis of the BDNF gray values revealed that although the BDNF level in the CCD + BO<sub>3</sub> group ( $0.76 \pm 0.18$ ) was lower than that in the sham group ( $1.01 \pm 0.25$ ) ( $P = 0.021$ ), it was higher than that in the CCD + AO<sub>3</sub> group ( $0.52 \pm 0.14$ ) ( $P = 0.026$ ), which in turn was higher than that in the CCD group ( $0.29 \pm 0.07$ ) ( $P < 0.001$ ). Analysis of Fos gray values revealed that the expression of CCD group ( $1.19 \pm 0.23$ ) was higher than that of the sham group ( $0.42 \pm 0.11$ ) ( $P < 0.001$ ), with downregulated levels in the CCD + AO<sub>3</sub> ( $0.96 \pm 0.10$ ) and CCD + BO<sub>3</sub> group ( $0.70 \pm 0.19$ ) ( $P < 0.05$ ). The expression of Fos in the CCD + BO<sub>3</sub> group was significantly lower than that in the CCD + AO<sub>3</sub> group ( $P = 0.014$ ); however, it was still higher than that in the sham group ( $P = 0.009$ ) (Figure 5).

## 4. Discussion

As the recognition of the effectiveness of medical ozone therapy in pain management increases, its detailed mechanism is also being investigated. The DRG is the aggregation site for primary sensory afferent neurons. Abnormal electrical activity after an injury triggers persistent neuropathic pain and is crucially involved in pain signal transduction [13]. Although clinical research has shown that the administration of ozone effectively alleviates neuropathic pain caused by damage to the DRG, its related mechanism has not yet been elucidated. Long-term chronic injury to the DRG has been reported to

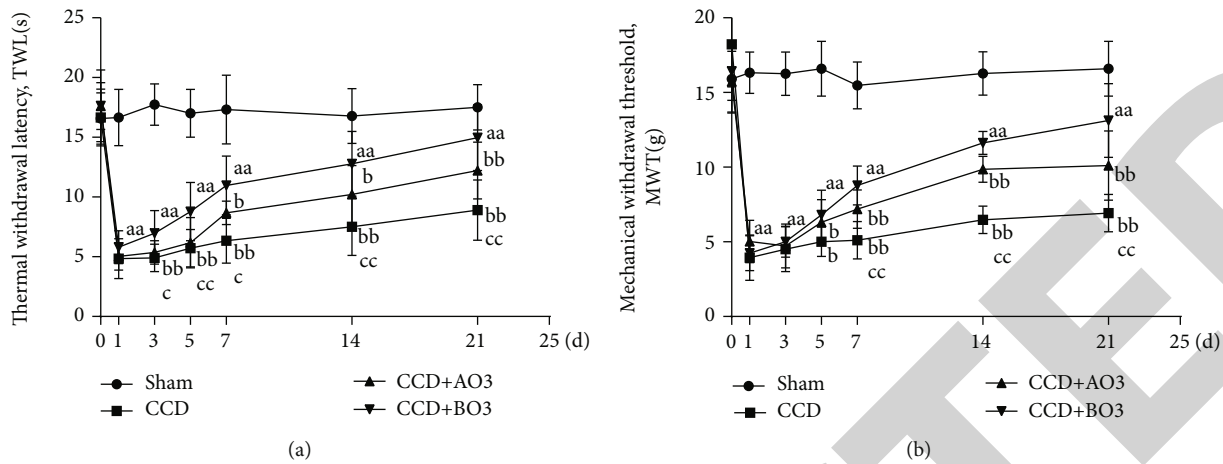


FIGURE 1: Effect of epidural ozone injection in alleviating pain in CCD model SD rats. With CCD, the thermal withdrawal latency (TWL) and mechanical withdrawal threshold (MWT) significantly reduced from day 1 to day 21 postsurgery ( $P < 0.001$  for both) ((a) and (b)). The thermosensitive pain was alleviated between day 7 and day 21 after surgery in the CCD + AO<sub>3</sub> group ( $P < 0.05$  for all except day 10, where  $P = 0.002$ ). The thermosensitive pain was significantly alleviated in the CCD + BO<sub>3</sub> group between day 3 and day 21 after surgery ( $P < 0.001$  for both). The thermosensitive pain-relieving effect between day 3 and day 21 postsurgery was more pronounced in the CCD + BO<sub>3</sub> group than in the CCD + AO<sub>3</sub> group ( $P < 0.001$  for both) (a). The mechanical allodynia was alleviated between day 7 and day 21 in the CCD + AO<sub>3</sub> group ( $P < 0.01$  for all except day 7, where  $P = 0.046$ ). The mechanical allodynia was also relieved significantly in the CCD + BO<sub>3</sub> group between day 5 and day 21 ( $P < 0.001$  for all except day 5, where  $P = 0.018$ ). The thermosensitive pain-relieving between day 7 to day 21 was more pronounced in the CCD + BO<sub>3</sub> group than in the CCD + AO<sub>3</sub> group ( $P < 0.001$ ) (b). Data are expressed as mean  $\pm$  SD (<sup>a</sup> $P < 0.05$  and <sup>aa</sup> $P < 0.01$ , vs. sham group; <sup>b</sup> $P < 0.05$  and <sup>bb</sup> $P < 0.01$ , vs. CCD group; <sup>c</sup> $P < 0.05$  and <sup>cc</sup> $P < 0.01$ , vs. CCD + AO<sub>3</sub> group).

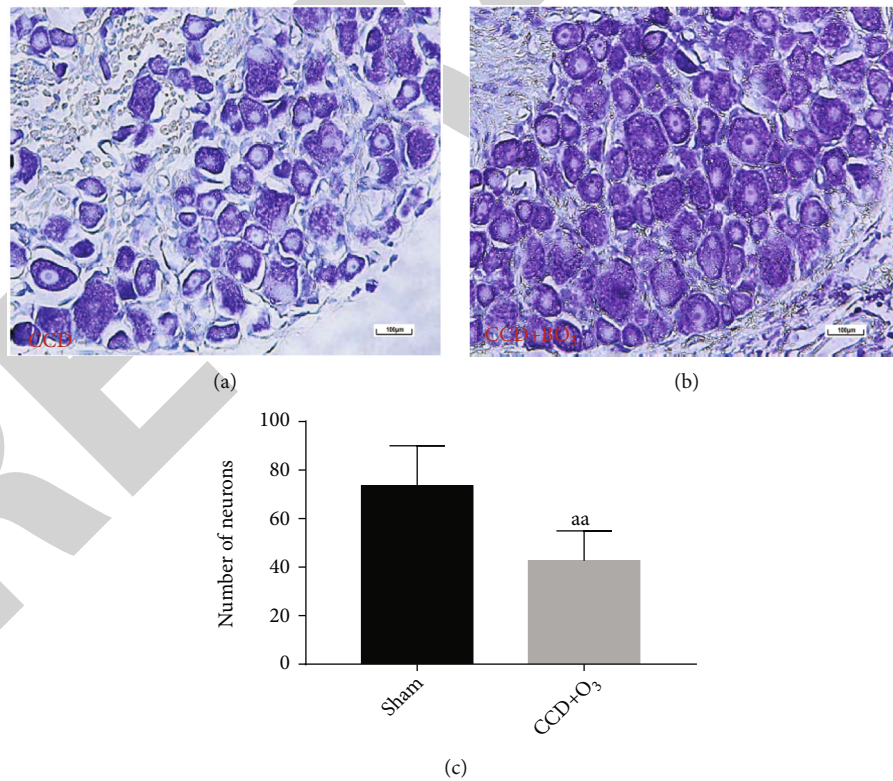


FIGURE 2: In the CCD group, DRG cells were shrunken with indistinct cytoplasm, loose arrangement, and faint staining (Figure 2(a)). After ozone intervention, the number of DRG cells increased, while the Nissl staining became darker compared to those of the CCD group (Figure 2(b)). The number of DRG neurons in the CCD + BO<sub>3</sub> group was significantly higher than that in the CCD group ( $P < 0.01$ ) (Figure 2(c)).

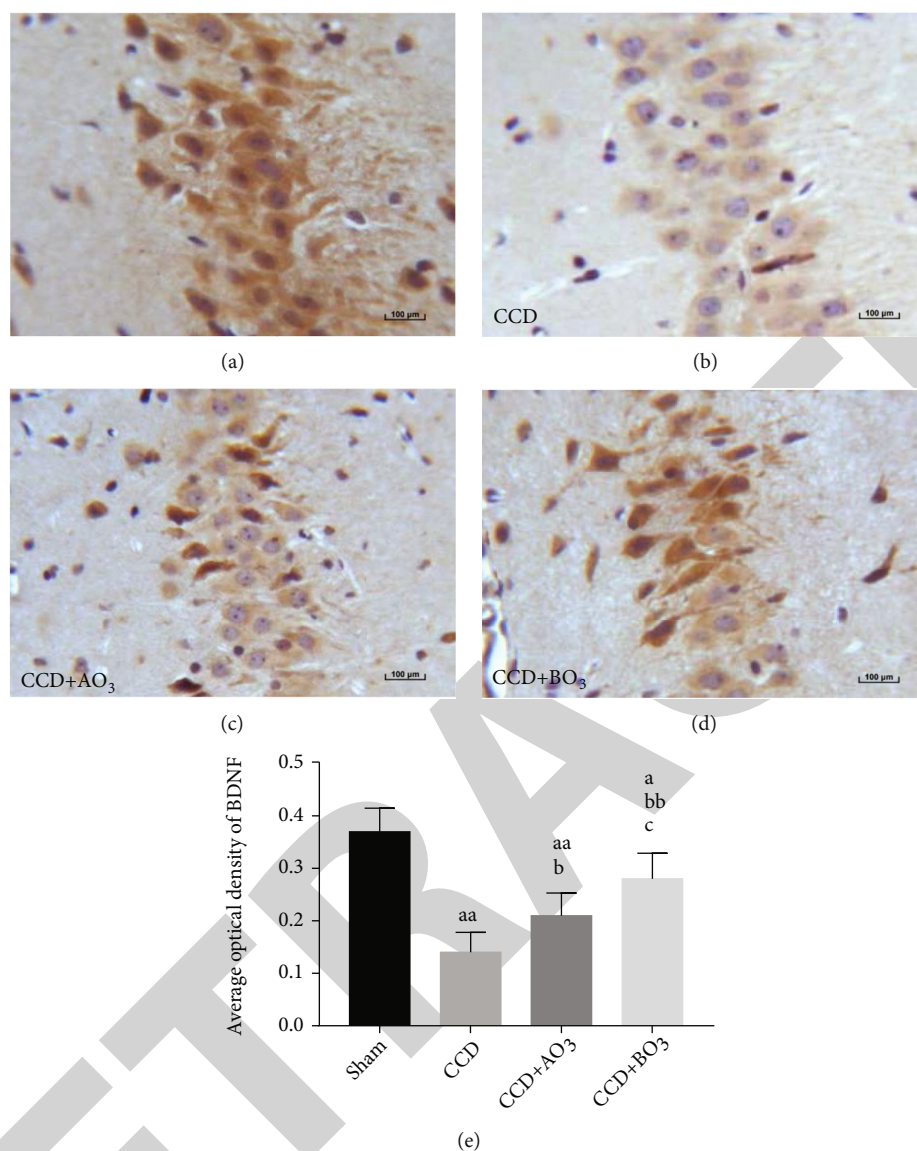


FIGURE 3: BDNF was mainly expressed in the cytoplasm and on the membrane of hippocampal cells in each group, as represented by brown staining. The average optical density of BDNF in the CCD group was lower than that in the sham group ( $P < 0.001$ ), whereas those in the ozone intervention groups were higher than that in the CCD group (CCD + AO<sub>3</sub>,  $P < 0.05$ ; CCD + BO<sub>3</sub>,  $P < 0.01$ ). The average optical density of BDNF in the CCD + BO<sub>3</sub> group was higher than that in the CCD + AO<sub>3</sub> group ( $P < 0.05$ ); however, it was still lower than that of the sham group ( $P < 0.05$ ). Data are expressed as mean  $\pm$  SD (<sup>a</sup> $P < 0.05$  and <sup>aa</sup> $P < 0.01$ , vs. sham group; <sup>b</sup> $P < 0.05$  and <sup>bb</sup> $P < 0.01$ , vs. CCD group; <sup>c</sup> $P < 0.05$  and <sup>cc</sup> $P < 0.01$ , vs. CCD + AO<sub>3</sub> group).

be involved in central sensitization closely related to hyperalgesia and allodynia [14, 15]. The hippocampus, which is the limbic system of the brain, is an important structure involved in the relevant integrative processing of this pain information. Therefore, this study assessed the damage to the DRG and the alteration of crucial hippocampal protein levels after ozone intervention to elucidate the mechanism by which ozone reduces pain.

In this study, once the CCD model was established, the rats exhibited pain-induced abnormalities such as toe apposition, lifting, and licking. The threshold between the thermal and mechanical paw withdrawal responses of rats in the CCD group was significantly lower than that in the sham group at all observed time points after the surgery, suggest-

ing the occurrence of thermal and mechanical pain sensitivity, thereby indicating the successful establishment of the model. Numerous studies have shown that although ozone exhibits antioxidation and anti-inflammatory effects to treat diseases, it can also aggravate oxidative stress or lead to disease [16]. In this preliminary study found that 20 μg/ml of O<sub>3</sub> did not affect the survival of spinal cord cells, whereas ozone concentrations of 30 to 100 μg/ml have been shown to be concentration-dependently neurotoxic to spinal cord neurons [17]. Intrathecal injection of ozone at concentrations of 10, 20, or 30 μg/mL has been shown to significantly reduce mechanical PWT; ozone concentration of 20 μg/ml could not induce nerve damage and was reported to have an anti-inflammatory effect [18]. Ozone at high concentrations



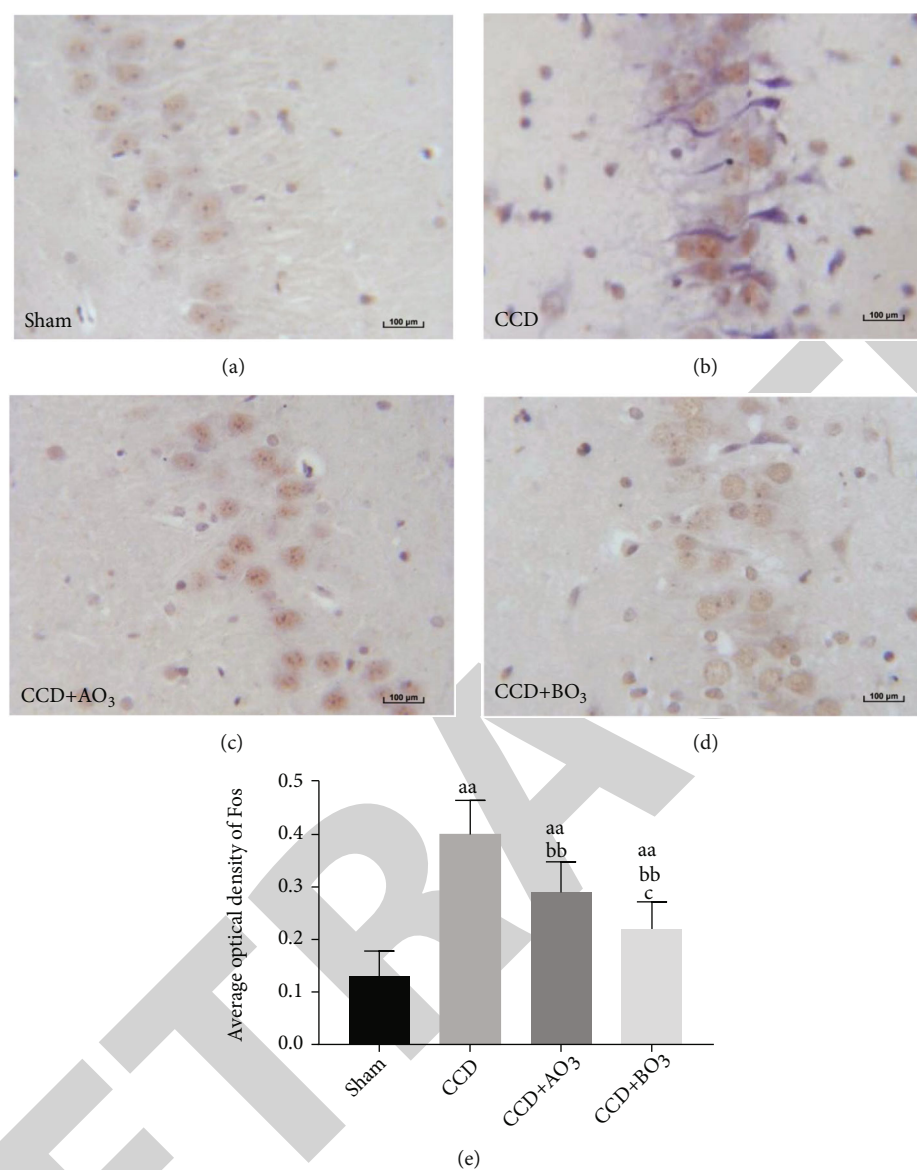


FIGURE 4: Fos staining, shown in brown, was mainly concentrated in the nucleus. Although it was lower than that in the CCD group ( $P < 0.01$ ), the average optical density of Fos in hippocampal cells in the CCD + AO<sub>3</sub> group was higher than that in the CCD + BO<sub>3</sub> group ( $P < 0.05$ ), which in turn was higher than that in the sham group ( $P < 0.01$ ). Data are expressed as mean  $\pm$  SD (<sup>aa</sup> $P < 0.01$  compared with the sham group; <sup>b</sup> $P < 0.05$  and <sup>bb</sup> $P < 0.01$ , compared with the CCD group; <sup>c</sup> $P < 0.05$  and <sup>cc</sup> $P < 0.01$ , compared with the CCD + AO<sub>3</sub> group).

of 40, 60, and 80  $\mu\text{g/ml}$  can cause neural apoptosis and peroxide damage through the JNK/MAPK signalling pathway, causing significant neurotoxicity. Therefore, this study selected epidural ozone injection that increased the arachnoid barrier. The effects of ozone at concentrations of 20 and 40  $\mu\text{g/ml}$  on the operative toe pain threshold were assessed after damaging the DRG.

The results of this study suggested that the thermal paw withdrawal response period of the operated rat foot was significantly longer, and the threshold of mechanical paw withdrawal response was significantly improved after ozone intervention compared to those of the CCD group, suggesting that ozone intervention alleviated thermal and mechanical pain sensitivity in rats. Our results also suggested that

ozone at a concentration of 40  $\mu\text{g/ml}$  increased the pain threshold more significantly than that at 20  $\mu\text{g/ml}$ . We believe that 40  $\mu\text{g/ml}$  ozone has a protective effect rather than a toxic effect because of the arachnoid as a barrier.

Expression of Fos is the central response to various noxious stimuli, and its expression levels are positively correlated with the intensity of the stimulation [19]. As a marker of nociceptive pain conduction, Fos can be widely used to explore pain conduction pathways and investigate pain modulation [20, 21]. In this study, the protein expression levels of Fos in the CCD model group were significantly higher than those in the control and ozone intervention groups. Fos expression in the CCD model was downregulated by ozone intervention. The degree of downregulation

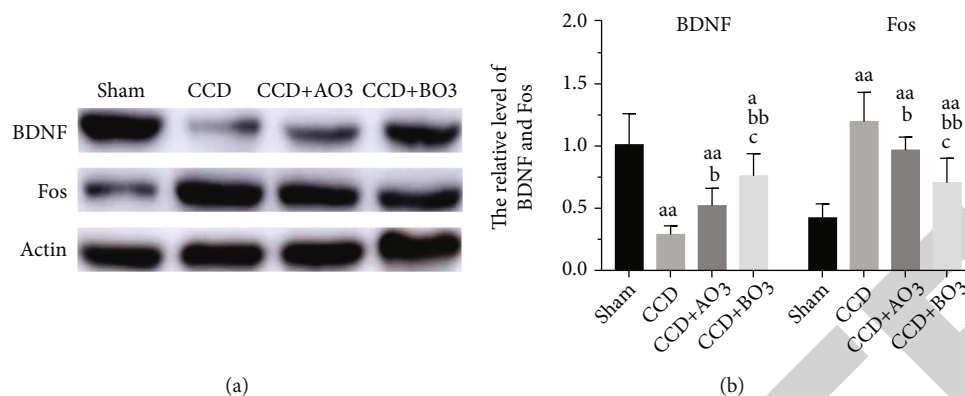


FIGURE 5: Western blot band images and quantitative determination of relative densities revealed that CCD of DRG significantly decreased the expression of BDNF in hippocampi compared to that in the sham group ( $n = 6/\text{group}$ ). Epidural injection of ozone (20 or 40  $\mu\text{g}/\text{ml}$ ) increased the protein expression of BDNF compared with that in the sham group ( $n = 6/\text{group}$ ) ( $P < 0.05$ ). Quantitatively, BDNF relative densities were calculated as the ratio of BDNF protein band intensity to that of actin. Ozone reduced the hippocampal expression of Fos. Western blot images and quantitatively calculated relative densities revealed that CCD of DRG significantly increased the hippocampal expression of Fos compared with that in the sham group ( $n = 6/\text{group}$ ). Epidural injection of ozone (20 or 40  $\mu\text{g}/\text{ml}$ ) decreased the protein expression of Fos compared to that in the CCD group ( $n = 6/\text{group}$ ) ( $P < 0.05$ ). Quantitatively, relative densities of Fos were calculated as the ratios of Fos protein band intensities to those of actin. Data are presented as mean  $\pm$  SD (<sup>aa</sup> $P < 0.01$  vs. sham group; <sup>b</sup> $P < 0.05$  and <sup>bb</sup> $P < 0.01$ , vs. CCD group; <sup>c</sup> $P < 0.05$  and <sup>cc</sup> $P < 0.01$ , vs. CCD + AO<sub>3</sub> group).

by ozone concentration of 40  $\mu\text{g}/\text{ml}$  was more pronounced than that by 20  $\mu\text{g}/\text{ml}$ , which was consistent with the changes in thermal and mechanical hyperalgesia in each group. These results suggested that the pain induced by CCD can alter the levels of pain-related factors in the hippocampus.

Levels of BDNF, which are abundant in the hippocampus, also change significantly by the process of chronic pain. BDNF has been shown as a critical mediator of central sensitization and an important regulator of neuronal excitability and plasticity [22–24]. BDNF is also involved in different pain models such as inflammation-induced hyperalgesia [25], complete Freund's adjuvant-induced thermal hyperalgesia [26], mechanical hyperalgesia in an L5 anterior rhizotomy model [27], and a spinal nerve ligation model [28]. Currently, chronic pain in peripheral tissues is believed to be equivalent to persistent stressors, which can cause apoptosis of neurons and decrease hippocampal BDNF expression; this indicates that peripheral noxious stimulation can regulate BDNF expression in the higher brain centre [29, 30]. Our results revealed that the BDNF protein expression in the CCD model group was significantly lower than that in the control group. Ozone concentration of 40  $\mu\text{g}/\text{ml}$  induced a more pronounced upregulation than that by 20  $\mu\text{g}/\text{ml}$ . This result indicated that ozone probably increased the pain threshold by upregulating hippocampal BDNF expression. However, BDNF expression levels in the DRG, spinal cord, and brain centre are different. In an SNI model, the BDNF levels in the DRG neurons of damaged nerves are upregulated, whereas that of undamaged nerves is downregulated [31]. CFA has been shown to increase BDNF expression and phosphorylated ERK in the spinal dorsal horn; the ERK inhibitor, U0126, has also been reported to reverse the increase in pain sensitivity [32]. In a chronic constriction injury (CCI) state, BDNF and MAPK expression levels in the spinal dorsal horn have been shown to increase, which could be inhibited by a MAPK inhibitor, thereby hindering pain sensitization [33,

34]. Ma et al. [35] have shown that elevating BDNF expression levels has been shown to reverse electrophysiological disturbances in vCA1-IL connectivity, alleviating spontaneous pain, thereby promoting a full recovery from pain.

Studies have found that there is some correlation between BDNF and Fos. c-fos, which forms a heterodimer with c-Jun, acts on the AP-1 site of target genes to regulate target gene expression, while BDNF contains an AP-1 site in its gene regulatory sequence, which may be regulated by Fos [36, 37]. Kim et al. [38] found that the addition of BDNF to spinal neuron culture fluid caused a rapid increase in c-fos mRNA. Spinal c-fos expression was also markedly increased 3 h after intrathecal BDNF injection in adult rats [39]. However, another study found that deletion of c-fos did not affect the expression of BDNF mRNA in CA1 and CA2 regions compared with c-fos mutated mice and wild type [40]. Thus, the interrelationship of BDNF and Fos expression is not clear. In this experiment, whether there is a correlation between the increase of BDNF expression and the decrease of Fos under the intervention of ozone remains to be further studied.

In conclusion, Epidural ozone could reduce chronic pain caused by long-term damage to the dorsal root ganglia, which is likely associated with hippocampal BDNF and Fos expression. Future studies will explore the signal pathway through which ozone interferes with the expression of BDNF and Fos.

### Data Availability

The data used to support the findings of this study are available from the corresponding author upon request.

### Conflicts of Interest

All authors declare no conflicts of interest.

## Authors' Contributions

All authors were involved in either writing or revising this paper. This paper was written by Lingling Zhu. All coauthors made important improvements to the article. Zhijian Fu had full access to all data in the study and takes responsibility for the integrity of the data as well as the accuracy of the data analysis. All authors approve the submission of this article for publication.

## Acknowledgments

This research was funded by grants from the National Natural Science Foundation of China (81771199).

## References

- [1] X. J. Song, S. J. Hu, K. W. Greenquist, J. M. Zhang, and R. H. LaMotte, "Mechanical and thermal hyperalgesia and ectopic-neuronal discharge after chronic compression of dorsal root ganglia," *Journal of Neurophysiology*, vol. 82, no. 6, pp. 3347–3358, 1999.
- [2] H. Kim, L. Chen, G. Lim et al., "Brain indoleamine 2,3-dioxygenase contributes to the comorbidity of pain and depression," *Journal of Clinical Investigation*, vol. 122, no. 8, pp. 2940–2954, 2012.
- [3] S. Khanna and F. Zheng, "Morphine reversed formalin-induced CA1 pyramidal cell suppression via an effect on septohippocampal neural processing," *Neuroscience*, vol. 89, no. 1, pp. 61–71, 1999.
- [4] M. Zhang, W. B. Li, J. X. Geng et al., "The upregulation of glial glutamate transporter-1 participates in the induction of brain ischemic tolerance in rats," *Journal of Cerebral Blood Flow & Metabolism*, vol. 27, no. 7, pp. 1352–1368, 2007.
- [5] R. Schmidt-Kastner and T. F. Freund, "Genomic approach to selective vulnerability of the hippocampus in brain ischemia-hypoxia," *Neuroscience*, vol. 309, no. 3, pp. 259–279, 2015.
- [6] X. Y. Zhaon, M. G. Liu, D. L. Yuan et al., "Nociception-induced spatial and temporal plasticity of synaptic connection and function in the hippocampal formation of rats: a multi-electrode array recording," *Molecular Pain*, vol. 5, 2009.
- [7] V. Duric and K. E. Mccarson, "Hippocampal neurokinin-1 receptor and brain-derived neurotrophic factor gene expression is decreased in rat models of pain and stress," *Neuroscience*, vol. 133, no. 4, pp. 999–1006, 2005.
- [8] K. Han, Y. Zhou, Z. H. Gan et al., "p21-activated kinase 7 is an oncogene in human osteosarcoma," *Cell Biology International*, vol. 38, no. 12, pp. 1394–1402, 2014.
- [9] J. Zhang, X. Zhu, H. Li et al., "Piperine inhibits proliferation of human osteosarcoma cells via G2/M phase arrest and metastasis by suppressing MMP-2/-9 expression," *International Immunopharmacology*, vol. 24, no. 1, pp. 50–58, 2015.
- [10] T. Nishiyama, "A rat model of chronic lumbar epidural catheterisation," *Canadian Journal of Anaesthesia*, vol. 45, no. 9, pp. 907–912, 1998.
- [11] K. Hargreaves, R. Dubner, F. Brown, C. Flores, and J. Joris, "A new and sensitive method for measuring thermal nociception in cutaneous hyperalgesia," *Pain*, vol. 32, no. 1, pp. 77–88, 1988.
- [12] S. R. Chaplan, F. W. Bach, J. W. Pogrel, J. M. Chung, and T. L. Yaksh, "Quantitative assessment of tactile allodynia in the rat paw," *Journal of Neuroscience Methods*, vol. 53, no. 1, pp. 55–63, 1994.
- [13] L. Ferhatovic, A. Banozic, S. Kostic et al., "Expression of calcium/calmodulin-dependent protein kinase II and pain-related behavior in rat models of type 1 and type 2 diabetes," *Anesthesia Analgesia*, vol. 116, no. 3, pp. 712–721, 2013.
- [14] R. H. Gracely, S. A. Lynch, and G. J. Bennett, "Painful neuropathy: altered central processing maintained dynamically by peripheral input," *Pain*, vol. 51, no. 2, pp. 175–194, 1992.
- [15] H. E. Torebjörk, L. E. Lundberg, and R. H. LaMotte, "Central changes in processing of mechanoreceptive input in capsaicin-induced secondary hyperalgesia in humans," *The Journal of Physiology*, vol. 448, no. 1, pp. 765–780, 1992.
- [16] A. Alexandre, J. Buric, and R. Paradiso, "Intradiscal injection of O<sub>2</sub>-O<sub>3</sub> to treat lumbar disc herniations," *Rivista Italiana di Ossigeno-Ozonoterapia*, vol. 1, pp. 165–169, 2002.
- [17] Y. Li, X. Lin, X. Zhao et al., "Ozone (O<sub>3</sub>) elicits neurotoxicity in spinal cord neurons (SCNs) by inducing ER Ca<sup>2+</sup> release and activating the CaMKII/MAPK signaling pathway," *Toxicology and Applied Pharmacology*, vol. 280, no. 3, pp. 493–501, 2014.
- [18] J. Wang, M. Wu, X. Lin, Y. Li, and Z. Fu, "Low-concentration oxygen/ozone treatment attenuated radiculitis and mechanical allodynia via PDE2A-cAMP/cGMP-NF-κB/p65 signaling in chronic radiculitis rats," *Pain Research and Management*, vol. 2018, 8 pages, 2018.
- [19] V. M. King and R. Apps, "Somatotopical organization of fos-like immunoreactivity in rat cervical spinal cord following noxious stimulation of the forelimb," *Neuroscience*, vol. 101, no. 1, pp. 179–188, 2000.
- [20] S. P. Hunt, A. Pini, and G. Evan, "Induction of c-*fos*-like protein in spinal cord neurons following sensory stimulation," *Nature*, vol. 328, no. 6131, pp. 632–634, 1987.
- [21] R. W. Presley, D. Menetrey, J. D. Levine, and A. I. Basbaum, "Systemic morphine suppresses noxious stimulus-evoked Fos protein-like immunoreactivity in the rat spinal cord," *Journal of Neuroscience*, vol. 10, no. 1, pp. 323–335, 1990.
- [22] A. R. Santos, D. Comprido, and C. B. Duarte, "Regulation of local translation at the synapse by BDNF," *Progress in Neurobiology*, vol. 92, no. 4, pp. 505–516, 2010.
- [23] Y. Yajima, M. Narita, A. Usui et al., "Direct evidence for the involvement of brain-derived neurotrophic factor in the development of a neuropathic pain-like state in mice," *Journal of Neurochemistry*, vol. 93, no. 3, pp. 584–594, 2005.
- [24] S. M. Todorovic and V. Jevtovic-Todorovic, "Targeting of CaV3.2 T-type calcium channels in peripheral sensory neurons for the treatment of painful diabetic neuropathy," *Pflugers Archiv-European Journal of Physiology*, vol. 466, no. 4, pp. 701–706, 2014.
- [25] R. Groth and L. Aanonsen, "Spinal brain-derived neurotrophic factor (BDNF) produces hyperalgesia in normal mice while antisense directed against either BDNF or trkB, prevent inflammation-induced hyperalgesia," *Pain*, vol. 100, no. 1, pp. 171–181, 2002.
- [26] H. H. Zhang, X. Q. Zhang, Q. S. Xue et al., "The BDNF/TrkB signaling pathway is involved in heat hyperalgesia mediated by Cdk5 in rats," *PLoS One*, vol. 9, no. 1, article e85536, 2014.
- [27] H. S. Chen, Z. H. Zhou, M. Li, J. X. Wang, B. J. Liu, and Y. Lu, "Contribution of brain-derived neurotrophic factor to mechanical hyperalgesia induced by ventral root transection in rats," *Neuroreport*, vol. 24, no. 4, pp. 167–170, 2013.
- [28] X. Zhang, Y. Xu, J. Wang et al., "The effect of intrathecal administration of glial activation inhibitors on dorsal horn

## Research Article

# Crosstalk between Heart Failure and Cognitive Impairment via hsa-miR-933/RELB/CCL21 Pathway

Wenxiao Feng,<sup>1,2</sup> Jie Yang,<sup>3</sup> Wenchao Song,<sup>4</sup> and Yitao Xue<sup>3</sup> 

<sup>1</sup>First Clinical Medical College, Shandong University of Traditional Chinese Medicine, Shandong, China

<sup>2</sup>Jinan Changqing District People's Hospital, China

<sup>3</sup>Department of Cardiovascular, Affiliated Hospital of Shandong University of Traditional Chinese Medicine, Shandong, China

<sup>4</sup>Department of Encephalopathy, Zouping Hospital of Traditional Chinese Medicine, Shandong, China

Correspondence should be addressed to Yitao Xue; mxdgi2967@t.edu.vn

Received 18 May 2021; Revised 26 July 2021; Accepted 8 August 2021; Published 21 September 2021

Academic Editor: Yuzhen Xu

Copyright © 2021 Wenxiao Feng et al. This is an open access article distributed under the Creative Commons Attribution License, which permits unrestricted use, distribution, and reproduction in any medium, provided the original work is properly cited.

**Background.** The association between heart failure (HF) and cognitive impairment has received increasing attention from scholars and researchers in recent years. However, no systematic studies have been carried out yet focused on the crosstalk between heart failure and cognitive impairment via miRNAs. **Methods.** GSE104150, GSE53473, GSE120584, and GSE116250 with RNA-seq data and clinical data were downloaded from the GSE database. All data were statistically analysed using R software to detect DE-miRNAs and DE-mRNAs associated with both HF and cognitive impairment. Protein-protein interaction (PPI) networks were mapped, and a logistic regression model for cognitive impairment prediction was developed. Furthermore, the TTRUST database and miRWalk were used to map miRNA-transcription factor (TF) and messenger RNA (mRNA) regulatory pathways. Finally, core TFs were enriched for analysis. **Results.** Differentially enriched DE-miRNAs and DE-mRNAs both present in HF and cognitive impairment were determined. A logistic regression model established based on DE-miRNAs was validated to have a strong performance in cognitive impairment prediction. The core miRNA-TF-mRNA pathway was formed by mapping the PPI networks associated with the two diseases. Further GSEA was performed with V-rel reticuloendotheliosis viral oncogene homolog B (RELB) as the core TF, and the retinol metabolism and gap junction pathways were analysed. **Conclusions.** This study was the first attempt to predict the crosstalk and examine underlying mechanisms between HF and cognitive impairment applying bioinformatics. The findings suggested a potential hsa-miR-933/RELB/CCL21 regulatory axis correlated with HF and neurological disorders (or cognitive impairment), according to PPI networks.

## 1. Introduction

Chronic heart failure (HF), alternatively known as chronic congestive heart failure, is the most advanced form of most cardiovascular diseases and a primary cause leading to patients' death. HF has largely resulted from myocardial damage caused by myocardial infarction, cardiomyopathy, haemodynamic overload, or inflammation. HF will weaken the contractility of heart muscles, preventing the maintenance of normal cardiac output [1]. The prevalence of HF in the general population is about 1-2%, but it exceeds 10% among the elderly aged over 70 [2, 3]. Statistics estimated that the number of patients suffering from cognitive impairment will reach around 74.7 million worldwide by 2030 [4].

Interestingly, approximately 25-75% of HF patients are accompanied by cognitive impairment [5]. Such a potential association between HF and cognitive impairment has attracted growing research attention [6].

Currently, though clinical indicators related to chronic HF have been identified, we still face a lack of more sensitive and accurate markers for early diagnosis, treatment, and prognostic assessment of chronic HF. miRNAs are small, endogenous RNAs of approximately 20 to 24 nucleotides in length with important regulatory roles in cells. miRNAs are involved in various pathological and physiological processes during HF development and cognitive impairment [7-10]. Disease diagnosis and prediction of prognosis could be based on testing certain miRNAs, as different compositions of



miRNA components are often indicative of disease types [11]. For example, as one of the most widely studied miRNAs, miR-206 has been identified to be closely associated with the development of HF and cognitive impairment [12]. HF is also related to changes in the microenvironment of the circulatory system [13]. Interestingly, these changes are present in cognitive impairment progression [14]. However, so far, no previous research has investigated the potential crosstalk between HF and cognitive impairment via miRNAs.

Bioinformatics allows the detection of specific signaling pathways via which diseases occur and analysis on the disease-target correlation, showing a strong potential of its use in predicting target mRNA binding sites potentially associated with cognitive impairment and HF. The present research is aimed at investigating the relationship between HF and cognitive impairment based on miRNA crosstalk and the underlying mechanisms, hoping to provide a theoretical basis for clinical translation.

## 2. Materials and Methods

**2.1. Data Collection and Preprocessing.** Microarray data was downloaded from GEO (<http://www.ncbi.nlm.nih.gov/geo/>). Microarray data of miRNA expression in peripheral blood derived from HF patients were downloaded from GSE104150 [15] and GSE53473 [16], while those of cognitive impairment patients were downloaded from GSE120584 [17]. Subsequently, the RNA-seq data of HF myocardial tissues were acquired from GSE116250 [18] to obtain mRNA expression. mRNA expression microarray data in brain tissues of cognitive impairment came from GSE140831 [19]. The GSE120584 dataset contained serum miRNA and corresponding clinical data of 1569 cases of cognitive impairment patients and normal controls; the GSE116250 dataset contained the mRNA expression data of 64 HF patients and normal controls; the GSE140831 dataset contained the mRNA expression data of 1129 patients with cognitive impairment and normal controls. Corresponding clinical information of patients in each GEO dataset was downloaded. RT-PCR data of the corresponding miRNAs in the predictive model were acquired. In addition, the corresponding clinical data were obtained. Informed consent was gained. Finally, RT-PCR data and clinical data from 95 patients who attended our hospital were acquired and served as a test set to evaluate the performance of the prediction model. The study procedure was reviewed and approved by the local ethical committee.

**2.2. Analysis of Variances.** The miRNA and mRNA microarray gene IDs were converted to gene symbols based on the microarray platform files. According to data types and sizes, the expression matrix was further log-transformed to obtain the miRNA and mRNA gene expression matrix. The limma [20] package was used to remove batch effects from the merged datasets when the same type of data was obtained from different platforms.

The Fragments Per Kilobase Million (FPKM) and Transcripts Per Kilobase Million (TPM) type data were analysed

to reveal mRNA/miRNA differences between HF and healthy control (HC) and between cognitive impairment and HC according to the clinical sample grouping using the limma package. Differentially expressed RNA between the two groups was filtered based on a threshold value.  $|FC > 1.1|$  was the threshold of miRNA differential analysis. DE-miRNAs and DE-mRNAs of HF and HC, as well as cognitive impairment and HC, were intersected to obtain common DE-miRNAs and DE-mRNAs. The results were presented in a Venn diagram using the VennDiagram package.

**2.3. miRNA-TF-mRNA and PPI Network and Subnetwork Construction.** TF and its target mRNA were acquired from the TTRUST database. The TF and corresponding mRNAs in the shared DE-mRNA database were compared to develop a DE-TF-mRNA regulatory relationship network. Target mRNAs of the shared DE-miRNAs were predicted by the miRWalk (<http://mirwalk.umm.uni-heidelberg.de/>) database. The results were analysed with the DE-TF-mRNAs to acquire the intersection of the miRNA-TF/mRNA relationship network. Cytoscape (version 3.8.2) was employed for the visualisation of the miRNA-TF-mRNA regulatory PPI network. Finally, the MCODE plugin (degree cutoff = 2, node score cutoff = 0.2,  $k$ -core = 2, and max.depth = 100) was used to create an aggregation of core genes and subnetworks in the network. The top two core subnetworks were selected according to the enrichment score, and their relational pairs and nodes were acquired for further analysis.

**2.4. Construction of a Logistic Regression Model to Predict the Incidence of Cognitive Impairment Patterns.** Shared DE-miRNAs and clinical information were analysed by univariate and multivariate logistic regression analyses. Factors from the common dataset and public database predictive of cognitive impairment onset were screened to develop two prediction models by logistic regression. A nomogram was created using the “rms” package to calculate and predict cognitive impairment incidence. Furthermore, a calibration curve was plotted to determine the calibration of the model. Public dataset and clinically acquired data served as the training group and the test group, respectively, for model training. The receiver operating characteristic (ROC) curve was plotted using the ROCR package [21] and the Hmisc package, and the C-index was calculated to assess the predictive and discriminatory performance of the model in the training, overall, and test groups. A C-index between 0.7 and 1 represented a high predictive performance. Finally, to evaluate the prediction range of the model, decision curves were plotted using the “rmda” package. The package was also used to assess the nomogram as well as clinical applicability and safety of the model.

**2.5. Thermal and Volcanic Mapping.** Heatmap and volcano maps of the DE-miRNAs and their target mRNAs in the prediction model for cognitive impairment and for normal controls were, respectively, intersected using the pheatmap and gplots packages. Furthermore, the miRNAs and target



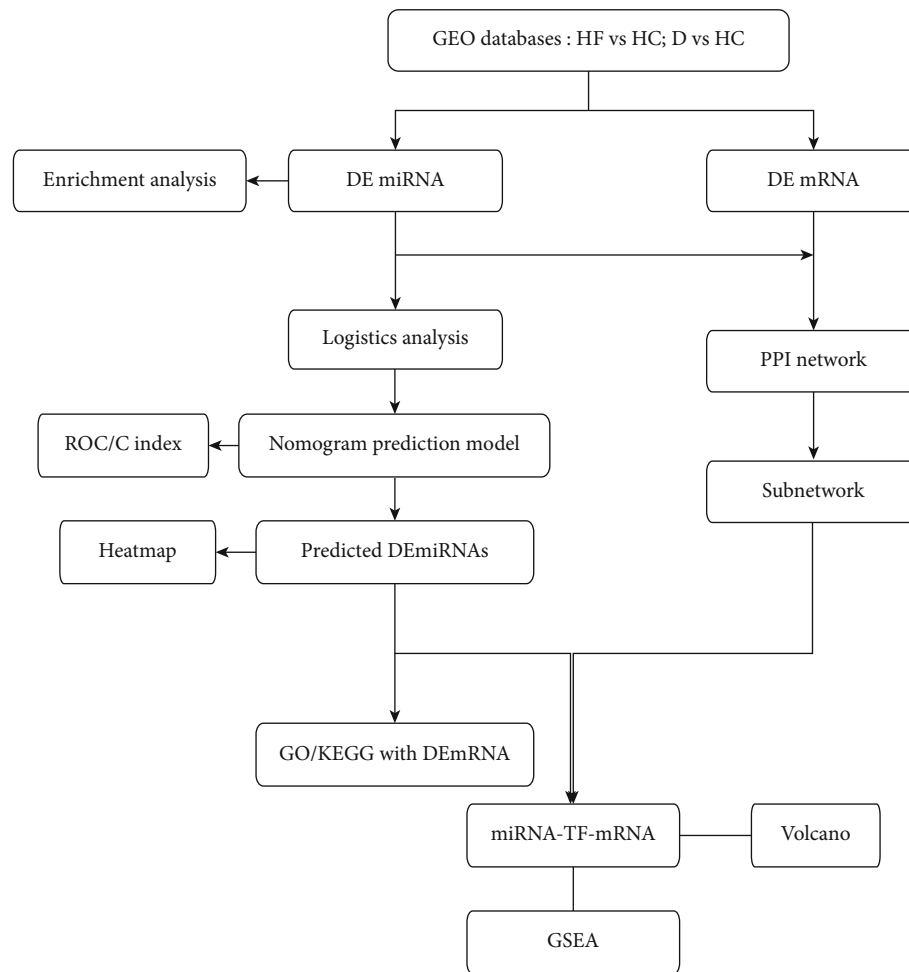


FIGURE 1: Flow chart of the analysis process.

mRNAs shared by both the core genes of the PPI subnetwork and the prediction model were marked in the volcano map. The ggalluvial and ggplot2 packages were employed to develop a mulberry map of differential miRNA-TF/mRNA axes, which were considered to play a regulatory role in the pathogenesis of cognitive impairment.

**2.6. Functional Enrichment Analysis and Statistical Analysis.** Functional enrichment analysis was carried out using FunRich (v.3.1.3) for DE-miRNAs shared by both HF and cognitive impairment. Upregulated and downregulated genes were identified from the differential mRNAs targeted by key miRNAs in the prediction model for cognitive impairment and further subjected to functional GO and KEGG pathway enrichment mapping. Enrichment analysis of GO and KEGG pathways was conducted using the org.Hs.eg.db and clusterProfiler packages, and bar graphs were created [22]. The pathways were filtered by  $P$  value ( $<0.05$ ). The TF factors were selected according to the fold change value and enriched by GSEA software (version 4.1.0), based on the obtained miRNA-TF-mRNA axis. The gene set “c2.cp.kegg.v7.4.symbols.gmt” was used for pathway enrichment annotation.

Statistical analysis was performed in R software (version 4.0.5). Hypothesis testing was conducted using a two-sided test.

### 3. Results

**3.1. Analysis of Variances and Network Construction.** The flow chart of the study analysis is shown in Figure 1. DE-miRNA and DE-mRNA were acquired from the downloaded datasets, and miRNA-TF/mRNA network and cognitive impairment prediction model were built. Finally, the core miRNAs and TFs were analysed.

The Venn diagrams showed DE-miRNAs (including hsa-miR-342-3p, hsa-miR-1246, hsa-miR-615-3p, hsa-miR-1224-5p, hsa-miR-636, hsa-miR-1257, hsa-miR-551a, hsa-miR-486-5p, hsa-miR-485-3p, hsa-miR-933, and hsa-miR-296-3p) incorporating 3097 common DE-mRNAs in HF and cognitive impairment (see Figures 2(a) and 2(b)). Functional enrichment analysis of DE-miRNA transcription factors showed enrichment in EGR1, MEF2A, NKX6-1, FOXD1, ESX1, and RORA (see Figure 2(c)). Table 1 exhibits the enrichment of DE-miRNAs in biological processes,

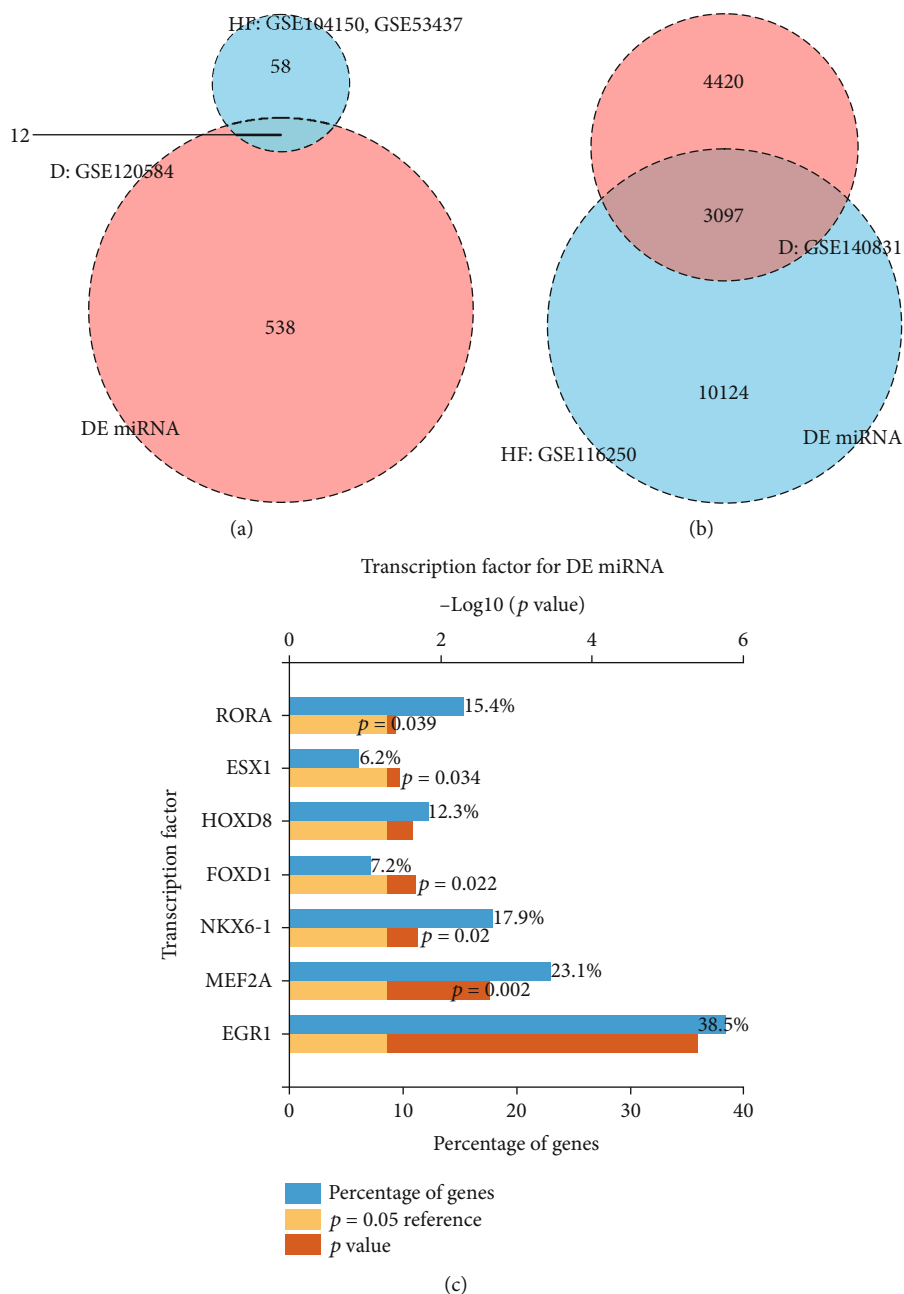


FIGURE 2: Venn diagram of mRNA and miRNA differential analysis results and differential miRNA pathway enrichment analysis. (a) Venn diagram shows the number of DE-miRNAs in HF and cognitive impairment, respectively, and the common differentially expressed miRNAs. (b) Venn diagram depicts the number of DE-mRNAs in HF and cognitive impairment, respectively, and the common differentially expressed mRNAs. (c) The bar chart exhibits the 11 DE-miRNAs targeted to TFs in cognitive impairment.

TABLE 1: Results of miRNA enrichment.

miRNA enrichment item	Percentage of genes	P value
Regulation of nucleobase, nucleoside, nucleotide, and nucleic acid metabolism (biological process)	25	0.044
Nucleus (cellular component)	56	0.007
Transcription factor activity (molecular function)	11	0.032
Integrin-linked kinase signaling (biological pathway)	27	0.041

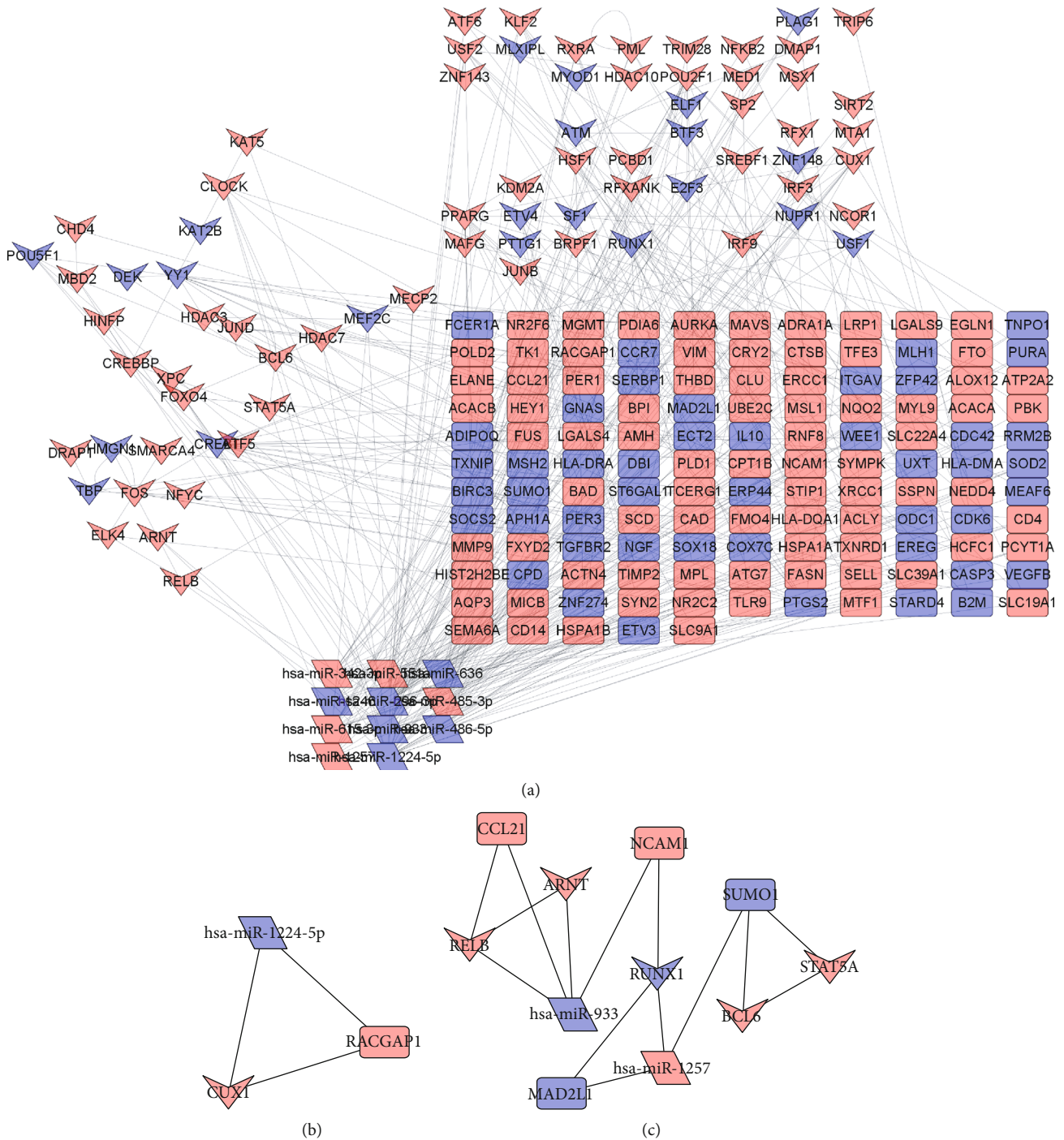


FIGURE 3: Protein interaction networks mapped from DE-miRNA, DE-mRNA, and predicted miRNA target gene prediction sites. (a) miRNA-TF-mRNA-regulated protein interaction network. (b, c) The top 2 aggregator network modules predicted according to MCODE. It represents the core group of genes involved in the disease process. The rectangles represent general protein mRNAs, the inner quadrilateral represents TF, and the rhombus represents miRNAs.

cellular components, molecular functions, and biological pathways.

Figure 3(a) displays the PPI mapping and construction of regulatory networks for DE-miRNAs and their predicted target DE-mRNAs. Based on the MCODE and filtering conditions, the top two aggregated subnetworks and core genes were obtained (see Figures 3(b) and 3(c)).

3.2. Single and Multifactor Logistic Regression Analyses. In cognitive impairment and normal control datasets, univariate and multivariate logistic regression analyses were performed on the above 11 DE-miRNAs together with two important clinical factors age and gender. The results of the univariate analysis were filtered by *P* value (<0.05) and showed statistical significance of the factors (see Table 2).

TABLE 2: Uni- and multilogistic regression analyses for predicting cognitive impairment.

Variables	Unilogistic regression			Multilogistic regression		
	$\beta$	Odds ratio (95% CI)	<i>P</i> value	$\beta$	Odds ratio (95% CI)	<i>P</i> value
Age	0.183	1.201 (1.173-1.231)	$P \leq 0.001$	0.185	1.204 (1.174-1.236)	$P \leq 0.001$
Sex	-0.783	0.457 (0.352-0.592)	$P \leq 0.001$	-0.510	0.6 (0.442-0.816)	0.001
hsa-miR-636	-0.678	0.508 (0.401-0.637)	$P \leq 0.001$	0.099	1.104 (0.826-1.471)	0.499
hsa-miR-485-3p	0.387	1.472 (1.255-1.726)	$P \leq 0.001$	0.340	1.405 (1.121-1.765)	0.003
hsa-miR-486-5p	-0.373	0.689 (0.591-0.803)	$P \leq 0.001$	-0.263	0.769 (0.6-0.985)	0.038
hsa-miR-933	-0.301	0.74 (0.652-0.839)	$P \leq 0.001$	-0.355	0.701 (0.584-0.84)	$P \leq 0.001$
hsa-miR-551a	0.468	1.597 (1.312-1.958)	$P \leq 0.001$	0.299	1.348 (1.038-1.762)	0.027
hsa-miR-296-3p	-0.405	0.667 (0.55-0.806)	$P \leq 0.001$	-0.129	0.879 (0.666-1.159)	0.361
hsa-miR-342-3p	0.359	1.432 (1.206-1.701)	$P \leq 0.001$	0.1925	1.212 (0.962-1.531)	0.105
hsa-miR-615-3p	0.315	1.37 (1.174-1.596)	$P \leq 0.001$	-0.0618	0.94 (0.749-1.178)	0.530
hsa-miR-1224-5p	-0.360	0.698 (0.569-0.845)	$P \leq 0.001$	-0.2666	0.766 (0.593-0.979)	0.037
hsa-miR-1257	0.583	1.792 (1.305-2.65)	0.001	0.30883	1.362 (0.941-2.103)	0.128
hsa-miR-1246	-0.110	0.896 (0.831-0.968)	0.005	0.05926	1.061 (0.946-1.192)	0.314

Note:  $\beta$  is the regression coefficient.

TABLE 3: Prediction factors for prevalence of cognitive impairment.

Variables	$\beta$	Prediction model Odds ratio (95% CI)	<i>P</i> value
(Intercept)	-10.561	0 (0-0)	$P \leq 0.001$
Age	0.184	1.202 (1.172-1.234)	$P \leq 0.001$
Sex	-0.511	0.6 (0.443-0.812)	$P \leq 0.001$
hsa-miR-485-3p	0.368	1.445 (1.178-1.774)	$P \leq 0.001$
hsa-miR-486-5p	-0.189	0.828 (0.678-1.011)	0.064
hsa-miR-933	-0.392	0.676 (0.575-0.792)	$P \leq 0.001$
hsa-miR-551a	0.356	1.427 (1.123-1.827)	0.004
hsa-miR-1224-5p	-0.290	0.748 (0.591-0.939)	0.014

Note:  $\beta$  is the regression coefficient.

Moreover, all the factors were subjected to multifactorial analysis. Here, we found that age, sex, hsa-miR-485-3p, hsa-miR-486-5p, hsa-miR-933, hsa-miR-551a, and hsa-miR-1224-5p were independent predictors.

### 3.3. Logistic Regression Model Construction and Testing.

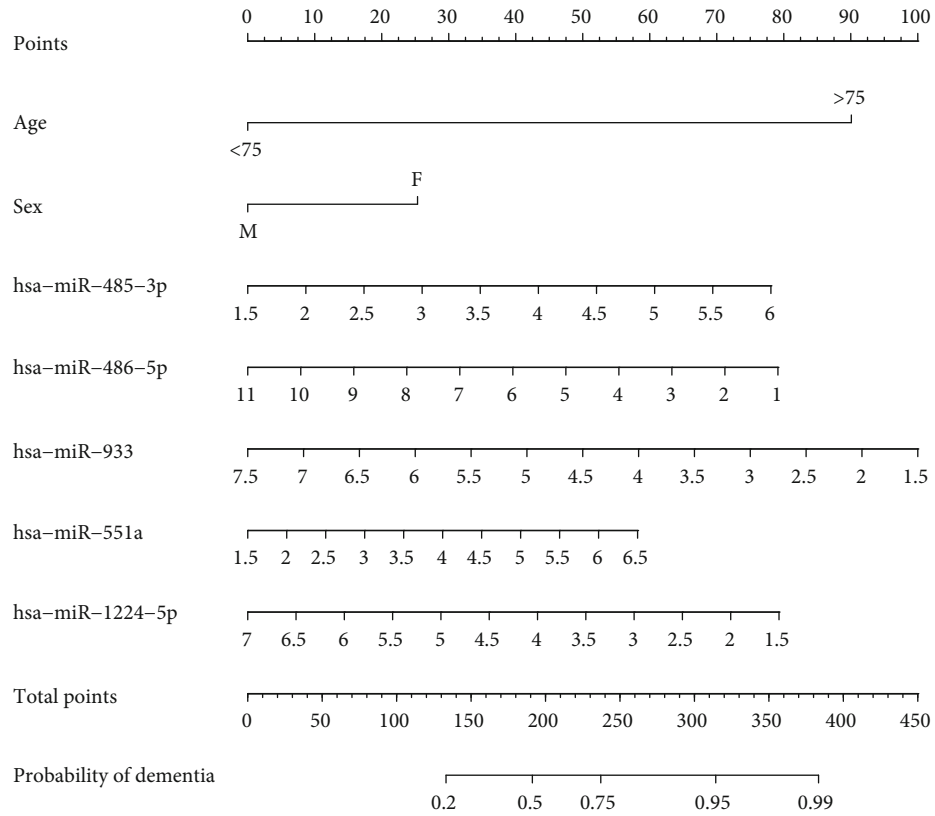
Table 3 shows the weights of the coefficients in the constructed model and the results of the statistical test of variance. Based on the constructed logistic regression model, the nomogram was plotted as a predictive model (see Figure 4(a)). Information on clinical patient characteristics was shown in Supplementary Table 1, and these data were the validation group for the predictive model. Figure 4(b) shows the calibration assessment of the predictive model in a calibration graph. Figure 4(c) shows the ROC and AUC of the model in the training, test, and overall groups. Table 4 displays the C-index values that ranged from 0.812 to 0.816 for the three groups. This indicated that the model had good predictive classification performance. Figure 4(d)

shows a wide clinical applicability and high safety of the prediction model in the training, test, and overall groups, according to the decision curve analysis (DCA) curves.

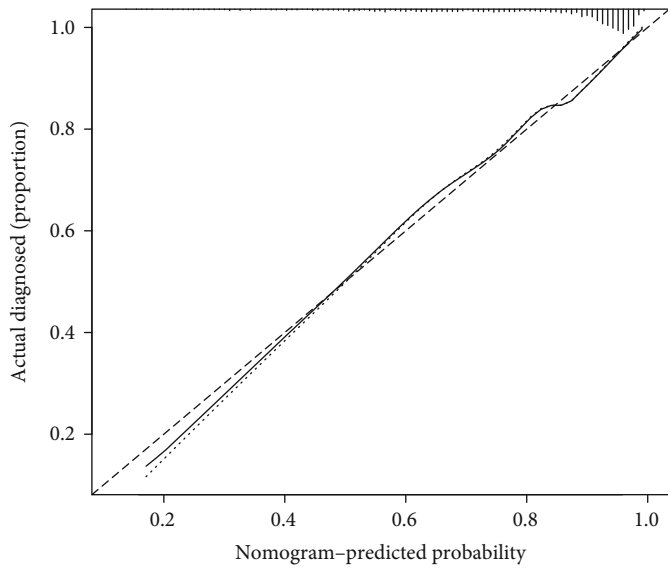
### 3.4. Heatmap of DE-miRNA and Targeted DE-mRNA in Logistic Prediction Model.

Based on the coefficients of the prediction model, the expression of five of the miRNAs in each cognitive impairment group and normal samples was presented as a heatmap (see Figure 5(a)). In relation to overall miRNA expression, factors such as age and gender were also shown. Based on the previously calculated PPI network, the expression of the target DE-mRNAs of these 5 miRNAs (hsa-miR-485-3p, hsa-miR-486-5p, hsa-miR-933, hsa-miR-551a, and hsa-miR-1224-5p) was presented in a heatmap (see Figure 5(b)).

**3.5. Functional Enrichment Analysis.** The GO and KEGG pathways were enriched to the five miRNA-targeted DE-mRNA genes in the model. The upregulated and downregulated GO pathways in cognitive impairment patients are



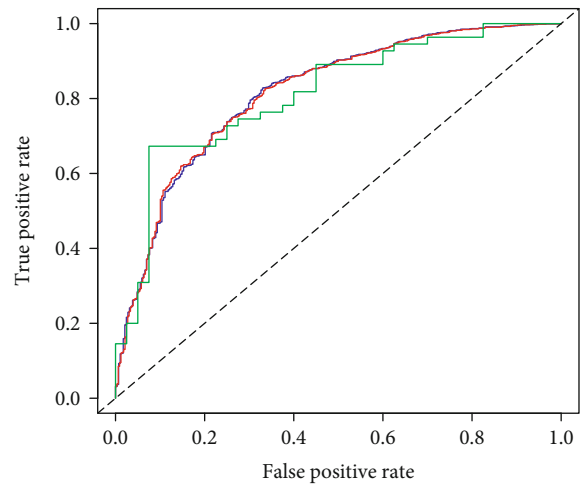
(a)



$B = 1000$  repetitions, boot Mean absolute error = 0.009  $n = 1569$

..... Apparent  
 — Bias-corrected  
 - - - Ideal

(b)



— Training\_set, AUC = 0.816  
 — Entire\_cohort, AUC = 0.815  
 — Validation\_set, AUC = 0.812

(c)

FIGURE 4: Continued.

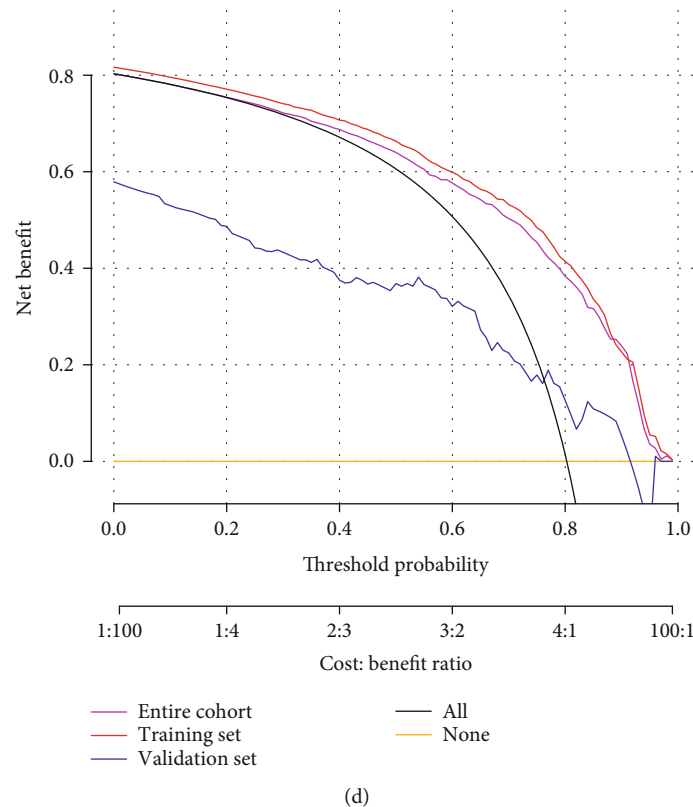


FIGURE 4: Logistic model based on DE-miRNA prediction of cognitive impairment. (a) Nomogram shows column plots for calculating the predicted incidence of cognitive impairment. (b) The calibration plot shows the calibration of the prediction results of the model. (c) The ROC curves show the classification and prediction performance of the prediction models. The training group, the clinical test group, and the overall group were evaluated separately. (d) Reliable range of model prediction probabilities demonstrated by DCA curves.

TABLE 4: C-index of the nomogram prediction model.

Dataset group	C-index of the prediction model	
	C-index	The C-index (95% CI)
Training set	0.816	0.788-0.843
Validation set	0.815	0.789-0.841
Entire cohort	0.812	0.725-0.899

shown in Figure 6, and the upregulated KEGG pathways are shown in Figure 7.

**3.6. Volcano Map and Sankey.** The significance of miRNA differential analysis and fold change in cognitive impairment and normal controls was shown in a volcano plot (see Figure 8(a)). Figure 8 also demonstrates the differential expression of DE-miRNAs in HF and cognitive impairment both in the cognitive impairment prediction model and in the core PPI subnetwork. Some miRNAs, such as hsa-miR-933 and hsa-miR-1224-5p, were present in both the cognitive impairment prediction model and PPI subnetwork which could be found in Figure 8(b). The DE-mRNA expression in cognitive impairment and normal controls was integrated in volcano plots. Furthermore, the DE-mRNAs targeted by the DE-miRNAs shared by both the cognitive impairment prediction model and PPI subnetwork were labelled. In Table 5, the results of the differential anal-

ysis of the two miRNAs mentioned above and their targeted DE-mRNAs could be found. The miRNA-TF-mRNA axes of these 2 miRNAs and their target genes were presented in a mulberry map (see Figure 8(c)).

**3.7. GSEA of Core Genes.** The mulberry map was constructed based on the targeted DE-mRNA of miRNAs selected. Combined with Table 5, the transcription factor RELB with the largest differential fold was determined, and the hsa-miR-933/RELB/CCL21 regulatory axis was developed, according to the prediction model and subnetwork. GSEA was performed on RELB in high- and low-expression groups (see Figures 9(a) and 9(b)). The results showed that the RELB high-expression group was enriched to KEGG\_RETINOL\_METABOLISM ( $P = 0.032$ ) and KEGG\_GAP\_JUNCTION ( $P = 0.032$ ), suggesting that the role of the regulatory axis may be similar in the development of HF and cognitive impairment.

## 4. Discussion

The treatment of HF is highly challenging in modern medicine. The present study was the first to investigate the correlation between HF and cognitive disorders from the perspective of miRNA-mRNA via a potential vascular-neural pathway. The crosstalk between HF and cognitive impairment as well as the underlying mechanisms was



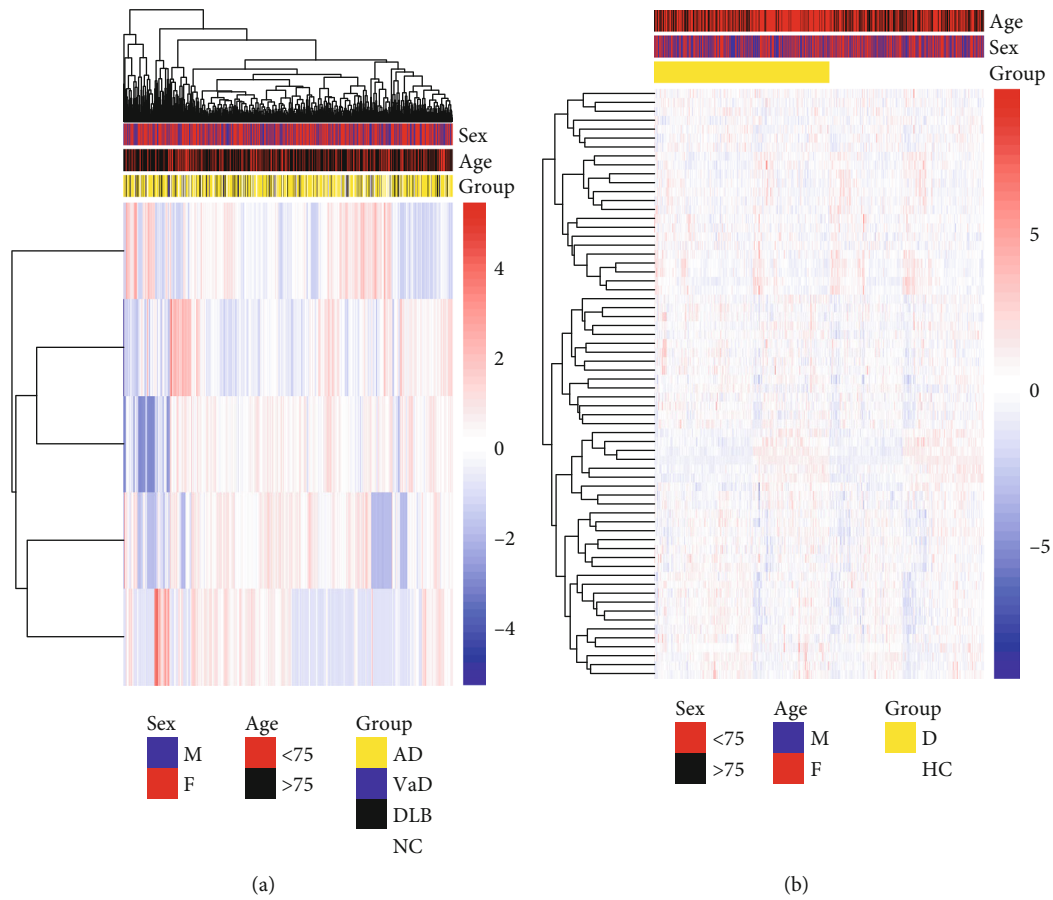
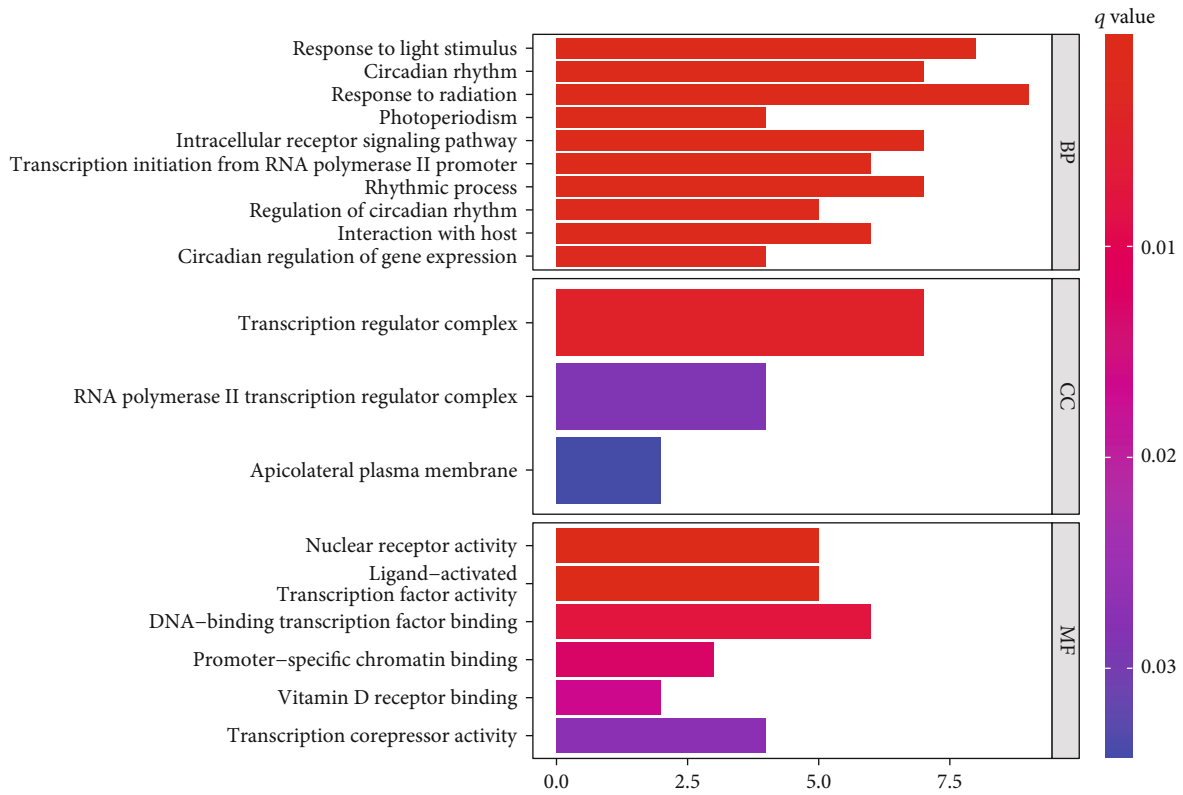


FIGURE 5: Heatmap of DE-miRNAs’ factor in predicting cognitive impairment and the expression of their targeted DE-mRNAs in the models. (a) Heatmap of DE-miRNA expression shows the expression of 5 DE-miRNAs predictive of cognitive impairment in the prediction model. (b) Heatmap of DE-mRNA expression shows the expression of DE-mRNA targeted by the five predictors in the model of patients with cognitive impairment, Alzheimer’s disease (AD), vascular dementia (VaD), Dementia with Lewy Bodies (DLB), Mild Cognitive Impairment (MCI), and dementia (D).

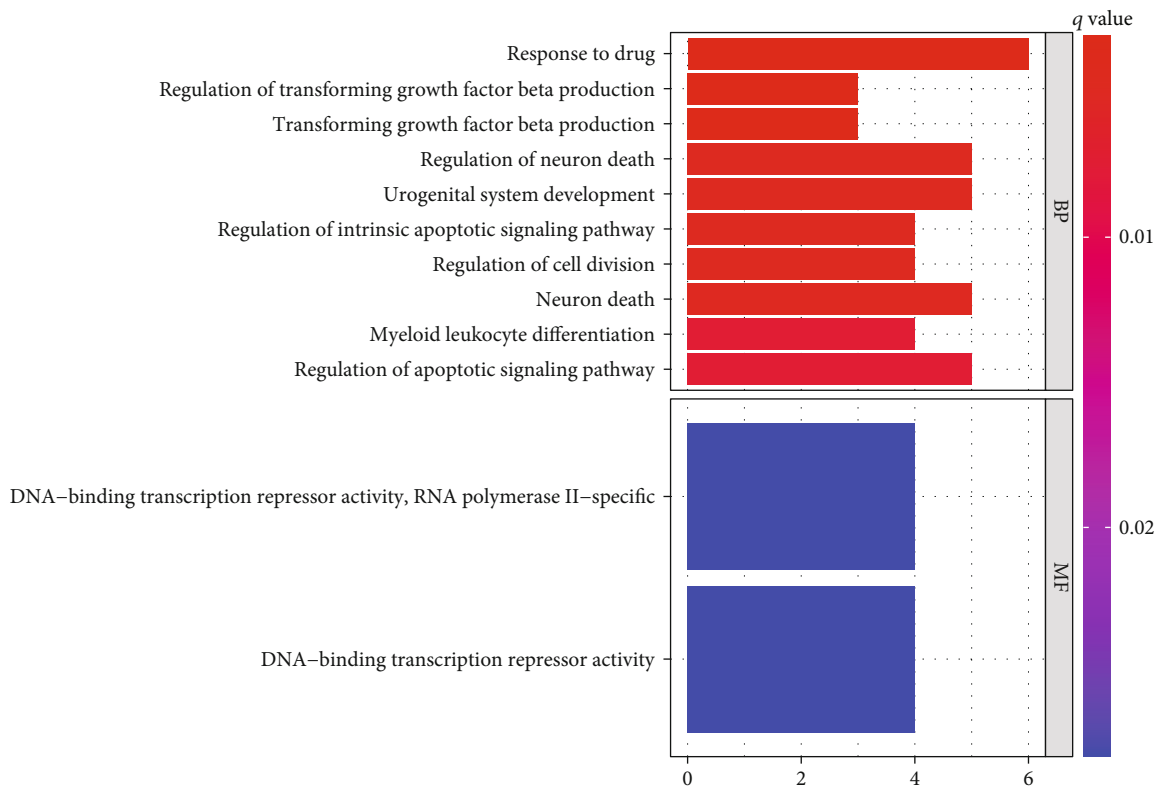
comprehensively investigated. This work will generate fresh insight into the theoretical basis for clinical translation by demonstrating that the hsa-miR-933/RELB/CCL21 regulatory axis played an important role in HF and cognitive disorders.

In this study, based on the GEO dataset, serum DE-miRNAs and DE-mRNAs in brain tissue from cognitive impairment patients and normal controls were obtained. Similarly, corresponding subjects were also acquired from HF patients and their controls. DE-miRNAs and DE-mRNAs present in both HF and cognitive impairment were detected to map a PPI network jointly associated with the two diseases. At the same time, a logistic regression model for predicting cognitive impairment incidence was established and further validated by comparing the results with clinical observations; here, the prediction model was verified to have a strong predictive performance. Moreover, the key miRNAs in the logistic regression model and the core TF in the PPI subnetwork were used to build a miRNA-TF-mRNA pathway. Further GSEA on the cores was performed, and the retinol metabolism and gap junction pathways were found to play similar regulatory roles in the development of HF and cognitive impairment.

The hsa-miR-933/RELB/CCL21 regulatory axis was speculated to function critically in HF and cognitive disorders. Also, the intron microRNA hsa-miR-933 is potentially associated with the development of neurodegenerative diseases and diabetes, and its important role in regulating ATF2 target genes could explain the observed association to some extent [23]. In addition, the miR-933 expression is correlated with numerous cancers, including oral squamous cell carcinoma, breast cancer, and colon cancer [24–26]. RELB, a TF for NF-kappaB, plays an important function in endothelial cells [27], which are vital components of the circulatory system and are partially involved in the development of HF and cognitive impairment [28]. The study also indicated the active role of RELB in neurodevelopment and central nervous system functions [29]. Our enrichment analysis revealed that the group with higher RELB expression was enriched to retinol metabolism and gap junction. In the present study, RELB as a TF regulating CCL21 expression was found to be possibly regulated by hsa-miR-933. Moreover, a previous study observed that RELB is positively correlated with CCL21 expression in dendritic cells [30, 31]. In cardiac tissues, CCL21 is considered a possible biomarker for the development of HF [32]. Previous



(a)



(b)

FIGURE 6: GO enrichment analysis bubble plots of DE-mRNAs targeted by five DE-miRNA factors predicting cognitive impairment in the prediction model. (a) Bubble map shows upregulated GO-enriched functional pathways. (b) Bubble diagram depicts downregulated GO-enriched functional pathways.



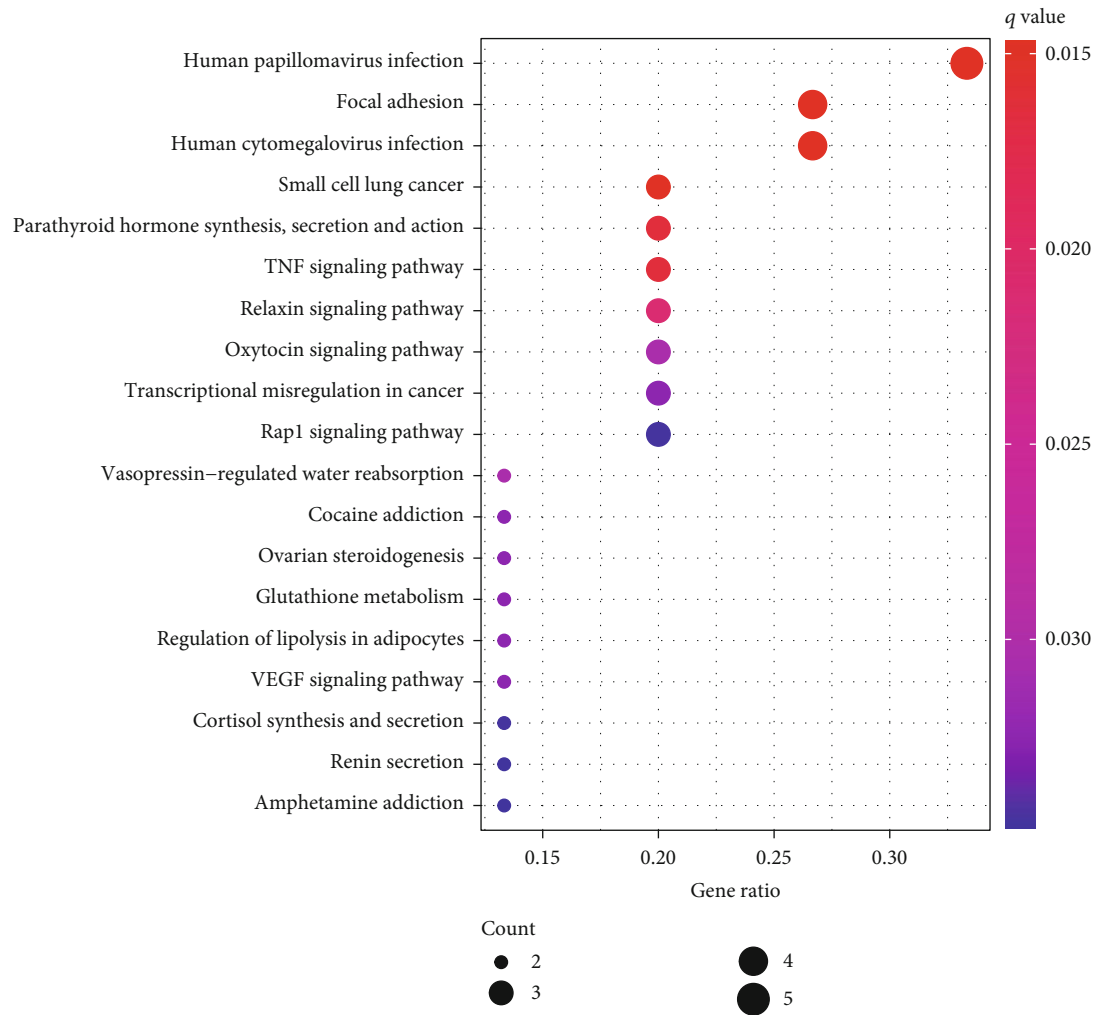


FIGURE 7: Bar graph of KEGG enrichment analysis of DE-mRNAs targeted by 5 DE-miRNA factors predicting cognitive impairment in the prediction model.

findings demonstrated a regulatory role of chemokines vital in physiological or pathological conditions of the central nervous system [33]. As a well-studied neuronal chemokine, the pathological expression of CCL21 has been detected in cerebral ischemia [34], axonal injury [35], amyotrophic lateral sclerosis [36], and spinal cord injury [37]. Thus, hsa-miR-933, RELB, and CCL21 may be correlated with HF and neurological disorders.

Previous studies have found that miRNAs in circulating blood alone also have the potential to predict dementia and HF [38–40]. This is because the information in circulating blood miRNAs is suggestive of essential organismal conditions such as ischemic, cardiomyopathy, diabetes, and valvular [41–44]. Thus, heart failure may influence the development of dementia by affecting miRNA expression in the blood microenvironment, a speculation that was first tentatively confirmed in this study. Moreover, severity of HF was found to be associated with the expression profile of circulating blood miRNAs [45]. Notably, miR-485-3p was also found to be potentially relevant to severity of HF in a previous study [46]. High expression of miR-485-3p was also found to be associated with dementia risk in the

present study. In this research, the chi-squared test also showed that the severity of heart failure was significantly associated with the risk of developing cognitive impairment; that is, as the degree of heart failure increased, the risk of developing cognitive impairment increased, which is consistent with the results of previous studies [47, 48]. Thus, this study suggested that the severity of HF is also related to dementia. In addition, miR-486-5p was also found to be a biomarker for the development of heart failure and dementia in a previous study [49, 50]. In conclusion, the present study is a preliminary one, and although we identified some interesting targets, further studies are necessary in the future.

In this study, based on the GEO dataset, DE-miRNAs and DE-mRNAs present in both HF and cognitive impairment were acquired and analysed. A logistic regression model with a high performance in predicting cognitive impairment incidence was established using the DE-miRNAs. The core miRNA-TF-mRNA pathway was built by mapping the PPI network jointly associated with cognitive impairment and HF. Moreover, GSEA showed that RELB as a core TF was enriched in retinol metabolism and gap junction pathways. Investigating the potential relevancy of the

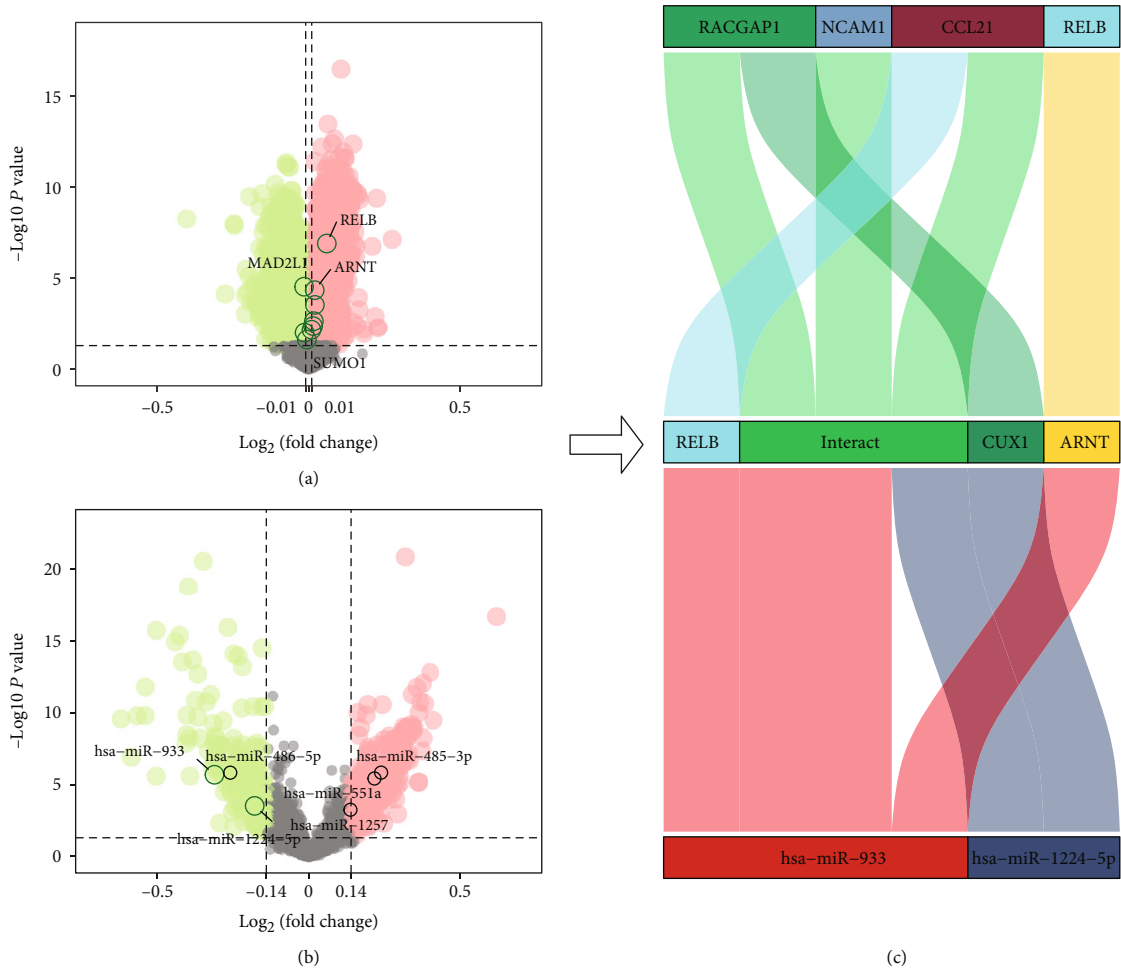
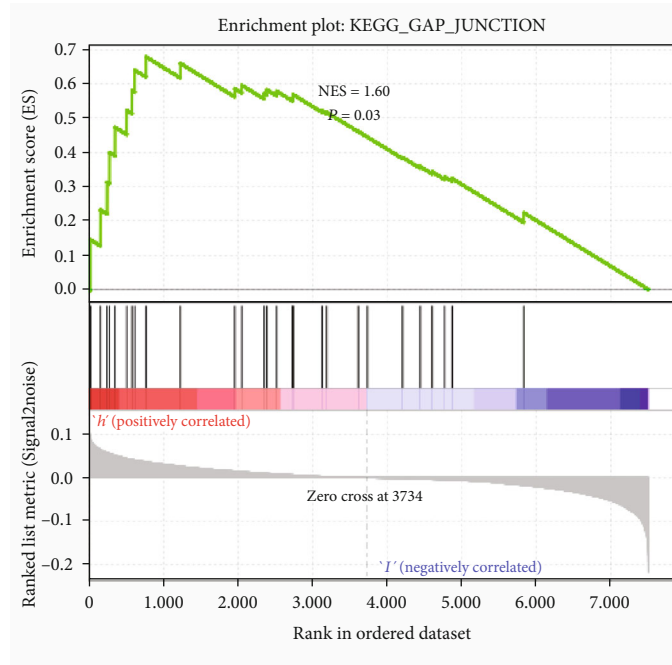


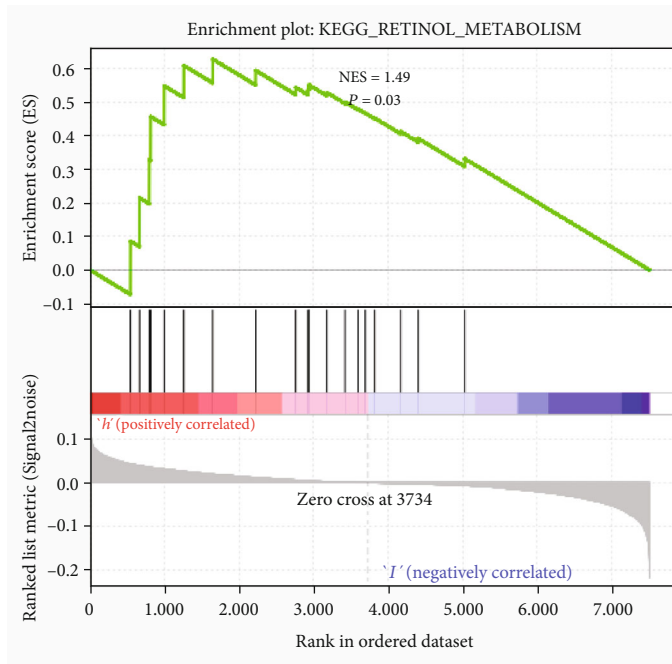
FIGURE 8: Volcano plot of DE-mRNA and DE-miRNA and Sankey plot of miRNA-TF-mRNA. (a) Volcano plots show the presence of DE-miRNAs in cognitive impairment and normal controls. The marked circles are for DE-miRNAs cooccurring in HF and cognitive impairment, present in both the cognitive impairment prediction model and the core PPI subnetwork. The miRNAs in the larger font are those miRNAs cooccurring in the cognitive impairment prediction model and the PPI subnetwork. (b) Volcano plot depicts DE-mRNA expression in cognitive impairment and normal controls. The marked circles are the DE-mRNAs targeted by miRNAs, which cooccur in HF and cognitive impairment and cooccur in the cognitive impairment prediction model and PPI subnetwork. (c) Mulberry diagram exhibits DE-miRNAs cooccurring in the model and core network and the regulatory axis of their target TF/mRNA.

TABLE 5: Two DE-miRNAs and nine DE-mRNAs.

id	logFC	<i>t</i>	<i>P</i> value	Adjusted <i>P</i> value	<i>B</i>
hsa-miR-933	-0.31	-4.77	$P \leq 0.001$	$P \leq 0.001$	4.47
hsa-miR-1224-5p	-0.18	-3.62	$P \leq 0.001$	0.002	-0.21
RELB	0.06	5.32	$P \leq 0.001$	$P \leq 0.001$	5.85
MAD2L1	-0.02	-4.2	$P \leq 0.001$	$P \leq 0.001$	0.61
ARNT	0.02	4.10	$P \leq 0.001$	$P \leq 0.001$	0.19
CCL21	0.02	3.63	$P \leq 0.001$	0.003	-1.56
CUX1	0.02	3.06	0.002	0.015	-3.48
NCAM1	0.01	2.87	0.004	0.025	-4.04
RACGAP1	0.01	2.72	0.007	0.035	-4.46
RUNX1	-0.01	-2.59	0.010	0.045	-4.78
SUMO1	-0.01	-2.27	0.023	0.087	-5.56



(a)



(b)

FIGURE 9: The target DE-mRNAs of miRNAs were selected according to the prediction model and subnetwork, and the TF RELB with the largest difference ploidy is selected for GSEA. The results show that the higher RELB expression group is enriched on KEGG\_RETINOL\_METABOLISM ( $P = 0.032$ ) and KEGG\_GAP\_JUNCTION ( $P = 0.032$ ).

hsa-miR-933/RELB/CCL21 in more clinical samples is highly necessary in the future. We will also explore the mechanisms of the hsa-miR-933/RELB/CCL21 regulatory axis in the development of HF and cognitive disorders by performing animal and cellular experiments.

## 5. Conclusion

In summary, this study was the first to examine the crosstalk between HF and cognitive impairment and the underlying mechanisms applying bioinformatics analysis. Based on PPI networks, the hsa-miR-933/RELB/CCL21 regulatory axis was considered a potential culprit in the development of both HF and cognitive disorders. The current findings provide a theoretical and experimental basis, but the mechanisms of the hsa-miR-933/RELB/CCL21 regulatory axis in the development of HF and neurological disorders should be validated by cellular and animal experiments.

## Abbreviations

DE: Differentially expressed  
 GO: Gene Ontology  
 GEO: Gene Expression Omnibus  
 GSEA: Gene set enrichment analysis  
 HC: Healthy control  
 HF: Heart failure.

## Data Availability

The miRNA expression microarray data from peripheral blood of HF patients were downloaded from GSE104150 and GSE53473. Peripheral blood miRNA expression microarray data of cognitive impairment patients was downloaded from GSE120584. RNA-seq data from myocardial tissue of HF patients were downloaded from GSE116250 to obtain mRNA expression files. mRNA expression microarray data from brain tissue of cognitive impairment patients were downloaded from GSE140831. Clinical data can be obtained by contacting the corresponding author.

## Conflicts of Interest

The authors declare that they have no conflicts of interest.

## Authors' Contributions

All authors worked together to collect data and specimens, performed data analysis and predictions, wrote the manuscript, and finally approved the manuscript.

## Acknowledgments

This research was funded by a project entitled "Study on Mitochondrial Damage and Repairing Mechanism of Qi-qi-yang-yang in Improving Exercise Tolerance of Heart Failure from Mitochondrial Dynamics (81774247)."

## Supplementary Materials

Supplementary Table 1: basic characteristics of patients. (*Supplementary Materials*)

## References

- [1] M. Prince, R. Bryce, E. Albanese, A. Wimo, W. Ribeiro, and C. P. Ferri, "The global prevalence of dementia: a systematic review and metaanalysis," *Alzheimer's & dementia*, vol. 9, no. 1, pp. 63–75.e2, 2013.
- [2] A. Wimo, L. Jonsson, J. Bond, M. Prince, B. Winblad, and Alzheimer Disease International, "The worldwide economic impact of dementia 2010," *Alzheimer's & dementia*, vol. 9, no. 1, pp. 1–11.e3, 2013.
- [3] K. Wallin, G. Bostrom, M. Kivipelto, and Y. Gustafson, "Risk factors for incident dementia in the very old," *International Psychogeriatrics*, vol. 25, no. 7, pp. 1135–1143, 2013.
- [4] M. Kivipelto, T. Ngandu, L. Fratiglioni et al., "Obesity and vascular risk factors at midlife and the risk of dementia and Alzheimer disease," *Archives of Neurology*, vol. 62, no. 10, pp. 1556–1560, 2005.
- [5] W. Huang, C. Qiu, E. von Strauss, B. Winblad, and L. Fratiglioni, "APOE genotype, family history of dementia, and Alzheimer disease risk: a 6-year follow-up study," *Archives of neurology*, vol. 61, no. 12, pp. 1930–1934, 2004.
- [6] J. Lovell, T. Pham, S. Q. Noaman, M. C. Davis, M. Johnson, and J. E. Ibrahim, "Self-management of heart failure in dementia and cognitive impairment: a systematic review," *BMC Cardiovascular Disorders*, vol. 19, no. 1, p. 99, 2019.
- [7] D. Jeong, J. Yoo, P. Lee et al., "miR-25 tough decoy enhances cardiac function in heart failure," *Molecular Therapy*, vol. 26, no. 3, pp. 718–729, 2018.
- [8] A. Wojciechowska, A. Braniewska, and K. Kozar-Kamińska, "MicroRNA in cardiovascular biology and disease," *Advances in Clinical and Experimental Medicine*, vol. 26, no. 5, pp. 865–874, 2017.
- [9] J. Zhang, P. Sun, C. Zhou et al., "Regulatory microRNAs and vascular cognitive impairment and dementia," *CNS Neuroscience & Therapeutics*, vol. 26, no. 12, pp. 1207–1218, 2020.
- [10] R. Zhou, L. Wang, G. Zhao et al., "Circulating exosomal microRNAs as emerging non-invasive clinical biomarkers in heart failure: mega bio-roles of a nano bio-particle," *IUBMB Life*, vol. 72, no. 12, pp. 2546–2562, 2020.
- [11] C. Backes, E. Meese, and A. Keller, "Specific miRNA disease biomarkers in blood, serum and plasma: challenges and prospects," *Molecular Diagnosis & Therapy*, vol. 20, no. 6, pp. 509–518, 2016.
- [12] J. Novák, P. Kružliak, J. Bienertová-Vašků, O. Slabý, and M. Novák, "MicroRNA-206: a promising therapeutic marker," *Theranostics*, vol. 4, no. 2, pp. 119–133, 2014.
- [13] M. Xiao, W. Zeng, J. Wang et al., "Exosomes protect against acute myocardial infarction in rats by regulating the renin-angiotensin system," *Stem Cells and Development*, vol. 30, no. 12, pp. 622–631, 2021.
- [14] P. Denver, H. D'Adamo, S. Hu et al., "A novel model of mixed vascular dementia incorporating hypertension in a rat model of Alzheimer's disease," *Frontiers in Physiology*, vol. 10, p. 1269, 2019.
- [15] W. Liu, J. Zheng, J. Dong et al., "Association of miR-197-5p, a circulating biomarker for heart failure, with myocardial

- fibrosis and adverse cardiovascular events among patients with stage C or D heart failure,” *Cardiology*, vol. 141, no. 4, pp. 212–225, 2019.
- [16] L. L. Wong, A. Armugam, S. Sepramaniam et al., “Circulating microRNAs in heart failure with reduced and preserved left ventricular ejection fraction,” *European Journal of Heart Failure*, vol. 17, no. 4, pp. 393–404, 2015.
- [17] D. Shigemizu, S. Akiyama, Y. Asanomi et al., “Risk prediction models for dementia constructed by supervised principal component analysis using miRNA expression data,” *Communications biology*, vol. 2, no. 1, p. 77, 2019.
- [18] M. E. Sweet, A. Cocciolo, D. Slavov et al., “Transcriptome analysis of human heart failure reveals dysregulated cell adhesion in dilated cardiomyopathy and activated immune pathways in ischemic heart failure,” *BMC Genomics*, vol. 19, no. 1, p. 812, 2018.
- [19] S. Rayaprolu, L. Higginbotham, P. Bagchi et al., “Systems-based proteomics to resolve the biology of Alzheimer’s disease beyond amyloid and tau,” *Neuropsychopharmacology*, vol. 46, no. 1, pp. 98–115, 2021.
- [20] M. E. Ritchie, B. Phipson, D. Wu et al., “limma powers differential expression analyses for RNA-sequencing and microarray studies,” *Nucleic acids research*, vol. 43, no. 7, p. e47, 2015.
- [21] T. Sing, O. Sander, N. Beerenwinkel, and T. Lengauer, “ROCR: visualizing classifier performance in R,” *Bioinformatics*, vol. 21, no. 20, pp. 3940–3941, 2005.
- [22] G. Yu, L. G. Wang, Y. Han, and Q. Y. He, “clusterProfiler: an R package for comparing biological themes among gene clusters,” *OMICS*, vol. 16, no. 5, pp. 284–287, 2012.
- [23] A. B. M. M. K. Islam, E. Mohammad, and M. A. Khan, “Aberration of the modulatory functions of intronic microRNA hsa-miR-933 on its host gene ATF2 results in type II diabetes mellitus and neurodegenerative disease development,” *Human Genomics*, vol. 14, no. 1, p. 34, 2020.
- [24] X. Zhu, P. Shao, Y. Tang, M. Shu, W. W. Hu, and Y. Zhang, “hsa\_circRNA\_100533 regulates GNAS by sponging hsa-miR\_933 to prevent oral squamous cell carcinoma,” *Journal of Cellular Biochemistry*, vol. 120, no. 11, pp. 19159–19171, 2019.
- [25] B. Zhou, H. Guo, and J. Tang, “Long non-coding RNA TFAP2A-AS1 inhibits cell proliferation and invasion in breast cancer via miR-933/SMAD2,” *Medical Science Monitor*, vol. 25, pp. 1242–1253, 2019.
- [26] J. H. Lu, Z. X. Zuo, W. Wang et al., “A two-microRNA-based signature predicts first-line chemotherapy outcomes in advanced colorectal cancer patients,” *Cell death discovery*, vol. 4, no. 1, p. 116, 2018.
- [27] O. A. Stone, M. El-Brolosy, K. Wilhelm et al., “Loss of pyruvate kinase M2 limits growth and triggers innate immune signaling in endothelial cells,” *Nature Communications*, vol. 9, no. 1, p. 4077, 2018.
- [28] E. Bosseboeuf and C. Raimondi, “Signalling, metabolic pathways and iron homeostasis in endothelial cells in health, atherosclerosis and Alzheimer’s disease,” *Cells*, vol. 9, no. 9, p. 2055, 2020.
- [29] C. Engelmann, M. Riemann, S. Carlstedt et al., “Identification of undescribed Relb expression domains in the murine brain by new Relb:cre-katushka reporter mice,” *Developmental Dynamics*, vol. 249, no. 8, pp. 983–997, 2020.
- [30] L. Valiño-Rivas, L. Gonzalez-Lafuente, A. B. Sanz, M. Ruiz-Ortega, A. Ortiz, and M. D. Sanchez-Niño, “Non-canonical NFκB activation promotes chemokine expression in podocytes,” *Scientific Reports*, vol. 6, no. 1, p. 28857, 2016.
- [31] G. Rodgers, C. D. Doucette, D. A. Soutar, R. S. Liwski, and D. W. Hoskin, “Piperine impairs the migration and T cell-activating function of dendritic cells,” *Toxicology Letters*, vol. 242, pp. 23–33, 2016.
- [32] S. H. Nymo, P. Aukrust, J. Kjekshus et al., “Limited added value of circulating inflammatory biomarkers in chronic heart failure,” *JACC: Heart Failure*, vol. 5, no. 4, pp. 256–264, 2017.
- [33] D. Gomez-Nicola, N. Pallas-Bazarra, B. Valle-Argos, and M. Nieto-Sampedro, “CCR7 is expressed in astrocytes and upregulated after an inflammatory injury,” *Journal of Neuroimmunology*, vol. 227, no. 1–2, pp. 87–92, 2010.
- [34] D. Harhausen, V. Prinz, G. Ziegler et al., “CD93/AA4.1: a novel regulator of inflammation in murine focal cerebral ischemia,” *Journal of Immunology*, vol. 184, no. 11, pp. 6407–6417, 2010.
- [35] F. A. White, J. Sun, S. M. Waters et al., “Excitatory monocyte chemoattractant protein-1 signaling is up-regulated in sensory neurons after chronic compression of the dorsal root ganglion,” *Proceedings of the National Academy of Sciences of the United States of America*, vol. 102, no. 39, pp. 14092–14097, 2005.
- [36] J. S. Henkel, D. R. Beers, L. Siklós, and S. H. Appel, “The chemokine MCP-1 and the dendritic and myeloid cells it attracts are increased in the mSOD1 mouse model of ALS,” *Molecular and Cellular Neurosciences*, vol. 31, no. 3, pp. 427–437, 2006.
- [37] K. Honjoh, H. Nakajima, T. Hirai, S. Watanabe, and A. Matsumine, “Relationship of inflammatory cytokines from M1-type microglia/macrophages at the injured site and lumbar enlargement with neuropathic pain after spinal cord injury in the CCL21 knockout (plt) mouse,” *Frontiers in Cellular Neuroscience*, vol. 13, p. 525, 2019.
- [38] M. Wang, L. Qin, and B. Tang, “MicroRNAs in Alzheimer’s disease,” *Frontiers in Genetics*, vol. 10, p. 153, 2019.
- [39] B. Martinez and P. V. Peplow, “MicroRNAs as diagnostic and therapeutic tools for Alzheimer’s disease: advances and limitations,” *Neural Regeneration Research*, vol. 14, no. 2, pp. 242–255, 2019.
- [40] R. Mir, I. Elfaki, N. Khullar et al., “Role of selected miRNAs as diagnostic and prognostic biomarkers in cardiovascular diseases, including coronary artery disease, myocardial infarction and atherosclerosis,” *Journal of Cardiovascular Development and Disease*, vol. 8, no. 2, p. 22, 2021.
- [41] B. Dewdney, A. Trollope, J. Moxon, D. Thomas Manapurathe, E. Biros, and J. Golledge, “Circulating microRNAs as biomarkers for acute ischemic stroke: a systematic review,” *Journal of Stroke and Cerebrovascular Diseases*, vol. 27, no. 3, pp. 522–530, 2018.
- [42] R. Guo and S. Nair, “Role of microRNA in diabetic cardiomyopathy: from mechanism to intervention,” *Biochimica et Biophysica Acta - Molecular Basis of Disease*, vol. 1863, no. 8, pp. 2070–2077, 2017.
- [43] C. Roma-Rodrigues, L. R. Raposo, and A. R. Fernandes, “MicroRNAs based therapy of hypertrophic cardiomyopathy: the road traveled so far,” *BioMed Research International*, vol. 2015, Article ID 983290, 8 pages, 2015.
- [44] J. Ryu, Y. Ahn, H. Kook, and Y. K. Kim, “The roles of non-coding RNAs in vascular calcification and opportunities as therapeutic targets,” *Pharmacology & Therapeutics*, vol. 218, p. 107675, 2021.

- [45] L. Papadimitriou and A. P. Kalogeropoulos, "Inflammatory biomarkers and therapeutic targets in heart failure," *Current Medicinal Chemistry*, vol. 22, no. 23, pp. 2716–2726, 2015.
- [46] D. Scrutinio, F. Conserva, A. Passantino, M. Iacoviello, R. Lagioia, and L. Gesualdo, "Circulating microRNA-150-5p as a novel biomarker for advanced heart failure: a genome-wide prospective study," *The Journal of Heart and Lung Transplantation*, vol. 36, no. 6, pp. 616–624, 2017.
- [47] S. Graham, S. Ye, M. Qian et al., "Cognitive function in ambulatory patients with systolic heart failure: insights from the warfarin versus aspirin in reduced cardiac ejection fraction (WARCEF) trial," *PLoS One*, vol. 9, no. 11, article e113447, 2014.
- [48] G. Kozdağ, P. Işeri, G. Gökçe et al., "Treatment with enhanced external counterpulsation improves cognitive functions in chronic heart failure patients," *Türk Kardiyoloji Derneği Arşivi*, vol. 41, no. 5, pp. 418–428, 2013.
- [49] A. Bayés-Genis, D. E. Lanfear, M. W. J. de Ronde et al., "Prognostic value of circulating microRNAs on heart failure-related morbidity and mortality in two large diverse cohorts of general heart failure patients," *European Journal of Heart Failure*, vol. 20, no. 1, pp. 67–75, 2018.
- [50] P. Prabhakar, S. R. Chandra, and R. Christopher, "Circulating microRNAs as potential biomarkers for the identification of vascular dementia due to cerebral small vessel disease," *Age and Ageing*, vol. 46, no. 5, pp. 861–864, 2017.



## Retraction

# Retracted: Effects of Different Intervention Time Points of Early Rehabilitation on Patients with Acute Ischemic Stroke: A Single-Center, Randomized Control Study

### BioMed Research International

Received 12 March 2024; Accepted 12 March 2024; Published 20 March 2024

Copyright © 2024 BioMed Research International. This is an open access article distributed under the Creative Commons Attribution License, which permits unrestricted use, distribution, and reproduction in any medium, provided the original work is properly cited.

This article has been retracted by Hindawi following an investigation undertaken by the publisher [1]. This investigation has uncovered evidence of one or more of the following indicators of systematic manipulation of the publication process:

- (1) Discrepancies in scope
- (2) Discrepancies in the description of the research reported
- (3) Discrepancies between the availability of data and the research described
- (4) Inappropriate citations
- (5) Incoherent, meaningless and/or irrelevant content included in the article
- (6) Manipulated or compromised peer review

The presence of these indicators undermines our confidence in the integrity of the article's content and we cannot, therefore, vouch for its reliability. Please note that this notice is intended solely to alert readers that the content of this article is unreliable. We have not investigated whether authors were aware of or involved in the systematic manipulation of the publication process.

Wiley and Hindawi regrets that the usual quality checks did not identify these issues before publication and have since put additional measures in place to safeguard research integrity.

We wish to credit our own Research Integrity and Research Publishing teams and anonymous and named external researchers and research integrity experts for contributing to this investigation.

The corresponding author, as the representative of all authors, has been given the opportunity to register their agreement or disagreement to this retraction. We have kept a record of any response received.

### References

- [1] L. L. Liu, Y. Q. Lu, Q. Q. Bi, W. Fu, X. Y. Zhou, and J. Wang, "Effects of Different Intervention Time Points of Early Rehabilitation on Patients with Acute Ischemic Stroke: A Single-Center, Randomized Control Study," *BioMed Research International*, vol. 2021, Article ID 1940549, 7 pages, 2021.

## Research Article

# Effects of Different Intervention Time Points of Early Rehabilitation on Patients with Acute Ischemic Stroke: A Single-Center, Randomized Control Study

LiLi Liu <sup>1</sup>, YanQin Lu <sup>2</sup>, QianQian Bi <sup>3</sup>, Wang Fu <sup>3</sup>, XiaoYu Zhou <sup>3</sup>,  
and Jue Wang <sup>3</sup>

<sup>1</sup>Department of Neurology, Shanghai Hongkou District Jiangwan Hospital, The First Rehabilitation Hospital Affiliated to Shanghai University of Medicine & Health Sciences, 1878 Sichuan North Road, Shanghai 200081, China

<sup>2</sup>Department of Infectious, Shanghai Tenth People's Hospital, Tongji University School of Medicine, 301 Middle Yanchang Road, Shanghai 200072, China

<sup>3</sup>Department of Neurology, Shanghai Tenth People's Hospital, Tongji University School of Medicine, 301 Middle Yanchang Road, Shanghai 200072, China

Correspondence should be addressed to XiaoYu Zhou; [xiaoyuzhou1979@163.com](mailto:xiaoyuzhou1979@163.com) and Jue Wang; [wangjueshiyuan@163.com](mailto:wangjueshiyuan@163.com)

Received 12 May 2021; Revised 2 August 2021; Accepted 9 August 2021; Published 29 August 2021

Academic Editor: Qian Wang

Copyright © 2021 LiLi Liu et al. This is an open access article distributed under the Creative Commons Attribution License, which permits unrestricted use, distribution, and reproduction in any medium, provided the original work is properly cited.

**Objective.** To investigate effects of different intervention time points of early rehabilitation on patients with acute ischemic stroke. **Methods.** We enrolled patients diagnosed with acute ischemic stroke in our hospital's rehabilitation ward from November 2013 to December 2015. Patients were randomly assigned to an ultraearly rehabilitation program (started within 72 hours of onset) or an early rehabilitation program (started from 72 hours to 7 days after onset). The efficacy was assessed by the NIH Stroke Scale (NIHSS) International, Barthel Index, and Fugl-Meyer Assessment at one and three months after rehabilitation. Data were analyzed by variance analysis of two-factor repeated measurement. Covariance analysis was used to adjust confounding factors for the determination of statistical differences. **Results.** 41 patients were enrolled in the ultraearly rehabilitation group, while 45 patients were in the early rehabilitation group. There were no differences between the two groups at baseline data. Compared with the early rehabilitation group, patients in the ultraearly rehabilitation group have significantly improved NIHSS score, BMI score, and FMA score at one month and three months ( $P < 0.001$ ). After adjusting for confounding factors (gender, age, severity of NIHSS score, location of stroke, hypertension, diabetes, atrial fibrillation, and coronary heart disease), the significant difference still existed between the two groups at one month and three months ( $P < 0.001$ ). **Conclusion.** Our study indicated a higher efficacy in the ultraearly rehabilitation group than the early rehabilitation group. The result suggests an important practical significance in favor of the clinical treatment of stroke.

## 1. Introduction

AS the leading cause of disability, stroke imposes a heavy burden on health care system. Epidemiological data shows the prevalence of stroke in China is approximately 336.3 in 100,000 people, and disability-adjusted life years (DALYS) reaches -27.3 to -23.0/100,000 [1]. Therefore, it is imperative to reduce the disability rate following stroke. The modern rehabilitation theory considers early rehabilitation intervention is essential for cerebral ischemic stroke patients [2].

Early rehabilitation plays a critical role in improving post-stroke disability and helping patients return to society [3]. Studies demonstrated patients with acute ischemic stroke entered a stable period after 24 to 48 hours of onset [4–6]. Therefore, it laid the theoretical foundation for the safety of early rehabilitation. Moreover, early rehabilitation improves the rehabilitation effect and reduced other complications [7–9]. Emerging evidence suggested early rehabilitation following stroke should be initiated as early as possible [10, 11]. American Heart Association (AHA)/American

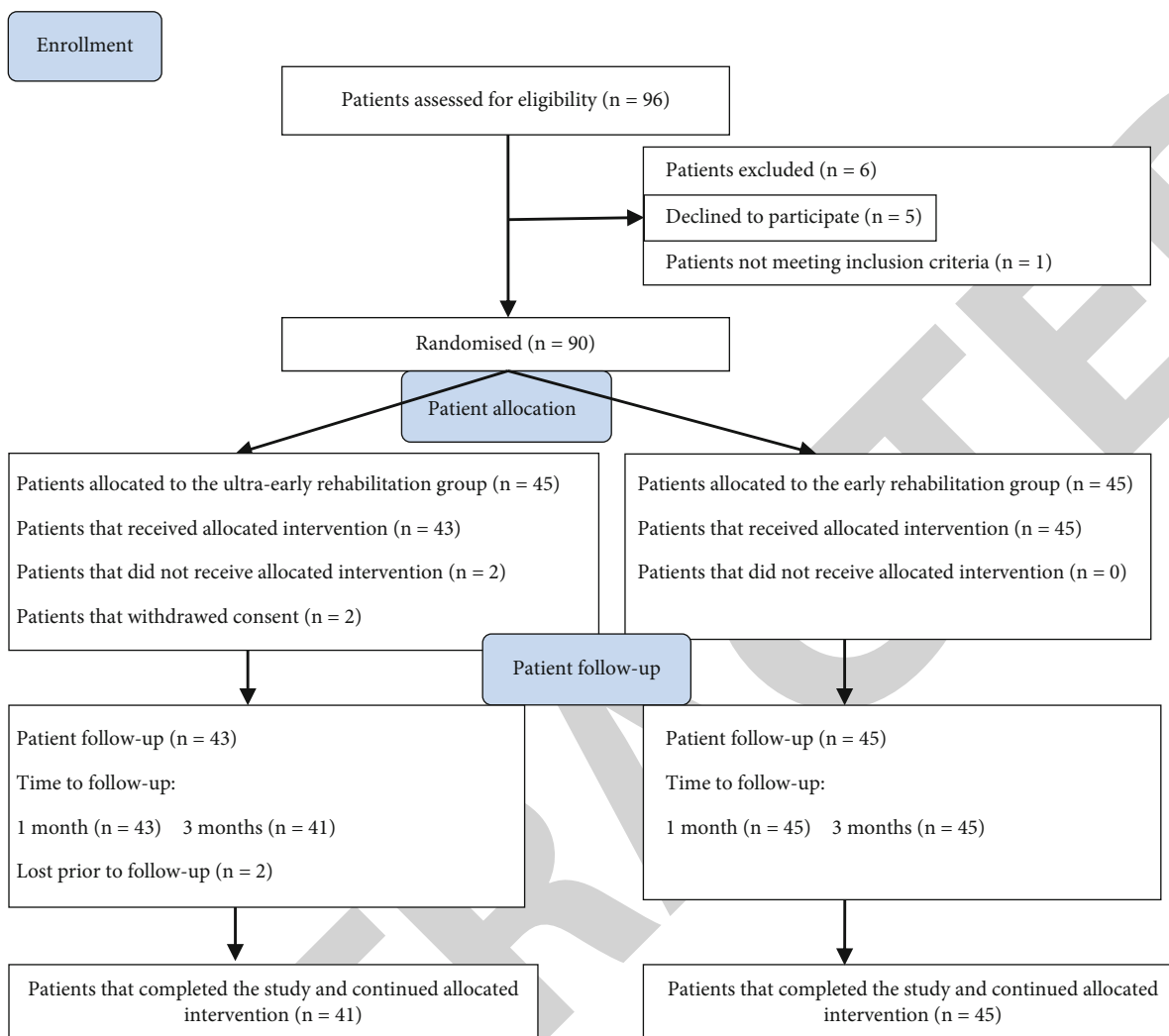


FIGURE 1: Flowchart of the study population.

Stroke Association (ASA) recommended early rehabilitation to the patients hospitalized for stroke [12, 13]. Bernhardt et al. brought forward the concept of early rehabilitation 24 hours after the stroke [14]. AVERT trial demonstrated the efficacy and safety of very early mobilization within 24 hours of stroke onset [15]. An observational study indicated the early rehabilitation, as early as 48-72 hours after stroke onset, was safe and effective in patients with ischemic stroke [16].

However, the optimal intervention time point for early rehabilitation is unclear. To date, the definite theory on the time point of early activities after stroke is not elucidated. Likewise, the researches in this field are insufficient. A study by Bernhardt et al. confirmed the effectiveness and safety of ultraearly activities in either hemorrhagic stroke or ischemic stroke patients [14]. The importance of improving activity levels and effectiveness of interventions to increase physical activity after stroke need to be tested further [17]. A survey investigated the attitudes of medical practitioners showing that 77% of experts recognized the early rehabilitation within 24 hours after the stroke [18-20].

TABLE 1: Basic characteristics of the ultraearly rehabilitation group and the early rehabilitation group with acute ischemic stroke.

Variables	Ultraearly group (n = 41)	Early group (n = 45)	P value
Gender (m/f)	25/16	29/16	0.740
Age at admission (mean $\pm$ SD)	76.5 $\pm$ 6.36	71.5 $\pm$ 14.8	0.961
Location of stroke			
The left hemisphere	20	25	
The right hemisphere	18	18	0.752
Brain stem	3	2	
Severity of NIHSS score			
Light	9	6	
Moderate	30	38	0.487
Severe	2	1	

TABLE 2: Comparison of neurological deficits (NIHSS score) between ultraearly rehabilitation group and the early rehabilitation group ( $\bar{x} \pm s$ ).

Group	Cases	NIHSS		
		At admission	Treatment after 1 month	Treatment after 3 months
Ultraearly group	41	10.02 $\pm$ 5.88	5.02 $\pm$ 3.37	3.10 $\pm$ 2.26
Early group	45	8.40 $\pm$ 4.21	6.71 $\pm$ 3.83	4.98 $\pm$ 3.31

Intragroup (repeated interaction) comparison:  $F = 253.433$  ( $P < 0.001$ ). Intergroup comparison:  $F = 35.710$  ( $P < 0.001$ ).

Therefore, we launched the study to explore the efficacy and timing of early rehabilitation in stroke patients.

## 2. Methods

**2.1. Participants.** The clinical trial registration number was ChiCTR1800019305. The Ethics Committee of Shanghai Jiangwan Hospital approved the study. All participants recruited from Shanghai City Hospital of Jiangwan between November 2013 and December 2015 signed written informed consent. The inclusion criteria in this study were as follows: (1) ischemic stroke is confirmed by cranial CT or MRI; (2) patients present with hemiplegia or hemiparesis with muscle power less than or equal to IV class; (3) patients' vital signs and nervous system are stable; and (4) patients consent to participation in rehabilitation training. The exclusion criteria were as follows: (1) subarachnoid hemorrhage or intracranial venous thrombosis patients; (2) patients suffering from a severe lung infection, liver disease, kidney disease, heart disease, or other essential organ damages; (3) unable to receive rehabilitation training for severe cognitive impairment; (4) unable to receive rehabilitation training for mental retardation or conscious disturbance; and (5) patients having neurological or musculoskeletal disorders affecting functional recovery.

**2.2. Grouping.** The patients were randomly divided into the ultraearly rehabilitation group (started within 72 hours) and early rehabilitation group (started from 72 hours to 7 days). All patients accepted rehabilitation from professional physical therapists. Rehabilitation of both groups did not start until the patients reached stable conditions. Except for intervention time points, the rehabilitation programs conducted in both groups were the same. Rehabilitation programs mainly included Bobath rehabilitation technique, brain circulation therapy apparatus, and electromyographic biofeedback technique. Bobath rehabilitation technology included the following:

- (1) Good positioning: families and nursing staff counseled patients using correct posture. Patients were decubitus lateral or supine lateral and were guided to turn over every 2 hours. Patients were asked to avoid abnormal patterns of upper limb flexion, lower limb extension, and varus foot alignment.
- (2) Bed position and joint training activities: hands and ten fingers cross each other on the ipsilateral hand grip, with the thumb placed on the top; with the healthy limb to limb disease, do elbow lift move-

ment; upper limb joint activity includes side to lift, lower limb flexion, and legs and the bed support hips, namely, the bridge movement.

- (3) Balance sitting and sit up training: correct hand, arm, and leg movements were shown.
- (4) Sit up and standing balance training: patients with lower limb muscle strength of grade 3 and above were trained to stand. Patients began stand training using parallel bars, and the standing time gradually increased.
- (5) Walk training: patients that showed an increase in the weight-bearing strength of their lower limbs started walk training. Gradually, patients were trained to step over different obstacles and up and down stairs.

Brain circulation therapy apparatus and EMG biofeedback technique were used to increase cerebral blood supply, activate brain cells, and improve local muscle spasticity, tic, and paralysis to improve muscle strength and motor function. The above rehabilitation exercises were performed 20-30 min per day, 2-3 times a day, and 4-5 days a week for a total of three months.

Besides rehabilitation, the other therapies followed the guidelines of treatment of acute ischemic cerebrovascular disease. Two weeks after treatment in the ward, the patient continued rehabilitation treatment in outpatient.

**2.3. Clinical Assessments.** The U.S. National Institutes of Health Stroke Scale (NIHSS) assessed the severity of neurological deficit. The modified Barthel Index (MBI) was introduced to evaluate daily life activity, and the simple Fugl-Meyer Assessment (FMA) was adopted to determine motor function. Neurologists and rehabilitation physicians in this study accepted specific training in NIHSS, MBI, and FMA assessments. We collected characteristics of patients, including gender, age, NIHSS score, location of the lesion, history of hypertension, history of diabetes, history of coronary heart disease, and history of atrial fibrillation. According to NIHSS 0-5, NIHSS 6-20, or NIHSS greater than 20, respectively, all patients were defined as mild, moderate, or severe neurologic deficit. The locations of the lesions included the right hemisphere, left hemisphere, and brain stem. All data were recorded in a unified form.

**2.4. Randomization, Masking, and Procedures.** All eligible patients with acute ischemic stroke were randomized to receive either ultraearly rehabilitation or early rehabilitation

TABLE 3: Comparison of Barthel Index (MBI) between the ultraearly rehabilitation group and the early rehabilitation group ( $\bar{x} \pm s$ ).

Group	Cases	MBI		
		At admission	Treatment after 1 month	Treatment after 3 months
Ultraearly group	41	47.32 ± 10.07	62.31 ± 10.37	73.90 ± 12.48
Early group	45	48.10 ± 9.90	55.78 ± 8.05	62.24 ± 8.77

Intragroup (repeated interaction) comparison:  $F = 758.093$  ( $P < 0.001$ ). Intergroup comparison:  $F = 86.333$  ( $P < 0.001$ ).

TABLE 4: Comparison of motor function (FMA) between the ultraearly rehabilitation group and the early rehabilitation group ( $\bar{x} \pm s$ ).

Group	Cases	FMA		
		At admission	Treatment after 1 month	Treatment after 3 months
Ultraearly group	41	47.73 ± 11.08	62.80 ± 11.26	78.12 ± 13.19
Early group	45	50.69 ± 7.34	57.98 ± 7.46	63.91 ± 8.74

Intragroup (repeated interaction) comparison:  $F = 842.880$  ( $P < 0.001$ ). Intergroup comparison:  $F = 130.962$  ( $P < 0.001$ ).

TABLE 5: ANCOVA of the factors that affected change of NIHSS score in one month and three months following rehabilitation.

$\Delta$ NIHSS	Factors	DF	MS	F value	P value
1 month	Group	1	265.670	85.199	.000
	Gender	1	15.029	4.820	.031
	Age	1	1.504	.482	.489
	Severity of NIHSS score	1	117.400	37.650	.000
	Location of stroke	1	.062	.020	.888
	Hypertension	1	.329	.105	.746
	Diabetes	1	2.498	.801	.374
	Coronary heart disease	1	5.973	1.915	.170
	Atrial fibrillation	1	.744	.239	.627
	3 months	Group	1	307.883	58.531
Gender		1	28.635	5.444	.022
Age		1	3.033	.577	.450
Severity of NIHSS score		1	263.925	50.174	.000
Location of stroke		1	2.371	.451	.504
Hypertension		1	.037	.007	.934
Diabetes		1	10.733	2.040	.157
Coronary heart disease		1	8.396	1.596	.210
Atrial fibrillation		1	.016	.003	.956

$\Delta$ NIHSS: change of NIHSS score; DF: degree of freedom; MS: mean square. Significance:  $P < 0.05$ .

with the ratio of 1 : 1. NIHSS, BMI, and FMA were assessed at baseline, one month, and three months by the evaluators who were blind to the outcome of randomization.

**2.5. Statistical Analysis.** SPSS19.0 statistical analysis software was used for analysis. The differences in baseline demographic and clinical characteristics were analyzed by a chi-square test and *t*-test. The analyses of repeated measurement data used variance analysis of two-factor repeated measurement. Covariance analysis was used to adjust the confounding factors and determine the statistical significance of dependent variables.  $P < 0.05$  was accepted as indicative of significant differences.

### 3. Results

90 out of 96 eligible participants were recruited and assigned randomly to one of two groups. Among the 96 participants, 88 completed the 1-month trial, and 86 patients completed the 3-month trial. There were two patient dropouts in the ultraearly rehabilitation group at the beginning of rehabilitation. Two cases were lost at follow-up in the ultraearly rehabilitation group at three months (Figure 1).

At baseline, there were no significant differences in the severity of disability, age, gender, locations of lesions, and medicine between the two groups (Table 1). Neurologic function, daily living activities, and motor function

TABLE 6: ANCOVA of the factors that affected change of MBI score in one month and three months following rehabilitation.

$\Delta$ MBI	Factors	DF	MS	F value	P value
1 month	Group	1	1092.659	27.541	.000
	Gender	1	2.455	.062	.804
	Age	1	1.144	.029	.866
	Severity of NIHSS score	1	3.908	.099	.754
	Location of stroke	1	20.868	.526	.471
	Hypertension	1	4.387	.111	.740
	Diabetes	1	43.801	1.104	.297
	Coronary heart disease	1	13.906	.351	.556
	Atrial fibrillation	1	17.214	.434	.512
	Group	1	3184.419	59.851	.000
	Gender	1	.094	.002	.967
3 months	Age	1	1.135	.021	.884
	Severity of NIHSS score	1	52.374	.984	.324
	Location of stroke	1	2.293	.043	.836
	Hypertension	1	28.252	.531	.468
	Diabetes	1	41.375	.778	.381
	Coronary heart disease	1	96.928	1.822	.181
	Atrial fibrillation	1	5.585	.105	.747

$\Delta$ MBI: change of NIHSS score; DF: degree of freedom; MS: mean square. Significance:  $P < 0.05$ .

TABLE 7: ANCOVA of the factors that affected change of FMA score in one month and three months following rehabilitation.

$\Delta$ FMA	Factors	DF	MS	F value	P value
1 month	Group	1	1252.803	103.570	.000
	Gender	1	.119	.010	.921
	Age	1	16.233	1.342	.250
	Severity of NIHSS score	1	7.172	.593	.444
	Location of stroke	1	11.948	.988	.323
	Hypertension	1	3.915	.324	.571
	Diabetes	1	14.156	1.170	.283
	Coronary heart disease	1	18.662	1.543	.218
	Atrial fibrillation	1	.654	.054	.817
	Group	1	6182.668	209.557	.000
	Gender	1	10.327	.350	.556
3 months	Age	1	15.514	.526	.471
	Severity of NIHSS score	1	14.890	.505	.480
	Location of stroke	1	2.609	.088	.767
	Hypertension	1	19.168	.650	.423
	Diabetes	1	44.121	1.495	.225
	Coronary heart disease	1	23.142	.784	.379
	Atrial fibrillation	1	2.306	.078	.781

$\Delta$ NIHSS: change of FMA score; DF: degree of freedom; MS: mean square. Significance:  $P < 0.05$ .

improved after rehabilitation in both groups. As shown in Tables 2–4, NIHSS scores were lower in the ultraearly rehabilitation group than in the early rehabilitation group at one month and three months [intragroup (repeated interaction) comparison:  $F = 253.433$  ( $P < 0.001$ )], while MBI scores and FMA were higher in the ultraearly rehabilitation group than

in the early rehabilitation group [intragroup (repeated interaction) comparison for MBI:  $F = 758.093$  ( $P < 0.001$ ); intragroup (repeated interaction) comparison for FMA:  $F = 842.880$  ( $P < 0.001$ )]. Covariance analysis showed the differences remained statistically significant after adjusting for confounding factors at 1-month and 3-month (Tables 5–7).



Moreover, gender and the severity of neurology deficit at onset were independently correlated to NIHSS, MBI, and FMA at one month and three months.

#### 4. Discussion

Our results indicated the efficacy of ultraearly patient rehabilitation within 72 hours outmatched that of early restoration. Previous studies supported our conclusions [2]. It is consistent with Bernhardt, et al.'s study which showed the validity and safety of ultraearly events, and results confirmed the effectiveness and safety of ultraearly events [14].

The theory of neural plasticity and functional reorganization accounts for our result [21–23]. In these two theoretical studies, early rehabilitation training facilitates neuroplasticity and functional reorganization. Moreover, changes in the brain tissue structure provide the foundation for neuroplasticity and functional recovery after stroke. In animal models, ischemia induces sprouting of new dendrites and axons, primarily in the perilesional cortex and in regions of molecular plasticity remote from the lesion [24]. Growth factor signals promoting synaptogenesis can be detected as early as three days poststroke and reaches the highest between 7 and 14 days [25, 26]. Compared with the recovery stage, acute stroke leads to distinct remote inhibitory effects, inflammatory reactions and inflammatory factors (such as hs-CRP, IL-1, and IL-6). With brain cell damaging, remote inhibitory effects may be independently associated with immediate neurological deficits. In the acute phase of stroke, the inflammatory response on brain cells is neurotoxic, which blocks nerve remodeling and inhibits nerve conduction. Therefore, inhibition of neuron recovery is more in the acute phase than in the recovery phase. Ultraearly intervention treatment reduces remote inhibitory effects and inflammatory response, thereby accelerating the rehabilitation and improving the rehabilitation effect.

In addition, early rehabilitation improves the early survival of brain cells by increasing cerebral blood flow (CBF) and reducing the penumbra around the lesion. Increasing CBF contributes to reducing ischemic necrosis of neurons in the penumbra zone. Sensory impulse is repeatedly introduced into the central nervous system, which plays an essential role in axon sprouting of neurons, transmission of latent pathways, and synapses. Therefore, ultraearly rehabilitation increases the CBF in the penumbra area and revitalizes a part of the neuron [27]. A study using a rat model of cerebral infarction indicated physical activities within 14 days of onset reduced dendritic branching and prevented the aggravation of nerve conduction [24]. Early rehabilitation intervention promotes dendritic sprouting, stimulates synaptic transmission, and increases CBF. Schallert et al. [28] proposed that early stroke rehabilitation intervention results in better recovery of neurological function after stroke. Natural recovery leads to further residual dysfunction, misuse gives rise to residual limb function, and subsequential deterioration of nerve function contributes to wasting. Therefore, earlier rehabilitation training prevents injured brain cells, misuse, and wasting of limbs and promotes the reconstruction of normal motion mode.

The limitations of our study were that it is a single-center study and the sample was relatively small. Therefore, the introduction of bias was possible. However, strict randomized design in our study partly reduced the possibility of bias.

#### 5. Conclusion

Our study showed the efficacy of ultraearly rehabilitation in neurological function, activities of daily living, and motor function in patients with acute ischemic stroke. Further large sample trial is clearly warranted.

#### Data Availability

The data are available from the corresponding author on reasonable request.

#### Ethical Approval

The Ethics Committee of Shanghai Jiangwan Hospital approved the present project. The project is registered through clinical trials, and the registration number is ChiCTR1800019305.

#### Conflicts of Interest

The authors declare no potential conflicts of interest with respect to the financial, consultant, institutional and authorship, and/or publication of this article.

#### Authors' Contributions

LiLi Liu and YanQin Lu contributed equally to this work.

#### Acknowledgments

Our work was supported by the Excellent Youth Backbone Project of Hongkou District Wei Planning Commission in Shanghai (2014-2016). Our work has also been supported by Shanghai Science and Technology Commission (19401972804). We thank the rehabilitation and nursing team who helped with patient treatment at Shanghai Hongkou District Jiangwan Hospital. We thank the patients and their families for their participation.

#### References

- [1] V. L. Feigin, M. H. Forouzanfar, R. Krishnamurthi et al., "Global and regional burden of stroke during 1990-2010: findings from the Global Burden of Disease Study 2010," *Lancet*, vol. 383, no. 9913, pp. 245–255, 2014.
- [2] M. Yagi, H. Yasunaga, H. Matsui et al., "Impact of rehabilitation on outcomes in patients with ischemic stroke: a nationwide retrospective cohort study in Japan," *Stroke*, vol. 48, no. 3, pp. 740–746, 2017.
- [3] M. Zhang, Q. Wang, Y. Jiang, H. Shi, T. Peng, and M. Wang, "Optimization of early mobilization program for patients with acute ischemic stroke: an orthogonal design," *Frontiers in Neurology*, vol. 12, 2021.

## *Retraction*

# **Retracted: Downregulation of LHPP Expression Associated with AFP Acts as a Good Prognostic Factor in Human Hepatocellular Carcinoma**

### **BioMed Research International**

Received 12 March 2024; Accepted 12 March 2024; Published 20 March 2024

Copyright © 2024 BioMed Research International. This is an open access article distributed under the Creative Commons Attribution License, which permits unrestricted use, distribution, and reproduction in any medium, provided the original work is properly cited.

This article has been retracted by Hindawi following an investigation undertaken by the publisher [1]. This investigation has uncovered evidence of one or more of the following indicators of systematic manipulation of the publication process:

- (1) Discrepancies in scope
- (2) Discrepancies in the description of the research reported
- (3) Discrepancies between the availability of data and the research described
- (4) Inappropriate citations
- (5) Incoherent, meaningless and/or irrelevant content included in the article
- (6) Manipulated or compromised peer review

The presence of these indicators undermines our confidence in the integrity of the article's content and we cannot, therefore, vouch for its reliability. Please note that this notice is intended solely to alert readers that the content of this article is unreliable. We have not investigated whether authors were aware of or involved in the systematic manipulation of the publication process.

Wiley and Hindawi regrets that the usual quality checks did not identify these issues before publication and have since put additional measures in place to safeguard research integrity.

We wish to credit our own Research Integrity and Research Publishing teams and anonymous and named external researchers and research integrity experts for contributing to this investigation.

The corresponding author, as the representative of all authors, has been given the opportunity to register their agreement or disagreement to this retraction. We have kept a record of any response received.

### **References**

- [1] X. Chao, W. Zhang, J. Wu et al., "Downregulation of LHPP Expression Associated with AFP Acts as a Good Prognostic Factor in Human Hepatocellular Carcinoma," *BioMed Research International*, vol. 2021, Article ID 1971048, 9 pages, 2021.

## Research Article

# Downregulation of LHPP Expression Associated with AFP Acts as a Good Prognostic Factor in Human Hepatocellular Carcinoma

Xu Chao<sup>1,2</sup>, Wei Zhang<sup>1</sup>, Jieqiong Wu<sup>1</sup>, Xuesong Feng<sup>2</sup>, Hailong Shi<sup>2</sup>, Luyan Zhao<sup>1</sup>, Haiyu Shen<sup>2</sup>, and Chao Jiang<sup>3</sup>

<sup>1</sup>The Second Affiliated Hospital of Shaanxi University of Chinese Medicine, Xianyang 712000, China

<sup>2</sup>The College of Basic Medicine Sciences, Shaanxi University of Chinese Medicine, Xianyang 712046, China

<sup>3</sup>The Second Affiliated Hospital of Xi'an Medical University, Xi'an, Shaanxi 710038, China

Correspondence should be addressed to Chao Jiang; 280165056@qq.com

Received 13 May 2021; Accepted 12 August 2021; Published 27 August 2021

Academic Editor: Qian Wang

Copyright © 2021 Xu Chao et al. This is an open access article distributed under the Creative Commons Attribution License, which permits unrestricted use, distribution, and reproduction in any medium, provided the original work is properly cited.

**Background.** Phospholysine phosphohistidine inorganic pyrophosphate phosphatase (LHPP) serves as a tumor suppressor in hepatocellular carcinoma (HCC), but the correlation between the expression of LHPP and the clinical parameters of oncogenic progression is still not well defined. This study is to reveal the correlation between the expression of LHPP in HCC and their clinical parameters. **Methods.** Immunohistochemical analysis was used to assess the correlation between the expression of LHPP and the clinical parameters of HCC. Expressions of LHPP in HCC tissues and cultured HCC cells were detected by Western blot and quantitative real-time polymerase chain reaction (qRT-PCR). LHPP, gamma-glutamyl transferase (GGT), and  $\alpha$ -fetoprotein (AFP) expression levels in blood or HCC tissues were detected by enzyme-linked immunosorbent assay (ELISA). The Spearman rank correlation coefficient was used to evaluate the correlation of the expression of LHPP and the clinical index of HCC. Correlation of survival and expression of LHPP were analyzed using the Kaplan-Meier method and the log-rank test. **Results.** Expressions of LHPP in HCC tissues were significantly downregulated than their paired adjacent normal tissues. A significant positive correlation was found between the cytoplasm and nuclear expression of LHPP in both HCC and their paired adjacent normal tissues. The expression of LHPP negatively correlated with the levels of GGT in the cytoplasm of adjacent tissues and with the AFP level in the nucleus of HCC cells. Relative levels of LHPP in HCC tissues were markedly lower than those of the paired adjacent normal tissues. Relative levels of LHPP in LO-2 cells were higher than those of HepG2, BEL-7404, and SMMC-7721 cell lines. The overall survival and DSF survival of patients with the high expression of LHPP were much higher than those with the low expression of LHPP in paired adjacent normal tissue. **Conclusions.** LHPP is associated with the AFP level and acts as a good prognostic factor in HCC.

## 1. Background

Liver cancer was predicted to be the sixth most commonly diagnosed cancer and the fourth leading cause of cancer death worldwide in 2018, with about 841,000 new cases and 782,000 deaths annually [1]. In China, liver cancer is a common primary cancer in adults and a malignant tumor due to its high morbidity. It is also the second leading cause of cancer mortality [2, 3]. Invasion and intrahepatic metastasis are the main factors leading to poor prognosis of patients with hepatocellular carcinoma (HCC) [4]. Detecting the molecular mechanism of hepatocellular carcinoma

might have a significant value in diagnosing and treating HCC [5].

LHPP encodes an enzyme known as phospholysine phosphohistidine inorganic pyrophosphate phosphatase (LHPP), which was originally purified from swine brain tissue [6]. Deregulated histidine phosphorylation has been found in various diseases [7]. LHPP gene variation is associated with the oral cavity and pharyngeal cancer [8]. LHPP may interact with serotonin receptor 1A (Htr1a) in the pathogenesis of major depression [9]. Patients with major depressive disorder having LHPP rs35936514 CT/TT genotype have increased activity in certain brain regions [6]. Recently, it

has been reported that LHPP plays an essential role in inhibiting human HCC progression by regulating the phosphatidylinositol-3-kinase/protein kinase B (PI3K/Akt) signaling pathway [10]. LHPP serves as a tumor suppressor in liver cancer, and the loss of the expression of LHPP is associated with reduced survival in HCC [11, 12]. However, the correlation between the expression of LHPP and the clinical parameters of HCC in oncogenic progression is still not well defined.

This study is aimed at exploring the expression of LHPP in HCC and evaluating the correlation between the expression of LHPP and the clinical parameters of HCC. The findings might provide a new insight to improve the prognosis of patients and the survival rate of patients with HCC.

## 2. Methods

**2.1. Materials.** HepG2, BEL-7404, SMMC-7721, and LO-2 cells were purchased from the National Collection of Authenticated Cell Culture (Shanghai, China). RPMI-1640 media and fetal bovine serum were purchased from Gibco Co., Ltd. (NY, USA). Mouse anti-human  $\beta$ -actin and LHPP were purchased from Santa Cruz Biotechnology, Inc. (CA, USA). Human alpha-fetoprotein (AFP) and ELISA Kit were purchased from Abcam Biotechnology, Inc. (Shanghai, China). A GGT Activity Assay Kit was purchased from Amy Jet Scientific, Inc. (Wuhan, China).

**2.2. Patients and Specimens.** Two tissue microarrays (TMAs) of HCC samples were used to assess the correlation between the expression of LHPP and the clinical parameters of HCC. One was a survival liver cancer tissue chip (HLivH180Su14, Shanghai Outdo Biotech, Shanghai, China), which included 90 liver cancer and paired paracancerous samples with death and recurrence information and followed up for 3.8-4.6 years. The other was the HCC tissue microarray (HLivH060CD03, Shanghai Outdo Biotech), which included 2 normal liver specimens, liver samples of 6 patients with cirrhosis, 17 primary tumors and paired adjacent cancer samples (3 cases with distal normal liver tissue), and 15 liver cancer metastases cases. Conventional clinicopathological variables, including gender, age, hepatitis history, liver cirrhosis, AFP, GGT, tumor number, size, encapsulation, differentiation, vascular invasion, stage, therapy, and status, were recorded and are displayed in Table 1.

Five liver cancer and paired paracancerous samples used for WB and qRT-PCR experiments and the blood used for enzyme-linked immunosorbent assay (ELISA) come from the pathology department of Xijing Hospital of Air Force Military Medical University.

**2.3. Cell Culture.** HepG2, BEL-7404, SMMC-7721, and LO-2 cells were obtained from the National Collection of Authenticated Cell Culture (Shanghai, China). All cells were cultured in RPMI-1640 medium supplemented with 10% (*v/v*) heat-inactivated fetal bovine serum, 100  $\mu$ g/mL streptomycin, and 100 U/mL penicillin. The cultures were maintained at 37°C in a humidified atmosphere of 5% CO<sub>2</sub>. Cells in the exponential growth phase were used for all experiments.

TABLE 1: The HCC patients' clinical information in detail.

	Clinical index	N	Total N
Gender	Male	80	90
	Female	10	
Age	≤60 years	71	90
	>60 years	19	
Tumor size	≤5 cm	62	90
	>5 cm	28	
T staging	T1	58	90
	T2-T3	32	
Clinical staging	Stage I	58	90
	Stage II	28	
	Stage III	4	

**2.4. Immunohistochemical Analysis.** Immunohistochemical analysis was employed to detect the differential expression of LHPP in HCC tissues and paired adjacent normal tissue. Briefly, the sections were dewaxed, hydrated, and washed. After the neutralization of endogenous peroxidase and the microwave antigen retrieval, the slides were preincubated with blocking serum and then incubated overnight with the mouse anti-human LHPP monoclonal antibody (1:500) at 4°C. Subsequently, the sections were serially rinsed, incubated with second horseradish peroxidase-(HRP-) labeled anti-mouse antibody, and treated with horseradish peroxidase-conjugated streptavidin. The reaction products were visualized with 3,3-diaminobenzidine tetrahydrochloride and counterstained with hematoxylin after washing with phosphate-buffered saline.

The staining intensity was observed by two pathologists for immunohistochemical analysis. The scoring in detail was as follows: negative for 0, "+" for 1, "++" for 2, and "+++" for 3. The positive staining rate according to the proportion of positively stained cancer cells was defined as follows: "negative" for 0, "1%-20%" for 1, "21%-40%" for 2, "41%-60%" for 3, "61%-80%" for 4, and "81%-100%" for 5. The total score was the product of "dying intensity" score and "dying positive rate" score.

The HCC tissues and their paired adjacent normal tissues were grouped separately because the expression of LHPP in cancer tissues was significantly lower than that in adjacent tissues. In HCC tissues, the total LHPP expression score ≤ 1.25 was considered as the low expression of LHPP, and the total LHPP expression score > 1.25 was considered as the high expression of LHPP. However, in adjacent normal tissues, the total LHPP expression score ≤ 6.25 was considered as the low expression of LHPP, and the total LHPP expression score > 6.25 was considered as the high expression of LHPP [13].

**2.5. RNA Extraction and qRT-PCR Analysis.** Total RNA was extracted from cultured cells or tissues using the Trizol Kit (Invitrogen, Carlsbad, CA, USA). Briefly, 3 mL cell suspension plated into 6-well plates (1 × 10<sup>7</sup> cells/well) were



harvested and washed with cold PBS. Or 50 mg HCC tissues or their adjacent normal tissues were frozen by liquid nitrogen and ground very fine. Subsequently, 1 mL Trizol was added to the harvested cells or ground tissues and maintained 1 min at 4°C for cell lysis. Then, 0.2 mL chloroform was added to lysis and shaken for 15 s. Samples were centrifugated for 15 min at 12000g rpm at 4°C, and supernatant contained total RNA was transferred to a 1.5 mL tube, and add 0.5 ml isopropanol, mix the liquid gently, and let it stand for 10 min at room temperature. And then, samples were centrifugated for 10 min at 12000g rpm at 4°C and the supernatant was discarded. Finally, 100  $\mu$ L of sterile-filtered water treated with diethyl pyrocarbonate (DEPC) was added to dissolve total RNA.

cDNA was obtained through reverse transcription using the Promega M-MLV Kit (Promega, Madison, WI, USA). Quantitative real-time PCR (qRT-PCR) was performed using the 7500 Real-Time PCR System (ABI, California, USA). The SYBR Master Mixture Kit (Takara, Japan) and RNA reverse transcription were performed to determine expression.

**2.6. Western Blot Analysis.** The cells or tissues frozen by liquid nitrogen and ground were lysed and centrifuged at 12,000g for 15 min at 4°C. Then, total protein was extracted from the resulting supernatant, and the concentration was quantified through the bicinchoninic acid (BCA) assay. Equal amounts (30  $\mu$ g) of proteins were separated using 10% sodium dodecyl sulfate-polyacrylamide gel (SDS), followed by transfer onto polyvinylidene difluoride membranes. After blocking with defatted milk powder, the membranes were treated with rabbit monoclonal anti-human  $\beta$ -actin and LHPP antibodies (1:1000 dilution) overnight at 4°C. This was followed by incubation with appropriate HRP-conjugated secondary antibodies at room temperature for 1 h and detected using an enhanced chemiluminescence (ECL) kit (GE Healthcare, Beijing, China).

**2.7. Detection of AFP and GGT of Blood.** The levels of AFP and GGT of blood were detected by enzyme-linked immunosorbent assay (ELISA) using a chemiluminescence immune analysis system (Dxl800Access, Beckman, USA). All procedures were strictly in accordance with the standard operating procedure.

**2.8. Statistical Analysis.** The differential expression of LHPP in HCC tissues and their adjacent normal tissues was evaluated using the nonparametric tests. The survival curves depending on the expression of LHPP and clinical characteristics were drawn by the Kaplan-Meier method and log-rank test. Subsequently, all the potential predictive factors were involved in the Cox multivariate regression survival analysis. The Spearman rank correlation coefficient was used to evaluate the correlation between the expression of LHPP and some clinical immunohistochemical factors. All statistical analyses were conducted using SPSS 17.0 software.  $P < 0.05$  was considered significant.

### 3. Results

**3.1. Participant Characteristics.** 90 paired HCC and paired adjacent normal tissues were obtained from patients who underwent primary surgery in the Taizhou Hospital of Zhejiang Province (Taizhou, China) between January 2010 and November 2015. In this study, there were 90 participants including 80 males (88.8%) and 10 females (11.2%) and 71(88.7%) with mean age  $\leq$  60 years. There were 62 (68.9%) patients with tumor size  $<$  5 cm. 58 (64.4%) cases were T1 stage, and patients with clinical Stage I, II, and III were 58 (64.4%), 28 (31.1%), and 4 (4.44%), respectively (Table 1).

**3.2. Result of Immunohistochemical Analysis.** The result of immunohistochemical analysis showed that the expression of LHPP in HCC was significantly downregulated compared with paired adjacent normal tissues ( $3.63 \pm 2.75$  vs.  $8.63 \pm 1.25$ ,  $P < 0.001$ ) (Figure 1(a)). Also, it is found that expressions of LHPP of cytoplasm or cell nucleus in HCC were significantly downregulated than those in paired adjacent normal tissues (Figures 1(b) and 1(c)).

**3.3. Expressions of mRNA and Protein of LHPP in Tissues and Cells.** Relative mRNA levels of LHPP in HCC tissues and paired adjacent samples and cultured cells were examined through qRT-PCR. The results showed relative mRNA levels of LHPP in tumor samples were markedly lower than those of the adjacent normal tissues (Figure 2(a)). Also, relative mRNA levels of LHPP in HepG2, BEL-7404, and SMMC-7721 cell lines were significantly lower than those of LO-2 cells (Figure 2(c)).

Protein levels of LHPP in tissues and cells were detected by Western blot analysis (WB). As showed in Figure 2(b), the protein expression levels of LHPP in HCC tissues were significantly lower than those in the adjacent normal tissues. Additionally, the data showed that the expression of LHPP in HepG2, BEL-7404, and SMMC-7721 cell lines was much lower than that in LO-2 cells (Figure 2(d)).

**3.4. Correlation of the Expression of LHPP with the Clinical Index of HCC.** The expression of LHPP negatively correlated with tumor size in HCC ( $r = 0.303$ ;  $P = 0.005$ ). The nuclear expression of LHPP in paired adjacent normal tissue negatively correlated with tumor size ( $r = 0.261$ ;  $P = 0.023$ ), while the cytoplasmic expression of LHPP in nontumor tissues correlated with vascular invasion ( $r = 0.300$ ;  $P = 0.012$ ) or recurrence ( $r = 0.348$ ;  $P = 0.002$ ). No significant correlation was found between LHPP expression and gender age pathological grading, vascular invasion, T clinical stages, recurrence, or liver cirrhosis (Table 2).

**3.5. Correlation between the Expression of LHPP and the Expression Levels of GGT and AFP.** To further investigate the correlation between the expression of LHPP and the expression levels of LHPP, GGT and AFP were detected in plasma and HCC tissue by ELISA and Spearman's rho test. Results showed that expression of LHPP of the plasma and HCC tissue of patients negatively correlated with GGT and AFP levels in blood and HCC tissues (Table 3).

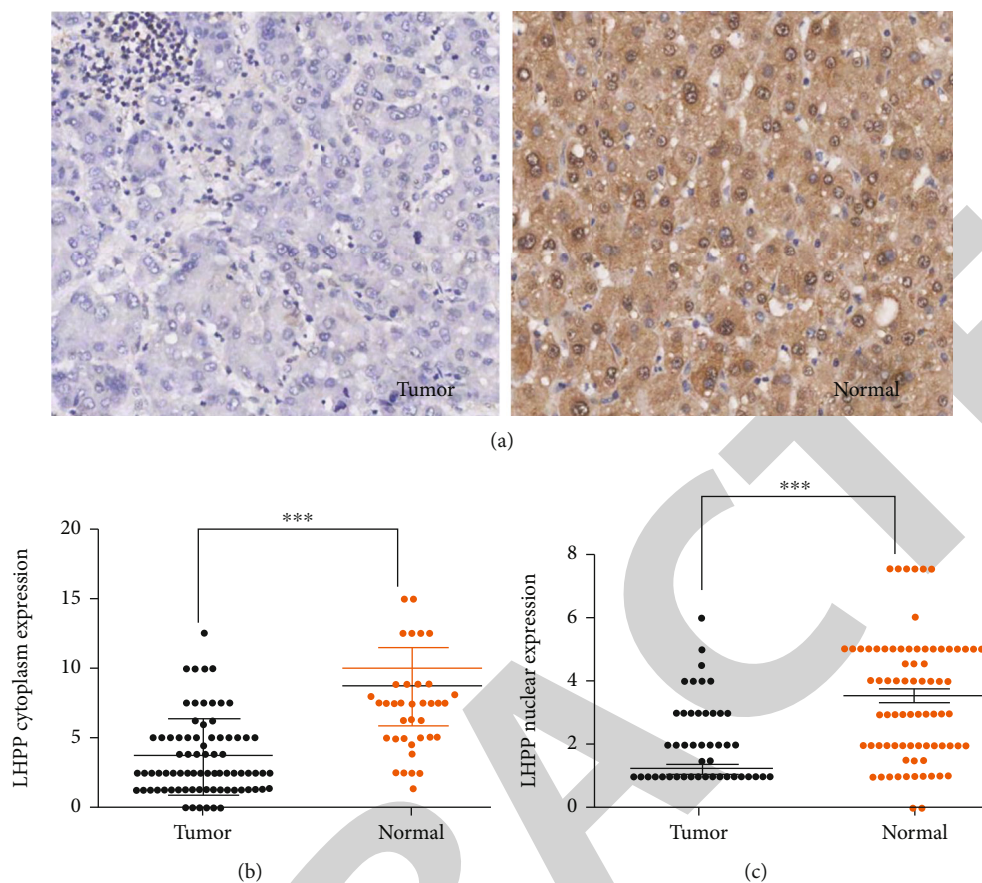


FIGURE 1: Expression of LHPP in the nucleus and plasma of tumor and normal samples. Expressions of LHPP in 90 liver cancer and paired adjacent normal tissue were detected through immunohistochemical staining, and staining intensities were calculated for immunohistochemical analysis. (a) Representative immunohistochemical images of the expression of LHPP in tumor and adjacent normal tissue. (b) Cytoplasmic expression of LHPP in tumor and adjacent normal tissue. (c) Nuclear expression of LHPP in tumor and adjacent normal tissue. \*\*\*  $P < 0.001$  vs. the corresponding control.

### 3.6. Correlation between Survival and Expression of LHPP.

Correlation between survival and expression of LHPP in HCC cancer or paired adjacent normal tissue was analyzed using the Kaplan-Meier method and the log-rank test. Results showed the overall survival of a patient with higher expression of LHPP and lower expression of LHPP in HCC tissue has no difference statistically ( $P = 0.369$ ) (Figure 3(a)). However, disease-free (DSF) survival of patients with the high expression of LHPP was significantly higher than patients with the low expression of LHPP in HCC tissue (53.4% vs. 25.9%,  $P = 0.012$ ) (Figure 3(b)). The overall survival of patients with the high expression of LHPP was much higher than those with the low expression of LHPP in adjacent normal tissue (71.7% vs. 31.3%,  $P = 0.004$ ) (Figure 3(c)). Also, it was found DSF survival of patients with the high expression of LHPP was markedly higher than those with the low expression of LHPP in adjacent normal tissue (55.0% vs. 12.5%,  $P = 0.008$ ) (Figure 3(d)).

## 4. Discussion

Histidine phosphorylation, also known as the hidden phosphoproteome, is a poorly characterized posttransla-

tional modification of proteins. LHPP is a protein histidine phosphatase and a tumor suppressor, suggesting that deregulated histidine phosphorylation is oncogenic [6]. A previous study suggested that LHPP acted as a tumor suppressor in various cancers, such as hepatocellular carcinoma, cervical cancer, bladder cancer, pancreatic cancer, and melanoma. In hepatocellular carcinoma (HCC), decreased expression of LHPP is positively correlated with larger tumor size and reduced overall survival [11]. But the correlation between the expression of LHPP and the clinical parameters of oncogenic progression is not fully studied.

In this study, the Spearman rank correlation coefficient was used to evaluate the correlation of the expression of LHPP and the clinical index of HCC. Results showed that LHPP expression in HCC was correlated with tumor size, indicating the potential function of LHPP on tumor proliferation. The expression of LHPP in paired adjacent normal tissue significantly negatively correlated with vascular invasion and recurrence. A comparison of the expression of LHPP in HCC tissues and their paired adjacent normal tissue suggested that the expression of LHPP in HCC and adjacent normal tissue might inhibit the progression of HCC *via* different mechanisms.



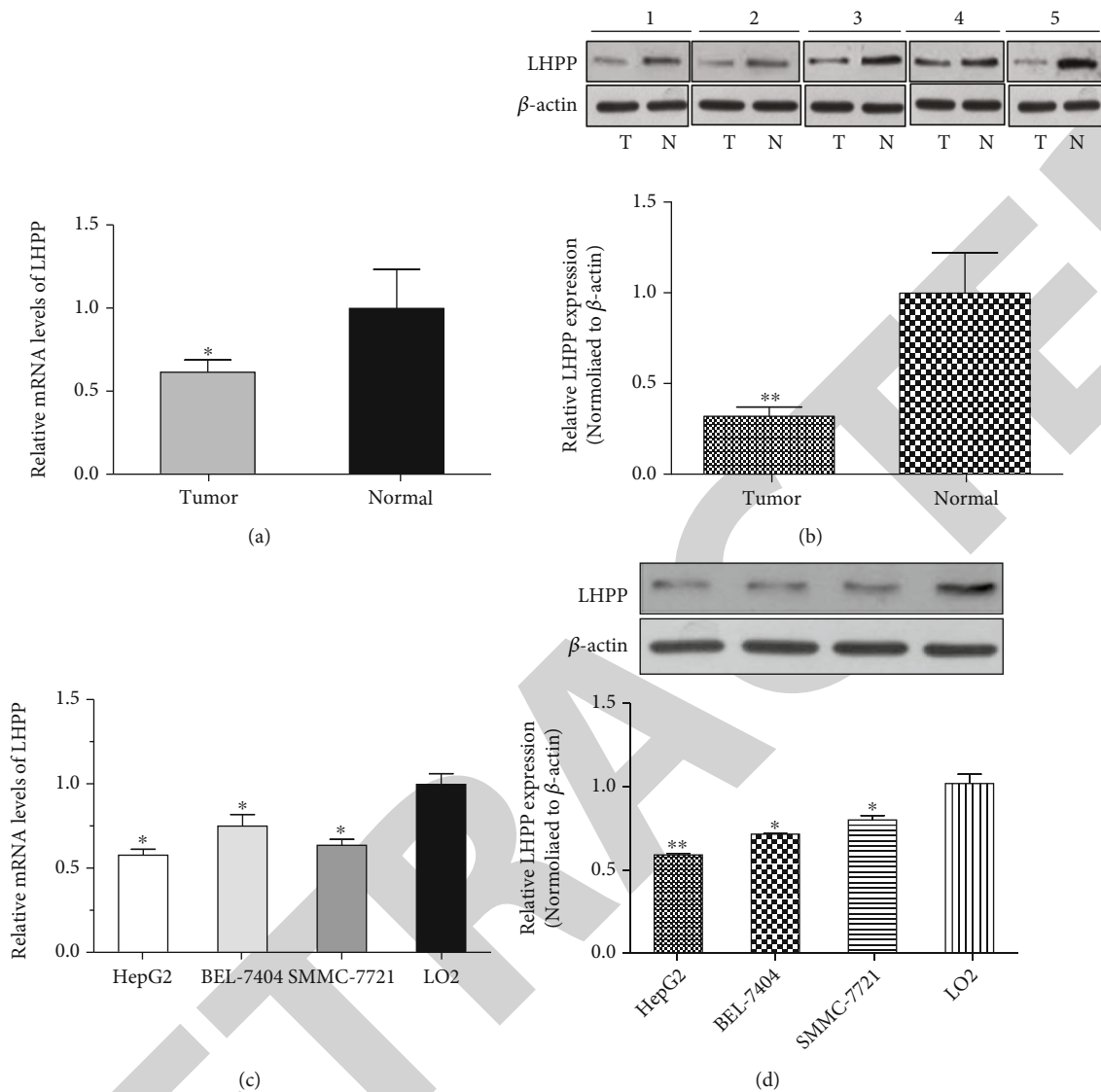


FIGURE 2: Expressions of mRNA and protein of LHPP in tissues and cells *in vitro*. (a) Relative mRNA levels of LHPP in cancer and paired adjacent normal tissue. Total RNA of 5 liver cancer and adjacent normal tissue were extracted, and relative mRNA levels of LHPP were examined through qRT-PCR. (b) Relative protein expressions of LHPP in cancer and paired adjacent normal tissue. Total protein of 5 liver cancer and adjacent normal tissue was extracted, and protein expressions of LHPP were examined through WB. (c) Relative mRNA levels of LHPP in HepG2, BEL-7404, SMMC-7721, and LO-2 cell lines. Total RNA of HepG2, BEL-7404, SMMC-7721, and LO-2 cells were extracted, and relative mRNA levels of LHPP were examined through qRT-PCR. (d) Relative LHPP expressions in HepG2, BEL-7404, SMMC-7721, and LO-2 cell lines. Total protein of HepG2, BEL-7404, SMMC-7721, and LO-2 cell lines was extracted, and protein expressions of LHPP were examined through WB. \* $P < 0.05$  and \*\* $P < 0.01$  vs. the corresponding control.

AFP and GGT, as two important HCC markers, have clinical significance in the diagnosis of HCC [14, 15]. To further investigate the role of LHPP in HCC, the expression levels of GGT and AFP were detected in the blood and tissue. Spearman's rho test results showed that expression of LHPP of the plasma and HCC tissues of patients negatively correlated with GGT and AFP levels. The present study validated that the expression of LHPP correlated with the expression of AFP and GGT in blood and HCC tissue, suggesting that LHPP correlated with the incidence of HCC or served as a complementary biomarker for AFP and GGT in diagnosing HCC.

LHPP gene variation is associated with the oral cavity and pharyngeal cancer [9]. In this study, the results of HCC microarray showed that the expression of LHPP was the lowest in HCC tissue, with lower expression in primary liver cancer and higher expression in paired adjacent normal tissue, illustrating that LHPP might inhibit the distant metastasis of HCC. The present study demonstrated that LHPP could inhibit the progression and the distant metastasis of HCC. As metastasis has been reported a leading cause of cancer-related death [11], it was speculated that the expression of LHPP was associated with tumor severity, and LHPP could act as a tumor suppressor.

TABLE 2: Correlation of the expression of LHPP and the clinical index of HCC.

	Gender	Age	Pathological grading	Tumor size	Tumor number	Cirrhotic nodule	Tumor cell membrane	Vascular invasion	T	Clinical stages	Recurrence	Liver cirrhosis
LHPP expression in the nucleus of HCC	0.019	-0.033	0.057	-0.274*	0.175	0.202	-0.064	-0.007	0.075	0.075	-0.056	-0.023
	0.874	0.776	0.626	0.017	0.130	0.082	0.585	0.954	0.518	0.518	0.633	0.845
Spearman's rho	76	76	76	76	76	75	75	70	76	76	76	75
	Correlation coefficient	-0.079	0.013	-0.108	0.150	0.163	-0.010	-0.116	-0.053	-0.053	-0.181	0.089
LHPP expression in adjacent normal tissue	0.497	0.910	0.354	0.036	0.196	0.163	0.932	0.338	0.650	0.650	0.117	0.446
	76	76	76	76	76	75	75	70	76	76	76	75
	N											

\*Correlation is significant at the 0.05 level (2-tailed).

TABLE 3: The relationship between the expression of LHPP and the GGT and AFP expression levels in blood and HCC tissues.

		HBsAg	HBcAb	TB	ALT	ALB	AFP	GGT	PTT
LHPP level in the plasma	Correlation coefficient	-0.027	-0.069	0.196	-0.033	0.114	-0.063	0.044	0.053
	Sig. (2-tailed)	0.808	0.536	0.075	0.763	0.301	0.571	0.691	0.630
	N	84	82	84	84	84	84	84	84
	Correlation coefficient	-0.017	0.187	-0.046	-0.144	0.111	-0.150	-0.269*	-0.174
Spearman's rho	Normal	0.882	0.113	0.692	0.219	0.342	0.200	0.020	0.136
	N	75	73	75	75	75	75	75	75
	Correlation coefficient	0.035	0.022	0.039	-0.042	-0.052	-0.232*	0.047	0.185
	Sig. (2-tailed)	0.766	0.851	0.738	0.720	0.655	0.045	0.686	0.112
LHPP expression in the tissues	Tumor	0.766	0.851	0.738	0.720	0.655	0.045	0.686	0.112
	N	75	73	75	75	75	75	75	75
	Correlation coefficient	-0.117	0.147	0.062	-0.223	0.093	-0.121	-0.193	-0.142
	Sig. (2-tailed)	0.317	0.216	0.599	0.054	0.426	0.300	0.097	0.223
Paratumor	N	75	73	75	75	75	75	75	75

\*Correlation is significant at the 0.05 level (2-tailed).

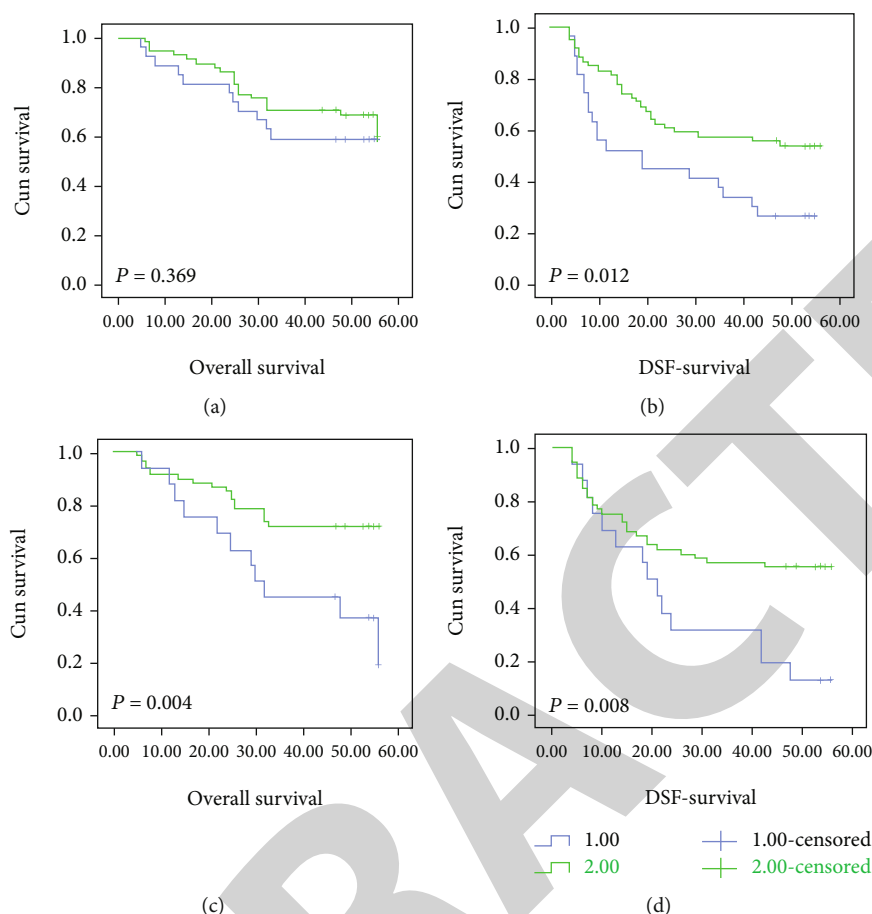


FIGURE 3: Correlation of survival and expression of LHPP in HCC tissue and paired adjacent normal tissue. Immunohistochemical analysis was employed to detect the differential expression of LHPP in HCC tissues or paired adjacent normal tissue, and the Kaplan-Meier method and the log-rank test were used to analyze the correlation of survival and expression of LHPP. (a) Correlation of overall survival and expression of LHPP in HCC tissue. (b) Correlation of disease-free survival and expression of LHPP in HCC tissue. (c) Correlation of overall survival and expression of LHPP in adjacent normal tissue. (d) Correlation of disease-free survival and expression of LHPP in paired adjacent normal tissue. \* $P < 0.05$  vs. the corresponding control.

The Kaplan-Meier method and the log-rank test were employed to reveal the correlation between the expression of LHPP in HCC tissue or adjacent normal tissue and the prognosis of HCC. Results showed DSF survival of patients with the high expression of LHPP was significantly higher than patients with the low expression of LHPP in HCC tissue. Also, it was verified that overall survival and DSF survival of patients with the high expression of LHPP were markedly higher than those with the low expression of LHPP in paired adjacent normal tissue.

Our study suggests that LHPP plays an important role in the occurrence and development of HCC and provides a potential marker of HCC. However, due to the limited number of samples, whether it can be used as an occurrence and development marker of HCC and as a diagnostic indicator of HCC needs further study.

## 5. Conclusions

The present study has validated there was a significant differential expression of LHPP in HCC tissues and their paired

adjacent normal tissue. It is suggested that the expression of LHPP was associated with the AFP level and good prognosis in HCC, and LHPP is expected to be a potential marker of HCC.

## Data Availability

Dataset can be accessed from the corresponding author upon reasonable request.

## Disclosure

The funder played no role in the design of the study and collection, analysis, and interpretation of data and in writing the manuscript.

## Conflicts of Interest

All authors declare that they have no conflicts of interest.

## Retraction

# Retracted: High-Throughput Screen of Natural Compounds and Biomarkers for NSCLC Treatment by Differential Expression and Weighted Gene Coexpression Network Analysis (WGCNA)

### BioMed Research International

Received 12 March 2024; Accepted 12 March 2024; Published 20 March 2024

Copyright © 2024 BioMed Research International. This is an open access article distributed under the Creative Commons Attribution License, which permits unrestricted use, distribution, and reproduction in any medium, provided the original work is properly cited.

This article has been retracted by Hindawi following an investigation undertaken by the publisher [1]. This investigation has uncovered evidence of one or more of the following indicators of systematic manipulation of the publication process:

- (1) Discrepancies in scope
- (2) Discrepancies in the description of the research reported
- (3) Discrepancies between the availability of data and the research described
- (4) Inappropriate citations
- (5) Incoherent, meaningless and/or irrelevant content included in the article
- (6) Manipulated or compromised peer review

The presence of these indicators undermines our confidence in the integrity of the article's content and we cannot, therefore, vouch for its reliability. Please note that this notice is intended solely to alert readers that the content of this article is unreliable. We have not investigated whether authors were aware of or involved in the systematic manipulation of the publication process.

Wiley and Hindawi regrets that the usual quality checks did not identify these issues before publication and have since put additional measures in place to safeguard research integrity.

We wish to credit our own Research Integrity and Research Publishing teams and anonymous and named external researchers and research integrity experts for contributing to this investigation.





The corresponding author, as the representative of all authors, has been given the opportunity to register their agreement or disagreement to this retraction. We have kept a record of any response received.

### References

- [1] L. Kui, M. Li, X. Yang et al., "High-Throughput Screen of Natural Compounds and Biomarkers for NSCLC Treatment by Differential Expression and Weighted Gene Coexpression Network Analysis (WGCNA)," *BioMed Research International*, vol. 2021, Article ID 5955343, 20 pages, 2021.

## Research Article

# High-Throughput Screen of Natural Compounds and Biomarkers for NSCLC Treatment by Differential Expression and Weighted Gene Coexpression Network Analysis (WGCNA)

Ling Kui <sup>1,2,3</sup>, Min Li,<sup>4</sup> Xiaonan Yang,<sup>5,6</sup> Ling Yang,<sup>7</sup> Qinghua Kong,<sup>8</sup> Yunbing Pan,<sup>9</sup> Zetan Xu,<sup>9</sup> Shouling Wang,<sup>9</sup> Dandan Mo,<sup>5,6</sup> Yang Dong <sup>5,10,11</sup>, Yao Liu <sup>12</sup> and Jianhua Miao <sup>5,13</sup>

<sup>1</sup>Shenzhen Qianhai Shekou Free Trade Zone Hospital, Shenzhen 518067, China

<sup>2</sup>School of Pharmacy, Jiangsu University, Zhenjiang 212013, China

<sup>3</sup>Dana-Farber Cancer Institute, Harvard Medical School, Brookline MA02215, USA

<sup>4</sup>Department of Biology Chemistry, Institute of Science, Nanchang University College of Science and Technology, Jiujiang 332020, China

<sup>5</sup>Guangxi Key Laboratory of Medicinal Resources Protection and Genetic Improvement, Guangxi Medicinal Botanical Garden, Nanning 530023, China

<sup>6</sup>Guangxi Engineering Research Center of TCM Resource Intelligent Creation, Guangxi Botanical Garden of Medicinal Plants, Nanning 530023, China

<sup>7</sup>Faculty of Food Science and Technology, Yunnan Agricultural University, Kunming 650201, China

<sup>8</sup>State Key Laboratory of Phytochemistry and Plant Resources in West China, Kunming Institute of Botany, Chinese Academy of Sciences, Kunming 650201, China

<sup>9</sup>Nowbio Biotechnology Company, Kunming 650000, China

<sup>10</sup>State Key Laboratory for Conservation and Utilization of Bio-Resources in Yunnan, Yunnan Agricultural University, Kunming 650201, China

<sup>11</sup>Yunnan Research Institute for Local Plateau Agriculture and Industry, Kunming 650201, China

<sup>12</sup>Baoji High-Tech Hospital, Baoji 721006, China

<sup>13</sup>School of Pharmacy, Guangxi Medical University, Nanning 530021, China

Correspondence should be addressed to Yao Liu; [baojiliuyao@163.com](mailto:baojiliuyao@163.com) and Jianhua Miao; [mjh1962@vip.163.com](mailto:mjh1962@vip.163.com)

Received 19 May 2021; Revised 24 June 2021; Accepted 13 July 2021; Published 27 August 2021

Academic Editor: Yuzhen Xu

Copyright © 2021 Ling Kui et al. This is an open access article distributed under the Creative Commons Attribution License, which permits unrestricted use, distribution, and reproduction in any medium, provided the original work is properly cited.

Lung cancer is known as the leading cause which presents the highest fatality rate worldwide; non-small-cell lung cancer (NSCLC) is the most prevalent type of lung carcinoma with high severity and affects 80% of patients with lung malignancies. Up to now, the general treatment for NSCLC includes surgery, chemotherapy, and radiotherapy; however, some therapeutic drugs and approaches could cause side effects and weaken the immune system. The combination of conventional therapies and traditional Chinese medicine (TCM) significantly improves treatment efficacy in lung cancer. Therefore, it is necessary to investigate the chemical composition and underlying antitumor mechanisms of TCM, so as to get a better understanding of the potential natural ingredient for lung cancer treatment. In this study, we selected 78 TCM to treat NSCLC cell line (A549) and obtained 92 transcriptome data; differential expression and WGCNA were applied to screen the potential natural ingredient and target genes. The sample which was treated with *A. pierreana* generated the most significant DEG set, including 6130 DEGs, 2479 upregulated, and 3651 downregulated. KEGG pathway analyses found that four pathways (MAPK, NF-kappa B, p53, and TGF-beta signaling pathway) were significantly enriched; 16 genes were significantly regulated in these four pathways. Interestingly, some of them such as EGFR, DUSP4, IL1R1, IL1B, MDM2, CDKN1A, and IDs have been used as the target biomarkers for cancer diagnosis and therapy. In addition, classified samples into 14 groups based on their pharmaceutical



effects, WGCNA was used to identify 27 modules. Among them, green and darkgrey were the most relevant modules. Eight genes in the green module and four in darkgrey were identified as hub genes. In conclusion, we screened out three new TCM (*B. fruticose*, *A. piirreana*, and *S. scandens*) that have the potential to develop natural anticancer drugs and obtained the therapeutic targets for NSCLC therapy. Our study provides unique insights to screen the natural components for NSCLC therapy using high-throughput transcriptome analysis.

## 1. Introduction

Lung cancer remained the leading cause which presents the highest fatality rate worldwide, with an estimated 1.8 million deaths (18%) in each year reported by the International Agency for Research on Cancer/World Health Organization [1]. Particularly, lung cancer is the highest incidence of cancer and the high fatality rate in men, in 93 countries [2]. Approximately 85% of patients have a group of histological subtypes collectively known as non-small-cell lung cancer (NSCLC), which is the most prevalent type of lung carcinoma with high severity and affects 80% of patients with lung malignancies [3–5]. Up to now, the general treatment for NSCLC includes surgery, chemotherapy, and radiotherapy [6], but most chemotherapy drugs kill both cancer and normal cells [7–10]. The side effects of chemotherapies somewhat impact the quality of patients' life. Therefore, it is urgent necessity to investigate the novel therapeutic strategies, to identify the prognostic markers based on better understanding of molecular mechanism of NSCLC. It helps to improve the precision rate for diagnosis and therapy and contributes to take the further steps for NSCLC research [3, 4].

Traditional Chinese medicine (TCM) presented significant advantages in disease treatment special in cancer therapy; it was reported that the function of relieving adverse effects and enhancing the efficacy of drugs is presented [11–13]. Importantly, it has cytoprotective properties without hindering the anticancer activity of conventional drugs during combinational chemotherapy [14]. Finding active anticancer ingredients from TCM and reported their anticancer mechanisms became more and more popular for medical practitioners [15, 16]. A new trend in research of the new drug development for cancer treatment is obtaining natural ingredients with low toxicity and high efficiency from TCM [17, 18]. However, the anticancer compounds and molecular mechanisms of TCM are still unclear; the systemic methods need to be established. Undoubtedly, high-throughput screening is an effective and systematic approach to analyze TCM-mediated gene expression modifications in cells. Based on gene expression and pathway enrichment variations in different treatments, the underlying anticancer mechanisms of both conventional drugs and traditional medicines can be analyzed. Finally, it would indicate the potential TCM for lung cancer therapy according to the pharmaceutical effect and effective component comprehensively. Moreover, it may help to explain the molecular mechanism and screen the anticancer compounds, providing the new sight for the natural anticancer drug development on cancer treatment.

The transcriptome is all the genes expressed in a certain cell in a certain functional status, and it can be used to compare differences in gene expression levels among various

tissues or under various physiological conditions [19, 20]. The regulatory mechanisms for cancers are closely tied with differential genes and changes in signal pathways within the transcriptome. Comparative transcriptome analysis of cell lines with drug intervention allows the molecular mechanisms of cell growth conditions and physical sign changes following drug treatment to be holistically understood, and the interaction between drugs and cellular activities to be probed; the functional genes and their expression patterns can be analyzed, regulatory mechanisms mastered, and cancer-related signal pathways and key genes identified to find the target genes on which the drugs act [21–25]. These data can be used for targeted screening of medicinal ingredients, which can be verified and analyzed to find potential drugs and provide scientific, accurate, and comprehensive data for drug research and development [23].

Weighted gene coexpression network analysis (WGCNA) is a bioinformatics data mining method that has been used to explore relationships between different gene modules of various cancer cell lines [26, 27]. The modules of coexpressing genes are found to maintain a consistent phenotype-independent expression relationship, and they may coregulate and share common biological functions [27]. Using WGCNA, expression alterations in gene sets, intrinsic properties of gene sets, correlation between gene modules, phenotype-correlated modules, candidate biomarker genes, and the targets for therapeutic drugs can be analyzed [28]. In previous studies, WGCNA was used to analyze biomarkers and targets of various diseases like schizophrenia, Alzheimer's disease, sickle cell disease, and cancers [29–32]. As a systematical biological method, WGCNA has been used in various cancer studies including non-small-cell lung cancer (NSCLC), bladder cancer, clear cell renal cell carcinoma (ccRCC), acute myeloid leukemia (AML), and pancreatic ductal adenocarcinoma (PDAC) [28, 33–36].

In this study, high-throughput transcriptome sequencing is used to provide the transcriptome data of NSCLC cell line distilled with 78 TCM and 10 chemical compounds (positive control) aforesaid. High-quality data sets are obtained from transcriptome assembly and comparative analysis. Then, identified and validated key genes were significantly associated with proinflammatory effects and metastasis process in NSCLC cancer by differential expression and WGCNA. We propose to establish a high-throughput method to screen potential natural compounds and identify the target genes, providing new sight on natural anticancer drug development for NSCLC cancer therapy.

## 2. Materials and Methods

*2.1. Preparation of Medicinal Plant Extracts.* All the 78 medicinal plants were provided by Guangxi Botanical

Garden of Medicinal Plants. Plant materials were collected to dry and ground into fine powder for preparation of extracts. Some of the plant materials were boiled by hot water, then freeze dried; the obtained extracts were named as "W." The extraction method named by "GX" refers to the medicinal plants extracted by 60% ethanol for 2 h. The extracted samples were vacuum concentrated and loaded on macroporous resin column, and the product of interest was eluted by water. The eluted fractions were concentrated by vacuum evaporation, and the completely dried samples were used for drug preparation. The dried fruit of *Myristica fragrans* was extracted using the CO<sub>2</sub> supercritical extraction method, and the obtained extract was named as "C." The remaining plant materials were firstly extracted by petroleum ether for 2 h and filtered, the remained residue was then extracted by ethyl acetate for another 2 h, and the extracts were vacuum concentrated to dry powder for drug preparation and named as "S." More description of samples is shown in Supplemental Table 1. Ten conventional anticancer drugs purchased from various companies were set as positive control (Table 1). All the plant samples and drugs were dissolved in DMSO for further experiments, marked as fractions and positive control, respectively.

**2.2. Cell Culture and Drug Preparation.** Purchased from the Shanghai Cell Bank of the Chinese Academy of Sciences, the A549 cell line was cultured in DMEM containing 10% fetal bovine serum and placed in a cell incubator with 5% CO<sub>2</sub> at 37°C. Then, the cells with complete culture media when their growth density reached 80%-90% trypsin (0.125%) were subcultured. We selected logarithmic growth phase to test and screen the anticancer activity of A549 cell line, which was treated with 78 TCM and 10 conventional anticancer drugs (Supplemental Table 1, Supplemental Table 6, Table 1). The samples, which were treated with 10 conventional anticancer drugs, were considered as positive control, while 4 samples without any treatment were regarded as negative control. The fractions were extracted from the TCM species mainly including Leguminosae, Compositae, Araliaceae, Euphorbiaceae, and Rutaceae, all of which have been reported to have antitumor effects through previous studies. The positive control was conventional anticancer drugs purchased from the companies (Table 1).

After the treatment experiments of fractions and positive control, a concentration of 100 µg/ml and a final volume of 200 µl per well were prepared for first screening; then, the cell survival rate after 24 h of drug treatment was calculated. A 6-well plate with the same concentration was applied to screen the cells whose survival rate was more than 80%. If the survival rate was less than 80%, the 96-well plate screening was carried out again with a reduced concentration. A gradient of 2 times was set to screen the fractions; the screen concentration was set base on the cell survival rate during first screening. Finally, we selected the concentration at which the cell survival rate reached about 80% to carry out the 6-well plate screening. Subsequently, the cell growth conditions under a microscope were observed and this concentration as the final administration concentration was recorded.

TABLE 1: The list of positive control.

Drug	Source (company)
Sorafenib	Beijing Solarbio Science & Technology Co., Ltd
cis-Platinum	Beijing Solarbio Science & Technology Co., Ltd
Lenvatinib	Shanghai Topscience Bio-Technology Co., Ltd
Cabozantinib	Shanghai Yuanye Bio-Technology Co., Ltd
Doxorubicin hydrochloride	Shanghai Yuanye Bio-Technology Co., Ltd
Gefitinib	Shanghai Macklin Biological Co., Ltd
Paclitaxel	Shanghai Macklin Biological Co., Ltd
Docetaxel	Shanghai Macklin Biological Co., Ltd
Vinorelbine	Shanghai Aladdin Reagent Co., Ltd
Gemcitabine	Beijing OKA Bio-Technology Co., Ltd

**2.3. RNA Quality Control, Library Preparation, and Sequencing.** In our study, the FastPure Cell/Tissue Total RNA Isolation Mini Kit (Vazyme, Nanjing, China) was applied to extract the total RNA of the cell lines. NanoDrop 2000 and Agilent 2100 Bioanalyzer (Agilent, USA) were used to obtain the OD<sub>260/280</sub>; the value is 1.8~2.0. The RIN (RNA Integrity Number) values and concentration of all total RNA samples were quantified; RIN values reached 8. mRNA libraries were constructed by the MGIEasy kit; cDNA libraries with an insert size of 200-300 bp were prepared according to standard BGISEQ protocol with total RNA samples. Paired-end sequencing with 100 bp read length was sequenced using the BGISEQ-500 instrument and BGISEQ-500RS high-throughput sequencing kit.

**2.4. RNA-seq Clean Data Preparation and Quality Checking.** After sequencing, raw data were obtained in the fastq format. FastQC has been used to perform the quality control detecting the quality of sequencing data [37] according to the standards: filtering the low-quality reads with low base-call scores, the adapter sequences, the reads including N, and a shift from the expected GC content. The generated high-quality data were moved forward to the alignment step. Afterwards, the read sequences were trimmed and filtered by Trimmomatic software (v.0.36), which was included in the Trinity package [38, 39]; more detailed information about quality checking is shown in Supplemental Table 2; the generated clean data has been uploaded to NCBI Sequence Read Archive (SRA). Take multiple correlation analyses and screen the potential natural component for lung cancer therapy (Supplemental Table 1). Among these groups, groups 1-10 refer to the samples treated with TCM fractions, group 11 was mixed by samples treated with unclassified fractions, and groups 12 and 13 refer to positive controls and negative controls, respectively. Group 14 represents the samples treated with TCM which may include anticancer ingredient.

**2.5. Alignment and Transcript Assembly.** When quality control was finished, the general RNA-seq analyses would be carried out. There are four main steps that need to be done: aligning the reads to the reference; assembling the alignments

TABLE 2: Detailed information of RNA-seq analysis pipeline.

Step	Analyses	Software	Script	Input	Main output
1	Prepare raw data	Trimmomatic ver.0.36	trimmomatic-0.36.jar PE -threads 12 -phred33 -trimlog xx.log xx.fq1 xx.fq2 -baseout	FASTQ file	FASTQ file
2	Quality control	FastQC	fastqc -t 10 -f fastq -o out xx.fq	FASTQ file from step 1	FASTQ file, multiqc_report.html
3	Alignment	HISAT	hisat2 -p 20 -x hg38.fa -1 xx_clean_1P.fq.gz -2 xx_clean_2P.fq.gz -S XX.sam	FASTQ file from step 2	Sam file
4	Sort	Samtools	samtools sort -@ 20 -O bam -o xx.bam xx.sam	Sam file from step 3	Bam file
5	Transcript assembly	StringTie	stringtie -e -p 30 -G hg38.gff -o xx.gtf xx.bam	Bam file from step 4	gtf file
6	Merged transcripts	StringTie-merge	stringtie -merge -o merged.gtf gtflist	All gtf file from step 5	gtf file
7	Reads count	StringTie-eB	stringtie -B -e -p 30 -G merged.gtf -o xx.gtf xx.bam	gtf file from step 6 and Bam file from step 4	Gallgown input file and gtf file
8	Generated gene expression (FPKM)	Ballgown	gene_expression = gexpr(bg)	Output files from StringTie-eB	Gene expression tables
9	Differential expression analysis	DESeq2 Wrapper of TBtools	Selection criteria of DEGs: $p.adjust \leq 0.05$ and $ \log 2FC  \geq 1$	Gene expression tables	Volcano plot and differential gene list
10	KEGG pathway analysis	R package clusterProfiler and <a href="http://org.Hs.eg.dbdata.set">http://org.Hs.eg.dbdata.set</a>	Parameter: $p.valueCutoff = 0.05$ , $p.AdjustMethod = "BH"$ , $qvalueCutoff = 0.1$	Differential gene list	KEGG pathway tables
11	Gene expression visualization	TBtools	Default parameters	Expression of top genes	Heatmaps
12	General analysis of WGCNA	"WGCNA" R package	Power of $\beta = 7$ (scale free $R^2 = 0.9$ )	FPKM table	Plots and forms of module connectivity
13	Selecting module and hub genes	"WGCNA" R package	$cor.geneModuleMembership > 0.8$ and $cor.geneTraitSignificance > 0.2$	Output files from WGCNA	Module and gene list
14	Network	Cytoscape	Default parameters The criteria for edge filter: weight value $> 0.13$ and weight value $> 0.06$	Output files from WGCNA	Network plots

The table lists analysis steps, software, and main scripts in our pipeline. Starting from the input FASTQ files produced by sequencing and finally generating the results of candidate medicine and genes for NSCLC cancer research.

on the alignment into a full-length transcript; quantitative expression of genes and transcripts; calculating the expression difference of all genes under different experimental conditions. The "new Tuxedo" package including HISAT, StringTie, and Ballgown has been used to perform this process. During this process, HISAT [40] has been used to align RNA-seq reads to the genome, and StringTie [41] is responsible for assembling transcripts and constructing isoforms to estimate gene expression. Ballgown [42] uses the results of StringTie splicing to calculate gene expression, then obtained the FPKM (Fragments Per Kilobase Million) results. The input data was generated by the BGISEQ-500 instrument; after running our pipeline, useful outputs were produced, including transcripts, gene expression values (FPKM), differentially expressed gene (DEG) list, and the merged statistical results. The detailed steps are shown in Table 2.

**2.6. Differential Expression and KEGG Pathway Analysis.** TBtools is a Toolkit for Biologists integrating various biological data-handling tools [43]; we applied it to perform differ-

ential expression analysis. Differentially expressed genes (DEGs) were filtered according to the criteria of  $p.adjust \leq 0.05$  and  $|\log 2FC| \geq 1$ , and a volcano plot was used to visualize the distribution of each gene. Subsequently, DEGs were imported to complete KEGG pathway analysis based on R package clusterProfiler and <http://org.Hs.eg.dbdata.set> with the parameter of  $p.valueCutoff = 0.05$ ,  $p.AdjustMethod = "BH"$ , and  $qvalueCutoff = 0.1$ . Based on KEGG results, the top 10 significant pathways and their enriched genes were selected as the candidate pathways and targets. They may be associated with inflammatory and metastasis processes in cancer. Furthermore, the expression of these genes was visualized by heat map through TBtools and the common genes were screened according to the high significance of differential expression. The analysis steps, software, and main scripts in our pipeline are listed in Table 2.

**2.7. Weighted Gene Coexpression Network Analysis (WGCNA).** The "WGCNA" R package with default parameters was applied to construct the weighted coexpressed networks



TABLE 3: Differential gene expression of top 10 sets.

Compare	Significant	Upregulated	Downregulated	Sample name	Note
Treat53_vs_CK	6130	2479	3651	<i>Argyreia pierreana</i>	Candidate TCM
Treat91_vs_CK	1865	966	899	<i>Excoecaria cochinchinensis</i> Lour.	
Treat8_vs_CK	1651	867	784	<i>Breynia fruticosa</i>	Candidate TCM
Treat56_vs_CK	1541	566	975	<i>Tabernaemontana divaricata</i>	
Treat63_vs_CK	1162	550	612	<i>Senecio scandens</i>	Candidate TCM
Treat6_vs_CK	956	350	606	<i>Melia azedarach</i>	
Treat59_vs_CK	814	527	287	<i>Phyllanthus reticulatus</i> Poir. var. <i>glaber</i> Muell.-Age.	
Treat44_vs_CK	745	266	479	<i>Chromolaena odorata</i>	
Treat27_vs_CK	645	186	459	<i>Sorafenib</i>	
Treat90_vs_CK	627	259	368	<i>Excoecaria cochinchinensis</i> Lour.	

and identify the coexpression modules. The modified WGCNA pipeline used in this study is shown in Table 2. The expression data generated by previous analyses were log<sub>2</sub> normalized and imported into the “WGCNA” R package; sample information of 14 groups was summarized in the table. The soft thresholding was set according to the power of  $\beta = 7$  (scale free  $R^2 = 0.9$ ), and MEDissThres was set as 0.25 to merge similar modules, so as to ensure a scale-free network. Finally, edges were screened by the criteria of weight value, then inputted them into Cytoscape to visualize the coexpression network and identify the nodes and hub genes [44]. These genes, which may play an important role in tumorigenesis process, can be selected as the potential targets in the future research on cancer therapy.

### 3. Results

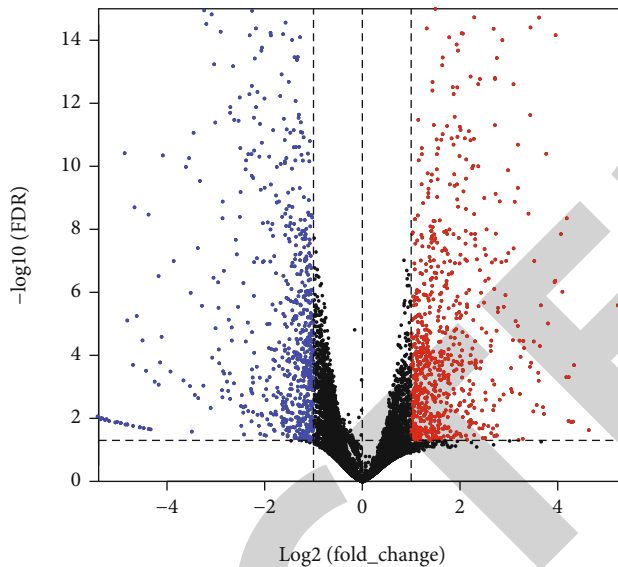
**3.1. Data Preprocessing and Differentially Expressed Gene (DEG) Screening.** In this study, 92 cDNA libraries were sequenced and produced about 806.67 Gb raw data, consisting of 8,066,731,626 reads with an average read length of 100 bp (Supplemental Table 3). Clean sequencing reads (785.50 Gb and 7,855,046,204 reads) are available at NCBI Sequence Read Archive. After quality control, obtained sequencing reads were mapped to reference genome using STAR and sorted using Samtools. Subsequently, the gene expression (FPKM, Fragments Per Kilobase Million) was generated using RSEM. Differential expression analysis was performed by DESeq2 Wrapper included in TBTools; the selection criteria for differentially expressed genes (DEGs) are  $p.adjust \leq 0.05$  and  $|\log_2 FC| \geq 1$ . We obtained 92 DEG set; the set contained most DEGs is Treat53 vs. CK, including 6130 DEGs, 2479 upregulated, and 3651 downregulated. We list the top 10 set shown in Tables 3, and selected the DEG set of three TCM candidates, which were *Breynia fruticosa* (*B. fruticosa*), *Argyreia pierreana* (*A. pierreana*), and *Senecio scandens* (*S. scandens*), illustrated by a volcano plot (Figures 1(b), 1(e), and 1(h)). The detailed DEG information is shown in Supplemental Table 4.

**3.2. KEGG Pathway Analysis and Candidate TCM Screening.** In order to identify biologic pathways, functional categories,

and networks of DEGs, we used the R package clusterProfiler and <http://org.Hs.dbdata> set to complete KEGG pathway analysis. The results indicated four key pathways associated with the biological processes of proinflammatory effects, and the metastasis process is significantly enriched, including the MAPK signaling pathway, NF-kappa B signaling pathway, p53 signaling pathway, and TGF-beta signaling pathway (Figures 1(c), 1(f), and 1(i)). Among all, the MAPK signaling pathway was enriched by the three plant samples *B. fruticosa*, *A. pierreana*, and *S. scandens*. The NF-kappa B signaling pathway was enriched by *B. fruticosa* and *S. scandens*. It indicated these three TCM may significantly regulate the expression of key genes in MAPK and NF-kappa B signaling pathways; they may include the potential ingredient for NSCLC therapy and should be screened as the effective TCM candidates (Figure 1). On the other hand, the p53 signaling pathway was enriched by 4 TCM samples and 5 positive control samples, while the TGF-beta signaling pathway was enriched by 8 TCM samples. It is still unknown whether they are associated with NSCLC or not.

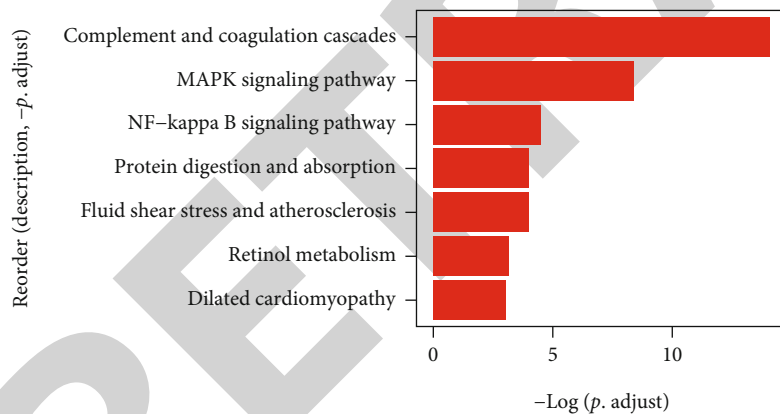
The detailed pathway results of other TCM are shown in Supplemental Table 5.

Additionally, *B. fruticosa* possesses the pharmaceutical effect of rheumatism treatment, *A. pierreana* and *S. scandens* possess the pharmaceutical effect of heat-clearing (Supplemental Table 6), and it is worth to explore the potential mechanism of NSCLC with rheumatism treatment and heat-clearing effect. We investigated and surveyed previous research; excitingly, *B. fruticosa* was reported including anti-inflammatory effect in cancer, which is one of the main factors with carcinogenesis. *B. fruticosa* widely grows in South China and was used to cure chronic bronchitis, sore throat, wounds, and gastroenteritis and presented an anticancer effect [45, 46]. *B. fruticosa* contains almost 10 bioactive compounds; among them, zizyberanolic acid and isoceanothic acid possess strong cytotoxic activity against five human cancer cell lines [46]. Meanwhile, it reported that the main active constituents of *B. fruticosa* include tannins, triterpenes, sterol derivatives, and lignins. Some compounds such as breynins presented the pharmacologic action of reducing inflammation through inhibiting NF-kappa B DNA-binding activity and expression of iNOS and



(a)

(b)

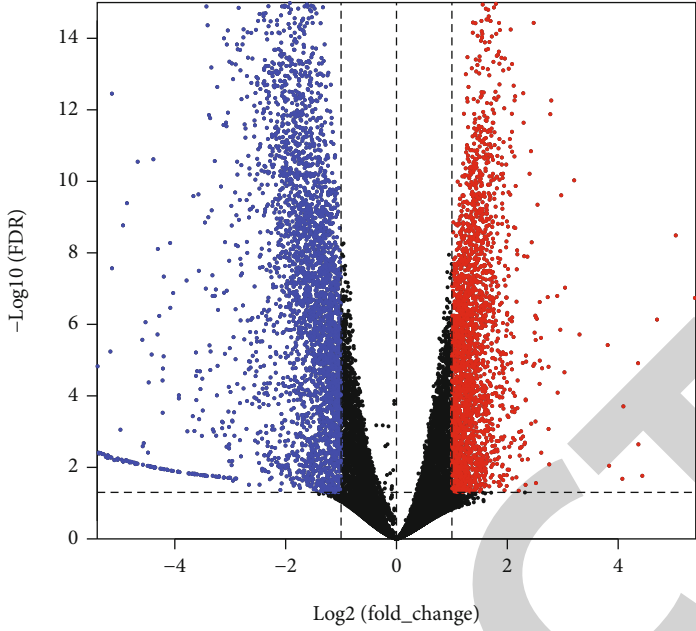


(c)

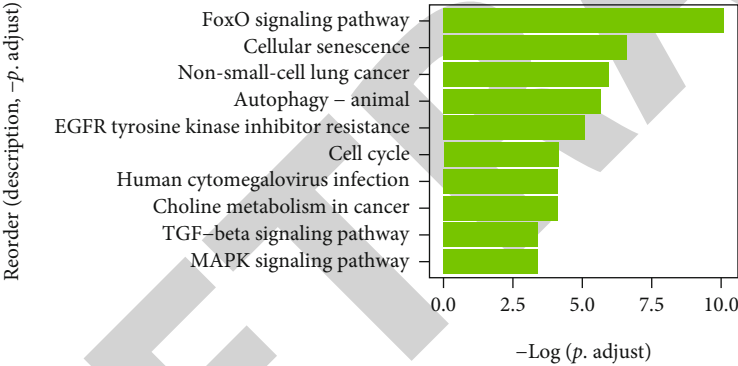


(d)

FIGURE 1: Continued.



(e)



(f)



(g)

FIGURE 1: Continued.



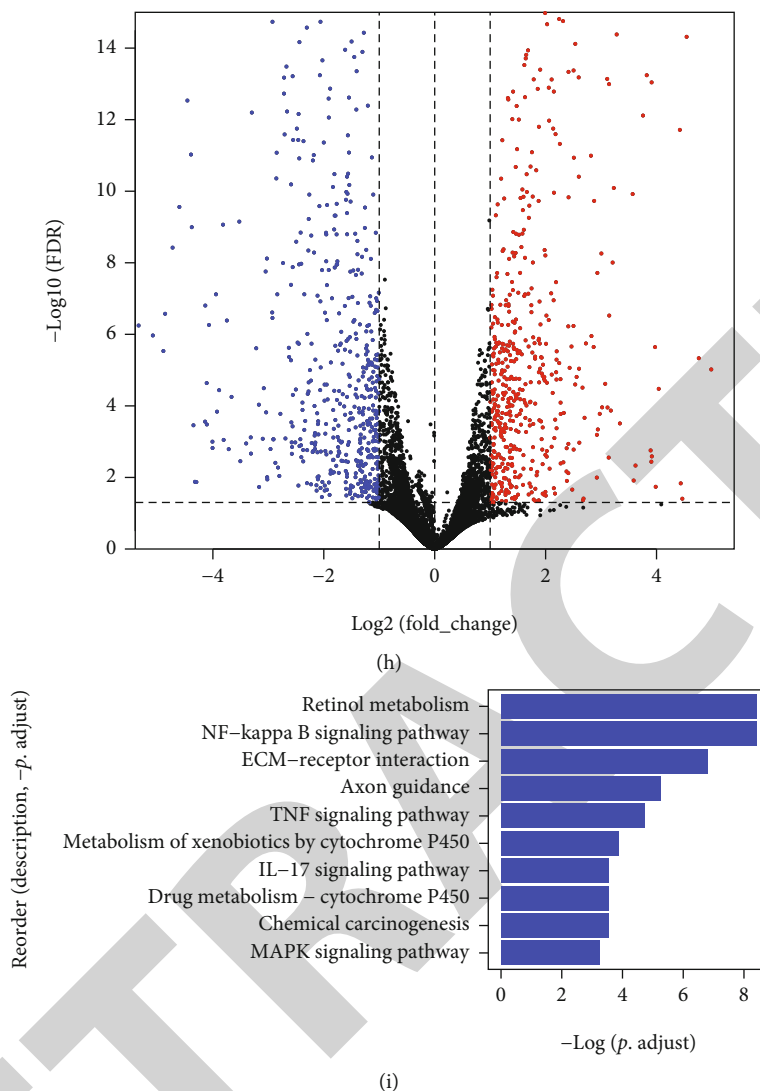
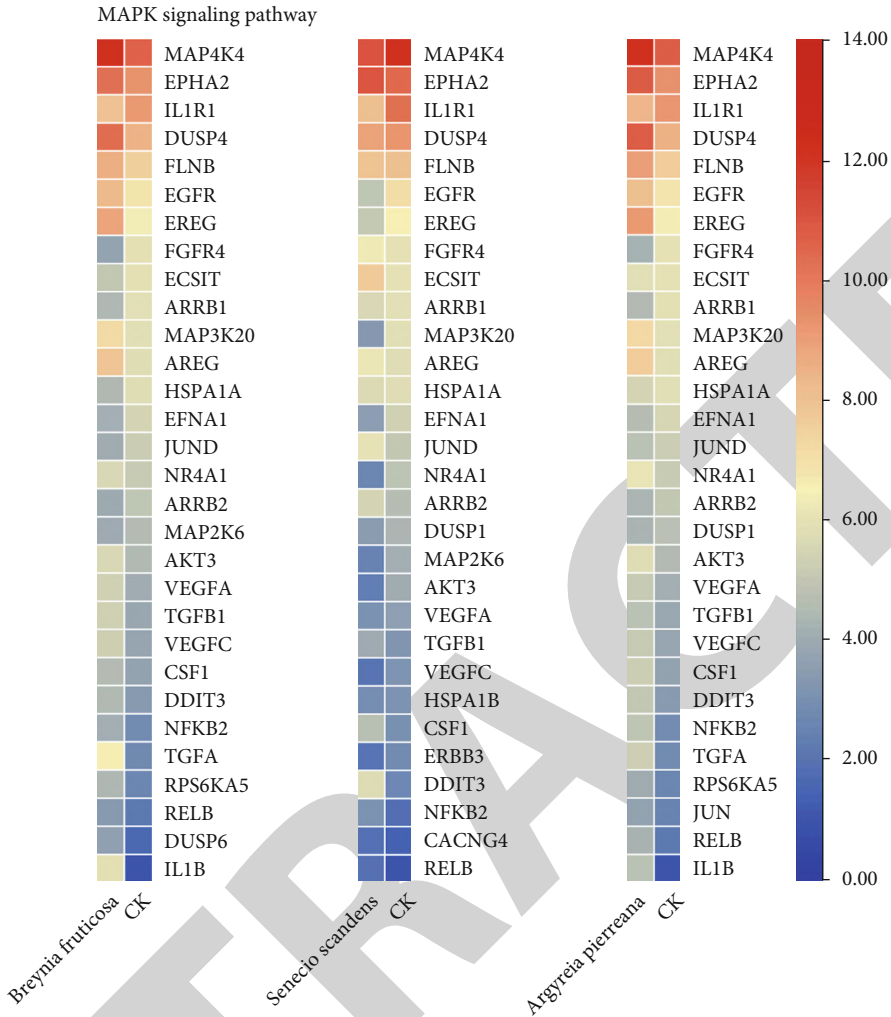


FIGURE 1: Plant morphology, differentially expressed genes (DEGs), and KEGG pathways of samples treated with three candidate TCM. (a–c) *Breynia fruticosa*, (d–f) *Argyreia pierreana*, and (g–i) *Senecio scandens*. Plant morphology pictures cited from Flora of China (source: <http://www.iplant.cn>). In volcano plots, the horizontal line at  $|\log_2 \text{FC}| = 1$ ; vertical line at false discovery rate (FDR) = 0.05. In bar plots of KEGG pathways, red block represented the key pathways.

COX-2; it is similar with thiacremonone [47]. Furthermore, it reported that the chloroplast genome of *B. fruticosa* has been completed; it helps to take the further research on genomic resources of *Breynia* species [45]. *S. scandens* is known as “Qianliguang” in Chinese; the active constituents include flavonoids, terpenes, alkaloids, carotenoids, volatile oils, chlorogenic acids, phenolic acids, and vitamins [48]. Among them, the main constituent is PAs and the main typical ingredients are adonifoline [48, 49]. Additionally, previous studies stated that some components isolated from *Senecio scandens* presented various pharmacological activities, such as antitumoral, anti-inflammatory, mutagenic, antiviral, antioxidant, and abirritation activities [49, 50]. However, there is almost no research on *A. pierreana*; we will plan to study on its pharmacological activities especially anticancer in the next research.

**3.3. Expression and Regulation of Top Genes Enriched on These Key Pathways.** In this study, we list the genes which were regulated significantly in MAPK and NF-kappa B signaling pathways in three candidate TCM, as well as other TCM enriched on p53 and TGF-beta signaling pathway (Figure 2). The common significantly regulated genes in three candidate TCM associated with the MAPK signaling pathway are IL1R1, DUSP4, EGFR, EREG, and MAP3K20. Among them, IL1R1 was downregulated and DUSP4 was upregulated in all three candidate TCM; other genes present different regulations. In the NF-kappa B signaling pathway, BIRC3, TRIM25, TAB3, PLAU, and IL1B are common significantly upregulated; only IL1R1 was downregulated, the same as in the MAPK signaling pathway. MDM2 was upregulated and CDKN1A was downregulated in the p53 signaling pathway; ID1, ID2, and ID4 present different



(a)

FIGURE 2: Continued.

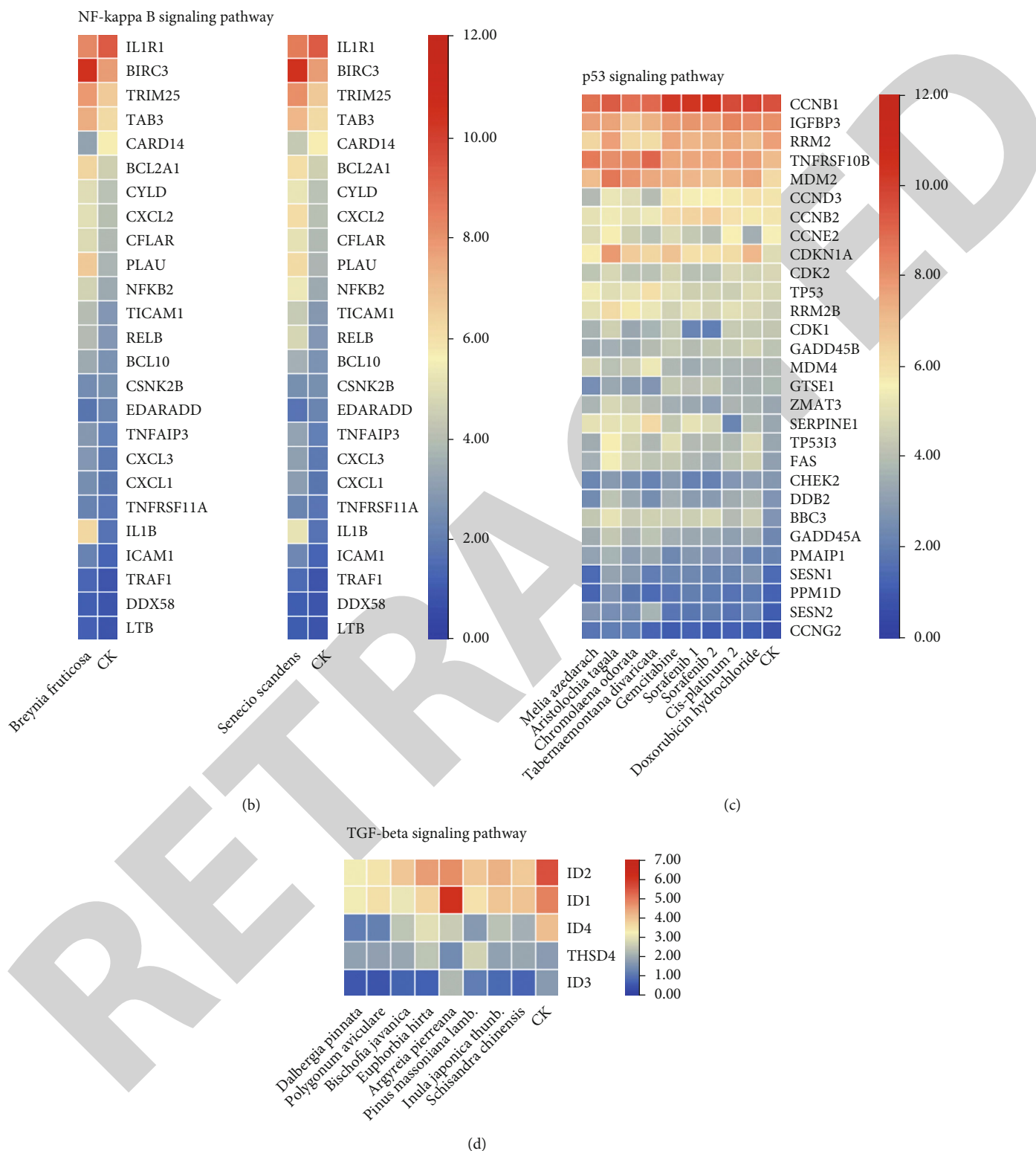


FIGURE 2: Expression and regulation of top genes enriched on the key pathways. (a) MAPK signaling pathway; (b) NF-kappa B signaling pathway; (c) p53 signaling pathway; (d) TGF-beta signaling pathway. CK: the negative control.

regulations in the TGF-beta signaling pathway. The regulated results of the common genes are shown in Table 4; the expression of common genes in all the samples is shown in Figure 2.

It is worth noting that some of the common genes were demonstrated to play an important role in inflammatory or metastasis processes in cancers, especially in NSCLC. What is more, some of them interacted on the key pathways, such

TABLE 4: The regulated results of the common genes.

Pathway	Common genes in medicine	Regulate
MAPK signaling pathway	IL1R1	Downregulated
	DUSP4	Upregulated
	EGFR	Upregulated in <i>B. fruticosa</i> and <i>A. pierreana</i> , downregulated in <i>S. scandens</i>
	EREG	Upregulated in <i>B. fruticosa</i> and <i>A. pierreana</i> , downregulated in <i>S. scandens</i>
	MAP3K20	Upregulated in <i>B. fruticosa</i> and <i>A. pierreana</i> , downregulated in <i>S. scandens</i>
NF-kappa B signaling pathway	IL1R1	Downregulated
	BIRC3	Upregulated
	TRIM25	Upregulated
	TAB3	Upregulated
	PLAU	Upregulated
	IL1B	Upregulated
p53 signaling pathway	MDM2	Upregulated
	CDKN1A	Upregulated
TGF-beta signaling pathway	ID2	Downregulated
	ID1	Upregulated in <i>A. pierreana</i> , downregulated in others
	ID4	Downregulated

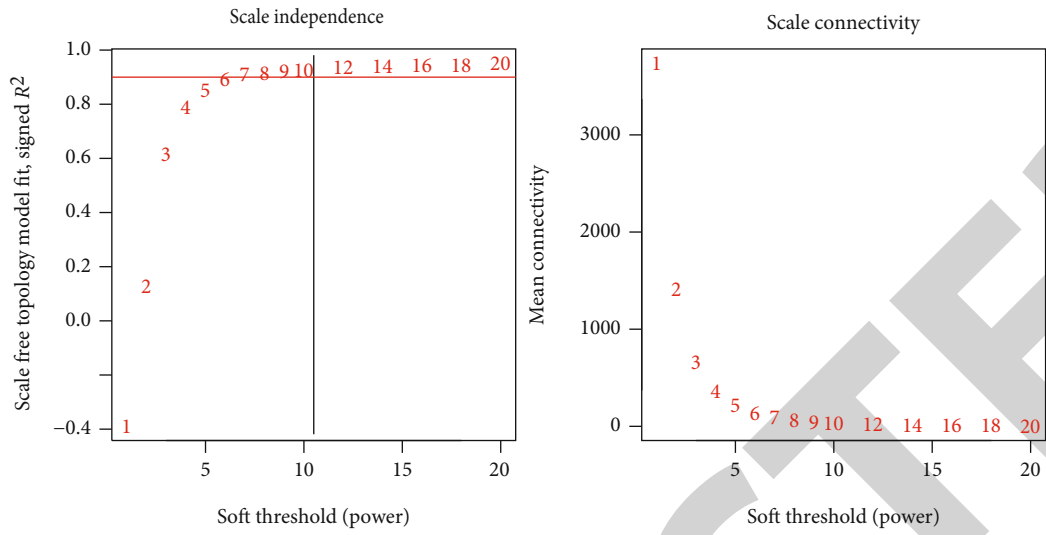
as EGFR, DUSP4, IL1R1, IL1B, MDM2, CDKN1A, and IDs; they all have been used as the target biomarkers for cancer diagnosis and therapy. The result indicated that the TCM candidates significantly inhibited the NSCLC by regulating various common genes of different signaling pathways. Overall, this study inferred that our TCM candidates probably possessed the significant curative effects for NSCLC. In the subsequent studies, identification of effective compounds and functional investigation of common genes would be considered.

As shown in Figure 2 and Table 4, IL1R1 was included in both MAPK and NF-kappa B signaling pathways; it is IL-1 receptor type I. IL-1 is a master regulator which contributed to inflammation, hematopoiesis, and innate immunity. IL-1 $\alpha$  and IL-1 $\beta$  are the representative proinflammatory cytokines, and both of them bonded to IL1R1 which also possesses pro-inflammatory effects. Besides, nuclear factor-kB (NF-kappa B), p38, and MAPKs are the key transcription factors involved in inflammatory and immune response activities [51, 52]. The epidermal growth factor receptor (EGFR) is one of the mutated signaling proteins in NSCLC, and the EGFR gene is one of the first molecules to be selected for targeted gene therapy [53]. EGFR is the kinase inhibitor and has successfully been used in targeted therapies of various oncogenic driver mutations [54]. DUSP4 is a negative regulator of the MAPK pathway [55]. It reported that the loss of complex heterozygosity between DOK2 and DUSP4 leads to the occurrence of lung adenocarcinomas, with a short incubation period and high incidence rate. Their codeletion can activate MAPK signaling and promote cell proliferation [56]. On the other hand, DUSP4 is involved in negative feedback control of EGFR signaling, and it proved the loss of DUSP4 associated with p16/CDKN2A deletion in the lung cancer patients [57].

MDM2 as an oncoprotein and a major negative regulator of the p53 pathway possesses the function of activating the

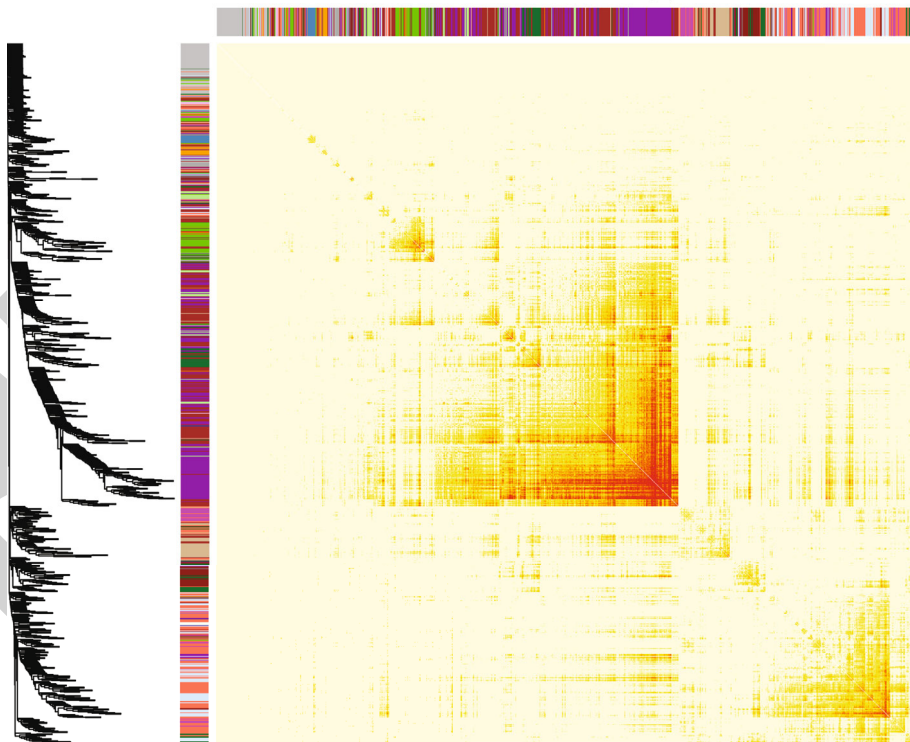
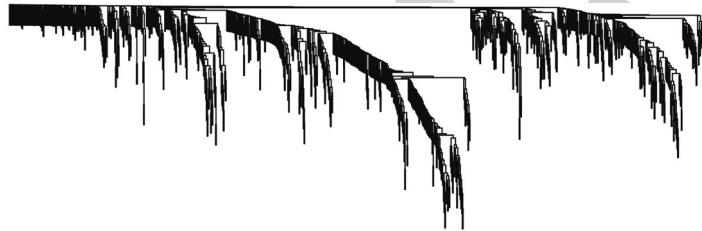
p53 target gene and target p53 protein for the degradation of proteasome. A previous study proved that chromatin-bound MDM2 also plays the p53-independent role to control the transcriptional genes associated in cell fate and metabolism [58]. MDM2 also presented the function of promoting degradation for ubiquitination and proteasomal dependence of wild-type p53, which is the regulator associated with cell cycle, senescence, apoptosis, DNA repair, and angiogenesis-related pathways. Xing et al. found that TNFAIP8 can regulate p53, MDM2, and cyclin D1 to induce cell proliferation and tumor growth in NSCLC [59]. The cyclin-dependent kinase inhibitor 1A (CDKN1A) gene is reported associated with drug (e.g., gefitinib) resistance and regulated the cell cycle in cancer, as its function of involving cell differentiation, DNA repair, and apoptosis. Besides, CDKN1A's activities are closely related to p53 status. For example, when p53 lost mutate function, CDKN1A overexpression will induce cells to present the aggressive phenotype to avoid cell block, senescence, and apoptosis. In Zamagni et al.'s study, it found that CDKN1A is an oncogene which can inhibit apoptosis and promote cancer cell proliferation, so it is used as a response indicator of NSCLC chemotherapy; the regulation of CDKN1A is a potential therapy to reverse the acquisition of resistance to drug such as gefitinib. What is more, for KRAS- and TP53-mutated NSCLC, CDKN1A also can be used as a predictive biomarker of response [60–62].

ID belongs to the helix-loop-helix (HLH) transcription factor family, was known as the inhibitor of differentiation/DNA-binding, and reported that it is involved in tumorigenesis, angiogenesis, and invasiveness. The ID family includes four members: ID1, ID2, ID3, and ID4. ID family member proteins contributed to proliferation, invasion, differentiation, metastasis, apoptosis, and angiogenesis in various human cancers; they may provide new targets and biomarkers for the treatment and prognosis of lung cancer



(a)

Network heat map plot, selected genes



(b)

FIGURE 3: Continued.

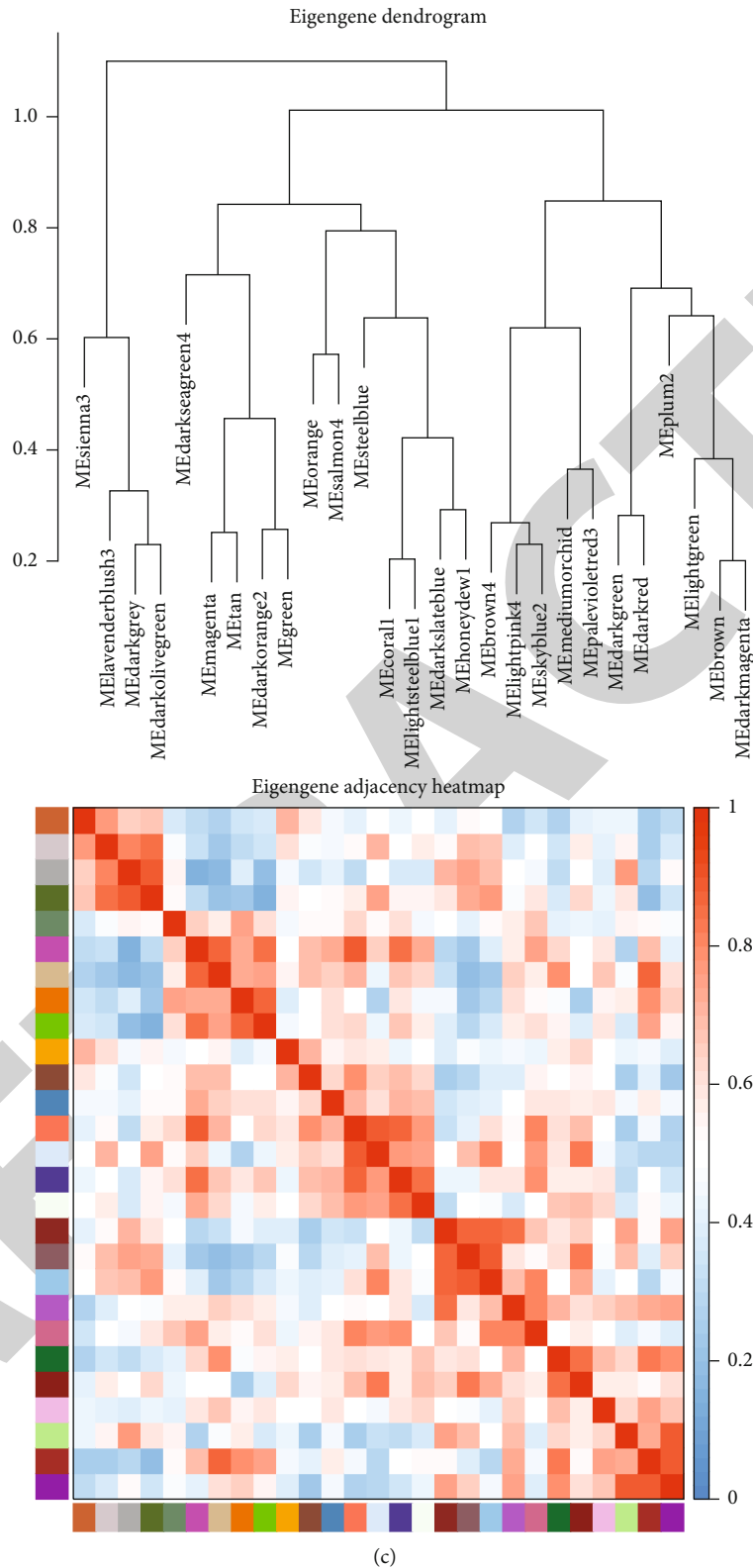


FIGURE 3: Estimation of soft-thresholding values, network heat map plot, and clustered correlation. (a) Scale independence and mean connectivity, power of  $\beta = 7$  (scale free  $R^2 = 0.9$ ). (b) The topological overlap heat map of coexpression genes summarized the interaction relationship of selected genes. Each module is represented by different colors. The brightness of yellow and red represented the high connectivity of modules. (c) Module eigengene dendrogram and eigengene adjacency heat map presented the relationship of the modules generated by the clustering analysis.



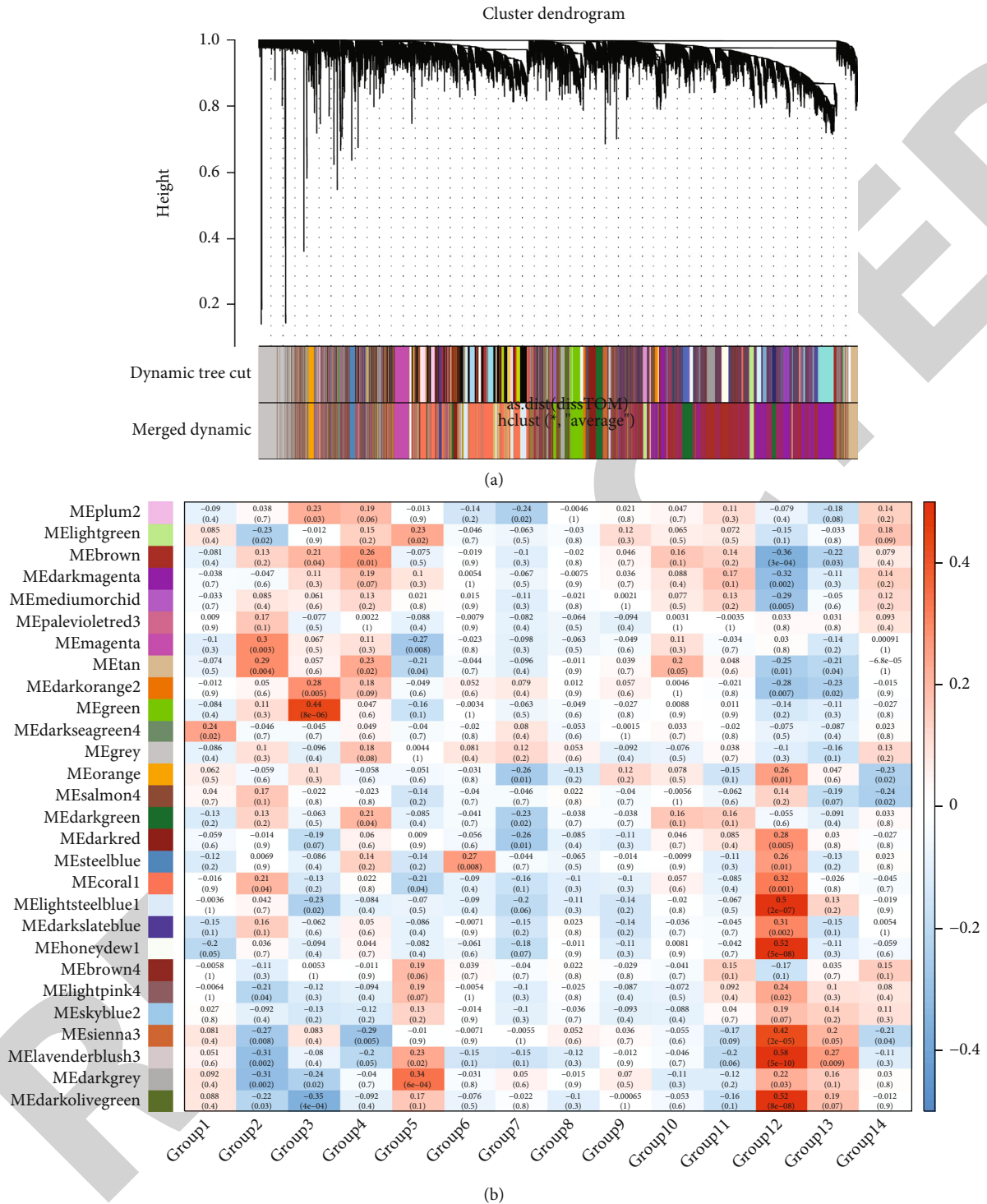
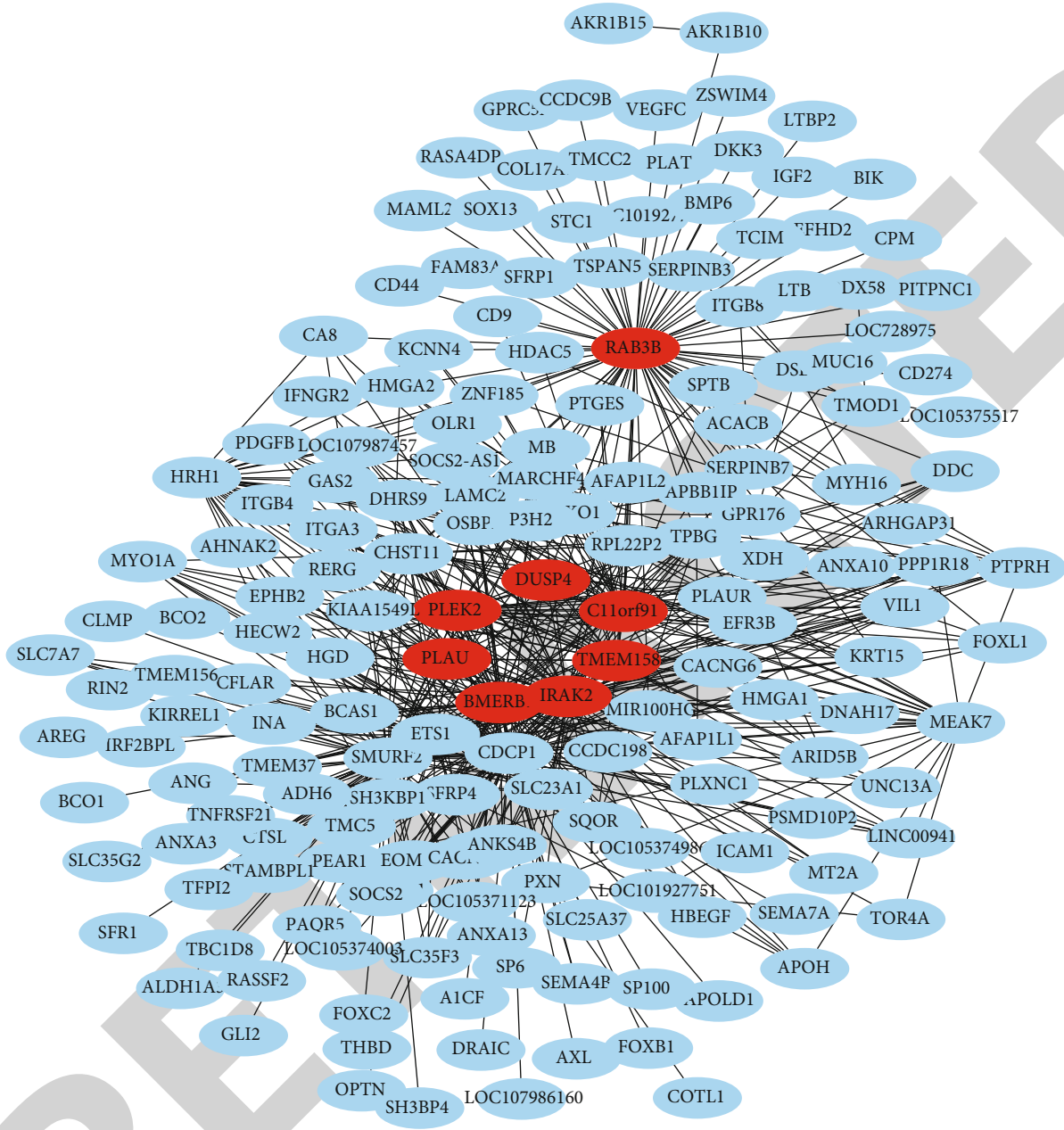


FIGURE 4: The gene set enrichment analysis and the identification of modules. (a) Dendrogram of dissimilarity between all filtered gene sets, which enriched according to a dissimilarity measure (1-TOM), and the cluster modules were marked as different colors. Dynamic tree cut algorithm generated the first set, then merged the correlated modules together. Each gene was represented by a branch, and each module was represented by one color. (b) Heat map of the correlation between the pharmaceutical effect of TCM fractions and MEs in NSCLC. The dark degree of the module color represented the significance of their relationship.

[63–65]. In this study, we found ID1, ID2, and ID4 present significant differences; they may be involved in the physiological activity of NSCLC cells. There are plenty of evidences to support it: Rollin et al. found that ID2 may be developed as

the biomarker for the prognosis of poorly differentiated tumors as it is associated with dedifferentiation [5]; Li et al. demonstrated that ID1 may activate the NF-kappa B signaling pathway to promote the process of proliferation,



(a)

FIGURE 5: Continued.

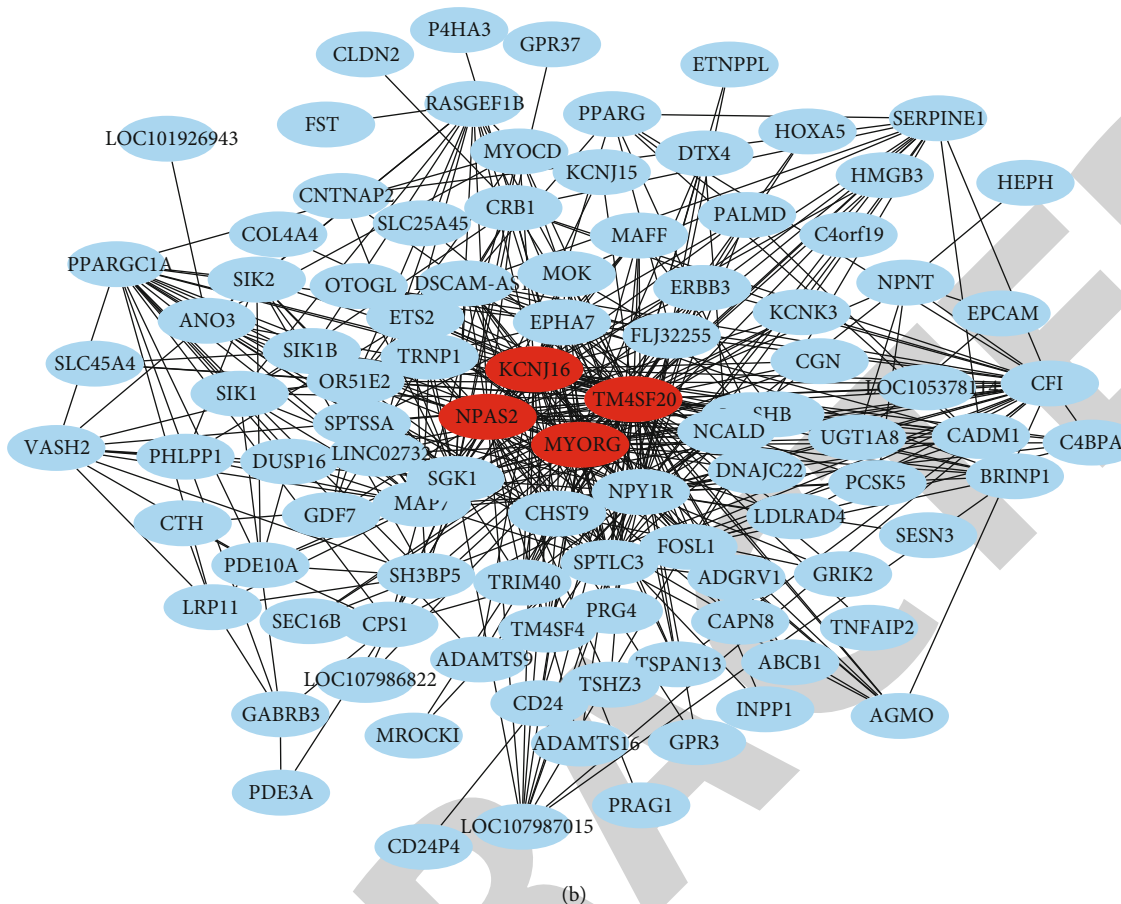


FIGURE 5: The coexpression network. (a) The coexpression network of the significant genes in the green module, including 132 nodes. (b) The coexpression network of the significant genes in the darkgrey module, including 81 nodes. The hub genes were represented in red color.

migration, and invasion in NSCLC cells [66]; Qi et al. found that ID4 impacted on the p38 MAPK pathway to inhibit cisplatin-induced apoptosis [67]. These two pathways also were proved very important in NSCLC in our study.

**3.4. Coexpression Network Constructing and Significant Modules Identifying.** In order to investigate the connectivity between the pharmaceutical effect of TCM fractions and module eigengene (ME), the “WGCNA” R package has been applied to construct weighted coexpressed networks and identify coexpression modules. In this research, the power of  $\beta = 7$  (scale free  $R^2 = 0.9$ ) was set to ensure low mean connectivity and high scale independence (Figure 3(a)), setting the dissimilarity of modules as 0.2 and generating 27 modules in total (Figure 4(a)). The module trait relationship is shown in Figure 4(b), and group 3, group 5, and group 12 were exhibited higher connectivity in several modules. Group 3 and group 5 were treated with TCM; group 12 was treated with conventional anticancer drugs (positive control). In TCM groups, the colors of green and darkgrey modules were the deepest; it suggested that it is suitable to identify the hub genes from these two modules which may be associated with the staging of cancer. The interaction relationship of 27 modules is shown in Figure 3(b); it indicated a high-scale independence and differential gene expressions between the

modules as all the modules were independent with each other. 27 modules enriched into five clusters based on the eigengene adjacency heat map (Figure 3(c)).

**3.5. Hub Gene Identification in the Selected Modules.** Generally, genes included in the coexpression modules and with high connectivity were selected as hub genes. In this study, 12 hub genes (8 in green module and 4 in darkgrey module) were obtained (Figure 5, Supplemental Table 7). Among them, PLAU and DUSP4 were the common genes identified by differential analysis. What is more, PLAU was included in the MAPK signaling pathway and DUSP4 was in the NF-kappa B signaling pathway; both of them were identified as the key pathways in KEGG analysis. The edges signifying the correlations in the green module were filtered by the criteria that weight value  $> 0.13$ ; then, a total of 132 nodes were identified after importing to Cytoscape (Figure 5(a), Supplemental Table 6). Meanwhile, darkgrey module was filtered by a condition of the weight value  $> 0.06$ ; 81 nodes were identified (Figure 5(b), Supplemental Table 7).

## 4. Discussion and Conclusions

Guangxi Botanical Garden of Medicinal Plants (Nanning, China) has collected and conserved various plant species

belonging to different families including Euphorbiaceae (*Ricinus*, *Mallotus*, *Euphorbia*, etc.), Araliaceae (*Panax*), Asteraceae (*Acmella*, *Arctium*, *Gynura*, etc.), Fabaceae, Malvaceae, and Solanaceae. There are almost 78 kinds of fractions (Supplemental Table 1) with remarkable medical effect, including promoting blood circulation and removing stasis; heat-clearing; rheumatism treatment; hemostatic; tonic; asthmatics, expectorants, and antitussives; water-disinhibiting and damp-percolating; Qi-regulating; heat-clearing astringent; and detoxifying, analgesia, antipruritic, etc. Some of the plant materials with potential anticancer effects were analyzed in previous studies, such as *Senecio scandens*, *Breynia fruticosa*, *Salvia miltiorrhiza* Bunge, *Gynura procumbens*, *Euphorbia hirta*, *Forsythia suspensa*, *Senecio scandens*, *Polygonum perfoliatum*, *Malva verticillata* var. *crispa*, *Mallotus apelta*, *Pteris semipinnata*, *Acmella paniculate*, *Aristolochia tagala*, *Schisandra chinensis*, *Gelsemium elegans*, and *Ligustrum confusum* [46, 47, 68–71]. Most of them were found to contain anticancer compounds like terpenoid, flavonoid, alkaloid, quercetin, epigallocatechin-3-gallate (EGCG), epicatechin, oleanolic acid, ursolic acid, and tanshinone, which are involved in multiple important pathways in cancers such as epithelial to mesenchymal transition (EMT), TGF- $\beta$ , PTEN/PI3K/Akt, NF-kappa B, MAPK, p53 signaling pathway, and Wnt/ $\beta$ -catenin pathway [72–75].

Some pathways which are mainly enriched by the TCM play an important role in cancer. Mitogen-activated protein kinase (MAPK) plays a crucial role in cellular signal transduction pathways as it involved not only cell proliferation, differentiation, and apoptosis but also the deregulation of cancer [76]. MAPK dysregulation may cause various cancer formations, including lungs, breast, oral, colorectal, ovarian, and thyroid [77]. It will improve the effectiveness of drugs through targeting MAPK pathways which contributed to conventional anticancer drugs [78]. The nuclear factor  $\kappa$ B (NF-kappa B) complex was constructed from a family which induced transcription factors and can be found in almost all cells. Some inflammatory cytokine genes are IL-6, IL-8, and TNF- $\alpha$ ; their expression would be improved by activating NF-kappa B [79]. It proved that NF-kappa B is involved in the initiation and progression of inflammation tumor tissues [80]; it even presented the function of harmonizing the key endogenous tumor promoter and inflammation. In addition to promoting tumor cell growth, NF-kappa B also activated the relative elements such as adhesion molecules, inflammatory cytokines, and angiogenic factors which expedited the cell proliferation in cancer [81, 82]. The NF-kappa B pathway has been regarded as the inflammation-mediated pathways, as it presented the capacity of escaping the apoptosis to cause emergency resistance to chemotherapy therapy [83].

p53 is one of the most intensive tumor suppressor proteins, and TP53 is reported as the most commonly mutated gene in human cancer, and the mutations induced the high expression of mutant p53 proteins. Previous genomic studies indicated that the function of p53 was compromised by its altfrequency in different cancer cell lines [84]. The development of most cancers required perturbations in p53 signaling pathways; more and more evidences indicated that restored

or reactivated function of p53 will benefit to cancer therapy [85]. The p53 signaling pathway is the key pathway involved in cell division, cell proliferation, and signal transduction in NSCLC; Tu et al. proved it via comparative analysis of 221 DEGs and constructing the PPI network [86]. Transforming Growth Factor beta (TGF-beta) is a tumor-suppressive factor in early stage tumors, as aberrant activation of TGF-beta will induce angiogenesis, invasion, immunosuppression, and self-renewal of cancer-initiating [87]. TGF-beta is associated with poor prognosis and aggressive disease progression in NSCLC, as its ability of driving cell proliferation, metastasis, angiogenesis, emergence of drug resistance, and immune evasion. Some processes such as lung organogenesis, tissue remodeling after lung injury, and postnatal lung homeostasis all required the attendance of TGF-beta [54]; it is the reason why it has been reported as one of the most commonly indispensable and activated pathways in the metastasis process of various cancers. Particularly, activating TGF- $\beta$  signaling induced progression and metastasis in NSCLC [54, 87, 88].

In this research, we provide the better understanding and evidence to support the exploration of anticancer potential of the natural ingredient from TCM. Based on our results, we can probe the interaction between medicinal plant ingredients and NSCLC cells, to explore the differential gene activation mechanisms for pharmacodynamic substances to identify medicinal compositions and action mechanisms. Furthermore, we will be able to not only identify novel makers and screen out NSCLC therapeutic targets but also develop new natural drug groups against lung cancer, bringing new ideas for the development of new methods to screen out new drugs.

## Data Availability

The clean sequence reads and analysis results in the study were deposited in the Sequence Read Archive (SRA) database of the National Center for Biotechnology Information (NCBI).

## Conflicts of Interest

The authors declare no conflict of interest.

## Authors' Contributions

YL and JM conceived this study. ML, XY, LY, QK, ZX, SW, and DM performed the experiments. YP and LK performed the bioinformatics analyses, LK wrote the manuscript, and YD edited the manuscript. All authors read and approved the final manuscript. Ling Kui and Min Li have contributed equally to this work and share first authorship.

## Acknowledgments

This work was supported by the grants from the Key Project of TCM Modernization Research (2019YFC1711000), Jiangsu University (No. 20JDG47), and Guangxi Science and Technology Research Project (GuiKeAA18242040 and GuiKeAD17129044).



## Supplementary Materials

The provided supplementary file includes the seven supplementary tables. Supplemental Table 1 Description of samples and classification. Supplemental Table 2 Summary of RNA-seq data quality control. Table 3 RNA-seq data statistics. Supplemental Table 4 Differential gene expression. Supplemental Table 5 Pathway results of traditional Chinese medicine and positive control. Supplemental Table 6 The efficacy and representative compounds of samples. Supplemental Table 7 Hub gene list. (*Supplementary Materials*)

## References

- [1] H. Sung, J. Ferlay, R. L. Siegel et al., "Global Cancer Statistics 2020: GLOBOCAN estimates of incidence and mortality worldwide for 36 cancers in 185 countries," *CA: a Cancer Journal for Clinicians*, vol. 71, no. 3, pp. 209–249, 2021.
- [2] M. Arnold, M. J. Rutherford, A. Bardot et al., "Progress in cancer survival, mortality, and incidence in seven high-income countries 1995–2014 (ICBP SURVMARK-2): a population-based study," *The Lancet Oncology*, vol. 20, no. 11, pp. 1493–1505, 2019.
- [3] R. S. Herbst, D. Morgensztern, and C. Boshoff, "The biology and management of non-small cell lung cancer," *Nature*, vol. 553, no. 7689, pp. 446–454, 2018.
- [4] Y. Li, L. Zhao, P. Zhao, and Z. Liu, "Long non-coding RNA LINC00641 suppresses non-small-cell lung cancer by sponging miR-424-5p to upregulate PLSCR4," *Cancer Biomarkers*, vol. 26, no. 1, pp. 79–91, 2019.
- [5] J. Rollin, C. Blechet, S. Regina, A. Tenenhaus, S. Guyetant, and X. Gidrol, "The intracellular localization of ID2 expression has a predictive value in non small cell lung cancer," *PLoS One*, vol. 4, no. 1, article e4158, 2009.
- [6] C. Zappa and S. A. Mousa, "Non-small cell lung cancer: current treatment and future advances," *Transl Lung Cancer Res*, vol. 5, no. 3, pp. 288–300, 2016.
- [7] T. Hata, H. Rajabi, H. Takahashi et al., "MUC1-C activates the NuRD complex to drive dedifferentiation of triple-negative breast cancer cells," *Cancer Research*, vol. 79, no. 22, pp. 5711–5722, 2019.
- [8] M. Ezzati, B. Yousefi, K. Velaei, and A. Safa, "A review on anti-cancer properties of quercetin in breast cancer," *Life Sciences*, vol. 248, p. 117463, 2020.
- [9] T. Hata, H. Rajabi, M. Yamamoto et al., "Targeting MUC1-C inhibits TWIST1 signaling in triple-negative breast cancer," *Molecular Cancer Therapeutics*, vol. 18, no. 10, pp. 1744–1754, 2019.
- [10] N. Harbeck and M. Gnant, "Breast cancer," *The Lancet*, vol. 389, no. 10074, pp. 1134–1150, 2017.
- [11] D. Zhao, J. P. Hamilton, G. M. Pham et al., "De novo genome assembly of *Campotheca acuminata*, a natural source of the anti-cancer compound camptothecin," *Gigascience*, vol. 6, no. 9, pp. 1–7, 2017.
- [12] L. Caputi, J. Franke, S. C. Farrow et al., "Missing enzymes in the biosynthesis of the anticancer drug vinblastine in Madagascar periwinkle," *Science*, vol. 360, no. 6394, pp. 1235–1239, 2018.
- [13] E. B. Khalid, E. E. Ayman, H. Rahman, G. Abdelkarim, and A. Najda, "Natural products against cancer angiogenesis," *Tumour Biology*, vol. 37, no. 11, pp. 14513–14536, 2016.
- [14] S. Xing, Y. Wang, K. Hu, F. Wang, T. Sun, and Q. Li, "WGCNA reveals key gene modules regulated by the combined treatment of colon cancer with PHY906 and CPT11," *Bioscience Reports*, vol. 40, no. 9, 2020.
- [15] S. L. Robinson, J. K. Christenson, and L. P. Wackett, "Biosynthesis and chemical diversity of  $\beta$ -lactone natural products," *Natural Product Reports*, vol. 36, no. 3, pp. 458–475, 2019.
- [16] J. A. Beutler, "Natural products as a foundation for drug discovery," *Current Protocols in Pharmacology*, vol. 46, no. 1, 2009.
- [17] R. A. S. T. S. F. M. S. A. D. R. N. I. Y. O. T.-K. O. K. C. C. A. A. F., "Natural products are the future of anticancer therapy: pre-clinical and clinical advancements of *Viscum album* phytometabolites," *Cell Mol Biol*, vol. 61, no. 6, pp. 62–68, 2015.
- [18] S. Goyal, N. Gupta, S. Chatterjee, and S. Nimesh, "Natural plant extracts as potential therapeutic agents for the treatment of cancer," *Current Topics in Medicinal Chemistry*, vol. 17, no. 2, pp. 96–106, 2017.
- [19] J. Cao, "Joint profiling of chromatin accessibility and gene expression in thousands of single cells," *Science*, vol. 361, no. 6409, pp. 1380–1385, 2018.
- [20] Z. Wang, M. Gerstein, and M. Snyder, "RNA-Seq: a revolutionary tool for transcriptomics," *Nature Reviews. Genetics*, vol. 10, no. 1, pp. 57–63, 2009.
- [21] D. Carrella, I. Manni, B. Tumaini et al., "Computational drugs repositioning identifies inhibitors of oncogenic PI3K/AKT/P70S6K-dependent pathways among FDA-approved compounds," *Oncotarget*, vol. 7, no. 37, pp. 58743–58758, 2016.
- [22] S. Chen, B. B. Lake, and K. Zhang, "High-throughput sequencing of the transcriptome and chromatin accessibility in the same cell," *Nature Biotechnology*, vol. 37, no. 12, pp. 1452–1457, 2019.
- [23] X. Yang, L. Kui, M. Tang et al., "High-throughput transcriptome profiling in drug and biomarker discovery," *Frontiers in Genetics*, vol. 11, p. 19, 2020.
- [24] Y.-H. Cheng, Y.-C. Chen, E. Lin et al., "Hydro-Seq enables contamination-free high-throughput single-cell RNA-sequencing for circulating tumor cells," *Nature Communications*, vol. 10, no. 1, p. 2163, 2019.
- [25] Y. Wei, M. Li, S. Cui et al., "Shikonin inhibits the proliferation of human breast cancer cells by reducing tumor-derived exosomes," *Molecules*, vol. 21, no. 6, p. 777, 2016.
- [26] X. Liu, A. X. Hu, J. L. Zhao, and F. L. Chen, "Identification of key gene modules in human osteosarcoma by co-expression analysis weighted gene co-expression network analysis (WGCNA)," *Journal of Cellular Biochemistry*, vol. 118, no. 11, pp. 3953–3959, 2017.
- [27] C. Clarke, S. F. Madden, P. Doolan et al., "Correlating transcriptional networks to breast cancer survival: a large-scale coexpression analysis," *Carcinogenesis*, vol. 34, no. 10, pp. 2300–2308, 2013.
- [28] Y. Luo, D. Shen, L. Chen et al., "Identification of 9 key genes and small molecule drugs in clear cell renal cell carcinoma," *Aging*, vol. 11, no. 16, pp. 6029–6052, 2019.
- [29] F. F. Liu, T. T. Tu, H. F. Zhang et al., "Coexpression network analysis of platelet genes in sickle cell disease," *Platelets*, vol. 30, no. 8, pp. 1022–1029, 2019.
- [30] J. W. Liang, Z. Y. Fang, Y. Huang et al., "Application of weighted gene co-expression network analysis to explore the key genes in Alzheimer's disease," *Journal of Alzheimer's Disease*, vol. 65, no. 4, pp. 1353–1364, 2018.

- [31] C. Chen, L. Cheng, K. Grennan, F. Pibiri, C. Zhang, and J. A. Badner, "Two gene co-expression modules differentiate psychotics and controls," *Molecular Psychiatry*, vol. 18, no. 12, pp. 1308–1314, 2013.
- [32] R. Jia, H. Zhao, and M. Jia, "Identification of co-expression modules and potential biomarkers of breast cancer by WGCNA," *Gene*, vol. 750, p. 144757, 2020.
- [33] M. Niemira, F. Collin, A. Szalkowska et al., "Molecular signature of subtypes of non-small-cell lung cancer by large-scale transcriptional profiling: identification of key modules and genes by weighted gene co-expression network analysis (WGCNA)," *Cancers (Basel)*, vol. 12, no. 1, 2020.
- [34] J.-D. Wang, H.-S. Zhou, X.-X. Tu et al., "Prediction of competing endogenous RNA coexpression network as prognostic markers in AML," *Ageing*, vol. 11, no. 10, pp. 3333–3347, 2019.
- [35] Y. Di, D. Chen, W. Yu, and L. Yan, "Bladder cancer stage-associated hub genes revealed by WGCNA co-expression network analysis," *Hereditas*, vol. 156, no. 1, p. 7, 2019.
- [36] J. Qian, J. Yang, X. Liu et al., "Analysis of lncRNA-mRNA networks after MEK1/2 inhibition based on WGCNA in pancreatic ductal adenocarcinoma," *Journal of Cellular Physiology*, vol. 235, no. 4, pp. 3657–3668, 2020.
- [37] S. W. Wingett and S. Andrews, "FastQ Screen: a tool for multi-genome mapping and quality control," *F1000Research*, vol. 7, 2018.
- [38] X. T. Xie, A. M. Kropinski, B. Tapscott, J. S. Weese, and P. V. Turner, "Prevalence of fecal viruses and bacteriophage in Canadian farmed mink (*Neovison vison*)," *Microbiology*, vol. 8, no. 1, article e00622, 2019.
- [39] R. T. K. Poluri, C. J. Beauparlant, A. Droit, and E. Audet-Walsh, "RNA sequencing data of human prostate cancer cells treated with androgens," *Data in Brief*, vol. 25, p. 104372, 2019.
- [40] D. Kim, B. Langmead, and S. L. Salzberg, "HISAT: a fast spliced aligner with low memory requirements," *Nature Methods*, vol. 12, no. 4, pp. 357–360, 2015.
- [41] M. Pertea, G. M. Pertea, C. M. Antonescu, T. C. Chang, J. T. Mendell, and S. L. Salzberg, "StringTie enables improved reconstruction of a transcriptome from RNA-seq reads," *Nature Biotechnology*, vol. 33, no. 3, pp. 290–295, 2015.
- [42] A. C. Frazee, G. Pertea, A. E. Jaffe, B. Langmead, S. L. Salzberg, and J. T. Leek, "Ballgown bridges the gap between transcriptome assembly and expression analysis," *Nature Biotechnology*, vol. 33, no. 3, pp. 243–246, 2015.
- [43] C. Chen, H. Chen, Y. Zhang et al., "TBtools: an integrative toolkit developed for interactive analyses of big biological data," *Molecular Plant*, vol. 13, no. 8, pp. 1194–1202, 2020.
- [44] G. Su, J. H. Morris, B. Demchak, and G. D. Bader, "Biological network exploration with Cytoscape 3," *Current Protocols in Bioinformatics*, vol. 47, no. 1, 2014.
- [45] Z. Zhou, R. Cao, D. Hu, and J. Liu, "Characterization of the complete plastid genome sequence of *Breynia fruticosa* (L.) Mull.Arg. (Phyllanthaceae), a traditional Chinese medicine plant," *Mitochondrial DNA B Resour*, vol. 5, no. 3, pp. 3510–3511, 2020.
- [46] Y. P. Liu, X. H. Cai, T. Feng, Y. Li, X. N. Li, and X. D. Luo, "Triterpene and sterol derivatives from the roots of *Breynia fruticosa*," *Journal of Natural Products*, vol. 74, no. 5, pp. 1161–1168, 2011.
- [47] X. L. He, J. J. Lv, X. Wang et al., "The identification and isolation of anti-inflammatory ingredients of ethno medicine *Breynia fruticosa*," *Journal of Ethnopharmacology*, vol. 239, p. 111894, 2019.
- [48] Z. Sun, L. Chen, Q. Liu et al., "Effects of dietary *Senecio scandens* buch-ham extracts on growth performance, plasma biochemical, histology and the expression of immune-related genes in hybrid grouper (*Epinephelus lanceolatus* ♂ × *Epinephelus fuscoguttatus* ♀)," *Fish & Shellfish Immunology*, vol. 98, pp. 681–690, 2020.
- [49] D. Wang, L. Huang, and S. Chen, "*Senecio scandens* Buch-Ham.: a review on its ethnopharmacology, phytochemistry, pharmacology, and toxicity," *Journal of Ethnopharmacology*, vol. 149, no. 1, pp. 1–23, 2013.
- [50] J. Yu, M. Hu, Y. Wang, Q. Zhang, W. Xu, and W. Su, "Extraction, partial characterization and bioactivity of polysaccharides from *Senecio scandens* Buch.-Ham.," *International Journal of Biological Macromolecules*, vol. 109, pp. 535–543, 2018.
- [51] A. Carey, D. K. Edwards, C. A. Eide et al., "Identification of interleukin-1 by functional screening as a key mediator of cellular expansion and disease progression in acute myeloid leukemia," *Cell Reports*, vol. 18, no. 13, pp. 3204–3218, 2017.
- [52] G. Cavalli, S. Colafrancesco, G. Emmi et al., "Interleukin 1 $\alpha$ : a comprehensive review on the role of IL-1 $\alpha$  in the pathogenesis and treatment of autoimmune and inflammatory diseases," *Autoimmunity Reviews*, vol. 20, no. 3, p. 102763, 2021.
- [53] S. Subat, K. Inamura, H. Ninomiya, H. Nagano, S. Okumura, and Y. Ishikawa, "Unique microRNA and mRNA interactions in EGFR-mutated lung adenocarcinoma," *Journal of Clinical Medicine*, vol. 7, no. 11, p. 419, 2018.
- [54] F. Stappenbeck, F. Wang, L. Y. Tang, Y. E. Zhang, and F. Parhami, "Inhibition of Non-Small Cell Lung Cancer Cells by Oxy210, an Oxysterol-Derivative that Antagonizes TGF $\beta$  and Hedgehog Signaling," *Cell*, vol. 8, no. 10, 2019.
- [55] J. M. Balko, L. J. Schwarz, N. E. Bhola et al., "Activation of MAPK pathways due to DUSP4 loss promotes cancer stem cell-like phenotypes in basal-like breast cancer," *Cancer Research*, vol. 73, no. 20, pp. 6346–6358, 2013.
- [56] M. Chen, J. Zhang, A. H. Berger et al., "Compound haploinsufficiency of Dok2 and Dusp4 promotes lung tumorigenesis," *The Journal of Clinical Investigation*, vol. 129, no. 1, pp. 215–222, 2019.
- [57] D. Chitale, Y. Gong, B. S. Taylor et al., "An integrated genomic analysis of lung cancer reveals loss of DUSP4 in EGFR-mutant tumors," *Oncogene*, vol. 28, no. 31, pp. 2773–2783, 2009.
- [58] G. Arena, M. Y. Cissé, S. Pyrdziak et al., "Mitochondrial MDM2 regulates respiratory complex I activity independently of p53," *Molecular Cell*, vol. 69, no. 4, pp. 594–609.e8, 2018.
- [59] Y. Xing, Y. Liu, T. Liu et al., "TNFAIP8 promotes the proliferation and cisplatin chemoresistance of non-small cell lung cancer through MDM2/p53 pathway," *Cell Communication and Signaling: CCS*, vol. 16, no. 1, p. 43, 2018.
- [60] A. Zamagni, A. Pasini, F. Pirini et al., "CDKN1A upregulation and cisplatin-pemetrexed resistance in non-small cell lung cancer cells," *International Journal of Oncology*, vol. 56, no. 6, pp. 1574–1584, 2020.
- [61] T. Xu, S. Yan, M. Wang et al., "LncRNA UCA1 induces acquired resistance to gefitinib by epigenetically silencing CDKN1A expression in non-small-cell lung cancer," *Frontiers in Oncology*, vol. 10, p. 656, 2020.
- [62] E. Siebring-van Olst, M. Blijlevens, R. X. de Menezes, I. H. van der Meulen-Muileman, E. F. Smit, and V. W. van Beusechem, "A genome-wide siRNA screen for regulators of tumor suppressor p53 activity in human non-small cell lung cancer cells identifies components of the RNA splicing machinery as



## Research Article

# A Potential ceRNA Network for Neurological Damage in Preterm Infants

Jin Huang , Xuejing Liang, and Zhenyu Cai 

Department of Obstetrics and Gynecology, Aviation General Hospital of China Medical University, Beijing, China

Correspondence should be addressed to Zhenyu Cai; [cai415419@163.com](mailto:cai415419@163.com)

Jin Huang and Xuejing Liang contributed equally to this work.

Received 13 May 2021; Revised 5 July 2021; Accepted 3 August 2021; Published 23 August 2021

Academic Editor: Yuzhen Xu

Copyright © 2021 Jin Huang et al. This is an open access article distributed under the Creative Commons Attribution License, which permits unrestricted use, distribution, and reproduction in any medium, provided the original work is properly cited.

**Objective.** This study is aimed at identifying key genes involved in neurological damage in preterm infants and at determining their potential circRNA-miRNA-mRNA regulatory mechanisms. **Methods.** Differentially expressed miRNAs, mRNAs, and circRNAs were downloaded from the GEO database. GO and KEGG enrichment analyses were used to determine possible relevant functions of differentially expressed mRNAs. The TTRUST database was used to predict differential TF-mRNA regulatory relationships. Then, CircMIR, miRDB, TargetScan and miRTarBase were then used to map circRNA/miRNA-TF/mRNA interaction networks. Finally, GSEA enrichment analysis was performed on the core transcription factors. **Results.** A total of 640 mRNAs, 139 circRNAs, and 206 differentially expressed miRNAs associated with neurological injury in preterm infants were obtained. Based on the findings of Cytoscape and PPI network analysis, the *hsa\_circ\_0008439-hsa-mir-3665-STAT3-MMP3* regulatory axis was established. GSEA analysis revealed that suppressed expression levels of STAT3 were associated with upregulated oxidative phosphorylation pathways in the neurological injury group of preterm infants. **Conclusions.** The circRNA-miRNA-TF-mRNA regulatory network of neurological injury in preterm infants can be used to elucidate on the pathogenesis of brain injury and help us with the early detection of brain injury in preterm infants.

## 1. Introduction

Infants born at less than 37 weeks of gestational age are referred to as premature and often have a birth weight of less than 2500 g. Due to the immaturity of their systemic organs, they are far more likely to suffer from complications when compared to full-term babies, especially neurological damage [1]. About 10% of preterm infants may have varying degrees of motor impairments [2] while about 25-50% present with cognitive impairments [3], visual and auditory impairments [4], and social behaviour, attention, and learning deficits [5, 6]. With advances in medical technology, the survival rates of preterm babies have significantly increased; however, incidences of neurological complications have not exhibited a proportional decrease [7]. Moreover, mechanisms involved in the development of neurological damage in preterm infants have not been elucidated. Studies have evaluated the roles of inflammatory factors [8], oxidative stress [9], and

the amino acid accumulation [10], in the molecular mechanisms of neurological damage; however, findings have not been conclusive. Therefore, elucidation of the molecular mechanisms involved in neurological damage in preterm infants will inform the development of appropriate diagnostic and therapeutic options.

miRNAs, as noncoding RNAs, act by targeting proteins [11] and are involved in disease development through the ceRNA mechanism [12]. Sequenced peripheral blood of pregnant mothers of preterm infants was found to exhibit differences in expressions of 164 miRNAs, compared to full-term infants [13]. miRNAs regulate protein expression levels mainly by targeting with mRNAs. Analysis of placental tissues from preterm infants revealed a number of mRNAs that are associated with brain damage [14]. Another similar study sequenced fetal placental tissue, grouped according to the presence or absence of cognitive impairment, found 117 differentially expressed mRNAs and identified significantly

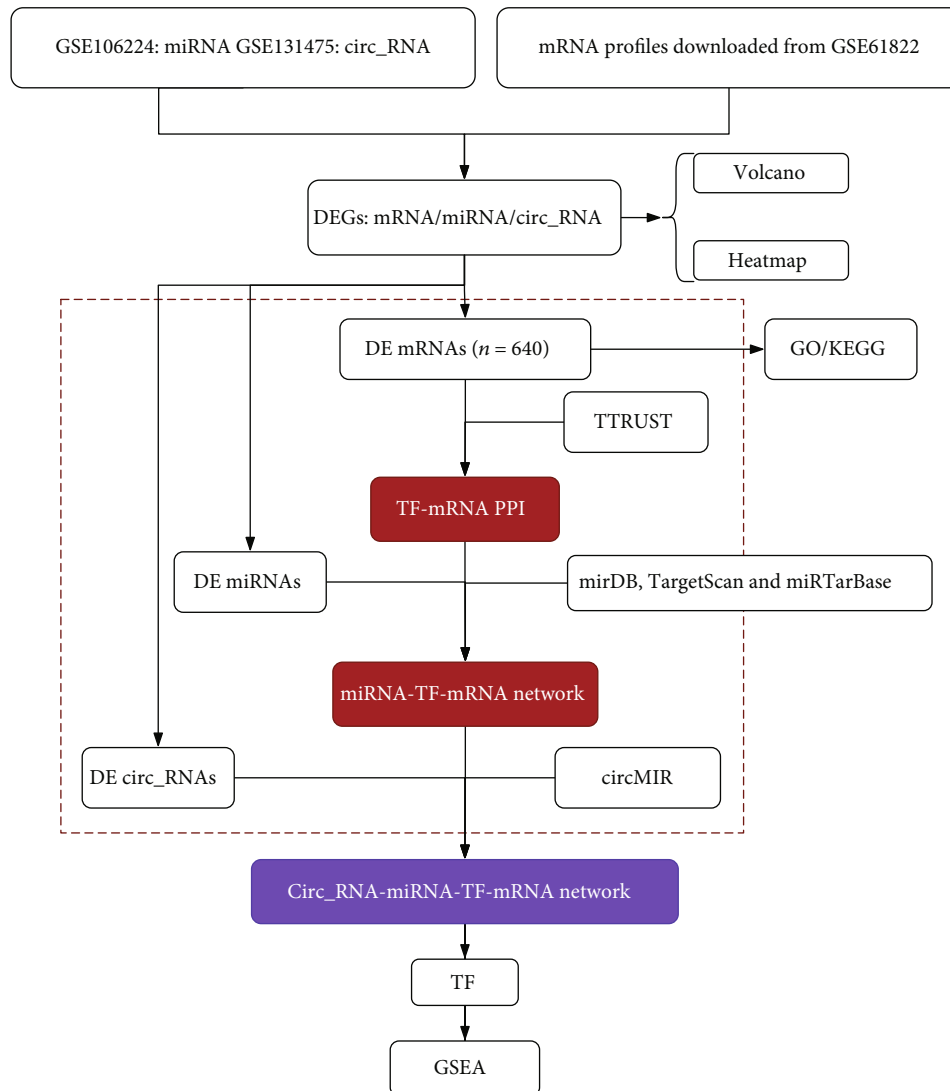


FIGURE 1: Schematic presentation of the analysis process.

affected pathways including oxidative phosphorylation, Parkinson's disease, and Alzheimer's disease [15]. In addition to its targeted regulatory relationship with mRNA, miRNA can also form ceRNA, circRNA-miRNA-mRNA, or a competitive binding miRNA mechanism of circRNA-miRNA-lncRNA to mRNA and genes including circRNA and lncRNA, which is thought to play an important role in biological behaviour. Comparisons of peripheral blood circRNA sequencing data from patients with premature ventricular white matter injury revealed 119 differentially expressed circRNAs, with the same preliminary construction of a miRNA-circRNA network [16]. The above studies revealed differential genetic changes during brain injury among preterm infants, with the exact mechanisms being unclear.

Therefore, we downloaded three datasets from the GEO database, including one mRNA dataset (GSE61822), one miRNA dataset (GSE106224), and one circRNA dataset (GSE131475). Using the downloaded datasets, we used bioin-

formatics approaches to explore the probable molecular mechanisms of neurological damage in preterm infants.

## 2. Methods

**2.1. Data Download and Preprocessing.** Gene expression transcriptomic microarray data for chorioamniotic membrane samples of placental tissue in preterm infants with and without neurological impairment, along with the corresponding clinically relevant information data, were downloaded from GSE61822 [15]. Peripheral blood miRNA expression data for pregnant women who had and for those who did not have preterm labour were obtained from the GSE106224 dataset [13]. The miRNA expression matrix of peripheral blood between the two groups and the corresponding clinical information was downloaded collated from the GSE106224 dataset. The GSE131475 dataset was used to compare circRNA expression levels in peripheral blood of

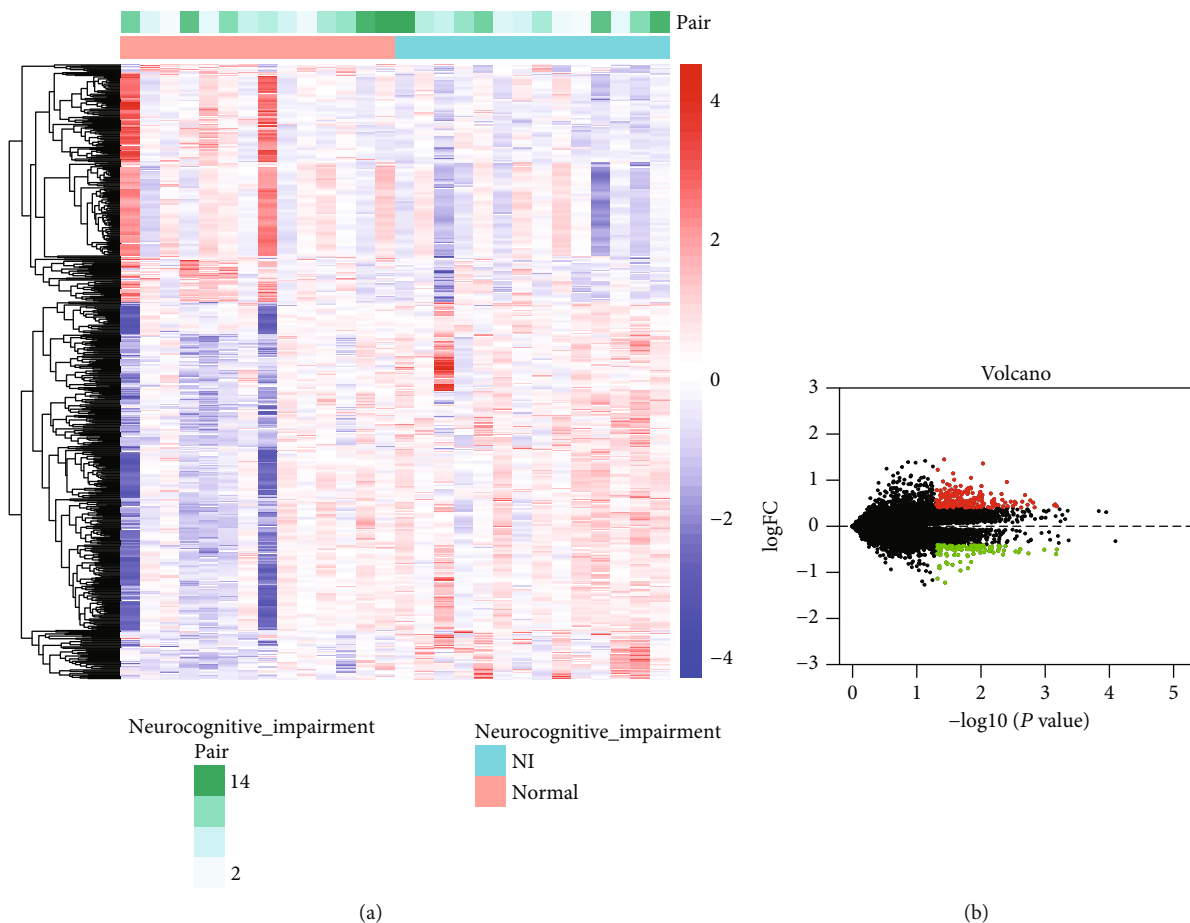


FIGURE 2: mRNA differential analysis and volcano plot results. (a) Heat map showing differential mRNA expression levels between the neurological impairment group and the normal group. (b) Volcano plot showing fold differences in gene expression between the two groups and  $p$  value relationship for the significance test. Red represents upregulated expression, and blue/green represents downregulated gene expression.

preterm infants with periventricular white matter damage (PWMD) and without damage. [16].

**2.2. Analysis of Variances.** Based on the microarray platform file, the mRNA microarray gene IDs were converted to gene symbol and further logarithmically transformed to obtain the mRNA gene expression matrix. Based on paired information from clinical samples, a moderated paired  $t$ -test was performed on the mRNA expression matrix using the limma package based on paired information from clinical samples [17]. The thresholds,  $p < 0.05$  and  $|\log_2FC| > 0.3$  ( $FC > 1.35$ ), were used to filter differentially expressed mRNAs between the two groups. To obtain differentially expressed miRNAs and a corrected miRNA expression matrix, differential analysis of miRNA expression matrix was performed using the edgeR package [18]. For the circRNA expression matrix of GSE131475 dataset, samples with more than 80% missing values were excluded, and circRNAs with missing values were deleted. The collated expression matrix was log-transformed after which the limma package was used to analyze the differences between the two groups based on the paired information of the clinical samples. Filtering of differentially expressed miRNAs and circRNAs expression

between the two groups was performed at the threshold of  $p < 0.05$  and  $FC > 1.5$ .

Heat mapping of differentially expressed mRNAs, miRNAs, and circRNAs was, respectively, performed using pheatmap and gplots packages. Plot function in the base package was applied to make a volcano plot on the above variance expressions.

**2.3. Enrichment Analysis.** Based on up- and downregulated differentially expressed mRNA transcripts, functional GO and KEGG pathways enrichment analyses were performed for up- and downregulated genes, respectively. Enrichment analysis and drawing of bar graphs of GO and KEGG pathways were performed using the org.Hs.eg.db package and clusterProfiler [19]. The pathways were filtered at  $p < 0.05$ .

**2.4. TF-mRNA Network Construction.** The TF-mRNA relationship pair data were downloaded from the TTRUST database. Findings of the RNA differential analysis were intersected with the TF and corresponding mRNAs in the relationship pairs to obtain differential TF-mRNA regulatory relationship pairs. Mulberry mapping of differential TF-mRNA relationships was performed using the ggalluvial and ggplot2 packages.

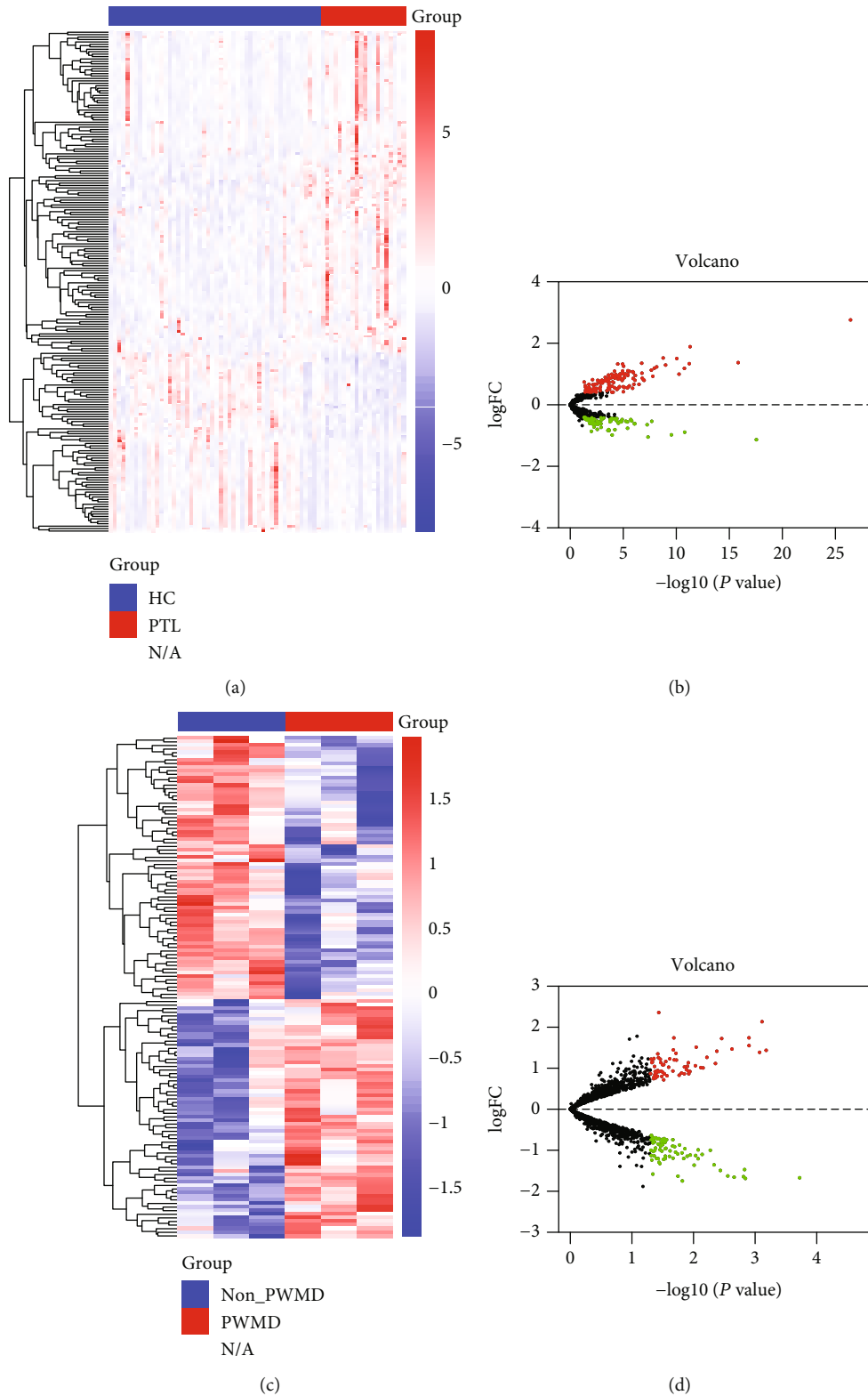
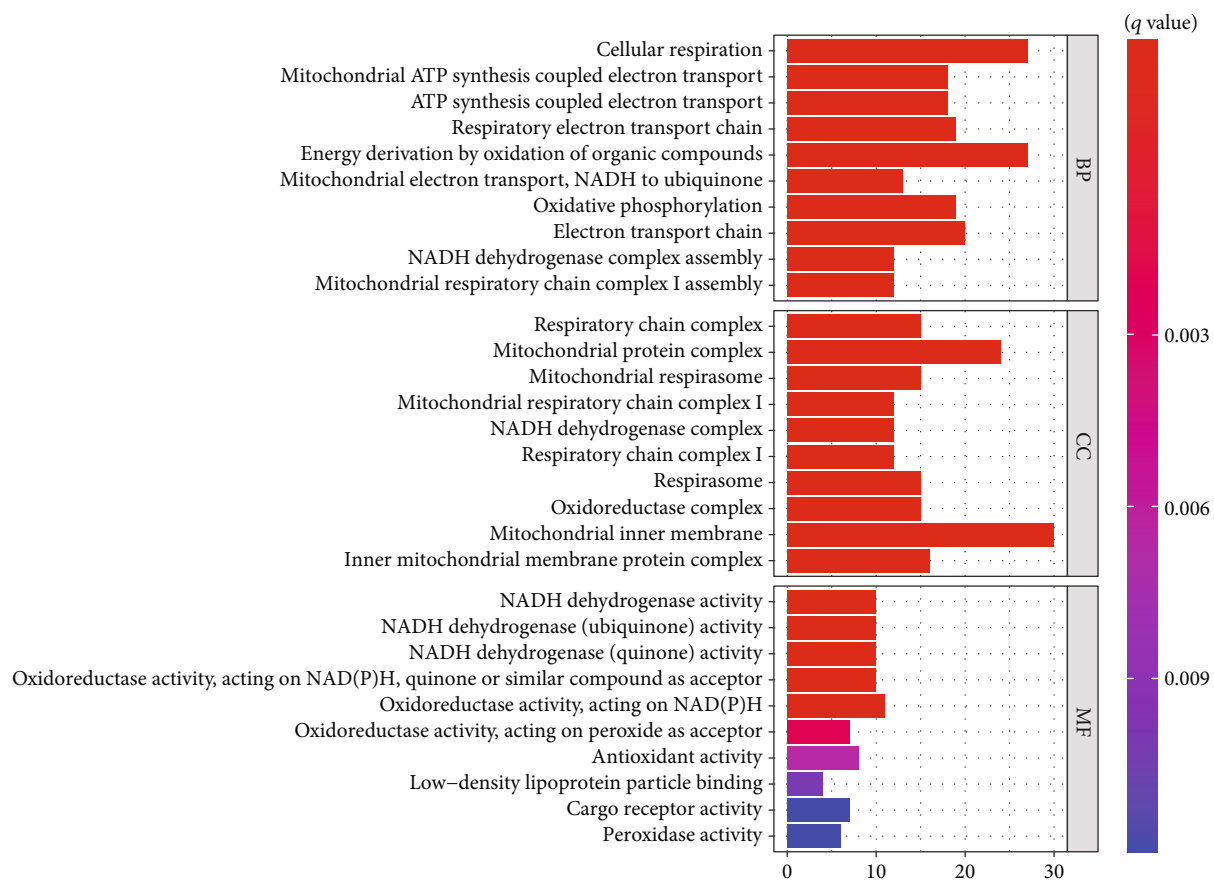


FIGURE 3: Results of differential analysis and volcano plot for miRNA and circRNA. (a) Heat map showing differences in miRNA expression levels in the peripheral blood of mothers in the normal delivery group and in the preterm group. (b) Volcano plot showing fold differences in miRNA expression levels between the two groups and the  $p$  value. (c) Heat map showing differences in circRNA expression in the peripheral blood of mothers in the two groups, with and without periventricular white matter injury. (d) Volcano plot showing fold differences in circRNA expression levels between the two groups.



(a)

FIGURE 4: Continued.

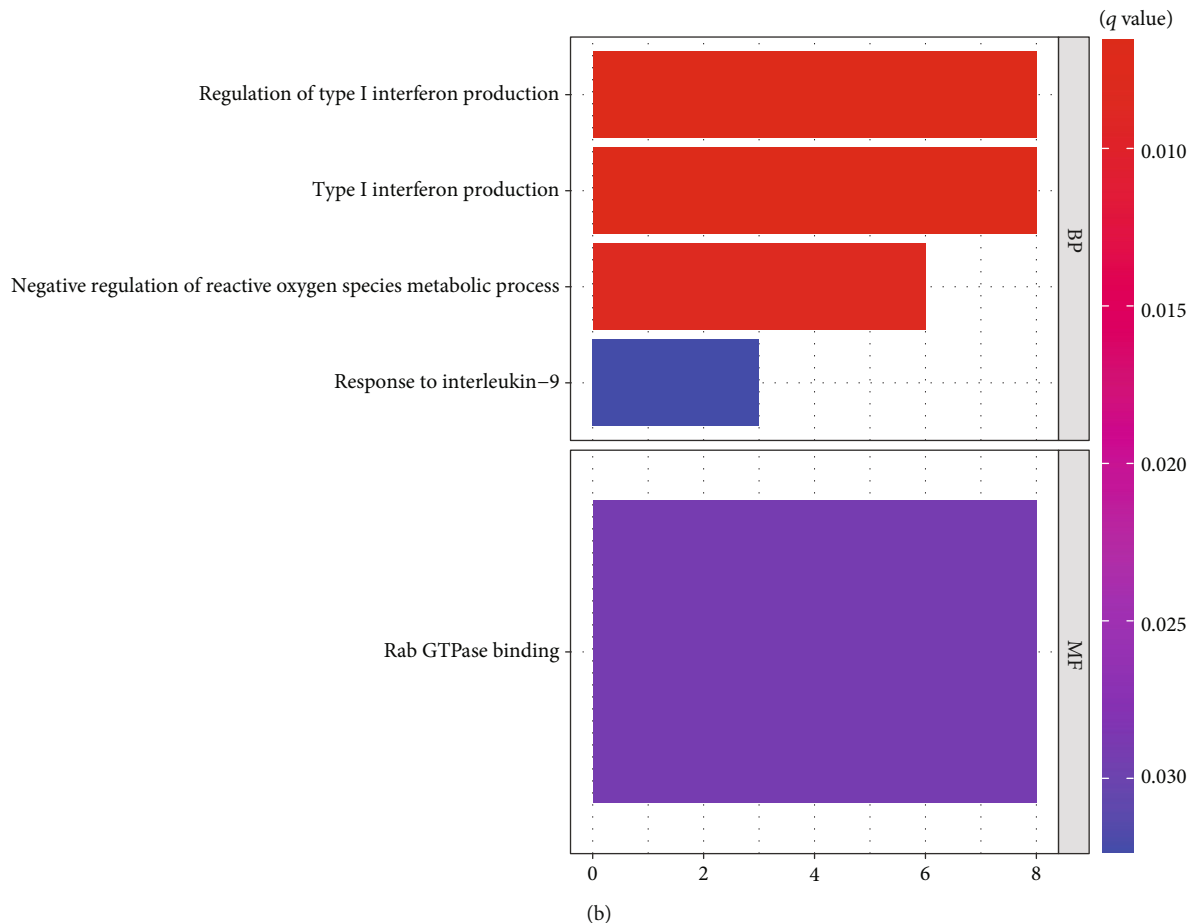


FIGURE 4: GO enrichment analysis of differential mRNA in preterm infants with and without neurological impairment. (a) GO enrichment pathways that were upregulated in placental tissues in the presence of neurological impairment. (b) GO enrichment pathways that were downregulated in placental tissues in the presence of neurological impairment. (c) GO enrichment pathways that were upregulated in placental tissue in the presence of neurological impairment.

### 2.5. Construction of miRNA-TF-mRNA Regulatory Network.

The miRNA-mRNA regulatory relationship pairs were downloaded from the miRDB database (<http://mirdb.org/>), TargetScan database ([http://www.targetscan.org/vert\\_72/](http://www.targetscan.org/vert_72/)), and miRTarBase (<https://mirtarbase.cuhk.edu.cn/>) ([php/index.php](http://php/index.php)). The intersection was used to select the differentially expressed miRNAs and the corresponding target mRNAs that were present in the miRNA differential analysis results of the relationship pairs. Then, target mRNAs of differentially expressed miRNAs were intersected with the TF and mRNAs of the TF-mRNAs that had been constructed in the previous step. Then, the final miRNA-TF-mRNA regulatory relationship network was obtained.

### 2.6. Prediction of circRNA and miRNA Relationships.

The miRNAs in the miRNA-TF-mRNA network obtained in the previous step and the differentially expressed circRNAs obtained from the differential analysis were predicted one by one using the CircMIR ([http://www.bioinf.com.cn/?page\\_id=10](http://www.bioinf.com.cn/?page_id=10)) software. Using miRanda (<http://www.microrna.org/microrna/getDownloads.do>) and RNAhybrid (<https://bibiserv.cebitec.uni-bielefeld.de/rnahybrid/>) algorithms, the

corresponding predictions were calculated for each pair of action relations, and the results are presented as circle plots.

### 2.7. Construction of circRNA-miRNA-TF-mRNA Interaction Network.

The Cytoscape (version 3.8.2) software was used to map the circRNA-miRNA-TF-mRNA regulatory network. The MCODE plugin (degree cutoff = 2, node score cutoff = 0.2, k-core = 2, and max.depth = 100) was also applied in the establishment of core genes and subnetworks in the network. Based on their enrichment scores, the top two core subnetworks were selected for presentation and subsequent analysis based on their enrichment scores.

### 2.8. GSEA Gene Set Functional Enrichment Analysis.

Based on the core subnetwork obtained, the TF factors within it were selected and used to construct the circRNA-miRNA-TF-mRNA axis that may be important in the regulation of neurological impairment. The selected core TF was analyzed using the GSEA software (version 4.1.0). Then, the selected gene sets "c2.cp.kegg.v7.4.symbols.gmt" were used for pathway enrichment annotation.



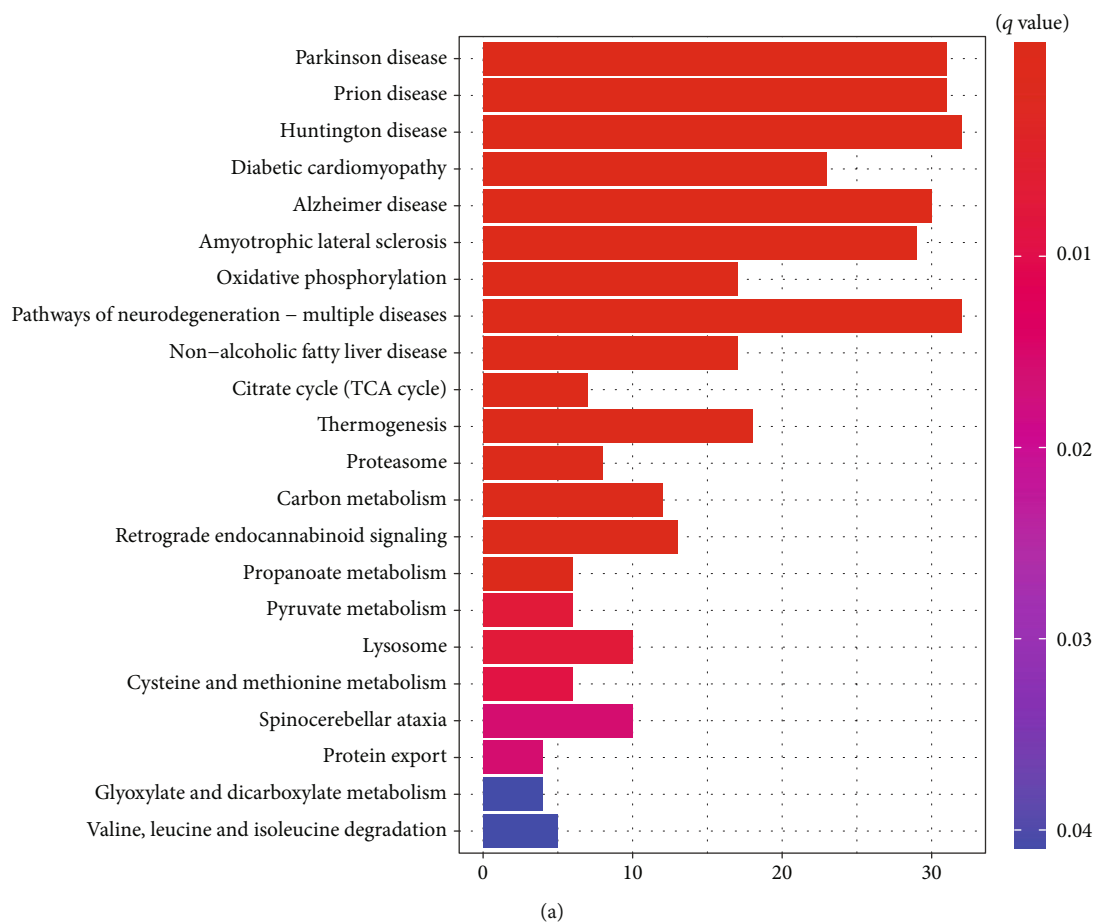


FIGURE 5: Continued.

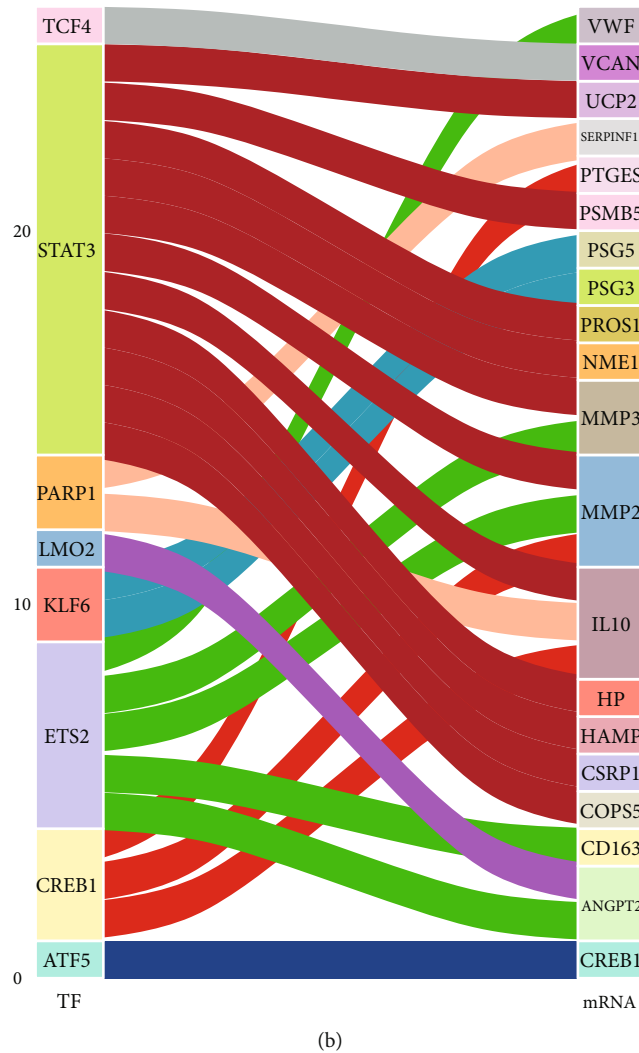


FIGURE 5: (a) KEGG enrichment analysis of differential mRNA in preterm infants with and without neurological impairment. KEGG enrichment pathways were found to be upregulated in the neurological impairment group. No downregulated enrichment pathways were found. (b) A Sankey diagram showing the predicted differential TF-mRNA regulatory relationships according to the TTRUST database.

### 3. Results

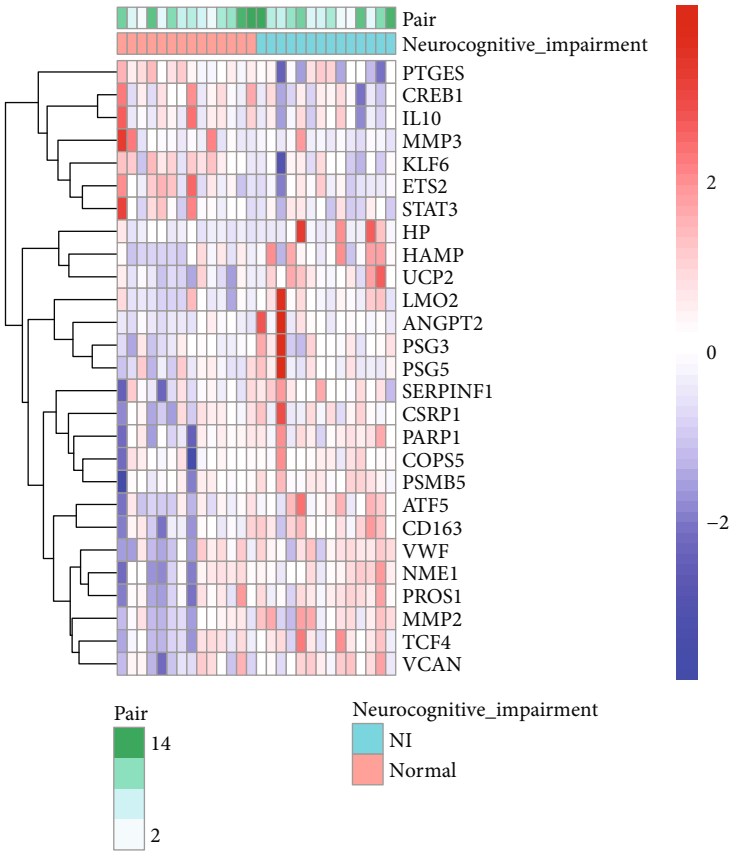
A schematic presentation of this study is shown in Figure 1. The three datasets were used for the differential analysis of mRNA, miRNA, and circRNA, while the circRNA-miRNA-TF-mRNA network was constructed based on the results of database interactions.

**3.1. Data Download.** A total of 28 placental tissue transcriptomic data and the corresponding clinical information for preterm infants were downloaded from the GSE61822 dataset for preterm infants. Fourteen of these cases were associated with neurological impairments while and the other 14 were not. Peripheral blood miRNA expression matrices for 20 preterm and 50 nonpreterm pregnant women were downloaded from the GSE106224 dataset for miRNA analysis. circRNA expression data files for six

preterm infants were downloaded from the GSE131475 dataset. Three of them had PWMD while the other three did not.

**3.2. Variance Analysis.** Results of mRNA differential expression analysis are shown in Figure 2. A total of 640 differentially expressed mRNAs were obtained by filtering at  $p < 0.05$  and  $\text{FoldChange} > 1.35$ . Results of miRNA and circRNA differential analysis are shown in heat and volcano plots (Figure 3), filtered by  $p < 0.05$  and  $\text{FoldChange} > 1.5$  to obtain 206 DE miRNAs and 139 DE circRNAs, respectively.

**3.3. Functional Enrichment Analysis.** The GO and KEGG pathways enrichment analyses for differentially expressed mRNA genes were performed. Figure 4 shows GO pathways for up- and downregulated genes. In preterm infants with neurological impairments, five GO pathways with the



(a)

FIGURE 6: Continued.

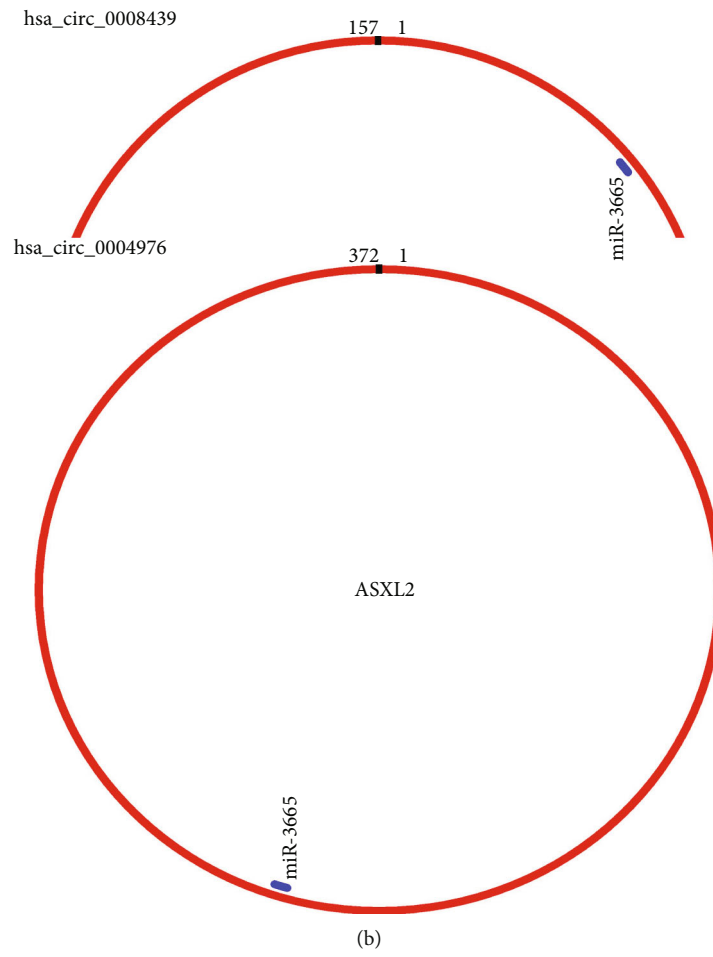


FIGURE 6: Continued.

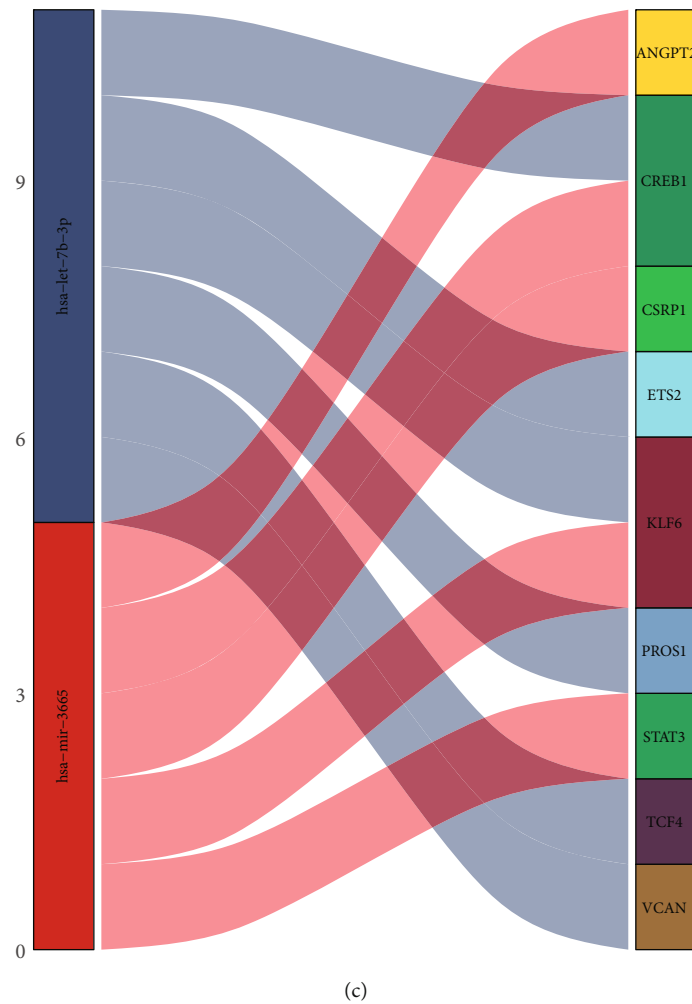


FIGURE 6: Construction of circRNA-miRNA-TF-mRNA regulatory network. (a) Heat map showing expression of individual gene transcripts in the TF-mRNA regulatory network with and without neurological impairment groups with differences. (b) Predicted results of differential miRNA as well as circRNA regulatory relationships according to CircMIR. (c) Results of miRNA and TF and mRNA (containing TF) regulation.

most significant differences in upregulation were “cellular respiration,” “mitochondrial ATP synthesis coupled electron transport,” “ATP synthesis coupled electron transport,” “respiratory electron transport chain,” and “energy derivation by oxidation of organic compounds.” The five GO pathways with most significant differences in down-regulation were “regulation of type I interferon production,” “type I interferon production,” “negative regulation of reactive oxygen species metabolic process,” “response to interleukin-9,” and “Rab GTPase binding.” KEGG pathway analysis (Figure 5(a)) revealed that the five most significant upregulated pathways were the “Parkinson disease,” “Prion disease,” “Huntington disease,” “diabetic cardiomyopathy,” and “Alzheimer disease”.

**3.4. TF-mRNA Action Relationship.** From the TTRUST database, a total of 27 TF-mRNA regulatory pairs were obtained after intersecting with differentially expressed mRNAs. Figure 5(b) shows the relationship between mRNA expression levels of 8 TFs and their target genes. Figure 6(a) shows the expression of individual gene transcripts in the TF-

mRNA regulatory network with and without neurological impairments.

**3.5. miRNA-TF-mRNA Action Relationship.** The miRNA-mRNA regulatory relationships were extracted from the miRDB, TargetScan, and miRTarBase databases. From intersections in the above differential TF-mRNA regulatory network, 2 differential miRNAs and their corresponding target mRNAs (containing TF) were obtained. Figure 6(c) shows the differential miRNA-mRNA/TF regulatory relationship.

**3.6. circRNA-miRNA Relationships.** The CircMIR software and its miRanda and RNAhybrid algorithms were used to predict miRNAs and differentially expressed circRNAs in the above miRNA-mRNA/TF regulatory relationship. Two circRNAs and 1 miRNA were obtained (Figure 6(b)). The corresponding analysis of the forecast results was reported in sup.tab1.

**3.7. Network Construction and Subnetwork Construction.** The Cytoscape software was used to map and construct

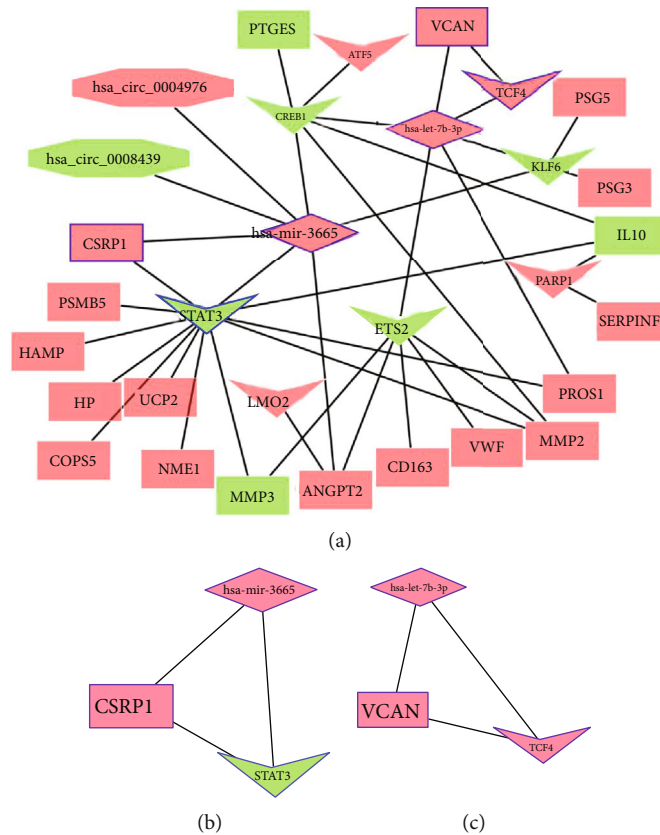


FIGURE 7: Protein interaction networks. (a) circRNA-miRNA-TF-mRNA regulated protein interaction networks. (b, c) Top 2 aggregator network modules predicted from MCODE. Rectangles represent mRNA, inner quadrilateral represents TF, rhombus represents miRNA, and octagon represents circRNA.

the regulatory network for the above regulatory pairs (Figure 7(a)). Further analyses based on MCODE and filtering conditions resulted in 2 subnetworks and core genes (Figures 7(b) and 7(c)).

**3.8. GSEA Enrichment Analysis of Core Genes.** Based on the obtained transcription factor STAT3 in the aggregated subnetwork and the corresponding ceRNA regulatory rules, we constructed the hsa\_circ\_0008439/hsa-mir-3665/STAT3/MMP3 regulatory axis (hsa\_circ\_0008439 and MMP3 were selected because, together with STAT3, they were downregulated in the network and, according to ceRNA rules, are more likely to be within the same regulatory axis) (supplementary table 1). A related regulatory axis was further constructed around hsa-mir-3665/STAT3 (Figure 8(a)). GSEA analysis was performed on high- and low-expressed STAT3. Figure 8(b) shows that STAT3 expression was suppressed in the group of preterm infants with neurological impairments, while the KEGG\_OXIDATIVE\_PHOSPHORYLATION pathway was upregulated ( $p=0.04$ ). This pathway may have a role in regulation of neurofunctional development in preterm infants.

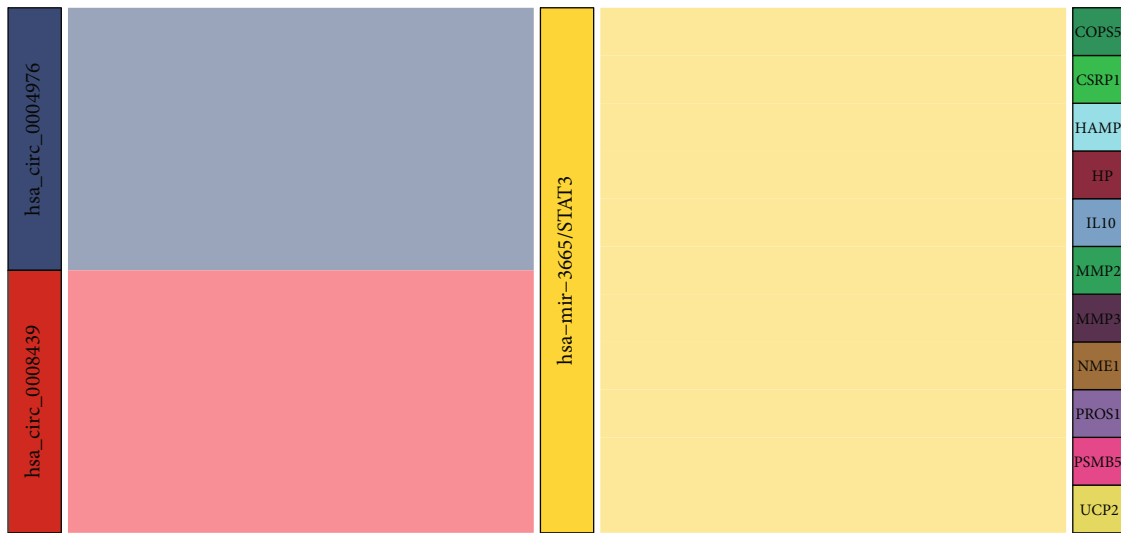
#### 4. Discussion

Due to advances in perinatal medicine, survival outcomes for preterm babies have considerably improved, especially

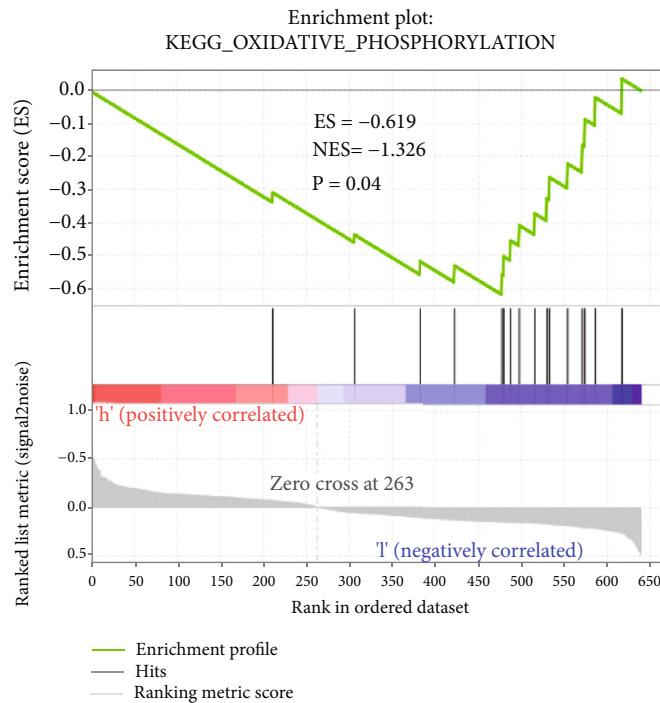
for very early preterm babies. However, not only does late complications of brain injury in preterm babies cause suffering to the child, they also place a great burden on the family and society [20]. Therefore, it is extremely important to establish the molecular mechanisms of brain damage in preterm infants. In addition, most studies nowadays are evaluating the miRNA-mRNA and TF-mRNA regulatory networks, and there are fewer studies on regulatory networks of TF and miRNA. We used the differentially expressed mRNA; miRNA constructs the miRNA-TF/mRNA regulatory network, which we combined with circRNA to synthesize the circRNA-miRNA-TF-mRNA regulatory network. These networks may be helpful in disease diagnosis and treatment.

We identified a total of 640 mRNAs that were differentially expressed in preterm infants with brain injury. The GO and KEGG pathway enrichment analyses of differentially expressed mRNA genes revealed that the five GO pathways that were most significantly differentially upregulated in preterm infants with neurological impairments were “cellular respiration,” “mitochondrial ATP synthesis coupled electron transport,” “ATP synthesis coupled electron transport,” “respiratory electron transport chain,” and “energy derivation by oxidation of organic compounds.” Neural damage in preterm infants were found to be associated with energy metabolism. It has been suggested that the function of the mitochondria is related to that of





(a)



(b)

FIGURE 8: Potential hsa\_circ\_0008439-hsa-mir-3665-STAT3-MMP3 regulatory pathway and enrichment analysis. (a) A Sankey diagram showing the transcription factor, STAT3, in the core genes selected according to the subnetwork, demonstrating the circRNA-STAT3 regulatory network constructed around hsa-mir-3665/STAT3. (b) Results of GSEA enrichment analysis of selected STAT3 transcription factors showing enrichment in the lower STAT3 expression group upon KEGG\_OXIDATIVE\_PHOSPHORYLATION ( $p = 0.04$ ).

the hippocampus [21]. Moreover, reducing energy metabolism suppresses white matter damage in the brain [22]. Five downregulated significant GO pathways were also revealed, including “regulation of type I interferon production,” “type I interferon production,” “negative regulation of reactive oxygen species metabolic process,” “response to interleukin-9,” and “Rab GTPase binding.” These findings show that inflammatory pathways are involved in neurological damage in preterm infants. The KEGG pathway analysis revealed that the five most significantly

upregulated pathways were the “Parkinson disease,” “Prion disease,” “Huntington disease,” “diabetic cardiomyopathy,” and “Alzheimer disease.” Early brain damage in preterm infants is not usually characterized by specific features [23] and is not detectable. The later stages of neurological damage are often more noteworthy. The above results reveal that molecules associated with brain damage in preterm infants are also involved in other neurological disorders; therefore, preterm birth is a risk factor for neurological damage in later life.

For differentially expressed mRNAs, we used the TTRUST database to obtain TF-mRNA, through a classical mode of action, in which we obtained 27 pairs of TF-mRNA regulatory relationship pairs. Combining differentially expressed miRNAs, circRNA, we obtained 2 differentially expressed miRNAs and 9 mRNAs/TFs. Based on one of the miRNAs, miR-3665, circ\_0004976-miR-3665, and miR-3665-ASXL2 regulatory axes were achieved. One of the key molecules in the aforementioned regulatory axis, miR-3665, which is associated with neurocognitive function in addition to tumour development, is involved in the development of neurological functions [24]. miR-3665 targets the regulatory protein, ASXL2, which can link various histamine modifying enzymes and link transcription factors to specific genetic loci by encoding a series of epistatic regulators [25]. This gene plays an important role in neurological development, cardiac function, adipogenesis, and cell formation [26]. Therefore, miR-3665 may be an important miRNA molecule that is involved in the mechanism of neurological injury in preterm infants.

Combining the above differentially expressed mRNAs, miRNAs, and circRNAs, PPI network analysis was performed to construct two miRNA-TF-mRNA networks, has-miR-3665-STAT3-CSPR1 and has-let-7b-3p-TCF4-VCAN. It has been reported that let-7b is downregulated in children with autism [27] and that it can target STAT3 and inhibit hippocampal glial cell activation in epilepsy [28]. Regarding its target protein, TCF3 has been found to be involved in neurodevelopment, and it inhibits neuroectodermal differentiation in mice [29]. miR-3665 is closely associated with neurodevelopment, and its target is STAT3, an important transcription factor involved in many biological processes, including neurodevelopment [30]. Therefore, we targeted the transcription factor, STAT3, and combined it with ceRNA regulatory rules to establish the hsa\_circ\_0008439-hsa-mir-3665-STAT3-MMP3 regulatory axis. The final effector, MMP3, accelerates the inflammatory process to promote neurodevelopmental damage. In addition, through GSEA analysis, oxidative phosphorylation was found to be upregulated in low-expression STAT3. Oxidative phosphorylation is associated with neurological damage and is involved in the development of various neurological disorders [31–33]. From the above findings, we identified molecular mechanisms regulating the hsa\_circ\_0008439-hsa-mir-3665-STAT3-MMP3 axis that may be associated with neurological damage in preterm infants. However, given the complexity of the regulatory network, further in vitro and in vivo experiments are needed to validate its possible regulatory mechanisms as a novel diagnostic marker. Experimental validation will elucidate on the mechanisms involved in neurological damage in preterm infants and provide a theoretical basis for disease diagnosis and treatment.

## 5. Conclusion

We identified 620 mRNAs, 206 miRNAs, and 139 circRNAs that are differentially expressed in preterm infants with neurological injury. Based on regulatory network

analysis, two key has-miR-3665 and has-let-7b-3p were derived. Coregulatory relationship of hsa\_circ\_0008439-hsa-mir-3665-STAT3-MMP3 was derived in conjunction with the key transcription factor, STAT3. However, this study has some limitations. The small sample size of this study was subject to significant sampling error, and therefore, the sample size should be expanded in future studies to increase data credibility. Besides, this study is also limited by the lack of experimental validation of the regulatory relationships and functions of the above key genes. It is clear that the complexity of the regulatory mechanisms does not allow for direct clinical use of regulatory axes we have identified for diagnosis and treatment but requires more practical support from in vivo and ex vivo experiments.

## Data Availability

Raw data and codes are available on request from the corresponding author.

## Conflicts of Interest

There are no potential conflicts of interest.

## Authors' Contributions

Jin Huang and Xuejing Liang contributed equally to this work.

## Supplementary Materials

Table S1: hsa-miR-3665 vs. hsa\_circ\_0008439. (*Supplementary Materials*)

## References

- [1] L. Liu, S. Oza, D. Hogan et al., "Global, regional, and national causes of under-5 mortality in 2000-15: an updated systematic analysis with implications for the Sustainable Development Goals," *The Lancet*, vol. 388, no. 10063, pp. 3027–3035, 2016.
- [2] A. Spittle, J. Orton, P. J. Anderson, R. Boyd, and L. W. Doyle, "Early developmental intervention programmes provided post hospital discharge to prevent motor and cognitive impairment in preterm infants," *Cochrane Database of Systematic Reviews*, vol. 11, article CD005495, 2015.
- [3] A. T. Bhutta, M. A. Cleves, P. H. Casey, M. M. Cradock, and A. KJS, "Cognitive and behavioral outcomes of school-aged children who were born preterm: a meta-analysis," *Journal of the American Medical Association*, vol. 288, no. 6, pp. 728–737, 2002.
- [4] M. Hirvonen, R. Ojala, P. Korhonen et al., "Visual and hearing impairments after preterm birth," *Pediatrics*, vol. 142, no. 2, article e20173888, 2018.
- [5] M. Peralta-Carcelen, J. Schwartz, and A. C. Carcelen, "Behavioral and socioemotional development in preterm children," *Clinics in Perinatology*, vol. 45, no. 3, pp. 529–546, 2018.
- [6] S. E. Berger, R. T. Harbourne, and C. L. Guallpa Lliguichuzhca, "Sit still and pay attention! Trunk movement and attentional resources in infants with typical and delayed development,"

- Physical & Occupational Therapy in Pediatrics*, vol. 39, no. 1, pp. 48–59, 2019.
- [7] D. Wilson-Costello, H. Friedman, N. Minich, A. A. Fanaroff, and M. Hack, “Improved survival rates with increased neurodevelopmental disability for extremely low birth weight infants in the 1990s,” *Pediatrics*, vol. 115, no. 4, pp. 997–1003, 2005.
- [8] J. P. Boardman, G. Ireland, G. Sullivan et al., “The cerebrospinal fluid inflammatory response to preterm birth,” *Frontiers in Physiology*, vol. 9, p. 1299, 2018.
- [9] O. Baud, A. E. Greene, J. Li, H. Wang, J. J. Volpe, and P. A. Rosenberg, “Glutathione peroxidase-catalase cooperativity is required for resistance to hydrogen peroxide by mature rat oligodendrocytes,” *The Journal of Neuroscience*, vol. 24, no. 7, pp. 1531–1540, 2004.
- [10] I. Paine, J. E. Posey, C. M. Grochowski et al., “Paralog Studies Augment Gene Discovery: *DDX* and *DHX* Genes,” *American Journal of Human Genetics*, vol. 105, no. 2, pp. 302–316, 2019.
- [11] A. Freischmidt, A. Goswami, K. Limm et al., “A serum microRNA sequence reveals fragile X protein pathology in amyotrophic lateral sclerosis,” *Brain*, vol. 144, no. 4, pp. 1214–1229, 2021.
- [12] Y. Tay, J. Rinn, and P. P. Pandolfi, “The multilayered complexity of ceRNA crosstalk and competition,” *Nature*, vol. 505, no. 7483, pp. 344–352, 2014.
- [13] S. Fallen, D. Baxter, X. Wu et al., “Extracellular vesicle RNAs reflect placenta dysfunction and are a biomarker source for preterm labour,” *Journal of Cellular and Molecular Medicine*, vol. 22, no. 5, pp. 2760–2773, 2018.
- [14] S. K. Tilley, R. M. Joseph, K. C. K. Kuban, O. U. Dammann, T. M. O’Shea, and R. C. Fry, “Genomic biomarkers of prenatal intrauterine inflammation in umbilical cord tissue predict later life neurological outcomes,” *PLoS One*, vol. 12, no. 5, article e0176953, 2017.
- [15] A. Pappas, T. Chaiworapongsa, R. Romero et al., “Transcriptomics of maternal and fetal membranes can discriminate between gestational-age matched preterm neonates with and without cognitive impairment diagnosed at 18-24 months,” *PLoS One*, vol. 10, no. 3, article e0118573, 2015.
- [16] L. Qiao, S. Mo, Y. Zhou et al., “Circular RNA expression alteration in whole blood of premature infants with periventricular white matter damage,” *Genomics*, vol. 112, no. 4, pp. 2875–2885, 2020.
- [17] M. E. Ritchie, B. Phipson, D. Wu et al., “limma powers differential expression analyses for RNA-sequencing and microarray studies,” *Nucleic Acids Research*, vol. 43, no. 7, p. e47, 2015.
- [18] M. D. Robinson, D. J. McCarthy, and G. K. Smyth, “edgeR: a bioconductor package for differential expression analysis of digital gene expression data,” *Bioinformatics*, vol. 26, no. 1, pp. 139–140, 2010.
- [19] G. Yu, L. G. Wang, Y. Han, and Q. Y. He, “clusterProfiler: an R package for comparing biological themes among gene clusters,” *OMICS*, vol. 16, no. 5, pp. 284–287, 2012.
- [20] V. Pierrat, L. Marchand-Martin, S. Marret et al., “Neurodevelopmental outcomes at age 5 among children born preterm: EPIPAGE-2 cohort study,” *BMJ*, vol. 373, p. n741, 2021.
- [21] M. Ramani, K. Miller, J. Brown et al., “Early life supraphysiological levels of oxygen exposure permanently impairs hippocampal mitochondrial function,” *Scientific Reports*, vol. 9, no. 1, p. 13364, 2019.
- [22] K. Wegleiter, M. Hermann, A. Posod et al., “The sigma-1 receptor agonist 4-phenyl-1-(4-phenylbutyl) piperidine (PPBP) protects against newborn excitotoxic brain injury by stabilizing the mitochondrial membrane potential in vitro and inhibiting microglial activation in vivo,” *Experimental Neurology*, vol. 261, pp. 501–509, 2014.
- [23] Z. Niatsetsykaya, S. Sosunov, A. Stepanova et al., “Cyclophilin D-dependent oligodendrocyte mitochondrial ion leak contributes to neonatal white matter injury,” *The Journal of Clinical Investigation*, vol. 130, no. 10, pp. 5536–5550, 2020.
- [24] E. L. Asahchop, S. M. Akinwumi, W. G. Branton, E. Fujiwara, M. J. Gill, and C. Power, “Plasma microRNA profiling predicts HIV-associated neurocognitive disorder,” *AIDS*, vol. 30, no. 13, pp. 2021–2031, 2016.
- [25] H. A. Baskind, L. Na, Q. Ma, M. P. Patel, D. L. Geenen, and Q. T. Wang, “Functional conservation of *Asxl2*, a murine homolog for the *Drosophila* enhancer of trithorax and polycomb group gene *Asx*,” *PLoS One*, vol. 4, no. 3, article e4750, 2009.
- [26] T. Izawa, N. Rohatgi, T. Fukunaga et al., “ASXL2 regulates glucose, lipid, and skeletal homeostasis,” *Cell Reports*, vol. 11, no. 10, pp. 1625–1637, 2015.
- [27] M. Ragusa, M. Santagati, F. Mirabella et al., “Potential associations among alteration of salivary miRNAs, saliva microbiome structure, and cognitive impairments in autistic children,” *International Journal of Molecular Sciences*, vol. 21, no. 17, article 6203, 2020.
- [28] C. L. Han, Y. P. Liu, C. J. Guo et al., “The lncRNA H19 binding to let-7b promotes hippocampal glial cell activation and epileptic seizures by targeting Stat3 in a rat model of temporal lobe epilepsy,” *Cell Proliferation*, vol. 53, no. 8, article e12856, 2020.
- [29] Y. Atlasi, R. Noori, C. Gaspar et al., “Wnt signaling regulates the lineage differentiation potential of mouse embryonic stem cells through Tcf3 down-regulation,” *PLoS Genetics*, vol. 9, no. 5, article e1003424, 2013.
- [30] U. Schmidt-Edelkraut, A. Hoffmann, G. Daniel, and D. Spengler, “Zac1 regulates astroglial differentiation of neural stem cells through Socs3,” *Stem Cells*, vol. 31, no. 8, pp. 1621–1632, 2013.
- [31] S. Wang, B. Li, V. Solomon et al., “Calcium-dependent cytosolic phospholipase A2 activation is implicated in neuroinflammation and oxidative stress associated with ApoE4,” *Molecular Neurodegeneration*, vol. 16, no. 1, p. 26, 2021.
- [32] C. Gu, F. Wang, Y. T. Zhang et al., “Microglial MT1 activation inhibits LPS-induced neuroinflammation via regulation of metabolic reprogramming,” *Aging Cell*, vol. 20, no. 6, article e13375, 2021.
- [33] A. Adlimoghaddam, G. G. Odero, G. Glazner, R. S. Turner, and B. C. Albensi, “Nilotinib improves bioenergetic profiling in brain astroglia in the 3xTg mouse model of Alzheimer’s disease,” *Aging and Disease*, vol. 12, no. 2, pp. 441–465, 2021.

## Retraction

# Retracted: Celastrol Attenuates Learning and Memory Deficits in an Alzheimer's Disease Rat Model

### BioMed Research International

Received 12 March 2024; Accepted 12 March 2024; Published 20 March 2024

Copyright © 2024 BioMed Research International. This is an open access article distributed under the Creative Commons Attribution License, which permits unrestricted use, distribution, and reproduction in any medium, provided the original work is properly cited.

This article has been retracted by Hindawi following an investigation undertaken by the publisher [1]. This investigation has uncovered evidence of one or more of the following indicators of systematic manipulation of the publication process:

- (1) Discrepancies in scope
- (2) Discrepancies in the description of the research reported
- (3) Discrepancies between the availability of data and the research described
- (4) Inappropriate citations
- (5) Incoherent, meaningless and/or irrelevant content included in the article
- (6) Manipulated or compromised peer review

The presence of these indicators undermines our confidence in the integrity of the article's content and we cannot, therefore, vouch for its reliability. Please note that this notice is intended solely to alert readers that the content of this article is unreliable. We have not investigated whether authors were aware of or involved in the systematic manipulation of the publication process.

Wiley and Hindawi regrets that the usual quality checks did not identify these issues before publication and have since put additional measures in place to safeguard research integrity.

We wish to credit our own Research Integrity and Research Publishing teams and anonymous and named external researchers and research integrity experts for contributing to this investigation.

The corresponding author, as the representative of all authors, has been given the opportunity to register their agreement or disagreement to this retraction. We have kept a record of any response received.

### References

- [1] Y. Xiao, X. Wang, S. Wang et al., "Celastrol Attenuates Learning and Memory Deficits in an Alzheimer's Disease Rat Model," *BioMed Research International*, vol. 2021, Article ID 5574207, 11 pages, 2021.

## Research Article

# Celastrol Attenuates Learning and Memory Deficits in an Alzheimer's Disease Rat Model

Yao Xiao, Xifeng Wang, Siyi Wang, Jun Li, Xueyu Xu, Min Wang, Gang Li , and Wei Shen 

Department of Neurology, Wuhan Fourth Hospital, Puai Hospital, Tongji Medical College, Huazhong University of Science and Technology, Wuhan, China

Correspondence should be addressed to Gang Li; [ligang666946@163.com](mailto:ligang666946@163.com) and Wei Shen; [shenwei1971@126.com](mailto:shenwei1971@126.com)

Received 27 February 2021; Revised 19 May 2021; Accepted 8 July 2021; Published 26 July 2021

Academic Editor: Yuzhen Xu

Copyright © 2021 Yao Xiao et al. This is an open access article distributed under the Creative Commons Attribution License, which permits unrestricted use, distribution, and reproduction in any medium, provided the original work is properly cited.

Alzheimer's disease (AD) is a chronic progressive neurodegenerative disorder that is associated with learning, memory, and cognitive deficits. Neuroinflammation and synapse loss are involved in the pathology of AD. Diverse measures have been applied to treat AD, but currently, there is no effective treatment. Celastrol (CEL) is a pentacyclic triterpene isolated from *Tripterygium wilfordii* Hook F that has been shown to enhance cell viability and inhibit amyloid- $\beta$  production induced by lipopolysaccharides *in vitro*. In the present study, the protective effect of CEL on  $A\beta_{25-35}$ -induced rat model of AD was assessed. Our results showed that CEL administration at a dose of 2 mg/kg/day improved spatial memory in the Morris water maze. Further biochemical analysis showed that CEL treatment of intrahippocampal  $A\beta_{25-35}$ -microinjected rats attenuated hippocampal NF- $\kappa$ B activity; inhibited proinflammatory markers, namely, IL-1 $\beta$ , IL-6, and TNF- $\alpha$ ; and upregulated anti-inflammatory factors, such as IL-4 and IL-10. Furthermore, CEL upregulated hippocampal neurexin-1 $\beta$ , neuroligin-1, CA1, and PSD95 expression levels, which may improve synaptic function. Simultaneously, CEL also increased glucose metabolism in  $A\beta_{25-35}$ -microinjected rats. In conclusion, CEL could exert protective effects against learning and memory decline induced by intrahippocampal  $A\beta_{25-35}$  through anti-inflammation, promote synaptic development, and maintain hippocampal energy metabolism.

## 1. Introduction

Alzheimer's disease (AD) is a neurodegeneration disorder that is the most common form of dementia in the older population, affecting almost 44 million people living with dementia worldwide [1]. The neuropathology of AD is characterized by synaptic loss and the presence of aggregates formed by amyloid- $\beta$  ( $A\beta$ ) peptide and phosphorylated tau, accompanied by progressive memory and learning impairment [2].

Diverse pathogenic factors are linked to AD; however, the precise mechanism of AD is unknown. Among these factors, neuroinflammation (the inflammatory process in the brain) plays a critical role in the pathogenesis of AD [3, 4]. Neuroinflammation alters neuronal synaptic proteins, such as decreasing drebrin, which is correlated with cognitive impairment in patients with AD [5]. Synapses are the fundamental units of information transfer and storage in the brain,

and they have pre- and postsynaptic compartments. Synapse transmission or neurotransmission consists of the release of neurotransmitters, which in turn bind to and activate receptors located at postsynaptic or presynaptic sites. Moreover, synapse loss and synaptic dysfunction are pathological processes already involved in the early stages of AD [6]. Accumulating evidence has shown that neurexins and neuroligins are synaptic cell adhesion molecules that are essential for normal synapse specification and function [7].

Neuroinflammation can be triggered by various biological mechanisms, including glial reactions. Despite the large number of agents that have been applied to control neuroinflammation, the effects of these agents are unsatisfactory. Strong supporting evidence exists for the hypothesis that the inflammatory response in AD is in part driven by the interactions of  $A\beta$ . Celastrol (CEL) is a chemical compound isolated from the root extracts of *Tripterygium wilfordii* and *Celastrus regelii*. Recently, studies have shown that CEL has



potent immunosuppressive and anti-inflammatory effects in incision-induced acute pain and inflammatory pain [8, 9], as well as having an effect in neurodegenerative diseases [10, 11]. A number of studies have shown the anti-inflammatory effects of CEL are mediated in part through the inhibition of NF- $\kappa$ B activity and regulation of the production or release of proinflammatory cytokines [9, 12–14]. Moreover, Zhao et al. [15] demonstrated that CEL reduced LPS-induced cell death and A $\beta$  production *in vitro* by increasing HSP-70 and Bcl-2 expression levels and reducing NF- $\kappa$ B, COX-2, and GSK-3 $\beta$  expression levels and oxidative stress. However, little is known about the possible protective effect of CEL in an AD rat model.

Therefore, this study is aimed at investigating the protective effect of CEL on the development of A $\beta$ -induced learning and memory deficits and its possible mechanism. We hypothesized that A $\beta$ -induced neuroinflammation contributes to learning and memory deficits in rats and that CEL improves cognitive dysfunction by inhibiting A $\beta$ -induced neuroinflammation, promoting synapse development, and maintaining hippocampal energy metabolism. These results provide preclinical evidence to support the use of CEL in the treatment of AD.

## 2. Methods

**2.1. Animals.** Male Sprague-Dawley rats (200–250 g) from the Experimental Animal Research Center of Hubei Province, Wuhan, PR China (Certificate No. 42000600006344/SCXK(E)2008-0005), were housed in a standard environment (22–25°C, light–dark cycle: 12 h alternating) with free access to food and water. All experimental protocols and animal handling procedures were approved by the Ethics Committee of Puai Hospital, Tongji Medical College, Huazhong University of Science and Technology, and were conducted in accordance with the National Institute of Health Guide for the Care and Use of Laboratory Animals (NIH Publications No. 80e23, revised in 1996).

**2.2. Preparation of the Animal Model.** The rats ( $n = 80$ ) were randomly divided into the following four groups: vehicle-treated sham (vehicle+sham, sham), vehicle-treated model group (vehicle+A $\beta_{25-35}$ , A $\beta_{25-35}$ ), CEL-treated sham (CEL+sham), and CEL-treated model group (CEL+A $\beta_{25-35}$ ). The experimenters were blinded to the treatment. The AD model in rats was induced as previously described with minor modifications [16]. Briefly, the rats were first anaesthetized with phenobarbital and fixed in a stereotaxic apparatus (RWD Life Science, Shenzhen, China). After a midline sagittal incision, the coordinates for the hippocampal CA1 region were defined with reference to a standard brain stereotaxic atlas [17] as follows: anteroposterior -3.5 mm from bregma, mediolateral  $\pm 2.0$  mm from the midline, and dorsoventral -2.8 mm from the skull. After drilling the marked points on the skull, 2  $\mu$ l sterile normal saline solution containing 10  $\mu$ g aggregated A $\beta_{25-35}$  (5  $\mu$ g/ $\mu$ l; Sigma Aldrich, USA) was injected bilaterally into the CA1 of the dorsal hippocampus.

**2.3. Drug Administration.** In the CEL-treated model group, rats were intraperitoneally administered CEL (2 mg/kg) one day before the A $\beta_{25-35}$  microinjection. In the other groups, the rats were given intraperitoneal injections of an equal volume of corn oil (vehicle, 2 mg/kg) in the same manner.

**2.4. Morris Water Maze Test.** The Morris water maze (MWM) test was performed as described previously [18]. The MWM (Institute of Materia Medica, Chinese Academy of Medical Sciences, Beijing, China) uses a circular tank with a diameter of 150 cm, height of 50 cm, water depth of 30 cm, and temperature of  $22 \pm 2^\circ\text{C}$ . The water was made opaque by adding Chinese ink [19] so that the rats could not see the position of the submerged platform. The maze was conceptually divided into four equal-sized quadrants, and a clear plastic platform (10 cm in diameter) was submerged 1.5 cm below the water surface and placed in the center of the designated quadrant throughout the training phase. Visual cues (geometric figures: square, triangle, circle, and star) were placed on the room walls. Behavioural testing was performed between 9:00 and 12:00 a.m. under standard laboratory conditions.

The rats ( $n = 10$  per group) were subjected to 4 consecutive trials per day with 10 min intervals for 5 days. The trials began on day 14 post A $\beta_{25-35}$  microinjection. The protocol of training for the MWM task involved 3 trials (120 s maximum, interval 20 min) each day and lasted for 5 consecutive days. At 1 h following the fifth day of training, the test trial was performed. The time spent searching for the platform (latency), the path length, and the duration of time spent in each quadrant and platform crossing were calculated.

**2.5. Quantitative Real-Time Polymerase Chain Reaction (RT-PCR).** After the behavioural test, the rats were deeply anaesthetized with sodium pentobarbital and the hippocampus was quickly removed and stored in liquid nitrogen. Quantitative RT-PCR was used to examine changes in the mRNA levels of IL-1 $\beta$ , IL-6, TNF $\alpha$ , IL-4, and IL-10. Total RNA from the samples was isolated according to the manufacturer's protocol (Invitrogen, Carlsbad, CA, USA). The fold change was calculated from the target gene and the  $\beta$ -actin loading control using the following formula: mRNA relative expression =  $2^{-\Delta\Delta\text{Ct}}$ . The primers used in this study are described in Table 1.

**2.6. Enzyme-Linked Immunosorbent Assay.** For the enzyme-linked immunosorbent assay, the rats ( $n = 4$ ) were deeply anaesthetized and decapitated after the behavioural test. The CA1 tissue was quickly removed and completely ground into brain tissue homogenate with saline (0.9% NaCl) and then centrifuged at 10,000 rpm for 15 min. The liquid above the lipid layer was collected, and competitive ELISA was performed as previously described [20]. IL-1 $\beta$ , IL-6, TNF- $\alpha$ , IL-4, and IL-10 ELISA kits were obtained from Elabscience (Wuhan, China).

**2.7.  $^{18}\text{F}$ -Labelled Fluorodeoxyglucose Positron-Emission Tomography.** PET scans of the spine and brain were performed on day 10 [21]. Briefly, all rats were fasted for 12 h prior to FDG injection. Before and during the PET imaging,



TABLE 1: The PCR primers of the inflammatory factors.

Gene	Forward	Reverse
IL-1 $\beta$	5'-CCTGTGTGATGAAAGACGG-3'	5'-TATGTCCCACCATTGCTG-3'
IL-6	5'-GTTGCCCTTCTGGGACTGAT-3'	5'-TACTGGTCTGTTGTGGGTGG-3'
TNF- $\alpha$	5'-CCGATTTGCCATTCATACC-3'	5'-TCACAGAGCAATGACTCAA-3'
IL-4	5'-CACCTTGCTGCACCCTGTT-3'	5'-CCTGCAGATGAGCTCGTTCT-3'
L-10	5'-GCCAGAAATCAAGGAGCA-3'	5'-CGTAGGCTTCTATGCAGTT-3'
$\beta$ -Actin	5'-CACGATGGAGGGGCCGAC-3'	5'-TAAAGACCTCTATGCCAAC-3'

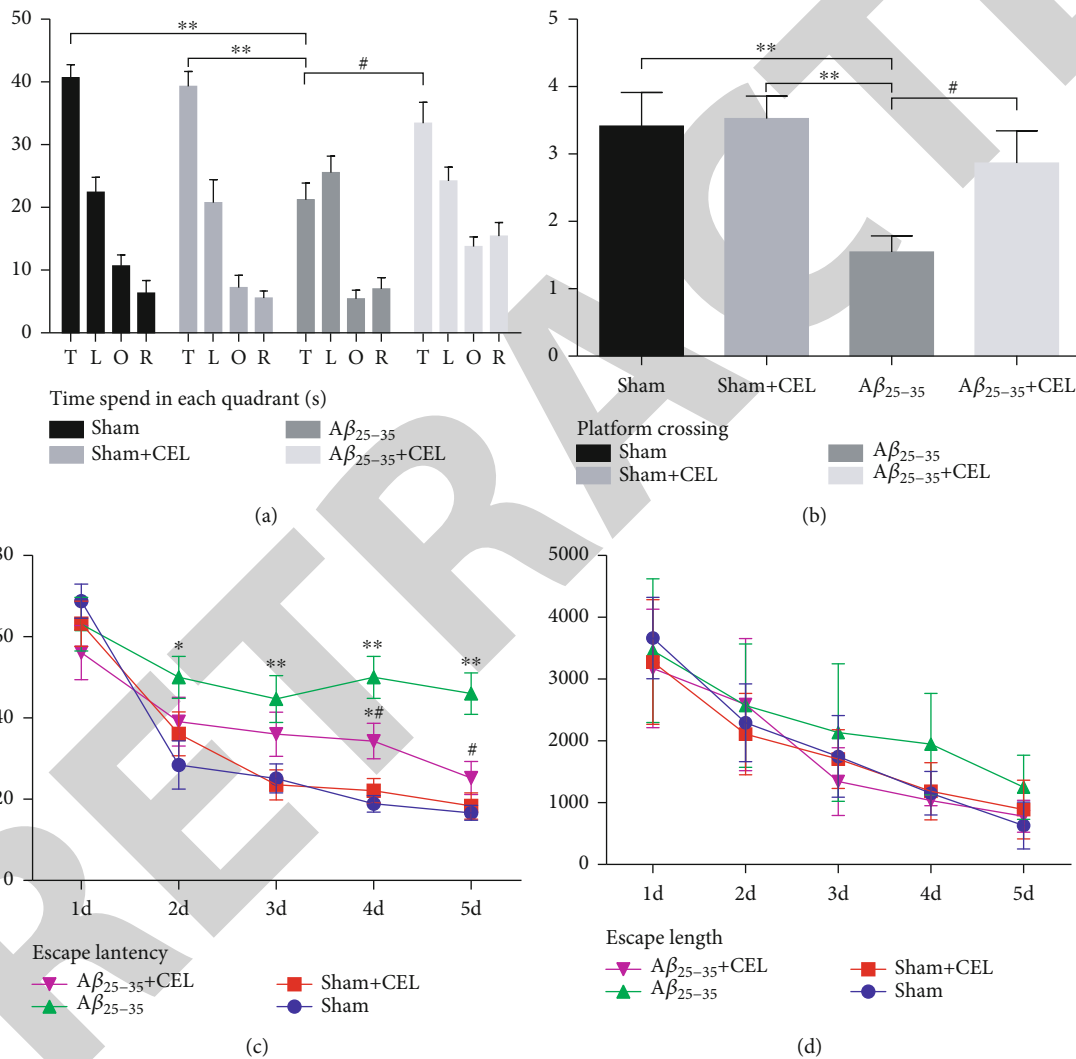


FIGURE 1: Celastrol alleviated A $\beta_{25-35}$ -induced spatial memory deficits. (a) Analysis time spent in each quadrant during the probe test of MWM, \*\* $p < 0.01$  compared with the sham group and # $p < 0.05$  compared with the A $\beta_{25-35}$  group. Data are shown as the mean  $\pm$  SD ( $n = 8$ ). (b) The platform crossing times during probe trial of MWM test. Compared with the sham group, # $p < 0.05$  compared with the A $\beta_{25-35}$  group. Data are shown as the mean  $\pm$  SD ( $n = 8$ ). (c) Escape latency in MWM plotted against the training days. Repeated measures ANOVA followed by a post hoc Bonferroni multiple comparison test. \* $p < 0.05$  and \*\* $p < 0.01$  compared with the sham group and # $p < 0.05$  compared with the A $\beta_{25-35}$  group. Data are shown as the mean  $\pm$  SD ( $n = 8$ ). (d) Escape path length in MWM plotted against the training days. No significant difference was observed in these groups. Data are shown as the mean  $\pm$  SD ( $n = 8$ ).

the rats were anaesthetized using 2.0% isoflurane in 100% oxygen (1.5l/min flow rate), and the temperature was maintained at  $\pm 37^{\circ}\text{C}$ . The tail veins were catheterized for injection

of  $22.0 \pm 3.0$  MBq [18F]FDG (specific activity range 83–760 GBq/ $\mu\text{mol}$ ). Static 30 min acquisitions were performed 60 min postinjection (Raycan Technology Co., Ltd., Suzhou,

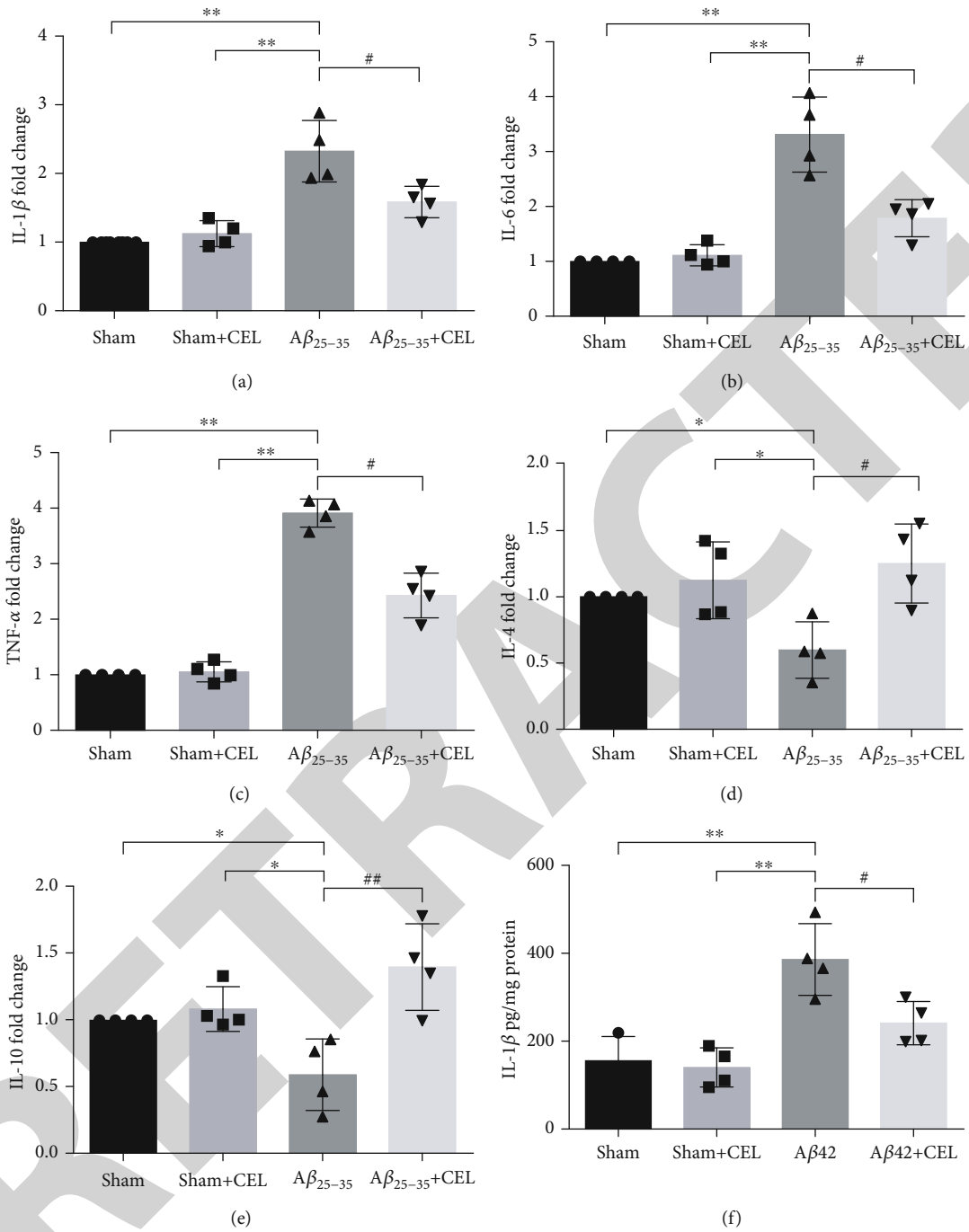


FIGURE 2: Continued.

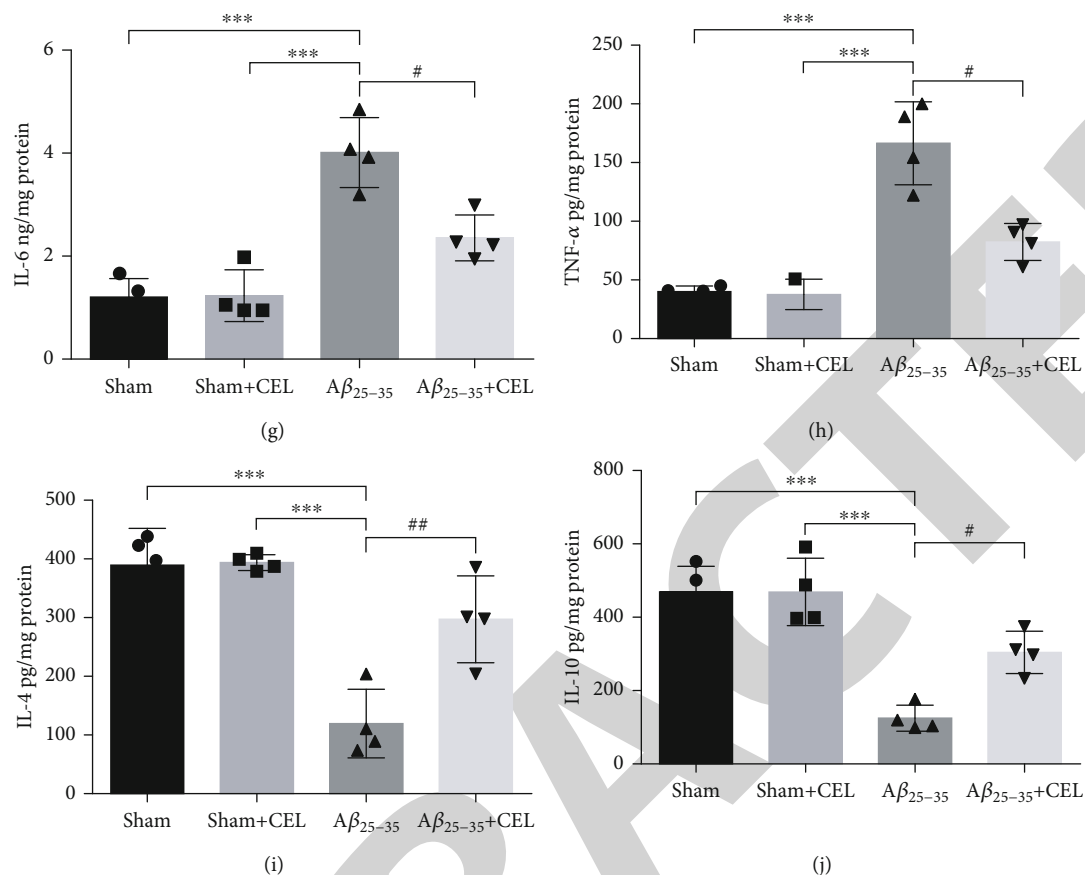


FIGURE 2: Celastrol inhibited the production of IL-1β, IL-6, and TNFα messenger RNA (mRNA) expression levels and contents and upregulated IL-4 and IL-10 messenger RNA (mRNA) expression levels and contents. (a-c) Aβ<sub>25-35</sub> increased the expression levels of IL-1β, IL-6, and TNFα (mRNA) from the CA1 region relative to the sham group, whereas CEL downregulated their expression levels. Data are represented as mean ± SD (n = 4). \*\*p < 0.001 vs. sham group and #p < 0.05 vs. Aβ<sub>25-35</sub> group. (d, e) Aβ<sub>25-35</sub> decreased the expression levels of IL-4 and IL-10 (mRNA), whereas CEL increased their expression levels. Data are represented as mean ± SD (n = 4). \*p < 0.001 vs. sham group and #p < 0.05 and ##p < 0.01 vs. Aβ<sub>25-35</sub> group. (f-h) Aβ<sub>25-35</sub> increased the contents of IL-1β, IL-6, and TNFα from CA1 region, whereas CEL downregulated their expression levels. Data are represented as mean ± SD (n = 4). \*\*p < 0.01 and \*\*\*p < 0.001 vs. sham group and #p < 0.05 vs. Aβ<sub>25-35</sub> group. (i, j) Aβ<sub>25-35</sub> decreased the expression of IL-4 and IL-10 contents, whereas CEL increased their levels. Data are represented as mean ± SD (n = 4). \*\*\*p < 0.001 vs. sham group and #p < 0.05 and ##p < 0.01 vs. Aβ<sub>25-35</sub> group.

China), which is a widely used small-animal PET system. The mean SUV was calculated using the following formula: mean pixel value with the decay – corrected region – of – interest activity (μCi/kg)/(injected dose [μCi]/weight [kg]). A single investigator reads the scans and was blinded to both the subject and the timing of the image.

2.8. *Western Blot Analysis.* Proteins from the hippocampal tissue samples were harvested after the behavioural testing. The samples were homogenized in RIPA buffer at 4°C for 30 min. Then, centrifugation and protein levels in the supernatant were determined by using a BCA protein assay kit (Boster, Wuhan, China). Equal amounts of these extracts (30-50 μg protein each) were separated by 10% SDS-PAGE and transferred to polyvinylidene difluoride membranes (Millipore, Bedford, MA, USA). The membranes were blocked with 5% BSA or 5% nonfat milk in Tris-buffered saline and Tween 20 (TBST) for 1-1.5 h and then incubated

overnight at 4°C with the primary antibodies, as indicated: mouse anti-β-actin (1 : 1000; Boster, Wuhan, China), rabbit anti-p65 (1 : 800; Abclonal, Cambridge, MA, USA), rabbit anti-p-p65 (1 : 800; Abclonal, Cambridge, MA, USA), rabbit anti-IBKα (1 : 1000; Cell Signalling Technology, Danvers, MA, USA), rabbit anti-p-IBKα (1 : 1000; Cell Signalling Technology, Danvers, MA, USA), rabbit anti-iNOS (1 : 800; Abcam, Cambridge, MA, USA), goat anti-neurexin-1β (1 : 1000; Abcam, Cambridge, UK) and rabbit anti-neuroigin-1 (1 : 1000; Abcam, Cambridge, UK), mouse anti-PSD95 (1 : 2000; Cell Signalling Technology, Danvers, MA, USA), and rabbit anti-synapsin (1 : 1000; Abcam, Cambridge, UK). The membranes were then washed and incubated with horseradish peroxidase-conjugated goat anti-mouse or anti-rabbit IgG antibody (1 : 5000; Boster, Wuhan, China), as appropriate, for 2 h at room temperature. The labelled proteins were detected by enhanced chemiluminescence reagents (Thermo Scientific, Waltham, MA, USA) with

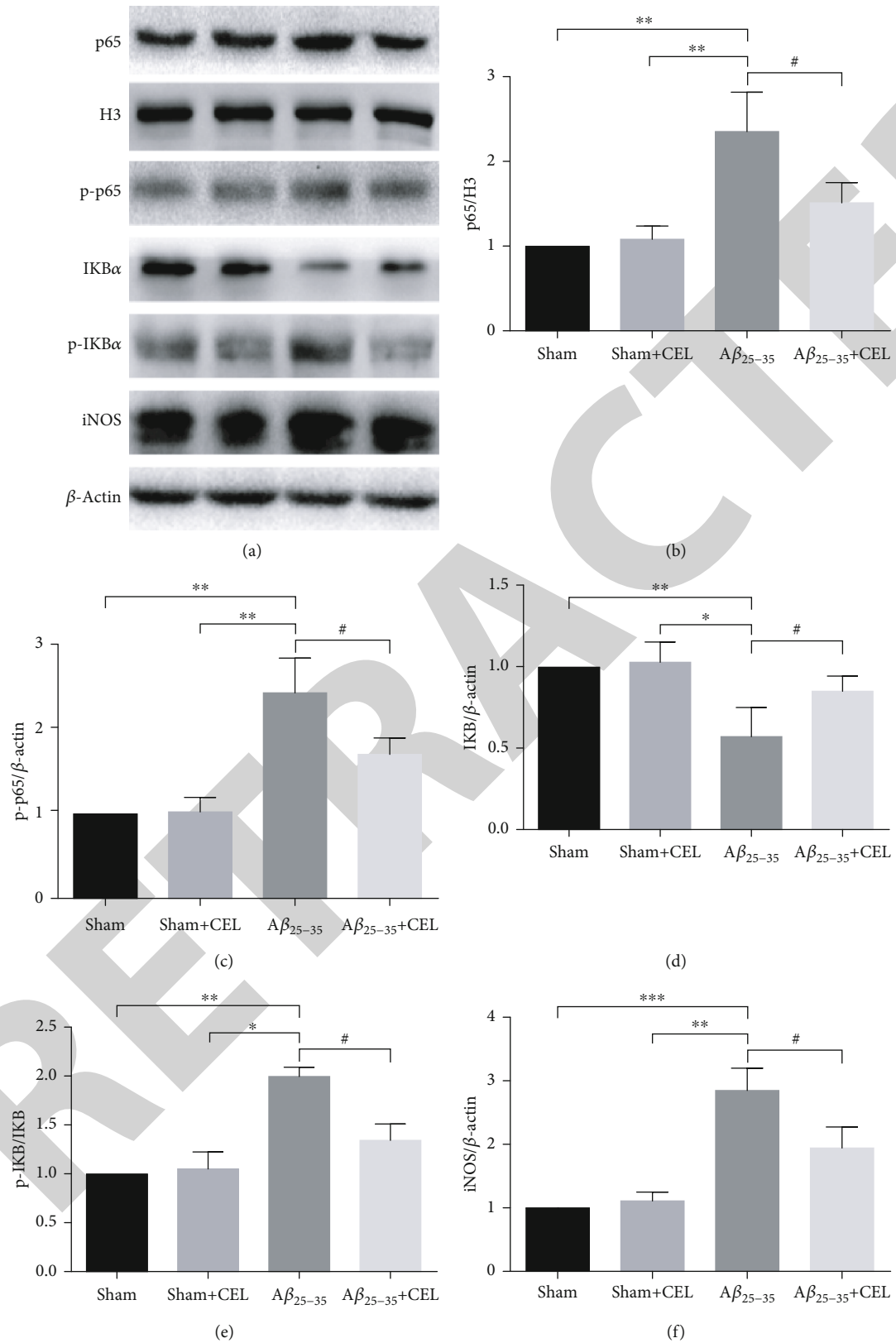


FIGURE 3: Continued.

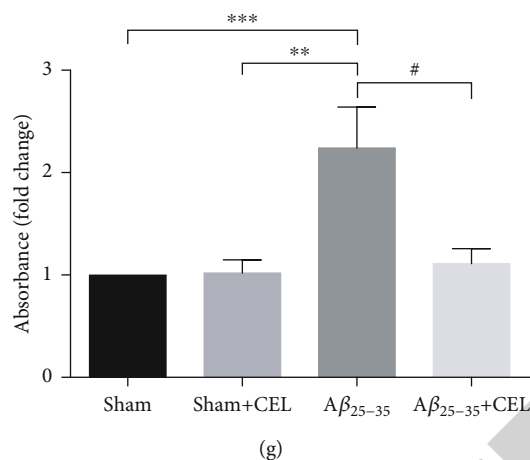


FIGURE 3: Celastrol inhibited A $\beta_{25-35}$ -induced NF- $\kappa$ B signalling pathway activation. (a–c) Quantitative analysis using western blot showed that cytoplasmic p-p65 expression and nuclear p65 levels were significantly downregulated by CEL. Data are represented as mean  $\pm$  SD ( $n = 4$ ). \*\* $p < 0.01$  vs. sham group and # $p < 0.05$  vs. A $\beta_{25-35}$  group. (a, d, e) CEL markedly upregulated IKB $\alpha$  expression and decreased p-IKB $\alpha$  levels. Data are represented as mean  $\pm$  SD ( $n = 4$ ). \* $p < 0.05$  and \*\* $p < 0.01$  vs. sham group and # $p < 0.05$  vs. A $\beta_{25-35}$  group. (a, f). CEL markedly downregulated iNOS expression in CA1 region. Data are represented as mean  $\pm$  SD ( $n = 4$ ). \*\* $p < 0.01$  and \*\*\* $p < 0.001$  compared with the sham group and # $p < 0.05$  vs. A $\beta_{25-35}$  group. (g) ELISA assay showing a more pronounced decrease of NF- $\kappa$ B p65-DNA binding in CEL group. \*\* $p < 0.01$  and \*\*\* $p < 0.001$  compared with the sham group and # $p < 0.05$  vs. A $\beta_{25-35}$  group. Data are represented as mean  $\pm$  SD ( $n = 6$ ).

a ChemiDocXRS Chemiluminescence imaging system (BioRad, Hercules, CA, USA). The protein bands were quantified using laboratory imaging software.

2.9. *Statistical Analysis.* All values are presented as the mean  $\pm$  SD and were analysed by using SPSS 19.0 (SPSS Inc., Armonk, New York, USA). The statistical analysis of the behavioural results was conducted using a two-way ANOVA with repeated measures followed by *post hoc* Bonferroni tests. One-way ANOVA followed by the Bonferroni *post hoc* test was used for RT-PCR, western blot, and [18F]FDG data. A  $p$  value  $< 0.05$  was considered statistically significant.

### 3. Results

3.1. *CEL Attenuates Amyloid- $\beta$  (A $\beta$ ) Peptide-Induced Learning and Memory Function Deficits.* To determine whether CEL improved learning and memory function, we first evaluated the spatial and learning memory in rats using the MWM test at day 28 after intrahippocampal A $\beta_{25-35}$  injection. Our results showed that rats microinjected with A $\beta_{25-35}$  showed evidence of cognitive impairment compared with the sham group, whereas pretreatment with CEL attenuated learning and memory dysfunction. These mice also exhibited prolonged escape latencies in the MWM test. CEL decreased the latencies (Figure 1(c),  $n = 10$  per group, from the training trials) and decreased the target quadrant residence times, whereas CEL increased the target times (Figure 1(a),  $n = 10$  per group, from the probe trials). A $\beta_{25-35}$  injection decreased the platform crossings, whereas CEL increased the crossing times (Figure 1(b),  $n = 10$  per group, from the probe trials). No significant differences were found

among the escape durations (Figure 1(d)). There was no significant difference between the sham and sham+CEL groups.

#### 3.2. CEL Decreases Hippocampal CA1 Inflammatory Factors.

To confirm the effects of CEL on the expression of proinflammatory cytokines, IL-1 $\beta$ , IL-6, and TNF- $\alpha$  mRNA and the expression levels of anti-inflammatory factors, namely, IL-4 and IL-10, were determined by using quantitative RT-PCR. Their expression levels were detected by using ELISA. We found that intrahippocampal A $\beta_{25-35}$  increased the mRNA expression levels of the proinflammatory cytokines IL-1 $\beta$ , IL-6, and TNF- $\alpha$  (Figures 2(a)–2(c),  $n = 4$  per group) and their protein levels (Figures 2(f)–2(h),  $n = 4$  per group), whereas pretreatment with CEL downregulated proinflammatory cytokine expression, accompanied by upregulated levels of anti-inflammatory factors, namely, IL-4 and IL-10 (Figures 2(d), 2(e), 2(i), and 2(j),  $n = 4$  per group). There was no significant difference between the sham and sham+CEL groups.

#### 3.3. CEL Alleviates Hippocampal CA1 Neuroinflammation by Inhibiting NF- $\kappa$ B Activation.

To determine whether the anti-inflammatory effects of CEL were associated with inhibition of the NF- $\kappa$ B signalling pathway, we performed western blot analysis. CEL significantly inhibited the nuclear translocation of p65 and increased the retention of p65 in the cytoplasm (Figures 3(a)–3(c),  $n = 4$  per group). Simultaneously, CEL upregulated the expression of IKB $\alpha$ , an endogenous NF- $\kappa$ B inhibitor, and decreased the p-IKB $\alpha$  level (Figures 3(a), 3(d), and 3(e),  $n = 4$  per group). Moreover, previous studies have shown that iNOS contributes to inflammatory factor production. Therefore, we observed changes in iNOS in our study and observed that CEL downregulated the expression of the iNOS protein (Figures 3(a) and 3(f),  $n = 4$  per group).

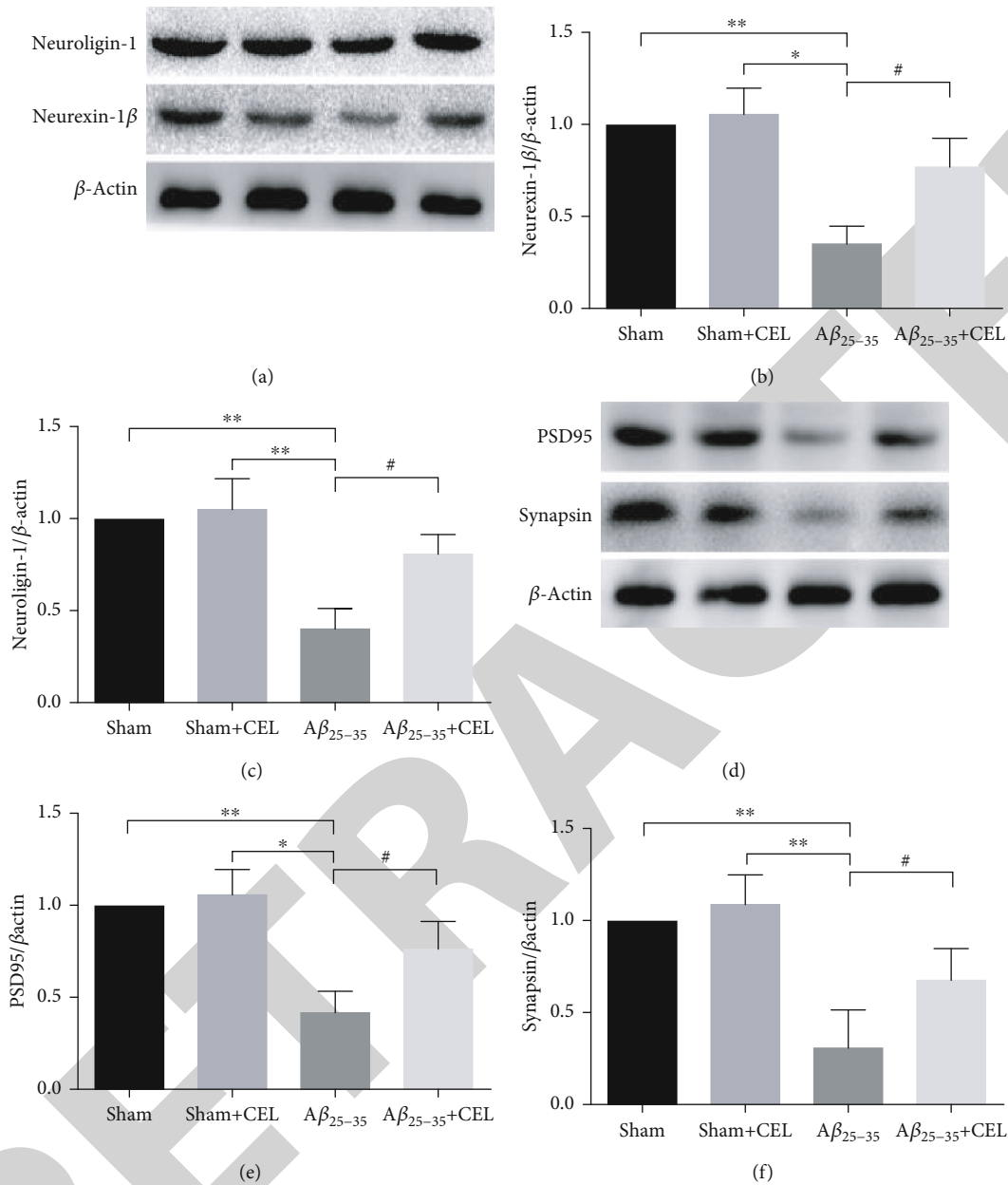


FIGURE 4: Celastrol upregulated neurexin-1 $\beta$ , neuroigin-1, PSD95, and synapsin expression levels. (a) Representative western blot images of neurexin-1 $\beta$  and neuroigin-1 proteins. (b, c) CEL markedly upregulated neurexin-1 $\beta$  and neuroigin-1 expression levels. Data are represented as mean  $\pm$  SD ( $n=4$ ). \* $p < 0.05$  and \*\* $p < 0.01$  compared with the sham group and # $p < 0.05$  vs. A $\beta_{25-35}$  group. (d) Representative western blot images of PSD95 and synapsin proteins. (e, f) CEL markedly upregulated PSD95 and synapsin expression levels. Data are represented as mean  $\pm$  SD ( $n=4$ ). \* $p < 0.05$  and \*\* $p < 0.01$  compared with sham group and # $p < 0.05$  vs. A $\beta_{25-35}$  group.

Furthermore, the NF- $\kappa$ B p65-DNA binding assay indicated that CEL mediated NF- $\kappa$ B inhibition (Figure 3(g),  $n=4$  per group). There was no significant difference between the sham and sham+CEL groups.

**3.4. CEL Upregulates Hippocampal CA1 Neurexin-1 $\beta$  and Neuroigin-1, PSD95, and Synapsin Expression.** To further confirm whether intrahippocampal A $\beta_{25-35}$  destroyed synapses in the CA1 region, we tested the protein expression of synapse-associated proteins using western blot analysis. We found that intrahippocampal A $\beta_{25-35}$  decreased the neur-

exin-1 $\beta$ , neuroigin-1, synapsin, and PSD95 expression levels in CA1 at 28 days after A $\beta_{25-35}$  was injected, and CEL pretreatment reversed these changes (Figures 4(a)–4(f),  $n=4$  per group). There was no significant difference between the sham and sham+CEL groups.

**3.5. CEL Increases Glucose Metabolism in the Hippocampus of A $\beta_{25-35}$  Rats.** We further investigated the effect of A $\beta_{25-35}$  on glucose metabolism in SD rats by 18F-labelled fluorodeoxyglucose positron-emission tomography (18F-FDG-PET) using the regional hippocampal metabolic rate for glucose.



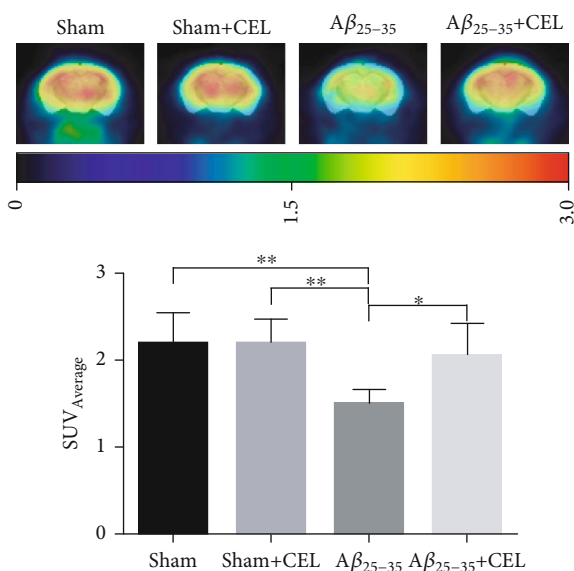


FIGURE 5: CEL increases the glucose metabolism in  $A\beta_{25-35}$  rat's hippocampus. Values of hippocampus (standardized uptake value (SUV) average) are shown as mean  $\pm$  SD, one-way ANOVA, followed by LSD multiple comparison post hoc tests,  $n = 3$  in each group. \* $p < 0.05$  and \*\* $p < 0.01$  vs.  $A\beta_{25-35}$  group.

We found that intrahippocampal  $A\beta_{25-35}$  decreased SUV in the hippocampus of SD rats; however, 2 mg/kg CEL increased the SUV in the hippocampus (Figures 5(a) and 5(b),  $n = 3$  per group). There was no significant difference between the sham and sham+CEL groups.

#### 4. Discussion

The present study evaluated the effect of CEL on learning and memory deficits in an  $A\beta_{25-35}$ -induced AD rat model and determined its protective effect and possible role in neuroinflammation, synapse dysfunction, and hippocampal energy metabolism. The results of the behavioural tests showed that CEL improved spatial memory in the MWM and learning and memory in the passive avoidance task. Further biochemical analysis showed that CEL pretreatment of intrahippocampal  $A\beta$ -microinjected rats attenuated hippocampal inflammation and downregulated inflammatory markers, such as IL-1 $\beta$ , IL-6, and TNF $\alpha$ , with a significant decrease in NF- $\kappa$ B activity. This downregulation was accompanied by the upregulation of anti-inflammatory factors, such as IL-4 and IL-10. Furthermore, CEL upregulated hippocampal CA1 neurexin-1 $\beta$ , neuroligin-1, PSD95, and synapsin expression levels, and these increased levels may improve synaptic function. Taken together, the protective effect of CEL on  $A\beta_{25-35}$ -induced learning and memory deficits occurs via anti-inflammatory effects and improvements in synaptic function.

CEL, which is the main bioactive compound of celastraceae, is a potent anti-inflammatory and immunosuppressive agent. Inflammatory disorders and acute immune-mediated demyelinating neuropathy could cause reduced signal transmission, which leads to neurodegenerative disease [22]. Pre-

vious studies have shown that CEL reduces LPS-induced cell death and  $A\beta$  production *in vitro* [15]. However, few reports have evaluated the effect of CEL on AD rat models. Therefore, we observed the protective effect of CEL on  $A\beta_{25-35}$ -induced learning and memory deficits in a rat model. Our results showed that CEL attenuated  $A\beta_{25-35}$ -induced learning and memory deficits. Recently, the evidence has demonstrated that neuroinflammatory responses contribute to AD; moreover, many studies have shown that CEL exhibits antioxidant, anti-inflammatory, and anticancer activities *in vitro* and *in vivo* in animal experiments [9, 23, 24]. The NF- $\kappa$ B pathway is important in chronic inflammatory and autoimmune diseases [25, 26]. Additionally, NF- $\kappa$ B has been suggested as an important mechanism linking learning and memory dysfunction [27, 28]. In addition, CEL has been shown to have (by inhibition of NF- $\kappa$ B in the hypothalamus) antidiabetic effects on diabetic nephropathy and to improve whole-body insulin resistance [29, 30]. However, no current evidence exists regarding the mechanism of action of NF- $\kappa$ B inhibition in AD. Therefore, we aimed to investigate the effects of the novel NF- $\kappa$ B inhibitor CEL on  $A\beta_{25-35}$ -induced learning and memory deficits by inhibiting the NF- $\kappa$ B pathway. Interestingly, we found that CEL can alleviate neuroinflammation in the hippocampal CA1 region, and this effect was mainly mediated by NF- $\kappa$ B pathway inhibition.

Synapses are fundamental components of normal brain function, such as learning and memory. The integrated synapse requires coordination between presynaptic and postsynaptic proteins [31]. Among these molecules are the synaptic adhesion molecules neurexins and neuroligins. Neurexin is a presynaptic protein that helps connect neurons at the synapse, and it has longer Nr $x1\alpha$  and shorter Nr $x1\beta$  (Nr $x1b$ ) isoforms, which are crucial for synaptic strength. Neuroligin-1 acts as a splice site-specific ligand for  $\beta$ -neurexins and has been shown to localize to the postsynaptic compartment at excitatory synapses [32]. Moreover, neuroligin-1 is involved in the formation and remodelling of central nervous system synapses. Previous studies have shown that transsynaptic Nr $x1b$ -NL1 interactions enhance the PSD95-dependent recruitment of postsynaptic molecules in the hippocampus [33–35]. Additionally, synaptic protein synapsin and postsynaptic protein PSD95 are indicators of synaptic structure and have previously been used to evaluate neuroplasticity [36].

Therefore, we observed the expression of neurexins, neuroligins, synapsin, and PSD95. Overexpression of neurexins, neuroligins, synapsin, and PSD95 proteins causes an increase in synapse formation, thus proving that they have functional roles in synaptogenesis. Conversely, the blockade of  $\beta$ -neurexin interactions reduces the number of excitatory and inhibitory synapses [37, 38]. Therefore, we investigated the expression levels of neurexin-1 $\beta$ , neuroligin-1, synapsin, and PSD95 because these indicators of synaptic structure have previously been used to evaluate neuroplasticity in other models of AD. We found that  $A\beta_{25-35}$ -induced learning and memory deficits downregulated the expression levels of neurexin-1 $\beta$ , neuroligin-1, synapsin, and PSD95. However, pretreatment with CEL upregulated neurexin-1 $\beta$ , neuroligin-1, synapsin, and PSD95 and alleviated cognitive dysfunction.

Thus, CEL is important in presynaptic and postsynaptic structure reconstruction.

It has been demonstrated that sustaining energy dynamics within the aged hippocampus can boost memory storage by sustaining synaptic functioning and long-term potentiation (LTP) and increase learning and memory function [39]. Medical imaging, such as MRI, can help clinicians diagnose status epilepticus when there is a strong suspicion based on medical examination [40]. Our results showed that  $A\beta_{25-35}$ -induced hippocampal energy metabolism was impaired; however, pretreatment with CEL increased the hippocampal SUV value and improved learning and memory function.

Some limitations exist in the present study. First, various strategies, including knockout animals, may be used to assess the direct relationship of neurexin-1 $\beta$ -, neuroligin-1-, synapsin-, PSD95-, and  $A\beta_{25-35}$ -induced learning and memory deficits that were not performed in this study. Second, it is not clear whether CEL is a targeted change specifically related to the brain CA1 region or instead has a systemic action.

In conclusion, CEL could exert a protective effect against learning and memory decline induced by intrahippocampal  $A\beta_{25-35}$  through anti-inflammation and promote synaptic development. This result improved our understanding of the relationship between CEL and  $A\beta_{25-35}$ -induced learning and memory deficits and may provide a basis for the development of novel neuroprotective treatment strategies.

## Data Availability

The data used to support the findings of this study are available from the corresponding author upon request.

## Conflicts of Interest

The authors declare no conflict of interest.

## Acknowledgments

Funding for this research was received from the Wuhan Municipal Health and Family Planning Commission Fund Project (Grant No. WX18Y03).

## References

- [1] J. B. Hopkinson, R. Milton, A. King, and D. Edwards, "People with dementia: what is known about their experience of cancer treatment and cancer treatment outcomes? A systematic review," *Psychooncology*, vol. 25, no. 10, pp. 1137–1146, 2016.
- [2] J. Michael, J. Marschallinger, and L. Aigner, "The leukotriene signaling pathway: a druggable target in Alzheimer's disease," *Drug Discovery Today*, vol. 24, no. 2, pp. 505–516, 2019.
- [3] M. Wiciński, E. Wódkiewicz, M. Słupski et al., "Neuroprotective Activity of Sitagliptin via Reduction of Neuroinflammation beyond the Incretin Effect: Focus on Alzheimer's Disease," *BioMed Research International*, vol. 2018, Article ID 6091014, 9 pages, 2018.
- [4] W. Y. Fu, X. Wang, and N. Y. Ip, "Targeting neuroinflammation as a therapeutic strategy for Alzheimer's disease: mechanisms, drug candidates, and new opportunities," *ACS Chemical Neuroscience*, vol. 10, no. 2, pp. 872–879, 2019.
- [5] J. Jebelli, C. Hooper, and J. M. Pocock, "Microglial p53 activation is detrimental to neuronal synapses during activation-induced inflammation: implications for neurodegeneration," *Neuroscience Letters*, vol. 583, pp. 92–97, 2014.
- [6] E. K. Pickett, J. Rose, C. McCrory et al., "Region-specific depletion of synaptic mitochondria in the brains of patients with Alzheimer's disease," *Acta Neuropathologica*, vol. 136, no. 5, pp. 747–757, 2018.
- [7] Q. Jiang, S. Chen, C. Hu, P. Huang, H. Shen, and W. Zhao, "Neuregulin-1 (Nrg1) signaling has a preventive role and is altered in the frontal cortex under the pathological conditions of Alzheimer's disease," *Molecular Medicine Reports*, vol. 14, no. 3, pp. 2614–2624, 2016.
- [8] W. Wang, C. Ha, T. Lin, D. Wang, Y. Wang, and M. Gong, "Celestrol attenuates pain and cartilage damage via SDF-1/CXCR4 signalling pathway in osteoarthritis rats," *The Journal of Pharmacy and Pharmacology*, vol. 70, no. 1, pp. 81–88, 2018.
- [9] X. Chen, B. Zhang, J. Li et al., "Celestrol attenuates incision-induced inflammation and pain associated with inhibition of the NF-kappaB signalling pathway via SARM," *Life Sciences*, vol. 205, pp. 136–144, 2018.
- [10] L. Gu, J. M. K. Kwong, D. Yadegari, F. Yu, J. Caprioli, and N. Piri, "The effect of celestrol on the ocular hypertension-induced degeneration of retinal ganglion cells," *Neuroscience Letters*, vol. 670, pp. 89–93, 2018.
- [11] B. S. Choi, H. Kim, H. J. Lee et al., "Celestrol from 'Thunder God Vine' protects SH-SY5Y cells through the preservation of mitochondrial function and inhibition of p38 MAPK in a rotenone model of Parkinson's disease," *Neurochemical Research*, vol. 39, no. 1, pp. 84–96, 2014.
- [12] Y. Kim, H. Kang, S. W. Jang, and J. Ko, "Celestrol inhibits breast cancer cell invasion via suppression of NF-kB-mediated matrix metalloproteinase-9 expression," *Cellular Physiology and Biochemistry*, vol. 28, no. 2, pp. 175–184, 2011.
- [13] S. H. Venkatesha, S. Dudics, B. Astry, and K. D. Moudgil, "Control of autoimmune inflammation by celestrol, a natural triterpenoid," *Pathogens and Disease*, vol. 74, no. 6, p. ftw059, 2016.
- [14] D. Luo, Y. Guo, Y. Cheng, J. Zhao, Y. Wang, and J. Rong, "Natural product celestrol suppressed macrophage M1 polarization against inflammation in diet-induced obese mice via regulating Nrf2/HO-1, MAP kinase and NF-kappaB pathways," *Aging (Albany NY)*, vol. 9, no. 10, pp. 2069–2082, 2017.
- [15] Y. Zhao, H. Zhao, N. Lobo, X. Guo, S. M. Gentleman, and D. Ma, "Celestrol enhances cell viability and inhibits amyloid-beta production induced by lipopolysaccharide in vitro," *Journal of Alzheimer's Disease*, vol. 41, no. 3, pp. 835–844, 2014.
- [16] W. Lu, J. Huang, S. Sun et al., "Changes in lactate content and monocarboxylate transporter 2 expression in Abeta(2)(5)-(3)(5)-treated rat model of Alzheimer's disease," *Neurological Sciences*, vol. 36, no. 6, pp. 871–876, 2015.
- [17] H. Benveniste, M. B. Jørgensen, M. Sandberg, T. Christensen, H. Hagberg, and N. H. Diemer, "Ischemic damage in hippocampal CA1 is dependent on glutamate release and intact innervation from CA3," *Journal of Cerebral Blood Flow and Metabolism*, vol. 9, no. 5, pp. 629–639, 1989.
- [18] X. Fang, S. Li, Q. Han et al., "Overexpression cdc42 attenuates isoflurane-induced neurotoxicity in developmental brain of rats," *Biochemical and Biophysical Research Communications*, vol. 490, no. 3, pp. 719–725, 2017.

## Research Article

# A Potential miRNA-mRNA Network for Dementia and Hernia Crosstalk

De-jian Chen and Da-peng Li 

Department of Day Care (Hernia Center), Shanghai General Hospital, Shanghai Jiao Tong University School of Medicine, China

Correspondence should be addressed to Da-peng Li; [dpli@inu.edu.vn](mailto:dpli@inu.edu.vn)

Received 5 May 2021; Revised 11 June 2021; Accepted 8 July 2021; Published 24 July 2021

Academic Editor: Yuzhen Xu

Copyright © 2021 De-jian Chen and Da-peng Li. This is an open access article distributed under the Creative Commons Attribution License, which permits unrestricted use, distribution, and reproduction in any medium, provided the original work is properly cited.

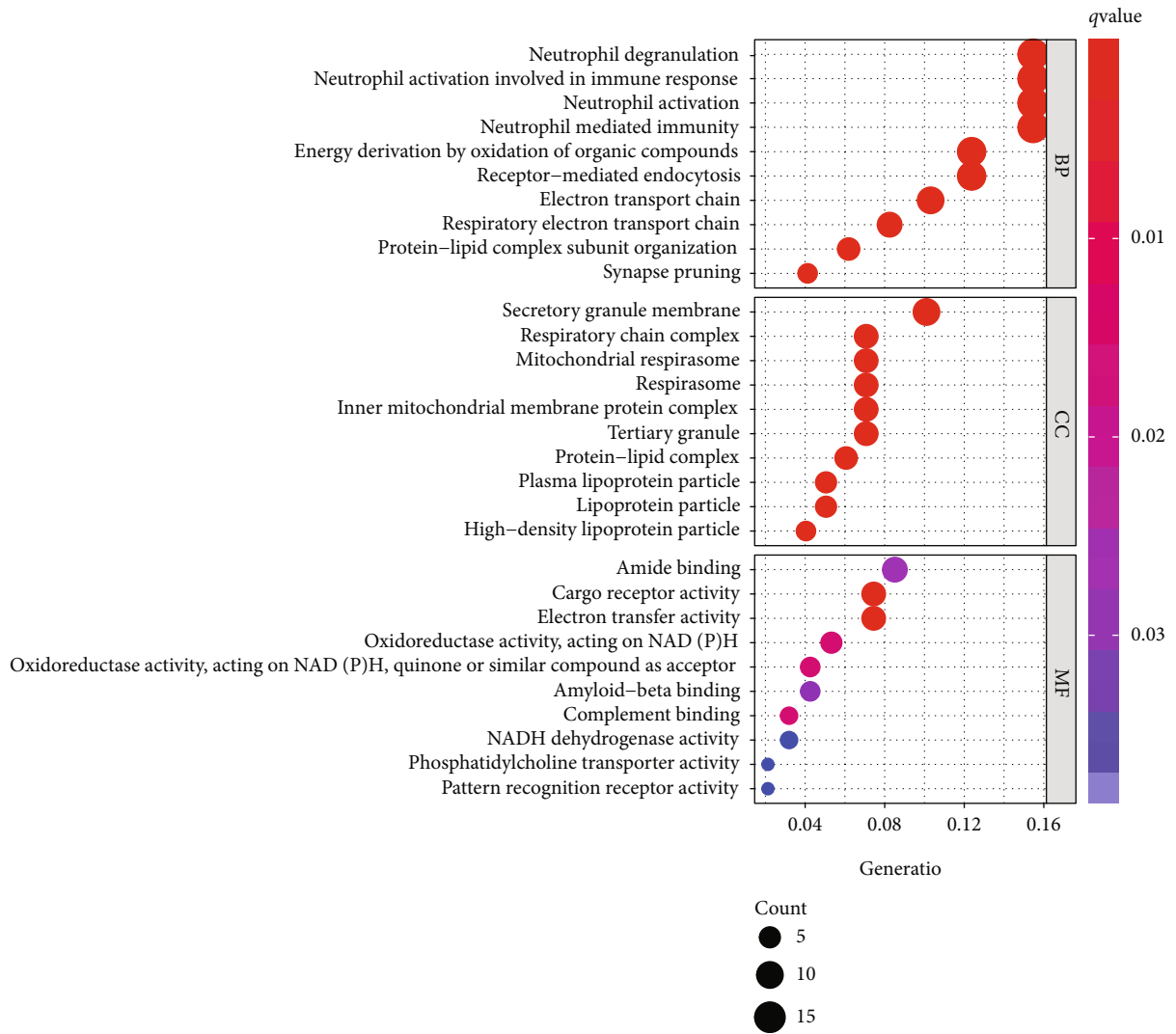
**Background.** It has been reported that there may be a potential link between hernia and dementia. However, the exact mechanisms of their association have not been established. This study is aimed at constructing miRNA-mRNA networks to elucidate on the potential link between dementia and hernia. **Methods.** Gene expression profiles for dementia, herniation, and skeletal muscle were downloaded from the GEO database after which differentially expressed mRNAs and miRNAs were obtained. In addition, fascia tissue samples were obtained during surgery. A total of 41 patients were recruited in this study, and expression levels of candidate genes were examined using quantitative RT-PCR. Luciferase reporter gene assays were used to identify potential miRNA-mRNA regulatory pathways. **Results.** Differentially expressed mRNAs and miRNAs were screened. A potential miRNA-mRNA network revealing the crosstalk mechanism between herniation and dementia was identified. Single cell analysis revealed that PI16 was highly enriched in adipose tissues, skeletal muscles, and in the skin. GSEA enrichment analysis showed that PI16 is involved in adipose metabolism, muscle functions, and energy metabolism. In clinical samples, PI16 was found to be upregulated in hernia, while miR-4451 was found to be downregulated. The luciferase reporter gene assay revealed that downregulation of circulating miR-4451 may be responsible for the upregulated PI16 expression in hernia sacs. **Conclusions.** We constructed an miRNA-mRNA network that shows the potential association between dementia and hernia. We also found that miR-4451 regulates the PI16 expression, which may be a key target and biomarker for hernia pathogenesis and dementia crosstalk.

## 1. Introduction

Ageing is a global social issue, and the number of people with dementia is expected to reach 75 million by 2030 and could exceed 100 million by 2050 [1]. The prevalence of dementia is positively correlated with age and various diseases including cardiac failure, depression, dyslipidemia, chronic obstructive pulmonary disease, stroke, and head injury among others, which are risk factors for dementia [2–4]. Formation of an abdominal wall hernia may be associated with various factors. A previous cohort study reported that there may be a potential link between hernias and dementia [5]. However, the possible mechanisms underlying the potential link between hernias and dementia have not been established.

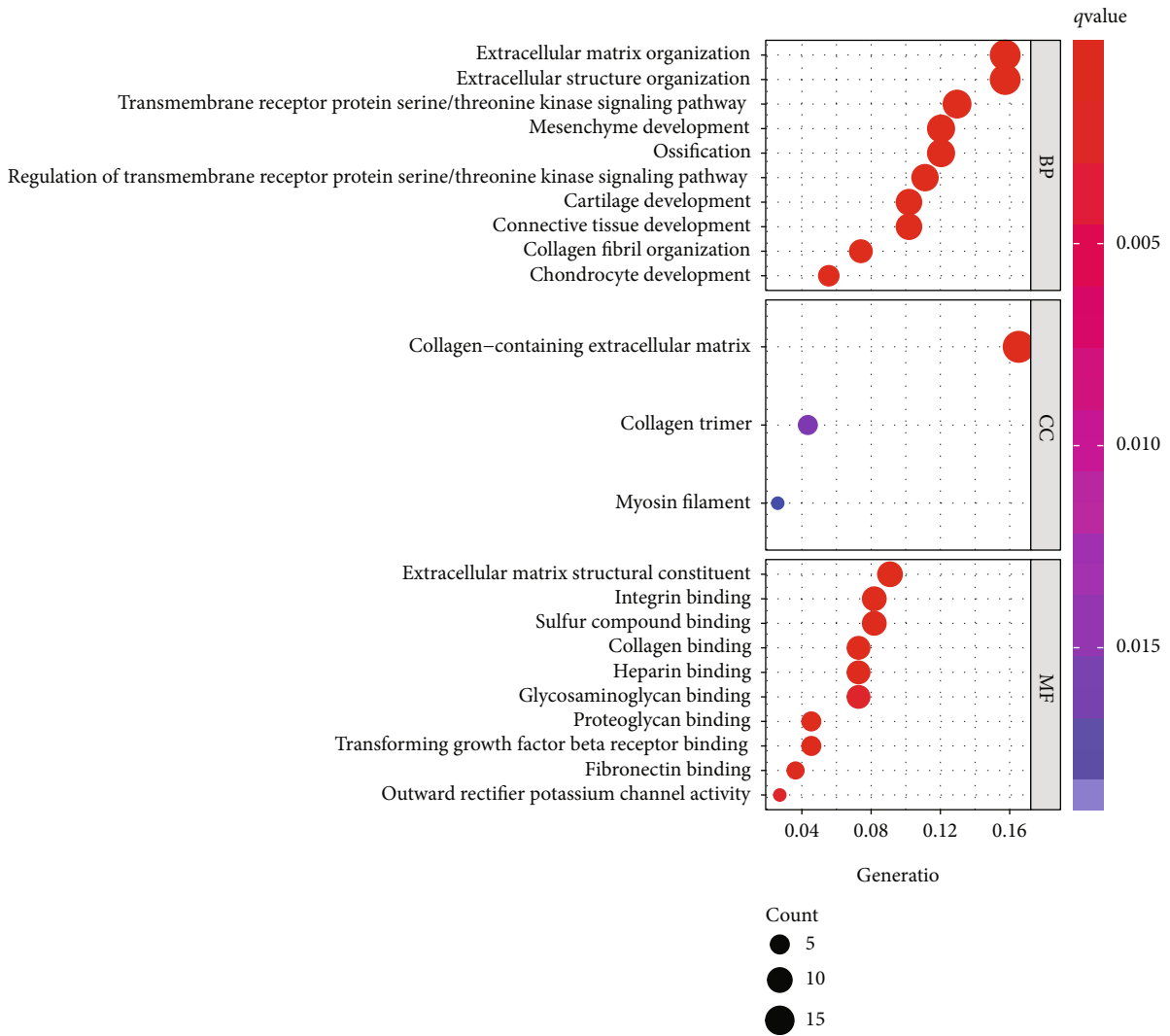
MiRNAs regulate the gene expression by complementary pair binding to transcript regions of mRNAs. In some cogni-

tive impairment-related diseases, expressions of miRNAs are altered [5, 6]. Based on microRNAs analysis, there is a link between age-related muscle atrophy and cognitive impairment [7]. Regulatory effects of microRNAs on muscles have been confirmed [8–10]. Older people with weak abdominal muscles and fascia are prone to hernia. In addition, changes in circulating microRNA levels are associated with development of congenital hernias [11]. Aberrant regulation of let-7b-5p, miR-1307-3p, miR-185-3p, miR-8084, miR-331-3p, and miR-210-3p may also contribute to the development of congenital diaphragmatic hernia [11]. Therefore, we hypothesized that some miRNAs are differentially expressed in the blood of dementia and hernia patients, and that these miRNAs could be markers for organismal weakness, acting as a link between dementia, muscle weakness, and hernia development.



(a)

FIGURE 1: Continued.



(b)

FIGURE 1: Continued.

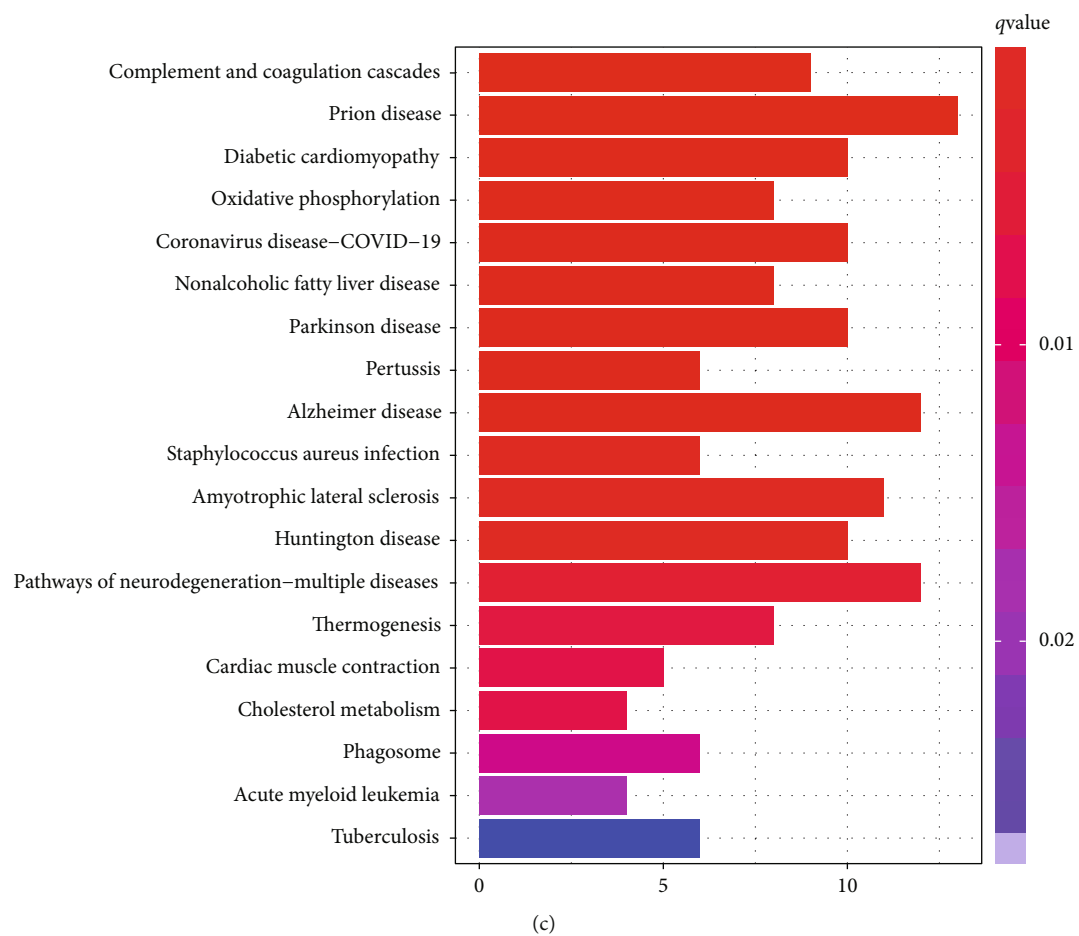
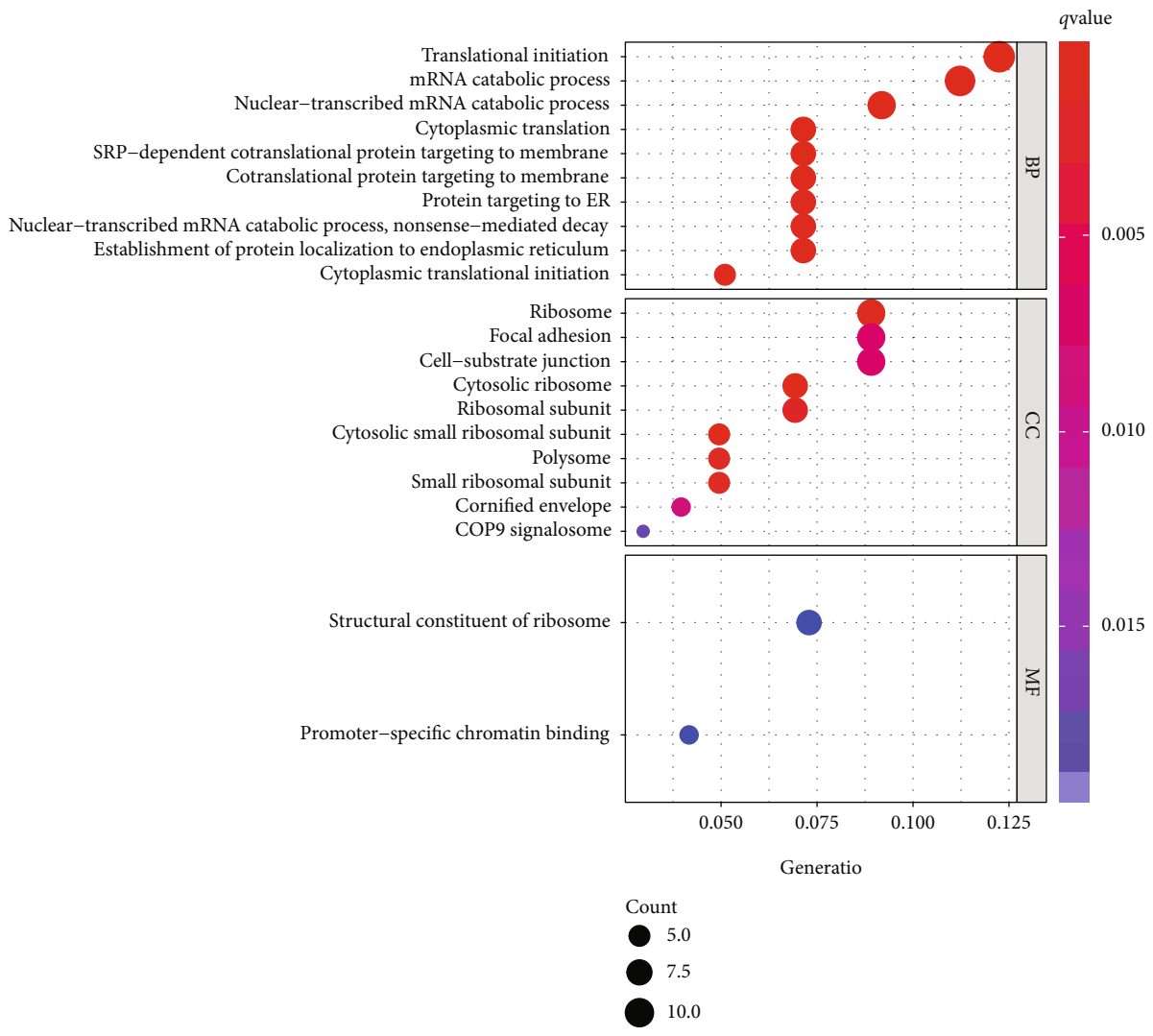


FIGURE 1: Continued.





(d)

FIGURE 1: Enrichment analysis of DEMs. GO enrichment analysis of DEMs in the fascia tissue (a, b). KEGG enrichment analysis of DEMs in the fascia tissue (c). Enrichment analysis of DEMs in the skin tissue.

This study is aimed at constructing miRNA-mRNA networks to elucidate on the potential link between dementia and hernia.

## 2. Materials and Methods

**2.1. Microarray Data.** To retrieve target gene expression profiles from the GEO dataset (<http://www.ncbi.nlm.nih.gov/geo>), we downloaded the hernia dataset GSE196374, the cognitive injury miRNA dataset GSE120584, and the skeletal muscle miRNA dataset GSE165632. The gene expression profile GSE19637 consisted of 17 samples from the skin tissue (8 from the normal tissue and 9 from the hernia tissue) and 17 samples from the fascia tissue (8 from the normal tissue and 9 from the hernia tissue). The gene expression dataset GSE120584 included 1021 sera samples from Alzheimer’s disease patient sera and 288 sera samples from healthy people. The gene expression dataset GSE165632 included 5 samples from sedentary patients and 9 samples trained for long-

term endurance and resistance. The full matrix file and sample information files were downloaded for further bioinformatic analysis.

**2.2. Screening of DEMs and DE-miRNAs.** Analysis of the difference in mRNA expression matrix was realized using the LIMMA package moderated paired *t*-test difference test [12]. EdgeR package was used for differential analysis of miRNA expression matrix [13]. The plot function from the “base” package was used to plot the volcanoes and mark key mRNAs or miRNAs on the volcanoes. GO and KEGG enrichment analysis was then performed on the differentially expressed mRNAs (DEMs) obtained using the aforementioned methods. Bar graphs of the enrichment analysis were plotted ( $p < 0.05$ ).

**2.3. miRNA-mRNA Regulatory Network.** The miRWalk3.0 database (<http://mirwalk.umm.uni-heidelberg.de/>), which includes 10 databases (RNA22, PITA, PICTAR5, PICTAR4,

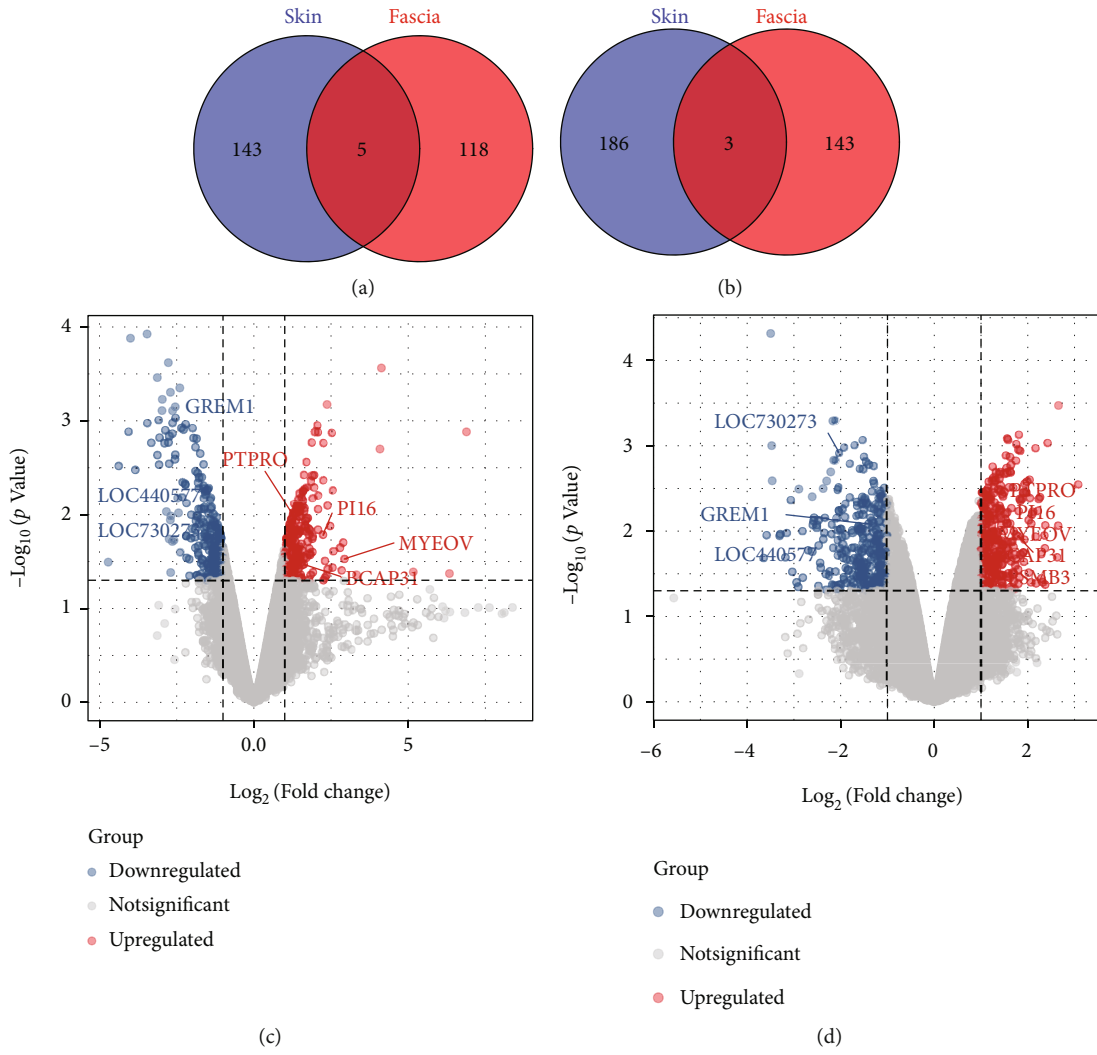
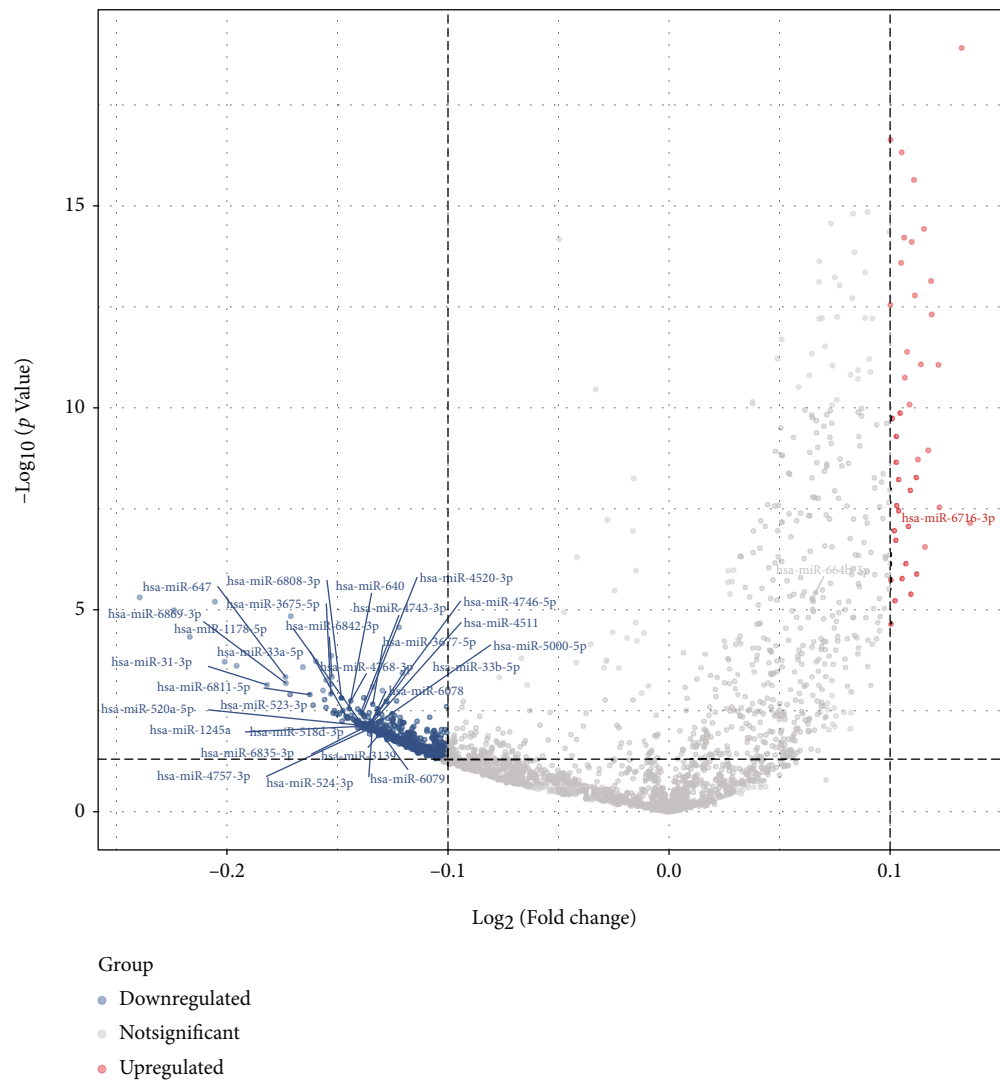


FIGURE 2: Continued.



(e)

FIGURE 2: Identification of co-DEMs and DE-miRNAs. Venn plot intersection analysis identified mRNAs that were codifferentially expressed in hernia (both skin and fascia) (a, b). Volcano plots were used to demonstrate codifferentially expressed genes (c, d). Differentially expressed miRNAs were screened from the cognitive damage miRNA dataset (GSE120584) (e).

Targetscan, RNAhybrid, miRWalk, miRDB, miRanda, and DIANAmt, was used to construct the miRNA-mRNA regulatory network.

**2.4. Functional Validation.** Gene set enrichment analysis (GSEA) was performed based on the core mRNAs obtained from the screening. The GSEA software (version 4.1.0) was employed to perform GSEA enrichment analysis, and a random sample size of 1000,  $p < 0.05$ , was set as the threshold of statistical significance. Immunohistochemical data were obtained from the Human Protein Atlas (THPA) (<https://www.proteinatlas.org/>). The HPA is licensed under the Creative Commons Attribution-ShareAlike 3.0 International License [14].

**2.5. Quantitative Real-Time PCR (qRT-PCR) and Sample Collection.** A total of 41 patients were recruited for this study.

Out of the total patients, 21 belonged to the hernia group while 20 belonged to the normal group. Ethical review and consent for this study were obtained from the Ethics Committee of Shanghai General Hospital. Fascia tissue samples were obtained during surgery. Isolation of total RNA from the tissues was done using the Mini-BEST Universal RNA Extraction Kit (TaKaRa, Kyoto, Japan) as guided by the manufacturer. Subsequently, RNA was converted to cDNA using reverse transcription with Prime-ScriptRT (TaKaRa). Then, the qPCR was performed on a Cyler 480 (Roche Diagnostics, Basel, Switzerland) using SYBR Green Master Mix (TaKaRa). In parallel, we isolated total miRNA from cell cultures using TRIzol® Reagent. The quantity and quality of miRNA were determined using stem-loop quantitative RT-PCR (TaqMan probe method). The first strand cDNA of purified MIRNA was synthesized using M-MLV reverse transcriptase and primers according to the instructions in

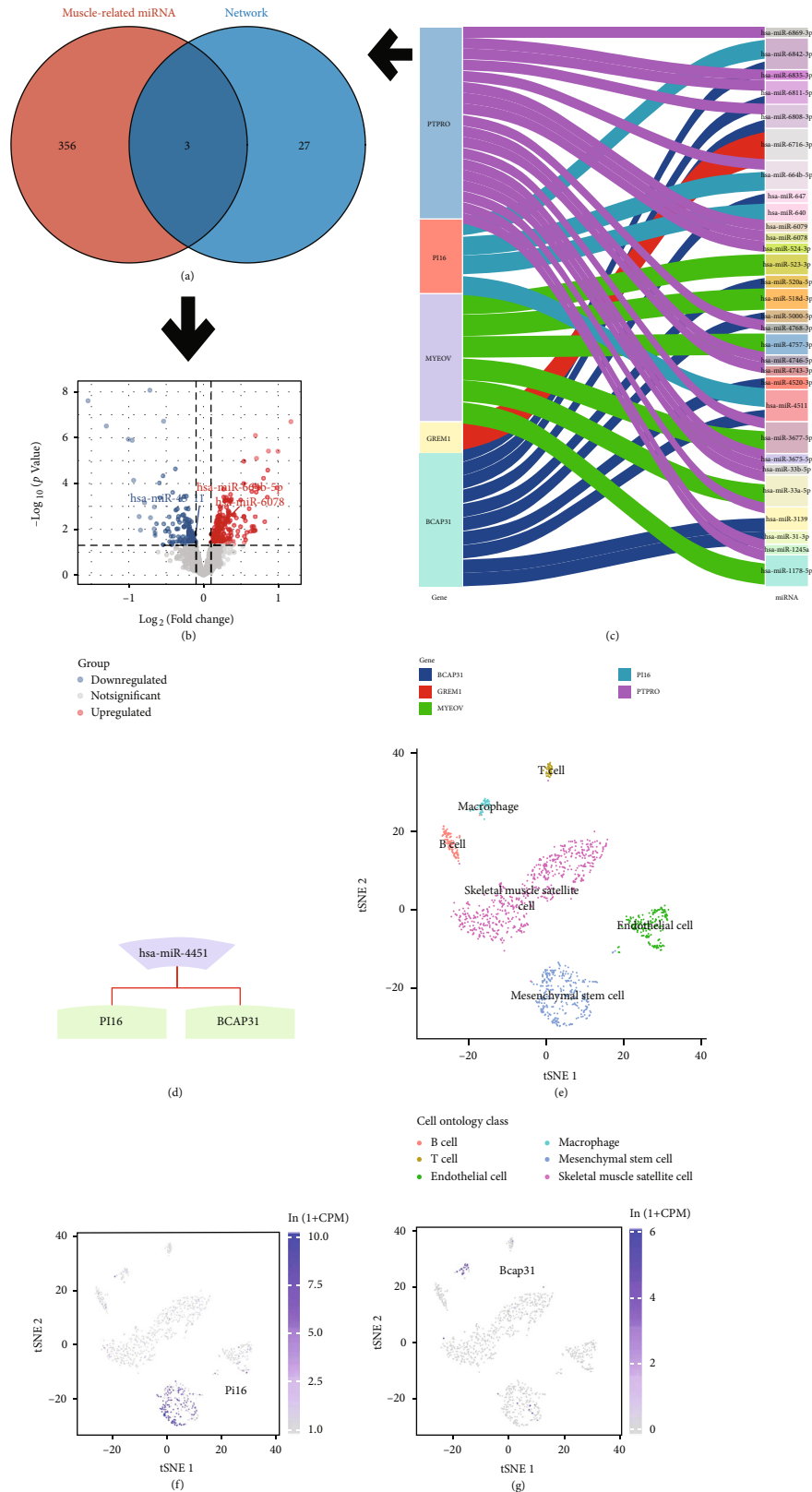


FIGURE 3: Construction of miRNA-mRNA regulatory networks and single-cell expression profiling. The intersections of 359 muscle-related miRNAs and 30 DE-miRNAs in the miRNA-mRNA network were determined by mapping Wayne plots (a). Volcano plot of intersecting genes (b). Sankey plots showing miRNA-mRNA networks constructed based on the miRWalk3.0 database (c). miR-4451 regulates PI16 and BCAP31 expressions (d). Annotated map of the single cell expression from mouse tissues (e). Pi16 was found to be highly enriched in mesenchymal stem cells (f). Bcap31 was found to be enriched in most cell types (g).

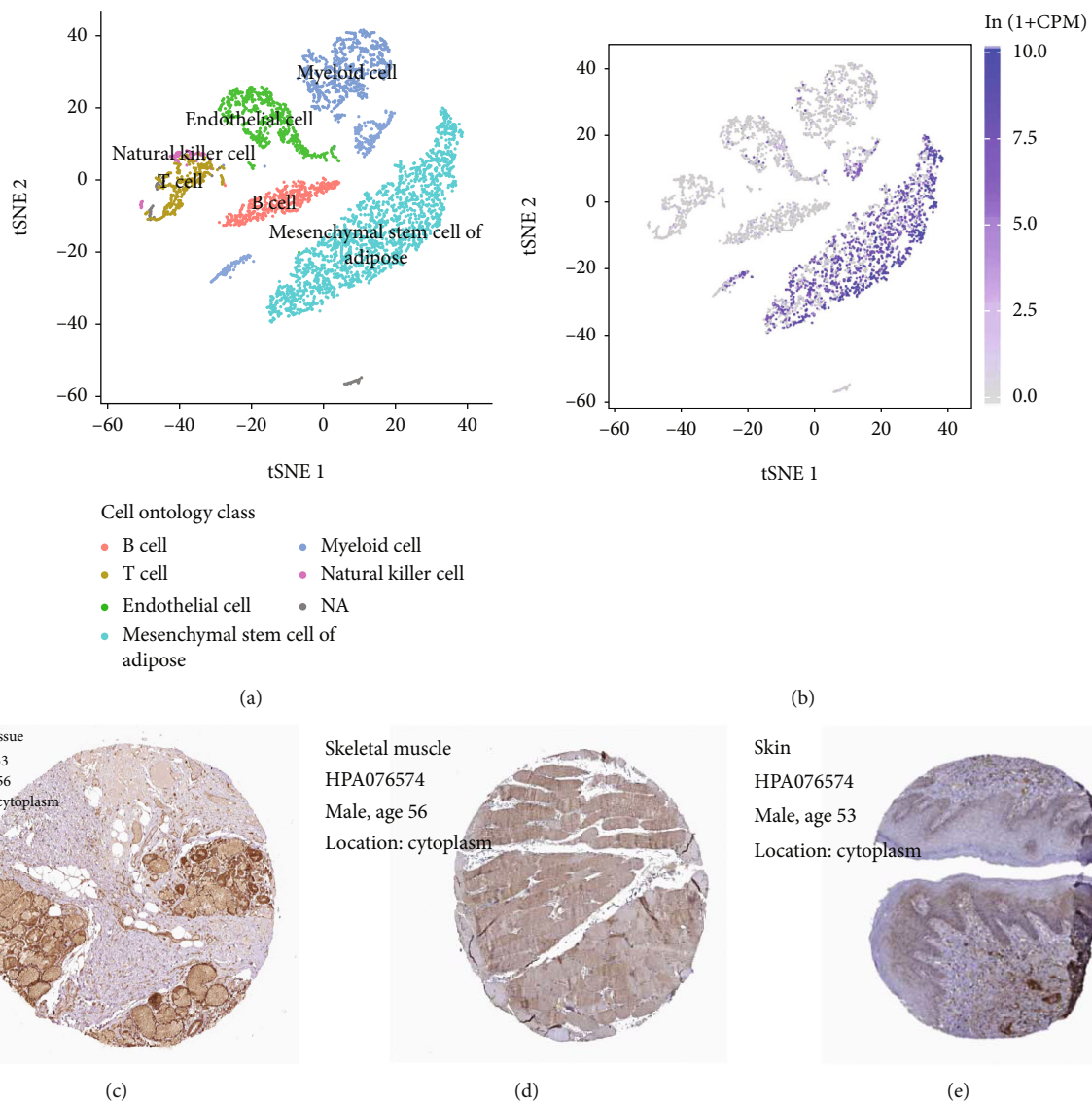


FIGURE 4: Expression of PI16 in the adipose tissue. In the adipose tissue, Pi16 was found to be enriched in mesenchymal stem cells of adipose (a, b). In the immunohistochemical profile of the THPA database, Pi16 was found to be widely enriched in the adipose tissue, skeletal muscle, and skin (c, d).

the protocol provided by the manufacturer (Promega, Fitchberg, MA, USA). The relative gene expression was determined using the U6 gene as an internal standard. All qRT-PCR analyses were carried out in triplicates.

**2.6. Dual Luciferase Reporter Gene Assay.** The HEK293 cell line is a highly efficient and easy to culture cell line for transfection. The PI16 reporter plasmids were obtained from GeneChem (Shanghai, China). Cotransfection of the reporter vector with PI16-WT or PI16-Mut into HEK293 cells was conducted with the Lipofectamine 2000 system (Invitrogen, Carlsbad, CA, USA). Cotransfection of the reporter vector with PI16-WT or PI16-Mut into HEK293 cells was conducted with the Lipofectamine 2000 system (Invitrogen, Carlsbad, CA, USA) for 48 h. Thereafter, the luciferase reporter system was then used to assess luciferase activity.

**2.7. Statistical Analysis and Gene Single Cell Expression Database.** Statistical analyses were completed using R software (version 4.0.2) and GraphPad software (version 7.0). Differences between the two groups were compared by two-tailed Student's *t*-test ( $p < 0.05$  was considered statistically different). Analysis of the gene expression within cells was completed based on previous studies [15]. Tabula Muris is a compilation of single cell transcriptional data from *Mus musculus* containing nearly 100,000 cells from 20 organs and tissues.

### 3. Results

**3.1. Identification of DEMs and Enrichment Analysis.** In the hernia dataset, GSE196374, we identified 148 genes and 123 genes that were upregulated in skin and fascia tissues where hernia occurred, respectively. In addition, 189 genes and

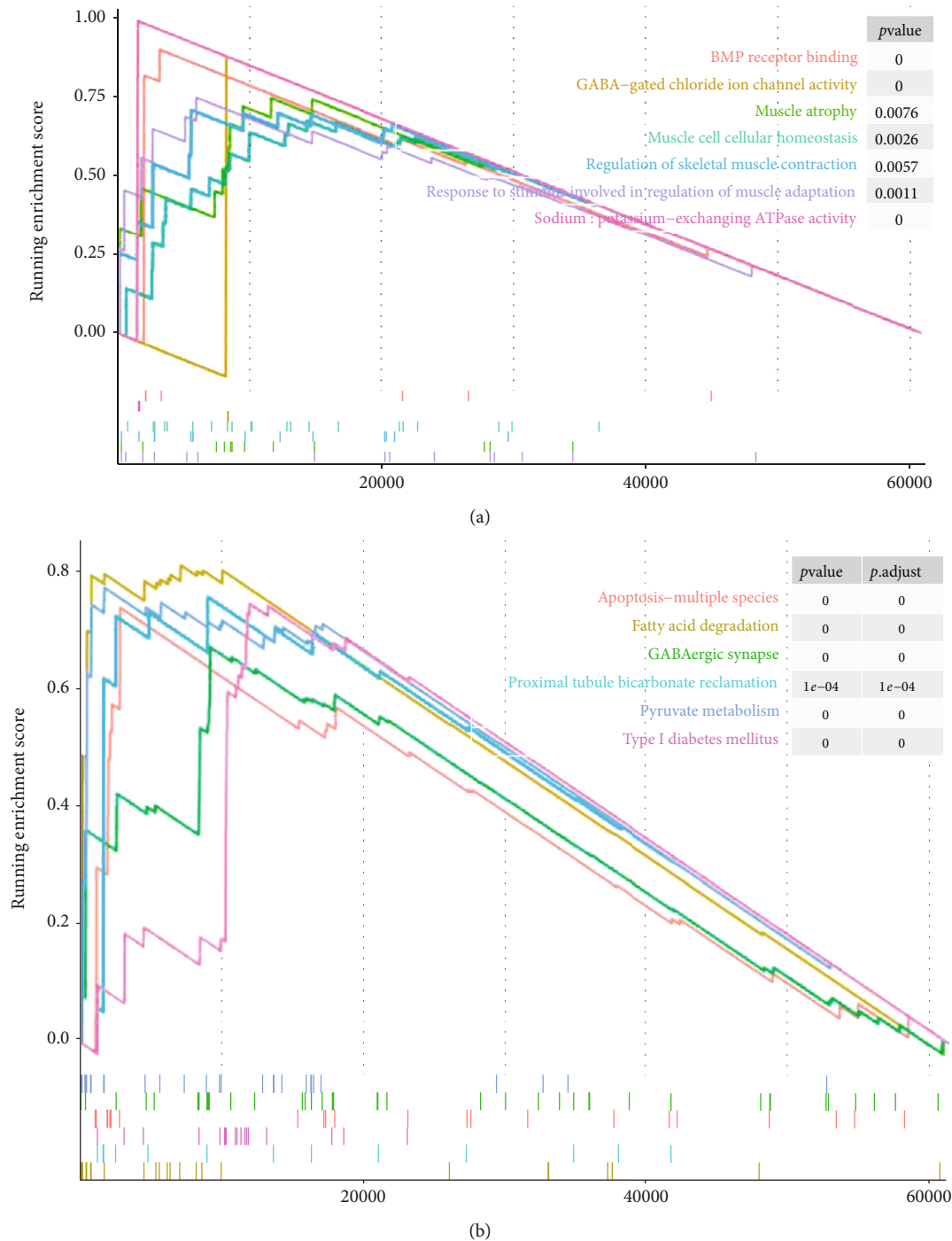


FIGURE 5: GSEA enrichment analysis showing GO functional analysis and KEGG pathway analysis associated with PI16. GO enrichment analysis (a). KEGG enrichment analysis (b).

146 genes were downregulated in the skin and fascia tissues where hernias occurred, respectively. GO and KEGG enrichment analyses were performed for these up- and downregulated DEMs, respectively. GO enrichment analyses of DEMs in fascia tissues are shown in Figures 1(a) and 1(b). The KEGG enrichment analyses of DEMs in fascia tissues are shown in Figure 1(c). Enrichment analyses of DEMs in skin tissues are shown in Figure 1(d).

**3.2. Identification of Co-DEMs and DE-miRNAs.** To identify mRNAs that are codifferentially expressed in hernia sacs (both skin and fascia), we performed veen plot intersection analysis (Figures 2(a) and 2(b)). These coexpressed differential genes were presented in a volcano plot (Figures 2(c) and 2(d)). We found that PTPTO, PI16, BCAP31, MYEOV, and PSMB3 were upregulated in the fascia and skin while LOC730273, GREM1, and LOC440577 were downregulated



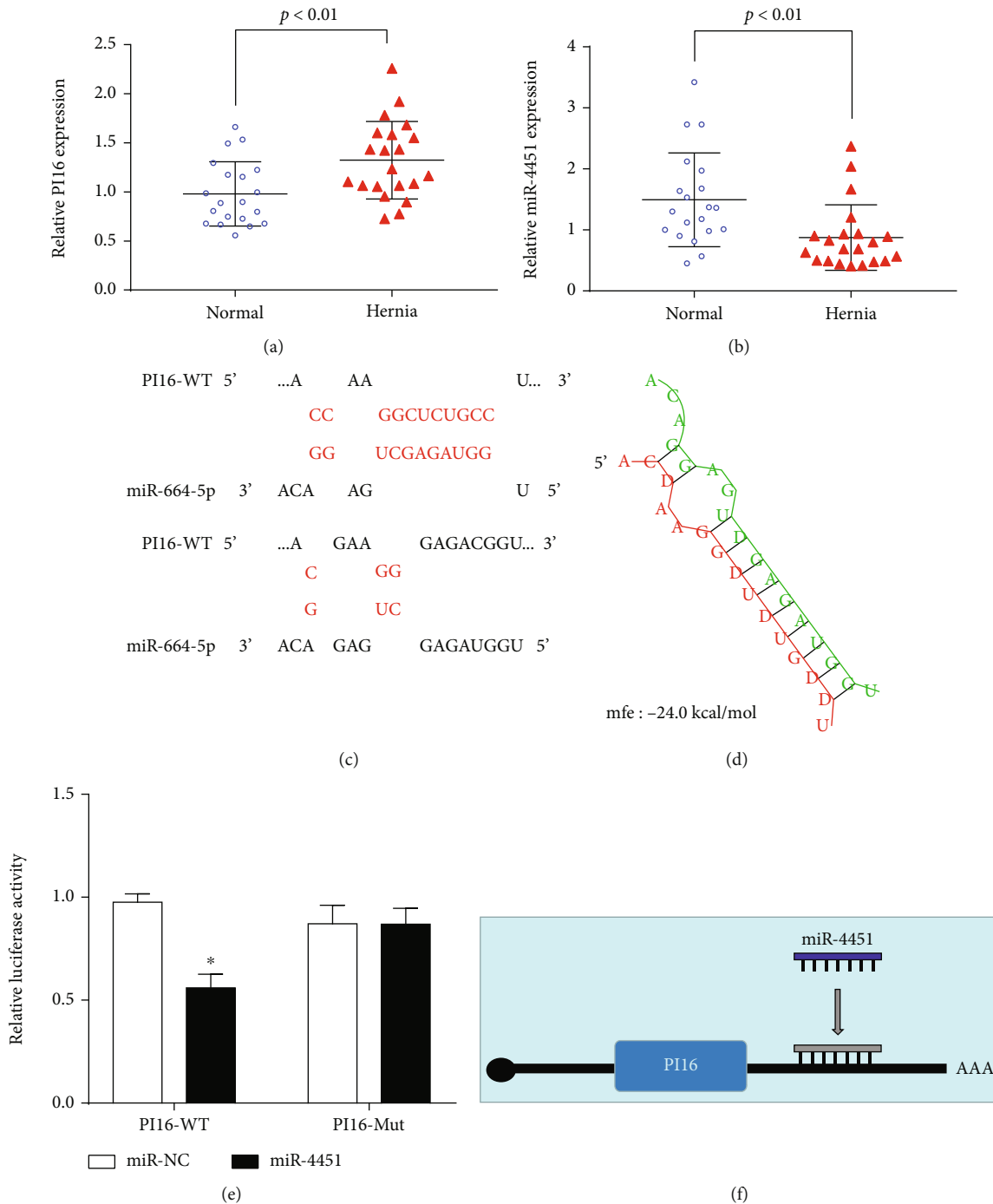


FIGURE 6: miR-4451 downregulates the expression of PI16. The relative expression of miR-4451 and PI16 in normal and hernia, respectively, was detected by qPCR (a, b). Pattern plots of PI16 wild type and miR-4451 binding with PI16 mutant groups (c). miR-4451 was determined as a target miRNA for PI16 using RNAhybrid 2.12. The minimum free energy was 24 kcal/mol (d). Expression levels of mir-32-3p in HEK-293 cells were detected by RT-qPCR after transfection of cells with mir-32-3p mimics (e). Pattern diagram of miR-4451 possibly acting as a sponge for PI16 and downregulating PI16 expression (f).

in the fascia and skin. Differentially expressed miRNAs (DE-miRNAs) in the cognitive impairment miRNA dataset GSE120584 were also screened out (Figure 2(e)).

3.3. Construction of the miRNA-mRNA Regulatory Network. To construct the miRNA-mRNA regulatory network, we

constructed a miRNA-mRNA network (Figure 3(c)) based on the miRWalk 3.0 database. The network is composed of DE-miRNAs and DEMs. A total of 30 DE-miRNAs and 5 mRNAs were included. The skeletal muscle miRNA dataset GSE165632 (samples from participants serum) was used to obtain 359 muscle-related miRNAs. These muscle-related

miRNAs may be associated with abdominal wall muscle weakness. Three miRNAs (hsa-miR-4511, hsa-miR-664b-5p, and hsa-miR-6078) were obtained by plotting these 359 muscle-related miRNAs against 30 DE-miRNAs in the miRNA-mRNA network (Figure 3(a)). These results are presented in the volcano plot, as shown in Figure 3(b). Therefore, miR-4451 was found to be coassociated with muscle atrophy and cognitive ageing. Based on the results in Figures 3(c) and 3(d), hsa-miR-4451 is suggested as a possible sponge regulating PI16 and BCAP31.

**3.4. Expression Distribution of Core mRNAs.** We analyzed the expression of Pi16 and Bcap31 in skeletal muscles at the single cell level based on Tabula Muris. The single cell expression annotation profile is shown in Figure 3(e). Pi16 was found to be predominantly enriched in mesenchymal stem cells (Figure 3(f)). Bcap31 was not found to be specifically enriched in any of the analyzed cell types (Figure 3(g)). In adipose tissues, Pi16 was found to be enriched in mesenchymal stem cells, whereas the Bcap31 expression was not detected (Figures 4(a) and 4(b)). Mesenchymal stem cells have an important role in skeletal muscle development, and therefore, we selected Pi16 for further analysis. Figures 4(c) and 4(d) show immunohistochemical profiles from the THPA database. Pi16 was found to be highly enriched in adipose tissues, in the skeletal muscle, and in the skin. In addition, Pi16 was also enriched in the cytoplasm.

**3.5. Functional Characterization of PI16.** GO functional enrichment analysis of GSEA revealed PI16-related signaling functions, including BMP receptor binding, GABA-gated chloride ion channel activity, muscle atrophy, muscle cell cellular homeostasis, regulation of skeletal muscle contraction, and response to stimuli involved in regulation of muscle adaptation (Figure 5(a)). In addition, KEGG enrichment analysis revealed the functions associated with PI16 isoforms, including apoptosis-multiple species, fatty acid degradation, GABAergic synapse, proximal tubule bicarbonate reclamation, pyruvate metabolism, and type I diabetes mellitus (Figure 5(b)). Enrichments of these functions and pathways implied that PI16 may play a role in fat metabolism, muscle function, and energy metabolism.

**3.6. Cognitive Impairment Upregulates PI16 by Downregulating miRNA-4451 and Is Associated with Hernia Development.** Expression levels of miR-4451 and PI16 in tissue samples were determined by qRT-PCR (Figures 6(a) and 6(b)). PI16 was found to be upregulated in hernia ( $p < 0.01$ ) while miR-4451 was downregulated ( $p < 0.01$ ). We hypothesized that miR-4451 may be involved in hernia pathogenesis by regulating PI16 transcription. To test this hypothesis, we predicted the potential binding site of miR-4451 to PI16 using RNAhybrid (Figure 6(d)). Luciferase reporter assays revealed that HEK-293 cells cotransfected with PLA2G4A-mut and the MIR-NC control had lower luciferase activity, while HEK-293 cells cotransfected with PI16-WT and miR-4451 had higher luciferase activities (Figures 6(c) and 6(e)). Moreover, miR-4451 acts as a sponge for PI16 to downregulate its expression (Figure 6(f)). We added Table 1 to present

TABLE 1: Differences of clinical characteristics between effective And ineffective groups.

Characteristics	Normal [N = 20]	Hernia [N = 21]
Gender		
Female	11 [55%]	9 [43%]
Male	9 [45%]	12 [57%]
Age		
Mean [SD]	70.7 [7.8]	65.6 [5.5]
Median [Min, Max]	70 [60, 90]	64 [60, 81]
BMI		
Mean [SD]	22.7 [2.5]	24.7 [3.2]
Median [Min, Max]	22.8 [19.2, 29.1]	24.3 [18.5, 31.5]
Hypertension		
Yes	8 [40%]	8 [38%]
No	12 [60%]	13 [62%]
Diabetes		
Yes	4 [20.0%]	3 [14%]
No	16 [80%]	18 [86%]
Hyperlipidemia		
Yes	4 [20%]	6 [29%]
No	16 [80%]	15 [71%]

the lack of significant differences in clinical characteristics between patients who developed a hernia and those who did not. These findings imply that downregulation of circulating miR-4451 may be responsible for upregulated PI16 in hernia sacs.

## 4. Discussion

Weak abdominal muscles and fascia among elderly individuals predispose them to hernia. In this study, miRNAs, which are commonly associated with muscle atrophy and dementia, were identified, and the potential miRNA-mRNA regulatory networks were established. miR-4451 may inhibit PI16 transcription, which may be a potential link between herniation and dementia development. In conclusion, this study revealed a potential link between dementia and herniation at the molecular regulatory level.

We identified DEMs that are codifferentially expressed in the hernia dataset. These DEMs were also analyzed for enrichment. Then, the dementia miRNA dataset (GSE120584) and the muscle atrophy miRNA dataset (GSE165632) were combined to construct a potential miRNA-mRNA regulatory network. The Tabula Muris and THPA web databases were used to evaluate the distribution of hub mRNA in cells and tissues. Pi16 was found to be highly enriched in adipose tissues, in skeletal muscles, and in the skin. GSEA enrichment analysis revealed a possible role of P16 in adipose metabolism, muscle function, and energy metabolism. In clinical samples, PI16 was found to be upregulated in hernia, while miR-4451 was downregulated. The luciferase reporter gene assay showed that mR-4451 may act as a sponge for P116, downregulating the P116 expression.

Therefore, downregulation of circulating miR-4451 may be responsible for upregulated PI16 in hernia sacs.

The peptidase inhibitor 16 (PI16) is a member of the CAP protein superfamily, a group of proteins that are evolutionarily highly conserved [16, 17]. PI16, a secretory protein that is mainly localized in the endoplasmic reticulum and secretory vesicles of fibroblasts, plays an important role in the cardiovascular system [18]. The overexpression of PI16 inhibits MMP activity, and MMPs, including MMP1, MMP2, MMP9, and MMP13, are associated with abdominal hernia development [19–22]. In this study, PI16 was found to be highly enriched in adipose tissues, skeletal muscles, and in the skin. GSEA revealed that PI16 functions in fat metabolism, muscle, and energy metabolism. These findings confirm a previously documented hypothesis [23].

The potential of miR-4451 as a cancer biomarker has been reported [24–26]. We postulated that miR-4451 may be a biomarker for the development of hernia and cognitive impairment. Cognitive impairment may be associated with hernia development by downregulating miR-4451 to upregulate PI16. However, other biological roles of miR-4451 should be further investigated.

A previous cohort study found that there may be a potential link between hernias and dementia; although, the exact mechanism is unknown [23]. Bioinformatics is a powerful research method for predicting molecular mechanisms and associations between genes. We used bioinformatic approach to investigate the crosstalk between abdominal hernias and cognitive impairment. A potential miRNA-mRNA network for dementia and hernia was constructed. It was found that miR-4451 is involved in the regulation of the PI16 expression. This study is associated with some limitations, and therefore, caution should be exercised before referring to our findings. Further studies should include more factors and involve more clinical samples to determine the effect of miR-4451 on PI16. This is because the pathogenesis of abdominal hernias is complex, and alterations in abdominal muscles and adipose tissues are unlikely to be the only factors involved. The most significant DE-miRNAs and DEMs were the only ones included in this study. In future, we will perform animal and cellular experiments to elucidate on the mechanisms of miR-4451's action on PI16.

## 5. Conclusion

The constructed miRNA-mRNA network reveals the potential association between dementia and hernia. miR-4451 is involved in the regulation of the PI16 expression, which may be a key target and biomarker for evaluating hernia pathogenesis and dementia crosstalk.

## Abbreviations

DEMs:	Differentially expressed mRNAs
DE-miRNAs:	Differentially expressed micro-RNAs
GO:	Gene ontology
GEO:	The Gene Expression Omnibus
GSEA:	Gene-set enrichment analysis
KEGG:	Kyoto Encyclopedia of Genes and Genomes

miRNA:	Micro-RNA
NC:	Normal control
qPCR:	Quantitative real-time PCR.

## Data Availability

If raw data is required, please contact the corresponding author for further access.

## Conflicts of Interest

All authors report no conflicts of interest.

## Acknowledgments

All authors worked together to collect data, specimens, perform data analysis and predictions, write the manuscript, and finally approve the manuscript.

## References

- [1] L. Robinson, E. Tang, and J. P. Taylor, "Dementia: timely diagnosis and early intervention," *BMJ*, vol. 350, article h3029, 2015.
- [2] S. Köhler, F. Buntinx, K. Palmer, and M. van den Akker, "Depression, vascular factors, and risk of dementia in primary care: a retrospective cohort study," *Journal of the American Geriatrics Society*, vol. 63, no. 4, pp. 692–698, 2015.
- [3] B. Poblador-Plou, A. Calderón-Larrañaga, J. Marta-Moreno et al., "Comorbidity of dementia: a cross-sectional study of primary care older patients," *BMC Psychiatry*, vol. 14, no. 1, p. 84, 2014.
- [4] R. Sahathevan, A. Brodtmann, and G. A. Donnan, "Dementia, stroke, and vascular risk factors; a review," *International Journal of Stroke*, vol. 7, no. 1, pp. 61–73, 2012.
- [5] D. Shigemizu, S. Akiyama, Y. Asanomi et al., "Risk prediction models for dementia constructed by supervised principal component analysis using miRNA expression data," *Communications Biology*, vol. 2, no. 1, p. 77, 2019.
- [6] K. Maiese, "c," *Current Neurovascular Research*, vol. 16, no. 1, pp. 1–2, 2019.
- [7] J. Zhang, Y. Yu, and J. Wang, "Protein nutritional support: the classical and potential new mechanisms in the prevention and therapy of sarcopenia," *Journal of Agricultural and Food Chemistry*, vol. 68, no. 14, pp. 4098–4108, 2020.
- [8] A. Zhang, M. Li, B. Wang, J. D. Klein, S. R. Price, and X. H. Wang, "miRNA-23a/27a attenuates muscle atrophy and renal fibrosis through muscle-kidney crosstalk," *Journal of Cachexia, Sarcopenia and Muscle*, vol. 9, no. 4, pp. 755–770, 2018.
- [9] A. Barbiera, L. Pelosi, G. Sica, and B. M. Scicchitano, "Nutrition and microRNAs: novel insights to fight sarcopenia," *Antioxidants (Basel)*, vol. 9, no. 10, p. 951, 2020.
- [10] Y. Wang, Z. J. Zhao, X. R. Kang et al., "lncRNA DLEU2 acts as a miR-181a sponge to regulate SEPP1 and inhibit skeletal muscle differentiation and regeneration," *Aging (Albany NY)*, vol. 12, no. 23, article 104095, pp. 24033–24056, 2020.
- [11] M. Herrera-Rivero, R. Zhang, S. Heilmann-Heimbach et al., "Circulating microRNAs are associated with pulmonary hypertension and development of chronic lung disease in

- congenital diaphragmatic hernia,” *Scientific Reports*, vol. 8, no. 1, article 10735, 2018.
- [12] M. E. Ritchie, B. Phipson, D. Wu et al., “Limma powers differential expression analyses for RNA-sequencing and microarray studies,” *Nucleic Acids Research*, vol. 43, no. 7, p. e47, 2015.
- [13] M. D. Robinson, D. J. McCarthy, and G. K. Smyth, “edgeR: a Bioconductor package for differential expression analysis of digital gene expression data,” *Bioinformatics*, vol. 26, no. 1, pp. 139–140, 2010.
- [14] M. Uhlen, L. Fagerberg, B. M. Hallstrom et al., “Tissue-based map of the human proteome,” *Science*, vol. 347, no. 6220, article 1260419, 2015.
- [15] The Tabula Muris Consortium, Overall coordination, Logistical coordination et al., “Single-cell transcriptomics of 20 mouse organs creates a *Tabula Muris*,” *Nature*, vol. 562, no. 7727, pp. 367–372, 2018.
- [16] M. Deng, S. Yang, Y. Ji et al., “Overexpression of peptidase inhibitor 16 attenuates angiotensin II-induced cardiac fibrosis via regulating HDAC1 of cardiac fibroblasts,” *Journal of Cellular and Molecular Medicine*, vol. 24, no. 9, pp. 5249–5259, 2020.
- [17] M. Regn, B. Laggerbauer, C. Jentzsch et al., “Peptidase inhibitor 16 is a membrane-tethered regulator of chemerin processing in the myocardium,” *Journal of Molecular and Cellular Cardiology*, vol. 99, pp. 57–64, 2016.
- [18] G. G. Hazell, A. M. Peachey, J. E. Teasdale et al., “PI16 is a shear stress and inflammation-regulated inhibitor of MMP2,” *Scientific Reports*, vol. 6, no. 1, article 39553, 2016.
- [19] G. A. Antoniou, G. S. Georgiadis, S. A. Antoniou, F. A. Granderath, A. D. Giannoukas, and M. K. Lazarides, “Abdominal aortic aneurysm and abdominal wall hernia as manifestations of a connective tissue disorder,” *Journal of Vascular Surgery*, vol. 54, no. 4, pp. 1175–1181, 2011.
- [20] S. A. Antoniou, G. A. Antoniou, F. A. Granderath, and C. Simopoulos, “The role of matrix metalloproteinases in the pathogenesis of abdominal wall hernias,” *European Journal of Clinical Investigation*, vol. 39, no. 11, pp. 953–959, 2009.
- [21] M. G. Franz, “The biology of hernia formation,” *The Surgical Clinics of North America*, vol. 88, no. 1, pp. 1–15, 2008.
- [22] N. A. Henriksen, D. H. Yadete, L. T. Sorensen, M. S. Agren, and L. N. Jorgensen, “Connective tissue alteration in abdominal wall hernia,” *The British Journal of Surgery*, vol. 98, no. 2, pp. 210–219, 2011.
- [23] K. C. Hung, C. K. Sun, J. Y. Chen, H. C. Wang, and C. H. Kao, “Association between abdominal hernia and the risk of subsequent dementia,” *Brain and Behavior: A Cognitive Neuroscience Perspective*, vol. 9, no. 11, article e01434, 2019.
- [24] X. Xu, H. Liu, N. Gross et al., “Overexpression of miRNA 4451 is associated with a poor survival of patients with hypopharyngeal cancer after surgery with postoperative radiotherapy,” *Translational Oncology*, vol. 11, no. 5, pp. 1244–1250, 2018.
- [25] X. Xu, Z. Lu, N. Gross et al., “A 3-miRNA signature predicts survival of patients with hypopharyngeal squamous cell carcinoma after post-operative radiotherapy,” *Journal of Cellular and Molecular Medicine*, vol. 23, no. 12, pp. 8280–8291, 2019.
- [26] Y. Mao, J. Shen, Y. Lu et al., “RNA sequencing analyses reveal novel differentially expressed genes and pathways in pancreatic cancer,” *Oncotarget*, vol. 8, no. 26, pp. 42537–42547, 2017.

## Research Article

# Single-Cell Transcriptomics-Based Study of Transcriptional Regulatory Features in the Mouse Brain Vasculature

Wei-Wei Lin <sup>1</sup>, Lin-Tao Xu,<sup>1</sup> Yi-Sheng Chen,<sup>2</sup> Ken Go,<sup>3</sup> Chenyu Sun,<sup>4</sup> and Yong-Jian Zhu <sup>1</sup>

<sup>1</sup>Department of Neurosurgery, Second Affiliated Hospital of Zhejiang University School of Medicine, Zhejiang University, 88 Jiefang Road, Hangzhou, 310009 Zhejiang, China

<sup>2</sup>Department of Orthopedics, Shanghai General Hospital, Shanghai Jiao Tong University School of Medicine, Shanghai Jiao Tong University, 100 Haining Road, Shanghai 200080, China

<sup>3</sup>Clinical Training Centre, St. Marianna Hospital, Japan

<sup>4</sup>Internal Medicine, AMITA Health Saint Joseph Hospital Chicago, 2900 N. Lake Shore Drive, Chicago, 60657 Illinois, USA

Correspondence should be addressed to Yong-Jian Zhu; neurosurgery@zju.edu.cn

Wei-Wei Lin and Lin-Tao Xu contributed equally to this work.

Received 18 May 2021; Revised 18 June 2021; Accepted 6 July 2021; Published 23 July 2021

Academic Editor: Yuzhen Xu

Copyright © 2021 Wei-Wei Lin et al. This is an open access article distributed under the Creative Commons Attribution License, which permits unrestricted use, distribution, and reproduction in any medium, provided the original work is properly cited.

**Background.** The critical role of vascular health on brain function has received much attention in recent years. At the single-cell level, studies on the developmental processes of cerebral vascular growth are still relatively few. Techniques for constructing gene regulatory networks (GRNs) based on single-cell transcriptome expression data have made significant progress in recent years. Herein, we constructed a single-cell transcriptional regulatory network of mouse cerebrovascular cells. **Methods.** The single-cell RNA-seq dataset of mouse brain vessels was downloaded from GEO (GSE98816). This cell clustering was annotated separately using singleR and CellMarker. We then used a modified version of the SCENIC method to construct GRNs. Next, we used a mouse version of SEEK to assess whether genes in the regulon were coexpressed. Finally, regulatory module analysis was performed to complete the cell type relationship quantification. **Results.** Single-cell RNA-seq data were used to analyze the heterogeneity of mouse cerebrovascular cells, whereby four cell types including endothelial cells, fibroblasts, microglia, and oligodendrocytes were defined. These subpopulations of cells and marker genes together characterize the molecular profile of mouse cerebrovascular cells. Through these signatures, key transcriptional regulators that maintain cell identity were identified. Our findings identified genes like *Lmo2*, which play an important role in endothelial cells. The same cell type, for instance, fibroblasts, was found to have different regulatory networks, which may influence the functional characteristics of local tissues. **Conclusions.** In this study, a transcriptional regulatory network based on single-cell analysis was constructed. Additionally, the study identified and profiled mouse cerebrovascular cells using single-cell transcriptome data as well as defined TFs that affect the regulatory network of the mouse brain vasculature.

## 1. Introduction

The critical role of vascular health on brain function has received much attention in recent years [1]. There is a close correlation between the expression of cerebrovascular-specific genes and neurovascular-related diseases. On the other hand, the blood-brain barrier (BBB) is a unique feature of the cerebrovascular system, and it is necessary for the functioning of the nervous system. By developing tissue-specific

properties, the vascular system forms a selective BBB that allows passage of essential molecules to the brain and locks the penetration of potentially harmful compounds or cells. Nonetheless, BBB may be a key barrier to the treatment of brain diseases as revealed in humans and animal models [2, 3]. Research into the characteristics of vascular cells is critical and advances diagnostic and therapeutic techniques for the cerebrovascular system [1]. Even so, the transcriptional regulatory features between cerebrovascular cells remain unclear.



Transcription factors (TFs) have long been recognized as important aspects in the maintenance of cellular identity and function [4]. Increased or decreased TF expression can significantly affect cellular function and can recode cells into different cell types [5–7]. However, the process of cerebral vascular growth and development, at the single-cell level, is still poorly studied. For example, the ability of vascular smooth muscle cells (VSMCs) to contract is critical to the regulation of blood pressure and flow. Nonetheless, there is a lack of prior research on the transcriptional regulation of VSMC contractile function at the individual cell level [8]. Significant progress has been made in recent years in the construction of gene regulatory networks (GRNs) based on single-cell transcriptome expression data [4, 9]. With advances in single-cell sequencing, we can begin to understand the transcriptional regulatory networks in cells.

In this study, we utilized a comprehensive atlas of obtained mouse cerebrovascular single-cell data [1] to construct a single-cell transcriptional regulatory network of mouse cerebrovascular cells. To realize this, the study used single-cell transcriptome data in conjunction with the GRN approach. In the study, we initially defined the TFs that affect the regulatory network of the mouse brain vasculature where it was revealed that even similar cell types have different regulatory networks.

## 2. Materials and Methods

**2.1. Datasets.** A single-cell RNA-seq dataset of mouse brain vasculature was downloaded from GEO (GSE98816) [1]. For each batch of cells, we calculated the number of genes expressed per cell. Genes that expressed less than 0.1% of the cell count were excluded from the study. Such batch of cells did not contain the mitochondrial gene. Ultimately, all cells in this dataset met quality control criteria, and a total of 3186 cells were included for analysis.

**2.2. Dimensional Reduction and Clustering.** Principal component analysis (PCA) together with JackStraw and PCElbow-Plot functions was performed using the Seurat package (version 3.2.2), in R software (version 4.0.2), to select important principal components (PCs) [10, 11]. Seurat's FindAllMarkers function was used to identify specific genes for each cell subpopulation. The RunUMAP function was then used for cell clustering and visual analysis of UMAP. The marker genes were thereafter annotated with the singleR package and corrected with CellMarker according to their characteristics [12, 13].

**2.3. Inference of Regulons and Activity.** A number of methods have been developed to predict GRNs from single-cell gene expression data. This study adapted the SCENIC method as previously described with slight modification [9, 14]. In the SCENIC analysis process, three steps were considered. First, there was the establishment of a gene coexpression network through gene coexpression analysis. Second, we established possible TF-target regulatory relationships based on the gene coexpression network. In this step, the direct regulatory relationship was established using motif analysis. Any direct

downstream genes occurring for each TF were profiled as regulon. It is important to note that, currently, SCENIC only supports transcriptional positive regulation analysis. Third, based on the results of step 2, a regulon activity score (RAS) was calculated for each cell. As described in previous studies, the Avg20 method was repeated three times to assess the variability of random sampling. Thereafter, a *t*-test was used to assess whether the Avg20 method performed better than using all individual cells [4].

**2.4. Functional Validation.** As in previous studies, we used SEEK analysis to verify whether the predicted regulons correlated with their cell type [15]. In brief, we used the mouse version of SEEK to assess whether genes in the regulons were coexpressed. Significantly coexpressed genes in multiple datasets associated with a particular cell type scored positive for high relevance of the function of the regulon to that cell type.

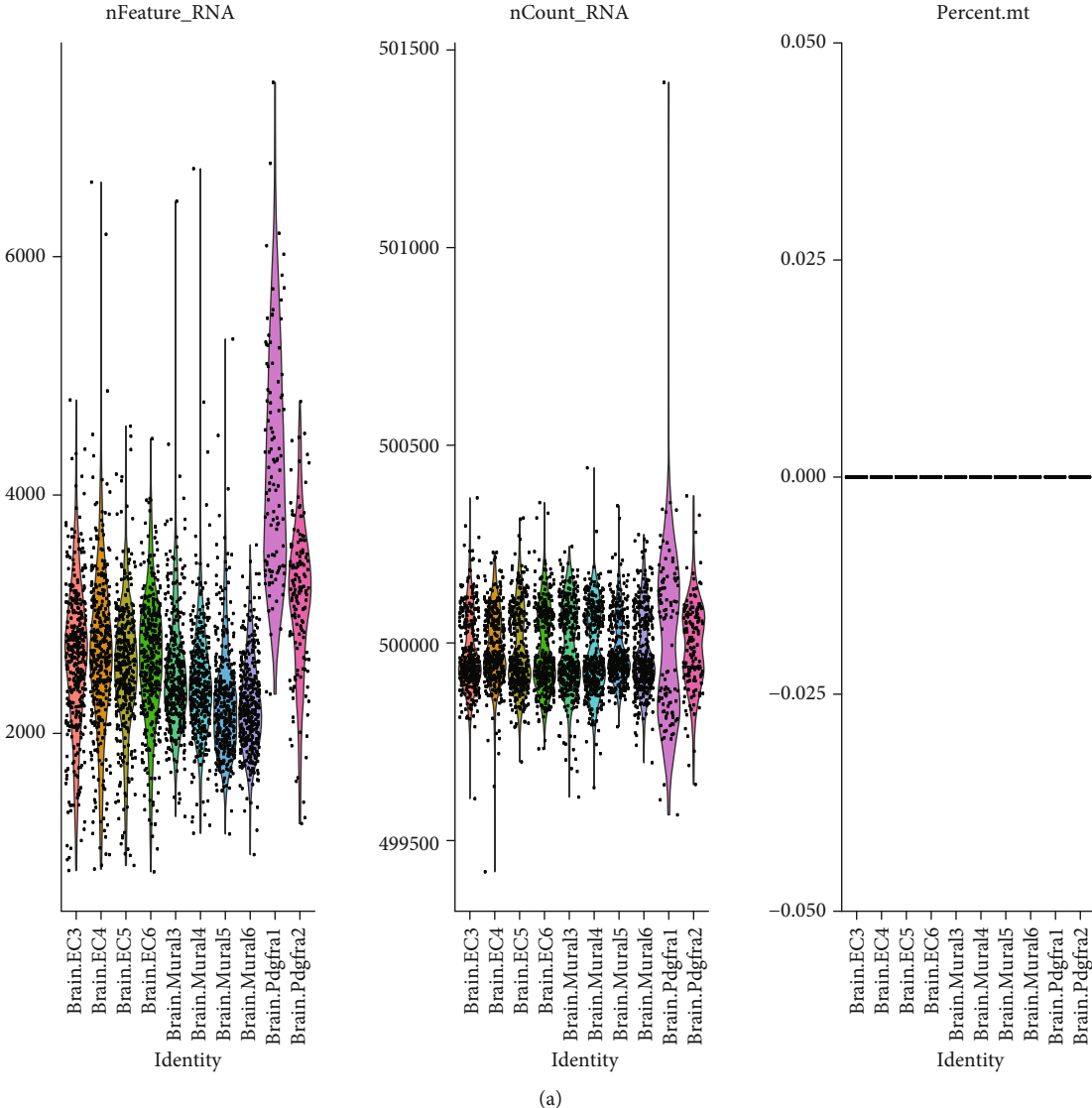
**2.5. Regulon Module Analysis and Quantifying Cell Type Relationship.** To identify regulon modules, we employed two main steps [4, 16]. First, each pair of regulatory relationships was analyzed for Pearson's correlation coefficient. The activity score of each regulon module in relation to a cell type was then defined as the average of the activity scores of its regulon members in all cells of that cell type. The highest ranked units were then filtered for each module. We quantified the relationship between different cell types based on the similarity of overall regulon activity. A pair of cell types was linked if their Spearman correlation coefficient was greater than 0.8. Finally, we used the Markov Clustering Algorithm (MCL) to identify related cell types [17].

## 3. Result

**3.1. Cell Heterogeneity in the Brain Vasculature.** Ten copies of cells from mouse brain vasculature were checked for quality control (GSE98816), and the resultant 3186 cells were included in the study (Figure 1(a)). The correlation of gene expression in the mouse cerebrovascular cells using ANOVA revealed Lum, Spp1, Apod, Moxd1, Acta2, Csf1r, and Mbp as the most variable genes (Figure 1(b)). Analysis with PCA (PC 1 and PC 2) showed that there was no significant separation of mouse cerebrovascular cells (Figure 1(c)). As shown in Figure 1(d), the model having the best clustering results of 10 PCs was selected. The heat map showed that it identified the 10 most important genes in each of these 10 clusters (Figure 1(e)).

**3.2. Cellular Subpopulation Distribution and Marker Genes in Mouse Cerebrovascular Cells.** The nine cell clusters were annotated separately using singleR and CellMarker according to the expression profile of the marker genes. Mouse cerebrovascular cells showed 10 clusters (Figure 2(a)). The majority of cerebrovascular cell clusters observed belonged to normal tissue and known vascular cell types such as endothelial cells, fibroblasts, oligodendrocytes, and microglia (Figure 2(a)). Four major marker genes, namely, Bsg, Atp1b2, Mbp, and Lum, distinguished these four cell types as shown in Figure 2(b). Significant differences were seen in





(a) FIGURE 1: Continued.

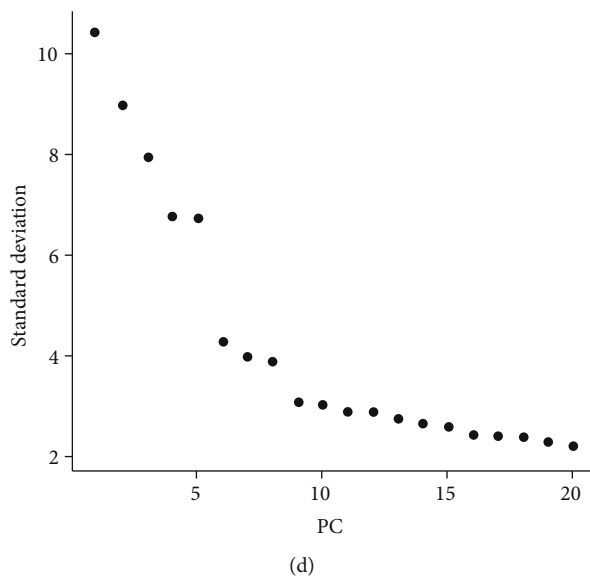
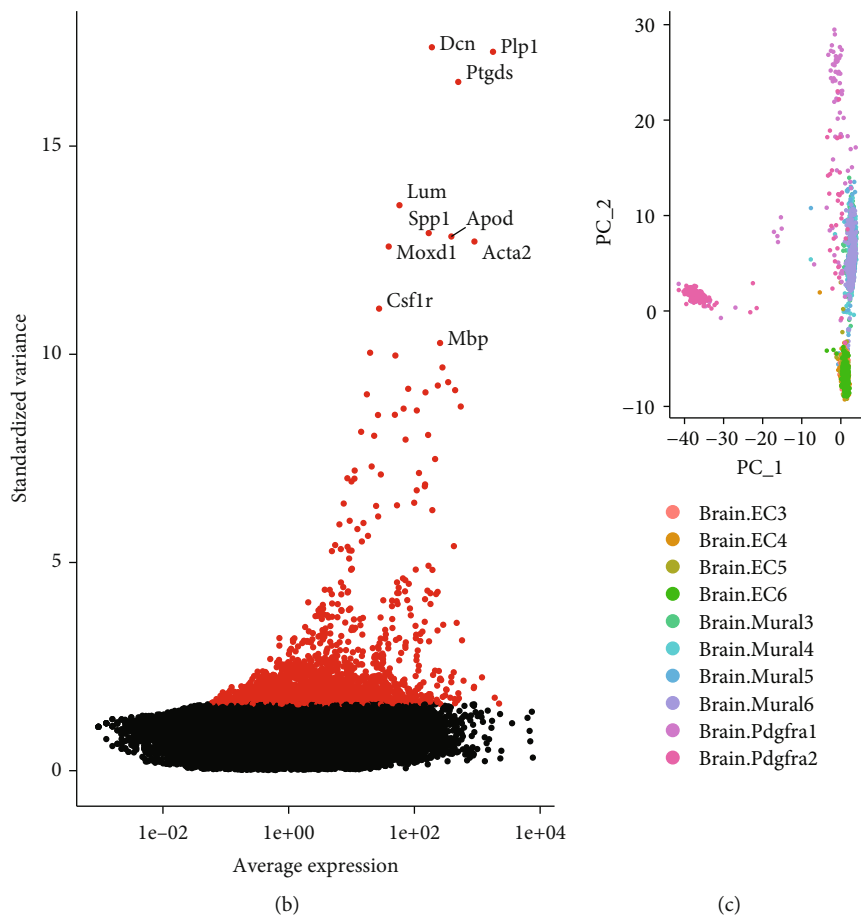
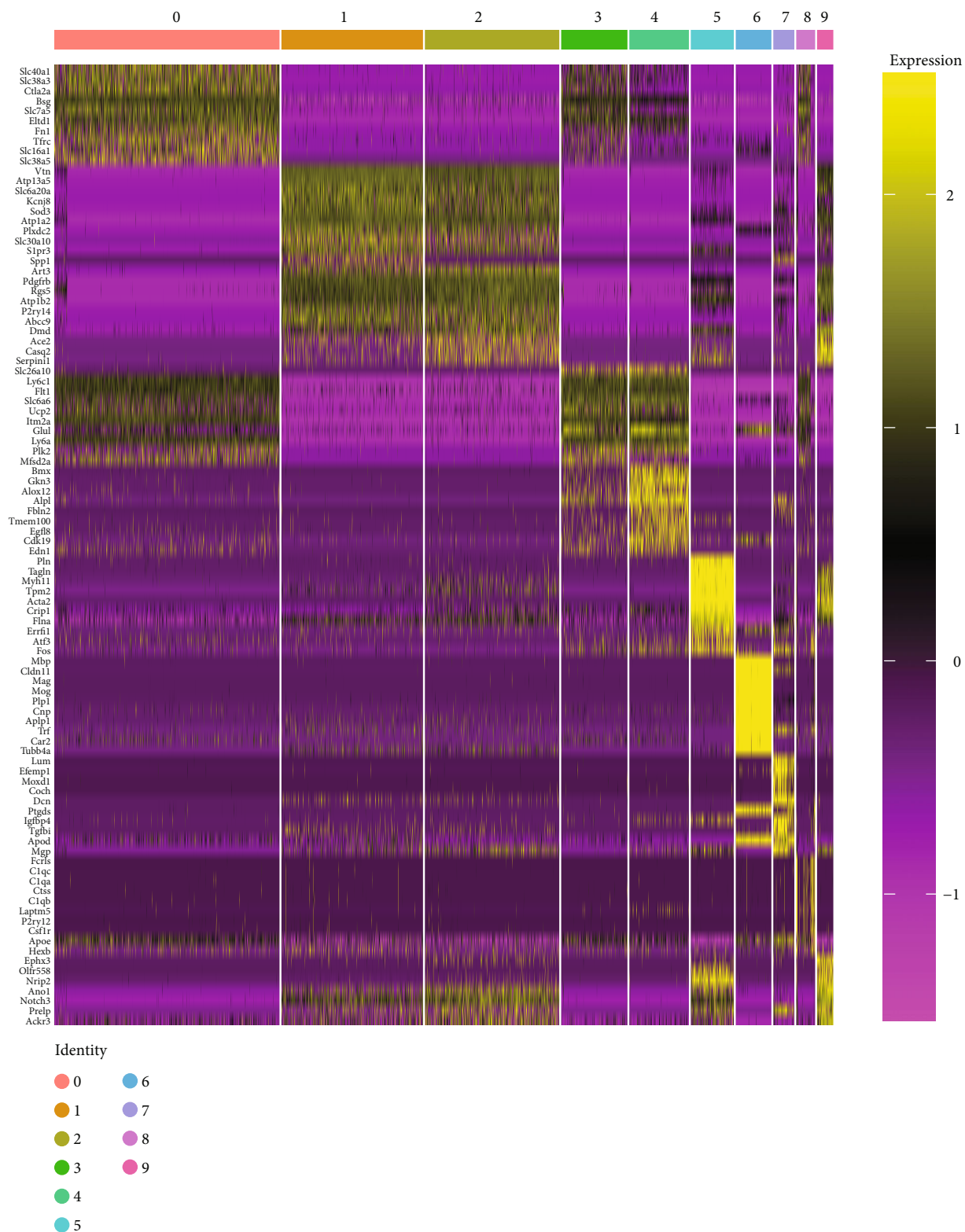
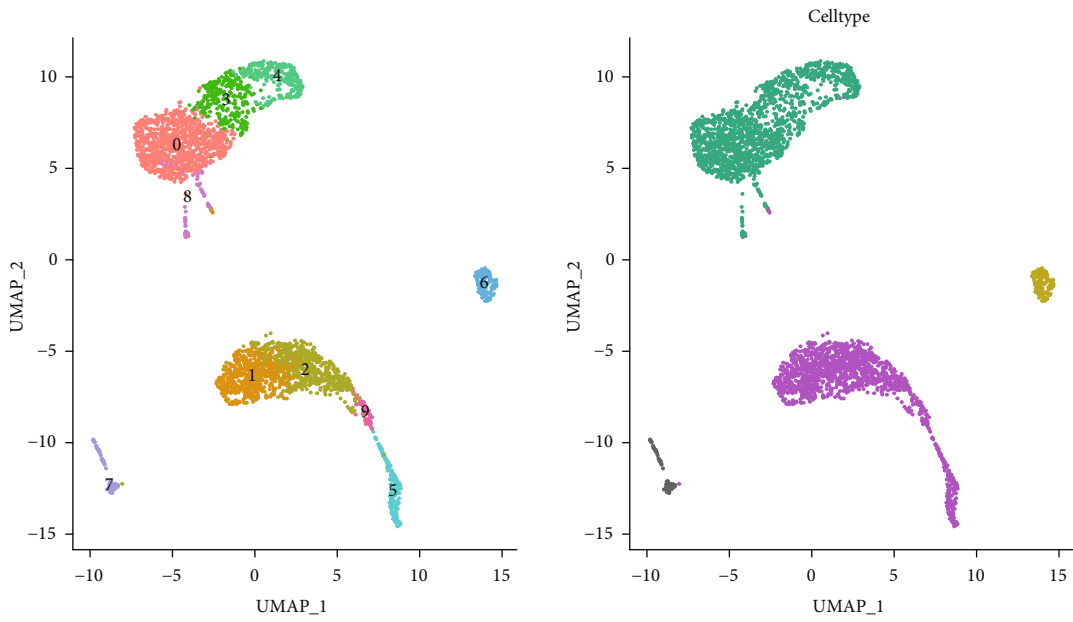


FIGURE 1: Continued.

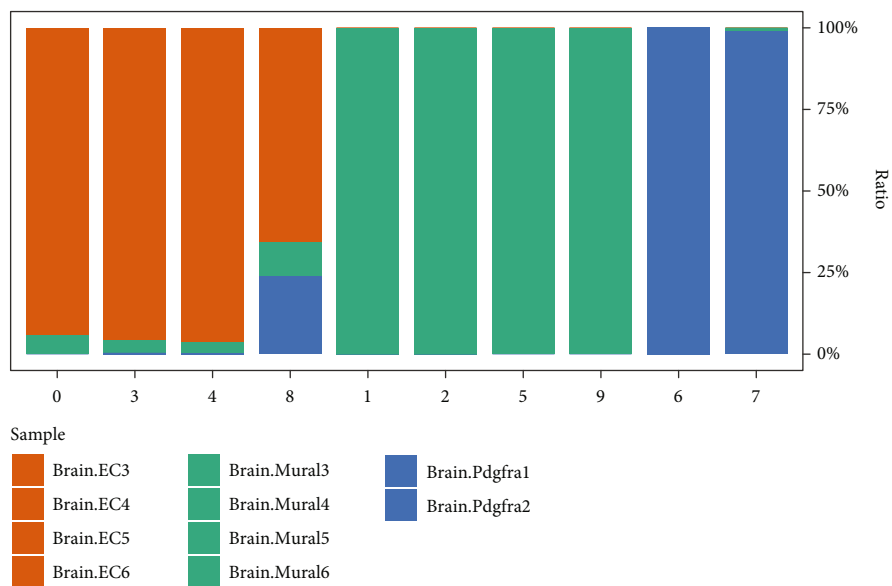
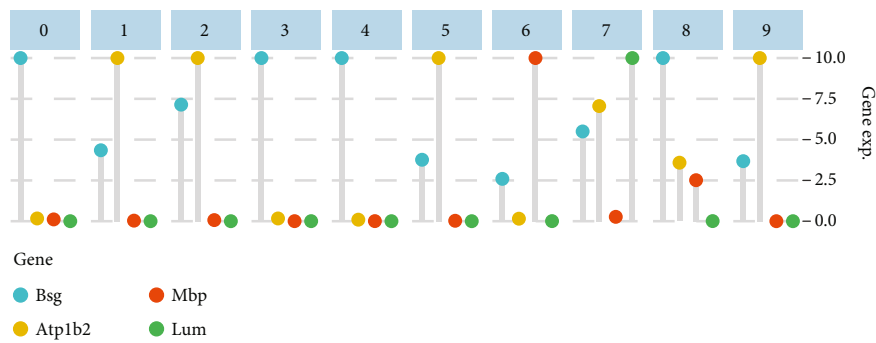


(e)

FIGURE 1: RNA-seq data revealed cell heterogeneity in the brain vasculature. (a) Quality control of 10 copies of cells from mouse brain vasculature, resulting in the inclusion of 3186 cells; (b) ANOVA analysis demonstrates the correlation of the expression of genes in mouse brain vasculature cells. Highly variable genes are indicated by red dots, and nonvariable genes are indicated by black dots. The most variable genes (Dcn, Plp1, Ptgsd, Lum, Spp1, Apod, Moxd1, Acta2, Csf1r, and Mbp) are indicated in the figure; (c) analysis with PCA shows that no significant separation of brain vasculature cells occurred in mice; (d) PCA identified 10 PCs as the best differentiation; (e) a heat map showing the top 10 marker genes for each cell cluster.

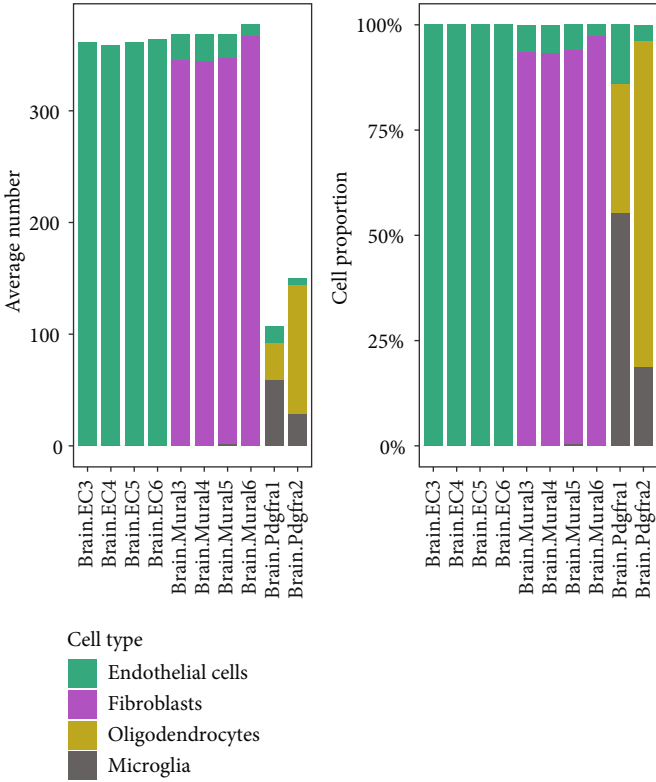


(a)



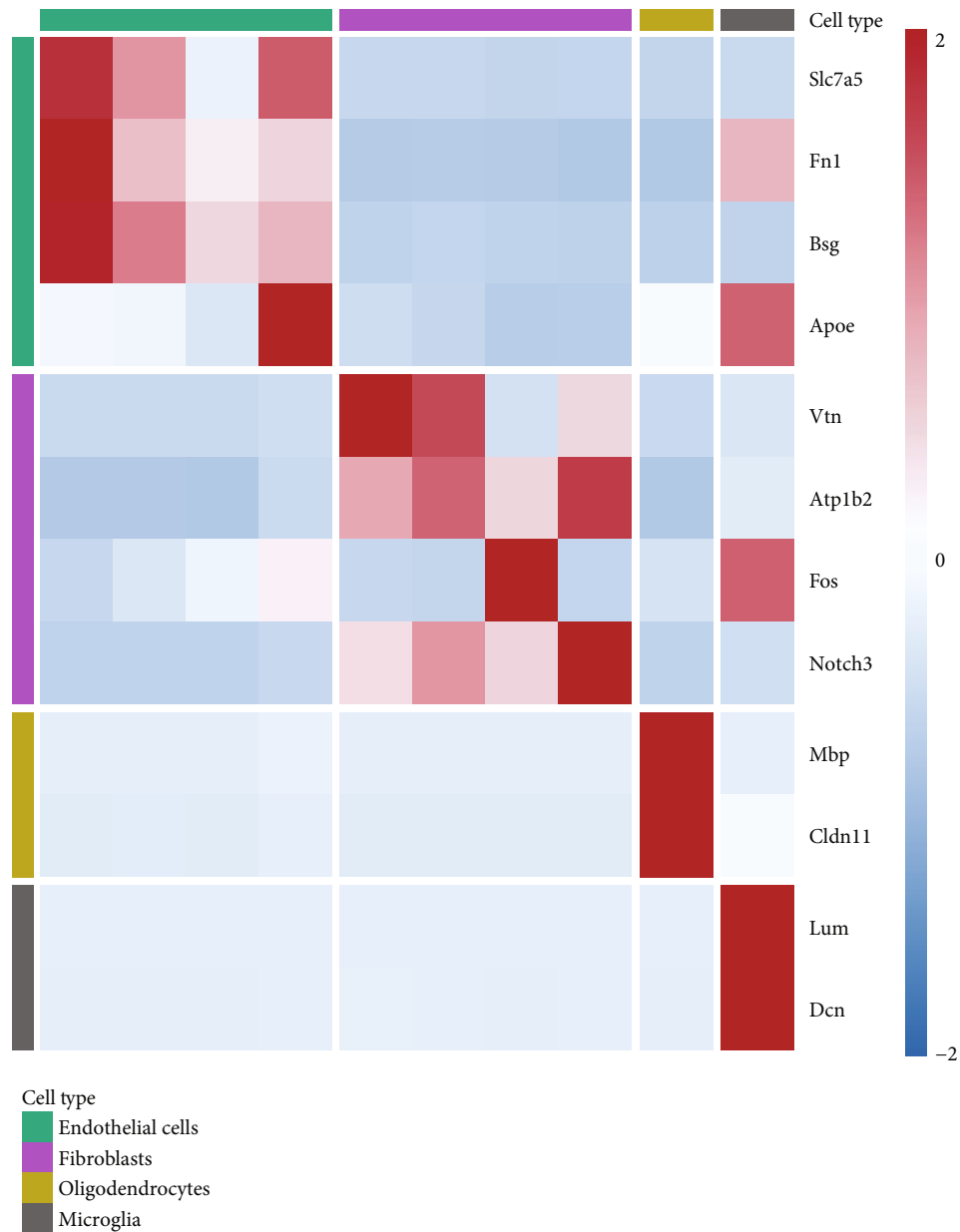
(b)

FIGURE 2: Continued.



(c)

FIGURE 2: Continued.



(d)

FIGURE 2: Tumor endothelial cells, fibroblasts promoting angiogenesis, and tissue remodeling. (a) UMAP and cell annotation figures showing mouse brain vasculature cells, colour coded with cell clusters and cell subpopulations (endothelial cells, fibroblasts, oligodendrocytes, and microglia). (b) Sample preference of each cluster. (c) Mean cell numbers and relative proportions of subpopulations of mouse brain vasculature cells derived from each tissue. Brain EC,  $n = 4$  samples; brain mural,  $n = 4$  samples; brain Pdgfra,  $n = 2$  samples. (d) Heat map showing selected mouse brain vasculature cells in each cell cluster. The relative expression profiles of marker genes associated with each cell subpopulation are known. The average expression values are adjusted by averaging and converted from high to low on a scale from -2 to 2 according to expression.

the mean cell numbers and relative proportions of subpopulations of mouse cerebrovascular cells derived from each tissue (Figures 2(b) and 2(c)). Marker genes for endothelial cells mainly included *Slc7a5*, *Fn1*, *Apoe*, and *Bsg*. The main marker genes for fibroblasts included *Vtn*, *Atp1b2*, *Fos*, and *Notch3*. The main marker genes for oligodendrocytes included *Mbp* and *Cldn11*, while those for microglia included *Lum* and *Dcn* (Figure 2(d)).

**3.3. Analysis of Cell Type-Specific Regulation in the Mouse Brain Vasculature.** We systematically analyzed key transcriptional regulators in each mouse cerebrovascular cell. For each pair of regulatory relationships, we defined a regulon specificity score (RSS) based on the Jensen-Shannon scatter [4, 18]. We then selected the specific regulatory factors with the highest RSS values and further examined their functional properties. Our network analysis identified *Cebpa*, *Zic1*,



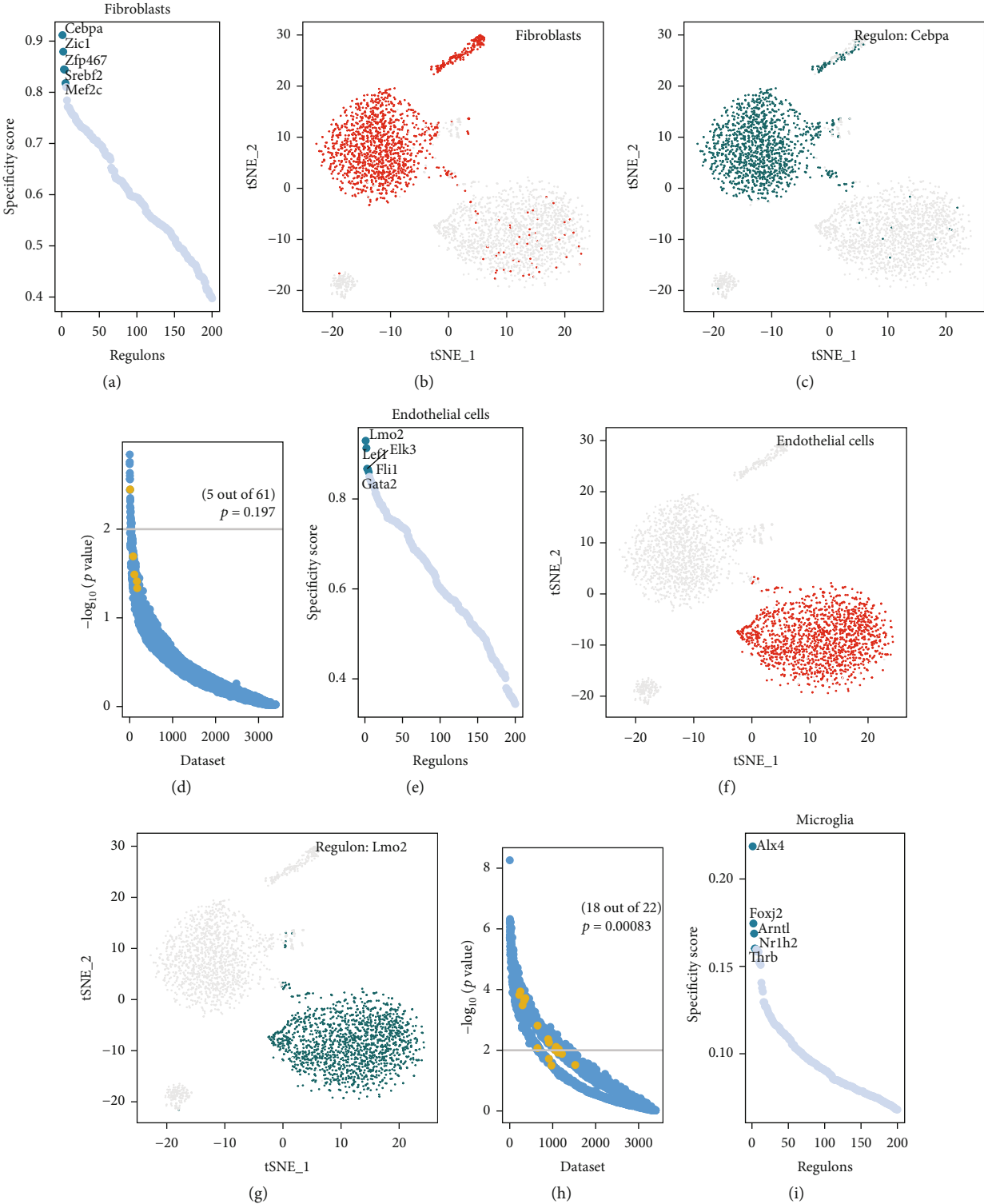


FIGURE 3: Continued.

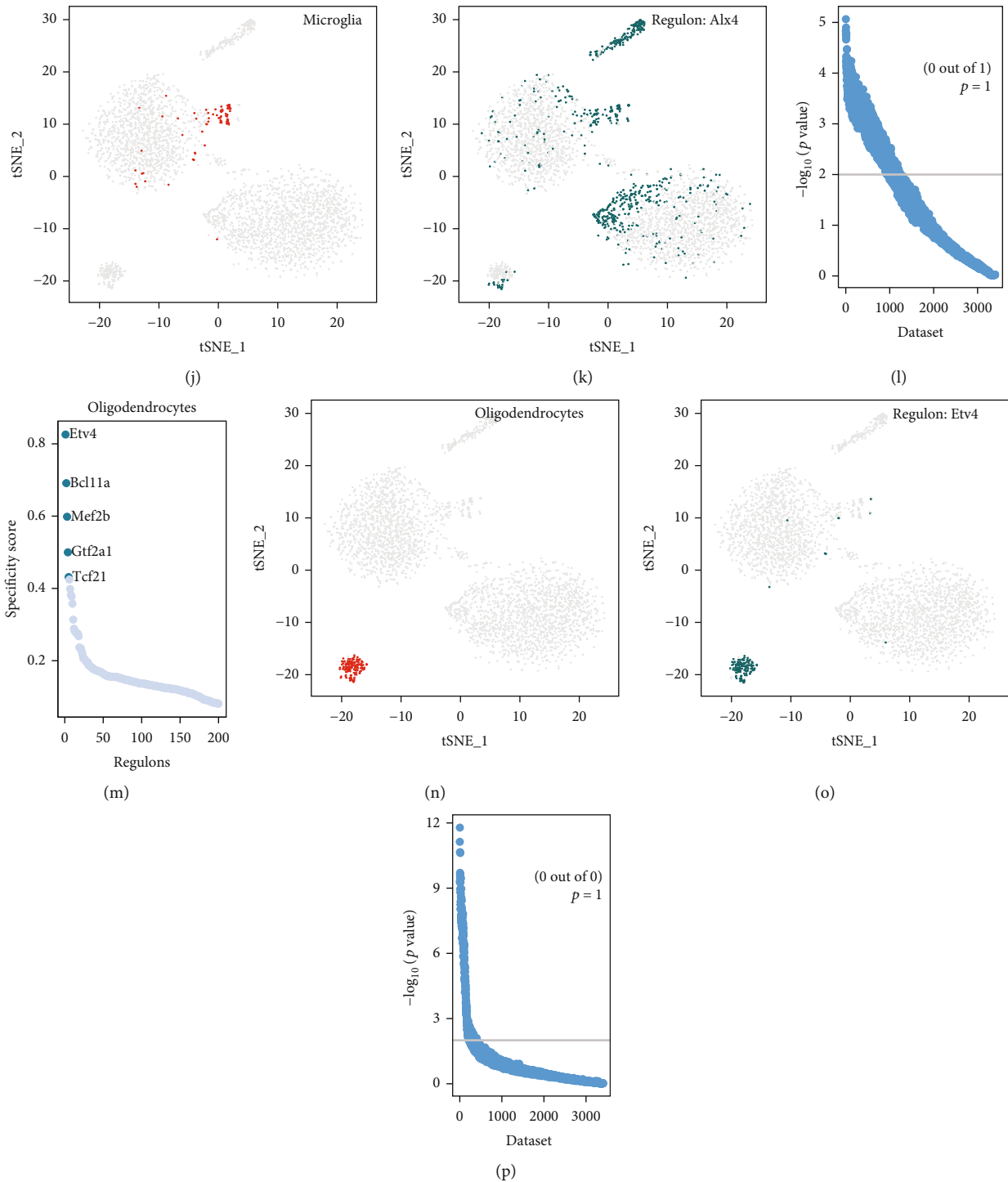


FIGURE 3: Analysis of cell type-specific regulation in the mouse brain vasculature. (a–d) Fibroblasts: (a) rank for regulons in mouse brain vasculature cells based on regulon specificity scores; (b) endothelial cells are highlighted as red dots in the tSNE plot; (c) the expression values of the genes with the highest regulon activity scores are presented in the tSNE plot; (d) the SEEK analysis is used to find coexpression results of the top regulated genes in different GEO datasets. The  $x$ -axis represents the different datasets, and the  $y$ -axis represents the coexpression significance of the target gene in each dataset. Relevant datasets with significant correlation ( $p$  value  $< 0.05$ ) are highlighted with yellow dots. (e–h) Same as (a–d) but for endothelial cells. (i–l) Same as (a–d) but for microglia. (m–p) Same as (a–d) but for oligodendrocytes.

Zfp467, Srebf2, and Mef2c as specific regulators associated with fibroblasts (Figure 3(a)). The tSNE plot further demonstrated that the expression of Cebpa was highly specific in

fibroblasts (Figures 3(b) and 3(c)). To test the validity of the above analysis, we applied SEEK analysis to determine GEO datasets with significant coexpression of the regulatory

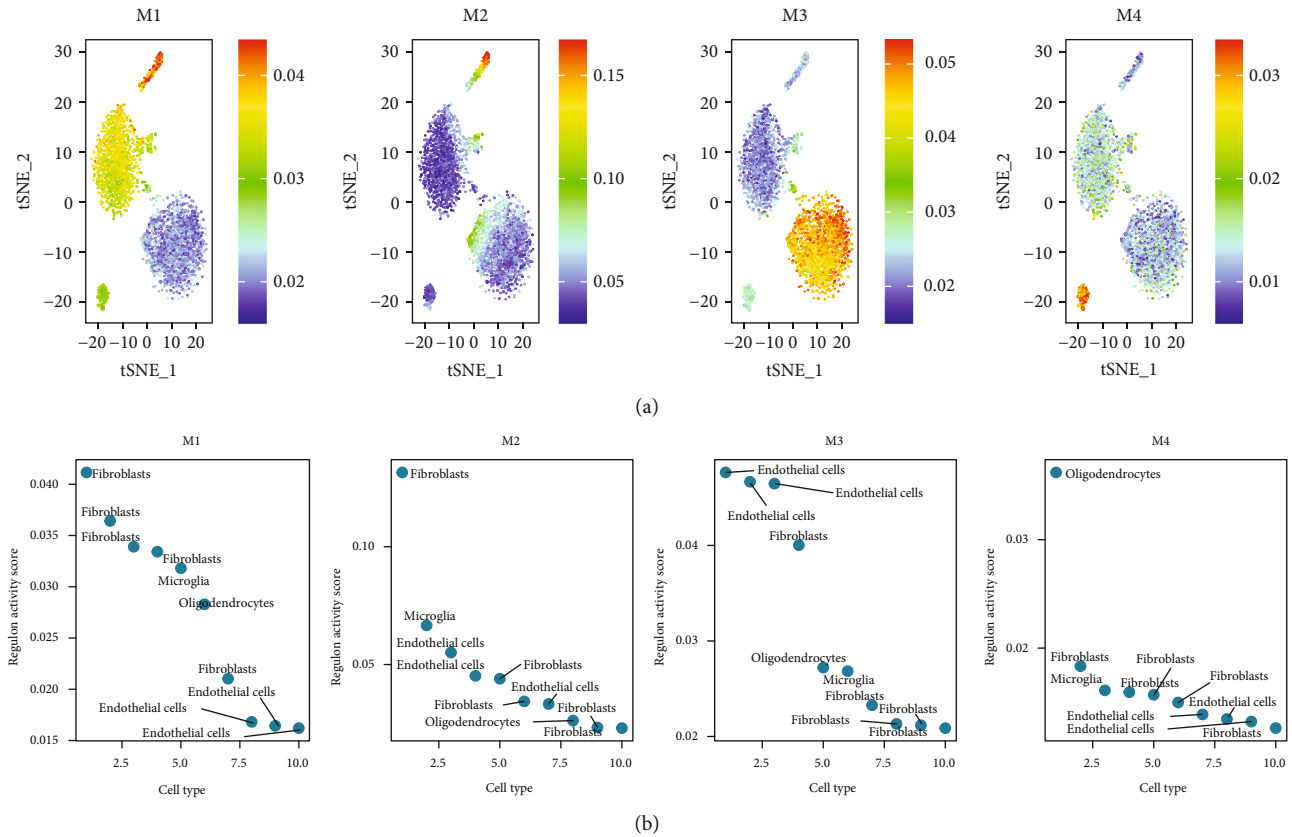


FIGURE 4: Activity of regulatory modules in different types of mouse brain vasculature cells. (a) Identified regulatory modules (M1-M4) based on the regulatory CSI matrix and mapped average activity of each module onto the tSNE; (b) rank for regulons in mouse brain vasculature cells based on regulon specificity scores. The y-axis represents the regulon activity score; the x-axis represents the cell type.

gene *Cebpa* (Figure 3(d); Fisher’s exact test,  $p = 0.197$ ). Using the same approach, we identified *Lmo2*, *Lef1*, *Elk3*, *Fli1*, and *Gata2* as specific regulators associated with endothelial cells (Figure 3(e)). The tSNE plot further demonstrated that the expression of the regulatory factor *Lmo2* was highly specific in endothelial cells (Figures 3(f) and 3(g)). To test the validity of the above analysis, we applied SEEK analysis to find GEO datasets that significantly coexpressed the regulatory gene *Lmo2*, with significant correlation (Figure 3(h); Fisher’s exact test,  $p = 0.00083$ ). Second, the most relevant specific regulators of microglia were *Alx4*, *Foxj2*, *Arntl*, *Nr1h2*, and *Thrb* (Figure 3(i)). *Alx4* expression was not found to be significantly specific in microglia (Figures 3(j) and 3(k)). The most relevant specific regulators of oligodendrocytes were found to be *Etv3*, *Bcl11a*, *Mef2b*, *Gtf2a1*, and *Tcf21* (Figure 3(m)). *Etv4* expression was found to be significantly specific in oligodendrocytes (Figures 3(n) and 3(o)). The SEEK analysis did not reveal significant coexpression of the regulatory genes *Alx4* and *Etv4* in the GEO dataset (Figures 3(l) and 3(p)).

**3.4. Organizing Regulons into Combinatorial Modules.** To systematically describe regulatory relationships of TFs, we compared the regulon activity scores of each regulatory relationship pair based on the connection specificity index (CSI) [16]. Thereafter, basing on the regulatory CSI matrix modules identified (M1-M4), we mapped the average activity of

each module onto the tSNE (Figure 4(a)). The mouse cerebrovascular cells were then ranked depending on regulon specificity scores (Figure 4(b)). The results showed that each module occupied a different region, with all highlighted regions suggesting the location of high transcriptional activity for different modules (Figure 4(a)). Among them, the M1 and M2 modules showed higher transcriptional activity mainly in fibroblast cells. In addition, the M2 module showed greater specificity. The M3 and M4 modules showed higher transcriptional activity primarily in endothelial cells and in oligodendrocytes, respectively. Gene Ontology (GO) and Kyoto Encyclopedia of Genes and Genomes (KEGG) enrichment analysis was also performed on the differentially expressed genes (DEGs) in each model. Bar graphs of the enrichment analysis were plotted ( $p < 0.05$ ; Supplementary Figures 1 and 2). Figure 5(a) shows the determination of the regulation module based on the regulation CSI matrix, along with associated cell types, corresponding binding motifs, and representative transcription factors. Interestingly, fibroblasts were found to be involved in all three major modules (M1, M2, and M3). The protein-protein interaction network of regulator factors in each module is shown in Figure 5(b) and Supplementary Figure 3. The M1 module contained the regulatory factors *Cebpa*, *Zic1*, *Srebf2*, and *Mef2c*, as well as regulator factor *Nr1h2*, which were transcriptional regulators of fibroblasts

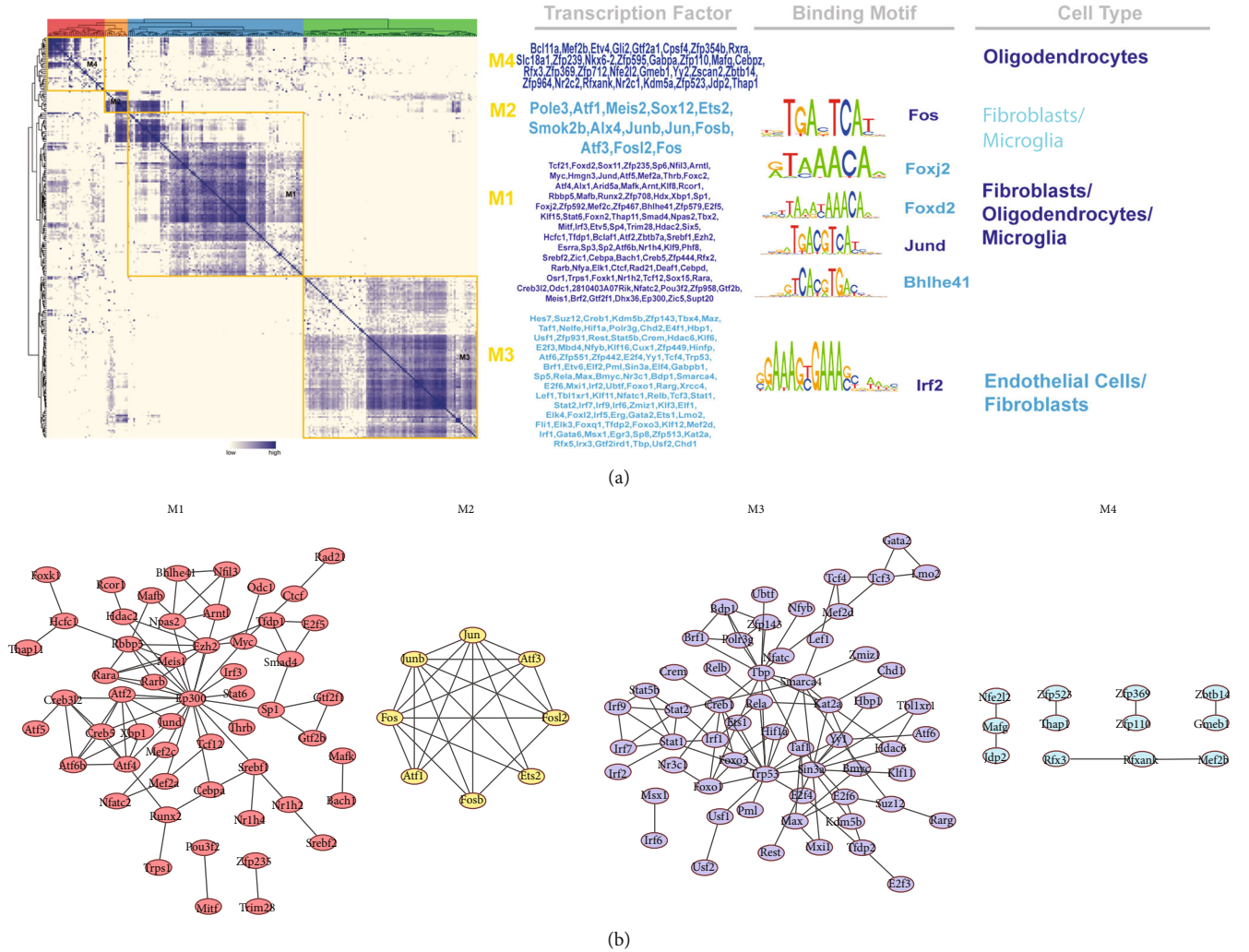


FIGURE 5: Identification of combinatorial regulon modules. (a) Determination of the regulon modules based on the regulation CSI matrix, along with associated cell types, corresponding binding motifs, and representative transcription factors. (b) Protein-protein interaction networks of regulator factors in each module.

and microglia in that order. Alx4 was included in the M2 module, which was a transcriptional regulator of microglia. Lmo2 was included in module M3, which was a transcriptional regulator of endothelial cells. Elsewhere, Etv4, Bcl11a, Mef2b, and Gtf2a1 were included in module M4, which were transcriptional regulators of oligodendrocytes. Combining the results in Figures 3 and 5(a), we speculated that Lmo2 may play an important role in endothelial cells.

**4. Discussion**

In the present study, we used retrieved single-cell RNA-seq to analyze the heterogeneity of mouse cerebrovascular cells, and four cell types (endothelial cells, fibroblasts, microglia, and oligodendrocytes) were defined. Together, these cell subpopulations and marker genes characterize the molecular profile of mouse cerebrovascular cells. Through these features, key transcriptional regulators that maintain cell identity are identified.

Our findings reveal that genes including Lmo2 play an important role in endothelial cells.

Significant progress has been made in recent years in the construction of GRNs based on single-cell transcriptome expression data [4, 9]. However, the process of cerebral vascular growth and development at the single-cell level is still poorly studied. In this study, we utilized a comprehensive atlas of obtained mouse cerebrovascular single-cell data [1] and constructed a single-cell transcriptional regulatory network of mouse cerebrovascular cells using single-cell transcriptome data in conjunction with the GRN approach. Four main marker genes distinguished four cell types (endothelial cells, fibroblasts, microglia, and oligodendrocytes): Bsg, Atp1b2, Mbp, and Lum in the present study. There was no significant difference revealed in the mean cell numbers and relative proportions of subpopulations of mouse cerebrovascular cells derived from each tissue. The expression of BSG in endothelial cells has been found to be positively correlated with age in humans, which may explain

the increased risk of cardiovascular disease with advancing age [19]. *Atp1b2* was found to be associated with changes in the microenvironment within the brain, and we hypothesize that the expression of fibroblasts may affect the microenvironment within the brain [20, 21]. The main marker genes for oligodendrocytes in the present study were *Mbp* and *Cldn11*. Similar findings were reported in previous studies [22]. The main marker genes of microglia included *Lum* and *Dcn*, both of which have been found to be associated with the development and progression of a variety of tumors [23].

Among the transcription factor regulatory networks, *Lmo2* was noted as the most important possible regulator of endothelial cells. The transcriptional regulatory relevance of *Lmo2* was significantly defined in 18 datasets (out of 22). In other studies, the transcription factor *Lmo2* was found to be an important transcription factor in determining the angiogenic properties of tumors, and it can significantly affect the growth and development of neurovascular cells [24–26]. Several other TFs (*Lef1*, *Elk3*, *Fli1*, and *Gata2*) have also been found to be associated with the characteristics of endothelial cells. *Alx4* has recently been found to be associated with cognitive impairment, congenital disorders of the brain, and normal function of the nervous system [27–29]. However, there are no studies on the interrelationship between microglia and *Alx4*. In the present study, *Alx4* was identified as a potential microglia regulator. The main function of oligodendrocytes in central nervous cells is to provide support and isolation for axons. Although oligodendrocyte development is associated with a variety of factors, its most important regulation is still unknown. *Etv4* was identified in the present study as possibly one of the most important regulators of oligodendrocytes. Previous studies have found that mutations in *CIC* promote malignant progression of gliomas and that *Etv4* is implicated in the transcriptional regulation of *CIC* [30, 31].

Interestingly, fibroblasts were covered in all three main modules (M1, M2, and M3). Crosstalk of fibroblasts in the three modules suggests that they may be important cells affecting the cerebrovascular microenvironment in mice. The transcriptional profile of fibroblasts may also greatly influence the cerebrovascular microenvironment, as has been demonstrated in previous studies [32–35]. In addition, through network analysis, we identified *Cebpa*, *Zic1*, *Zfp467*, *Srebf2*, and *Mef2c* as specific regulators associated with fibroblasts. The *Cebpa*, *Zic1*, *Srebf2*, and *Mef2c* have been found to be associated with the development of fibroblasts in many studies [36, 37]. High expression of *ZFP467* was found to be associated with altered vascular morphology and the presence of an inflammatory microenvironment [38].

Knowledge of cellular heterogeneity has greatly increased with the recent availability of single-cell sequencing technology. However, information about mechanisms by which these cellular heterogeneities are established and maintained is rare. The present study provides a new approach to understanding the developmental and functional relationships between vascular cell types in mice. Through the development of a transcriptional regulatory network of major cell

types in the mouse brain vasculature, the study further presents protocols and recommendations for prospect studies on neurovascular disease. In the current study, we fully acknowledge that the predicted results remain hypothetical, and further cellular and animal experiments are needed to justify our findings. In addition, prospect studies will need to employ multiple datasets to investigate commonalities between mice and humans to facilitate clinical translation of the research.

## 5. Conclusion

In this study, a transcriptional regulatory network based on single-cell analysis was constructed. In the process, we identified and profiled mouse cerebrovascular cells and incorporated a GRN approach using single-cell transcriptome data. In the study, TFs that affect the regulatory network of the mouse brain vasculature were defined. Further TFs, including *Lmo2*, which may play an important role in brain endothelial cells, were defined. In addition, we found that even similar cell types have different regulatory networks, which may affect the functional characteristics of local tissues.

## Abbreviations

BBB:	Blood-brain barrier
CSI:	Connection specificity index
GRNs:	Gene regulatory networks
PCA:	Principal component analysis
RSS:	Regulon specificity score
RAS:	Regulon activity score
SEEK:	Search-based Exploration of Expression Kompendia
SCENIC:	Single-cell regulatory network inference and clustering.

## Data Availability

All data used in this paper are from the GSE98816 dataset of the GEO database.

## Conflicts of Interest

The authors declare that they have no conflicts of interest.

## Authors' Contributions

Wei-Wei Lin and Lin-Tao Xu contributed equally to this work.

## Supplementary Materials

Supplementary Figure 1: Gene Ontology enrichment pathways of transcription factors in modules M1-M4 (A-D). Supplementary Figure 2: KEGG functional pathways of transcription factors in modules M1-M3 (A-C). Supplementary Figure 3: protein-protein interaction networks of regulator factors in modules M1-M4 (A-D) based on STRING. (*Supplementary Materials*)



## References

- [1] M. Vanlandewijck, L. He, M. A. Mäe et al., "A molecular atlas of cell types and zonation in the brain vasculature," *Nature*, vol. 554, no. 7693, pp. 475–480, 2018.
- [2] N. J. Abbott, L. Rönnbäck, and E. Hansson, "Astrocyte-endothelial interactions at the blood-brain barrier," *Nature Reviews Neuroscience*, vol. 7, no. 1, pp. 41–53, 2006.
- [3] B. V. Zlokovic, "The blood-brain barrier in health and chronic neurodegenerative disorders," *Neuron*, vol. 57, no. 2, pp. 178–201, 2008.
- [4] S. Suo, Q. Zhu, A. Saadatpour, L. Fei, G. Guo, and G. C. Yuan, "Revealing the critical regulators of cell identity in the mouse cell atlas," *Cell Reports*, vol. 25, no. 6, pp. 1436–1445.e3, 2018.
- [5] X. Han, R. Wang, Y. Zhou et al., "Mapping the mouse cell atlas by microwell-Seq," *Cell*, vol. 173, no. 5, p. 1307, 2018.
- [6] M. Ieda, J. D. Fu, P. Delgado-Olguin et al., "Direct reprogramming of fibroblasts into functional cardiomyocytes by defined factors," *Cell*, vol. 142, no. 3, pp. 375–386, 2010.
- [7] J. Riddell, R. Gazit, B. S. Garrison et al., "Reprogramming committed murine blood cells to induced hematopoietic stem cells with defined factors," *Cell*, vol. 157, no. 3, pp. 549–564, 2014.
- [8] A. Armulik, G. Genové, and C. Betsholtz, "Pericytes: developmental, physiological, and pathological perspectives, problems, and promises," *Developmental Cell*, vol. 21, no. 2, pp. 193–215, 2011.
- [9] M. W. E. J. Fiers, L. Minnoye, S. Aibar, C. Bravo González-Blas, Z. Kalender Atak, and S. Aerts, "Mapping gene regulatory networks from single-cell omics data," *Briefings in Functional Genomics*, vol. 17, no. 4, pp. 246–254, 2018.
- [10] A. Butler, P. Hoffman, P. Smibert, E. Papalexi, and R. Satija, "Integrating single-cell transcriptomic data across different conditions, technologies, and species," *Nature Biotechnology*, vol. 36, no. 5, pp. 411–420, 2018.
- [11] P. Lin, M. Troup, and J. W. Ho, "CIDR: ultrafast and accurate clustering through imputation for single-cell RNA-seq data," *Genome Biology*, vol. 18, no. 1, p. 59, 2017.
- [12] D. Aran, A. P. Looney, L. Liu et al., "Reference-based analysis of lung single-cell sequencing reveals a transitional profibrotic macrophage," *Nature Immunology*, vol. 20, no. 2, pp. 163–172, 2019.
- [13] X. Zhang, Y. Lan, J. Xu et al., "CellMarker: a manually curated resource of cell markers in human and mouse," *Nucleic Acids Research*, vol. 47, no. D1, pp. D721–D728, 2019.
- [14] S. Aibar, C. B. González-Blas, T. Moerman et al., "SCENIC: single-cell regulatory network inference and clustering," *Nature Methods*, vol. 14, no. 11, pp. 1083–1086, 2017.
- [15] Q. Zhu, A. K. Wong, A. Krishnan et al., "Targeted exploration and analysis of large cross-platform human transcriptomic compendia," *Nature Methods*, vol. 12, no. 3, pp. 211–214, 2015.
- [16] J. I. F. Bass, A. Diallo, J. Nelson, J. M. Soto, C. L. Myers, and A. J. Walhout, "Using networks to measure similarity between genes: association index selection," *Nature Methods*, vol. 10, no. 12, pp. 1169–1176, 2013.
- [17] S. van Dongen and C. Abreu-Goodger, "Using MCL to extract clusters from networks," *Methods in Molecular Biology*, vol. 804, pp. 281–295, 2012.
- [18] M. N. Cabili, C. Trapnell, L. Goff et al., "Integrative annotation of human large intergenic noncoding RNAs reveals global properties and specific subclasses," *Genes & Development*, vol. 25, no. 18, pp. 1915–1927, 2011.
- [19] B. Ahmetaj-Shala, R. Vaja, S. S. Atanur, P. M. George, N. S. Kirkby, and J. A. Mitchell, "Cardiorenal tissues express SARS-CoV-2 entry genes and basigin (BSG/CD147) increases with age in endothelial cells," *JACC: Basic to Translational Science*, vol. 5, no. 11, pp. 1111–1123, 2020.
- [20] K. Murata, T. Kinoshita, T. Ishikawa, K. Kuroda, M. Hoshi, and Y. Fukazawa, "Region- and neuronal-subtype-specific expression of Na,K-ATPase alpha and beta subunit isoforms in the mouse brain," *The Journal of Comparative Neurology*, vol. 528, no. 16, pp. 2654–2678, 2020.
- [21] M. Borggrewe, C. Grit, I. D. Vainchtein et al., "Regionally diverse astrocyte subtypes and their heterogeneous response to EAE," *Glia*, vol. 69, no. 5, pp. 1140–1154, 2021.
- [22] I. Kalafatakis, K. Kalafatakis, A. Tsimpolis et al., "Using the Allen gene expression atlas of the adult mouse brain to gain further insight into the physiological significance of TAG-1/Contactin-2," *Brain Structure & Function*, vol. 225, no. 7, pp. 2045–2056, 2020.
- [23] T. A. Järvinen and S. Prince, "Decorin: a growth factor antagonist for tumor growth inhibition," *BioMed Research International*, vol. 2015, Article ID 654765, 11 pages, 2015.
- [24] D. Gratzinger, S. Zhao, R. West et al., "The transcription factor LMO2 is a robust marker of vascular endothelium and vascular neoplasms and selected other entities," *American Journal of Clinical Pathology*, vol. 131, no. 2, pp. 264–278, 2009.
- [25] S. H. Kim, E. J. Kim, M. Hitomi et al., "The LIM-only transcription factor LMO2 determines tumorigenic and angiogenic traits in glioma stem cells," *Cell Death and Differentiation*, vol. 22, no. 9, pp. 1517–1525, 2015.
- [26] B. Herberth, K. Minkó, A. Csillag, T. Jaffredo, and E. Madarász, "SCL, GATA-2 and Lmo2 expression in neurogenesis," *International Journal of Developmental Neuroscience*, vol. 23, no. 5, pp. 449–463, 2005.
- [27] Y. Z. Ren, B. Z. Zhang, X. J. Zhao, and Z. Y. Zhang, "Resolvin D1 ameliorates cognitive impairment following traumatic brain injury via protecting astrocytic mitochondria," *Journal of Neurochemistry*, vol. 154, no. 5, pp. 530–546, 2020.
- [28] N. Gopal, A. Jain, S. J. S. Sandhu, A. A. Bhatt, and E. H. Middlebrooks, "A rare congenital cause of epilepsy," *Cureus*, vol. 12, no. 10, article e11204, 2020.
- [29] D. Zhang, C. Liu, H. Li, and J. Jiao, "Deficiency of STING signaling in embryonic cerebral cortex leads to neurogenic abnormalities and autistic-like behaviors," *Advanced Science*, vol. 7, no. 23, 2020.
- [30] V. Gleize, A. Alentorn, L. Connen de Kérillis et al., "CICinactivating mutations identify aggressive subset of 1p19q codeleted gliomas," *Annals of Neurology*, vol. 78, no. 3, pp. 355–374, 2015.
- [31] Z. Z. Li, P. F. Liu, T. T. An, H. C. Yang, W. Zhang, and J. X. Wang, "Construction of a prognostic immune signature for lower grade glioma that can be recognized by MRI radiomics features to predict survival in LGG patients," *Translational Oncology*, vol. 14, no. 6, article 101065, 2021.
- [32] S. Masi, M. Uliana, and A. Virdis, "Angiotensin II and vascular damage in hypertension: role of oxidative stress and sympathetic activation," *Vascular Pharmacology*, vol. 115, pp. 13–17, 2019.
- [33] S. Crnko, M. Cour, L. W. Van Laake, and S. Lecour, "Vasculature on the clock: circadian rhythm and vascular dysfunction," *Vascular Pharmacology*, vol. 108, pp. 1–7, 2018.



- [34] R. Upadhyaya, W. Zingg, S. Shetty, and A. K. Shetty, "Astrocyte-derived extracellular vesicles: neuroreparative properties and role in the pathogenesis of neurodegenerative disorders," *Journal of Controlled Release*, vol. 323, pp. 225–239, 2020.
- [35] J. Silpanisong and W. J. Pearce, "Vasotrophic regulation of age-dependent hypoxic cerebrovascular remodeling," *Current Vascular Pharmacology*, vol. 11, no. 5, pp. 544–563, 2013.
- [36] J. Kosla, M. Dvorak, and V. Cermak, "Molecular analysis of the TGF-beta controlled gene expression program in chicken embryo dermal myofibroblasts," *Gene*, vol. 513, no. 1, pp. 90–100, 2013.
- [37] H. Hirai, B. Yang, M. T. Garcia-Barrio et al., "Direct reprogramming of fibroblasts into smooth muscle-like cells with defined transcription factors-brief report," *Arteriosclerosis, Thrombosis, and Vascular Biology*, vol. 38, no. 9, pp. 2191–2197, 2018.
- [38] E. Bressan, L. Ferroni, C. Gardin et al., "Metal nanoparticles released from dental implant surfaces: potential contribution to chronic inflammation and peri-implant bone loss," *Materials*, vol. 12, no. 12, p. 2036, 2019.

## Retraction

# Retracted: Modified Prehospital Acute Stroke Severity (mPASS) Scale to Predict Emergent Large Arterial Occlusion

### BioMed Research International

Received 12 March 2024; Accepted 12 March 2024; Published 20 March 2024

Copyright © 2024 BioMed Research International. This is an open access article distributed under the Creative Commons Attribution License, which permits unrestricted use, distribution, and reproduction in any medium, provided the original work is properly cited.

This article has been retracted by Hindawi following an investigation undertaken by the publisher [1]. This investigation has uncovered evidence of one or more of the following indicators of systematic manipulation of the publication process:

- (1) Discrepancies in scope
- (2) Discrepancies in the description of the research reported
- (3) Discrepancies between the availability of data and the research described
- (4) Inappropriate citations
- (5) Incoherent, meaningless and/or irrelevant content included in the article
- (6) Manipulated or compromised peer review

The presence of these indicators undermines our confidence in the integrity of the article's content and we cannot, therefore, vouch for its reliability. Please note that this notice is intended solely to alert readers that the content of this article is unreliable. We have not investigated whether authors were aware of or involved in the systematic manipulation of the publication process.

Wiley and Hindawi regrets that the usual quality checks did not identify these issues before publication and have since put additional measures in place to safeguard research integrity.

We wish to credit our own Research Integrity and Research Publishing teams and anonymous and named external researchers and research integrity experts for contributing to this investigation.

The corresponding author, as the representative of all authors, has been given the opportunity to register their agreement or disagreement to this retraction. We have kept a record of any response received.

### References

- [1] X. Si, J. Ruan, L. Li et al., "Modified Prehospital Acute Stroke Severity (mPASS) Scale to Predict Emergent Large Arterial Occlusion," *BioMed Research International*, vol. 2021, Article ID 5568696, 6 pages, 2021.

## Research Article

# Modified Prehospital Acute Stroke Severity (mPASS) Scale to Predict Emergent Large Arterial Occlusion

Xiaoli Si,<sup>1</sup> Jie Ruan,<sup>2</sup> Lingfei Li,<sup>3</sup> Shan Lu,<sup>3</sup> Huan Huang,<sup>3</sup> Wenqing Xia,<sup>3</sup> Keqin Liu,<sup>3</sup> Tianwen Chen,<sup>3</sup> Lin Jiang ,<sup>3</sup> and Congguo Yin <sup>3</sup>

<sup>1</sup>Department of Neurology, Second Affiliated Hospital, College of Medicine, Zhejiang University, Hangzhou, Zhejiang, China

<sup>2</sup>Department of Neurology, Hangzhou Geriatric Hospital, Hangzhou, China

<sup>3</sup>Department of Neurology, Affiliated Hangzhou First People's Hospital, Zhejiang University School of Medicine, Hangzhou, China

Correspondence should be addressed to Lin Jiang; [jianglin760229@126.com](mailto:jianglin760229@126.com) and Congguo Yin; [yincg716@aliyun.com](mailto:yincg716@aliyun.com)

Received 14 January 2021; Revised 21 June 2021; Accepted 6 July 2021; Published 20 July 2021

Academic Editor: Yuzhen Xu

Copyright © 2021 Xiaoli Si et al. This is an open access article distributed under the Creative Commons Attribution License, which permits unrestricted use, distribution, and reproduction in any medium, provided the original work is properly cited.

**Introduction.** To date, identifying emergent large vessel occlusion (ELVO) patients in the prehospital stage is important but still challenging. In this present study, we aimed to design a modified prehospital acute stroke severity (mPASS) scale to identify ELVO patients and compared the scale to the PASS scale which has been published. **Methods.** We retrospectively evaluated a consecutive cohort of acute ischemic stroke (AIS) in our stroke unit who visited the emergency department. These patients underwent CT angiography (CTA), MR angiography (MRA), or digital subtraction angiography (DSA) at admission. The mPASS scale was calculated based on the National Institutes of Health Stroke Scale (NIHSS) items retrospectively, including the level of consciousness commands, gaze, arm weakness, and aphasia/dysarthria. Receiver operating characteristic (ROC) analysis was used to obtain the area under the curve (AUC) of the mPASS scale, NIHSS, and PASS scale. *U*-statistics was used to compare the AUC of the mPASS scale to the NIHSS and PASS scale. **Results.** A total of 382 AIS patients were enrolled. The AUC and specificity of the mPASS scale (0.92, 84.4) were all higher than those of the PASS scale. Cortical symptoms such as gaze palsy and consciousness disorder were more specific indicators for ELVO than motor deficits. **Conclusions.** The mPASS scale had a better discrimination for identifying ELVO than the PASS scale in our retrospective cohort. It might predict ELVO in an effective and simple way for paramedics in the prehospital triage stage or emergency stage. Moreover, cortical symptoms might have relatively high specificities to predict ELVO on their own.

## 1. Introduction

Reperfusion with the intravenous tissue plasminogen activator (recombinant tissue-type plasminogen activator (rt-PA)) and endovascular therapy (EVT) improve outcomes in acute ischemic stroke (AIS) patients [1]. Both treatment efficiencies are highly time dependent [2]. Intravenous thrombolysis can be administered in Primary Stroke Centers (PSCs) while endovascular treatment can only be administered in EVT-capable centers in Comprehensive Stroke Centers (CSCs) [3]. Several recent studies have demonstrated that patients may have a better outcome by shortening the delay to EVT. Therefore, a simple and accurate assessment for paramedics to precisely identify emergent large vessel occlusion (ELVO) in the setting of prehospital triage stage or emergency stage is urgent.

Computed tomography angiography (CTA), magnetic resonance angiography (MRA), or digital subtraction angiography (DSA) allow a rapid assessment of the vessel status in AIS. However, they are not broadly available 24 hours per day, particularly for PSCs with imaging resources limited [4]. Thus, surrogate clinic markers of vessel occlusion will be helpful. The National Institutes of Health Stroke Scale (NIHSS) has a relatively strong relationship between neurological deficit and vessel status [5]. However, it is complex for emergency assessment and necessitating regular training for primary paramedics.

There have been several prehospital stroke scales to identify patients experiencing ELVO [6–9]. Among them, the Prehospital Acute Severity Scale (PASS) simplifies the parameters and has been shown to improve the predictive

TABLE 1: The mPASS scale and its correspondence to the PASS scale and NIHSS.

Item	mPASS	NIHSS
LOC commands		
Both correct	0	0
One correct	1	1
Neither correct	2	2
Gaze		
Normal	0	0
Partial deviation	1	1
Forced deviation	2	2
Arm weakness		
No drift/drift but does not hit bed	0	0–1
Drift and hit bed/no effort against gravity/no movement	1	2–4
Aphasia/dysarthria		
Normal	0	0
Aphasia and/or dysarthria	1	1–3/1–2

LOC: level of consciousness; mPASS: modified Prehospital Acute Stroke Severity; NIHSS: National Institutes of Health Stroke Scale.

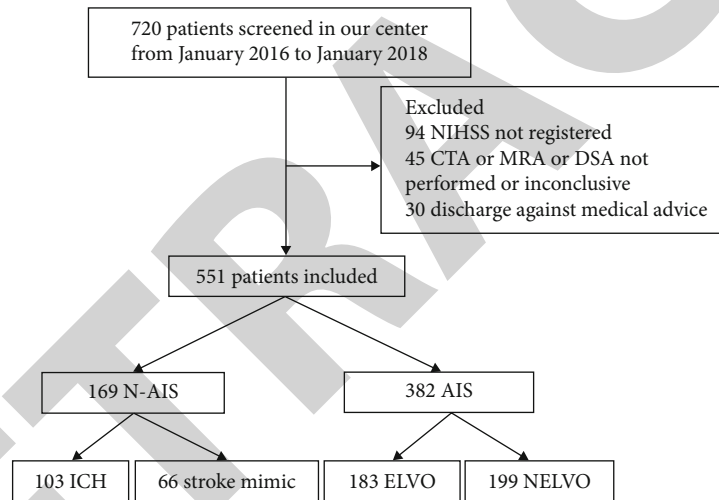


FIGURE 1: Flowchart of the study population. NIHSS: National Institutes of Health Stroke Scale; CTA: computed tomography angiography; MRA: magnetic resonance angiography; DSA: digital subtraction angiography; AIS: acute ischemic stroke; N-AIS: nonacute ischemic stroke; ELVO: emergent large vessel occlusion; NELVO: non-emergent large vessel occlusion; ICH: intracerebral hemorrhage.

capability of ELVO when compared to other reported scales [10]. The PASS scale (level of consciousness (LOC) questions, which combined both assessments of language and consciousness (scored 0–1), gaze palsy and/or deviation (0–1), and arm weakness (scored 0–1)) is derived from the NIHSS. The PASS scale score  $\geq 2$  predicts ELVO. However, patients with basal ganglia infarction (non-emergent large vessel occlusion) may get a PASS score = 2, if they have slurred speech and arm weakness. Therefore, it is unsuitable to evaluate the level of consciousness (LOC) through LOC questions in the PASS scale. In this present study, we replaced the item “LOC questions” by the item “LOC commands—open/close eyes, grip, and release non-paretic hand” to evaluate LOC in our scale. And we add the item “aphasia” separately. However, in emergency evaluation, paramedics could not accurately distinguish speech ambiguity as aphasia or dysarthria and cortical symptoms of some patients with

right hemisphere infarction could also be manifested as dysarthria. Therefore, aphasia and dysarthria are both included in language evaluation indicators. Here, we developed a new scale—the modified Prehospital Acute Stroke Severity (mPASS) Scale, which is derived from the PASS scale. We posit that the modification of the PASS scale might increase the predictive ability of ELVO. Then, we retrospectively evaluated whether the mPASS scale could achieve a better predictive performance than the PASS scale for identifying ELVO.

## 2. Subjects and Methods

We retrospectively reviewed a historical cohort of 720 patients who visited the emergency room from January 2016 to January 2018 in Hangzhou First People’s Hospital, Zhejiang University. We enrolled patients who (1) were clinically suspected of AIS (symptom onset  $\leq 24$  hours, including

patients who have intracerebral hemorrhage (ICH) or with a final nonvascular diagnosis like status epilepticus, syncope, metabolic disturbance, and other reasons) at emergency, (2) were examined by 2 experienced stroke neurologists and assessed with the NIHSS at the emergency room (the assessment of the NIHSS was written on sheets detailed to each parameter), (3) were AIS patients confirmed by magnetic resonance imaging (MRI) diffusion-weighted imaging (DWI) at admission, and (4) were ELVO patients confirmed by CTA, MRA, or DSA at admission. Participants' baseline demographic (age, gender, and smoking), clinical characteristics (diabetes, hyperlipidemia, hypertension, and atrial fibrillation), laboratory data (serum glucose at admission, low-density lipoprotein, and homocysteine), and images were recorded.

The mPASS was calculated based on NIHSS retrospectively by 2 experienced neurologists. This scale assessed 4 parameters: (1) LOC commands—open/close eyes, grip, and release the nonparetic hand (scored 0 and 2); (2) gaze (scored 0 and 2); (3) arm weakness (scored 0 and 1); and (4) aphasia/dysarthria (scored 0 and 1) (Table 1).

ELVO is defined as occlusion of the internal carotid artery (ICA), anterior cerebral artery (ACA), horizontal segment (M1), and insula segment (M2) of middle cerebral artery (MCA), posterior cerebral artery (PCA), basilar artery (BA), and vertebral artery (VA). Two experienced neurologists blinded to patients' information assessed the occlusion on CTA, MRA, or DSA with rater discrepancies settled by consensus. Patients with inconclusive or missing information on NIHSS or were not eligible for imaging assessment were excluded. The flowchart of the study population is shown in Figure 1. This study was approved by the ethics committee of the Affiliated Hangzhou First People's Hospital, Zhejiang University School of Medicine, and written consent was obtained from each participant.

**2.1. Statistical Analysis.** Patients were divided into the AIS-ELVO group and AIS-non-ELVO (NELVO) group. Data were entered into Microsoft Excel, and statistical analyses were performed with Statistical Package for the Social Sciences 18.0 (IBM, Chicago, IL, USA). Statistical plots were generated using GraphPad Prism 7.0a (GraphPad Inc., San Diego, CA, USA). Categorical or binary datum was summarized by proportion ( $n$ , %), clinical characteristics were presented as mean  $\pm$  standard deviation (mean  $\pm$  SD) and as median (interquartile range (IQR)). The Kolmogorov-Smirnov test was used to determine the normality of the distribution of the variables. Demographic data, clinical variables, and scale scores were compared using independent  $t$ -tests for normally distributed continuous variables, and Mann-Whitney  $U$  test and Kruskal-Wallis  $H$  test for continuous variables that were not normally distributed. Receiver operating curves (ROC) and areas under receiver operating curve (AUC) were calculated as measures of predictive ability for ELVO among AIS patients (ELVO and AIS-ELVO) of the mPASS scale, PASS scale, and NIHSS and for different items of the mPASS scale. ROC-derived optimal cutoff was determined at the maximal Youden index. Cross tables for different cutoff values of the mPASS scale were used to evaluate

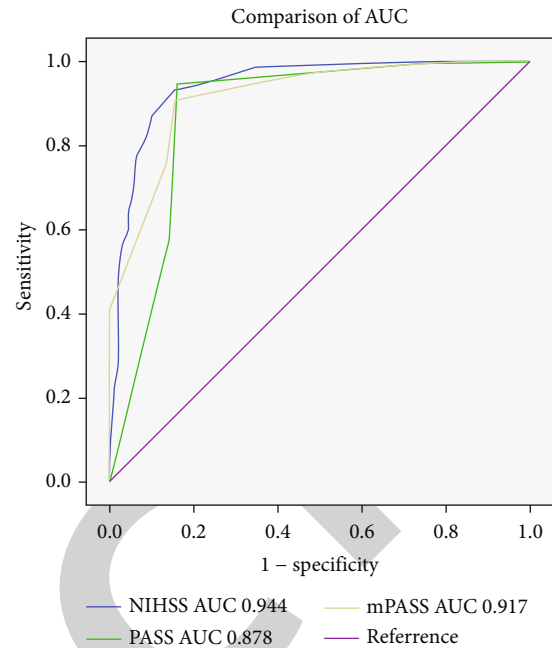


FIGURE 2: Discrimination and calibration analysis: mPASS scale showed AUC 0.917, sensitivity 90.7%, and specificity 84.4%; the PASS scale showed AUC 0.878, sensitivity 94.5%, and specificity 83.9%; the NIHSS showed AUC 0.944, sensitivity 92.9%, and specificity 84.9%.

sensitivity, specificity, positive predictive value (PPV), and negative predictive value (NPV). A value with  $p < 0.05$  was regarded as statistically significant.

### 3. Results

Totally, we screened 720 patients in our stroke unit from January 2016 to January 2018. Finally, 382 AIS patients were included. Figure 1 summarized the flowchart of the study population. In the ELVO group, the mean age was  $70.3 \pm 11.2$  years, males were 111 (60.7%), median time between symptom onset and assessment was  $4.7 \pm 4.0$  hours, and median NIHSS score was  $17.2 \pm 8.0$ . In the NELVO group, the mean age was  $71.0 \pm 11.2$  years, males were 118 (59.3%), median time between symptom onset and assessment was  $9.7 \pm 5.1$  hours, and median NIHSS score was  $4.6 \pm 4.6$ . The AUC of the mPASS scale to predict ELVO from AIS (ELVO and AIS-NELVO patients) was 0.917. The highest Youden index was 0.751, which was achieved for a mPASS score  $\geq 3$ , with sensitivity, specificity, PPV, and NPV of 0.907, 0.844, 0.843, and 0.908, respectively. The AUC of the PASS scale was 0.878. The highest Youden index was 0.785, which was achieved for a PASS score  $\geq 2$ , with sensitivity, specificity, PPV, and NPV of 0.945, 0.839, 0.844, and 0.944, respectively. The AUC of the NIHSS was 0.944. The highest Youden index was 0.778, which was achieved for a NIHSS score  $\geq 9$ , with sensitivity, specificity, PPV, and NPV of 0.929, 0.849, 0.841, and 0.923, respectively. The AUC of the mPASS scale was significantly higher than that of the PASS scale ( $p < 0.05$ ) (Figure 2, Table 2).



TABLE 2: Sensitivity, specificity, PPV, NPV, and overall accuracy of different scales.

Scale	AUC	95% CI	Sensitivity (%)	Specificity (%)	PPV (%)	NPV (%)	Youden (%)	Accuracy (%)
mPASS $\geq 3$	0.917	0.889–0.944	90.7	84.4	84.3	90.8	75.1	87.4
Pass $\geq 2$	0.878	0.833–0.916	94.5	83.9	84.4	94.4	78.5	89.0
NIHSS $\geq 9$	0.944	0.921–0.967	92.9	84.9	84.1	92.3	77.8	88.7

mPASS: modified Prehospital Acute Stroke Severity; PASS: Prehospital Acute Stroke Severity; NIHSS: National Institutes of Health Stroke Scale; AUC: area under the curve; CI: confidence interval; PPV: positive predictive value; NPV: negative predictive value.

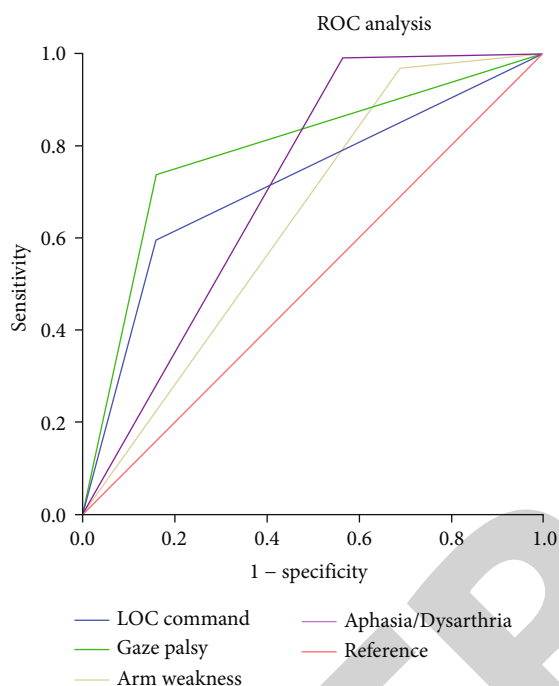


FIGURE 3: Discrimination and calibration analysis: level of consciousness showed AUC=0.717, sensitivity 56.9%, and specificity 83.9%; gaze palsy and/or deviation showed AUC=0.788, sensitivity 73.8%, and specificity 83.9%; aphasia/dysarthria showed AUC=0.713, sensitivity 98.9%, and specificity 43.7%; arm weakness showed AUC=0.639, sensitivity 96.7%, and specificity 31.2%.

Figure 3 showed that the strongest predictor of ELVO through mPASS scale's four parameters was gaze palsy and/or deviation, with AUC = 0.788 (95% confidence interval (CI) 0.741-0.836), sensitivity 73.8%, and specificity 83.9%. The second strongest predictor was LOC command, with AUC = 0.717 (95% CI, 0.665-0.770), sensitivity 59.6%, and specificity 83.9%. Then comes aphasia/dysarthria which showed AUC = 0.713 (95% CI, 0.661-0.765), sensitivity 98.9%, and specificity 43.7%. The last is arm weakness, which showed AUC = 0.639 (95% CI, 0.584-0.695), sensitivity 96.7%, and specificity 31.2%. The ELVO group had a higher percentage of LOC command and gaze palsy than the AIS-NELVO group (Mann-Whitney  $U$  test,  $p < 0.001$ ). ACI had a higher percentage of gaze palsy (Mann-Whitney  $U$  test,  $p < 0.001$ ), and PCI had a higher percentage of consciousness disorder (Mann-Whitney  $U$  test,  $p = 0.003$ ). Detailed vessel occlusion types were ACA 2 (1.1%), ICA 54 (29.5%), MCA 95 (51.9%), PCA 2 (1.1%), BA 29 (15.8%), and VA 1

(0.5%). We ran a separate analysis using only ICA/M1 occlusions as the ELVO definition. The AUC of the mPASS scale to predict ELVO from AIS (ELVO and AIS-NELVO patients) was 0.926. The highest Youden index was 0.763, which was achieved for mPASS score  $\geq 3$ , with sensitivity, specificity, PPV, and NPV of 0.919, 0.844, 0.815, and 0.933, respectively. The AUC of the PASS scale was 0.883. The highest Youden index was 0.785, which was achieved for PASS score  $\geq 2$ , with sensitivity, specificity, PPV, and NPV of 0.946, 0.839, 0.815, and 0.954, respectively. The AUC of the NIHSS was 0.941. The highest Youden index was 0.782, which was achieved for a NIHSS score  $\geq 9$ , with sensitivity, specificity, PPV, and NPV of 0.939, 0.849, 0.822, and 0.944, respectively (in supplementary materials).

#### 4. Discussion

The NIHSS has demonstrated to be predictive of ELVO, but is difficult and time-consuming for PSC paramedics who are inexperienced in performing assessment. Moreover, right hemispheric ELVO may present mild to moderate symptoms underrepresented with the NIHSS which would be ignored. Currently, a European group has designed and demonstrated the PASS scale as a simple tool that highly predicts ELVO emergency. The current study indicates that our novel mPASS in retrospective cohort had a good discrimination ability and could be an easily memorized tool to identify ELVO, as the AUC of the mPASS scale showed a higher predictive value compared with the NIHSS and PASS scale. Atherosclerotic intracranial stenosis is found commonly among stroke patients of Asian, Black, and Hispanic ancestry [11], especially in China [12]. Thus, the mPASS scale would be a useful and necessary tool to detect ELVO patients, especially for Asian patients.

There are several advantages of the mPASS scale over existing scales. First, parameters in the mPASS are easily observed and objective to evaluate. LOC commands are objective and could be separated with evaluation of aphasia/dysarthria which the PASS scale ignored [10]. Gaze palsy can be easily observed by paramedics in emergency conditions rather than neglect or field of vision in RACE, FAST-ED, and VAN scales [13, 14]. Second, the different forms of the PASS, 3ISS, LAMS, and mPASS scales give a higher weight to cortical symptoms (consciousness disorder 0/2, gaze palsy, and/or deviation 0/2) rather than motor symptoms (arm weakness 0/1), which are typical signs of ELVO, because motor symptoms can also occur in lacunar stroke and may not be good indicators for ELVO. This study also indicated that the strongest predictor was cortical symptoms



(consciousness disorder and gaze palsy and/or deviation). Recently, gaze palsy and/or deviation has been the only parameter in an ELVO screen as an ideal prehospital scale [11]. Thus, we may further design a simpler and faster scale which just focuses on cortical symptoms and validates prospectively in the field by trained paramedics prehospital in the future.

Our study has several limitations. First, this model was made from a single retrospective cohort. Perspective and large multicenter data would be more believable and compelling. Second, as a global scale with a limited range (0 to 6), the mPASS scale is insensitive to small differences between patients and to small changes in clinical status for individual patients. However, the complexity of the NIHSS scale is responsible for its infrequent use in clinical routine. In contrast, the mPASS scale is relatively more simple and faster to apply. Moreover, the mPASS score in ACI was higher than that in PCI; however, NIHSS score was higher in PCI than ACI. The accuracy of the mPASS scale in PCI needs further investigation and improvement.

## 5. Conclusion

In summary, the mPASS scale might be an easily memorized and effective tool to identify AIS with high likelihood of ELVO. The mPASS scale might achieve a better predictive performance than the PASS scale for identifying ELVO. Additional studies concerning utility and accuracy of the mPASS scale in prehospital setting and its ability to predict stroke outcome are warranted, which may change destination triage decisions and transfer appropriate patients to a CSC more quickly.

## Data Availability

We confirm that our article contains a data availability statement. We confirm that we have included a citation for available data in our reference section. The data that support the findings of this study are openly available.

## Ethical Approval

The consent we obtained from study participants was verbal and this was approved by the ethics committee. This study has required ethic approval.

## Disclosure

The submission of the manuscript is in a preprint (<https://www.researchsquare.com/article/rs-1795/v1>), which is a preliminary version of a manuscript that has not completed peer review at a journal. Research Square does not conduct peer review prior to posting preprints. The posting of a preprint on this server should not be interpreted as an endorsement of its validity or suitability for dissemination as established information or for guiding clinical practice.

## Conflicts of Interest

The authors have no financial conflicts of interest.

## Authors' Contributions

Xiaoli Si, Jie Ruan, Lin Jiang, and Congguo Yin contributed equally to this work.

## Acknowledgments

We thank the patients and their relatives for their generous donation of samples. The study was approved by Zhejiang Province Public Welfare Technology Application Research Project (LGF20H090008) and Natural Science Foundation of Zhejiang Province (LQ21H090007) and Hangzhou Science and Technology Plan Guidance Project (20181228Y01).

## Supplementary Materials

We ran a separate analysis using only ICA/M1 occlusions as the ELVO definition. Tables 3, 4, and 5 are sensitivity, specificity, PPV, NPV, and overall accuracy of different scales. Figure 4: discrimination and calibration analysis: the mPASS showed AUC 0.917, sensitivity 90.7%, and specificity 84.4%; the PASS showed AUC 0.876, sensitivity 92.6%, and specificity 83.9%; the NIHSS showed AUC 0.935, sensitivity 88.9%, and specificity 89.9% (AIS-ICA/NELVO). Figure 5: discrimination and calibration analysis: the mPASS showed AUC 0.931, sensitivity 92.6%, and specificity 84.4%; the PASS showed AUC 0.887, sensitivity 95.8%, and specificity 83.9%; the NIHSS showed AUC 0.944, sensitivity 93.7%, and specificity 84.9% (AIS-MCA-M1/NELVO). Figure 6: discrimination and calibration analysis: the mPASS showed AUC 0.926, sensitivity 91.9%, and specificity 84.4%; the PASS showed AUC 0.883, sensitivity 94.6%, and specificity 83.9%; the NIHSS showed AUC 0.941, sensitivity 93.3%, and specificity 84.9% (AIS – ICA + MCA – M1/NELVO). (*Supplementary Materials*)

## References

- [1] B. C. V. Campbell, G. A. Donnan, K. R. Lees et al., "Endovascular stent thrombectomy: the new standard of care for large vessel ischaemic stroke," *Lancet Neurology*, vol. 14, no. 8, pp. 846–854, 2015.
- [2] B. C. V. Campbell, A. Meretoja, G. A. Donnan, and S. M. Davis, "Twenty-year history of the evolution of stroke thrombolysis with intravenous Alteplase to reduce long-term disability," *Stroke*, vol. 46, no. 8, pp. 2341–2346, 2015.
- [3] P. de la Ossa, "Design and validation of a prehospital stroke scale to predict large arterial occlusion," *Stroke*, vol. 45, no. 1, pp. 87–91, 2014.
- [4] D. P. Briley, T. Meagher, and D. King, "Practical limitations of acute stroke MRI due to patient-related problems," *Neurology*, vol. 64, no. 2, pp. 400–401, 2005.
- [5] L. Derex, N. Nighoghossian, M. Hermier, P. Adeleine, J. C. Froment, and P. Trouillas, "Early detection of cerebral arterial occlusion on magnetic resonance angiography: predictive value of the baseline NIHSS score and impact on neurological outcome," *Cerebrovascular Diseases*, vol. 13, no. 4, pp. 225–229, 2002.
- [6] C. S. Kidwell, S. Starkman, M. Eckstein, K. Weems, and J. L. Saver, "Identifying stroke in the field. Prospective validation

## *Retraction*

# **Retracted: Constructing a Predictive Model of Depression in Chemotherapy Patients with Non-Hodgkin's Lymphoma to Improve Medical Staffs' Psychiatric Care**

### **BioMed Research International**

Received 12 March 2024; Accepted 12 March 2024; Published 20 March 2024

Copyright © 2024 BioMed Research International. This is an open access article distributed under the Creative Commons Attribution License, which permits unrestricted use, distribution, and reproduction in any medium, provided the original work is properly cited.

This article has been retracted by Hindawi following an investigation undertaken by the publisher [1]. This investigation has uncovered evidence of one or more of the following indicators of systematic manipulation of the publication process:

- (1) Discrepancies in scope
- (2) Discrepancies in the description of the research reported
- (3) Discrepancies between the availability of data and the research described
- (4) Inappropriate citations
- (5) Incoherent, meaningless and/or irrelevant content included in the article
- (6) Manipulated or compromised peer review

The presence of these indicators undermines our confidence in the integrity of the article's content and we cannot, therefore, vouch for its reliability. Please note that this notice is intended solely to alert readers that the content of this article is unreliable. We have not investigated whether authors were aware of or involved in the systematic manipulation of the publication process.

Wiley and Hindawi regrets that the usual quality checks did not identify these issues before publication and have since put additional measures in place to safeguard research integrity.

We wish to credit our own Research Integrity and Research Publishing teams and anonymous and named external researchers and research integrity experts for contributing to this investigation.

The corresponding author, as the representative of all authors, has been given the opportunity to register their agreement or disagreement to this retraction. We have kept a record of any response received.

### **References**

- [1] C. Hu, Q. Li, J. Shou et al., "Constructing a Predictive Model of Depression in Chemotherapy Patients with Non-Hodgkin's Lymphoma to Improve Medical Staffs' Psychiatric Care," *BioMed Research International*, vol. 2021, Article ID 9201235, 12 pages, 2021.

## Research Article

# Constructing a Predictive Model of Depression in Chemotherapy Patients with Non-Hodgkin's Lymphoma to Improve Medical Staffs' Psychiatric Care

Cheng Hu,<sup>1</sup> Qian Li ,<sup>2</sup> Ji Shou,<sup>3</sup> Feng-xian Zhang,<sup>1</sup> Xia Li,<sup>4</sup> Min Wu,<sup>2</sup> Meng-jing Xu,<sup>1</sup> and Li Xu<sup>1</sup>

<sup>1</sup>Quality Control Department, The Third Hospital of Quzhou, China

<sup>2</sup>Psychiatry Department, The Third Hospital of Quzhou, China

<sup>3</sup>Nursing Department, The Third Hospital of Quzhou, China

<sup>4</sup>Rehabilitation Department, The Second Affiliated Hospital and Yuying Children's Hospital of Wenzhou Medical University, China

Correspondence should be addressed to Qian Li; [s01279062@acad.tri-c.edu](mailto:s01279062@acad.tri-c.edu)

Received 5 May 2021; Revised 10 June 2021; Accepted 29 June 2021; Published 19 July 2021

Academic Editor: Yuzhen Xu

Copyright © 2021 Cheng Hu et al. This is an open access article distributed under the Creative Commons Attribution License, which permits unrestricted use, distribution, and reproduction in any medium, provided the original work is properly cited.

**Objectives.** Depression is highly prevalent in non-Hodgkin's lymphoma (NHL) patients undergoing chemotherapy. The social stress associated with malignancy induces neurovascular pathology promoting clinical levels of depressive symptomatology. The purpose of this study was to establish an effective depressive symptomatology risk prediction model to those patients. **Methods.** This study included 238 NHL patients receiving chemotherapy, 80 of whom developed depressive symptomatology. Different types of variables (sociodemographic, medical, and psychosocial) were entered in the models. Three prediction models (support vector machine-recursive feature elimination model, random forest model, and nomogram prediction model based on logistic regression analysis) were compared in order to select the one with the best predictive power. The selected model was then evaluated using calibration plots, ROC curves, and C-index. The clinical utility of the nomogram was assessed by the decision curve analysis (DCA). **Results.** The nomogram prediction has the most efficient predictive ability when 10 predictors are included (AUC = 0.938). A nomogram prediction model was constructed based on the logistic regression analysis with the best predictive accuracy. Sex, age, medical insurance, marital status, education level, per capita monthly household income, pathological stage, SSRS, PSQI, and QLQ-C30 were included in the nomogram. The C-index was 0.944, the AUC value was 0.972, and the calibration curve also showed the good predictive ability of the nomogram. The DCA curve suggested that the nomogram had a strong clinical utility. **Conclusions.** We constructed a depressive symptomatology risk prediction model for NHL chemotherapy patients with good predictive power and clinical utility.

## 1. Introduction

Non-Hodgkin lymphoma (NHL) is a common hematological malignancy, originating from the lymphoid tissues. Chemotherapy is one of the common treatment options for non-Hodgkin lymphomas. However, chemotherapy is considered a stressor causing psychological problems in patients with NHL [1]. Compared with patients not receiving chemotherapy, patients receiving chemotherapy are more likely to experience depression [2]. Previous studies report that the incidence of

depression among patients undergoing chemotherapy is 16.8-45% [1, 3, 4].

As we all know, disease itself may also be a stressor for psychological burden. And stress also associated with malignancy induces neurovascular pathology promoting depression [5]. Depression can not only reduce the quality of life of the patients but also increase the recurrence rate as well as the risk of death [5-7]. Therefore, exploring potential risk factors related to depression in NHL patients undergoing chemotherapy is important, to help in promoting mental health care.

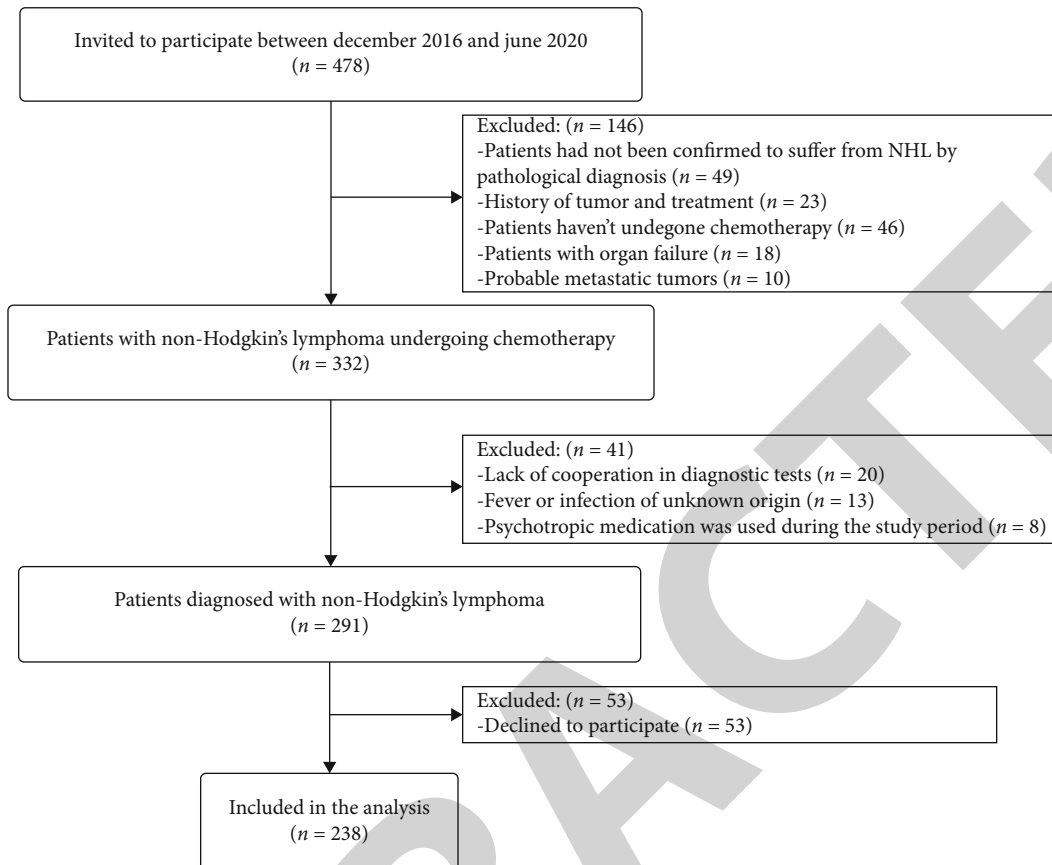


FIGURE 1: Flow chart of the study design.

Previous research points out that depression relates to physical conditions, diseases, sociodemographic characteristics, treatments, psychosocial factors, and so on [8]. Despite numerous research have identified many factors associated with depressive symptomatology in NHL patients undergoing chemotherapy, no systematic assessment aimed at predicting the risk of depressive symptomatology in NHL patients undergoing chemotherapy exists. Fortunately, studies have also pointed out that the nomogram can be used as a predictive tool to predict the risk of disease occurrence [9]. Psychological-based self-report tools, such as Hamilton Depression Scale (HAMD) [10], Depression Self-Rating Scale [11], and Beck Depression Scale [12], are often used in clinical practice to assess depressive symptomatology [13]. Therefore, we hypothesized that based on clinical and epidemiological characteristics as well as those scoring systems of depression, an effective prediction model could be developed in predicting the likelihood of depressive symptomatology for NHL patients.

This study is aimed at establishing a nomogram predictive model of depressive symptomatology in patients with NHL to improve medical staffs' psychiatric care. This model can provide information suitable for clinical decision-making, identification of individuals at high risk of depressive symptomatology. This research provides new ideas for improving the life quality of the NHL.

## 2. Materials and Methods

**2.1. Patients.** We conducted a cross-sectional study of patients diagnosed with NHL in The Third Hospital of Quzhou from December 2016 to June 2020. Combined with preoperative medical information, telephone questionnaire surveys and community follow-up were conducted. Community follow-up is a survey of patient information in the community where the patient lives in order to improve patient compliance with the survey. Informed consent was obtained from the patients before the start of the study. Participants were required to fill the questionnaire under the guidance of a designated researcher who had received psychology training to ensure they accurately understood the content of the questionnaire. The study was approved by the Institutional Ethics Review Board of The Third Hospital of Quzhou (approval no. 2016003), and all patients were Chinese residents. The inclusion criteria were as follows: non-Hodgkin's lymphoma was confirmed by pathological diagnosis, no history of tumor and treatment, no psychotropic medication was used during the study period, the patient had undergone chemotherapy, and the patient did not have any organ failure. The exclusion criteria were as follows: lack of compliance, declined to participate, tumors of uncertain origin, probable metastatic tumors (this is because the

TABLE 1: Patient characteristics.

Variables	Depressive symptomatology ( <i>n</i> = 80)	No depressive symptomatology ( <i>n</i> = 158)	<i>p</i> value
Age	57.4 ± 9.7	53.7 ± 14.5	0.041*
Gender			<i>p</i> ≤ 0.001**
Male	12 (15)	128 (81)	
Female	68 (85)	30 (19)	
Education level			<i>p</i> ≤ 0.001**
Primary school or below	49 (61.2)	58 (36.7)	
Junior high school	21 (26.3)	61 (38.6)	
Senior high school or higher	10 (12.5)	39 (24.7)	
Marital status			0.014*
Single	1 (1.3)	9 (5.7)	
Married	70 (87.4)	144 (91.1)	
Divorce	9 (11.3)	5 (3.2)	
Medical insurance			0.059
Self-paying	11 (13.8)	17 (10.8)	
Social security payments	57 (71.2)	105 (66.4)	
Commercial insurance payment	12 (15)	36 (22.8)	
Home place			0.32
Rural areas	33 (41.3)	57 (36.1)	
Urban areas	47 (58.7)	101 (63.9)	
Per capita monthly household income			0.027*
≤4000 yuan/month	13 (16.3)	16 (10.1)	
400-8000 yuan/month	37 (46.3)	51 (32.3)	
>8000 yuan/month	30 (37.4)	91 (57.6)	
Doctor patient communication frequency			0.197
Less	15 (18.8)	43 (27.2)	
Normal	59 (73.7)	98 (62)	
Frequent	6 (7.5)	17 (10.8)	
Hypertension			0.788
No	63 (78.7)	122 (77.2)	
Yes	17 (21.3)	36 (22.8)	
Diabetes			0.977
No	73 (91.2)	144 (91.1)	
Yes	7 (8.8)	14 (8.9)	
Hypercholesterolemia			0.549
No	64 (80)	121 (76.6)	
Yes	16 (20)	37 (23.4)	
Psychiatric history			0.599
No	77 (96.2)	155 (98.1)	
Yes	3 (3.8)	3 (1.9)	
Family history of NHL			0.544
No	75 (93.7)	152 (96.2)	
Yes	5 (6.3)	6 (3.8)	
Targeted drug			0.334
No	60 (75)	109 (69)	
Yes	20 (25)	49 (31)	
Pathological stage			0.372
No	31 (38.7)	52 (32.9)	
Yes	49 (61.3)	106 (67.1)	



TABLE 1: Continued.

Variables	Depressive symptomatology (n = 80)	No depressive symptomatology (n = 158)	p value
IPI			0.067
Score 0 to 2	28 (35)	75 (47.5)	
Score 3 to 5	52 (65)	83 (52.5)	
Palindromia			0.791
No	19 (23.8)	40 (25.3)	
Yes	61 (76.2)	118 (74.7)	
The first time in hospital			0.874
No	22 (27.5)	45 (28.5)	
Yes	58 (72.5)	113 (71.5)	
Disclosure of NHL diagnosis			$p \leq 0.001^{**}$
No	7 (8.8)	58 (36.7)	
Yes	73 (91.2)	100 (63.3)	
SSRS			$p \leq 0.001^{**}$
Low	20 (25)	57 (36)	
Medium	42 (52.5)	96 (60.8)	
High	18 (22.5)	5 (3.2)	
BAI			$p \leq 0.001^{**}$
Negative	30 (37.5)	112 (70.9)	
Positive	50 (62.5)	46 (29.1)	
PSQI	9.3 ± 2.3	4.8 ± 3.3	$p \leq 0.001^{**}$
Social Impact Scale	60.1 ± 8.1	62.6 ± 7.6	0.017*
Total score QLQ-C30	51.7 ± 8.8	59 ± 12	$p \leq 0.001^{**}$

\* $p < 0.05$  and \*\* $p < 0.01$ . Values are presented as the mean ± SD or number (percent (%)). IPI: International Prognostic Index; SSRS: Social Support Rate Scale; BAI: Beck Anxiety Inventory; PSQI: Pittsburgh Sleep Quality Index.

condition of patients with metastatic tumors is complex and easily misdiagnosed), and fever or infection of unknown origin.

**2.2. Diagnosis of Depressive Symptomatology.** The 17-item HAMD (HAMD-17) was used to assess the severity of depressive symptomatology in non-Hodgkin's lymphoma. The score for each item was 0-4 or 0-2 (distinct/severe, doubtful/mild, absent, and obvious, respectively) [14]. The total score of HAMD-17 was 0 to 54. As previously described, a total score of HAMD-17  $\geq 8$  indicates depression and patients were assigned to the depression group [15, 16]. The internal consistency of HAMD-17 is 0.83, the interrater reliability is 0.97, and the test-retest reliability was 0.81 [17-19]. Therefore, the HAMD-17 score demonstrates good reproducibility and strong feasibility for follow-up investigations.

**2.3. Demographic and Clinical Information.** The patient's demographic information (medical insurance, home place, marital status, per capita monthly household income, doctor-patient communication frequency, age, gender, education level, income level, etc.) and clinical data (hypertension, diabetes, hypercholesterolemia, psychiatric history, family history of NHL, targeted drug, pathological stage, and palindromia) were obtained for the included patients.

Relevant data were obtained from the NHL's medical records.

**2.4. Data Collection and Psychological Status Assessment System.** The Social Support Rate Scale (SSRS) was used to measure the dimensions of social support. The total score of SSRS ranges between 12 and 65 points (0-33 points, low social support; 33-45 points, medium social support; and 46-65 points, high level of social support) [20]. The test-retest reliability of SSRS is 0.89-0.94, and Cronbach's coefficient is 0.92 [21]. The anxiety state was measured using the 21-item Beck Anxiety Inventory (BAI). Each item's score ranges from 0 to 3, with a maximum score of 63, and the total BAI score of 45 points is considered as a diagnostic indicator of anxiety [22]. The internal consistency of the questionnaire is 0.92 [12]. The sleep state was measured using the Pittsburgh Sleep Quality Index (PSQI) [23], with a Cronbach's coefficient of 0.805 [24]. The PSQI score ranges from 0 to 21, with higher scores indicating poorer sleep quality. The Social Impact Scale was used for further evaluation, including the four dimensions of social exclusion, economic discrimination, inherent shame, and social isolation [25]. Using the four-level scoring method, the scale was divided into the total score of 4 dimensions. The higher the score, the greater the social impact that the individual perceives. Cronbach's coefficient is 0.85~0.90, and the correlation coefficient of each dimension is 0.28~0.66 [25].



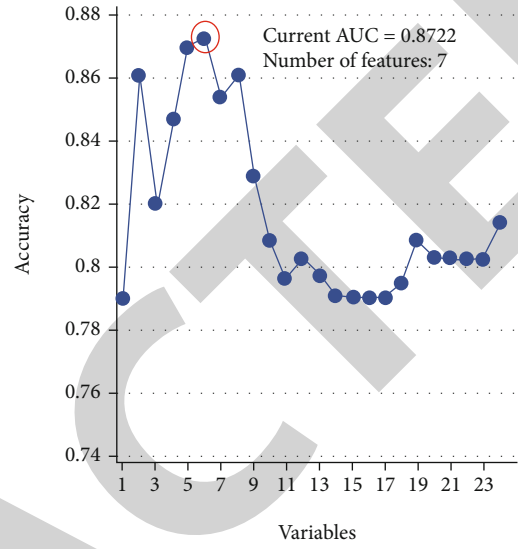
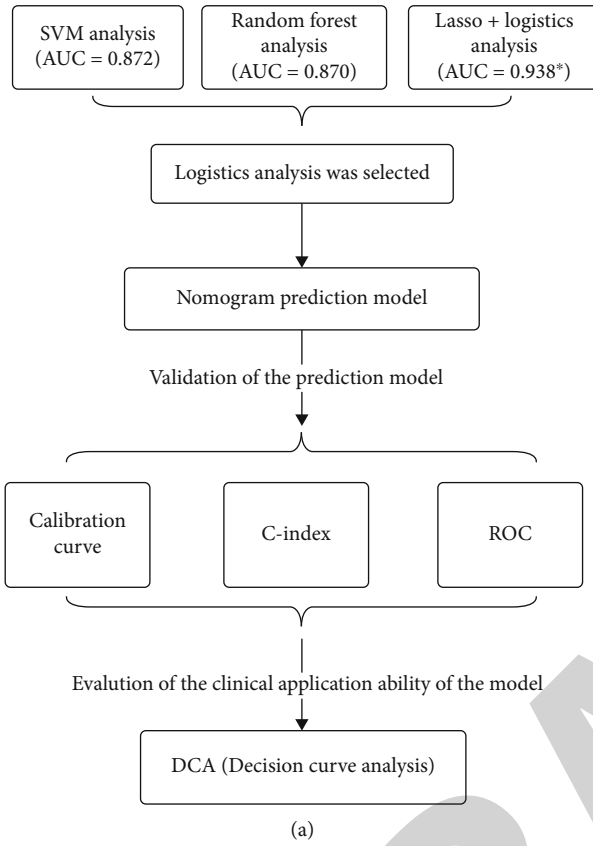


FIGURE 2: Continued.

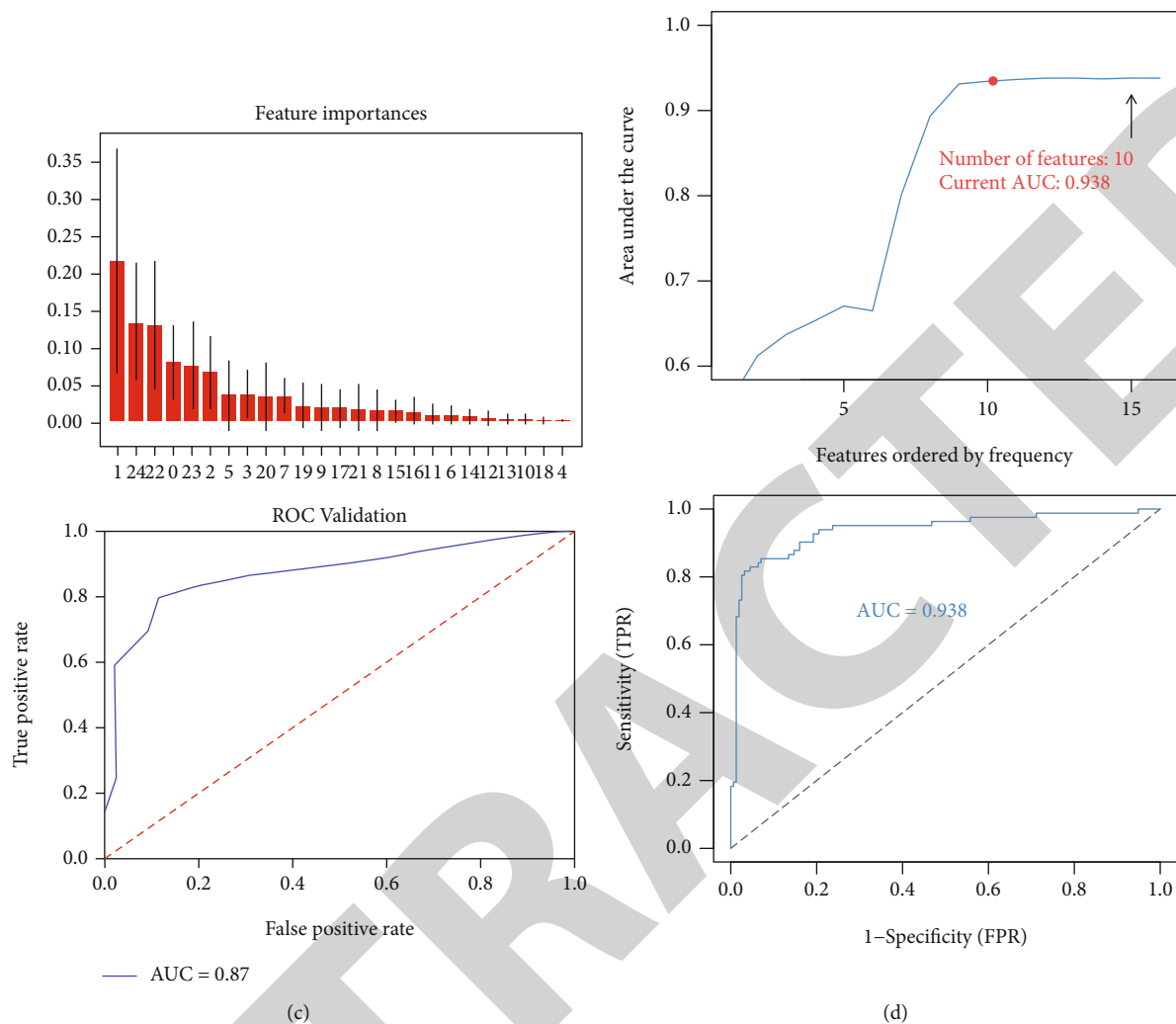


FIGURE 2: Prediction model selection. (a) Flow chart of model screening and evaluation design. (b) The support vector machine-recursive feature elimination (SVM-RFE) was used to build a prediction model. The SVM-RFE model had the highest accuracy (AUC = 0.8722) when it included 7 predictive factors. (c) Importance values of each factor in the random forest model (the picture above). And the ROC curve (AUC = 0.87) demonstrated the accuracy of the random forest model (the picture below). (d) Based on the number of occurrences of each factor, it is incorporated into the logic model to obtain a pattern diagram of the AUC values (the picture above). Ultimately, the simplest predictive model with good predictive power can be constructed using only 10 predictors (the picture below).

The European Organization for Research and Treatment Cancer Quality of Life Department C30 (EORTC QLQ C30) was used to determine the quality of life of NHL patients. The Chinese version of EORTC QLQ-C30 has a total of 30 items, which is divided into 15 areas, namely, 5 functional areas (physical, role, cognitive, emotional, and social function), 3 multi-item symptom areas (fatigue, pain, nausea, and vomiting), 1 general health status, and 6 single items (shortness of breath, insomnia, loss of appetite, constipation, diarrhea, and financial difficulties). The items on the scale 1 to 28 use a 4-level Likert scoring method. The 29th and 30th items are scored into 7 levels, from 1 to 7 points. The scale score ranges from 30 to 126 points. The higher the score, the worse the quality of life. The Chinese version of EORTCQLQ-C30 has good reliability and validity [26].

**2.5. Statistical Analysis.** The patients were randomly divided into the training and validation (7:3) groups. The training

group was used for diagnosis and prognostic analysis. The validation group was used to validate the prediction model. All statistical analyses were performed in R software (version 3.5.3).

Support vector machines and random forest models are also becoming more widely used in biology [27–29]. The SVM-RFE algorithm may be superior to linear discriminant analysis and mean square error methods in selecting relevant features and removing redundant features, especially when the sample size is small [30]. The random forest model also has been shown to have better advantages on many datasets [31]. It is also able to handle data at high latitudes and can calculate the importance of each feature, and it can balance errors for unbalanced datasets. Therefore, randomForest was also used as an alternative model. Besides, to prevent overfitting of the clinical prediction model, all preset factors were incorporated into the LASSO analysis, dimensionality reduction was done, and suitable predictive factors were

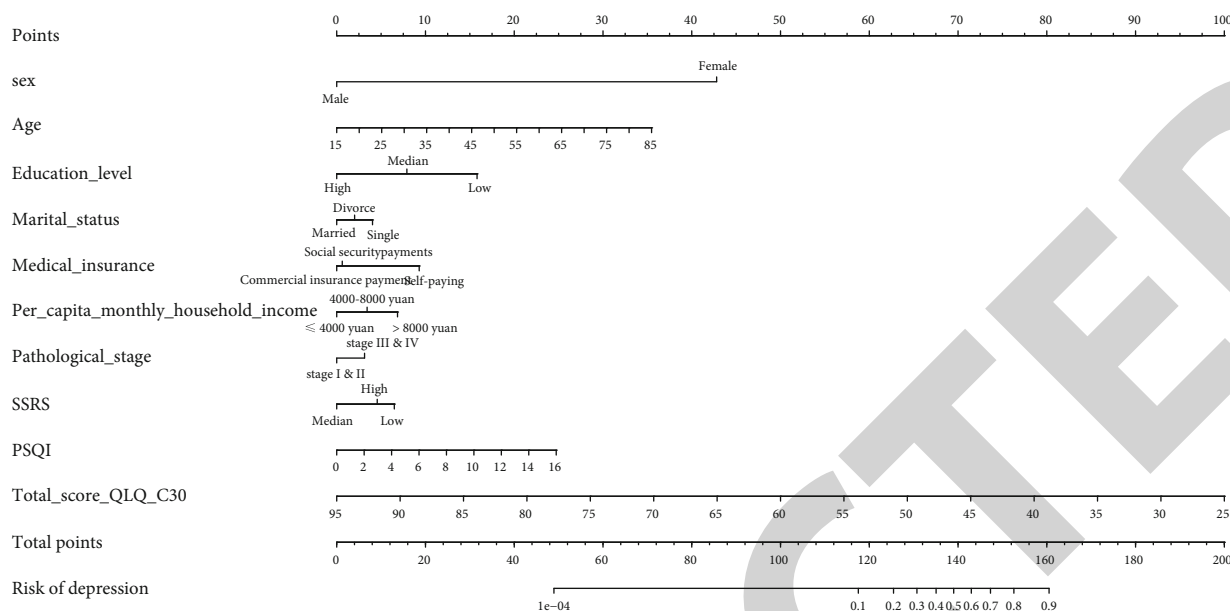


FIGURE 3: Establishing a predictive model. The predictive model of depressive symptomatology in patients with NHL. Sex, age, medical insurance, marital status, education level, per capita monthly household income, pathological stage, SSRS, PSQI, and QLQ-C30 are significant factors affecting the occurrence of depressive symptomatology in patients with NHL ( $p < 0.05$ ).

TABLE 2: Prediction factors for depressive symptomatology.

Variable	Prediction model		
	$\beta$	Odds ratio (95% CI)	$p$ value
(Intercept)	1.744	5.719 (0.108-315.986)	0.390
Sex	4.348	77.361 (24.273-313.424)	$p \leq 0.001$
Age	0.056	1.058 (1.015-1.106)	0.011
Education_level	-0.833	0.435 (0.214-0.84)	0.016
Marital_status	0.136	1.145 (0.207-6.633)	0.878
Medical_insurance	-0.460	0.631 (0.276-1.416)	0.266
Per_capita_monthly_household_income	0.310	1.364 (0.726-2.61)	0.338
Pathological_stage	-0.311	0.733 (0.279-1.908)	0.523
SSRS	-0.335	0.715 (0.339-1.492)	0.373
PSQI	0.170	1.185 (1.023-1.387)	0.027
Total_score_QLQ_C30	-0.144	0.866 (0.808-0.918)	$p \leq 0.001$

$\beta$  is the regression coefficient.

screened [32]. Multivariate logistic regression model was used to establish the predictive model. The nomogram included the most significant factors to predict the risk of depressive symptomatology in patients with NHL [28, 29, 33]. A calibration curve was used to evaluate the accuracy of the nomogram [34]. To further quantify the identification performance of the nomogram, the C-index was calculated and the ROC curve was plotted [35]. The AUC value was between 0.7 and 1, indicating that the model had a good prediction accuracy [36]. To improve medical staffs' psychiatric care (i.e., the ability to make better decisions using the model) by quantifying the net income under different threshold probabilities from patient's information, the DCA was used to evaluate the clinical applicability of the nomogram [9].

All statistical tests were two-sided, and  $p$  values less than 0.05 were considered statistically significant. This study proposed a visual multivariate prediction model to predict the incidence of depressive symptomatology in NHL patients [37].

### 3. Results

**3.1. Clinicopathological Characteristics.** The recruitment process is illustrated in Figure 1. The clinical information of 238 NHL patients (140 males and 98 females) obtained between December 2016 and June 2020 was evaluated. The patients were divided into the depressive symptomatology group (80 patients) and nondepressed group (158 patients). Table 1

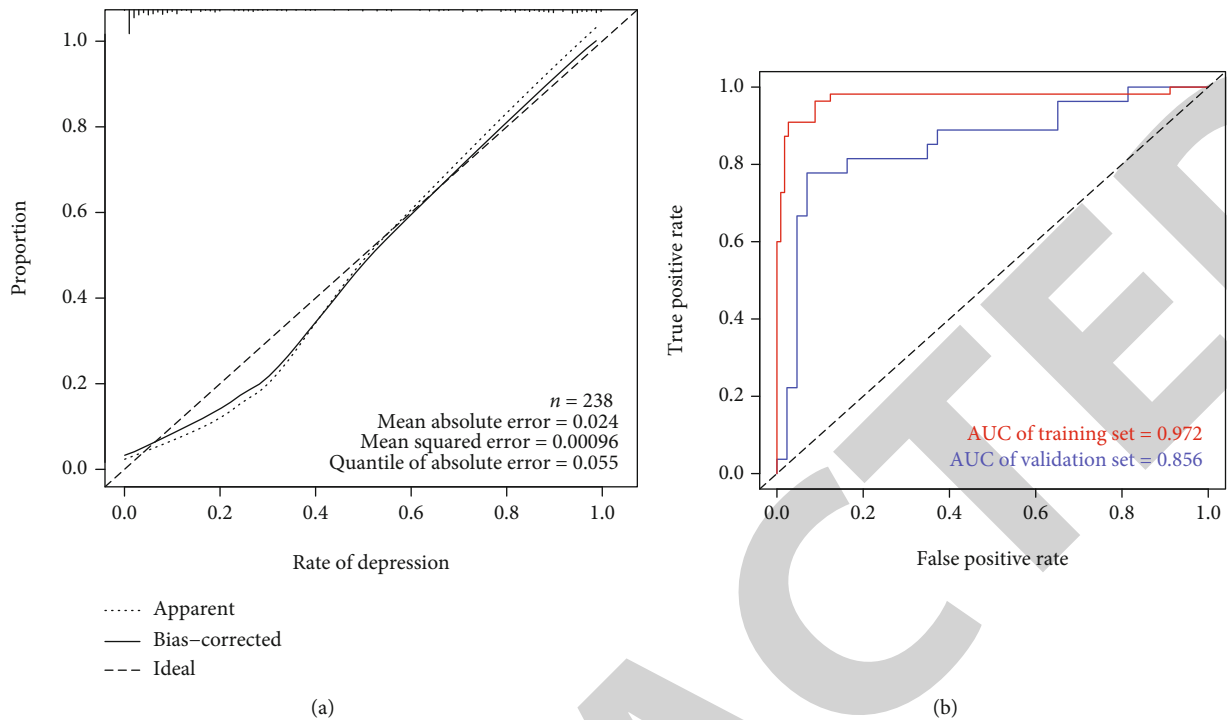


FIGURE 4: Validation of the prediction model. (a) Calibration curve of the prediction model of depressive symptomatology in patients with NHL ( $B = 10000$ ). The x-axis is the predicted risk of depressive symptomatology in patients with non-Hodgkin's lymphoma. The y-axis represents the actual incidence of depressive symptomatology in patients with non-Hodgkin's lymphoma. The solid line represents the actual prediction of the prediction model. The more consistent the solid line and the dotted line are, the better the predictive ability of the predictive model. (b) AUC represents the accurate prediction of the risk of depressive symptomatology in patients with NHL in randomly selected cases. The AUC values of the training set (red) and validation set (blue) are 0.972 and 0.856, respectively.

TABLE 3: C-index of the prediction model.

Dataset group	C-index of the prediction model	
	C-index	The C-index (95% CI)
Training set	0.972	0.938-1.000
Validation set	0.885	0.796-0.974
Entire cohort	0.944	0.907-0.981

shows the general characteristics of patient data. There were no significant differences between medical insurance, home place, doctor patient communication frequency, hypertension, diabetes, hypercholesterolemia, psychiatric history, family history of NHL, targeted drug, pathological stage, International Prognostic Index (IPI), palindromia, and the first time in hospital in NHL patients with and without depressive symptomatology. There were statistically significant differences between age, gender, education level, marital status, per capita monthly household income, disclosure of NHL diagnosis, SSRS, BAI, PSQI, and Social Impact Scale in the two groups.

**3.2. Prediction Model Selection and Screening Predictors.** The flow chart of model screening and evaluation design is illustrated in Figure 2(a). There were 167 cases in the training group and 71 cases in the validation group. The support vector machine-recursive feature elimination (SVM-RFE) was used to build a prediction model which may be better than

linear discriminant analysis in selecting correlated features and removing redundant features. The SVM-RFE model had the highest accuracy (AUC = 0.8722) when it included 7 predictive factors (Figure 2(b)). The order of features in SVM-RFE method was ranked in Supplementary Table 1. In addition, random forest models were also constructed to assess predictive ability (Figure 2(c)). Importance values of each factor in the random forest model were showed. And the ROC curve (AUC = 0.87) demonstrated the accuracy of the random forest model. We believe that the model can be further optimized. Overfitting of models is a challenge in machine learning. Therefore, we used the minimum absolute contraction selection operator (LASSO) method to further reduce the number of features to prevent overfitting of the prediction model. In this study, we randomly performed 1000 LASSO regressions and obtained the best combination of predictors. The predictors were then sequentially included in the logistic model based on the number of occurrences of the predictors. It was found that the model must have the most efficient predictive ability when 10 predictors are included (AUC = 0.938) (Figure 2(d)). In summary, we find that the model based on LASSO analysis combined with logistic regression has the strongest predictive power.

Therefore, the LASSO regression model (Supplementary Figures 1(A) and 1(B)) was used to reduce the factors in this study from 24 predictors to 10 predictive parameters, thereby establishing a predictive model containing 10

predictors. The 10 predictive factors included education level, sex, age, marital status, medical insurance, per capita monthly household income, pathological stage, SSRS, PSQI, and QLQ-C30. Principal component analysis (PCA) revealed that these predictors could potentially distinguish between the depressed and nondepressed groups (Supplementary Figure 1(C)).

**3.3. Establishment of the Prediction Model.** The logistic model was used to analyze and determine the 10 predictive factors, and the nomogram is constructed in R software as shown in Figure 3. Among them, sex, age, education level, PSQI, and QLQ-C30 were found to be the most significant factors associated with the occurrence of depressive symptomatology in patients with NHL ( $p < 0.05$ ). The specific performance of various factors in the prediction model of depressive symptomatology in patients with NHL is shown in Table 2.

**3.4. Validation of the Prediction Model.** The calibration curve of the nomogram showed good agreement between the observation and prediction (Figure 4(a)), indicating that the model can be used to assess the risk of depressive symptomatology in NHL patients. Besides, the AUC in the training group of the prediction model was 0.972, and the AUC in the verification group was 0.856 (Figure 4(b)). The *C*-index in the overall sample and verification group indicated the good predictive performance of the nomogram (the *C*-index of the overall sample was 0.944, and the *C*-index of the verification group was 0.885) (Table 3).

**3.5. Evaluation of Clinical Application.** The decision curve analysis (DCA) of the nomogram is shown in Supplementary Figure 2. The results show that the decision curve based on the nomogram predictive model can help in making better clinical decisions. This means that the established predictive model can improve medical staffs' psychiatric care, promote early planning of a clinical intervention, and better predict the risk of disease, hence support individualized intervention.

## 4. Discussion

Nomograms are widely used for prognostic predictive analysis in cancer prognosis, due to their ability to comprehensively integrate risk factors in multiple dimensions. Besides, the logistic regression analysis results can be graphed and visualized, and this greatly improves the accuracy of the predictions, which can be easily interpreted, hence suitable in clinical decision-making [38]. Obviously, there is no research on the application of a nomogram model to predict the risk of depressive symptomatology in NHL patients undergoing chemotherapy. Based on a total of 10 predictive factors, including the patients' general clinical data and evaluation of various dimensions of the quality of life, this study for the first time established and verified a nomogram prediction model as a predictive tool for depressive symptomatology in non-Hodgkin's lymphoma patients.

LASSO regression model was used in this study to screen and predict related factors and reduced the main factors from 24 to 10, and the factors included sex, age, education level, marital status, medical insurance, per capita monthly house-

hold income, pathological stage, SSRS, PSQI, and QLQ-C30. Based on the predicted factors, a nomogram prediction model containing 10 optimal features was established as a predictive tool for the occurrence of depressive symptomatology in non-Hodgkin's lymphoma patients. Similar to previous studies, most of these variables have been reported to be related to the occurrence of depression [39]. Internal validation of the nomogram using the validation cohort showed that the prediction tool had a good predictive ability. Therefore, the nomogram can help in the early prediction of non-Hodgkin's lymphoma patients with a high risk of depressive symptomatology and provide targeted medical care to improve the prognosis of patients.

This study suggests that the risk factors for depressive symptomatology in patients with NHL undergoing chemotherapy include female, elderly, low education level, good marital status, medical insurance, high household income, lower pathological stage, SSRS, PSQI, and QLQ-C30. Numerous previous studies have reported that these factors are associated with a higher risk of depressive symptomatology in patients with lymphoma, similar to the results of previous systematic reviews [8]. Polikandrioti et al. pointed out that the elderly group has a higher risk of depressive symptomatology compared to the younger population [40]. Four studies with 1,149 participants reported that female participants had a higher risk of depressive symptomatology compared to male participants [1, 3, 41, 42]. Good marital status also helps to prevent depressive symptomatology. Previous research reports that reduced sex life is significantly related to depression in cancer patients undergoing chemotherapy [43]. The type of medical insurance is also an important factor influencing depression in patients with NHL. This study showed that patients using agricultural insurance and self-financed payment methods were at a higher risk of developing depressive symptomatology. Anticancer treatment is expensive, and the economic burden placed on the patients has a greater negative impact on the patients' emotional and mental health [44]. Research reports that patients with higher cancer stages are at higher risk of depressive symptomatology [3, 45–48]. Numerous studies have reported that sleep disorders are positively related to increased risk of depressive symptomatology [49–51]. Two studies, with 366 participants, provided evidence that patients with sleep disorders had higher depression scores than those with no sleep disorders [50, 51]. Consistent with previous studies, this study found that lack of social support was significantly associated with depression [52, 53]. Depression can be prevented through good social relationships, which can buffer against stressful environments [54]. Depression also restricts social interaction activities, leading to a decline in the quality of life. Studies have reported that the self-evaluation of cancer patients can greatly affect the patient's mental health and disease prognosis [9]. Self-evaluation is likely to affect how people feel, think, and act, and also affect their assessment of stress stimuli [55].

Therefore, medical workers should take some preventive measures to improve psychiatric care for patients at high risk for depressive symptomatology. Psychological interventions for such patients should be strengthened to ease their



negative emotions, strengthen their awareness of the disease and treatment, and enhance their confidence in overcoming the disease, hence face life and the disease with a more positive and optimistic attitude [8, 56]. Besides, the patients' relatives and friends should play an active role in providing social support to the patients, which further improves their psychological conditions. At the same time, the psychological condition of the patients should be regularly monitored for prevention and early diagnosis of depressive symptomatology.

The proposed nomogram is innovative in the following aspects. Firstly and most importantly, this was the first prognostic nomogram established for patients with non-Hodgkin's lymphoma, making individualized screening possible. Secondly, as the new net benefit analysis method, DCA analysis was applied to our nomogram, and the results showed that the model had a good clinical application value. Finally, early intervention can reduce the risk of depressive symptomatology in NHL patients. The significance of the findings was encouraging, and the predictive model has satisfactory clinical utility. However, some potential limitations should be considered. And the predictive model requires further external validation and multicenter studies to confirm its clinical applicability. Besides, it also remains unknown if the model is acceptable by medical workers and patients.

In this study, we established and validated a nomogram for predicting the risk of depressive symptomatology in patients with NHL undergoing chemotherapy. Our study also found that risk factors for depressive symptomatology in NHL patients receiving chemotherapy included the following: female, elderly, low education level, good marital status, medical insurance, high household income, lower pathological stage, SSRS, PSQI, and QLQ-C30. The significance of the findings was encouraging, and the predictive model has satisfactory clinical utility.

By using this predictive model, individuals at high risk for NHL can be identified prior to clinical manifestation. Medical staffs could take some preventive measures for high-risk depressive symptomatology at early time. Psychological interventions for such patients should be strengthened to ease their negative emotions, strengthen their awareness of the disease and treatment, and enhance their confidence in overcoming the disease, hence face life and the disease with a more positive and optimistic attitude. Therefore, early intervention can reduce the risk of depressive symptomatology in patients with NHL, reduce the consumption of precious medical resources, facilitate further clinical research, and provide personalized care plans to improve quality of life.

## 5. Conclusion

In conclusion, we established and validated a nomogram for predicting the risk of depressive symptomatology in patients with NHL undergoing chemotherapy. The proposed nomogram showed relatively high accuracy. The model can help doctors and medical staff to determine the risk of depressive symptomatology in patients with NHL, and provide individualized care to improve the quality of life of the patients.

## Abbreviations

BAI:	Beck Anxiety Inventory
DCA:	Decision curve analyses
HAMD-17:	The 17-item HAMD
IPI:	International Prognostic Index
LASSO:	Least absolute shrinkage and selection operator
NHL:	Non-Hodgkin's lymphoma
PCA:	Principal component analysis
PSQI:	Pittsburgh Sleep Quality Index
QLQ-C30:	European Organization for Research and Treatment Cancer Quality of Life Department C30
ROC:	The receiver operating characteristic curve
SIS:	Social Impact Scale
SVM-RFE:	Support vector machine-recursive feature elimination
SSRS:	Social Support Rate Scale

## Data Availability

The datasets generated and analyzed during the present study are available from the corresponding author on reasonable request.

## Ethical Approval

This study was approved by the Institutional Ethics Review Board of The Third Hospital of Quzhou (approval no. 2016003).

## Consent

All data published here are under the consent for publication. Informed written consent was obtained from all the patients.

## Conflicts of Interest

The authors declare that there are no competing interests.

## Authors' Contributions

CH, QL, JS, FZ, XL, and LX performed the data curation and analysis. CH, QL, JS, MW, MX, and LX analyzed and interpreted the results. CH and QL drafted and reviewed the manuscript. All authors read and approved the final manuscript.

## Acknowledgments

The authors wish to thank all the patients and staff who participated in this study.

## Supplementary Materials

This section contains the raw data from all patients participated in the study. (*Supplementary Materials*)

## References

- [1] C. D. Bergerot, H. R. Mitchell, K. T. Ashing, and Y. Kim, "A prospective study of changes in anxiety, depression, and



- problems in living during chemotherapy treatments: effects of age and gender," *Support Care Cancer*, vol. 25, no. 6, pp. 1897–1904, 2017.
- [2] Tian Mei, "A survey and analysis of depression state of cancer patients undergoing chemotherapy," *Chinese General Practice Nursing*, vol. 6, pp. 1601–1603, 2008.
  - [3] S. Duc, M. Rainfray, P. Soubeyran et al., "Predictive factors of depressive symptoms of elderly patients with cancer receiving first-line chemotherapy," *Psychooncology*, vol. 26, no. 1, pp. 15–21, 2017.
  - [4] A. J. Mitchell, M. Chan, H. Bhatti et al., "Prevalence of depression, anxiety, and adjustment disorder in oncological, haematological, and palliative-care settings: a meta-analysis of 94 interview-based studies," *The Lancet Oncology*, vol. 12, no. 2, pp. 160–174, 2011.
  - [5] C. Menard, M. L. Pfau, G. E. Hodes et al., "Social stress induces neurovascular pathology promoting depression," *Nature Neuroscience*, vol. 20, no. 12, pp. 1752–1760, 2017.
  - [6] T. Saevardottir, N. Fridriksdottir, and S. Gunnarsdottir, "Quality of life and symptoms of anxiety and depression of patients receiving cancer chemotherapy: longitudinal study," *Cancer Nursing*, vol. 33, no. 1, pp. E1–e10, 2010.
  - [7] S. Schneider and A. Moyer, "Depression as a predictor of disease progression and mortality in cancer patients: a meta-analysis," *Cancer*, vol. 116, no. 13, pp. 3304; author reply 3304–3304; author reply 3305, 2010.
  - [8] S. Wen, H. Xiao, and Y. Yang, "The risk factors for depression in cancer patients undergoing chemotherapy: a systematic review," *Support Care Cancer*, vol. 27, no. 1, pp. 57–67, 2019.
  - [9] E. W. Steyerberg and Y. Vergouwe, "Towards better clinical prediction models: seven steps for development and an ABCD for validation," *European Heart Journal*, vol. 35, no. 29, pp. 1925–1931, 2014.
  - [10] M. Hamilton, "A rating scale for depression," *Journal of Neurology, Neurosurgery, and Psychiatry*, vol. 23, no. 1, pp. 56–62, 1960.
  - [11] W. W. Zung, "A self-rating depression scale," *Archives of General Psychiatry*, vol. 12, no. 1, pp. 63–70, 1965.
  - [12] A. T. Beck, C. H. Ward, M. Mendelson, J. Mock, and J. Erbaugh, "An inventory for measuring depression," *Archives of General Psychiatry*, vol. 4, no. 6, pp. 561–571, 1961.
  - [13] L. K. Sharp and M. S. Lipsky, "Screening for depression across the lifespan: a review of measures for use in primary care settings," *American Family Physician*, vol. 66, no. 6, pp. 1001–1008, 2002.
  - [14] M. Hamilton, "Development of a rating scale for primary depressive illness," *The British Journal of Social and Clinical Psychology*, vol. 6, no. 4, pp. 278–296, 1967.
  - [15] E. Frank, R. F. Prien, R. B. Jarrett et al., "Conceptualization and rationale for consensus definitions of terms in major depressive disorder. Remission, recovery, relapse, and recurrence," *Archives of General Psychiatry*, vol. 48, no. 9, pp. 851–855, 1991.
  - [16] Y. Jia, W. Zhang, S. You, M. Li, L. Lei, and L. Chen, "A nomogram for predicting depression in patients with hepatocellular carcinoma: an observational cross-sectional study," *International Journal of Psychiatry in Clinical Practice*, vol. 23, no. 4, pp. 273–280, 2019.
  - [17] A. J. Rush, M. H. Trivedi, H. M. Ibrahim et al., "The 16-Item Quick Inventory of Depressive Symptomatology (QIDS), clinician rating (QIDS-C), and self-report (QIDS-SR): a psychometric evaluation in patients with chronic major depression," *Biological Psychiatry*, vol. 54, no. 5, pp. 573–583, 2003.
  - [18] K. A. Kobak, J. D. Lipsitz, and A. Feiger, "Development of a standardized training program for the Hamilton Depression Scale using internet-based technologies: results from a pilot study," *Journal of Psychiatric Research*, vol. 37, no. 6, pp. 509–515, 2003.
  - [19] J. B. Williams, "A structured interview guide for the Hamilton Depression Rating Scale," *Archives of General Psychiatry*, vol. 45, no. 8, pp. 742–747, 1988.
  - [20] S. Y. Xiao, "The theoretical basis and applications of Social Support Rate Scale," *Journal of Clinical Psychiatry*, vol. 4, pp. 98–100, 1994.
  - [21] J. Deng, J. Hu, W. Wu, B. Dong, and H. Wu, "Subjective well-being, social support, and age-related functioning among the very old in China," *International Journal of Geriatric Psychiatry*, vol. 25, no. 7, pp. 697–703, 2010.
  - [22] A. Osman, J. Hoffman, F. X. Barrios, B. A. Kopper, J. L. Breitenstein, and S. K. Hahn, "Factor structure, reliability, and validity of the Beck Anxiety Inventory in adolescent psychiatric inpatients," *Journal of Clinical Psychology*, vol. 58, no. 4, pp. 443–456, 2002.
  - [23] D. J. Buysse, C. F. Reynolds 3rd, T. H. Monk, S. R. Berman, and D. J. Kupfer, "The Pittsburgh Sleep Quality Index: a new instrument for psychiatric practice and research," *Psychiatry Research*, vol. 28, no. 2, pp. 193–213, 1989.
  - [24] F. Hita-Contreras, E. Martínez-López, P. A. Latorre-Román, F. Garrido, M. A. Santos, and A. Martínez-Amat, "Reliability and validity of the Spanish version of the Pittsburgh Sleep Quality Index (PSQI) in patients with fibromyalgia," *Rheumatology International*, vol. 34, no. 7, pp. 929–936, 2014.
  - [25] A. W. Pan, L. Chung, B. L. Fife, and P. C. Hsiung, "Evaluation of the psychometrics of the Social Impact Scale: a measure of stigmatization," *International Journal of Rehabilitation Research*, vol. 30, no. 3, pp. 235–238, 2007.
  - [26] T. J. Gong Yu, C. Pan, Z. Kai, and Z. Lei, "Evaluation of the Chinese version of EORTCQLQ-C30, QLQ-BN20 for brain tumor patients," vol. 35, pp. 90–494, 2020.
  - [27] N. Q. K. Le, E. K. Y. Yapp, Q. T. Ho, N. Nagasundaram, Y. Y. Ou, and H. Y. Yeh, "iEnhancer-5Step: identifying enhancers using hidden information of DNA sequences via Chou's 5-step rule and word embedding," *Analytical Biochemistry*, vol. 571, pp. 53–61, 2019.
  - [28] X. R. Kang, B. Chen, Y. S. Chen et al., "A prediction modeling based on SNOT-22 score for endoscopic nasal septoplasty: a retrospective study," *PeerJ*, vol. 8, article e9890, 2020.
  - [29] Y. S. Chen, Y. X. Cai, X. R. Kang et al., "Predicting the risk of sarcopenia in elderly patients with patellar fracture: development and assessment of a new predictive nomogram," *PeerJ*, vol. 8, article e8793, 2020.
  - [30] M. L. Huang, Y. H. Hung, W. M. Lee, R. K. Li, and B. R. Jiang, "SVM-RFE based feature selection and Taguchi parameters optimization for multiclass SVM classifier," *The Scientific World Journal*, vol. 2014, Article ID 795624, 10 pages, 2014.
  - [31] R. T. Buxton, M. F. McKenna, M. Clapp et al., "Efficacy of extracting indices from large-scale acoustic recordings to monitor biodiversity," *Conservation Biology*, vol. 32, no. 5, pp. 1174–1184, 2017.
  - [32] A. C. Kidd, M. McGettrick, S. Tsim, D. L. Halligan, M. Bylesjo, and K. G. Blyth, "Survival prediction in mesothelioma using a scalable Lasso regression model: instructions for use and initial

## Retraction

# Retracted: A Predictive Model for the Risk of Cognitive Impairment in Patients with Gallstones

### BioMed Research International

Received 12 March 2024; Accepted 12 March 2024; Published 20 March 2024

Copyright © 2024 BioMed Research International. This is an open access article distributed under the Creative Commons Attribution License, which permits unrestricted use, distribution, and reproduction in any medium, provided the original work is properly cited.

This article has been retracted by Hindawi following an investigation undertaken by the publisher [1]. This investigation has uncovered evidence of one or more of the following indicators of systematic manipulation of the publication process:

- (1) Discrepancies in scope
- (2) Discrepancies in the description of the research reported
- (3) Discrepancies between the availability of data and the research described
- (4) Inappropriate citations
- (5) Incoherent, meaningless and/or irrelevant content included in the article
- (6) Manipulated or compromised peer review

The presence of these indicators undermines our confidence in the integrity of the article's content and we cannot, therefore, vouch for its reliability. Please note that this notice is intended solely to alert readers that the content of this article is unreliable. We have not investigated whether authors were aware of or involved in the systematic manipulation of the publication process.

Wiley and Hindawi regrets that the usual quality checks did not identify these issues before publication and have since put additional measures in place to safeguard research integrity.

We wish to credit our own Research Integrity and Research Publishing teams and anonymous and named external researchers and research integrity experts for contributing to this investigation.

The corresponding author, as the representative of all authors, has been given the opportunity to register their agreement or disagreement to this retraction. We have kept a record of any response received.

### References

- [1] Z. Liu and C. Li, "A Predictive Model for the Risk of Cognitive Impairment in Patients with Gallstones," *BioMed Research International*, vol. 2021, Article ID 3792407, 13 pages, 2021.

## Research Article

# A Predictive Model for the Risk of Cognitive Impairment in Patients with Gallstones

Zhaofang Liu  and Chuanyan Li

Department of General Surgery, The First Affiliated Hospital of USTC, China

Correspondence should be addressed to Zhaofang Liu; zhaofangliu@seu.edu.cn

Received 18 May 2021; Revised 13 June 2021; Accepted 7 July 2021; Published 19 July 2021

Academic Editor: Yuzhen Xu

Copyright © 2021 Zhaofang Liu and Chuanyan Li. This is an open access article distributed under the Creative Commons Attribution License, which permits unrestricted use, distribution, and reproduction in any medium, provided the original work is properly cited.

**Objectives.** Gallstones can cause malnutrition in patients and further lead to cognitive impairment. This study is aimed at constructing a validated clinical prediction model for evaluating the risk of developing cognitive impairment from gallstones. **Methods.** The study was a single-centre cross-sectional study. Four models or methods (SVM-RFE, random forest model, Lasso model, and logistics analysis) were analyzed and compared regarding their predictive performance. The model with the best classification performance and predictive power was selected. The AUC index, C-index, and calibration curves were applied to the chosen model to further evaluate its classification and prediction performance. Finally, the nomogram was plotted, and the clinical usability, efficacy, and safety of the nomogram were assessed using decision curve analysis (DCA). **Results.** This study included a total of 294 patients with gallstones, of which 110 had cognitive impairment. Factors such as gender, age, education, place of birth, history of alcohol consumption, abdominal circumference, sarcopenia, diabetes, anaemia, depression, and Pittsburgh Sleep Quality Index (PSQI) were incorporated into the model for nomogram construction. The calibration curve showed that the nomogram had good classification performance. Furthermore, the C-index of the model was 0.778 (95% CI, 0.674-0.882) in the test group. The DCA curves indicated that the constructed model had strong clinical applicability, efficacy, and safety. **Conclusions.** This study constructed a cognitive impairment risk prediction model for patients with gallstones with good classification and predictive power. The constructed predictive model allows us to screen patients with gallstones and at high risk of cognitive impairment. These efforts might also help to further increase patient compliance, assist healthcare professionals to better manage patients with gallstones, and ultimately improve their overall health status and quality of life. Future clinical studies should further evaluate the accuracy and clinical usability of this model.

## 1. Introduction

Although most gallstone carriers are asymptomatic, up to 20% of adults develop gallstones at some point in their lives, and more than 20% of these patients have complications [1, 2]. The known risk factors for gallstones are getting older, pregnancy, lack of physical activity, obesity, and metabolic changes such as overnutrition [1]. Gallstones and cognitive disorders can cause anorexia, leading to weight loss, malnutrition, and other problems [3]. Malnutrition also plays a role in the development of sarcopenia [4]. This finding is in agreement with a meta-analysis study, showing that the prevalence of sarcopenia was between 41% and 46% in older people (aged >60 years), with malnutrition being an independent

risk factor [5]. In addition, several studies have revealed that sarcopenia is also a risk factor for cognitive impairment and cognitive impairment [6, 7]. By reducing appetite, cognitive impairment can continue to exacerbate the severity of malnutrition. Thus, cognitive impairment and malnutrition usually operate in a vicious cycle. Treatment of gallstones is still predominantly invasive and relies mainly on surgery [1]. Cognitive impairment is considered to be an important factor that hinders patients from undergoing surgery [8]. Hence, it is important to examine the risk factors associated with cognitive impairment in patients with gallstones. This would help healthcare professionals manage the disease in patients with gallstones, allowing them to make appropriate and timely surgical decisions.

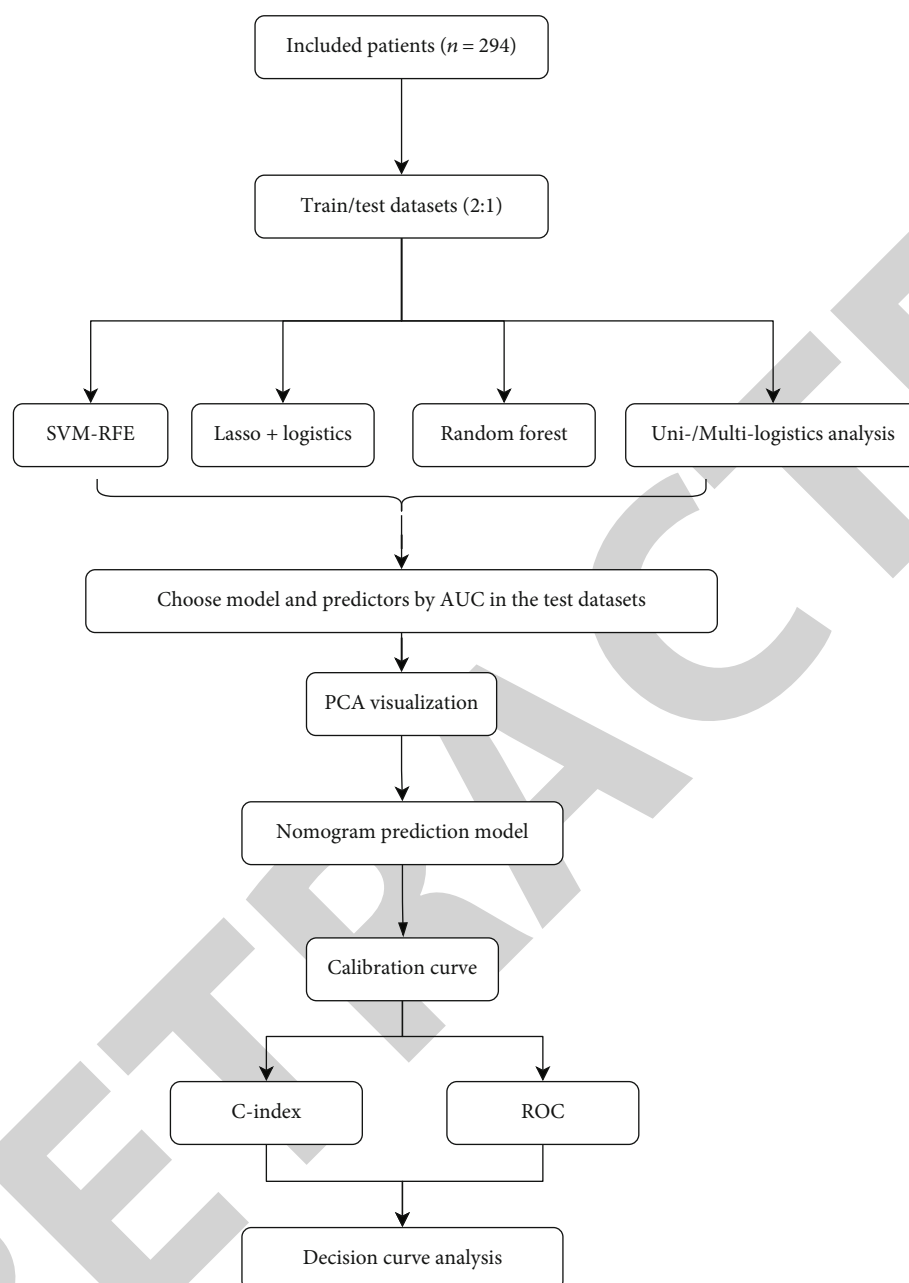


FIGURE 1: Flow chart of this research programme.

Previous studies have indicated that the prevalence of cognitive impairment in older people (aged  $\geq 65$  years) is between 5% and 10%. Various factors are known to be associated with cognitive impairment, including hypertension, diabetes, anaemia, cerebrovascular disease, smoking, alcohol consumption, and lack of exercise [9–12]. A closer look at the literature on risk factors for cognitive impairment, however, reveals a number of gaps and shortcomings. Namely, there is a lack of systematic assessment and, in particular, a lack of knowledge of risk factors for cognitive impairment in patients with gallstones. Thus, a risk prediction tool is needed for assessing risk factors and visualizing the results to solve these problems. Previous studies have suggested that nomogram-based clinical prediction models can be

employed to assist clinicians in visually calculating and assessing the incidence of disease for each patient [13, 14]. The development of a clinical risk prediction tool requires the collection of raw data and the extensive screening of clinical characteristics and models. However, a number of scales already exist that can be used for cognitive impairment, such as the Mini-Mental State Examination (MMSE) and Clinical Dementia Rating (CRD) [15, 16]. By using these scales together, a specialist psychiatrist can easily make a diagnosis of cognitive impairment. We, therefore, hypothesized that a valid predictive model could be developed to predict the likelihood of cognitive impairment in people with gallstones based on clinical and epidemiological characteristics and these scoring scales for cognitive impairment.

TABLE 1: Demographic and clinical characteristics of patients with or without cognitive impairment.

Variables	Normal (n = 184)	Dementia (n = 110)	P value
Age (year)	67.85 ± 6.25	71.83 ± 7.40	<0.001**
Sex			
Female	110 (59.78)	82 (74.55)	0.010*
Male	74 (40.22)	28 (25.45)	
Heart rate (bpm)	78.70 ± 10.22	77.74 ± 8.87	0.412
BMI (kg/m <sup>2</sup> )	24.39 ± 3.11	24.11 ± 3.39	0.471
Waist (cm)	86.09 ± 8.50	93.58 ± 86.20	0.243
Sarcopenia			
No	169 (91.85)	76 (69.09)	<0.001**
Yes	15 (8.15)	34 (30.91)	
Marital status			
Married	173 (94.02)	103 (93.64)	0.894
Single	11 (5.98)	7 (6.36)	
Education level			
Illiteracy	50 (27.17)	35 (31.82)	<0.001**
Primary education or below	77 (41.85)	63 (57.27)	
Secondary education or above	57 (30.98)	12 (10.91)	
Homeplace			
Rural areas	76 (41.30)	56 (50.91)	0.109
Urban areas	108 (58.70)	54 (49.09)	
Smoking			
No	168 (91.30)	105 (95.45)	0.181
Yes	16 (8.70)	5 (4.55)	
Drinking			
No	181 (98.37)	97 (88.18)	<0.001**
Yes	3 (1.63)	13 (11.82)	
Hypertension			
No	95 (51.63)	44 (40.00)	0.053
Yes	89 (48.37)	66 (60.00)	
Diabetes			
No	161 (87.50)	83 (75.45)	0.008**
Yes	23 (12.50)	27 (24.55)	
Anemia			
No	165 (89.67)	85 (77.27)	0.004**
Yes	19 (10.33)	25 (22.73)	
Exercise			
Less than 3 times a week	70 (38.04)	50 (45.45)	0.042*
More than 3 times a week	50 (27.17)	16 (14.55)	
No	64 (34.78)	44 (40.00)	
Medical insurance			
Commercial insurance payment	174 (94.57)	104 (94.55)	0.994
Self-paying	10 (5.43)	6 (5.45)	
Depression			
No	120 (65.22)	47 (42.73)	<0.001**
Yes	64 (34.78)	63 (57.27)	
PSQI	6.47 ± 3.77	7.81 ± 3.39	0.003**
Social Impact Scale	62.43 ± 8.54	62.22 ± 7.04	0.823
Total score QLQ-C30	56.69 ± 11.91	55.38 ± 10.87	0.347

\*P &lt; 0.05; \*\*P &lt; 0.01. Values are mean ± SD or number (percents%). Pittsburgh Sleep Quality Index (PSQI).

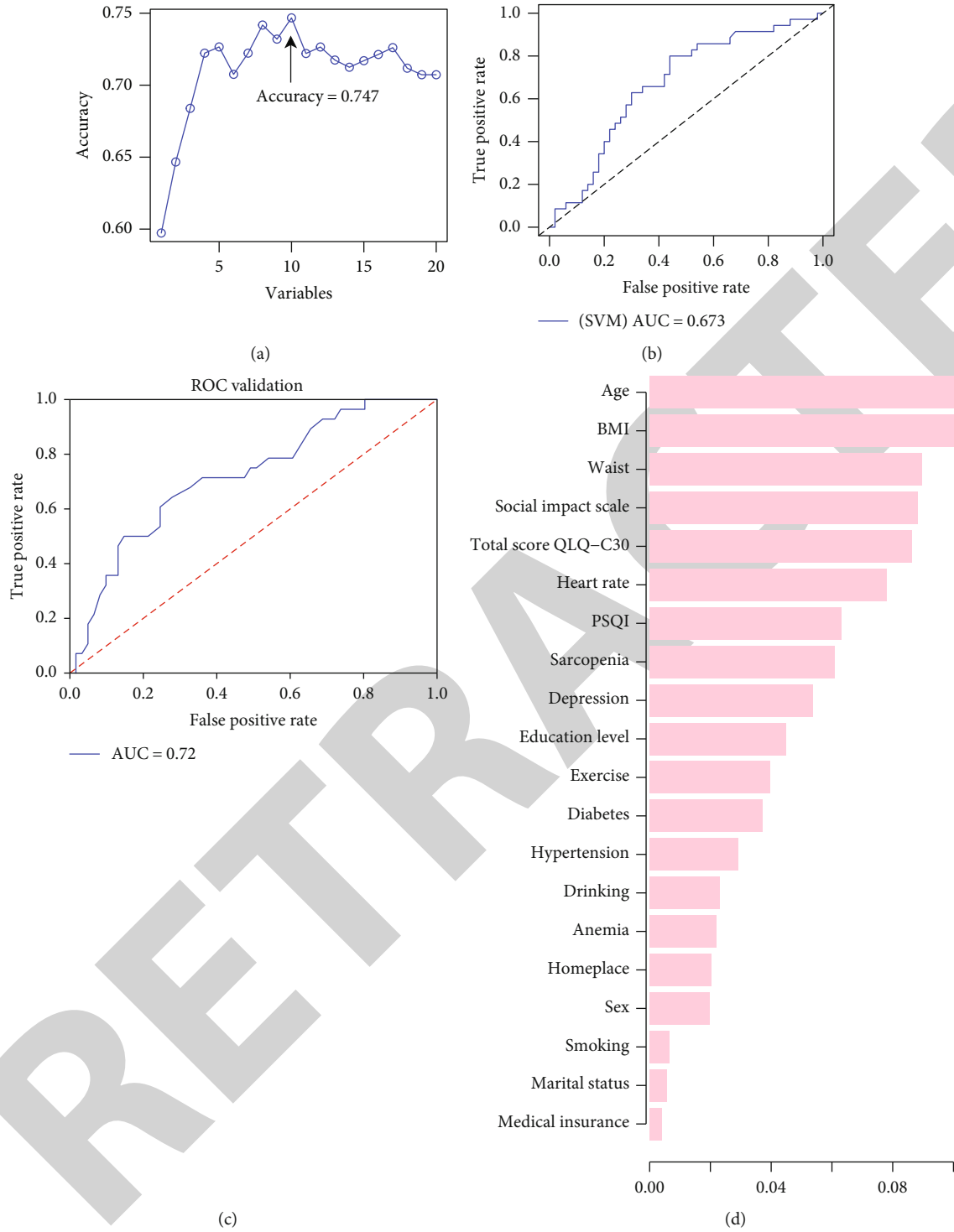


FIGURE 2: Continued.



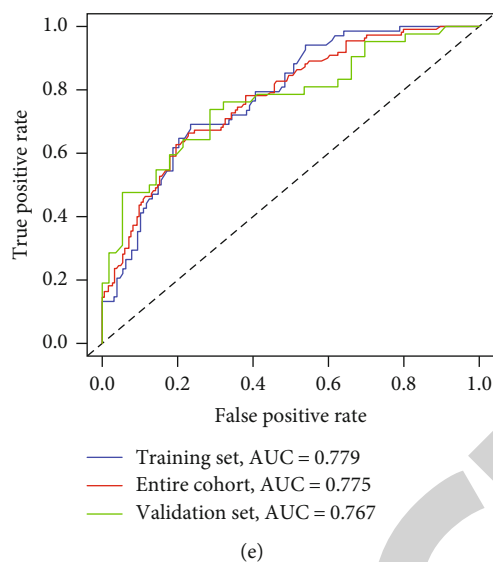


FIGURE 2: Multiple model training prediction results are shown along with the selection process and prediction feature factor screening. (a) Line graph of the process of hyperparameter selection for the support vector machine model. The horizontal axis is the number of features incorporated into the support vector machine model, and the vertical axis is the accuracy of the corresponding model's classification predictions. The model has the highest prediction accuracy in the training group when 10 features are included, with an accuracy of 0.747. (b) Based on the relationship between the model performance and the corresponding hyperparameters, the 10 features corresponding to the best model performance are included in the support vector machine model for training, and its classification prediction performance is evaluated in the test group. AUC = 0.673; (c) the ROC curve shows that the random forest model has good classification performance in the test group (AUC = 0.72). (d) This bar graph shows the importance ranking of each factor incorporated in the random forest model modelling. Pittsburgh Sleep Quality Index (PSQI); Quality of Life Questionnaire Core 30 (QLQ-C30); (e) eight factors were obtained by single and multifactor logistic regression analysis. The ROC curve shows that the logistic regression prediction model constructed based on these eight factors had good classification prediction ability in both the training group (AUC = 0.779) and the test group (0.767).

This study is aimed at building a nomogram prediction model for cognitive impairment in patients with gallstones. The model is expected to lead to more proper psychiatric care for patients. This study also sheds light on the importance of care and social support for elderly cognitive impairment patients with gallstones.

## 2. Materials and Methods

**2.1. Patients.** We selected patients diagnosed with gallstones at the First Affiliated Hospital of USTC from January 2018 to January 2021 for a cross-sectional study. Inclusion criteria were age > 60 years, documented preoperative, and absence of any organ failure. Exclusion criteria were patients with malignant diseases such as gallbladder cancer, patients taking relevant psychotropic drugs, and patients with missing clinical features of the relevant study or no outcome indicators recorded. This study was approved by our institutional ethics committee, and informed consent was obtained from the patients.

**2.2. General Clinical Data of the Patients.** The medical case record data included demographic and clinically relevant information on the patients. Demographic information, including sex, age, abdominal circumference, BMI, marital status, educational attainment, smoking history, alcohol history, place of birth, and exercise status, was collected. The data on clinical characteristics include heart rate, hyperten-

sion, sarcopenia, diabetes, and anaemia, as well as psychosocial score ratings such as depression status and social impact scores. History and demographic data on hypertension, diabetes mellitus, and anaemia were collected through medical records. Patients were also contacted via telephone if there were missing values. The diagnosis of sarcopenia was based on the Asian Working Group for Sarcopenia (AWGS) 2019 consensus: sarcopenia is diagnosed as a loss of muscle mass and a reduction in muscle strength and somatic function [17].

**2.3. Diagnosis of Cognitive Impairment and Related Psychiatric Diagnoses.** The Mini-Mental State Examination (MMSE) scale was used to screen cognitive impairment. The selection of relevant thresholds was consistent with previous studies in the literature [16]. The Clinical Dementia Rating (CDR) Scale was also used to evaluate the mental status of the patients [15, 18]. The Hamilton Rating Scale for Depression (17-item version, HAMD-17) was employed to measure the severity of depression in patients with gallstones who had not undergone surgical treatment [19]. Patients with a total score of  $\geq 8$  on the HAMD-17 were identified as having depression [20].

**2.4. Other Social Behaviour Assessment Scales.** The Pittsburgh Sleep Quality Index (PSQI) was used to evaluate the quality of sleep in patients with gallstones [21]. PSQI scores range from 0 to 21, with higher scores representing poorer sleep

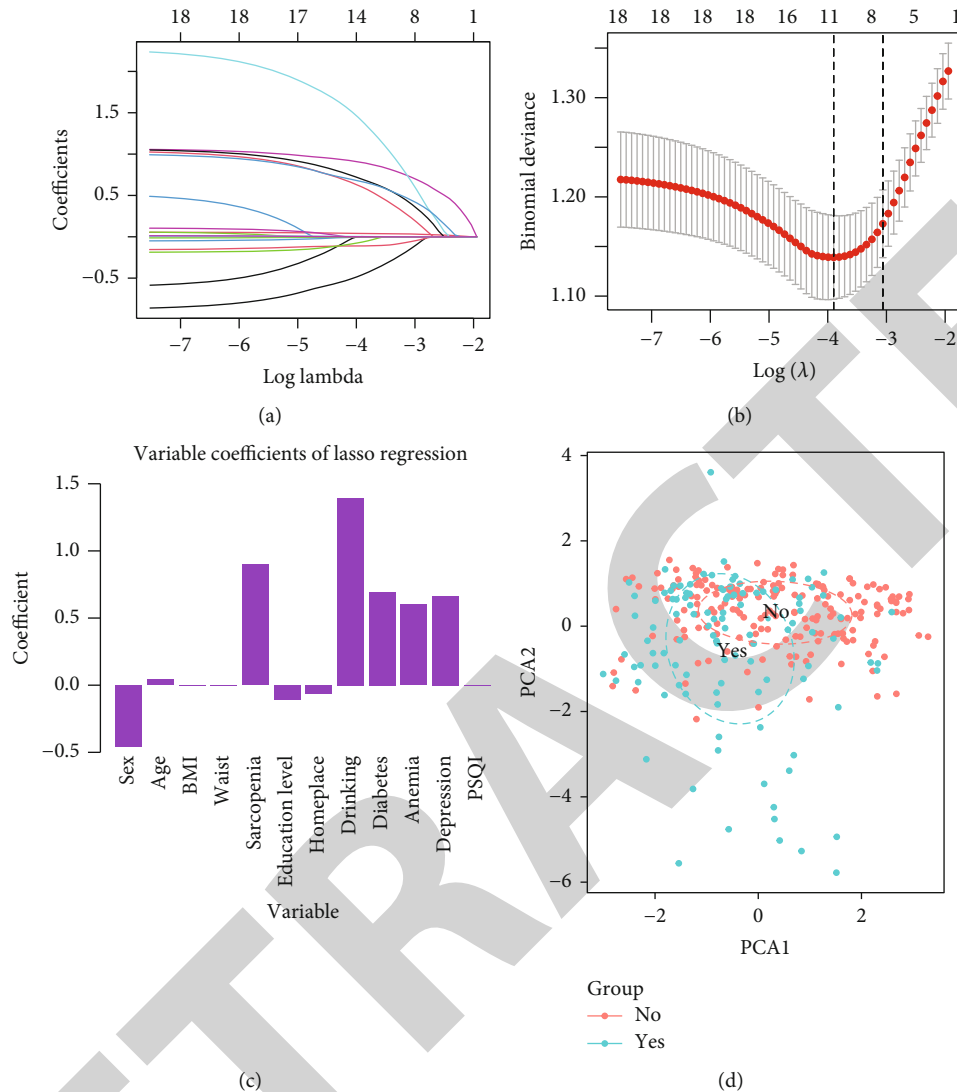


FIGURE 3: The Lasso regression model is based on a default 10-fold crossvalidation for the process of variable screening and initial assessment. (a) This graph shows the relationship between the penalty coefficient  $\log(\lambda)$  and the retained variables. The number of intersecting curves is the number of variables retained at that  $\log(\lambda)$  value. (b) Using the 10-fold crossvalidation method, the relationship between binomial deviance and  $\log(\lambda)$  is plotted. (c) This bar graph displays the names of the 11 variables selected and their corresponding coefficient values. (d) Scatter plot exhibits the unsupervised clustering of the 11 variables using PCA, which allows a good differentiation between the presence and absence of cognitive impairment in patients with gallstones. The pink dots represent patients without cognitive impairment, and the blue dots represent patients with cognitive impairment.

quality. It is important to note that the internal consistency of the PSQI measured by Cronbach's alpha is excellent [22]. The Social Impact Scale (SIS) was used to evaluate patients' psychological coping skills in response to social stigma [23]. The European Organisation for Research and Treatment of Cancer's (EORTC) Quality of Life Questionnaire (QLQ-C30) was performed to assess the quality of life of patients with gallstones and tumours, bearing in mind that both groups of patients suffer from chronic diseases. Core 30 (QLQ-C30) was also employed to evaluate the quality of life of patients [24, 25]. It must be stated that a higher score on this scale indicates a poorer quality of life.

**2.5. Predictive Model and Predictor Screening.** Patients were randomly divided into training and validation groups in a

ratio of 2 : 1. The training group was used to train the parameters of each model. On the other hand, the validation group was used to validate and compare the performance of each prediction model. A total of four models or methods were applied for predictive model construction, namely, the random forest model, SVM-RFE, Lasso model, and logistics analysis. The model with the strongest predictive power was selected based on its AUC value. The random forest model has several advantages, including its handling of high-dimensional data, the ability to build predictive models, and the ability to estimate the importance of each variable [26]. Support Vector Machine-Recursive Feature Elimination (SVM-RFE) is advantageous for small sample size datasets [27]. The SVM-RFE also has the ability to remove redundant factors and retain only the outcome related

TABLE 2: Uni- and multilogistics regression analysis.

Variables	Uni-logistics regression			Multilogistics regression		
	$\beta$	Odds ratio (95% CI)	<i>P</i> value	$\beta$	Odds ratio (95% CI)	<i>P</i> value
Sex	-0.678	0.508 (0.298-0.847)	0.011	-0.831	0.436 (0.211-0.86)	0.020
Age	0.084	1.088 (1.05-1.129)	<i>P</i> ≤ 0.001	0.052	1.053 (1.008-1.102)	0.022
Heart rate	-0.010	0.99 (0.966-1.014)	0.411			
BMI	-0.027	0.973 (0.902-1.047)	0.470			
Waist	0.003	NA	0.408			
Sarcopenia	1.617	5.04 (2.636-10.049)	<i>P</i> ≤ 0.001	0.982	2.669 (1.244-5.838)	0.012
Marital status	0.067	1.069 (0.383-2.801)	0.894			
Education level/illiterate						
Primary education or below	0.156	1.169 (0.679-2.024)	0.575			
Second education or above	-1.201	0.301 (0.137-0.627)	0.002			
Homeplace	-0.388	0.679 (0.421-1.091)	0.110			
Smoking	-0.693	0.5 (0.16-1.319)	0.189			
Drinking	2.090	8.086 (2.533-35.887)	0.001	2.251	9.498 (2.153-54.008)	0.005
Hypertension	0.471	1.601 (0.995-2.594)	0.054	0.141	1.151 (0.648-2.041)	0.630
Diabetes	0.823	2.277 (1.232-4.245)	0.009	0.960	2.611 (1.305-5.296)	0.007
Anemia	0.938	2.554 (1.337-4.953)	0.005	0.989	2.69 (1.199-6.14)	0.017
Exercise/less than 3 times a week						
More than 3 times a week	-0.803	0.448 (0.224-0.862)	0.019	-0.691	0.501 (0.226-1.075)	0.081
No	-0.038	0.962 (0.567-1.633)	0.887	0.056	1.057 (0.574-1.949)	0.858
Medical insurance	0.004	1.004 (0.333-2.784)	0.994			
Depression	0.922	2.513 (1.553-4.099)	<i>P</i> ≤ 0.001	0.923	2.517 (1.293-4.997)	0.007
PSQI	0.102	1.107 (1.036-1.186)	0.003	0.017	1.017 (0.927-1.116)	0.714
Social Impact Scale	-0.003	0.997 (0.967-1.027)	0.822			
Total score QLQ-C30	-0.010	0.99 (0.969-1.011)	0.347			

$\beta$  is the regression coefficient.

variables. The least absolute shrinkage and selection operator (Lasso) regression analysis is often employed to filter variables to prevent overfitting [28]. It uses the default tenfold crossvalidation. Multifactor logistic regression models are created for the screened variables based on the lambda.min value corresponding to the smallest loss. These analyses (both univariate and multifactorial logistic analyses) are often performed in medical research to screen for independent prognostic factors. Factors with  $P < 0.1$  on the univariate logistic analysis were included in the multifactor logistic analysis. Similarly, the factors were further filtered by  $P < 0.1$  in the subsequent multifactor logistic analyses. The final filtered variables were subjected to multifactor logistics prediction model construction.

**2.6. Nomogram Validation.** AUC values were calculated to evaluate each model's classification performance, and ROC curves were plotted for visualisation. Finally, the model with the highest AUC value was selected for nomogram plotting and further evaluation [13, 14]. Correction curves were plotted for visualising the model prediction accuracy. The C-index was calculated to quantitatively assess the model prediction accuracy. DCA curves were plotted to judge the clinical usability and safety of the model [29].

**2.7. Statistical Analysis.** R software (version 3.5.3) was employed for all statistical analyses. Two-tailed *t*-tests were used for significance testing of continuous variables. Pearson chi-square tests were used for categorical variables. For all statistical tests, a  $P < 0.05$  was considered to be statistically significant.

### 3. Results

**3.1. Patient Demographics and Clinical Characteristics.** Figure 1 depicts the flow chart and patient inclusion process. A total of 294 patients with gallstones (192 females and 102 males) were included in the study, of whom 110 had been previously diagnosed with cognitive impairment. Table 1 reveals the differences between the general and clinical characteristics of patients with or without cognitive impairment. Factors such as age, gender, sarcopenia, education, history of alcohol consumption, the prevalence of diabetes, proportion of anaemia, frequency of exercise, proportion of depression, and PSQI scores were statistically significantly different between the two groups ( $P < 0.05$ ). However, there were no statistical differences in factors such as BMI, heart rate, marital status, place of birth, smoking history, hypertension history, health insurance status, Social Impact Scale score, and total score of QLQ-C30 ( $P > 0.05$ ).

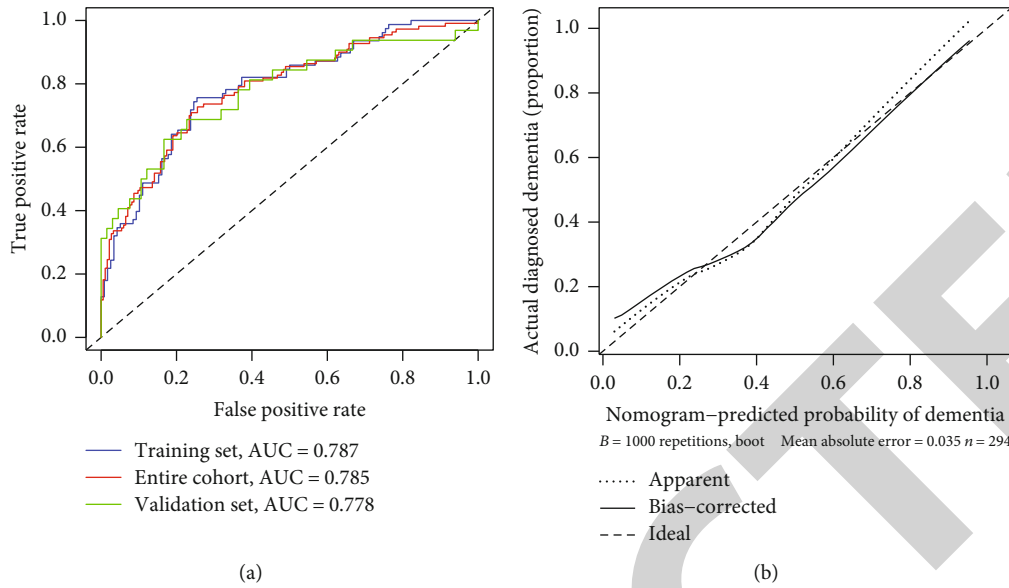


FIGURE 4: Model predictive power validation and assessment. (a) The ROC curve shows that the logistic regression model constructed from the variables screened by lasso regression has optimal predictive power. The AUCs were 0.787, 0.778, and 0.785 in the training, test, and whole cohorts, respectively; (b) calibration curve displays the predictive ability of the model for cognitive impairment prevalence in patients with gallstones. The dashed line represents the predictive ability of the model to show a 100% match under optimal expectations. The solid line represents the predictive ability that the trained model would exhibit in a real situation. The closer the solid and dashed lines are to each other, the better the predictive ability of the chosen model ( $B = 1000$ ).

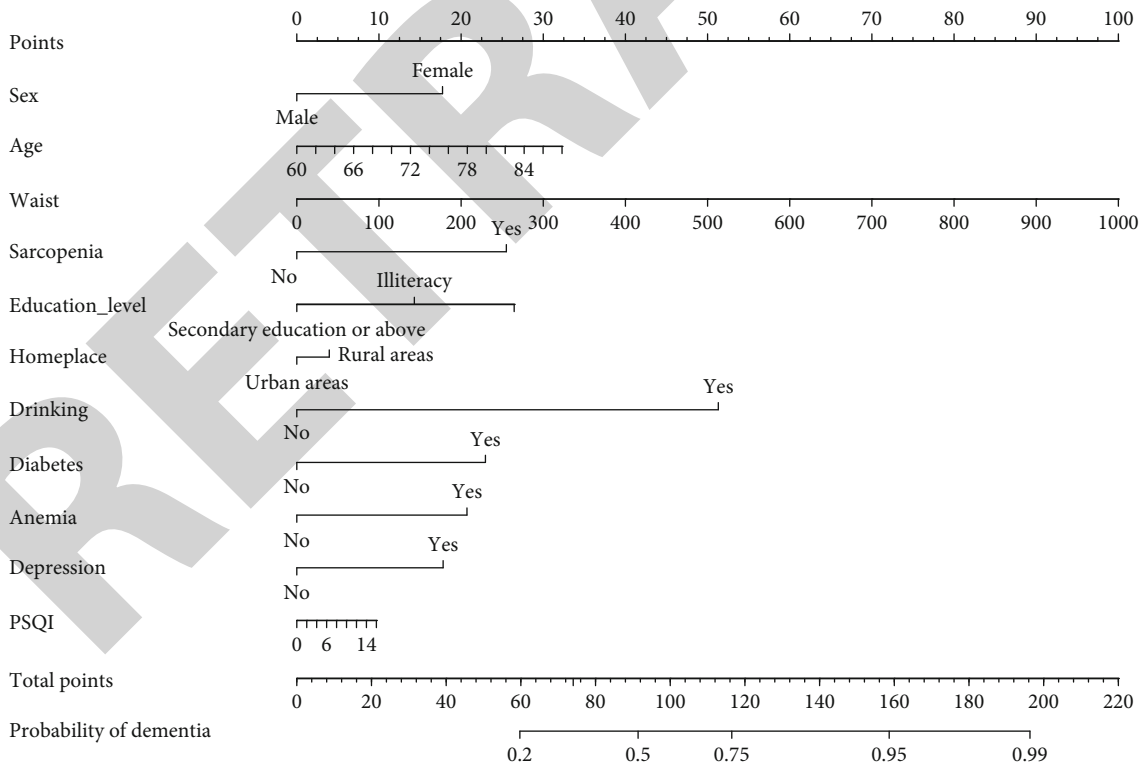


FIGURE 5: A predictive model was constructed using 11 variables screened by lasso regression, and a nomogram was created to calculate and predict the likelihood of cognitive impairment in patients with gallstones.

3.2. Predictive Model and Predictor Screening. Figures 2 and 3 exhibit the model screening process. The SVM-RFE model has nonlinear discriminatory properties, which allows the

comparison of results after modelling different numbers of variables to screen for the best combination of variables (see Figure 2(a)). In this study, the SVM-RFE

TABLE 3: Prediction factors for prevalence of cognitive impairment.

Variables	$\beta$	Odds ratio (95% CI)	P value
(Intercept)	-5.455	0.004 (0-0.127)	0.002
Sex	-0.777	0.46 (0.214-0.953)	0.041
Age	0.050	1.052 (1.005-1.102)	0.030
Waist	0.004	NA	0.435
Sarcopenia	1.117	3.055 (1.391-6.894)	0.006
Education level (illiterate)			
Primary education or below	0.532	1.702 (0.875-3.375)	0.121
Secondary education or above	-0.627	0.534 (0.174-1.557)	0.259
Homeplace (rural areas)	-0.173	0.841 (0.45-1.566)	0.585
Drinking	2.247	9.456 (2.284-50.568)	0.004
Diabetes	1.005	2.733 (1.341-5.665)	0.006
Anemia	0.907	2.477 (1.099-5.682)	0.030
Depression	0.780	2.181 (1.117-4.336)	0.024
PSQI	0.027	1.027 (0.933-1.13)	0.585

$\beta$  is the regression coefficient.

TABLE 4: C-index of the nomogram prediction model.

Dataset	C-index of the prediction model	
	C-index	The C-index (95% CI)
Training set	0.787	0.723-0.852
Validation set	0.778	0.674-0.882
Entire cohort	0.785	0.73-0.839

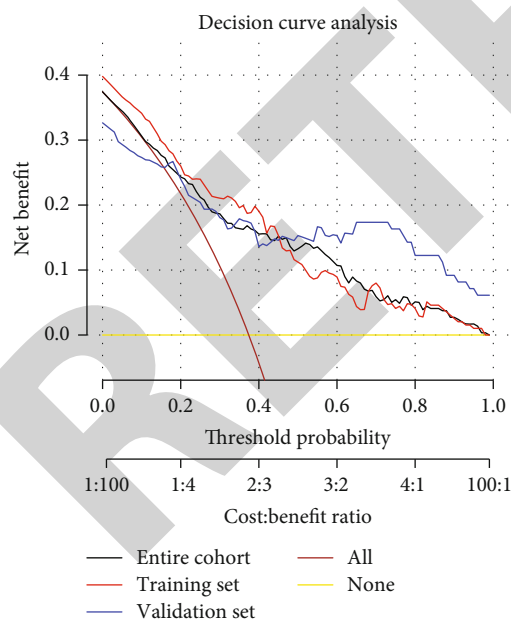


FIGURE 6: Clinical usability and safety of the model. Application of clinical decision analysis curves to assess the range of clinical applicability and safety of the model in predicting the likelihood of cognitive impairment in patients with gallstones.

hyperparameter selection of 10 variables produced the most accurate model (AUC = 0.673, Figure 2(b)). Then, the random forest model was constructed to evaluate its classifica-

tion and prediction performance (AUC = 0.72, Figure 2(c)). Also, based on the factors of the random forest model, the importance of the variables were ranked in the model (see Figure 2(d)). Furthermore, univariate and multivariate logistic regression analyses were applied to identify factors that independently predicted the outcome (see Table 2). The results indicated that factors such as female, advanced age, sarcopenia, alcohol consumption, history of diabetes, anaemia, and depression were independent risk factors for cognitive impairment patients with gallstones ( $P < 0.05$ ). The variables obtained from the screening were modelled in a multifactorial logistic regression prediction model based on a preset filter of  $P$  values. Figure 2(e) displays that the model had AUCs of 0.779, 0.767, and 0.775 for the training group, the test group, and the whole cohort, respectively. Figure 3(a) shows the relationship between the penalty coefficient log (lambda) and the variables retained by the model in the Lasso regression analysis. A total of 11 variables were filtered out based on the lambda.min value corresponding to the smallest loss value loss (see Figure 3(b)). Figure 3(c) presents the names of these 11 variables and the corresponding coefficients. PCA for unsupervised cluster analysis was applied for these 11 variables. It was found that these 11 variables could be well differentiated for the presence or absence of cognitive impairment in patients with gallstones (see Figure 3(d)). The variables screened by lasso analysis were used to construct a multifactorial logistic prediction model to assess the predictive performance of the model in the validation set (AUC = 0.778, Figure 4(a)). This logistic regression model was constructed with the best predictive performance. Thus, this model was used for further follow-up analyses.

3.3. Clinical Visualisation Prediction Tool Construction. Based on logistic regression prediction models, a nomogram was plotted in R for the 11 characteristic variables obtained from the lasso analysis screening (see Figure 5). In this constructed model, gender, age, sarcopenia, history of alcohol



consumption, diabetes, anaemia, and depression were found to be statistically significant difference factors associated with the development of cognitive impairment ( $P < 0.05$ , Table 3).

**3.4. Nomogram Validation.** The calibration curve assessing the predictive accuracy of the nomogram showed good agreement between the constructed model's prediction of cognitive impairment prevalence in patients with gallstones and the true observation (see Figure 4(b)). The ROC curve revealed that the constructed logistic regression model had AUCs of 0.787, 0.778, and 0.785 in the training group, the test group, and the whole cohort, respectively. In addition, the C-index of the model's predictions was also calculated for the three groups, at 0.787 (95% CI, 0.723-0.852), 0.778 (95% CI 0.778 (95% CI, 0.674-0.882), and 0.785 (95% CI, 0.73-0.839) (Table 4). These results indicate that the constructed nomogram had good predictive power. Moreover, the DCA revealed that the constructed model had a good level of clinical application and safety (see Figure 6). The results confirm that the nomogram and DCA can be tailored to patient needs and characteristics to help healthcare providers make better clinical decisions and provide a basis for safety and reliability for individualised interventions.

#### 4. Discussion

In this study, four models were evaluated and compared to predict cognitive impairment in patients with gallstones. By comparing the predictive performance of each model or method, the best method was selected for model construction. Consequently, the clinical computational tool nomogram was drawn.

The results indicate that a multifactor logistic regression model based on 11 factors screened by LASSO regression analysis had the best predictive performance. These 11 factors were gender, age, education, place of birth, history of alcohol consumption, abdominal circumference, sarcopenia, diabetes, anaemia, depression, and PSQI. Based on the constructed logistic regression model, gender, age, history of alcohol consumption, sarcopenia, diabetes, anaemia, and depression were considered to be the factors associated with the development of cognitive impairment in patients with gallstones. The nomogram was built as a predictive tool for the development of cognitive impairment in patients with gallstones based on the best model constructed for the predictors. The accuracy of the model was further validated in both the training and test groups. The level of safety and reliability of the model was also evaluated in clinical applications. This predictive model was developed to assist healthcare providers in predicting the onset of cognitive impairment in patients with gallstones in advance based on risk factors. Thus, this model can help them provide appropriate and timely care, support, and treatment for patients.

This study suggests that female gender, advanced age, alcohol consumption, history of diabetes, sarcopenia, anaemia, and depression are all risk factors for developing cognitive impairment in patients with gallstones. The correlation between these factors and cognitive impairment has also been explored in several previous studies [10–12, 30]. The

known risk factors for gallstone are female gender, increasing age, and metabolic syndromes such as obesity and overnutrition [1, 31–34]. Interestingly, Langa et al. showed that the risk of cognitive impairment increases with age and appears to be higher in men than in women [30]. Our findings also suggest that advanced age is a risk predictor for the development of cognitive impairment. However, our study found that female patients with gallstones were more likely to develop cognitive impairment than their male counterparts. This finding might be related to the fact that women are more likely to develop gallstones. Gallstones can lead to anorexia, whereby patients suffer from weight loss and malnutrition [3]. Malnutrition or mineral deficiencies are also found to be playing a role in the formation of gallstones [33, 35]. In addition, several previous studies have pointed out malnutrition as an independent risk factor for the development of sarcopenia [4, 5]. Consistent with our findings, sarcopenia is also reported to be a risk factor for cognitive impairment and cognitive impairment [6, 7]. Thus, cognitive impairment may exacerbate anorexia and further lead to malnutrition, perpetuating a vicious cycle of the disease. In summary, there seems to be a complex interaction between gallstones, malnutrition, sarcopenia, and cognitive impairment.

Frequent and heavy alcohol consumption is found to alter brain function, resulting in reduced cognition and even neurodegenerative diseases [36, 37]. Moreover, excessive alcohol consumption can also lead to mineral and vitamin deficiencies such as magnesium and folic acid deficiencies [38, 39]. Deficiencies in haematopoietic trace elements may cause anaemia. This is important since it has been shown that cognitive impairment is associated with anaemia [40]. This study also revealed that alcohol consumption was a significant predictor of developing cognitive impairment in patients with gallstones. Diabetes has also been found to be associated with cognitive impairment. Previous studies indicate that people with diabetes, especially those with poor blood sugar control, are at higher risk for developing cognitive impairment [41]. Another systematic review that included seven clinical studies came to similar conclusions, and they recommended testing and controlling patients' blood sugar to prevent or delay cognitive impairment [42].

It is also known that depression is an important cause of cognitive impairment [43]. Interestingly, loneliness was reported as an important factor in older patients for depression, contributing to the progression of cognitive impairment [44]. Social support is found to reduce depression in older people. Family support, in particular, is known to have a greater impact on depression in older people living in Asian communities [45]. Therefore, support groups such as family and friends can play an important role in improving elderly people's mental well-being by actively interacting and communicating with them [46]. Early detection and treatment are critical for optimal clinical outcome in patients with cognitive impairment, especially those at high risk of cognitive impairment. Potentially effective interventions for patients with cognitive impairment include meals with caregivers, family-style meals, soothing mealtime music, formal and informal caregiver support, and multifunctional interventions [47]. In summary, health workers can employ a myriad



of preventive and therapeutic measures to alleviate the illness and enhance the psychological care of patients at risk of cognitive impairment. The current treatment of gallstones relies mainly on surgery [1]. Cognitive impairment often prevents patients from undergoing surgery [8]. Thus, it is crucial to screen for, prevent, and treat cognitive impairment in patients with gallstones as early as possible.

Cognitive impairment is known to be a significant challenge for society and families. In order to properly address this challenge, in this study, we developed and validated a nomogram to predict the risk of cognitive impairment in patients with gallstones. This is the first nomogram to be constructed for the prediction of cognitive impairment in patients with gallstones, thus offering the possibility of individualised screening. Furthermore, this model allows for the early intervention and treatment of patients, potentially reducing the risk of exacerbation of cognitive impairment. Analysing the net benefit to patients also revealed that the model has good levels of clinical application and safety. The clinical prediction model, based on the present statistical characteristics, has satisfactory classification performance and clinical application. However, there were some limitations in this study. Firstly, the prediction model lacked external data sets for validation. The research results show that the performance of logistic regression model is better than that of random forest. It may also be because the amount of data does not meet the requirements. Moreover, conducting a multicentre prospective study would allow us to obtain a higher level of evidence for clinical application and provide better generalisable findings. Secondly, the study should have been further developed to include more cognitive impairment-related characteristics, for example, by adding a multimodal database. Third, the evaluation result of C-index is low, so it is difficult to prove that it is an accurate prediction. Also, the model should be further optimised through further multicentre studies and increased sample size. In future work, investigating the ease with which the model can be mastered by health professionals and accepted by patients in clinical practice might prove important.

Both early intervention and social support play a vital role in reducing the risk of cognitive impairment in older patients, the consumption of valuable healthcare resources, and the cost to society. The constructed predictive model allows us to screen patients with gallstones and at high risk of cognitive impairment. Surgeons can employ the nomogram to make appropriate and timely decisions about the indications for surgery. Prediction results also enable healthcare professionals to intervene with families and the community for patients at high risk of cognitive impairment in the early stages. These efforts might also help to further increase patient compliance, assist healthcare professionals to better manage patients with gallstones, and ultimately improve their overall health status and quality of life.

## 5. Conclusion

In summary, this study developed and validated a highly accurate nomogram for predicting the risk of cognitive impairment in patients with gallstones. The constructed

model provides a clinical basis for individualised diagnosis and treatment of patients with gallstones who are at risk of developing cognitive impairment. The nomogram was constructed to assist physicians in determining the need, suitability, and optimal time for surgery in patients with gallstones. It might also help caregivers and family members better monitor patients' conditions and ultimately improve the quality of life of patients with gallstones.

## Abbreviations

DCA:	Decision curve analyses
HAMD-17:	Hamilton Rating Scale for Depression (17-item version)
LASSO:	The least absolute shrinkage and selection operator
PCA:	Principal component analysis
PSQI:	Pittsburgh Sleep Quality Index
MMSE:	Mini-Mental State Examination
CRD:	Clinical Dementia Rating
SIS:	The Social Impact Scale
EORTC:	The European Organisation for Research and Treatment of Cancer
QLQ-C30:	Quality of Life Questionnaire Core 30
SVM-RFE:	Support Vector Machine-Recursive Feature Elimination
ROC:	The receiver operating characteristic curve
AUC:	Area under the curve.

## Data Availability

The datasets generated and analyzed during the present study are available from the corresponding author on reasonable request.

## Ethical Approval

This study was approved by the Institutional Ethics Review Board of The First Affiliated Hospital of USTC.

## Consent

All data published here are under the consent for publication. Informed written consent was obtained from all the patients.

## Conflicts of Interest

The authors declare that there are no competing interests.

## Authors' Contributions

Zhaofang Liu and Chuanyan Li performed the data curation and analysis. Zhaofang Liu and Chuanyan Li analyzed and interpreted the results. Zhaofang Liu and Chuanyan Li drafted and reviewed the manuscript. All authors read and approved the final manuscript.

## Acknowledgments

The authors wish to thank all the patients and staff who participated in this study. We thank Yitao Xue for his contribution to this study. Zhaofang Liu and Chuanyan Li are employed by The First Affiliated Hospital of USTC.

## References

- [1] F. Lammert, K. Gurusamy, C. W. Ko et al., "Gallstones," *Nature Reviews Disease Primers*, vol. 2, no. 1, article 16024, 2016.
- [2] D. M. Shabanzadeh, "Incidence of gallstone disease and complications," *Current Opinion in Gastroenterology*, vol. 34, no. 2, pp. 81–89, 2018.
- [3] J. E. Morley and D. Kraenzle, "Causes of weight loss in a community nursing home," *Journal of the American Geriatrics Society*, vol. 42, no. 6, pp. 583–585, 1994.
- [4] T. Cederholm, R. Barazzoni, P. Austin et al., "ESPEN guidelines on definitions and terminology of clinical nutrition," *Clinical Nutrition*, vol. 36, no. 1, pp. 49–64, 2017.
- [5] Y. Shen, J. Chen, X. Chen, L. Hou, X. Lin, and M. Yang, "Prevalence and associated factors of sarcopenia in nursing home residents: a systematic review and meta-analysis," *Journal of the American Medical Directors Association*, vol. 20, no. 1, pp. 5–13, 2019.
- [6] S. Nishiguchi, M. Yamada, H. Shirooka et al., "Sarcopenia as a risk factor for cognitive deterioration in community-dwelling older adults: a 1-year prospective study," *Journal of the American Medical Directors Association*, vol. 17, no. 4, pp. 372.e5–372.e8, 2016.
- [7] Y. Ogawa, Y. Kaneko, T. Sato, S. Shimizu, H. Kanetaka, and H. Hanyu, "Sarcopenia and muscle functions at various stages of Alzheimer disease," *Frontiers in Neurology*, vol. 9, p. 710, 2018.
- [8] F. J. García-Alonso, M. de Lucas Gallego, D. Bonillo Cambrodón et al., "Gallstone-related disease in the elderly: is there room for improvement?," *Digestive Diseases and Sciences*, vol. 60, no. 6, pp. 1770–1777, 2015.
- [9] L. A. Zilliox, K. Chadrsekaran, J. Y. Kwan, and J. W. Russell, "Diabetes and cognitive impairment," *Current Diabetes Reports*, vol. 16, no. 9, p. 87, 2016.
- [10] M. H. Cho, D. W. Shin, S.-A. Chang et al., "Association between cognitive impairment and poor antihypertensive medication adherence in elderly hypertensive patients without dementia," *Scientific Reports*, vol. 8, no. 1, article 11688, 2018.
- [11] K. L. Campbell, J. W. Y. Kam, S. E. Neil-Sztramko et al., "Effect of aerobic exercise on cancer-associated cognitive impairment: a proof-of-concept RCT," *Psycho-Oncology*, vol. 27, no. 1, pp. 53–60, 2018.
- [12] A. Andreev, B. Erdinc, K. Shivaraj et al., "The association between anemia of chronic inflammation and Alzheimer's disease and related dementias," *Journal of Alzheimer's Disease Reports*, vol. 4, no. 1, pp. 379–391, 2020.
- [13] K. Han, K. Song, and B. W. Choi, "How to develop, validate, and compare clinical prediction models involving radiological parameters: study design and statistical methods," *Korean Journal of Radiology*, vol. 17, no. 3, pp. 339–350, 2016.
- [14] S. W. Grant, G. S. Collins, and S. A. M. Nashef, "Statistical primer: developing and validating a risk prediction model," *European Journal of Cardio-Thoracic Surgery*, vol. 54, no. 2, pp. 203–208, 2018.
- [15] C. P. Hughes, L. Berg, W. L. Danziger, L. A. Coben, and R. L. Martin, "A new clinical scale for the staging of dementia," *The British Journal of Psychiatry*, vol. 140, no. 6, pp. 566–572, 1982.
- [16] M. Sugishita, Y. Koshizuka, S. Sudou et al., "The validity and reliability of the Japanese version of the Mini-Mental State Examination (MMSE-J) with the original procedure of the Attention and Calculation Task (2001)," *Japanese Journal of Cognitive Neuroscience*, vol. 20, pp. 91–110, 2018.
- [17] L.-K. Chen, J. Woo, P. Assantachai et al., "Asian working group for sarcopenia: 2019 consensus update on sarcopenia diagnosis and treatment," *Journal of the American Medical Directors Association*, vol. 21, no. 3, pp. 300–307.e2, 2020.
- [18] J. Hugo and M. Ganguli, "Dementia and cognitive impairment: epidemiology, diagnosis, and treatment," *Clinics in Geriatric Medicine*, vol. 30, no. 3, pp. 421–442, 2014.
- [19] M. Hamilton, "Development of a rating scale for primary depressive illness," *The British Journal of Social and Clinical Psychology*, vol. 6, no. 4, pp. 278–296, 1967.
- [20] E. Frank, R. F. Prien, R. B. Jarrett et al., "Conceptualization and rationale for consensus definitions of terms in major depressive disorder. Remission, recovery, relapse, and recurrence," *Archives of General Psychiatry*, vol. 48, no. 9, pp. 851–855, 1991.
- [21] D. J. Buysse, C. F. Reynolds, T. H. Monk, S. R. Berman, and D. J. Kupfer, "The Pittsburgh sleep quality index: a new instrument for psychiatric practice and research," *Psychiatry Research*, vol. 28, no. 2, pp. 193–213, 1989.
- [22] T. Mollayeva, P. Thurairajah, K. Burton, S. Mollayeva, C. M. Shapiro, and A. Colantonio, "The Pittsburgh sleep quality index as a screening tool for sleep dysfunction in clinical and non-clinical samples: a systematic review and meta-analysis," *Sleep Medicine Reviews*, vol. 25, pp. 52–73, 2016.
- [23] A.-W. Pan, L. Chung, B. L. Fife, and P.-C. Hsiung, "Evaluation of the psychometrics of the social impact scale: a measure of stigmatization," *International Journal of Rehabilitation Research*, vol. 30, no. 3, pp. 235–238, 2007.
- [24] J. M. Giesinger, J. M. Kieffer, P. M. Fayers et al., "Replication and validation of higher order models demonstrated that a summary score for the EORTC QLQ-C30 is robust," *Journal of Clinical Epidemiology*, vol. 69, pp. 79–88, 2016.
- [25] O. Husson, B. H. de Rooij, J. Kieffer et al., "The EORTC QLQ-C30 summary score as prognostic factor for survival of patients with cancer in the "real-world": results from the population-based PROFILES registry," *The Oncologist*, vol. 25, no. 4, pp. e722–e732, 2020.
- [26] L. Blanchet, R. Vitale, R. van Vorstenbosch et al., "Constructing bi-plots for random forest: tutorial," *Analytica Chimica Acta*, vol. 1131, pp. 146–155, 2020.
- [27] M.-L. Huang, Y.-H. Hung, W. M. Lee, R. K. Li, and B.-R. Jiang, "SVM-RFE based feature selection and Taguchi parameters optimization for multiclass SVM classifier," *ScientificWorldJournal*, vol. 2014, article 795624, 10 pages, 2014.
- [28] R. Tibshirani, "Regression shrinkage and selection via the Lasso," *Journal of the Royal Statistical Society: Series B (Methodological)*, vol. 58, no. 1, pp. 267–288, 1996.
- [29] E. W. Steyerberg and Y. Vergouwe, "Towards better clinical prediction models: seven steps for development and an ABCD for validation," *European Heart Journal*, vol. 35, no. 29, pp. 1925–1931, 2014.

## *Retraction*

# **Retracted: Facial Nerve Monitoring under Different Levels of Neuromuscular Blockade with Cisatracurium Besilate in Parotid Tumour Surgery**

### **BioMed Research International**

Received 12 March 2024; Accepted 12 March 2024; Published 20 March 2024

Copyright © 2024 BioMed Research International. This is an open access article distributed under the Creative Commons Attribution License, which permits unrestricted use, distribution, and reproduction in any medium, provided the original work is properly cited.

This article has been retracted by Hindawi following an investigation undertaken by the publisher [1]. This investigation has uncovered evidence of one or more of the following indicators of systematic manipulation of the publication process:

- (1) Discrepancies in scope
- (2) Discrepancies in the description of the research reported
- (3) Discrepancies between the availability of data and the research described
- (4) Inappropriate citations
- (5) Incoherent, meaningless and/or irrelevant content included in the article
- (6) Manipulated or compromised peer review

The presence of these indicators undermines our confidence in the integrity of the article's content and we cannot, therefore, vouch for its reliability. Please note that this notice is intended solely to alert readers that the content of this article is unreliable. We have not investigated whether authors were aware of or involved in the systematic manipulation of the publication process.

Wiley and Hindawi regrets that the usual quality checks did not identify these issues before publication and have since put additional measures in place to safeguard research integrity.

We wish to credit our own Research Integrity and Research Publishing teams and anonymous and named external researchers and research integrity experts for contributing to this investigation.

The corresponding author, as the representative of all authors, has been given the opportunity to register their agreement or disagreement to this retraction. We have kept a record of any response received.

### **References**

- [1] H. Huang, H. Jiang, J. Liu et al., "Facial Nerve Monitoring under Different Levels of Neuromuscular Blockade with Cisatracurium Besilate in Parotid Tumour Surgery," *BioMed Research International*, vol. 2021, Article ID 5655061, 11 pages, 2021.

## Research Article

# Facial Nerve Monitoring under Different Levels of Neuromuscular Blockade with Cisatracurium Besilate in Parotid Tumour Surgery

Huimin Huang, Hong Jiang , Jinxing Liu, Jie Chen , Lin Qiu, Jiayi Wang, Wenhui Liu, and Huan Chen

Department of Anesthesiology, Shanghai 9th People's Hospital, Shanghai Jiao Tong University School of Medicine, Shanghai, China

Correspondence should be addressed to Hong Jiang; [drjianghongji@163.com](mailto:drjianghongji@163.com) and Jie Chen; [jenney\\_chen0806@163.com](mailto:jenney_chen0806@163.com)

Received 1 May 2021; Revised 13 June 2021; Accepted 23 June 2021; Published 13 July 2021

Academic Editor: Yuzhen Xu

Copyright © 2021 Huimin Huang et al. This is an open access article distributed under the Creative Commons Attribution License, which permits unrestricted use, distribution, and reproduction in any medium, provided the original work is properly cited.

**Background.** Anaesthesia can alter neuronal excitability and vascular reactivity and ultimately lead to neurovascular coupling. Precise control of the skeletal muscle relaxant doses is the key in reducing anaesthetic damage. **Methods.** A total of 102 patients with the normal functioning preoperative facial nerve who required parotid tumour resection were included in this study. Facial nerve monitoring was conducted intraoperatively. The surgeon stimulated the facial nerve at different myorelaxation intervals at TOF% (T4/T1) and T1% (T1/T0) and recorded the responses and the amplitude of electromyogram (EMG). Body movements (BM) or patient-ventilator asynchrony (PVA) was recorded intraoperatively. **Results.** In parotid tumour resection, T1% should be maintained at a range of 30 to 60% while TOF% should be maintained at a range of 20 to 30%. Analysis of the decision tree model for facial nerve monitoring suggests a partial muscle relaxation level of  $30% < T1% \leq 50%$  and  $TOF \leq 60%$ . A nomogram prediction model, while incorporating factors such as sex, age, BMI, TOF%, and T1%, was constructed to predict the risk of BM/PVA during surgery, showing good predictive performance. **Conclusions.** This study revealed an adequate level of neuromuscular blockade in intraoperative parotid tumour resection while conducting facial nerve monitoring. A visual nomogram prediction model was constructed to guide anaesthetists in improving the anaesthetic plan.

## 1. Introduction

Anaesthesia can alter neuronal excitability and vascular reactivity and ultimately lead to neurovascular coupling [1]. Skeletal muscle relaxants are widely used in anaesthesia. However, numerous studies have linked skeletal muscle relaxants to neurovascular side effects [2, 3]. Therefore, precise control of the skeletal muscle relaxants dose is the key in reducing anaesthetic damage [4].

Facial nerve injury is a relatively common and major complication of parotidectomy that is disheartening to surgeons and the patients. Intraoperative facial nerve monitoring can significantly reduce postoperative facial nerve injury [5–8]. It is traditionally held that skeletal muscle relaxants should be avoided in general anaesthetic procedures requiring neuromonitoring. However, general anaesthesia without the use of skeletal muscle relaxants may aggravate anaesthetic damage and lead to intraoperative BM and PVA, affecting the surgical process [9]. To avoid BM/PVA, anaesthetists often

need to increase the dose of intraoperative analgesics and sedative drugs. However, this may increase the risk of anaesthesia-related complications such as neurovascular injury, intraoperative circulatory depression, and delayed postoperative awakening.

In this study, nondepolarizing skeletal muscle relaxant, Cisatracurium besilate, was used in total intravenous anaesthesia during parotid tumour resection requiring facial nerve monitoring. The study is aimed at determining the appropriate level of muscular relaxation and providing a reference for general anaesthetic procedures requiring facial nerve monitoring by exploring the feasibility of facial nerve monitoring under partial muscular relaxation.

## 2. Materials and Methods

**2.1. Basic Characteristics.** This was a prospective study done between 2019 and 2020 at the Ninth People's Hospital. The study was approved by the Ethics Committee of the Clinical

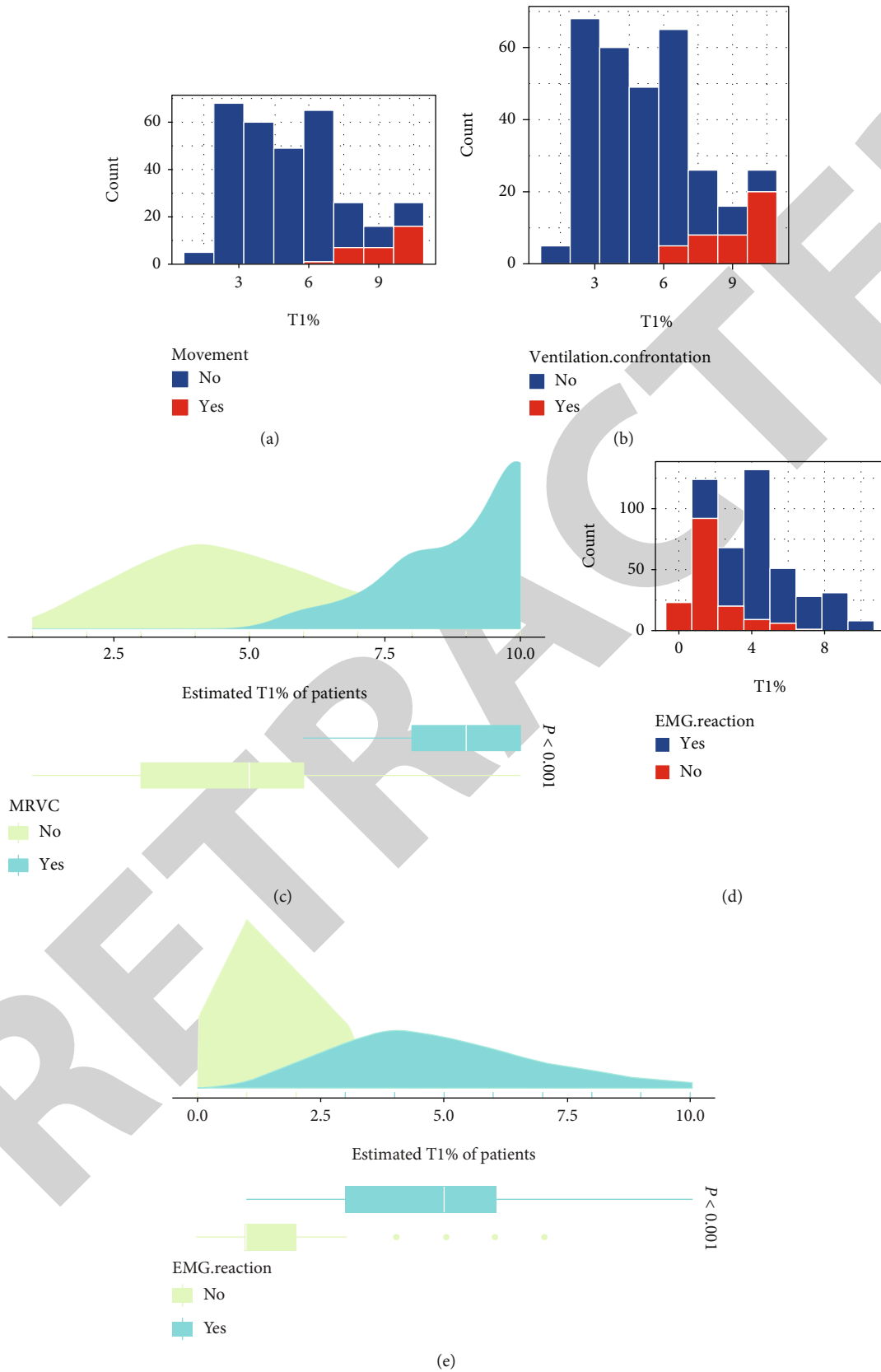


FIGURE 1: Relationship between T1% and the degree of muscle relaxation with skeletal muscle relaxants in facial nerve monitoring: (a) T1% and body movement score relationship; (b) T1% and patient-ventilator asynchrony relationship; (c) estimated T1% with/without BM/PVA; (d) T1% and positive facial nerve EMG reaction relationship; (e) comparison of estimated T1% between positive EMG reaction and negative EMG reaction.

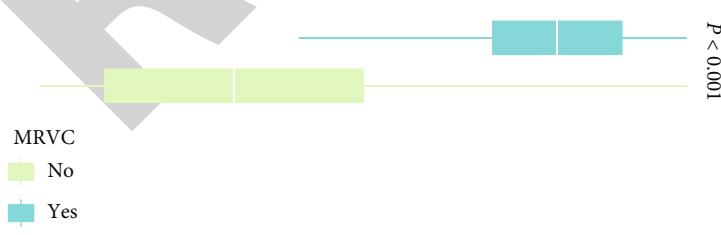
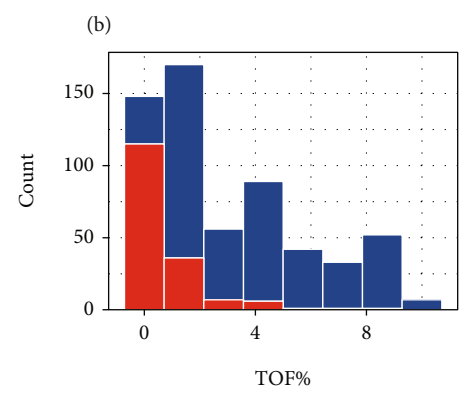
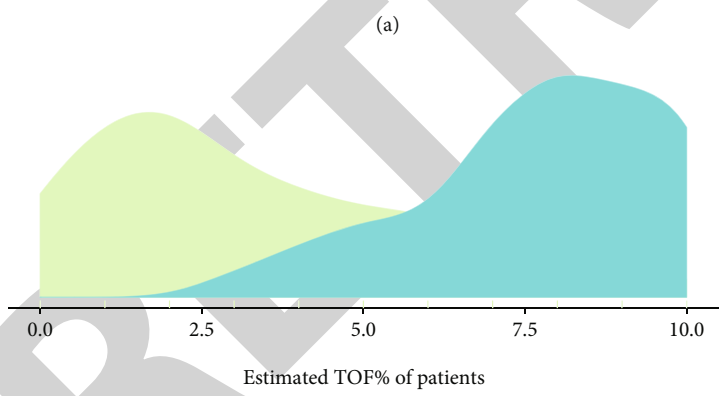
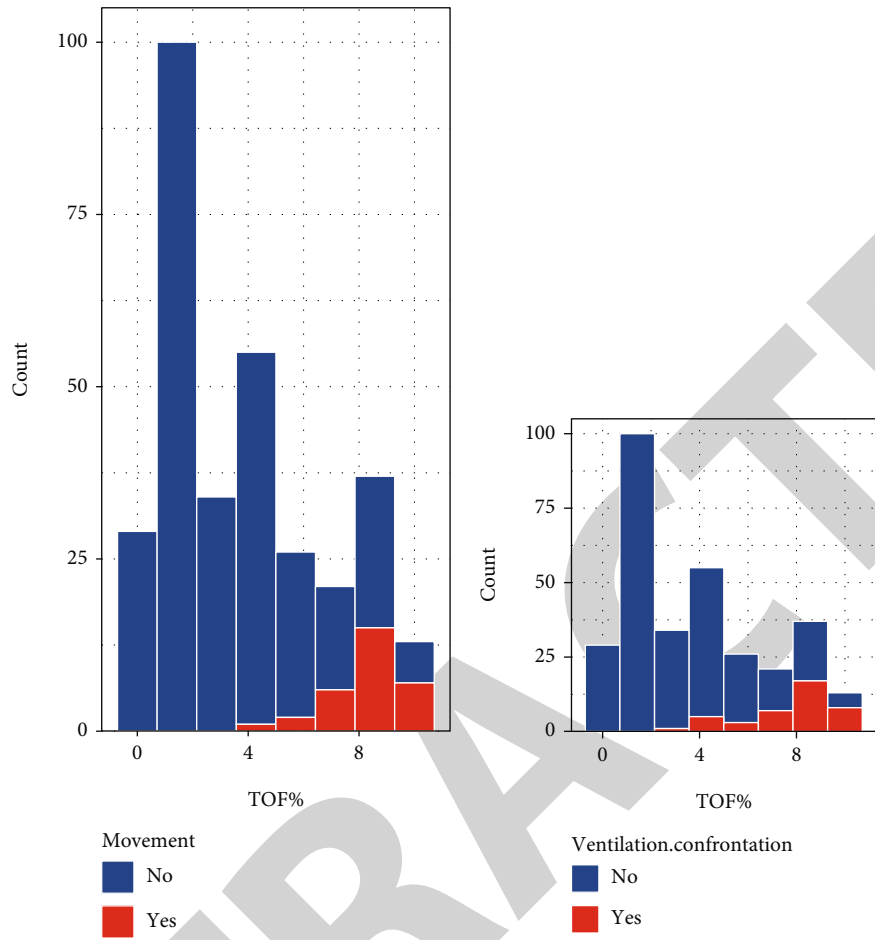


FIGURE 2: Continued.



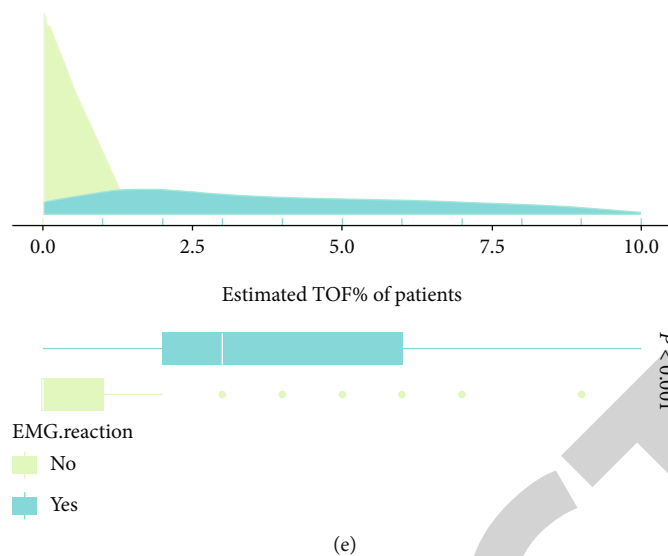


FIGURE 2: Relationship between TOF% and the cut-off value for the effect of facial nerve anaesthesia for muscle relaxation: (a) the relationship between TOF% and body movement score; (b) the relationship between TOF% and patient-ventilator asynchrony; (c) comparison of estimated TOF% with/without BM/PVA; (d) the relationship between TOF% and positive EMG reaction of the facial nerve; (e) comparison of estimated TOF% between positive EMG reaction and negative EMG reaction.

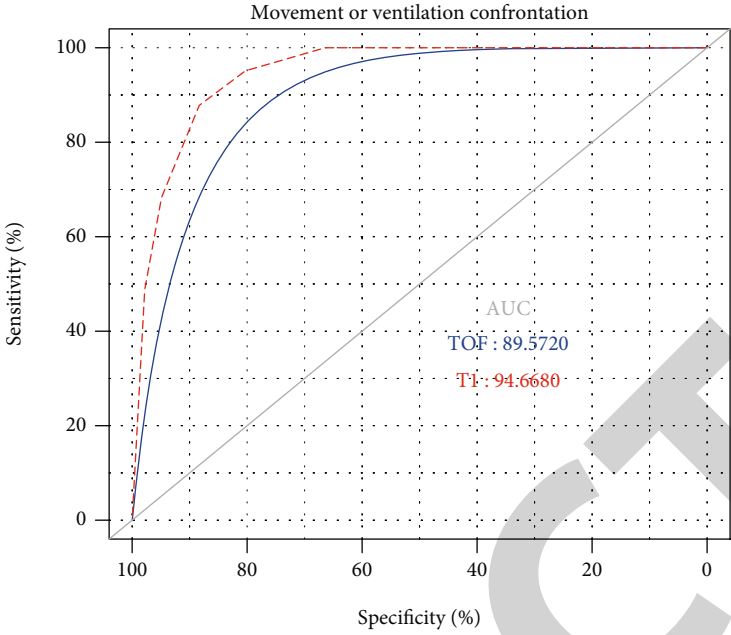
Trial Center of the Ninth People's Hospital of Shanghai Jiao Tong University (Ethics No. 2017-405-T302). Patients requiring parotid tumour resection who were classified under American Society of Anesthesiologists (ASA) grade I to II ( $n = 102$ ) were selected for the inclusion to the study. Exclusion criteria are comprised of patients with Cisatracurium besilate allergy, facial palsy, or other neuromuscular diseases, history of diabetes mellitus, epilepsy, and craniotomy that may affect neuromonitoring. Anaesthesia was intravenously administered, with routine ECG monitoring, bispectral index (BIS) monitoring for the depth of anaesthesia, facial nerve EMG, and muscle relaxation monitoring (TOF%, T1%) carried out. Cisatracurium besilate was used intermittently during the operation. The surgeon recorded the facial nerve EMG at different levels of myorelaxation while stimulating the facial nerve or adjacent tissues to the operative area during the excision of the parotid tumour. BM and PVA were also recorded intraoperatively.

**2.2. General Anaesthesia and Muscle Relaxation Monitoring.** Patients admitted to the operating room underwent routine cardiac monitoring and received preoperative medication 30 min before the surgery. Before induction of the general anaesthesia, the Veriark-TOF muscle relaxation monitor (Willie's Ark, China) was connected to the ulnar nerve on the left upper forearm. The muscle tone sensor was placed at the tiger's mouth of the hand while the temperature sensor was placed at the inner thumb muscle and secured with an adhesive tape. The muscle relaxation monitoring was set up in the train-of-four stimulation (TOF) mode with one-minute repetitive stimulation time, and the TOF% (T4/T1) and T1% (T1/T0) values were recorded. In the induction of general anaesthesia, patients were sedated by intravenous administration of midazolam 0.05 mg/kg, fentanyl 2  $\mu$ g/kg, and propofol 2 mg/kg. T0 value and the appropriate stimula-

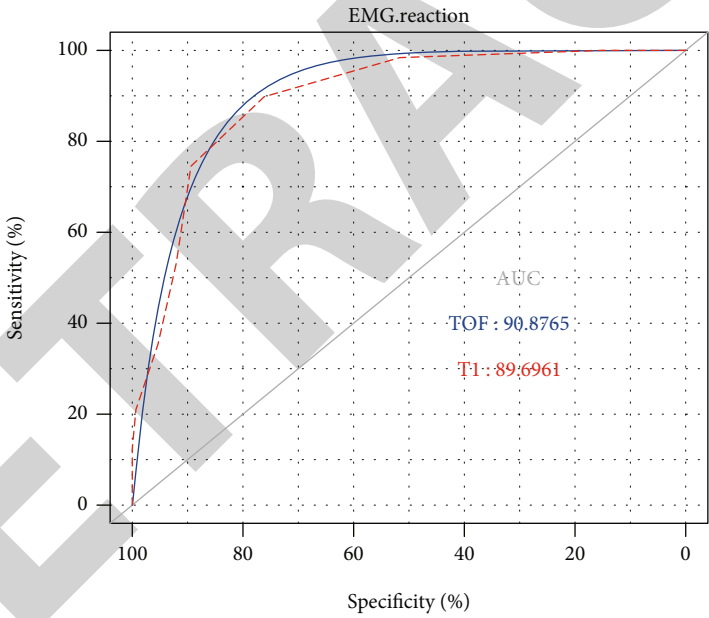
tion current were determined. Cisatracurium besilate 0.15 mg/kg ( $3 \times$  ED95) was then administered intravenously, and the tracheal tube was inserted. The BIS electrodes were connected to monitor the depth of anaesthesia. For the maintenance of general anaesthesia, continuous propofol 2-10 mg/(kg·h) and remifentanyl 0.1-2  $\mu$ g/(kg·min) were administered with real-time regulation to maintain intraoperative vital signs, BIS between 40 and 60, and End-Tidal Carbon Dioxide (ETCO<sub>2</sub>) between 35 and 45. Single additional doses of Cisatracurium besilate 0.025 mg/kg ( $0.5 \times$  ED95) were also given intraoperatively to maintain partial muscle relaxation in the following cases: (a) patients developed BM/PVA, (b) intraoperative electrokinetic stimulation of the patient's muscle twitching was too pronounced to interfere with the procedure, and (c) patients' TOF% or T1% was >91%.

**2.3. Facial Nerve Monitoring.** A Medtronic NIM-Neuro 3.0 neuromonitor (Medtronic Xomed, Inc., USA) was used to record the facial nerve EMG upon induction of general anaesthesia. Stimulating electrodes were inserted into the frontalis, orbicularis oculi, orbicularis orientalis, and chin muscles, while the grounding electrodes were inserted to the thorax and then connected to the mainframe of the facial nerve monitor. The facial nerve or adjacent tissues were stimulated with bipolar electrodes. To ensure accuracy of the facial nerve stimulation, the main trunk of the facial nerve or main branches, the mandibular margin branch and the temporal branch, was selected. Stimulation intensity was 0.20 mA, and the event threshold was 100  $\mu$ V. Facial nerve stimulation was considered positive at an EMG wave amplitude > 100  $\mu$ V and an abrupt rise in EMG changes.

**2.4. Observation Parameters.** Patients' facial nerve EMG responses and specific wave amplitude values were recorded at different muscle relaxation intervals. The TOF% (T4/T1)



(a)



(b)

FIGURE 3: Continued.

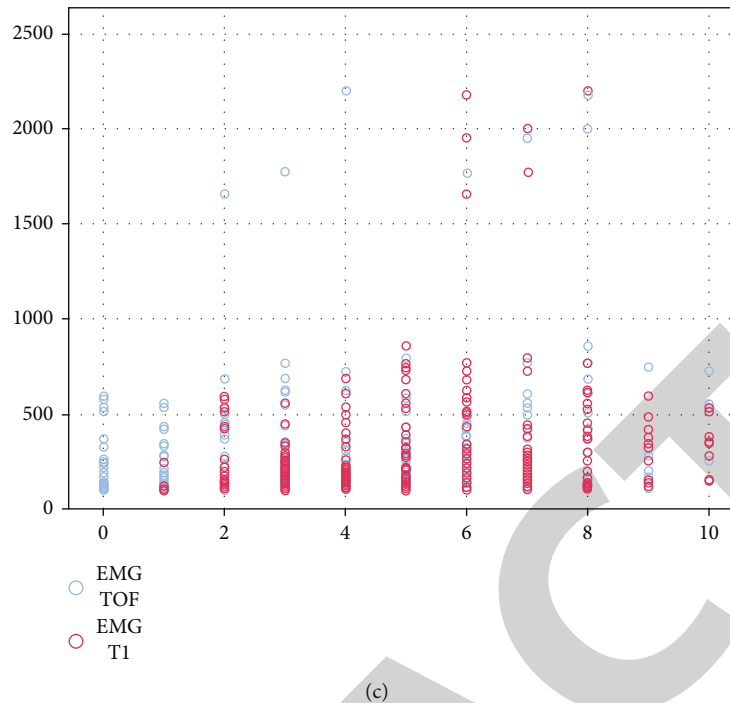


FIGURE 3: ROC curves of TOF% and T1% for predicting the effect of facial nerve anaesthesia on muscle relaxation: (a) ROC curve of TOF% and T1% for body movement or patient-ventilator asynchrony; (b) ROC curve of TOF% and T1% for body movement or positive EMG reaction of the facial nerve; (c) correlation of EMG values with TOF% and T1%.

and T1% (T1/T0) were divided into eleven different muscle relaxation intervals, such as 0%, 1-10%, 11-20%, 21-30%, 31-40%, 41-50%, 51-60%, 61-70%, 71-80%, 81-90%, and 91-100%. Patients were continuously monitored for muscle relaxation. The facial nerve was stimulated intraoperatively at different intervals of TOF% and T1%, and the response to facial nerve monitoring was recorded and the wave amplitude of the EMG was recorded when there was a positive reaction. Patients were continuously observed for limb and swallowing movements, under different levels of muscle relaxation. The BM score was calculated by dividing stimulus with BM by stimulus without BM. The presence of autonomic respiratory waveform on the monitor and anaesthetic machine was recorded under different levels of muscle relaxation.

**2.5. Statistical Analysis.** Statistical analyses were done using R software (version 3.6.0). Visualization of the decision tree was done with the treehearer package, as described in a previous study [10]. The receiver operating characteristic curve (ROC) was used to assess the predictive accuracy of T1% and TOF% [11]. Nomogram was used to construct predictive models to assess the risk of BM/PVA. The calibration curve and C-index were further used to assess the predictive power of the nomogram [12, 13]. One-way ANOVA or two-tailed *t*-test was used to determine significance between groups. Values of  $P < 0.05$  were considered statistically significant.

### 3. Results

**3.1. Demographic and Clinical Characteristics.** A total of 102 patients (48 males and 54 females) undergoing parotid mass

resection were included in this study. All patients included in the study were in ASA classification grade I to II. Patients had a mean age of  $44.49 \pm 13.02$  years, weight of  $65.54 \pm 13.51$  kg, and height of  $167.21 \pm 8.62$  cm.

**3.2. T1% Relationship to the Optimal Dose of the Neuromuscular Relaxant.** A histogram of BM/PVA and T1% is shown in Figures 1(a) and 1(b). The chi-square test revealed a significant correlation between T1% and BM/PVA ( $P < 0.001$ ) (Figure 1(c)). Patients experienced significantly elevated BM/PVA at  $T1\% \geq 60\%$ . The correlation between different intraoperative muscle relaxation conditions (T1%) and positive EMG reaction of the facial nerve was shown to be significant using chi-square analysis ( $P < 0.001$ ) (Figures 1(d) and 1(e)). As shown in Figure 1(d), EMG monitoring of the facial nerve was largely unaffected at  $T1\% > 30\%$  when the muscle relaxation was maintained with Cisatracurium besilate in TIVA. This suggests that T1% should be controlled at a range of between 30 and 60% in parotidectomy.

**3.3. TOF% Relationship to Neuromuscular Blockade Levels in Facial Nerve Monitoring.** A histogram of BM/PVA and TOF% is shown in Figures 2(a) and 2(b). The relationship between different intraoperative muscle relaxation levels (TOF%) and the occurrence of BM/PVA was calculated using the chi-square test, which revealed a significant correlation ( $P < 0.001$ ) (Figure 2(c)). Patients were shown to experience significantly elevated BM/PVA when  $TOF\% \geq 30\%$ . The correlation between different intraoperative muscle relaxation levels (TOF%) and positive EMG reaction of the facial nerve using chi-square analysis was shown to be significant ( $P < 0.001$ ) (Figures 2(d) and 2(e)). As seen in

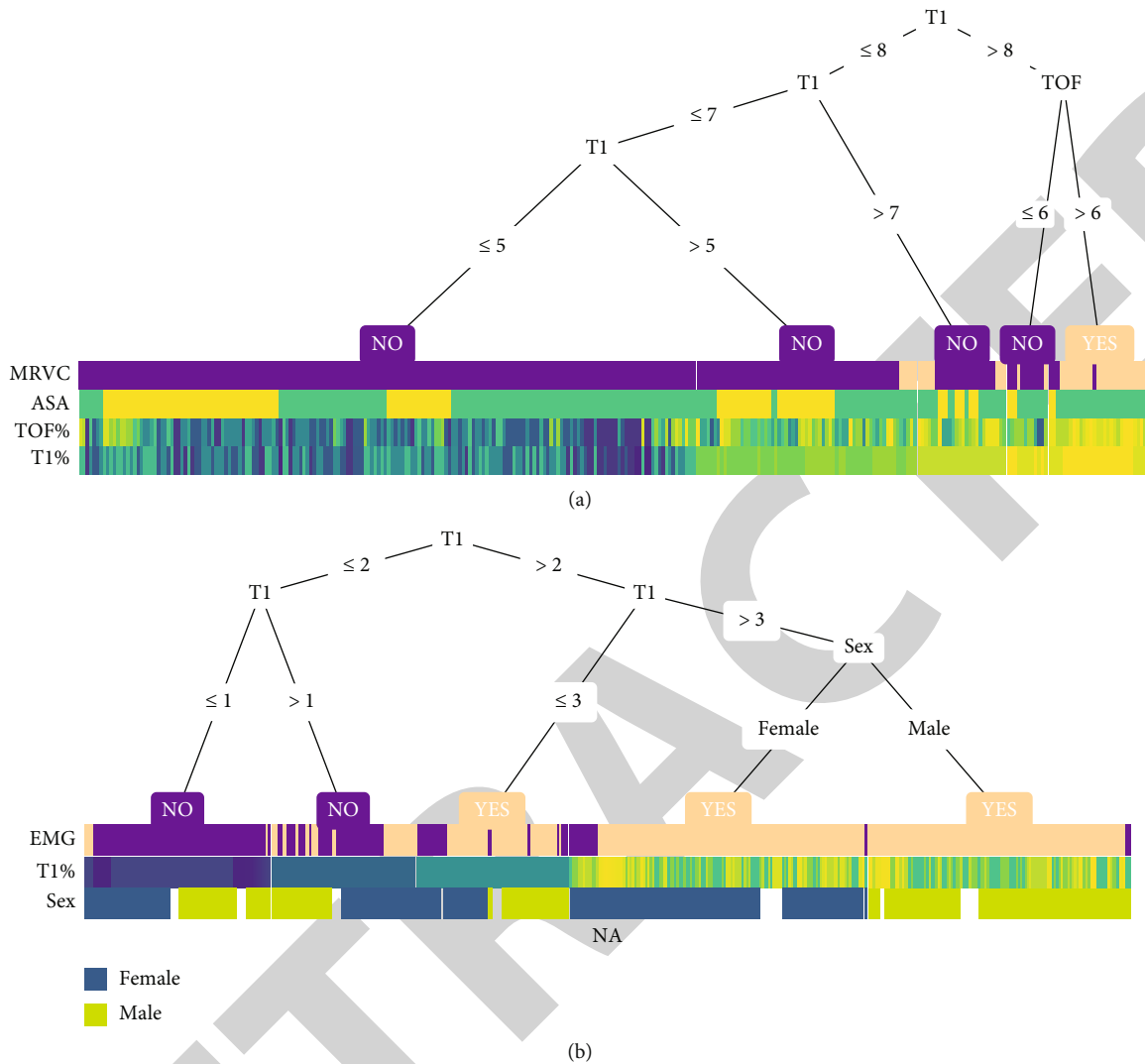


FIGURE 4: Visualization of the decision tree. (a) A decision tree-heat map for predicting the occurrence of BM or PVA during surgery. MRVC: movement or ventilation confrontation has occurred; ASA: American Society of Anesthesiologists. (b) A decision tree-heat map for predicting a positive EMG response of the facial nerve during surgery. EMG: electromyogram. Note: the heat map colours present the relative value of a sample compared to the rest of the group.

Figure 2(d), EMG monitoring of the facial nerve was largely unaffected at  $TOF\% > 20\%$  when muscle relaxation was maintained with Cisatracurium besilate in TIVA. This suggests that  $TOF\%$  should be controlled at a range of 20 to 30% in parotidectomy.

**3.4. ROC Curves of  $TOF\%$  and  $T1\%$  for Predicting the Effect of Facial Nerve Anaesthesia on Muscle Relaxation.** As shown in Figure 3(a), the ROC curve had an AUC of 0.896 for  $TOF\%$  and 0.947 for  $T1\%$ , both close to 1. It can be concluded that the different intervals of  $TOF\%$  and  $T1\%$  values are ideal for determining the presence of BM/PVA, with  $T1\%$  being relatively better than  $TOF\%$ . Figure 3(b) shows a ROC curve plotted against the facial nerve EMG showing an AUC of 0.909 for  $TOF\%$  and 0.897 for  $T1\%$ , which were also close to 1. It can be concluded that the different intervals of  $TOF\%$  and  $T1\%$  values are ideal for determining effectiveness

of facial nerve monitoring. It is worth noting that the magnitude of facial nerve EMG values did not correlate linearly with  $TOF\%$  and  $T1\%$ . EMG amplitude values in most patients were below  $1000 \mu V$  and did not increase as the muscle relaxation lessened (Figure 3(c)).

**3.5. Visualization of the Decision Tree.** Decision trees were drawn to guide visualization for better clinical application. As shown in Figure 4(a), the decision tree-heat map for predicting BM/PVA occurrence during surgery reflects that  $T1\% \leq 50\%$  does not result in BM/PVA, while  $TOF\% > 60\%$  is a high-risk factor for BM/PVA occurrence. Therefore, in parotidectomy,  $T1\%$  should be maintained  $\leq 50\%$  and  $TOF \leq 60\%$ . As shown in Figure 4(b), a decision tree-heat map for predicting the incidence of a positive EMG response of the facial nerve during surgery revealed a good positive EMG reaction of the facial nerve at  $T1\% > 30\%$ . Women were seen

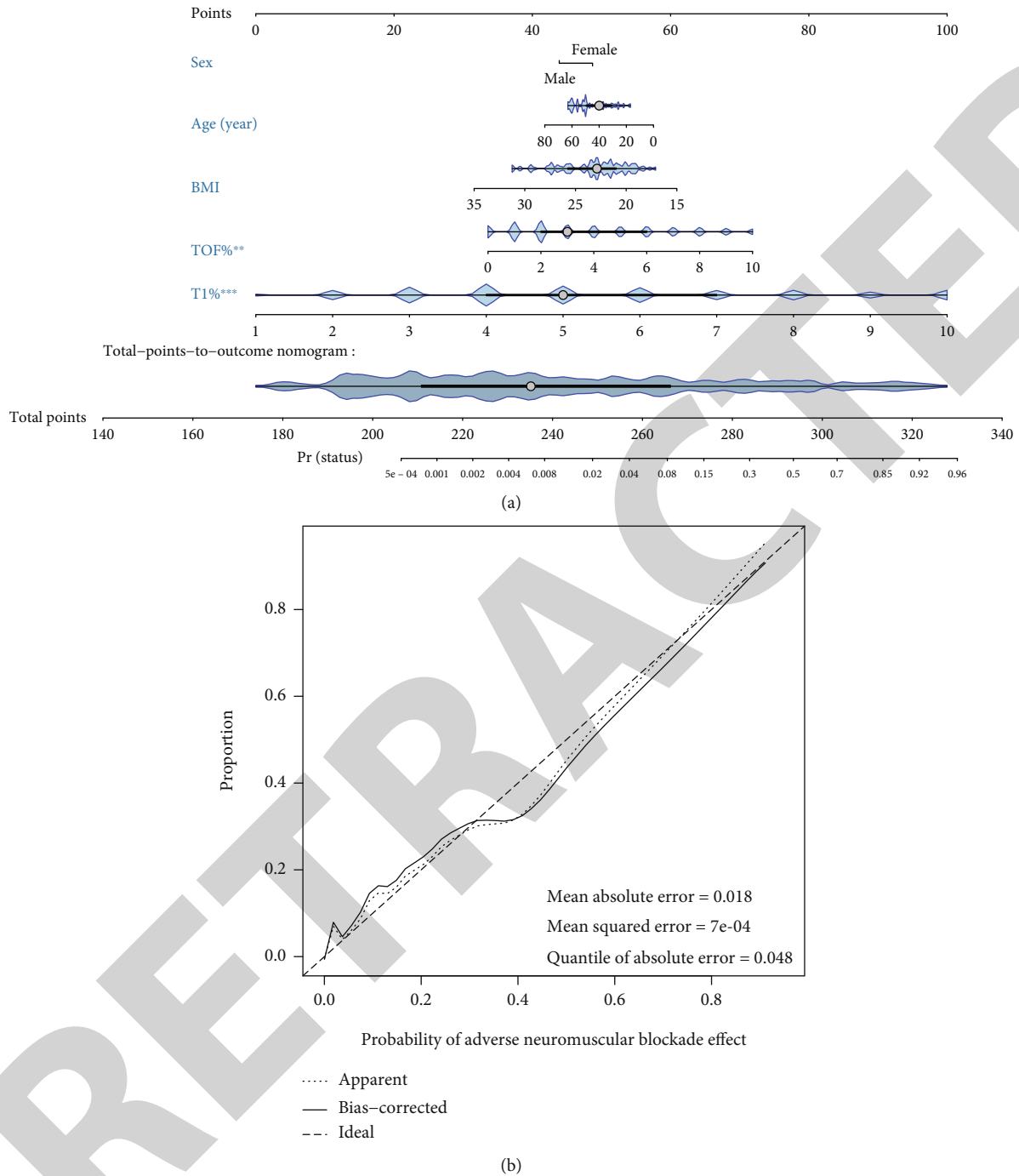


FIGURE 5: A visual nomogram prediction model. (a) Nomogram prediction model for predicting the occurrence of BM or PVA during surgery. (b) Calibration curve of the BM/PVA model for predicting the occurrence of BM/PVA during surgery. The closer the solid line to the dashed line, the better the predictive power.

to be less likely to have a negative EMG reaction of the facial nerve compared to men. In conclusion,  $30% < T1\% \leq 50%$  and  $TOF \leq 60%$  should be maintained.

**3.6. A Visual Nomogram Prediction Model.** In clinical practice, the final anaesthetic outcome may be influenced by several factors. Therefore, a visual nomogram prediction model was constructed to predict the likelihood of patients developing BM/PVA during surgery, while incorporating factors

such as sex, age, BMI, TOF%, and T1% (Figure 5(a)). The specific parameters of the visual nomogram prediction model are shown in Table 1. The overall prediction performance of the prediction model was good as the solid line was very close to the dashed line in the calibration curve (Figure 5(b)). The C-index was 0.959 (95% CI, 0.935-0.982, entire cohort) (Table 2). The model also had a good internal validation. This model shows that a low BMI, young age, and female gender were more likely to be associated with BM/PVA

TABLE 1: Chart showing the prediction factors.

Variable	Prediction model		P value
	$\beta$	Odds ratio (95% CI)	
Intercept	0.034	0.001 (0-0.119)	0.007
TOF%	-0.059	1.396 (1.123-1.768)	0.004
T1%	-0.678	2.633 (1.909-3.888)	$P < 0.001$
Sex (male)	2.189	0.657 (0.203-2.053)	0.472
Age (years)	-2.003	0.983 (0.944-1.022)	0.391
BMI	-0.001	0.88 (0.723-1.048)	0.172

Note:  $\beta$  is the regression coefficient.

TABLE 2: C-index of the nomogram prediction model.

Features	C-index (95% confidence interval)
Entire cohort	0.959 (0.935-0.982)
Train set	0.977 (0.957-0.997)
Validation set	0.905 (0.84-0.97)

during surgery, and patients should be anaesthetized at an increased depth.

#### 4. Discussion

In this study, we explored the optimal cut-off value for neurovascular anaesthesia on muscle relaxation in local surgery involving parotid tumour resection. Appropriate level of muscle relaxation should be maintained in parotidectomy with facial nerve monitoring. TOF% and T1% are useful markers of the degree of muscle relaxation during facial nerve monitoring. We recommend a partial muscle relaxation level of  $30\% < T1\% \leq 50\%$  and  $TOF \leq 60\%$  for facial nerve monitoring, and the operator should be aware of the presence of a negative EMG reaction of the facial nerve when dealing with female patients. Construction of a visual nomogram prediction model was done to guide anaesthetists in the anaesthetic plan.

Due to the proximity of the anatomical structures to the facial nerve, the use of facial nerve monitoring can significantly reduce the incidence of postoperative facial nerve injury in a large number of craniomaxillofacial surgical operations including auditory neuroma at the base of the skull, middle ear, and parotid area surgery [5–8, 14, 15]. Facial nerve monitoring tools have resulted in increased use of facial nerve monitoring thus avoiding or reducing the chances of facial paralysis in patients undergoing surgery. The use of skeletal muscle relaxants in general anaesthesia may affect EMG or contraction of the facial muscles by reducing the transmission of electrical signals from the neuromuscular junction thus affecting facial nerve monitoring. For this reason, surgeons recommend that skeletal muscle relaxants be avoided during general anaesthetic procedures requiring facial nerve monitoring. However, avoiding use of skeletal muscle relaxants in general anaesthesia requires anesthesiologists to increase the dose of intraoperative analgesics and sedative drugs so as to avoid BM and PVA. This increases the risk of intraoperative circulatory depression,

delayed postoperative awakening, hypothermia, and other anaesthetic complications. The use of a higher dose of the analgesic, remifentanyl, under general anaesthesia was shown to decrease the incidence of intraoperative BM from 44 to 20%. However, the highest dose of remifentanyl (0.21 mg/kg.min) did not completely prevent BM and was associated with increased intraoperative hypotension and bradycardia and circulatory depression [16]. Maintaining partial muscle relaxation in general anaesthesia has been shown to be a more effective strategy. In recent years, skeletal muscle relaxants have been used during general anaesthesia in a variety of procedures requiring neuromonitoring to induce a partially muscle relaxed state [17–21].

In this study, the nondepolarizing skeletal muscular relaxant, Cisatracurium besilate, was used. The study revealed that facial nerve monitoring could be effectively performed under partial muscle relaxation. The suitable range of partial muscle relaxation was determined as TOF% between 20 and 30% or T1% between 30 and 50%. Noteworthy, the TOF% value is considered a classical indicator of the degree of muscle relaxation. In this study, a positive EMG reaction in facial nerve monitoring was seen in some patients in muscle relaxation recovery with a TOF% of 0 and a partial recovery at T1%. There was no reaction to facial nerve stimulation in all patients when T1% was 0. T1% was more sensitive in facial nerve monitoring during the initial phase of myosin recovery which is consistent with the findings of Chung et al. Chung et al. recommended using T1% as the control target in determining the required degree of partial muscle relaxation when monitoring facial muscle lateral spread response (LSR) during microvascular decompression as opposed to using TOF% [21]. Additionally, surgeons are often interested in the amplitude of the facial nerve EMG when isolating the facial nerve. The present study shows that the amplitude of the facial nerve EMG does not increase linearly as the muscle relaxation is restored. The EMG response values may be more relevant to individual differences than the degree of muscle relaxation recovery.

There are several other factors that affect facial nerve monitoring. Firstly, the use of inhalation drugs in general anaesthesia may inhibit neuromuscular function and have synergistic effects with skeletal muscle relaxants, thus affecting recovery [22, 23]. To control this, general anaesthesia was maintained under TIVA. The correlation between maintenance and recovery time from muscle relaxation and facial nerve monitoring needs to be confirmed by further clinical studies. Secondly, there has been opposition to carry out facial nerve monitoring during parotid surgery, due to false-positive and false-negative results occasioned by unfamiliarity with facial nerve anatomy, mechanical failure, and anaesthetic drugs [5, 24–26]. When using a facial nerve monitor during parotidectomy and stimulating the facial nerve with a bipolar electroacupuncture needle, if the anatomy of the stimulated facial nerve branch is abnormal, the muscle into which the electrode is inserted is not within the innervation of the stimulated nerve, resulting in a false-negative result. In this study, the surgeon chose to stimulate mainly the main trunk of the facial nerve or its main branches, the mandibular marginal branch and the temporal branch, to



avoid false negatives. Patients with superficial location of the tumour with the inaccessible target nerve or with excessive intraoperative bleeding were excluded from the study.

This study had some limitations. (1) Due to the limited number of parotid tumour cases, the line graphs could not be externally validated, and thus, another study with a large sample size is required. (2) The study population was all Asian, and thus, the study findings may not be generalizable to other populations. (3) Construction of the predictive models needs to be enriched further. In future studies, we need to collect more data and further refine the multicentre study to construct more accurate predictive models.

## 5. Conclusion

In summary, we explored the optimal cut-off value for the effect of neurovascular anaesthesia on muscle relaxation in local parotid tumour surgery with facial nerve monitoring. TOF% and T1% are good indicators of the degree of muscle relaxation during facial nerve monitoring, with T1% being more sensitive compared to TOF%. We recommend a partial muscle relaxation level of  $30\% < T1\% \leq 50\%$  and  $TOF \leq 60\%$  for facial nerve monitoring, and the operator should be aware of the presence of a negative EMG reaction of the facial nerve when dealing with female patients. A visual nomogram prediction model is also available to provide the anaesthetist with a detailed guide to improve the anaesthetic plan.

## Abbreviations

AUC: Area under the curve  
 ASA: American Society of Anesthesiologists  
 BM: Body movement  
 BIS: Bispectral index  
 EMG: Electromyogram  
 PVA: Patient-ventilator asynchrony  
 ROC: The receiver operating characteristic curve  
 TOF: Train-of-four stimulation  
 TIVA: Total intravenous anaesthesia.

## Data Availability

Raw data are available on request from the corresponding author.

## Conflicts of Interest

The authors declare no conflict of interest.

## Authors' Contributions

Huimin Huang and Jinxing Liu contributed equally to this work.

## Acknowledgments

This project was funded by the Shanghai Science and Technology Commission (project number 16DZ191110B).

## References

- [1] K. Masamoto and I. Kanno, "Anesthesia and the quantitative evaluation of neurovascular coupling," *Journal of Cerebral Blood Flow and Metabolism*, vol. 32, no. 7, pp. 1233–1247, 2012.
- [2] H. J. Schneck and J. Ruprecht, "Central anticholinergic syndrome (CAS) in anesthesia and intensive care," *Acta Anaesthesiologica Belgica*, vol. 40, no. 3, pp. 219–228, 1989.
- [3] A. M. Amin, M. Y. Mohammad, and M. F. Ibrahim, "Comparative study of neuromuscular blocking and hemodynamic effects of rocuronium and cisatracurium under sevoflurane or total intravenous anesthesia," *Middle East Journal of Anaesthesiology*, vol. 20, no. 1, pp. 39–51, 2009.
- [4] B. Plaud, C. Baillard, J. L. Bourgain et al., "Guidelines on muscle relaxants and reversal in anaesthesia," *Anaesth Crit Care Pain Med.*, vol. 39, no. 1, pp. 125–142, 2020.
- [5] E. Savvas, S. Hillmann, D. Weiss, M. Koopmann, C. Rudack, and J. Alberty, "Association between facial nerve monitoring with postoperative facial paralysis in parotidectomy," *JAMA Otolaryngology. Head & Neck Surgery*, vol. 142, no. 9, pp. 828–833, 2016.
- [6] P. Pieńkowski, W. Golusiński, A. Wiertel-Krawczuk, and J. Huber, "Śródoperacyjne monitorowanie czynności nerwu twarzowego w chirurgii ślinianki przyusznej," *Otolaryngologia Polska*, vol. 64, no. 5, pp. 302–306, 2010.
- [7] C. M. Chiesa-Estomba, E. Larruscain-Sarasola, J. R. Lechien et al., "Facial nerve monitoring during parotid gland surgery: a systematic review and meta-analysis," *European Archives of Oto-Rhino-Laryngology*, vol. 278, no. 4, pp. 933–943, 2021.
- [8] C. T. Haring, S. E. Ellsperman, B. M. Edwards et al., "Assessment of intraoperative nerve monitoring parameters associated with facial nerve outcome in parotidectomy for benign disease," *JAMA Otolaryngology. Head & Neck Surgery*, vol. 145, no. 12, pp. 1137–1143, 2019.
- [9] T. B. Sloan, "Muscle relaxant use during intraoperative neurophysiologic monitoring," *Journal of Clinical Monitoring and Computing*, vol. 27, no. 1, pp. 35–46, 2013.
- [10] T. T. Le and J. H. Moore, "treeheat: an R package for interpretable decision tree visualizations," *Bioinformatics*, vol. 37, no. 2, pp. 282–284, 2021.
- [11] F. E. Harrell Jr., K. L. Lee, R. M. Califf, D. B. Pryor, and R. A. Rosati, "Regression modelling strategies for improved prognostic prediction," *Statistics in Medicine*, vol. 3, no. 2, pp. 143–152, 1984.
- [12] A. A. Kramer and J. E. Zimmerman, "Assessing the calibration of mortality benchmarks in critical care: the Hosmer-Lemeshow test revisited," *Critical Care Medicine*, vol. 35, no. 9, pp. 2052–2056, 2007.
- [13] M. J. Pencina and R. B. D'Agostino, "Overall C as a measure of discrimination in survival analysis: model specific population value and confidence interval estimation," *Statistics in Medicine*, vol. 23, no. 13, pp. 2109–2123, 2004.
- [14] B. Sc and J. Dl, "Surgery of the ear and the lateral skull base: pitfalls and complications," *GMS Current Top Otorhinolaryngol Head Neck Surgery*, vol. 12, 2013.
- [15] O. Guntinas-Lichius and D. W. Eisele, "Facial nerve monitoring," *Advances in Oto-Rhino-Laryngology*, vol. 78, pp. 46–52, 2016.
- [16] A. M. Marco, A. De, H. B. Mohamed et al., "Dosing of remifentanyl to prevent movement during craniotomy in the absence

## *Retraction*

# **Retracted: The Conditioned Medium of *Lactobacillus rhamnoides* GG Regulates Microglia/Macrophage Polarization and Improves Functional Recovery after Spinal Cord Injury in Rats**

### **BioMed Research International**

Received 12 March 2024; Accepted 12 March 2024; Published 20 March 2024

Copyright © 2024 BioMed Research International. This is an open access article distributed under the Creative Commons Attribution License, which permits unrestricted use, distribution, and reproduction in any medium, provided the original work is properly cited.

This article has been retracted by Hindawi following an investigation undertaken by the publisher [1]. This investigation has uncovered evidence of one or more of the following indicators of systematic manipulation of the publication process:

- (1) Discrepancies in scope
- (2) Discrepancies in the description of the research reported
- (3) Discrepancies between the availability of data and the research described
- (4) Inappropriate citations
- (5) Incoherent, meaningless and/or irrelevant content included in the article
- (6) Manipulated or compromised peer review

The presence of these indicators undermines our confidence in the integrity of the article's content and we cannot, therefore, vouch for its reliability. Please note that this notice is intended solely to alert readers that the content of this article is unreliable. We have not investigated whether authors were aware of or involved in the systematic manipulation of the publication process.

Wiley and Hindawi regrets that the usual quality checks did not identify these issues before publication and have since put additional measures in place to safeguard research integrity.

We wish to credit our own Research Integrity and Research Publishing teams and anonymous and named

external researchers and research integrity experts for contributing to this investigation.

The corresponding author, as the representative of all authors, has been given the opportunity to register their agreement or disagreement to this retraction. We have kept a record of any response received.

### **References**

- [1] F. Lin, B. Zhang, Q. Shi et al., "The Conditioned Medium of *Lactobacillus rhamnoides* GG Regulates Microglia/Macrophage Polarization and Improves Functional Recovery after Spinal Cord Injury in Rats," *BioMed Research International*, vol. 2021, Article ID 3376496, 13 pages, 2021.

## Research Article

# The Conditioned Medium of *Lactobacillus rhamnoides* GG Regulates Microglia/Macrophage Polarization and Improves Functional Recovery after Spinal Cord Injury in Rats

Fangqi Lin , Baokun Zhang, Qiang Shi, Jiaming Liang, Xin Wang, Xiaofeng Lian , and Jianguang Xu 

Department of Orthopedic Surgery, Shanghai Jiao Tong University Affiliated No.6 People's Hospital, 600 Yishan Road, Shanghai 200233, China

Correspondence should be addressed to Xiaofeng Lian; [xf909@126.com](mailto:xf909@126.com) and Jianguang Xu; [xjgn6spine@126.com](mailto:xjgn6spine@126.com)

Received 7 April 2021; Accepted 25 June 2021; Published 12 July 2021

Academic Editor: Yuzhen Xu

Copyright © 2021 Fangqi Lin et al. This is an open access article distributed under the Creative Commons Attribution License, which permits unrestricted use, distribution, and reproduction in any medium, provided the original work is properly cited.

*Lactobacillus rhamnoides*, a human intestinal colonizer, can act through various pathways to induce microglia/macrophages to produce cytokines and to polarize microglia/macrophages to different phenotypes to reduce the inflammatory response. In this article, we evaluated the treatment potential of the *Lactobacillus rhamnoides* GG conditioned medium (LGG-CM) in rat model with SCI (acute spinal cord injury), including functional, neurophysiological, and histological outcomes and the underlying neuroprotective mechanisms. In our experiment, LGG-CM (30 mg/kg) was injected directly into the injury site in rats immediately after SCI. Measured by the BBB scale (Basso, Beattie, and Bresnahan locomotor rating scale) and inclined plane test, rats in the LGG-CM-treated group showed better locomotor scores. Moreover, compared to the vehicle treatment group, LGG-CM increased the mRNA level of the M2 marker (CD206), and decreased that of the M1 marker (iNOS). Western blot assays showed that LGG-CM-treated SCI rats had a higher grayscale ratio of p65 and a lower ratio of p-I $\kappa$ B $\alpha$ /I $\kappa$ B $\alpha$ . Our study shows that local injection of LGG-CM after acute SCI can inhibit inflammatory responses and improve motor function recovery. These effects may be related with the inhibition to the NF- $\kappa$ B (The nuclear factor-kappa B) signal pathway which leads to M2 microglia/macrophage polarization.

## 1. Introduction

SCI (spinal cord injury), which is often secondary to spinal injury, is the most severe complication of spinal trauma and often leads to serious limb dysfunction [1]. SCI can cause local tissue destruction and microcirculation disturbances, resulting in the exacerbation of local damage and extensive necrosis of peripheral nerve cells, which in turn can cause motor, sensory, and autonomic dysfunction in the human body, greatly reducing the quality of life of patients [2, 3]. A previous study has proved that timely medication and intervention after spinal cord injury can attenuate long-term functional impairment and pathological damage [4]. So it is essential to develop effective methods to promote locomotor function recovery after SCI. Methylprednisolone is currently most commonly used clinically, but it must be carefully mon-

itored to prevent arrhythmia, circulatory failure, and cardiac arrest, as well as complications of gastrointestinal bleeding [5]. Other drugs such as naloxone, nerve growth factor, and thyrotropin-releasing hormone have been shown to be effective in the recovery of spinal cord function in experiments, but they have yet to be confirmed by their extensive clinical application [6–8].

Within a few hours after spinal cord injury, microglia/macrophages, as the first immune cells to react to injury, polarize into M1 microglia/macrophages, releasing inflammatory factors (TNF- $\alpha$ , IL-6, and IL-1 $\beta$ ), exacerbating the inflammatory response, inhibiting axonal regeneration, and finally leading to apoptosis of residual neurons [9, 10]. At later stages of spinal cord injury, the inflammatory response gradually weakens, and inflammatory factors secreted by M1 microglia/macrophages gradually decrease, and M2

microglia/macrophages play a key gradually. M2 microglia/macrophages can make regeneration and functional recovery of residual nerves by modifying the microglia/macrophage phenotype, reducing the secretion of proinflammatory factors, increasing the secretion of neurotrophic factors, and increasing stimulatory factors in the microenvironment, such as TGF- $\beta$ 1 [11, 12]. The predominance of the M1 phenotype instead of M2 phenotype after SCI may contribute to secondary damage of the spinal cord. But, it is still unclear which factors in SCI can lead to microglia/macrophage phenotype switching. The switch of microglia/macrophage has been successfully applied in the treatment of chronic inflammatory renal disease, type 1 diabetes, and autoimmune encephalomyelitis in animal models [13–17], but the reports about this method applied in SCI treating are yet not so complete.

*Lactobacillus rhamnoides*, a kind of Gram-positive bacterium, can produce a large amount of lactic acid from fermentable carbohydrates [18]. Moderate intervention to the NF- $\kappa$ B signal pathway can reduce inflammatory response. Studies have shown that the conditioned medium of *Lactobacillus rhamnoides* GG (LGG-CM) can promote microglia/macrophage polarization to M2 by inhibiting the NF- $\kappa$ B signal pathway; this has been proven in the context of *Salmonella infantis*-induced inflammation in a pig model and colitis in mice [19, 20]. However, it has not been reported whether lactic acid bacteria can promote the repair of SCI by regulating the polarization of microglia/macrophages. Given its ability to regulate cytokines secreted by microglia/macrophages and microglia/macrophage polarization, we used LGG-CM in the treatment of SCI rats for the first time, to investigate whether it can reduce the nerve damage caused by SCI and promote the recovery of behavioral motor function.

## 2. Materials and Methods

**2.1. Ethical Approval.** All rats were operated on by the same surgeon. The animals were anesthetized by using 30 mg/kg pentobarbital administered intraperitoneally. The anesthetic effect was expected to begin within 5 min and to last approximately 2 hours, which was enough time to complete the spinal cord injury procedure. The withdrawal reflex to tail compression was used to evaluate the level of anesthesia.

**2.2. Drugs.** *Lactobacillus rhamnoides* was inoculated in MRS medium and cultured for 24 h at 37°C. We centrifuged the supernatant and filtered out the bacteria with a 0.22  $\mu$ m filter membrane, loaded them into an enrichment tube, and centrifuged them at 4000 r/min for 40 min at 4°C. From previous studies, we can know that the active ingredient of LGG-CM has a relative molecular weight  $\geq$  30000 kDa, and our preexperimental results also showed that the LGG-CM component with a relative molecular weight  $\geq$  30000 kDa significantly promoted microglia/macrophage polarization from M1 to M2 state. Therefore, we used the LGG-CM component with a molecular weight of  $\geq$ 30000 kDa in this study.

**2.3. Animals.** Female rats (200–220 g, approximately 2 months) were reared in cages (every cage had 4 rats) in an

environment with controlled temperature (25°C) and light/dark cycle (12/12 h). All rats had sufficient water and food during the whole study, and we made lots of efforts to alleviate the rats' suffering.

The rats were divided into the 3 groups randomly, in which SCI or laminectomy was performed. In clinical practice, some doctors inject methylprednisolone into the local area of nerve decompression surgery and administer it in the form of local infiltration, which has played a good auxiliary role in surgical treatment. Similarly, the mice were directly administered LGG-CM (30 mg/kg) or saline at the site of injury by intrathecal injection within the first hour. The animal groups were as follows:

- (1) SCI+saline (SCI+vehicle)
- (2) SCI+2 ml/kg LGG-CM (SCI+LGG-CM)
- (3) Sham+saline (sham; same surgical operation as the other 2 groups, except that weight dropping to the dura was not applied)

At 1, 2, 3, 4, 5, 6, and 7 days postsurgery, each rat was subjected to behavioral function assessment. And at 1, 3, and 7 days after surgery, we sacrificed 3 rats from each group and excised their spinal cords for follow-up biochemical studies and staining.

### 2.4. In Vitro Experiments

**2.4.1. Cell Counting Kit-8.** The degrees of cell viability of different LGG-CM concentrations were assessed with CCK-8 (Cell Counting Kit-8). Briefly, LGG-CM (LGG-CM: PBS (phosphate buffer saline) at 4 concentrations: 0, 1:100, 1:50, and 1:25) was added to 96-well plates, and each well was seeded with 200  $\mu$ l cells at a concentration of  $1 \times 10^4$  cells/ml. Incubated for 0 and 24 hours, the cells were added with 10  $\mu$ l CCK-8 reagent. Then, the plates would be incubated for 1 hour. Finally, we used a microplate reader to measure spectrophotometric absorbance at 450 nm.

**2.4.2. Flow Cytometric Measurement.** THP-1 cells were incubated or differentiated in media containing different concentrations of LGG-CM (0  $\mu$ l/ml, 10  $\mu$ l/ml, and 20  $\mu$ l/ml). The microglia/macrophages were detached with trypsin. The collected microglia/macrophages were washed twice in PBS (phosphate buffer saline) and then resuspended in PBS again at a concentration of  $1 \times 10^7$  cells/ml. We transferred 100  $\mu$ l of suspended cells to a flow tube. After that, we stained the cells with fluorescent dye-conjugated antibodies against CD206, CD86, and the corresponding isotype controls at 4°C. Washed twice in PBS again, the stained cells were then analyzed by FACS Aria flow cytometry on a flow cytometer. The software we used for analyzing results was FlowJo. Flow cytometry and fluorescence microscopy were used to measure apoptosis. We used PBS to wash the cells twice and then used trypsin to detach. We centrifuged the THP-1 cells at 1000 rpm for 3 min, washed them in PBS twice, and added Annexin V Binding Solution (1 $\times$ ) to the cells, which were maintained at a fixed concentration of  $1 \times 10^6$  cells/ml; then,



we transferred 100  $\mu\text{l}$  of the cell-containing solution to prepared flow tubes. We added FITC Annexin V (5  $\mu\text{l}$ ) and propidium iodide (PI, 5  $\mu\text{l}$ ) to each tube, incubated the tubes for 15 min in the dark, and then added 400  $\mu\text{l}$  of 1 $\times$  Annexin V Binding Solution to each tube. The results were analyzed by a FACSAria flow cytometer and fluorescence microscopy.

## 2.5. In Vivo Experiments

**2.5.1. Animal Surgery.** Animals were anaesthetized by pentobarbital (30 mg/kg body weight). After the hair at the surgical area was shaved, the skin of the surgical area was disinfected with medical alcohol (70%) and povidone-iodine. Under aseptic conditions, we made a longitudinal incision on the midline of the rat back to expose the paravertebral muscles. The T5–T8 vertebrae were exposed after dissecting the paravertebral muscles away. After exposing the spinal cord by T5–T8 laminectomy, we performed extradural compression by dropping a rod (diameter: 2 mm; weight: 10 g; height: 20 mm) to the dura rapidly to produce SCI. The rats in the sham group were only subjected to laminectomy. Ten minutes after SCI, rats in the LGG-CM group were administered direct injections of LGG-CM (2 ml/kg) at the injured segment of the spinal column, and the same volume of PBS was injected into rats in the vehicle group. We set the pH of the LGG-CM solution at between 7.2 and 7.4 to match the normal tissue pH. To replenish the blood lost in the surgery, 1 ml of saline was injected subcutaneously. The rats were placed in an area with warm heating lights during the recovery from anesthesia. During the whole experiment, sufficient food and water were provided. We manually voided rat bladders twice daily until bladder function returned to normal.

**2.5.2. Basso, Beattie, and Bresnahan Locomotor Rating Scale.** We used the BBB scale (Basso, Beattie, and Bresnahan locomotor rating scale) to evaluate the locomotor function of rats. Based on paw placement, limb movement, coordination and gait, the BBB scale is a detailed classification system of functional scores ranging from 0 to 21 (0 for no hindlimb movement and 21 for normal hindlimb movement) [21]. From day 1 to day 7 after the surgery, each rat was observed by at least two different experimenters who were blinded to the treating methods received for each rat. During a 5 min walk, the rats were positioned in an open and smooth field so that they could be observed on both sides.

**2.5.3. Inclined Plane Test.** We used an inclined plane test to assess the muscle strength of the rat hind paws [22]. The rats were observed and evaluated by two different experimenters who were blinded to the treating methods received for each rat. The rats were placed on an inclined plane that was then gradually raised from 0° by 1° at a time, and the maximum angle at which the rat could remain on the inclined plane was observed. Each rat was tested at least 3 times, and the data would be averaged for subsequent analysis.

**2.5.4. Tissue Preparation.** At 1, 3, and 7 days post-SCI, the rats were sacrificed with overdose pentobarbital (100 mg/kg; Nembutal). The rats, whose spinal cords would be used for staining, were perfused transcardially with cold normal saline

and 4% paraformaldehyde in sequence. After careful dissection, the spinal cords were fixed in 4% paraformaldehyde at 4°C overnight, dehydrated with 30% sucrose, embedded in paraffin wax, and then sectioned (5  $\mu\text{m}$ ). For the spinal cords which were used for PCR and Western blot analysis, we made a dissection for segments of approximately 1 cm concluding the area of injury, washed them with PBS (ice-cold phosphate-buffered saline), and then snap-frozen and stored in liquid nitrogen until analysis.

**2.6. Hematoxylin-Eosin Staining and Nissl Staining.** We stained the spinal cord sections (20  $\mu\text{m}$ ) with conventional hematoxylin-eosin (H&E) staining and Nissl staining and observed the stained sections through an optical microscope. In hematoxylin-eosin staining, after deparaffinization and rehydration, we stained 5  $\mu\text{m}$  longitudinal sections with hematoxylin solution for 5 min, then immersed the sections in 1% acid ethanol (1% HCl in 70% ethanol) solution, and then rinse in distilled water totally. Then, the sections were stained with eosin solution for 3 min, and then dehydrated with gradient alcohol and clarified in xylene. In Nissl staining, we first heated the sections at room temperature for 30 min, then immersed the sections in 100% ethanol, 75% ethanol and distilled water for 30 seconds, and then stained them with 0.1% cresyl violet solution at 37°C for 5 min. After the sections were completely washed in distilled water, they would be immersed in 95% ethanol for 30 seconds and then immersed in absolute ethanol, absolute ethanol, and xylene for 5 minutes. Finally, seal the sections with neutral glue and observe under a microscope.

**2.7. Immunohistochemistry.** Spinal cord sections were stained for: MMPs (matrix metalloproteinases). After fixation, the sections were washed with PBST (30 min) and then incubated in normal goat serum (10%, 30 min) for blocking. The transverse sections were then incubated with the primary antibodies MMPs, at 4°C for 12 h. Subsequently, the sections were washed again in PBST (30 min) and then incubated with the secondary antibodies for 8 h. Finally, the sections were washed with PBST (30 min) and then incubated with DAPI for 30 s and cover-slipped. Images were captured by a laser scanning confocal microscope. Three consecutive slices from each animal were analyzed, and three random visual fields were counted in each slice. Table 1 shows the information of antibodies.

**2.8. Real-Time PCR.** Following the standard manufacturer's instructions, we used an RNA simple total RNA kit to isolate total RNAs from the injured spinal cords. The concentration and quality of total RNA were assessed by spectrophotometric determination at 260/280 nm, and equal amounts of RNA from each sample were reverse-transcribed into complementary DNA (cDNA) for RT-qPCR. For miRNA reverse transcription, cDNA was synthesized using the miRNA First-Strand cDNA Synthesis (Tailing Reaction) Kit (Sangon Biotech, Shanghai). For mRNA reverse transcription, cDNA was synthesized using the PrimeScript RT Reagent Kit with gDNA Eraser (TaKaRa Biomedical Technology Co. Ltd., Beijing, China). cDNA was further applied as a template for RT-

TABLE 1: Primers used for real-time PCR.

Genes	Forward primers	Reverse primers
$\beta$ -Actin	5' CCT CTA TGC CAA CAC AGT 3'	5' AGC CAC CAA TCC ACA CAG 3'
IL-6	5' AAT CTG CTC TGG TCT TCT GGA 3'	5' ATT GCT CTG AAT GAC TCT GGC 3'
IL-1 $\beta$	5' GTT CTT TGA GGC TGA CAG ACC 3'	5' GAT GCT GCT GTG AGA TTT GAA 3'
TNF- $\alpha$	5' CCA ATC TGT GTC CTT CTA ACT 3'	5' TGT GTT TCT GAG CAT CGT 3'
iNOS	5' CTC AGG CTT GGG TCT TGT TAG 3'	5' TCT GTG ACT TTG TGC TTC TGC 3'
CD206	5' CCT TCT GTG CCT ATC TCT CCA 3'	5' TAT TTC TCT GCT TCG TGC CAT 3'
TGF- $\beta$ 1	5' CCT GGA TAC CAA CTA CTG CTT 3'	5' AGG TCC TTC CTA AAG TCA ATG T 3'
MMP-9	5' GAC TCG GTC TTT GAG GAG CC 3'	5' GAA CTC ACG CGC CAG TAG AA 3'

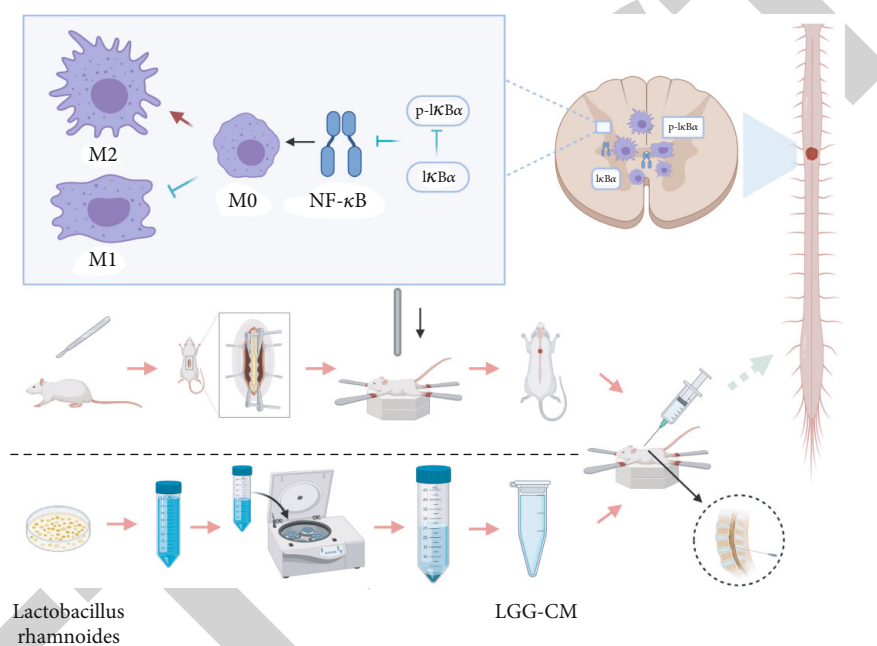


FIGURE 1: The scheme of our article.

qPCR following the manufacturer's instructions (Mastecycler Gradient; Eppendorf, Germany). The primers are shown in Table 1.

**2.9. Western Blot Analysis.** Microglia/macrophages isolated from mice treated with or without LGG-CM were homogenized with ice-cold RIPA buffer (25 mM Tris-HCl pH 7.6, 150 mM NaCl, 1% NP-40, 1% sodium deoxycholate, and 0.1% SDS) containing protease and phosphatase inhibitors (Complete Protease Inhibitor Cocktail and PhosSTOP Phosphatase Inhibitor Cocktail; both from Roche). After centrifugation at 12,000 g for 10 min at 4°C, the supernatants were collected. The protein concentration was determined using a bicinchoninic acid (BCA) assay (QuantiPro BCA Assay Kit, Sigma-Aldrich) according to the manufacturer's instructions. Protein samples were separated by SDS-polyacrylamide gel electrophoresis and transferred onto polyvinylidene fluoride (PVDF) membranes (Millipore Corporation, USA). The membranes were blocked with 5%

skimmed milk for 1 h at room temperature and then incubated with primary antibodies at 4°C overnight: rabbit anti-p-I $\kappa$ B $\alpha$  (1:1000; Cell Signaling Technology), rabbit anti-I $\kappa$ B $\alpha$  (1:1000; Abcam), and rabbit anti- $\beta$ -actin (1:1000; Abcam). After three washes, the membranes were incubated with an HRP-coupled secondary antibody (1:20000; Jackson) at room temperature for 1 h and washed three times for 10 min each at room temperature. Finally, all the membranes were imaged using densitometry (ChemiScope 6100) and quantified using densitometric analysis (ImageJ software, NIH).

**2.10. Statistical Analysis.** We used GraphPad Prism software 8.0 to perform statistical analysis. Two-tailed unpaired Student's *t*-test was used to compare the two groups. Unless otherwise stated, the rest of the data were analyzed by either one-way or two-way analysis of variance with post hoc Tukey's multiple comparisons tests. *P* values of < 0.05 were considered significant.



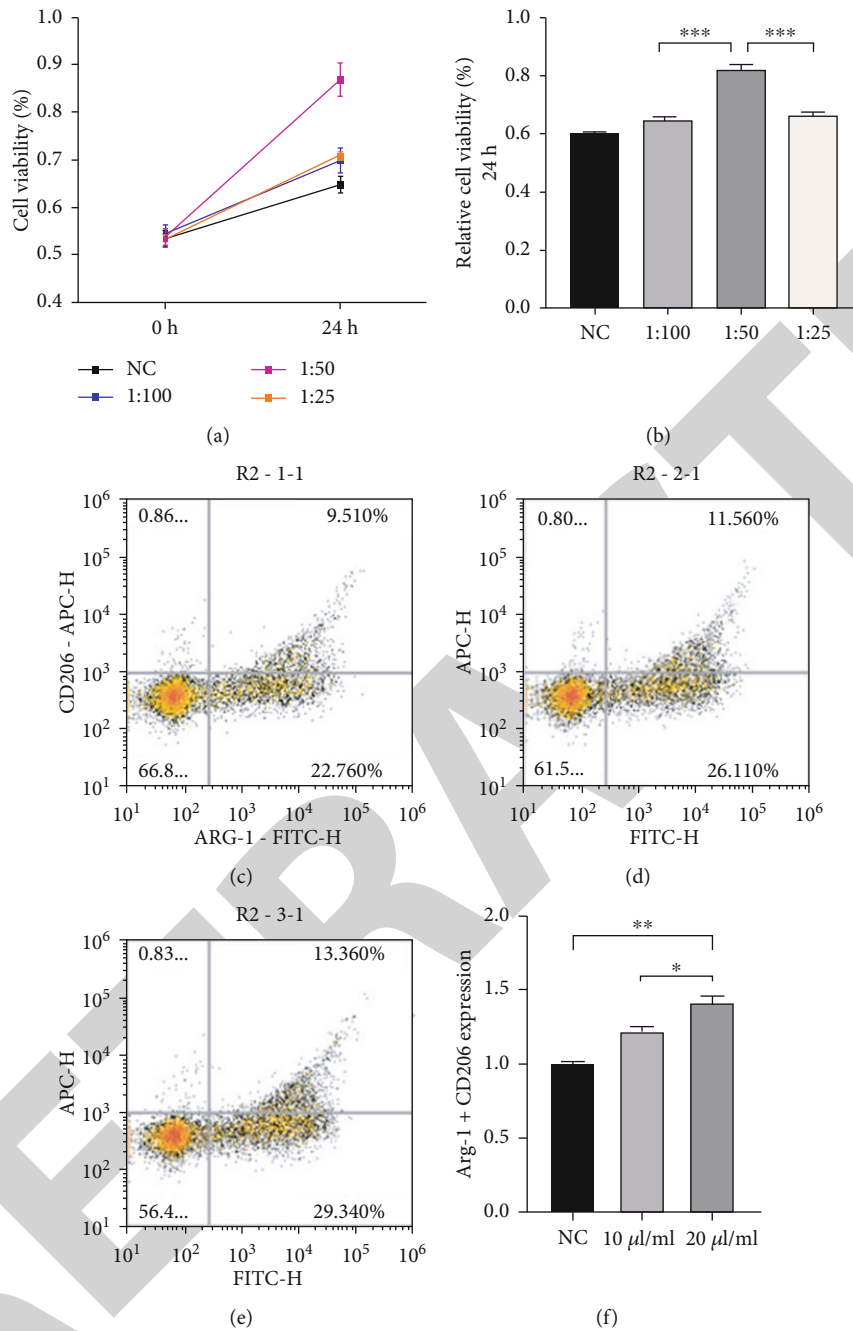


FIGURE 2: (a, b) Cell viability of in different percentage of LGG-CM and PBS at 0 h and 24 h (NC, 1 : 100, 1 : 50, and 1 : 25). (c-e) Flow cytometric measurement. (f) The expression of Arg-1 and CD206 at different concentrations of LGG-CM (NC, 10  $\mu$ l/ml, and 20  $\mu$ l/ml).

### 3. Results

**3.1. Experimental Protocol.** The scheme of our article explains the protocol (Figure 1).

**3.2. Cell Survival Assay.** To determine the appropriate dose of LGG-CM, microglia/macrophage cells were incubated with 0 (control), 1 : 25, 1 : 50, and 1 : 100 LGG-CM : PBS for 24 h. We can find from the CCK-8 results assay that LGG-CM significantly increased cell viability compared to the control. The 1 : 50 concentration had a greater effect on viability than the other concentrations and also promoted the most microglia/-

macrophage polarization to M2. Thus, 1 : 50 (20  $\mu$ l/ml) was selected for use in the subsequent experiments (Figure 2).

**3.3. LGG-CM Improves Functional Restoration after Acute SCI.** We performed BBB and inclined plane tests daily from 1 to 7 days after SCI to evaluate the functional restoration of mice in different groups. As the higher BBB scores indicated, the LGG-CM-treated group showed improved recovery from day 3 after SCI. Compared to the rats of the vehicle-treated group, the rats of the LGG-CM-treated group showed better locomotor function recovery in inclined plane

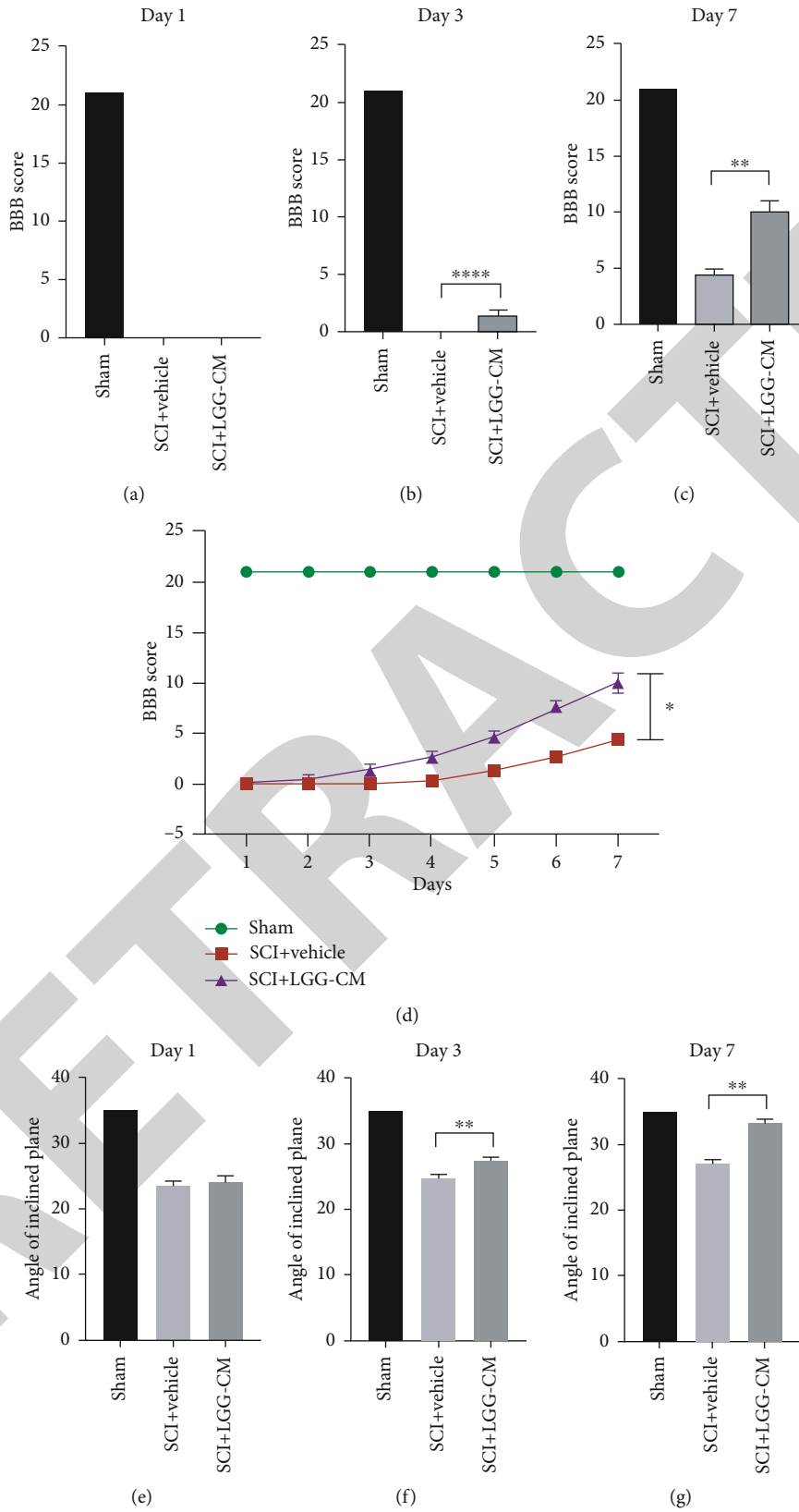
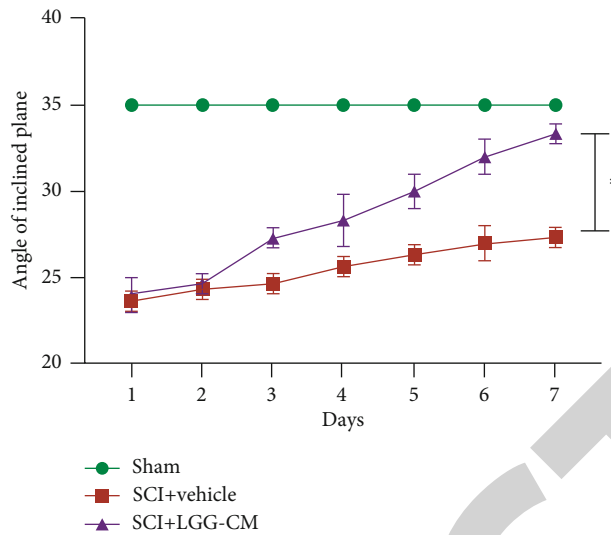


FIGURE 3: Continued.



(h)

FIGURE 3: LGG-CM treatment promotes the recovery of locomotor functions after SCI. (a–d) Quantification of BBB score from day 1 to day 7 after surgery. (e–h) Quantification tested by inclined plane test from day 1 to day 7 after surgery.

test, with a significantly increased angle of the inclined plane that the rats could stay (Figure 3).

**3.4. LGG-CM Reduces Lesion Size.** At 7 days post-SCI, the area of spinal cord damage on the specimens in the LGG-CM-treated group was noticeably less than that in the vehicle-treated group. Moreover, Nissl staining suggested that the density of Nissl bodies in the LGG-CM-treated group was significantly higher than that in the vehicle-treated group at 7 days after SCI (Figure 4).

**3.5. LGG-CM Polarization to M2 Microglia/Macrophages and Reduce Inflammation.** At 7 days after surgery, we used immunochemistry and immunofluorescence staining to observe the spinal cord slices of rats with spinal cord injury to study the changes of matrix metalloproteinases (MMPs) near the slices. We found that the expression of MMPs was low in the sham group. In both the LGG-CM group and vehicle group, the expression of MMPs was higher than that in the sham group significantly; the expression of MMPs was less in the LGG-CM compared with the vehicle group. Then, we used qPCR to value the mRNA levels of MMP-9 and characteristic surface markers (TNF- $\alpha$ , IL-6, IL-1 $\beta$ , TGF- $\beta$ 1, CD206, and iNOS) at day 7 after surgery. As expected, LGG-CM treatment reduced the mRNA expression of MMP-9, iNOS, IL-6, IL-1 $\beta$ , and TNF- $\alpha$ . On the contrary, the mRNA expression CD206 and TGF- $\beta$  was significantly increased in LGG-CM-treated rats. The mRNA marker expressions of both M1 and M2 in the vehicle-treated group were significantly higher than that in the sham group. Compared to vehicle treatment, LGG-CM treatment can increase the mRNA expression of M2 markers and decreased that of M1 markers (Figure 5).

**3.6. LGG-CM Inhibits the NF- $\kappa$ B Signal Pathway by Reducing the Phosphorylation of I $\kappa$ B $\alpha$ .** The NF- $\kappa$ B (nuclear factor-

kappa B) signal pathway is crucial in the process of producing inflammatory cytokines to perform proinflammatory functions. We hypothesized that LGG-CM can protect rats against SCI by inhibiting NF- $\kappa$ B-mediated inflammation. To verify our hypothesis, we used immunoblotting to assess the NF- $\kappa$ B activation and assessed the expression of NF- $\kappa$ B in microglia/macrophages by immunostaining. In the LGG-CM treatment group, we could observe an inhibition of NF- $\kappa$ B p65, suggesting that LGG-CM can suppress the transcriptional activity of NF- $\kappa$ B p65. Moreover, the ratio of p-I $\kappa$ B $\alpha$ /I $\kappa$ B $\alpha$  was significantly lower in rats with LGG-CM treatment, which means that the NF- $\kappa$ B signaling pathway was inhibited by reducing the phosphorylation of I $\kappa$ B $\alpha$  (Figure 6).

## 4. Discussion

After ensuring the safety of LGG-CM by CCK-8 test and the effectiveness by flow cytometric measurement, we applied LGG-CM locally at the injured site after SCI in rats. From the observation of the treatment group, we can find a less damage area of spinal cord specimens and a higher density of Nissl bodies. Evaluated by BBB test and inclined plane test, functional recovery was improved significantly in the treatment group, which shows that LGG-CM do provide a protective effect against SCI in rats. The results of PCR and Western blot experiments showed that the therapeutic effect was associated with the inhibition of the NF- $\kappa$ B signal pathway, which promoted the polarization of microglia/macrophages to M2 rather than M1 and thereby reduced related inflammatory processes and improved locomotor function recovery.

With the mediation of inflammatory mediators, matrix metalloproteinases (MMPs) can cause the dissolution of extracellular matrix and the destruction of basement membrane, aggravating the inflammatory response and

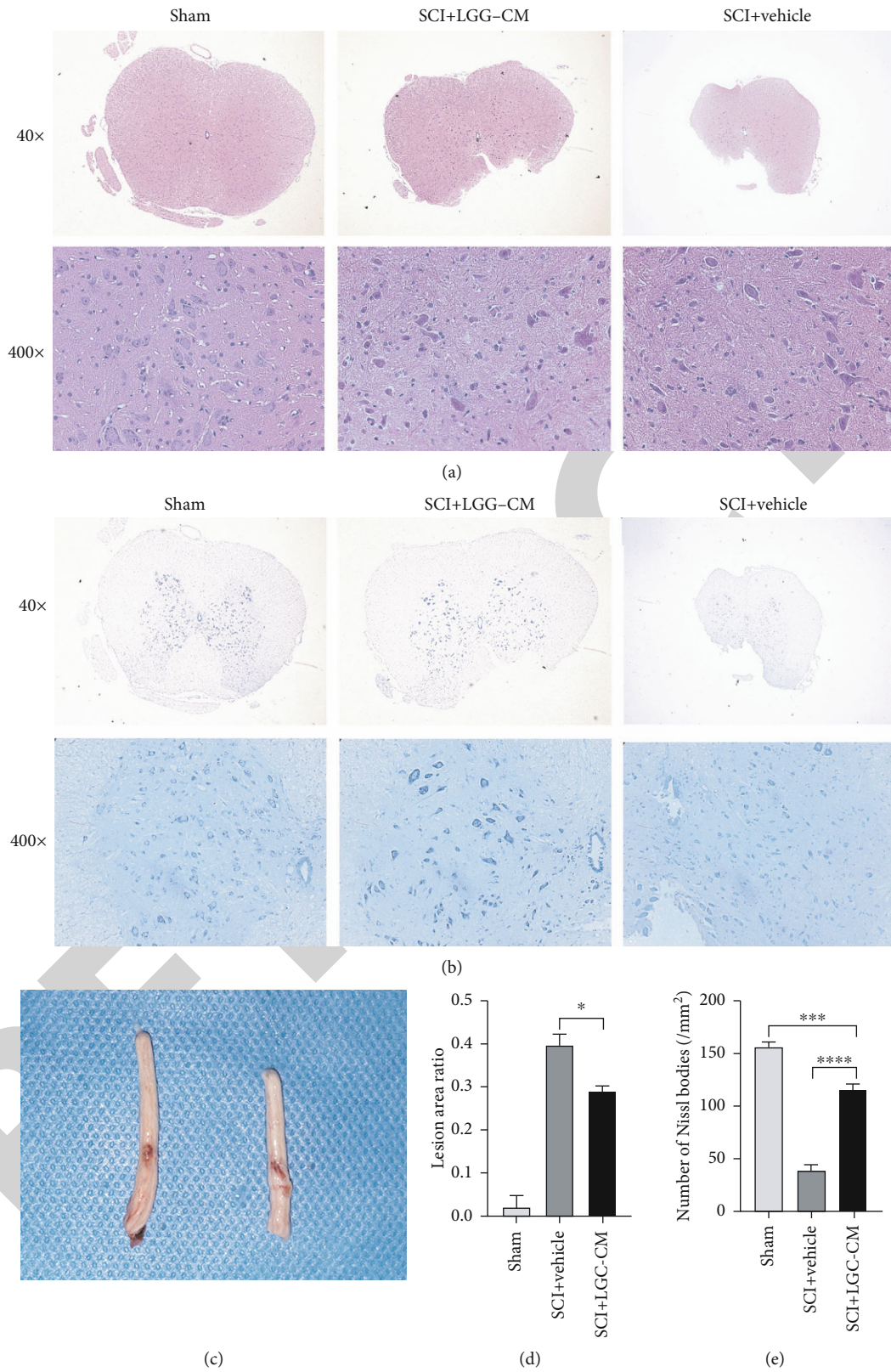


FIGURE 4: LGG-CM attenuates tissue damage. (a) H&E staining of transverse spinal cord sections near the injury at day 7 after SCI. (b) Nissl staining of transverse spinal cord sections near the injury at day 7 after SCI. (c) The area of injury site in SCI rats who were treated with LGG-CM or vehicle. (d) Quantification of lesion as a ratio to whole area at the epicenter in each SCI group. (e) Numbers of Nissl bodies (/mm<sup>2</sup>) in transverse spinal cord sections near the injury at day 7 after SCI.



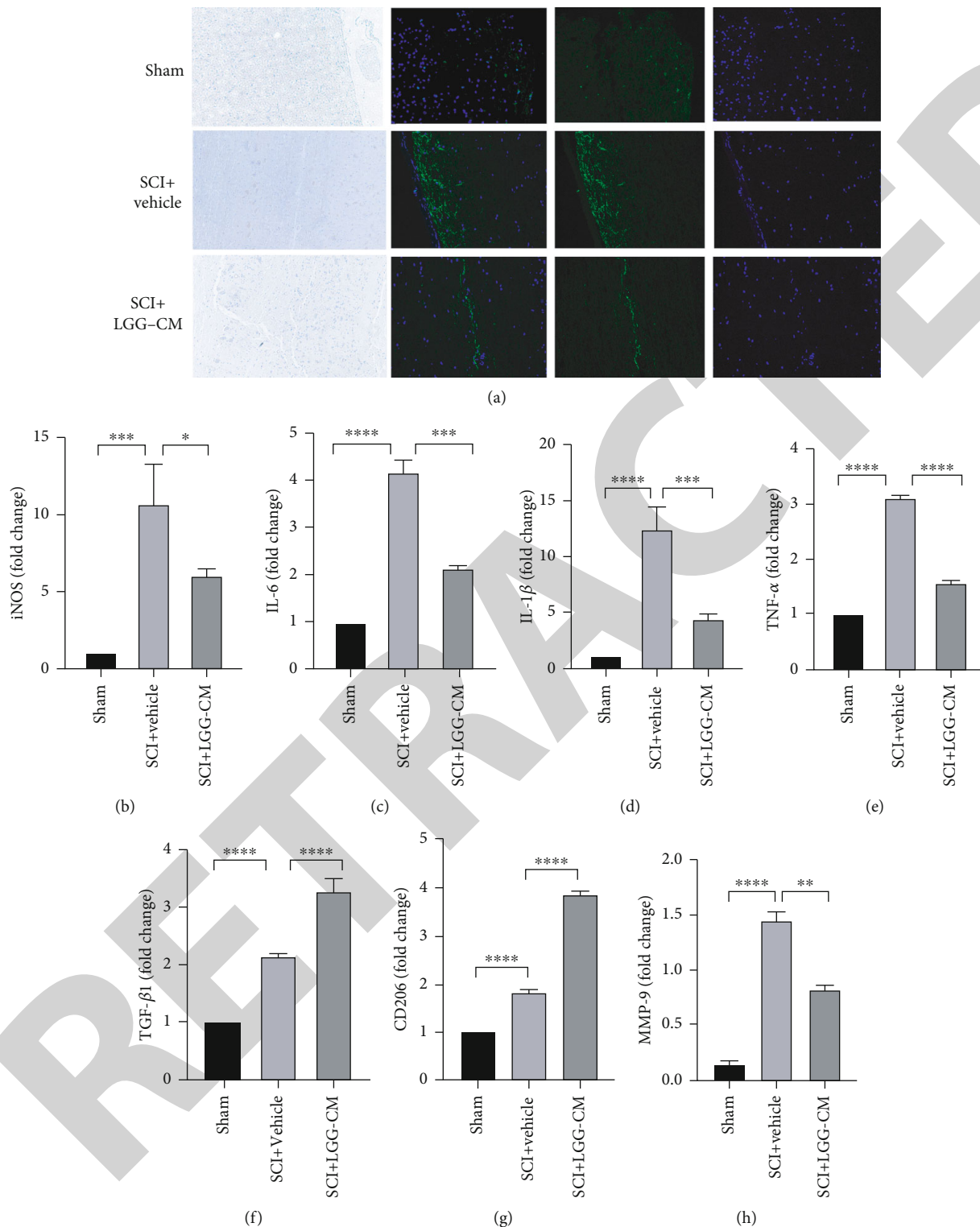


FIGURE 5: LGG-CM treatment reduces neuroinflammation in the spinal cord after SCI. (a) Immunohistochemistry and immunofluorescence images of MMPs in the spinal cord at 7 days post-SCI. (b–e) The mRNA levels of iNOS (b), IL-6 (c), IL-1 $\beta$  (d), and TNF- $\alpha$  (e) near the injury section at day 7 post-SCI of the sham operation, SCI+vehicle, and SCI+LGG-CM treatments. (f, g) The mRNA levels of TGF- $\beta$ 1 (f) and CD206 (g) near the injury section at day 7 post-SCI of the sham operation, SCI+vehicle, and SCI+LGG-CM treatments. (h) Upregulation of MMP-9 activity after SCI is demonstrated. After LGG-CM treatment, the activity was downregulated.

destroying normal cell tissues. What is more, the expression of MMPs is positive with the inflammatory mediators. So MMPs can be used to assess the severity of inflammatory

response [23–25]. From the results of immunohistochemistry and immunofluorescence staining, we found that in the sham operation group, the expression of MMPs was low,

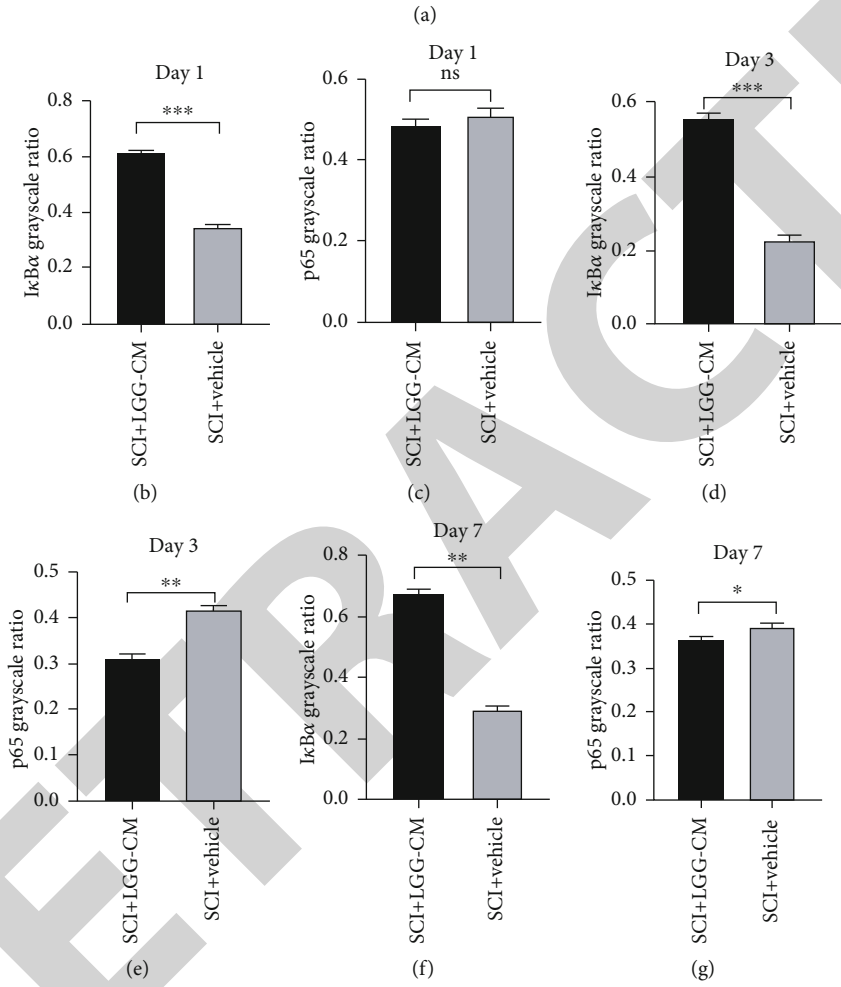
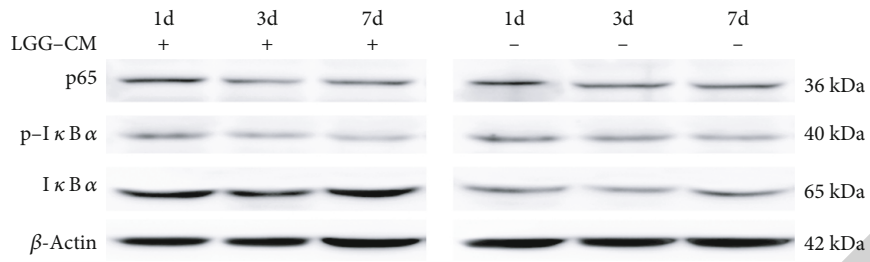


FIGURE 6: Continued.



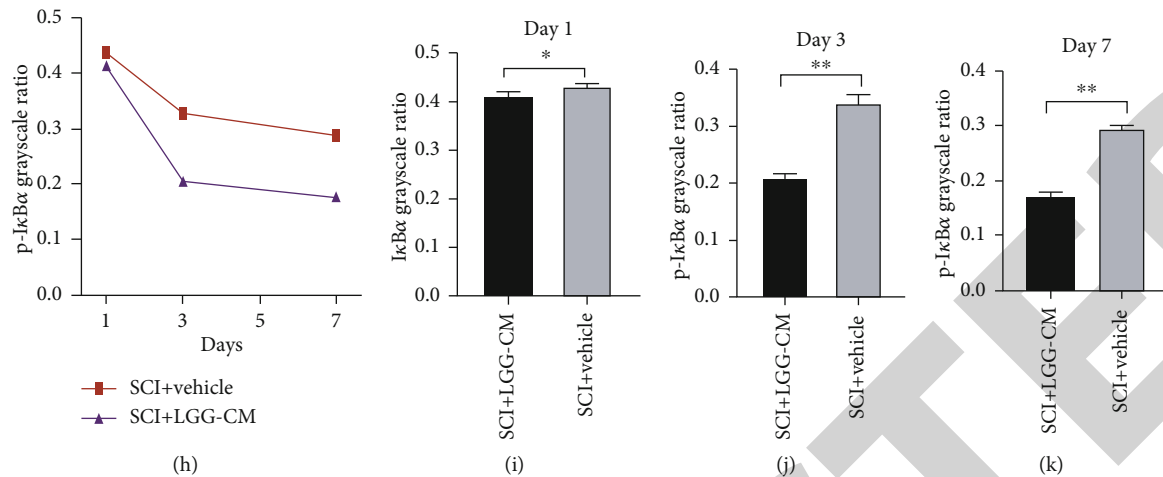


FIGURE 6: LGG-CM treatment could inhibit NF- $\kappa$ B signal pathway by reducing the phosphorylation of I $\kappa$ B $\alpha$ . (a) Western blot images show the expression of I $\kappa$ B $\alpha$ , p-I $\kappa$ B $\alpha$ , and p65 in microglia/macrophage. (b, d, f) The grayscale ratio of I $\kappa$ B $\alpha$  in the spinal cord of mice at 1 (b), 3 (d), and 7 (f) days post-SCI. (c, e, g) The grayscale ratio of p65 in the spinal cord of mice at 1 (c), 3 (e), and 7 (g) days post-SCI. (i–k) The grayscale ratio of p-I $\kappa$ B $\alpha$  in the spinal cord of mice at 1 (i), 3 (j), and 7 (k) days post-SCI. (h) The ratio of p-I $\kappa$ B $\alpha$ /I $\kappa$ B $\alpha$  in the spinal cord of mice.

which is in line with the description in the literature review: the expression of MMPs in normal tissues was low or even not expressed. In the LGG-CM group and the vehicle group, the expression of MMPs was higher than that in sham group, and the expression of MMPs in the LGG-CM group was lower than that in the vehicle group. This indicates that the intervention of LGG-CM can reduce the inflammatory response of spinal cord injury tissue, and its effect may be related to the reduction of inflammatory mediators.

The inflammatory response plays an important role during the process of local tissue injury after SCI. In well-defined in vitro situations, microglia/macrophages can be divided into the M1 (proinflammatory) phenotype and M2 (anti-inflammatory) phenotype by the presence of different surface markers. The dominance of the M1 or M2 phenotype can determine the trend of immune responses [26]. The proinflammatory M1 state may be related to the dominant expression of proinflammatory factors (TNF- $\alpha$ , IL-6, IL-1 $\beta$ , and iNOS) that exacerbate local inflammation. On the contrary, the anti-inflammatory M2 state is associated with the dominance of anti-inflammatory factors (TGF- $\beta$ 1 and CD206), which is beneficial for tissue repair [27, 28]. In our research, we observed the changes of inflammatory factors and microglia/macrophage markers by real-time PCR. We can find that in the first few hours after SCI, microglia/macrophages polarized to the M1 phenotype, and proinflammatory factors increased and remained a high level for 3 days after SCI. In the late stage of SCI, microglia/macrophages polarized to M2, with a significant increase of anti-inflammatory factors (i.e., TGF- $\beta$ 1 and CD206). These results offer a possible therapeutic strategy that regulates the polarization of microglia/macrophages to decrease excess neuroinflammatory factor levels and block inflammatory responses which may down-regulate the production of inflammatory cytokines and inhibited inflammation, to promote neural functional repair after SCI.

LGG is currently one of the most widely studied probiotics, and it has been proven effective in preventing and treat-

ing certain conditions, such as intestinal infections, diarrhea, systemic inflammation, and allergic diseases [29, 30]. Studies have shown that LGG-CM can reduce intestinal damage caused by pathogenic bacteria and oxidative stress [31, 32]; moreover, LGG-CM reduced allergic reactions and enhanced the immune function of mononuclear microglia/macrophages when administered to mice [33, 34]. In a previous study, it was found that LGG-CM can directly act on brain microvascular cells to inhibit the activation of the NF- $\kappa$ B signal pathway. [35] We applied LGG-CM to SCI rats and found that LGG-CM can reduce the occurrence of inflammation in SCI and do exert a therapeutic effect. During in vitro experiments, we ensured the safety of LGG-CM by CCK-8 test. And then, we treated microglia/macrophages with different concentrations of LGG-CM and found that the effect of LGG-CM on polarization was concentration dependent. From the real-time PCR results, we can find that compared to vehicle treatment, LGG-CM treatment significantly decreased the mRNA levels of M1 state markers (iNOS) near the injury section of SCI rats, which shows that LGG-CM administration may inhibit polarization to M1. Conversely, the mRNA levels of markers of M2 were increased, which means that polarization to M2 was promoted. As indicated by our behavioral analyses, LGG-CM can promote the polarization of microglia/macrophage to M2 phenotype rather than M1 phenotype and thus improve the recovery of motor function.

In fact, the dominance of the M1 or M2 phenotype in vivo may be associated with many conflicting factors from the physiological environment. As a key transcription factor, NF- $\kappa$ B plays an important role in microglia/macrophage polarization. NF- $\kappa$ B pathways are activated by extracellular stimuli. Extracellular signaling factors bind to the corresponding receptors on the cell membrane, initiating a series of downstream responses. The stimulated receptor protein activates I $\kappa$ B kinase (IKK). IKK phosphorylates the serine within the amino-terminal domain of I $\kappa$ B in the intracellular NF- $\kappa$ B I $\kappa$ B complex so that the I $\kappa$ B subunit is modified by

ubiquitination and then degraded by proteases, thereby releasing the NF- $\kappa$ B dimer. The activated NF- $\kappa$ B dimer is mainly composed of the p50 subunit and p65 subunit. In the NF- $\kappa$ B pathway, the activation of p65 can initiate inflammation in the human body and induce microglia/macrophage polarization to M1. Our Western blot assay indicated that the grayscale ratio of p65 was lower in the LGG-CM-treated SCI rats, suggesting that LGG-CM can inhibit the transcriptional activity of NF- $\kappa$ B p65. Moreover, the ratio of p-I $\kappa$ B $\alpha$ /I $\kappa$ B $\alpha$  was significantly lower in LGG-CM-treated SCI rats, which indicates that the phosphorylation of I $\kappa$ B $\alpha$  was reduced. Collectively, these findings suggest that LGG-CM inhibited the NF- $\kappa$ B pathway by reducing the phosphorylation of I $\kappa$ B $\alpha$ , which can promote microglia/macrophage polarizing to the anti-inflammatory M2 state to repair injury tissue and reduce inflammation.

## 5. Conclusion

Our study suggests a novel treatment strategy: early LGG-CM administration immediately after SCI reduced the extent of posttraumatic inflammation near the injured site and promoted locomotor function recovery after SCI. This occurred through a mechanism in which LGG-CM inhibited the NF- $\kappa$ B pathway by reducing the phosphorylation of I $\kappa$ B $\alpha$ , which promoted microglia/macrophage polarization to M2 and inhibited polarization to M1. Thus, LGG-CM is expected to be a candidate therapeutic drug for exerting neuroprotection after SCI.

## Data Availability

The data used to support the findings of this study are included within the article.

## Conflicts of Interest

The authors declare no conflict of interest.

## Authors' Contributions

F.L. carried out the experiments, and drafted the manuscript. B.Z. performed the statistical analysis, and helped to perform the experiments. J.X. and X.L. advised on the experimental procedures, and designed the study. Q.S., J. L. and X.W. helped to perform the experiments. All authors have read and approved the final manuscript.

## Acknowledgments

This work is supported by the National Natural Science Foundation of China (81672217).

## References

- [1] B. T. Lang, J. M. Cregg, M. A. DePaul et al., "Modulation of the proteoglycan receptor PTP $\sigma$  promotes recovery after spinal cord injury," *Nature*, vol. 518, no. 7539, pp. 404–408, 2015.
- [2] M. S. Beattie, "Inflammation and apoptosis: linked therapeutic targets in spinal cord injury," *Trends in Molecular Medicine*, vol. 10, no. 12, pp. 580–583, 2004.
- [3] R. Galeiras Vázquez, P. Rascado Sedes, M. Mourelo Fariña, A. Montoto Marqués, and M. E. Ferreira Velasco, "Respiratory management in the patient with spinal cord injury," *BioMed Research International*, vol. 2013, Article ID 168757, 2013.
- [4] C. Wang, Q. Wang, Y. Lou et al., "Salidroside attenuates neuroinflammation and improves functional recovery after spinal cord injury through microglia polarization regulation," *Journal of Cellular and Molecular Medicine*, vol. 22, no. 2, pp. 1148–1166, 2018.
- [5] M. Teşiorowski, T. Potaczek, B. Jasiewicz, J. Sapa, and M. Zygmunt, "Metylprednizolon – ostre urazy rdzeniarkęgowego, korzyści czy zagrożenia?," *Postępy Higieny i Medycyny Doświadczalnej*, vol. 67, pp. 601–609, 2013.
- [6] E. Hayta and H. Elden, "Acute spinal cord injury: a review of pathophysiology and potential of non-steroidal anti-inflammatory drugs for pharmacological intervention," *Journal of Chemical Neuroanatomy*, vol. 87, pp. 25–31, 2018.
- [7] L. L. Wu, X. M. Pan, H. H. Chen, X. Y. Fu, J. Jiang, and M. X. Ding, "Repairing and analgesic effects of umbilical cord mesenchymal stem cell transplantation in mice with spinal cord injury," *BioMed Research International*, vol. 2020, Article ID 7650354, 2020.
- [8] BioMed Research International, "Retracted: study of effect of salvianolic acid B on motor function recovery in rats with spinal cord injury," *BioMed Research International*, vol. 2017, Article ID 8234878, 2017.
- [9] E. Talamonti, A. M. Pauter, A. Asadi, A. W. Fischer, V. Chiurchiù, and A. Jacobsson, "Impairment of systemic DHA synthesis affects microglia/macrophage plasticity and polarization: implications for DHA supplementation during inflammation," *Cellular and Molecular Life Sciences*, vol. 74, no. 15, pp. 2815–2826, 2017.
- [10] O. Manzhulo, A. Tyrtysnaia, Y. Kipyryushina, I. Dyuzhen, and I. Manzhulo, "Docosahexaenoic acid induces changes in microglia/macrophage polarization after spinal cord injury in rats," *Acta Histochemica*, vol. 120, no. 8, pp. 741–747, 2018.
- [11] A. Etzerodt and S. K. Moestrup, "CD163 and inflammation: biological, diagnostic, and therapeutic aspects," *Antioxidants & Redox Signaling*, vol. 18, no. 17, pp. 2352–2363, 2013.
- [12] R. Yang, J. He, and Y. Wang, "Activation of the niacin receptor HCA<sub>2</sub> reduces demyelination and neurofilament loss, and promotes functional recovery after spinal cord injury in mice," *European Journal of Pharmacology*, vol. 791, pp. 124–136, 2016.
- [13] R. Parsa, P. Andresen, A. Gillett et al., "Adoptive transfer of immunomodulatory M2 microglia/macrophages prevents type 1 diabetes in NOD mice," *Diabetes*, vol. 61, no. 11, pp. 2881–2892, 2012.
- [14] Y. Wang, Y. P. Wang, G. Zheng et al., "Ex vivo programmed macrophages ameliorate experimental chronic inflammatory renal disease," *Kidney International*, vol. 72, no. 3, pp. 290–299, 2007.
- [15] X. M. Zhang, H. Lund, S. Mia, R. Parsa, and R. A. Harris, "Adoptive transfer of cytokine-induced immunomodulatory adult microglia attenuates experimental autoimmune encephalomyelitis in DBA/1 mice," *Glia*, vol. 62, no. 5, pp. 804–817, 2014.
- [16] D. Han, Z. Yu, W. Liu et al., "Plasma hemopexin ameliorates murine spinal cord injury by switching microglia from the

## Retraction

# Retracted: The Prognostic Value of Leucine-Rich $\alpha 2$ Glycoprotein 1 in Pediatric Spinal Cord Injury

### BioMed Research International

Received 12 March 2024; Accepted 12 March 2024; Published 20 March 2024

Copyright © 2024 BioMed Research International. This is an open access article distributed under the Creative Commons Attribution License, which permits unrestricted use, distribution, and reproduction in any medium, provided the original work is properly cited.

This article has been retracted by Hindawi following an investigation undertaken by the publisher [1]. This investigation has uncovered evidence of one or more of the following indicators of systematic manipulation of the publication process:

- (1) Discrepancies in scope
- (2) Discrepancies in the description of the research reported
- (3) Discrepancies between the availability of data and the research described
- (4) Inappropriate citations
- (5) Incoherent, meaningless and/or irrelevant content included in the article
- (6) Manipulated or compromised peer review

The presence of these indicators undermines our confidence in the integrity of the article's content and we cannot, therefore, vouch for its reliability. Please note that this notice is intended solely to alert readers that the content of this article is unreliable. We have not investigated whether authors were aware of or involved in the systematic manipulation of the publication process.

Wiley and Hindawi regrets that the usual quality checks did not identify these issues before publication and have since put additional measures in place to safeguard research integrity.

We wish to credit our own Research Integrity and Research Publishing teams and anonymous and named external researchers and research integrity experts for contributing to this investigation.




The corresponding author, as the representative of all authors, has been given the opportunity to register their agreement or disagreement to this retraction. We have kept a record of any response received.

### References

- [1] H. Ma, F. Lu, Y. Guo, Z. Shen, and Y. Chen, "The Prognostic Value of Leucine-Rich  $\alpha 2$  Glycoprotein 1 in Pediatric Spinal Cord Injury," *BioMed Research International*, vol. 2021, Article ID 7365204, 5 pages, 2021.

## Research Article

# The Prognostic Value of Leucine-Rich $\alpha 2$ Glycoprotein 1 in Pediatric Spinal Cord Injury

Hong Ma,<sup>1</sup> Fengshan Lu,<sup>1</sup> Yueming Guo ,<sup>1</sup> Zhaoxiong Shen ,<sup>1</sup> and Yuanzhen Chen <sup>2</sup>

<sup>1</sup>Foshan Hospital of Traditional Chinese Medicine, Foshan, 528000 Guangdong Province, China

<sup>2</sup>Neck-Shoulder and Lumbocrural Pain Hospital, Shandong First Medical University & Shandong Academy of Medical Sciences, Jinan, 250014 Shandong Province, China

Correspondence should be addressed to Yueming Guo; guo\_yueming2008@126.com, Zhaoxiong Shen; 591340219@qq.com, and Yuanzhen Chen; chenyanzhen2011@163.com

Received 21 May 2021; Accepted 26 June 2021; Published 9 July 2021

Academic Editor: Yuzhen Xu

Copyright © 2021 Hong Ma et al. This is an open access article distributed under the Creative Commons Attribution License, which permits unrestricted use, distribution, and reproduction in any medium, provided the original work is properly cited.

**Objective.** Leucine-rich  $\alpha 2$  glycoprotein 1 (LRG1) is a novel cytokine, which is believed to be involved in the inflammatory process of a series of diseases. However, the relationship between LRG1 and spinal cord injury (SCI) has not been reported. The purpose of our study is to determine the predictive value of LRG1 for the prognosis of pediatric SCI (PSCI). **Methods.** This study recruited 64 patients with confirmed PSCI and 40 healthy controls at Foshan Traditional Chinese Medicine Hospital from January 2016 to December 2020. The clinical information of all participants at the time of admission was recorded. Peripheral blood was collected, and commercial reagents were used to detect the level of serum LRG1. At the same time, the International Standards for Neurological Classification of Spinal Cord Injury (ISNCSCI) was used to assess the severity of PSCI. **Results.** All participants were divided into PSCI group ( $n = 64$ ) and NC group ( $n = 40$ ). There was no significant difference in clinical information (age, gender, heart rate, systolic blood pressure, diastolic blood pressure, sampling time from injury, white blood cells, and C-reactive protein) between the two groups ( $p > 0.05$ ). According to the interquartile range of serum LRG1, we compared the motor and sensory scores of ISNCSCI and found that serum LRG1 levels were negatively correlated with the prognosis of PSCI patients ( $p < 0.001$ ). The results of receiver operating curve (ROC) showed that the sensitivity, specificity, and AUC (Area Under the Curve) of serum LRG1 level in predicting the prognosis of PSCI were 68.4%, 69.1%, and 0.705, respectively. The cut-off value of serum LRG1 level predicting the prognosis of PSCI is 21.1  $\mu\text{g/ml}$ . **Conclusions.** Serum LRG1 level is significantly increased in PSCI patients, and the elevated LRG1 level is negatively correlated with the prognosis of PSCI patients. Serum LRG1 may be a potentially useful biomarker for predicting PSCI.

## 1. Introduction

Spinal cord injury (SCI) can be defined as complete or incomplete damage to motor function, sensory function, autonomic nerves, reflexes, etc. caused by spinal cord structure or function damage [1, 2]. In the United States, there are approximately 17,000 new cases of SCI patients each year, and reports on the incidence of SCI in China range from 25 per million to 60 per million [3, 4]. It is estimated that the total annual cost of SCI in Australia is about 2 billion Australian dollars, and as the life expectancy of SCI patients increases, the economic burden caused by it has become heavier [5]. Among children, the incidence of SCI is relatively

low, and the reported incidence in the United States is 1.99 per 100,000 [6, 7]. In addition to rehabilitation, there is currently a lack of effective cures for SCI [8]. Therefore, looking for early targets to predict the prognosis of SCI may be of great significance to the prevention and treatment of SCI.

Leucine-rich  $\alpha 2$ -glycoprotein 1 is a glycoprotein with a molecular weight of 38-50 kDa encoded by the LRG1 gene [9]. It was first identified in human serum by German scientists Haupt and Baudner in 1977 [10]. LRG1 is composed of 312 amino acid residues, 66 of which are leucine residues. Its leucine-rich repeat sequence family provides a functional domain for protein interaction, which provides the possibility to exert a variety of biological functions in vivo and



in vitro [11]. LRG1 is widely distributed in the body, and it is reported to be expressed in endothelial cells, neutrophils, macrophages, and hepatocytes [12]. However, in the central nervous system, LRG1 is mainly expressed in the deep cortex, vasculature, and astrocytes, and its expression increases with age [13]. LRG1 is involved in and is increasingly expressed in various physiological reactions, especially inflammation-related reactions [14]. However, the regulation and pathogenic mechanism of LRG1 is not yet fully understood.

In recent years, the role of LRG1 in neurological diseases has been gradually discovered. LRG1 is likely to become a neurobiomarker with clinical application potential. The purpose of our study is to determine whether LRG1 can be used as an indicator for the diagnosis of PSCI. If the correlation between LRG1 and PSCI is confirmed, it will provide a new way for the early diagnosis and effective prevention and treatment of PSCI.

## 2. Methods

**2.1. The Participant.** From January 2016 to December 2020, 64 PSCI patients and 40 healthy controls who were treated in Foshan Hospital of Traditional Chinese Medicine were continuously included in the study. The diagnosis of SCI is based on the diagnostic criteria established by the guidelines [15, 16]. The PSCI entry criteria are as follows: (1) age between 6 and 15 years, (2) met the diagnostic criteria of SCI and the onset of SCI within 24 hours, (3) clear consciousness, and (4) stable vital signs. The PSCI exclusion criteria are as follows: (1) with a history of brain injury, (2) with a history of mental illness, (3) with a physical disability, (4) with a history of congenital cerebral palsy and epilepsy, (5) with a history of dementia or speech disorder, and (6) with malignant tumors or severe infections. All participants or their guardians were informed of the purpose and plan of the study and signed a consent form. The study was approved by Foshan Hospital of Traditional Chinese Medicine. And this clinical study complies with the Declaration of Helsinki.

**2.2. Clinical Information.** Once a participant is enrolled in the group, their clinical information is collected. The clinical information includes age, gender, heart rate, body temperature, and blood pressure. We also collect peripheral blood and use the standard biochemical method of the hospital laboratory to detect the concentration of white blood cells and C-reactive protein. At the same time, we record the time from the patient's injury to the sample collection.

**2.3. Serum LRG1 Concentration.** The venous blood of the participants was collected in a serum separation tube (SST) immediately after enrollment. The sample was allowed to clot for 2 hours at room temperature or overnight at 4°C and then centrifuged at 1000 g in a low-temperature centrifuge for 15 minutes. The serum was taken out and used immediately in the experiment. The samples can also be stored in aliquots at -80°C to avoid damage to the samples caused by repeated freezing. Serum LRG1 was detected by enzyme-linked immunosorbent assay (ELISA), and the reagents were purchased from a biological reagent company (Mybioscience, Beverly,

TABLE 1: The clinical information of all participants.

	NC ( $n = 40$ )	PSCI ( $n = 64$ )	$p$
Age (years)	9.3 ± 2.1	9.5 ± 2.3	0.657
Gender, male/female	29/11	42/22	0.464
HR (beats/min)	80.4 ± 7.6	79.8 ± 8.1	0.708
Body temperature (°C)	36.5 ± 0.2	36.6 ± 0.3	0.065
SBP (mmHg)	101.7 ± 8.9	102.0 ± 8.4	0.863
DBP (mmHg)	72.2 ± 6.5	72.3 ± 6.7	0.940
Sampling time from injury (h)	3.4 ± 1.9	3.6 ± 2.3	0.646
WBC ( $10^9/L$ )	7.4 ± 1.2	7.7 ± 1.3	0.241
CRP ( $\mu g/ml$ )	4.3 ± 0.7	4.5 ± 0.6	0.124
LRG1 ( $\mu g/ml$ )	18.3 ± 3.7	25.4 ± 3.2	<0.001

HR: heart rate; SBP: systolic blood pressure; DBP: diastolic blood pressure; WBC: white blood cells; CRP: C-reactive protein; LRG1: leucine-rich  $\alpha 2$  glycoprotein 1.

MA, USA). For the ELISA test of each serum sample, we take 3 replicate wells. The experimental procedures of ELISA are based on the instructions of the reagents.

**2.4. Motor and Sensory Scores of PSCI Patients.** The International Standards for Neurological Classification of Spinal Cord Injury (ISNCSCI) established by The American Spinal Injury Association (ASIA) is a general standard for evaluating the severity of spinal cord injury [17]. Our study also used this method to evaluate the degree of motor and sensory impairment of PSCI. The total scores of the motor function and sensory scores in ISNCSCI are 100 points and 224 points, respectively. The higher the score, the less severe the damage. According to the degree of damage to sensory and motor functions, SCI can be divided into five grades: Grades A, B, C, D, and E. From A to E, Grade A has the heaviest damage and Grade E has the least damage. Each side of the body is scored independently.

**2.5. Statistical Analysis.** The statistics of the data was obtained using SPSS 20.0 (SPSS Inc., Chicago, IL, USA). The description of continuous variables uses the mean ± standard deviation (SD), and the description of categorical variables uses numbers or percentages (%). The comparison of continuous variables between the two groups uses the  $t$  test, while the comparison of categorical variables uses the chi-square test. In the regression model, the trend test of the quartile of serum LRG1 was analyzed by entering the quartile as the ordinal number. The cut-off value of serum LRG1 as a biomarker for the prognosis of PSCI patients was calculated according to Youden's index. Two-tailed  $p < 0.05$  was used as a statistically significant standard.

## 3. Results

**3.1. The Clinical Information of All Participants.** The results of the clinical information of all participants are shown in Table 1. The clinical information includes age, gender, heart rate, body temperature, systolic blood pressure, diastolic

TABLE 2: Relationship between serum LRG1 and PSCI.

Variable	Serum LRG1 levels ( $\mu\text{g/ml}$ )				<i>P</i>
	Q1	Q2	Q3	Q4	
ASIA sensation score	148.2 $\pm$ 19.3	142.1 $\pm$ 16.4	133.5 $\pm$ 12.6	125.9 $\pm$ 11.0	<0.001
ASIA motor score	81.7 $\pm$ 8.5	76.3 $\pm$ 6.1	69.8 $\pm$ 5.7	63.4 $\pm$ 4.9	<0.001

LRG1: leucine-rich  $\alpha 2$  glycoprotein 1; PSCI: pediatric spinal cord injury; ASIA: American Spinal Injury Association.

blood pressure, time from injury to sampling, white blood cells, C-reactive protein, and serum LRG1 concentration. The results showed that there was no statistically significant difference between the age, gender, heart rate, body temperature, systolic blood pressure, diastolic blood pressure, time from injury to sampling, white blood cells, and C-reactive protein between the PSCI group and the NC group ( $p > 0.05$ ). The serum LRG1 concentration of the PSCI group and NC group was  $18.3 \pm 3.7 \mu\text{g/ml}$  and  $25.4 \pm 3.2 \mu\text{g/ml}$ , respectively. The concentration of serum LRG1 in the PSCI group was significantly higher than that in the NC group ( $p < 0.001$ ).

**3.2. Relationship between Serum LRG1 and PSCI.** According to the serum LRG1 quantile, the ASIA sensory and motor function scores of PSCI patients are shown in Table 2. The results showed that the ASIA sensory and motor function scores of PSCI patients had a linear relationship with the serum LRG1 quantile; that is, the ASIA sensory and motor function scores of PSCI patients decreased with the increase of serum CCL21 levels ( $p < 0.001$ ).

**3.3. ROC Curve Analysis.** In order to evaluate serum LRG1 as a potential biomarker for the diagnosis of PSCI, we performed receiver operating characteristic (ROC) curve analysis. The ROC curve is shown in Figure 1. The results showed that the sensitivity and specificity of serum LRG1 in diagnosing PSCI were 68.4% and 69.1%, and the area under the curve was 0.705. The diagnostic cut-off value of serum LRG1 calculated using Youden's index was  $21.1 \mu\text{g/ml}$ .

## 4. Discussions

The main finding of this study is that compared with that in the NC group, the serum LRG1 concentration in the PSCI group was significantly higher, and the serum LRG1 concentration was inversely correlated with the AISA motor and sensory function scores. Further studies have found that serum LRG1 may be used as an early biomarker for diagnosing the prognosis of PSCI. Our study confirmed for the first time that the serum LRG1 concentration of PSCI patients is correlated with the prognosis of sensory and motor function.

Recent studies have shown that LRG1 is closely related to the pathogenesis of a variety of tumors. Andersen and colleagues found that serum LRG1 levels in patients with ovarian cancer were significantly increased, and it was moderately correlated with the traditional tumor marker CA125 [18]. Kakisaka et al. reported the first increase in plasma LRG1 levels in patients with pancreatic cancer through plasma proteomics technology and verified this

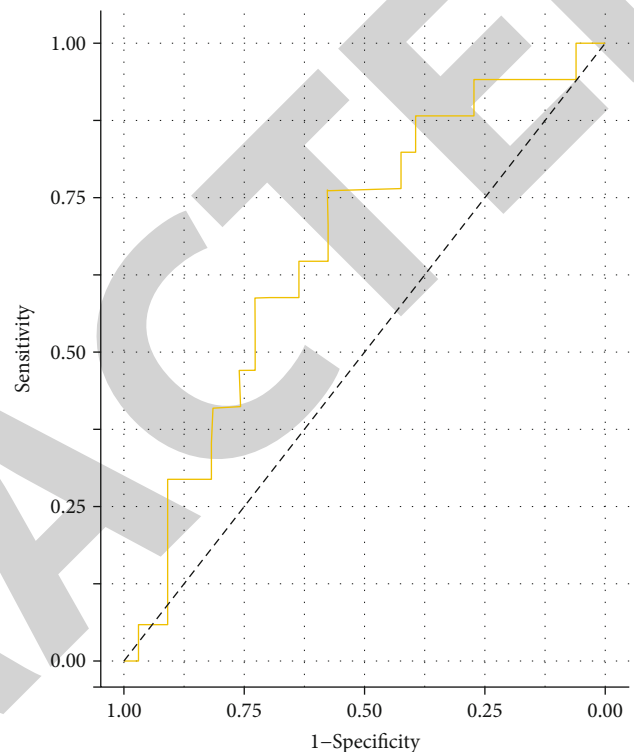


FIGURE 1: ROC curve analysis for serum LRG1 levels as a potential biomarker for the diagnosis of PSCI. ROC: operating characteristic curve; LRG1: leucine-rich  $\alpha 2$  glycoprotein 1; PSCI: pediatric spinal cord injury.

new finding through Western blotting [19]. Scholars from China have found that LRG1 is elevated in patients with colorectal cancer and may act as a tumor promoter, which is consistent with the conclusions of Japanese scholars [20, 21]. In addition, the latest research results show that LRG1 can predict the diagnosis and prognosis of glioblastoma, and it has the potential to become a biomarker of glioblastoma [22].

In addition to tumors, the role of LRG1 in immune system diseases and inflammation has gradually gained attention. Serada's team found that LRG concentration is closely related to the disease activity of ulcerative colitis, and its mechanism may involve an IL-6 independent pathway [23]. This result suggests that LRG can be used as a new serum biomarker for monitoring the disease activity of ulcerative colitis. On this basis, Japanese scholar Shinichiro Shinzaki further concluded that serum LRG can be used as a biomarker for mucosal repair in the course of ulcerative colitis disease activity [24]. LRG not only in peripheral blood but also in saliva can also be used as a noninvasive biomarker



of airway inflammation in asthma patients [25]. In humans, the serum LRG level of pulmonary tuberculosis patients is significantly increased, but decreased after anti-tuberculosis treatment [26]. These findings indicate that LRG is a promising biomarker for predicting pulmonary tuberculosis activity. A study in South Korea showed that serum LRG may be a new biomarker for evaluating the inflammatory activity of patients with rheumatoid arthritis, and it may be involved in the inflammatory process independently of TNF- $\alpha$  [27]. Unlike the above results, a Brazilian study showed that serum LRG1 cannot be used as a biomarker for the diagnosis of appendicitis [28]. Interestingly, another study on LRG1 and appendicitis in the United States showed that urine LRG1 can distinguish patients with acute appendicitis from patients with nonacute appendicitis [29].

There are also reports on the involvement of LRG1 in neurological diseases. Research from Fukuoka Children's Hospital shows that LRG1 in cerebrospinal fluid can be used as a potential inflammatory biomarker for meningitis [30]. The research of Juntendo University suggests that the cerebrospinal fluid organism LRG1 may be a potential biomarker for diagnosing idiopathic normal pressure hydrocephalus [31]. The level of LRG1 in the cerebrospinal fluid of patients with Parkinson's disease combined with dementia (PDD) and progressive supranuclear palsy (PSP) is significantly increased, while the deposition of LRG1 in the cerebral cortex increases with age. Further observation of transgenic mice overexpressing LRG1 can show neuronal degeneration and decline, suggesting that LRG1 is involved in the process of neurodegenerative diseases [32]. Malaysian scholars have found that serum LRG1 levels in patients with severe traumatic brain injury are elevated, suggesting that it can be used as a biomarker for assessing the severity of traumatic brain injury [33]. In addition, LRG1 is also believed to be related to diabetes, myocardial ischemia, and infarction [34, 35]. However, the role of LRG1 in PSCI has not been reported yet.

Our study confirmed for the first time that the serum LRG1 level of PSCI patients is related to the prognosis. Nevertheless, our research has some limitations. First of all, our patients are confined to southern China, and the sample size is small. Secondly, we did not dynamically monitor the level of serum LRG1. Thirdly, we have not done a long-term follow-up study of serum LRG1 and the prognosis of PSCI. Fourthly, we did not detect the level of LRG1 in cerebrospinal fluid. Finally, we did not conduct research on the mechanism of LRG1 involved in the pathogenesis of PSCI.

## 5. Conclusions

Our research shows that serum LRG1 levels in PSCI patients are significantly increased, which is significantly related to the motor and sensory scores of spinal cord injury. In other words, the more severe the motor and sensory function of spinal cord injury is, the higher the serum LRG1 level. At the same time, serum LRG1 can be used as a biomarker for the diagnosis of PSCI. This conclusion is worthy of our further confirmation and may provide a new way for the treatment of PSCI.

## Data Availability

The data used to support the findings of this study are available from the corresponding authors upon request.

## Conflicts of Interest

All the authors declare no conflict of interests.

## Authors' Contributions

Yueming Guo, Zhaoxiong Shen, and Yuanzhen Chen are the corresponding authors.

## References

- [1] Y. Chen, L. Liang, S. Cao et al., "Serum CCL21 as a potential biomarker for cognitive impairment in spinal cord injury," *BioMed Research International*, vol. 2020, Article ID 6692802, 5 pages, 2020.
- [2] N. Wang, Y. Yang, M. Pang et al., "MicroRNA-135a-5p promotes the functional recovery of spinal cord injury by targeting SP1 and rock," *Molecular Therapy - Nucleic Acids*, vol. 22, pp. 1063–1077, 2020.
- [3] S. Yuan, Z. Shi, F. Cao, J. Li, and S. Feng, "Epidemiological features of spinal cord injury in China: a systematic review," *Frontiers in Neurology*, vol. 9, p. 683, 2018.
- [4] Y. Chen, D. Wang, S. Cao, G. Hou, H. Ma, and B. Shi, "Association between serum IL-37 and spinal cord injury: a prospective observational study," *BioMed Research International*, vol. 2020, Article ID 6664313, 5 pages, 2020.
- [5] B. P. Vaikuntam, J. W. Middleton, P. McElduff et al., "Identifying predictors of higher acute care costs for patients with traumatic spinal cord injury and modeling acute care pathway redesign: a record linkage study," *Spine*, vol. 44, no. 16, pp. E974–E983, 2019.
- [6] H. Darain, A. Arsh, A. Zeb, S. Muhammad Ilyas, D. Muhammad, and M. Naseem Khan, "Epidemiology, clinical features and consequences of spinal cord injury in children," *Journal of the College of Physicians and Surgeons-Pakistan : JCPSP*, vol. 28, no. 7, pp. 532–535, 2018.
- [7] K. Zebracki, M. Hwang, P. L. Patt, and L. C. Vogel, "Autonomic cardiovascular dysfunction and vitamin D deficiency in pediatric spinal cord injury," *Journal of Pediatric Rehabilitation Medicine*, vol. 6, no. 1, pp. 45–52, 2013.
- [8] N. Wang, L. He, Y. Yang et al., "Integrated analysis of competing endogenous RNA (ceRNA) networks in subacute stage of spinal cord injury," *Gene*, vol. 726, p. 144171, 2020.
- [9] C. Akiba, M. Nakajima, M. Miyajima et al., "Leucine-rich  $\alpha$ 2-glycoprotein overexpression in the brain contributes to memory impairment," *Neurobiology of Aging*, vol. 60, pp. 11–19, 2017.
- [10] H. Haupt and S. Baudner, "Isolierung und charakterisierung eines bisher unbekanntes leucinreichen 3.1S- $\alpha$ 2-Glykoproteins aus humanserum," *Hoppe-Seyler's Zeitschrift für physiologische Chemie*, vol. 358, no. 1, pp. 639–646, 1977.
- [11] Y. Yang, R. Luo, Y. Cheng et al., "Leucine-rich  $\alpha$ 2-glycoprotein-1 upregulation in plasma and kidney of patients with lupus nephritis," *BMC Nephrology*, vol. 21, no. 1, p. 122, 2020.
- [12] L. J. Druhan, A. Lance, S. Li et al., "Leucine rich  $\alpha$ -2 glycoprotein: a novel neutrophil granule protein and modulator of myelopoiesis," *PLoS One*, vol. 12, no. 1, article e0170261, 2017.

## Research Article

# A Single-Center Clinical Study to Evaluate Shenxiong Glucose Injection Combined with Edaravone in the Treatment of Acute Large-Area Cerebral Infarction

Zongqin Li <sup>1</sup>, Xiaoxia Rong,<sup>2</sup> Jun Luo,<sup>1</sup> Tao Zeng,<sup>3</sup> Pan Huang <sup>4</sup>, and Xuejie Xu <sup>1</sup>

<sup>1</sup>Department of Neurology, The Sichuan Mianyang 404 Hospital, No. 56 Yuejin Road, Mianyang, Sichuan, China

<sup>2</sup>Department of Operations Management Division, The Sichuan Mianyang 404 Hospital, No. 56 Yuejin Road, Mianyang, China

<sup>3</sup>Department of Thoracic Surgery, The Sichuan Mianyang 404 Hospital, No. 56 Yuejin Road, Mianyang, China

<sup>4</sup>Pan Huang's department is Neurology, Deyang People's Hospital, 173 Taishan North Road, Deyang, China

Correspondence should be addressed to Xuejie Xu; xuxj404@126.com

Received 18 March 2021; Revised 27 May 2021; Accepted 21 June 2021; Published 30 June 2021

Academic Editor: Qian Wang

Copyright © 2021 Zongqin Li et al. This is an open access article distributed under the Creative Commons Attribution License, which permits unrestricted use, distribution, and reproduction in any medium, provided the original work is properly cited.

**Objectives.** To investigate the clinical efficacy and safety of Shenxiong glucose injection combined with edaravone in the treatment of acute large-area cerebral infarction. **Methods.** 156 patients with acute large-area cerebral infarction admitted to our hospital from July 2015 to January 2017 were included in the analysis. The patients were randomly divided into experimental (78 cases) and control (78 cases) groups. Patients in the experimental group were given a 30 mg injection of edaravone in 100 ml of 0.9% sodium chloride solution by intravenous drip, twice a day within 30 minutes and a daily 200 ml injection of Shenxiong glucose by intravenous drip. Patients in the control group were given a 30 mg edaravone injection in 100 ml of 0.9% sodium chloride solution by intravenous drip, twice a day, and the drip was completed within 30 minutes. Patients in both groups were treated for 2 weeks. The levels of fibrinogen (FIB), D-dimer, interleukin 6 (IL-6), P-selectin (CD62P), and hypersensitive C-reactive protein (hs-CRP) were evaluated in the two groups of patients. Neurological disability was evaluated using the modified Rankin scale (mRS) and the neurological deficit score (National Institute of Health Stroke Scale, NIHSS). Adverse reactions to the treatments were also recorded. **Results.** No significant differences in age, gender, medical histories, and blood biochemical indices were observed between the two groups before treatment ( $P > 0.05$ ). After treatment, the levels of FIB, D-dimer, IL-6, CD62P, and hs-CRP were significantly lower following treatment and compared to the control group ( $P < 0.05$ ). Also, the mRS and NIHSS scores were significantly lower after treatment and compared with the control group ( $P < 0.05$ ). The total effective rate of the treatment in the experimental group was significantly higher compared to the control group ( $P < 0.05$ ). During the treatment period, no obvious adverse reactions were observed in the two groups of patients. **Conclusions.** In addition to the routine basic treatment of acute large-area cerebral infarction, the addition of Shenxiong glucose injection combined with edaravone injection can improve platelet aggregation and reduce inflammation by affecting P-selectin, D-dimer, and FIB. This treatment approach promotes the recovery of nerve defect function without obvious adverse reactions in patients with acute large-area cerebral infarction.

## 1. Introduction

Recent epidemiological studies have shown that cerebrovascular diseases have surpassed cancer as the number one cause of death in humans. The pathophysiological processes involved in the development of strokes are irreversible, and so the disease has a very high rate of disability that imposes a major public health burden in China [1]. Currently, arterial

and venous thrombolysis and mechanical thrombectomy techniques have delivered improved outcomes for the majority of patients with acute cerebral infarction. However, for patients who cannot be treated with thrombolysis or mechanical thrombectomy, conservative medications are mainly adopted that include supportive therapy, improvement of ischemia tissue perfusion, and protection of brain cells [2, 3].

Edaravone is a free radical scavenger that can be used to protect the brain from injury by improving cerebral blood flow around the infarct and inhibiting lipid peroxidation [4]. The main components of Shenxiong glucose injection are Danshensu and ligustrazine hydrochloride which affects antiplatelet aggregation and dilation of the coronary artery and improves the microcirculation [5]. To date, there have been no reports on the efficacy and safety of these drugs in combination in the treatment of acute large-area cerebral infarction. This study is aimed at exploring the clinical efficacy, mechanism, and potential use of Shenxiong glucose injection combined with edaravone injection in the treatment of large-area cerebral infarction.

## 2. Information and Methods

**2.1. Experiment Methods.** The experiment method is a prospective randomized controlled study.

**2.2. Inclusion Criteria.** The inclusion criteria are as follows: (1) acute cerebral infarction caused on the basis of arteriosclerosis, diabetes, and hypertension, that is, TOAST classification is aortic atherosclerosis; (2) onset time < 48 d; (3) patients with first onset; and (4) all patients were diagnosed with large-area cerebral infarction by MRI or CT examination. Large area is defined as the largest slice diameter of cerebral infarction measured by MRI, or CT examination is greater than 5.0 cm, or the infarction spreads to two brain lobes, or the spread of cerebral infarction is larger than 1/2 or 2/3 of the area on the same side.

**2.3. Exclusion Criteria.** The exclusion criteria are as follows: (1) severe dementia, (2) severe mental symptoms or mental illness who cannot cooperate, (3) severe liver and kidney failure, (4) heart disease, (5) combined severe infection, and (6) those who are allergic to the drugs used in this study.

**2.4. Research Subjects Selected.** This study included 156 patients admitted to the Sichuan Mianyang 404 Hospital from July 2015 to January 2017 with acute large-area cerebral infarction. All patients met the diagnostic criteria for cerebral infarction in the Acute Ischemic Stroke Treatment Guidelines [6]. Using the random table method, all patients were randomized into experimental (78 cases) and control groups (78 cases). The experimental group consisted of 42 males and 36 females, aged between 50 and 80 years with an average of 61.74 ( $\pm 4.67$ ) years. The experimental group consisted of 44 males and 34 females, aged between 52 and 81 years with an average age of 62.82 ( $\pm 4.83$ ) years. No significant differences in the general patient characteristics were observed between the two groups ( $P > 0.05$ ). The time from onset to admission for blood collection in both groups ranged from 1 to 48 hours with an average time of 18.25 ( $\pm 1.14$ ) hours. The research protocol was reviewed and approved by the medical ethics committee of the hospital, and all participants were recruited under written informed consent document. The experimental flow used in the study is shown in Figure 1.

**2.5. Treatment Methods.** After admission, the two groups of patients were dehydrated to reduce cerebral edema and

treated with antiplatelet aggregation and other basic treatments. In addition to the basic treatment, patients in the experimental group were given a 30 mg edaravone injection in 100 ml of 0.9% sodium chloride solution by intravenous drip, twice a day within 30 minutes and a daily injection of 200 ml of Shenxiong glucose. Patients in the control group were given a 30 mg injection of edaravone in 100 ml of 0.9% sodium chloride solution by intravenous drip, twice a day within 30 minutes, and treatment was continued for two weeks. The Shenxiong glucose injection was obtained from the Guizhou Yibai Injection Pharmaceutical Co., Ltd. (Approval Number: National Medicine Zhunzi H52020703, specification 100 ml/bottle). The edaravone injection was obtained from the Sinopharm Guorui Pharmaceutical Co., Ltd. (Approval Number: National Medicine Standard H20080056, specification 20 ml: 30 mg).

**2.6. Specimen Collection and Testing.** All blood samples were collected from the anterior cubital venous blood on an empty stomach within 24 hours after admission. The plasma was separated and extracted by the EDTA anticoagulant tube. The serum was separated and extracted from the tube without anticoagulant and stored in a freezer at  $-20^{\circ}\text{C}$ . The serum levels of CD62p were determined by flow cytometry (American Applied Biosystems). A flow cytometry kit was used for analysis (Shanghai Xuanhao Technology Co., Ltd) according to the manufacturer's instructions. Serum D-dimer levels were detected using a magnetic bead method (normal value =  $0-1 \mu\text{g/ml}$ ). Serum hs-CRP levels were determined using an immunoturbidimetric method with a Deling's BN-Prospec special protein instrument for detection. IL-6 levels were determined by ELISA using test kits purchased from the R&D company production.

**2.7. Observation Indices.** The neurological deficit scores of the two groups were obtained before and after treatment which included the mRS and NIHSS scores. The levels of P-selectin (CD62P), D-dimer, hs-CRP, IL-6, and FIB were evaluated before and after treatment in the two groups. The occurrence of adverse reactions was also recorded in the two groups.

**2.8. Efficacy Evaluation [6].** The efficacy of treatment was defined as follows: (1) cure: when the degree of disability was zero, and the NIHSS score was reduced by  $\geq 90\%$  compared to that before treatment; (2) significantly effective: when the degree of disability was one to three, and the NIHSS score was reduced by  $46\% - < 90\%$  compared to that before treatment; (3) effective: when the degree of disability was one to three, and the NIHSS score was reduced by  $> 18\% - 45\%$  compared to before treatment; (4) ineffective: when the symptoms of the patient and signs of disease did not change significantly or worsened before and after medication, and when the NIHSS score was reduced by  $\leq 18\%$  compared to before treatment; and (5) totally effective: when the cure + markedly effective + effective.

**2.9. Statistical Analysis.** The SPSS 21.0 software was used for statistical analysis. Measurement data were expressed as  $\bar{x} \pm s$  and analyzed using a  $t$ -test. Counting data were expressed as

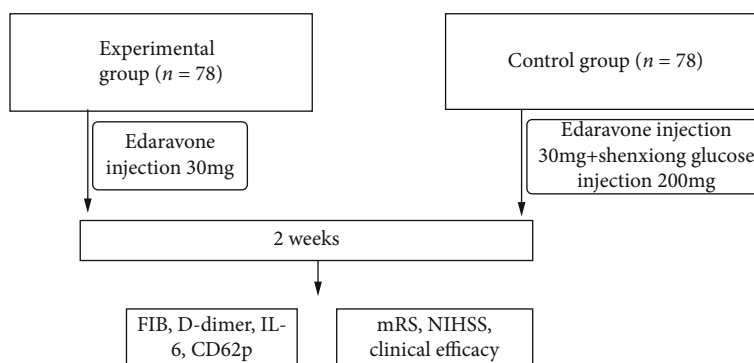


FIGURE 1: The experimental flow chart.

the number of cases and analyzed using a  $\chi^2$  test. Grade data were expressed as the number of cases or rates and analyzed using a rank-sum test.  $P$  values  $< 0.05$  were used to indicate statistical significance.

### 3. Results

**3.1. Comparison of General Data in the Two Patient Groups before Treatment.** No significant differences were detected in the age, past medical histories, and blood biochemical examinations between the two groups before treatment ( $P > 0.05$ ). The patient characteristics are summarized in Table 1.

There was no significant difference in age, past medical history, and blood biochemical examinations between the two groups before treatment ( $P > 0.05$ ), indicating that the two groups are comparable (Table 1).

**3.2. Comparison of CD62P, D-Dimer, IL-6, FIB, and hs-CRP Levels before and after Treatment in the Two Patient Groups.** Before treatment, the two groups of patients had no significant differences in the levels of CD62P, D-dimer, hs-CRP, FIB, and IL-6 ( $P > 0.05$ ). After treatment, the levels of these biomarkers were all significantly lower than before treatment ( $P < 0.05$ ) with larger decreases observed in the experimental group. The data are summarized in Table 2.

**3.3. Comparison of the Neurological Deficit Scores between the Two Groups before and after Treatment.** Before treatment, no significant differences were observed between the mRS and NIHSS scores of the two groups of patients ( $P > 0.05$ ). After treatment, the mRS and NIHSS scores of the two groups of patients were significantly lower than before treatment. The level of improvement in each score in the experimental group was significantly higher than in the control group ( $P < 0.05$ ). The data are summarized in Table 3.

**3.4. Comparison of Clinical Efficacy between Two Groups of Patients.** After the combined treatment with the two drugs, the total effective rate of the experimental group was 89% which was significantly higher than the 77% total effective rate observed in the control group ( $P < 0.05$ ). The data are summarized in Table 4.

TABLE 1: Comparison of general information of the two groups of patients.

Item	Experimental group (n = 78)	Control group (n = 78)	P
Age (years)	60.74 ± 4.67	62.82 ± 4.83	0.15
Sex (M/F)	40/38	41/37	0.52
Smoke (n, %)	28 (35.89%)	30 (38.46%)	0.48
Hypertension (n, %)	18 (23.07%)	21 (26.92%)	0.39
Diabetes (n, %)	11 (14.10%)	12 (15.38%)	0.62
SCr ( $\mu\text{mol/l}$ )	52.24 ± 6.47	51.81 ± 6.20	0.67
UA ( $\mu\text{mol/l}$ )	354.85 ± 37.25	361.23 ± 38.96	0.29
TC (mmol/l)	4.82 ± 0.41	4.90 ± 0.42	0.23
TG (mmol/l)	1.23 ± 0.25	1.26 ± 0.28	0.48
HDL-C (mmol/l)	0.95 ± 0.23	0.96 ± 0.22	0.78
LDL-C (mmol/l)	2.88 ± 0.43	2.87 ± 0.41	0.88
AST/ALT	0.72 ± 0.22	0.73 ± 0.21	0.77
BMI ( $\text{kg/m}^2$ )	22.51 ± 1.21	22.73 ± 1.24	0.26
Coronary heart disease	12 (15.38)	13 (16.67)	0.64
Atrial fibrillation	8 (10.25)	9 (11.53)	0.62

BMI: body mass index; TG: triglyceride; TC: total cholesterol; HDL-C: high density lipoprotein-cholesterol; LDL-C: low high density lipoprotein-cholesterol.

**3.5. Comparison of Adverse Reactions between the Two Groups of Patients.** During the entire treatment period, no adverse reactions such as skin rash, nausea, vomiting, fever, or headache were observed in the patients. No obvious abnormalities were detected by electrocardiogram, routine blood and urine analysis, and liver and kidney function tests.

### 4. Discussion

Acute cerebral infarction is caused by obstructions of brain blood supply that lead to cerebral ischemia, hypoxic necrosis, and corresponding neurological deficits. In China, acute cerebral infarction has surpassed cancer as the leading threat to human health. Studies have confirmed that cerebral infarction is closely related to platelet aggregation [7, 8] which is caused by platelet activation [9]. P-selectin (CD62P) is a glycoprotein that has a molecular mass of 140,000 and is mainly



TABLE 2: Comparison of CD62P, D-dimer, FIB, IL-6, and hs-CRP content between 2 groups before and after treatment.

(a)

	CD62P (ng/l)		D-dimer ( $\mu\text{g/ml}$ )		Hs-CRP (mg/l)	
	Bef Tre	Aft Tre	Bef Tre	Aft Tre	Bef Tre	Aft Tre
Experimental group	36.70 $\pm$ 2.45	34.23 $\pm$ 2.21*	2.99 $\pm$ 0.71	0.85 $\pm$ 0.22*	10.65 $\pm$ 1.22	8.56 $\pm$ 0.85*
Control group	37.45 $\pm$ 2.49	36.56 $\pm$ 2.32*	3.01 $\pm$ 0.75	1.23 $\pm$ 0.41*	11.02 $\pm$ 1.33	9.75 $\pm$ 1.12*
<i>T</i>	1.89	6.42	0.17	7.21	1.81	7.47
<i>P</i>	0.59	0.00	0.86	0.00	0.07	0.00

(b)

	FIB (ng/l)		IL-6 (pg/ml)	
	Bef Tre	Aft Tre	Bef Tre	Aft Tre
Experimental group	3.85 $\pm$ 0.86	3.43 $\pm$ 0.56*	14.27 $\pm$ 1.25	10.23 $\pm$ 1.02*
Control group	3.65 $\pm$ 0.78	3.27 $\pm$ 0.41*	13.89 $\pm$ 1.45	11.45 $\pm$ 1.15*
<i>T</i>	1.52	2.03	1.75	7.00
<i>P</i>	0.13	0.04	0.08	0.00

Compared with before treatment, \* $P < 0.05$ . Bef Tre: before treatment; Aft Tre: after treatment.

TABLE 3: Comparison of neurologic impairment degree scores between 2 groups before and after treatment.

	NIHSS		mRS	
	Before Tre	Aft Tre	Bef Tre	Aft Tre
Experimental group	38.26 $\pm$ 2.78	24.53 $\pm$ 1.7	3.89 $\pm$ 0.85	1.84 $\pm$ 0.45
Control group	37.79 $\pm$ 1.50	28.98 $\pm$ 1.89	3.85 $\pm$ 0.82	2.21 $\pm$ 0.56
<i>T</i>	1.30	15.13	0.29	0.00
<i>P</i>	0.19	0.00	0.76	0.00

Bef Tre: before treatment; Aft Tre: after treatment.

TABLE 4: Comparison of clinical efficacy rate between 2 groups.

Item	Cure	Significantly effective	Effective	Ineffective	Total effective (%)
Experimental group	14	18	38	9	89%
Control group	10	15	35	18	77%#

Compared with the experimental group, # $P < 0.05$ .

distributed on  $\alpha$  particles in stationary platelets. When platelets are activated,  $\alpha$  particles quickly fuse with the platelet membrane and are released to allow redistribution of CD62p on the platelet surface [10]. The concentration of CD62p reaches a peak 10 minutes after platelet activation and can be used as a specific marker for evaluating platelet activation and thrombosis [11]. Animal experiments have shown that the expression of CD62P increases significantly 1 hour after cerebral infarction and reaches a peak at 8 to 24 hours that can last for 3 to 5 days. Also, CD62P can promote the activation of granulocytes to aggravate inflammation and coagulation reactions which can promote the formation of thrombus [12].

The fibrinolytic function in the body also changes when cerebral infarction occurs [13, 14]. D-dimer is a specific degradation product formed by fibrin cross-linking and redissolving. D-dimer reflects the fibrinolytic function in the body.

After thrombosis, the level of D-dimer in the body changes, and so it can be used as a biomarker in clinical practice [15] for the early diagnosis of cerebral infarction and to evaluate thrombolytic effects. FIB is a coagulation protein that participates in platelet aggregation and the coagulation processes and can also promote the occurrence of cerebral infarction [16].

After cerebral infarction, the focal area is composed of a necrotic center and an ischemic penumbra. Damage to brain cells located in the ischemic penumbra can be reversed, and these cells can potentially be protected from damage [17]. Brain protective drugs include free radical scavengers, opioid receptor blockers, and excitatory amino acid receptor blockers. However, neuroprotective agents have made significantly less progress compared to reperfusion therapy [18, 19]. The American Stroke Treatment Development Roundtable (STAIR) reviewed the experience and lessons of

the past 30 years and put proposed future areas for neuroprotective research and development including more adequate preclinical trials, multitarget protection, and combined reperfusion therapy [20, 21].

Under the guidance of STAIR principles, two exciting developments in neuroprotective agents have been reported in the past two years: firstly, the ESCAPE-NA1 study in which a PSD-95 inhibitor was obtained in the subgroup of combined perfusion therapy positive result [22, 23] and, secondly, TASTE research which uses multitarget protection as an important theoretical principle [24]. Multitarget protection is aimed at the cascade reaction after cerebral ischemia. This complex pathophysiological process results in damage to brain cells and is driven by energy metabolism disorders, hypoxic depolarization around the infarction, calcium overload, excitatory amino acid toxicity, oxidative stress damage, and the inflammatory response and other signaling pathways [25]. Multiple pathways may be involved at different points during the development of brain damage, and a single drug targeting a single mechanism is unlikely to effectively control the disease. Edaravone is a free radical scavenger that has a 3-methyl-1-phenyl-2-pyrazoline-5-one structure with lipophilic groups and a good ability to cross the blood-brain barrier [26]. In the central nervous system, edaravone mainly protects nerve cells by scavenging oxygen free radicals, inhibiting lipid peroxidation, regulating inflammatory factors, and inhibiting apoptosis [27–31].

Shenxiong glucose injection is a compound preparation that is composed of Danshensu, ligustrazine, glucose, and glycerin. Studies have confirmed that Danshensu and ligustrazine hydrochloride can resist platelet aggregation, reduce blood viscosity, improve brain microcirculation, and protect vascular endothelial function. Studies have found that Shenxiong glucose injection can improve neuronal tolerance to ischemia, promote the recovery of damaged neurons, reduce infarct volume, and improve prognosis [32].

The results of this study show that the FIB, D-dimer, IL-6, P-selectin, and hs-CRP levels and the mRS and NIHSS scores in the two groups of patients decreased after a two-week treatment compared to before treatment and the control group. The decreases were more obvious in the experimental group ( $P < 0.05$ ) suggesting that Shenxiong glucose injection combined with edaravone can improve the symptoms of neurological impairment in patients. Also, the effective rate in the experimental group was significantly higher than the control, and no obvious adverse reactions were observed during treatment.

In summary, Shenxiong glucose injection combined with edaravone is a safe and effective treatment for acute large-area cerebral infarction. However, the data reported in this study requires further validation due to the small sample size and investigation of a single-center study. Also, the follow-up was relatively short, and further studies should include larger patient cohorts in a multicenter study.

## Data Availability

All data, models, and code generated or used during the study appear in the submitted article.

## Conflicts of Interest

The authors declare that they have no financial or other conflicts of interest in relation to this research and its publication.

## Acknowledgments

The article is supported by the Primary Health Development Research Center of Sichuan Province in 2019 Year, North Sichuan Medical College (Project Number: SWFZ19-Q-15).

## References

- [1] GBD 2016 Stroke Collaborators, “Global, regional, and national burden of stroke, 1990–2016: a systematic analysis for the global burden of disease study 2016,” *The Lancet Neurology*, vol. 18, no. 5, pp. 439–458, 2019.
- [2] M. Zhou, H. Wang, J. Zhu et al., “Cause-specific mortality for 240 causes in China during 1990–2013: a systematic subnational analysis for the global burden of disease study 2013,” *The Lancet*, vol. 387, no. 10015, pp. 251–272, 2016.
- [3] Y. Z. Xu, Q. Wang, Z. H. Wu et al., “The effect of lithium chloride on the attenuation of cognitive impairment in experimental hypoglycemic rats,” *Brain Research Bulletin*, vol. 149, pp. 168–174, 2019.
- [4] T. Watanabe, M. Tahara, and S. Todo, “The novel antioxidant edaravone: from bench to bedside,” *Cardiovascular Therapeutics*, vol. 26, no. 2, p. 114, 2008.
- [5] Q. Wang, H. P. Sun, L. Yu et al., “Pharmacokinetic behaviors of ligustrazine after single- and multiple-dose intravenous Shenxiong glucose injection in rats by high-performance liquid chromatography,” *Naunyn-Schmiedeberg's Archives of Pharmacology*, vol. 392, no. 5, pp. 565–572, 2019.
- [6] X. Wang, W. U. Chengji, L. I. Hongying, J. Wang, J. Yang, and H. Pan, “Clinical observation of Shuxuetong injection in the treatment of acute cerebral infarction,” *China Pharmacy*, vol. 27, no. 3, pp. 316–318, 2016.
- [7] P. Järemo, M. Eriksson-Franzen, and M. Milovanovic, “Platelets, gender and acute cerebral infarction,” *Journal of Translational Medicine*, vol. 13, no. 1, 2015.
- [8] P. Järemo, M. Eriksson, T. L. Lindahl, S. Nilsson, and M. Milovanovic, “Platelets and acute cerebral infarction,” *Platelets*, vol. 24, no. 5, pp. 407–411, 2013.
- [9] J. Nojima, H. Kuratsune, E. Suehisa, T. Kitani, Y. Iwatani, and Y. Kanakura, “Strong correlation between the prevalence of cerebral infarction and the presence of anti-cardiolipin/ $\beta$ 2-glycoprotein I and anti-phosphatidylserine/prothrombin antibodies,” *Thrombosis and Haemostasis*, vol. 91, pp. 967–976, 2004.
- [10] Z. Cai, Y. S. Yan, J. Zhou, Y. Yang, Y. Zhang, and J. Chen, “Multifunctionalized brush-like glycopolymers with high affinity to P-selectin and antitumor metastasis activity,” *Bio-macromolecules*, vol. 22, no. 3, pp. 1177–1185, 2021.
- [11] H. Zhang, H. X. Zhou, Y. Bai et al., “Changes in the levels of vascular endothelial adhesion molecule-1 and P-selectin in patients with cerebral infarction,” *International Journal of Laboratory Medicine*, vol. 35, no. 24, pp. 3417–3418, 2014.
- [12] Y. Okada, B. R. Copeland, E. Mori, M. M. Tung, W. S. Thomas, and G. J. Del Zoppo, “P-selectin and intercellular adhesion



- molecule-1 expression after focal brain ischemia and reperfusion,” *Stroke*, vol. 25, no. 1, pp. 202–211, 1994.
- [13] S. H. Wang, Q. Li, Z. H. Deng et al., “Neanthes japonica (Iznka) fibrinolytic enzyme reduced cerebral infarction, cerebral edema and increased antioxidation in rat models of focal cerebral ischemia,” *Neuroscience Letters*, vol. 489, no. 1, pp. 16–19, 2011.
- [14] D. Ogton and H. W. Fullerton, “Plasma fibrinolytic activity following recent myocardial and cerebral infarction,” *The Lancet*, vol. 286, no. 7403, pp. 99–101, 1965.
- [15] M. Xu, X. Y. He, and P. Huang, “The value of combined detection of D-dimer and CD62p in judging the severity of acute cerebral infarction and short-term prognosis,” *BioMed Research International*, vol. 2021, Article ID 6620311, 6 pages, 2021.
- [16] L. Gao, P. Liu, J. X. Song et al., “Study on the correlation of tongue manifestation with fibrinogen and neutrophil in acute cerebral infarction patients,” *Chinese Journal of Integrative Medicine*, vol. 18, no. 12, pp. 942–945, 2012.
- [17] J. Hofmeijer, L. J. Kappelle, A. Algra, G. J. Amelink, J. Van Gijn, and H. B. Van Der Worp, “Surgical decompression for space-occupying cerebral infarction (the Hemicraniectomy After Middle Cerebral Artery infarction with Life-threatening Edema Trial [HAMLET]): a multicentre, open, randomised trial,” *The Lancet Neurology*, vol. 8, no. 4, pp. 326–333, 2009.
- [18] X. Yi, J. Lin, J. Li, Q. Zhou, and Z. Han, “Epoxyeicosatrienoic acids are mediated by EPHX2 variants and may be a predictor of early neurological deterioration in acute minor ischemic stroke,” *Journal of Atherosclerosis and Thrombosis*, vol. 24, no. 12, pp. 1258–1266, 2017.
- [19] Y. Pan, W. Chen, Y. Xu et al., “Genetic polymorphisms and clopidogrel efficacy for acute ischemic stroke or transient ischemic attack: a systematic review and meta-analysis,” *Circulation*, vol. 135, no. 1, pp. 21–33, 2017.
- [20] X. Yi, Q. Zhou, J. Lin, and L. F. Chi, “Aspirin resistance in Chinese stroke patients increased the rate of recurrent stroke and other vascular events,” *International Journal of Stroke*, vol. 8, no. 7, pp. 535–539, 2013.
- [21] S. P. Feinklestein, M. Fisher, A. J. Furland et al., “Recommendations for standards regarding preclinical neuroprotective and restorative drug development,” *Stroke*, vol. 30, 1999.
- [22] A. Rizwan, C. Adams, and M. Tymianski, “Abstract WP412: use of interactive cluster heatmaps and text analytics in the Escape-na1 phase 3 clinical trial for pharmacovigilance of adverse events and site performance,” *Stroke*, vol. 50, Supplement\_1, 2019.
- [23] Z. Miao, X. Tang, M. Schultzberg, Y. Zhao, and X. Wang, “Plasma resolvin D2 to leukotriene B4 ratio is reduced in diabetic patients with ischemic stroke and related to prognosis,” *BioMed Research International*, vol. 2021, Article ID 6657646, 8 pages, 2021.
- [24] J. Xu, A. Wang, X. Meng et al., “Edaravone dextran versus edaravone alone for the treatment of acute ischemic stroke,” *Stroke*, vol. 52, no. 3, pp. 772–780, 2021.
- [25] H. Kaur, A. Prakash, and B. Medhi, “Drug therapy in stroke: from preclinical to clinical studies,” *Pharmacology*, vol. 92, no. 5–6, pp. 324–334, 2013.
- [26] H. P. Adams Jr., R. J. Adams, T. Brott et al., “Guidelines for the early management of patients with ischemic stroke: a scientific statement from the Stroke Council of the American Stroke Association,” *Stroke*, vol. 34, no. 10, pp. 1056–1083, 2013.
- [27] Y. Z. Xu, Q. Wang, Z. S. Qu, J. Yang, X. Zhang, and Y. Zhao, “Protective effect of hyperbaric oxygen therapy on cognitive function in patients with vascular dementia,” *Cell Transplantation*, vol. 28, no. 8, pp. 1071–1075, 2019.
- [28] Edaravone Acute Infarction Study Group, “Effect of a novel free radical scavenger, edaravone (MCI-186), on acute brain infarction. Randomized, placebo-controlled, double-blind study at multicenters,” *Cerebrovascular Diseases*, vol. 15, pp. 222–229, 2003.
- [29] N. Zhang, M. Komine-Kobayashi, R. Tanaka, M. Liu, Y. Mizuno, and T. Urabe, “Edaravone reduces early accumulation of oxidative products and sequential inflammatory responses after transient focal ischemia in mice brain,” *Stroke*, vol. 36, no. 10, pp. 2220–2225, 2005.
- [30] S. Kobayashi, S. Fukuma, T. Ikenoue, S. Fukuhara, S. Kobayashi, and on behalf of the Japan Stroke Data Bank, “Effect of edaravone on neurological symptoms in real-world patients with acute ischemic stroke,” *Stroke*, vol. 50, no. 7, pp. 1805–1811, 2019.
- [31] J. Xu, Y. Wang, A. Wang et al., “Safety and efficacy of Edaravone Dextran versus edaravone for patients with acute ischaemic stroke: a phase II, multicentre, randomised, double-blind, multiple-dose, active-controlled clinical trial,” *Stroke and Vascular Neurology*, vol. 4, no. 3, pp. 109–114, 2019.
- [32] X. D. Chen, C. F. Liu, Y. J. Cao, Y. M. Wang, and Z. Tao, “Effects of the *Salvia miltiorrhiza* ligustrazine hydrochloride and glucose injection on the inflammatory factors changes after focal cerebral ischemiareperfusion in rats,” *Chinese Journal of Practical Internal Medicine*, vol. 27, no. 13, pp. 1017–1020, 2007.

## Review Article

# Relationship of Neutrophil-to-Lymphocyte Ratio with Carotid Plaque Vulnerability and Occurrence of Vulnerable Carotid Plaque in Patients with Acute Ischemic Stroke

Xin Li , Jing Li , and Guode Wu 

Department of Neurology, Lanzhou University Second Hospital, Lanzhou, 730000 Gansu Province, China

Correspondence should be addressed to Guode Wu; [wgdzh@163.com](mailto:wgdzh@163.com)

Received 5 April 2021; Revised 1 June 2021; Accepted 11 June 2021; Published 21 June 2021

Academic Editor: Yuzhen Xu

Copyright © 2021 Xin Li et al. This is an open access article distributed under the Creative Commons Attribution License, which permits unrestricted use, distribution, and reproduction in any medium, provided the original work is properly cited.

**Background.** Carotid plaque is an undefined risk factor in ischemic stroke and is driven by inflammation. Mounting evidence suggests that neutrophil-to-lymphocyte ratio (NLR) is crucial not only for cerebrovascular events but also in atherosclerosis progression. Here, we aimed to explore the association between the admission NLR and carotid plaque vulnerability as well as the occurrence of vulnerable carotid plaque detected by carotid ultrasonography in patients with acute ischemic stroke (AIS) among Chinese. **Methods.** We conducted a retrospective study composed of 588 patients with AIS and 309 healthy controls free of carotid plaque in the Department of Neurology in The Second Hospital of Lanzhou University from March 2014 to February 2015. All patients were classified as nonplaque, stable plaque, and vulnerable plaque groups on the basis of carotid ultrasonography results. The baseline information was collected and compared among the four different groups. The correlation between variables and carotid plaque vulnerability was tested by Spearman linear correlation analysis. To identify the independent predictors for vulnerable carotid plaque, univariate and multivariate logistic regression analysis was performed. **Results.** The comparisons of age, sex proportion, history of hypertension, diabetes, and smoking, the levels of HDL-C, Lp(a), BMI, SBP, DBP, Fib, CRP, leukocyte, and NLR among the four groups showed a statistically significant difference ( $P < 0.05$ ); in particular, the NLR was significantly higher in the vulnerable plaque group as compared to the control ( $P = 0.043$ ), nonplaque ( $P = 0.022$ ), and stable plaque groups ( $P = 0.015$ ). The Spearman correlation analysis presented a positive correlation between carotid plaque vulnerability and age ( $r = 0.302$ ;  $P < 0.001$ ), SBP ( $r = 0.163$ ;  $P < 0.001$ ), and NLR ( $r = 0.087$ ;  $P = 0.034$ ), while the lymphocyte was negatively related to the carotid plaque vulnerability ( $r = -0.089$ ;  $P = 0.030$ ). The multivariate logistic regression analysis adjusted for confounding factors revealed that age (odds ratio [OR], 1.042; 95% confidence interval [CI], 1.025-1.060;  $P < 0.001$ ), male gender (OR, 2.005; 95% CI, 1.394-2.884;  $P < 0.001$ ), diabetes (OR, 1.481; 95% CI, 1.021-2.149;  $P = 0.039$ ), SBP (OR, 1.012; 95% CI, 1.003-1.021;  $P = 0.010$ ), and NLR (OR, 1.098; 95% CI, 1.018-1.184;  $P = 0.015$ ) are independent predictors of vulnerable carotid plaque in patients with AIS. **Conclusion.** The admission NLR is a novel and meaningful biomarker that can be used in predicting carotid plaque vulnerability and the presence of vulnerable carotid plaque assessed by carotid ultrasonography in patients with AIS among Chinese.

## 1. Introduction

Stroke affects 33 million individuals worldwide annually, of whom 87% are ischemic [1]. The burden of stroke is greater in Asian countries than in the Western world, which is attributed to the higher incidence of stroke than coronary heart disease in Asians [2]. In China, ischemic stroke is a leading cause of mortality and disability and is projected to increase year by year. Atherosclerosis is the important pathologic

basis of ischemic stroke and 30% of which results from carotid atherosclerotic disease [3]. Arterioarterial emboli caused by carotid vulnerable plaque rupture, ulceration, platelet activation, and thrombosis is considered to be the pathogenesis of ischemic stroke [4], and even the risk of vulnerable plaque rupture is more crucial than the severity of stenosis in ischemic stroke. For this reason, compared to patients with a stable 70% asymptomatic stenosis, the patient who has a low-grade stenosis but with an ulcerated plaque

may benefit more from a revascularization procedure [5]. Therefore, judging the vulnerability of carotid plaque accurately contributes to stroke risk assessment and guides individualized treatment further, so as to prevent stroke effectively.

An increasing body of evidence suggests atherosclerosis is a concomitant inflammatory disease, which occurs firstly in the endothelium of the arterial wall [6]. As a subclinical sign of atherosclerosis, atherosclerotic plaque was found to hold various inflammatory cells, like activated T lymphocytes, macrophages, and mast cells [7]. What is more, it has been shown that circulating inflammatory markers including high-sensitivity C-reactive protein (hs-CRP), pentraxin 3 (PTX3), E-selectin, interleukin (IL)-6, tumor necrosis factor- $\alpha$  (TNF- $\alpha$ ), and matrix metalloproteinases (MMPs)-9 are consistently associated with carotid plaque vulnerability [8, 9]. Thus, it is easy to see an apparent relevance regarding inflammation and plaque progression, and it is particularly critical to seek for sensitive biochemical indicators related to inflammation to distinguish the vulnerable carotid plaque.

As key elements of the immune system, leukocytes and their subtypes, neutrophils and lymphocytes, play a critical role in the immune response and inflammatory reaction. Neutrophil-to-lymphocyte ratio (NLR) can be readily calculated from the leukocytes related parameters, which combines neutrophils' nonspecific inflammation and lymphocytes' specific immune response into a single inflammatory biomarker. Previous investigations of NLR have reported that it can be used as a predictor of cancer [10, 11] and cardiovascular disease [12–15]. More recently, several studies have been carried out in cerebrovascular disease and shown strong predictive value of NLR for short-term prognosis in patients with AIS or transient ischemic attack [16–19]. However, the relationship between NLR and the evolution of carotid atherosclerotic plaque in patients with acute ischemic stroke (AIS) has been poorly understood to date.

Ultrasound is recognized to be an ideal tool for diagnosis and evaluation of atherosclerosis at present due to the advantages of noninvasive, convenient, and repeatability. Color Doppler ultrasound of carotid artery is applied to explore the information about the degree of stenosis, and the composition/surface of the carotid plaque, and to determine the pathology [20], has become the main imaging method for the examination of carotid plaque lesions. The purpose of this study was to investigate whether admission NLR is associated with carotid plaque vulnerability and the occurrence of vulnerable carotid plaque detected by carotid ultrasonography in patients with AIS among Chinese.

## 2. Methods

**2.1. Study Population.** We studied 588 consecutive AIS patients admitted to the Department of Neurology in The Second Hospital of Lanzhou University within seven days of stroke onset and underwent carotid ultrasonography imaging from March 2014 to February 2015. All the patients were in accordance with the Fourth National Stroke Conference revised cerebral infarction diagnostic standard, and the

new ischemic lesions were confirmed by brain computed tomography (CT) and/or magnetic resonance imaging (MRI). Patients meeting any of the following criteria were excluded: (1) the patients who without a clear onset time, (2) patients with other cerebrovascular events rather than AIS, (3) patients who are suffering from serious cardiovascular diseases, blood disorders, and liver and kidney dysfunction; (4) patients who have severe infection, sepsis, malignant or autoimmune diseases, and who are taking immunosuppressants, glucocorticoid, or cytotoxic drugs; and (5) patients with missing data. The AIS patients were divided into nonplaque, stable plaque, and vulnerable plaque groups according to the carotid ultrasonography examination results below. In addition, another 309 healthy subjects without carotid plaque confirmed by carotid ultrasonography who were selected from the population simultaneously participated in a medical examination at the Center of Physical Examination in The Second Hospital of Lanzhou University were regarded as controls. The exclusion criteria of controls are the same as the AIS patients. Ultimately, a total of 588 consecutive AIS patients and 309 healthy subjects were recruited in this study.

The present study was approved by the Ethics Committee of the Second Hospital of Lanzhou University. Each participant was given a written and an oral description of the study and provided written informed consent before participating in this research.

**2.2. Data Collection.** A complete case history collecting, neurological examination, and demographic data recording were carried out by professional neurologists in all the patients within four hours after admission; electrocardiography (ECG), chest X-ray, brain CT or MRI, transcranial color-coded Doppler (TCD), and carotid ultrasonography were done in all the patients within 24 hours after admission. Clinical information was obtained from all patients, including age, sex, height, weight, the history of hyperlipidemia, hypertension, diabetes, coronary heart disease (CHD), atrial fibrillation (AF), smoking, and drinking. The body mass index (BMI) was calculated by dividing weight in kilograms by height in squared meters ( $\text{Kg}/\text{m}^2$ ). We also investigated the whole clinical data mentioned above and below of healthy subjects from their physical examination records.

**2.3. Risk Factor Definitions.** Hyperlipidemia was defined as total cholesterol (TC)  $\geq 5.72$  mmol/L and/or triglyceride  $\geq 1.70$  mmol/L, or use of lipid-lowering medications. Hypertension was described as systolic blood pressure (SBP)  $\geq 140$  mmHg and/or diastolic blood pressure (DBP)  $\geq 90$  mmHg, or a history of taking hypertension drugs. The diagnosis of diabetes depended on previous history of diabetes treated with or without antidiabetic agents or insulin, or fasting blood glucose (FBG)  $\geq 7.00$  mmol/L and/or 2-hour postprandial blood glucose  $\geq 11.10$  mmol/L. The patients who with a typical clinical manifestation of CHD and confirmed before or a previous history of CHD were considered as CHD. The diagnosis of AF was based on the ECG manifestations. Smoking was determined as the average amount of cigarettes  $\geq 10$  per day and sustained more than one year.

The patients who have an average amount of ethanol intake  $\geq 30$  g/d in the previous more than one year period were taken as drinking.

**2.4. Laboratory Tests.** The blood samples were taken from an antecubital vein after a 12-hour overnight fast and then stored at  $-80^{\circ}\text{C}$  refrigerator before assay. Leukocyte counts and its different subtypes were determined by an automated blood cell counter (XE-2100, Sysmex, Kobe, Japan) according to the manufacturer's instructions, and NLR was calculated based on the results afterwards. An automatic biochemical analyzer (Cobas-8000, Roche, Basel, Switzerland) was used to measure many biochemical indexes, such as TC, triglyceride, high-density lipoprotein cholesterol (HDL-C), apolipoprotein AI (ApoAI), apolipoprotein B (ApoB), lipoprotein(a) [Lp(a)], fasting blood glucose (FBG.), homocysteine (Hcy), and C-reactive protein (CRP). The concentration of low-density lipoprotein cholesterol (LDL-C) was calculated as TC minus cholesterol in the supernatant by precipitation method. Fibrinogen (Fib) was quantified using the Beckman automatic coagulation analyzer (ACL-2000, Beckman Coulter, California, USA). SBP and DBP were measured at the right brachial artery of the subject using a standard mercury sphygmomanometer after five minutes of rest in the supine position.

**2.5. Carotid Ultrasonography.** The evaluation of carotid plaque was performed by using a color Doppler ultrasound with an 5~12 MHz linear-array probe (Philips-IU22, Royal Dutch Philips Electronics, Amsterdam, Holland) after a rest in the supine position for about 15 minutes. Putting a pillow below the subject's neck and making the head back with a slightly lateral rotation. Next, we scanned the bilateral common carotid artery, bifurcation, and internal and external carotid artery along the direction of vessel to determine the intima-media thickness (IMT). IMT was defined as the distance from the lumen-intima interface to the media-adventitia interface, and  $\text{IMT} > 1.5$  mm protruding into the arterial lumen was regarded as carotid plaque formation, observing and recording the plaque characteristics including size, morphology, and property.

According to the morphological and acoustic characteristics of the plaques, they can be divided into (1) low-echo plaque: the fibrous cap is thin or unclear, and the interior is rich in lipid components, which is soft plaque, (2) medium-echo plaque: the fibrous cap is thick and mainly composed of collagen tissue, which is a fibrous flat plaque, (3) strong-echo plaque: the surface is smooth, but it can be accompanied by sound shadow in the rear, which is calcified hard plaque, and (4) mixed-echo plaque: the echoes vary in strength in more than 20% of the intraplaque area, suggesting that it is ulcerous plaque or mixed plaque with hemorrhage. Among them, medium-echo plaque and strong-echo plaque belong to stable plaques, while low-echo plaque and mixed-echo plaque were vulnerable plaques. Those with both stable plaques and vulnerable plaques were classified as vulnerable plaques.

**2.6. Statistical Analysis.** Baseline data of all participants is expressed as mean  $\pm$  standard deviation (SD) for continuous variables and as percentages (proportions) for categorical

variables. The Kolmogorov-Smirnov test was used to verify the normality of distribution of continuous variables. Multiple group comparisons of continuous variables were performed by one-way analysis of variance, followed by Tukey-Kramer posthoc analysis. The chi-square test was used to compare the categorical variables. The correlation between variables and carotid plaque vulnerability was tested by Spearman linear correlation analysis. To identify the independent predictors for vulnerable carotid plaque, multivariate logistic regression analysis was made by including the parameters that show significant values of  $<0.05$  in univariate analysis, the odds ratios (OR) and 95% confidence intervals (CI) were calculated.

All statistical analyses were conducted by using SPSS for windows (version 19.0, Chicago, Illinois, USA). A two-tailed  $P$  value of  $<0.05$  was considered as statistically significant.

### 3. Results

Our study population comprised 588 consecutive AIS patients and 309 healthy subjects totally. Of the 588 patients, 357 (60.71%) males, 231 (39.29%) females—with a mean age of  $65.32 \pm 11.43$  years, 247(42.01%), 93(15.82%), and 248(42.18%) were in the non-, stable, and vulnerable plaque group, respectively. The mean age of 309 controls was  $65.63 \pm 10.63$  years, and 53.72% of the subjects were male. The baseline characteristics of all study population are summarized in Table 1. The patients with vulnerable carotid plaque were obviously older and demonstrated higher prevalences of male gender, hypertension, diabetes, and smoking. Furthermore, they were more likely to present with increased Lp(a), BMI, SBP, DBP, Fib, CRP, and leukocyte and tended to have a lower HDL-C. The mean NLR of 588 patients was  $2.86 \pm 2.53$ , and the NLR was significantly higher in the vulnerable plaque group when compared to the control ( $P = 0.043$ ), nonplaque ( $P = 0.022$ ), and stable plaque groups ( $P = 0.015$ ).

Table 2 shows the Spearman correlation analysis results of the associations between influence factors and the degree of carotid plaque vulnerability. Significant positive associations were observed for age ( $r = 0.302$ ;  $P < 0.001$ ), SBP ( $r = 0.163$ ;  $P < 0.001$ ), NLR ( $r = 0.087$ ;  $P = 0.034$ ), and carotid plaque vulnerability, and the age, SBP, and NLR increased progressively with aggravating of carotid plaque instability, whereas the lymphocyte was negatively related to the carotid plaque vulnerability ( $r = -0.089$ ;  $P = 0.030$ ), i.e., the lower level of lymphocyte and the poorer stability of carotid plaque (Table 2).

Univariate logistic regression analysis was performed for all the variables measured in this study. In order to determine the independent predictors of vulnerable carotid plaque, the variables found to be statistically significant in the univariate analysis were included in the multivariate logistic regression analysis. As a result, age (odds ratio [OR], 1.042; 95% confidence interval [CI], 1.025-1.060;  $P < 0.001$ ), male gender (OR, 2.005; 95% CI, 1.394-2.884;  $P \leq 0.001$ ), diabetes (OR, 1.481; 95% CI, 1.021-2.149;  $P = 0.039$ ), SBP (OR, 1.012; 95% CI, 1.003-1.021;  $P = 0.010$ ), and NLR (OR, 1.098; 95% CI, 1.018-1.184;  $P = 0.015$ ) were found to be the independent predictors of vulnerable carotid plaque (Table 3).



TABLE 1: Baseline characteristics of all study population in different groups.

Item	Control ( <i>n</i> = 309)	Non-plaque ( <i>n</i> = 247)	Stable plaque ( <i>n</i> = 93)	Vulnerable plaque ( <i>n</i> = 248)	$\chi^2/F$ value	<i>P</i> value
Age, years	65.63 ± 10.63	60.72 ± 12.03 <sup>a</sup>	69.74 ± 9.70 <sup>ab</sup>	68.25 ± 9.71 <sup>ab</sup>	26.752	<0.001
Male, <i>n</i> (%)	166 (53.7)	138 (55.9)	50 (53.8)	169 (68.1) <sup>abc</sup>	13.939	0.003
Hyperlipidemia, <i>n</i> (%)	67 (21.7)	63 (25.5)	22 (23.7)	61 (24.6)	1.249	0.741
Hypertension, <i>n</i> (%)	195 (63.1)	176 (71.3) <sup>a</sup>	75 (80.6) <sup>a</sup>	200 (80.6) <sup>ab</sup>	24.842	<0.001
Diabetes, <i>n</i> (%)	64 (20.7)	61 (24.7)	27 (29.0)	87 (35.1) <sup>ab</sup>	15.345	0.002
CHD, <i>n</i> (%)	12 (3.9)	13 (5.3)	4 (4.3)	21 (8.5) <sup>a</sup>	5.955	0.114
AF, <i>n</i> (%)	8 (2.6)	17 (6.9) <sup>a</sup>	5 (5.4)	14 (5.6)	5.960	0.114
Smoking, <i>n</i> (%)	28 (9.1)	37 (15.0) <sup>a</sup>	21 (22.6) <sup>a</sup>	43 (17.3) <sup>a</sup>	14.013	0.003
Drinking, <i>n</i> (%)	21 (6.8)	28 (11.3)	14 (15.1) <sup>a</sup>	30 (12.1) <sup>a</sup>	7.486	0.058
TC, mmol/L	4.10 ± 1.01	3.86 ± 0.89 <sup>a</sup>	4.20 ± 2.38 <sup>b</sup>	4.00 ± 1.12	2.491	0.059
TG, mmol/L	1.41 ± 0.88	1.46 ± 0.93	1.56 ± 1.25	1.47 ± 0.85	0.683	0.563
HDL-C, mmol/L	1.28 ± 0.66	1.12 ± 0.29 <sup>a</sup>	1.19 ± 0.33	1.16 ± 0.57 <sup>a</sup>	5.178	0.001
LDL-C, mmol/L	2.57 ± 0.85	2.41 ± 0.85 <sup>a</sup>	2.39 ± 0.83	2.50 ± 0.79	2.242	0.082
ApoAI, g/L	1.16 ± 0.29	1.08 ± 0.23 <sup>a</sup>	1.17 ± 0.32 <sup>b</sup>	1.07 ± 0.24 <sup>ac</sup>	8.024	<0.001
ApoB, g/L	0.79 ± 0.21	0.76 ± 0.21 <sup>a</sup>	0.77 ± 0.19	0.79 ± 0.22	1.635	0.180
Lp(a), nmol/L	34.09 ± 26.47	36.64 ± 27.67	44.41 ± 46.96 <sup>a</sup>	41.07 ± 39.31 <sup>a</sup>	3.405	0.017
BMI, kg/m <sup>2</sup>	20.40 ± 3.10	21.70 ± 3.18 <sup>a</sup>	21.65 ± 3.20 <sup>a</sup>	22.15 ± 3.13 <sup>a</sup>	16.038	<0.001
SBP, mmHg	136.44 ± 17.60	136.53 ± 19.62	141.61 ± 18.23 <sup>ab</sup>	143.55 ± 19.87 <sup>ab</sup>	8.694	<0.001
DBP, mmHg	78.93 ± 11.04	81.05 ± 11.74 <sup>a</sup>	80.52 ± 9.37	81.95 ± 12.08 <sup>a</sup>	3.498	0.015
FBG, mmol/L	5.37 ± 2.06	5.75 ± 2.77	5.81 ± 2.43	5.79 ± 2.15 <sup>a</sup>	2.026	0.109
Hcy, μmol/L	20.91 ± 12.35	23.10 ± 24.24	22.66 ± 16.37	24.00 ± 16.45 <sup>a</sup>	1.499	0.213
Fib, g/L	2.88 ± 0.64	3.04 ± 0.65 <sup>a</sup>	3.11 ± 0.54 <sup>a</sup>	3.06 ± 0.60 <sup>a</sup>	6.270	<0.001
CRP, mg/L	21.31 ± 10.43	17.55 ± 12.27 <sup>a</sup>	19.18 ± 17.08	19.80 ± 14.43	3.931	0.008
Leukocyte (×10 <sup>9</sup> /L)	6.05 ± 2.00	6.66 ± 3.02 <sup>a</sup>	6.32 ± 1.99	6.71 ± 2.55 <sup>a</sup>	4.237	0.006
Neutrophil (×10 <sup>9</sup> /L)	4.05 ± 1.75	4.19 ± 1.96	3.91 ± 1.36	4.24 ± 2.26	0.910	0.435
Lymphocyte (×10 <sup>9</sup> /L)	1.67 ± 0.59	1.79 ± 0.61 <sup>a</sup>	1.74 ± 0.49	1.67 ± 0.59 <sup>b</sup>	2.406	0.066
NLR	2.77 ± 1.93	2.69 ± 1.97	2.48 ± 1.43	3.17 ± 3.22 <sup>abc</sup>	2.837	0.037

Abbreviations: CHD: coronary heart disease; AF: atrial fibrillation; TC: total cholesterol; TG: triglyceride; HDL-C: high-density lipoprotein cholesterol; LDL-C: low-density lipoprotein cholesterol; ApoAI: apolipoprotein AI; ApoB: apolipoprotein B; Lp(a): lipoprotein(a); BMI: body mass index; SBP: systolic blood pressure; DBP: diastolic blood pressure; FBG: fasting blood glucose; Hcy: homocysteine; Fib: fibrinogen; CRP: C-reactive protein; NLR: neutrophil-to-lymphocyte ratio. <sup>a</sup>*P* < 0.05, as compared to control; <sup>b</sup>*P* < 0.05, as compared to nonplaque; <sup>c</sup>*P* < 0.05, as compared to stable plaque.

TABLE 2: Correlation of influence factors and the degree of carotid plaque vulnerability.

Variables	<i>r</i> value	<i>P</i> value
Age	0.302	<0.001
SBP	0.163	<0.001
Lymphocyte	-0.089	0.030
NLR	0.087	0.034

Abbreviations: SBP: systolic blood pressure; NLR: neutrophil-to-lymphocyte ratio.

#### 4. Discussion

In the current study, we demonstrated the relation between admission NLR with the extent of carotid plaque vulnerability and the presence of vulnerable carotid plaque evaluated by

carotid ultrasonography in patients with AIS. The principal findings of this analysis were as follows: (1) there was an obvious trend of increased NLR levels in the vulnerable carotid plaque group compared to other groups, (2) NLR levels were positively correlated with the degree of carotid plaque vulnerability, and the stable carotid plaque was more likely to shift to vulnerable carotid plaque with the rise of NLR, and (3) elevated NLR significantly portended an increased risk of vulnerable carotid plaque in AIS patients, and the effect remained after adjusting the classical atherosclerotic risk factors, such as age, sex, diabetes, and blood pressure.

The pathogenesis of atherosclerosis is quite complex, the key processes of which involve vascular inflammation, lipid accumulation, intima thickening and fibrosis, arterial stiffness, remodeling, and plaque rupture or erosion [21]. The vulnerable plaque refers to that it is more prone to rupture

TABLE 3: Univariate/multivariate logistic regression analysis to determine the independent predictors of vulnerable carotid plaque.

Variables	Univariate			Multivariate		
	OR	95% CI	P value	OR	95% CI	P value
Age	1.042	1.026-1.058	<0.001	1.042	1.025-1.060	<0.001
Male gender	1.730	1.228-2.435	0.002	2.005	1.394-2.884	<0.001
Diabetes	1.547	1.084-2.210	0.016	1.481	1.021-2.149	0.039
SBP	1.015	1.006-1.023	0.001	1.012	1.003-1.021	0.010
Lymphocyte	0.740	0.556-0.984	0.038	0.968	0.676-1.387	0.861
NLR	1.091	1.017-1.171	0.015	1.098	1.018-1.184	0.015

Abbreviations: SBP: systolic blood pressure; NLR: neutrophil-to-lymphocyte ratio.

and subsequently results in the distal embolization. Pathological characteristics of vulnerable plaque include a thin or ruptured fibrous cap, lipid-rich necrotic core, intraplaque hemorrhage, and intraplaque active inflammation [22]. Inflammation was recognized to be a key factor in influencing plaque vulnerability [23]. Besides, Biscetti et al. [24] found that proinflammatory genetic profiles were prominently more universal in subjects with vulnerable carotid plaque. Thus, we have reason to believe that inflammation biomarkers and proinflammatory cytokines are involved in the progression of carotid plaque and are closely related to plaque vulnerability. For example, Shindo et al. [8] studied 58 patients with carotid stenosis and observed that the levels of hs-CRP, PTX3, E-selectin, IL-6, and TNF- $\alpha$  were increased in the vulnerable plaque group compared with the stable plaque group; on the contrary, the anti-inflammatory cytokines IL-10 and adiponectin in the vulnerable plaque group were lower than those in the stable plaque group. However, as a marker of subclinical inflammation, the clinical relevance regarding NLR with carotid plaque vulnerability in patients with AIS has not been elucidated until now.

Neutrophil infiltration in the atherosclerotic plaque has been visualized immediately *in vivo* in animal models [25], and neutrophils mediate the inflammatory reaction by releasing numerous bioactive substances like arachidonic acid metabolites, platelet-aggravating factors, cytotoxic oxygen-derived free radicals, myeloperoxidase, elastase, and acid phosphatases, [12], leading to plaque evolution and vulnerability gradually [26]; on the other hand, lymphocytes have been reported to be associated with the development of atherosclerosis [27, 28], and endogenous glucocorticoid secretes excessively in a stress state caused by inflammation, which brings about immunosuppression [29] and lymphocytes apoptosis [30]. Furthermore, the lymphocyte apoptosis tends to increase progressively with the intensification of atherosclerosis [31], while lymphocytes take part in anti-inflammation and endothelium protection. Hence, elevated NLR can objectively reflect systemic inflammation state because of the imbalance between neutrophils and lymphocytes, and the higher level of NLR suggests the more severe inflammation response [32]. In the present study, NLR was the highest in patients with vulnerable carotid plaque, and additionally, elevated NLR and decreasing lymphocyte were found to be correlated with exacerbation of carotid plaque vulnerability. As a consequence, NLR can express valuable information about the intergrated inflammatory activity of

the vascular bed and reflects the degree of plaque burden in patients with atherosclerosis.

In a study which consisted of 399 coronary artery disease (CAD) patients with coronary lesions who underwent virtual histology-intravascular ultrasound, CAD patients with a raised NLR were observed to have more vulnerable plaque components [33], whereas Açar et al. [34] found that NLR was related to luminal stenosis rather than plaque morphology in coronary artery. Our finding was compatible with the former, and we focused on patients with AIS and demonstrated that NLR but not neutrophil or lymphocyte even leukocyte appears to be a powerful predictor in determining the carotid plaque vulnerability in patients with AIS, which indicates a key role for NLR in the occurrence of vulnerable carotid plaque. A previous study reported that a higher NLR to be independently associated with arterial stiffness measured by brachial-ankle pulse wave velocity in the general population [35]. Lately, Hyun et al. [36] evaluated 252 cases of acute to subacute ischemic stroke assessing the carotid stenosis by carotid artery intima-media thickening (IMT), and they believed that NLR can be used to predict the degree of carotid stenosis in male patients with ischemic stroke. The results described above reveal a significant relationship between NLR and atherosclerosis collectively and prove that the inflammatory mechanisms are involved in the initiation and evolution of atherosclerosis as well as carotid plaques indeed. Therefore, our finding suggests NLR is more likely a risk factor than the differential leukocyte count being a predictor for vulnerable carotid plaque, independent of traditional risk factors of atherosclerosis. In addition, Świtońska et al. [37] have reported that NLR at admission can accurately predict the risk of symptomatic hemorrhagic transformation in AIS patients undergoing revascularization. In a systematic review and meta-analysis published in 2017 [38], the authors confirmed that an elevated pretreatment NLR value is effective in predicting the risk of mortality or major adverse cardiac events in patients with a recent acute coronary syndrome. Therefore, NLR is expected to be an effective predictor for the prognosis of cardiovascular and cerebrovascular diseases.

Except for the results listed above, this research showed a positive correlation of carotid plaque vulnerability with age and SBP, as shown for NLR, age, male gender, diabetes, and SBP that are also found to be independent markers of vulnerable carotid plaque in AIS diseases. It is widely known that age, sex, hypertension, and diabetes are acknowledged risk



factors of atherosclerosis [39, 40]. It has been suggested that carotid plaque morphology characteristics like plaque hemorrhage or thin fibrous caps vary with age and differ in sex [41]; Matsumoto et al. [42] observed that thicker and stiffer carotid arteries are more common in patients with type 2 diabetes than in the general population; moreover, hypertensive was reported to have a significantly higher carotid stiffness rate when compared to normotensive individuals [43]. Based on correlational clinical investigations aforementioned, we may speculate that various risk factors influence each stage of atherosclerotic progression process [44], for instance, IMT, plaque formation and stability shifting, carotid stenosis, or stiffness, in different manners.

To our knowledge, this is the first report examining the relationship between admission NLR and carotid plaque vulnerability as well as the occurrence of vulnerable carotid plaque in patients with AIS. In addition, our findings are persuasive and easy to be accepted due to the fact that we also included important covariates including well-established atherosclerosis risk factors such as age, sex, hyperlipidemia, hypertension, diabetes, and smoking; various blood lipid profiles, blood pressure, and glucose level; and kinds of serum index, for example, Hcy, Fib, CRP, and different leukocyte subtypes all that can reflect the systemic inflammatory information of the body to a variable extent. Adjustment for these potential confounders in multivariate models did not weaken the power of NLR in predicting vulnerable carotid plaque. The last but not the least, unlike other inflammatory markers such as hs-CRP, IL-6, TNF- $\alpha$ , and MMP-9, NLR can be readily and quickly obtained from blood routine text except cheapness. Meanwhile, it also conduces to assess the degree of carotid plaque vulnerability and stroke risk.

There are several limitations that should be taken into consideration. First, this is a retrospective and single-center study without a big enough sample size, which suggests that further large-scale randomized controlled trials are required to confirm the causality and generalize to all populations. Second, the property of carotid plaque was assessed by carotid ultrasonography, which has a limitation to detect individual plaque components and characteristics in detail on account of low sensitivity and specificity compared with MRI and CT [45]. Furthermore, NLR is a dynamic and time-varying marker result of the neutrophil and lymphocyte counts change over time. Beyond that, the level of NLR is likely to be affected by the body's own metabolism and external environmental factors, and so it would be particularly important to conduct the continuous follow-up of the NLR value, and we are on the point of performing it. Finally, despite the emerging evidence including our findings for the contribution of NLR to the atherosclerosis, the concrete mechanism of the influence of NLR on the atherosclerotic plaque remains to be clarified.

It is worth noting that the hemodynamic damage caused by carotid atherosclerosis is also the pathological mechanism of stroke, and inflammatory factors are also involved in this process. In recent years, vascular reactivity and cognitive dysfunction in patients with severe internal carotid artery stenosis after carotid endarterectomy have been investigated and

discussed, and the association between the two has been explored [46, 47]. After the carotid revascularization, the diameter of the local stenosis can be significantly improved, so that the blood flow is unobstructed, the perfusion of the intracranial blood is increased, the reserve capacity of cerebral vascular is improved, the hemodynamics tends to be stable, and inflammatory factors may have corresponding changes in this process. Therefore, the correlation between NLR and cerebrovascular hemodynamic status and vascular reactivity will be the target of our further study.

In conclusion, our findings support the hypotheses that NLR can serve as a potentially useful indicator of the degree of carotid plaque vulnerability and that a higher NLR may be a clinically modifiable predictor of vulnerable carotid plaque among patients with AIS. The determination of NLR in patients with carotid plaque helps to identify those who are at risk and may benefit from vascular health management in clinical practice and also provides reference for stroke risk stratification and etiological prevention, as well.

## 5. Conclusion

The NLR is a novel and meaningful biomarker that is independently associated with the carotid plaque vulnerability and the presence of vulnerable carotid plaque detected by carotid ultrasonography in patients with AIS in Chinese.

## Conflicts of Interest

The author(s) declared no potential conflicts of interest with respect to the research, authorship, and/or publication of this article.

## References

- [1] D. Mozaffarian, E. J. Benjamin, A. S. Go et al., "Heart disease and stroke statistics—2015 update: a report from the American Heart Association," *Circulation*, vol. 131, no. 4, pp. e29–322, 2015.
- [2] K.-L. Chien, T.-C. Su, J.-S. Jeng et al., "Carotid artery intima-media thickness, carotid plaque and coronary heart disease and stroke in Chinese," *PLoS One*, vol. 3, no. 10, pp. e3435–e3435, 2008.
- [3] R. Magge, B. C. Lau, B. P. Soares et al., "Clinical risk factors and CT imaging features of carotid atherosclerotic plaques as predictors of new incident carotid ischemic stroke: a retrospective cohort Study," *AJNR. American Journal of Neuroradiology*, vol. 34, no. 2, pp. 402–409, 2013.
- [4] T. Freilinger, K. Dimitriadis, K. Nikolaou, M. F. Reiser, M. Dichgans, and T. Saam, "Stroke while squeezing a pimple: traumatic rupture of a vulnerable carotid artery plaque," *Neurology*, vol. 76, no. 3, pp. 305–306, 2011.
- [5] W. Brinjikji, J. Huston 3rd, A. A. Rabinstein, G. M. Kim, A. Lerman, and G. Lanzino, "Contemporary carotid imaging: from degree of stenosis to plaque vulnerability," *Journal of Neurosurgery*, vol. 124, no. 1, pp. 27–42, 2016.
- [6] K. Husain, W. Hernandez, R. A. Ansari, and L. Ferder, "Inflammation, oxidative stress and renin angiotensin system

- in atherosclerosis," *World Journal of Biological Chemistry*, vol. 6, no. 3, pp. 209–217, 2015.
- [7] J. A. Chalela, "Evaluating the carotid plaque: going beyond stenosis," *Cerebrovascular Diseases*, vol. 27, no. 1, pp. 19–24, 2009.
- [8] A. Shindo, H. Tanemura, K. Yata et al., "Inflammatory biomarkers in atherosclerosis: pentraxin 3 can become a novel marker of plaque vulnerability," *PLoS One*, vol. 9, no. 6, article e100045, 2014.
- [9] D. Silvello, L. B. Narvaes, L. C. Albuquerque et al., "Serum levels and polymorphisms of matrix metalloproteinases (MMPs) in carotid artery atherosclerosis: higher MMP-9 levels are associated with plaque vulnerability," *Biomarkers*, vol. 19, no. 1, pp. 49–55, 2014.
- [10] J. Wang, Y. Jia, N. Wang et al., "The clinical significance of tumor-infiltrating neutrophils and neutrophil-to-CD8+ lymphocyte ratio in patients with resectable esophageal squamous cell carcinoma," *Journal of Translational Medicine*, vol. 12, no. 1, p. 7, 2014.
- [11] P. Xue, M. Kanai, Y. Mori et al., "Neutrophil-to-lymphocyte ratio for predicting palliative chemotherapy outcomes in advanced pancreatic cancer patients," *Cancer Medicine*, vol. 3, no. 2, pp. 406–415, 2014.
- [12] U. U. Tamhane, S. Aneja, D. Montgomery, E. K. Rogers, K. A. Eagle, and H. S. Gurm, "Association between admission neutrophil to lymphocyte ratio and outcomes in patients with acute coronary syndrome," *The American Journal of Cardiology*, vol. 102, no. 6, pp. 653–657, 2008.
- [13] T. Bhat, S. Teli, J. Rijal et al., "Neutrophil to lymphocyte ratio and cardiovascular diseases: a review," *Expert Review of Cardiovascular Therapy*, vol. 11, no. 1, pp. 55–59, 2013.
- [14] A. Kaya, M. Kurt, I. H. Tanboga et al., "Relation of neutrophil to lymphocyte ratio with the presence and severity of stable coronary artery Disease," *Clinical and Applied Thrombosis/Hemostasis*, vol. 20, no. 5, pp. 473–477, 2014.
- [15] V. A. Benites-Zapata, A. V. Hernandez, V. Nagarajan, C. A. Cauthen, R. C. Starling, and W. H. Wilson Tang, "Usefulness of neutrophil-to-lymphocyte ratio in risk stratification of patients with advanced heart failure," *The American Journal of Cardiology*, vol. 115, no. 1, pp. 57–61, 2015.
- [16] S. Tokgoz, M. Kayrak, Z. Akpınar, A. Seyithanoğlu, F. Güney, and B. Yürüten, "Neutrophil lymphocyte ratio as a predictor of stroke," *Journal of Stroke and Cerebrovascular Diseases*, vol. 22, no. 7, pp. 1169–1174, 2013.
- [17] S. Gökhan, A. Ozhasenekler, H. Mansur Durgun, E. Akil, M. Ustündag, and M. Orak, "Neutrophil lymphocyte ratios in stroke subtypes and transient ischemic attack," *European Review for Medical and Pharmacological Sciences*, vol. 17, no. 5, pp. 653–657, 2013.
- [18] A. Celikbilek, S. Ismailogullari, and G. Zararsiz, "Neutrophil to lymphocyte ratio predicts poor prognosis in ischemic cerebrovascular disease," *Journal of Clinical Laboratory Analysis*, vol. 28, no. 1, pp. 27–31, 2014.
- [19] S. Tokgoz, S. Keskin, M. Kayrak, A. Seyithanoglu, and A. Ogmegul, "Is neutrophil/lymphocyte ratio predict to short-term mortality in acute cerebral infarct independently from infarct volume?," *Journal of Stroke and Cerebrovascular Diseases*, vol. 23, no. 8, pp. 2163–2168, 2014.
- [20] F. Accorsi, "Color Doppler of the extracranial and intracranial arteries in the acute phase of cerebral ischemia," *Journal of Ultrasound*, vol. 16, no. 4, pp. 187–193, 2013.
- [21] D. Fairweather, "Sex differences in inflammation during atherosclerosis," *Clinical Medicine Insights: Cardiology*, vol. 8, Supplement 3, pp. 49–59, 2014.
- [22] L. Saba, M. Anzidei, B. C. Marincola et al., "Imaging of the carotid artery vulnerable plaque," *Cardiovascular and Interventional Radiology*, vol. 37, no. 3, pp. 572–585, 2014.
- [23] M. Marnane, S. Prendeville, C. McDonnell et al., "Plaque inflammation and unstable morphology are associated with early stroke recurrence in symptomatic carotid stenosis," *Stroke*, vol. 45, no. 3, pp. 801–806, 2014.
- [24] F. Biscetti, G. Straface, G. Bertolotti et al., "Identification of a potential proinflammatory genetic profile influencing carotid plaque vulnerability," *Journal of Vascular Surgery*, vol. 61, no. 2, pp. 374–381, 2015.
- [25] E. E. Eriksson, X. Xie, J. Werr, P. Thoren, and L. Lindbom, "Direct viewing of atherosclerosis in vivo: plaque invasion by leukocytes is initiated by the endothelial selectins," *The FASEB Journal*, vol. 15, no. 7, pp. 1149–1157, 2001.
- [26] G. Huang, X. N. Zhong, B. Zhong et al., "Significance of white blood cell count and its subtypes in patients with acute coronary syndrome," *European Journal of Clinical Investigation*, vol. 39, no. 5, pp. 348–358, 2009.
- [27] A. S. Major, S. Fazio, and M. F. Linton, "B-lymphocyte deficiency increases atherosclerosis in LDL receptor-null Mice," *Arteriosclerosis, Thrombosis, and Vascular Biology*, vol. 22, no. 11, pp. 1892–1898, 2002.
- [28] D. Ducloux, B. Challier, P. Saas, P. Tiberghien, and J. M. Chalopin, "CD4 cell lymphopenia and atherosclerosis in renal transplant Recipients," *Journal of the American Society of Nephrology*, vol. 14, no. 3, pp. 767–772, 2003.
- [29] A. Soop, L. Hällström, C. Frostell, H. Wallén, F. Mobarrez, and D. S. Pisetsky, "Effect of lipopolysaccharide administration on the number, phenotype and content of nuclear molecules in blood microparticles of normal human Subjects," *Scandinavian Journal of Immunology*, vol. 78, no. 2, pp. 205–213, 2013.
- [30] D. H. Wyllie, I. C. Bowler, and T. E. Peto, "Relation between lymphopenia and bacteraemia in UK adults with medical emergencies," *Journal of Clinical Pathology*, vol. 57, no. 9, pp. 950–955, 2004.
- [31] J. Núñez, J. Sanchis, V. Bodí et al., "Relationship between low lymphocyte count and major cardiac events in patients with acute chest pain, a non-diagnostic electrocardiogram and normal troponin levels," *Atherosclerosis*, vol. 206, no. 1, pp. 251–257, 2009.
- [32] F. Imtiaz, K. Shafique, S. S. Mirza, Z. Ayoob, P. Vart, and S. Rao, "Neutrophil lymphocyte ratio as a measure of systemic inflammation in prevalent chronic diseases in Asian population," *International Archives of Medicine*, vol. 5, no. 1, p. 2, 2012.
- [33] Y. H. Choi, Y. J. Hong, Y. Ahn, I. H. Park, and M. H. Jeong, "Relationship between neutrophil-to-lymphocyte ratio and plaque components in patients with coronary artery disease: virtual histology intravascular ultrasound analysis," *Journal of Korean Medical Science*, vol. 29, no. 7, pp. 950–956, 2014.
- [34] G. Açar, S. Fidan, Z. A. Uslu et al., "Relationship of neutrophil-lymphocyte ratio with the presence, severity, and extent of coronary atherosclerosis detected by coronary computed tomography angiography," *Angiology*, vol. 66, no. 2, pp. 174–179, 2015.
- [35] B.-J. Park, J.-Y. Shim, H.-R. Lee et al., "Relationship of neutrophil-lymphocyte ratio with arterial stiffness and

- coronary calcium score,” *Clinica Chimica Acta*, vol. 412, no. 11-12, pp. 925–929, 2011.
- [36] S. Hyun, S. Kwon, S. Cho et al., “Can the neutrophil-to-lymphocyte ratio appropriately predict carotid artery stenosis in patients with ischemic stroke?—a retrospective study,” *Journal of Stroke and Cerebrovascular Diseases*, vol. 24, no. 11, pp. 2646–2651, 2015.
- [37] M. Świtońska, N. Piekus-Słomka, A. Słomka, P. Sokal, E. Żekanowska, and S. Lattanzi, “Neutrophil-to-lymphocyte ratio and symptomatic hemorrhagic transformation in ischemic stroke patients undergoing revascularization,” *Brain Sciences*, vol. 10, no. 11, p. 771, 2020.
- [38] C.-H. Dong, Z.-M. Wang, and S.-Y. Chen, “Neutrophil to lymphocyte ratio predict mortality and major adverse cardiac events in acute coronary syndrome: A systematic review and meta-analysis,” *Clinical Biochemistry*, vol. 52, pp. 131–136, 2018.
- [39] A. J. Lusis, “Atherosclerosis,” *Nature*, vol. 407, no. 6801, pp. 233–241, 2000.
- [40] J. C. Wang and M. Bennett, “Aging and Atherosclerosis,” *Circulation Research*, vol. 111, no. 2, pp. 245–259, 2012.
- [41] C. Wendorff, H. Wendorff, J. Pelisek et al., “Carotid plaque morphology is significantly associated with sex, age, and history of neurological symptoms,” *Stroke*, vol. 46, no. 11, pp. 3213–3219, 2015.
- [42] K. Matsumoto, Y. Sera, H. Nakamura, Y. Ueki, and S. Miyake, “Correlation between common carotid arterial wall thickness and ischemic stroke in patients with type 2 diabetes mellitus,” *Metabolism*, vol. 51, no. 2, pp. 244–247, 2002.
- [43] C. Giannarelli, E. Bianchini, R. M. Bruno et al., “Local carotid stiffness and intima-media thickness assessment by a novel ultrasound-based system in essential hypertension,” *Atherosclerosis*, vol. 223, no. 2, pp. 372–377, 2012.
- [44] G. Douglas and K. M. Channon, “The pathogenesis of atherosclerosis,” *Medicine*, vol. 38, no. 8, pp. 397–402, 2010.
- [45] A. Huibers, G. J. de Borst, S. Wan et al., “Non-invasive carotid artery imaging to identify the vulnerable plaque: current status and future goals,” *European Journal of Vascular and Endovascular Surgery*, vol. 50, no. 5, pp. 563–572, 2015.
- [46] S. Lattanzi, L. Carbonari, G. Pagliariccio et al., “Predictors of cognitive functioning after carotid revascularization,” *Journal of the Neurological Sciences*, vol. 405, 2019.
- [47] S. Lattanzi, L. Carbonari, G. Pagliariccio et al., “Neurocognitive functioning and cerebrovascular reactivity after carotid endarterectomy,” *Neurology*, vol. 90, no. 4, pp. e307–e315, 2018.

## Research Article

# C-Reactive Protein Levels and Clinical Prognosis in LAA-Type Stroke Patients: A Prospective Cohort Study

Qingjia Zeng,<sup>1</sup> Yaying Zeng,<sup>2</sup> Mark Slevin,<sup>3</sup> Baoqiang Guo,<sup>3</sup> Zhipeng Shen ,<sup>4</sup>  
Binbin Deng ,<sup>2</sup> and Wenbo Zhang ,<sup>4</sup>

<sup>1</sup>University College London, Institute of Health Informatics, UK

<sup>2</sup>Department of Neurology, The First Affiliated Hospital of Wenzhou Medical University, Wenzhou, China

<sup>3</sup>Department of Life Science Faculty of Science and Engineering, Manchester Metropolitan University, Manchester M1 5GD, UK

<sup>4</sup>Department of Neurosurgery, The Children's Hospital of Zhejiang University School of Medicine, National Clinical Research Center for Child Health, Hangzhou, China

Correspondence should be addressed to Zhipeng Shen; shenzp@zju.edu.cn, Binbin Deng; dbinbin@aliyun.com, and Wenbo Zhang; zhangwenbozero@163.com

Received 11 December 2020; Revised 10 March 2021; Accepted 17 May 2021; Published 8 June 2021

Academic Editor: Juan Yang

Copyright © 2021 Qingjia Zeng et al. This is an open access article distributed under the Creative Commons Attribution License, which permits unrestricted use, distribution, and reproduction in any medium, provided the original work is properly cited.

**Background and Purpose.** There are increasing evidences that show that the prognosis of patients with acute ischemic stroke (AIS) is closely related to the inflammatory response. In the inflammation caused by AIS, plasma C-reactive protein (CRP) will increase and is associated with prognosis in these patients; few studies have looked at the relationship between CRP and large artery atherosclerosis- (LAA-) type AIS. We aim to investigate the role of CRP in predicting the functional outcome of LAA-type AIS patients. **Methods.** We prospectively included 200 patients with LAA-type AIS and tested their CRP levels on admission. We followed these patients consecutively. The primary outcome was an adverse event, defined as a modified Rankin Scale score of 2-6 at months 3, 6, and 12 after discharge. A logistic regression model was used to analyze the relationship between CRP and the functional outcome of LAA stroke. **Results.** We divided 200 patients into 3 groups evenly based on CRP level. After adjustment for gender, age, smoking history, drinking history, history of hyperlipidemia, history of diabetes, lipid levels, and blood glucose levels, logistic regression showed that the incidence of LAA-type AIS poor outcome was positively associated with CRP level at admission, whether it was 3 months, 6 months, or 12 months after discharge, respectively (OR: 2.574, 95% CI: 1.213-5.463; OR: 2.806, 95% CI: 1.298-6.065; OR: 2.492, 95% CI: 1.167-5.321. In the highest tertile vs. the lowest tertile as a reference), and both were statistically different. **Conclusions.** High CRP level predicts poor functional outcome in LAA-type AIS patients, which provides a strong basis for clinicians to make treatment decisions for these patients.

## 1. Introduction

Stroke is one of the most common causes of disability and death and is associated with a remarkable economic and social burden [1, 2]. Acute ischemic stroke (AIS) is the most common type of stroke, accounting for 87% of all strokes [3]. There is growing evidence that ischemic stroke is related to the systemic inflammatory response, and diverse inflammatory cytokines are being investigated as potential predictors of cardiovascular and functional prognosis after AIS [4, 5].

It is increasingly recognized that inflammation plays a central role in atherosclerosis and cardiovascular disease

[6]. Inflammation plays a crucial role in the pathogenesis of ischemic stroke, with mechanisms of action including atherosclerosis, plaque instability, and plaque rupture triggering [7, 8]. In the case of an acute stroke, inadequate blood flow to the brain leads to an interruption in the supply of oxygen and glucose to the neurons, resulting in massive cell death within the infarcted core [9]. Damage signals are released from dying cells in the ischemic core and peri-infarct region [10]; these signals activate leukocytes and microglia, leading to a substantial release of proinflammatory cytokines, upregulate the expression of leukocyte adhesion molecules, and stimulate the formation of chemokines. Combined with increased



TABLE 1: Characteristics of the cohort by C-reactive protein (CRP) levels.

	Group A (n = 66) CRP: <1.68	Group B (n = 67) CRP: 1.70-5.46	Group C (n = 67) CRP: >5.50
mRS 3 months	1.12 ± 1.34	1.63 ± 1.58	2.16 ± 1.68
mRS 6 months	1.06 ± 1.29	1.57 ± 1.63	2.06 ± 1.68
mRS 12 months	1.11 ± 1.31	1.73 ± 1.82	2.28 ± 1.97
NIHSS	3.26 ± 2.79	4.02 ± 3.72	5.81 ± 5.26
Age	64.06 ± 10.57	65.78 ± 11.59	66.34 ± 11.16
SBP	151.39 ± 20.51	163.54 ± 20.66	159.22 ± 24.69
DBP	80.41 ± 14.32	84.39 ± 13.03	82.16 ± 14.23
WBC	6.39 ± 1.53	6.70 ± 1.88	7.82 ± 2.59
Neutrophils	3.86 ± 1.38	4.14 ± 1.52	5.93 ± 6.72
Lymphocyte	1.89 ± 0.50	1.84 ± 0.56	1.76 ± 0.74
RBC	5.53 ± 0.52	4.61 ± 0.56	4.40 ± 0.61
PLT	208.35 ± 63.93	210.72 ± 60.57	241.32 ± 68.40
Albumin	38.33 ± 2.74	38.49 ± 4.08	36.91 ± 3.89
ALT	22.42 ± 12.33	22.18 ± 11.82	27.61 ± 45.50
AST	23.00 ± 9.29	24.16 ± 8.13	25.42 ± 12.99
Bilirubin	11.11 ± 4.02	11.54 ± 4.96	12.03 ± 6.85
Cr	69.15 ± 19.68	76.31 ± 38.45	69.61 ± 18.77
Bun	4.73 ± 1.92	5.80 ± 5.31	5.18 ± 1.69
TC	4.52 ± 1.00	4.60 ± 1.29	4.65 ± 1.35
TG	1.76 ± 0.81	1.83 ± 0.76	1.74 ± 1.06
HDL	1.06 ± 0.26	1.06 ± 0.24	1.06 ± 0.39
LDL	2.65 ± 0.80	2.72 ± 0.90	2.74 ± 1.01
Blood glucose	6.47 ± 1.60	6.60 ± 1.62	6.73 ± 1.61
Thyroxine	1.22 ± 0.24	1.23 ± 0.23	1.08 ± 0.29
Gender (female)	71.20%	67.20%	62.70%
DM	33.30%	37.30%	53.70%
Hyperlipidemia	54.50%	56.70%	70.10%
Smoking	57.60%	44.80%	40.30%
Drinking	47.00%	37.30%	31.10%

Abbreviation: NIHSS: the National Institutes of Health Stroke Scale; SBP: systolic pressure; DBP: diastolic pressure; WBC: white blood cell; RBC: red blood cell; PLT: platelet; AST: aspartate aminotransferase; ALT: alanine aminotransferase; Cr: creatinine; Bun: blood urea nitrogen; TC: total cholesterol; TG: triglyceride; HDL: high-density lipoprotein; LDL: low-density lipoprotein; DM: diabetes mellitus.

blood-brain barrier (BBB) permeability, this allows leukocytes to enter the ventricles in large numbers and remove the large amount of debris caused by cell death [11, 12].

Among the inflammatory markers of peripheral blood, CRP is the most widely used and well established [12]. Previous studies have shown that in the general population, elevated serum or plasma CRP may lead to future vascular events [13–16]. A study reports high levels of CRP associated

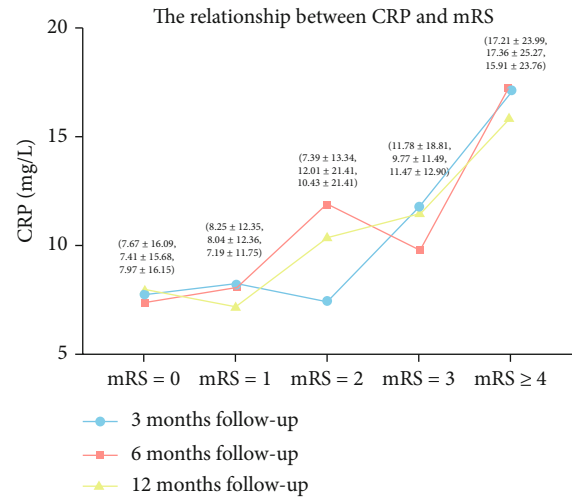


FIGURE 1: Plasma C-reactive protein levels and modified Rankin Scale. Note: at 3 months, 6 months, and 12 months of follow-up, CRP levels increased with increasing mRS. CRP: C-reactive protein; mRS: modified Rankin Scale.

with clinical prognosis in the time window between 12 and 72 hours after ischemic stroke [17, 18]. CRP is of clinical importance as an early prognostic factor after stroke because it is an easily measured and clinically common indicator of inflammation. However, the vast majority of current studies address the relationship between AIS and CRP and are mostly retrospective. AIS has different subtypes, and large artery atherosclerosis (LAA) is a key subtype of the Trial of Org 10172 in Acute Stroke Treatment (TOAST) classification system. Elevated CRP often indicates a worse prognosis in AIS patients, but it is not clear whether it can predict the patient's functional outcome in LAA patients. We explored this topic.

## 2. Materials and Methods

**2.1. Study Design.** We enrolled patients with AIS between January 2016 and January 2017. Stroke is an acute cerebrovascular disease with acute or focal brain dysfunction caused by various vascular etiologies lasting longer than 24 hours. We use brain imaging data (computed tomography and/or magnetic resonance imaging) to diagnose AIS. According to TOAST criteria, AIS can be divided into four subtypes: LAA, small vessel occlusion, cardioembolic, and others [19]. This study included patients with LAA according to TOAST criteria.

**2.2. Exclusion Criteria.** The exclusion criteria are as follows: (1) excluding other vascular infarction, cerebral venous thrombosis; (2) on anti-inflammatory therapy prior to hospitalization; (3) any factor that would affect indicators of inflammation, including serious infection or use of antibiotics prior to admission, hematologic disorders, immune system disorders, glucocorticoid use, or severe liver or kidney disease, and recent trauma or major surgery; (4) patients lost to follow-up. All patients were admitted within 7 days of



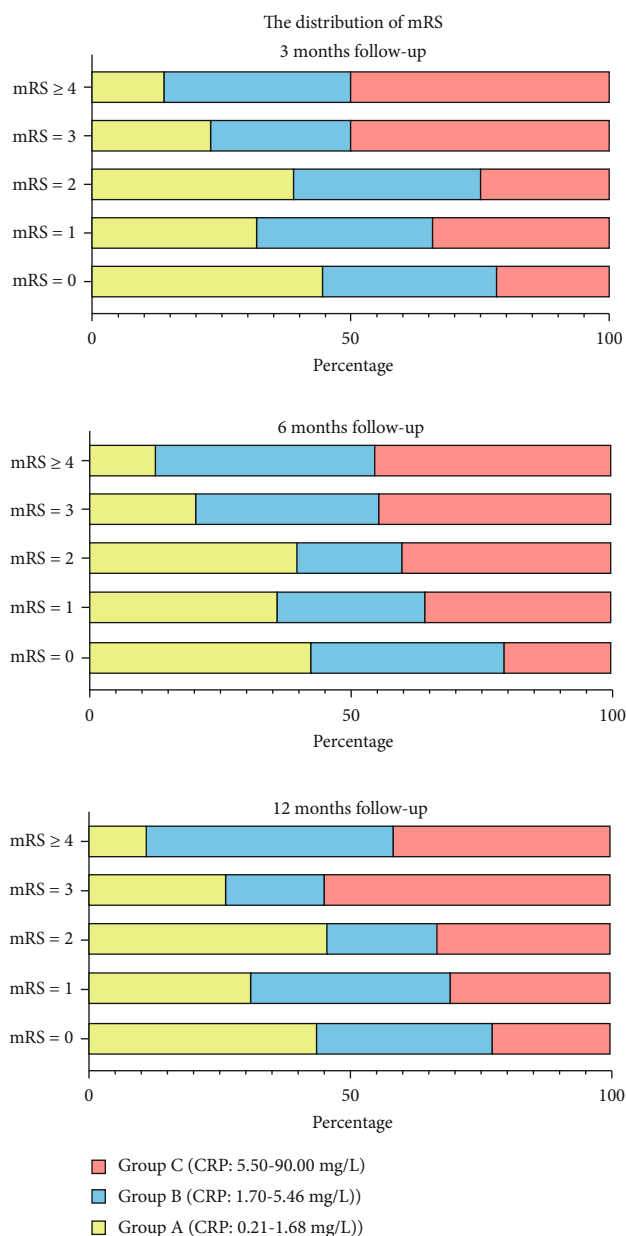


FIGURE 2: The percentage of three groups at different modified Rankin Scale scores.

stroke onset, and their baseline data were collected using standardized data records. Therefore, 200 remained for analysis. We evenly divided 200 patients into 3 groups according to CRP from low to high. There were 66 patients, 67 patients, and 67 patients in each group. We defined them as group A, group B, and group C. In this way, we have 3 subgroups with different CRP levels and roughly equal numbers of patients.

**2.3. Clinical and Laboratory Assessments.** All blood indicators were assessed on the morning of the second day of admission after overnight fasting. CT examinations were completed within 24 hours of admission; confirmation of AIS relies on repeat CT and MRI exams prior to hospital discharge.

**2.4. Follow-Up.** The National Institutes of Health Stroke Scale (NIHSS) score was used for assessment at admission and on the first day after admission and at discharge. Patients who survived the acute phase and were discharged or hospitalized for rehabilitation were assessed for functional outcome every 3 months by follow-up using a modified Rankin Scale (mRS) score. Good outcomes were defined as mRS scores 0-1, while poor outcomes were defined as mRS scores 2-6. Two investigators evaluated all clinical data alone. In case of disagreement, a third party intervened to assess it. Each patient was followed up for at least 1 year.

**2.5. Statistical Analysis.** All data were counted by SPSS 22.0 and R. Univariate analysis was performed using the chi-square test, *t*-test, or Kruskal-Wallis rank-sum test. Logistic regression analysis was used to estimate the multivariate-adjusted odds ratio (OR) and 95% confidence intervals (95% CI). Multivariate models included age, gender, dyslipidemia, diabetes, smoking, drinking, lipid levels, and blood glucose levels. Heterogeneity *P* was calculated by adding the CRP tertile × subgroup variable interaction term to the model. Probability values of *P* < 0.05 were considered statistically different.

### 3. Results

**3.1. Patient Characteristics.** Patient demographic information and vascular risk factors were recorded within 48 hours of admission. Table 1 shows the baseline demographic and clinical characteristics of LAA patients based on CRP levels. A total of 200 patients with LAA were collected in this study, of which 134 (67.0%) were males, with a mean age of 63.9 years, and 66 (33.0%) were females, with a mean age of 68.4 years. The median plasma CRP level on admission was 2.90 mg/L (the tertile range of all patients: 1.70-5.46 mg/L). At 3-month follow-up, the mean mRS for these patients was 1.64, while at 6- and 12-month follow-up, their mean mRS was 1.57 and 1.71, respectively (Table 1).

**3.2. CRP Levels and Clinical Outcomes.** We considered mRS ≥ 2 as the occurrence of an adverse outcome. At 3-month follow-up, the incidence of adverse outcomes was 45.0% (CRP level, 7.89 vs. 12.59); at 6 months, it was 42.5% (CRP level, 7.64 vs. 13.69); at 12 months, a total of 43.5% of patients had adverse outcomes (CRP level, 7.68 vs. 13.02).

In Figure 1, regardless of the time period of follow-up, when mRS was elevated, CRP levels overall also increased. However, at these three follow-up time points, when the mRS was the same, CRP levels did not show significant differences. Figure 2 shows the percentage of each CRP level at different mRS levels. As mRS increased, the percentage of group C gradually increased.

After adjustment for gender, age, smoking history, drinking history, history of dyslipidemia, history of diabetes, lipid levels, and blood glucose levels, CRP levels were significantly associated with patient outcomes (Table 2). In a multifactorial logistic regression analysis, we found that the age of the patients was also a risk factor for adverse outcomes, and the older the patients, the more likely they were to have an

TABLE 2: Plasma C-reactive protein levels and functional outcomes during follow-up.

	Events%	OR	Model 1 95% CI	P	OR	Model 2 95% CI	P	OR	Model 3 95% CI	P
Outcome 1 (3-month follow-up)										
Group A	33.33%	Ref	Ref	Ref	Ref	Ref	Ref	Ref	Ref	Ref
Group B	44.78%	1.559	0.762-3.192	0.224	1.548	0.752-3.187	0.236	1.400	0.673-2.915	0.368
Group C	56.72%	2.545	1.241-5.221	0.011*	2.611	1.241-5.496	0.011*	2.574	1.213-5.463	0.014*
P				0.038*			0.040*			0.044*
Outcome 2 (6-month follow-up)										
Group A	30.30%	Ref	Ref	Ref	Ref	Ref	Ref	Ref	Ref	Ref
Group B	41.79%	1.572	0.754-3.276	0.228	1.553	0.741-3.253	0.243	1.384	0.651-2.940	0.399
Group C	55.22%	2.756	1.324-5.734	0.007*	2.751	1.290-5.865	0.009*	2.806	1.298-6.065	0.009*
P				<0.001*			0.031*			0.026*
Outcome 3 (12-month follow-up)										
Group A	33.33%	Ref	Ref	Ref	Ref	Ref	Ref	Ref	Ref	Ref
Group B	40.30%	1.299	0.632-2.669	0.476	1.267	0.611-2.626	0.524	1.093	0.519-2.303	0.815
Group C	56.72%	2.57	1.253-5.269	0.010*	2.446	1.165-5.135	0.018*	2.492	1.167-5.321	0.018*
P				0.027*			0.047*			0.033*

Note: in the logistic regression analysis, Model 1 adjusted for gender and age. Model 2 incorporates gender, age, smoking history, drinking history, history of dyslipidemia, and history of diabetes as confounding factors, and Model 3 incorporates lipid levels and blood glucose levels on the basis of Model 2. We can see that after adjusting for various confounding factors, CRP still significantly affects the prognosis of patients.

adverse outcome. The patients' gender ( $P = 0.318$ ), history of drinking ( $P = 0.461$ ), history of smoking ( $P = 0.448$ ), lipid level ( $P = 0.496$ ), and blood glucose level ( $P = 0.888$ ) were not significantly associated with the prognosis (Figure 3). Figure 4 shows the linear region of diagnosis of CRP and AIS patients. Based on the two risk factors, CRP and age, we plotted a nomogram accordingly (Figure 5). Based on the nomogram, we can easily calculate the cumulative risk score of patients with LAA-type AIS and use this to calculate the corresponding probability of having an adverse outcome.

#### 4. Discussion

In terms of disability and mortality, the major factors contributing to poor poststroke outcomes, such as age or baseline stroke severity, can not be modified. However, alterations in biomarkers may occur after stroke that may correlate with certain clinical outcomes, providing researchers and clinicians with a unique opportunity for interventions to improve stroke outcomes. Biomarkers serve as indicators of physiological or pathological biological processes that can be objectively measured and assessed. CRP is easily measured and commonly used and may be important in predicting functional prognosis after stroke [12]. Elevated CRP may reflect the degree of stroke, tissue damage, or systemic inflammatory response to concurrent infection [20]. The major finding of this study is that a higher level of CRP is an independent predictor of poor outcomes in patients with LAA-type AIS. Therefore, this study will give clinicians the insight that CRP is a widely available and easily accessible biomarker;

early intervention with CRP in patients with LAA-type AIS may help these patients achieve a better clinical outcome.

Neuroinflammation is a unique pathophysiological feature of AIS patients [21, 22]. After an ischemic attack, the accumulation of inflammatory cells and mediators in the ischemic brain tissue triggers neuroinflammation. The inflammatory process is ignited by inflammatory cells such as leukocytes and activated microglia. A growing body of research suggests that CRP may be an inflammatory factor in response to ischemic stroke [23, 24]. Based on neuroinflammatory pathogenesis, patients with AIS are significantly associated with CRP [25]. Usually, in patients with severe stroke, CRP levels correlate with stroke severity and can be used as a marker of stroke prognosis [20, 26]. Studies have shown that the percentage of AIS patients with aortic sclerosis increases with increasing CRP levels; initial NIHSS scores, acute infection rates, and age increase with increasing CRP levels on admission; and the rate of neurological improvement increases with decreasing CRP levels [27]. CRP levels are elevated in the first 48 hours after onset and remain high for 3-6 months after stroke [18] [26].

In a meta-analysis, it was found that AIS patients with high CRP levels had an almost 2-fold increased risk of poor prognosis compared to patients with low CRP levels. This finding suggests that baseline CRP levels may predict the functional prognosis of patients after AIS [28]. Similarly, in our study, patients with the highest levels of CRP were 2.492 times more likely to have an adverse outcome than those with low levels of CRP at 12-month follow-up. In addition, a study found that at 90-day follow-up, an elevated each unit log-transformed CRP level was associated with a 2.5-fold higher risk of poor functional outcome [29]. In our 200

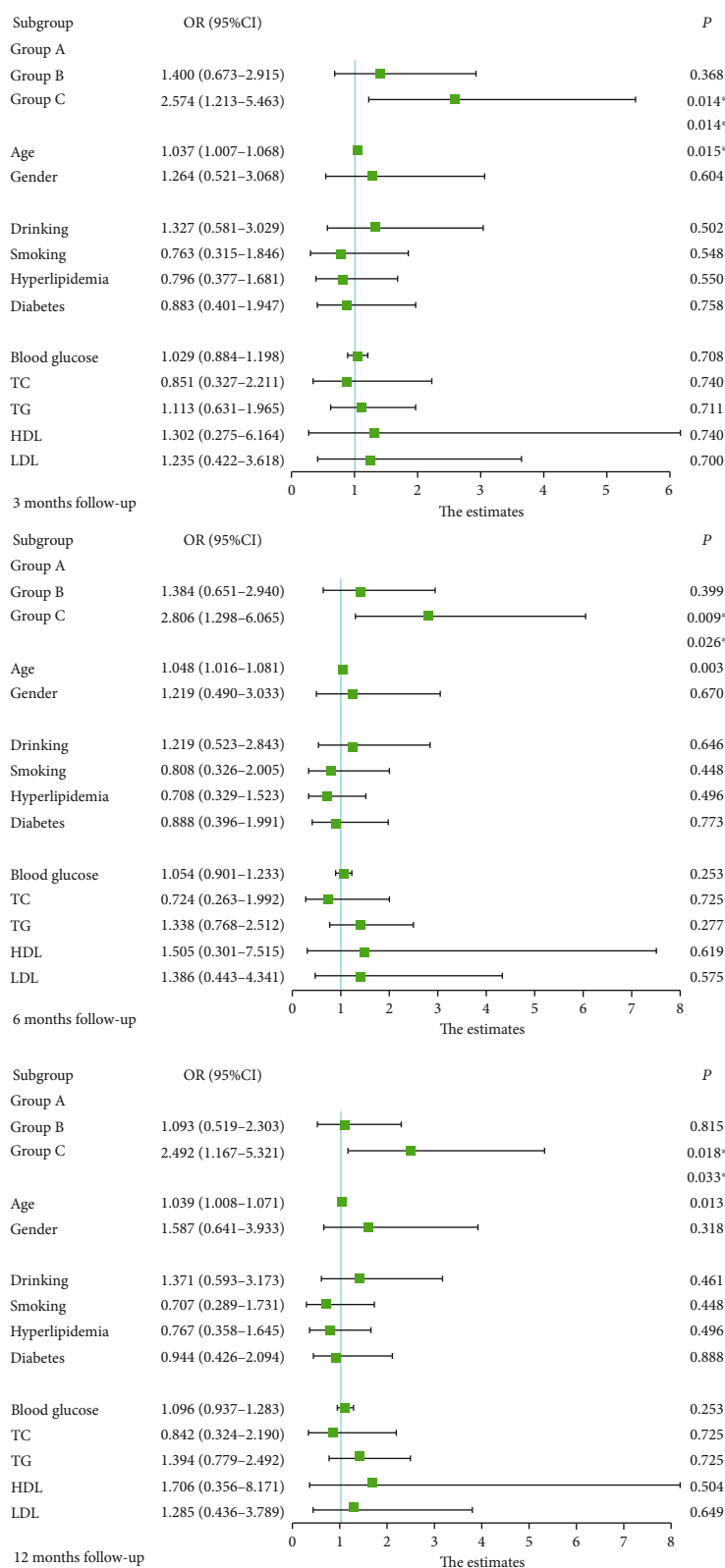


FIGURE 3: Multivariable-adjusted forest plot of each C-reactive protein tertile for poor functional outcome.

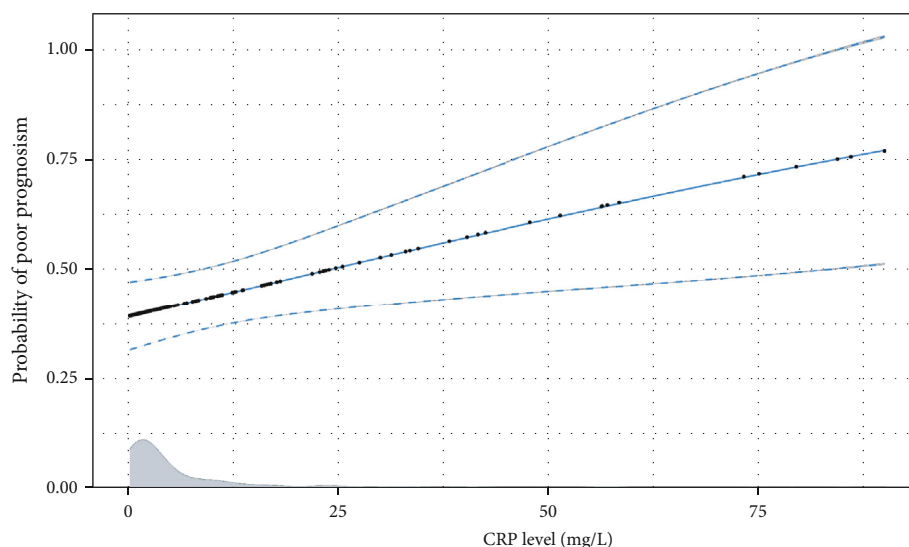


FIGURE 4: The linear regression of prognosis of C-reactive protein levels and acute ischemic stroke patients. Note: the abscissa represents C-reactive protein levels, and the ordinate shows the probability of poor prognosis. It can be seen that with the increase of C-reactive protein levels, the probability of poor prognosis is higher.

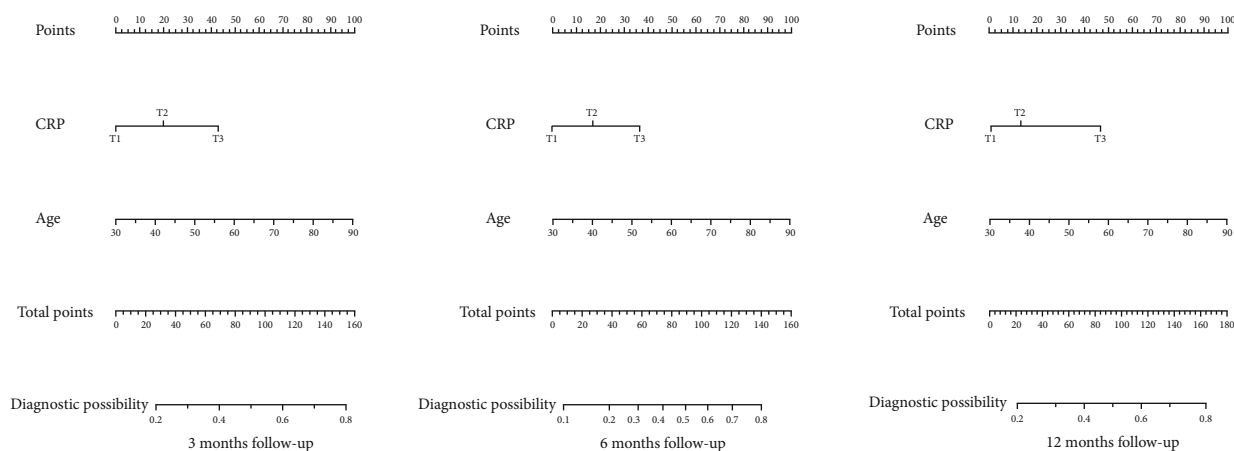


FIGURE 5: A nomogram model based on C-reactive protein and age. Note: the values on each variable axis have corresponding points, and the sum of these points on the survival axis has a probability of large artery atherosclerosis stroke corresponding to it.

patients, at 90-day follow-up, high CRP was 2.574 times more likely to have an adverse outcome than patients with low CRP levels. Welsh et al. found that a one-unit increase in CRP levels was associated with an 18% increase in the risk of 1-year adverse functional outcome, and baseline CRP levels were a predictor of poor functional prognosis at 1 month postadmission [30].

A study found that artificial administration of CRP caused significantly greater infarcts than controls in a model of middle cerebral artery occlusion in adult rats [31]. In addition, in a rat model of acute myocardial infarction, artificial injection of CRP increased infarct size and exacerbated cardiac insufficiency, whereas the use of CRP inhibitors eliminated this effect [32]. These studies suggest that CRP has the inherent property of exacerbating ischemic injury. In patients with acute stroke, CRP was shown to be associated with poststroke functional outcome [32]. These studies sug-

gest that intervening with CRP in patients early in stroke may improve ischemia-induced injury and shed new light on clinical treatment.

The paper still has several shortcomings. First, patients who were lost to follow-up were excluded, which may lead to selection bias. Second, our patient sample size remains inadequate, and single-center studies make the results insufficient for further generalization. Third, the follow-up period is one year; although it is longer than most similar studies, it is still insufficient. Stroke recurrence and patient death are very meaningful endpoint. However, this study is a small-sample prospective study with a follow-up time of 1 year. Due to the small sample size, the confidence interval in statistical analysis is extremely large, making the statistical results unreliable. However, we have been conducting a longer-term prospective study with a larger sample size, and we believe it can make up for this shortcoming.

## 5. Conclusion

High CRP levels in LAA-type AIS patients were associated with worse outcomes, both with short-term follow-up (3 months) and relative long-term follow-up (12 months). Early intervention on CRP levels in these patients may lead to more favorable outcomes and bring new thinking to the treatment of LAA-type AIS.

## Data Availability

The raw data used to support the findings of this study are made available from the corresponding author upon reasonable request.

## Conflicts of Interest

The authors declare that they have no competing interests.

## Acknowledgments

We acknowledge all the authors who participated in this research. We thank all the authors who participated in this research.

## References

- [1] C. J. Murray and A. D. Lopez, "Measuring the global burden of disease," *The New England Journal of Medicine*, vol. 369, no. 5, pp. 448–457, 2013.
- [2] V. L. Feigin, B. Norrving, and G. A. Mensah, "Global burden of stroke," *Circulation Research*, vol. 120, no. 3, pp. 439–448, 2017.
- [3] J. R. Shiber, E. Fontane, and A. Adewale, "Stroke registry: hemorrhagic vs ischemic strokes," *The American Journal of Emergency Medicine*, vol. 28, no. 3, pp. 331–333, 2010.
- [4] P. Libby, "Inflammation in atherosclerosis," *Nature*, vol. 420, no. 6917, pp. 868–874, 2002.
- [5] W. Whiteley, W. L. Chong, A. Sengupta, and P. Sandercock, "Blood markers for the prognosis of ischemic stroke: a systematic review," *Stroke*, vol. 40, no. 5, pp. e380–e389, 2009.
- [6] G. K. Hansson, "Inflammation, atherosclerosis, and coronary artery disease," *The New England Journal of Medicine*, vol. 352, no. 16, pp. 1685–1695, 2005.
- [7] B. M. Scirica and D. A. Morrow, "Is C-reactive protein an innocent bystander or proatherogenic culprit? The verdict is still out," *Circulation*, vol. 113, no. 17, pp. 2128–2151, 2006.
- [8] F. C. Barone and G. Z. Feuerstein, "Inflammatory mediators and stroke: new opportunities for novel therapeutics," *Journal of Cerebral Blood Flow and Metabolism*, vol. 19, no. 8, pp. 819–834, 1999.
- [9] S. L. Mehta, N. Manhas, and R. Raghuram, "Molecular targets in cerebral ischemia for developing novel therapeutics," *Brain Research Reviews*, vol. 54, no. 1, pp. 34–66, 2007.
- [10] A. Liesz, A. Dalpke, E. Mracsko et al., "DAMP signaling is a key pathway inducing immune modulation after brain injury," *The Journal of Neuroscience*, vol. 35, no. 2, pp. 583–598, 2015.
- [11] S. Fumagalli, C. Perego, F. Pischiutta, E. R. Zanier, and M. G. de Simoni, "The ischemic environment drives microglia and macrophage function," *Frontiers in Neurology*, vol. 6, p. 81, 2015.
- [12] L. Li, A. Lundkvist, D. Andersson et al., "Protective role of reactive astrocytes in brain ischemia," *Journal of Cerebral Blood Flow and Metabolism*, vol. 28, no. 3, pp. 468–481, 2008.
- [13] P. M. Ridker, M. Cushman, M. J. Stampfer, R. P. Tracy, and C. H. Hennekens, "Inflammation, aspirin, and the risk of cardiovascular disease in apparently healthy men," *The New England Journal of Medicine*, vol. 336, no. 14, pp. 973–979, 1997.
- [14] J. J. Cao, C. Thach, T. A. Manolio et al., "C-reactive protein, carotid intima-media thickness, and incidence of ischemic stroke in the elderly: the Cardiovascular Health Study," *Circulation*, vol. 108, no. 2, pp. 166–170, 2003.
- [15] Y. Wakugawa, Y. Kiyohara, Y. Tanizaki et al., "C-reactive protein and risk of first-ever ischemic and hemorrhagic stroke in a general Japanese population: the Hisayama Study," *Stroke*, vol. 37, no. 1, pp. 27–32, 2006.
- [16] P. M. Ridker, J. E. Buring, N. Rifai, and N. R. Cook, "Development and validation of improved algorithms for the assessment of global cardiovascular risk in women: the Reynolds risk score," *JAMA*, vol. 297, no. 6, pp. 611–619, 2007.
- [17] H. Christensen and G. Boysen, "C-reactive protein and white blood cell count increases in the first 24 hours after acute stroke," *Cerebrovascular Diseases*, vol. 18, no. 3, pp. 214–219, 2004.
- [18] K. Winbeck, H. Poppert, T. Etgen, B. Conrad, and D. Sander, "Prognostic relevance of early serial C-reactive protein measurements after first ischemic stroke," *Stroke*, vol. 33, no. 10, pp. 2459–2464, 2002.
- [19] H. P. Adams Jr., B. H. Bendixen, L. J. Kappelle et al., "Classification of subtype of acute ischemic stroke. Definitions for use in a multicenter clinical trial. TOAST. Trial of Org 10172 in Acute Stroke Treatment," *Stroke*, vol. 24, no. 1, pp. 35–41, 1993.
- [20] H. M. Hertog, J. A. Rossum, H. B. Worp et al., "C-reactive protein in the very early phase of acute ischemic stroke: association with poor outcome and death," *Journal of Neurology*, vol. 256, no. 12, pp. 2003–2008, 2009.
- [21] K. Yamashiro, R. Tanaka, T. Urabe et al., "Gut dysbiosis is associated with metabolism and systemic inflammation in patients with ischemic stroke," *PLoS One*, vol. 12, no. 2, p. e0171521, 2017.
- [22] Z. Sternberg, T. Chichelli, D. Sternberg et al., "Relationship between inflammation and aspirin and clopidogrel antiplatelet responses in acute ischemic stroke," *Journal of Stroke and Cerebrovascular Diseases*, vol. 25, no. 2, pp. 327–334, 2016.
- [23] A. Bustamante, A. Simats, A. Vilar-Bergua, T. García-Berrosco, and J. Montaner, "Blood/brain biomarkers of inflammation after stroke and their association with outcome: from C-reactive protein to damage-associated molecular patterns," *Neurotherapeutics*, vol. 13, no. 4, pp. 671–684, 2016.
- [24] J. M. Luna, Y. P. Moon, K. M. Liu et al., "High-sensitivity C-reactive protein and interleukin-6-dominant inflammation and ischemic stroke risk: the northern Manhattan study," *Stroke*, vol. 45, no. 4, pp. 979–987, 2014.
- [25] G. Y. Lip, J. V. Patel, E. Hughes, and R. G. Hart, "High-sensitivity C-reactive protein and soluble CD40 ligand as indices of inflammation and platelet activation in 880 patients with nonvalvular atrial fibrillation: relationship to stroke risk factors, stroke risk stratification schema, and prognosis," *Stroke*, vol. 38, no. 4, pp. 1229–1237, 2007.
- [26] J. W. Eikelboom, G. J. Hankey, R. I. Baker et al., "C-reactive protein in ischemic stroke and its etiologic subtypes," *Journal of Stroke and Cerebrovascular Diseases*, vol. 12, no. 2, pp. 74–81, 2003.



- [27] Z. Cai, W. He, F. J. Zhuang, and Y. Chen, "The role of high high-sensitivity C-reactive protein levels at admission on poor prognosis after acute ischemic stroke," *The International Journal of Neuroscience*, vol. 129, no. 5, pp. 423–429, 2019.
- [28] Z. Hu, J. Lai, L. Chen, Y. Yi, R. Li, and W. Liao, "Can baseline C-reactive protein level predict functional outcome in acute ischaemic stroke? A meta-analysis," *Biomarkers*, vol. 25, no. 7, pp. 525–532, 2020.
- [29] W. J. Tu, S. J. Zhao, T. G. Liu, D. G. Yang, and H. Chen, "Combination of high-sensitivity C-reactive protein and homocysteine predicts the short-term outcomes of Chinese patients with acute ischemic stroke," *Neurological Research*, vol. 35, no. 9, pp. 912–921, 2013.
- [30] P. Welsh, M. Barber, P. Langhorne, A. Rumley, G. D. O. Lowe, and D. J. Stott, "Associations of inflammatory and haemostatic biomarkers with poor outcome in acute ischaemic stroke," *Cerebrovascular Diseases*, vol. 27, no. 3, pp. 247–253, 2009.
- [31] R. Gill, J. A. Kemp, C. Sabin, and M. B. Pepys, "Human C-reactive protein increases cerebral infarct size after middle cerebral artery occlusion in adult rats," *Journal of Cerebral Blood Flow and Metabolism*, vol. 24, no. 11, pp. 1214–1218, 2004.
- [32] M. B. Pepys, G. M. Hirschfield, G. A. Tennent et al., "Targeting C-reactive protein for the treatment of cardiovascular disease," *Nature*, vol. 440, no. 7088, pp. 1217–1221, 2006.

## Corrigendum

# Corrigendum to “Potential Factors for Psychological Symptoms at Three Months in Patients with Young Ischemic Stroke”

**Dongjuan Xu** <sup>1</sup>, **Xi Chu**<sup>2</sup>, **Kun Wang**<sup>3,4</sup>, **Lianyan Wei**<sup>1</sup>, **Yunyun Xu**<sup>1</sup>, **Xiaomin Huang**<sup>5</sup>, **Jinna Li**<sup>6</sup>, **Lina Xu**<sup>6</sup>, **Lu Yin** <sup>7</sup>, **Hong Liu**<sup>8</sup>, **Xiaolei Liu**<sup>9</sup>, **Haixia Leng**<sup>4</sup>, **Qing Xue**<sup>4</sup>, **Mao Peng**<sup>4</sup>, **Longbin Jia**<sup>6</sup> and **Hongxing Wang**<sup>4,10,11</sup>

<sup>1</sup>Department of Neurology, Dongyang People’s Hospital, Wenzhou Medical University, Zhejiang 322100, China

<sup>2</sup>Health Management Department, Xuanwu Hospital, Capital Medical University, Beijing 100053, China

<sup>3</sup>Department of Neurology, Beijing Puren Hospital, Beijing 100062, China

<sup>4</sup>Department of Neurology, Xuanwu Hospital, Capital Medical University, Beijing 100053, China

<sup>5</sup>Department of Neurology, Ningcheng Center Hospital, Inner Mongolia 024200, China

<sup>6</sup>Department of Neurology, Jincheng People’s Hospital, Shanxi 048026, China

<sup>7</sup>Medical Research & Biometrics Centre, National Centre for Cardiovascular Diseases, Fuwai Hospital, Peking Union Medical College & Chinese Academy of Medical Sciences, Beijing, China Beijing, 102300, China

<sup>8</sup>Department of Neurology, Heping Hospital Affiliated to Changzhi Medical College, Shanxi 046000, China

<sup>9</sup>Department of Neurology, The First Affiliated Hospital of Kunming Medical University, Yunnan 650032, China

<sup>10</sup>Beijing Psychosomatic Disease Consultation Center, Xuanwu Hospital, Capital Medical University, Beijing 100053, China

<sup>11</sup>Institute of Sleep and Consciousness Disorders, Beijing Institute for Brain Disorders, Capital Medical University, Beijing 100053, China

Correspondence should be addressed to Hongxing Wang; wanghongxing@xwh.ccmu.edu.cn

Received 24 May 2021; Accepted 24 May 2021; Published 7 June 2021

Copyright © 2021 Dongjuan Xu et al. This is an open access article distributed under the Creative Commons Attribution License, which permits unrestricted use, distribution, and reproduction in any medium, provided the original work is properly cited.

In the article titled “Potential Factors for Psychological Symptoms at Three Months in Patients with Young Ischemic Stroke” [1], the authors identified two errors in Table 3 where “cm<sup>3</sup>” should be “mm<sup>3</sup>”. The corrected Table 3 is shown below.

TABLE 3

Variables	OR (95% CI)	P
Model for SCL-90-R		
Family function (moderate and serious dysfunction vs. good)	2.50 (1.71, 3.54)	<0.01
Hypertension (yes vs. no)	3.27 (1.92, 4.27)	0.02
Infarct size ( $\geq 20$ vs. $< 20$ mm <sup>3</sup> )	2.39 (1.53, 3.45)	<0.01
Model for depression		
Marital status (single vs. married)	1.23 (1.03, 1.54)	0.01
Family function (moderate and serious dysfunction vs. good)	1.21 (1.05, 1.45)	0.03
Infarct size ( $\geq 20$ vs. $< 20$ mm <sup>3</sup> )	1.74 (1.14, 3.13)	0.02
Model for somatization		
Family function (moderate and serious dysfunction vs. good)	2.32 (1.51, 2.80)	<0.01
Model for anxiety		
Hypertension (yes vs. no)	2.41 (1.54, 3.46)	0.03

Abbreviations: OR: odds ratio; CI: confidence interval; SCL-90-R: Symptom Checklist 90 Revised.

## References

- [1] D. Xu, X. Chu, K. Wang et al., "Potential Factors for Psychological Symptoms at Three Months in Patients with Young Ischemic Stroke," *BioMed Research International*, vol. 2021, Article ID 5545078, 7 pages, 2021.

## *Retraction*

# **Retracted: The Impact of Study Setting on Clinical Characteristics in Older Chinese Adults with Subjective Cognitive Decline: Baseline Investigation of Convenience and Population-Based Samples**

### **BioMed Research International**

Received 12 March 2024; Accepted 12 March 2024; Published 20 March 2024

Copyright © 2024 BioMed Research International. This is an open access article distributed under the Creative Commons Attribution License, which permits unrestricted use, distribution, and reproduction in any medium, provided the original work is properly cited.

This article has been retracted by Hindawi following an investigation undertaken by the publisher [1]. This investigation has uncovered evidence of one or more of the following indicators of systematic manipulation of the publication process:

- (1) Discrepancies in scope
- (2) Discrepancies in the description of the research reported
- (3) Discrepancies between the availability of data and the research described
- (4) Inappropriate citations
- (5) Incoherent, meaningless and/or irrelevant content included in the article
- (6) Manipulated or compromised peer review

The presence of these indicators undermines our confidence in the integrity of the article's content and we cannot, therefore, vouch for its reliability. Please note that this notice is intended solely to alert readers that the content of this article is unreliable. We have not investigated whether authors were aware of or involved in the systematic manipulation of the publication process.

Wiley and Hindawi regrets that the usual quality checks did not identify these issues before publication and have since put additional measures in place to safeguard research integrity.

We wish to credit our own Research Integrity and Research Publishing teams and anonymous and named external researchers and research integrity experts for contributing to this investigation.







The corresponding author, as the representative of all authors, has been given the opportunity to register their agreement or disagreement to this retraction. We have kept a record of any response received.

### **References**

- [1] M. Zhao, G. Chen, T. Li, C. Sheng, Y. Li, and Y. Han, "The Impact of Study Setting on Clinical Characteristics in Older Chinese Adults with Subjective Cognitive Decline: Baseline Investigation of Convenience and Population-Based Samples," *BioMed Research International*, vol. 2021, Article ID 5538323, 9 pages, 2021.

## Research Article

# The Impact of Study Setting on Clinical Characteristics in Older Chinese Adults with Subjective Cognitive Decline: Baseline Investigation of Convenience and Population-Based Samples

Mingyan Zhao <sup>1,2</sup>, Guanqun Chen <sup>1,3</sup>, Taoran Li <sup>1</sup>, Can Sheng <sup>1</sup>, Yuxia Li <sup>1</sup>,  
and Ying Han <sup>1,4,5</sup>

<sup>1</sup>Department of Neurology, Xuanwu Hospital of Capital Medical University, Beijing, China 100053

<sup>2</sup>Department of Neurology, Tangshan Gongren Hospital, Tangshan, China 063000

<sup>3</sup>National Clinical Research Center for Geriatric Disease, Beijing, China 100053

<sup>4</sup>School of Biomedical Engineering, Hainan University, Haikou, China 570228

<sup>5</sup>Center of Alzheimer's Disease, Beijing Institute for Brain Disorders, Beijing, China 100053

Correspondence should be addressed to Ying Han; [hanying@xwh.ccmu.edu.cn](mailto:hanying@xwh.ccmu.edu.cn)

Received 25 January 2021; Revised 27 March 2021; Accepted 26 May 2021; Published 7 June 2021

Academic Editor: Yuzhen Xu

Copyright © 2021 Mingyan Zhao et al. This is an open access article distributed under the Creative Commons Attribution License, which permits unrestricted use, distribution, and reproduction in any medium, provided the original work is properly cited.

**Background.** Subjective cognitive decline (SCD) is the earliest symptom stage of Alzheimer's disease (AD). Previous studies have shown that the study setting is an important influence factor of SCD. However, the effect of this factor among a Chinese population with SCD is not clear. Here, we aim to compare the clinical characteristics of SCD between a convenience and a population-based sample in China. **Methods.** We included a convenience sample of 212 SCD subjects and a population-based sample of 110 SCD subjects. We performed univariate analysis to evaluate the between-group differences in sociodemographic characteristics, neuropsychological performance, psychiatric conditions, different cognitive domains, and the SCD-plus criteria. Multiple linear regression model was established, adjusted for sex, age, and education, and compared the neuropsychological performance between the groups. **Results.** The convenience sample had more years of education, a higher family history of dementia, and higher neuropsychological and anxiety depression score than the population-based sample. Using sex, age, education, group as the independent variables, and neuropsychological score as the dependent variable, multiple linear regression model was established; a statistically significant neuropsychological score difference (MoCA-B, AVLT-H-N4, AVLT-H-N5, AVLT-H-N7, AFT, and STT-B) was found between the two samples. In the SCD cognitive domains, the population-based sample had more complaints about declines in their language and planning domains. For SCD-plus criteria in memory domain, the convenience sample had more complaints, worry, and cognitive decline within the last 5 years, along with medical help-seeking. **Conclusion.** There were some different characteristics among SCD individuals between convenience samples and population-based samples in China.

## 1. Introduction

Dementia is a serious public health problem. In 2015, the World Alzheimer Report showed that approximately 47 million people have dementia, and this number is expected to increase to 131 million by 2050 [1]. However, there is currently no effective therapeutic agent for mild cognitive impairment (MCI) and Alzheimer's disease (AD) [2, 3]. Effective

interventions to delay or prevent pathologic cognitive decline should be targeted at the earliest symptomatic stages of subjective cognitive decline (SCD) [4].

Cognitive decline was initially described in 1982 [5] and later was conceptualized as subjective cognitive impairment, subjective memory impairment, subjective memory decline, and so on [6]. Epidemiological studies have shown that cognitively normal elderly with SCD is more likely to develop



MCI or AD dementia [7–12]. However, SCD is not consistently associated with future cognitive impairment [13–15]. This discrepancy may be related to different definitions and research methods. Settings of recruitment lead to differences in SCD, including sociodemographic characteristics, clinical manifestations, *apolipoprotein E (APOE) ε4* status, and biological markers [16–20]. Some studies have shown that cognitively normal volunteers recruited in the community or in memory clinics were younger, better educated, and had a higher rate of a family history of AD than population-based samples [16, 17]. Subjects from clinical cohort with more memory concerns tend to have more severe AD pathology and have shown a higher annual rate of conversion to MCI or dementia than their community counterparts [12, 21]. One study showed that the recruitment methods influenced the associated biomarkers and affective symptomatology [22]. These above studies showed that different research environments lead to different characteristics. However, there are no previous studies that compared samples of a population with SCD across different study settings in China.

The aim of our study was to compare the clinical features, neuropsychological performance, and the decline in different cognitive domains as well as the SCD-plus criteria between a convenience sample and a population-based sample of SCD subjects in China. We hypothesized that there are different characteristics among Chinese SCD individuals in different study settings.

## 2. Materials and Methods

**2.1. Participants.** The convenience sample is part of the Sino Longitudinal Study on Cognitive Decline (SILCODE) project, which is a longitudinal cohort study aiming to develop a model for the ultraearly diagnosis of AD. Participants are continuously recruited through public advertisements and referrals from physicians, memory clinics, or informants. After demographic, clinical, and laboratory screening, subjects meeting the inclusion criteria were selected. Neuropsychological assessments, imaging examinations, and laboratory examinations were completed at baseline and follow-up. For details of the implementation process, see the SILCODE study published in 2019 [23]. The study recruited 579 eligible baseline subjects from March 2017 to September 2018, and from these, we selected 212 subjects who were diagnosed with SCD (Figure 1).

Population-based samples were selected from an epidemiological survey conducted in ShunYi District in Beijing, China. The purpose of this study was to investigate the incidence and characteristics of SCD in a Chinese population. Shunyi District consists of 12 towns, 7 district offices, and 6 subdistricts, with a total of 426 villagers' committees and 85 subdistrict committees. At the end of 2015, the region had registered 80,000 permanent residents aged 60 to 80. Sixteen committees were selected by stratified cluster random sampling, and 4,505 people were selected by preliminary questionnaire screening. Ultimately, 2,689 people took part in the survey. After applying the inclusion and exclusion criteria, 814 residents completed the clinical and neuropsychological assessments between September and

November 2016. Details of the design and data collection of the study have been published previously [24]. We selected 110 SCD subjects based on the study objectives and diagnostic criteria (Figure 1).

**2.2. Subject Selection Criteria.** The diagnostic criteria are based on a SCD diagnostic framework published by Frank Jessen in 2014 [25]. SCD is defined as a self-experienced persistent decline in cognitive capacity in comparison with a previously normal status, unrelated to an acute event. The patient has normal age-, gender-, and education-adjusted performance on standardized cognitive tests, and they do not meet the diagnostic criteria for MCI and AD. An MCI diagnosis conforms to the criteria proposed by Jak and Bondi: meeting any of the following three criteria: (1) two indexes of the same cognitive domains were damaged ( $>1.0$  SD); (2) all 3 cognitive domains were impaired ( $>1.0$  SD); or (3) the Functional Activities Questionnaire (FAQ)  $\geq 9$  [26]. A diagnosis of AD was based on the Diagnostic and Statistical Manual of Mental Disorders, fourth edition (DSM-IV) [27], and a CDR score  $\geq 1$ .

The inclusion criteria include the following: Han ethnicity, 60–80 years old.

The exclusion criteria include the following: (1) other nervous system diseases that can lead to cognitive decline, such as cerebrovascular disease, Parkinson's disease, brain tumors, brain trauma, and epilepsy; (2) other systemic diseases that can cause cognitive decline: anemia, thyroid dysfunction, and metabolic encephalopathy; (3) a general anesthesia history, a history of poisoning with carbonic oxide, a psychiatric disease, a serious physical disease, substance use, visual and auditory disorders, and/or cannot complete the neuropsychological examination.

**2.3. Neuropsychological and Clinical Assessment.** The neuropsychological assessment includes (1) neuropsychiatric assessment: HAMA (Hamilton Anxiety) and HAMD (Hamilton Depression); (2) global cognition: MoCA-B (Montreal Cognitive Assessment-Basic) [28]; (3) memory: AVLT-H (Auditory Verbal Learning Test-Huashan version) [29]; (4) executive function: STT-B (Trail Making Test B) and STT-A (Trail Making Test A) [30]; (5) language: AFT (Animal Fluency Test) [31] and BNT (Boston Naming Test) [32]; (6) daily life ability: ADL (Activities of Daily Living) [33]; and (7) except for a vascular disease etiology: HIS (the Hachinski Ischemic Index) [34]. Sociodemographic characteristics, medical history, lifestyle (smoking and drinking history), personal history (marital status and profession), and SCD-questionnaire 9 were obtained with a questionnaire [35]. The epidemiological survey of ShunYi district did not include the STT-A and BNT but include some other substitute indexes, executive function: Clock-Drawing Test (CDT-30); language: Verbal Fluency Test (animals and fruits) [24, 36].

A semistructured interview was used to evaluate the details of SCD. The interview was administered face to face by trained physicians. Our assessment of subjective cognitive decline covered five different cognitive domains, including memory, language, planning, attention, and any other

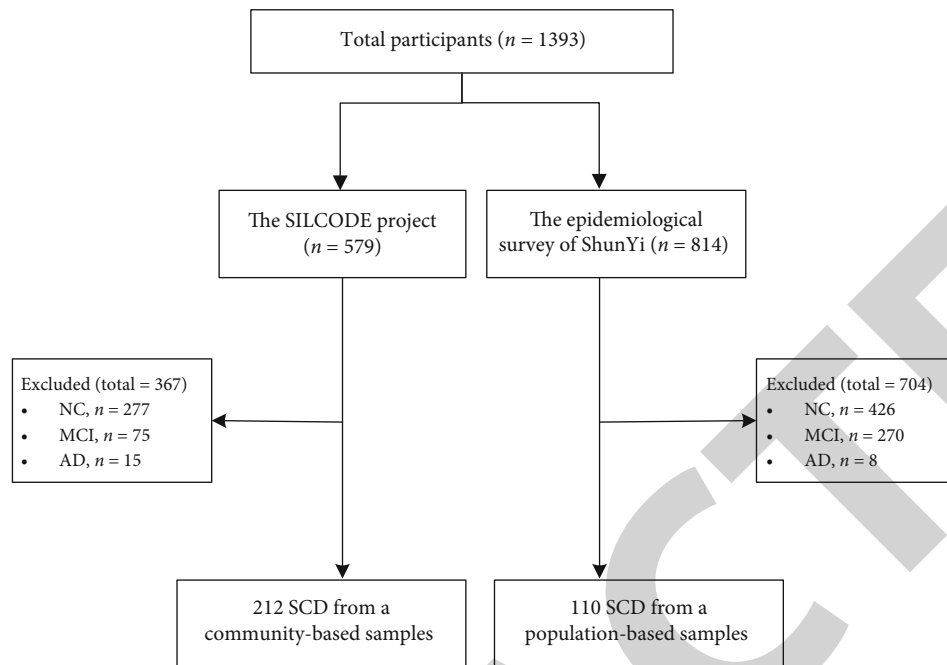


FIGURE 1: The flow charts of this study. NC: normal controls; SCD: subjective cognitive decline; MCI: mild cognitive impairment; AD: Alzheimer's disease.

cognitive decline. For each domain, the physician asked the patient if they had noticed a deterioration in function, i.e., do you think your memory has become worse? If the participant answered this question with yes, the physician further questioned about the SCD-plus features, i.e., associated worry ("Does this worry you?"), onset ("How long ago did you start to notice the decline?"), the performance in comparison to peers ("Compared to other people of your age, would you say that your performance is worse?"), and medical help-seeking ("Have you ever been to a doctor for these problems?") [37].

**2.4. Statistical Analyses.** All statistical analyses were performed with SPSS (version 17.0);  $p < 0.05$  was considered to be statistically significant. For the quantitative data, the Kolmogorov-Smirnov test and a Q-Q plot were used to test for normality. The first model was univariable. Nonnormal distribution data (age, education, MoCA-B, AVLT-H-N4, AVLT-H-N5, AVLT-H-N7, AFT, HAMD, and HAMA) are described with the median and interquartile, and the Mann-Whitney  $U$  tests were used to compare the differences between groups. Normal distribution data (STT-B) are described with the mean  $\pm$  standard deviation (SD), and  $t$  tests were used to compare the differences between groups. Categorical variables (sex, medical history, smoking, drinking, personal history, SCD-plus features, and SCD-I domains) are described as percentages; the chi-squared ( $\chi^2$ ) test was employed to assess differences between groups. The second model was multivariable; multiple linear regression analyses was established, adjusted for sex, age, and education, and compared the differences between the study setting and the neuropsychological scales (MoCA-B, AVLT-H-N4, AVLT-H-N5, AVLT-H-N7, AFT, and STT-B).

### 3. Results

**3.1. Sociodemographic, Clinical, and Neuropsychological Characteristics of the Groups.** A total of 322 SCD cases were analysed. The convenience sample included 212 cases from the SILCODE, and the population-based sample included 110 cases from the epidemiological survey data of ShunYi district (Figure 1). Both groups were more likely to be female, and the convenience sample was younger than the population-based sample, but there were no group differences. Compared with the population-based sample, the convenience sample had more years of education (12 [10–15] versus 6 [4–9],  $p < 0.001$ ) and a higher rate of a family history of dementia (49 [23.1%] versus 3 [2.7%],  $p < 0.001$ ) (Table 1).

The neuropsychological assessment (MoCA-B, AVLT-H-N4, AVLT-H-N5, AVLT-H-N7, AFT, and STT-B) in the convenience sample was superior to that in the population-based samples ( $p < 0.001$ ) (Table 1). Using sex, age, education, group as the independent variables, and neuropsychological score as the dependent variable, multiple linear regression model was established; there were still significant differences between the two groups ( $p < 0.001$ ) (Table 2). The convenience sample had higher anxiety and depression scores (HAMD 3 [1–5.75] versus 1.5 [0–4],  $p = 0.002$ ; HAMA 4 [2–6] versus 1 [0–4],  $p < 0.001$ ). In the convenience sample, an *APOE* examination was performed in 209 of 212 SCD, and 50 (23.92%) subjects had *APOE*  $\epsilon 4$ . The population-based samples were not assessed for *APOE*. Because of the experimental design, some of the low-education subjects did not complete the STT. In the population-based sample, STT test was conducted by 41 subjects. (Table 1).

TABLE 1: Demographics and neuropsychological assessments.

	Convenience sample ( <i>n</i> = 212)	Population sample ( <i>n</i> = 110)	$\chi^2/t/Z$	<i>p</i>
Age, y	65 (63-69)	67 (63-70)	-1.940	0.052 <sup>d</sup>
Female, <i>n</i> (%)	140 (66%)	74 (67.3%)	0.050	0.824 <sup>c</sup>
Education, y	12 (10-15)	6 (4-9)	-12.801	<0.001 <sup>d</sup>
MoCA-B	26 (24-27)	20 (17-22)	-12.484	<0.001 <sup>d</sup>
AVLT-H-N4	7 (6-9)	4 (3-5)	-11.787	<0.001 <sup>d</sup>
AVLT-H-N5	7 (5.25-8)	3 (2-4)	-12.276	<0.001 <sup>d</sup>
AVLT-H-N7	23 (22-24)	20 (19-22)	-8.438	<0.001 <sup>d</sup>
AFT	19 (16-22)	13 (11-16)	-9.758	<0.001 <sup>d</sup>
STT-B <sup>b</sup>	135.85 ± 33.77	176.24 ± 41.33	-6.749	<0.001 <sup>e</sup>
HAMD	3 (1-5.75)	1.5 (0-4)	-3.100	0.002 <sup>d</sup>
HAMA	4 (2-6)	1 (0-4)	-6.647	<0.001 <sup>d</sup>
APOEε4 <sup>a</sup>	50 (23.92%)	—		
Hypertension, <i>n</i> (%)	79 (37.3%)	57 (51.8%)	6.288	0.012 <sup>c</sup>
Diabetes, <i>n</i> (%)	29 (13.7%)	12 (10.9%)	0.500	0.479 <sup>c</sup>
Dyslipidemia, <i>n</i> (%)	78 (37%)	27 (24.5%)	5.068	0.024 <sup>c</sup>
Smoking, <i>n</i> (%)	46 (21.7%)	26 (23.6%)	0.157	0.692 <sup>c</sup>
Drinking, <i>n</i> (%)	50 (23.6%)	27 (24.5%)	0.037	0.848 <sup>c</sup>
Married, <i>n</i> (%)	181 (85.4%)	96 (87.3%)	0.216	0.642 <sup>c</sup>
Job category, <i>n</i> (%)				
Mental	148 (69.8%)	11 (10%)	150.082	<0.001 <sup>c</sup>
Physical	30 (14.2%)	92 (83.6%)		
Mental+physical	34 (16%)	7 (6.4%)		
Family history	49 (23.1%)	3 (2.7%)	22.227	<0.001 <sup>c</sup>

All continuous variables in the table were nonnormally distributed and described as median (interquartile). <sup>a</sup>APOE genotype results were included in the convenience sample SCD subjects (*N* = 209), ε4<sup>+</sup> (*N* = 50). <sup>b</sup>STT-B results were included in the convenience sample (*N* = 212) and in population-based samples (*N* = 41). <sup>c</sup>The *p* value was calculated using Chi-square. <sup>d</sup>The *p* value was calculated using the Mann-Whitney *U*. <sup>e</sup>The *p* value was calculated using independent samples *t* tests. MoCA-B: Montreal Cognitive Assessment-Basic; AVLT-H-N4: Auditory Verbal Learning Test-Huashan version short-delayed free recall (5 min); AVLT-H-N5: Auditory Verbal Learning Test-Huashan version long-delayed free recall (20 min); AVLT-H-N7: Auditory Verbal Learning Test-Huashan version long-delayed recognition (20 min); AFT: Verbal Fluency Test (animal); STT-B: Shape Trail Test B; HAMD: Hamilton Depression Rating Scale; HAMA: Hamilton Anxiety Scale.

TABLE 2: Multivariable compared the neuropsychological assessments.

	<i>B</i> (95%CI)	<i>t</i>	<i>P</i>
MoCA-B	-3.662 (-4.483, -2.842)	-8.782	<0.001
AVLT-H-N4	-2.605 (-3.238, -1.972)	-8.093	<0.001
AVLT-H-N5	-2.719 (-3.359, -2.079)	-8.359	<0.001
AVLT-H-N7	-1.633 (-2.204, -1.061)	-5.622	<0.001
AFT	-2.995 (-4.334, -1.656)	-4.401	<0.001
STT-B	32.143 (20.035, 44.250)	5.229	<0.001

MoCA-B: Montreal Cognitive Assessment-Basic; AVLT-H-N4: Auditory Verbal Learning Test-Huashan version short-delayed free recall (5 min); AVLT-H-N5: Auditory Verbal Learning Test-Huashan version long-delayed free recall (20 min); AVLT-H-N7: Auditory Verbal Learning Test-Huashan version long-delayed recognition (20 min); AFT: Verbal Fluency Test (animal); STT-B: Shape Trail Test B.

**3.2. SCD Domains and SCD-Plus Characteristics of the Groups.** The differences in the SCD domains and the SCD-plus characteristics are given in Table 3. Due to the inclusion criteria, the 322 included participants (100%) reported a memory decline. Compared with the convenience sample,

more subjects complained of a decline in the language (46.4% versus 30.7%, *p* = 0.005) and planning domains (30% versus 15.1%, *p* = 0.002) in the population-based samples, and there was a statistically significant between-group difference. For memory, the convenience sample had more SCD patients reporting worries (62.7% versus 22.7%, *p* < 0.001), cognitive decline within the last 5 years (82.5% versus 65.5%, *p* = 0.001), and medical help-seeking (7.5% versus 0.9%, *p* = 0.012).

## 4. Discussion

In the study, we compared the demographic, neuropsychological, cognitive domains, and SCD-plus features between a convenience sample and a population-based sample. The main findings of our study are (1) the convenience sample had more years of education and higher neuropsychological score, and (2) the convenience sample was more consistent with the SCD-plus features.

The recruitment settings usually include population-based samples, community-based volunteer samples, clinical

TABLE 3: SCD-plus features and SCD-I domains.

	Convenience sample ( <i>n</i> = 212)	Population sample ( <i>n</i> = 110)	$\chi^2$	<i>p</i>
Decline in memory	212 (100%)	110 (100%)		
Particular concerns/worries	133 (62.7%)	25 (22.7%)	46.386	<0.001
Onset within 5 years	175 (82.5%)	72 (65.5%)	11.843	0.001
Feeling worse than peers	59 (27.8%)	27 (24.5%)	0.399	0.528
Medical help-seeking	16 (7.5%)	1 (0.9%)	6.381	0.012
Decline in language	65 (30.7%)	51 (46.4%)	7.749	0.005
Particular concerns/worries	35 (53.8%)	15 (29.4%)	6.957	0.008
Onset within 5 years	56 (86.2%)	36 (70.6%)	4.220	0.040
Feeling worse than peers	19 (29.2%)	20 (39.2%)	1.277	0.259
Medical help-seeking	1 (1.5%)	0 (0%)		1.000*
Decline in planning	32 (15.1%)	33 (30%)	9.987	0.002
Particular concerns/worries	14 (43.8%)	10 (30.3%)	1.261	0.261
Onset within 5 years	28 (87.5%)	21 (63.6%)	4.986	0.026
Feeling worse than peers	4 (12.5%)	15 (45.5%)	8.529	0.003
Medical help-seeking	1 (3.1%)	0 (0%)		0.492*
Decline in attention	66 (31.1%)	30 (27.3%)	0.516	0.473
Particular concerns/worries	34 (51.5%)	11 (36.7%)	1.826	0.177
Onset within 5 years	55 (83.3%)	20 (66.7%)	3.352	0.067
Feeling worse than peers	12 (18.2%)	10 (33.3%)	2.680	0.102
Medical help-seeking	2 (3%)	0 (0%)		1.000*
Decline in other	13 (6.1%)	1 (0.9%)		0.059*

\*The *p* value was calculated using Fisher's Exact Test.

samples, convenience samples, and mixed samples. In the convenience samples and mixed samples, it is normal to find mixtures of two types, it is also normal to find mixtures of clinical characteristics. The differences among samples are mostly the initiative of seek medical help (self-selection bias) [38]. The convenience sample was partly community- and partly clinically based. The results suggest that the convenience sample had more years of education, a higher rate of a family history of dementia and higher neuropsychological score. The population-based sample had a greater proportion of decline in the nonmemory cognitive domains, and the convenience sample was more consistent with the SCD-plus features. There were different characteristics among SCD individuals between different study settings.

This is the first study to compare the characteristics of SCD between different recruitment settings of the Chinese population. In regard to the sociodemographic characteristics, a previous researcher showed that subjects from the Open House Initiative which can be considered partly medical help seeking and partly community-based were more likely to be women and had a higher educational level and a higher rate of a family history of dementia than those from the Memory Unit [39]. Some studies have found that cognitively healthy control volunteers recruited through community-based cohorts or memory clinics are younger, better educated, and more likely to have a family history of AD than population-based control samples [16, 17].

Our results are consistent with these studies. Our convenience sample was younger than the population-based sam-

ples, but there were no group differences. This may be related to the fact that we chose people 60–80 years old. The convenience sample had a significantly higher rate of a family history of dementia. One possible explanation for this is a worry associated with a family history of dementia triggered medical help-seeking [18]. It is possible that highly educated individuals are more sensitive to subtle declines in cognitive function and pay more attention to cognition declines, leading to more help-seeking, so the convenience sample is better educated than the population-based samples. This may also be related to the fact that the target population of the convenience samples is biased depending on the channel of recruitment. In the convenience sample, most participants are highly educated individuals which are recruited through public advertisements and referrals. In the population sample, as the result of the stratification, we selected 2 subdistrict areas, 3 regional offices, and 4 towns; the sample represents the education of the general population. The convenience sample also had a lower proportion of hypertension, a higher proportion of dyslipidemia, and a lower proportion employed in physical labor. Their effects on cognitive decline are inconclusive.

SCD subjects compared to controls had lower scores on neuropsychological performance but within the normal range, which is predictive of a future decline [7]. A previous study showed different neuropsychological characteristics depending on the recruitment method. The Open House Initiative sample showed better overall neuropsychological performance than the Memory Unit sample on global cognition,



two executive tasks, and on recognition memory [39]. It has been demonstrated that memory clinic patients with MCI have poorer cognitive performance and a higher risk of progression to dementia than population-based samples [17]. Our results are different from previous studies in this regard. It may be related to the difference in educational level between these two groups. Although we adjusted for education, the underlying pathological basis may still influence the results. In less-educated individuals, a degree of underlying brain pathology might lead to clinical symptoms. Highly educated individuals may be able to compensate for longer periods of time and appear clinically normal because of a higher cognitive reserve. Cognitive reserve has the potential to delay or slow cognitive decline in individuals with SCD [40]. SCD individuals with more years of education have a stronger amyloid burden compared with less-educated individuals. The association between SCD and  $A\beta$  burden becomes stronger in greater educational individuals [41].

Most psychiatric disorders and subclinical psychiatric conditions can affect cognition. Recruitment methods influence the affective symptomatology. Depression, for example, is specifically associated with medical help-seeking. There are higher rates of depression/anxiety symptomatology in clinical-based SCD samples compared with community-based SCD samples [18, 42]. Despite not meeting the criteria for a clinical diagnosis of depression, a cross-sectional study showed that subclinical depression was more prevalent in medical-help seeking SCD individuals compared to community-recruited older adults [22]. In our study, people with significant anxiety and depression were excluded, but the anxiety and depression scores of the convenience sample were significantly higher than the population-based samples. This is because the convenience samples are seeking medical help more actively.

Several community-based studies have revealed that the rate of cognitive complaints is relatively high in the typical older adult population and could represent complaints about normal aging [43–45]. This may result in false-positive diagnoses of SCD. In memory clinics, cognitive complaints are more likely to reflect nonnormal aging, which eliminates false-positives [46]. Thus, the evaluation of the SCD concept in preclinical AD population remains to be further explored. In 2014, the SCD-Initiative proposed the “SCD-plus criteria” as an enrichment strategy for the likelihood of preclinical AD in individuals with SCD [25]. In addition, current research suggests the SCD assessments should involve additional cognitive domains [47].

In our study, we used a semistructured interview to assess SCD features. The semistructured interview includes five different cognitive domains (memory, language, planning, attention, and any other cognitive decline) and comprises all five SCD-plus features. Due to the inclusion criteria, all SCD patients reported a decline in memory. In the other domains, language complaints were the most frequent, followed by an attention, planning, and any other cognitive decline. A recent study showed the prevalence for SCD of affected different cognitive domains was language (82.9%), planning (21%), attention (46.7%), and any other cognitive decline (37.1%) [37]. The use of different inclusion criteria

and research methods can lead to a different result. One study showed word finding difficulties accounted for three-quarters of SCD individuals, which reflect its association with a better cognitive performance [37]. The incidence is similar in MCI and community cognitively healthy older adults, suggesting that subjective word finding difficulty is a part of normal aging rather than a possible sign of AD pathology [48]. In our study, the population-based samples had more subjective complaints of declines in the language domain than did the convenience sample. The decline of cognitive domains in the population-based samples has greater consistency with normal aging. This supports the potential of convenience samples to have greater consistency with preclinical SCD.

The two participant groups differed in their decline of SCD-plus features. Longitudinal and cross-sectional studies acknowledge complaints of memory changes are nonspecific, unless associated with a progressive nature or worry [49, 50]. In our study, the proportion of SCD individuals with worry in the convenience sample is much higher than that in the population-based sample. A study reported 81% SCD participants reported the onset of their decline within the last 5 years. This is based on direct testing, and it validated the SCD-plus criterion “onset within the last 5 years” was significantly associated with amyloid pathology [37]. The reported onset within the last 5 years in the SCIENCE SCD-cohort was 83% [51]. These findings are completely consistent with the reported onset in our study, where 82.5% reported an onset within the last 5 years in the convenience sample. Memory changes and a worse memory in comparison to peers are useful for identifying individuals at preclinical and prodromal stages of AD [52]. In our study, the proportion of SCD participants reported they had a worse memory in comparison to peers was 27.8% in the convenience sample and 24.5% in the population-based samples. The former is closer to the previous results of 29.5% [37]. It has been reported that medical help-seeking groups have more pronounced markers of neurodegeneration at a higher prevalence than healthy community-dwelling volunteers [22, 50]. The above research confirmed that the convenience sample is more closely associated with SCD-plus features than the population-based samples.

Our study of cognitive domains and SCD-plus features indicated that the population-based samples are more consistent with normal aging, and the convenience sample is more closely associated with SCD-plus features. But the population-based samples performed significantly worse in neuropsychological performance compared to the convenience samples. It may be related to the fact that different levels of education result in neuropsychological performance and underlying pathological basis. This may also be related to the fact that the target population of the convenience samples are biased depending on the channel of recruitment. We should consider the representativeness of the samples in future SCD studies. Longitudinal studies of different samples are necessary; SCD-plus features or worse neuropsychological performance is better predictors of future cognitive decline in certain samples. We acknowledge that there are some limitations of this study. First, this is a retrospective study, and some details of the two samples were not

identical, but the principles of diagnosis are consistent. Second, there were no genetic or imaging data available for the population-based samples, so we cannot compare their biomarkers of AD. We will perform a follow-up of this cohort in the future.

## 5. Conclusions

There are differences in demographic, neuropsychological, cognitive domains and SCD-plus features among SCD subjects from different recruitment settings in China. The convenience sample was more consistent with SCD-plus features than the population-based sample. Thus, the impact of study setting on SCD individuals also needs to be considered in the future. Study setting is an essential factor result in the heterogeneity of SCD. When choosing the subjects or analyzing research results, the role of study setting should be taken into account.

## Data Availability

The data used to support the findings of this study are available from the corresponding author upon request.

## Conflicts of Interest

The authors declare that the research was conducted in the absence of any commercial or financial relationships that could be construed as a potential conflict of interest.

## Acknowledgments

We appreciate Kun Yang of the Xuanwu Hospital for the guidance of statistics. We appreciate volunteers' participation and the support of the government. We thank every participant of this study. This article was supported by the National Natural Science Foundation of China (Grant 61633018).

## References

- [1] M. J. Prince, A. Wimo, M. M. Guerchet, G. C. Ali, Y. T. Wu, and M. Prina, *The World Alzheimer Report 2015, The Global Impact of Dementia: an analysis of prevalence, incidence, cost and trends* Alzheimer's Disease International.
- [2] R. S. Doody, R. G. Thomas, M. Farlow et al., "Phase 3 trials of solanezumab for mild-to-moderate Alzheimer's disease," *The New England Journal of Medicine*, vol. 370, no. 4, pp. 311–321, 2014.
- [3] R. A. Sperling, C. R. Jack Jr., and P. S. Aisen, "Testing the right target and right drug at the right stage," *Science Translational Medicine*, vol. 3, no. 111, p. 111cm33, 2011.
- [4] B. Dubois, H. Hampel, H. H. Feldman et al., "Preclinical Alzheimer's disease: definition, natural history, and diagnostic criteria," *Alzheimers Dement*, vol. 12, no. 3, pp. 292–323, 2016.
- [5] B. Reisberg, S. H. Ferris, M. J. de Leon, and T. Crook, "The Global Deterioration Scale for assessment of primary degenerative dementia," *The American Journal of Psychiatry*, vol. 139, no. 9, pp. 1136–1139, 1982.
- [6] K. Abdulrab and R. Heun, "Subjective memory impairment. A review of its definitions indicates the need for a comprehensive set of standardised and validated criteria," *European Psychiatry*, vol. 23, no. 5, pp. 321–330, 2008.
- [7] B. Reisberg, M. B. Shulman, C. Torossian, L. Leng, and W. Zhu, "Outcome over seven years of healthy adults with and without subjective cognitive impairment," *Alzheimers Dement*, vol. 6, no. 1, pp. 11–24, 2010.
- [8] F. Jessen, S. Wolfgruber, B. Wiese et al., "AD dementia risk in late MCI, in early MCI, and in subjective memory impairment," *Alzheimers Dement*, vol. 10, no. 1, pp. 76–83, 2014.
- [9] A. J. Mitchell, H. Beaumont, D. Ferguson, M. Yadegarfar, and B. Stubbs, "Risk of dementia and mild cognitive impairment in older people with subjective memory complaints: meta-analysis," *Acta Psychiatrica Scandinavica*, vol. 130, no. 6, pp. 439–451, 2014.
- [10] A. R. Kaup, J. Nettiksimmons, E. S. LeBlanc, and K. Yaffe, "Memory complaints and risk of cognitive impairment after nearly 2 decades among older women," *Neurology*, vol. 85, no. 21, pp. 1852–1858, 2015.
- [11] M. Rönnlund, A. Sundström, R. Adolfsson, and L. G. Nilsson, "Subjective memory impairment in older adults predicts future dementia independent of baseline memory performance: evidence from the Betula prospective cohort study," *Alzheimers Dement*, vol. 11, no. 11, pp. 1385–1392, 2015.
- [12] Y. Chen, K. G. Denny, D. Harvey et al., "Progression from normal cognition to mild cognitive impairment in a diverse clinic-based and community-based elderly cohort," *Alzheimers Dement*, vol. 13, no. 4, pp. 399–405, 2017.
- [13] S. Hollands, Y. Y. Lim, R. Buckley et al., "Amyloid- $\beta$  related memory decline is not associated with subjective or informant rated cognitive impairment in healthy adults," *Journal of Alzheimer's Disease*, vol. 43, no. 2, pp. 677–686, 2015.
- [14] M. E. Mol, M. P. van Boxtel, D. Willems, and J. Jolles, "Do subjective memory complaints predict cognitive dysfunction over time? A six-year follow-up of the Maastricht Aging Study," *International Journal of Geriatric Psychiatry*, vol. 21, no. 5, pp. 432–441, 2006.
- [15] R. Gallassi, F. Oppi, R. Poda et al., "Are subjective cognitive complaints a risk factor for dementia?," *Neurological Sciences*, vol. 31, no. 3, pp. 327–336, 2010.
- [16] M. Ganguli, M. E. Lytle, M. D. Reynolds, and H. H. Dodge, "Random versus volunteer selection for a community-based study," *The Journals of Gerontology. Series A, Biological Sciences and Medical Sciences*, vol. 53A, no. 1, pp. M39–M46, 1998.
- [17] H. Brodaty, A. Mothakunnel, M. de Vel-Palumbo et al., "Influence of population versus convenience sampling on sample characteristics in studies of cognitive aging," *Annals of Epidemiology*, vol. 24, no. 1, pp. 63–71, 2014.
- [18] I. H. Ramakers, P. J. Visser, A. J. Bittermann, R. W. H. M. Ponds, M. P. J. van Boxtel, and F. R. J. Verhey, "Characteristics of help-seeking behaviour in subjects with subjective memory complaints at a memory clinic: a case-control study," *International Journal of Geriatric Psychiatry*, vol. 24, no. 2, pp. 190–196, 2009.
- [19] P. K. Crane, L. E. Gibbons, S. M. McCurry et al., "Importance of home study visit capacity in dementia studies," *Alzheimers Dement*, vol. 12, no. 4, pp. 419–426, 2016.
- [20] J. A. Schneider, N. T. Aggarwal, L. Barnes, P. Boyle, and D. A. Bennett, "The neuropathology of older persons with and



- without dementia from community versus clinic cohorts," *Journal of Alzheimer's Disease*, vol. 18, no. 3, pp. 691–701, 2009.
- [21] B. E. Snitz, T. Wang, Y. K. Cloonan et al., "Risk of progression from subjective cognitive decline to mild cognitive impairment: the role of study setting," *Alzheimers Dement*, vol. 14, no. 6, pp. 734–742, 2018.
- [22] A. Perrotin, R. la Joie, V. de la Sayette et al., "Subjective cognitive decline in cognitively normal elders from the community or from a memory clinic: differential affective and imaging correlates," *Alzheimers Dement*, vol. 13, no. 5, pp. 550–560, 2017.
- [23] X. Li, X. Wang, L. Su, X. Hu, and Y. Han, "Sino Longitudinal Study on Cognitive Decline (SILCODE): protocol for a Chinese longitudinal observational study to develop risk prediction models of conversion to mild cognitive impairment in individuals with subjective cognitive decline," *BMJ Open*, vol. 9, no. 7, article e028188, 2019.
- [24] L. Hao, X. Wang, L. Zhang et al., "Prevalence, risk factors, and complaints screening tool exploration of subjective cognitive decline in a large cohort of the Chinese population," *Journal of Alzheimer's Disease*, vol. 60, no. 2, pp. 371–388, 2017.
- [25] F. Jessen, R. E. Amariglio, M. van Boxtel et al., "A conceptual framework for research on subjective cognitive decline in pre-clinical Alzheimer's disease," *Alzheimers Dement*, vol. 10, no. 6, pp. 844–852, 2014.
- [26] for the Alzheimer's Disease Neuroimaging Initiative, M. W. Bondi, E. C. Edmonds et al., "Neuropsychological criteria for mild cognitive impairment improves diagnostic precision, biomarker associations, and progression rates," *Journal of Alzheimer's Disease*, vol. 42, no. 1, pp. 275–289, 2014.
- [27] American Psychiatric Association, *Diagnostic and Statistical Manual of Mental Disorders*, American Psychiatric Association, Washington, DC, USA, 4th edition, 1994.
- [28] K. L. Chen, Y. Xu, A. Q. Chu et al., "Validation of the Chinese version of Montreal cognitive assessment basic for screening mild cognitive impairment," *Journal of the American Geriatrics Society*, vol. 64, no. 12, pp. e285–e290, 2016.
- [29] Q. Zhao, Y. Lv, Y. Zhou, Q. Guo, and Z. Hong, "Short-term delayed recall of auditory verbal learning test is equivalent to long-term delayed recall for identifying amnesic mild cognitive impairment," *PLoS One*, vol. 7, no. 12, article e51157, 2012.
- [30] Q. Zhao, Q. Guo, F. Li, Y. Zhou, B. Wang, and Z. Hong, "The Shape Trail Test: application of a new variant of the Trail making test," *PLoS One*, vol. 8, no. 2, article e57333, 2013.
- [31] Q. Guo, L. Jin, and Z. Hong, "A specific phenomenon of animal fluency test in Chinese elderly," *Chinese Mental Health Journal*, vol. 21, 2007.
- [32] Q. H. Guo, Z. Hong, and W. X. Shi, "Boston naming test in Chinese elderly, patient with mild cognitive impairment and Alzheimer's dementia," *Chinese Mental Health Journal*, vol. 20, pp. 81–84, 2006.
- [33] Y. He, X. Xiong, Y. Chi, M. Zhang, and M. Zhang, "Evaluation of the ability of daily living activities of the elderly," *Journal of Gerontology*, vol. 10, pp. 266–269, 1990.
- [34] I. V. C. Hachinski, L. D. Iliff, E. Zilhka et al., "Cerebral blood flow in dementia," *Archives of Neurology*, vol. 32, no. 9, pp. 632–637, 1975.
- [35] K. A. Gifford, D. Liu, R. R. Romano, R. N. Jones, and A. L. Jefferson, "Development of a subjective cognitive decline questionnaire using item response theory: a pilot study," *Alzheimer's & Dementia: Diagnosis, Assessment & Disease Monitoring*, vol. 1, no. 4, pp. 429–439, 2015.
- [36] Q. Guo, F. U. Jianhui, J. Yuan, Q. Zhao, X. Cao, and Z. Hong, "A study of validity of a new scoring system of clock drawing test," *Chinese Journal of Neurology*, vol. 41, pp. 234–237, 2008.
- [37] L. Miebach, S. Wolfsgruber, A. Polcher et al., "Which features of subjective cognitive decline are related to amyloid pathology? Findings from the DELCODE study," *Alzheimer's Research & Therapy*, vol. 11, 2019.
- [38] O. Rodríguez-Gómez, C. Abdelnour, F. Jessen, S. Valero, and M. Boada, "Influence of sampling and recruitment methods in studies of subjective cognitive decline," *Journal of Alzheimer's Disease*, vol. 48, Supplement 1, pp. S99–S107, 2015.
- [39] C. Abdelnour, O. Rodríguez-Gómez, M. Alegret et al., "Impact of recruitment methods in subjective cognitive decline," *Journal of Alzheimer's Disease*, vol. 57, no. 2, pp. 625–632, 2017.
- [40] K. Yang, G. Chen, C. Sheng et al., "Cognitive reserve, brain reserve, APOE  $\epsilon$ 4, and cognition in individuals with subjective cognitive decline in the SILCODE study," *Journal of Alzheimer's Disease*, vol. 76, no. 1, pp. 249–260, 2020.
- [41] S. L. Aghjayan, R. F. Buckley, P. Vannini et al., "The influence of demographic factors on subjective cognitive concerns and beta-amyloid," *International Psychogeriatrics*, vol. 29, no. 4, pp. 645–652, 2017.
- [42] C. S. Hurt, A. Burns, R. G. Brown, and C. Barrowclough, "Why don't older adults with subjective memory complaints seek help?," *International Journal of Geriatric Psychiatry*, vol. 27, no. 4, pp. 394–400, 2012.
- [43] C. Cooper, P. Bebbington, J. Lindesay et al., "The meaning of reporting forgetfulness: a cross-sectional study of adults in the English 2007 Adult Psychiatric Morbidity Survey," *Age and Ageing*, vol. 40, no. 6, pp. 711–717, 2011.
- [44] C. Jonker, M. I. Geerlings, and B. Schmand, "Are memory complaints predictive for dementia? A review of clinical and population-based studies," *International Journal of Geriatric Psychiatry*, vol. 15, pp. 983–991, 2000.
- [45] M. J. Slavin, H. Brodaty, N. A. Kochan et al., "Prevalence and predictors of "subjective cognitive complaints" in the Sydney Memory and Ageing Study," *The American Journal of Geriatric Psychiatry*, vol. 18, no. 8, pp. 701–710, 2010.
- [46] the Alzheimer's Disease Neuroimaging Initiative, L. A. Rabin, C. M. Smart et al., "Subjective cognitive decline in older adults: an overview of self-report measures used across 19 international research studies," *Journal of Alzheimer's Disease*, vol. 48, no. s1, Supplement 1, pp. S63–S86, 2015.
- [47] J. L. Molinuevo, L. A. Rabin, R. Amariglio et al., "Implementation of subjective cognitive decline criteria in research studies," *Alzheimers Dement*, vol. 13, no. 3, pp. 296–311, 2017.
- [48] E. Pravatà, J. Tavernier, R. Parker, H. Vavro, J. E. Mintzer, and M. V. Spampinato, "The neural correlates of anomia in the conversion from mild cognitive impairment to Alzheimer's disease," *Neuroradiology*, vol. 58, no. 1, pp. 59–67, 2016.
- [49] F. Jessen, B. Wiese, C. Bachmann et al., "Prediction of dementia by subjective memory impairment: effects of severity and temporal association with cognitive impairment," *Archives of General Psychiatry*, vol. 67, no. 4, pp. 414–422, 2010.

## Review Article

# The Influence of Serum Uric Acid Level on Alzheimer's Disease: A Narrative Review

Mengyuan Qiao , Chongli Chen , Yuqing Liang , Yuxi Luo , and Wenbin Wu 

Department of Geriatrics, Hospital of Chengdu University of Traditional Chinese Medicine, Chengdu City, Sichuan Province, China

Correspondence should be addressed to Wenbin Wu; [wwb1201@vip.sina.com](mailto:wwb1201@vip.sina.com)

Received 14 February 2021; Revised 21 May 2021; Accepted 27 May 2021; Published 3 June 2021

Academic Editor: Yuzhen Xu

Copyright © 2021 Mengyuan Qiao et al. This is an open access article distributed under the Creative Commons Attribution License, which permits unrestricted use, distribution, and reproduction in any medium, provided the original work is properly cited.

As a powerful antioxidant in the human body, uric acid (UA) has been the subject of increasing research that focused on its influence on Alzheimer's disease (AD) in recent years. The latest literature was gathered to describe the influence of serum uric acid (SUA) level on the onset and progression of AD and to analyze the possibility that SUA is a biomarker of Alzheimer's disease. A large number of existing studies suggested that the SUA level was lower or tended to decrease in patients with AD, and increased SUA level may have a protective effect in AD, which could reduce the risk of onset and slowing the course of the disease. However, some Mendelian randomization analyses suggested that genetically determined uric acid was not associated with AD risk. Existing research results are contradictory due to the high inconsistency of the studies, the selection of subjects, and other factors. UA also showed a strong association with cognitive function, and there appeared to be a gender-selective neuroprotective action. Due to its potent antioxidant properties, the low uric acid level may contribute to oxidative stress to accelerate disease progression. But some preclinical data showed a possibility that in some special cases, UA had a prooxidant properties. The possibility was raised in the discussion of the underlying mechanism that both the low uric acid level and the rapidly progressive course of the disease were the consequence of malnutrition. This paper reviews recent advances in the study of SUA and AD which offers the possibility of new biomarker, new prevention, and treatment strategies for Alzheimer's disease.

## 1. Introduction

Uric acid (UA) is a product of purine metabolism, which is a natural and powerful antioxidant that helps remove superoxide by blocking the degradation of superoxide dismutase, the enzyme responsible for purine removal [1]. The SUA level is altered according to the balance between dietary purine intake, xanthine oxidase activity, and renal UA excretion [2]. When the equilibrium is disturbed, hyperuricemia or hypouricemia occurs. In the past, uric acid was mainly considered to be related to gout. But in recent years, there has been a proliferation of studies between uric acid and neurodegenerative disease, mainly including dementia, Parkinson's disease, amyotrophic lateral sclerosis, and multiple system atrophy.

Current trends indicate that early detection of AD by noninvasive approaches is a popular area of research. A growing number of studies have demonstrated that UA was linked with the risk, progress, and prognosis of AD, through

its neuroprotective effect, antioxidant capacity, metal complexation, and other mechanisms [3]. However, due to the inconsistency of research types and limitations of various research types, existing research results are contradictory. This article reviewed the progress of epidemiological and other studies on the influence of SUA on AD, aiming at exploring the possibility of SUA as a peripheral marker of AD and providing a reference for future research on peripheral markers of AD.

## 2. Method

On December 04, 2020, we performed a search of PubMed and Web of Science. Language and regional restrictions were not imposed. We searched the database above using search terms including "Alzheimer" AND "uric acid", "dementia" AND "uric acid", and "cognitive" AND "uric acid". The reference lists of included studies and relevant reviews were studied manually to minimize the omission of potentially

eligible articles. We mainly selected literature from 2016 to 2020 and included older literature that was commonly cited and highly valued (Figure 1).

### 3. Level of SUA Was Relevant to the Risk of AD

In recent years, there has been an increasing interest in studying the risk of developing AD in populations with different concentrations of SUA. However, the relationship between level of SUA and the risk of AD has been conflicting in different types of studies, and the evidence is weak in elderly subjects.

**3.1. Results from Epidemiological Studies.** In recent years, several prospective cohort studies with large sample size and long follow-up period have been published. A prospective cohort study in Sweden enrolled a population-based sample of 1462 females who were followed for up to 44 years. During the follow-up period, serum uric acid levels were measured twice. They found that a higher SUA concentration (per standard deviation of 76.5 mmol/L) was related to a lower risk for incident dementia ( $n = 320$ ; hazard ratio (HR) 0.81; confidence interval (CI) 0.72–0.91) and both AD ( $n = 152$ ; HR 0.78; CI 0.66–0.91) and vascular dementia (VD;  $n = 52$ ; HR 0.66; CI 0.47–0.94) [4]. This finding suggested the protective effect of SUA in the onset of incident dementia regardless of subtype. For the present literature, this cohort had the longest follow-up years and was a strong evidence. However, the limitation was that the sample population included only women. So whether the conclusions are also applicable to men is yet to be confirmed by other studies.

Latourte et al. evaluated the longitudinal link between the level of SUA and incident dementia in a large cohort followed for 12 years. This study enrolled 1598 individuals (mean (SD) age 72.4 (4.1) years, 61.7% female). The result showed that 110 participants developed dementia. After multivariate adjustment, the multivariate HR of the highest versus lowest SUA levels was 1.79. The correlation was stronger with other subtypes compared to AD, including VD and mixed dementia (MD) [5]. The elderly with a high level of SUA may mark the higher risk of incident dementia, especially VD or MD. The conflicting findings of these two studies may be due to the different gender structures of the participants and the duration of follow-up years.

Because of the difficulty of follow-up and other factors, only a few studies have considered the subtype classification in the cohort study of dementia. Alam et al. studied 11,169 participants in communities (ARIC) cohort with 24.1-year median follow-up period. As the study progressed, a total of 2005 cases of incident dementia were detected. They conducted adjustments including cardiovascular risk factors. After that, SUA and incident dementia showed an uncorrelated outcome (HR, 1.03; 95% CI, 0.88, 1.21). Elevated baseline levels of SUA were relevant to faster decline of cognition (25-year global z-score difference, -0.149; 95% CI, -0.246, -0.052) [6]. The results of this study may be due to the different influences of SUA on the onset of different subtypes of incident dementia. There was no separate subtype analysis of AD and VD in data analysis, which may lead to the cancel-

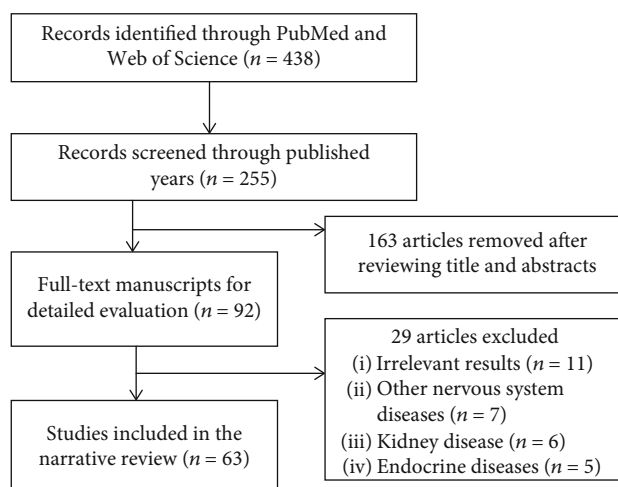


FIGURE 1: A flowchart shows the selection of study in the narrative review, which includes the final results of the initial search.

lation of positive and negative effects, resulting in the final result of no correlation. Another prospective study conducted in the UK without subgroup analysis showed that people in the lowest level group of SUA had a 25% increased risk of dementia compared to those in the highest SUA level group (HR = 0.75, 95% CI: 0.64–0.87). SUA was an independent predictor of dementia [7]. These studies did not include the analysis of the subtypes of incident dementia. AD and VD were analyzed together, which would have some impact on the results and conclusions.

Two population-based cohort studies [8, 9] indicated that gout was inversely relevant to the onset of AD. Gout patients had lower risks of AD. Among them, Hong et al. [9] took into account the effects of vascular dementia. According to sensitivity analysis in the study, after classifying patients with stroke before AD as vascular dementia, the conclusion remained the same. However, this inverse association could not be definitively attributed to the neuroprotective effect of uric acid, since uric acid levels were not directly analyzed in these studies. It remains to be seen whether this represents a definitive causal relationship.

In addition to the cohort study, there were more retrospective and cross-sectional analysis. Boccardi et al. did a retrospective study of UA and late-onset AD. A total of 232 subjects were divided into three groups, including healthy controls (HC), mild cognitive impairment (MCI) group, and AD group ( $n = 65, 95, \text{ and } 72$ , respectively). SUA levels were significantly lower in the AD group ( $4.84 \pm 1.30$  mg/mL) than in the healthy control group ( $5.82 \pm 1.76$  mg/mL;  $P = 0.001$ ). After adjusting for age, sex, body mass index, and creatinine levels, the correlation that existed between SUA and AD showed that the level of SUA was independently relevant to the diagnosis of AD [10]. The results showed that AD patients had a decreased level of SUA. UA may have a protective effect on elderly AD patients. Gonzalez-Dominguez et al. investigated metabolic differences in serum of AD patients and healthy controls by using gas chromatography coupled to mass spectrometry. As a result, SUA was markedly reduced in the AD group compared to

HC [11]. The same finding has been found in four investigations in recent years [12–16]. However, in a cross-sectional analysis, Zuliani et al. concluded that UA levels of LOAD (late-onset AD;  $357 \pm 95 \mu\text{mol/L}$ ) were elevated compared to the control group ( $300 \pm 96 \mu\text{mol/L}$ ;  $P < 0.01$ ) [17]. They concluded that a combination of markers including SUA may be a possible tool for the diagnosis of LOAD. In addition, three studies have reported increases or no change of UA in AD blood [18–20]. Observational evidence is susceptible to a large number of biases that limit causal inference, both residual confounding and reverse causation. It is required to conduct more studies to ascertain whether this is a causal relationship.

**3.2. Results from Other Studies.** Scholefield et al. systematically analyzed the results of various biochemical pathways in AD. The analysis showed the decrease of uric acid in biological fluids of AD cases and suggested that the decline in serum UA could be used as part of a generic biomarker for dementia [21]. In a meta-analysis, 21 case-control studies that included UA measurements were included to analyze plasma antioxidant status in AD patients and cognitively intact older adults. The result showed that plasma UA was markedly decreased in AD with a pooled mean difference (PMD)  $-27.37 \mu\text{mol/L}$  (95% CI:  $-49.75, -5.00$ ,  $P = 0.02$ ) compared to the control group [22]. The meta-analysis of Khan et al. also showed that the level of SUA in dementia patients was markedly decreased compared to HC, especially in patients with AD [23]. Paradoxically, another analysis suggested that there was no significant difference in levels of SUA between AD patients and HC, but with proper interpretation, there may be a trend toward decreased UA in AD [24]. The above analysis suggested that high uric acid could be relevant to low risk of AD, which was also confirmed in an animal experiment. In an experimental study, Wang et al. observed differences in the expression of AD biomarkers (APP and BACE1) in rats with different serum uric acid levels. The results showed that rats in the high-SUA-level group had significantly lower protein levels of APP and BACE1 in the hippocampus [25].

Over the past few years, four two-sample Mendelian randomized analyses have been performed to investigate the relationship between genetically determined circulating UA levels and risk of AD. Mendelian randomization is a statistical method that uses genetic variants like single nucleotide polymorphisms as genetic tools to make causal inferences about the nature of exposure-outcome relationships [26]. Williams et al. extracted genotype-AD risk association statistics from data from a genome-wide association study of LOAD subjects ( $n = 17,008$ ) and controls ( $n = 37,154$ ) [27]. The result suggested that genetically determined UA was not associated with AD risk and higher exposure to UA does not reduce the risk of AD. Similar results could be found in the study of Efstathiadou et al. [26] and Yuan and Yang [8]. But interestingly, Wang et al. came to the opposite conclusion in the latest research in 2020. The study found that for every standard deviation, increase in levels of UA ( $1.33 \text{ mg/dL}$ ) was related to a 0.09-fold increase in the risk of AD [28]. This analysis suggested that genetically predicted higher level of UA may lead to a higher risk of AD. The MR method

prevents bias caused by reverse causality and minimizes bias caused by measured and unmeasured confounding factors. These findings can make up for shortcomings of causality in observational studies and enrich the existing evidence.

**3.3. Summary of This Section.** Among the related studies on SUA and the risk of AD, existing cohort studies and an animal experiment suggested that high SUA level indicated a low risk of AD, and the evidence was stronger in women. Consistent with this, a large number of retrospective studies, cross-sectional analyses, and systematic meta-analyses showed that AD patients had lower SUA level than healthy controls. Conflicting conclusions of other studies may be due to the selection of subjects and the absence of subgroup analysis of dementia. Some Mendelian-random analysis indicated that gene-determined UA was not related to the risk of AD, suggesting the importance of the influence of acquired confounders.

## 4. Level of SUA Was Relevant to the Progression of AD

**4.1. Related Studies.** With the progression of AD, cognitive impairment becomes more and more serious. In recent years, only one cohort has observed cognitive decline in patients with AD at different baseline uric acid levels. Ye et al. used the AD Neuroimaging Initiative database to evaluate the cognitive decline of MCI and AD patients ( $n = 1064$ , including 271 HC, 596 MCI, and 197 AD). SUA and AD biomarkers in cerebrospinal fluid (CSF) were recorded once for baseline. Cognitive assessment scales were assessed continuously. The result showed that higher SUA level was related to slower cognitive decline, particularly in MCI and AD subgroups, and this association was more significant among female participants ( $P < 0.001$ ). Cerebrospinal fluid biomarker models showed that high concentrations of UA attenuated the adverse effects of  $A\beta_{1-42}$  and tau on cognitive decline in female subjects. However, it was noteworthy that in male subjects, the interaction was limited to resistance to the adverse effects of  $A\beta_{1-42}$  only, and there was no significant interaction with tau [29]. These findings suggested that UA had protective actions against longitudinal decline of cognition and can interact with  $A\beta$  and tau. Higher level of SUA may indicate slower progression of AD. The results also showed sex-related differences in uric acid's protective effects on cognition, which may partially explain the conflicting results and conclusions of the two cohort studies mentioned above.

This sex-related effect has also been observed in some other studies. A study of 1451 cognitively healthy adults found that elevated baseline SUA was relevant to decreased attention and visuospatial abilities in males. But in females, there were no marked findings [30]. A longitudinal cohort study of SUA and cognitive change showed that elevated level SUA at baseline was relevant to faster decline of cognition by using the visual memory/visuoconstruction ability test. UA only had a potential benefit for attention filed in older men [31]. Lin et al. found that the high level of SUA had different actions on spontaneous brain activities and cognitive



TABLE 1: Latest prospective studies that assessed the relationship between SUA and AD.

First author, journal year [Ref]	Population	Duration	Main results
Scheepers et al. 2019 [4]	1462 females	44 years	Lower risk of AD in women with higher SUA (HR 0.78; CI 0.66–0.91).
Latourte et al. 2018 [5]	1598 individuals	12 years	Significant risk of VD or mixed dementia in patients with higher SUA levels (HR 3.66, 95% CI: 1.29–10.41, $P = 0.015$ ), compared to AD (HR 1.55 (95% CI 0.92 to 2.61), $P = 0.10$ ).
Alam et al. 2020 [6]	11,169 individuals	24.1-year median follow-up period	After adjustment including cardiovascular risk factors, SUA and incident dementia showed an uncorrelated outcome (HR, 1.03; 95% CI, 0.88, 1.21). Elevated baseline levels of SUA were relevant to faster decline of cognition (25-year global z-score difference, -0.149; 95% CI, -0.246, -0.052).
Cao et al. 2020 [7]	502,528 individuals	8.1-year median follow-up period	People in the lowest level group of SUA had a 25% increased risk of dementia compared to those in the highest SUA level group (HR = 0.75, 95% CI: 0.64-0.87).
Ye et al.2016 [29]	1064 subjects (197 AD, 596 MCI, and 271 HC)	Mean duration 2.9 years	Higher levels of uric acid were associated with slower cognitive decline, particularly in the MCI and AD subgroups and more prominently in female subjects ( $P < 0.01$ ).

function in men and women [32]. This sex-dependent effect was also suggested in a cross-sectional analysis from the ELSA Brazil cohort [33].

Some scholars have pointed out that the conclusions of these studies may be due to the different standard SUA levels of men and women. Many studies have shown that women and men have different optimal SUA cutoff values for predicting metabolic syndrome, insulin resistance, cardiovascular status, the development of gout, etc. [34, 35]. Since the cutoff value for hyperuricemia in women is lower than that in men, at a certain high uric acid level, men and women actually have different elevations. If this had been taken into account in the data analysis, different results might have been found [36]. Honarpisheh et al. [37] also pointed out that sex was a biological variable in the pathological studies of neurodegenerative diseases. In future research, this factor should be considered in data analysis.

There were some studies on the influence of SUA on cognitive function, which were not AD targeted. In a cross-sectional analysis, Xue et al. found that levels of SUA were markedly decreased in MCI patients ( $292.28 \pm 63.71 \mu\text{mol/L}$ ) compared to HC ( $322.49 \pm 78.70 \mu\text{mol/L}$ ;  $P < 0.05$ ). Markedly positive correlations were shown between the Mini-mental State Examination (MMSE) scores and levels of SUA ( $P < 0.05$ ). UA was a protective factor for MCI (odds ratio = 0.999, 95% CI = 0.987-0.999) [38]. Similar results were found in a cross-sectional study of 10,016 individuals in Beijing, China [39].

Wang et al. enrolled 12798 middle-aged and elderly people over 45 years old in the follow-up study of health and pension in China. They measured the baseline plasma UA level, and the cognitive function was evaluated by a variety of methods. The results showed that middle-aged and older Chinese with high UA levels at baseline had better cognitive function, but not with rates of cognitive decline [40]. Xu et al. found that lower serum UA levels were related to cognitive dysfunction and could serve as a potential predictor for VD [41]. In a cross-sectional study in South Korea, Kim

et al. observed the association along SUA, AD brain changes, and cognitive impairment. 430 dementia-free elderly subjects were enrolled in this study. The results suggested that levels of SUA were markedly relevant to AD-characteristic area cerebral glucose metabolism (AD-CM) and borderline associated with MMSE. AD-CM was the link of UA and cognitive measure scores. A decreased level of SUA was relevant to AD-related cerebral hypometabolism [42]. In previous studies, few studies had included multimodal brain imaging to observe the relationship between uric acid and brain changes. Subsequent research is needed to prove whether this represents a causal relationship or not. And only after this relationship has been confirmed by more studies can experiments and clinical trials be designed from this point to using SUA as a therapeutic target.

In contrast, in a case-control study, higher levels of circulating UA were considered to be relevant to impairment of cognition in pharmacologically untreated elderly subjects [43]. In a two-center study of 180 elderly maintenance hemodialysis (MHD), Zhang et al. found that SUA levels were independently and negatively correlated with MMSE scores [44]. High SUA level may lead to impairment of cognition in the elderly MHD patients. A cross-sectional study from Japan showed that the high level of SUA was independently related to deterioration of cognition, and UA had an adverse influence on cognition [45].

**4.2. Summary of This Section.** Existing cohort studies have suggested that the high SUA level was associated with slower cognitive decline in AD patients, and high concentration of SUA could attenuate the effects of  $A\beta 1-42$  and tau on decline of cognition in female subjects. This gender-related effect has also been observed in some other studies, which may be due to the fact that the standard SUA level of men and women is different. A large number of cross-sectional studies found that the elderly with high UA level had better cognitive function and SUA was considered to be a protective factor of MCI. The decreased level of SUA was relevant to AD-



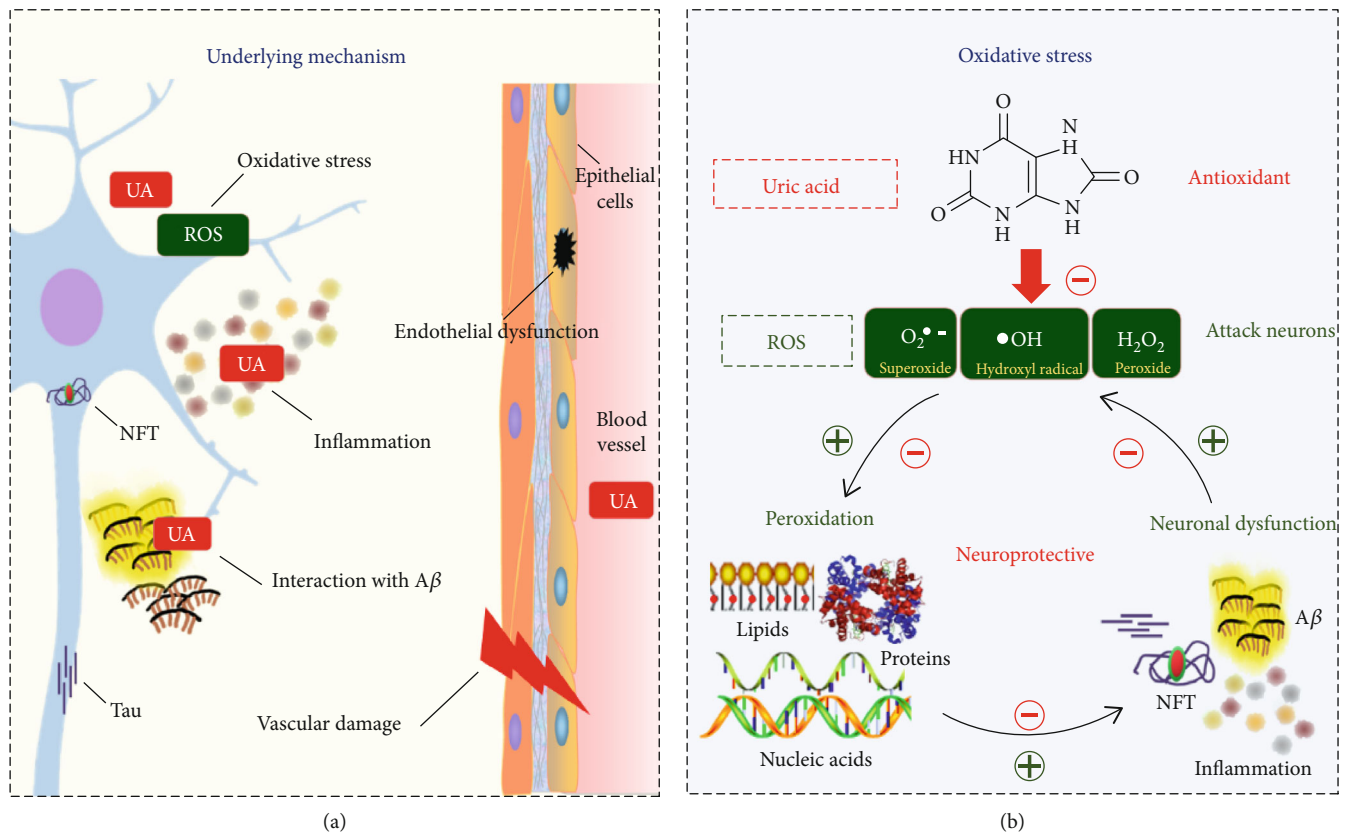


FIGURE 2: The underlying mechanism of uric acid on AD: (a) a summary figure on potential mechanisms; (b) SUA and AD were connected by oxidative stress.

related cerebral hypometabolism, but it is still uncertain whether there is a causal relationship. Still, some studies have shown that UA had an adverse influence on cognition (Table 1).

### 5. UA Was Related to AD through Multiple Mechanisms

Based on former research, UA had a dual effect on cognition including neuroprotective action and neurotoxic action. The dual effect of UA is reflected in a variety of hypotheses, including oxidative stress (OS), interaction with  $\beta$ -amyloid ( $A\beta$ ), inflammation, endothelial dysfunction, and vascular damage [3].

Current research indicates that OS has a crucial part to play in these mechanisms. The influence of OS is particularly important in neurodegenerative diseases. The brain is especially vulnerable to reactive oxygen species (ROS). Lipids, proteins, and nucleic acids of neurons can be attacked by ROS, causing inevitable neuronal dysfunction [11]. Evidence showed that the brain tissue of AD patients is exposed to OS, which leads to peroxidation of lipid, protein, DNA, and RNA and glycoxidation [46]. These peroxidation products could promote the production of key pathological changes of AD, including  $A\beta$ , neurofibrillary tangles (NFT), and inflammation. In turn, pathological changes of AD could promote oxidative stress, which has been experimentally demonstrated in postmortem brain tissues in AD patients and AD transgenic

mouse models [47]. Therefore, the two aspects interacted with each other and accelerated the development of AD. Additionally, it has been demonstrated that increasing antioxidant potential correlated with a reduction of white matter injury [42].

UA is a natural and powerful antioxidant of humans. The antioxidant effect of UA is attributed to its capacity to chelate transition metal ions to make stable complexes [48, 49] and to act as a powerful cleaner of oxygen and hydroperoxyl radicals. The level of UA in cerebrospinal fluid was positively correlated with SUA level, especially when the blood-brain barrier was damaged [50]. Therefore, a higher serum uric acid level indicates a higher antioxidant capacity and may reduce the damage to the brain from oxidative stress. However, the antioxidant properties have also been challenged by some studies. Some scholars have suggested that under some specific conditions, uric acid even had an oxidation-promoting effect [51–53]. And there was insufficient data to analyze uric acid levels in the brain, and the limited available data did not suggest a significant change [54, 55] (Figure 2).

An in vivo experiment conducted by Shao et al. showed that UA induced hippocampal inflammation through the TLR4/NF- $\kappa$ B pathway and led to dysfunction of cognition. They also found that hyperuricemia in rats and people was relevant to gliosis in the hippocampus by using magnetic resonance imaging [56]. Another laboratory study showed that ITM2B was a regulator of GLUT9-mediated urate transport, which was a molecular link between UA homeostasis and

neurodegenerative diseases [57]. Mazumder et al. [58] pointed out that uric acid was the most potent inhibitor of AChE, which was associated with dementia and cognitive impairment. In the Framingham Study, Chouraki et al. found the association with AD and hypoxanthine and taurine, which could be evidence that UA is neuroprotective [59].

Other potential links between uric acid and cognitive impairment can be suggested from the perspective of genetic syndromes and malnutrition. Some genetic syndromes are characterized by congenital uric acid disorders and neurological deficits, for example, primary renal hypouricemia [60, 61] and Lesch-Nyhan syndrome [62]. Therefore, it can be inferred that patients with the congenital uric acid disorder may have a genetic tendency to cognitive dysfunction. Since high uric acid levels increase cardiovascular risk, the relation between uric acid level and neurologic disorders could be like U- or J-shaped [61], which means if the UA level is extremely high or low, the risk of AD may both increase.

Hypouricemia is recognized as a sign of poor nutritional status, and some studies showed that poor nutritional status can cause faster cognitive decline in people with dementia [63]. There is a possibility that the correlation between low uric acid and cognitive impairment shown in the above study may include the influence of malnutrition. Cognitive frailty is a clinical syndrome in elderly individuals, which is characterized by physiological weakness and potentially reversible cognitive impairment, and dementia is excluded. The concept describes a preclinical cognitive status caused by physical frailty rather than neurodegenerative disorders [64]. The emergence of the concept of cognitive frailty supported this point. It provided a possibility that cognitive impairment may be caused by frailty or other comorbidities, and UA level is the manifestation of malnutrition, frailty, or other comorbidities rather than the main determinant.

## 6. Conclusions

The relationship between SUA and AD remains controversial, while current evidence supports the hypothesis that elevated UA levels could reduce the risk of AD, slow down the decline of cognition, and delay the progression of AD, and high SUA level may related to lower risk and progression of AD. But findings of some studies contradicted it. The main reasons for contradiction between the results are study inconsistency, the difference in subject selection (sex and age), and the lack of subtype analysis of incident dementia.

The current studies have some shortcomings, such as only recorded the UA level at baseline, one-time record could not reflect long-term uric acid levels, the small number of large-sample, AD-targeted cohort studies, and inadequate adjustment of confounding factors like nutritional status and comorbidity.

Whether the dual effect of UA can be selectively controlled, whether it has different effects on men or women, and whether there is a causal relationship between low SUA and AD-related cerebral hypometabolism are questions that need to be considered in the design of future studies. Future epidemiological studies should measure the SUA level several times to record dynamic changes and analyze the actual

increase of SUA in different genders, carry out the assessment of nutrition, frailty, and comorbidity to fully exclude the influence of confounding factors, and combine imaging examinations in the study design.

## Conflicts of Interest

The authors declare no conflicts of interest.

## Acknowledgments

This work was supported by grants from the “Xing-lin Scholars” Project of Chengdu University of Traditional Chinese Medicine (No. QNXZZ2018004), and “Hundred Talents Program” and Science and Technology Developmental Foundation from the Hospital of Chengdu University of Traditional Chinese Medicine (grant No. 20-Y02).

## References

- [1] P. Pacher, J. S. Beckman, and L. Liaudet, “Nitric oxide and peroxynitrite in health and disease,” *Physiological Reviews*, vol. 87, no. 1, pp. 315–424, 2007.
- [2] C. Tana, L. Busetto, A. Di Vincenzo et al., “Management of hyperuricemia and gout in obese patients undergoing bariatric surgery,” *Postgraduate Medicine*, vol. 130, no. 6, pp. 523–535, 2018.
- [3] C. Tana, A. Ticinesi, B. Prati, A. Nouvenne, and T. Meschi, “Uric acid and cognitive function in older individuals,” *Nutrients*, vol. 10, no. 8, 2018.
- [4] L. E. Scheepers, L. T. Jacobsson, S. Kern, L. Johansson, M. Dehlin, and I. Skoog, “Urate and risk of Alzheimer's disease and vascular dementia: a population-based study,” *Alzheimer's & Dementia*, vol. 15, no. 6, pp. 754–763, 2019.
- [5] A. Latourte, A. Soumaré, T. Bardin, F. Perez-Ruiz, S. Debette, and P. Richette, “Uric acid and incident dementia over 12 years of follow-up: a population-based cohort study,” *Annals of the rheumatic diseases*, vol. 77, no. 3, pp. 328–335, 2018.
- [6] A. B. Alam, A. Wu, M. C. Power, N. A. West, and A. Alonso, “Associations of serum uric acid with incident dementia and cognitive decline in the ARIC-NCS cohort,” *Journal of the Neurological Sciences*, vol. 414, p. 116866, 2020.
- [7] Z. Cao, C. Xu, H. Yang et al., “Associations of BMI and serum urate with developing dementia: a prospective cohort study,” *The Journal of Clinical Endocrinology & Metabolism*, vol. 105, no. 12, 2020.
- [8] H. Yuan and W. Yang, “Genetically determined serum uric acid and Alzheimer's disease risk,” *Journal of Alzheimer's Disease*, vol. 65, no. 4, pp. 1259–1265, 2018.
- [9] J. Y. Hong, T. Y. Lan, G. J. Tang, C. H. Tang, T. J. Chen, and H. Y. Lin, “Gout and the risk of dementia: a nationwide population-based cohort study,” *Arthritis research & therapy*, vol. 17, p. 139, 2015.
- [10] V. Boccardi, S. Carino, E. Marinelli et al., “Uric acid and late-onset Alzheimer's disease: results from the ReGAI 2.0 project,” *Aging clinical and experimental research*, vol. 33, no. 2, pp. 361–366, 2021.
- [11] R. Gonzalez-Dominguez, T. Garcia-Barrera, and J. L. Gomez-Ariza, “Metabolite profiling for the identification of altered metabolic pathways in Alzheimer's disease,” *Journal of pharmaceutical and biomedical analysis*, vol. 107, pp. 75–81, 2015.

- [12] F. Mangialasche, M. Baglioni, R. Cecchetti et al., "Lymphocytic mitochondrial aconitase activity is reduced in Alzheimer's disease and mild cognitive impairment," *Journal of Alzheimer's Disease*, vol. 44, no. 2, pp. 649–660, 2015.
- [13] E. Al-Khateeb, A. Althaher, M. Al-Khateeb et al., "Relation between uric acid and Alzheimer's disease in elderly Jordanians," *Journal of Alzheimer's Disease*, vol. 44, no. 3, pp. 859–865, 2015.
- [14] H. Hatanaka, H. Hanyu, R. Fukasawa et al., "Differences in peripheral oxidative stress markers in Alzheimer's disease, vascular dementia and mixed dementia patients," *Geriatrics & gerontology international*, vol. 15, pp. 53–58, 2015.
- [15] M. Cankurtaran, Y. Yesil, M. E. Kuyumcu et al., "Altered levels of homocysteine and serum natural antioxidants links oxidative damage to Alzheimer's disease," *Journal of Alzheimer's Disease*, vol. 33, no. 4, pp. 1051–1058, 2013.
- [16] Z. Pu, W. Xu, Y. Lin, J. He, and M. Huang, "Oxidative stress markers and metal ions are correlated with cognitive function in Alzheimer's disease," *American Journal of Alzheimer's Disease & Other Dementias*, vol. 32, no. 6, pp. 353–359, 2017.
- [17] G. Zuliani, A. Passaro, C. Bosi et al., "Testing a combination of markers of systemic redox status as a possible tool for the diagnosis of late onset Alzheimer's disease," *Disease markers*, vol. 2018, Article ID 2576026, 9 pages, 2018.
- [18] C. Cervellati, A. Romani, D. Seripa et al., "Oxidative balance, homocysteine, and uric acid levels in older patients with late onset Alzheimer's disease or vascular Dementia," *Journal of the Neurological Sciences*, vol. 337, no. 1-2, pp. 156–161, 2014.
- [19] E. Trushina, T. Dutta, X. M. Persson, M. M. Mielke, and R. C. Petersen, "Identification of altered metabolic pathways in plasma and CSF in mild cognitive impairment and Alzheimer's disease using metabolomics," *PloS one*, vol. 8, no. 5, p. e63644, 2013.
- [20] K. Nazef, M. Khelil, H. Chelouti et al., "Hyperhomocysteinemia is a risk factor for Alzheimer's disease in an Algerian population," *Archives of medical research*, vol. 45, no. 3, pp. 247–250, 2014.
- [21] M. Scholefield, R. D. Unwin, and G. J. S. Cooper, "Shared perturbations in the metallome and metabolome of Alzheimer's, Parkinson's, Huntington's, and dementia with Lewy bodies: a systematic review," *Ageing Research Reviews*, vol. 63, p. 101152, 2020.
- [22] K. Mullan, C. R. Cardwell, B. McGuinness, J. V. Woodside, and G. J. McKay, "Plasma antioxidant status in patients with Alzheimer's disease and cognitively intact elderly: a meta-analysis of case-control studies," *Journal of Alzheimer's Disease*, vol. 62, no. 1, pp. 305–317, 2018.
- [23] A. A. Khan, T. J. Quinn, J. Hewitt, Y. Fan, and J. Dawson, "Serum uric acid level and association with cognitive impairment and dementia: systematic review and meta-analysis," *Age (Dordrecht, Netherlands)*, vol. 38, no. 1, p. 16, 2016.
- [24] X. Chen, X. Guo, R. Huang, Y. Chen, Z. Zheng, and H. Shang, "Serum uric acid levels in patients with Alzheimer's disease: a meta-analysis," *PLoS One*, vol. 9, no. 4, article e94084, 2014.
- [25] L. Q. Wang Junxia and X. Xinxing, "The effects of serum uric acid on expression of APP and BACE1 in rats," *Chinese Journal of Nervous and Mental Diseases*, vol. 2014, no. 8, pp. 479–482, 2014.
- [26] A. Efstathiadou, D. Gill, F. McGrane, T. Quinn, and J. Dawson, "Genetically determined uric acid and the risk of cardiovascular and neurovascular diseases: a Mendelian randomization study of outcomes investigated in randomized trials," *Journal of the American Heart Association*, vol. 8, no. 17, p. e012738, 2019.
- [27] D. M. Williams, S. Hagg, and N. L. Pedersen, "Circulating antioxidants and Alzheimer disease prevention: a Mendelian randomization study," *The American Journal of Clinical Nutrition*, vol. 109, no. 1, pp. 90–98, 2019.
- [28] Z. Wang, L. Meng, L. Shen, and H. F. Ji, "Impact of modifiable risk factors on Alzheimer's disease: a two-sample Mendelian randomization study," *Neurobiology of aging*, vol. 91, pp. 167.e11–167.e19, 2020.
- [29] B. S. Ye, W. W. Lee, J. H. Ham, J. J. Lee, P. H. Lee, and Y. H. Sohn, "Does serum uric acid act as a modulator of cerebrospinal fluid Alzheimer's disease biomarker related cognitive decline?," *European journal of neurology*, vol. 23, no. 5, pp. 948–957, 2016.
- [30] A. M. Kueider, Y. An, T. Tanaka et al., "Sex-dependent associations of serum uric acid with brain function during aging," *Journal of Alzheimer's Disease*, vol. 60, no. 2, pp. 699–706, 2017.
- [31] M. A. Beydoun, J. A. Canas, G. A. Dore et al., "Serum uric acid and its association with longitudinal cognitive change among urban adults," *Journal of Alzheimer's Disease*, vol. 52, no. 4, pp. 1415–1430, 2016.
- [32] L. Lin, L. J. Zheng, U. Joseph Schoepf et al., "Uric acid has different effects on spontaneous brain activities of males and females: a cross-sectional resting-state functional MR imaging study," *Frontiers in neuroscience*, vol. 13, p. 763, 2019.
- [33] C. P. Baena, C. K. Suemoto, S. M. Barreto, P. A. Lotufo, and I. Benseñor, "Serum uric acid is associated with better executive function in men but not in women: baseline assessment of the ELSA-Brasil study," *Experimental gerontology*, vol. 92, pp. 82–86, 2017.
- [34] S. Seki, K. Tsutsui, T. Fujii, K. Yamazaki, R. Anzawa, and M. Yoshimura, "Association of uric acid with risk factors for chronic kidney disease and metabolic syndrome in patients with essential hypertension," *Clinical and Experimental Hypertension*, vol. 32, no. 5, pp. 270–277, 2010.
- [35] M. L. Zhang, Y. X. Gao, X. Wang, H. Chang, and G. W. Huang, "Serum uric acid and appropriate cutoff value for prediction of metabolic syndrome among Chinese adults," *Journal of Clinical Biochemistry and Nutrition*, vol. 52, no. 1, pp. 38–42, 2013.
- [36] P. Soysal, *Comment on Serum uric acid is associated with better executive function in men but not in women: baseline assessment of the ELSA-Brasil study*, vol. 96, p. 99, 2017.
- [37] P. Honarpisheh and L. D. McCullough, "Sex as a biological variable in the pathology and pharmacology of neurodegenerative and neurovascular diseases," *British Journal of Pharmacology*, vol. 176, no. 21, pp. 4173–4192, 2019.
- [38] L. Xue, Y. Liu, H. Xue et al., "Low uric acid is a risk factor in mild cognitive impairment," *Neuropsychiatric Disease and Treatment*, vol. Volume 13, pp. 2363–2367, 2017.
- [39] S. Xiu, Z. Zheng, S. Guan, J. Zhang, J. Ma, and P. Chan, "Serum uric acid and impaired cognitive function in community-dwelling elderly in Beijing," *Neuroscience letters*, vol. 637, pp. 182–187, 2017.
- [40] T. Wang, Y. Wu, Y. Sun, L. Zhai, and D. Zhang, "A prospective study on the association between uric acid and cognitive function among middle-aged and older Chinese," *Journal of Alzheimer's Disease*, vol. 58, no. 1, pp. 79–86, 2017.

- [41] Y. Xu, Q. Wang, R. Cui, K. Lu, Y. Liu, and Y. Zhao, "Uric acid is associated with vascular dementia in Chinese population," *Brain and behavior*, vol. 7, no. 2, p. e00617, 2017.
- [42] J. W. Kim, M. S. Byun, D. Yi et al., "Serum uric acid, Alzheimer-related brain changes, and cognitive impairment," *Frontiers in Aging Neuroscience*, vol. 12, p. 160, 2020.
- [43] A. F. Cicero, G. Desideri, G. Grossi et al., "Serum uric acid and impaired cognitive function in a cohort of healthy young elderly: data from the Brisighella Study," *Internal and emergency medicine*, vol. 10, no. 1, pp. 25–31, 2015.
- [44] J. Zhang, L. Tang, J. Hu, Y. Wang, and Y. Xu, "Uric acid is associated with cognitive impairment in the elderly patients receiving maintenance hemodialysis—a two-center study," *Brain and behavior*, vol. 10, no. 3, p. e01542, 2020.
- [45] K. Suzuki, D. Koide, K. Fujii, T. Yamazaki, S. Tsuji, and A. Iwata, "Elevated serum uric acid levels are related to cognitive deterioration in an elderly Japanese population," *Dementia and geriatric cognitive disorders extra*, vol. 6, pp. 580–588, 2017.
- [46] A. Gella and N. Durany, "Oxidative stress in Alzheimer disease," *Cell adhesion & migration*, vol. 3, no. 1, pp. 88–93, 2009.
- [47] C. M. Feitosa and O. G. L. Da Silva, "Determination of parameters of oxidative stress in vitro models of neurodegenerative diseases—a review," *Current Clinical Pharmacology*, vol. 13, no. 2, pp. 100–109, 2018.
- [48] C. X. Santos, E. I. Anjos, and O. Augusto, "Uric acid oxidation by peroxynitrite: multiple reactions, free radical formation, and amplification of lipid oxidation," *Archives of Biochemistry and Biophysics*, vol. 372, no. 2, pp. 285–294, 1999.
- [49] K. J. Davies, A. Sevanian, S. F. Muakkassah-Kelly, and P. Hochstein, "Uric acid-iron ion complexes. A new aspect of the antioxidant functions of uric acid," *The Biochemical Journal*, vol. 235, no. 3, pp. 747–754, 1986.
- [50] G. L. Bowman, J. Shannon, B. Frei, J. A. Kaye, and J. F. Quinn, "Uric acid as a CNS antioxidant," *Journal of Alzheimer's disease*, vol. 19, no. 4, pp. 1331–1336, 2010.
- [51] G. Desideri, R. Gentile, A. Antonosante et al., "Uric acid amplifies A $\beta$  amyloid effects involved in the cognitive dysfunction/dementia: evidences from an experimental model in vitro," *Journal of cellular physiology*, vol. 232, no. 5, pp. 1069–1078, 2017.
- [52] W. Lu, Y. Xu, X. Shao et al., "Uric acid produces an inflammatory response through activation of NF- $\kappa$ B in the hypothalamus: implications for the pathogenesis of metabolic disorders," *Scientific reports*, vol. 5, article 12144, 2015.
- [53] A. So and B. Thorens, "Uric acid transport and disease," *The Journal of clinical investigation*, vol. 120, no. 6, pp. 1791–1799, 2010.
- [54] N. McFarland, T. Burdett, C. A. Desjardins, M. P. Frosch, and M. A. Schwarzschild, "Postmortem brain levels of urate and precursors in Parkinson's disease and related disorders," *Neurodegenerative Diseases*, vol. 12, no. 4, pp. 189–198, 2013.
- [55] M. Zabel, A. Nackenoff, W. M. Kirsch, F. E. Harrison, G. Perry, and M. Schrag, "Markers of oxidative damage to lipids, nucleic acids and proteins and antioxidant enzymes activities in Alzheimer's disease brain: a meta-analysis in human pathological specimens," *Free Radical Biology & Medicine*, vol. 115, pp. 351–360, 2018.
- [56] X. Shao, W. Lu, F. Gao et al., "Uric acid induces cognitive dysfunction through hippocampal inflammation in rodents and humans," *The Journal of Neuroscience*, vol. 36, no. 43, pp. 10990–11005, 2016.
- [57] A. K. Mandal and D. B. Mount, "Interaction between ITM2B and GLUT9 links urate transport to neurodegenerative disorders," *Frontiers in physiology*, vol. 10, article 1323, 2019.
- [58] M. K. Mazumder, B. C. Phukan, A. Bhattacharjee, and A. Borah, "Disturbed purine nucleotide metabolism in chronic kidney disease is a risk factor for cognitive impairment," *Medical hypotheses*, vol. 111, pp. 36–39, 2018.
- [59] V. Chouraki, S. R. Preis, Q. Yang et al., "Association of amine biomarkers with incident dementia and Alzheimer's disease in the Framingham Study," *Alzheimers Dement*, vol. 13, no. 12, pp. 1327–1336, 2017.
- [60] I. Sebesta and B. J. P. Stiburkova, "Purine disorders with hypouricemia," *Prilozi*, vol. 35, no. 1, pp. 87–92, 2014.
- [61] A. Latourte, T. Bardin, and P. Richette, "Uric acid and cognitive decline: a double-edge sword?," *Current Opinion in Rheumatology*, vol. 30, no. 2, pp. 183–187, 2018.
- [62] S. Bell, I. Kolobova, L. Crapper, and C. Ernst, "Lesch-Nyhan syndrome: models, theories, and therapies," *Molecular syndromology*, vol. 7, no. 6, pp. 302–311, 2016.
- [63] C. Sanders, S. Behrens, S. Schwartz et al., "Nutritional status is associated with faster cognitive decline and worse functional impairment in the progression of dementia: the Cache County Dementia Progression Study1," *Journal of Alzheimer's disease*, vol. 52, no. 1, pp. 33–42, 2016.
- [64] C. Chen, J. Park, C. Wu et al., "Cognitive frailty in relation to adverse health outcomes independent of multimorbidity: results from the China health and retirement longitudinal study," *Aging*, vol. 12, no. 22, pp. 23129–23145, 2020.



## Retraction

# Retracted: Osmotic Demyelination Syndrome: Clinical, Neuroimaging Characteristics, and Outcomes in a Series of 18 Cases

### BioMed Research International

Received 12 March 2024; Accepted 12 March 2024; Published 20 March 2024

Copyright © 2024 BioMed Research International. This is an open access article distributed under the Creative Commons Attribution License, which permits unrestricted use, distribution, and reproduction in any medium, provided the original work is properly cited.

This article has been retracted by Hindawi following an investigation undertaken by the publisher [1]. This investigation has uncovered evidence of one or more of the following indicators of systematic manipulation of the publication process:

- (1) Discrepancies in scope
- (2) Discrepancies in the description of the research reported
- (3) Discrepancies between the availability of data and the research described
- (4) Inappropriate citations
- (5) Incoherent, meaningless and/or irrelevant content included in the article
- (6) Manipulated or compromised peer review

The presence of these indicators undermines our confidence in the integrity of the article's content and we cannot, therefore, vouch for its reliability. Please note that this notice is intended solely to alert readers that the content of this article is unreliable. We have not investigated whether authors were aware of or involved in the systematic manipulation of the publication process.

Wiley and Hindawi regrets that the usual quality checks did not identify these issues before publication and have since put additional measures in place to safeguard research integrity.

We wish to credit our own Research Integrity and Research Publishing teams and anonymous and named

external researchers and research integrity experts for contributing to this investigation.

The corresponding author, as the representative of all authors, has been given the opportunity to register their agreement or disagreement to this retraction. We have kept a record of any response received.

### References

- [1] X. Lv, Q. Hong, X. Lin, W. Chen, and Y. Tian, "Osmotic Demyelination Syndrome: Clinical, Neuroimaging Characteristics, and Outcomes in a Series of 18 Cases," *BioMed Research International*, vol. 2021, Article ID 9944632, 9 pages, 2021.



## Research Article

# Osmotic Demyelination Syndrome: Clinical, Neuroimaging Characteristics, and Outcomes in a Series of 18 Cases

Xinhuang Lv <sup>1</sup>, Qian Hong <sup>1</sup>, Xiuxiu Lin <sup>2</sup>, Weian Chen <sup>1</sup>, and Yuan Tian <sup>3</sup>

<sup>1</sup>Department of Neurology, First Affiliated Hospital of Wenzhou Medical University, Wenzhou, 325000 Zhejiang, China

<sup>2</sup>Department of Respiratory Medicine, First Affiliated Hospital of Wenzhou Medical University, Wenzhou, 325000 Zhejiang, China

<sup>3</sup>Department of Hematopathology, First Affiliated Hospital of Wenzhou Medical University, Wenzhou, 325000 Zhejiang, China

Correspondence should be addressed to Weian Chen; [wzanan@126.com](mailto:wzanan@126.com) and Yuan Tian; [wztymm@163.com](mailto:wztymm@163.com)

Received 26 March 2021; Revised 23 April 2021; Accepted 18 May 2021; Published 28 May 2021

Academic Editor: Yuzhen Xu

Copyright © 2021 Xinhuang Lv et al. This is an open access article distributed under the Creative Commons Attribution License, which permits unrestricted use, distribution, and reproduction in any medium, provided the original work is properly cited.

**Objective.** To investigate the etiology, clinical as well as neuroimaging characteristics, and outcomes after proper treatment in a series of 18 patients with osmotic demyelination syndrome. **Methods.** Medical records, including video records, of 18 patients with osmotic demyelination syndrome were retrospectively examined. Demographic and clinical information, imaging results, plans of management, and outcomes during the follow-up period were collected and analyzed. **Results.** Eighteen patients, including 10 males and 8 females, were included in the present study. The mean age at diagnosis of CNS insult was  $47.4 \pm 13.3$  years (ranged from 30 to 78 years). Etiologies included rapidly corrected hyponatremia (50%), alcoholism (27.8%), and others. Neurological manifestations included encephalopathy (61.1%), dysphonia (50%), extrapyramidal symptoms (38.9%), and seizures (22.2%). Neuroimaging results showed that 6 patients (33.3%) had central pontine myelinolysis, 5 (27.8%) had extrapontine myelinolysis, and 7 (38.9%) had both. After treatment, 12 patients showed improvement and the other 6 did not. Among these patients, those who showed symptoms of encephalopathy had a favorable outcome. The majority of those who presented with mental retardation, seizures, and no other symptoms recovered better than their counterparts who had other symptoms. Nine out of 11 patients with pseudobulbar paralysis and/or extrapyramidal symptoms showed improvement, but the other 2 did not show improvement. Five patients who did not improve after treatment during admission were followed up for 1-3 months with rehabilitation training recommended, and it was found that 3 showed significant improvement after training, and the other 2 did not respond to this training. **Conclusions.** Osmotic demyelination syndrome is a complex disease entity due to a variety of etiologies, manifesting with symptoms involving diverse systems of the brain. Early identification and removal/correction of conditions leading to osmotic demyelination syndrome are the key to prevent and/or manage this disease.

## 1. Introduction

Osmotic demyelination syndrome (ODS), including central pontine myelinolysis (CPM) and extrapontine myelinolysis (EPM), is a rare condition and was first described by Adams et al. in 1959 as a noninflammatory, demyelinating condition involving the pons of the hindbrain [1]. In 1962, another 2 studies reported that other brain areas like the basal ganglia, thalamus, cerebral cortex, and the subcortical white matter were also involved in addition to the pons [2, 3]. In the 1970s and 1980s, it was recognized that chronic alcoholism, long-lasting malnutrition, and rapid correction of hyponatremia

were the primary causes of ODS, especially when the level of sodium increased by more than 12 mmol/l/d [4].

Although the underlying mechanism of ODS is unclear, it is widely accepted that the pathologic changes observed in ODS were due to compression of fiber tracts by the fluctuating osmotic forces and the subsequent demyelination of these fiber tracts [5].

Clinical manifestations of ODS vary depending on the brain regions afflicted, ranging from symptoms of encephalopathy, pseudobulbar palsy (including dysarthria and dysphagia), to paralysis and extrapyramidal symptoms. The typical radiological findings on MRI are hyperintensities in

the central pons and/or other brain regions like the basal ganglia and the thalamus on T2-weighted (T2W) and fluid-attenuated inversion recovery (FLAIR) images and hypointensities on T1-weighted (T1W) images [6–8]. Diffusion-weighted imaging (DWI) also showed increased signal intensity and ADC values [9]. Surprisingly, radiological changes were still present for a period even after clinical improvement was observed.

Currently, the diagnosis of ODS primarily depends on the detailed medical history and imaging findings of suspected patients [7]: (1) a clear history of patients presenting with new neurological symptoms after a rapid increase in the level of serum sodium; (2) characteristic MRI findings include hypointensities on T1-weighted images and hyperintensities on T2-weighted, DWI, proton density-weighted, and FLAIR images. These demyelinated lesions are frequently confined to the central pons and are trident in shape, sparing fiber tracts traveling in the ventrolateral pons, such as the corticospinal tracts.

Though pharmacologic treatment is initiated for patients with ODS immediately after the diagnosis is confirmed, patients do not show consistent improvement as reported by previous studies [1, 10]. Recently, studies suggested that early diagnosis and intensive medical treatment may improve patients' outcomes [9, 11]. Since the 1970s, diverse etiologies have been revealed and treatments for ODS slowly shifted to focus on correcting these conditions apart from correcting patients' symptoms [10]. However, due to the fact that the majority of previous studies were case reports and the underlying conditions were different from each other, no consensus on the prognosis of ODS patients has been reached. In China, a few studies have reported the clinical manifestations of patients with ODS, but only a small number of patients in each study were reported. Here, we presented a large series of 18 patients with ODS in China, summarizing their etiologies, manifestations, neuroimaging findings, treatments, and prognosis after proper management.

## 2. Materials and Methods

**2.1. Study Participants and Data Collection.** Medical records, neuroimaging results, and videotapes of 18 patients with ODS who presented to the First Affiliated Hospital of Wenzhou Medical University from July 1996 to November 2019 were retrospectively reviewed and analyzed.

The diagnosis of ODS was made based on symptoms at admission and additional symptoms during their hospital stay, new hypointensities, or hyperintensities on MR images of different modalities [5]. Diagnostic criteria of ODS were (1) a clear history of patients presenting with new neurological symptoms after a rapid increase in the level of serum sodium; (2) characteristic MRI findings including hypointensities on T1-weighted images and hyperintensities on T2-weighted, DWI, proton density-weighted, and FLAIR images [7]. Demographic information including sex and age, neurological symptoms at presentation, CNS lesions shown on MRI, etiology, locations of new CNS lesions, characteristics of ODS, accompanying neurologic symptoms, and outcomes after treatments were reviewed and extracted. Outcomes

TABLE 1: Etiologies of ODS.

Etiologies	N (%) n = 18
Hyponatremia	9 (50.0)
Alcoholism	5 (27.8)
Multiple myeloma	1 (5.6)
Uremia	1 (5.6)
Terlipressin used	1 (5.6)
Hypokalemia	1 (5.6)
After general anesthesia	1 (5.6)
Hypernatremia	1 (5.6)
Diabetes insipidus	1 (5.6)

were assessed by viewing medical records of patients with ODS and their videos before and after their treatments.

## 3. Results

**3.1. Demographic Information about Patients with ODS.** A total of 18 patients were included in the present study, including 8 males and 10 females with a mean age of  $47.4 \pm 13.3$  years (ranging from 30 to 78 years). Among them, 8 patients showed new neurological symptoms before presenting to our hospital, and the other 10 patients demonstrated new symptoms during their admission (Supplementary Table 1).

**3.2. Etiologies of Patients with ODS.** Eight patients demonstrated new neurological symptoms before arriving at our hospital, and 5 were due to habitual drinking of alcohol, 1 due to uremia, 1 due to myeloma, and 1 due to hypokalemia. The other 10 patients presented new symptoms during their admission. One presented with neurological symptoms after a liver surgery. The other 9 had hyponatremia which was rapidly corrected. As a result, these patients showed neurological deficits. The average level of serum sodium before and after sodium supplementation was  $111.2 \pm 9.4$  mmol/l and  $136.1 \pm 5.1$  mmol/l, respectively, and the median of serum sodium before and after sodium supplementation was 117 mmol/l (in the range of 99–122 mmol/l) and 138 mmol/l (in the range of 127.5–142 mmol/l), respectively. The daily increase in serum sodium exceeded 12 mmol/l. Patient 6 was admitted to our hospital due to hypokalemia (2.8 mmol/l). The most common causes of ODS were the rapidly corrected hyponatremia in (9 patients), followed by alcoholism (5 patients). Three patients had both the rapidly corrected hyponatremia and alcoholism. Other causes included multiple myeloma (1 patient), uremia (1 patient), use of terlipressin (1 patient), hypokalemia (1 patient), post-liver surgery (1 patient), hypernatremia (1 patient), and diabetes insipidus (1 patient) (Table 1).

**3.3. Neurological Manifestations of Patients with ODS.** Clinical manifestations of ODS varied depending on the brain regions involved. The most common one was encephalopathy, which was observed in 11 (61.1%) patients, followed by dysphonia in 9 patients (50%), extrapyramidal symptoms in 7 patients (38.9%), and seizures in 4 patients (22.2%). The most common manifestation of those 9 patients with rapidly

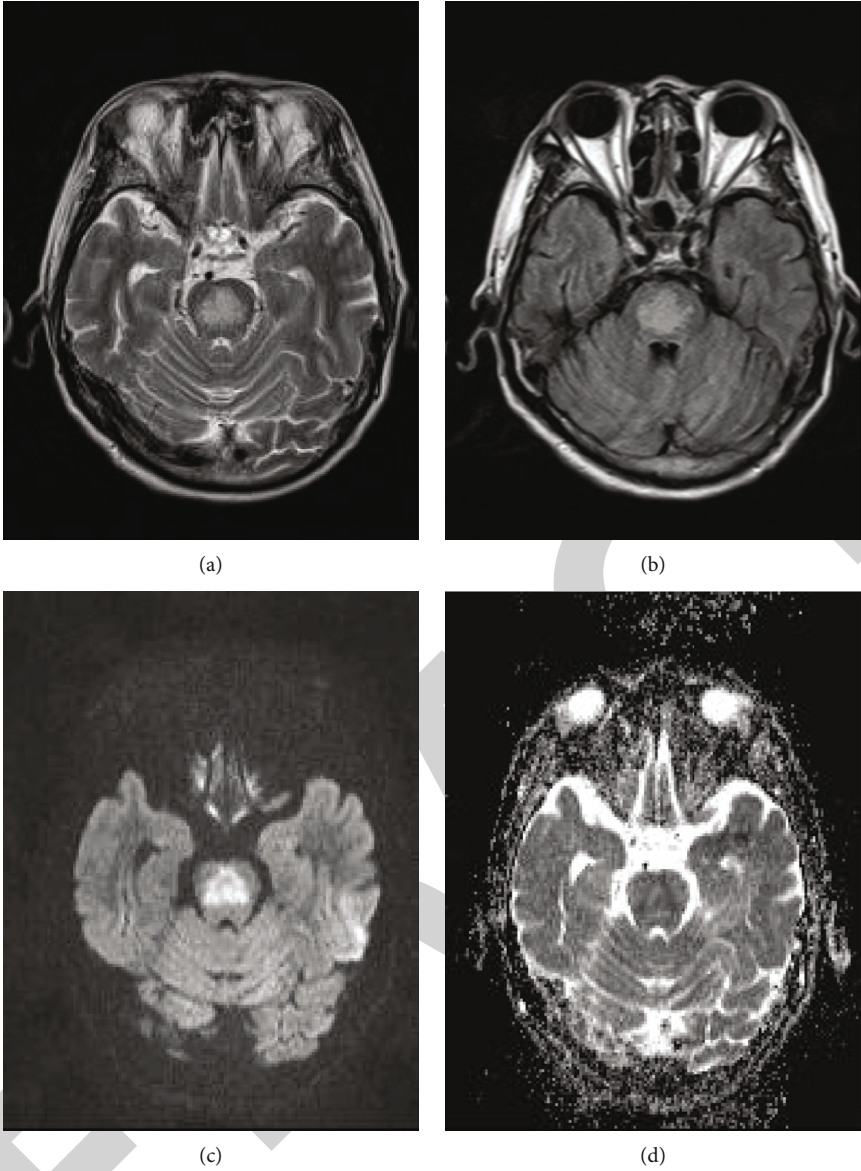
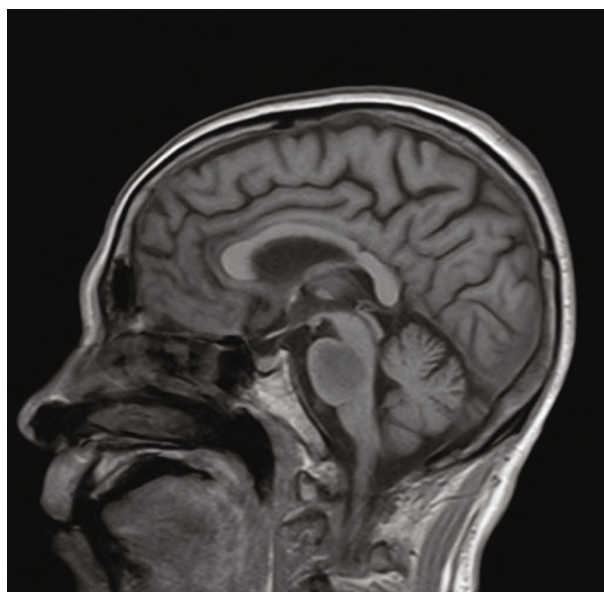


FIGURE 1: Continued.



(e)

FIGURE 1: Central pontine myelinolysis: (a) T2 and (b) T2 FLAIR images demonstrating symmetric hyperintensities in the central pons; (c) axial diffusion weighted image; (d) ADC map demonstrating restricted diffusion changes in the central pons; (e) sagittal T1 image demonstrating hypointensities in the pons.

corrected hyponatremia was encephalopathy (8/9), followed by severe coma and epilepsy which were observed in 3 patients. Among 5 patients with alcoholism, the most common symptom was dysphonia (4/5), followed by encephalopathy (3/5) and sensory disturbances (3/5) (Supplementary Table 1).

**3.4. Neuroimaging Data.** MRI scan was completed to confirm the diagnosis of ODS for these 18 patients. Among them, 6 showed CPM, evidenced by hyperintensities in the central pons on T2W as well as FLAIR images and hypointensities on T1W; 5 showed EPM involving the basal ganglia and the thalamus; and the other 7 showed both CPM and EPM (Figures 1 and 2). Three out of 5 patients with alcoholism showed CPM. Among 9 patients with their serum sodium rapidly corrected, 8 showed EPM or EPM plus CPM, and 1 showed CPM. The patient with hypokalemia showed CPM. The patient with myeloma and the one with uremia demonstrated CPM, whereas the one treated with terlipressin showed EPM and the one who underwent liver surgery showed CPM and EPM (Figures 1 and 2). The most frequently inflicted brain region was the pons (13/18), followed by the basal ganglia (10/18), the cerebral cortex (6/18), the thalamus, the midbrain, the hippocampus (2/18), and the cerebellum (1/18) (Table 2).

**3.5. Etiology Oriented Management.** The aim of treatment was to remove/correct the conditions that led to ODS. Apart from the specific management plan for patients with concomitant diseases, all of them were managed to sustain their blood volume, to restore levels of electrolytes and the acid-base balance, to provide nutritional support, and to improve their symptoms. For those with rapidly corrected hyponatremia,

the speed of supplementing sodium was decreased. For patients with severe symptoms, they were empirically managed with dexamethasone 10 mg once a day for a week. For a patient who was taking terlipressin, this medication was discontinued due to the suspected effect on water and electrolyte disturbance (Supplementary Table 1).

**3.6. Prognosis.** The prognosis of patients with different clinical manifestations was also different. Among these 18 patients with ODS, 12 showed improvement after treatment. Among these 12 patients, 6 completely recovered from ODS. The other 6 did not show significant improvement after treatment, and 1 of them completely failed to respond to the treatment. Patient 4 showed symptoms of respiratory failure and was supported with a ventilator (Table 3, Supplementary Table 1).

In general, patients with symptoms of encephalopathy had a favorable outcome after correcting electrolyte imbalance and supplementing necessary nutrients. The majority of these patients presented only with mental retardation and seizures. These patients recovered better after receiving proper treatment than their counterparts with other symptoms. Among 11 patients with pseudobulbar paralysis and/or extrapyramidal symptoms, 9 showed improvement, and the other 2 did not show significant improvement. Eight of these patients still had mild to moderate neurological deficits.

For patients with pseudobulbar palsy and/or extrapyramidal symptoms, 5 patients were followed up for 1-3 months with their rehabilitation training continued, which included soft palate function training and limb movement-related training. It was found that patients 5, 8, and 12 showed significant improvement in swallowing and speech, whereas patients 13 and 15 did not show significant improvement.



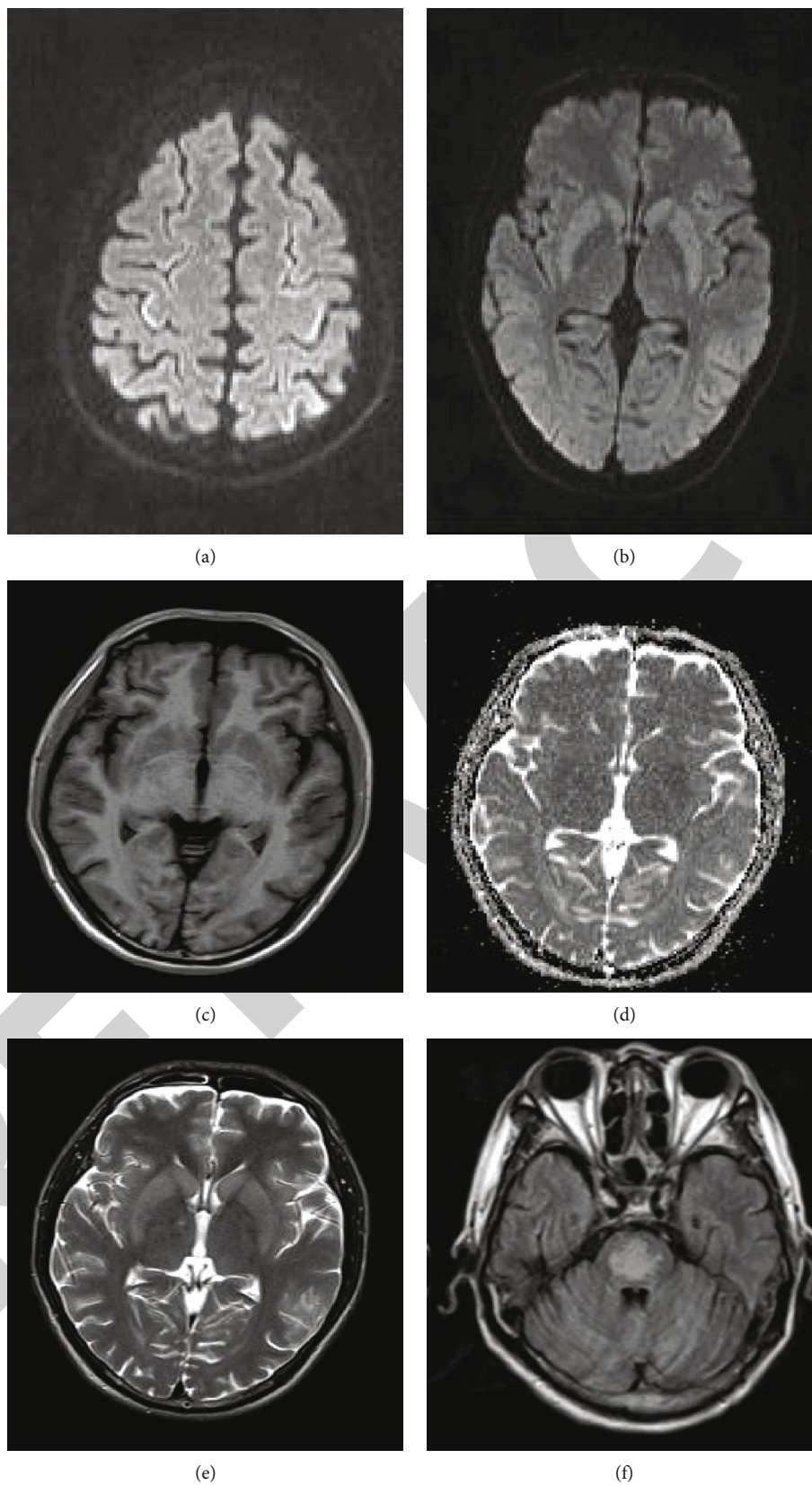


FIGURE 2: Extrapontine myelinolysis with central pontine myelinolysis: (a, b) axial diffusion-weighted images demonstrating restricted diffusion in the cerebral cortex and the basal ganglia; (c) T1 and (d) ADC map showing hypointensities in the basal ganglia; (e) T2 image demonstrating symmetric hyperintensities in the basal ganglia; (f) T2 FLAIR image demonstrating symmetric hyperintensities in the central pons.



TABLE 2: Distribution of lesions in the brain.

Lesion site (s)	N (%) n = 18
Pons	13 (55.6)
Basal ganglia	10 (55.6)
Cerebral cortex	6 (33.3)
Midbrain	2 (11.1)
Thalamus	2 (11.1)
Hippocampus	2 (11.1)
Cerebellum	1 (5.6)

#### 4. Discussion

ODS, a rare neurological condition, was poorly understood about its pathogenic mechanism and optimal managements. Though it was first reported in 1959 [1], the majority of available publications about it were case reports. The present study summarized findings from 18 patients with ODS, a large case series study in China, and presented their etiologies, clinical manifestations, neuroimaging results, treatments, and prognosis.

In the present study, it was found that the leading causes were rapidly corrected hyponatremia (50%) and alcoholism (27.8%), followed by other uncommon causes, which is consistent with findings from previous studies [2, 12, 13]. In a study, 292 patients were admitted because of suspected metabolic encephalopathy and 8.56% of them were confirmed ODS patients [5], suggesting that ODS might be closely related to abnormal metabolism. In our study, apart from 6 patients who had ODS after rapidly correcting hyponatremia alone, 5 patients had ODS due to alcoholism (including 3 patients with both the rapidly corrected hyponatremia and alcoholism). Among these alcoholic patients, alcohol might serve as a trigger resulting in vitamin B deficiency, which increases the susceptibility of these patients to demyelinating damage. Furthermore, diagnosing ODS in alcoholic patients is challenging as symptoms of ODS can overlap with alcohol withdrawal. Therefore, extra care should be taken in correcting hyponatremia and in early identification of ODS symptoms in alcoholics [14]. However, a study found that ODS was nearly cured after overcorrecting hyponatremia [15]. Hypokalemia has been reported to be a risk factor of OSD [16]. It was found that 89% of OSD patients who presented with hyponatremia also had hypokalemia [15, 16]. The authors believe that hypokalemia may also increase the susceptibility of nerve fibers to demyelination. In the present study, among the 9 patients who were rapidly corrected for hyponatremia, 6 had serum potassium below 3.5 mmol/l and 1 patient had only hypokalemia during the biochemical examination at the time of onset with a normal level of blood sodium. Specific mechanisms require further research.

The onset of ODS is usually acute and can progress rapidly. Different etiologies lead to different clinical manifestations of ODS. It has been reported that the major neurological symptoms include encephalopathy, parkinsonism, pseudobulbar palsy, and other movement disorder-related symptoms [5, 7, 17]. In our study, encephalopathy (61.1%),

dysphonia (50%), extrapyramidal symptoms (38.9%), and seizures (22.2%) were frequently observed, which is similar to findings of previous studies. Due to the fact that the majority of publications reported a small number of patients, predominantly from Caucasian populations, there might be a slight difference in the clinical manifestations between them and Chinese people, which might be confirmed by pooling reports from different ethnic groups.

Neuroimaging is key to the diagnosis of ODS. Based on the location of demyelinating lesions, ODS is divided into CPM and EPM [18]. These two categories of lesions can be observed in the same brain or in different ones. A study reported that 10% of patients with CPM can have concomitant EPM [19]. However, another study reported that CPM plus EPM, CPM alone, and EPM alone accounted for 50%, 30%, and 20%, respectively, of patients with ODS [20]. Among 18 patients with ODS in the present study, 7 (38.9%) had both CPM and EPM, 6 (33.3%) had CPM alone, and 5 (27.8%) had EPM alone. In our study, 3 out of 5 patients with alcoholism had CPM, whereas 8 out of 9 patients with rapidly corrected hyponatremia had EPM or EPM plus CPM. Again, due to the small number of patients studied, the predominance of CPM or EPM cannot be clearly differentiated based on the difference in the underlying causes.

Regarding the brain regions that are commonly inflicted by ODS, it is recognized that the pons in the brainstem is the primary lesion site, followed by the basal ganglia and the thalamus. A study on 58 patients with ODS suggested that the cerebellum and the lateral geniculate body were the most frequently affected extrapontine regions [20]. Another study on 25 patients showed that the pons and the basal ganglia were the most frequently affected regions [5]. Our results are consistent with those of previous reports in that the brainstem, basal ganglia, and the thalamus accounted for 72.2%, 55.6%, and 11.1% of lesion sites, respectively. This might be related to the presence of densely packed fiber tracts in these regions. A rapid increase in osmotic pressure in these regions is more likely to compress these fiber tracts, leading to lesions observed on MR images.

Current treatments for ODS are mainly to remove or correct underlying conditions and to improve symptoms. Acute electrolyte disturbance is fatal under certain circumstances [21]. For all patients, removing or correcting the underlying conditions should be the first step. In general, life-threatening symptoms will be improved after increasing the concentration of serum sodium by 5%. To minimize the risk of developing ODS, serum sodium should not be increased by more than 8-12 meq/l per day. For those who have accompanying risk factors like alcoholism, malnutrition, or hypokalemia in addition to hyponatremia, serum sodium should not be increased by more than 8 meq/l per 24 h [7, 22].

In the present study, 12 out of 18 patients with ODS showed improvement after correcting the underlying conditions, adjusting the speed of supplementing sodium as well as providing nutritional support. When patients were grouped by the time they received treatments, it was found that 2 out of 4 patients who received treatments 24 hours after symptom onset showed improvement during the follow-up period, whereas 10 out of 14 patients who were

TABLE 3: Clinical characters of participants.

Patient	Age (y)	Sex	Treatment	MMSE (before)	MMSE (after)	Water swallowing test (before)	Water swallowing test (after)	GCS (before)	GCS (after)	Water swallowing test (after rehab)
1	54	M	Symptomatic treatment	29						
2	30	M	Symptomatic treatment	29						
3	53	F	Symptomatic treatment	18	29					
4	78	F	Symptomatic treatment+ dexamethasone 10 mg	Not cooperative	Not cooperative	Not cooperative		6	10	
5	30	M	Symptomatic treatment+ dexamethasone 10 mg			4	3			2
6	38	F	Symptomatic treatment	20	29	1	1			
7	52	M	Symptomatic treatment	17	28	4	2			
8	47	F	Symptomatic treatment	20	29	4	3			2
9	34	F	Symptomatic treatment	15	26	4	3			
10	61	M	Symptomatic treatment							
11	60	M	Symptomatic treatment			3	2			
12	26	F	Symptomatic treatment			3	2			1
13	55	M	Symptomatic treatment			4	3			3
14	40	M	Symptomatic treatment	16	27	2	2			2
15	39	M	Symptomatic treatment	20	29					
16	58	F	Symptomatic treatment	18	29					
17	49	M	Symptomatic treatment	18	28	3	2			
18	50	F	Symptomatic treatment	19	29					

managed within 24 hours after symptom onset showed improvement and 6 of them completely recovered. This might be explained by the early removal of underlying conditions and consequently halting the progression of ODS. Therefore, early identification of new neurological symptoms and the underlying conditions is key to good outcomes of these patients.

In addition, a relationship between the therapeutic effect and clinical manifestations was observed. For example, patients who showed symptoms of encephalopathy and seizures tended to have better outcomes after treatment than those who had dysarthria and/or extrapyramidal symptoms. This might be related to the extent of brain damage. For patients with severe clinical symptoms, it was suggested that

corticosteroid might be effective [5]. In the present study, 2 patients with poor therapeutic response received short-term intravenous administration of 10 mg dexamethasone. One patient showed improvement while the other did not. It is unclear whether this difference is related to the use of corticosteroid or related to the nature and duration of the disease.

Furthermore, rehabilitation training was recommended to patients with unsatisfactory functional recovery. During the follow-up period, 3 out of 5 patients showed improvement in swallowing and speech. This suggests that continued rehabilitation is beneficial to the recovery of patients. Other potential therapeutics such as immunoglobulin injection and plasma exchange are suggested, but further research is required to confirm their usefulness for ODS [23–26].

In conclusion, ODS has diverse etiologies and discrete clinical manifestations as well as neuroimaging characters. Treatments are mainly targeting to correct the underlying conditions and to improve the symptoms. Outcomes are related to various factors. Further research is needed to comprehend this condition.

### Data Availability

Data are available from the corresponding author upon reasonable request.

### Ethical Approval

Study procedures of the present study were approved by the Human Research Ethics Committee of First Affiliated Hospital of Wenzhou Medical University.

### Conflicts of Interest

The authors declare that there is no conflict of interests.

### Acknowledgments

The present study was supported by a grant from Wenzhou Municipal Science and Technology Bureau, Zhejiang Province (No. Y20180874).

### Supplementary Materials

Supplementary Table 1: clinicoradiologic information of ODS patients. (*Supplementary Materials*)

### References

- [1] R. D. Adams, M. Victor, and E. L. Mancall, "Central pontine Myelinolysis," *A.M.A. Archives of Neurology and Psychiatry*, vol. 81, no. 2, pp. 154–172, 1959.
- [2] S. A. Howard and J. A. Barletta, "Best cases from the AFIP osmotic demyelination syndrome," *Radiographics*, vol. 29, no. 3, pp. 933–938, 2009.
- [3] B. K. Kleinschmidt-DeMasters, A. M. Rojiani, and C. M. Filley, "Central and extrapontine myelinolysis: then ... and now," *Journal of Neuropathology and Experimental Neurology*, vol. 65, no. 1, pp. 1–11, 2006.
- [4] D. M. Snell and C. Bartley, "Osmotic demyelination syndrome following rapid correction of hyponatraemia," *Anaesthesia*, vol. 63, no. 1, pp. 92–95, 2008.
- [5] R. N. Kallakatta, A. Radhakrishnan, R. K. Fayaz, J. P. Unnikrishnan, C. Kesavadas, and S. P. Sarma, "Clinical and functional outcome and factors predicting prognosis in osmotic demyelination syndrome (central pontine and/or extrapontine myelinolysis) in 25 patients," *Journal of Neurology Neurosurgery and Psychiatry*, vol. 82, no. 3, pp. 326–331, 2011.
- [6] G. M. Miller and H. L. Baker, "Central pontine myelinolysis and its imitators: MR findings," *Radiology*, vol. 168, no. 3, pp. 795–802, 1988.
- [7] J. D. King and M. H. Rosner, "Osmotic demyelination syndrome," *The American Journal of the Medical Sciences*, vol. 339, no. 6, p. 567, 2010.
- [8] J. Laubenberger, B. Schneider, O. Ansorge et al., "Central pontine myelinolysis: clinical presentation and radiologic findings," *European Radiology*, vol. 6, no. 2, pp. 177–183, 1996.
- [9] R. Abbott, E. Silber, J. Felber, and E. Ekpo, "Osmotic demyelination syndrome," *British Medical Journal*, vol. 331, no. 7520, pp. 829–830, 2005.
- [10] D. G. Wright, R. Laureno, and M. Victor, "Pontine and extrapontine myelinolysis," *Brain: A Journal of Neurology*, vol. 102, no. 2, pp. 361–385, 1979.
- [11] H. Menger and J. Jörg, "Outcome of central pontine and extrapontine myelinolysis (n =44)," *Journal of Neurology*, vol. 246, no. 8, p. 705, 1999.
- [12] F. Gankam Kengne, C. Nicaise, A. Soupart et al., "Astrocytes are an early target in osmotic demyelination syndrome," *Journal of American Society of Nephrology*, vol. 22, no. 10, pp. 1834–1845, 2011.
- [13] K. A. Ruzek, N. G. Campeau, and G. M. Miller, "Early diagnosis of central pontine myelinolysis with diffusion-weighted Imaging," *American Journal of Neuroradiology*, vol. 25, no. 2, pp. 210–213, 2004.
- [14] M. Jahan, S. Sharma, and R. Rehmani, "Osmotic demyelination syndrome despite appropriate hyponatremia correction," *Cureus*, vol. 12, no. 5, 2020.
- [15] J. W. Lohr, "Osmotic demyelination syndrome following correction of hyponatremia: association with hypokalemia," *The American Journal of Medicine*, vol. 96, no. 5, pp. 408–413, 1994.
- [16] P. A. Koul, U. H. Khan, R. A. Jan et al., "Osmotic demyelination syndrome following slow correction of hyponatremia: possible role of hypokalemia," *Indian Journal of Critical Care Medicine: peer-reviewed, official publication of Indian Society of Critical Care Medicine*, vol. 17, no. 4, pp. 231–233, 2013.
- [17] A. Seiser, S. Schwarz, M. M. Aichinger-Steiner, G. Funk, P. Schnider, and M. Brainin, "Parkinsonism and dystonia in central pontine and extrapontine myelinolysis," *Journal of Neurology, Neurosurgery & Psychiatry*, vol. 65, no. 1, pp. 119–121, 1998.
- [18] S. W. Cheo, Q. J. Low, Y. A. Tan, and Y. K. Chia, "Trident sign in osmotic demyelination syndrome," *QJM: An International Journal of Medicine*, vol. 113, no. 2, pp. 131–132, 2019.
- [19] A. Uchino, T. Yuzuriha, M. Murakami et al., "Magnetic resonance imaging of sequelae of central pontine myelinolysis in chronic alcohol abusers," *Neuroradiology*, vol. 45, no. 12, p. 880, 2003.

## Research Article

# Score for Predicting Active Cancer in Patients with Ischemic Stroke: A Retrospective Study

Jiwei Jiang <sup>1</sup>, Xiuli Shang <sup>2</sup>, Jinming Zhao,<sup>3</sup> Meihui Cao,<sup>4</sup> Jirui Wang,<sup>2</sup> Runzhi Li <sup>1</sup>, Yanli Wang <sup>1</sup> and Jun Xu <sup>1</sup>

<sup>1</sup>Department of Neurology, Beijing Tiantan Hospital, Capital Medical University, Beijing, China

<sup>2</sup>Department of Neurology, The First Affiliated Hospital, China Medical University, Shenyang, China

<sup>3</sup>Department of Pathology, The First Affiliated Hospital and College of Basic Medical Sciences, China Medical University, China

<sup>4</sup>Department of Oncology, Cancer Hospital of China Medical University, Liaoning Cancer Hospital & Institute, China

Correspondence should be addressed to Jun Xu; [neurojun@126.com](mailto:neurojun@126.com)

Received 3 March 2021; Revised 1 April 2021; Accepted 18 May 2021; Published 25 May 2021

Academic Editor: Yuzhen Xu

Copyright © 2021 Jiwei Jiang et al. This is an open access article distributed under the Creative Commons Attribution License, which permits unrestricted use, distribution, and reproduction in any medium, provided the original work is properly cited.

**Background.** We aimed to examine the differences of clinical characteristics between patients with ischemic stroke with active cancer and those without cancer to develop a clinical score for predicting the presence of occult cancer in patients with ischemic stroke. **Methods.** This retrospective study enrolled consecutive adult patients with acute ischemic stroke who were admitted to our department between December 2017 and January 2019. The demographic, clinical, laboratory, and neuroimaging characteristics were compared between patients with ischemic stroke with active cancer and those without cancer. Multivariate analysis was performed to identify independent factors associated with active cancer. Subsequently, a predictive score was developed using the areas under the receiver operating characteristic curves based on these independent factors. Finally, Bayesian decision theory was applied to calculate the posterior probability of active cancer for finding the best scoring system. **Results.** Fifty-three (6.63%) of 799 patients with ischemic stroke had active cancer. The absence of a history of hyperlipidemia (odds ratio (OR) = 0.17, 95% confidence interval (CI): 0.06–0.48,  $P < 0.01$ ), elevated serum fibrinogen (OR = 1.72, 95% CI: 1.33–2.22,  $P < 0.01$ ) and D-dimer levels (OR = 1.43, 95% CI: 1.24–1.64,  $P < 0.01$ ), and stroke of undetermined etiology (OR = 22.87, 95% CI: 9.91–52.78,  $P < 0.01$ ) were independently associated with active cancer. A clinical score based on the absence of hyperlipidemia, serum fibrinogen level of  $\geq 4.00$  g/L, and D-dimer level of  $\geq 2.00$   $\mu\text{g/mL}$  predicted active cancer with an area under the curve of 0.83 (95% CI: 0.77–0.89,  $P < 0.01$ ). The probability of active cancer was 59% at a supposed prevalence of 6.63%, if all three independent factors were present in a patient with ischemic stroke. **Conclusions.** We devised a clinical score to predict active cancer in patients with ischemic stroke based on the absence of a history of hyperlipidemia and elevated serum D-dimer and fibrinogen levels. The use of this score may allow for early intervention. Further research is needed to confirm the implementation of this score in clinical settings.

## 1. Introduction

Malignant tumors and stroke are the most common causes of disability and mortality worldwide [1]. The concomitance of both conditions has serious repercussions on the quality of life, with a substantial increase in the socioeconomic burden at both the individual and societal levels. Previous studies have reported that approximately 15% of patients with cancer are at risk of developing ischemic stroke (IS) later in

life [2], and 10% of patients hospitalized with IS could have cancer as a comorbidity [3]. Sometimes, IS could even represent the initial manifestation of occult cancer [4]. A systematic review revealed that the short-term risk of stroke was considerably increased after a new diagnosis of a solid tumor, and correspondingly, the probability of diagnosing cancer was significantly high in the first few months after a stroke [5]; moreover, the risk of stroke varies with the type of cancer, histopathological features, and stage [6]. This



evidence demonstrates a close association between cancer and stroke, revealing an opportunity for occult cancer screening in specific populations, such as patients with cryptogenic stroke. Thus, discerning occult malignancies at an early stage in patients with IS and treatment with appropriate interventions could help improve the chances of survival and functional outcomes [7].

However, there is no consensus on the characteristics of patients with IS at a higher risk of developing malignancies, despite the increasing interest in the relationship between IS and cancer [6, 8]. Some studies have shown that higher rates of stroke of undetermined etiology (SUE), elevated C-reactive protein (CRP) and D-dimer levels, and lesions involving multiple vascular territories as shown on diffusion-weighted imaging (DWI) are relatively specific characteristics of patients with cancer-associated IS [9–11]. However, other studies did not find significant differences in these stroke-related characteristics between IS patients with and without cancer [12–14]. Currently, research focusing on the appropriate time and approach for screening cancer in patients with IS is lacking. To the best of our knowledge, only one study has reported a score for predicting occult malignancies in patients with IS; however, in terms of overall predictive strength, that score had an area under the curve (AUC) of 0.73 [15]. Therefore, we conducted a retrospective study to identify the differences in clinical, laboratory, and neuroimaging characteristics between IS patients with active cancer or without cancer and to develop a more reliable, clinically relevant predictive score for cancer screening in patients with IS.

## 2. Materials and Methods

**2.1. Patient Selection and Data Collection.** This retrospective study enrolled consecutive patients with acute IS from the Department of Neurology at the First Affiliated Hospital of China Medical University, a comprehensive academic hospital in a large urban area, between December 2017 and January 2019. The inclusion criteria were as follows: (1) age  $\geq 18$  years, (2) IS that met the Baltimore-Washington Cooperative Young Study Criteria, (3) neurologic deficit lasting longer than 24 h, and (4) computed tomography (CT) or magnetic resonance imaging (MRI) scans depicting infarctions consistent with clinical findings [16]. Patients were excluded from the study if they (1) lacked information regarding the etiological examination for stroke, including data from Holter electrocardiography (ECG), transthoracic or transesophageal echocardiography, magnetic resonance angiography (MRA), CT angiography (CTA), or Doppler ultrasonography; (2) were diagnosed with transient ischemic attack (TIA) or cerebral hemorrhage; (3) had a previous history of brain tumor, cerebral metastases, or intracranial surgery; and (4) had indications of inactive cancer (patients with IS and cancer that did not meet the description of active cancer) or hematological malignancies. Active cancer was defined as the diagnosis of cancer or administration of cancer treatment within the past 6 months or the metastasis or recurrence of known cancers [17, 18]. Patients with IS and active cancer were categorized into the cancer group, while those without cancer were assigned to the control group.

**2.2. Clinical Assessment.** Trained personnel reviewed the patients' demographic data (age, sex, and medical history); vascular risk factors (hypertension: previous diagnosis and treatment or blood pressure  $\geq 140/90$  mmHg); diabetes mellitus (previous diagnosis and treatment or fasting glucose level of  $\geq 7.00$  mmol/L); hyperlipidemia (previous diagnosis and treatment; fasting total serum cholesterol level of  $\geq 5.72$  mmol/L, triglyceride level of  $\geq 1.7$  mmol/L, or low-density lipoprotein level of  $\geq 3.64$  mmol/L); atrial fibrillation (previous diagnosis and treatment or suggestive ECG findings); history of coronary heart disease, IS, or TIA; obesity (body mass index  $\geq 28$  kg/m<sup>2</sup>); current smoking habits; stroke severity on admission (based on the National Institute of Health Stroke Scale (NIHSS) score) [19]; and results of diagnostic investigations. Two board-certified neurologists consensually determined the stroke etiology as large-artery atherosclerosis (LAA), cardioembolism (CE), small vessel occlusion (SVO), stroke of other determined etiology (SOE), or SUE, according to the Trial of Org 10172 in Acute Stroke Treatment (TOAST) criteria [20].

Routine investigations included neuroimaging (MRI, especially contrast-enhanced MRI and DWI, and angiography, including MRA, CTA, and Doppler ultrasonography), ECG or 24 h ECG, and transthoracic or transesophageal echocardiography. The presence of acute multiple cerebral infarctions (AMCI) was determined based on DWI findings, and AMCI were defined as multiple acute infarcts, either in the bilateral anterior or posterior circulation or simultaneously in the anterior and posterior circulations, suggesting an embolic etiology. Data on routine laboratory parameters, including serum platelet counts and hemoglobin, fibrinogen, D-dimer, CRP, lipid, and glucose levels, were also obtained. The diagnosis of cancer was confirmed based on histopathological evidence and the oncologist's opinion. Furthermore, oncological records were carefully reviewed for cancer-specific details, including tumor type, histology, and stage.

**2.3. Statistical Analysis.** All statistical analyses were performed using SPSS 22.0 statistical software (SPSS Inc., Chicago, IL, USA). Categorical variables are presented as the total number ( $n$ ) and percentage (%) per group, and the  $\chi^2$  or Fisher's exact test was used to assess statistical differences. The mean and standard deviations (SDs) were calculated for continuous variables with normal distribution, while the median and interquartile range (IQR) were used for continuous variables lacking normal distribution. Similarly, the Student  $t$ -test was used for normally distributed data. The Mann-Whitney  $U$  test was used for data without normal distribution. Risk factors ( $P \leq 0.05$ ) were further analyzed using univariate and multivariate logistic regression. Risk factors independently associated with active cancer were included in our clinical scoring system, which were dichotomized using cut-off points prior to score entry based on clinical experience and previously published evidence. We compared the diagnostic performance of different scores using the area under the receiver operating characteristic (AUC-ROC) curve. Bayesian decision theory was used to calculate the posterior probability of active cancer for different scores. All  $P$  values were two-tailed.  $P$  values  $< 0.05$  were considered statistically significant.



### 3. Results

**3.1. Baseline Characteristics of Patients with Ischemic Stroke in Both Groups.** Of the initial 1,889 patients with IS, 799 were included in the final analysis (Figure 1). Of these, 53 (6.63%) were diagnosed with active cancer at the time of stroke onset and were assigned to the cancer group, while 746 (93.37%) did not have a history of cancer and were assigned to the control group.

Table 1 shows the patient characteristics for both groups. Patients in the cancer group had a significantly higher mean age than those without cancer (mean  $\pm$  SD: 67.21  $\pm$  10.11 years vs. 62.11  $\pm$  12.09 years;  $t = 3.00$ ,  $P < 0.01$ ). The frequency of hyperlipidemia was lower in the cancer group than in the control group (22.6% vs. 49.3%;  $\chi^2 = 14.13$ ,  $P < 0.01$ ). The prevalence of other vascular risk factors did not differ significantly between the two groups. We observed that 35 (66.04%) patients in the cancer group had SUE compared to 31 (4.16%) patients in the control group ( $\chi^2 = 250.06$ ,  $P < 0.01$ ), while the LAA subtype was less common in the cancer group than in the control group (9.43% vs. 60.99%;  $\chi^2 = 53.85$ ,  $P < 0.01$ ), as per the TOAST criteria. There were no significant differences in prevalence of the CE, SVO, and SOE subtypes. We found that the average NIHSS score at admission was higher in the cancer group than in the control group (mean  $\pm$  SD: 6.13  $\pm$  4.10 vs. 4.30  $\pm$  4.48;  $t = 2.89$ ,  $P < 0.01$ ). AMCI were observed more frequently in the cancer group than in the control group (56.60% vs. 19.84%;  $\chi^2 = 38.63$ ,  $P < 0.01$ ). The incidence of deep vein thrombosis or pulmonary embolism during hospitalization was higher in the cancer group than in the control group (13.21% vs. 3.75%;  $\chi^2 = 10.56$ ,  $P < 0.01$ ). Patients with active cancer had significantly higher serum levels of fibrinogen (mean  $\pm$  SD: 4.44  $\pm$  1.82 g/L vs. 3.56  $\pm$  1.02 g/L;  $t = 3.49$ ,  $P < 0.01$ ), D-dimer (median [IQR]: 2.23 mg/mL [0.98–10.76] vs. 0.35 mg/mL [0.27–0.48];  $Z = -9.55$ ,  $P < 0.01$ ), and CRP (median [IQR]: 18.40 mg/L [5.45–46.00] vs. 3.90 mg/L [2.80–6.33];  $Z = -7.35$ ,  $P < 0.01$ ) but significantly lower levels of hemoglobin (mean  $\pm$  SD: 119.79  $\pm$  25.68 g/L vs. 143.61  $\pm$  18.57 g/L;  $t = -6.63$ ,  $P < 0.01$ ) than those without.

**3.2. Type, Histology, and Stage of Active Cancer.** The most commonly observed cancer diagnoses among patients with IS and active cancer were as follows: lung cancer ( $n = 16$ , 30.19%); gastric cancer ( $n = 8$ , 15.09%); liver cancer ( $n = 6$ , 11.32%); colorectal cancer ( $n = 5$ , 9.43%); breast cancer ( $n = 5$ , 9.43%); genitourinary cancers (bladder, prostate, and ovarian cancers;  $n = 5$ , 9.43%); biliary tract cancer ( $n = 4$ , 7.55%); and pancreatic cancer, nasopharyngeal cancer, renal cancer, and adrenal cancer ( $n = 1$ , 1.89% each). Thirty-one (58.49%) patients were diagnosed with adenocarcinoma, and 21 (39.62%) were diagnosed with metastatic disease (Table 2).

**3.3. Univariate and Multivariate Logistic Regression Analyses.** We assessed all risk factors with  $P$  values  $\leq 0.05$  (Table 1) using a univariate logistic regression model (including age, hyperlipidemia, LAA, SUE, NIHSS score, AMCI, hemoglobin, fibrinogen, D-dimer, and CRP). The results are shown in Table 3. Notably, the odds ratios (OR) for age, NIHSS score, hemoglobin, and CRP were approximately 1 on uni-

variate logistic regression analysis. Therefore, we considered only the remaining risk factors, including hyperlipidemia, SUE, AMCI, presence of venous thromboembolism or pulmonary embolism, and fibrinogen and D-dimer levels, in the multivariate logistic regression model. Multivariate analysis showed that the absence of a history of hyperlipidemia (OR = 0.17, 95% confidence interval (CI): 0.06–0.48,  $P < 0.01$ ), elevated serum fibrinogen levels (OR = 1.72, 95% CI: 1.33–2.22,  $P < 0.01$ ), elevated D-dimer levels (OR = 1.43, 95% CI 1.24–1.64,  $P < 0.01$ ), and SUE (OR = 22.87, 95% CI: 9.91–52.78,  $P < 0.01$ ) were independently associated with active cancer (Table 3).

**3.4. Development of a Predictive Score Using Areas under the Receiver Operating Characteristic Curves.** We developed a scoring system to predict active cancer in patients with IS, based on the findings of multivariate analysis, particularly in the subset of patients with SUE. The final score, ranging from 0 to 3, comprised the sum of individual scores for the history of hyperlipidemia, serum D-dimer levels, and serum fibrinogen levels. We reviewed and compared several studies to determine the appropriate cut-off values for D-dimer and fibrinogen levels for the scoring system. The OASIS-CANCER study conducted by Lee et al. determined the first quartile of the pre-treatment D-dimer concentration as 2.08  $\mu$ g/mL and the median fibrinogen concentration as 399 mg/dL [21]. Moreover, Quintas et al. found that the median fibrinogen level of patients with IS without cancer was 408.5 mg/dL [22]. They demonstrated that fibrinogen values were associated with the diagnosis of cancer after IS. Therefore, we analyzed multiple data conditions and assigned the following final scores, according to the findings of previous studies, our clinical experience, and the findings of this study: history of hyperlipidemia = 0 points, no history of hyperlipidemia = 1 point; D-dimer level  $\leq 2.00$   $\mu$ g/mL = 0 points, D-dimer level  $> 2.00$   $\mu$ g/mL = 1 point; and fibrinogen level  $\leq 4.00$  g/L = 0 points, fibrinogen level  $> 4.00$  g/L = 1 point. Table 4 presents the sensitivity, specificity, and posterior probability of each cut-off point based on the supposed cancer prevalence value of 6.63% in our study. Figure 2 shows that the probability of active cancer was 59% if a patient with IS had a clinical score of 3 points, with a reliable AUC-ROC value of 0.83 (95% CI: 0.77–0.89,  $P < 0.01$ ).

### 4. Discussion

This study showed that the absence of a history of hyperlipidemia, increased serum levels of D-dimer and fibrinogen, and SUE were independent risk factors associated with active cancer in patients with IS. Adenocarcinoma was the most commonly observed histological manifestation, consistent with the results of several previous studies [21, 23, 24]. However, recent studies evaluating underlying cancer in patients with IS have simply focused on differences in epidemiological and biochemical parameters. There is no consensus on the optimal method or time for identifying occult cancer in patients with acute IS. Thus, in light of our findings, we developed a reliable predictive score that can help clinical neurologists to rapidly screen the possibility of occult cancer

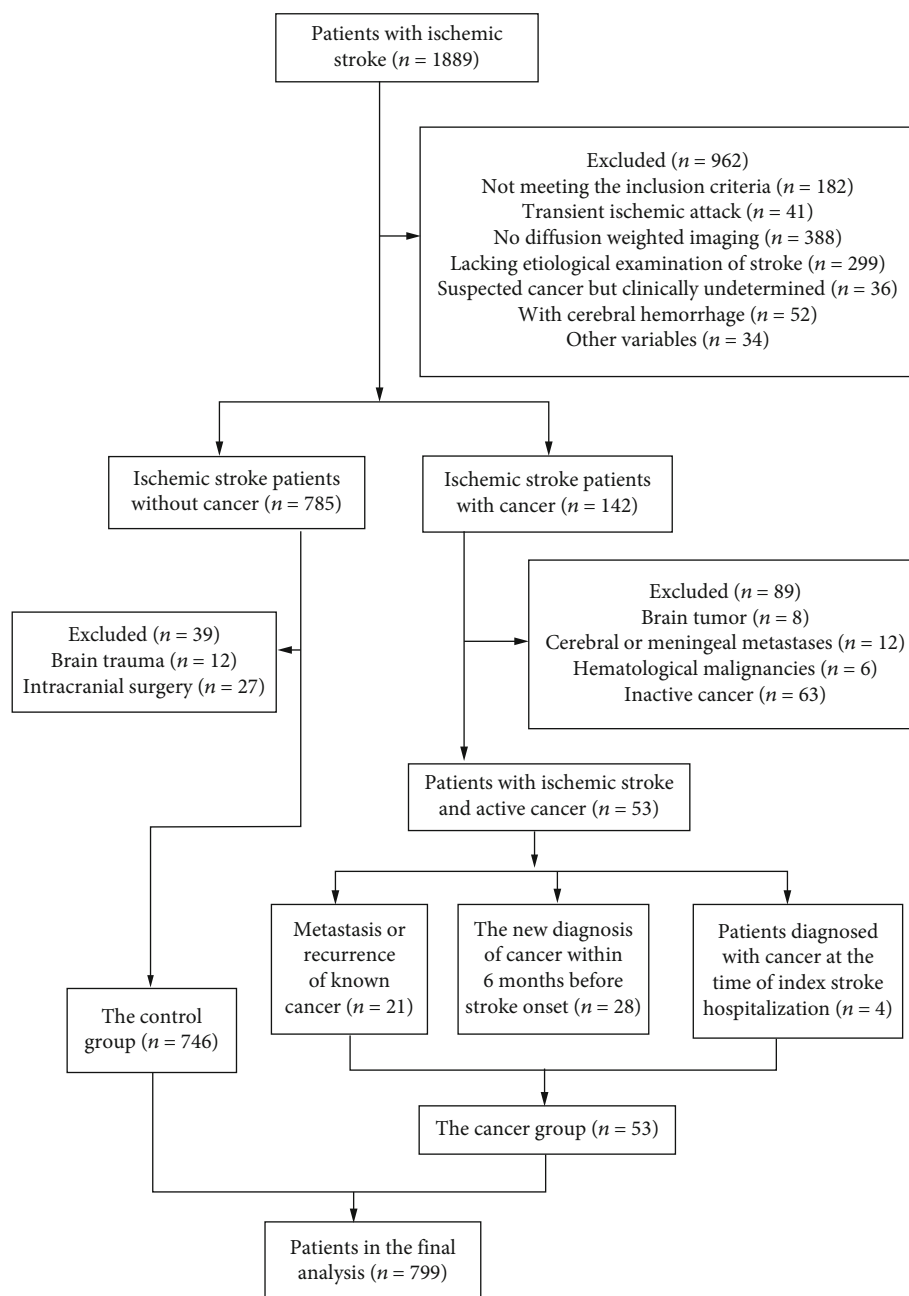


FIGURE 1: Flow diagram explaining the inclusion and exclusion criteria.

in patients with IS at an early stage, which could ultimately improve patients' quality of life and survival outcomes.

Our systematically developed predictive score consisted of increased serum levels of D-dimer and fibrinogen and the absence of a history of hyperlipidemia, especially in patients with SUE. Our final scoring system demonstrated that if a patient with IS had a total score of 3/3, the probability of active cancer was 59% (with high specificity [99%]), based on an assumed cancer prevalence of 6.63%, which was similar to that in previous studies [22, 25, 26]. The probability of active cancer was 27% if the score was 2 points. We compared the predictive capabilities of our scoring system with those of a previously reported system and found that our system was

significantly superior; the AUC of the score described by Selvik et al. was 0.73 [15], while the AUC of our score was 0.83.

The differences in classical vascular risk factors between patients with IS with and without cancer remain unclear. Some studies have reported that the prevalence of classical vascular risk factors was similar between these patient groups [18, 27, 28], while others have demonstrated that the frequency of vascular risk factors, especially hyperlipidemia, was lower in patients with IS and active cancer [29, 30]. Our analyses demonstrated that the absence of a history of hyperlipidemia was independently associated with the presence of active cancer in patients with IS. Previous studies have suggested that low total cholesterol levels were associated with

TABLE 1: Comparison of baseline characteristics between patients with ischemic stroke and active cancer and those without cancer.

Variables	Cancer group <i>n</i> = 53	Control group <i>n</i> = 746	<i>t</i> / $\chi^2$	<i>P</i> value
<i>Demographics</i>				
Age (years)	67.21 ± 10.11	62.11 ± 12.09	3.00	<0.01
Sex (% male)	34 (64.2)	522 (70.0)	0.79	0.37
<i>Vascular risk factors</i>				
Hypertension	30 (56.6)	508 (68.1)	2.97	0.09
Diabetes mellitus	14 (26.4)	286 (38.3)	3.00	0.08
Hyperlipidemia	12 (22.6)	368 (49.3)	14.13	<0.01
Atrial fibrillation	4 (7.6)	46 (6.2)		0.57
Coronary heart disease	8 (15.1)	106 (14.2)	0.03	0.86
Previous stroke/TIA	7 (13.2)	129 (17.3)	0.59	0.45
Current smoking	25 (47.2)	351 (47.1)	0.00	0.99
Obesity	6 (11.3)	121 (16.2)	0.89	0.35
<i>TOAST classification</i>				
Large-artery atherosclerosis	5 (9.4)	455 (61.0)	53.85	<0.01
Cardioembolism	2 (3.8)	33 (4.4)		1.00
Small vessel occlusion	9 (17.0)	216 (29.0)	3.51	0.06
Other determined etiology	2 (3.8)	11 (1.5)		0.21
Undetermined etiology	35 (66.0)	31 (4.2)	250.6	<0.01
<i>Ischemic stroke characteristics</i>				
Initial NIHSS score	6.13 ± 4.10	4.30 ± 4.48	2.89	<0.01
AMCI	30 (56.6)	148 (19.8)	38.63	<0.01
VTE or PE	7 (13.2)	28 (3.8)	10.56	<0.01
<i>Laboratory markers</i>				
Hemoglobin (g/L)	119.79 ± 25.68	143.61 ± 18.58	-6.63	<0.01
Platelets (/10 <sup>9</sup> )	213.28 ± 99.86	222.17 ± 66.55	-0.64	0.53
Fibrinogen (g/L)	4.44 ± 1.82	3.56 ± 1.02	3.49	<0.01
D-dimer (mg/mL)	2.23 (0.98–10.76)	0.35 (0.27–0.48)	-9.55	<0.01
CRP (mg/L)	18.40 (5.45–46.00)	3.90 (2.80–6.33)	-7.35	<0.01

Data are presented as the mean ± standard deviation, median (interquartile range), or *n* (%). Abbreviations: AMCI: acute multiple cerebral infarctions; VTE: venous thromboembolism; PE: pulmonary embolism; CRP: C-reactive protein; NIHSS: National Institute of Health Stroke Scale; TOAST: Trial of Org 10172 in Acute Stroke Treatment; TIA: transient ischemic attack.

an elevated risk of cancer incidence and mortality [31–33], and this inverse association has been well demonstrated in patients with stomach, breast, and prostate cancers [32, 34]. The findings of these studies are generally in accordance with those of our study. Moreover, we found a significant difference in the classification of stroke etiology between the two groups. Similar to previous studies, we observed a lower frequency of the LAA subtype and a higher prevalence of SUE in patients with IS and active cancer than in those without cancer [12, 29]. Thus, previous studies and our study indicate that a specific stroke mechanism, differing from that associated with traditional IS, may exist in patients with active cancer.

We compared the differences in blood coagulation biomarkers between the two groups, including an analysis of platelet, fibrinogen, and D-dimer levels to further explore the possible mechanisms underlying cancer-associated IS. We found higher serum levels of fibrinogen and D-dimer in patients with IS and active cancer than in those without

cancer, similar to most recent studies [11, 21, 22]. These factors are even considered to be predictors of active cancer in patients with IS [35]. Earlier studies have reported that D-dimer levels, which reflect excessive fibrin turnover associated with an activated coagulation system, were correlated with the degree of hypercoagulability [21] and widespread dissemination of microthrombi [36]. Moreover, malignancies can induce a hypercoagulable state and promote the formation of microthrombi by promoting the secretion of mucins, release of tissue factors, and production of procoagulant cytokines [37], which may explain the elevated levels of blood coagulation biomarkers in the present study. Therefore, it is necessary to identify the specific cancer types that tend to induce hypercoagulable states and thrombosis. Our data demonstrated that active lung cancer and gastric cancer were the most common cancer types in IS patients, and adenocarcinoma was the most commonly observed histopathological subtype. These findings are also consistent with

TABLE 2: Characteristics of patients with ischemic stroke and active cancer.

Cancer location	Histological type	Number
Lung cancer	Adenocarcinoma	15
	Small cell carcinoma	1
Gastric cancer	Adenocarcinoma	8
Liver cancer	Hepatocellular carcinoma	6
Colon cancer	Adenocarcinoma	3
Rectal cancer	Adenocarcinoma	2
Breast cancer	Infiltrating ductal carcinoma	4
	Medullary carcinoma	1
Biliary tract cancer	Epithelial cell carcinoma	3
	Adenocarcinoma	1
Bladder cancer	Transitional epithelial carcinoma	3
Prostate cancer	Adenocarcinoma	1
Ovarian cancer	Serous carcinoma	1
Pancreatic cancer	Adenocarcinoma	1
Nasopharyngeal cancer	Squamous cell carcinoma	1
Renal cancer	Clear cell carcinoma	1
Adrenal cancer	Cortical carcinoma	1
Metastatic disease		21

TABLE 3: Univariate and multivariate logistic regression analyses of risk factors in patients with ischemic stroke with active cancer and those without cancer.

Variables	Univariate logistic regression analysis		Multivariate logistic regression analysis	
	OR (95% CI)	<i>P</i> value	OR (95% CI)	<i>P</i> value
Age	1.04 (1.01–1.07)	<0.01		
Hyperlipidemia	0.30 (0.16–0.58)	<0.01	0.16 (0.06–0.45)	<0.01
LAA	0.07 (0.02–0.17)	<0.01		
SUE	44.85 (22.89–87.88)	<0.01	19.30 (7.93–48.96)	<0.01
NIHSS score	1.06 (1.02–1.11)	<0.01		
AMCI	5.27 (2.97–9.34)	<0.01	1.58 (0.66–3.81)	0.31
VTE or PE	4.56 (1.97–10.58)	<0.01	0.92 (0.21–3.94)	0.91
Hemoglobin (g/L)	0.95 (0.94–0.96)	<0.01		
Fibrinogen (g/L)	1.63 (1.35–2.00)	<0.01	1.70 (1.31–2.21)	<0.01
D-dimer ( $\mu\text{g/mL}$ )	1.72 (1.45–2.03)	<0.01	1.42 (1.23–1.65)	<0.01
CRP	1.03 (1.02–1.04)	<0.01		

LAA: large-artery atherosclerosis; SUE: stroke of undetermined etiology; NIHSS: National Institute of Health Stroke Scale; AMCI: acute multiple cerebral infarctions; VTE: venous thromboembolism; PE: pulmonary embolism; CRP: C-reactive protein.

TABLE 4: Performance and posterior probabilities of the predictive score for cancer in patients with ischemic stroke.

Score	Sensitivity	Specificity	Posterior probability
1	0.96	0.37	0.09
2	0.68	0.88	0.27
3	0.19	0.99	0.59

those of previous studies, which revealed a higher prevalence of thromboembolic events in patients with lung cancer and adenocarcinoma [25, 38, 39]. Furthermore, studies have shown that patients with adenocarcinoma were prone to

developing cancer-mediated hypercoagulability and micro-emboli [18, 40]. Several studies have suggested that some epithelium-derived tumors, such as those originating from the lung, stomach, and bile ducts, were frequently adenocarcinomas and could systematically secrete mucins that bind to P- and L-selectins, inducing the formation of platelet-rich micro-thrombi [41, 42]. Moreover, these cancers usually remain undiagnosed until they reach an advanced or metastatic stage. The histologic and natural characteristics of these tumors underline the potential increase in the risk of IS, further revealing the role of hypercoagulability in cancer-related IS.

Our study has several limitations. First, this was a single-center retrospective study performed using consecutively

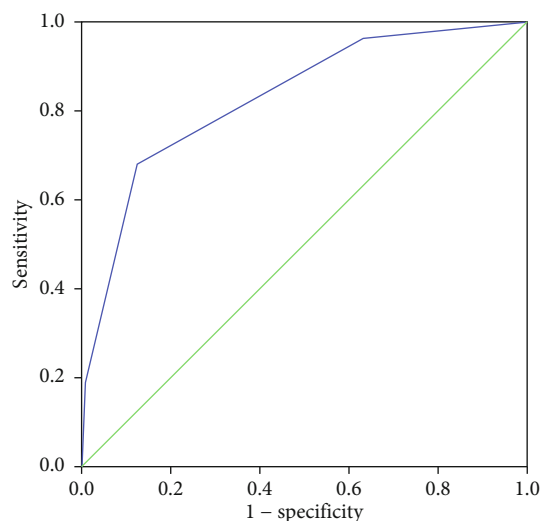


FIGURE 2: Receiver operating characteristic curves of the clinical scores. The final scores were as follows: history of hyperlipidemia = 0 points, no history of hyperlipidemia = 1 point; D-dimer level  $\leq 2.00 \mu\text{g/mL}$  = 0 points, D-dimer level  $> 2.00 \mu\text{g/mL}$  = 1 point; and fibrinogen level  $\leq 4.00 \text{ g/L}$  = 0 points, fibrinogen level  $> 4.00 \text{ g/L}$  = 1 point.

collected data. Therefore, our findings may not be applicable to other settings due to the inherent selection bias. Second, comparing the characteristics of patients according to different cancer types would have been ideal, as patients with IS may have different types of cancer. However, further categorization by cancer type did not allow for appropriate subgroup analyses, because this study included a relatively limited number of patients with active cancer. Third, we could not clarify the relationship between the value of hypercoagulation biomarkers and tumor markers, as this is difficult to achieve for a retrospective study; furthermore, tumor markers were not routinely tested in the Department of Neurology due to Chinese national conditions and the high cost of examination.

## 5. Conclusions

This study systematically developed a scoring system comprising the history of hyperlipidemia and fibrinogen and D-dimer levels for the prediction of active cancer in patients with IS, especially in those with SUE. Our findings indicate the importance of hypercoagulability in assessing active cancer in patients with IS, which could support early decision-making for intervention and management at the time of admission. Prospective multicenter studies are needed to evaluate the effectiveness of this clinical scoring system prior to implementation in clinical practice.

## Data Availability

Data has not been made accessible in the interest of protecting patients' privacy.

## Ethical Approval

This study was performed in accordance with the principles of the Declaration of Helsinki. The Medical Science Research Ethics Committee of the First Affiliated Hospital of China Medical University approved this study (committee's reference number [2019]325).

## Consent

The need for informed consent (prior to participation) was waived because of the retrospective nature of this study and the minimal risk posed to patients in this study.

## Conflicts of Interest

The authors have no competing interests to declare.

## Authors' Contributions

Jiwei Jiang contributed in conceptualization and design of the study, interpretation of data, and drafting and revising the manuscript. Xiuli Shang contributed in conceptualization and critical revision of the manuscript. Jinming Zhao contributed in data collection and analyses and ethics submission. Meihui Cao contributed in data analyses and data collection. Jirui Wang contributed in data analyses. Runzhi Li contributed in data analyses. Yanli Wang contributed in data analyses. Jun Xu contributed in critical revision of the manuscript for important intellectual content, study supervision, and funding support.

## Acknowledgments

This study was supported by the National Natural Science Foundation of China (81870821 and 82071187) and Beijing Youth Talent Team Support Program (2018000021223TD08), both of which were from the corresponding author Jun Xu. The funding body provided funding for data collection, analysis, and interpretation, as well as writing of the manuscript. We would like to thank Editage (<http://www.editage.cn>) for English language editing.

## References

- [1] GBD 2013 Mortality and Causes of Death Collaborators, "Global, regional, and national age-sex specific all-cause and cause-specific mortality for 240 causes of death, 1990-2013: a systematic analysis for the Global Burden of Disease Study 2013," *The Lancet*, vol. 385, pp. 117-171, 2015.
- [2] W. Grisold, S. Oberndorfer, and W. Struhal, "Stroke and cancer: a review," *Acta Neurologica Scandinavica*, vol. 119, no. 1, pp. 1-16, 2009.
- [3] N. Sanossian, C. Djabiras, W. J. Mack, and B. Ovbiagele, "Trends in cancer diagnoses among inpatients hospitalized with stroke," *Journal of Stroke and Cerebrovascular Diseases*, vol. 22, no. 7, pp. 1146-1150, 2013.
- [4] B. B. Navi, A. S. Reiner, H. Kamel et al., "Association between incident cancer and subsequent stroke," *Annals of Neurology*, vol. 77, no. 2, pp. 291-300, 2015.



- [5] B. Rioux, L. Touma, A. Nehme, G. Gore, M. R. Keezer, and L. C. Gioia, "Frequency and predictors of occult cancer in ischemic stroke: a systematic review and meta-analysis," *International Journal of Stroke*, vol. 16, no. 1, pp. 12–19, 2021.
- [6] R. A. Salazar-Camelo, E. A. Moreno-Vargas, A. F. Cardona, and H. F. Bayona-Ortiz, "Ischemic stroke: a paradoxical manifestation of cancer," *Critical Reviews in Oncology/Hematology*, vol. 157, p. 103181, 2021.
- [7] H. H. G. Castro, A. P. Alencar, I. M. Benseñor, P. A. Lotufo, and A. C. Goulart, "Multimorbidities are associated to lower survival in ischaemic stroke: results from a Brazilian Stroke Cohort (EMMA study)," *Cerebrovascular Diseases*, vol. 44, no. 3-4, pp. 232–239, 2017.
- [8] J. L. Dearborn, V. C. Urrutia, and S. R. Zeiler, "Stroke and cancer—a complicated relationship," *Journal of Neurology & Translational Neuroscience*, vol. 2, p. 1039, 2015.
- [9] J.-y. Wang, G.-j. Zhang, S.-x. Zhuo et al., "D-dimer >2.785 µg/ml and multiple infarcts ≥3 vascular territories are two characteristics of identifying cancer-associated ischemic stroke patients," *Neurological Research*, vol. 40, no. 11, pp. 948–954, 2018.
- [10] Y. Gon, M. Sakaguchi, J. Takasugi et al., "Plasma D-dimer levels and ischaemic lesions in multiple vascular regions can predict occult cancer in patients with cryptogenic stroke," *European Journal of Neurology*, vol. 24, no. 3, pp. 503–508, 2017.
- [11] A. G. Karlińska, G. Gromadzka, M. A. Karliński, and A. Członkowska, "The activity of malignancy may determine stroke pattern in cancer patients," *Journal of Stroke and Cerebrovascular Diseases*, vol. 24, pp. 348–353, 2015.
- [12] S. G. Kim, J. M. Hong, H. Y. Kim et al., "Ischemic stroke in cancer patients with and without conventional mechanisms: a multicenter study in Korea," *Stroke*, vol. 41, no. 4, pp. 798–801, 2010.
- [13] D. M. Cestari, D. M. Weine, K. S. Panageas, A. Z. Segal, and L. M. DeAngelis, "Stroke in patients with cancer: incidence and etiology," *Neurology*, vol. 62, no. 11, pp. 2025–2030, 2004.
- [14] Y. Y. Zhang, D. Cordato, Q. Shen, A. Z. Sheng, W. T. Hung, and D. K. Chan, "Risk factor, pattern, etiology and outcome in ischemic stroke patients with cancer: a nested case-control study," *Cerebrovascular Diseases*, vol. 23, no. 2-3, pp. 181–187, 2007.
- [15] H. A. Selvik, A. T. Bjerkreim, L. Thomassen, U. Waje-Andreassen, H. Naess, and C. E. Kvistad, "When to screen ischaemic stroke patients for cancer," *Cerebrovascular Diseases*, vol. 45, no. 1-2, pp. 42–47, 2018.
- [16] C. J. Johnson, S. J. Kittner, R. J. McCarter et al., "Interrater reliability of an etiologic classification of ischemic stroke," *Stroke*, vol. 26, no. 1, pp. 46–51, 1995.
- [17] J. Yoo, H. S. Nam, Y. D. Kim, H. S. Lee, and J. H. Heo, "Short-term outcome of ischemic stroke patients with systemic malignancy," *Stroke*, vol. 50, no. 2, pp. 507–511, 2019.
- [18] B. B. Navi, S. Singer, A. E. Merkler et al., "Recurrent thromboembolic events after ischemic stroke in patients with cancer," *Neurology*, vol. 83, no. 1, pp. 26–33, 2014.
- [19] L. Goldstein and G. Samsa, "Reliability of the national institutes of health stroke scale," *Stroke*, vol. 28, no. 2, pp. 307–310, 1997.
- [20] H. P. Adams, B. H. Bendixen, L. J. Kappelle et al., "Classification of subtype of acute ischemic stroke. Definitions for use in a multicenter clinical trial. TOAST. Trial of Org 10172 in acute stroke treatment," *Stroke*, vol. 24, no. 1, pp. 35–41, 1993.
- [21] M. J. Lee, J. W. Chung, M. J. Ahn et al., "Hypercoagulability and mortality of patients with stroke and active cancer: the OASIS-CANCER study," *J Stroke*, vol. 19, no. 1, pp. 77–87, 2017.
- [22] S. Quintas, J. Rogado, P. Gullón et al., "Predictors of unknown cancer in patients with ischemic stroke," *Journal of Neuro-Oncology*, vol. 137, no. 3, pp. 551–557, 2018.
- [23] K. W. Nam, C. K. Kim, T. J. Kim et al., "D-dimer as a predictor of early neurologic deterioration in cryptogenic stroke with active cancer," *European Journal of Neurology*, vol. 24, no. 1, pp. 205–211, 2017.
- [24] S. Grazioli, M. Paciaroni, G. Agnelli et al., "Cancer-associated ischemic stroke: a retrospective multicentre cohort study," *Thrombosis Research*, vol. 165, pp. 33–37, 2018.
- [25] H. A. Selvik, L. Thomassen, A. T. Bjerkreim, and H. Naess, "Cancer-associated stroke: the Bergen NORSTROKE study," *Cerebrovasc Dis Extra*, vol. 5, no. 3, pp. 107–113, 2015.
- [26] M. H. Sorgun, M. Kuzu, I. S. Ozer et al., "Risk factors, biomarkers, etiology, outcome and prognosis of ischemic stroke in cancer patients," *Asian Pacific Journal of Cancer Prevention*, vol. 19, no. 3, pp. 649–653, 2018.
- [27] B. Sun, S. Fan, Z. Li et al., "Clinical and neuroimaging features of acute ischemic stroke in cancer patients," *European Neurology*, vol. 75, no. 5-6, pp. 292–299, 2016.
- [28] P. Corraini, A. G. Ording, V. W. Henderson, S. Szépligeti, E. Horváth-Puhó, and H. T. Sørensen, "Cancer, other comorbidity, and risk of venous thromboembolism after stroke: a population-based cohort study," *Thrombosis Research*, vol. 147, pp. 88–93, 2016.
- [29] S. Oberndorfer, V. Nussgruber, O. Berger, H. Lahrmann, and W. Grisold, "Stroke in cancer patients: a risk factor analysis," *Journal of Neuro-Oncology*, vol. 94, pp. 221–226, 2009.
- [30] A. Carrilho Romeiro, A. Valadas, and J. Marques, "Acute ischemic stroke on cancer patients, a distinct etiology? A case-control study," *Acta Médica Portuguesa*, vol. 28, no. 5, pp. 613–618, 2015.
- [31] M. Li, J. Lu, J. Fu et al., "The association and joint effect of serum cholesterol, glycemic status with the risk of incident cancer among middle-aged and elderly population in China cardiometabolic disease and cancer cohort (4C)-study," *American Journal of Cancer Research*, vol. 10, no. 3, pp. 975–986, 2020.
- [32] V. A. Katzke, D. Sookthai, T. Johnson, T. Kühn, and R. Kaaks, "Blood lipids and lipoproteins in relation to incidence and mortality risks for CVD and cancer in the prospective EPIC-Heidelberg cohort," *BMC Medicine*, vol. 15, no. 1, p. 218, 2017.
- [33] B. Wu, L. Teng, D. He, D. D. Yu, and F. Jiang, "Dose-response relation between serum total cholesterol levels and overall cancer risk: evidence from 12 prospective studies involving 1,926,275 participants," *International Journal of Food Sciences and Nutrition*, vol. 70, no. 4, pp. 432–441, 2019.
- [34] K. Asano, M. Kubo, K. Yonemoto et al., "Impact of serum total cholesterol on the incidence of gastric cancer in a population-based prospective study: the Hisayama study," *International Journal of Cancer*, vol. 122, no. 4, pp. 909–914, 2008.
- [35] Y. J. Guo, M. H. Chang, P. L. Chen, Y. S. Lee, Y. C. Chang, and Y. C. Liao, "Predictive value of plasma (D)-dimer levels for cancer related stroke: a 3-year retrospective study," *Journal of*

- Stroke and Cerebrovascular Diseases*, vol. 23, no. 4, pp. e249–e254, 2014.
- [36] J. M. Seok, S. G. Kim, J. W. Kim et al., “Coagulopathy and embolic signal in cancer patients with ischemic stroke,” *Annals of Neurology*, vol. 68, no. 2, pp. 213–219, 2010.
- [37] A. Varki, “Trousseau’s syndrome: multiple definitions and multiple mechanisms,” *Blood*, vol. 110, no. 6, pp. 1723–1729, 2007.
- [38] R. Kassubek, L. Bullinger, J. Kassubek et al., “Identifying ischemic stroke associated with cancer: a multiple model derived from a case-control analysis,” *Journal of Neurology*, vol. 264, no. 4, pp. 781–791, 2017.
- [39] J. Lin, S. Wu, R. Xu et al., “Clinical characteristics and risk factors of lung cancer-associated acute ischemic stroke,” *BioMed Research International*, vol. 2019, Article ID 6021037, 7 pages, 2019.
- [40] E. J. Lee, H. W. Nah, J. Y. Kwon, D. W. Kang, S. U. Kwon, and J. S. Kim, “Ischemic stroke in patients with cancer: is it different from usual strokes?,” *International Journal of Stroke*, vol. 9, no. 4, pp. 406–412, 2014.
- [41] L. E. Neilson, L. R. Rogers, and S. Sundararajan, “Evaluation and treatment of a patient with recurrent stroke in the setting of active malignancy,” *Stroke*, vol. 50, 2019.
- [42] R. Bhatia, S. K. Gautam, A. Cannon et al., “Cancer-associated mucins: role in immune modulation and metastasis,” *Cancer Metastasis Reviews*, vol. 38, no. 1-2, pp. 223–236, 2019.

## Research Article

# Decreased Levels of Serum IL-34 Associated with Cognitive Impairment in Vascular Dementia

Yang Wang,<sup>1</sup> Wei Lu,<sup>2</sup> Wenjing Ning,<sup>3,4</sup> Yan Chen ,<sup>5</sup> and Lingxing Li <sup>6</sup>

<sup>1</sup>Department of Neurology, Qingpu Branch of Zhongshan Hospital, Fudan University, Shanghai 201700, China

<sup>2</sup>Department of Intensive Rehabilitation, Shandong Provincial Third Hospital, Cheeloo College of Medicine, Shandong University, Jinan, Shandong Province 250000, China

<sup>3</sup>Department of Geriatric, Shandong Provincial Hospital, Cheeloo College of Medicine, Shandong University, Jinan, Shandong Province 250021, China

<sup>4</sup>Department of Neurology, Jinan First People's Hospital, Shandong Traditional Chinese Medicine University, Jinan, Shandong Province 250013, China

<sup>5</sup>Department of Geriatric Medicine, Shandong Provincial Third Hospital, Cheeloo College of Medicine, Shandong University, Jinan, Shandong Province 250000, China

<sup>6</sup>Department of Cardiovascular Medicine, Taian City Central Hospital, Shandong First Medical University & Shandong Academy of Medical Sciences, Taian, Shandong Province. 271000, China

Correspondence should be addressed to Yan Chen; [chenyan2004925@163.com](mailto:chenyan2004925@163.com) and Lingxing Li; [luckykeyan@163.com](mailto:luckykeyan@163.com)

Received 16 April 2021; Revised 5 May 2021; Accepted 13 May 2021; Published 21 May 2021

Academic Editor: Juan Yang

Copyright © 2021 Yang Wang et al. This is an open access article distributed under the Creative Commons Attribution License, which permits unrestricted use, distribution, and reproduction in any medium, provided the original work is properly cited.

**Objective.** Interleukin- (IL-) 34 is a new type of cytokine with neuroprotective effects discovered in recent years. However, the relationship between IL-34 and vascular dementia (VaD) has not yet been elucidated. The purpose of this study is to determine whether IL-34 is involved in cognitive impairment of VaD. **Methods.** From January 2017 to December 2020, 84 VaD patients and 60 healthy controls who attended Qingpu Branch of Zhongshan Hospital were prospectively included in the study. Once included in the study, demographic features of all research subjects are collected. They include age, gender, education, white blood cells (WBC), neutrophil, lymphocyte, systolic blood pressure (SBP), diastolic blood pressure (DBP), fasting blood glucose (FBG), triglycerides (TG), and total cholesterol (TC). Meanwhile, the Montreal Cognitive Assessment (MoCA) scale was used to assess the cognitive function of participants. The serum IL-34 level was determined by enzyme-linked immunosorbent assay (ELISA). **Results.** There was no significant difference between the demographic features of VaD patients and healthy controls ( $p > 0.05$ ). However, the serum IL-34 levels of VaD patients and healthy controls are  $27.6 \pm 3.9$  pg/ml and  $41.8 \pm 6.0$  pg/ml, respectively, and there is a significant statistical difference between them ( $p < 0.001$ ). The results of bivariate correlation analysis showed that serum IL-34 levels were significantly positively correlated with MoCA scores ( $r = 0.371$ ,  $p = 0.023$ ). Further regression analysis showed that IL-34 was still correlated with MoCA after adjusting for demographic features ( $\beta = 0.276$ ,  $p = 0.038$ ). **Conclusions.** Serum IL-34 levels in VaD patients were significantly reduced, which may be an independent predictor of cognitive impairment in VaD patients.

## 1. Introduction

Vascular dementia (VaD) is a common type of dementia. The main cause of VaD is cerebrovascular disease, which leads to impaired cerebral blood flow and further damages neurons in the hippocampus or cortex [1, 2]. According to statistics from the World Health Organization (WHO), there are cur-

rently about 36 million people with dementia in the world. By 2050, this number will reach to 115 million, and VaD accounts for about 20% of them, second only to Alzheimer's disease (AD) [3]. It is reported that the prevalence of VaD in developed countries ranges from 1% to 4%, while the prevalence of VD in developing countries is about 8%, and the prevalence of VD in the elderly is rising rapidly [4]. The annual

cost of VaD is as high as 200 billion US dollars, and with the extension of human life expectancy, VaD has gradually become one of the main health problems that need to be solved urgently in countries all over the world [5]. Our existing treatment may alleviate some of the symptoms of VaD in the short term, but it cannot fundamentally slow down the disease progression or reverse the disease process [6]. Therefore, it is particularly urgent to continue to explore the potential pathogenic mechanism and therapeutic targets of VaD.

Interleukin- (IL-) 34 was first discovered by Lin's team in 2008 and is considered to be a nonspecific ligand for colony stimulating factor- (CSF-) 1 receptor (CSF-1R) [7]. In addition to CSF-1R, IL-34 can also bind to protein-tyrosine phosphatase- (PTP-)  $\zeta$  and syndecan-1. IL-34 is a homoglycan protein secreted mainly by brain neuron cells and skin keratinocytes, and it is highly conserved in vertebrates [8]. The human IL-34 gene is located on the 16q22.1 chromosome, while the mouse IL-34 gene is located on the 8E1 chromosome, which has high homology among different species [9]. More and more evidences show that IL-34 is involved in the etiology of various diseases, such as inflammation, infection, autoimmune diseases, and tumors [10].

Recent studies have shown that IL-34 has a certain neuroprotective effect in certain special diseases. However, it is not clear whether IL-34 is involved in the disease process of VaD. Therefore, the main purpose of our study is to explore the relationship between IL-34 and cognitive impairment in VaD patients, in order to provide potential targets and drugs for the treatment of VaD.

## 2. Methods

**2.1. Study Participants.** From January 2017 to December 2020, 84 VaD patients treated at Qingpu Branch of Zhongshan Hospital were included in the study. At the same time, 60 age- and gender-matched healthy controls were included. The diagnosis of VaD was completed by experienced physicians with reference to the National Institute of Nervous System Diseases and Stroke (NINDSAIREN) and the 11th edition of the International Classification of Diseases (ICD-11) [11, 12]. The exclusion criteria are as follows: combined with AD or Lewy body dementia; severe infectious diseases; taking anti-infective drugs; severe trauma; recent history of surgery; suffering from severe liver disease, kidney disease, or tumor; alcoholism; and severe mental illness. The patients or family members are written informed of the current research and agree to participate in the research. The study was approved by the ethics committee of our hospital and abides by the Declaration of Helsinki.

**2.2. Demographic Features of the Participants.** Of the 144 study participants, 84 were VaD patients, and the other 60 were healthy controls. The demographic features of all participants were carefully recorded by dedicated personnel, including age, gender, education, white blood cells (WBC), neutrophil, lymphocyte, systolic blood pressure (SBP), diastolic blood pressure (DBP), fasting blood glucose (FBG), triglycerides (TG), and total cholesterol (TC). Demographic feature information is obtained in the form of questionnaires.

**2.3. MoCA Scale Evaluation.** The Montreal Cognitive Assessment (MoCA) is used as a tool to evaluate cognitive function. Dr. Ziad Nasreddine of Canada invented the MoCA scale in 1996, which was later translated into multiple languages and widely used because of its good accuracy. MoCA evaluated the following cognitive areas: short-term memory, visuospatial abilities, executive functions, attention, language, abstract reasoning, and orientation. The MoCA score ranges from 0 to 30, and a score of 26 or more is considered normal [13, 14].

**2.4. Serum ELISA Test.** Enzyme-linked immunosorbent assay (ELISA) is a popular immunoassay method that can quickly and easily analyze the same indicator in a large number of samples. In this experiment, we used an ELISA kit (MyBioSource, San Diego, CA, USA) to detect the concentration of IL-34 in the serum. Fasting venous blood of all participants was collected within 24 hours of enrollment. The collected whole blood was placed in the refrigerator overnight at 4°C and then centrifuged at 3000 rpm for 10 minutes, and the supernatant was immediately taken to be tested and stored in the refrigerator at -80°C. The specific experimental steps refer to previous reports and product manuals [15].

**2.5. Statistical Analysis.** In this study, categorical variables are represented by numbers, and continuous variables are represented by mean  $\pm$  standard deviation. The comparison between the two groups used *t*-test or chi-square test. Spearman's rank was used to assess the bivariate correlation, and multivariate regression analysis was used to clarify the causal relationship between the variables. All data were analyzed using the SPSS 22.0 software (SPSS Inc., IL, USA), and a two-tailed *p* value  $< 0.05$  was considered statistically significant.

## 3. Results

**3.1. Demographic Features of the Participants.** Of the 144 study participants, 84 were VaD patients, and the other 60 were healthy controls. The demographic features of the participants are shown in Table 1. There was no significant difference between the demographic features (age, gender, education, WBC, neutrophil, lymphocyte, SBP, DBP, FBG, TG, and TC) of VaD patients and healthy controls ( $p > 0.05$ ). However, the serum IL-34 levels of VaD patients and healthy controls are  $27.6 \pm 3.9$  pg/ml and  $41.8 \pm 6.0$  pg/ml, respectively, and there is a significant statistical difference between them ( $p < 0.001$ ). The comparison of the MoCA score and serum IL-34 levels of VaD patients and healthy controls is shown in Figure 1.

**3.2. Bivariate Correlation Analysis.** In order to clarify the potential factors affecting the cognitive function of VaD patients, we conducted a bivariate correlation analysis of the MoCA score and the variables of the demographic features. The results of the bivariate correlation analysis are summarized in Table 2. From the results in Table 2, it can be seen that the MoCA score of VaD patients is significantly positively correlated with serum IL-34 levels

TABLE 1: Demographic features of the participants.

	VaD (N = 84)	Controls (N = 60)	p value
Age (year, mean $\pm$ SD)	70.3 $\pm$ 8.9	70.5 $\pm$ 9.2	0.896
Gender (male/female)	50/34	38/22	0.644
Education (year, mean $\pm$ SD)	8.4 $\pm$ 1.5	8.6 $\pm$ 1.8	0.469
WBC ( $\times 10^9/L$ , mean $\pm$ SD)	7.6 $\pm$ 1.3	7.4 $\pm$ 1.6	0.410
Neutrophil ( $\times 10^9/L$ , mean $\pm$ SD)	5.2 $\pm$ 1.4	5.0 $\pm$ 1.1	0.358
Lymphocyte ( $\times 10^9/L$ , mean $\pm$ SD)	1.8 $\pm$ 0.6	1.9 $\pm$ 0.7	0.359
SBP (mmHg, mean $\pm$ SD)	140.6 $\pm$ 12.2	139.8 $\pm$ 12.9	0.705
DBP (mmHg, mean $\pm$ SD)	87.7 $\pm$ 8.8	87.1 $\pm$ 8.5	0.683
FBG (mmol/L, mean $\pm$ SD)	7.3 $\pm$ 0.6	7.1 $\pm$ 0.8	0.089
TG (mmol/L, mean $\pm$ SD)	1.6 $\pm$ 0.2	1.6 $\pm$ 0.1	1.000
TC (mmol/L, mean $\pm$ SD)	4.6 $\pm$ 0.5	4.5 $\pm$ 0.4	0.202
MoCA (points, mean $\pm$ SD)	22.5 $\pm$ 2.6	28.1 $\pm$ 1.2	<0.001
IL-34 (pg/ml, mean $\pm$ SD)	27.6 $\pm$ 3.9	41.8 $\pm$ 6.0	<0.001

Abbreviations: VaD, vascular dementia; WBC, white blood cells; SBP, systolic blood pressure; DBP, diastolic blood pressure; FBG, fasting blood glucose; TG, triglycerides; TC, total cholesterol; MoCA, Montreal Cognitive Assessment; IL-34, interleukin-34.

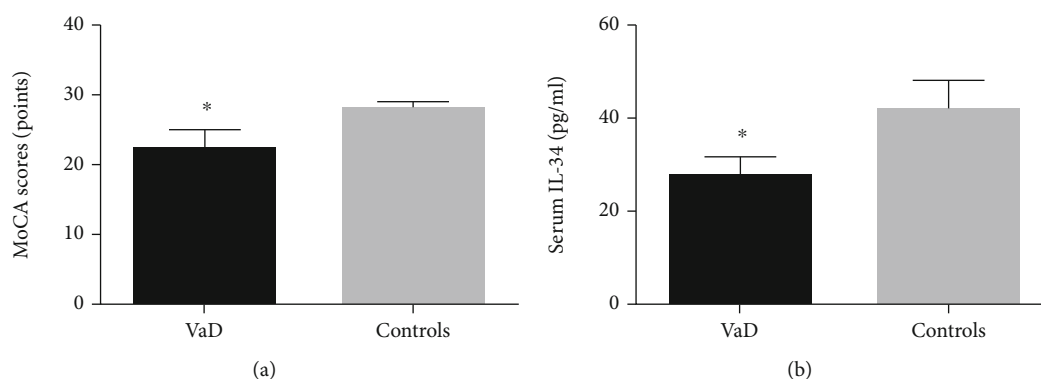


FIGURE 1: The MoCA scores and serum IL-34 levels of VaD patients and healthy controls. (a) MoCA scores; (b) serum IL-34 levels. Compared with the controls, \* $p < 0.05$ .

( $r = 0.371$ ,  $p = 0.023$ ). However, there is no significant correlation between MoCA score and age, gender, education, WBC, neutrophil, lymphocyte, SBP, DBP, FBG, TG, and TC ( $p > 0.05$ ).

**3.3. Multivariate Regression Analysis.** In order to understand the relationship between IL-34 levels and the cognitive function of VaD patients, we conducted a multivariate logistic regression analysis between the MoCA score and demographic features including IL-34. The results of the multivariate logistic regression analysis are summarized in Table 3. After adjusting for various demographic features, the relationship between IL-34 and the cognitive impairment of VaD patients is still significant, with an OR of 2.171 ( $\beta = 0.276$ ,  $p = 0.0038$ ). These results indicate that IL-34 levels are positively correlated with VaD MoCA scores. In other words, VaD patients with low serum IL-34 levels may have more severe cognitive impairment.

## 4. Discussion

This study mainly explored the correlation between the cognitive function of VaD patients and the level of serum IL-34. The preliminary results showed that the serum IL-34 level and MoCA score of VaD patients were significantly lower than those of healthy controls. The results of correlation analysis showed that the MoCA score of VaD patients was significantly positively correlated with serum IL-34 levels and was not related to age, gender, education, WBC, neutrophil, lymphocyte, SBP, DBP, FBG, TG, and TC and other demographic features. Regression analysis, after correcting for interference factors, further confirmed the correlation between serum IL-34 and MoCA in VaD patients. As far as we know, this is the first research report that uses serum IL-34 as an index to predict cognitive impairment in VaD patients.

Cytokines are a group of secreted proteins, and its members include interleukins, lymphokines, chemokines, tumor



TABLE 2: Correlation between demographic features and MoCA in VaD.

	<i>r</i>	<i>p</i> value
Age (year, mean $\pm$ SD)	-0.287	0.134
Gender (male/female)	0.329	0.399
Education (year, mean $\pm$ SD)	-0.173	0.097
WBC ( $\times 10^9/L$ , mean $\pm$ SD)	0.418	0.283
Neutrophil ( $\times 10^9/L$ , mean $\pm$ SD)	0.556	0.431
Lymphocyte ( $\times 10^9/L$ , mean $\pm$ SD)	0.314	0.262
SBP (mmHg, mean $\pm$ SD)	-0.205	0.305
DBP (mmHg, mean $\pm$ SD)	-0.231	0.338
FBG (mmol/L, mean $\pm$ SD)	-0.270	0.196
TC (mmol/L, mean $\pm$ SD)	-0.402	0.583
TG (mmol/L, mean $\pm$ SD)	-0.357	0.677
IL-34 (ng/ml, mean $\pm$ SD)	0.371	0.023

Abbreviations: MoCA, Montreal Cognitive Assessment; VaD, vascular dementia; WBC, white blood cells; SBP, systolic blood pressure; DBP, diastolic blood pressure; FBG, fasting blood glucose; TG, triglycerides; TC, total cholesterol; IL-34, interleukin-34.

TABLE 3: Multivariable analyses of demographic features and MoCA in VaD.

	Regression coefficient	<i>p</i> value
Age (year, mean $\pm$ SD)	0.213	0.569
Gender (male/female)	0.217	0.117
Education (year, mean $\pm$ SD)	0.139	0.209
WBC ( $\times 10^9/L$ , mean $\pm$ SD)	0.296	0.318
Neutrophil ( $\times 10^9/L$ , mean $\pm$ SD)	0.245	0.167
Lymphocyte ( $\times 10^9/L$ , mean $\pm$ SD)	0.197	0.388
SBP (mmHg, mean $\pm$ SD)	0.115	0.271
DBP (mmHg, mean $\pm$ SD)	0.168	0.226
FBG (mmol/L, mean $\pm$ SD)	0.103	0.309
TC (mmol/L, mean $\pm$ SD)	0.186	0.275
TG (mmol/L, mean $\pm$ SD)	0.153	0.224
IL-34 (ng/ml, mean $\pm$ SD)	0.276	0.038

Abbreviations: MoCA, Montreal Cognitive Assessment; VaD, vascular dementia; WBC, white blood cells; SBP, systolic blood pressure; DBP, diastolic blood pressure; FBG, fasting blood glucose; TG, triglycerides; TC, total cholesterol; IL-34, interleukin-34.

necrosis factor, and interferon. Cytokines produced by a variety of cells can mediate cell-cell signal transduction through autocrine and paracrine and play a key role in the communication between different cells, tissues, and organs. The combination of cytokines and specific receptors not only controls the growth, proliferation, and migration of main cells at the cellular level but also participates in the body's inflammation, tumor, immunity, and angiogenesis [16]. Therefore, research on cytokines as diagnostic markers and therapeutic targets has been in the ascendant for a long time, and some progress has been made in predicting the severity and prognosis of the disease. IL-34 was identified as the second ligand of CSF1R in 2008. The full length of human IL-34

contains 242 amino acids. The first 182 amino acids are essential for the stability and proper folding of IL-34, and the last 50 residues are a large number of disordered and Pro-Ser-Thr-rich amino acids [17]. It has a similar active region to CSF-1, but their sequence does not have homology. IL-34 is a hematopoietic cytokine, which is widely distributed in the neurons, skin, heart, lung, liver, kidney, testes, and lymph nodes. It is a key regulator of the survival, proliferation, and differentiation of myeloid cells [18].

Recent studies have found that IL-34 is involved in the process of many diseases. Scholars from Dalian Medical University found that IL-34 increases the expression of IL-6 and then upregulates Th17 to participate in the course of rheumatoid arthritis [19]. Researchers from Chongqing Medical University found that serum IL-34 is elevated in patients with systemic lupus erythematosus (SLE), which may be used as a diagnostic marker for SLE [20]. In addition, Polish studies have shown that IL-34 can be used as a potential inflammatory biomarker for predicting the risk of diabetes complications [21]. Interestingly, the scientific research team of Shanghai Jiao tong University found that increased levels of IL-34 in the acute phase are associated with increased risk of heart failure and poor prognosis after myocardial infarction [22]. IL-34 is also believed to be related to psoriasis, psoriatic arthritis, obesity, liver disease, kidney disease, and inflammatory bowel disease [23–28].

The role of IL-34 in neurological diseases has gradually attracted attention in recent years. IL-34 can act on a variety of cells such as neurons, microglia, and endothelial cells to maintain the homeostasis of the central nervous system [29, 30]. A professor at Stanford University found that IL-34 provides a powerful neuroprotective and survival signal for neurons in brain injury and neurodegeneration [31]. Recently, Iranian scientists have found that serum IL-34 levels in patients with acute and chronic inflammatory demyelinating polyneuropathies (AIDP and CIDP) are elevated, suggesting that IL-34 may participate in the pathogenesis of autoimmune diseases [32]. In addition, West Nile virus infection can cause cognitive impairment, and IL-34 knockout mice can reduce the synaptic loss caused by this virus infection, suggesting that IL-34 may participate in the course of cognitive impairment [33]. Canadian researchers initially revealed the mechanism by which IL-34 is involved in the pathogenesis of AD [34], but its relationship with VaD has not been reported yet.

Our research has some limitations. First of all, we are a single-center small sample study; secondly, our VaD patients may have mixed types of dementia; and finally, we have not done interventional mechanism research. However, we have studied the relationship between serum IL-34 and VaD for the first time, which is the advantage of our research.

## 5. Conclusions

In summary, we found that serum IL-34 levels in VaD patients were significantly reduced. We report for the first time the role of serum IL-34 in VaD. IL-34 may be used in clinical services as a diagnosis and treatment target of VaD.

## Data Availability

The data used to support the findings of this study are available from the corresponding authors upon request.

## Conflicts of Interest

All the authors declare no conflict of interests.

## Authors' Contributions

Yang Wang and Wei Lu are co-first authors, and they contributed equally to this work.

## References

- [1] Q. Wang, W. Yang, J. Zhang, Y. Zhao, and Y. Xu, "TREM2 overexpression attenuates cognitive deficits in experimental models of vascular dementia," *Neural Plasticity*, vol. 2020, Article ID 8834275, 10 pages, 2020.
- [2] M. Xu, X. Y. He, and P. Huang, "The relationship between serum amyloid A level and cognitive dysfunction in patients with vascular dementia: preliminary findings," *BioMed Research International*, vol. 2021, Article ID 6676144, 6 pages, 2021.
- [3] J. Li, S. Li, Y. Song et al., "Association of serum FAM19A5 with cognitive impairment in vascular dementia," *Disease Markers*, vol. 2020, Article ID 8895900, 5 pages, 2020.
- [4] K. Yang, L. Zeng, A. Ge, Y. Yi, S. Wang, and J. Ge, "Exploring the oxidative stress mechanism of Buyang Huanwu decoction in intervention of vascular dementia based on systems biology strategy," *Oxidative Medicine and Cellular Longevity*, vol. 2021, Article ID 8879060, 29 pages, 2021.
- [5] E. E. Smith, "Clinical presentations and epidemiology of vascular dementia," *Clinical Science*, vol. 131, no. 11, pp. 1059–1068, 2017.
- [6] L. Wang, J. W. Yang, L. T. Lin et al., "Acupuncture attenuates inflammation in microglia of vascular dementia rats by inhibiting miR-93-mediated TLR4/MyD88/NF- $\kappa$ B signaling pathway," *Oxidative Medicine and Cellular Longevity*, vol. 2020, Article ID 8253904, 15 pages, 2020.
- [7] H. Lin, E. Lee, K. Hestir et al., "Discovery of a cytokine and its receptor by functional screening of the extracellular proteome," *Science*, vol. 320, no. 5877, pp. 807–811, 2008.
- [8] T. L. Tay, J. C. Savage, C. W. Hui, K. Bisht, and M. Tremblay, "Microglia across the lifespan: from origin to function in brain development, plasticity and cognition," *The Journal of Physiology*, vol. 595, no. 6, pp. 1929–1945, 2017.
- [9] E. Franzè, C. Stolfi, E. Troncone, P. Scarozza, and G. Monteleone, "Role of interleukin-34 in cancer," *Cancers*, vol. 12, no. 1, p. 252, 2020.
- [10] Y. Nakamichi, N. Udagawa, and N. Takahashi, "IL-34 and CSF-1: similarities and differences," *Journal of Bone and Mineral Metabolism*, vol. 31, no. 5, pp. 486–495, 2013.
- [11] O. Lopez, M. Larumbe, J. Becker et al., "Reliability of NINDS-AIREN clinical criteria for the diagnosis of vascular dementia," *Neurology*, vol. 44, no. 7, pp. 1240–1240, 1994.
- [12] M. Zaudig, "Behavioral and psychological symptoms of dementia in the International Classification of Diseases (ICD)-10 and Beyond (ICD-11)," *International Psychogeriatrics*, vol. 12, p. 29, 2000.
- [13] Y. Chen, L. Liang, S. Cao et al., "Serum CCL21 as a potential biomarker for cognitive impairment in spinal cord injury," *BioMed Research International*, vol. 2020, Article ID 6692802, 5 pages, 2020.
- [14] X. Wang, F. Zhang, W. Ma, D. Feng, J. Zhang, and J. Xu, "Increased levels of serum neuregulin 1 associated with cognitive impairment in vascular dementia," *BioMed Research International*, vol. 2020, Article ID 6683747, 5 pages, 2020.
- [15] L. Wang, Y. Chen, D. Feng, and X. Wang, "Serum ICAM-1 as a predictor of prognosis in patients with acute ischemic stroke," *BioMed Research International*, vol. 2021, Article ID 5539304, 6 pages, 2021.
- [16] M. Baghdadi, H. Endo, Y. Tanaka, H. Wada, and K. I. Seino, "Interleukin 34, from pathogenesis to clinical applications," *Cytokine*, vol. 99, pp. 139–147, 2017.
- [17] M. Baghdadi, Y. Umeyama, N. Hama et al., "Interleukin-34, a comprehensive review," *Journal of Leukocyte Biology*, vol. 104, no. 5, pp. 931–951, 2018.
- [18] I. Lelios, D. Cansever, S. G. Utz, W. Mildenerberger, S. A. Stifter, and M. Greter, "Emerging roles of IL-34 in health and disease," *The Journal of Experimental Medicine*, vol. 217, no. 3, 2020.
- [19] B. Wang, Z. Ma, M. Wang et al., "IL-34 upregulated Th17 production through increased IL-6 expression by rheumatoid fibroblast-like Synoviocytes," *Mediators of Inflammation*, vol. 2017, Article ID 1567120, 10 pages, 2017.
- [20] H. Wang, J. Cao, and X. Lai, "Serum interleukin-34 levels are elevated in patients with systemic lupus erythematosus," *Molecules*, vol. 22, 2017.
- [21] K. Zorena, O. Jachimowicz-Duda, and P. Wąż, "The cut-off value for interleukin 34 as an additional potential inflammatory biomarker for the prediction of the risk of diabetic complications," *Biomarkers: biochemical indicators of exposure, response, and susceptibility to chemicals*, vol. 21, no. 3, pp. 276–282, 2016.
- [22] Q. Fan, R. Tao, H. Zhang et al., "Interleukin-34 levels were associated with prognosis in patients with acute myocardial infarction," *International Heart Journal*, vol. 60, no. 6, pp. 1259–1267, 2019.
- [23] J. Li, L. Liu, W. Rui et al., "New interleukins in psoriasis and psoriatic arthritis patients: the possible roles of interleukin-33 to interleukin-38 in disease activities and bone erosions," *Dermatology*, vol. 233, pp. 37–46, 2017.
- [24] N. Li, L. Jiang, Y. Cai et al., "The correlation between interleukin-34 and bone erosion under ultrasound in rheumatoid arthritis," *Modern Rheumatology*, vol. 30, no. 2, pp. 269–275, 2020.
- [25] E. J. Chang, S. K. Lee, Y. S. Song et al., "IL-34 is associated with obesity, chronic inflammation, and insulin resistance," *The Journal of Clinical Endocrinology and Metabolism*, vol. 99, no. 7, pp. E1263–E1271, 2014.
- [26] F. Al-Shaebi, L. Wenzhang, K. Hezam, M. Almezgagi, and L. Wei, "Recent insights of the role and signalling pathways of interleukin-34 in liver diseases," *International Immunopharmacology*, vol. 89, p. 107023, 2020.
- [27] J. H. Baek, R. Zeng, J. Weinmann-Menke et al., "IL-34 mediates acute kidney injury and worsens subsequent chronic kidney disease," *The Journal of Clinical Investigation*, vol. 125, no. 8, pp. 3198–3214, 2015.
- [28] S. Zwicker, G. L. Martinez, M. Bosma et al., "Interleukin 34: a new modulator of human and experimental inflammatory

- bowel disease,” *Clinical science*, vol. 129, no. 3, pp. 281–290, 2015.
- [29] S. Jin, Y. Sonobe, J. Kawanokuchi et al., “Interleukin-34 restores blood-brain barrier integrity by upregulating tight junction proteins in endothelial cells,” *PLoS One*, vol. 9, no. 12, article e115981, 2014.
- [30] P. W. Lee, A. Selhorst, S. G. Lampe, Y. Liu, Y. Yang, and A. E. Lovett-Racke, “Neuron-specific vitamin D signaling attenuates microglia activation and CNS autoimmunity,” *Frontiers in Neurology*, vol. 11, p. 19, 2020.
- [31] J. Luo, F. Elwood, M. Britschgi et al., “Colony-stimulating factor 1 receptor (CSF1R) signaling in injured neurons facilitates protection and survival,” *The Journal of Experimental Medicine*, vol. 210, no. 1, pp. 157–172, 2013.
- [32] S. Rezaei, S. Ghafouri-Fard, A. Komaki, M. Mazdeh, M. Taheri, and M. M. Eftekharian, “Increased levels of IL-34 in acquired immune-mediated neuropathies,” *Journal of molecular neuroscience*, vol. 71, no. 1, pp. 137–141, 2021.
- [33] M. J. Vasek, C. Garber, D. Dorsey et al., “A complement-microglial axis drives synapse loss during virus-induced memory impairment,” *Nature*, vol. 534, no. 7608, pp. 538–543, 2016.
- [34] V. Pons, P. Lévesque, M. M. Plante, and S. Rivest, “Conditional genetic deletion of CSF1 receptor in microglia ameliorates the pathophysiology of Alzheimer’s disease,” *Alzheimer’s Research & Therapy*, vol. 13, no. 1, p. 8, 2021.

## Review Article

# Repulsive Guidance Molecule-a and Central Nervous System Diseases

Jinhua Tang, Xiaopeng Zeng, Hang Li, Lu Ju, Jinzhou Feng , and Jun Yang 

Department of Neurology, The First Affiliated Hospital of Chongqing Medical University, Chongqing 400016, China

Correspondence should be addressed to Jinzhou Feng; fengjinzhou@hotmail.com and Jun Yang; yangweixiao222@sina.com

Received 5 February 2021; Accepted 27 April 2021; Published 4 May 2021

Academic Editor: Yuzhen Xu

Copyright © 2021 Jinhua Tang et al. This is an open access article distributed under the Creative Commons Attribution License, which permits unrestricted use, distribution, and reproduction in any medium, provided the original work is properly cited.

Repulsive guidance molecule-a (RGMa) is a member of glycosylphosphatidylinositol- (GPI-) anchored protein family, which has axon guidance function and is widely involved in the development and pathological processes of the central nervous system (CNS). On the one hand, the binding of RGMa and its receptor Neogenin can regulate axonal guidance, differentiation of neural stem cells into neurons, and the survival of these cells; on the other hand, RGMa can inhibit functional recovery of CNS by inhibiting axonal growth. A number of studies have shown that RGMa may be involved in the pathogenesis of CNS diseases, such as multiple sclerosis, neuromyelitis optica spectrum diseases, cerebral infarction, spinal cord injury, Parkinson's disease, and epilepsy. Targeting RGMa can enhance the functional recovery of CNS, so it may become a promising target for the treatment of CNS diseases. This article will comprehensively review the research progression of RGMa in various CNS diseases up to date.

## 1. Introduction

RGMa (repulsive guidance molecule-a) is a member of glycosylphosphatidylinositol (GPI)-anchored protein family [1]. It was first found in the visual system of chicken embryo, with axon guidance function [1]. Three members of the RGM family, RGMa, RGMb, and RGMc were found in vertebrates [2]. Their 3D structures have been partially discovered [2, 3]. RGMa and RGMb are expressed in the central nervous system (CNS) and other tissues (heart, lung, liver, small intestine, etc.) with a nonoverlapping form, while RGMc is only expressed in the skeletal muscle, liver, and blood [2]. The RGMa gene is located on chromosome 15q26.1 and encodes a protein of 450 amino acids [1, 2]. RGMa consists of GPI-anchored C-terminal signal peptide, N-terminal signal peptide, and RGD motif (only found in RGMa and RGMc) and partial von Willebrand factor type D [2, 4, 5]. RGMa exists in CNS such as neural stem cells, neuron cells, and myelin sheath in both soluble and membrane-bound forms [4, 5]. It binds with type I transmembrane protein Neogenin and plays the biological functions of axon guidance and neuron survival through the FAK-RhoA signaling pathway [4, 5]. In addition, as a coreceptor of bone

morphogenetic proteins (BMPs), RGMa can bind to BMP-2, BMP-4, and other BMP family molecules and participate in iron metabolism, bone development, and axon regeneration through the BMP-BMPR signaling pathway [2, 5]. Currently, a number of studies have shown that RGMa is highly expressed in the injured lesions in patients with multiple sclerosis, neuromyelitis optica spectrum diseases, cerebral infarction, spinal cord injury, and Parkinson's disease [6–11]. It has also been reported that it can promote the functional recovery of the nervous system by inhibiting RGMa [6–11]. However, the expression of RGMa is low in patients with epilepsy [12]. Upregulation of RGMa can reduce epileptic seizures [12]. These data indicated that RGMa may be involved in the pathogenesis of the above diseases and may become a potential target for the treatment of CNS diseases.

## 2. Role of RGMa in CNS Physiology

**2.1. Cell Proliferation and Differentiation.** Both RGMa and Neogenin are highly expressed in intestinal neural stem cells during proliferation and differentiation [13]. The loss of

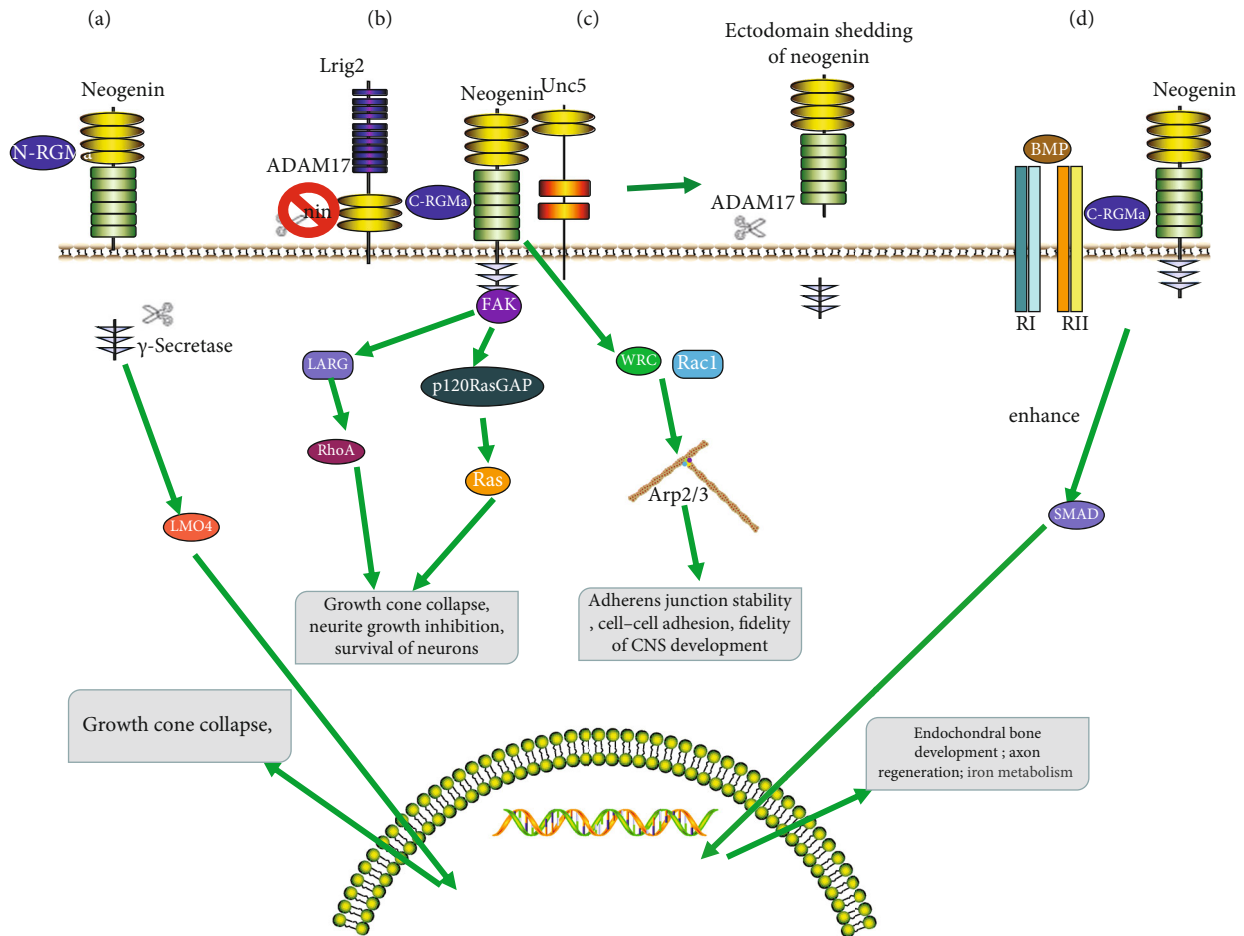


FIGURE 1: Mechanisms for RGMa Signal Transduction. (a) The role of N-RGMa depends on the release of Neogenin intracellular domain by  $\gamma$ -secretase and LMO4. It has been suggested that Neogenin intracellular domain may enter the nucleus together with LMO4 and regulates gene transcription and growth cone collapse. (b) In general, C-RGMa-Neogenin binding can activate RhoA through Unc5 and LARG and inactivate Ras through FAK and p120 RasGAP, thus inducing growth cone collapse and playing the role of axon guidance and regulation of neuronal survival. The binding of C-RGMa with Neogenin inhibits the interaction between Lrig2 and Neogenin. At this time, ADAM17 can cleave Neogenin and cause the extracellular domain of Neogenin to fall off, eventually leading to signal termination. Therefore, LRIG2 and ADAM17 can regulate the sensitivity of neurons to RGMa. (c) In epithelial cells, Neogenin binds to and localizes the wave regulatory complex (WRC), leading to actin nucleation via Arp2/3, which also requires Rac1 to activate the stability of adhesion junctions. (d) RGMa acts as a coreceptor of bone morphogenetic protein (BMP) and has been proposed as a structural bridge between BMP and Neogenin. A recently proposed model suggests that RGMa induces endocytosis of BMP receptor complexes, thereby activating classical Smad signaling. The interaction between RGMa and BMP signal transduction has been involved in iron metabolism, bone development, axon regeneration, and so on.

RGMa and Neogenin resulted in the decrease of neurons, glial cells, and ganglia in the intestinal system, indicating that RGMa is involved in the proliferation and differentiation of intestinal neural stem cells [13]. RGMa had a rejection effect on differentiating progenitors via Neogenin [13, 14]. In the midbrain of a chicken embryo, RGMa overexpression can temporarily inhibit cell proliferation [15]. In addition, RGMa promotes neuronal differentiation in the midbrain through Neogenin signal transduction [15].

**2.2. Cell Adhesion and Migration.** RGMa can improve the adhesion of embryonic cells *in vitro*, and RGMa overexpression can also induce the migration defects in early embryonic ectodermal cells, indicating that RGMa is related to the adhesion and migration of embryonic cells [16]. RGMa increases

the adhesion between cells through Neogenin, recruiting cell adhesion molecules [17]. Moreover, RGMa and Neogenin jointly act on adhesion junctions (AJ) to regulate actin and maintain epithelial fidelity. In epithelial cells, Neogenin binds to and localizes the wave regulatory complex (WRC), leading to actin nucleation via Arp2/3 (Figure 1(c)) [2]. RGMa induces cell migration through Neogenin, independent of the BMP pathway [17]. Recent studies have shown that Neogenin-Netrin-1-RGMa complex regulates neuron migration [18]. The vWF and RGD domains in RGMa play a functional role in cell adhesion and cell migration [17].

**2.3. Neurogenesis and Neural Tube Closure.** RGMa and Neogenin can coregulate the differentiation and migration of embryonic neurogenesis, and they can also coregulate the



development of an adult central nervous system (Figures 1(a) and 1(b)) [15, 17]. In addition, RGMa can induce Neogenin protein hydrolysis and promote neural tube morphogenesis [19]. The closure defects of neural tube may occur if RGMa is exhausted [19]. Neogenin-Netrin-1-RGMa complex may regulate neurogenesis and neural tube closure through the RhoA/ROCK pathway [18]. In addition, whether the RGMa-BMP pathway plays a role in neurogenesis is a hot topic in future research [17].

### 3. Role of RGMa in CNS Pathology

**3.1. Survival of Neurons.** On the one hand, inhibition of RGMa in adult dentate gyrus can increase the number of new neurons; on the other hand, inhibition of Neogenin can improve neuron survival and behavioral recovery after spinal cord injury [20, 21]. It has been proved that both RGMa and Neogenin regulate the survival of neurons [20, 21]. Some scholars believe that RGMa binds to Neogenin on neural stem cells and regulates neuron survival by regulating caspase-3 and Rock [15, 17]. Other scholars believe that the combination of RGMa and Neogenin affects the survival of neurons in the CNS through death-associated protein kinase (DAPK) and LMO4. DAPK affects cell survival by activating the apoptotic pathway, while LMO4 affects the cytoskeleton and gene expression [2, 22].

**3.2. Synapse Formation.** RGMa can inhibit synapse formation by interfering with the expression of presynaptic protein synapsin-1 and postsynaptic protein PSD-95 in cortical neurons [23]. Inhibition of RGMa can increase the coexpression of the above two proteins, thus enhancing the synaptic formation after spinal cord injury [23]. RGMa, especially C-RGMa, may inhibit synaptic formation through Neogenin [24]. The latest research shows that RGMa can regulate neuronal branching through the RhoA pathway to mediate synaptic plasticity [25].

**3.3. Growth Cone Collapse and Axon Growth Inhibition.** RGMa can inhibit the axon growth after CNS injury, but the specific mechanism is not clear. It may inhibit the axon growth by stimulating neurons to induce RhoA and ROCK (Rho-associated coiled-coil protein kinase) expression [5]. It has been confirmed that RGMa may cause cone collapse by activating downstream Rho-GTPase activity [26]. In addition, RGMa can regulate the phosphorylation of collapse response mediator protein-2 (CRMP-2) by activating Rho-kinase and glycogen synthase kinase 3  $\beta$  (GSK-3 $\beta$ ) signaling pathways, thus regulating the axonal shortening [26]. Two independent c-RGMa and n-RGMa can activate different intracellular pathways to regulate neuronal survival: (1) in general, c-RGMa combines with Neogenin to activate RhoA through Unc5 and LARG (Figure 1(b)) [27–29]. C-RGMa can inhibit axon growth through the Rho-GEF (LARG)/Rho/ROCK signaling pathway and also inactivate Ras through FAK and p120 Ras-GAP to induce growth collapse (Figure 1(b)) [27–29]. (2) When C-RGMa and Neogenin bind to inhibit the interaction between LRIG2 and Neogenin, then, C-RGMa can promote ADAM17 specific cleavage of

Neogenin, resulting in signal termination (Figure 1(b)) [27–29]. (3) N-RGMa mainly depends on  $\gamma$ -secretase to cleave the intracellular part of Neogenin to generate intracellular domain [27]. This domain can inhibit axonal growth by binding to LIM protein 4 (LMO4) (Figure 1(a)) [27]. Inhibition of RGMa with specific antibodies can promote axonal germination, regeneration, and motor recovery after spinal cord injury (SCI) in primates [30].

**3.4. Immunoregulation.** RGMa can regulate T cell activation and autoimmunity through dendritic cells (DCS) [31]. RGMa in dendritic cells can also bind to Neogenin on CD4<sup>+</sup> T cells to activate inflammatory cells, enhance the adhesion between inflammatory cells and ICAM-1, and indirectly regulate the release and diffusion of cytokines [31]. Treatment with RGMa neutralizing antibody can cause dendritic cell tolerance and immunomodulatory function; reduce the levels of MHC II, CD86, CD80, and CD40; decrease the levels of IL-12, IL-1  $\beta$ , and TNF- $\alpha$ ; and increase the secretion of IL-10, resulting in reducing T cell proliferation and enhancing the T cell differentiation into Th2 cells [32].

**3.5. Inhibition of Angiogenesis.** RGMa is a negative regulator of angiogenesis [33]. The binding of recombinant RGMa with Neogenin on endothelial cells can significantly reduce endothelial cell proliferation, migration, and formation of vascular endothelium, as well as the level of phosphorylated focal adhesion kinase (p-FAK Tyr397) [5, 33, 34]. In addition, F-actin assembled in the cytoskeleton was also significantly inhibited, thereby inhibiting cytoskeleton reorganization [5]. Removal of Neogenin or Unc5b could significantly reduce the effect of RGMa [5, 34]. RGMa can inhibit angiogenesis by down-regulating VEGF and p-FAK (Tyr397) in vitro [34, 35]. Recombinant RGMa can also inhibit angiogenesis [36].

## 4. RGMa as a Therapeutic Target in CNS Disorders

**4.1. Multiple Sclerosis (MS).** Many researches have shown that RGMa plays an important role in MS. Demicheva et al. reported that the expression of RGMa was significantly increased in acute and chronic damaged plaques and normal white matter of CNS in MS patients [22]. The level of RGMa in the baseline blood was negatively correlated with the changes of Expanded Disability Status Scale (EDSS) in MS patients, indicating that the level of RGMa was closely related to neurological function [2, 6, 37]. The possible pathogenesises of RGMa in MS include the following:

- (1) Abnormal signal transduction of immune cells: since IL-17-expressing CD4<sup>+</sup> T cells (Th17 cells) strongly expressed RGMa, so the combination of RGMa and Neogenin on immune cells can enhance the immune cell adhesion, promote their invasion to the brain, and enhance T cell response [5, 37]. Neutralizing RGMa antibody can reduce the severity of experimental autoimmune encephalomyelitis (EAE) in the

MS animal model; secondly, it can inhibit peripheral blood T cell proliferation, block the production of inflammatory cytokines such as IL-2, IFN- $\gamma$ , IL-17, and IL-4, and significantly reduce the level of CNS inflammatory cytokines in MS patients [5, 37].

- (2) Promotion of demyelinating production: in EAE, RGMa promotes the demyelination of CNS by enhancing the activation of CD4<sup>+</sup> T cells [38, 39]. Our previous work also found that the usage of RGMa neutralizing antibody can reduce the demyelination level of EAE mice, thereby inhibiting the neurological damage.
- (3) Promotion of neurodegeneration: RGMa has strong inhibitory activity on axon regeneration and also plays a role in MS neurodegeneration [40]. The possible mechanism involves RGMa inducing Akt dephosphorylation in neurons by binding to Neogenin on Th17 cells [40]. Neutralizing RGMa antibody can enhance the axonal regeneration ability of inflammatory lesions, reduce axonal degeneration and clinical severity, and promote the growth of corticospinal tract and motor recovery in EAE mice [5, 7, 22, 40].
- (4) Inhibition of angiogenesis: angiogenesis is another key factor involved in the pathophysiology of EAE [41]. RGMa can inhibit the formation of endothelial vessels [5, 41].
- (5) Alter the permeability of blood-brain barrier (BBB): the damage of BBB is an important pathological feature of MS [42, 43]. Studies have found that the level of RGMa in cerebrospinal fluid in patients with triamcinolone acetone treatment (its pharmacological effect is mainly on improving the BBB permeability) is reduced, which suggested that RGMa may be involved in the pathology of MS by regulating BBB permeability in MS patients (Table 1) [44, 45].

**4.2. Neuromyelitis Optica Spectrum Disorders (NMOSD).** Systemic administration of anti RGMa antibody can delay the onset time, alleviate its clinical symptoms, and reduce inflammatory cell infiltration and axon damage in NMOSD rat model, indicating that inhibiting RGMa can effectively treat NMOSD [8]. The possible pathogenesises of RGMa in NMOSD include the following: (1) the loss of aquaporin-4 (AQP4) and glial fibrillary acid protein (GFAP) often occurred before the demyelination of NMOSD [46]. Anti-RGMa antibody could partially restore the expression of AQP4 and GFAP in NMOSD rats, resulting in preventing astrogliosis and relieving clinical symptoms [8, 46]. (2) Anti-RGMa antibody can reduce the immune response of NMOSD rats, which may help to delay the attack and/or progress of NMOSD in the NMOSD rat model by reducing the number of activated microglia and reducing the infiltration of IL-17A<sup>+</sup> T cells [8, 47]. (3) Axonal injury is an early pathological feature of NMOSD, which can cause dyskinesia [40]. The treatment of anti RGMa antibody can reduce axonal degeneration and injury [8, 40, 48]. (4) Inhibition

of RGMa can promote the repair of damaged neural network and delay the secondary progression of NMOSD (Table 1) [8, 49].

**4.3. Cerebral Infarction.** Our previous study found that an adenovirus vector can reduce BBB dysfunction in rats with middle cerebral artery occlusion (MCAO)/reperfusion by inducing specific RGMa silencing [9]. The possible mechanism was that RGMa participates in BBB injury through the CDC-42/PAK-1 pathway (Table 1) [9, 50]. We also found that RGMa can inhibit axonal growth by phosphorylating CRMP-2 through the Rho kinase and GSK-3 $\beta$  signaling pathways (Table 1) [51, 52]. Both RGMa and Neogenin were expressed in neurons and vessel endothelial cells after ischemia/reperfusion injury in rats, and angiogenesis, coupled with functional recovery, was enhanced after RGMa RNA interference against RGMa [34, 35]. The mechanism may lie in RGMa inhibiting angiogenesis through VEGF, Ang2, Ang1, and BDNF (Table 1) [34, 35]. In addition, the increased RGMa in patients with MCAO may be related to leptomeningeal collateral damage, which can predict the pathological state of leptomeningeal collateral by measuring the expression of RGMa mRNA in the early stage of stroke (Table 1) [53].

**4.4. Spinal Cord Injury (SCI).** The treatment of spinal cord injury with anti-RGMa antibody can promote the recovery of hand agility and muscle strength [10, 30]. Possibly because the inhibition of RGMa promotes the survival and regeneration of neurons, it promotes the regeneration, repairs plasticity of corticospinal tract axons, improves motor function and gait recovery, and reduces nerve pain by reducing activated microglia (Table 1) [21].

**4.5. Parkinson's Disease (PD).** RGMa is upregulated in the substantia nigra of Parkinson's disease patients [11]. RGMa can induce neuropathological and behavioral changes similar to Parkinson's disease [11]. If RGMa in substantia nigra dopaminergic (DA) neurons of Parkinson's disease mouse is significantly increased, it can lead to progressive dyskinesia, including motor coordination and imbalance, which is a typical manifestation of DA reduction in striatum [11, 54–56]. The mechanism may be the selective degeneration of DA neurons and the activation of microglia and astrocytes in substantia nigra induced by elevated RGMa (Table 1) [11, 57]. These data suggested that RGMa dysfunction plays an important role in Parkinson's disease [11, 57].

**4.6. Epilepsy.** RGMa has been considered a potential therapeutic agent for epilepsy [12, 58]. Some studies found that the levels of RGMa are significantly decreased in both temporal lobe epilepsy patients and experimental rats [12, 58]. Some studies also confirmed that overexpression of RGMa can inhibit epileptic seizures [12, 58]. The possible mechanisms include the following: (1) in the organ slice model of epilepsy induced by magnesium deficiency, the overexpression of RGMa can inhibit the N-methyl-D-aspartate receptor- (NMDAR-) mediated current, thereby inhibiting the overexcitation of hippocampal neurons [58–60]. (2) Lentiviral vector-induced RGMa overexpression in the

TABLE 1: RGMa-related possible mechanisms involved in CNS diseases.

Disease	Expression site of RGMa	Possible mechanisms	Participants or models	Potential therapeutic target
MS	(1) Significantly upregulated in active and chronic MS lesions [22, 61] (2) Plasma RGMa is inversely related to delta EDSS [2, 6]	(1) Mediates immune responses [5, 37, 61–64] (2) Mediates CNS demyelination [38, 39] (3) Mediates neurodegeneration and inhibits neurite outgrowth [5, 7, 22, 40] (4) Inhibits neovascularization [5, 36, 65] (5) May be involved in BBB dysfunction [43–45, 66] (1) May involve loss of AQP4, GFAP, and astrocytes [8, 46, 67] (2) May aggravate immune responses [8, 47, 68, 69] (3) May induce neuronal damage [8, 48, 49]	(1) MS patients [6, 22, 44] (2) EAE rats [5, 61]	(1) Targeting RGMa can improve functional recovery [22] (2) Anti-RGMa antibody can promote neurite outgrowth and remyelination [5, 22] (3) Anti-RGMa antibody can reduce immune responses [5]
NMOSD	Unknown	(1) May involve loss of AQP4, GFAP, and astrocytes [8, 46, 67] (2) May aggravate immune responses [8, 47, 68, 69] (3) May induce neuronal damage [8, 48, 49]	NMOSD model in rats [8]	Inhibition of RGMa can (1) delay onset [8] (2) relieve symptoms [8] (3) delay progression of NMOSD [8]
Ischemic stroke	Upregulated in vascular endothelium and neurons after I/R injury [9, 36]	(1) Might inhibit angiogenesis by downregulating BDNF VEGF, AngI, and Ang2 [35] (2) Might impact LMC status [53] (3) May be involved in BBB dysfunction via the CDC-42/PAK-1 signal pathway [9]	(1) MCAO patients [53] (2) I/R injury model in rats [9, 35] (3) Endothelial cell in vitro [34]	(1) Anti-RGMa antibody or RGMa function-blocking peptide can significantly upregulate BDNF, VEGF, AngI, and Ang2 [34, 35] (2) Inhibition of RGMa promotes functional recovery by promoting angiogenesis [35] (2) RGMa may predict LMC status [53] (3) Silencing RGMa ameliorates infarct volume, brain edema, and BBB dysfunction [9]
SCI	Upregulated around SCI lesion [30, 70]	(1) Inhibits neuronal survival [30] (2) Activates microglia [21]	(1) Patients with SCI [21] (2) SCI model in monkey [10, 71] (3) SCI model in mice [30, 72]	(1) Anti-RGMa antibody can promote axon regeneration, plasticity, motor recovery, and manual dexterity [10, 21, 30, 72] (2) Anti-RGMa antibody can relieve neuralgia [21]
PD	Significantly upregulated in the SN of patients with PD [11, 73]	(1) Induces selective degeneration of dopaminergic neurons in the SN [11, 74] (2) Activates microglia and astrocyte strongly [11, 74] (3) May inhibit neuronal survival by activating RhoA [58, 74]	(1) Patients with PD [11, 73] (2) RGMa can model PD in mouse [11]	(1) Inhibition of RGMa may modify PD [11, 75] (2) Regulating RGMa-Neogenin may promote cell replacement [74] (3) Anti-RGMa antibody may offer neuroprotection [74]
Seizures	Significantly decreased in epileptic patients and rat models [12, 58, 76]	(1) Partly via the FAK-p120Ras GAP-Ras signaling pathway suppresses MFS [12, 76] (3) Inhibits hyperexcitability of hippocampal neurons via suppressing NMDAR-mediated currents [58]	(1) Epileptic patients [58] (2) Pentylentetrazol rat model [12] (3) Epileptic rat model [58] (4) Organotypic slice model [58]	Injection recombinant RGMa to intracerebroventricular or overexpression of RGMa suppresses MFS and seizures [12, 58, 76]

RGMa: repulsive guidance molecule-4; EAE: experimental autoimmune encephalomyelitis; NMOSD: neuromyelitis optica spectrum disorders; AQP4: aquaporin-4; MCAO: middle cerebral artery occlusion; I/R: ischemia-reperfusion; CRMP-2: collapsin response mediator protein 2; LMCs: leptomeningeal collaterals; SCI: spinal cord injury; PD: Parkinson's disease; SN: substantia nigra; PTZ: pentylentetrazol; MFS: mossy fiber sprouting.



hippocampus can inhibit seizures by inhibiting mossy fiber sprouting [12]. (3) Silencing miR-20a-5p, an upstream regulator of RGMA, inhibits neuronal branching and axon growth through the RGMA-RhoA pathway, thereby preventing epilepsy (Table 1) [25].

## 5. Summary

In conclusion, as an axon guidance molecule, RGMA widely participates in the development and pathological process of CNS to regulate cell proliferation, differentiation, adhesion, migration, neurogenesis, neural tube closure, neuronal apoptosis, synapse formation, growth cone collapse, axon growth inhibition, immune response, and neovascularization through RGMA-Neogenin, RGMA-BMPs, and other signaling pathways. Recent studies have found that RGMA can participate in the pathogenesis of MS, NMOSD, cerebral infarction, spinal cord injury, PD, epilepsy, and other CNS diseases. By regulating the expression of RGMA, it can reduce neural function damage and promote the recovery of neural function, indicating that RGMA may be a promising target molecule for the treatment of CNS diseases (Table 1). As the specific pathogenesis and signaling pathway of RGMA in CNS diseases are not fully clear, the randomized controlled clinical trials need to take years to conduct. Therefore, more in-depth analysis and large sample for randomized controlled clinical trials are required to elucidate the mechanism of RGMA in the guidance of clinical treatment of CNS diseases.

## Conflicts of Interest

The authors declare no conflicts of interest.

## Authors' Contributions

Jinhua Tang searched the literature and wrote the manuscript, Xiaopeng Zeng drew the figure, Hang Li made the table, Lu Ju edited format, and Feng Jinzhou and Yang Jun revised the manuscript. All authors read and approved the final manuscript.

## Acknowledgments

This work was supported by the National Natural Science Foundation of China (grant number 81701191).

## References

- [1] P. Monnier, A. Sierra, P. Macchi et al., "RGM is a repulsive guidance molecule for retinal axons," *Nature*, vol. 419, no. 6905, pp. 392–395, 2002.
- [2] C. Siebold, T. Yamashita, P. P. Monnier, B. K. Mueller, and R. J. Pasterkamp, "RGMs: structural insights, molecular regulation, and downstream signaling," *Trends in Cell Biology*, vol. 27, no. 5, pp. 365–378, 2017.
- [3] T. Malinauskas, T. V. Peer, B. Bishop, T. D. Mueller, and C. Siebold, "Repulsive guidance molecules lock growth differentiation factor 5 in an inhibitory complex," *Proceedings of the National Academy of Sciences of the United States of America*, vol. 117, no. 27, pp. 15620–15631, 2020.
- [4] S. Rajagopalan, L. Deitinghoff, D. Davis et al., "Neogenin mediates the action of repulsive guidance molecule," *Nature Cell Biology*, vol. 6, no. 8, pp. 756–762, 2004.
- [5] Y. Fujita and T. Yamashita, "The roles of RGMA-neogenin signaling in inflammation and angiogenesis," *Inflammation and Regeneration*, vol. 37, no. 1, p. 6, 2017.
- [6] A. Malekzadeh, C. Leurs, W. van Wieringen et al., "Plasma proteome in multiple sclerosis disease progression," *Annals of Clinical Translational Neurology*, vol. 6, no. 9, pp. 1582–1594, 2019.
- [7] S. Tanabe, Y. Fujita, K. Ikuma, and T. Yamashita, "Inhibiting repulsive guidance molecule-a suppresses secondary progression in mouse models of multiple sclerosis," *Cell Death & Disease*, vol. 9, no. 11, p. 1061, 2018.
- [8] K. Harada, Y. Fujita, T. Okuno et al., "Inhibition of RGMA alleviates symptoms in a rat model of neuromyelitis optica," *Scientific Reports*, vol. 8, no. 1, p. 34, 2018.
- [9] M. Li, Y. Wen, R. Zhang, F. Xie, G. Zhang, and X. Qin, "Adenoviral vector-induced silencing of RGMA attenuates blood-brain barrier dysfunction in a rat model of MCAO/reperfusion," *Brain Research Bulletin*, vol. 142, pp. 54–62, 2018.
- [10] H. Nakagawa, T. Ninomiya, T. Yamashita, and M. Takada, "Treatment with the neutralizing antibody against repulsive guidance molecule-a promotes recovery from impaired manual dexterity in a primate model of spinal cord injury," *Cerebral Cortex*, vol. 29, no. 2, pp. 561–572, 2019.
- [11] J. Korecka, E. Moloney, R. Eggers et al., "Repulsive guidance molecule a (RGMA) induces neuropathological and behavioral changes that closely resemble Parkinson's disease," *The Journal of Neuroscience*, vol. 37, no. 39, pp. 9361–9379, 2017.
- [12] M. Song, F. Tian, H. Xia, and Y. Xie, "Repulsive guidance molecule a suppresses seizures and mossy fiber sprouting via the FAK-p120RasGAP-Ras signaling pathway," *Molecular Medicine Reports*, vol. 19, no. 4, pp. 3255–3262, 2019.
- [13] M. Metzger, S. Conrad, T. Skutella, and L. Just, "RGMA inhibits neurite outgrowth of neuronal progenitors from murine enteric nervous system via the neogenin receptor in vitro," *Journal of Neurochemistry*, vol. 103, no. 6, pp. 2665–2678, 2007.
- [14] P. H. Neckel, R. Mohr, Y. Zhang, B. Hirt, and L. Just, "Comparative microarray analysis of proliferating and differentiating murine ENS progenitor cells," *Stem Cells International*, vol. 2016, Article ID 9695827, 13 pages, 2016.
- [15] T. J. Isaksen and T. Yamashita, "Repulsive guidance molecule a regulates adult neurogenesis via the neogenin receptor," *Neuroscience Insights*, vol. 15, article 2633105520948481, 2020.
- [16] G. Lah and B. Key, "Novel roles of the chemorepellent axon guidance molecule RGMA in cell migration and adhesion," *Molecular and Cellular Biology*, vol. 32, no. 5, pp. 968–980, 2012.
- [17] T. Isaksen, Y. Fujita, and T. Yamashita, "Repulsive guidance molecule a suppresses adult neurogenesis," *Stem Cell Reports*, vol. 14, no. 4, pp. 677–691, 2020.
- [18] R. A. Robinson, S. C. Griffiths, L. L. van de Haar et al., "Simultaneous binding of guidance cues NET1 and RGM blocks extracellular NEO1 signaling," *Cell*, vol. 184, no. 8, pp. 2103–2120.e31, 2021.
- [19] S. Brown, P. Jayachandran, M. Negesse, V. Olmo, E. Vital, and R. Brewster, "Rgma-induced Neol proteolysis promotes

- neural tube morphogenesis,” *The Journal of Neuroscience*, vol. 39, no. 38, pp. 7465–7484, 2019.
- [20] E. Matsunaga, S. Tauszig-Delamasure, P. Monnier et al., “RGM and its receptor neogenin regulate neuronal survival,” *Nature Cell Biology*, vol. 6, no. 8, pp. 749–755, 2004.
- [21] A. Mothe, N. Tassew, A. Shabanzadeh et al., “RGMa inhibition with human monoclonal antibodies promotes regeneration, plasticity and repair, and attenuates neuropathic pain after spinal cord injury,” *Scientific Reports*, vol. 7, no. 1, article 10529, 2017.
- [22] E. Demicheva, Y. Cui, P. Bardwell et al., “Targeting repulsive guidance molecule A to promote regeneration and neuroprotection in multiple sclerosis,” *Cell Reports*, vol. 10, no. 11, pp. 1887–1898, 2015.
- [23] J. Yoshida, T. Kubo, and T. Yamashita, “Inhibition of branching and spine maturation by repulsive guidance molecule in cultured cortical neurons,” *Biochemical and Biophysical Research Communications*, vol. 372, no. 4, pp. 725–729, 2008.
- [24] J. Nevoux, M. Alexandru, T. Bellocq et al., “An antibody to RGMa promotes regeneration of cochlear synapses after noise exposure,” *Scientific Reports*, vol. 11, no. 1, p. 2937, 2021.
- [25] Y. Feng, C. Duan, Z. Luo, W. Xiao, and F. Tian, “Silencing miR-20a-5p inhibits axonal growth and neuronal branching and prevents epileptogenesis through RGMa-RhoA-mediated synaptic plasticity,” *Journal of Cellular and Molecular Medicine*, vol. 24, no. 18, pp. 10573–10588, 2020.
- [26] X. Ye, Y. Qiu, Y. Gao, D. Wan, and H. Zhu, “A subtle network mediating axon guidance: intrinsic dynamic structure of the growth cone, attractive and repulsive molecular cues, and the intermediate role of signaling pathways,” *Neural Plasticity*, vol. 2019, Article ID 1719829, 26 pages, 2019.
- [27] P. Banerjee, H. Harada, N. G. Tassew et al., “Y-secretase and LARG mediate distinct RGMa activities to control appropriate layer targeting within the optic tectum,” *Cell Death and Differentiation*, vol. 23, no. 3, pp. 442–453, 2016.
- [28] Y. Okamura, E. Kohmura, and T. Yamashita, “TACE cleaves neogenin to desensitize cortical neurons to the repulsive guidance molecule,” *Neuroscience Research*, vol. 71, no. 1, pp. 63–70, 2011.
- [29] S. van Erp, D. van den Heuvel, Y. Fujita et al., “Lrig2 negatively regulates ectodomain shedding of axon guidance receptors by ADAM proteases,” *Developmental Cell*, vol. 35, no. 5, pp. 537–552, 2015.
- [30] T. Nakanishi, Y. Fujita, T. Tanaka, and T. Yamashita, “Anti-repulsive guidance molecule-a antibody treatment and repetitive transcranial magnetic stimulation have synergistic effects on motor recovery after spinal cord injury,” *Neuroscience Letters*, vol. 709, article 134329, 2019.
- [31] X. Xu, Y. Gao, F. Shan, and J. Feng, “A novel role for RGMa in modulation of bone marrow-derived dendritic cells maturation induced by lipopolysaccharide,” *International Immunopharmacology*, vol. 33, pp. 99–107, 2016.
- [32] X. Xu, Y. Gao, Z. Zhai, S. Zhang, F. Shan, and J. Feng, “Repulsive guidance molecule a blockade exerts the immunoregulatory function in DCs stimulated with ABP and LPS,” *Human Vaccines & Immunotherapeutics*, vol. 12, no. 8, pp. 2169–2180, 2016.
- [33] W. Lu, H. Liang, Y. Li et al., “MicroRNA-210-3p targets RGMa to enhance the angiogenic functions of endothelial progenitor cells under hypoxic conditions,” *Frontiers in Cellular Neuroscience*, vol. 13, p. 223, 2019.
- [34] G. Zhang, R. Wang, K. Cheng et al., “Repulsive guidance molecule a inhibits angiogenesis by downregulating VEGF and phosphorylated focal adhesion kinase In Vitro,” *Frontiers in Neurology*, vol. 8, p. 504, 2017.
- [35] Y. Wang, R. Zhang, X. Xing et al., “Repulsive guidance molecule a suppresses angiogenesis after ischemia/reperfusion injury of middle cerebral artery occlusion in rats,” *Neuroscience Letters*, vol. 662, pp. 318–323, 2018.
- [36] K. Harada, Y. Fujita, and T. Yamashita, “Repulsive guidance molecule A suppresses angiogenesis,” *Biochemical and Biophysical Research Communications*, vol. 469, no. 4, pp. 993–999, 2016.
- [37] T. Korn and A. Kallies, “T cell responses in the central nervous system,” *Nature Reviews. Immunology*, vol. 17, no. 3, pp. 179–194, 2017.
- [38] T. Kubo, S. Tokita, and T. Yamashita, “Repulsive guidance molecule-a and demyelination: implications for multiple sclerosis,” *Journal of Neuroimmune Pharmacology*, vol. 7, no. 3, pp. 524–528, 2012.
- [39] R. J. M. Franklin, J. Frisén, and D. A. Lyons, “Revisiting remyelination: towards a consensus on the regeneration of CNS myelin,” *Seminars in Cell & Developmental Biology*, 2020.
- [40] S. Tanabe and T. Yamashita, “Repulsive guidance molecule-a is involved in Th17-cell-induced neurodegeneration in autoimmune encephalomyelitis,” *Cell Reports*, vol. 9, no. 4, pp. 1459–1470, 2014.
- [41] R. Kant, S. Halder, J. Fernández, J. H. Griffin, and R. Milner, “Activated protein C attenuates experimental autoimmune encephalomyelitis progression by enhancing vascular integrity and suppressing microglial activation,” *Frontiers in Neuroscience*, vol. 14, p. 333, 2020.
- [42] L. Novakova, M. Axelsson, M. Khademi et al., “Cerebrospinal fluid biomarkers of inflammation and degeneration as measures of fingolimod efficacy in multiple sclerosis,” *Multiple Sclerosis*, vol. 23, no. 1, pp. 62–71, 2017.
- [43] J. Bell, J. Spencer, R. Yates, and G. DeLuca, “The cortical blood-brain barrier in multiple sclerosis: a gateway to progression?,” *Journal of Neurology*, vol. 265, no. 4, pp. 966–967, 2018.
- [44] T. Müller, S. Barghorn, S. Lütge et al., “Decreased levels of repulsive guidance molecule a in association with beneficial effects of repeated intrathecal triamcinolone acetone application in progressive multiple sclerosis patients,” *Journal of Neural Transmission (Vienna)*, vol. 122, no. 6, pp. 841–848, 2015.
- [45] K. Pitarokoili, M. Sgodzai, T. Grüter et al., “Intrathecal triamcinolone acetone exerts anti-inflammatory effects on Lewis rat experimental autoimmune neuritis and direct anti-oxidative effects on Schwann cells,” *Journal of Neuroinflammation*, vol. 16, no. 1, p. 58, 2019.
- [46] M. Watanabe, Y. Nakamura, Z. Michalak et al., “Serum GFAP and neurofilament light as biomarkers of disease activity and disability in NMOSD,” *Neurology*, vol. 93, no. 13, pp. e1299–e1311, 2019.
- [47] E. Flanagan, P. Cabre, B. Weinshenker et al., “Epidemiology of aquaporin-4 autoimmunity and neuromyelitis optica spectrum,” *Annals of Neurology*, vol. 79, no. 5, pp. 775–783, 2016.
- [48] C. Lucchinetti, R. Mandler, D. McGavern et al., “A role for humoral mechanisms in the pathogenesis of Devic’s neuromyelitis optica,” *Brain: A Journal of Neurology*, vol. 125, no. 7, pp. 1450–1461, 2002.



- [49] H. Zhang and A. Verkman, "Eosinophil pathogenicity mechanisms and therapeutics in neuromyelitis optica," *The Journal of Clinical Investigation*, vol. 123, no. 5, pp. 2306–2316, 2013.
- [50] L. Zhang, C. Liu, C. Huang, X. Xu, and J. Teng, "miR-155 knockdown protects against cerebral ischemia and reperfusion injury by targeting MafB," *BioMed Research International*, vol. 2020, Article ID 6458204, 11 pages, 2020.
- [51] T. Wang, X. Wu, C. Yin, D. Klebe, J. H. Zhang, and X. Qin, "CRMP-2 is involved in axon growth inhibition induced by RGMa in vitro and in vivo," *Molecular Neurobiology*, vol. 47, no. 3, pp. 903–913, 2013.
- [52] T. Xiong, J. Tang, J. Zhao et al., "Involvement of the Akt/GSK-3 $\beta$ /CRMP-2 pathway in axonal injury after hypoxic-ischemic brain damage in neonatal rat," *Neuroscience*, vol. 216, pp. 123–132, 2012.
- [53] Q. Wu, T. Li, B. Gong, J. Yang, and X. Qin, "Elevated repulsive guidance molecule-a mRNA in peripheral blood mononuclear cells are associated with impaired leptomeningeal collaterals in patients with middle cerebral artery occlusions," *Annals of Palliative Medicine*, vol. 9, no. 5, pp. 2933–2942, 2020.
- [54] L. Lu, K. Xu, L. Shi et al., "Measuring Subthalamic Nucleus Volume of Parkinson's Patients and Evaluating Its Relationship with Clinical Scales at Pre- and Postdeep Brain Stimulation Treatment: A Magnetic Resonance Imaging Study," *BioMed Research International*, vol. 2021, Article ID 6646416, 7 pages, 2021.
- [55] M. T. Gabr and S. Yahiaoui, "Multitarget therapeutics for neurodegenerative diseases," *BioMed Research International*, vol. 2020, Article ID 6532827, 2 pages, 2020.
- [56] S. Muthuraju, R. Zakaria, M. K. M. Karuppan, and B. Al-Rahbi, "The role of neuroinflammation in cellular damage in neurodegenerative diseases," *BioMed Research International*, vol. 2020, Article ID 9231452, 2 pages, 2020.
- [57] T. Müller, I. Trommer, S. Muhlack, and B. Mueller, "Levodopa increases oxidative stress and repulsive guidance molecule A levels: a pilot study in patients with Parkinson's disease," *Journal of Neural Transmission*, vol. 123, no. 4, pp. 401–406, 2016.
- [58] L. Chen, B. Gao, M. Fang et al., "Lentiviral vector-induced overexpression of RGMa in the hippocampus suppresses seizures and mossy fiber sprouting," *Molecular Neurobiology*, vol. 54, no. 2, pp. 1379–1391, 2017.
- [59] Y. Lu, Q. Su, M. Li et al., "Association of SCN1A, SCN2A, and UGT2B7 polymorphisms with responsiveness to valproic acid in the treatment of epilepsy," *BioMed Research International*, vol. 2020, Article ID 8096235, 8 pages, 2020.
- [60] X. Tan, Y. Zeng, Z. Tu et al., "TRPV1 contributes to the neuroprotective effect of dexmedetomidine in pilocarpine-induced status epilepticus juvenile rats," *BioMed Research International*, vol. 2020, Article ID 7623635, 9 pages, 2020.
- [61] R. Muramatsu, T. Kubo, M. Mori et al., "RGMa modulates T cell responses and is involved in autoimmune encephalomyelitis," *Nature Medicine*, vol. 17, no. 4, pp. 488–494, 2011.
- [62] B. Trapp and K. Nave, "Multiple sclerosis: an immune or neurodegenerative disorder?," *Annual Review of Neuroscience*, vol. 31, no. 1, pp. 247–269, 2008.
- [63] S. Conrad, H. Genth, F. Hofmann, I. Just, and T. Skutella, "Neogenin-RGMa signaling at the growth cone is bone morphogenetic protein-independent and involves RhoA, ROCK, and PKC," *The Journal of Biological Chemistry*, vol. 282, no. 22, pp. 16423–16433, 2007.
- [64] R. Nohra, A. D. Beyeen, J. P. Guo et al., "RGMa and IL21R show association with experimental inflammation and multiple sclerosis," *Genes and Immunity*, vol. 11, no. 4, pp. 279–293, 2010.
- [65] R. Muramatsu, C. Takahashi, S. Miyake, H. Fujimura, H. Mochizuki, and T. Yamashita, "Angiogenesis induced by CNS inflammation promotes neuronal remodeling through vessel-derived prostacyclin," *Nature Medicine*, vol. 18, no. 11, pp. 1658–1664, 2012.
- [66] T. Müller, "Role of intraspinal steroid application in patients with multiple sclerosis," *Expert Review of Neurotherapeutics*, vol. 9, no. 9, pp. 1279–1287, 2009.
- [67] T. Misu, K. Fujihara, A. Kakita et al., "Loss of aquaporin 4 in lesions of neuromyelitis optica: distinction from multiple sclerosis," *Brain: A Journal of Neurology*, vol. 130, no. 5, pp. 1224–1234, 2007.
- [68] N. Asavapanumas and A. Verkman, "Neuromyelitis optica pathology in rats following intraperitoneal injection of NMO-IgG and intracerebral needle injury," *Acta Neuropathologica Communications*, vol. 2, no. 1, p. 48, 2014.
- [69] B. Popescu, V. Lennon, J. Parisi et al., "Neuromyelitis optica unique area postrema lesions: nausea, vomiting, and pathogenic implications," *Neurology*, vol. 76, no. 14, pp. 1229–1237, 2011.
- [70] J. Schwab, S. Conrad, P. Monnier, S. Julien, B. K. Mueller, and H. J. Schluessener, "Spinal cord injury-induced lesional expression of the repulsive guidance molecule (RGM)," *The European Journal of Neuroscience*, vol. 21, no. 6, pp. 1569–1576, 2005.
- [71] H. Nakagawa and M. Takada, "Promoting functional recovery by inhibition of repulsive guidance molecule-a after spinal cord injury," *Neural Regeneration Research*, vol. 13, no. 6, pp. 981–982, 2018.
- [72] A. Kyoto, K. Hata, and T. Yamashita, "Synapse formation of the cortico-spinal axons is enhanced by RGMa inhibition after spinal cord injury," *Brain Research*, vol. 1186, pp. 74–86, 2007.
- [73] K. Bossers, G. Meerhoff, R. Balesar et al., "Analysis of gene expression in Parkinson's disease: possible involvement of neurotrophic support and axon guidance in dopaminergic cell death," *Brain Pathology*, vol. 19, no. 1, pp. 91–107, 2009.
- [74] A. J. Santiago-Lopez, "A repulsive environment induces neurodegeneration of midbrain dopaminergic neurons," *The Journal of Neuroscience*, vol. 38, no. 6, pp. 1323–1325, 2018.
- [75] E. Y. Van Battum, S. Brignani, and R. J. Pasterkamp, "Axon guidance proteins in neurological disorders," *Lancet Neurology*, vol. 14, no. 5, pp. 532–546, 2015.
- [76] M. Y. Song, F. F. Tian, Y. Z. Wang, X. Huang, J. L. Guo, and D. X. Ding, "Potential roles of the RGMa-FAK-Ras pathway in hippocampal mossy fiber sprouting in the pentylentetrazole kindling model," *Molecular Medicine Reports*, vol. 11, no. 3, pp. 1738–1744, 2015.

## Retraction

# Retracted: Predicting Decreased Activities of Daily Living in Patients with Moyamoya Disease after Revascularization: Development and Assessment of a New Predictive Nomogram

### BioMed Research International

Received 12 March 2024; Accepted 12 March 2024; Published 20 March 2024

Copyright © 2024 BioMed Research International. This is an open access article distributed under the Creative Commons Attribution License, which permits unrestricted use, distribution, and reproduction in any medium, provided the original work is properly cited.

This article has been retracted by Hindawi following an investigation undertaken by the publisher [1]. This investigation has uncovered evidence of one or more of the following indicators of systematic manipulation of the publication process:

- (1) Discrepancies in scope
- (2) Discrepancies in the description of the research reported
- (3) Discrepancies between the availability of data and the research described
- (4) Inappropriate citations
- (5) Incoherent, meaningless and/or irrelevant content included in the article
- (6) Manipulated or compromised peer review

The presence of these indicators undermines our confidence in the integrity of the article's content and we cannot, therefore, vouch for its reliability. Please note that this notice is intended solely to alert readers that the content of this article is unreliable. We have not investigated whether authors were aware of or involved in the systematic manipulation of the publication process.

Wiley and Hindawi regrets that the usual quality checks did not identify these issues before publication and have since put additional measures in place to safeguard research integrity.

We wish to credit our own Research Integrity and Research Publishing teams and anonymous and named external researchers and research integrity experts for contributing to this investigation.

The corresponding author, as the representative of all authors, has been given the opportunity to register their agreement or disagreement to this retraction. We have kept a record of any response received.

### References

- [1] Y. Zhao, D. Yang, G. Li, P. Zhao, X. Luan, and H. Li, "Predicting Decreased Activities of Daily Living in Patients with Moyamoya Disease after Revascularization: Development and Assessment of a New Predictive Nomogram," *BioMed Research International*, vol. 2021, Article ID 6624245, 8 pages, 2021.

## Research Article

# Predicting Decreased Activities of Daily Living in Patients with Moyamoya Disease after Revascularization: Development and Assessment of a New Predictive Nomogram

Yani Zhao <sup>1</sup>, Dongliang Yang <sup>2</sup>, Gang Li <sup>1</sup>, Peng Zhao <sup>1</sup>, Xiaorong Luan <sup>3</sup>,  
and Haiyan Li <sup>1</sup>

<sup>1</sup>Department of Neurosurgery, Qilu Hospital of Shandong University, Jinan 250012, China

<sup>2</sup>Cangzhou Medical College, Cangzhou 061000, China

<sup>3</sup>Department of Infection Management Office, Qilu Hospital of Shandong University, Jinan 250012, China

Correspondence should be addressed to Xiaorong Luan; 199162000814@sdu.edu.cn and Haiyan Li; 199462000306@sdu.edu.cn

Received 9 December 2020; Revised 1 March 2021; Accepted 12 March 2021; Published 30 April 2021

Academic Editor: Yuzhen Xu

Copyright © 2021 Yani Zhao et al. This is an open access article distributed under the Creative Commons Attribution License, which permits unrestricted use, distribution, and reproduction in any medium, provided the original work is properly cited.

The aim of this study was to develop and validate a nomogram model to predict the risk of decreased activities of daily living (ADLs) in patients with moyamoya disease (MMD) following revascularization. The nomogram model was constructed based on data from 292 patients with MMD that were treated at Qilu Hospital of Shandong University from January 2018 to June 2019. The prediction model was assessed using a dataset of 119 patients with MMD collected from July 2019 to June 2020. Patients were evaluated with a general information questionnaire and the Mini Mental Status Examination, Hospital Anxiety and Depression Scale, Social Support Rating Scale, and ADL Scale. Multivariable logistic regression analysis was applied to build a prediction model incorporating the features selected in the least absolute shrinkage and selection operator regression model. Discrimination, calibration, and clinical usefulness of the prediction model were assessed using receiver operating characteristic (ROC) curves, calibration plots, and decision curve analysis. Predictors contained in the nomogram included gender, age, monthly income, hypertension, and cognitive function and depression scores. The areas under the ROC curves of the training and testing datasets were 0.938 and 0.853, respectively. The prediction model displayed good calibration, and the decision curve analysis showed that it had a wide range of clinical applications. This novel predictive could be conveniently used to predict the risk of the decreased living activity ability in patients with MMD.

## 1. Introduction

Moyamoya disease (MMD) is a chronic occlusive cerebrovascular disease characterized by progressive stenosis or occlusion of the bilateral internal carotid arteries, anterior cerebral arteries, and middle cerebral arteries; it often manifests as single or repeated attack of hemorrhagic or ischemic stroke [1, 2]. MMD has a relatively high incidence in East Asia [3]. Studies demonstrated that vascular reconstruction can effectively decrease the incidence of stroke [4, 5], but neurological dysfunction due to stroke, postoperative complications, and other reasons significantly influence patients' activities of daily living (ADLs) and even lead to disability [6]. This requires considerable social resources for rehabilitation

and nursing, which places a heavy burden on both families and healthcare resources [7]. Therefore, it is important to predict and evaluate the postoperative ADLs of MMD patients.

ADLs are the daily activities that individuals perform to care for themselves and maintain their lives. The ability or inability to perform ADLs is an important functional measurement. It is also widely used to predict the prognosis and evaluate the self-care ability of stroke patients [8]. However, few studies have focused on the postoperative ADLs of patients with MMD. A model is needed to evaluate the survival status of patients after vascular reconstruction to determine which factors influence patient ADLs.

Nomograms are used to establish relevant prognostic models based on disease characteristics to predict patient

outcomes. They have been widely used to predict survival [9]. However, few groups have used nomograms to predict the quality of life of patients after surgery for MMD.

In our study, we aimed to (i) explore the influencing factors and weights of ADL in patients with MMD after vascular reconstruction, (ii) develop and validate a prediction model for Chinese MMD patients, and (iii) use simple and effective nomograms to predict postoperative ADL status in MMD patients. This will enable us to prevent or reduce the occurrence of inability to perform ADL in MMD patients.

## 2. Materials and Methods

**2.1. Patients.** Study subjects were selected with a convenience sampling method. All the patients included in our study were treated in the Department of Neurosurgery of Qilu Hospital of Shandong University from January 2018 to June 2020. A face-to-face questionnaire survey was administered 3 months after surgery. The inclusion criteria were as follows: (i) age  $\geq 18$ , (ii) diagnosed with MMD based on digital subtraction angiography, and (iii) vascular reconstruction with superficial temporal artery-middle cerebral artery bypass graft performed for the first time. Patients with other severe diseases, secondary vascular reconstruction, or severe cognitive dysfunction were excluded. The predictive model was constructed based on a training dataset including patients who met the inclusion criteria. The same inclusion criteria were used to select a testing dataset that included patients treated at Qilu Hospital of Shandong University between July 2019 and June 2020.

This study was approved by the Ethics Committee of Qilu Hospital of Shandong University (No. 2016.109), and informed consent was obtained from all patients.

**2.2. Sample Size.** The sample size was determined based on the principle that it should be 5-10 times the number of independent variables [10]. Our study included 21 variables, so the sample size should be at least 210. Based on the estimation that  $\sim 20\%$  of patients would reject the questionnaire, we determined the sample size should be at least 252.

### 2.3. Research Methods

**2.3.1. General Data Questionnaire.** We designed the general data questionnaire based on the information and characteristics of MMD. It included gender, age, monthly income, hypertension, diabetes, heart disease, and many other factors. The diagnosis of complications was confirmed by two doctors according to clinical diagnostic criteria.

**2.3.2. ADL Scale.** ADLs were evaluated with the ADL scale, which consists of 14 items including physical activity ability (including 6 items like eating and dressing) and instrumental daily activity ability (including 8 items such as taking buses and shopping). Each item was scored as 1-4 points. A score  $\geq 14$  was considered to indicate a decline of ADLs. The Cronbach's alpha of this scale was 0.940.

**2.3.3. Mini Mental Status Examination (MMSE).** The MMSE was used to test cognitive function. It has 30 items that

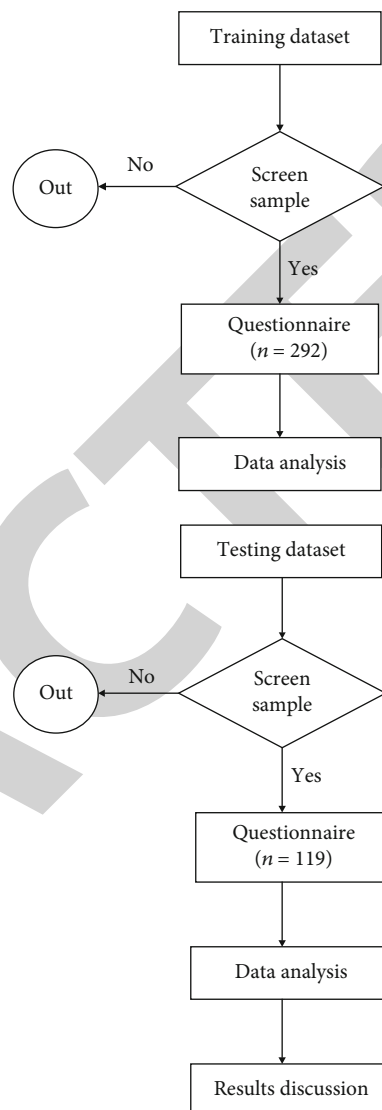


FIGURE 1: Research process flow chart.

queries abilities in 5 dimensions (orientation, attention, computing power, recall ability, and language ability). Each item is scored as 0 or 1 point, with a total score of 0 to 30 points. The Cronbach's alpha of this scale was 0.743.

**2.3.4. Hospital Anxiety and Depression Scale (HADS).** The HADS is a reliable tool for evaluating anxiety and depression. It is divided into two subscales (anxiety and depression), with seven items in each. The Cronbach's alpha of the anxiety and depression subscales were 0.817 and 0.832, respectively.

**2.3.5. Social Support Rating Scale (SSRS).** This scale has good reliability and validity in evaluating the degree of social support in patients with cerebrovascular disease. There are 3 dimensions (subjective support, objective support, and utilization of support) and 10 items. The Cronbach's alpha of the scale was 0.812.

TABLE 1: General characteristics of the training and testing sets.

Variables	Training set ( $n = 292$ )		Testing set ( $n = 119$ )	
	Number of cases/ $(\bar{x} \pm s)$	%	Number of cases	%
Gender				
Male	146	50	60	50.4
Female	146	50	59	49.6
Age				
$\leq 44$	87	29.8	35	29.4
45-59	140	47.9	59	49.6
$\geq 60$	65	22.3	25	21.0
Level of education				
Never attended school	36	12.3	13	10.9
Primary or junior high school	172	58.9	68	57.1
Senior high school and above	84	28.8	38	32.0
Marital status				
Married	283	96.9	113	95.0
Unmarried/divorced/widowed	9	3.1	6	5.0
Residence				
City	93	31.8	36	30.3
Village	114	39.0	48	40.3
County/town	85	29.1	35	29.4
Profession				
Physical labor	121	41.4	40	33.6
Professional worker	90	30.8	47	39.5
Retired/unemployed	19	6.5	12	10.1
Other career	62	21.2	20	16.8
Payment				
Worker healthcare	136	46.6	54	45.4
Resident healthcare	147	50.3	49	41.2
Other	9	3.1	16	13.4
Household per capita monthly income				
$\leq 1000$ RMB	112	38.4	45	37.8
1001-3000 RMB	80	27.4	30	25.2
$> 3000$ RMB	100	34.2	44	37.0
Lesion type				
Cerebral hemorrhage	124	42.5	52	43.7
Cerebral ischemia	168	57.5	67	56.3
Cerebral infarction				
Yes	88	30.1	34	28.6
Diabetes				
Yes	34	11.6	21	17.6
Hypertension				
Yes	94	32.2	41	34.5
Heart disease				
Yes	13	4.5	12	10.1
Time between disease onset and surgery				
$\leq 6$ weeks	74	25.3	31	26.1
6-12 weeks	115	39.4	49	41.2
$> 12$ weeks	103	35.3	39	32.8
Operation side				
Right	123	42.1	52	43.7



TABLE 1: Continued.

Variables	Training set ( $n = 292$ )		Testing set ( $n = 119$ )	
	Number of cases/ $(\bar{x} \pm s)$	%	Number of cases	%
Postoperative complications				
Yes	24	8.2	14	11.8
Regular exercise				
No	150	51.4	52	43.7
Cognitive function score	23.75 $\pm$ 5.00		23.98 $\pm$ 4.53	
Anxiety score	5.53 $\pm$ 3.34		5.10 $\pm$ 3.01	
Depression scores	6.78 $\pm$ 3.87		6.42 $\pm$ 3.46	
Social support score	37.58 $\pm$ 6.48		36.31 $\pm$ 6.95	
Decreased ability in daily life	178	61.0	67	56.3

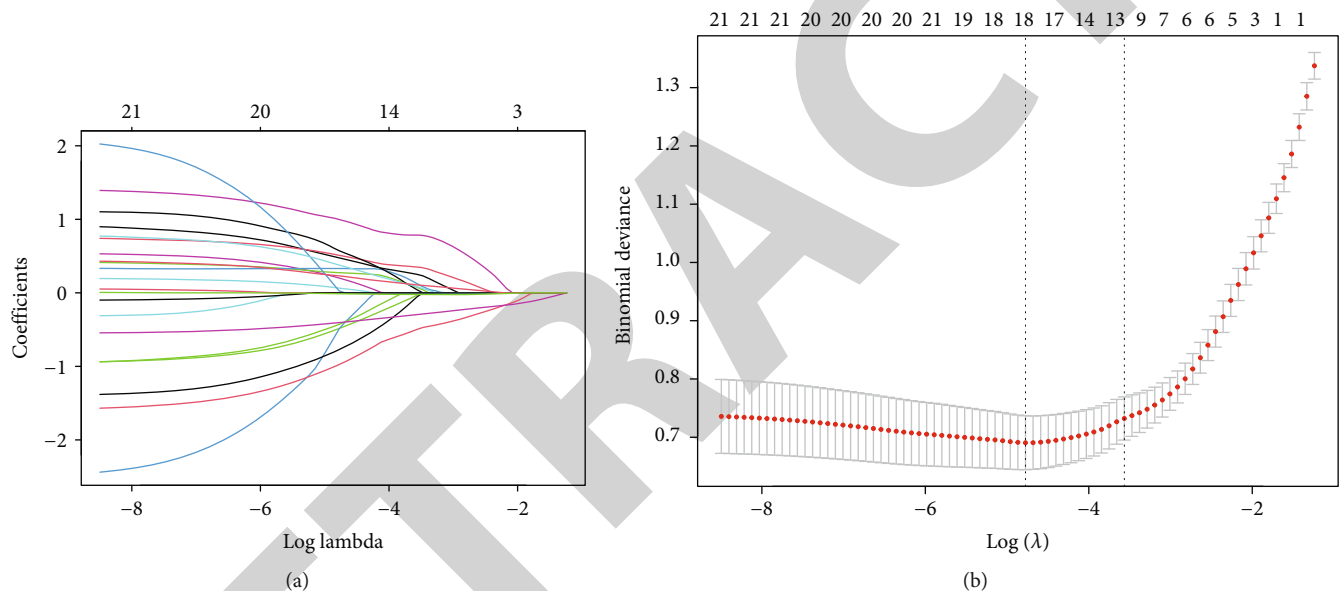


FIGURE 2: Variable selection using the LASSO regression model. (a) The selection of the best parameter in the LASSO model ( $\lambda$ ) uses a 10-fold cross-validation approach. (b) Seven variables with coefficients not equal to zero were selected through LASSO regression.

**2.4. Statistical Analysis.** Statistical analysis was performed using R software (Version 3.4.4). Normally distributed data are presented as the means and standard deviations ( $\bar{x} \pm s$ ), and quantitative data are expressed as frequency and percentage (%). The least absolute shrinkage and selection operator (LASSO) method was used to select optimal predictive features among risk factors. Features with nonzero coefficients in the LASSO regression model were selected; then multivariable logistic regression analysis was used to build a prediction model by incorporating the selected features. All potential predictors were applied to develop a model to predict decreased ADL risk. The discrimination, calibration, and clinical usefulness of the predicting model were assessed using receiver operative characteristic (ROC) curves, calibration plots, and decision curve analysis. The specific research process is shown in Figure 1.

### 3. Results

**3.1. Patient Characteristics.** A total of 411 patients with MMD were included in our study, with 292 patients in the training dataset and 119 patients in the testing dataset. The male:female ratio was balanced, and the patients ranged in age from 23 to 66, with a mean age of  $50.11 \pm 10.04$  years old. Nearly 60 percent of patients had decreased ADL post-operatively. The general characteristics of the patients in the training and testing sets are shown in Table 1.

**3.2. Identifying Independent Predictors.** Seven potential predictors were identified with LASSO regression, including gender, age, family per capita monthly income, hypertension, cognitive function, depression, and social support scores (Figure 2). These variables were incorporated into multivariate logistic regression, which revealed six independent

TABLE 2: Multivariate logistic regression results regarding decreased ADLs in patients with MMD.

Variable	Odds ratio (95% confidence interval)	P
Female gender	2.24 (1.06, 4.84)	0.037
Age	2.19 (1.30, 3.77)	0.004
Family per capita monthly income	0.44 (0.26, 0.72)	0.002
Hypertension	4.04 (1.74, 9.87)	0.001
Cognitive function score	0.61 (0.50, 0.73)	<0.001
Depression score	1.30 (1.12, 1.51)	0.001

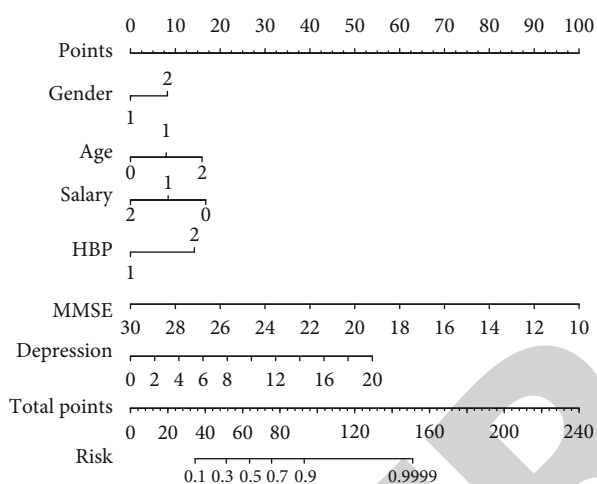


FIGURE 3: Nomogram for predicting declined ADLs.

predictors. As shown in Table 2, females, patients with hypertension, older age, and higher depression scores increased the risk of ADL decline. Conversely, patients with higher income and good cognitive function were at the lower risk of decreased ADL.

3.3. *Development and Evaluation of the Nomogram Prediction Model.* According to the multivariate logistic regression analysis, six independent predictors (gender, age, monthly income, hypertension, cognitive function, and depression scores) were combined to develop the nomogram risk prediction model (Figure 3). The assignment and scores of each predictor are shown in Table 3. In this study, the calibration curves (Figure 4) of the ADL risk prediction model for MMD patients were generated in both the training and testing datasets. The results showed good consistency and a high degree of calibration, indicating that the prediction model was more accurate. Then the ROC curves of the prediction model in the training and testing data sets were analyzed to evaluate the model’s diagnostic effect (Figure 5). The areas under the ROC curves in both groups were >0.8, suggesting that this model could predict postoperative ADLs in MMD patients. The decision curve analysis indicated that the prediction model had a wide range of applications

TABLE 3: Values assigned to each variable in the nomogram model.

Variable	Assignment	Score/risk factor
Gender	1 = male	0
	2 = female	8
Age	0 ≤ 44	0
	1 = 45-59	8
	2 ≥ 60	16
Household per capita monthly income	0 ≤ 1000 RMB	17
	1 = 1001-3000 RMB	8
	2 ≥ 3000 RMB	0
Hypertension	1 = no	0
	2 = yes	14
Cognitive function score	10	100
	20	50
	30	0
Depression score	0	0
	10	27
Total score	20	54
	35	Risk of ADL decline = 0.1
	57	Risk of ADL decline = 0.5
	66	Risk of ADL decline = 0.7

(Figure 6). Collectively, the findings show that the nomogram prediction model constructed with the above six indicators had an accurate predictive value for ADLs in MMD patients.

#### 4. Discussion

ADLs are an important indicator to evaluate the recovery of MMD patients who experienced a stroke. It is crucial to identify high-risk subjects in advance and provide timely interventions, therefore improving their quality of life. We developed and validated a prediction model for MMD patients by evaluating ADLs. Predictors contained in the nomogram included gender, age, monthly income, hypertension status, and cognitive function and depression scores; it can help clinicians determine the high-risk population and provide a foundation for sound medical treatment. We also validated our nomogram using ROC curves, calibration plots, and decision curve analysis.

Our study showed that ~60% of MMD patients with revascularization had decreased ADLs, which was in accordance with a previous study [11]. Because decreased ADLs significantly influence patient quality of life, it is important to clarify which factors are associated with the ADLs of MMD patients who underwent vascular reconstruction. However, few studies have focused on the postoperative prognosis of MMD patients. We evaluated the ADLs of MMD patients following revascularization and identified

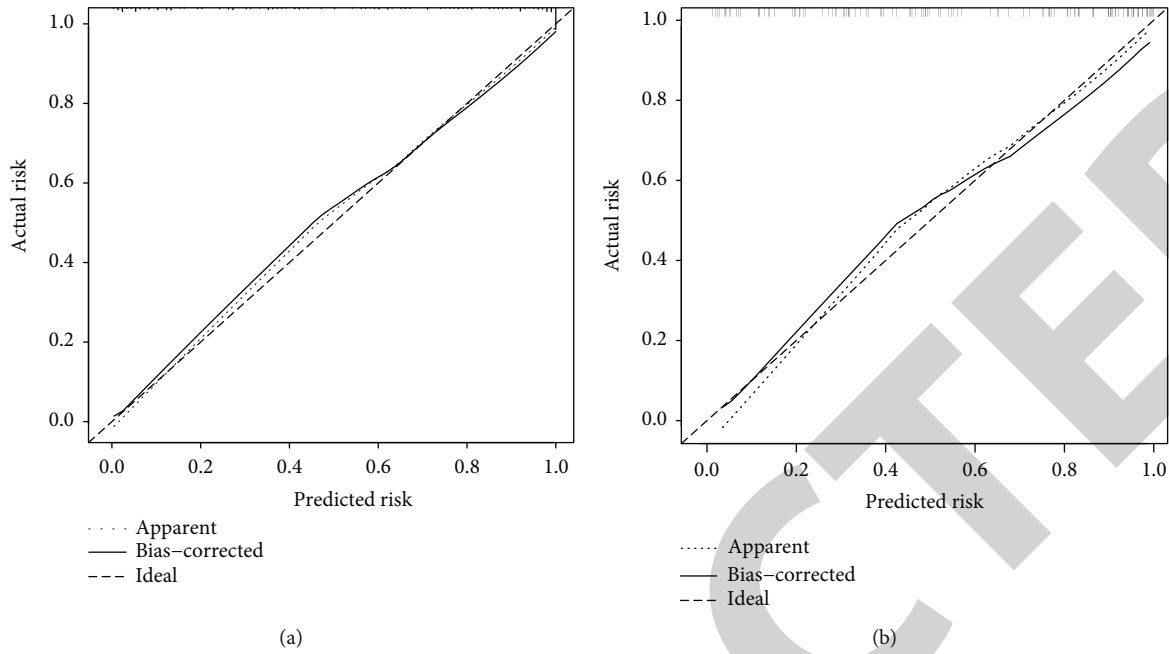


FIGURE 4: Establishment and validation of the prediction model. (a) The prediction model was calibrated in the training dataset. (b) The prediction model in the validation set of the calibration diagram. Note: the *x*-axis represents the prediction risk of ADL function decline, the *y*-axis represents the actual risk of ADL function decline, the diagonal dashed line represents the ideal prediction effect of the theoretical model, and the solid line represents the performance of the nomogram. A closer diagonal dashed line indicates a stronger prediction effect.

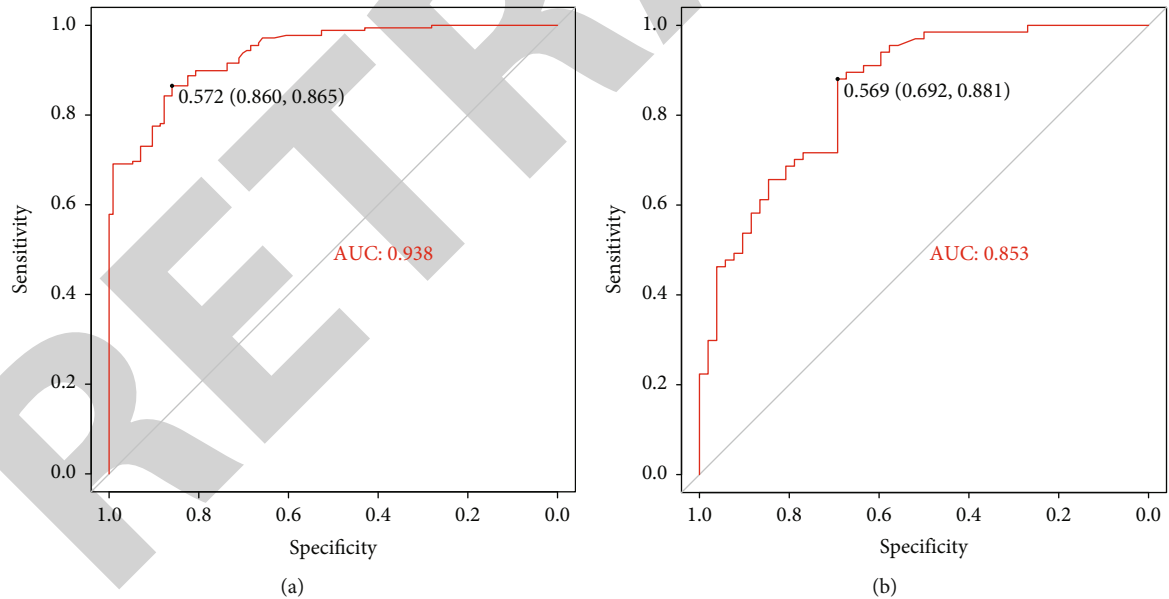


FIGURE 5: ROC curves of the predictive model. (a) Training dataset model. (b) Testing dataset model.

the factors that affected patient ADLs by focusing on general demographics, clinical data, psychology, and sociology. The variables of this model are easy to obtain and integrate multiple predictive variables into the line diagram, which is intuitive and convenient for calculation.

The six predictive factors included in the nomogram deserve more attention from medical workers, especially the

cognitive function and depression scores. We found that MMD patients with lower cognitive function were more likely to have decreased ADLs after surgery. Some researchers posited that cognitive dysfunction would influence ADLs in MMD patients [12]. Another study showed that cognitive impairment seriously affected patient quality of life [13]. A possible reason is that the typical pathological changes of

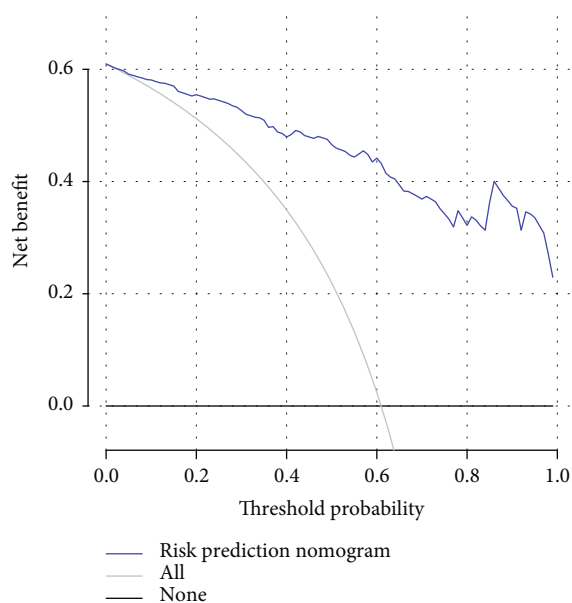


FIGURE 6: Decision curve of the prediction model.

MMD include stenosis or occlusion of critical arteries resulted in long-term chronic cerebral ischemia and stroke, therefore influencing cognitive function. Other studies reported that vascular reconstruction did not improve cognitive function [14, 15], and the patients usually had impairments in executive function, concentration, memory, computing power, and logistical ability, all of which decrease independent living abilities.

Depression is a common complication of cerebrovascular disease, especially stroke. As a unique chronic progressive cerebrovascular disease, MMD is likely to induce depression [16]. We found that depression was an important factor that contributed to decreased ADL, which was in accordance with Ezema et al.'s study [17]. Since depressed patients experience negative emotions and a lack of confidence, motivation, and enthusiasm to participate in daily activities, ADL recovery is changing. Moreover, depression is likely to contribute to cognitive impairment, which further influences ADL recovery [16, 17].

Previous studies based on normal populations demonstrated that patients with hypertension were more likely to have decreased ADLs [18, 19]. We also found that hypertension was an independent risk factor for decreased ADLs in MMD patients. A reasonable explanation may be that hypertensive patients face the risk of functional decline, and there are more complications leading to the decline of ADL function [18]. Furthermore, it was reported that hypertension could increase the risks of ADL decline, postoperative cerebral infarction, and complications, which can result in muscle strength decline, aphasia, and other neurological issues.

General demographic data such as gender, age, and income were identified as key predictive factors for ADL. We found that females were more likely to have decreased ADL after surgery for MMD. Several previous studies also

reported that female patients had worse prognoses and lower ADLs than male patients [20–22]. This may be due to the fact that female patients have weaker constitutions and are less able to withstand emergent events. MMD is more likely to be diagnosed in children and young adults, and the risk of postoperative ADL decline increases with age [23]. Conversely, higher family income was associated with a reduced likelihood of decreased ADL. This result was not completely in accordance with previous research, and the reason may be that most patients in our study were low-income residents from rural areas.

In view of the high rate of acute ADL decline in MMD patients and the current lack of predictive tools, clinicians can use this model to predict patient ADL status. The possible clinical application is to strengthen cognitive training, pay more attention to psychological factors, encourage patients to actively accept treatment, and address depression symptoms. Moreover, it is also important to control blood pressure in patients with MMD to maintain the cerebral perfusion. Furthermore, women, older patients, and those with low income should be considered high-risk populations and closely followed.

Our results should be considered in the context limitations. The data were collected at a single research center, although they were relatively systematic and complete. And the prediction model was validated using patient data from the same research center, which may partly reduce its generalizability.

## 5. Conclusion

We developed a novel prediction model to determine the risk of decreased ADLs in MMD patients following revascularization. This nomogram incorporates gender, age, monthly income, hypertension status, and cognitive function and depression scores and can be conveniently used to predict the risk of the decreased ADLs in patients with MMD. Based on this nomogram, interventions and treatments could be employed to prevent decreased ADLs and improve patient quality of life.

## Data Availability

Source data are available from the corresponding author upon reasonable request.

## Conflicts of Interest

The authors declare that they have no competing interests.

## Authors' Contributions

Yani Zhao and Dongliang Yang contributed equally to this work.

## References

- [1] L. Duan, X. Y. Bao, W. Z. Yang et al., "Moyamoya disease in China: its clinical features and outcomes," *Stroke*, vol. 43, no. 1, pp. 56–60, 2012.

## Research Article

# The Relationship of Large-Artery Atherothrombotic Stroke with Plasma Trimethylamine N-Oxide Level and Blood Lipid-Related Indices: A Cross-Sectional Comparative Study

Dongjuan Xu,<sup>1</sup> Wenfeng Zhao,<sup>2</sup> Juexian Song<sup>1</sup>,<sup>2</sup> Lu Yin,<sup>3</sup> Kun Wang,<sup>2,4,5</sup> Lianyan Wei,<sup>1</sup> Yunyun Xu,<sup>1</sup> Hongfei Li,<sup>1</sup> Baoquan Min,<sup>2,5</sup> Ning Tang,<sup>2,6</sup> Xiaoyan Jiang,<sup>2,7</sup> Hui Liu,<sup>2,8</sup> Shuo Yan,<sup>2,9</sup> Haixia Leng,<sup>2,5</sup> Qing Xue,<sup>2,5</sup> Mao Peng,<sup>2,5</sup> and Hongxing Wang<sup>1</sup>,<sup>2,5,10</sup>

<sup>1</sup>Department of Neurology, Dongyang People's Hospital, Wenzhou Medical University, Zhejiang, China 322100

<sup>2</sup>Department of Neurology, Xuanwu Hospital, Capital Medical University, Beijing, China 100053

<sup>3</sup>Medical Research & Biometrics Centre, National Centre for Cardiovascular Diseases, Fuwai Hospital, Peking Union Medical College & Chinese Academy of Medical Sciences, Beijing, China 102300

<sup>4</sup>Department of Neurology, Beijing Puren Hospital, Beijing, China 100062

<sup>5</sup>Beijing Psychosomatic Disease Consultation Center, Xuanwu Hospital, Capital Medical University, Beijing, China 100053

<sup>6</sup>Department of Neurology, The First People's Hospital of Yunnan Province, The Affiliated Hospital of Kunming University of Science and Technology, Yunnan, China 650032

<sup>7</sup>Department of Neurology, Shexian Hospital of Hebei Province, Hebei, China 056400

<sup>8</sup>Department of Neurology, Rongcheng Hospital of Hebei Province, Hebei, China 071700

<sup>9</sup>Department of Neurology, The Third Affiliated Hospital of Shenzhen University, Guangdong, China 518000

<sup>10</sup>Institute of Sleep and Consciousness Disorders, Beijing Institute for Brain Disorders, Capital Medical University, Beijing, China 100053

Correspondence should be addressed to Hongxing Wang; wanghongxing@xwh.ccmu.edu.cn

Dongjuan Xu and Wenfeng Zhao contributed equally to this work.

Received 8 February 2021; Revised 29 March 2021; Accepted 11 April 2021; Published 23 April 2021

Academic Editor: Yuzhen Xu

Copyright © 2021 Dongjuan Xu et al. This is an open access article distributed under the Creative Commons Attribution License, which permits unrestricted use, distribution, and reproduction in any medium, provided the original work is properly cited.

**Objective.** The role of trimethylamine N-oxide (TMAO) in cardiovascular diseases has been highlighted. Nevertheless, the associations of large-artery atherosclerotic (LAA) stroke with TMAO and blood lipid-related indices are little investigated. **Methods.** A cross-sectional comparative study was performed on 50 patients with LAA stroke and 50 healthy controls. Basic demographic data, common vascular risk factors, and blood lipid-related indices were collected. Plasma TMAO was detected through liquid chromatography tandem mass spectrometry. Multivariable unconditional logistic regression analyses were run to assess the associations of LAA stroke with plasma TMAO level and blood lipid-related indices. The area under the curve (AUC) of the receiver operating characteristic (ROC) was computed to assess the diagnostic performance of plasma TMAO level and blood lipid-related indices for LAA stroke. **Results.** Compared with healthy controls, the elevated plasma TMAO level (odds ratio [OR], 7.03; 95% confidence interval [CI], 2.86, 17.25;  $p < 0.01$ ) and Apo-B (OR, 1.74; 95% CI, 1.06, 2.85;  $p = 0.03$ ) were observed in LAA stroke patients, while lower Apo-A1 (OR, 0.56; 95% CI, 0.34, 0.91;  $p = 0.02$ ), Apo-A1 to Apo-B ratio (OR, 0.29; 95% CI, 0.15, 0.56;  $p < 0.01$ ), and HDL-C (OR, 0.56; 95% CI, 0.35, 0.91;  $p = 0.02$ ) were found in LAA stroke patients after adjusted for age and gender. Moreover, plasma TMAO (AUC, 0.89; 95% CI, 0.83, 0.95), Apo-A1 (AUC, 0.81; 95% CI, 0.72, 0.89), Apo-B (AUC, 0.81; 95% CI, 0.73, 0.90), Apo-A1 to Apo-B ratio (AUC, 0.85; 95% CI, 0.78, 0.93), and HDL-C (AUC, 0.81; 95% CI, 0.72, 0.89) showed good diagnostic values for LAA stroke in adjusted models. **Conclusions.** The plasma TMAO level, Apo-A1, Apo-B, and HDL-C are important biomarkers for LAA stroke patients.



## 1. Introduction

Stroke is a significant cause of death worldwide [1], and large-artery atherosclerosis is a significant cause of ischemic stroke [2, 3], approximately 15% of all ischemic strokes [2]. Large-artery atherosclerotic (LAA) stroke is one common stroke in China [3], and the most common areas orderly are the basilar artery, the internal carotid arteries, the middle cerebral arteries, the intracranial vertebral arteries, the posterior cerebral arteries, and the anterior cerebral arteries [3]. Atherosclerosis is a pathologic process causing LAA stroke and the most common cause of in situ regional diseases within the extracranial and intracranial arteries that provide the brain [3]. Many factors are involved in the pathogenesis of atherosclerosis [3, 4]. Of them, lipid abnormality plays a critical role in the development of atherosclerosis [4, 5].

Recently, more attention on the association of plasma trimethylamine *N*-oxide (TMAO) with the pathogenesis of cardiovascular disease has been attracted [6–10]. Previous reports showed that plasma TMAO, produced in the liver, has associations with cardiovascular disease [11], atherothrombotic diseases [7], ischemic brain injury secondary to carotid artery stenting [12], and stroke severity and infarct volume in patients with acute ischemia [13]. Plasma TMAO directly causes platelet hyperreactivity and increases thrombosis risks in animal models and healthy subjects [14]. It may also indicate coronary plaque vulnerability and development in patients with coronary artery disease [15]. Moreover, it is associated with atherosclerosis formation [10, 16–18], which causes the stenosis of large artery as the reason for LAA stroke.

On the above grounds, we speculate that plasma TMAO level and blood lipid-related indices may be associated with LAA stroke patients. Therefore, in this cross-sectional comparative study, we aimed to investigate whether circulating TMAO level and blood lipid-related indices are associated with LAA stroke.

## 2. Methods

**2.1. Study Design and Participants.** This comparative study was performed from October 2018 to November 2019. All subjects were enrolled from two research centers in China (Dongyang People's Hospital of Wenzhou Medical University and Xuanwu Hospital of Capital Medical University). The local Ethics Committees of Xuanwu Hospital, Capital Medical University (LYS2018008), and Dongyang People's Hospital, Wenzhou Medical University (2017-KY-036), approved the study protocols. All subjects and/or their legal representatives provided written informed consent.

The 50 LAA stroke patients who suffered acute cerebral ischemia, meeting the stroke diagnostic criteria formulated by the Chinese cerebrovascular disease classification and were validated by magnetic resonance imaging (MRI) and/or computed tomography (CT) scan [19], were sequentially enrolled. The inclusion criteria were as follows: (1) aged 18 years or older, (2) Han Chinese, (3) no limitation on gender, (4) LAA stroke was diagnosed based on the TOAST classification with evidence of cerebral infarction confirmed by

MRI and/or CT [20], and (5) carotid artery stenosis with a narrowing greater than 70% lumen were responsible for these LAA stroke patients [21]. The exclusion criteria included the following: (1) other types of cerebrovascular diseases (e.g., cerebral hemorrhage, transient ischemic attack, cerebral aneurysm, or cerebrovascular malformation), (2) severe systemic diseases (such as a tumor and infectious or inflammatory diseases), (3) known embolic source (aortic arch, cardiac, or carotid), (4) consumption with probiotics or antibiotics within one month before admission, contraindications to MRI (e.g., any implanted metal devices), (5) participation in any clinical study concurrently, (6) inability to understand the study, (7) severe physical diseases (including congestive cardiac failure, respiratory failure, renal failure, and liver dysfunction). The enrolled patients received the best medical management in the stroke centers. All patients received acute treatment and secondary prevention of stroke according to Chinese guidelines during hospitalization and after discharge.

50 healthy controls were recruited from relatives of outpatients or inpatients (including their immediate family members). Their inclusion criteria were as follows: (1) aged 18 years or older, (2) Han Chinese, (3) no limitation on gender, (4) no history of cerebrovascular diseases, (5) no history of atherosclerotic diseases in the carotid arteries, (6) no the atrial fibrillation, and (7) regular physical examinations. Exclusion criteria were not different from the exclusion criteria of the stroke patient group.

**2.2. Measurement of Blood Lipid-Related Indices and Plasma TMAO Level.** The overnight fasting blood samples were collected for routine blood lipid-related indices at 6: 00 to 7: 00 AM before breakfast. Plasma was prepared from the blood of EDTA tube and kept at  $-80^{\circ}\text{C}$  until examination. Plasma TMAO level was qualified via stable isotope dilution liquid chromatography tandem mass spectrometry, consistent with the previous reported [12, 13]. In brief, the mixture of  $80\ \mu\text{L}$ ,  $10\ \mu\text{mol/L}$  d9-TMAO, and  $20\ \mu\text{L}$  plasma was vortexed for 1 minute. The supernatant was centrifuged at  $15,000 \times g$  at  $4^{\circ}\text{C}$  for 25 min and then transferred to a new sample bottle for the check. The 10 mL of supernatant was injected directly into a silica column at a flow rate of  $0.8\ \text{mL/min}$  with 80% A (0.1% formic acid in water) and 20% B (methanol). TMAO and d9-TMAO were detected by the positive multiple reaction monitoring mass spectrometry mode by characteristic precursor–product transitions including  $m/z$  76/58 and  $m/z$  85/66. For detection of TMAO concentration, a standard curve using multiknown concentrations of TMAO was used. The median (interquartile range) of healthy participants' reference values was  $2.8$  ( $1.9$ – $4.8$ )  $\mu\text{mol/L}$ . The intra-assay and interassay coefficients of variation were 1.9%–5.6% and 2.9%–8.4%, respectively. Testers were blind to all subjects' clinical data.

**2.3. Calculation of the Volume of Infarct and the Area of Carotid Atherosclerotic Plaque.** Imaging acquisition details were standardized in both sites. The area of carotid artery plaque was measured via the common color Doppler ultrasound system by measuring the areas of unstable and stable

TABLE 1: General characteristics.

Characteristics	Stroke patients ( $n = 50$ )	Healthy controls ( $n = 50$ )	$p^1$
Male sex, % ( $n$ )	70.00 (35)	28.00 (14)	<0.01
Age, years, mean $\pm$ SD	63.20 $\pm$ 12.00	57.36 $\pm$ 10.65	0.01
Overweight or obesity, % ( $n$ )	32.00 (16)	20.00 (10)	0.43
Smoking, % ( $n$ )	38.00 (19)	4.00 (2)	<0.01
Alcohol, % ( $n$ )	32.00 (16)	10.00 (5)	<0.01
Diabetes, % ( $n$ )	42.00 (21)	8.00 (4)	<0.01
Hypertension, % ( $n$ )	72.00 (36)	26.00 (13)	<0.01
Volume of acute cerebral infarction, mm <sup>3</sup> , mean $\pm$ SD	25.02 $\pm$ 49.50	0.68 $\pm$ 0.82	<0.01
Area of carotid artery plaque, mm <sup>2</sup> , mean $\pm$ SD	61.42 $\pm$ 44.27	60.67 $\pm$ 42.71	0.95
TMAO, ng/mL, mean $\pm$ SD	2659.51 $\pm$ 976.81	1484.75 $\pm$ 648.87	<0.01
Lp-a, g/L, mean $\pm$ SD	131.52 $\pm$ 90.83	33.38 $\pm$ 10.50	<0.01
Apo-A1, g/L, mean $\pm$ SD	1.04 $\pm$ 0.22	1.18 $\pm$ 0.26	<0.01
Apo-B, g/L, mean $\pm$ SD	1.00 $\pm$ 0.26	0.83 $\pm$ 0.28	<0.01
Apo-A1/B ratio, mean $\pm$ SD	1.03 $\pm$ 0.27	1.43 $\pm$ 0.42	<0.01
TC, mmol/L, mean $\pm$ SD	4.70 $\pm$ 1.12	4.37 $\pm$ 0.81	0.12
HDL-C, mmol/L, mean $\pm$ SD	1.02 $\pm$ 0.25	1.16 $\pm$ 0.28	<0.01
LDL-C, mmol/L, mean $\pm$ SD	2.91 $\pm$ 1.02	2.57 $\pm$ 0.80	0.07
TG, mmol/L, mean $\pm$ SD	1.78 $\pm$ 1.08	1.49 $\pm$ 0.76	0.16
D-Dimer, IU/L, mean $\pm$ SD	0.88 $\pm$ 0.84	0.48 $\pm$ 0.33	<0.01
TT, s, mean $\pm$ SD	16.01 $\pm$ 0.88	16.15 $\pm$ 0.89	0.37

Abbreviations: SD: standard deviation; TMAO: trimethylamine N-oxide; Lp-a: lipoprotein-a; Apo-A1: apolipoprotein A1; Apo-B: apolipoprotein B; TC: total cholesterol; HDL-C: high-density lipoprotein cholesterol; LDL-C: low-density lipoprotein cholesterol; TG: triglycerides; TT: thrombin time. <sup>1</sup> $p$  value was obtained using chi-square tests or Fisher's exact tests for categorical variables and Mann-Whitney  $U$  tests for continuous variables.

carotid artery plaques. All patients received MRI within 24 hours of hospitalization with a 1.5 T or 3.0 T scanner. The sequence includes axial spin-echo T1-weighted sequence, T2-weighted sequence, fluid-attenuated inversion recovery sequence, DWI sequence ( $b = 1,000$  s/mm<sup>2</sup>, 2 mm isotropic resolution, and 30 diffusion directions), and 3D time-of-flight angiography. The slice layer of MRI was 5 mm, and the slice interval was 1.5 mm. Acute cerebral infarction was defined as high signal intensity on the DWI sequence. Infarct areas were manually qualified on DWI sequences. The images were collected and analyzed by experienced stroke neurologists who were blind to the participants' other characteristics. Infarct volumes were computed by slice layer multiplied by infarct area in each slice.

**2.4. Statistical Analysis.** Statistical tests were conducted using SAS, version 9.4 (SAS Institute Inc). Chi-square test or Fisher's exact test was used to compare group differences of categorical variables. Mann-Whitney  $U$  test was used to compare continuous variables. Multivariate unconditional logistic regressions were performed to evaluate the associations of LAA stroke with plasma TMAO and blood lipid-related indices (i.e., lipoprotein-a (Lp-a), apolipoprotein A1 (Apo-A1), apolipoprotein B (Apo-B), Apo-A1/B ratio, total cholesterol (TC), high-density lipoprotein cholesterol (HDL-C), low-density lipoprotein cholesterol (LDL-C), triglycerides (TG), D-Dime, and thrombin time (TT)). Model 1 was unadjusted.

Model 2 was adjusted for sex and age. The area under the curves (AUCs) of the receiver operating characteristic (ROC) were also calculated to assess their diagnostic performance of these abovementioned indices. Correlations between plasma TMAO and Lp-a, Apo-A1, Apo-B, Apo-A1/B ratio, TC, HDL-C, LDL-C, TG, D-Dimer, and TT were calculated using Spearman's correlation.

### 3. Results

**3.1. General Characteristics.** 50 LAA stroke patients and 50 healthy controls were included in the study. Table 1 demonstrated their demographics, vascular risk factors, plasma TMAO, and blood lipid-related indices in stroke patients and healthy controls. LAA stroke patients showed a higher TMAO than that of healthy controls (LAA vs. control: 2659.51  $\pm$  976.81 ng/mL vs. 1484.75  $\pm$  648.87 ng/mL,  $p < 0.01$ ). Significance was also observed between LAA stroke patients and healthy controls in age, gender, smoking, alcohol, diabetes, and hypertension, the volume of acute cerebral infarction, Lp-a, Apo-A1, Apo-B, the ratio of Apo-A1/B, HDL-C, and D-Dimer ( $p < 0.05$ ), while no statistical differences were found in obesity, area of carotid artery plaque, TC, LDL-C, TG, and TT ( $p > 0.05$ ).

**3.2. The Associations of the Risk of LAA Stroke with Plasma TMAO and Blood Lipid-Related Indices (Table 2).** The

TABLE 2: Odds ratios and areas under the curve for stroke risk per one sex-specific standard deviation increase of parameters.

Parameters	Unadjusted model			Adjusted model <sup>1</sup>		
	OR (95% CI)	<i>p</i> value	AUC (95% CI)	OR (95% CI)	<i>p</i> value	AUC (95% CI)
TMAO (ng/mL)	3.99 (2.16, 7.36)	<0.01	0.79 (0.70, 0.88)	7.03 (2.86, 17.25)	<0.01	0.89 (0.83, 0.95)
Area of carotid artery plaque (mm <sup>2</sup> )	1.07 (0.72, 1.59)	0.74	0.52 (0.40, 0.63)	1.00 (0.63, 1.59)	0.99	0.78 (0.69, 0.88)
Apo-A1 (g/L)	0.53 (0.34, 0.83)	0.01	0.67 (0.57, 0.78)	0.56 (0.34, 0.91)	0.02	0.81 (0.72, 0.89)
Apo-B (g/L)	1.43 (0.95, 2.17)	0.09	0.61 (0.50, 0.72)	1.74 (1.06, 2.85)	0.03	0.81 (0.73, 0.90)
Apo-A1 to Apo-B ratio	0.30 (0.17, 0.53)	<0.01	0.75 (0.66, 0.85)	0.29 (0.15, 0.56)	<0.01	0.85 (0.78, 0.93)
TC (mmol/L)	0.72 (0.54, 0.96)	0.02	0.65 (0.54, 0.76)	1.32 (0.83, 2.10)	0.24	0.79 (0.70, 0.88)
HDL-C (mmol/L)	0.61 (0.40, 0.93)	0.02	0.64 (0.54, 0.75)	0.56 (0.35, 0.91)	0.02	0.81 (0.72, 0.89)
LDL-C (mmol/L)	0.80 (0.56, 1.15)	0.23	0.59 (0.48, 0.70)	1.21 (0.77, 1.89)	0.41	0.78 (0.69, 0.88)
TG (mmol/L)	0.89 (0.62, 1.28)	0.52	0.55 (0.43, 0.66)	1.50 (0.91, 2.47)	0.11	0.80 (0.71, 0.89)

Abbreviations: OR: odds ratio; CI: confidence interval; AUC: area under the curve; TC: total cholesterol; HDL-C: high-density lipoprotein cholesterol; LDL-C: low-density lipoprotein cholesterol; TG: triglycerides. <sup>1</sup>Adjusted for age and gender.

multivariate unconditional logistic regression analyses revealed that elevated plasma TMAO was associated with higher risk of LAA stroke (odds ratio [OR], 3.99; 95% confidence interval [CI], 2.16, 7.36;  $p < 0.01$ ), while lower Apo-A1 (OR, 0.53; 95% CI, 0.34, 0.83;  $p = 0.01$ ), lower Apo-A1 to Apo-B ratio (OR, 0.30; 95% CI, 0.17, 0.53;  $p < 0.01$ ), lower TC (OR, 0.72; 95% CI, 0.54, 0.96;  $p < 0.01$ ), and lower HDL-C (OR, 0.61; 95% CI, 0.40, 0.93;  $p < 0.01$ ) were associated with higher risks of LAA stroke patients in an unadjusted model.

After adjusting for sex and age, logistic regression exhibited that higher plasma TMAO level (OR, 7.03; 95% CI, 2.86, 17.25;  $p < 0.01$ ) and higher Apo-B (OR, 1.74; 95% CI, 1.06, 2.85;  $p = 0.03$ ) were associated with higher risks of LAA stroke, while lower Apo-A1 (OR, 0.56; 95% CI, 0.34, 0.91;  $p = 0.02$ ), lower Apo-A1 to Apo-B ratio (OR, 0.29; 95% CI, 0.15, 0.56;  $p < 0.01$ ), and lower HDL-C (OR, 0.56; 95% CI, 0.35, 0.91;  $p = 0.02$ ) were observed in LAA stroke patients.

**3.3. The Diagnostic Performance of Plasma TMAO and Blood Lipid-Related Indices for LAA Stroke (Table 2).** The AUCs were calculated to assess the diagnostic ability of plasma TMAO and other blood lipid-related indices for vulnerable LAA stroke. The elevated plasma TMAO (AUC, 0.79; 95% CI, 0.70, 0.88) and lower Apo-A1 to Apo-B ratio (AUC, 0.75; 95% CI, 0.66, 0.85) were found to have good diagnostic performance for vulnerable LAA stroke in an unadjusted model.

While adjusted for sex and age in multivariate unconditional logistic regression, the elevated plasma TMAO (AUC, 0.89; 95% CI, 0.83, 0.95) and the increased Apo-B (AUC, 0.81; 95% CI, 0.73, 0.90) were of significant diagnostic values for vulnerable LAA stroke. By contrast, the lower Apo-A1 (AUC, 0.81; 95% CI, 0.72, 0.89), the lower Apo-A1 to Apo-B ratio (AUC, 0.85; 95% CI, 0.78, 0.93), and lower HDL-C (AUC, 0.81; 95% CI, 0.72, 0.89) showed good diagnostic ability for suffering LAA stroke.

**3.4. Correlation Analysis between Plasma TMAO Level and Blood Lipid-Related Indices in LAA Stroke Patients and Healthy Controls.** Spearman's correlation analysis revealed that plasma TMAO was not significantly correlated with vol-

ume of acute cerebral infarction and area of carotid artery plaque in LAA stroke patients, but positively correlated with area of carotid artery plaque in healthy controls ( $\beta = 4.49$ ,  $p = 0.04$ ) (Figure 1). Furthermore, there was no relationship between plasma TMAO and various blood lipid-related indices, including Lp-a, Apo-A1, Apo-B, the ratio of Apo-A1/B, TC, HDL-C, LDL-C, and TC ( $p > 0.05$ ) (Table 3).

#### 4. Discussion

The main findings of this study include plasma TMAO level in LAA stroke patients was significantly higher than that of the control group. Furthermore, for LAA stroke patients, the increased plasma TMAO level and Apo-B were risk factors, while lower Apo-A1, Apo-A1 to Apo-B ratio, and HDL-C were risk factors. Moreover, the increased plasma TMAO level and Apo-B were good diagnostic values for susceptible LAA stroke, but lower Apo-A1, Apo-A1 to Apo-B ratio, and HDL-C were good diagnostic values for suffering LAA stroke. Interestingly, the elevated plasma TMAO level was positively correlated with the area of carotid artery plaque in healthy controls, but not associated with the volume of acute cerebral infarction and area of carotid artery plaque in LAA stroke patients.

Our results also replicated the previous reports on the risk factors included age, smoking, alcohol drinking, diabetes, and hypertension [3, 22] and blood lipid abnormalities in LAA stroke patients [5, 10]. Most importantly, compared with healthy controls, LAA stroke patients had higher plasma TMAO levels, which indicated that TMAO might play a critical role in the pathophysiological mechanism of patients with stroke having large-artery atherosclerosis, and supported the need for further study of TMAO in the pathophysiological mechanism related to LAA stroke. This result aligned with the previous report [13] and the statement that the increased TMAO may promote platelet hyperreactivity and increase thrombosis risk [14].

In our study, the result that the elevated plasma TMAO and Apo-B were found to be risk factors for LAA stroke may be important manageable biological markers for exploring the potential of having LAA stroke in those with large-artery atherosclerosis. These markers combined with other

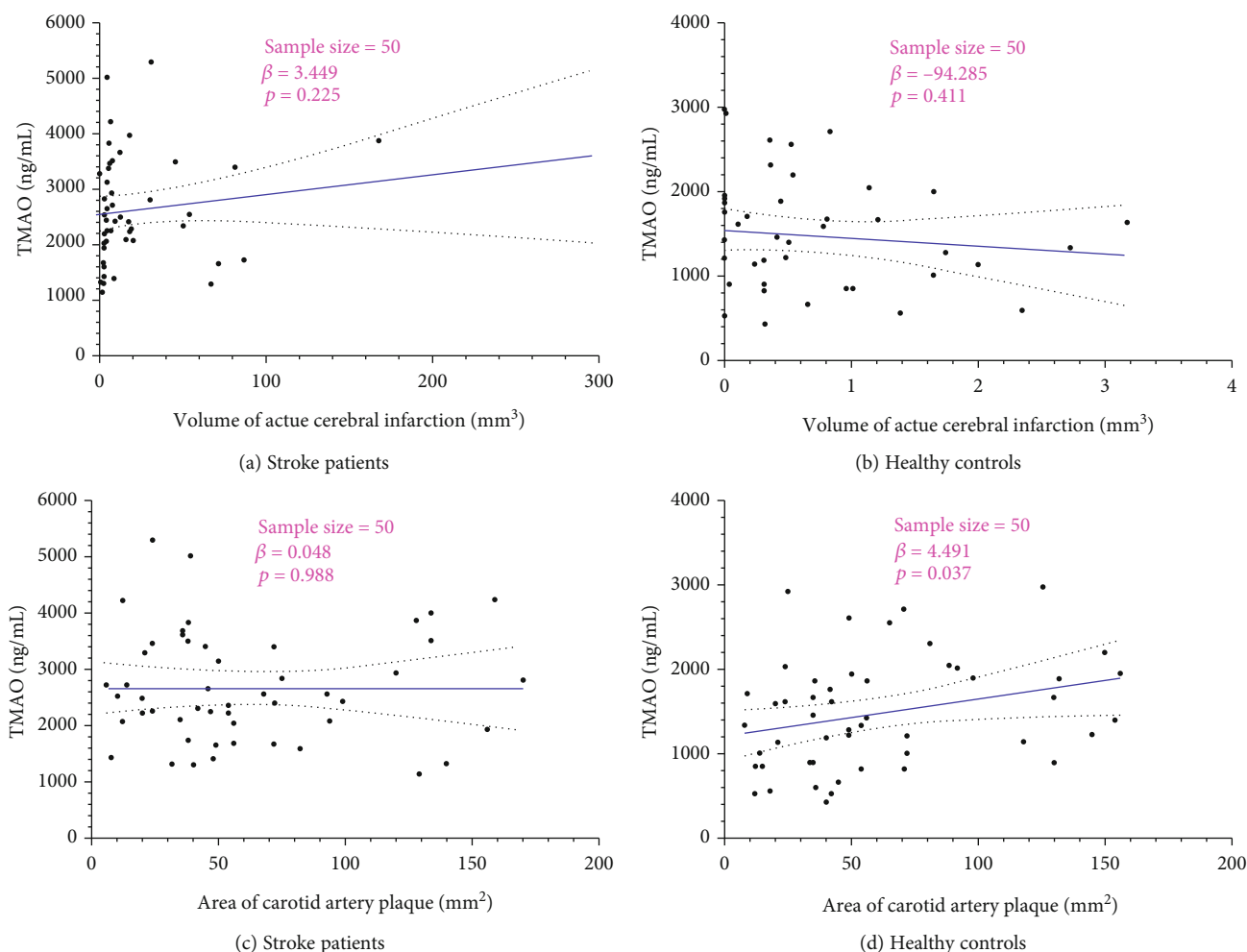


FIGURE 1: Scatter plots for plasma TMAO with volume of acute cerebral infarction and area of carotid artery plaque in LAA stroke patients and healthy controls by Spearman's correlation.

TABLE 3: Correlations between plasma TMAO and blood lipid-related indices in stroke patients and healthy participants.

Parameters	Stroke patients		Healthy participants	
	Beta ( $\beta$ )	<i>p</i> value	Beta ( $\beta$ )	<i>p</i> value
Lp-a (g/L)	1.44	0.36	-0.82	0.93
Apo-A1 (g/L)	-59.05	0.93	-513.08	0.16
Apo-B (g/L)	-255.90	0.64	-391.99	0.25
Apo-A1 to Apo-B ratio	578.09	0.27	-163.48	0.47
TC (mmol/L)	-57.75	0.65	-32.02	0.78
HDL-C (mmol/L)	335.33	0.55	-521.03	0.12
LDL-C (mmol/L)	-32.36	0.82	-132.46	0.26
TG (mmol/L)	-178.22	0.17	-81.93	0.51

Abbreviations: TMAO: trimethylamine N-oxide; Apo-A1: apolipoprotein A1; Apo-B: apolipoprotein B; TC: total cholesterol; HDL-C: high-density lipoprotein cholesterol; LDL-C: low-density lipoprotein cholesterol; TG: triglycerides.

factors on blood lipid-related indices, such as Apo-A1, Apo-A1 to Apo-B ratio, and HDL-C, may reflect the progress of pathogenesis of LAA stroke and be a panel of assessments for individuals with large-artery atherosclerosis without stroke. It has been reported that plasma TMAO is a potential mediator of the pathogenesis of atherosclerotic diseases,

including stroke and myocardial infarction [23]. Our findings further revealed that the elevated plasma TMAO and blood indicators reflecting the atherosclerosis such as Apo-A1, Apo-B, and HDL-C had good diagnostic performance for those vulnerably suffered LAA stroke, which added to the existing evidence presenting that TMAO level may regard



as a useful and potential prognostic biological indicator in LAA stroke, even beyond the currently clinic routine check.

Our study did not reveal that the elevated plasma TMAO was positively correlated with the area of carotid artery plaque in healthy controls but not significantly correlated with volume of acute cerebral infarction and area of carotid artery plaque in LAA stroke patients. The previous study supported this point of our results [24]. It showed no direct association between the increased plasma TMAO and the extent of atherosclerosis in mice and humans. Still, there was an association of the increased plasma TMAO levels with atherosclerotic plaque instability in a mouse model of plaque instability [24]. In contrast, other studies found that plasma TMAO has relations with atherosclerosis [25–27]. Interestingly, in our study, the elevated plasma TMAO levels were not associated with all blood lipid-related indices in our study in LAA stroke patients, suggesting the associations of plasma TMAO and blood lipids still need to be further noted and investigated for stroke.

The strengths of the study include a homogeneous LAA stroke population, blind evaluation on TMAO and imaging collection and analysis, and simultaneous detection of multiple blood lipid indicators. The study has limitations. Firstly, the sample was not big in both groups; the results of the current study should be confirmed in a large sample. Secondly, the positive control group, such as different stroke types, was a lack in this study. The positive control group of stroke, except for LAA stroke, should be designed for exploring the role of plasma TMAO and the associations of TMAO and blood lipid-related indices in various types of stroke, including different LAA strokes with various responsible large arteries. Lastly, the potential factors on plasma TMAO level, including diet, gut microbiota, drug management, and liver flavin monooxygenase [6, 7, 24, 28, 29], should be considered in different strokes of future studies.

## 5. Conclusions

To be our best knowledge, we firstly explored the association of LAA stroke with plasma TMAO and blood lipid-related indices. We demonstrated that plasma TMAO level, Apo-A1, Apo-B, and HDL-C could be as the potential biomarkers on LAA stroke and in blood will be beneficial for early managing and preventing stroke [30], especially LAA stroke.

## Data Availability

The data in this manuscript is available from the first or corresponding author on reasonable request.

## Conflicts of Interest

All authors declare that they have no conflict of interest.

## Authors' Contributions

Dongjuan Xu, Juexian Song, Kun Wang, Lianyan Wei, Yunyun Xu, Hongfei Li, Baoquan Min, Haixia Leng, Qing Xue, and Mao Peng collected the data. Wenfeng Zhao, Lu

Yin, Juexian Song, Ning Tang, Xiaoyan Jiang, Hui Liu, Shuo Yan, and Hongxing Wang analyzed and interpreted the data. Wenfeng Zhao drafted the manuscript. Hongxing Wang conceived, designed, and supervised the study.

## Acknowledgments

The study was supported by Zhejiang Provincial Natural Science Foundation of China (LGF18H090001), the National Key Technology R & D Program of China (2017YFC1310001), and Jinhua Science and Technology Plan Key Projects under Grant 2019-3-024.

## References

- [1] D. Xu, X. Chu, K. Wang et al., "Potential factors for psychological symptoms at three months in patients with young ischemic stroke," *Bio Med Research International*, vol. 2021, article 5545078, pp. 1–7, 2021.
- [2] J. W. Cole, "Large artery atherosclerotic occlusive disease," *Continuum (Minneapolis, Minn)*, vol. 23, no. 1, pp. 133–157, 2017.
- [3] A. I. Qureshi and L. R. Caplan, "Intracranial atherosclerosis," *Lancet*, vol. 383, no. 9921, pp. 984–998, 2014.
- [4] M. S. Rahman and K. Woollard, "Atherosclerosis," *Advances in Experimental Medicine and Biology*, vol. 1003, pp. 121–144, 2017.
- [5] D. Steinberg and J. L. Witztum, "Oxidized low-density lipoprotein and atherosclerosis," *Arteriosclerosis, Thrombosis, and Vascular Biology*, vol. 30, no. 12, pp. 2311–2316, 2010.
- [6] Z. Wang, E. Klipfell, B. J. Bennett et al., "Gut flora metabolism of phosphatidylcholine promotes cardiovascular disease," *Nature*, vol. 472, no. 7341, pp. 57–63, 2011.
- [7] R. A. Koeth, Z. Wang, B. S. Levison et al., "Intestinal microbiota metabolism of L-carnitine, a nutrient in red meat, promotes atherosclerosis," *Nature Medicine*, vol. 19, no. 5, pp. 576–585, 2013.
- [8] W. K. Wu, C. C. Chen, P. Y. Liu et al., "Identification of TMAO-producer phenotype and host-diet-gut dysbiosis by carnitine challenge test in human and germ-free mice," *Gut*, vol. 68, no. 8, pp. 1439–1449, 2019.
- [9] X. Wang, X. Li, and Y. Dong, "Vitamin D decreases plasma trimethylamine-N-oxide level in mice by regulating gut microbiota," *BioMed Research International*, vol. 2020, Article ID 9896743, 11 pages, 2020.
- [10] M. Canyelles, M. Tondo, L. Cedó, M. Farràs, J. Escolà-Gil, and F. Blanco-Vaca, "Trimethylamine N-oxide: a link among diet, gut microbiota, gene regulation of liver and intestine cholesterol homeostasis and HDL function," *International Journal of Molecular Sciences*, vol. 19, no. 10, p. 3228, 2018.
- [11] W. H. Tang, Z. Wang, B. S. Levison et al., "Intestinal microbial metabolism of phosphatidylcholine and cardiovascular risk," *The New England Journal of Medicine*, vol. 368, no. 17, pp. 1575–1584, 2013.
- [12] C. Wu, C. Li, W. Zhao et al., "Elevated trimethylamine N-oxide related to ischemic brain lesions after carotid artery stenting," *Neurology*, vol. 90, no. 15, pp. e1283–e1290, 2018.
- [13] C. Wu, F. Xue, Y. Lian et al., "Relationship between elevated plasma trimethylamine N-oxide levels and increased stroke injury," *Neurology*, vol. 94, no. 7, pp. e667–e677, 2020.



- [14] W. Zhu, J. C. Gregory, E. Org et al., "Gut microbial metabolite TMAO enhances platelet hyperreactivity and thrombosis risk," *Cell*, vol. 165, no. 1, pp. 111–124, 2016.
- [15] Q. Fu, M. Zhao, D. Wang et al., "Coronary plaque characterization assessed by optical coherence tomography and plasma trimethylamine-N-oxide levels in patients with coronary artery disease," *The American Journal of Cardiology*, vol. 118, no. 9, pp. 1311–1315, 2016.
- [16] M. Warrier, D. M. Shih, A. C. Burrows et al., "The TMAO-generating enzyme flavin monooxygenase 3 is a central regulator of cholesterol balance," *Cell Reports*, vol. 10, no. 3, pp. 326–338, 2015.
- [17] L. Ding, M. Chang, Y. Guo et al., "Trimethylamine-N-oxide (TMAO)-induced atherosclerosis is associated with bile acid metabolism," *Lipids in Health and Disease*, vol. 17, no. 1, p. 286, 2018.
- [18] B. J. Bennett, T. Q. A. Vallim, Z. Wang et al., "Trimethylamine-N-oxide, a metabolite associated with atherosclerosis, exhibits complex genetic and dietary regulation," *Cell Metabolism*, vol. 17, no. 1, pp. 49–60, 2013.
- [19] Chinese Society of Neurology, "Chinese cerebrovascular disease classification 2015," *Chinese Journal of Neurology*, vol. 50, pp. 168–171, 2017.
- [20] H. P. Adams Jr., B. H. Bendixen, L. J. Kappelle et al., "Classification of subtype of acute ischemic stroke. Definitions for use in a multicenter clinical trial. TOAST. Trial of Org 10172 in Acute Stroke Treatment," *Stroke*, vol. 24, no. 1, pp. 35–41, 1993.
- [21] H. J. M. Barnett, D. W. Taylor, R. B. Haynes, and North American Symptomatic Carotid Endarterectomy Trial Collaborators, "Beneficial effect of carotid endarterectomy in symptomatic patients with high-grade carotid stenosis," *The New England Journal of Medicine*, vol. 325, no. 7, pp. 445–453, 1991.
- [22] K. Ritz, N. P. Denswil, O. C. Stam, J. J. van Lieshout, and M. J. A. P. Daemen, "Cause and mechanisms of intracranial atherosclerosis," *Circulation*, vol. 130, no. 16, pp. 1407–1414, 2014.
- [23] Q. Zhai, X. Wang, C. Chen et al., "Prognostic value of plasma trimethylamine N-oxide levels in patients with acute ischemic stroke," *Cellular and Molecular Neurobiology*, vol. 39, no. 8, pp. 1201–1206, 2019.
- [24] Y. C. Koay, Y. C. Chen, J. A. Wali et al., "Plasma levels of trimethylamine-N-oxide can be increased with 'healthy' and 'unhealthy' diets and do not correlate with the extent of atherosclerosis but with plaque instability," *Cardiovascular Research*, vol. 117, no. 2, pp. 435–449, 2021.
- [25] T. Yamashita, "Intestinal immunity and gut microbiota in atherogenesis," *Journal of Atherosclerosis and Thrombosis*, vol. 24, no. 2, pp. 110–119, 2017.
- [26] A. Wilson, C. McLean, and R. B. Kim, "Trimethylamine-N-oxide: a link between the gut microbiome, bile acid metabolism, and atherosclerosis," *Current Opinion in Lipidology*, vol. 27, no. 2, pp. 148–154, 2016.
- [27] A. K. Duttaroy, "Role of gut microbiota and their metabolites on atherosclerosis, hypertension and human blood platelet function: a review," *Nutrients*, vol. 13, no. 1, p. 144, 2021.
- [28] M. H. Janeiro, M. J. Ramírez, F. I. Milagro, J. Martínez, and M. Solas, "Implication of trimethylamine N-oxide (TMAO) in disease: potential biomarker or new therapeutic target," *Nutrients*, vol. 10, no. 10, p. 1398, 2018.
- [29] B. C. Fu, M. A. J. Hullar, T. W. Randolph et al., "Associations of plasma trimethylamine N-oxide, choline, carnitine, and betaine with inflammatory and cardiometabolic risk biomarkers and the fecal microbiome in the multiethnic cohort adiposity phenotype study," *The American Journal of Clinical Nutrition*, vol. 111, no. 6, pp. 1226–1234, 2020.
- [30] A. Bustamante, E. López-Cancio, S. Pich et al., "Blood biomarkers for the early diagnosis of stroke: the stroke-chip study," *Stroke*, vol. 48, no. 9, pp. 2419–2425, 2017.

## Retraction

# Retracted: Mechanism of *Radix Astragali* and *Radix Salviae Miltiorrhizae* Ameliorates Hypertensive Renal Damage

### BioMed Research International

Received 12 March 2024; Accepted 12 March 2024; Published 20 March 2024

Copyright © 2024 BioMed Research International. This is an open access article distributed under the Creative Commons Attribution License, which permits unrestricted use, distribution, and reproduction in any medium, provided the original work is properly cited.

This article has been retracted by Hindawi following an investigation undertaken by the publisher [1]. This investigation has uncovered evidence of one or more of the following indicators of systematic manipulation of the publication process:

- (1) Discrepancies in scope
- (2) Discrepancies in the description of the research reported
- (3) Discrepancies between the availability of data and the research described
- (4) Inappropriate citations
- (5) Incoherent, meaningless and/or irrelevant content included in the article
- (6) Manipulated or compromised peer review

The presence of these indicators undermines our confidence in the integrity of the article's content and we cannot, therefore, vouch for its reliability. Please note that this notice is intended solely to alert readers that the content of this article is unreliable. We have not investigated whether authors were aware of or involved in the systematic manipulation of the publication process.

Wiley and Hindawi regrets that the usual quality checks did not identify these issues before publication and have since put additional measures in place to safeguard research integrity.

We wish to credit our own Research Integrity and Research Publishing teams and anonymous and named external researchers and research integrity experts for contributing to this investigation.

The corresponding author, as the representative of all authors, has been given the opportunity to register their agreement or disagreement to this retraction. We have kept a record of any response received.

### References

- [1] G. Hou, Y. Jiang, Y. Zheng et al., "Mechanism of *Radix Astragali* and *Radix Salviae Miltiorrhizae* Ameliorates Hypertensive Renal Damage," *BioMed Research International*, vol. 2021, Article ID 5598351, 7 pages, 2021.

## Research Article

# Mechanism of *Radix Astragali* and *Radix Salviae Miltiorrhizae* Ameliorates Hypertensive Renal Damage

Guangjian Hou,<sup>1</sup> Yuehua Jiang,<sup>2</sup> Yuekun Zheng,<sup>1</sup> Meng Zhao,<sup>3</sup> Yuanzhen Chen,<sup>1</sup>  
Yonghao Ren,<sup>4</sup> Congan Wang ,<sup>1</sup> and Wei Li <sup>4</sup>

<sup>1</sup>Neck-Shoulder and Lumbocrural Pain Hospital of Shandong First Medical University, Jinan 250062, China

<sup>2</sup>Central Laboratory, Affiliated Hospital of Shandong University of Traditional Chinese Medicine, Jinan 250011, China

<sup>3</sup>Rizhao Traditional Chinese Medicine Hospital, Rizhao 276826, China

<sup>4</sup>Department of Nephrology, Affiliated Hospital of Shandong University of Traditional Chinese Medicine, Jinan 250011, China

Correspondence should be addressed to Congan Wang; wangcongan2005@163.com and Wei Li; lweidw@163.com

Received 16 February 2021; Revised 26 March 2021; Accepted 8 April 2021; Published 22 April 2021

Academic Editor: Yuzhen Xu

Copyright © 2021 Guangjian Hou et al. This is an open access article distributed under the Creative Commons Attribution License, which permits unrestricted use, distribution, and reproduction in any medium, provided the original work is properly cited.

Hypertensive-induced renal damage (HRD) is an important public health and socioeconomic problem worldwide. The herb pair *Radix Astragali*- (*RA*-) *Radix Salviae Miltiorrhizae* (*RS*) is a common prescribed herbal formula for the treatment of HRD. However, the underlying mechanisms are unclear. The purpose of our study is to explore the mechanism of combination of *Radix Astragali* (*RA*) and *Radix Salviae Miltiorrhizae* (*RS*) ameliorating HRD by regulation of the renal sympathetic nerve. Thirty 24-week-old spontaneously hypertensive rats (SHRs) as the experimental group were randomly divided into the *RA* group, the *RS* group, the *RA*+*RS* group, the valsartan group, and the SHR group and six age-matched Wistar Kyoto rats (WKY) as the control group. After 4 weeks of corresponding drug administration, venipuncture was done to collect blood and prepare serum for analysis. A color Doppler ultrasound diagnostic instrument was used to observe renal hemodynamics. Enzyme-linked immunosorbent assay was used to detect norepinephrine (NE), epinephrine (E), angiotensin II (Ang II), and B-type brain natriuretic peptide (BNP). Simultaneously, the kidneys were removed immediately and observed under a transmission electron microscope to observe the ultrastructural changes. And the concentration of transforming growth factor- $\beta$ 1 (TGF- $\beta$ 1), angiotensin type 1 receptor (AT1), and nitric oxide (NO) was detected by immunohistochemistry. Our results showed that renal ultrasonography of rats showed no significant difference in renal size among groups. The *RA*+*RS* group had obviously decreased vascular resistance index. The levels of NE, E, BNP, Ang II, AT1, and TGF- $\beta$ 1 were decreased ( $P < 0.05$ ), and the density of NO was increased. Pathological damage of the kidney was alleviated. In conclusion, the results of the present study suggested sympathetic overexpression in the pathogenesis of HRD. The combination of *RA* and *RS* may inhibit the hyperexcitability of sympathetic nerves and maintain the normal physiological structure and function of kidney tissue and has a protective effect on the cardiovascular system.

## 1. Introduction

Hypertensive-induced renal damage (HRD) is a critical reason of end-stage renal disease [1]. Among the causes of end-stage renal disease, HRD accounts for nearly 34% of the total number of cases [2]. Studies have shown that the progression of HRD is closely related to renal sympathetic nerve hyperexcitability [3]. Renal sympathetic nerve hyperexcitability affects HRD patients mainly in three aspects, including changes in blood pressure, progression of kidney

disease, and cardiovascular complications [3, 4]. Sympathetic nerve hyperexcitability can lead to increased volume load, cause abnormal activation of RAS, ultimately increase blood pressure, and promote cardiovascular complications [5]. In addition, sympathetic nerve excitement directly acts on the kidneys, causing blood pressure to rise [6].

In traditional Chinese medicine, “invigorating qi and promoting blood circulation” is currently one of the most widely used treatments for hypertensive kidney damage. *Radix Astragali* (*RA*, Huangqi in Chinese) and *Radix Salviae*

*Miltiorrhizae* (RS, Danshen in Chinese) are the most commonly used compatibility drugs. In our previous research, we focused on investigating the role of traditional Chinese medicine in chronic kidney disease. Studies have shown that RA is commonly used for treating nephrotic syndrome [7]. RA is used in large amounts and can reduce blood pressure, increase renal nitric oxide level, improve the expression of NOS, scavenge oxygen free radicals, and block the oxidation reaction. To protect the structural and functional integrity of renal vascular and improve vascular endothelial function [8], RS exhibits multiple pharmacological activities such as vasorelaxation, antioxidation, and antiapoptotic effects in renal cells [9].

Based on the above understanding, the research on the efficacy of RA and RS against chronic kidney disease is relatively clear. However, the pharmacological effects of RA and RS on hypertensive kidney injury are still unclear. Therefore, this study is aimed at investigating the effects of herb pair RA and RS in spontaneously hypertensive rats (SHRs) and determining the underlying mechanism by regulation of the renal sympathetic nerve.

## 2. Materials and Methods

**2.1. Animals and Experimental Methods.** Thirty 17-week-old male SHRs and six age-matched Wistar Kyoto rats (WKY) were obtained from Beijing Weitong Lihua Experimental Animal Technology Co., Ltd., China (No. SCXK (Beijing) 2012-0001). They were fed in the Experiment Animal Center of Affiliated Hospital of Shandong University of Traditional Chinese Medicine. All procedures of the project were approved by the Faculty of Medicine and Health Sciences Ethics Committee for Animal Research, Affiliated Hospital of Shandong University of Traditional Chinese Medicine.

Studies have shown that SHR kidney damage occurs at an average age of 6 months, so after feed with food and water for 2 months. The random number table is divided into the RA group, the RS group, the RA+RS group, the valsartan group (used as positive control), the SHR group, and the WKY group. The SHR group and the WKY group were intragastrically administered with saline. SHRs in other groups (RA group, RS group, RA+RS group, and valsartan group) were intragastrically administered the corresponding drugs once daily for 28 days. The blood pressure was recorded at 7-day interval.

**2.2. Renal Ultrasonography and Tissue Collection.** The renal ultrasonography was performed on small animals under anesthesia with sodium pentobarbital (30 mg/kg, intraperitoneal injection) using a color Doppler ultrasound diagnostic instrument (M5Vet, Mindray, China) [10]. Computer software (M5Vet) was used to record and analyze renal hemodynamics.

After 4 weeks of drug administration, the rats were euthanized with intraperitoneal injection of sodium pentobarbital (40 mg/kg). Venipuncture was done to collect blood and prepare serum for analysis. Enzyme-linked immunosorbent assay (ELISA) was used to detect norepinephrine (NE), epinephrine (E), angiotensin II (Ang II), and B-type brain natri-

uretic peptide (BNP). Simultaneously, the kidneys were removed immediately, one part was fixed with 4% paraformaldehyde, and the concentration of transforming growth factor- $\beta$ 1 (TGF- $\beta$ 1), angiotensin type 1 receptor (AT1), and nitric oxide (NO) was detected by immunohistochemistry (IHC). In the second part, the ultrastructure changes were observed under a transmission electron microscope (TEM, JEOL 1200EX, Electron Optics Laboratory Co. Ltd., Japan). The remaining tissues were homogenized for western blot assay.

**2.3. IHC Staining of TGF- $\beta$ 1, AT1, and NO in Rat Renal Tissue.** Renal sections were stained with rabbit anti-rat TGF- $\beta$ 1, AT1, and NO (Abcam, 1:150 dilution, China; Ab92486, Ab18801, and Ab66127) at 4°C overnight. Then, sections were incubated with horseradish peroxidase-(HRP-) conjugated AffiniPure goat anti-rabbit IgG (ZSGB-Bio, ZB-2301, 1:100, China) at room temperature for 60 min [10]. Tissue sections were colored with diaminobenzidine (DAB, ZSGB-Bio, ZLI-9031, 1:100) and then counterstained with hematoxylin for 5 minutes [10]. The sections were observed under a microscope (Carl Zeiss Jena, Germany). Image-Pro Plus 6.0 image analysis system (Media Cybernetics, USA) was used to analyze, and 8 nonoverlapping fields of view were randomly read from each slice. The integrated optical density (IOD) was calculated and was taken for statistical analysis.

**2.4. Statistical Analysis.** Statistical analyses were performed with the Statistical Package for the Social Sciences, version 22.0 (SPSS Inc., Chicago, IL, USA). All data were described as mean  $\pm$  standard deviation ( $\bar{X} \pm s$ ) values. Differences between groups were analyzed by one-way analysis of variance (ANOVA), followed by Student-Newman-Keuls test. *P* values of less than 0.05 were considered to be statistically significant.

## 3. Results

**3.1. Renal Hemodynamics of Rats.** Renal ultrasonography of rats showed no significant difference in renal size among groups. However, compared with the WKY group, the vascular resistance index in the SHR group was higher ( $P < 0.05$ ), and each treatment significantly decreased the vascular resistance index ( $P < 0.05$ , Figure 1). The valsartan group and the RA+RS group obviously decreased (Table 1). We speculate that these two drugs may reduce renal blood flow resistance and protect renal function in clinical treatment.

**3.2. Biomarkers of Serum Renal Damage in Rats.** The serum levels of NE, E, BNP, and Ang II were all increased in the SHR group than in the WKY group ( $P < 0.05$ ). In addition, the RS group has decreased levels of E and BNP than the SHR group ( $P < 0.05$ ), and the RA group has decreased NE, E, and BNP levels ( $P < 0.05$ ). Simultaneously, the valsartan group had obviously reduced levels of NE, E, BNP, and Ang II ( $P < 0.05$ ), and the herb pair of RA and RS obviously decreased the levels of NE, E, BNP, and Ang II ( $P < 0.05$ , Table 2).



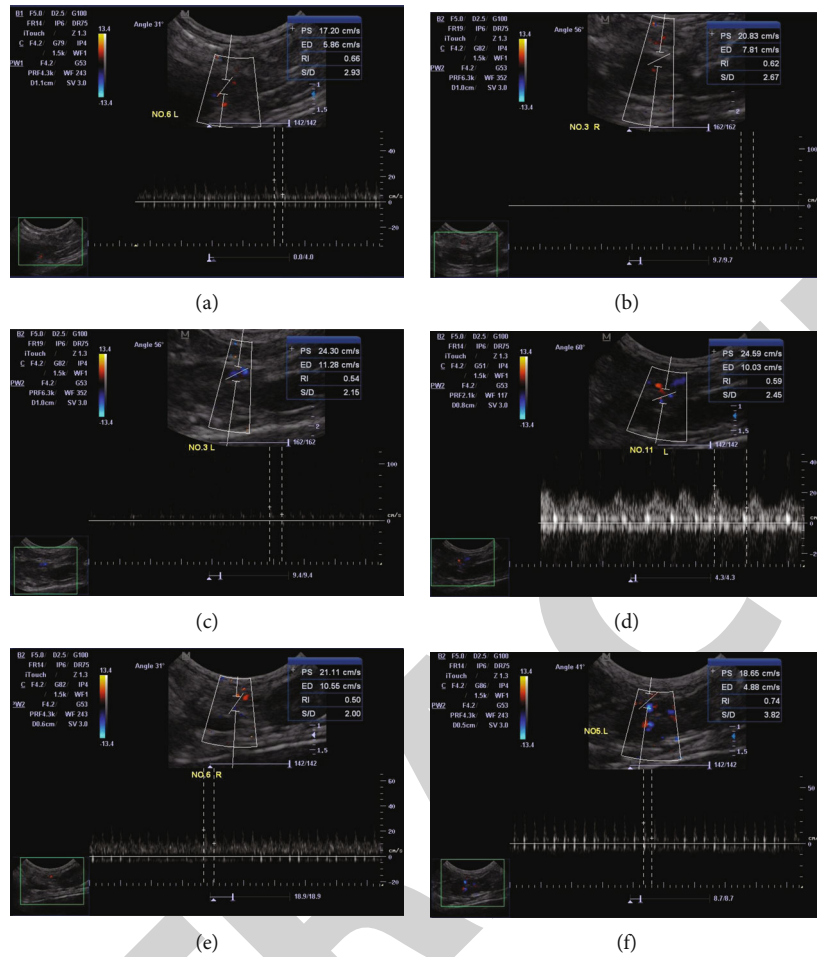


FIGURE 1: Renal ultrasonography of rat vascular resistance index: (a) RA group; (b) RS group; (c) RA+RS group; (d) valsartan group; (e) SHR group; (f) WKY group.

TABLE 1: The rat renal vascular resistance index.

Group	No.	Right renal	Left renal
RA group	6	0.65 ± 0.04*	0.67 ± 0.06*
RS group	6	0.62 ± 0.03*	0.67 ± 0.10*
RA+RS group	6	0.54 ± 0.04*	0.54 ± 0.05*
Valsartan group	6	0.54 ± 0.04*	0.57 ± 0.07*
SHR group	6	0.75 ± 0.02 <sup>△</sup>	0.80 ± 0.02 <sup>△</sup>
WKY group	6	0.51 ± 0.04	0.53 ± 0.03

No.: number; RA group: *Radix Astragali* treatment group; RS group: *Radix Salvia Miltiorrhiza* treatment group; RA+RS group: RA and RS combination treatment group; SHR group: spontaneously hypertensive rat group; WKY group: Wistar Kyoto rat group. Values are the mean ± SD. \* $P < 0.05$  vs. the SHR group; <sup>△</sup> $P < 0.05$  vs. the WKY group.

**3.3. Rat Renal Morphology.** Compared with that in the WKY group, the density of AT1 and TGF- $\beta$ 1 was increased in the SHR group, and the density of NO was significantly decreased. After 4-week different drug administration, compared with the SHR group, all the treatment groups had decreased AT1 and TGF- $\beta$ 1 density, and the density of NO was increased (Figure 2). Compared with the WKY group, transmission electron microscopy showed that the SHR group had irregular cell

morphology, endothelial cytoplasmic swelling, foot process fusion and foot process wide, organelle-rich, both atrophy of renal tubules, decreased cytoplasm, and thicker and crinkled basement membrane. Compared with the SHR group, after the drug treatment, all the groups have improved cell morphology, endothelial cytoplasmic swelling decreased, occasional fusion of foot process segmental fusion and neatly arranged, and the organelles were abundant (Figure 3). Among them, RA+RS proved to have the best efficacy.

#### 4. Discussion

TCM has received extensive attention and research due to its long-lasting efficacy and fewer side effects [11]. TCM not only pays attention to improving the symptoms of patients but also focuses on the adjustment of the patients' constitution and improve the quality of life [12]. HRD is usually related to the insufficiency of "qi" and "blood." Studies showed that RA can improve cardiovascular function and increase coronary blood flow [13, 14]. Simultaneously, treatment with RA may improve TGF- $\beta$ 1-induced renal fibrosis [15]. Studies reveal that RS can improve vascular function and structure and significantly improve the occurrence of hypertension [16], and RS and its extracts have been known to have an antioxidant



TABLE 2: Renal biomarkers in rat serum.

Group	NE	E	BNP	Ang II
RA group	11.84 ± 0.41*	0.92 ± 0.20*	200.68 ± 5.46*	152.76 ± 5.50
RS group	12.98 ± 0.97	0.89 ± 0.12*	193.30 ± 5.48*	153.26 ± 7.54
RA+RS group	8.57 ± 0.42*	0.68 ± 0.04*	186.13 ± 7.86*	126.36 ± 10.29*
Valsartan group	11.52 ± 0.65*	0.70 ± 0.11*	191.90 ± 6.43*	132.94 ± 9.14*
SHRs group	14.04 ± 1.39	1.40 ± 0.34	219.75 ± 9.33	157.87 ± 4.70
WKY group	8.14 ± 1.01*	0.60 ± 0.07*	159.58 ± 7.22*	115.58 ± 7.60*

RA group: *Radix Astragali* treatment group; RS group: *Radix Salvia Miltiorrhiza* treatment group; RA+RS group: RA and RS combination treatment group; SHR group: spontaneously hypertensive rat group; WKY group: Wistar Kyoto rat group; NE: norepinephrine; E: epinephrine; Ang II: angiotensin II; BNP: B-type brain natriuretic peptide. Values are the mean ± SD. \* $P < 0.05$  vs. the SHR group.

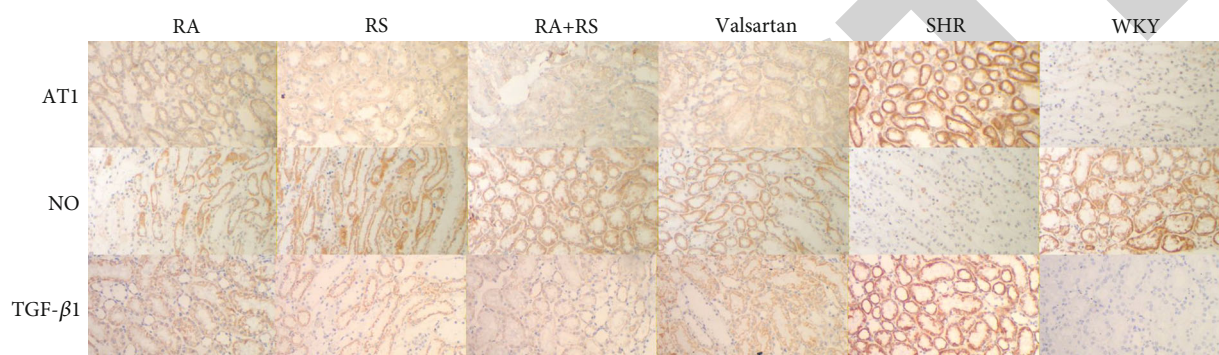


FIGURE 2: AT1, NO, and TGF- $\beta$ 1 density in the kidney determined by IHC staining ( $\times 400$ ). AT1: angiotensin type 1; NO: nitric oxide; TGF- $\beta$ 1: transforming growth factor- $\beta$ 1; RA: *Radix Astragali* treatment group; RS: *Radix Salvia Miltiorrhiza* treatment group; RA+RS: RA and RS combination treatment group; SHR: spontaneously hypertensive rat group; WKY: Wistar Kyoto rat group.

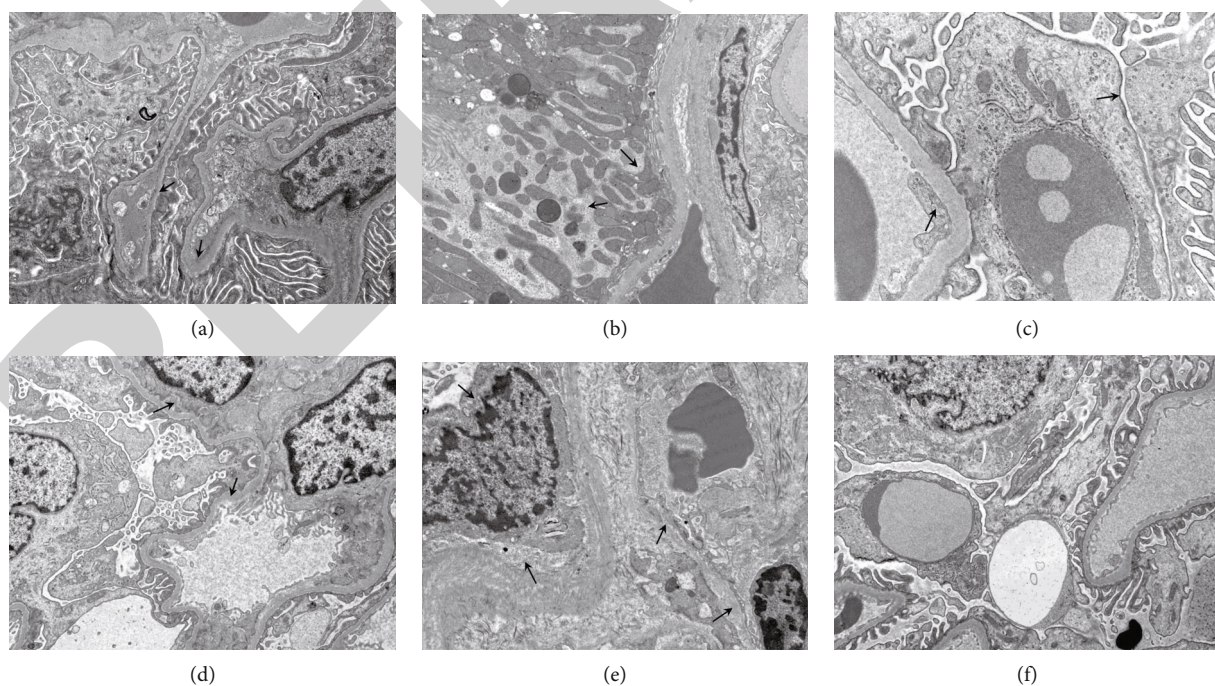


FIGURE 3: Renal sections were observed under a transmission electron microscope ( $\times 12000$ ): (a) RA group; (b) RS group; (c) RA+RS group; (d) valsartan group; (e) SHR group; (f) WKY group.

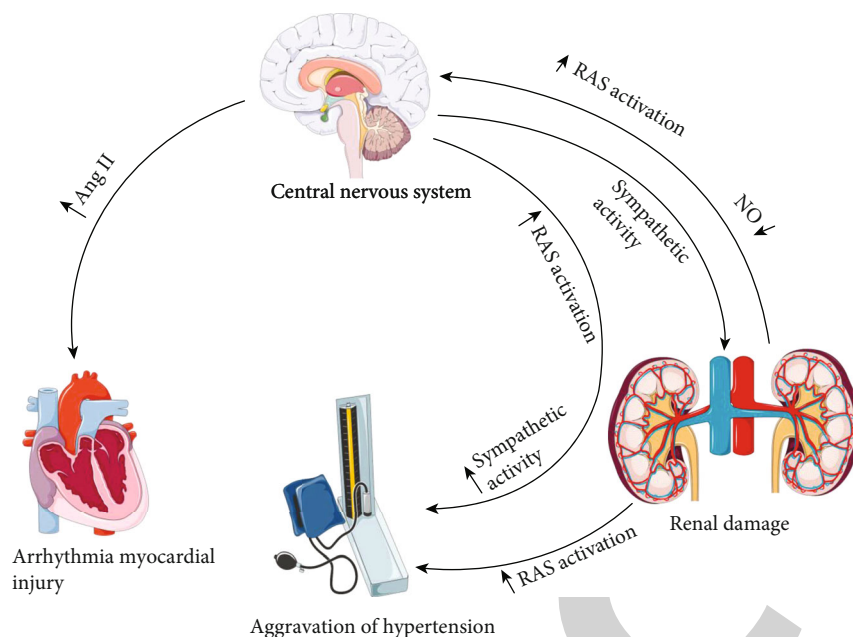


FIGURE 4: Mechanism of sympathetic activation in HRD.

property and neuroprotective effects [17]. The combination of RA and RS exerts synergistic effect on HRD.

Renal interstitial fibrosis (RIF) is the main pathological change from a variety of chronic kidney disease to end-stage renal disease [18]. Studies have found that for chronic kidney disease, tubulointerstitial damage is more important than glomerular disease [19]. Inhibiting epithelial-mesenchymal transition of renal tubular epithelial cells is considered an efficient approach for the treatment of renal interstitial fibrosis [20–22]. Currently, mechanisms of HRD have been paid more attention, such as hyperactivation of the renin-angiotensin system (RAS), small vessel lesions, and an increase in sodium and water retention. The kidney is densely innervated by sympathetic nerves, which are playing an important role in the regulation of blood pressure homeostasis [23]. Therefore, we discuss the mechanism of renal sympathetic nerve in HRD.

The main components of RAS such as Ang I and Ang II can be detected in normal human kidneys. Studies have found that aberrant RAS activation is closely related to RIF [24]. On the one hand, with the combination of Ang II and AT1 receptor, abnormal expression of Ang II can directly stimulate TGF- $\beta$ 1 activity and directly regulate the synthesis and degradation of extracellular matrix (ECM), regulating inflammatory mediators in the kidney and aggravating RIF [25, 26]. The second is that Ang II can activate signal pathways by stimulating the RAS system, which can induce cell proliferation and aggravate RIF. In our study, the combination of RA and RS obviously decreased the levels of BNP and Ang II. It is speculated that RA and RS can effectively reduce the expression of Ang II, block RAS activation and inhibit TGF- $\beta$ 1 expression, delay the progression of the RIF, and prevent hypertension and cardiac function injury (Figure 4).

Meanwhile, studies found that due to the decrease in renal vascular flow, stimulation of renal sympathetic nerves can cause hypertension [27]. Stimulation signals such as

ischemia, hypoxia, and NO can activate the receptors of the renal sympathetic afferent nerves and transmission to the central nervous system [28, 29] and increase central sympathetic nerve activity by activating neurons in the rostral ventrolateral medulla, causing vasoconstriction and increased blood pressure [30, 31]. At present, changes in plasma noradrenaline concentration are used as an evaluation index of sympathetic nerve activity [32]. In our study, we found that NE and E in the SHR group were significantly increased; it suggests that there is sympathetic hyperexcitability in HRD. And the combination of RA and RS obviously decreased the levels of NE and E. It is speculated that RA+RS can effectively inhibit the overexcited sympathetic nerve in HRD.

The sympathetic nervous system regulates blood pressure and heart and kidney functions by releasing catecholamines. Simultaneously, the sympathetic nervous system can activate  $\beta$ 1 receptors, leading to renin release and RAS activation. In addition, Ang II can promote the release of catecholamines, increase sympathetic nerve activity, and participate in the pathophysiological process of HRD [33].

In addition, this study still has limitations. The components of RA and RS are complex, and it is impossible to determine which specific active ingredients have played a role. The investigation of the pharmacological mechanism cannot be very clear. The follow-up research needs to be further verified.

In conclusion, the results of the present study suggested sympathetic overexpression in the pathogenesis of HRD. The combination of RA and RS may inhibit the hyperexcitability of sympathetic nerves, reduce Ang II overexpression, avoid abnormal activation of the RAS system, and improve rat renal blood flow resistance, accordingly maintaining the normal physiological structure and function of kidney tissue and having a protective effect on the cardiovascular system. Moreover, further comprehensive studies are required to examine other possible mechanisms.



## Data Availability

All data included in this study are available upon request by contact with the corresponding author.

## Conflicts of Interest

All authors declare they have no conflicts of interest.

## Authors' Contributions

All authors had access to the data and a role in writing the manuscript. All authors read and approved the final manuscript.

## Acknowledgments

This study was supported by the National Natural Science Foundation of China (No. 81673812), Academic Promotion Project of Shandong First Medical University (grant number 2019QL003), and Shandong Province Medical and Health Technology Development Plan (202002080788).

## References

- [1] P. M. Snijder, A. R. Frenay, A. M. Koning et al., "Sodium thio-sulfate attenuates angiotensin II-induced hypertension, proteinuria and renal damage," *Nitric Oxide*, vol. 42, pp. 87–98, 2014.
- [2] P. K. Whelton, R. M. Carey, W. S. Aronow et al., "2017 ACC/AHA/AAPA/ABC/ACPM/AGS/APhA/ASH/ASPC/NMA/PCNA guideline for the prevention, detection, evaluation, and management of high blood pressure in adults: a report of the American College of Cardiology/American Heart Association Task Force on Clinical Practice Guidelines," *Hypertension*, vol. 71, no. 6, pp. e13–e115, 2018.
- [3] L. Hering, M. Rahman, H. Hoch et al., " $\alpha$ 2A-adrenoceptors modulate renal sympathetic neurotransmission and protect against hypertensive kidney disease," *Journal of the American Society of Nephrology*, vol. 31, no. 4, pp. 783–798, 2020.
- [4] Y. Sata and M. P. Schlaich, "The potential role of catheter-based renal sympathetic denervation in chronic and end-stage kidney disease," *Journal of Cardiovascular Pharmacology and Therapeutics*, vol. 21, no. 4, pp. 344–352, 2016.
- [5] E. J. Johns, U. C. Kopp, and G. F. DiBona, "Neural control of renal function," *Comprehensive Physiology*, vol. 1, no. 2, pp. 731–767, 2011.
- [6] J. H. Jeong, I. T. Fonkoue, A. A. Quyyumi, D. DaCosta, and J. Park, "Nocturnal blood pressure is associated with sympathetic nerve activity in patients with chronic kidney disease," *Physiological Reports*, vol. 8, no. 20, article e14602, 2020.
- [7] A. P. Li, L. Yang, T. Cui et al., "Uncovering the mechanism of Astragali Radix against nephrotic syndrome by integrating lipidomics and network pharmacology," *Phytomedicine*, vol. 77, article 153274, 2020.
- [8] M. Shahzad, A. Shabbir, K. Wojcikowski, H. Wohlmuth, and G. C. Gobe, "The antioxidant effects of *Radix Astragali* (*Astragalus membranaceus* and related species) in protecting tissues from injury and disease," *Current Drug Targets*, vol. 17, no. 12, pp. 1331–1340, 2016.
- [9] J. Y. Han, J. Y. Fan, Y. Horie et al., "Ameliorating effects of compounds derived from *Salvia miltiorrhiza* root extract on microcirculatory disturbance and target organ injury by ischemia and reperfusion," *Pharmacology & Therapeutics*, vol. 117, no. 2, pp. 280–295, 2008.
- [10] W. Li, Y. H. Jiang, Y. Wang et al., "Protective effects of combination of *Radix Astragali* and *Radix Salviae Miltiorrhizae* on kidney of spontaneously hypertensive rats and renal intrinsic cells," *Chinese Journal of Integrative Medicine*, vol. 26, no. 1, pp. 46–53, 2020.
- [11] P. P. Hao, F. Jiang, Y. G. Chen et al., "Traditional Chinese medication for cardiovascular disease," *Nature Reviews. Cardiology*, vol. 12, no. 6, p. 318, 2015.
- [12] J. Qi, J. Yu, Y. Tan et al., "Mechanisms of Chinese Medicine Xinmailong's protection against heart failure in pressure-overloaded mice and cultured cardiomyocytes," *Scientific Reports*, vol. 7, no. 1, article 42843, 2017.
- [13] R. Han, F. Tang, M. Lu et al., "Astragalus polysaccharide ameliorates H2O2-induced human umbilical vein endothelial cell injury," *Molecular Medicine Reports*, vol. 15, no. 6, pp. 4027–4034, 2017.
- [14] J. Yu, X. Zhang, and Y. Zhang, "Astragaloside attenuates myocardial injury in a rat model of acute myocardial infarction by upregulating hypoxia inducible factor-1 $\alpha$  and Notch1/Jagged1 signaling," *Molecular Medicine Reports*, vol. 15, no. 6, pp. 4015–4020, 2017.
- [15] G. Shan, X. J. Zhou, Y. Xia, and H. J. Qian, "*Astragalus membranaceus* ameliorates renal interstitial fibrosis by inhibiting tubular epithelial-mesenchymal transition in vivo and in vitro," *Experimental and Therapeutic Medicine*, vol. 11, no. 5, pp. 1611–1616, 2016.
- [16] Y. Ma, W. Wang, J. Yang et al., "A network pharmacology technique to investigate the synergistic mechanisms of *Salvia miltiorrhiza* and *Radix puerariae* in treatment of cerebrovascular diseases," *Evidence-based Complementary and Alternative Medicine*, vol. 2020, Article ID 6937186, 18 pages, 2020.
- [17] Y. Li, H. Chen, Y. Yang et al., "Danshen formula granule and salvianic acid alleviate ethanol-induced neurotoxicity," *Journal of Natural Medicines*, vol. 74, no. 2, pp. 399–408, 2020.
- [18] H. Menn-Josephy, C. S. Lee, A. Nolin et al., "Renal interstitial fibrosis: an imperfect predictor of kidney disease progression in some patient cohorts," *American Journal of Nephrology*, vol. 44, no. 4, pp. 289–299, 2016.
- [19] P. Boor, T. Ostendorf, and J. Floege, "Renal fibrosis: novel insights into mechanisms and therapeutic targets," *Nature Reviews. Nephrology*, vol. 6, no. 11, pp. 643–656, 2010.
- [20] B. D. Humphreys, S. L. Lin, A. Kobayashi et al., "Fate tracing reveals the pericyte and not epithelial origin of myofibroblasts in kidney fibrosis," *The American Journal of Pathology*, vol. 176, no. 1, pp. 85–97, 2010.
- [21] R. Koesters, B. Kaissling, M. Lehir et al., "Tubular overexpression of transforming growth factor- $\beta$ 1 induces autophagy and fibrosis but not mesenchymal transition of renal epithelial cells," *The American Journal of Pathology*, vol. 177, no. 2, pp. 632–643, 2010.
- [22] T. Inoue, A. Umezawa, T. Takenaka, H. Suzuki, and H. Okada, "The contribution of epithelial-mesenchymal transition to renal fibrosis differs among kidney disease models," *Kidney International*, vol. 87, no. 1, pp. 233–238, 2015.

## Review Article

# Advances in the Development of Biomarkers for Poststroke Epilepsy

Mengke Liang <sup>1</sup>, Liren Zhang <sup>2</sup>, and Zhi Geng <sup>2</sup>

<sup>1</sup>Department of Neurology, Shanghai Jiao Tong University Affiliated Sixth People's Hospital South Campus, Shanghai 201499, China

<sup>2</sup>Department of Neurology, Shanghai Jiao Tong University Affiliated Sixth People's Hospital, Shanghai 200233, China

Correspondence should be addressed to Zhi Geng; gengzhi1998@163.com

Received 16 February 2021; Revised 26 March 2021; Accepted 9 April 2021; Published 19 April 2021

Academic Editor: Yuzhen Xu

Copyright © 2021 Mengke Liang et al. This is an open access article distributed under the Creative Commons Attribution License, which permits unrestricted use, distribution, and reproduction in any medium, provided the original work is properly cited.

Stroke is the main cause of acquired epilepsy in elderly people. Poststroke epilepsy (PSE) not only affects functional recovery after stroke but also brings considerable social consequences. While some factors such as cortical involvement, hemorrhagic transformation, and stroke severity are associated with increased seizure risk, so far that remains controversial. In recent years, there are an increasing number of studies on potential biomarkers of PSE as tools for diagnosing and predicting epileptic seizures. Biomarkers such as interleukin-6 (IL-6), tumor necrosis factor- $\alpha$  (TNF- $\alpha$ ), glutamate, and S100 calcium-binding protein B (S100B) in blood are associated with the occurrence of PSE. This review is aimed at summarizing the progress on potential biomarkers of PSE.

## 1. Introduction

The main cause of seizures in adults beyond the age of 60 is cerebrovascular disease [1], and the leading are hemorrhagic and ischemic strokes. Poststroke epilepsy (PSE) is one of the complications that lead to poorer quality of life, higher mortality, and greater health expenditures.

Seizures are defined as a transient, abnormally excessive synchronous neuronal activity in the brain. Poststroke seizures occur within 1 week of stroke onset (as early-onset seizures) or 1 week after a stroke (as late-onset seizures) [2]. Studies reporting on the rate of early postischemic stroke seizures range from 2% to 33%, while that of late seizures spans from 3 to 67% [3]. Seizure activity is present in up to 8–13% of patients following intracerebral hemorrhage [4]. This variability in the reported incidences is likely due to different study designs and length of follow-up. Seizures can be used as a predictor of poor functional outcome or longer hospital stays in patients with stroke [5]. The classical factors such as cortical involvement, hemorrhagic conversion of ischemic stroke, and stroke severity carry a higher risk of seizures [5–7].

However, the mechanism of poststroke epilepsy is not well understood. The majority of available studies agree cellular ionic imbalance and excitotoxic neurotransmitters are the main cause of the early seizure, while the late seizure is associated with glial scar formation resulting in increased nerve excitability [8]. The disruption of the blood-brain barrier and brain tissue ischemia/hypoxia injury all can lead to ion pump dysfunction. The elevation of the intracellular calcium ion, sodium, and extracellular potassium ion concentration will cause neural hyperexcitability and reduce seizure threshold [1, 9, 10]. Ischemic injury caused astrocyte and microglial activation, which will increase the production of inflammation mediators including tumor necrosis factor- $\alpha$ , interleukin-1 $\beta$ , and interleukin-6. Abnormal immune responses aggravate the damage to the BBB integrity that may promote epileptogenesis [11, 12]. Disruption of the neurovascular unit integrity also induced albumin extravasation, which results in significant accumulation of extracellular glutamate by activating the TGF $\beta$  signaling pathways [13]. Glutamate is the primary excitatory neurotransmitter in the central nervous system. The neurotransmitter glutamate is neurotoxic inducing or contributing to epileptogenesis when

it is accumulated in a massive amount in the extracellular fluid [14, 15].

Glial scar formation was closely associated with late seizures. Increased expression of gliosis in the ischemic area is accompanied by abnormal nerve conduction and heightened neural excitability [8]. Compared with ischemic stroke, those with hemorrhagic stroke had higher seizure frequency. This well-known phenomenon may account for the direct stimulation of blood components to the superficial cortex [16]. Animal models have emphasized the involvement of hemosiderin depositions in late seizure susceptibility and epileptogenesis. Besides, as the study of poststroke epilepsy is deepened, some epileptogenic genes are associated with seizure susceptibility and are possibly involved in epileptogenesis [17].

Diagnosis of poststroke epilepsy is often challenging because of the diversity of clinical manifestations and low recognition. Electroencephalography (EEG), not widely used at present in hospitals, is unable to provide definitive information to predict an impending seizure or to guide inpatient AED management [18]. In recent years, more researches have confirmed that the blood biomarkers are associated with the occurrence of PSE and even provide more accurate and reliable information for the prognostic of PSE. This review is aimed at summarizing the existing studies on potential biomarkers for PSE diagnosis and prognosis.

## 2. Inflammatory Biomarkers

Inflammatory mediators increasing amount of clinical studies suggest that it has a tight connection with the initiation and progression of poststroke epilepsy. Repeated seizures can trigger inflammatory response, which in turn stimulates the production of inflammatory factors. At the same time, a variety of inflammatory markers of the nervous system can increase neuronal excitability and induce seizures [19, 20].

**2.1. Interleukin.** Interleukin is a common cytokine that participates in inflammation and has a pivotal role in the systemic immunomodulatory. Although its content is at a low level in the human body, the expression of cytokines will increase rapidly when brain tissue suffers from ischemic injury and further result in an inflammatory reaction. Recent studies suggest that inflammatory mediators, such as interleukin- (IL-)  $1\beta$ , IL-6, and IL-10, play a significant role in the underlying pathophysiology of epilepsy, contributing to the onset and perpetuation of seizures [21, 22]. Interleukin-6 (IL-6), regarded as the upstream mediator of the inflammatory reaction [23], is rapidly upregulated after acute CNS injury. The determination of the IL-6 level is a good predictor of poststroke epilepsy. Previous studies have found that patients with seizures resulting from multiple etiologies are accompanied by elevated levels of IL-6 [22, 24]. Kegler et al. found that Ala16Val MnSOD (alanine to valine at the 16th amino acid manganese superoxide dismutase) polymorphism has an important role on neuroinflammation maintenance and its consequences, especially the VV genotype in epilepsy patients, increased levels of inflammatory cytokines such as IL- $1\beta$  and IL-6 [22]. This finding has also been con-

firmed in animal models [25]. Mice are highly vulnerable to seizures by intracranial injection of IL-6 into the neocortex [26, 27]. A cohort study of patients with acute ischemic stroke also found that the serum IL-6 levels in patients with poststroke epilepsy were significantly higher than those in patients without seizures, which could be regarded as an independent predictor of seizures in stroke patients. Jia et al. studied 209 patients with poststroke epilepsy who were diagnosed within 1 week of admission and found that serum IL-6 can be used as a biomarker of recurrent epilepsy after stroke. The results of the ROC curve showed that the possibility of predicting epilepsy recurrence by IL-6 was 70% [28]. Besides, IL-6 levels were also associated with the development of poststroke cognitive impairment, patients with higher levels of IL-6 had lower MMSE scores three months after stroke [29].

Interleukin- $1\beta$  is also a multifunctional cytokine produced by brain glial cells related to seizures. Multiple studies have found that various biological samples such as serum and cerebrospinal fluid of patients with epilepsy are accompanied by the increase of IL- $1\beta$  [30–32]. The level of interleukin- $1\beta$  in epileptogenic regions of the poststroke epileptic animal model was also significantly higher than that of normal tissue. The injection of exogenous IL- $1\beta$  antibodies into the brain will have a prominent anticonvulsant effect on epileptic mice. Zhang et al. found that IL-1 was overexpressed in patients with recurrent poststroke epilepsy compared to the patients without recurrence. Receiver operating characteristic (ROC) curve analysis showed that the area under curves was 0.808 when the best cut-off value of IL- $1\beta$  was 5.42, which could be used as a biomarker of recurrent epilepsy after stroke [33]. In addition, IL- $1\beta$  is also the intermediate medium for IL-10 to participate in the epileptic response. With a strong anti-inflammation effect, IL-10 is known to suppress seizures in epilepsy patients by reducing the expression of interleukin-1 [34]. There is a significant negative correlation between plasma IL-10 levels and the prolongation of seizure time, while the continuous decrease of IL-10 has a significant positive correlation with hippocampal sclerosis in patients with epilepsy [35]. The significance of IL-10 in epilepsy remains controversial because some studies have reported that the level of IL-10 in patients with epilepsy is increased instead of decreased. A recent meta-analysis has noted that IL-8, IL-17, and IL-22, several inflammatory mediators that can lead to blood-brain barrier disruption, are also crucial factors involved in seizures by evaluating the correlation between epilepsy and different subtypes of interleukin [32]. Different experiments have demonstrated that in patients with epilepsy, serum IL-17 levels were 5-15 times higher than in the control groups [36], but there was no research on the correlation between poststroke epilepsy and the above three subtypes, which need to be further studied.

**2.2. Tumor Necrosis Factor.** Tumor necrosis factor (TNF) has multiple subtypes, among which TNF- $\alpha$  is the most highly correlated to epilepsy. Extra-CNS TNF- $\alpha$  is inaccessible to the intracranial brain tissues. However, it will not only stimulate glial cells to excessively secrete tumor necrosis factor



TNF- $\alpha$  but also promote peripheral inflammatory cytokines transported from the blood into the brain when the integrity of the blood-brain barrier is impaired. The high level of tumor necrosis factor associated with the inflammatory response after stroke is an important cause of poststroke epilepsy [37]. Studies have noted increased TNF- $\alpha$  serum levels in individuals with epilepsy compared with normal subjects. The content of TNF- $\alpha$  in brain tissue of epilepsy rats similarly shows a significant upward trend [38]. Low-dose TNF- $\alpha$  (5.0  $\mu\text{g}/\text{kg}$ ) significantly increased the frequency of epilepsy and prolonged the duration of neuronal firing [39, 40]. The content of TNF- $\alpha$  was positively correlated with the severity of epilepsy, which was higher in the severe epilepsy group than in the mild group, while the nonepileptic group is at a minimum level [41]. Tumor necrosis factor is mainly involved in the pathological process of seizures through two receptors, which will induce seizures by binding receptor 1, while the activation of receptor 2 will exert anticonvulsant effects. Abaira noted that low levels of tumor necrosis factor receptor 1 are an independent predictor of early poststroke seizures. The optimal cut-off value in the ROC curve is 0.013 with the strongest prognostic value, which can be interpreted as evidence of the increase of TNF-R1 binding after stroke. The study also pointed out that the combination of TNF-R1 with existing clinical predictors will significantly improve the early identification of poststroke epilepsy [42]. Despite no relevant research that has reported that TNF-R2 could be used to predict epilepsy, receptor 1 inhibition and receptor 2 activations may be an effective means for preventing poststroke epilepsy.

### 3. Neurotransmitter Biomarkers

The imbalance of neurotransmitters is a crucial cause of seizures. Glutamate is the primary excitatory neurotransmitter in the CNS, while GABA is a main inhibitory transmitter that counterbalances the excitatory action of glutamate. On the one hand, glutamic acid decarboxylase can convert glutamic acid to  $\gamma$ -aminobutyric acid, while  $\gamma$ -aminobutyric acid can be converted to  $\alpha$ -keto succinate by a  $\gamma$ -aminobutyric acid transaminase. It will lead to the occurrence of poststroke epilepsy when stroke leads to the imbalance of the above circulatory metabolic pathways. High levels of glutamate in the acute phase of stroke are a biomarker for poststroke seizures [15, 43]. Xie et al. found that plasma glutamate levels in patients with poststroke epilepsy are significantly higher than those without seizures [14]. Animal experiments have similarly confirmed that the glutamate level in the central nervous system increased significantly when brain tissue suffering from ischemic damage especially the ischemic core region is most evident. Studies on patients with tumor-associated epilepsy also confirmed that glutamate in the epileptogenic hippocampus was significantly higher than that in other populations. Recent studies have found that the content of glutamate was significantly higher during the interictal period than during epileptic seizures in epilepsy patients who undergo surgical treatments. Thus, they suggest that increased levels of glutamate can result in the occurrence of spontaneous seizures. Stroke causes excessive glutamate

released from the presynaptic membrane into the synaptic, which produces excitotoxicity leading to the recurrence of abnormal neuronal discharge [44]. Therefore, glutamate could be an important target to prevent or treat epilepsy. On the other hand, the expression of GABA and its receptors is downregulated after stroke, which reduces the seizure threshold and leads to the occurrence of epilepsy [14]. Patients who received oral GABA within 14 days after a stroke had higher GABA and lower glutamate levels than those without any intervention when remeasured one month after drug withdrawal. GABA administration can effectively inhibit the occurrence of early poststroke epilepsy. The decrease in GABA production and GABA receptor expression equally provide reliable information for the prediction of poststroke epilepsy.

### 4. Genetic Biomarkers

Since the first seizure-related gene was found in animal experiments, more than 500 genes and loci have been confirmed to contribute to the seizures. To the best of our knowledge, approximately 30% of epilepsy syndromes have been shown to be related to genetic factors, several of which have been identified as causally related to poststroke epilepsy [17].

**4.1. ALDH2 rs671.** ALDH2 rs671 polymorphism, a reliable index that can be used to predict poststroke epilepsy, refers to the mutations in exon 12, which result in the substitution of glutamic acid by lysine. Therefore, ALDH2 can be divided into three different genotypes: homozygous mutations (AA genotype), heterozygous mutations (GA genotype), and wild-type mutations (GG genotype) [45]. The mutations of the A gene could lead to a decrease of 90% in the enzyme activity of ALDH. A case-control study found that rs671A allelic or genotypic frequencies in the PSE group were significantly higher than those in the IS group, and the difference between the two groups was striking. ALDH2 is a key enzyme in 4HN metabolism, inducing seizures by suppressing ALDH2 activity that may lead to decreased proteolysis of 4HN. The mutated genes induce seizures by suppressing ALDH2 activity that may lead to decreased proteolysis of 4HN. 4-HNE serves as a specific biomarker for oxidative stress. The continuous increase of 4-HNE promotes inflammatory reactions, which enhance free radical production, increase excitability of neurons, and induce epilepsy [46]. Increased 4-HNE levels were found in mice with middle cerebral artery occlusive cerebral infarction [47]. Zhang confirmed that patients with poststroke epilepsy showed a significantly higher 4-HNE level in the postacute phase compared with the levels in patients with stroke who did not develop PSE and in control patients. There is a positive correlation between 4-HNE and PSE, which suggests that the content of serum 4-HNE provides a convinced index for evaluating the risk of epileptic seizures after stroke [48]. ALDH2 is one of the best-characterized target proteins of daidzein. The combination of the two acts as an antiepileptic effect by multiple pathways [49].

**4.2. TRPM6 Polymorphism.** There is a close relationship between cell electrophysiological instabilities and epilepsy, and varying the concentration of the ion inside and outside of the cell has been identified to be the link between them. Decreased serum magnesium was demonstrated to reduce seizure threshold or increase seizure susceptibility, leading to an increased vulnerability to epilepsy [50]. Magnesium sulfate ( $MgSO_4$ ) is the most commonly used medication for the control of seizure in preeclampsia for which the patient is at risk. N-Methyl-D-aspartate-induced convulsions in experimental animals can be effectively controlled by oral magnesium supplementation [51].

Transient receptor potential cation channel subfamily M member 6 (TRPM6), belonging to nonselective cation channel families, is the key regulator responsible for the transportation of the body's  $Mg^{2+}$  balance [52]. Mutation of the gene encoding TRPM6 can decrease blood magnesium levels due to the imbalanced ion transport in intestinal and kidney tubule epithelia. Some studies have reported that a homozygous variant genotype of the polymorphism of TRPM6 was associated with an increased risk of poststroke epilepsy. TRPM6C genotype (CC) frequency was significantly higher in those patients than in controls ( $P = 0.006$ ). The mutant allele with the C variant is more common in patients with poststroke epilepsy. TRPM6 are essential regulators of  $Mg^{2+}$  transport. Mutated TRPM6 gene results in hereditary hypomagnesemia [53]. Therefore, the mechanisms of icogenesis may be achieved by decreasing the magnesium ion concentrations, which leads to a reduced seizure threshold and an increased vulnerability to epilepsy. This phenomenon that sera magnesium content generally decreased seems to be confirmed in vivo in epilepsy patients [54]. Compared with the TT genotype, the TRPM6rs2274924 CC genotype was significantly associated with an induced risk of poststroke epilepsy. The frequency of the C allele in poststroke epilepsy patients was significantly higher than that in the nonepilepsy group [55].

**4.3. CD40/CD40L System.** Mounting evidence implicates that inflammatory response and oxidative stress are implicated in the pathogenesis of poststroke epilepsy, while agents having antioxidant activity also exert neuroprotective effects in seizures. The interaction of CD40 with its ligand, CD40 ligand (CD40L), is the link between inflammation and immunity [56]. On the one hand, activated CD40 initiates the inflammatory response via activating JNK and nuclear factor-kappa B (NF- $\kappa$ B) pathways. On the other hand, it promotes the production of reactive oxygen species, which in turn causes the occurrence of oxidative stress [57]. Previous studies show that SCD40L is a surrogate biologic marker for the occurrence of cardiovascular risk [23, 58]. Recent retrospective studies have found that CD40 gene polymorphism is associated with seizure susceptibility. The T allele was associated with significantly increased poststroke epilepsy risk compared with the C allele. Furthermore, this CD40T gene exhibits a stronger expression of mRNA and the content of CD40 protein and the ligand in the carriers were significantly higher than those in other groups, which is particularly apparent in the TT group. CD40L is also thought to be a

prognostic marker for unfavorable outcomes [59]. Elevated CD40L levels were associated with a worse prognosis in post-stroke epilepsy patients. The CD40 system determination of stroke patients would provide more accurate and reliable information for the prediction of the occurrence and prognostic of poststroke epilepsy.

## 5. Neuroprotein Biomarkers

**5.1. S100B.** S100 calcium-binding protein B (S100B) is a  $Ca^{2+}$  binding protein that is expressed mainly in the brain by astrocytes, which participates in signal transduction, inflammatory reactions, and repair of neurons and glial cells after central nervous system injury. Previous research has highlighted the importance of S100B not only as the most useful biomarker for glial cell injury and central nervous system dysfunction but also as a tool for the diagnosis and prediction of epileptic seizures [60, 61]. Although the inclusion criteria are different, many studies have shown that the serum S100B in epilepsy patients is significantly higher than that in the control group regardless of the aetiology and location of the seizures, and this increases with increased frequency of seizures. The central nervous system damage and the inflammatory response caused by a stroke can stimulate the expression of S100B. The severity of the ischemic injury and the stimulation by microbial components that are risk factors for poststroke epilepsy has been widely acknowledged and endorsed. Therefore, it would be plausible for S100B to be increased in these patients. Before thrombolytic therapy in high-risk patients undergoing hemorrhagic transformation, elevated serum S100B levels were observed [62]. In 1070 days median follow-up for 90 patients on mechanical thrombectomy treatment, Eriksson proved that multiple serology indicators, including S100B in patients with poststroke epilepsy, are higher than normal. With a sensitivity of predicting post-stroke epilepsy being 100%, the best specificity can still reach 77%~93%. However, given the low incidence of poststroke epilepsy in this study, statistical analysis was not further performed [63]. Recent meta-analyses of several cohorts provide a multitude of evidence that support the elevation of S100B protein level in epilepsy patients. Two recent meta-analyses also provided evidence for the increase of serum S100B levels in patients with epilepsy. S100B is the most valuable biological marker for seizures and prognosis [64, 65].

Some researchers have come out with the opposite conclusion. Abaira concluded that reduced S100B levels were related to a greater risk of epilepsy after stroke. S100B level  $< 1.364$  ( $P = 0.001$ ) is an independent predictor of post-stroke epilepsy [66]. S100B plays a crucial role in maintaining the integrity of the blood-brain barrier function. The reduction of S100B not only causes the disorder of the blood-brain barrier function but also leads to the imbalance of microglia function that both will induce epilepsy [67]. Although there are many studies on S100B, the mechanism by which S100B leads to epilepsy is unclear. S100B in patients with ischemic stroke did not increase until eight hours after the ischemic damage, while the serological samples in Zhang et al.'s study were drawn within six hours after stroke [68].

Whether the levels at different times have different significance for poststroke seizures still needs to be confirmed by large-scale clinical trials.

5.2. *Hsc70*. Heat shock 70 kDa protein-8 (*Hsc70*) is a member of the heat shock protein 70 (*Hsp70*) family, which is a potential predictor of poststroke epilepsy. A retrospective study of 14 serological blood indicators in 1115 stroke patients found that heat shock protein levels in patients with early poststroke epilepsy were higher than those without seizures and the control group, although the difference did not reach statistical significance after adjusting for confounding factors [42, 63]. Another retrospective study of late poststroke epilepsy also found that the heat shock protein was significantly decreased in the epileptic group, and the low level of heat shock protein is a biomarker that can be used in the prediction and detection of poststroke epilepsy. ROC curve analysis showed that the optimal cut-off value of the seizure risk is 2.496. *Hsc70* has neuroprotective effects, which act as molecular chaperones, promoting the correct folding of proteins to maintain protein homeostasis [66, 69]. Decreasing *Hsc70* contributes to impairment of blood-brain barrier integrity, altering the susceptibility of poststroke epilepsy.

In addition, the decrease of *Hsc70* may be related to the increased expression of *Hsp70* in poststroke stress [70]. Heat shock protein 70 (*Hsp70*) is a stress protein and is expressed after exposure to various stress conditions, which is significantly higher in patients with temporal lobe epilepsy than in normal subjects. Some studies have also suggested that heat shock protein 70 is a stress marker of temporal lobe epilepsy. Those who had more frequent seizures also reported expressing more *Hsp70* compared to those who had less frequent seizures [71]. In particular, the expression levels of *Hsp70* in the hippocampus are positively correlated with epileptogenic power and negatively correlated with surgical treatment efficacy. This could be due to the hyperexcitability of cortical networks caused by the strong expression of heat shock proteins under stress. At present, reports on the study of *Hsp70* in poststroke epilepsy are scarce. In particular, the roles of *Hsp70* in seizure activity are still controversial.

The fact that specific alterations of different biomarkers were observed in epilepsy patients supports the notion that biomarkers can improve the prediction of patients who later experience acute or remote symptomatic seizures after stroke and could be valuable in addition to clinical or EEG factors. Besides, biomarkers may also have important reference significance for understanding the mechanism of epileptic seizures and evaluating prognosis.

## 6. Conclusions

In summary, due to progress in treatments of poststroke patients, the prevalence of stroke-related seizures is increasing. Although the EEG is strongly recommended to monitor epileptic activity, there are still many difficulties in clinical application. The current guidelines only give some weak recommendations on prevention of occurrence of poststroke seizures, and the use of antiepileptic drugs remains contro-

versial. Hence, the use of biomarkers in the prediction of poststroke epilepsy provides a complementary approach. In this review, it is divided into inflammatory biomarkers, neurotransmitter biomarkers, genetic biomarkers, and neuroprotein biomarkers. Changes in the levels of these biomarkers are largely related to the occurrence and prognosis of PSE. The discovery and application of biomarkers will identify new pharmacological targets and develop more therapies for the treatment of PSE. Further large-scale clinical randomized controlled trials are required to support the research results.

## Data Availability

The data used to support the findings of our study are included within the article (see References).

## Conflicts of Interest

The authors declare there are any potential conflicts of interest. The authors declare they have no actual or potential competing financial interests.

## Authors' Contributions

Mengke Liang and Liren Zhang wrote the paper. Zhi Geng made revisions to the manuscript. Mengke Liang and Liren Zhang contributed equally to this work and should be considered co-first authors.

## Acknowledgments

This study was supported by grants from the Science and Technology Committee of Fengxian District, Shanghai (20201605).

## References

- [1] A. M. Feyissa, T. F. Hasan, and J. F. Meschia, "Stroke-related epilepsy," *European Journal of Neurology*, vol. 26, no. 1, p. 18, 2019.
- [2] E. Beghi, A. Carpio, L. Forsgren et al., "Recommendation for a definition of acute symptomatic seizure," *Epilepsia*, vol. 51, no. 4, pp. 671–675, 2010.
- [3] O. Camilo and L. B. Goldstein, "Seizures and epilepsy after ischemic stroke," *Stroke*, vol. 35, no. 7, pp. 1769–1775, 2004.
- [4] S. Zou, X. Wu, B. Zhu, J. Yu, B. Yang, and J. Shi, "The pooled incidence of post-stroke seizure in 102 008 patients," *Topics in Stroke Rehabilitation*, vol. 22, no. 6, pp. 460–467, 2015.
- [5] M. Anadani, A. Lekoubou, E. Almallouhi et al., "Incidence, predictors, and outcome of early seizures after mechanical thrombectomy," *Journal of the Neurological Sciences*, vol. 396, pp. 235–239, 2019.
- [6] N. Shehta, R. Fahmi, B. Ramadan, E. M. Emad, and A. F. Elsaid, "Early post-stroke seizures in a sample of Egyptian patients with first-ever stroke," *Neurology India*, vol. 66, no. 4, pp. 1031–1035, 2018.
- [7] F. Rodríguez Lucci, M. Alet, and S. Ameriso, "Post-stroke epilepsy," *Medicina (B Aires)*, vol. 78, no. 2, pp. 86–90, 2018.



- [8] J. W. Doria and P. B. Forgacs, "Incidence, implications, and management of seizures following ischemic and hemorrhagic stroke," *Current Neurology and Neuroscience Reports*, vol. 19, no. 7, p. 37, 2019.
- [9] M. A. Kamp, M. Dibue, T. Schneider, H. J. Steiger, and D. Hanggi, "Calcium and potassium channels in experimental subarachnoid hemorrhage and transient global ischemia," *Stroke Research and Treatment*, vol. 2012, Article ID 382146, 8 pages, 2012.
- [10] C. F. Bladin, A. V. Alexandrov, A. Bellavance et al., "Seizures after stroke a prospective multicenter study," *Archives of Neurology*, vol. 57, no. 11, pp. 1617–1622, 2000.
- [11] G. Feher, Z. Gurdan, K. Gombos et al., "Early seizures after ischemic stroke: focus on thrombolysis," *CNS Spectrums*, vol. 25, no. 1, pp. 101–113, 2020.
- [12] S. Y. Kim, M. Buckwalter, H. Soreq, A. Vezzani, and D. Kaufer, "Blood-brain barrier dysfunction-induced inflammatory signaling in brain pathology and epileptogenesis," *Epilepsia*, vol. 53, Suppl 6, pp. 37–44, 2012.
- [13] T. Tanaka and M. Ihara, "Post-stroke epilepsy," *Neurochemistry International*, vol. 107, pp. 219–228, 2017.
- [14] W. J. Xie, M. Dong, Q. Liu, and H. M. Meng, "Early predictors and prevention for post-stroke epilepsy: changes in neurotransmitter levels," *Translational Neuroscience*, vol. 7, no. 1, pp. 1–5, 2016.
- [15] D. A. Sun, S. Sombati, and R. J. DeLorenzo, "Glutamate injury-induced epileptogenesis in hippocampal neurons: an in vitro model of stroke-induced "epilepsy"," *Stroke*, vol. 32, no. 10, pp. 2344–2350, 2001.
- [16] A. M. Lahti, P. Saloheimo, J. Huhtakangas et al., "Poststroke epilepsy in long-term survivors of primary intracerebral hemorrhage," *Neurology*, vol. 88, no. 23, pp. 2169–2175, 2017.
- [17] J. Noebels, "Pathway-driven discovery of epilepsy genes," *Nature Neuroscience*, vol. 18, no. 3, pp. 344–350, 2015.
- [18] R. Rao, D. J. Monlezun, T. Kimbrough, B. J. Burkett, A. Samai, and S. Martin-Schild, "Antiepileptic drug management in acute ischemic stroke: are vascular neurologists utilizing electroencephalograms? An observational cohort study," *BioMed Research International*, vol. 2020, Article ID 6250531, 6 pages, 2020.
- [19] K. M. Webster, M. Sun, P. Crack, T. J. O'Brien, S. R. Shultz, and B. D. Semple, "Inflammation in epileptogenesis after traumatic brain injury," *Journal of Neuroinflammation*, vol. 14, no. 1, p. 10, 2017.
- [20] A. Dey, X. Kang, J. Qiu, Y. Du, and J. Jiang, "Anti-inflammatory small molecules to treat seizures and epilepsy: from bench to bedside," *Trends in Pharmacological Sciences*, vol. 37, no. 6, pp. 463–484, 2016.
- [21] A. Vezzani, S. Balosso, and T. Ravizza, "Neuroinflammatory pathways as treatment targets and biomarkers in epilepsy," *Nature Reviews Neurology*, vol. 15, no. 8, pp. 459–472, 2019.
- [22] A. Kegler, A. L. F. Caprara, E. T. Pascotini et al., "Apoptotic Markers Are Increased in Epilepsy Patients: A Relation with Manganese Superoxide Dismutase Ala16Val Polymorphism and Seizure Type through IL-1 $\beta$  and IL-6 Pathways," *BioMed Research International*, vol. 2020, Article ID 6250429, 9 pages, 2020.
- [23] X. Y. Wang, F. Zhang, C. Zhang, L. R. Zheng, and J. Yang, "The biomarkers for acute myocardial infarction and heart failure," *BioMed Research International*, vol. 2020, Article ID 2018035, 2020.
- [24] H. Tao, Y. Gong, Q. Yu, H. Zhou, and Y. Liu, "Elevated serum matrix metalloproteinase-9, interleukin-6, hypersensitive C-reactive protein, and homocysteine levels in patients with epilepsy," *Journal of Interferon & Cytokine Research*, vol. 40, no. 3, pp. 152–158, 2020.
- [25] N. Chmielewska, P. Maciejak, B. Osuch, M. B. Kurska, and J. Szyndler, "Pro-inflammatory cytokines, but not brain- and extracellular matrix-derived proteins, are increased in the plasma following electrically induced kindling of seizures," *Pharmacological Reports*, vol. 73, no. 2, pp. 506–515, 2021.
- [26] A. Vezzani, S. Balosso, and T. Ravizza, "The role of cytokines in the pathophysiology of epilepsy," *Brain, Behavior, and Immunity*, vol. 22, no. 6, pp. 797–803, 2008.
- [27] M. Erta, A. Quintana, and J. Hidalgo, "Interleukin-6, a major cytokine in the central nervous system," *International Journal of Biological Sciences*, vol. 8, no. 9, pp. 1254–1266, 2012.
- [28] Q. Jia, F. Jiang, D. Ma, J. Li, F. Wang, and Z. Wang, "Association between IL-6 and seizure recurrence in patients with the first post-ischemic stroke seizure," *Neuropsychiatric Disease and Treatment*, vol. Volume 16, pp. 1955–1963, 2020.
- [29] A. Kulesh, V. Drobakha, E. Kuklina, I. Nekrasova, and V. Shestakov, "Cytokine response, tract-specific fractional anisotropy, and brain morphometry in post-stroke cognitive impairment," *Journal of Stroke and Cerebrovascular Diseases*, vol. 27, no. 7, pp. 1752–1759, 2018.
- [30] E. A. van Vliet, E. Aronica, A. Vezzani, and T. Ravizza, "Review: neuroinflammatory pathways as treatment targets and biomarker candidates in epilepsy: emerging evidence from preclinical and clinical studies," *Neuropathology and Applied Neurobiology*, vol. 44, no. 1, pp. 91–111, 2018.
- [31] L. M. Shi, R. J. Chen, H. Zhang, C. M. Jiang, and J. Gong, "Cerebrospinal fluid neuron specific enolase, interleukin-1 $\beta$  and erythropoietin concentrations in children after seizures," *Child's Nervous System*, vol. 33, no. 5, pp. 805–811, 2017.
- [32] E. E. de Vries, B. van den Munckhof, K. P. Braun, A. van Royen-Kerkhof, W. de Jager, and F. E. Jansen, "Inflammatory mediators in human epilepsy: A systematic review and meta-analysis," *Neuroscience and Biobehavioral Reviews*, vol. 63, pp. 177–190, 2016.
- [33] Q. Zhang, G. Li, D. Zhao, P. Yang, T. Shabier, and T. Tuerxun, "Association between IL-1 $\beta$  and recurrence after the first epileptic seizure in ischemic stroke patients," *Scientific Reports*, vol. 10, no. 1, article 13505, 2020.
- [34] Y. Sun, J. Ma, D. Li et al., "Interleukin-10 inhibits interleukin-1 $\beta$  production and inflammasome activation of microglia in epileptic seizures," *Journal of Neuroinflammation*, vol. 16, no. 1, p. 66, 2019.
- [35] P. Basnyat, M. Pesu, M. Söderqvist et al., "Chronically reduced IL-10 plasma levels are associated with hippocampal sclerosis in temporal lobe epilepsy patients," *BMC Neurology*, vol. 20, no. 1, p. 241, 2020.
- [36] J. Todd, P. Simpson, J. Estis, V. Torres, and A. H. Wub, "Reference range and short- and long-term biological variation of interleukin (IL)-6, IL-17A and tissue necrosis factor-alpha using high sensitivity assays," *Cytokine*, vol. 64, no. 3, pp. 660–665, 2013.
- [37] X. Deng, X. Zhang, B. Tang et al., "Design, synthesis, and evaluation of dihydrobenzo[cd]indole-6-sulfonamide as TNF- $\alpha$  inhibitors," *Frontiers in Chemistry*, vol. 6, p. 98, 2018.

- [38] S. Bauer, S. Cepok, A. Todorova-Rudolph et al., "Etiology and site of temporal lobe epilepsy influence postictal cytokine release," *Epilepsy Research*, vol. 86, no. 1, pp. 82–88, 2009.
- [39] L. Y. He, M. B. Hu, R. L. Li et al., "The effect of protein-rich extract from *Bombyx batryticatus* against glutamate-damaged PC12 cells via regulating  $\gamma$ -Aminobutyric acid signaling pathway," *Molecules*, vol. 25, no. 3, p. 553, 2020.
- [40] A. Shandra, L. Godlevsky, R. Vastyanov et al., "The role of TNF- $\alpha$  in amygdala kindled rats," *Neuroscience Research*, vol. 42, no. 2, pp. 147–153, 2002.
- [41] T. Kamaşak, B. Dilber, S. Ö. Yaman et al., "HMGB-1, TLR4, IL-1R1, TNF- $\alpha$ , and IL-1 $\beta$ : novel epilepsy markers?," *Epileptic Disorders*, vol. 22, no. 2, pp. 183–193, 2020.
- [42] L. Abraira, N. Giannini, E. Santamarina et al., "Correlation of blood biomarkers with early-onset seizures after an acute stroke event," *Epilepsy & Behavior*, vol. 104, article 106549, Pt B, 2020.
- [43] H. Luhmann, "Ischemia and lesion induced imbalances in cortical function," *Progress in Neurobiology*, vol. 48, no. 2, pp. 131–166, 1996.
- [44] K. Lippmann, L. Kamintsky, S. Y. Kim et al., "Epileptiform activity and spreading depolarization in the blood-brain barrier-disrupted peri-infarct hippocampus are associated with impaired GABAergic inhibition and synaptic plasticity," *Journal of Cerebral Blood Flow and Metabolism*, vol. 37, no. 5, pp. 1803–1819, 2017.
- [45] D. W. Crabb, H. J. Edenberg, W. F. Bosron, and T. K. Li, "Genotypes for aldehyde dehydrogenase deficiency and alcohol sensitivity. The inactive ALDH2(2) allele is dominant," *The Journal of Clinical Investigation*, vol. 83, no. 1, pp. 314–316, 1989.
- [46] H. Yang, Z. Song, G. P. Yang et al., "The ALDH2 rs671 polymorphism affects post-stroke epilepsy susceptibility and plasma 4-HNE levels," *PLoS One*, vol. 9, no. 10, article e109634, 2014.
- [47] W. C. Lee, H. Y. Wong, Y. Y. Chai et al., "Lipid peroxidation dysregulation in ischemic stroke: plasma 4-HNE as a potential biomarker?," *Biochemical and Biophysical Research Communications*, vol. 425, no. 4, pp. 842–847, 2012.
- [48] Z. Huang, M. C. Walker, and M. M. Shah, "Loss of dendritic HCN1 subunits enhances cortical excitability and epileptogenesis," *The Journal of Neuroscience*, vol. 29, no. 35, pp. 10979–10988, 2009.
- [49] Z. Kazmi, S. Zeeshan, A. Khan et al., "Anti-epileptic activity of daidzin in PTZ-induced mice model by targeting oxidative stress and BDNF/VEGF signaling," *Neurotoxicology*, vol. 79, pp. 150–163, 2020.
- [50] K. E. Osborn, R. D. Shytle, A. T. Frontera, J. R. Soble, and M. R. Schoenberg, "Addressing potential role of magnesium dyshomeostasis to improve treatment efficacy for epilepsy: a reexamination of the literature," *Journal of Clinical Pharmacology*, vol. 56, no. 3, pp. 260–265, 2016.
- [51] N. Pages, P. Maurois, B. Delplanque, P. Bac, and J. Vamecq, "Brain anticonvulsant protection of mice given chronic carbamazepine under various fatty acid and magnesium diet conditions," *Prostaglandins, Leukotrienes, and Essential Fatty Acids*, vol. 87, no. 2-3, pp. 63–70, 2012.
- [52] S. Lainez, K. P. Schlingmann, J. van der Wijst et al., "New TRPM6 missense mutations linked to hypomagnesemia with secondary hypocalcemia," *European Journal of Human Genetics*, vol. 22, no. 4, pp. 497–504, 2014.
- [53] J. S. Cuffe, S. Steane, K. M. Moritz, and T. M. Paravicini, "Differential mRNA expression and glucocorticoid-mediated regulation of TRPM6 and TRPM7 in the heart and kidney throughout murine pregnancy and development," *PLoS One*, vol. 10, no. 2, article e0117978, 2015.
- [54] A. E. Kirkland, G. L. Sarlo, and K. F. Holton, "The role of magnesium in neurological disorders," *Nutrients*, vol. 10, no. 6, p. 730, 2018.
- [55] C. Y. Fu, S. J. Chen, N. H. Cai et al., "Increased risk of post-stroke epilepsy in Chinese patients with a TRPM6 polymorphism," *Neurological Research*, vol. 41, no. 4, pp. 378–383, 2019.
- [56] C. Antoniadis, C. Bakogiannis, D. Tousoulis, A. S. Antonopoulos, and C. Stefanadis, "The CD40/CD40 ligand system: linking inflammation with atherothrombosis," *Journal of the American College of Cardiology*, vol. 54, no. 8, pp. 669–677, 2009.
- [57] M. Rizvi, D. Pathak, J. E. Freedman, and S. Chakrabarti, "CD40-CD40 ligand interactions in oxidative stress, inflammation and vascular disease," *Trends in Molecular Medicine*, vol. 14, no. 12, pp. 530–538, 2008.
- [58] G. Davì, A. Tuttolomondo, F. Santilli et al., "CD40 ligand and MCP-1 as predictors of cardiovascular events in diabetic patients with stroke," *Journal of Atherosclerosis and Thrombosis*, vol. 16, no. 6, pp. 707–713, 2009.
- [59] B. Zhang, M. Chen, H. Yang, T. Wu, C. Song, and R. Guo, "Evidence for involvement of the CD40/CD40L system in post-stroke epilepsy," *Neuroscience Letters*, vol. 567, pp. 6–10, 2014.
- [60] E. B. Bulduk, G. Kurt, S. Barun et al., "The effects of minocycline on the hippocampus in lithium-pilocarpine induced status epilepticus in rat: relations with microglial/astrocytic activation and serum S100B level," *Turkish Neurosurgery*, vol. 29, no. 1, pp. 95–105, 2019.
- [61] R. Maiti, B. R. Mishra, M. Jena, A. Mishra, S. Nath, and A. Srinivasan, "Effect of anti-seizure drugs on serum S100B in patients with focal seizure: a randomized controlled trial," *Journal of Neurology*, vol. 265, no. 11, pp. 2594–2601, 2018.
- [62] C. Foerch, M. T. Wunderlich, F. Dvorak et al., "Elevated serum S100B levels indicate a higher risk of hemorrhagic transformation after thrombolytic therapy in acute stroke," *Stroke*, vol. 38, no. 9, pp. 2491–2495, 2007.
- [63] H. Eriksson, P. Löwhagen Hendén, A. Rentzos et al., "Acute symptomatic seizures and epilepsy after mechanical thrombectomy," *Epilepsy & Behavior*, vol. 104, article 106520, Pt B, 2020.
- [64] L. Simani, M. Sadeghi, F. Ryan, M. Dehghani, and S. Niknazar, "Elevated blood-based brain biomarker levels in patients with epileptic seizures: a systematic review and meta-analysis," *ACS Chemical Neuroscience*, vol. 11, no. 24, pp. 4048–4059, 2020.
- [65] K. G. Liang, R. Z. Mu, Y. Liu, D. Jiang, T. T. Jia, and Y. J. Huang, "Increased serum S100B levels in patients with epilepsy: a systematic review and meta-analysis study," *Frontiers in Neuroscience*, vol. 13, p. 456, 2019.
- [66] L. Abraira, E. Santamarina, S. Cazorla et al., "Blood biomarkers predictive of epilepsy after an acute stroke event," *Epilepsia*, vol. 61, no. 10, pp. 2244–2253, 2020.
- [67] H. Wu, E. V. Brown, N. K. Acharya et al., "Age-dependent increase of blood-brain barrier permeability and neuron-binding autoantibodies in S100B knockout mice," *Brain Research*, vol. 1637, pp. 154–167, 2016.



- [68] K. Fassbender, R. Schmidt, A. Schreiner et al., "Leakage of brain-originated proteins in peripheral blood: temporal profile and diagnostic value in early ischemic stroke," *Journal of the Neurological Sciences*, vol. 148, no. 1, pp. 101–105, 1997.
- [69] K. Rejdak, J. Kuhle, S. Rüegg et al., "Neurofilament heavy chain and heat shock protein 70 as markers of seizure-related brain injury," *Epilepsia*, vol. 53, no. 5, pp. 922–927, 2012.
- [70] T. Liu, C. K. Daniels, and S. Cao, "Comprehensive review on the HSC70 functions, interactions with related molecules and involvement in clinical diseases and therapeutic potential," *Pharmacology & Therapeutics*, vol. 136, no. 3, pp. 354–374, 2012.
- [71] P. Gass, P. Prior, and M. Kiessling, "Correlation between seizure intensity and stress protein expression after limbic epilepsy in the rat brain," *Neuroscience*, vol. 65, no. 1, pp. 27–36, 1995.

## *Retraction*

# **Retracted: Pancancer Analysis of Neurovascular-Related NRP Family Genes as Potential Prognostic Biomarkers of Bladder Urothelial Carcinoma**

### **BioMed Research International**

Received 12 March 2024; Accepted 12 March 2024; Published 20 March 2024

Copyright © 2024 BioMed Research International. This is an open access article distributed under the Creative Commons Attribution License, which permits unrestricted use, distribution, and reproduction in any medium, provided the original work is properly cited.

This article has been retracted by Hindawi following an investigation undertaken by the publisher [1]. This investigation has uncovered evidence of one or more of the following indicators of systematic manipulation of the publication process:

- (1) Discrepancies in scope
- (2) Discrepancies in the description of the research reported
- (3) Discrepancies between the availability of data and the research described
- (4) Inappropriate citations
- (5) Incoherent, meaningless and/or irrelevant content included in the article
- (6) Manipulated or compromised peer review

The presence of these indicators undermines our confidence in the integrity of the article's content and we cannot, therefore, vouch for its reliability. Please note that this notice is intended solely to alert readers that the content of this article is unreliable. We have not investigated whether authors were aware of or involved in the systematic manipulation of the publication process.

Wiley and Hindawi regrets that the usual quality checks did not identify these issues before publication and have since put additional measures in place to safeguard research integrity.

We wish to credit our own Research Integrity and Research Publishing teams and anonymous and named external researchers and research integrity experts for contributing to this investigation.

The corresponding author, as the representative of all authors, has been given the opportunity to register their agreement or disagreement to this retraction. We have kept a record of any response received.

### **References**

- [1] C. Deng, H. Guo, D. Yan, T. Liang, X. Ye, and Z. Li, "Pancancer Analysis of Neurovascular-Related NRP Family Genes as Potential Prognostic Biomarkers of Bladder Urothelial Carcinoma," *BioMed Research International*, vol. 2021, Article ID 5546612, 31 pages, 2021.

## Research Article

# Pancancer Analysis of Neurovascular-Related NRP Family Genes as Potential Prognostic Biomarkers of Bladder Urothelial Carcinoma

Chao Deng, Hang Guo, Dongliang Yan , Tao Liang, Xuxiao Ye, and Zuwei Li

Department of Urology, Shanghai Jiao Tong University Affiliated Sixth People's Hospital, Shanghai, China

Correspondence should be addressed to Dongliang Yan; [dly1919@126.com](mailto:dly1919@126.com)

Chao Deng and Hang Guo contributed equally to this work.

Received 2 February 2021; Revised 8 March 2021; Accepted 20 March 2021; Published 15 April 2021

Academic Editor: Qian Wang

Copyright © 2021 Chao Deng et al. This is an open access article distributed under the Creative Commons Attribution License, which permits unrestricted use, distribution, and reproduction in any medium, provided the original work is properly cited.

**Background.** Neurovascular-related genes have been implicated in the development of cancer. Studies have shown that a high expression of neuropilins (NRPs) promotes tumorigenesis and tumour malignancy. **Method.** A multidimensional bioinformatics analysis was performed to examine the relationship between NRP genes and prognostic and pathological features, tumour mutational burden (TMB), microsatellite instability (MSI), and immunological features based on public databases and find the potential prognostic value of NRPs in pancancer. **Results.** Survival analysis revealed that a low NRP1 expression in adrenocortical carcinoma (ACC), cervical squamous cell carcinoma and endocervical adenocarcinoma (CESC), low-grade glioma (LGG), and stomach adenocarcinoma (STAD) was associated with poor prognosis. A high NRP2 expression in bladder urothelial carcinoma (BLCA), kidney renal papillary cell carcinoma (KIRP), and mesothelioma (MESO) was associated with poor prognosis. Moreover, NRP1 and NRP2 were associated with TMB and MSI. Subsequent analyses showed that NRP1 and NRP2 were correlated with immune infiltration and immune checkpoints. Genome-wide association analysis revealed that the NRP1 expression was strongly associated with kidney renal clear cell carcinoma (KIRC), whereas the NRP2 expression was closely associated with BLCA. Ultimately, NRP2 was found to be involved in the development of BLCA. **Conclusions.** Neurovascular-related NRP family genes are significantly correlated with cancer prognosis, TME, and immune infiltration, particularly in BLCA.

## 1. Introduction

The growth and development of neovascular tissue or angiogenesis are critical for normal physiological processes. Therefore, dysregulation of the angiogenic process has been linked to tumour development and progression [1]. The vascular endothelial growth factor (VEGF) is a key factor involved in angiogenesis. VEGF messenger RNA (mRNA) is widely overexpressed in tissues and is associated with metastasis, recurrence, and prognosis [2]. In recent years, several drugs that inhibit the VEGF signaling pathway have been designed to treat cancer, including anti-VEGF monoclonal antibodies [3–6]. And neurovascular-related genes have been implicated

in cancer development. There is a strong link between neural stem/progenitor cells (NSPCs) and endothelial cells (ECs) [7].

Evidence suggests that neuropilins (NRPs), the VEGF receptors, are involved in tumorigenesis [8, 9]. NRPs participate in the development of the nervous system by functioning as receptors for axon guidance factors [10]. Several signaling pathways regulate neuronal development by targeting NRPs [11]. High expression of NRPs is closely associated with tumorigenesis and malignancy [12].

NRP1 and NRP2 are two isoforms of NRPs in mammals; studies have demonstrated their cancer-promoting potential [13]. For example, NRP2 is highly expressed in triple-negative breast cancers [14]. In prostate cancer, NRP2 expression is

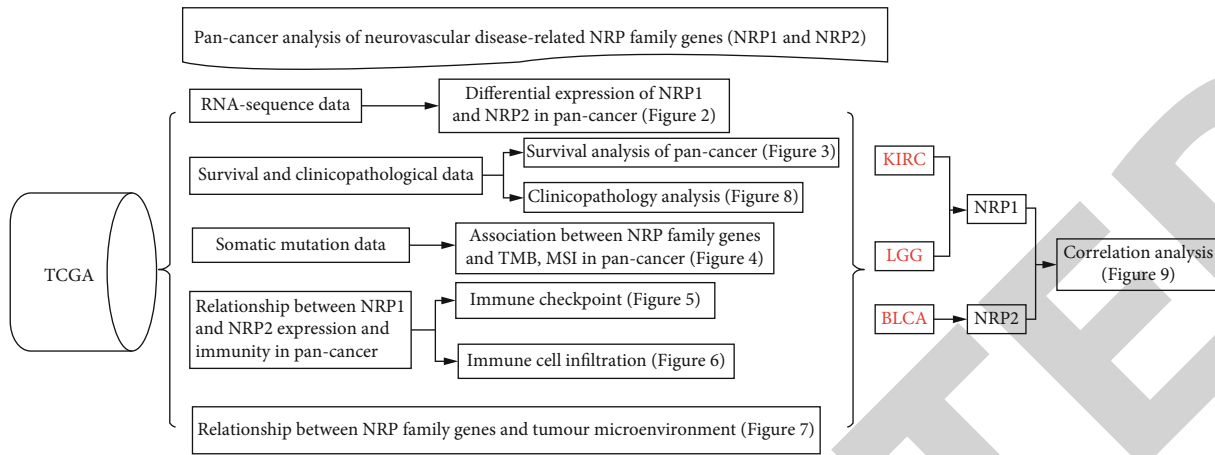


FIGURE 1: Flow chart for this study.

positively correlated with the Gleason grade [15]. In the bladder cancer, high expression of NRP2 is associated with chemoresistance and epithelial-to-mesenchymal transition and poor patient prognosis [16]. However, the expression and function of NRPs in different cancers are not fully known.

Herein, we comprehensively analysed the correlation of NRP expression with prognosis and tumour microenvironment landscape in 33 cancer types. Our findings reveal that NRPs may be a potential prognostic marker associated with immune infiltration, tumour mutations, and tumour microenvironment, particularly in bladder urothelial carcinoma (BLCA).

## 2. Materials and Methods

**2.1. Analysis of Differential NRP1 and NRP2 Gene Expression in Human Cancer.** RNA sequences, somatic mutations, and clinicopathological features of 33 cancers were downloaded from The Cancer Genome Atlas (TCGA) database. The data included 10,953 patients (10,967 samples). A pancancer analysis was performed on NRP1 and NRP2 mRNA expression levels in the Oncomine database (<http://www.ONCOMINE.org>). The threshold was set at  $p$  value  $< 0.05$  and  $|\text{fold change}| > 1.5$ . In addition, changes in NRP1 and NRP2 expression in different cancer types were determined using the R package “ggpubr” and the cBioPortal database (<https://www.cbioportal.org>). All data analyses were performed using version 4.0.3 of the R language package (<https://www.r-project.org/>).

**2.2. Survival Analysis.** The association of NRP1 and NRP2 with survival was assessed with the Kaplan-Meier method and log-rank test ( $p < 0.05$ ). Patients were divided into high- and low-risk groups based on median expression levels of NRP1 and NRP2. Survival curves were created using “survminer” and “survivor” packages of R. Cox analysis was performed to explore the association of NRP1 and NRP2 with the prognosis of different cancers. A “forestplot” function was used to draw a forest plot whereas the “ggplot2” function was used to analyse clinicopathological features.

**2.3. Association of NRP Family Genes with Tumour Mutational Burden (TMB) and Microsatellite Instability (MSI) in Various Cancers.** TMB was derived from a study published by Gentles et al. [17], and MSI was obtained from a study published by Bonneville et al. [18]. As in previous studies [19–21], statistical analyses were performed using the rank-sum test, and  $p$  values less than 0.05 were considered statistically significant; R software was used for plotting.

**2.4. Association of NRP1 and NRP2 Expression with Immune Checkpoint-Related Genes in Different Cancers.** As described in previous studies [22–27], the xCell method was used to perform immune score assessment. The immune checkpoint genes, *pDCD1*, *SIGLEC15*, *HAVCR2*, *IDO1*, *CD274*, *LAG3*, *CTLA4*, and *PDCD1LG2*, were analysed to examine the association of NRP1 and NRP2 with expression of immune checkpoint-related genes.

**2.5. DNAss, RNAss, StromalScore, and ImmuneScore among Subgroups.** The differentiated phenotype was rapidly lost during cancer progression, and progenitor and stem-cell-like characteristics were acquired [28]. RNAss based on mRNA expression and DNAss based on DNA methylation were utilized to measure the tumour stemness [29]. The ESTIMATE algorithm in the R language ESTIMATE package was used to estimate the ratio of immune to stromal components in the TME for each sample and is presented as two scores: ImmuneScore and StromalScore, which are positively correlated with immune and stromal components, respectively.

**2.6. Integrative Data Visualization.** The correlation of NRP1 and NRP2 with other genes was mapped using Cancer Regu- lome Tools (<http://explorer.cancerregulome.org/>). A  $p$  value  $> -\log_{10}$  was considered statistically significant.

## 3. Results

**3.1. NRP1 and NRP2 mRNA Levels in Pancancers.** The flow chart of this study is shown in Figure 1. NRP1 and NRP2 were found to be widely expressed in human tissues (Figure 2(a)). The overall expression level of NRP1 did not

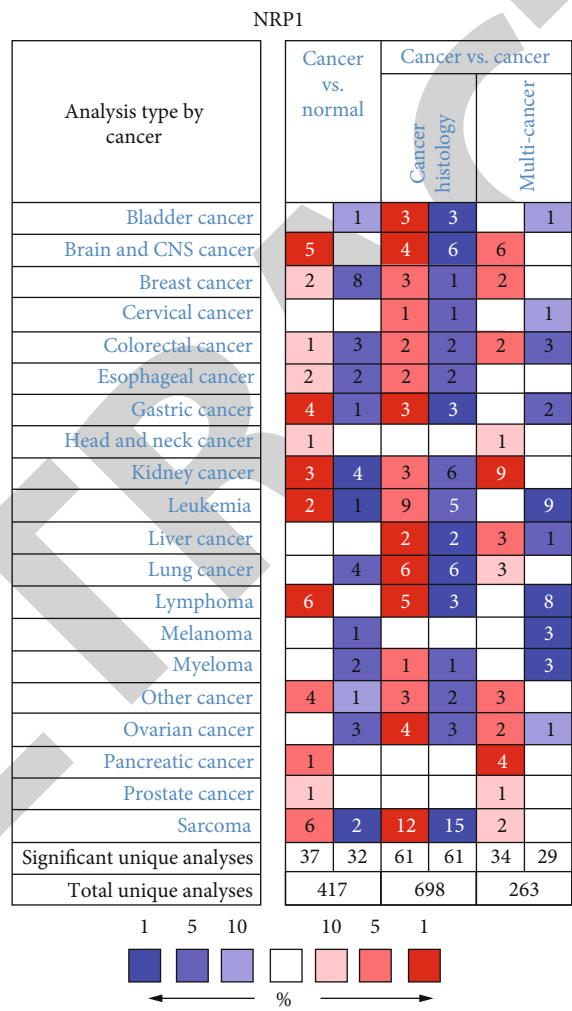
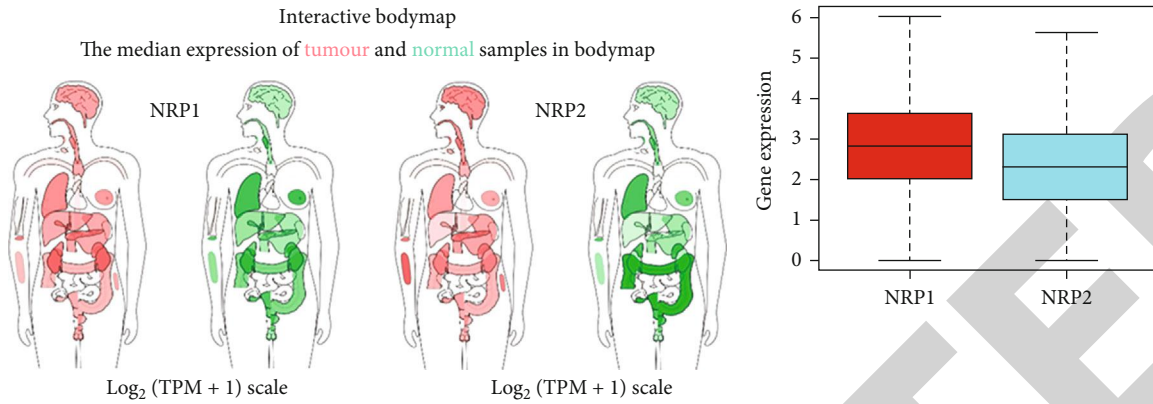
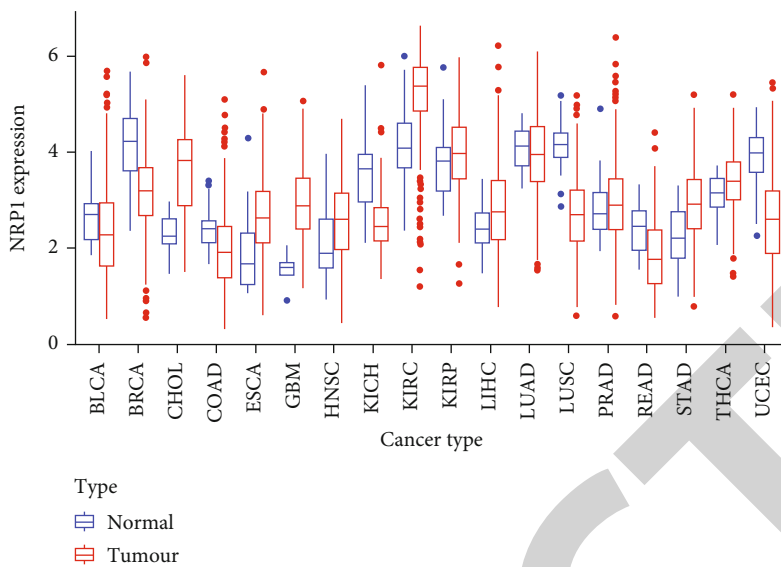
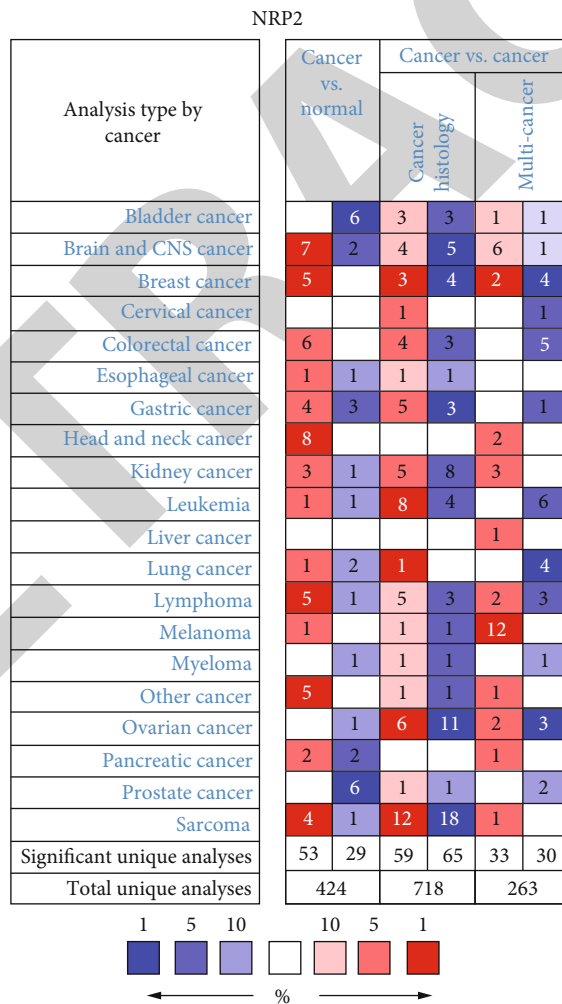


FIGURE 2: Continued.





(d)



(e)

FIGURE 2: Continued.

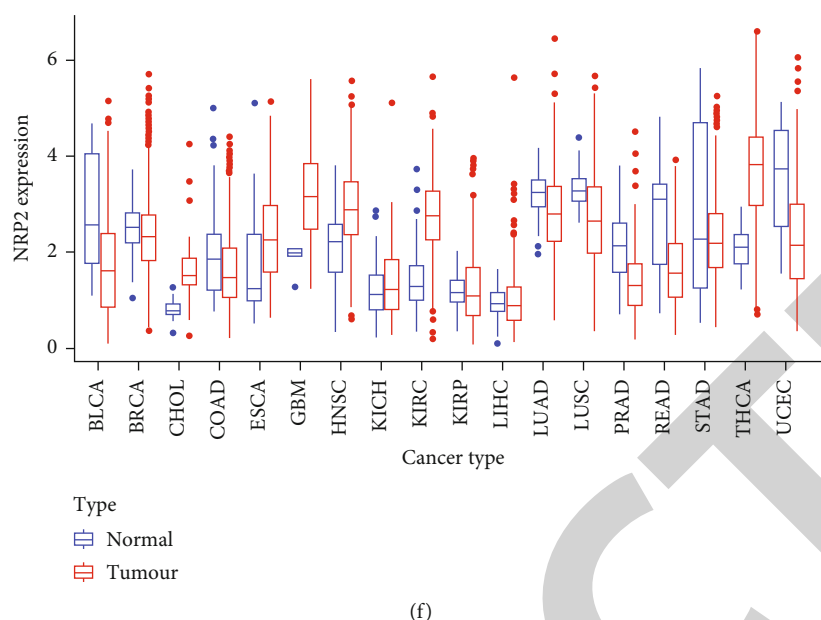


FIGURE 2: NRP1 and NRP2 mRNA levels in pancancers. (a) NRP1 and NRP2 expression levels in human tissues. Darker colours indicate higher levels of expression. (b) Overall expression of NRP1 and NRP2 in human tissues. (c) Differential in NRP1 expression in cancer and normal tissues in the Oncomine database. The number in each small rectangle represents the number of high or low expression of NRP genes in each cancer. Red (high expression) and blue (low expression) shading indicates the proportion in each cancer tissue. (d) Box plots from TCGA's database demonstrating differential expression of NRP1 expression in different tumour and normal samples. (e) Differential expression of NRP2 expression in cancer and normal tissues in the Oncomine database. (f) Box plots from TCGA's database demonstrating differential expression of NRP2 expression in different tumour and normal samples.

significantly differ from that of NRP2 in human tissues (Figure 2(b)), suggesting good concordance between NRP1 and NRP2 expression in humans. Results of NRP1 and NRP2 mRNA levels in the Oncomine database are shown in Figures 2(c) and 2(d). We further assessed the expression of NRP1 and NRP2 in different cancers by analysing 730 normal samples and 10,327 fractional tumour samples in TCGA data sets (Figures 2(e) and 2(f)). Overall, whether NRP1 and NRP2 are highly or lowly expressed in tumour tissue was difficult to establish. The expression of NRP1 and NRP2 was different between normal tissue and tumour tissues in the brain and central nervous system cancers. Of note, the expression of NRP1 and NRP2 genes in some cancers was inconsistent in different databases. These inconsistencies may be caused by different gene extraction methods and biological mechanisms. These results demonstrate that NRP1 and NRP2 are differentially expressed in different tissues, suggesting they may have distinct roles in different tissues.

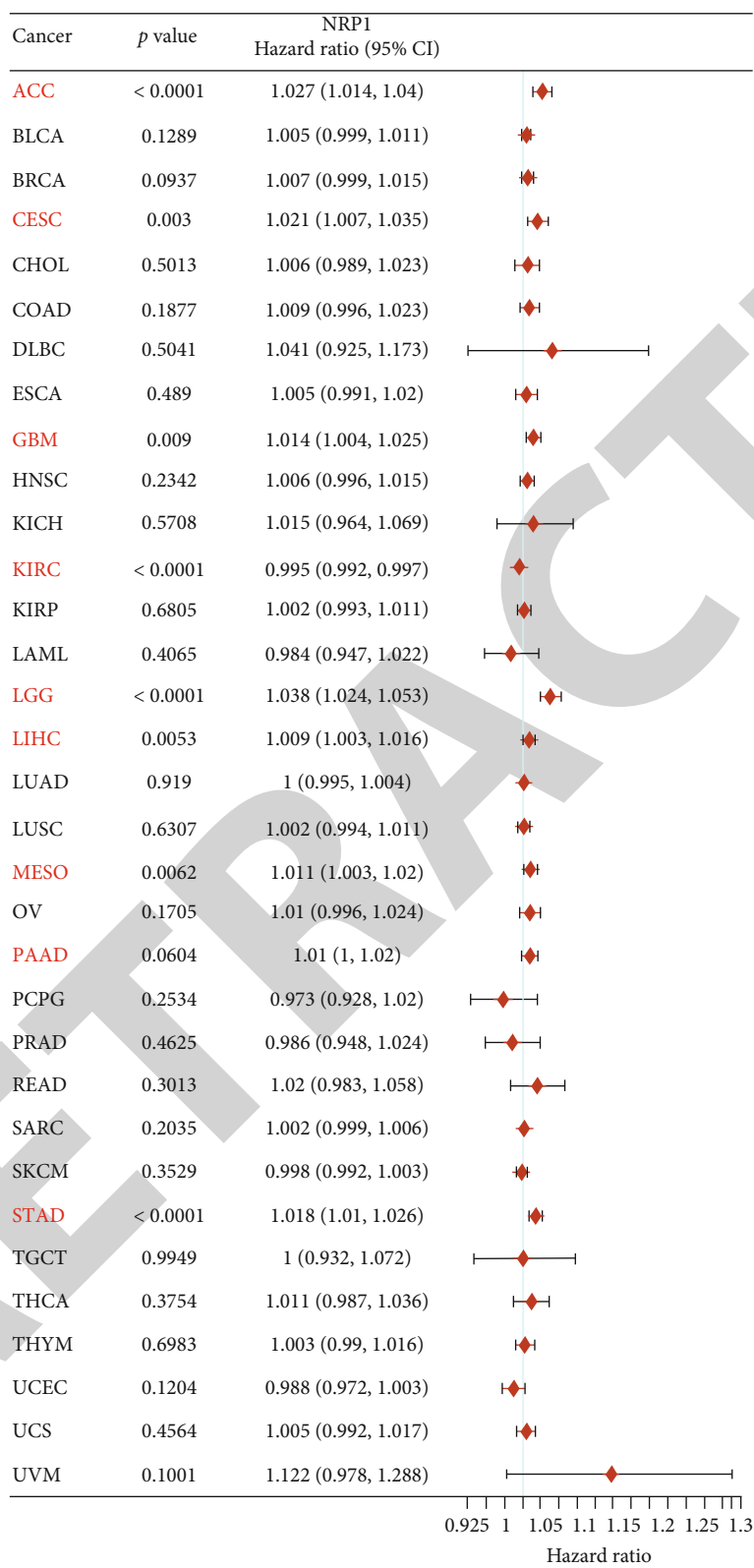
### 3.2. Prognostic Value of NRP1 and NRP2 in Various Cancers.

Next, we explored the prognostic value of NRP1 and NRP2 in various cancers in the TCGA database. We found that NRP1 and NRP2 expression was associated with the prognosis of various cancers. NRP1 was found to be a risk factor in different cancers, including ACC (HR 1.027, 95% CI 1.014-1.040,  $p < 0.001$ ), CESC (HR 1.021, 95% CI 1.007-1.035,  $p < 0.003$ ), GBM (HR 1.014, 95% CI 1.004-1.025,  $p = 0.009$ ), LGG (HR 1.038, 95% CI 1.024-1.053,  $p < 0.0001$ ), LIHC (HR 1.009, 95% CI 1.003-1.016,  $p = 0.0053$ ), MESO (HR 1.011, 95% CI 1.003-1.020,  $p = 0.0062$ ), and STAD (HR 1.018, 95% CI

1.010-1.026,  $p < 0.0001$ ) (Figure 3(a)). In contrast, NRP1 was a protective factor in KIRC (HR 0.995, 95% CI 0.992-0.997,  $p < 0.0001$ ). Further analysis showed that NRP2 was a risk factor in different cancers such as BLCA (HR 1.012, 95% CI 1.003-1.021,  $p = 0.0093$ ), KICH (HR 1.178, 95% CI 1.008-1.375,  $p = 0.0390$ ), KIRP (HR 1.048, 95% CI 1.015-1.081,  $p = 0.0040$ ), LAML (HR 1.127, 95% CI 1.031-1.232,  $p = 0.0086$ ), LGG (HR 1.012, 95% CI 1.002-1.021,  $p = 0.0168$ ), LIHC (HR 1.015, 95% CI 1.001-1.029,  $p = 0.0400$ ), MESO (HR 1.012, 95% CI 1.006-1.019,  $p = 0.0003$ ), PAAD (HR 1.017, 95% CI 1.006-1.029,  $p = 0.0027$ ), and STAD (HR 1.009, 95% CI 1.001-1.018,  $p = 0.0282$ ) (Figure 3(b)). Survival analysis suggested that low NRP1 expression in adrenocortical carcinoma (ACC), cervical squamous cell carcinoma and endocervical adenocarcinoma (CESC), low-grade glioma (LGG), and stomach adenocarcinoma (STAD) was associated with poor patient prognosis. However, high NRP1 expression in kidney renal clear cell carcinoma (KIRC) predicted good prognosis (Figures 3(c)–3(g)). High NRP2 expression in BLCA, kidney renal papillary cell carcinoma (KIRP), and mesothelioma (MESO) was associated with poor prognosis (Figures 3(h)–3(j)).

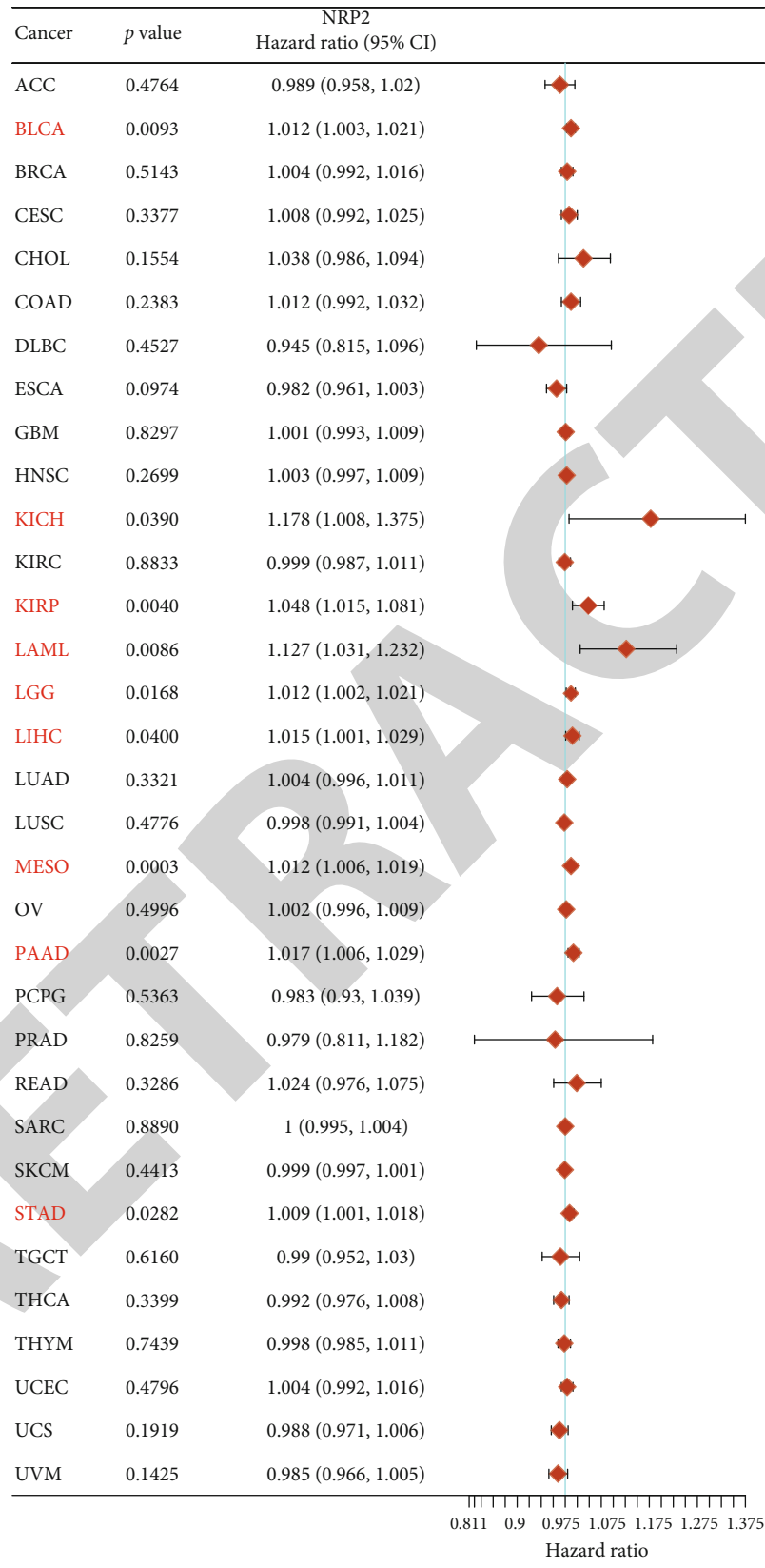
### 3.3. Association of NRP1 and NRP2 Expression with TMB and MSI in Different Cancers.

A high TMB influences immunotherapy sensitivity [28, 29]. Thus, we assessed the relationship between NRP2 expression levels and BLCA, kidney chromophobe (KICH), KIRP, acute myeloid leukemia (LAML), LGG, liver hepatocellular carcinoma (LIHC), MESO, pancreatic adenocarcinoma (PAAD), and STAD.



(a)

FIGURE 3: Continued.



(b)

FIGURE 3: Continued.

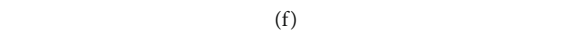
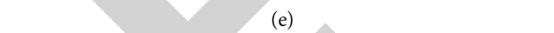
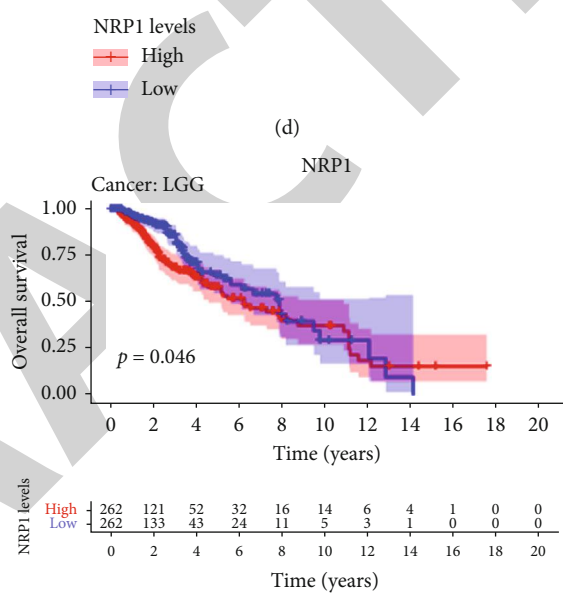
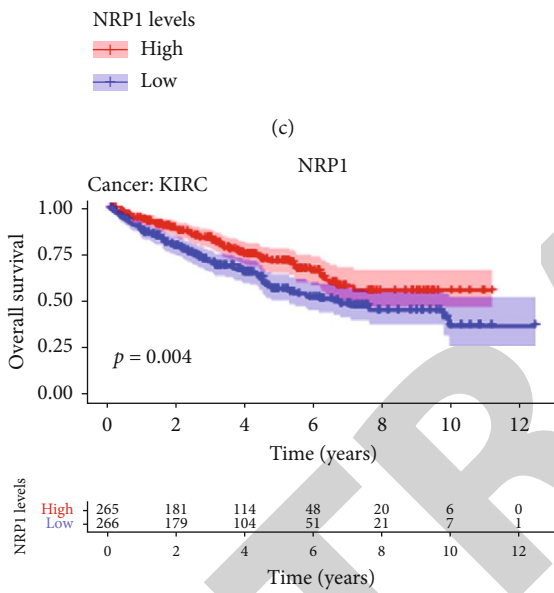
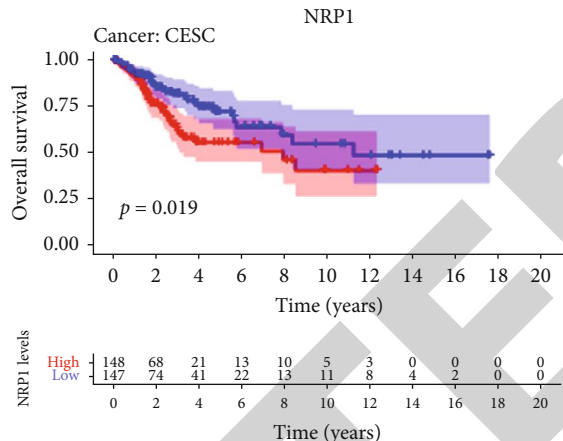
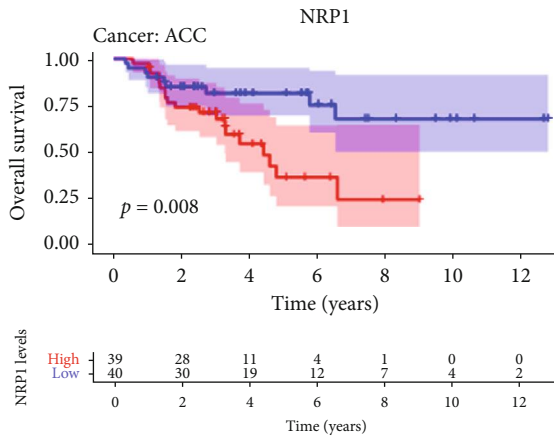


FIGURE 3: Continued.



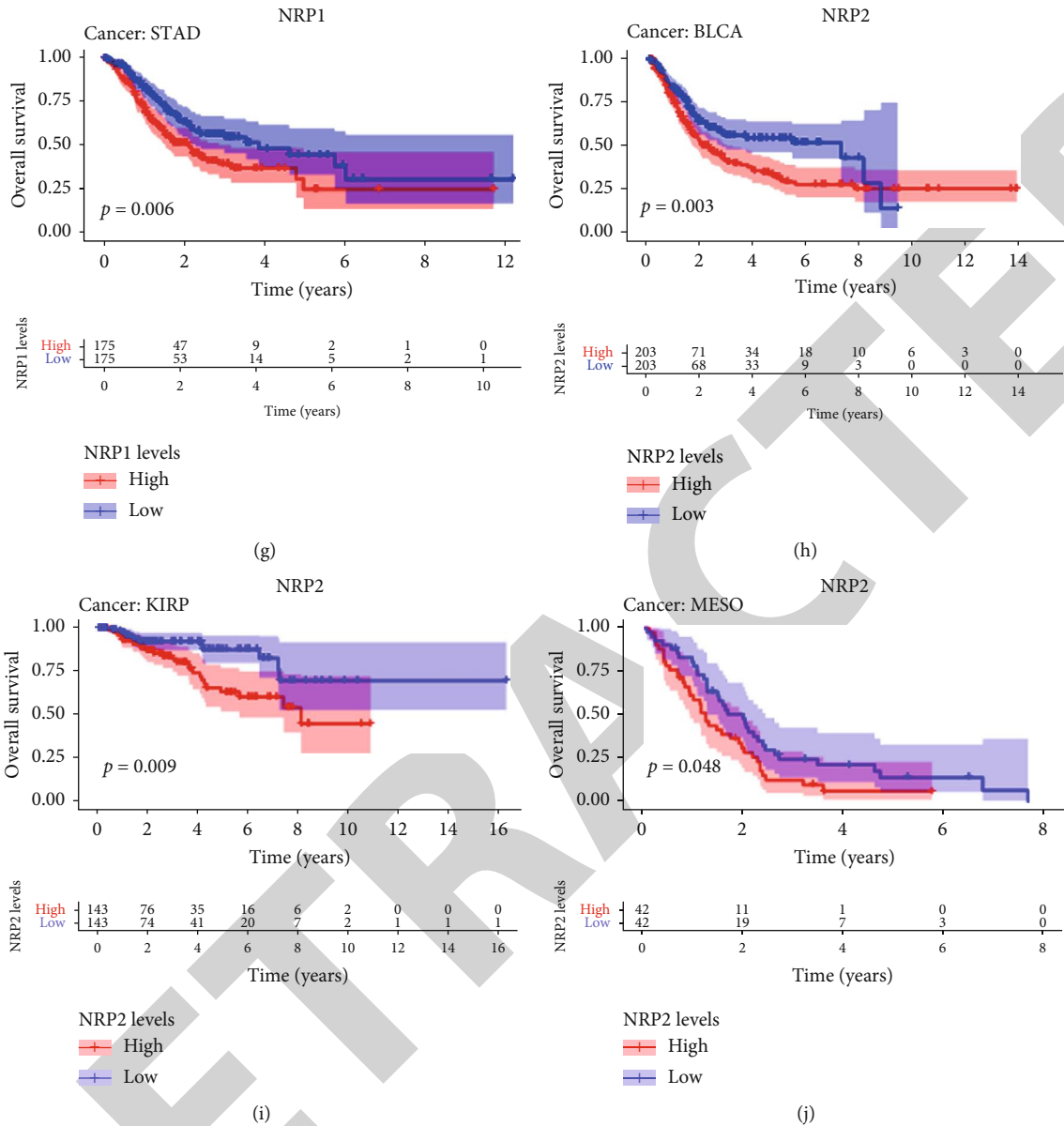


FIGURE 3: Prognostic value of NRP1 and NRP2 in pancreatic cancers (a, b). Association of NRP1 and NRP2 with the prognosis of different tumours in the univariate Cox analysis. (c–j) Association of NRP1 and NRP2 expression with the prognosis of different tumours as determined from Kaplan-Meier survival curves.

This is because the expression of NRP1 and NRP2 correlated with the overall survival of such cancers (according to the results of one-way Cox and Kaplan-Meier survival analyses). The results showed that NRP1 expression was positively correlated with TMB in ACC and LGG but negatively correlated with the TMB of MESO, LIHC, and STAD expression (Figure 4(a)). NRP2 expression was positively correlated with the TMB of LAML and PAAD but negatively correlated with the TMB of MESO, KIRP, STAD, and LIHC (Figure 4(c)).

In further analyses, it was found that NRP1 expression was significantly positively correlated with MSI in MESO but negatively correlated with MSI in STAD (Figure 4(b)). NRP2 expression was also significantly positively correlated with MSI in KIRC but negatively correlated with MSI in STAD (Figure 4(d)).

**3.4. Coexpression of Immune Checkpoint Genes with NRP1 and NRP2 in Different Cancers.** A coexpression analysis was performed to explore the correlation of NRP1 and NRP2 expression with immune checkpoint genes. In most cancers, NRP1 and NRP2 expression was found to be positively correlated with immune checkpoint genes (*CD274*, *CTLA4*, *HAVCR2*, *LAG3*, *PDCD1*, *PDCD1LG2*, *SIGLEC15*, and *TIGIT*) (Figures 5(a) and 5(b)). In BLCA, the NRP1 and NRP2 expression was negatively correlated with the *SIGLEC15* expression. In MESO, the *SIGLEC15* expression was negatively correlated with the NRP2 expression. In KIRC, *LAG3* and *PDCD1* expression levels were positively correlated with the NRP1 expression.

**3.5. Association of NRP1 and NRP2 Expression with Immune Infiltration.** Previously, we showed that low NRP1 expression

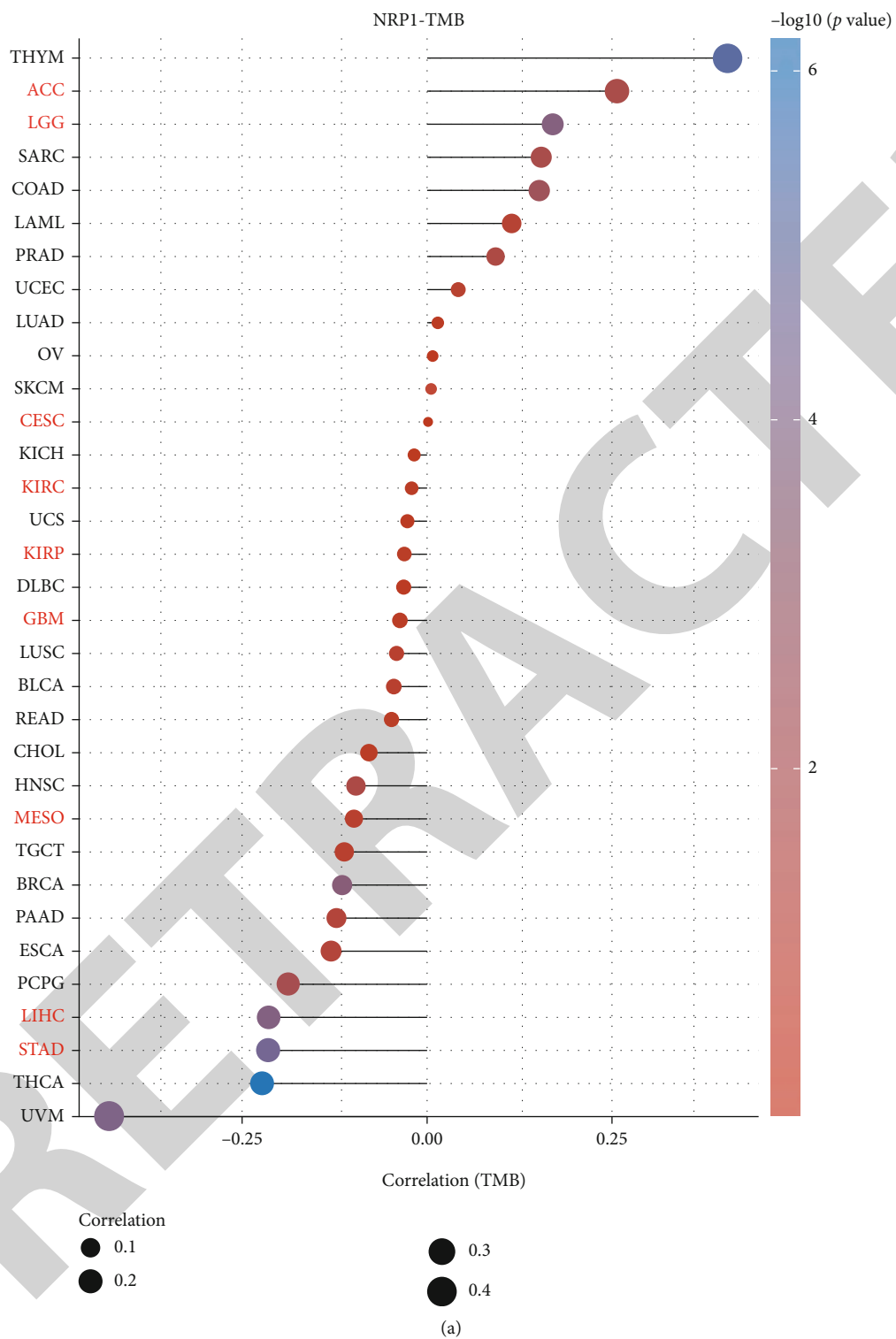
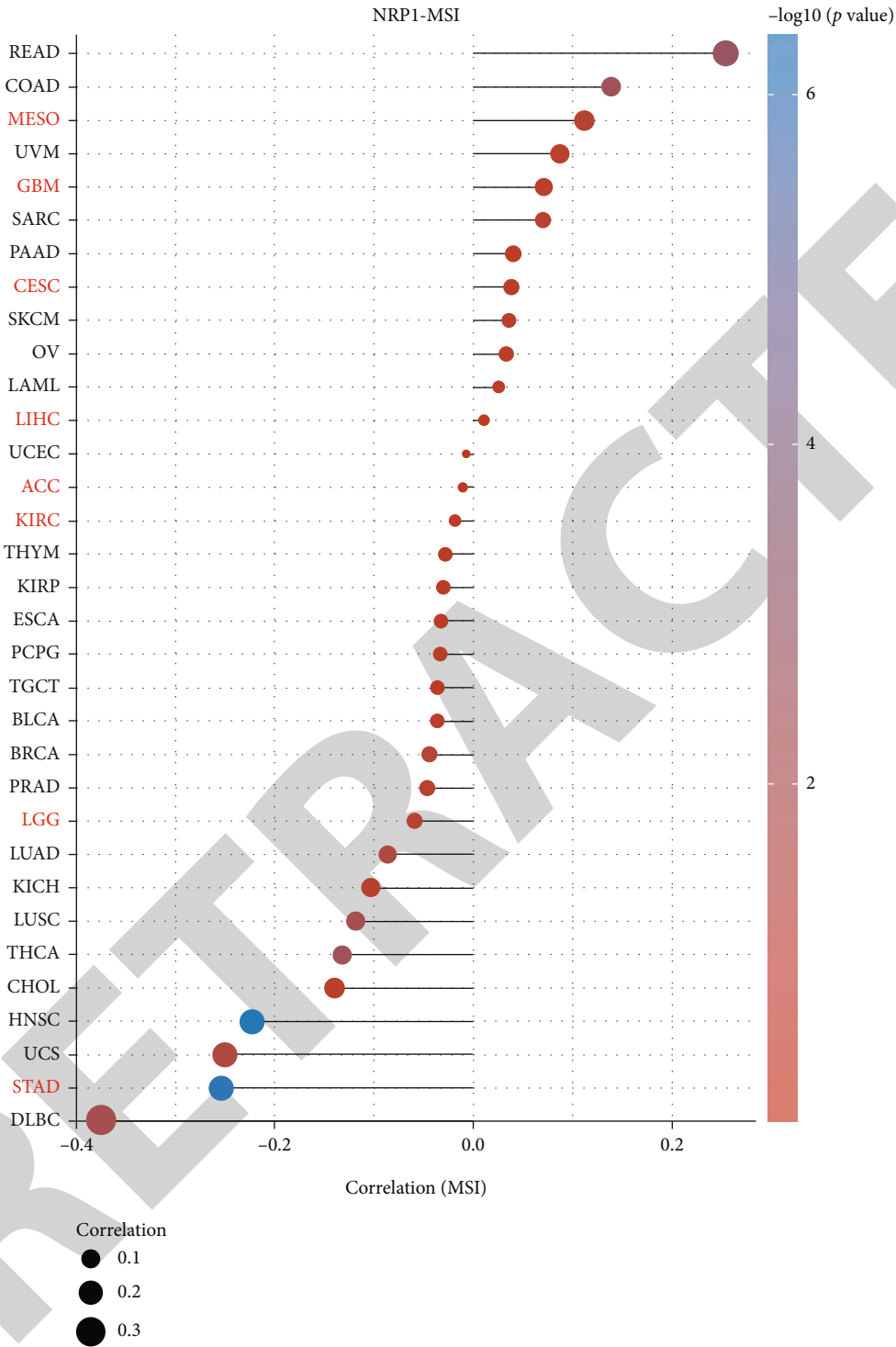
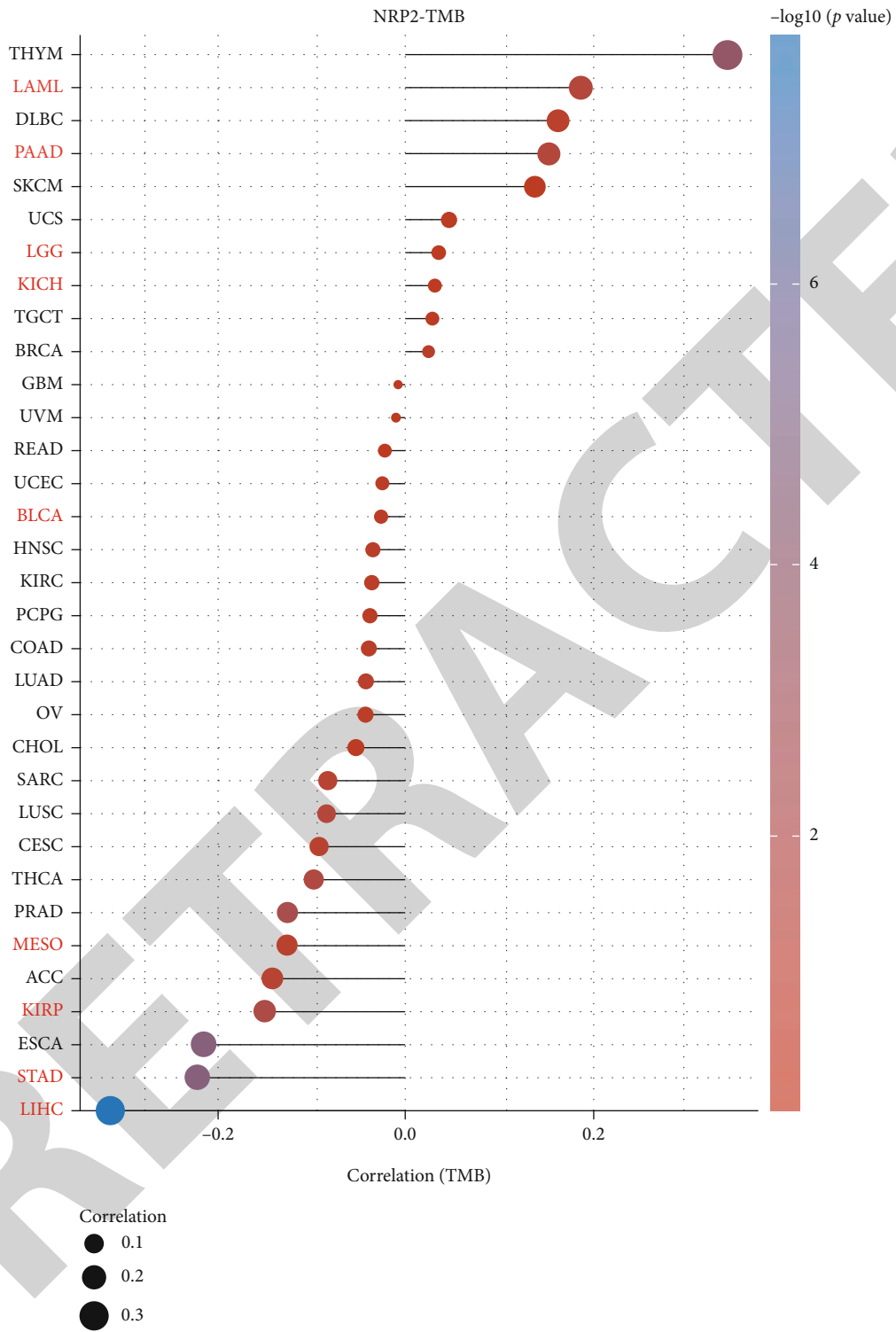


FIGURE 4: Continued.



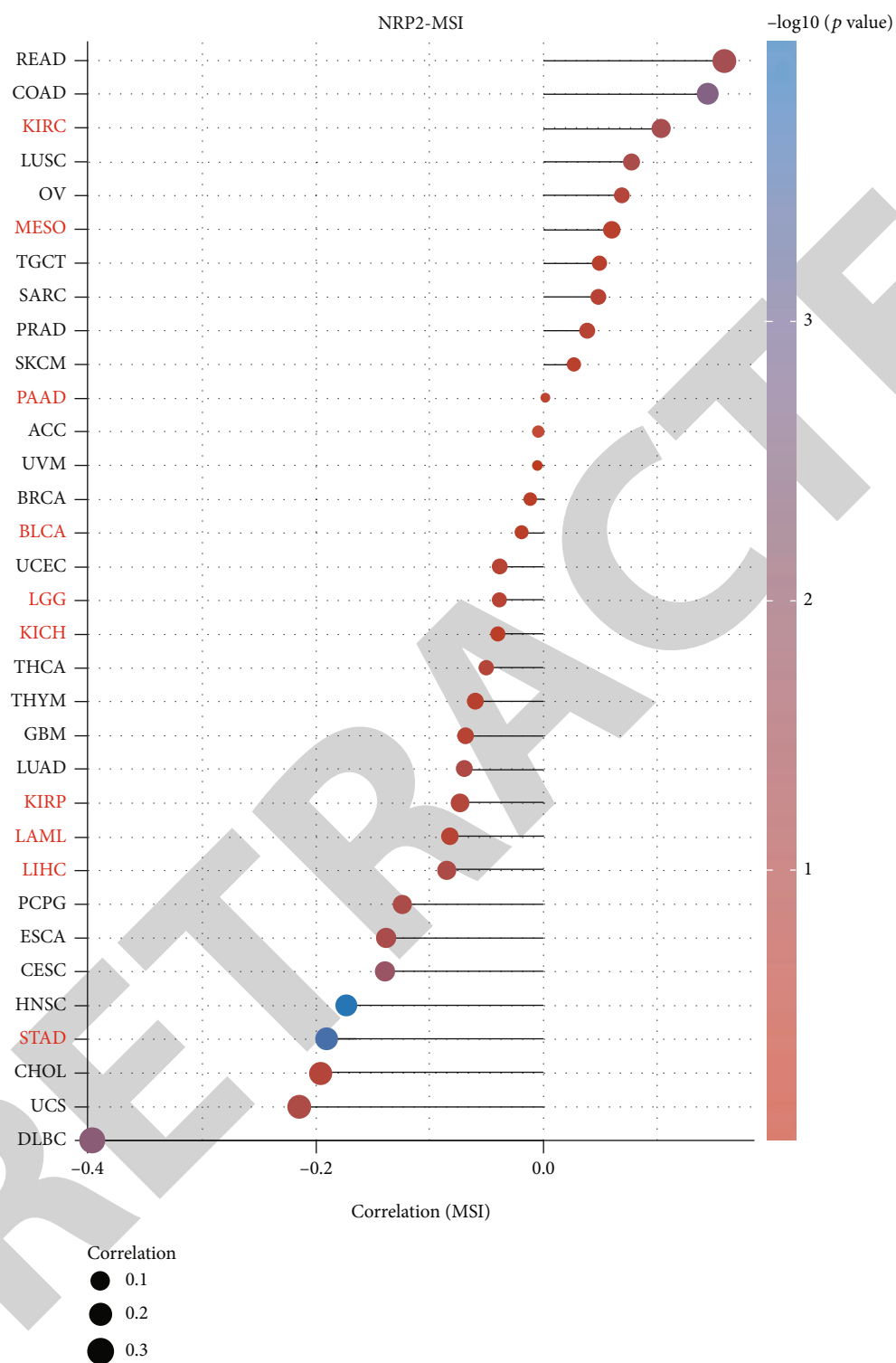
(b)

FIGURE 4: Continued.



(e)

FIGURE 4: Continued.



(d)

FIGURE 4: Correlation analysis between NRP1 and NRP2 gene expression and TMB and MSI in pancaner: (a) correlation between NRP1 and TMB; (b) correlation between NRP1 and MSI; (c) correlation between NRP2 and TMB; (d) correlation between NRP2 and MSI.

in ACC, CESC, LGG, and STAD was associated with poor prognosis, whereas high NRP1 expression in KIRC predicted good prognosis. Moreover, high NRP2 expression in BLCA, KIRP, and MESO was associated with poor prognosis.

Hence, the xCell approach was used to comprehensively assess the association of NRP family genes with immune infiltration (Figures 6(a) and 6(b)). We found that the NRP1 and NRP2 expression correlated significantly negatively with the





FIGURE 5: Coexpression of immune checkpoint genes with NRP1 (a) and NRP2 (b) in pancancers. Heat map of immune checkpoint-related gene expression in different tumour tissues, where the horizontal axis represents different tumour tissues and the vertical axis represents immune checkpoint-related gene expression.

T cell CD4+ Th1 expression in almost all of the cancer types. Infiltration of mast cells was positively correlated with the NRP1 expression in most of the cancer types. The high NRP1 expression in ACC, CESC, GBM, LGG, MESO, and STAD was associated with poor prognosis, suggesting that mast cell infiltration may be associated with NRP1 expression.

In addition, high NRP1 expression was associated with higher stroma, microenvironment, and immune scores, as well as more endothelial cell infiltration in most tumours. A high NRP2 expression in BLCA and KIRP was associated with poor patient prognosis, while a high NRP2 expression in BLCA and KIRP implied depletion of T cell CD4+ central memory.

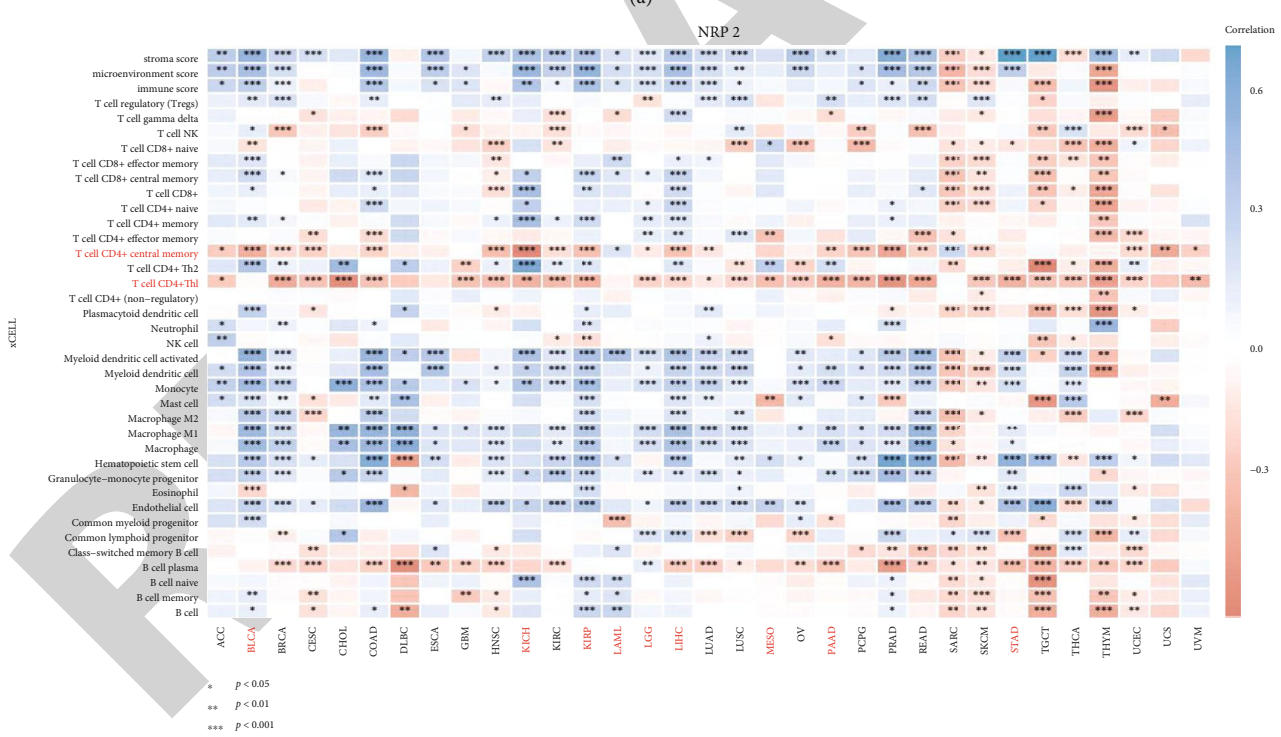
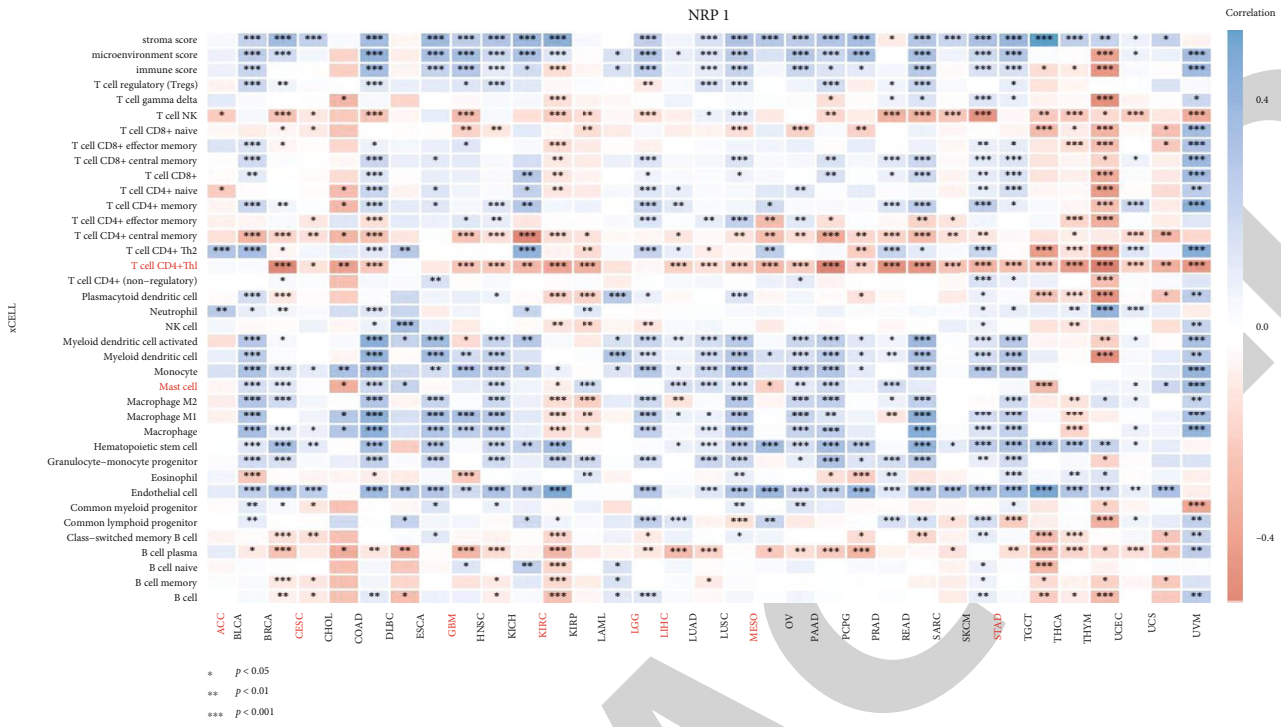


FIGURE 6: Heat map of Spearman correlation analysis between the xCell/EPIC immune score and the NRP family gene expression in multiple tumour tissues, where the horizontal axis represents different tumour tissues, the vertical axis represents different immune scores, different colours represent correlation coefficients, negative values represent negative correlation, and positive values represent positive correlation (\* $p < 0.05$ , \*\* $p < 0.01$ , \*\*\* $p < 0.001$ ). Significance of the two sample groups by Wilcoxon test.

Overall, these results suggest that the NRP1 and NRP2 expression is associated with alterations in immune gene expression and infiltration in different cancers.

3.6. Association of NRP1 and NRP2 Expression with the TME in Various Cancers. The heterogeneity of TME across different cancers affects tumour drug resistance and modulates

Cancer: LGG

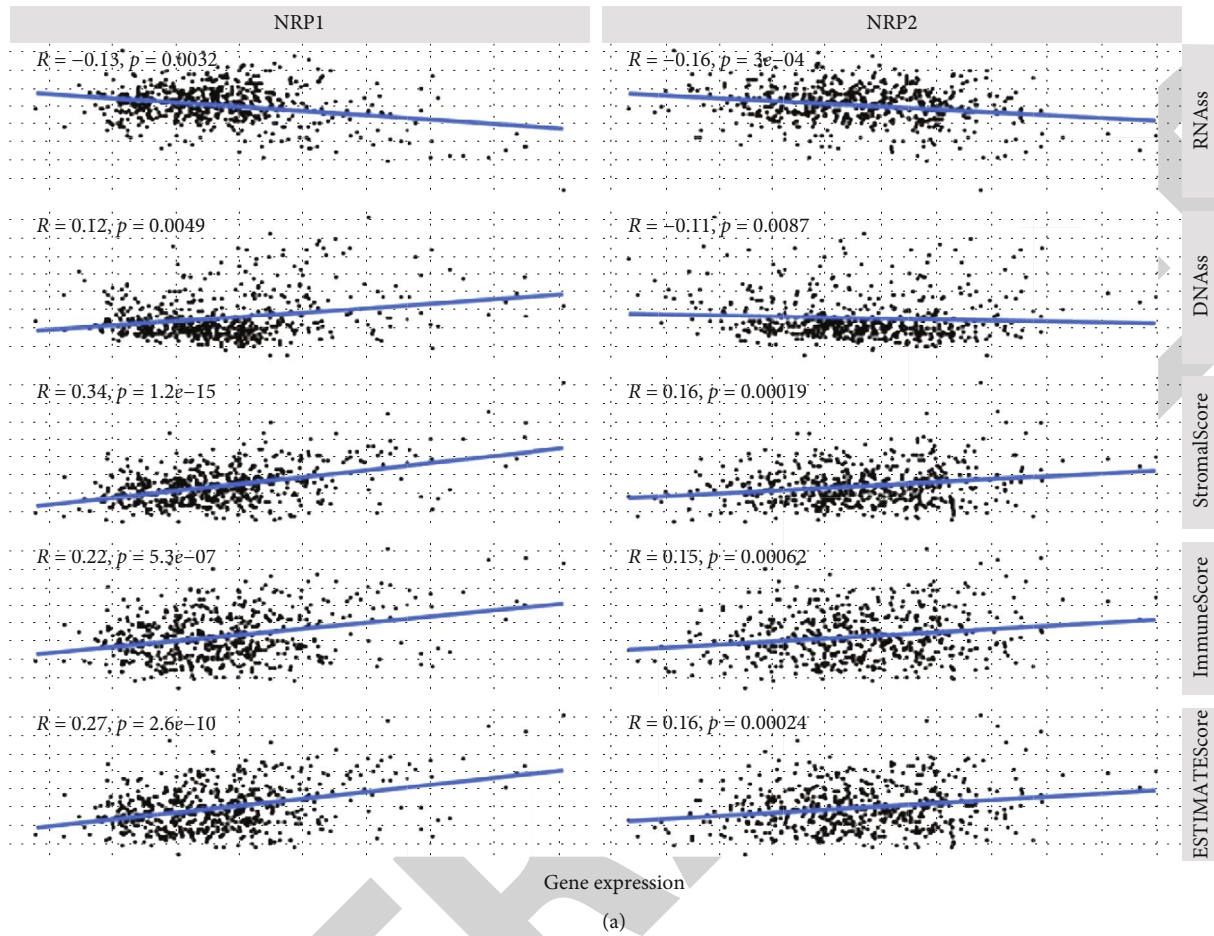
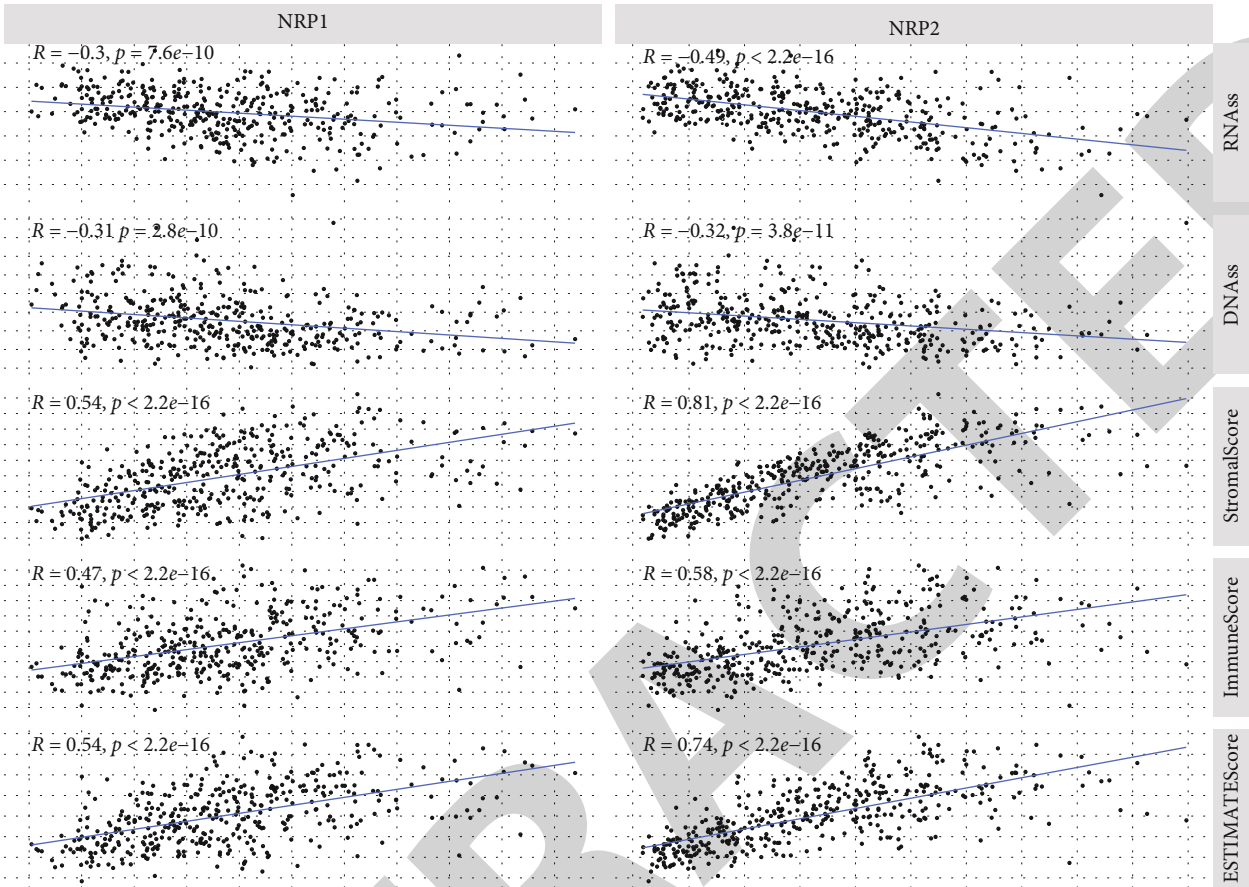


FIGURE 7: Continued.

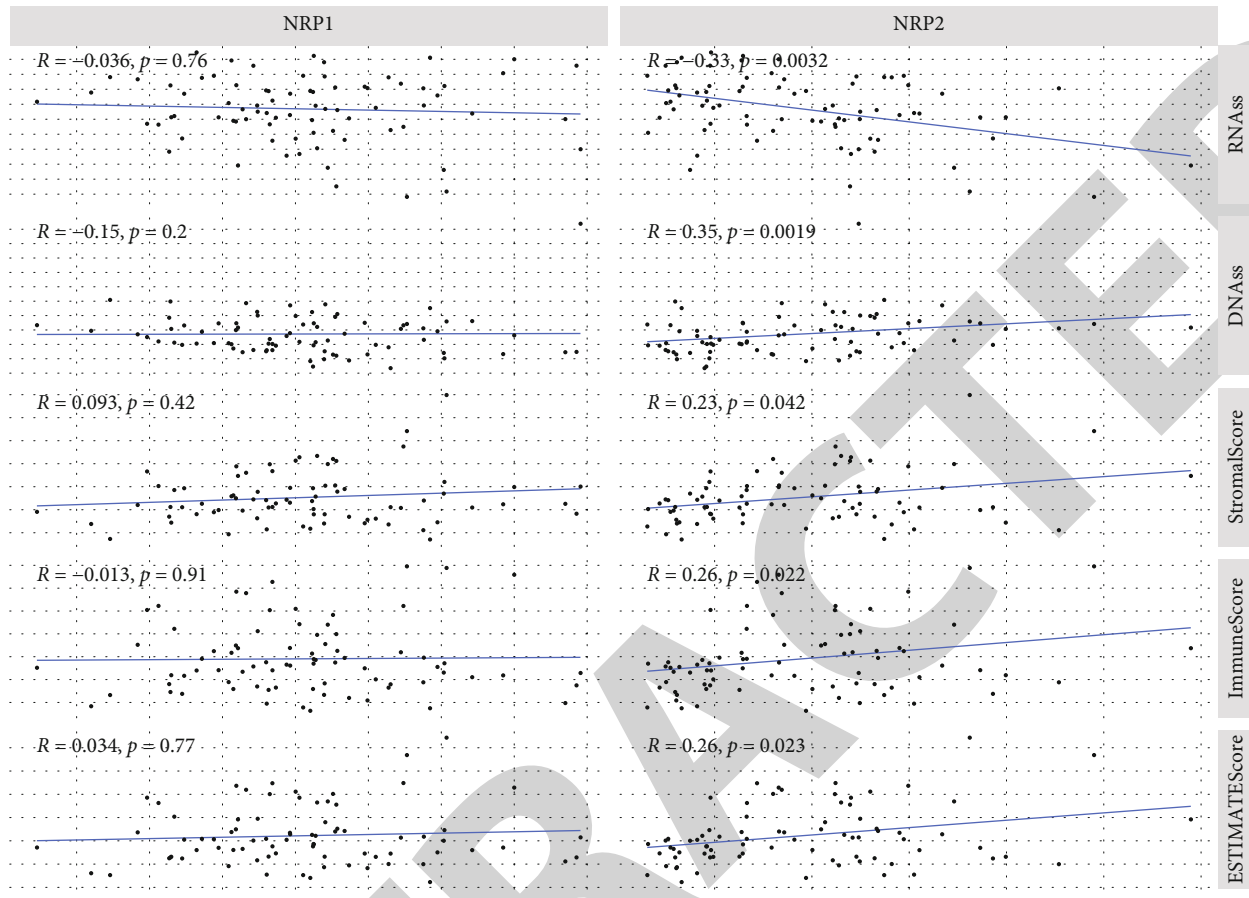
Cancer: BLCA



Gene expression  
(b)

FIGURE 7: Continued.

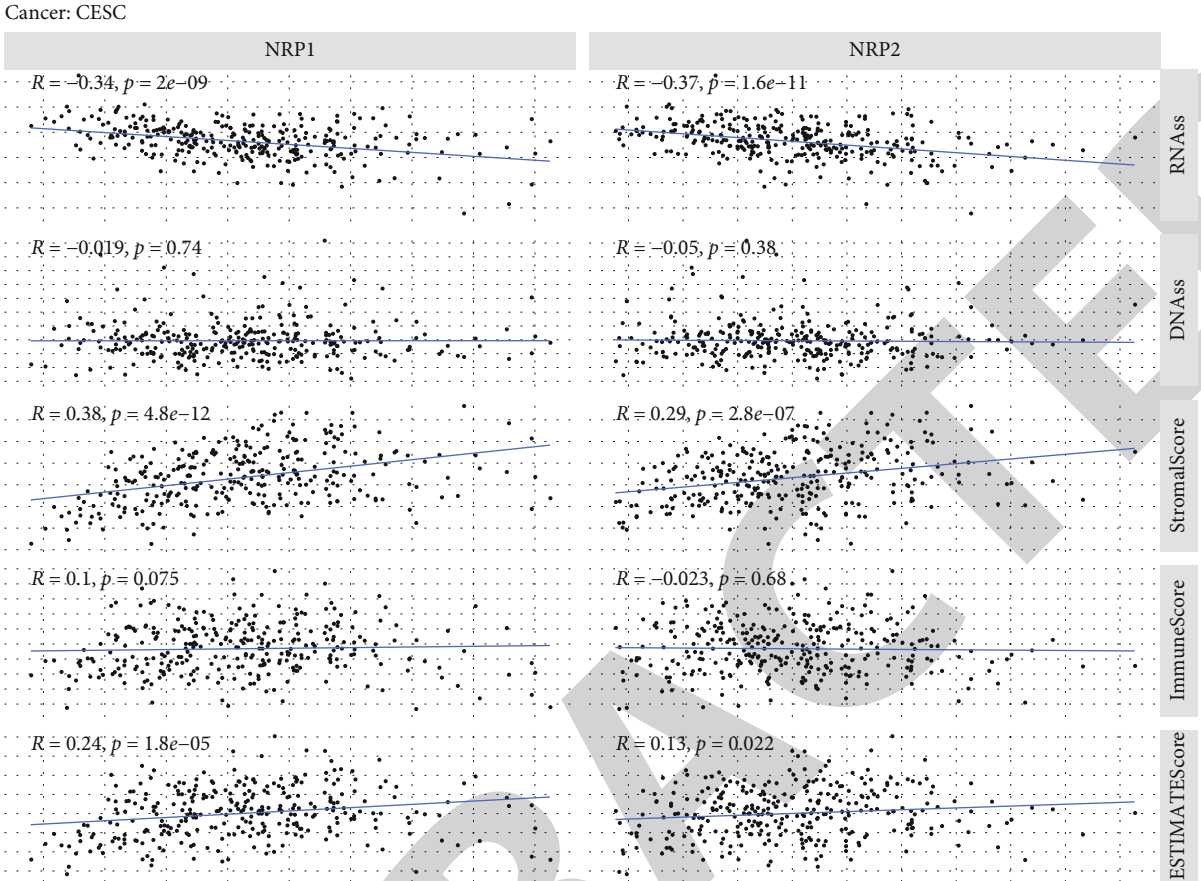
Cancer: ACC



Gene expression  
(c)

FIGURE 7: Continued.





Gene expression  
(d)

FIGURE 7: Continued.

Cancer: KIRC

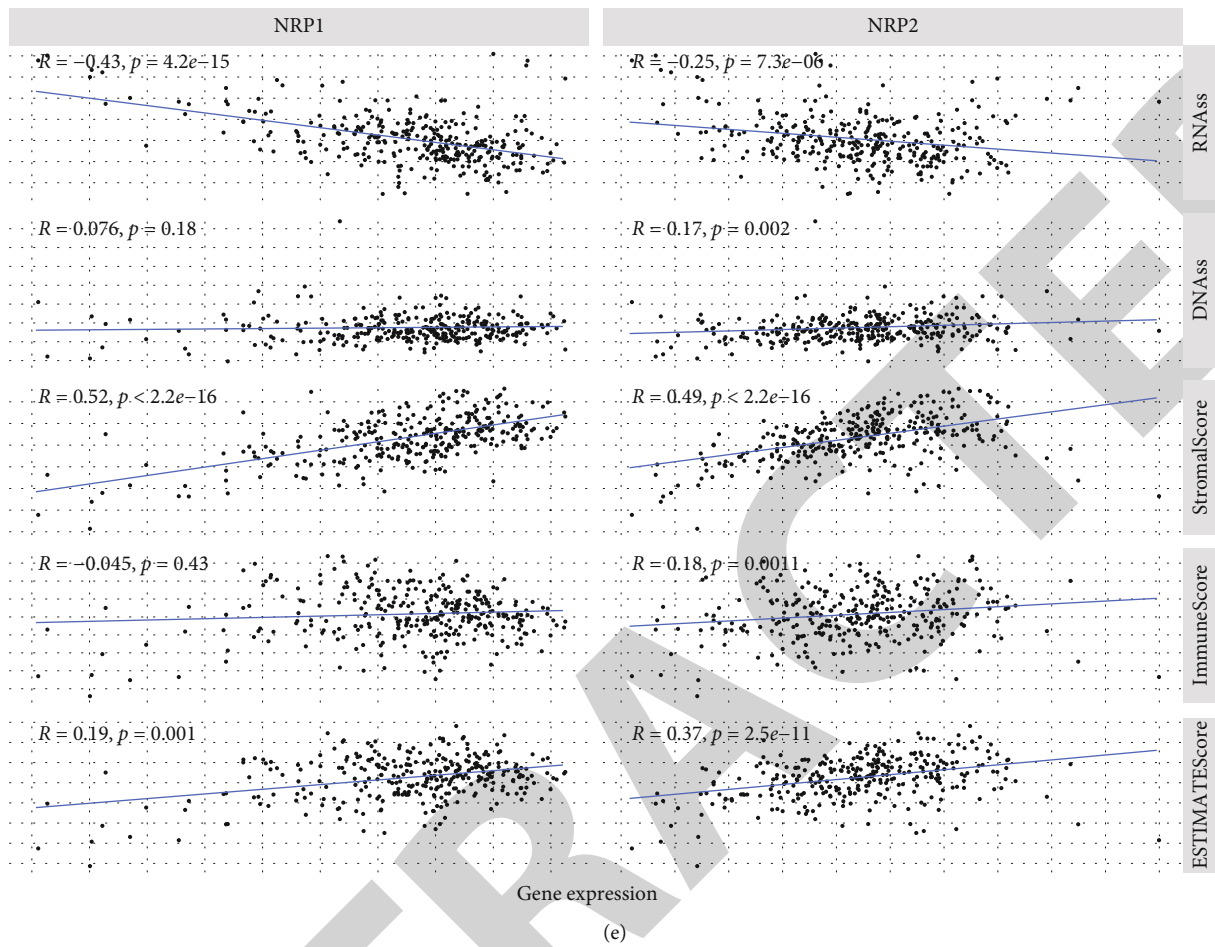


FIGURE 7: Continued.

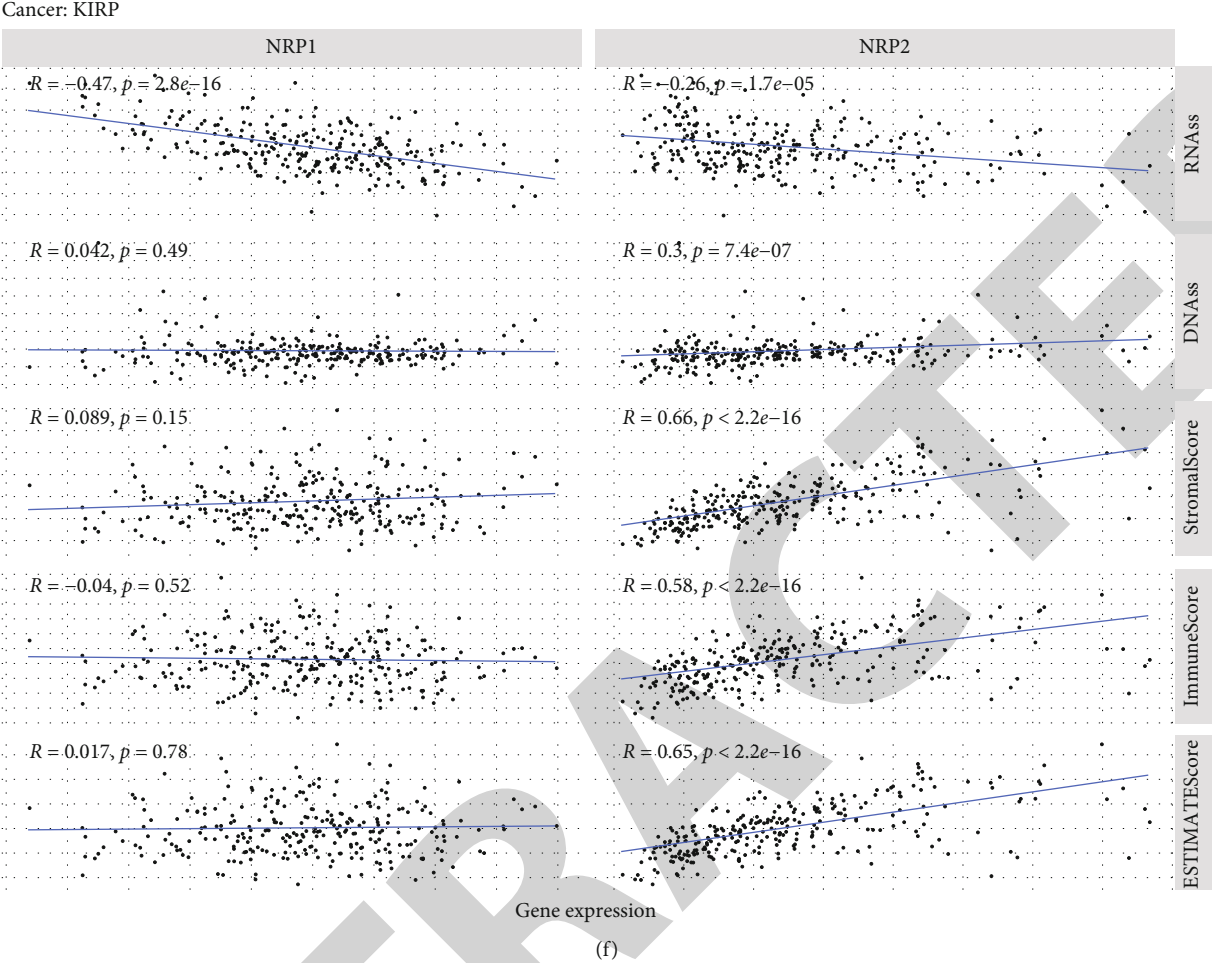


FIGURE 7: Continued.

Cancer: MESO

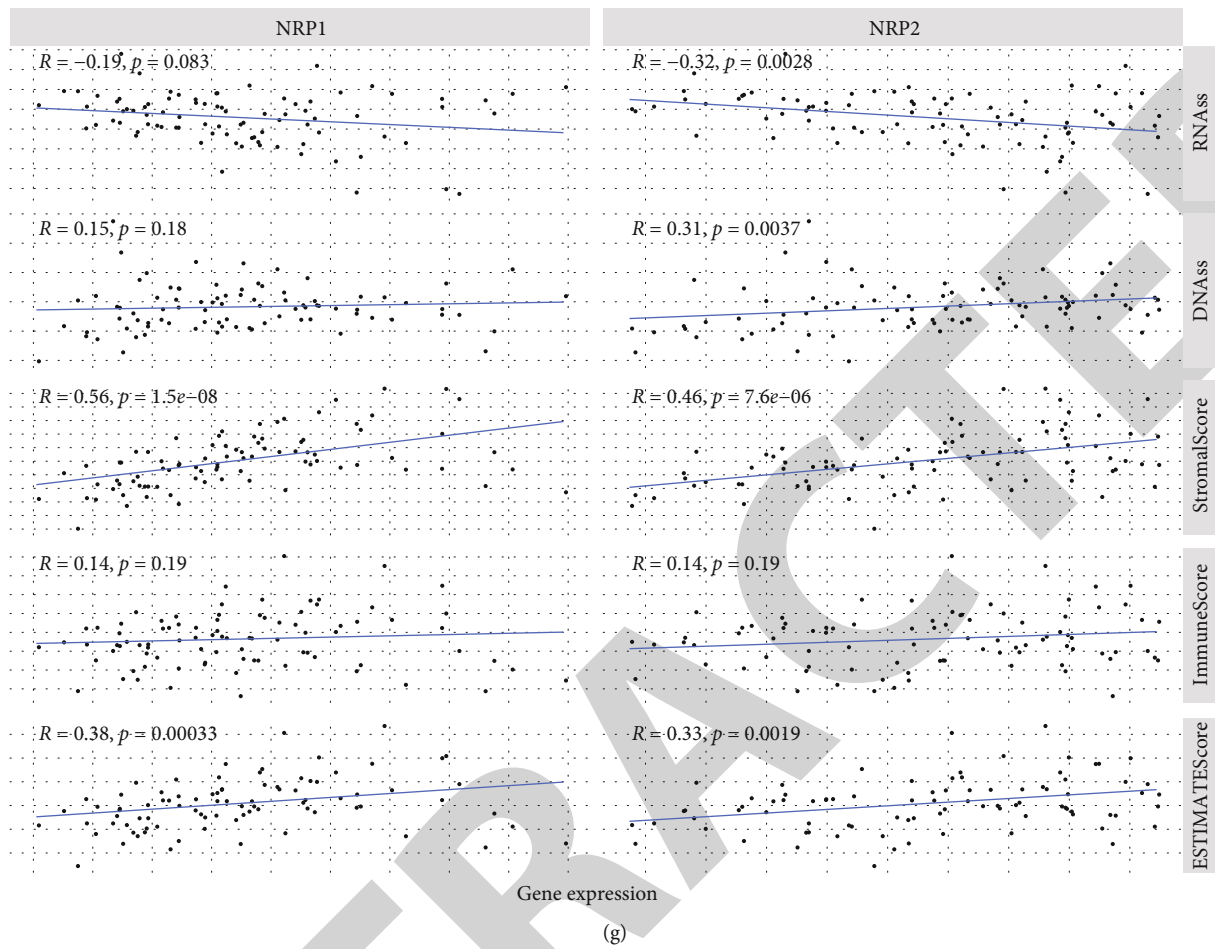


FIGURE 7: Continued.

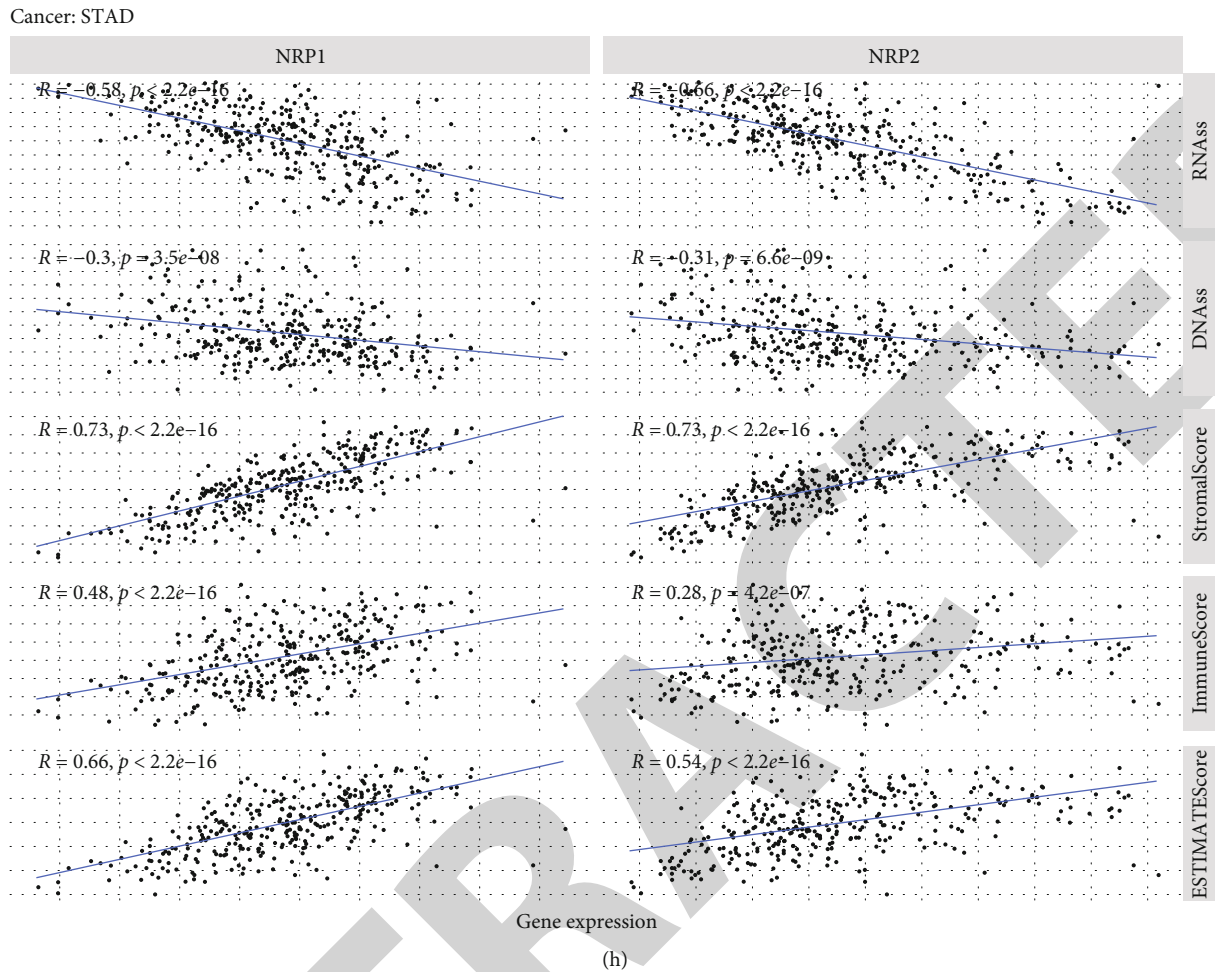


FIGURE 7: (a–h) Correlation analysis of NRP1 and NRP2 expression with tumour microenvironment in pancancer (LGG (a), BLCA (b), ACC (c), CESC (d), KIRC (e), KIRP (f), MESO (g), and STAD (h)).

cancer progression and metastasis [30, 31]. Here, we further explored the association of NRP1 and NRP2 expression with the immune microenvironment of some cancers (LGG, BLCA, ACC, CESC, KIRC, KIRP, MESO, and STAD). The ESTIMATE algorithm was used to calculate, among other things, stem cell and immune cell indices in tumour cells. The expression of NRP family genes in BLCA and LGG was found to be correlated most significantly with RNAss, DNAss, StromalScore, ImmuneScore, and ESTIMATEScore (Figures 7(a) and 7(b)). Overall, the NRP1 and NRP2 expression was positively correlated with StromalScore, ImmuneScore, and ESTIMATEScore in most prognosis-related cancers (Figures 7(a)–7(h)). Conversely, the correlation of the NRP1 and NRP2 expression with RNAss and DNAss was heterogeneous across cancer types. In conclusion, expression of NRP family genes is associated with the TME of various cancers.

**3.7. Association of NRP1 and NRP2 Expression with Clinicopathological Features in Various Cancers.** Further analysis demonstrated that the NRP1 and NRP2 expression was correlated with clinicopathological features of several cancers (KIRC, LGG, STAD, BLCA, and KIRP) (Figures 8(a)–8(e)). In patients with KIRC and STAD, NRP1 expression was signifi-

cantly correlated with ethnicity. The degree of NRP1 expression was higher in Blacks and Asians. In BLCA, NRP2 expression was higher in Asian populations compared to Caucasians. A high NRP1 and NRP2 expression was also found to be correlated with tumour diameter. In KIRC, a high NRP1 expression was associated with a larger tumour size, higher risk of distant metastases, and worse stage staging and grade staging. Similarly, a high NRP1 expression in STAD implied a worse grade staging. However, in LGG, a high NRP1 expression implied a better grade staging. Furthermore, in BLCA, NRP2 expression was associated with tumour size, stage staging, and worse grade staging. In KIRP, the NRP2 expression was higher in male patients.

**3.8. Genome-Wide Association of NRP1 and NRP2 mRNA in Various Cancers.** The previous results revealed that NRP1 might play important roles in KIRC and LGG, whereas NRP2 might play important roles in BLCA. Therefore, we analysed the association of KIRC, LGG, and BLCA with NRP1 and NRP2 in human genomic models (including gene expression, DNA methylation, somatic copy number, micro-RNA expression, somatic mutation, and protein level RPPA). The results showed that NRP1 was associated with genome-



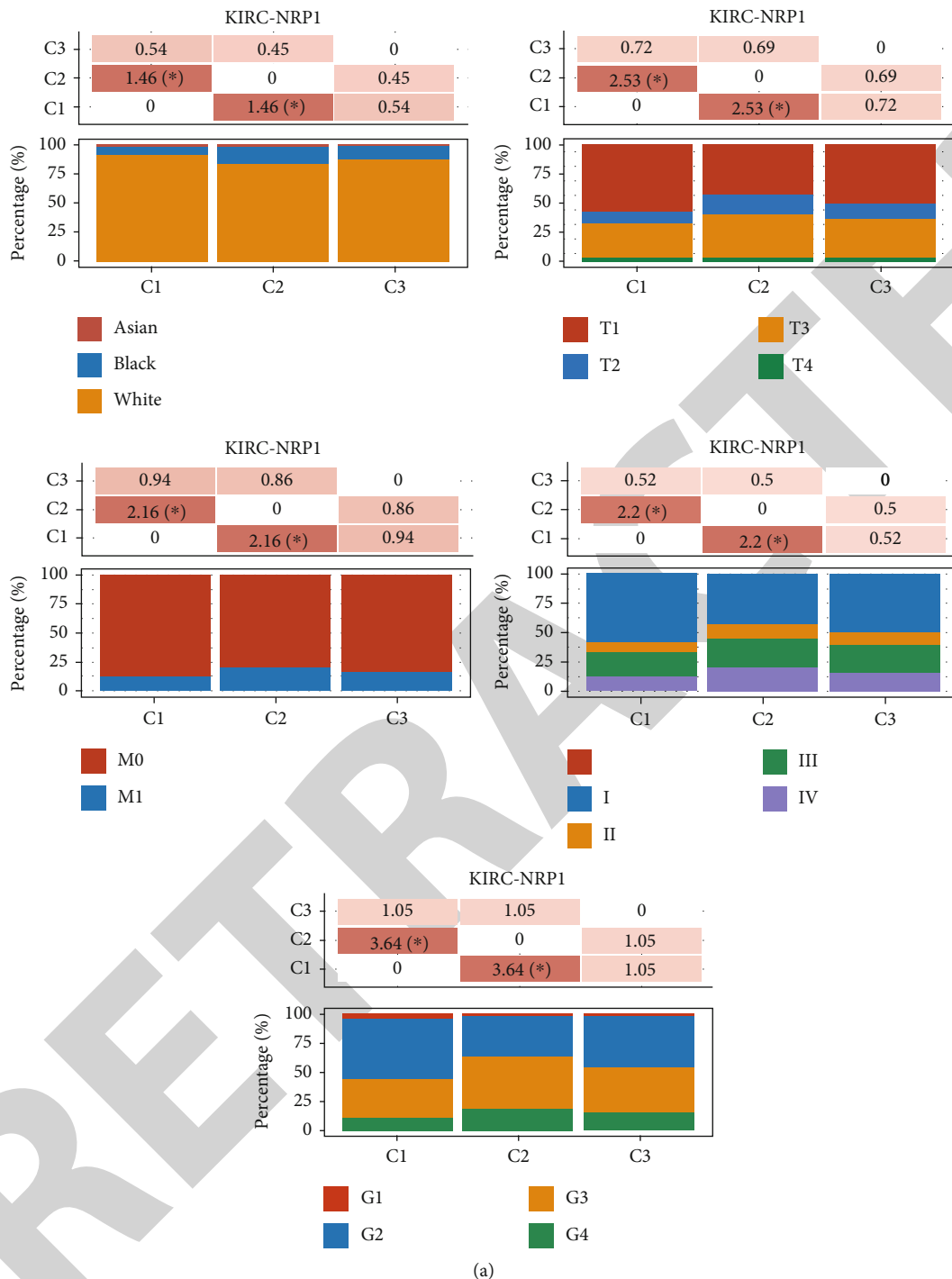


FIGURE 8: Continued.

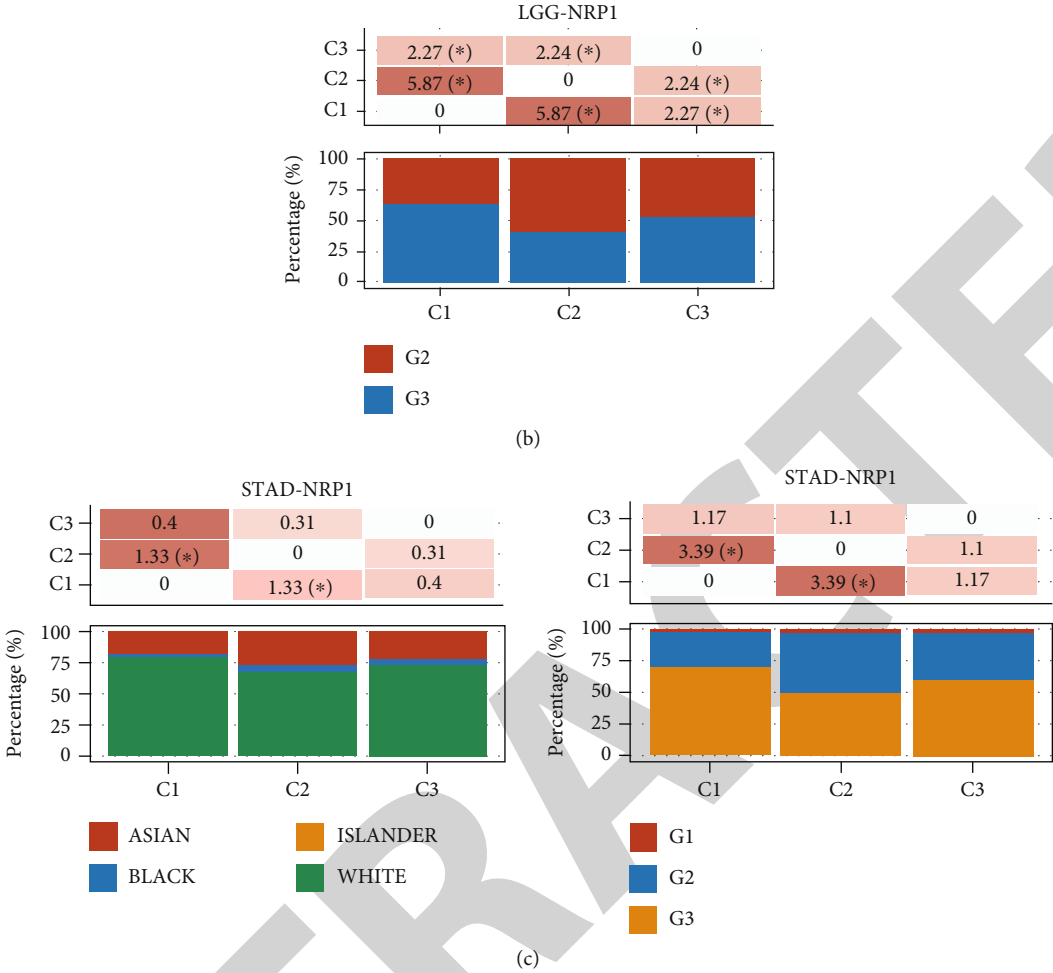


FIGURE 8: Continued.

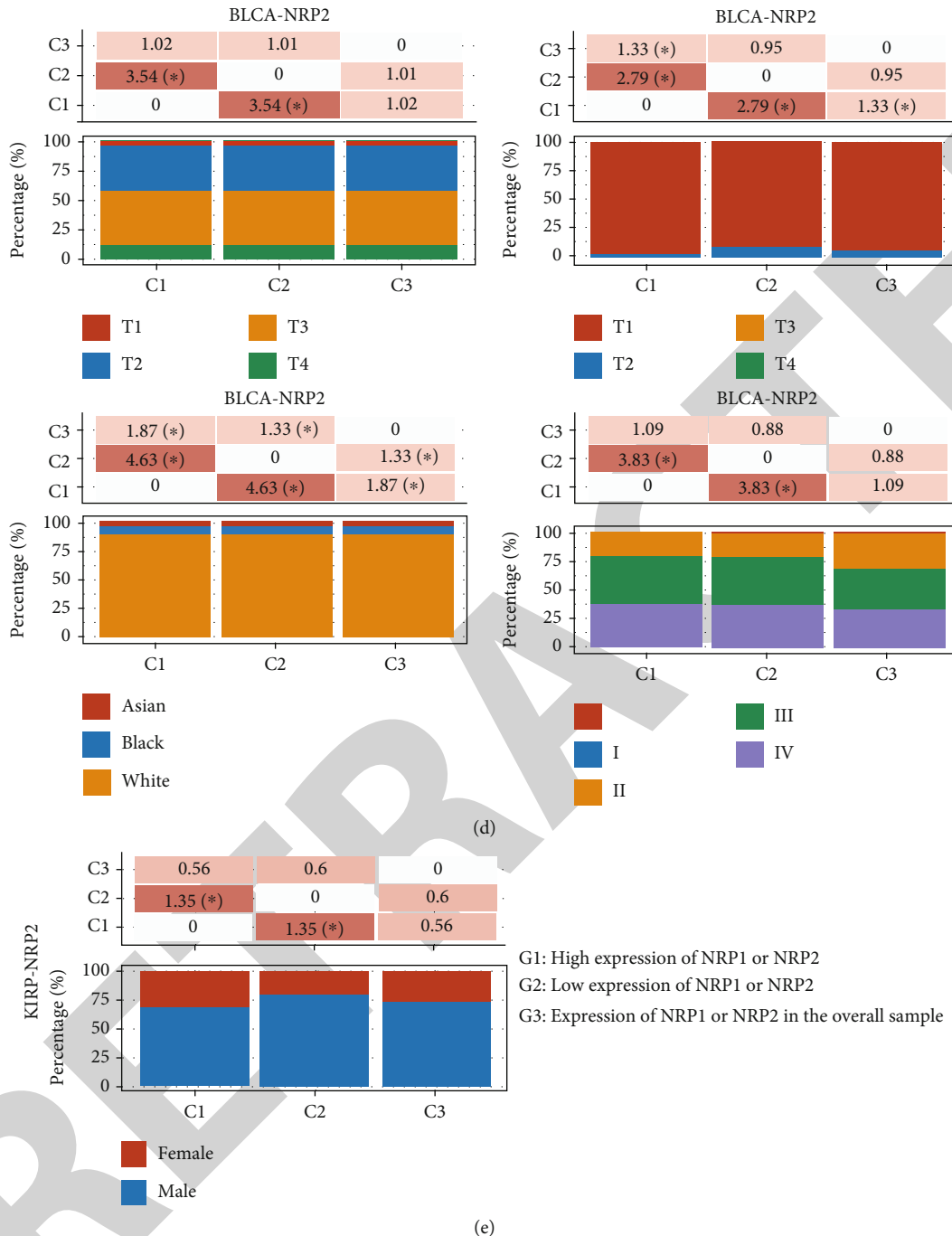


FIGURE 8: Correlation analysis of NRP1 and NRP2 expression with clinicopathological features in pancreatic cancer. The distribution of clinical characteristics in different groups of samples, where the horizontal axis represents the different groups of samples and the vertical axis represents the percentage of clinical information contained in the sample of the corresponding group. Significant differences were analysed by the chi-square test, where the magnitude of the value was taken as  $-\log_{10}(p \text{ value})$ ; \* means that there is a significant difference in the distribution of the clinical characteristic in the corresponding two groups ( $p < 0.05$ ).

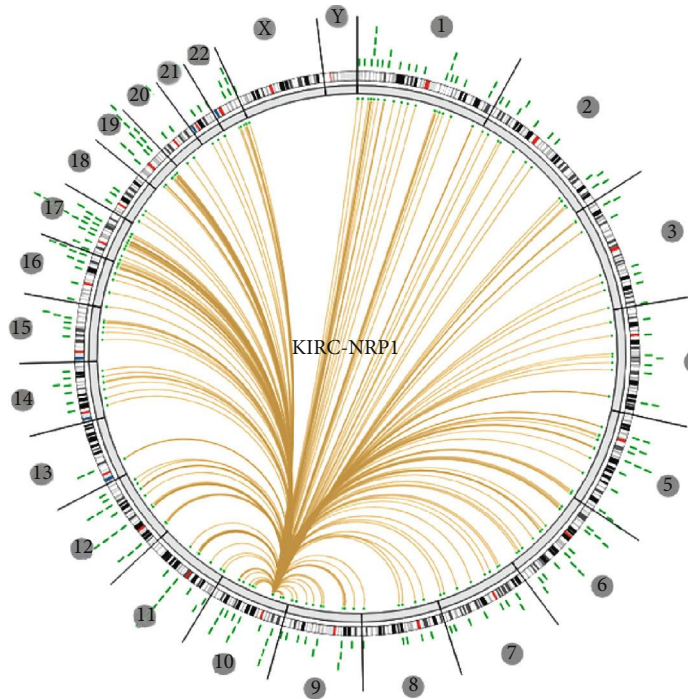
wide features in KIRC and LGG (Figures 9(a) and 9(b)), while NRP2 was broadly associated with genome-wide features in BLCA (Figure 9(c)).

#### 4. Discussion

Data obtained from pancancer analysis has the potential to guide tumour control strategies and design of therapies

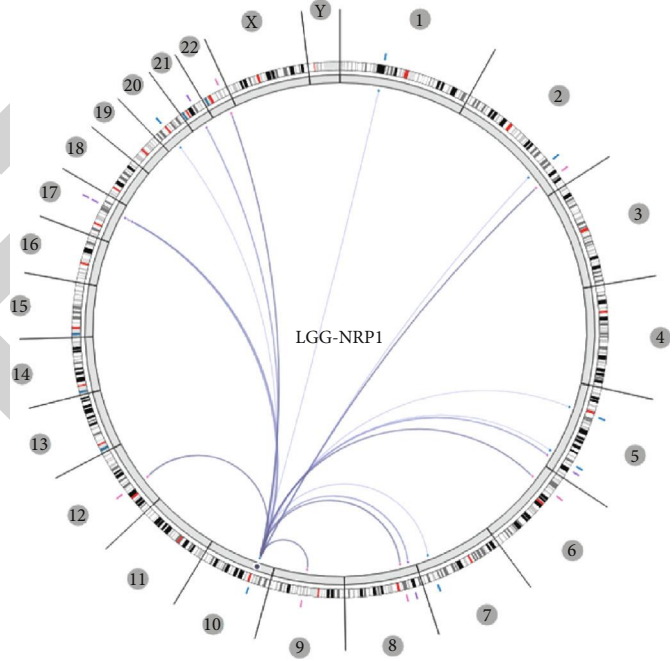
[32]. In recent years, genome-wide pancancer analysis has revealed mutations, RNA expression profiles, and immune profiles associated with tumour development. This has provided numerous biomarkers for the diagnosis and treatment of tumours [33].

In this study, we used different tools to analyse the expression of NRPs in different tumours and its association with mutations, TME, immune landscape, and prognosis.



Variable types  
■ Gene expression    ■ MicroRNA expression  
■ DNA methylation   ■ Somatic mutation  
■ Somatic copy number   ■ Protein level-RPPA

(a)



Variable types  
■ Gene expression    ■ MicroRNA expression  
■ DNA methylation   ■ Somatic mutation  
■ Somatic copy number   ■ Protein level-RPPA

(b)

FIGURE 9: Continued.

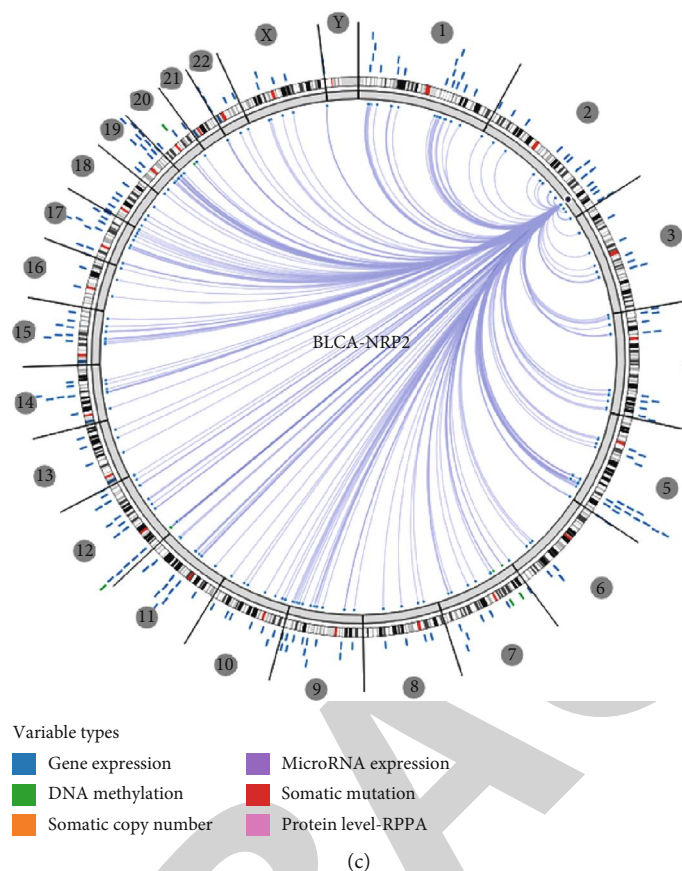


FIGURE 9: Genome-wide association of NRP1 and NRP2 mRNA in pancancer (Regulome program). NRP1 is broadly associated with genome-wide features in KIRC (a) and LGG (b). NRP2 is also found to be broadly associated with genome-wide features in BLCA (c).

We found that neurovascular-associated NRPs can predict the prognosis of many cancers. Moreover, NRP1 and NRP2 were differentially expressed levels in different tissues. This suggests that they may play distinct roles in different cancers. Survival analysis demonstrated that a low NRP1 expression in ACC, CESC, LGG, and STAD was associated with poor patient prognosis, whereas a high NRP1 expression in KIRC predicted good prognosis. A high NRP2 expression in BLCA, KIRP, and MESO was associated with poor patient prognosis. Further analysis revealed that NRP1 and NRP2 were significantly associated with TMB and MSI in various cancers. Moreover, the NRP1 and NRP2 expression was positively correlated with the expression of immune checkpoint genes and immune infiltration. The expression level of NRPs was associated with the TME and clinicopathological features of cancers. Finally, genome-wide association analysis suggested that the NRP1 expression was closely associated with KIRC, whereas the NRP2 expression was closely associated with BLCA. Together with previous studies, we suggest that NRP2 may be involved in the development of various cancers, particularly BLCA.

NRPs are highly conserved, multifunctional transmembrane proteins that are unique to vertebrates and are involved in various physiological and pathological processes in the body [34, 35]. In mammals, there are two isoforms of NRPs (NRP1 and NRP2) that are functionally distinct and complementary. These genes are involved various biological pro-

cesses such as neuroangiogenesis, cell migration, and immune regulation [36, 37].

A high NRP1 expression has been reported to be closely associated with tumorigenesis and progression, which is consistent with our findings [38, 39]. Using NRP1 antagonists, several studies have demonstrated the therapeutic potential of NRP1 in cancers [40]. Previous studies have also revealed that NRP1 modulates the function of various immune cells. In recent studies, NRP1 was found to regulate the stability and function of Tregs. It has also been reported to function as an antitumour immune inhibitor [41]. Anti-NRP1 treatment improved the efficacy of anti-PD-1 immunotherapy. This indicates that immunotherapy targeting NRP1 may have good clinical outcomes [42]. NRP1 has also been previously found to promote tumour angiogenesis, tumour proliferation, and migration [43–48]. Anti-NRP1 therapy can block tumour angiogenesis and upregulate the antitumour immune response [49–52]. Currently, anti-NRP1 therapy is used as a potential antitumour treatment option [42, 53]. In conclusion, the results of our study reveal that anti-NRP1 therapy has good clinical benefits.

A high NRP2 expression in BLCA, KIRP, and MESO was associated with poor prognosis. Similar to our study, a high NRP2 expression in the bladder has been associated with chemoresistance and epithelial-to-mesenchymal transition [16]. In addition, a higher NRP2 expression has been reported in triple-negative breast cancers indicating that the



NRP2 expression depends on the type of breast cancer [14]. Moreover, the NRP2 expression in prostate cancer is positively correlated with the Gleason grading [15]. NRP2 is closely related to the immune system [12]. The xCell algorithm was to first provide indirect data on the expression pattern of NRP2 in B cells, NPRs, natural killer cells, and T cells. Recent studies have shown that NRP2 regulates various processes such as cell migration and antigen migration in the immune system [12]. Similarly, this study reveals that NRP2 influences immune processes. NRP2 has also been found to be closely associated with metastasis and BRAFV600E in thyroid cancer [54]. Downregulation of NRP2 has been shown to influence epithelial-mesenchymal transition by affecting phosphorylation signaling pathways [54]. This suggests a potential association of NRP2 expression with the TME and gene mutations.

Energy metabolism is interconnected, coupled to insulin signaling, and linked to the release of metabolic hormones from adipose tissue. Understanding the diverse roles of energy metabolism should prevent and treat various human diseases such as diabetes, obesity, and cancer [55]. Previous studies have found that NRP1/2 may be involved in energy metabolism [56, 57]. Diabetes is an energy metabolism-related disease that can lead to multiple systemic pathologies [58–61]. And diabetes is closely associated with neurovascular disease [62–65]. Therefore, we propose the bold hypothesis that NRP1/2 may also influence tumour prognosis through energy metabolism-related pathways.

However, there are limitations to this study that warrant further exploration. Firstly, the present study does not demonstrate how NRPs influence tumour growth and developmental processes by affecting the immune microenvironment or the TME, as well as other pathways. Secondly, *in vivo* and *in vitro* experiments should be performed to substantiate our results and clarify the impact of NRP expression on tumourigenesis development. Further studies at cellular and molecular levels would be beneficial to elucidate the specific functional mechanisms of NRPs in different cancer types. Thirdly, future well-designed studies are needed such as single-cell RNA sequencing. Further improvements in precision would be beneficial to prevent systematic bias at the cellular level. Therefore, future cohort studies and population-based case-control studies are necessary to examine the mechanisms involved.

## 5. Conclusion

In conclusion, neurovascular-related NRP family genes are significantly correlated with the prognosis, TME, and immune profiles of tumours, especially in BLCA. Therefore, NRPs may be used as a marker for predicting the prognosis of various tumours. Besides, NRPs hold great promise as a potential target for tumour therapy.

## Abbreviations

ACC: Adrenocortical carcinoma  
 BLCA: Bladder urothelial carcinoma  
 BRCA: Breast invasive carcinoma

CESC: Cervical squamous cell carcinoma  
 CHOL: Cholangiocarcinoma  
 COAD: Colon adenocarcinoma  
 DLBC: Lymphoid neoplasm diffuse large B-cell lymphoma  
 ESCA: Esophageal carcinoma  
 GBM: Glioblastoma multiforme  
 LGG: Brain lower grade glioma  
 HNSC: Head and neck squamous cell carcinoma  
 KICH: Kidney chromophobe  
 KIRC: Kidney renal clear cell carcinoma  
 KIRP: Kidney renal papillary cell carcinoma  
 LAML: Acute myeloid leukemia  
 LIHC: Liver hepatocellular carcinoma  
 LUAD: Lung adenocarcinoma  
 LUSC: Lung squamous cell carcinoma  
 MESO: Mesothelioma  
 OV: Ovarian serous cystadenocarcinoma  
 PAAD: Pancreatic adenocarcinoma  
 PCPG: Pheochromocytoma and paraganglioma  
 PRAD: Prostate adenocarcinoma  
 READ: Rectum adenocarcinoma  
 SARC: Sarcoma  
 SKCM: Skin cutaneous melanoma  
 STAD: Stomach adenocarcinoma  
 TGCT: Testicular germ cell tumours  
 THCA: Thyroid carcinoma  
 THYM: Thymoma  
 UCEC: Uterine corpus endometrial carcinoma  
 UCS: Uterine carcinosarcoma  
 UVM: Uveal melanoma.

## Data Availability

All data was obtained from the public database described in Materials and Methods.

## Conflicts of Interest

No competing interests exist.

## Authors' Contributions

Chao Deng and Hang Guo contributed equally to this work.

## References

- [1] R. S. Apte, D. S. Chen, and N. Ferrara, "VEGF in signaling and disease: beyond discovery and development," *Cell*, vol. 176, no. 6, pp. 1248–1264, 2019.
- [2] R. S. Kerbel, "Tumor angiogenesis," *The New England Journal of Medicine*, vol. 358, no. 19, pp. 2039–2049, 2008.
- [3] N. Ferrara, "VEGF and intraocular neovascularization: from discovery to therapy," *Translational Vision Science & Technology*, vol. 5, no. 2, p. 10, 2016.
- [4] N. Ferrara and A. P. Adamis, "Ten years of anti-vascular endothelial growth factor therapy," *Nature Reviews. Drug Discovery*, vol. 15, no. 6, pp. 385–403, 2016.
- [5] G. C. Jayson, R. Kerbel, L. M. Ellis, and A. L. Harris, "Antiangiogenic therapy in oncology: current status and future directions," *Lancet*, vol. 388, no. 10043, pp. 518–529, 2016.

- [6] S. Soker, S. Takashima, H. Q. Miao, G. Neufeld, and M. Klagsbrun, "Neuropilin-1 is expressed by endothelial and tumor cells as an isoform-specific receptor for vascular endothelial growth factor," *Cell*, vol. 92, no. 6, pp. 735–745, 1998.
- [7] X. Wang, S. Li, Y. Ma et al., "Identification of miRNAs as the crosstalk in the interaction between neural stem/progenitor cells and endothelial cells," *Disease Markers*, vol. 2020, Article ID 6630659, 29 pages, 2020.
- [8] S. Soker, M. Kaefer, M. Johnson, M. Klagsbrun, A. Atala, and M. R. Freeman, "Vascular endothelial growth factor-mediated autocrine stimulation of prostate tumor cells coincides with progression to a malignant phenotype," *The American Journal of Pathology*, vol. 159, no. 2, pp. 651–659, 2001.
- [9] A. L. Elaimy and A. M. Mercurio, "Convergence of VEGF and YAP/TAZ signaling: implications for angiogenesis and cancer biology," *Science Signaling*, vol. 11, no. 552, article eaau1165, 2018.
- [10] H. Chen, A. Chédotal, Z. He, C. S. Goodman, and M. Tessier-Lavigne, "Neuropilin-2, a novel member of the neuropilin family, is a high affinity receptor for the semaphorins Sema E and Sema IV but not Sema III," *Neuron*, vol. 19, no. 3, pp. 547–559, 1997.
- [11] T. Takahashi, A. Fournier, F. Nakamura et al., "Plexin-neuropilin-1 complexes form functional semaphorin-3A receptors," *Cell*, vol. 99, no. 1, pp. 59–69, 1999.
- [12] S. Schellenburg, A. Schulz, D. M. Poitz, and M. H. Muders, "Role of neuropilin-2 in the immune system," *Molecular Immunology*, vol. 90, pp. 239–244, 2017.
- [13] H. L. Goel and A. M. Mercurio, "VEGF targets the tumour cell," *Nature Reviews. Cancer*, vol. 13, no. 12, pp. 871–882, 2013.
- [14] H. L. Goel, B. Pursell, C. Chang et al., "GLI1 regulates a novel neuropilin-2/ $\alpha 6 \beta 1$  integrin based autocrine pathway that contributes to breast cancer initiation," *EMBO Molecular Medicine*, vol. 5, no. 4, pp. 488–508, 2013.
- [15] H. L. Goel, C. Chang, B. Pursell et al., "VEGF/neuropilin-2 regulation of Bmi-1 and consequent repression of IGF-IR define a novel mechanism of aggressive prostate cancer," *Cancer Discovery*, vol. 2, no. 10, pp. 906–921, 2012.
- [16] A. Schulz, I. Gorodetska, R. Behrendt et al., "Linking NRP2 with EMT and chemoradioresistance in bladder cancer," *Frontiers in Oncology*, vol. 9, p. 1461, 2020.
- [17] V. Thorsson, D. L. Gibbs, S. D. Brown et al., "The immune landscape of cancer," *Immunity*, vol. 51, no. 2, pp. 411–412, 2019.
- [18] R. Bonneville, M. A. Krook, E. A. Kautto et al., "Landscape of microsatellite instability across 39 cancer types," *JCO Precision Oncology*, vol. 2017, 2017.
- [19] F. G. Frost, P. F. Cherukuri, S. Milanovich, and C. F. Boerkoel, "Pan-cancer RNA-seq data stratifies tumours by some hallmarks of cancer," *Journal of Cellular and Molecular Medicine*, vol. 24, no. 1, pp. 418–430, 2020.
- [20] V. Izzi, M. N. Davis, and A. Naba, "Pan-cancer analysis of the genomic alterations and mutations of the matrisome," *Cancers*, vol. 12, no. 8, p. 2046, 2020.
- [21] Q. Zhang, R. Huang, H. Hu et al., "Integrative analysis of hypoxia-associated signature in pan-cancer," *iScience*, vol. 23, no. 9, p. 101460, 2020.
- [22] G. Sturm, F. Finotello, F. Petitprez et al., "Comprehensive evaluation of transcriptome-based cell-type quantification methods for immuno-oncology," *Bioinformatics*, vol. 35, no. 14, pp. i436–i445, 2019.
- [23] G. Sturm, F. Finotello, F. Petitprez et al., "Comprehensive analyses of tumor immunity: implications for cancer immunotherapy," *Genome Biology*, vol. 17, no. 1, p. 174, 2016.
- [24] D. Aran, Z. Hu, and A. J. Butte, "xCell: digitally portraying the tissue cellular heterogeneity landscape," *Genome Biology*, vol. 18, no. 1, p. 220, 2017.
- [25] J. Wang, J. Sun, L. N. Liu et al., "TIMER2.0 for analysis of tumor-infiltrating immune cells," *Nucleic Acids Research*, vol. 48, no. W1, pp. W509–W514, 2020.
- [26] J. Wang, J. Sun, L. N. Liu et al., "Siglec-15 as an immune suppressor and potential target for normalization cancer immunotherapy," *Nature Medicine*, vol. 25, no. 4, pp. 656–666, 2019.
- [27] D. Zeng, M. Li, R. Zhou et al., "Tumor microenvironment characterization in gastric cancer identifies prognostic and immunotherapeutically relevant gene signatures," *Cancer Immunology Research*, vol. 7, no. 5, pp. 737–750, 2019.
- [28] X. Zhang, B. Klamer, J. Li, S. Fernandez, and L. Li, "A pan-cancer study of class-3 semaphorins as therapeutic targets in cancer," *BMC Medical Genomics*, vol. 13, Suppl.5, p. 45, 2020.
- [29] T. M. Malta, A. Sokolov, A. J. Gentles et al., "Machine learning identifies stemness features associated with oncogenic dedifferentiation," *Cell*, vol. 173, no. 2, pp. 338–354.e15, 2018.
- [30] Z. R. Chalmers, C. F. Connelly, D. Fabrizio et al., "Analysis of 100,000 human cancer genomes reveals the landscape of tumor mutational burden," *Genome Medicine*, vol. 9, no. 1, p. 34, 2017.
- [31] M. Yarchoan, A. Hopkins, and E. M. Jaffee, "Tumor mutational burden and response rate to PD-1 inhibition," *The New England Journal of Medicine*, vol. 377, no. 25, pp. 2500–2501, 2017.
- [32] F. X. Schaub, V. Dhankani, A. C. Berger, M. Trivedi, A. B. Richardson, R. Shaw et al., "Cancer Genome Atlas Network. Pan-cancer alterations of the MYC oncogene and its proximal network across The Cancer Genome Atlas," *Cell Systems*, vol. 6, no. 3, pp. 282–300.e2, 2018.
- [33] T. Schlomm, "Ergebnisse des "ICGC/TCGA pan-cancer analysis of the whole genomes"(PCWAG)-konsortiums," *Urologie A.*, vol. 59, no. 12, pp. 1552–1553, 2020.
- [34] X. Li, S. Fan, X. Pan et al., "Nordihydroguaiaretic acid impairs prostate cancer cell migration and tumor metastasis by suppressing neuropilin 1," *Oncotarget*, vol. 7, no. 52, pp. 86225–86238, 2016.
- [35] N. Gioelli, F. Maione, C. Camillo et al., "A rationally designed NRP1-independent superagonist SEMA3A mutant is an effective anticancer agent," *Science Translational Medicine*, vol. 10, no. 442, article eaah4807, 2018.
- [36] J. Wang, Y. Huang, J. Zhang et al., "NRP2 in tumor lymphangiogenesis and lymphatic metastasis," *Cancer Letters*, vol. 418, pp. 176–184, 2018.
- [37] W. P. Li, H. Zhao, X. Zhang et al., "Study on the white matter neuronal integrity in amnesic mild cognitive impairment based on automating fiber-tract quantification," *Zhonghua Yi Xue Za Zhi*, vol. 100, no. 3, pp. 172–177, 2020.
- [38] L. E. Jimenez-Hernandez, K. Vazquez-Santillan, R. Castro-Oropeza et al., "NRP1-positive lung cancer cells possess tumor-initiating properties," *Oncology Reports*, vol. 39, no. 1, pp. 349–357, 2018.
- [39] H. Al-Shareef, S. I. Hiraoka, N. Tanaka et al., "Use of NRP1, a novel biomarker, along with VEGF-C, VEGFR-3, CCR7 and SEMA3E, to predict lymph node metastasis in squamous cell

## Research Article

# A Novel Clinical Nomogram to Predict Transient Symptomatic Associated with Infarction: The ABCD3-SLOPE Score

YanQin Lu <sup>1</sup>, QianQian Bi <sup>1</sup>, Wang Fu <sup>1</sup>, LiLi Liu <sup>2</sup>, Yin Zhang <sup>3</sup>, XiaoYu Zhou <sup>1</sup>,  
and Jue Wang <sup>4</sup>

<sup>1</sup>Department of Neurology, Shanghai Tenth People's Hospital, Tongji University School of Medicine, Shanghai, China

<sup>2</sup>Department of Neurology, Shanghai Hongkou District Jiangwan Hospital, Rehabilitation Hospital Affiliated to Shanghai University of Medicine & Health Sciences, Shanghai, China

<sup>3</sup>Tongji University School of Medicine, Shanghai, China

<sup>4</sup>Educational Office, Shanghai Tenth People's Hospital, Tongji University School of Medicine, Shanghai, China

Correspondence should be addressed to XiaoYu Zhou; xiaoyuzhou1979@163.com and Jue Wang; wangjuedr@163.com

Received 1 March 2021; Revised 16 March 2021; Accepted 1 April 2021; Published 15 April 2021

Academic Editor: Qian Wang

Copyright © 2021 YanQin Lu et al. This is an open access article distributed under the Creative Commons Attribution License, which permits unrestricted use, distribution, and reproduction in any medium, provided the original work is properly cited.

**Background.** It is hard to differentiate transient symptoms associated with infarction (TSI) from transient ischemic stroke (TIA) without MRI in the early onset. However, they have distinct clinical outcomes and respond differently to therapeutics. Therefore, we aimed to develop a risk prediction model based on the clinical features to identify TSI. **Methods.** We enrolled 230 consecutive patients with transient neurologic deficit in the Department of Neurology, Tongji University Affiliated Tenth People's Hospital from March 2014 to October 2019. All the patients were assigned into TIA group (DWI-negative) or TSI group (DWI-positive) based on MRI conducted within five days of onset. We summarized the clinical characteristics of TSI by univariate and multivariate analyses. And then, we developed and validated a nomogram to identify TSI by the logistic regression equation. **Results.** Of the 230 patients, 41.3% were diagnosed with TSI. According to the multivariate analysis, four independent risk factors, including smoking history, low-density lipoprotein cholesterol, brain natriuretic peptide precursor, and ABCD3 score, were incorporated into a nomogram. We developed a predictive model named ABCD3-SLOPE. The calibration curve showed good agreement between nomogram prediction and observation. The concordance index (C-index) of the nomogram for TSI prediction was 0.77 (95% confidence interval, 0.70-0.83), and it was well-calibrated. **Conclusions.** Smoking history, low-density lipoprotein cholesterol, brain natriuretic peptide precursor, and ABCD3 score were reliable risk factors for TSI. ABCD3-SLOPE was a potential tool to quantify the likelihood of TSI.

## 1. Introduction

A transient episode of neurological dysfunction caused by focal brain, spinal cord, or retinal ischemia, without acute infarction, has been defined as a TIA [1, 2]. With the advent of diffusion-weighted imaging (DWI), it was reported that 29.3-41.5% percent of patients with transient clinical deficit had positive DWI [3-7]. To date, the normative definition for these DWI-positive cases was not yet well-established, while it was termed transient symptoms associated with infarction (TSI) [6]. They are two distinct entities and contribute to different prognoses, even

if they share the identical feature that neurological deficits fully recovered within 24 hours of onset. The risk of recurrent ischemic events is much higher in patients with TSI than those with TIA. One study found a rate of recurrent ischemic stroke of 10.8% among TSI patients in 90 days, while 4.3% in TIA [8]. What is more, TSI patients were ten times more likely to suffer from ischemic stroke in 7 days and 4.3 times in 12 months than TIA patients [9, 10]. Therefore, early identification of TSI and aggressive treatment may reduce the risk of recurrent stroke.

The TSI diagnosis is exceptionally dependent on DWI sequence, but the MR image is unavailable at the first one

or two days of onset in most medical facilities. Nowadays, there are ample studies of detection and early stroke risk prediction for TIA [8, 11–15], while few studies have investigated TSI's clinical characteristics. For this reason, it is imperative to make investigations on the specific clinical characteristics of TSI and to develop a prediction model derived from clinical features for the identification of TSI.

The purpose of this research is to develop a practical risk prediction tool that can aid in rapidly and accurately triaging patients with high positive predictive value.

## 2. Methods

**2.1. Patients and Study Design.** We collected consecutive 348 patients manifested with transient neurological deficits hospitalized in the Department of Neurology, Shanghai Tenth People's Hospital from March 2014 to October 2019. Patients with neurological dysfunction due to cerebral hemorrhage or other nonvascular causes (hypoglycemia, infection, space-occupying lesions, subdural hematoma, and epidural hematoma) were excluded. Also, patients without a brain MRI were excluded from this study. Two hundred and thirty patients were finally recruited. Brain MRI (Siemens 3.0T Avanto MRI) was required for all study participants. Standardized MRI sequences were necessary per protocol (at least T2-weighted, fluid-attenuated inversion recovery images and DWI sequences). All images were analyzed off-line centrally by two experienced readers blinded to clinical and demographic data. The patients were divided into TIA group (DWI-negative) and TSI group (DWI-positive) based on DWI sequence results. We retrospectively analyzed the demographic characteristics, clinical manifestations, risk factors, laboratory examinations, imaging examinations, and other variables.

**2.2. Grouping Standard.** A transient episode of neurological dysfunction caused by focal brain, spinal cord, or retinal ischemia, without acute infarction, was defined as a TIA [1, 2]. Correspondingly, the patient with acute infarction was diagnosed with TSI. According to the definition, all the patients were divided into the TIA group (DWI-negative) and TSI group (DWI-positive) based on the DWI sequence results.

**2.3. Statistical Analysis.** Statistical analysis was performed using IBM SPSS Statistics, Version 22.0 (IBM; Armonk, NY). Categorical variables are expressed as a number or percentage, and continuous variables are expressed as means and SDs. Statistical analysis of categorical variables was done using the chi-square test, while continuous variables were compared using the *t*-test or Mann-Whitney test, as appropriate.

First, a univariate analysis was performed. We used the forward stepwise regression method based on the maximum likelihood ratio to conduct multivariate logistic regression analysis of independent influencing factors in TSI patients. The odds ratio (OR) with 95% confidence intervals (CI) was calculated.  $P < 0.05$  indicates that the difference is statistically significant. We then established a risk prediction model and drawn the ROC curve of it and each clinical var-

iable, calculated the sensitivity, specificity, and positive and negative predictive values correspondingly.

We formulated the nomogram based on the multivariate Cox regression model for TSI prediction through the package of rms in R, Version 3.6.3. The prediction performance of the nomogram was measured using the C-index and calibration curves.

## 3. Results

**3.1. Clinical Features.** Of the 230 patients, 41.3% (95 of 230) were diagnosed with TSI. The demographic and clinical characteristics of the patients are listed in Table 1. Compared with the TIA group, there were more male (69.5 versus 51.9%;  $P = 0.007$ ), longer duration of symptoms (30 versus 10 min;  $P = 0.011$ ), higher SBP and DBP on admission ( $155.14 \pm 25.34$  versus  $144.73 \pm 20.65$  mmHg and  $87.23 \pm 12.85$  versus  $83.45 \pm 12.36$  mmHg;  $P = 0.001$  and  $0.026$ ), and higher incidences of unilateral weakness and speech impairment (72.6% versus 50.4% and 38.9% versus 21.5%;  $P = 0.001$  and  $0.006$ ) in TSI group, whereas there were less memory loss (5.3% versus 14.8%;  $P = 0.03$ ) of atrial fibrillation and smoking, and drinking was higher (12.6% versus 3.0% and 48.4% versus 24.4% and 25.3% versus 14.1%;  $P = 0.007$ ,  $<0.001$ , and  $0.049$ ).

Biomarker and imaging characteristics are shown in Table 2. It indicated that creatinine ( $P = 0.008$ ), uric acid ( $P = 0.006$ ), total cholesterol ( $P = 0.015$ ), low-density lipoprotein ( $P < 0.001$ ), brain natriuretic peptide precursor ( $P = 0.007$ ), red blood cell ( $P = 0.010$ ), hemoglobin ( $P = 0.023$ ), and hematocrit ( $P = 0.022$ ) in the group TSI are significantly higher than those in the TIA group, and the differences were statistically significant. Similarly, the percentages of patients with severe responsible vessel stenosis or occlusion (23.9% versus 14.0% and 9.1% versus 2.3%;  $P < 0.001$ ) and carotid plaque (76.3% versus 56.0%;  $P = 0.002$ ) were higher than that in the TIA group. Table 3 showed the multivariable analyses of clinical characteristics of TSI patients, and the smoking history, low-density lipoprotein cholesterol, brain natriuretic peptide precursor, and ABCD3 score are the independent risk factors of TSI.

**3.2. Model Evaluation.** Table 4 shows the performance of LDL, NT-pro-BNP, ABCD2 score, ABCD3 score, and our combined risk prediction model. We used the area under the ROC curve to evaluate the diagnosis efficacy (Figure 1). Compared with the other models, the combined model consisting of smoking history, low-density lipoprotein cholesterol, brain natriuretic peptide precursor, and ABCD3 score had the largest area under the ROC curve, whose AUC is 0.762 (95% CI 0.701–0.823), which means it shows better performance.

**3.3. Construction and Validation of the Nomogram.** As the combined model had the best predictive performance, we built a nomogram based on this final model: the ABCD3-SLOPE score (Figure 2). The performance of the nomogram was evaluated by the concordance index (C-index) with 1000 bootstrap resamples, and we measure the discrimination of the model by the area under the ROC curve. A value of 1



TABLE 1: Demographic and clinical characteristics of the patients.

Variables	TIA (N = 135)	TSI (N = 95)	P value
<i>Demographic characteristics</i>			
Gender (male, %)	70 (51.9)	66 (69.5)	0.007
Age (years)	65 (59.73)	64 (58.71)	0.516
<i>Clinical data</i>			
Duration of TIA (min)	10 (3.60)	30 (9.60)	0.011
Frequency in 24 h (%) 1	112 (83.6)	70 (73.7)	0.097
≥2	22 (16.4)	25 (26.3)	
SBPa (mmHg)	144.73 ± 20.65	155.14 ± 25.34	0.001
DBPa (mmHg)	83.45 ± 12.36	87.23 ± 12.85	0.026
<i>Clinical symptoms</i>			
Unilateral weakness (%)	68 (50.4)	69 (72.6)	0.001
Numbness or tingling (%)	41 (30.4)	33 (34.7)	0.579
Speech impairment (%)	29 (21.5)	37 (38.9)	0.006
Diplopia (%)	2 (1.5)	0 (0)	0.513
Dizzy (%)	43 (31.9)	22 (23.2)	0.196
Unconsciousness (%)	9 (6.7)	4 (4.2)	0.566
Bilateral amaurosis, hemianopia (%)	11 (8.1)	4 (4.2)	0.286
Memory loss (%)	20 (14.8)	5 (5.3)	0.030
Facial paralysis (%)	7 (5.2)	12 (12.6)	0.053
Torpor (%)	6 (4.4)	4 (4.2)	1.000
Unilateral amaurosis (%)	5 (3.7)	0 (0)	0.079
Weakness of upper limbs (%)	10 (7.4)	3 (3.2)	0.248
<i>PMH</i>			
Hypertension (%)	91 (67.4)	64 (67.4)	1.000
Diabetes mellitus (%)	32 (23.7)	26 (27.4)	0.634
Atrial fibrillation (%)	4 (3.0)	12 (12.6)	0.007
Hyperlipidemia (%)	27 (20.0)	19 (20.0)	1.000
Stroke (%)	21 (15.6)	17 (17.9)	0.772
TIA (%)	48 (35.6)	33 (34.7)	1.000
Dual TIAa (%)	28 (20.7)	28 (29.5)	0.173
Coronary heart disease (%)	10 (7.4)	7 (7.4)	1.000
Tumor (%)	6 (4.4)	5 (5.3)	0.776
Renal insufficiency (%)	8 (5.9)	2 (2.1)	0.202
Smoking (%)	33 (24.4)	46 (48.4)	<0.001
Drinking (%)	19 (14.1)	24 (25.3)	0.049
<i>Drug history</i>			
Antiplatelet drugs (%)	18 (13.3)	8 (8.4)	0.344
Statins (%)	10 (7.4)	3 (3.2)	0.278
Anticoagulants (%)	1 (1.1)	1 (0.7)	1.000
<i>ABCD scores</i>			
ABCD2	3 (2.4)	4 (3.5)	<0.001
ABCD3	4 (2.5)	5 (4.6)	<0.001

PMH: past medical history; SBPa: the first systolic blood pressure after admission; DBPa: the first diastolic blood pressure after admission; dual TIAa prompting medical attention plus at least one other TIA in the preceding 7 days.

indicates perfect discrimination, and 0.5 represents discriminative power equal to randomness. Furthermore, the calibration curve of the combined model (Figure 3) is close to the ideal curve, which demonstrated that it has a well-predictive performance.

#### 4. Discussion

Our study suggested 41.3% of the patients with transient neurologic deficits had positive DWI lesions on brain MRI. The rate of TSI in our research was



TABLE 2: Biomarker and imaging characteristics.

Variables	TIA (N = 135)	TSI (N = 95)	P value
<i>Biomarkers data</i>			
CRP (mg/L)	3.02 (3.02, 3.23)	3.02 (3.02, 3.40)	0.306
NSE (ng/ml)	14.27 (12.72, 16.38)	14.18 (12.88, 16.71)	0.484
Folic acid (ng/ml)	7.18 (5.63, 9.63)	7.24 (5.22, 9.68)	0.763
HbA1c (%)	5.85 (5.68, 6.25)	5.90 (5.60, 6.33)	0.700
ALT (U/L)	17.80 (10.80, 25.95)	17.10 (11.00, 23.30)	0.473
CR ( $\mu$ mol/L)	69.50 (59.60, 83.98)	76.90 (66.95, 85.24)	0.008
UA ( $\mu$ mol/L)	317.71 $\pm$ 75.57	346.82 $\pm$ 80.94	0.006
FBG (mmol/L)	5.10 (4.60, 5.55)	5.10 (4.80, 5.55)	0.195
AST (U/L)	18.00 (15.05, 23.35)	17.20 (14.65, 21.70)	0.283
TC (mmol/L)	4.16 $\pm$ 1.11	4.50 $\pm$ 0.94	0.015
TG (mmol/L)	1.27 (0.90, 1.65)	1.36 (1.07, 1.72)	0.175
HDL (mmol/L)	1.10 (0.94, 1.33)	1.05 (0.90, 1.25)	0.260
LDL-C (mmol/L)	2.39 $\pm$ 0.89	2.83 $\pm$ 0.82	<0.001
Calcium (mmol/L)	2.27 (2.22, 2.32)	2.26 (2.21, 2.31)	0.287
Hcy ( $\mu$ mol/L)	11.30 (9.45, 11.89)	11.20 (9.20, 15.15)	0.772
Fib (g/L)	2.59 (2.33, 3.05)	2.56 (2.38, 2.99)	0.837
D-dimer (mg/L)	0.28 (0.22, 0.46)	0.29 (0.22, 0.46)	0.614
NT-pro-BNP (pg/ml)	75.07 (31.04, 138.75)	99.42 (52.76, 239.55)	0.007
WBC ( $\times 10^9/L$ )	6.20 (5.24, 7.42)	6.38 (5.34, 7.58)	0.544
RBC ( $\times 10^{12}/L$ )	4.38 $\pm$ 0.54	4.56 $\pm$ 0.48	0.010
Hemoglobin (g/L)	133.27 $\pm$ 15.94	138.13 $\pm$ 15.77	0.023
Hematocrit (%)	40.19 $\pm$ 4.58	41.58 $\pm$ 4.34	0.022
PTL ( $\times 10^9/L$ )	216 (185, 254)	221 (176, 262)	0.853
Neutrophil (%)	3.50 (2.91, 4.55)	3.79 (3.13, 4.56)	0.172
Lymphocyte (%)	1.92 (1.55, 2.40)	1.89 (1.52, 2.20)	0.311
NLR	1.79 (1.36, 2.42)	2.02 (1.51, 2.65)	0.069
MPV (fL)	10.81 $\pm$ 0.96	10.80 $\pm$ 0.96	0.920
PCT (%)	0.23 (0.19, 0.28)	0.23 (0.20, 0.28)	0.665
PDW (%)	12.70 (11.35, 13.80)	12.70 (11.35, 14.15)	0.678
<i>Imaging data</i>			
<i>Degree of vascular stenosis (%)</i>			
Mild	99 (76.7)	44 (50.0)	<0.001
Moderate	9 (7.0)	15 (17.0)	
Severe	18 (14.0)	21 (23.9)	
Occlusion	3 (2.3)	8 (9.1)	
<i>Fazekas score (%)</i>			
0	31 (23.0)	15 (16.1)	0.136
1	74 (54.8)	52 (55.9)	
2	22 (16.3)	17 (18.3)	
3	8 (5.9)	9 (9.7)	
<i>Carotid plaque (%)</i>			
No	59 (44.0)	22 (23.7)	0.002
Yes	75 (56.0)	71 (76.3)	

concordant with those in previous studies which reported 29.3-41.5% of the patients with transient symptoms were found acute ischemic lesions by DWI [3-7]. The high incidence of TIS prompted us to develop a practical tool to

identify TSI in patients with transient symptoms at the onset of stroke.

Our study found TSI was independently associated with the smoking history, low-density lipoprotein cholesterol,

TABLE 3: The multivariable analyses of clinical characteristics of TSI patients.

Variables	$\beta$	P	OR	95% CI	
				Lower	Upper
Smoking history	1.220	<0.001	3.388	1.265	5.115
LDL	0.404	0.035	1.497	1.081	2.388
NT-pro-BNP	0.003	0.019	1.003	1.001	1.006
ABCD3 score	0.422	<0.001	1.525	1.233	1.853
Constant	-4.058	<0.001	0.017	-	-

TABLE 4: Performance of prediction models.

Predicting factors	AUC	95% CI		Cut-off value	P value
		Lower	Upper		
LDL	0.638	0.566	0.710	1.98	<0.001
NT-pro-BNP	0.601	0.527	0.676	48.515	0.009
ABCD2 score	0.681	0.613	0.750	2.5	<0.001
ABCD3 score	0.682	0.614	0.750	3.5	<0.001
Prediction model	0.762	0.701	0.823	0.325	<0.001

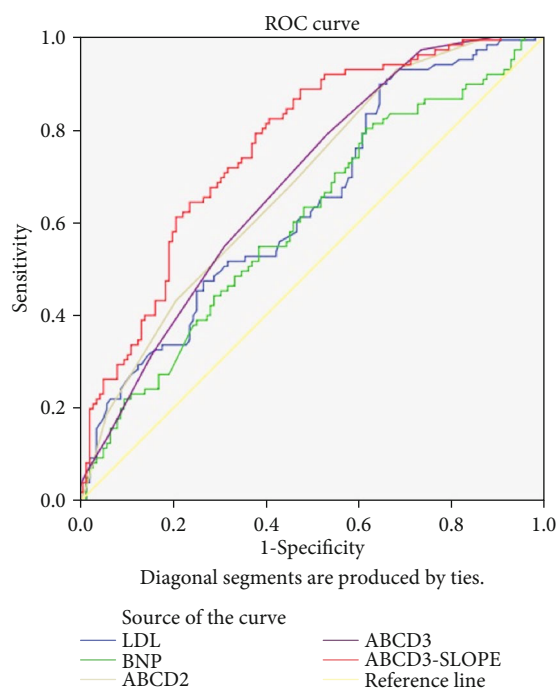


FIGURE 1: The AUC for the prediction of TSI risk of different models.

brain natriuretic peptide precursor, and ABCD3 score. We developed the model ABCD3-SLOPE, and it is a practical and convenient tool with the high prediction of TSI in patients with neurological deficits recovered within 24 hours of onset. The score had easy applicability due to the easy and rapid availability of these variables in emergency department at the onset of stroke, and the nomogram indicated the virtue of simplicity and intuition. As demonstrated in Table 4, compared with other models, the ABCD3-SLOPE model had

high sensitivity (82.1%) and specificity (59.3%) to identify TSI when the patients presented transient symptoms. The concordance index (C-index) was 0.77 (95% confidence interval, 0.70-0.83) in the internal validation with 1000 bootstrap resamples, and the calibration curve demonstrated that the ABCD3-SLOPE had a well-predictive performance.

TSI is not only an independent entity different from TIA and acute cerebral infarction, but it is associated with a higher risk of recurrent ischemic events as well [4, 16–18]. The patient with a DWI lesion on baseline MRI was 4.3 times (9.1% versus 2.1%;  $P = 0.19$ ) more likely to suffer a subsequent stroke in 1 year than TIA [9]. The 7-day risk of stroke was higher on DWI-positive than DWI-negative patients (1.2% versus 12.3%) [13]. The subsequent risk of ischemic stroke after TIA was 2.4% in 2 days, 3.8% in 7 days, 4.1% in 30 days, and 4.7% in 90 days according to a systematic review and meta-analysis of 206455 unique patients [19]. It is reasonable to assume higher rates of subsequent ischemic stroke in 30 or 90 days in the TSI population. There was a trend that minor stroke patients who received intravenous t-PA had favorable outcomes and the larger proportion of alive and independent defined as Oxfordshire Handicap Score of 0-2 [20]. In the Austrian Stroke Unit Registry, rt-PA-treated patients with mild stroke had a good outcome in comparison to subjects without rt-PA [21]. However, there is no evidence of evidence-based medicine on intravenous t-PA in TIA patients. Thrombolysis is warranted in the TSI population instead of TIA patients probably. Early initiation of existing treatments was associated with an 80% reduction in early recurrent stroke and reduced subsequent hospital bed-days, acute costs, and 6-month disability [22, 23]. Despite the fact that recognition of TSI is of much importance, it remains a challenge for the physician in emergency department, since the TSI diagnosis is exceptionally dependent on the DWI sequence. Chaturvedi et al. reported that no more than 51% of TIA or minor stroke had MR image within two days of initial presentation [24]. In another multicenter study, MRI was performed in 58.5% of patients with TIA or minor stroke [25]. Other validating and simple tools are needed for physicians to distinguish TSI from TIA as traditionally defined.

In our study, we obtained a high global accuracy with the combination of four items that built the model of ABCD3-SLOPE: the smoking history, low-density lipoprotein cholesterol, brain natriuretic peptide precursor, and ABCD3 score. These items were featured with easy and quick availability. It provided a practical risk prediction tool for clinicians in rapid and accurate identification of TSI from TIA population at the earliest when MRI is not available. In consequence, more appropriate and precise treatments could be taken in time.

Some risk factors were found their associations with TSI in recent years. Jia et al. found that dysphasia was associated with acute DWI lesions in patients with transient neurological symptoms [26]. In Crisostomo et al.’s study, patients with positive DWI were 9.6 times more likely to present with symptom duration greater than 1 hour [27], and longer duration of symptoms would yield a higher probability of persistent parenchymal damage that could be detected by MRI. Cigarette smoking has appreciable adverse effects on hemorheological parameters, plasma osmolality, and high

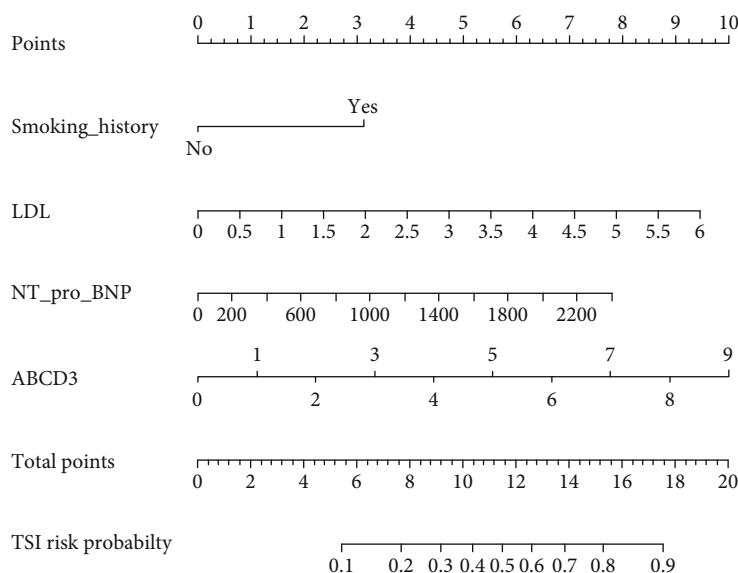


FIGURE 2: Nomogram for patients with symptoms of TIA. To use the nomogram, the value attributed to a patient is located on each variable axis, and a line is drawn upwards to determine the number of points received for each variable value. The sum of these numbers is located on the total point axis, and a line is then drawn downwards to the probability axis to predict the TSI risk likelihood.

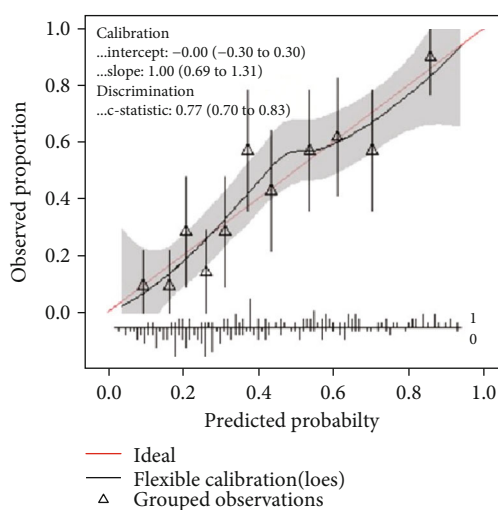


FIGURE 3: Calibration curve of the combined nomogram. The diagonal red line indicates the ideal prediction by a perfect model.

fibrinogen level. RBC aggregation in smokers promotes endothelial dysfunction through arterial wall inflammation and the impact of hematocrit on the blood vessel, and the increased blood viscosity may play an adverse role in the dissolution of thrombus [28]. Brain natriuretic peptide precursor is secreted by the cardiac ventricles, increasing serum levels correlate with the severity of left ventricle dysfunction. Left atrial appendage emptying flow velocity (LAAEV) can reflect the left atrial function, and it was independently associated with ischemic stroke in a prospective observational study [29]. As we have known that DOT score [11], Dawson score [12], and ABCD scoring system [30] are clinical diagnostic tools designed for and from TIA population, they fail to be fully applicable to TSI population. The ABCD3-

SLOPE model and nomogram is derived from the TSI population. Therefore, it is not only a simple risk assessment tool but of suitability to quantify the likelihood of TSI in the way of visualization.

Although the nomogram model demonstrated reasonable accuracy for the prediction of TSI, there are some limitations. First, the time delay from symptom onset to MRI examination is an essential factor that affects DWI positivity [3], and some patients might be underestimated if the MRI was performed within 24 hours of symptom onset. The time should be classified in the further study. Second, the current study was performed on the basis of a single-center, retrospective database, and it might not have the generalizability of a multicenter trial typically retains. However, we found the baseline characteristics of our patients such as age, gender, risk factors, and clinical symptoms were similar to a large sample size of 1910 patients [31], and we had reason to believe our cohort had a representative of a larger population. Third, although we had well internal validation, we did not have external validation. Hence, a further multicenter, larger validation study is clearly warranted.

## 5. Conclusions

Limb weakness, speech impairment, long duration of symptoms, high ABCD3 scores, and smoking history were the independent risk factors for TSI. The ABCD3-SLOPE and nomogram had a reasonable prediction performance on the recognition of TSI, and we need to design more robust research to explore the best critical ABCD3 scores and symptom duration to predict the risk of TSI and to provide more reliable evidence for other potential predictors.

## Data Availability

The data are available from the corresponding author on reasonable request.

## Conflicts of Interest

No conflict of interests by any of the authors.

## Authors' Contributions

LYQ and BQQ contributed equally. LYQ and WJ devised the study. LYQ and BQQ drafted the manuscript. LYQ and LLL analyzed and interpreted the data. FW and ZY collected the data. ZXY contributed to the critical revision of the manuscript. All authors read and approved the final manuscript. XiaoYu Zhou and Jue Wang are co-corresponding authors.

## Acknowledgments

The work was supported by Shanghai Municipal Key Clinical Specialty (shslczdzk06102), Shanghai Science and Technology Commission (19401972804), and Start-up Fund of Shanghai Tenth People's Hospital (04.03.16.002).

## References

- [1] W. N. Kernan, B. Ovbiagele, H. R. Black et al., "Guidelines for the prevention of stroke in patients with stroke and transient ischemic attack: a guideline for healthcare professionals from the American Heart Association/American Stroke Association," *Stroke*, vol. 45, no. 7, pp. 2160–2236, 2014.
- [2] T. Fitzpatrick, S. Gocan, C. Q. Wang et al., "How do neurologists diagnose transient ischemic attack: a systematic review," *International Journal of Stroke*, vol. 14, no. 2, pp. 115–124, 2019.
- [3] J. Yuan, Z. Jia, Y. Song et al., "Incidence and predictors of acute ischemic lesions on brain magnetic resonance imaging in patients with a clinical diagnosis of transient ischemic attack in China," *Frontiers in Neurology*, vol. 10, p. 764, 2019.
- [4] M. Al-Khaled and J. Eggers, "MRI findings and stroke risk in TIA patients with different symptom durations," *Neurology*, vol. 80, no. 21, pp. 1920–1926, 2013.
- [5] M. Brazzelli, F. M. Chappell, H. Miranda et al., "Diffusion-weighted imaging and diagnosis of transient ischemic attack," *Annals of Neurology*, vol. 75, no. 1, pp. 67–76, 2014.
- [6] H. Ay, W. J. Koroshetz, T. Benner et al., "Transient ischemic attack with infarction: a unique syndrome?," *Annals of Neurology*, vol. 57, no. 5, pp. 679–686, 2005.
- [7] S. Anticoli, F. R. Pezzella, C. Pozzessere et al., "Transient ischemic attack fast-track and long-term stroke risk: role of diffusion-weighted magnetic resonance imaging," *Journal of Stroke and Cerebrovascular Diseases*, vol. 24, no. 9, pp. 2110–2116, 2015.
- [8] B. Song, L. Pei, H. Fang et al., "Validation of the RRE-90 scale to predict stroke risk after transient symptoms with infarction: a prospective cohort study," *PLoS One*, vol. 10, no. 9, article e0137425, 2015.
- [9] J. M. Boulanger, S. B. Coutts, M. Eliasziw, S. Subramaniam, J. Scott, and A. M. Demchuk, "Diffusion-weighted imaging-negative patients with transient ischemic attack are at risk of recurrent transient events," *Stroke*, vol. 38, no. 8, pp. 2367–2369, 2007.
- [10] T. Tong, Z. Yao, and X. Feng, "Combined diffusion- and perfusion-weighted imaging: a new way for the assessment of hemispheric transient ischemic attack patients," *International Journal of Developmental Neuroscience*, vol. 29, no. 1, pp. 63–69, 2011.
- [11] D. Dutta, "Diagnosis of TIA (DOT) score—design and validation of a new clinical diagnostic tool for transient ischaemic attack," *BMC Neurology*, vol. 16, no. 1, p. 20, 2016.
- [12] J. Dawson, K. E. Lamb, T. J. Quinn et al., "A recognition tool for transient ischaemic attack," *QJM*, vol. 102, no. 1, pp. 43–49, 2009.
- [13] H. Ay, E. M. Arsava, S. C. Johnston et al., "Clinical- and imaging-based prediction of stroke risk after transient ischemic attack: the CIP model," *Stroke*, vol. 40, no. 1, pp. 181–186, 2009.
- [14] T. Kiyohara, M. Kamouchi, Y. Kumai et al., "ABCD3 and ABCD3-I scores are superior to ABCD2 score in the prediction of short- and long-term risks of stroke after transient ischemic attack," *Stroke*, vol. 45, no. 2, pp. 418–425, 2014.
- [15] L. S. Dolmans, E. R. Lebedeva, D. Veluponnar et al., "Diagnostic accuracy of the explicit diagnostic criteria for transient ischemic attack: a validation study," *Stroke*, vol. 50, no. 8, pp. 2080–2085, 2019.
- [16] S. B. Coutts and B. Cucchiara, "Stroke risk after TIA: DWI is only part of the answer," *Neurology*, vol. 80, no. 21, pp. 1914–1915, 2013.
- [17] A. Arhami Dolatabadi, A. Meisami, H. Hatamabadi et al., "Improving the prediction of stroke or death after transient ischemic attack (TIA) by adding diffusion-weighted imaging lesions and TIA etiology to the ABCD2 score," *Journal of Stroke and Cerebrovascular Diseases*, vol. 22, no. 7, pp. e25–e30, 2013.
- [18] F. Purroy, P. E. Jiménez-Caballero, G. Mauri-Capdevila et al., "Predictive value of brain and vascular imaging including intracranial vessels in transient ischaemic attack patients: external validation of the ABCD3-I score," *European Journal of Neurology*, vol. 20, no. 7, pp. 1088–1093, 2013.
- [19] S. Shahjouei, A. Sadighi, D. Chaudhary et al., "A 5-Decade analysis of incidence trends of ischemic stroke after transient ischemic attack: a systematic review and meta-analysis," *JAMA Neurology*, vol. 78, no. 1, p. 77, 2021.
- [20] P. Khatri, D. Tayama, G. Cohen et al., "Effect of intravenous recombinant tissue-type plasminogen activator in patients with mild stroke in the third international stroke trial-3: post hoc analysis," *Stroke*, vol. 46, no. 8, pp. 2325–2327, 2015.
- [21] S. Greisenegger, L. Seyfang, S. Kiechl, W. Lang, and J. Ferrari, "Thrombolysis in patients with mild Stroke," *Stroke*, vol. 45, no. 3, pp. 765–769, 2014.
- [22] R. Luengo-Fernandez, A. M. Gray, and P. M. Rothwell, "Effect of urgent treatment for transient ischaemic attack and minor stroke on disability and hospital costs (EXPRESS study): a prospective population-based sequential comparison," *Lancet Neurology*, vol. 8, no. 3, pp. 235–243, 2009.
- [23] P. M. Rothwell, M. F. Giles, A. Chandratheva et al., "Effect of urgent treatment of transient ischaemic attack and minor stroke on early recurrent stroke (EXPRESS study): a prospective population-based sequential comparison," *Lancet*, vol. 370, no. 9596, pp. 1432–1442, 2007.

- [24] S. Chaturvedi, S. Ofner, F. Baye et al., "Have clinicians adopted the use of brain MRI for patients with TIA and minor stroke?," *Neurology*, vol. 88, no. 3, pp. 237–244, 2017.
- [25] P. Amarenco, P. C. Lavallée, J. Labreuche et al., "One-year risk of stroke after transient ischemic attack or minor stroke," *The New England Journal of Medicine*, vol. 374, no. 16, pp. 1533–1542, 2016.
- [26] Z. Jia, Y. Song, and W. Hu, "Dysphasia is associated with diffusion-weighted MRI abnormalities in patients with transient neurological symptoms," *Neurological Sciences*, vol. 41, no. 7, pp. 1765–1771, 2020.
- [27] R. A. Crisostomo, M. M. Garcia, and D. C. Tong, "Detection of diffusion-weighted MRI abnormalities in patients with transient ischemic attack: correlation with clinical characteristics," *Stroke*, vol. 34, no. 4, pp. 932–937, 2003.
- [28] Y. Cai, W. Xu, H. Liu et al., "Effects of cigarette smoking on older Chinese men treated with clopidogrel monotherapy or aspirin monotherapy: a prospective study," *Platelets*, vol. 31, no. 5, pp. 667–673, 2020.
- [29] R. M. Melduni, H.-C. Lee, K. R. Bailey et al., "Real-time physiologic biomarker for prediction of atrial fibrillation recurrence, stroke, and mortality after electrical cardioversion: a prospective observational study," *American Heart Journal*, vol. 170, no. 5, pp. 914–922, 2015.
- [30] T. J. Quinn, A. C. Cameron, J. Dawson, K. R. Lees, and M. R. Walters, "ABCD2 scores and prediction of noncerebrovascular diagnoses in an outpatient population: a case-control study," *Stroke*, vol. 40, no. 3, pp. 749–753, 2009.
- [31] M. Al-Khaled, C. Matthis, T. F. Münte, J. Eggers, and QugSS2-Study, "The incidence and clinical predictors of acute infarction in patients with transient ischemic attack using MRI including DWI," *Neuroradiology*, vol. 55, no. 2, pp. 157–163, 2013.



## Retraction

# Retracted: Flat Panel CT Scanning Is Helpful in Predicting Hemorrhagic Transformation in Acute Ischemic Stroke Patients Undergoing Endovascular Thrombectomy

### BioMed Research International

Received 12 March 2024; Accepted 12 March 2024; Published 20 March 2024

Copyright © 2024 BioMed Research International. This is an open access article distributed under the Creative Commons Attribution License, which permits unrestricted use, distribution, and reproduction in any medium, provided the original work is properly cited.

This article has been retracted by Hindawi following an investigation undertaken by the publisher [1]. This investigation has uncovered evidence of one or more of the following indicators of systematic manipulation of the publication process:

- (1) Discrepancies in scope
- (2) Discrepancies in the description of the research reported
- (3) Discrepancies between the availability of data and the research described
- (4) Inappropriate citations
- (5) Incoherent, meaningless and/or irrelevant content included in the article
- (6) Manipulated or compromised peer review

The presence of these indicators undermines our confidence in the integrity of the article's content and we cannot, therefore, vouch for its reliability. Please note that this notice is intended solely to alert readers that the content of this article is unreliable. We have not investigated whether authors were aware of or involved in the systematic manipulation of the publication process.

Wiley and Hindawi regrets that the usual quality checks did not identify these issues before publication and have since put additional measures in place to safeguard research integrity.

We wish to credit our own Research Integrity and Research Publishing teams and anonymous and named

external researchers and research integrity experts for contributing to this investigation.

The corresponding author, as the representative of all authors, has been given the opportunity to register their agreement or disagreement to this retraction. We have kept a record of any response received.

### References

- [1] L. Chen, Y. Xu, R. Shen et al., "Flat Panel CT Scanning Is Helpful in Predicting Hemorrhagic Transformation in Acute Ischemic Stroke Patients Undergoing Endovascular Thrombectomy," *BioMed Research International*, vol. 2021, Article ID 5527101, 8 pages, 2021.

## Research Article

# Flat Panel CT Scanning Is Helpful in Predicting Hemorrhagic Transformation in Acute Ischemic Stroke Patients Undergoing Endovascular Thrombectomy

Liuwei Chen,<sup>1</sup> Yi Xu,<sup>1</sup> Rui Shen,<sup>1</sup> Jiping Sun,<sup>1</sup> Xiang Zhang ,<sup>1</sup> Quanbin Zhang ,<sup>1</sup> and Feng Wang <sup>2</sup>

<sup>1</sup>Department of Neurosurgery, Shanghai Tenth People's Hospital, Tongji University School of Medicine, Shanghai, China

<sup>2</sup>Departments of Neurology, Seventh People's Hospital of Shanghai University of Traditional Chinese Medicine, Shanghai, China

Correspondence should be addressed to Quanbin Zhang; [quanbinzhang@aliyun.com](mailto:quanbinzhang@aliyun.com) and Feng Wang; [13816566556@163.com](mailto:13816566556@163.com)

Received 13 January 2021; Revised 28 February 2021; Accepted 23 March 2021; Published 14 April 2021

Academic Editor: Qian Wang

Copyright © 2021 Liuwei Chen et al. This is an open access article distributed under the Creative Commons Attribution License, which permits unrestricted use, distribution, and reproduction in any medium, provided the original work is properly cited.

**Purpose.** Hyperdense lesions are frequently revealed on flat panel CT (FP-CT) immediately after endovascular thrombectomy in patients with acute ischemic stroke. This study is aimed at discriminating hyperdense lesions caused by extravasation plus hemorrhage from those caused by contrast extravasation alone. **Methods.** We retrospectively analyzed clinical and radiological data of patients who underwent an immediate postprocedure FP-CT scan and a follow-up noncontrast CT 24 hours after thrombectomy. We especially focused on the Maximum Hounsfield Units ( $HU_{max}$ ) of each hyperdense lesion. A hyperdense lesion was judged to be hemorrhagic when it persisted on noncontrast CT and/or developed a mass effect. **Results.** Of 81 patients included in this study, 32 (39.5%) patients presented 41 hyperdense lesions on FP-CT. The chance of hemorrhagic transformation is higher in patients with hyperdense lesions on FP-CT than that in patients without hyperdense lesions (23/32 vs. 1/49,  $p < 0.001$ ). The  $HU_{max}$  of hyperdensity on FP-CT can predict hemorrhagic transformation with an area under the curve of 0.805 (95% CI: 0.67-0.94,  $p = 0.02$ ). The sensitivity, specificity, positive, and negative predictive values of hyperdensity on FP-CT for hemorrhagic transformation were 96%, 84%, 72%, and 98%, respectively. A  $HU_{max}$  of  $>600$  predicted hemorrhagic transformation with a sensitivity of 50% and a specificity of 100%. **Conclusions.** The presence of hyperdensity on FP-CT can predict hemorrhagic transformation with a high sensitivity and negative predictive value. The measurement of  $HU_{max}$  of hyperdense lesion on FP-CT can be applied to the management of patients undergoing endovascular recanalization.

## 1. Introduction

Mechanical thrombectomy has been regarded as a milestone in the rescue of severe acute ischemic stroke (AIS) with high recanalization rates and dramatically improved results [1]. However, this endovascular treatment may result detrimental mainly because of hemorrhagic transformation (HT) [2]. Detection of intracerebral hemorrhage as early as possible is absolutely critical in the management of this intractable condition. Flat panel computed tomography (FP-CT) is a very useful tool for the detection of peri-interventional complications immediately after procedure without transferring patients to the CT unit [3, 4]. However, this imaging

modality poses challenges in diagnosing HT in patients undergoing mechanical thrombectomy as the presence of hyperdense lesions could be either contrast extravasation alone or plus hemorrhage. The goal of this study was to evaluate the potential of FP-CT in the detection of intraparenchymal hemorrhage through analyzing Hounsfield Units of hyperdense areas seen on FP-CT immediately after mechanical thrombectomy.

## 2. Methods and Materials

**2.1. Patients.** AIS patients who were treated with mechanical thrombectomy due to large vessel occlusion between January

2016 and March 2018 at our institution were retrospectively reviewed and analyzed. The inclusion criteria for the study were examined with an immediate postprocedure FP-CT and a follow-up noncontrast computed tomography (NC-CT) 24 hours after thrombectomy. Patients were excluded if their image data were incomplete or nondiagnostic due to motion or other artifacts. This study was approved by the ethics committee of our Institution, and the review board waived the need for written informed consent from the participants.

**2.2. Stroke Management.** In accordance with AHA/ASA guideline's acute ischemic stroke protocol, patients presenting large vessel occlusions within 6 hours from symptom onset received endovascular recanalization. A combination of Solitaire™ FR revascularization device and Navein guide catheter (ev3, Irvine, CA, USA) was employed for mechanical thrombectomy in all selected cases. Balloon or stent-assisted angioplasty as an alternative was performed only when stent retriever thrombectomy failed due to intracranial stenosis. Details on the arterial occlusion sites, median time from onset to puncture (onset-to-puncture time), procedure time, interval between FP-CT and NC-CT, and so on were recorded for each patient. Recanalization was considered to be successful when the thrombolysis in cerebral infarction (TICI) score was 2b or 3. Decompressive craniectomy was reserved for patients whose neurological condition deteriorated due to significant space-occupying effect. The neurologic outcomes were assessed using the modified Rankin scale (mRS) score at a three-month follow-up. Favorable outcomes were defined as scores  $\leq 2$ .

**2.3. Image Acquisition.** FP-CT scans were regularly performed at the end of thrombectomy, while follow-up NC-CT scans were finished about 24 hours after the procedure. FP-CT scans were performed with a biplane angiography system (Dyna CT, Siemens, Germany) using the following parameters: voltage, 84 kV; tube current, 253 mA; acquisition time, 11.6 ms per frame; projection on 48 cm flat panel size; angulation, frame speed, 30 frames per second, 0.4° per frame; total angle, 196°; exposure time, 20 s. NC-CT images were acquired on a 64-slice multidetector CT (GE LightSpeed VCT, GE Healthcare, USA) at 120 kV, 250 mA, and 1.0 s rotation time. Images were reconstructed with 5 mm section thickness, using a standard reconstruction kernel, a field of view of 250 mm, and a 512 × 512 matrix.

**2.4. Image Analysis.** Two experienced neurologists blinded to clinical data independently reviewed FP-CT images on a dedicated workstation (syngo Multi-Modality Workplace, Siemens, Germany) and NC-CT images on the PACS (Philips iSite PACS, Netherlands) in randomized order. Afterward, a consensus reading was performed to get a reference standard for statistical analyses.

Maximum Hounsfield Units ( $HU_{max}$ ) of hyperdense lesions in FP-CT were measured based on visually defined regions of interest.  $HU_{max}$  and location of each hyperdense lesion were separately recorded if there were multiple hyperdense lesions in the same patient. Hyperdense lesions that were no longer discernible on the follow-up NC-CT were

regarded as contrast extravasation. Hyperdensity was confirmed to be hemorrhagic transformation (HT) when it persisted on NC-CT and/or developed a mass effect [5, 6]. HT was further categorized as symptomatic and nonsymptomatic. We defined symptomatic hemorrhage according to the SITS-MOST definition [7]: when blood clot exceeds 30% of the infarcted volume with significant mass effect or leads to a decline in NIHSS of  $\geq 4$  points or causing death within 36 hours.

**2.5. Statistical Analysis.** Continuous variables are expressed as the mean  $\pm$  standard deviation, ordinal variables are expressed as median (interquartile), and categorical variables are expressed as numbers (frequencies). Bivariate comparisons were performed by the Mann-Whitney  $U$  test for continuous variables and the  $\chi^2$  test for categorical variables (or Fisher's exact test when the expected cell frequency was  $< 5$ ). The sensitivity, specificity, positive predictive value, and negative predictive value of FP-CT for the prediction of HT were calculated. In addition, receiver operating characteristic analysis was performed to indicate the predictive value of the  $HU_{max}$  of hyperdensity for identifying intraparenchymal hemorrhage. All the statistical analyses were performed with SPSS version 21.0 (SPSS, Chicago, IL, USA). A value of  $p < 0.05$  was considered to be significant.

### 3. Results

**3.1. The Study Sample and Clinical Outcomes.** Between January 2016 and March 2018, 87 patients underwent both FP-CT and follow-up NC-CT scans after mechanical thrombectomy but 6 were excluded due to poor image quality, yielding a cohort of 81 patients (49 males, 32 females). The mean age of this series was  $67.4 \pm 9.5$  years (ranging from 49 to 83 years), and patients presented with a median on-admission NIHSS score of 15 (ranging from 6 to 26). The rate of successful recanalization (TICI 2b and 3) was 88.9% (72/81). Hyperdense lesions were found on 32 patients on the FP-CT. However, HT was revealed in 24 patients on the follow-up NC-CT, among them, 7 were symptomatic. At the 3-month follow-up, we obtained a functional independence rate of 45.7% (37/81) and a mortality rate of 11.1% (9/81). 6 patients died of symptomatic intracranial hemorrhage and/or brain infarction edema; the remaining 3 died because of systematic infection.

According to the results of FP-CT scans, patients were divided into hyperdense lesion group (32 cases) and nonhyperdense lesion group (49 cases). There was no significant difference between the two groups regarding age, sex, occlusion sites, NIHSS scores, onset-to-puncture time, procedure time, interval between FP-CT and NC-CT, TICI scores, and so on (see Table 1); however, the rate of functional independence at 3 months was 53.1% (26/49) in the nonhyperdense lesion group and 34.3% (11/32) in the hyperdense lesion group ( $p = 0.12$ ); meanwhile, the mortality rate is 6.1% (3/49) in the nonhyperdense lesion group, in comparison to 18.8% (6/32) in the hyperdense lesion group ( $p = 0.14$ ), indicating that hyperdense lesion on FP-CT was related to

TABLE 1: Comparisons of hyperdensity versus no hyperdensity on flat panel CT performed immediately after mechanical thrombectomy.

	FP-CT+ (N = 32)	FP-CT- (N = 49)	p
HT	23 (71.9%)	1 (2.0%)	$p < 0.01$
Age in years	66.2 ± 10.9	66.9 ± 8.6	0.45
Male	19 (59.4%)	30 (61.2%)	>0.99
Baseline NIHSS score	15 (13-18)	15 (12-18)	0.54
Occluded circulation			0.85
Anterior	26 (81.2%)	39 (79.6%)	
Posterior	6 (18.8%)	10 (20.4%)	
Occluded arteries			0.98
MCA isolated	18 (56.2%)	27 (55.1%)	
ICA isolated or tandem with MCA	8 (25.0%)	12 (24.5%)	
Posterior circulation	6 (18.8%)	10 (20.4%)	
Time from symptom onset to puncture	210.2 ± 64.8	195.7 ± 80.9	0.15
Procedure time	103.0 ± 44.1	91.1 ± 32.2	0.24
Interval between FP-CT and NC-CT	25.1 ± 3.9	23.7 ± 3.5	0.37
Recanalization after treatment,			0.25
TICI < 2b	5 (15.6%)	3 (6.1%)	
TICI ≥ 2b	27 (84.4%)	46 (93.9%)	
3-month mRS			0.12
≤2	11 (34.4%)	26 (53.1%)	
>2	21 (65.6%)	23 (46.9%)	
Mortality rate	6 (18.8%)	3 (6.1%)	0.14

Data are *n* (%), median (interquartile), or mean ± standard deviation. Note: FP-CT indicates flat panel CT, HT indicates hemorrhagic transformation, NIHSS indicates National Institutes of Health Stroke Scale, MCA indicates middle cerebral artery, ICA indicates internal carotid artery, TICI indicates thrombolysis in cerebral infarction, mRS indicates modified Rankin scale.

unfavorable outcomes though statistical difference was not significant possibly due to sample size.

**3.2. Hyperdensity Could Predict HT.** The total number of HT was 24, most of them were from the hyperdense lesion group (23/32, 71.9%), and only one case was from the nonhyperdense lesion group (1/49, 2.0%). The difference was statistically significant ( $p < 0.001$ ). The sensitivity and specificity of hyperdensity on FP-CT for detecting hemorrhage transformation were 96% (23/24) and 84% (48/57), respectively, while positive and negative predictive value were 72% (23/32) and 98% (48/49). Among the 24 cases with HT, 7 cases were categorized as symptomatic and all of them were from the hyperdense lesion group. Sample cases are shown in Figure 1.

There was a total of 41 hyperdense lesions in 32 patients, with 9 patients harboring two isolated hyperdense lesions. As 13 hyperdense lesions disappeared on the following NC-CT scans, they were attributed to oozing of contrast agent. The remaining 28 lesions were judged as hemorrhagic. The clinical features of these hyperdense lesions are shown in Table 2. We further divided the hyperdense lesions into the hemorrhagic group and the nonhemorrhagic group. The  $HU_{max}$  of each hyperdense lesion was measured, as a result, the  $HU_{max}$  of the hemorrhagic group was much higher than that of the nonhemorrhagic group ( $867.3 \pm 667.1$  verse  $300.1 \pm 127.0$  HU,  $p = 0.02$ ). It was very impressive that in one

patient who had both hemorrhagic and nonhemorrhagic hyperdense lesions, the  $HU_{max}$  of the hemorrhagic one was much higher than that of the nonhemorrhagic one (Figure 2). The receiver operating characteristic analysis showed that the  $HU_{max}$  of the hyperdensity on FP-CT can predict HT with an area under the curve of 0.805 (95% CI: 0.67-0.94,  $p = 0.02$ ) (Figure 3). The lowest and highest  $HU_{max}$  was 169 and 2766, respectively, in the 41 hyperdense lesions. With the upregulation of the threshold values, the sensitivity of  $HU_{max}$  for detecting HT decreased, but the specificity increased meanwhile. The highest  $HU_{max}$  of hyperdense lesion finally judged to be contrast extravasation was 561 HU, so when we set  $HU_{max}$  600 by Youden index as a threshold value, it can predict HT with a sensitivity of 50% (14/28) and a specificity of 100%.

#### 4. Discussion

FP-CT has the advantage of immediately revealing periprocedural abnormal conditions without transferring patients, which is especially useful in the management of patients undergoing endovascular recanalization.

Our study found that 39.5% of patients (32/81) had hyperdense lesions after mechanical thrombectomy, which is in line with previous reports (from 30% to 87% using NC-CT [8-15] and 16% to 60% using FP-CT [16-18]). As HT is critical in the setting of therapy for AIS patients, we



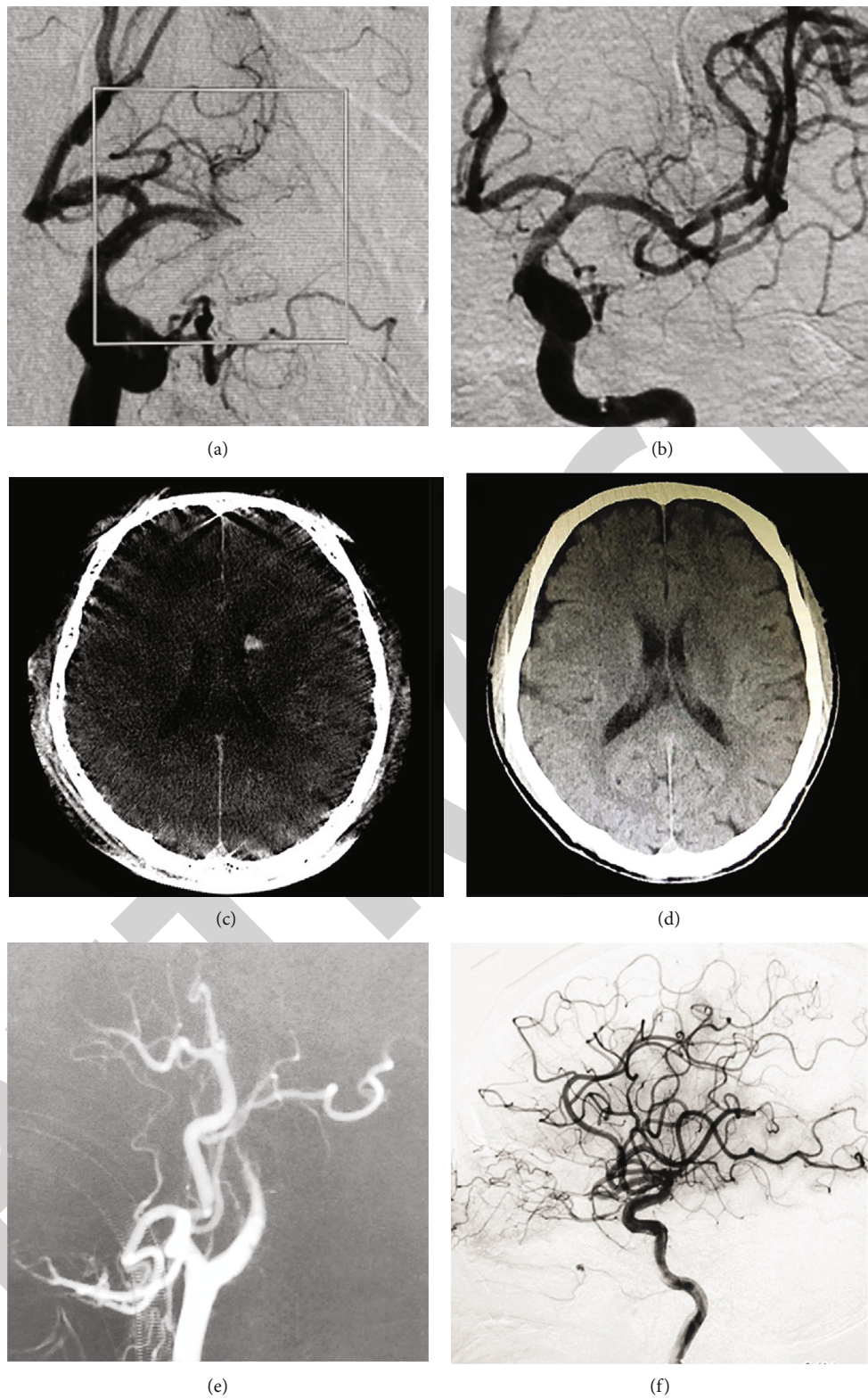


FIGURE 1: Continued.



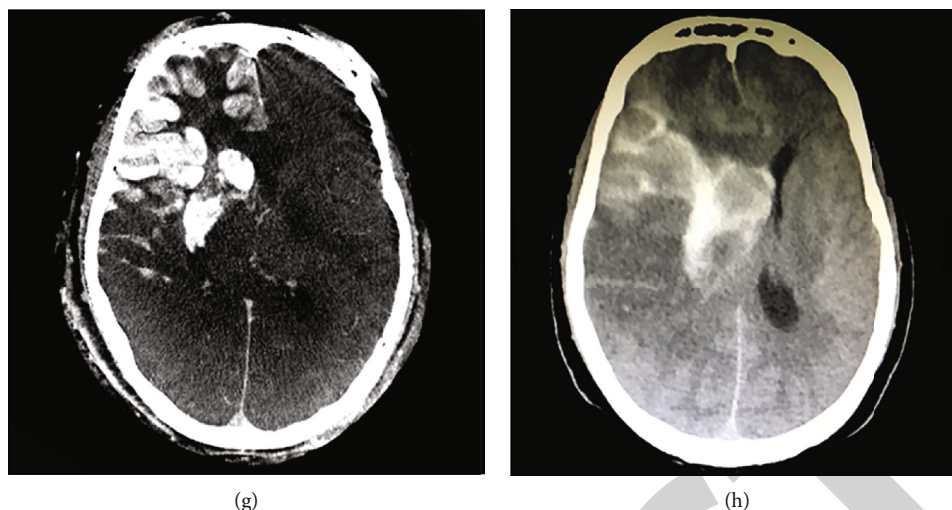


FIGURE 1: Images of sample patients. A 56-year-old man with acute occlusion of the left middle cerebral artery (a) received successful recanalization (b). Flat panel CT shows hyperdense lesion in the head of the left caudal nucleus (c), which resolved on noncontrast CT 24 hours after thrombectomy (d). A 67-year-old man with acute occlusion of the right internal carotid artery (e) received successful recanalization (f). Flat panel CT shows hyperdense lesion in the right basal ganglia and right middle cerebral artery territory (g), which persisted on noncontrast CT (h).

TABLE 2: The clinical features of patients with hyperdense lesions on FP-CT.

Variable	Total hyperdense lesions (n = 41)	Hemorrhagic lesions		p
		Yes (n = 28)	No (n = 13)	
Age	68.6 ± 11.2	67.5 ± 11.4	70.9 ± 10.8	0.34
Sex (male)	25 (61.0%)	19 (67.9%)	6 (46.2%)	0.18
Baseline NIHSS score	15 (12-18)	16 (13-20)	14 (11-14)	0.08
Occluded arteries (n, %)				0.05
MCA isolated	21 (51.2%)	11 (39.3%)	10 (76.9%)	
ICA isolated or tandem with MCA	14 (34.1%)	11 (39.3%)	3 (23.1%)	
Posterior circulation	6 (14.6%)	6 (21.4%)	0 (0.0%)	
Time from symptom onset to puncture	204.8 ± 66.3	211.9 ± 65.9	189.6 ± 67.4	0.31
Procedure time	105.1 ± 42.7	109.0 ± 45.8	96.5 ± 35.0	0.58
Interval between FP-CT and NC-CT	25.0 ± 4.1	24.5 ± 4.1	26.0 ± 4.1	0.20
Recanalization after treatment				0.39
TICI < 2b	6 (14.6%)	5 (17.9%)	1 (7.7%)	
TICI ≥ 2b	35 (85.4%)	23 (82.1%)	12 (92.3%)	
3-month mRS				0.55
≤2	12 (29.3%)	9 (32.1%)	3 (23.1%)	
>2	29 (70.7%)	19 (67.9%)	10 (76.9%)	
Mortality rate	8 (19.5%)	8 (28.6%)	0 (0.0%)	0.03
HU <sub>max</sub>	687.4 ± 613.7	867.3 ± 667.1	300.1 ± 127.0	0.02

Data are n (%), median (interquartile), or mean ± standard deviation. Note: HU<sub>max</sub> indicates maximum Hounsfield units.

attempted to investigate the potential of FP-CT in the prediction of HT. As a result, the hyperdense lesion on FP-CT demonstrated high sensitivity and negative predictive value for the detection of HT. When focusing on the HU<sub>max</sub> of hyperdense lesions, we found that, with the increase of the HU<sub>max</sub> value, the risk of HT enhanced accordingly. Berger et al. [19] reported that symptomatic intracranial hemorrhage was the

only HT that independently caused clinical deterioration and impacted prognosis. As far as symptomatic hemorrhage is concerned, all the symptomatic cases are from the FP-CT (+) group, indicating that FP-CT can reliably predict symptomatic intracranial hemorrhage.

As a dynamic interface between the peripheral circulation and the central nervous system, the blood-brain barrier

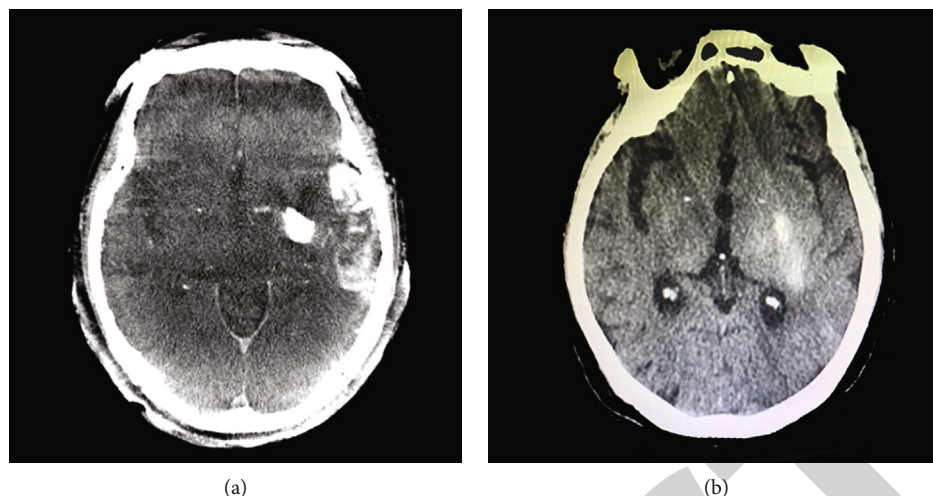


FIGURE 2: Images of post-procedure flat-panel CT (a) and non-contrast CT (b) in one patient. Flat panel CT shows hyperdensity in the left basal ganglia and left temporosphenoid lobe. The  $HU_{max}$  of left basal ganglia is 1405 and the  $HU_{max}$  of left temporosphenoid lobe is 474. Noncontrast CT revealed hemorrhage only in the left basal ganglia.

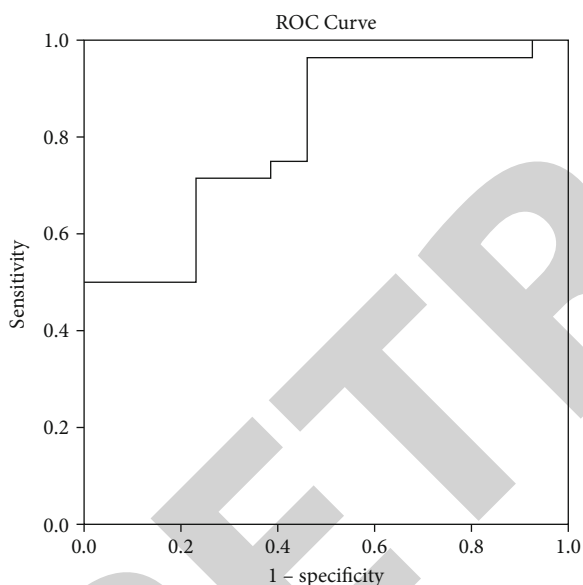


FIGURE 3: Receiver operating characteristic curve for the predictive value of  $HU_{max}$  for hemorrhagic transformation. The  $HU_{max}$  value was a predictor of hemorrhagic transformation with statistical significance (area under curve of 0.805; 95% CI: 0.67-0.94,  $p = 0.02$ ).

(BBB) controls the influx and efflux of biological substances needed for the brain metabolic processes, as well as for neuronal function. In the case of acute ischemic stroke, the damage to the BBB is initiated immediately after arterial occlusion, and the extent of BBB disruption is associated with the type, severity, and duration of ischemic insults. When the BBB disruption is relatively mild, the contrast agent is allowed to extravasate due to the increased permeability; however, with the progression of the ischemic/reperfusion injuries, the rupture of the blood-brain barrier takes place, leading to a massive extravasation of both contrast agent and blood elements [20]. Therefore, it is not difficult to

explain why patients with hyperdense lesions on FP-CT have more chance of HT than those without hyperdense lesions, and the higher the  $HU_{max}$  of the hyperdense lesions, the greater the risk of symptomatic intracranial hemorrhage.

The measurement of  $HU_{max}$  of the hyperdense lesions on FP-CT can be applied to the management of patients receiving endovascular recanalization. A large amount of data suggests that intracranial hemorrhage tends to occur within the first 12–24 hours after treatment [21]. It is proper to delay antiplatelet and anticoagulant drugs when a hyperdense lesion is found on FP-CT until a follow-up NC-CT is performed to rule out hemorrhage. Blood pressure management is another urgent consideration in these patients. Target blood pressure is set according to the recanalization level of the occluded circulation. A systolic blood pressure goal of less than 140 mmHg is recommended for those achieving successful recanalization [22]; however, if hyperdense lesions are presented, neurocritical care, including sedation, analgesia, and strict blood pressure control, is recommended to reduce the risk of HT. When  $HU_{max}$  of the hyperdense lesion breaks a threshold value (600 HU in our study), hemorrhage is almost inevitable, preparation for decompressive craniectomy in advance is strongly suggested when extensive hyperdense lesions are found on FP-CT, considering that the final infarction area can be evaluated on the basis of hyperdense lesions [23].

Recanalization of the responsible cerebral vessels is the primary target after the onset of AIS; however, the big gap between the high recanalization rate and the relatively low functional independence rate implies the revascularization in a large proportion of patients is actually futile or even detrimental. How to select the best candidates for recanalization is still a hot topic at present. As FP-CT has the advantage of providing real-time information on the integrity of the blood-brain barrier, the final decision to restore or not to restore the blood flow could be made by referring to the FP-CT image, especially in a dilemma moment. Takes it for example, after temporary blood flow restoration with the

deployment of a stent retriever, we can perform an FP-CT scan, if extensive hyperdense lesions already exist while stenting and antiplatelet administration are necessary to achieve a successful recanalization. It is sagacious to abandon recanalization, as the risk of symptomatic hemorrhage is very high after reperfusion.

## 5. Limitations

Our study has several limitations. First, our study was performed retrospectively with a small sample size from a single center, which might result in selection bias. In addition, the amount of contrast media and the number of recanalization attempts were reported to be risk factors for HT [24, 25]; in our study, the dose, volume, type of contrast media administered, and number of recanalization attempts were not available in some patients, which made the evaluation limited.

## 6. Conclusions

The presence of hyperdensity on FP-CT can predict HT with a high sensitivity and negative predictive value. The measurement of  $HU_{max}$  of hyperdense lesion on FP-CT can be applied to the management of patients undergoing endovascular recanalization.

## Data Availability

The data used to support the findings of this study are available from the corresponding author upon request.

## Ethical Approval

The study protocol was approved by the local ethics committee of the Shanghai Tenth People's Hospital. All procedures performed in studies involving human participants were in accordance with the ethical standards of the institutional and/or national research committee and with the 1964 Helsinki declaration and its later amendments or comparable ethical standards.

## Consent

Informed consent was obtained from all the patients or their relatives.

## Conflicts of Interest

The authors have no conflicts of interest to declare.

## Authors' Contributions

Liuwei Chen and Yi Xu contributed equally to this work. All authors have approved the manuscript and agree with its submission.

## Acknowledgments

This research was funded by the Outstanding Leaders Training Program of Pudong Health Bureau of Shanghai

(Grant No. PWR12020-03), 2020 Science and Technology Development Fund of Pudong New Area Special Fund for People's Livelihood Scientific Research (PKJ2020-Y-15), and General Project of Shanghai Natural Science Foundation (18ZR14307000).

## References

- [1] A. Rouchaud, M. Mazighi, J. Labreuche et al., "Outcomes of mechanical endovascular therapy for acute ischemic stroke: a clinical registry study and systematic review," *Stroke*, vol. 42, no. 5, pp. 1289–1294, 2011.
- [2] E. S. Sussman and E. S. Connolly, "Hemorrhagic transformation: a review of the rate of hemorrhage in the major clinical trials of acute ischemic stroke," *Frontiers in Neurology*, vol. 4, p. 69, 2013.
- [3] K. A. Hausegger, M. Fürstner, M. Hauser, F. Smetana, and T. Kau, "Klinische Anwendung der Flachdetektor-CT im Angio-OP," *Röfo*, vol. 183, no. 12, pp. 1116–1122, 2011.
- [4] Y. Shinohara, M. Sakamoto, H. Takeuchi et al., "Subarachnoid hyperattenuation on flat panel detector-based conebeam CT immediately after uneventful coil embolization of unruptured intracranial aneurysms," *AJNR. American Journal of Neuroradiology*, vol. 34, no. 3, pp. 577–582, 2013.
- [5] S. Payabvash, M. H. Qureshi, S. M. Khan et al., "Differentiating intraparenchymal hemorrhage from contrast extravasation on post-procedural noncontrast CT scan in acute ischemic stroke patients undergoing endovascular treatment," *Neuroradiology*, vol. 56, no. 9, pp. 737–744, 2014.
- [6] S. Dekeyser, O. Nikoubashman, B. Lutin et al., "Distinction between contrast staining and hemorrhage after endovascular stroke treatment: one CT is not enough," *Journal of NeuroInterventional Surgery*, vol. 9, no. 4, pp. 394–398, 2017.
- [7] N. Wahlgren, N. Ahmed, A. Dávalos et al., "Thrombolysis with alteplase for acute ischaemic stroke in the safe implementation of thrombolysis in stroke-monitoring study (SITS-MOST): an observational study," *Lancet*, vol. 369, no. 9558, pp. 275–282, 2007.
- [8] Y. M. Jang, D. H. Lee, H. S. Kim et al., "The fate of high-density lesions on the non-contrast CT obtained immediately after intra-arterial thrombolysis in ischemic stroke patients," *Korean Journal of Radiology*, vol. 7, no. 4, pp. 221–228, 2006.
- [9] M. Komiyama, Y. Nishijima, A. Nishio, and V. K. Khosla, "Extravasation of contrast medium from the lenticulostriate artery following local intracarotid fibrinolysis," *Surgical Neurology*, vol. 39, no. 4, pp. 315–319, 1993.
- [10] S. Nakano, T. Iseda, H. Kawano, T. Yoneyama, T. Ikeda, and S. Wakisaka, "Parenchymal hyperdensity on computed tomography after intra-arterial reperfusion therapy for acute middle cerebral artery occlusion: incidence and clinical significance," *Stroke*, vol. 32, no. 9, pp. 2042–2048, 2001.
- [11] S. L. Wildenhain, C. A. Jungreis, J. Barr, J. Mathis, L. Wechsler, and J. A. Horton, "CT after intracranial intraarterial thrombolysis for acute stroke," *AJNR. American Journal of Neuroradiology*, vol. 15, no. 3, pp. 487–492, 1994.
- [12] K. Yokogami, S. Nakano, H. Ohta, T. Goya, and S. Wakisaka, "Prediction of hemorrhagic complications after thrombolytic therapy for middle cerebral artery occlusion: value of pre- and post-therapeutic computed tomographic findings and angiographic occlusive site," *Neurosurgery*, vol. 39, no. 6, pp. 1102–1107, 1996.

## Retraction

# Retracted: Protective Effect of Triphala against Oxidative Stress-Induced Neurotoxicity

### BioMed Research International

Received 12 March 2024; Accepted 12 March 2024; Published 20 March 2024

Copyright © 2024 BioMed Research International. This is an open access article distributed under the Creative Commons Attribution License, which permits unrestricted use, distribution, and reproduction in any medium, provided the original work is properly cited.

This article has been retracted by Hindawi following an investigation undertaken by the publisher [1]. This investigation has uncovered evidence of one or more of the following indicators of systematic manipulation of the publication process:

- (1) Discrepancies in scope
- (2) Discrepancies in the description of the research reported
- (3) Discrepancies between the availability of data and the research described
- (4) Inappropriate citations
- (5) Incoherent, meaningless and/or irrelevant content included in the article
- (6) Manipulated or compromised peer review

The presence of these indicators undermines our confidence in the integrity of the article's content and we cannot, therefore, vouch for its reliability. Please note that this notice is intended solely to alert readers that the content of this article is unreliable. We have not investigated whether authors were aware of or involved in the systematic manipulation of the publication process.

Wiley and Hindawi regrets that the usual quality checks did not identify these issues before publication and have since put additional measures in place to safeguard research integrity.

We wish to credit our own Research Integrity and Research Publishing teams and anonymous and named external researchers and research integrity experts for contributing to this investigation.

The corresponding author, as the representative of all authors, has been given the opportunity to register their agreement or disagreement to this retraction. We have kept a record of any response received.

### References

- [1] W. Ning, S. Li, J. Tsering et al., "Protective Effect of Triphala against Oxidative Stress-Induced Neurotoxicity," *BioMed Research International*, vol. 2021, Article ID 6674988, 11 pages, 2021.



## Research Article

# Protective Effect of Triphala against Oxidative Stress-Induced Neurotoxicity

Wanchen Ning <sup>1</sup>, Simin Li <sup>2</sup>, Jokyab Tsering <sup>3</sup>, Yihong Ma <sup>4</sup>, Honghong Li <sup>3</sup>,  
Yuezhu Ma <sup>5</sup>, Anthony Chukwunonso Ogbuehi <sup>6</sup>, Hongying Pan <sup>7</sup>, Hanluo Li <sup>8</sup>,  
Shaonan Hu <sup>9</sup>, Xiangqiong Liu <sup>3</sup>, Yupei Deng <sup>3</sup>, Jianlin Zhang <sup>10</sup> and Xianda Hu <sup>3</sup>

<sup>1</sup>Department of Conservative Dentistry and Periodontology, Ludwig Maximilian University of Munich, Goethestrasse 70, Munich 80336, Germany

<sup>2</sup>Stomatological Hospital, Southern Medical University, Guangzhou 510280, China

<sup>3</sup>Laboratory of Cell and Molecular Biology, Beijing Tibetan Hospital, China Tibetology Research Center, 218 Anwaixiaoguanbeili Street, Chaoyang, Beijing 100029, China

<sup>4</sup>Department of Neurology, Graduate School of Medical Sciences, Kumamoto University, Kumamoto, Japan

<sup>5</sup>Peking University Third Yanqing Hospital, 28 East Shuncheng St., Yanqing District, Beijing 110229, China

<sup>6</sup>Faculty of Physics, University of Münster, Wilhelm-Klemm-Straße 9, Münster 48149, Germany

<sup>7</sup>School of Dentistry, University of Michigan, 1011 N University Ave, Ann Arbor, MI 48109, USA

<sup>8</sup>Department of Craniomaxillofacial Surgery, University Clinic Leipzig, Liebigstr. 12, Leipzig 04103, Germany

<sup>9</sup>Innovation Center Computer Assisted Surgery (ICCAS), Leipzig University, Semmelweisstraße 14, Leipzig 04103, Germany

<sup>10</sup>Department of Neurosurgery, Taian Central Hospital, Taian City, Shandong Province 271000, China

Correspondence should be addressed to Xianda Hu; [hellocean@hotmail.com](mailto:hellocean@hotmail.com)

Received 25 November 2020; Revised 4 March 2021; Accepted 27 March 2021; Published 9 April 2021

Academic Editor: Andrea Scribante

Copyright © 2021 Wanchen Ning et al. This is an open access article distributed under the Creative Commons Attribution License, which permits unrestricted use, distribution, and reproduction in any medium, provided the original work is properly cited.

**Background.** Oxidative stress is implicated in the progression of many neurological diseases, which could be induced by various chemicals, such as hydrogen peroxide (H<sub>2</sub>O<sub>2</sub>) and acrylamide. Triphala is a well-recognized Ayurvedic medicine that possesses different therapeutic properties (e.g., antihistamine, antioxidant, anticancer, anti-inflammatory, antibacterial, and anticariogenic effects). However, little information is available regarding the neuroprotective effect of Triphala on oxidative stress. **Materials and Methods.** An *in vitro* H<sub>2</sub>O<sub>2</sub>-induced SH-SY5Y cell model and an *in vivo* acrylamide-induced zebrafish model were established. Cell viability, apoptosis, and proliferation were examined by MTT assay, ELISA, and flow cytometric analysis, respectively. The molecular mechanism underlying the antioxidant activity of Triphala against H<sub>2</sub>O<sub>2</sub> was investigated dose dependently by Western blotting. The *in vivo* neuroprotective effect of Triphala on acrylamide-induced oxidative injury in *Danio rerio* was determined using immunofluorescence staining. **Results.** The results indicated that Triphala plays a neuroprotective role against H<sub>2</sub>O<sub>2</sub> toxicity in inhibiting cell apoptosis and promoting cell proliferation. Furthermore, Triphala pretreatment suppressed the phosphorylation of the mitogen-activated protein kinase (MARK) signal pathway (p-Erk1/2, p-JNK1/2, and p-p38), whereas it restored the activities of antioxidant enzymes (superoxide dismutase 1 (SOD1) and catalase) in the H<sub>2</sub>O<sub>2</sub>-treated SH-SY5Y cells. Consistently, similar protective effects of Triphala were observed in declining neuroapoptosis and scavenging free radicals in the zebrafish central neural system, possessing a critical neuroprotective property against acrylamide-induced oxidative stress. **Conclusion.** In summary, Triphala is a promising neuroprotective agent against oxidative stress in SH-SY5Y cells and zebrafishes with significant antiapoptosis and antioxidant activities.



## 1. Introduction

Oxidative stress is implicated in the progression of many inflammatory and malignant diseases, including neurodegenerative disease (such as Alzheimer's disease [1], Parkinson's disease [2], mild cognitive impairment [3, 4], and vascular dementia [5]), as well as oral disorders like dental caries, periodontal disease [6, 7], oral mucositis [8], and oral cancer [9]. The severe or prolonged oxidative stress is mainly induced by the excessive production of reactive oxygen species (ROS), which causes DNA damage, oxidative proteins, and peroxidation of lipids and thereby triggers cell apoptosis [10, 11]. ROS is composed of superoxide anion ( $O_2^-$ ), hydrogen peroxide ( $H_2O_2$ ), and hydroxyl radicals ( $OH^\cdot$ ) [12], of which  $H_2O_2$  is a culprit, destroying neurons, and thus is widely used as a stimulant of neutral cells to establish an *in vitro* oxidative injury model [13, 14]. In addition, acrylamide, a vinyl monomer formed in high-temperature foods [15], is applied as a neurotoxin in various cell and animal models for its overproduction of ROS. For instance, acrylamide was suggested to induce cell apoptosis in human neuroblastoma SH-SY5Y cells [16] and promote neurotoxicity in the zebrafish model [17].

Triphala, or 'Bras Bu gSum Thang' in Tibetan, is a well-recognized Ayurvedic medicine consisting of dried fruits of three plant species, including *Emblica officinalis* (family Euphorbiaceae), *Terminalia bellirica* (family Combretaceae), and *Terminalia chebula* (family Combretaceae). Modern studies have shown that Triphala has many properties, including antihistamine, antioxidant, antitumor, anti-inflammatory, antibacterial, antiviral, antifungal, and anticariogenic effects [18, 19]. In addition, Triphala has been investigated to be effective in treating many types of cancers and oral diseases, including prostate cancer [20], pancreatic cancer [21], colon cancer [22], and gynecological cancers [23], as well as periodontal diseases [24]. Regarding Triphala's neuroprotective ability, a research group from Taiwan has revealed the protective effect of *Terminalia chebula* extracts on a neuron-like rat pheochromocytoma (PC12) cell line [25, 26]. Thus, it is of note that Triphala has many possibilities to possess neuroprotective property. However, despite the recent report, current information regarding the neuroprotective effect of Triphala is still limited. Thus, the present study is aimed at investigating Triphala's neuroprotective property against oxidative stress-induced damage *in vitro* and *in vivo*.

## 2. Materials and Methods

**2.1. Cell Culture.** Human neuroblastoma (SH-SY5Y) cells were provided by China Infrastructure of Cell Line Resource. SH-SY5Y cells were cultured in Dulbecco's modified Eagle medium (DMEM) (Corning), supplemented with 10% fetal bovine serum (FBS) (Corning) and 1% penicillin-streptomycin (Beyotime Biotechnology Inc., Nantong, China). The cells were incubated at 37°C under a humidified atmosphere of 5% carbon dioxide.

**2.2. MTT Assay for Cell Viability Analysis.** SH-SY5Y cells were seeded in 96-well plates (CoStar, USA) separately at a density of 4,000 cells per well. Triphala extract power

(AL1675; Dabur India Ltd., Alwar, India) was prepared and diluted in the same way as our previous study [23, 27]. Firstly, to determine the optimal concentrations of Triphala and  $H_2O_2$ , higher concentrations (0.08, 0.4, 2, 10, 50, and 250  $\mu\text{g}/\text{mL}$ ) and lower concentrations (0.014, 0.041, 0.12, 0.37, 1.11, 3.33, and 10  $\mu\text{g}/\text{mL}$ ) of Triphala were applied to treat SH-SY5Y cells for 48 h. Meanwhile, cells were treated with 300, 400, 500, 600, 700, and 800  $\mu\text{mol}/\text{L}$  of hydrogen peroxide ( $H_2O_2$ ) for 20 h, separately. Then, cell viability was measured using 3-[4,5-dimethylthiazol-2-yl]-2,5-diphenyltetrazolium bromide (MTT) assay (Boster Biological Technology Company, Wuhan, Hubei, China). Briefly, each well was incubated with 10  $\mu\text{L}$  of MTT solution for 4 h at 37°C, added with 110  $\mu\text{L}$  formazan solvent, and the absorption at 490 nm was measured using a microplate reader (Beijing Pulang New Technology Co., Beijing, China).

Next, the neuroprotective effect of Triphala on  $H_2O_2$  toxicity was estimated by preincubating cells with increasing concentrations (0.014, 0.041, 0.12, 0.37, 1.11, 3.33, and 10  $\mu\text{g}/\text{mL}$ ) of Triphala for 24 h and then challenging the cells with 400  $\mu\text{mol}/\text{L}$   $H_2O_2$  for an additional 20 h. Cells treated without either  $H_2O_2$  or Triphala were considered as blank control, while the  $H_2O_2$ -induced injury cell model, in which only  $H_2O_2$  was added, was regarded as model control. After the drug intervention, cell viability was determined using the MTT assay as described above and the percentage of cell viability was calculated as follows:  $\text{viability (\%)} = (\text{OD}_{\text{experiment}} - \text{OD}_{\text{blank}}) / (\text{OD}_{\text{model}} - \text{OD}_{\text{blank}}) \times 100\%$ . The percentage of the protective effects was calculated; thus,  $\text{protective effects (\%)} = 1 - \text{viability (\%)}$ .

**2.3. ELISA Assay for Cell Apoptosis Analysis.** The Cell Death Detection Enzyme-Linked Immunosorbent Assay (ELISA) Plus Kit (Roche Diagnostics, Basel, Switzerland) was applied to examine the apoptosis inhibition activity of Triphala as our previous study [23]. Briefly, the cells were seeded and cultured using the same method described above. SH-SY5Y cells in the logarithmic growth phase were seeded in 96-well plates and pretreated with different concentrations (0.37, 1.1, and 3.3  $\mu\text{g}/\text{mL}$ ) of Triphala for 24 h. Then, cells were treated with 400  $\mu\text{mol}/\text{L}$   $H_2O_2$  for an additional 20 h. The setup of the blank control and model control was the same as above. After the drug intervention, the cells were collected and resuspended in lysis buffer and the lysate was centrifuged to remove the intact nuclei. The supernatant containing cytoplasmic histone-associated DNA fragments was transferred into a streptavidin-coated microplate and was then incubated with immunoreagent and substrate for quantitative immunoassay. The OD value was determined at 405 nm using a microplate reader, and the fold increase of DNA fragmentation, reflecting the number of programmed cell deaths, was calculated as  $\text{absorbance of treated cells} / \text{absorbance of negative control cells}$ .

**2.4. Flow Cytometric Analysis.** Flow cytometry assays were processed using monoclonal antibody Ki-67 and Annexin V/propidium iodide (PI) double staining, to evaluate the degree of proliferation apoptosis, as in our previous study [23]. Briefly, SH-SY5Y cells were seeded into 6-well plates

(Nest Biotech., China) at a density of  $1 \times 10^5$  cells per well. After pretreatment with different concentrations (0.37, 1.1, and  $3.3 \mu\text{g/mL}$ ) of Triphala for 24 h, the cells were treated with  $400 \mu\text{mol/L H}_2\text{O}_2$  for an additional 20 h. Then, the cells were harvested by trypsinization, incubated with  $-20^\circ\text{C}$  in absolute ethanol, washed, and resuspended in cell staining buffer. Subsequently, cells were fixed and the nuclear membrane was permeabilized using Foxp3/Transcription Factor Staining Buffer Set (eBioscience Inc., San Diego, CA) before staining with anti-Ki67 antibody (Miltenyi Biotec, Bergisch Gladbach, Germany) at  $4^\circ\text{C}$  for 1 h. To detect the apoptosis, cells were incubated using the FITC Annexin V Apoptosis Detection Kit with PI (Dojindo Molecular Technologies Inc.), at room temperature for 15 min. Afterwards, the fluorescent staining was detected and analyzed using a flow cytometer (BD Biosciences, San Jose, CA). The mean fluorescent intensity for Ki-67 was calculated using FlowJo VX software (Tree Star Inc., Ashland, OR).

**2.5. Western Blot Analysis.** SH-SY5Y cells were seeded in the 10 cm Petri dishes with a density of  $5 \times 10^5$  cells per dish. Firstly, the cells were pretreated with increasing concentrations (0.37, 1.1, and  $3.3 \mu\text{g/mL}$ ) of Triphala for 24 h and stimulated with  $400 \mu\text{mol/L H}_2\text{O}_2$ . The blank control and model control were established as described above. Then, the cultured cells were harvested by centrifugation and fractionated using the Nuclear and Cytoplasmic Protein Extraction Kit (Beyotime Biotechnology Inc., Nantong, China) following the manufacturer's instruction with the supplement of protease inhibitor cocktail and phosphatase inhibitor cocktail, offered by Sigma-Aldrich Corp. (St. Louis, MO). The protein concentrations were determined using the Pierce BCA Protein Assay Kit (Thermo Fisher Scientific, Waltham, MA). The total or nuclear proteins were separated by SDS-PAGE electrophoresis, transferred to a nitrocellulose membrane, and then incubated with monoclonal antibodies, including phospho-p44/42 mitogen-activated protein kinase (MAPK) extracellular signal-related kinase (ERK)1/2. (Thermo Fisher), phospho-c-Jun amino-terminal kinases (JNK)1/2 (Thermo Fisher), and phospho-p38 MAPK, superoxide dismutase 1 (SOD1), and catalase, which were purchased from Cell Signaling Technology (Danvers, USA). Afterwards, rabbit anti-mouse secondary antibody (Abcam, Cambridge, UK) and goat anti-rabbit secondary antibody (Abcam) were attached and expression levels of proteins were detected by chemiluminescence using a Pierce ECL Plus Western Blotting Substrate (Thermo Fisher).

**2.6. Zebrafish Embryos.** The wild-type AB strain of zebrafishes (*Danio rerio*) were obtained from Hunter Biotechnology (Hangzhou, China). The zebrafishes were maintained in the  $28^\circ\text{C}$  reverse osmosis water, incubating with  $200 \text{ mg/L}$  instant sea salt and  $50\text{--}100 \text{ mg/L CaCO}_3$ , at an electrical conductivity of  $450\text{--}550 \mu\text{S/cm}$  and a pH of 6.5–8.5. The embryos used in this study were generated by natural pairwise mating.

**2.7. In Vivo Maximum Tolerated Concentration (MTC) of Triphala.** A total of 270 wild-type AB strain zebrafishes were

randomly selected at 1 day postfertilization (dpf), and 30 zebrafishes per well were plated in 6-well plates (Nest Biotech., China). Acrylamide stock (L2028046; Aladdin, Shanghai, China) was dissolved with DMSO into  $1 \text{ mol/L}$ ,  $30 \mu\text{L}$  of which was then added into 3 mL fish water, reaching the final concentration ( $10 \text{ mmol/L}$ ). Triphala was prepared as described above. Prepared acrylamide was applied to establish a zebrafish neuroapoptosis model. Then, to explore the maximum tolerated concentration (MTC) of Triphala, we treated the acrylamide-stimulated zebrafishes together with different concentrations of 3 mL Triphala (0.123, 0.370, 1.11, 3.33, 10.0, 30.0, and  $90.0 \mu\text{g/mL}$ ) at the same time, for 24 h. The control group was incubated with neither Triphala nor acrylamide, while  $10 \text{ mM}$  acrylamide only stimulated the model group.

**2.8. In Vivo Neuroprotective Effect of Triphala.** A total of 240 wild-type AB strain zebrafishes were randomly selected at 1 dpf, and 30 zebrafishes per well were plated in 6-well plates. Control and model groups were established as described above. Five different concentrations of 3 mL water-soluble Triphala (0.123, 0.370, 1.11, 3.33, and  $10.0 \mu\text{g/mL}$ ) were applied to treat the  $10 \text{ mM}$  acrylamide-induced fishes at the same time. Glutathione (GSH) powder (SLCF2362; Sigma-Aldrich, Shanghai, China) was diluted into  $615 \mu\text{g/mL}$ , and 3 mL GSH was used to stimulate the acrylamide-induced fishes together, regarded as a positive control group to compare the effects of Triphala. Then, the eight groups of fishes were incubated at  $28^\circ\text{C}$  for 24 h. Then, the fishes were stained with acridine orange (AO) (494-38-2, Sigma, China). After that, ten zebrafishes from each group were randomly selected, which were observed and imaged using a fluorescence microscope (VertA1; Shanghai Tucson Vision Technology Co., China). The mean fluorescence intensity was analyzed using NIS-Elements D 3.20 image software. The statistical analysis of the fluorescence intensity was used to evaluate the neuroprotective efficacy of Triphala.

**2.9. In Vivo Antioxidant Effect of Triphala.** A total of 240 wild-type AB strain zebrafishes were randomly selected at 1 dpf, and 30 zebrafishes per well were plated in a 12-well plate (Nest Biotech., China). Control and model groups were established as described above. Five different concentrations of 3 mL water-soluble Triphala (0.123, 0.370, 1.11, 3.33, and  $10.0 \mu\text{g/mL}$ ) and  $615 \mu\text{g/mL}$  GSH were applied to treat the acrylamide-induced fishes together. Meanwhile, 2 mL E3 medium with ROS-specific fluorescent substrate (CM-H2DCFDA) (C6827/2146733; Invitrogen, USA) was added into each well. Subsequently, the fishes and medium were transferred into a 96-well plate (CoStar, USA) and incubated for 20 h at  $28^\circ\text{C}$  (protected from light). Next, the plate was scanned with the multifunctional enzyme marker (Spark; Tecan, Switzerland) and each group's fluorescence was measured. Finally, the fluorescence value of each group was collected and analyzed using SPARKCON TROL Dashboard software. The fluorescence value was used to evaluate the ability of Triphala in scavenging free radicals.

**2.10. Statistical Analysis.** All in vitro data were represented as means  $\pm$  SDs of a minimum of 3 independent experiments.

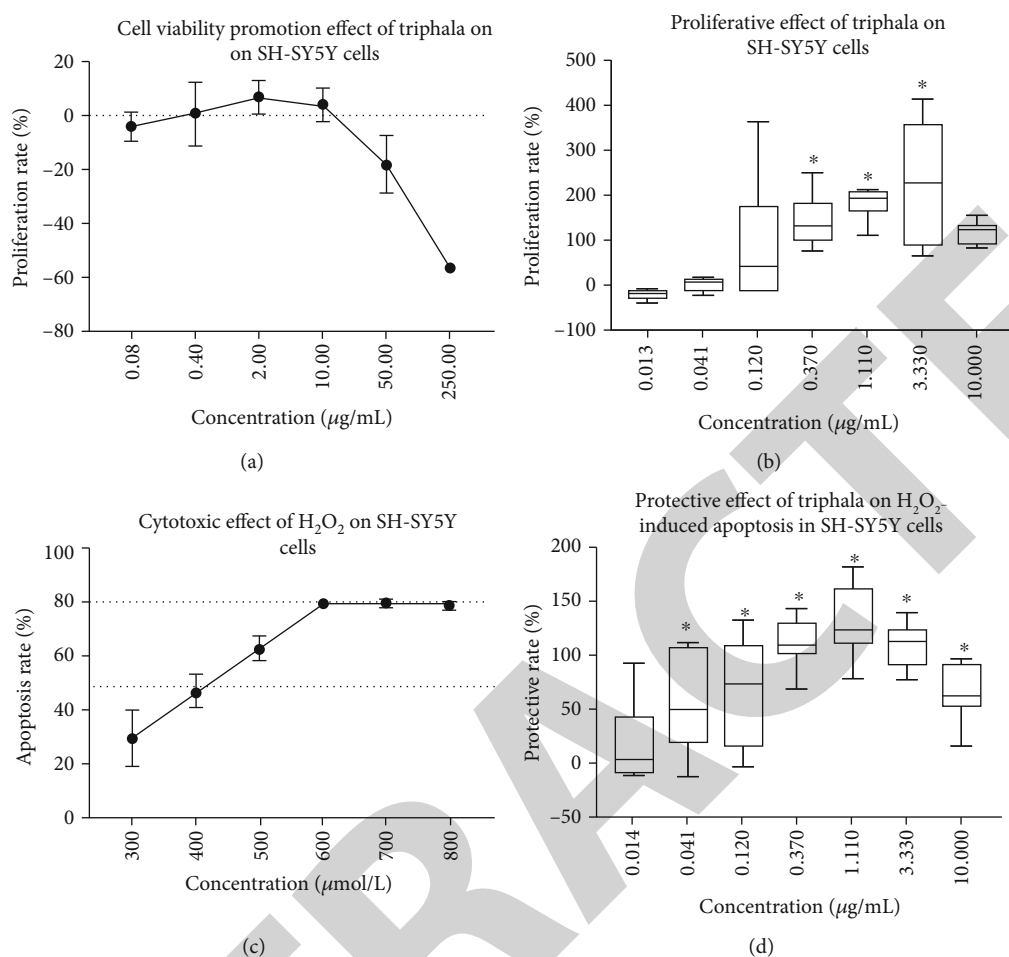


FIGURE 1: Effects of Triphala and hydrogen peroxide ( $\text{H}_2\text{O}_2$ ) on cell viability in SH-SY5Y cells. (a) Cell viability promotion effect of Triphala on SH-SY5Y cells. SH-SY5Y cells were treated with higher concentrations (0.08, 0.4, 2, 10, 50, and 250  $\mu\text{g/mL}$ ) of Triphala for 48 h. (b) Proliferative effect of Triphala on SH-SY5Y cells. SH-SY5Y cells were treated with lower concentrations (0.014, 0.041, 0.12, 0.37, 1.11, 3.33, and 10  $\mu\text{g/mL}$ ) of Triphala for 48 h. (c) Cytotoxic effect of  $\text{H}_2\text{O}_2$  on SH-SY5Y cells. SH-SY5Y cells were treated with different concentrations (300, 400, 500, 600, 700, and 800  $\mu\text{mol/L}$ ) of  $\text{H}_2\text{O}_2$  for 20 h. (d) Protective effect of Triphala on  $\text{H}_2\text{O}_2$ -induced apoptosis in SH-SY5Y cells. SH-SY5Y cells were pretreated with increasing concentrations (0.014, 0.041, 0.12, 0.37, 1.11, 3.33, and 10  $\mu\text{g/mL}$ ) of Triphala for 24 h and then exposed to 400  $\mu\text{mol/L}$  of  $\text{H}_2\text{O}_2$  for 20 h. The data are expressed as mean  $\pm$  SD ( $n = 3$ ). \* $p < 0.05$  as compared to control.

Statistical analyses were carried out by one-way ANOVA, with Bonferroni correction, via SPSS Statistics 26.0 software. A  $p$  value  $< 0.05$  was considered to be statistically significant.

### 3. Results

**3.1. Optimal Concentration of Triphala and Hydrogen Peroxide ( $\text{H}_2\text{O}_2$ ) in SH-SY5Y Cells.** In order to determine the optimal concentration of Triphala applied in the subsequent experiments, the proliferation rate of various concentrations of Triphala was firstly measured using MTT assay. Among the higher concentrations (from 0.08 to 250  $\mu\text{g/mL}$ ) of Triphala, only 50 and 250  $\mu\text{g/mL}$  Triphala significantly decreased cell viability, with the proliferation rates of  $-17.84\%$  and  $-56.38\%$  ( $p < 0.05$ ), compared to blank control (see Figure 1(a)). However, lower concentrations (from 0.014 to 10  $\mu\text{g/mL}$ ) of Triphala promoted cell viability in SH-SY5Y

cells, of which 0.37, 1.11, and 3.33  $\mu\text{g/mL}$  Triphala dramatically enhanced the proliferation rates to 142.55%, 183.12%, and 226.80% ( $p < 0.05$ ) (see Figure 1(b)). By virtue of these results, pretreatment with low concentrations of Triphala (from 0.014 to 10  $\mu\text{g/mL}$ ), especially 0.37, 1.11, and 3.33  $\mu\text{g/mL}$ , was considered as optimal to examine its neuroprotective effect against  $\text{H}_2\text{O}_2$ -induced damage.

Aimed at determining the optimal concentration of  $\text{H}_2\text{O}_2$  to exert neurotoxicity, the apoptosis rate of various concentrations of  $\text{H}_2\text{O}_2$  was measured using an MTT assay. Relative to 300, 400, 500, 600, 700, and 800  $\mu\text{mol/L}$  ( $\mu\text{M}$ ) of the  $\text{H}_2\text{O}_2$  apoptosis rate was upregulated to 30.14%, 47.65%, 63.53%, 80.41%, 80.36%, and 79.78%, respectively (see Figure 1(c)). Based on the above, the half-maximal inhibitory concentration ( $\text{IC}_{50}$ ) of  $\text{H}_2\text{O}_2$  was 400  $\mu\text{mol/L}$ ; thereby, stimulating 400  $\mu\text{mol/L}$   $\text{H}_2\text{O}_2$  for 20 h was considered as optimal and applied in subsequent experiments.



**3.2. Neuroprotective Effect of Triphala on SH-SY5Y Cells.** Aimed at determining Triphala's neuroprotective effect on H<sub>2</sub>O<sub>2</sub>-induced SH-SY5Y cells, cell viability was measured by the MTT assay. In a dose-dependent experiment, increasing concentrations of Triphala were applied to preincubate the SH-SY5Y cells which were then treated with H<sub>2</sub>O<sub>2</sub>. Corresponding to 0.014, 0.041, 0.12, 0.37, 1.11, 3.33, and 10 µg/mL Triphala pretreatment, the calculated protective rates were 17.82%, 54.98%, 61.08%, 109.22%, 125.65%, 108.34%, and 61.96%, respectively (see Figure 1(d)). Except the lowest concentration (0.014 µg/mL), other concentrations of Triphala markedly (0.041, 0.12, 0.37, 1.11, 3.33, and 10 µg/mL) upregulated the protective rates in the H<sub>2</sub>O<sub>2</sub>-induced SH-SY5Y cells ( $p < 0.05$ ), compared to the model control (see Figure 1(d)). Combined, Triphala played a protective role in attenuating the cell viability loss in SH-SY5Y cells treated with H<sub>2</sub>O<sub>2</sub>.

**3.3. Inhibition of Triphala on H<sub>2</sub>O<sub>2</sub>-Induced Apoptosis in SH-SY5Y Cells.** ELISA was used to determine the effect of Triphala on H<sub>2</sub>O<sub>2</sub>-induced apoptosis in SH-SY5Y cells. Compared to the model control, the apoptosis inhibitory rates of H<sub>2</sub>O<sub>2</sub>-induced SH-SY5Y cells were significantly upregulated to 22.53%, 23.66%, and 35.45%, by 0.37, 1.11, and 3.33 µg/mL Triphala, respectively ( $p < 0.05$ ) (see Figure 2(a)). The above results suggested an inhibitory effect of Triphala in suppressing the apoptosis stimulated by H<sub>2</sub>O<sub>2</sub>.

**3.4. Proliferative Effect of Triphala on H<sub>2</sub>O<sub>2</sub>-Induced SH-SY5Y Cells.** The cell proliferation rate was evaluated by flow cytometry analysis using the FITC Annexin V Apoptosis Detection Kit. As shown in Figure 2(b), the results revealed a significant reduction of 20.60% in the proliferation rate in SH-SY5Y cells exposed to H<sub>2</sub>O<sub>2</sub>, compared to the blank control. In contrast, 0.37, 1.11, and 3.33 µg/mL Triphala preincubation increased the proliferation rates by 17.93%, 15.11%, and 22.81%, in the H<sub>2</sub>O<sub>2</sub>-induced SH-SY5Y cells (see Figure 2(b)). The results suggested that H<sub>2</sub>O<sub>2</sub> is an inhibitor, but Triphala is a promoter in the SH-SY5Y cell proliferation.

**3.5. Investigation of Molecular Pathways.** To further determine the neuroprotective mechanisms of Triphala, the expression of p-ERK1/2, p-JNK1/2, p-p38 MAPK, SOD1, and catalase was examined in H<sub>2</sub>O<sub>2</sub>-induced SH-SY5Y cells by Western blotting. Higher levels of p-Erk1/2, p-JNK1/2, and p-p38 and lower levels of SOD1 and catalase were expressed in the model control, relative to blank control (see Figure 2(c)). Furthermore, the degrees of p-Erk1/2 and p-p38 in the H<sub>2</sub>O<sub>2</sub>-induced SH-SY5Y cells were decreased by 0.37 and 1.1 µg/mL Triphala pretreatment (see Figure 2(c)). On the contrary, in comparison with the model control, 3.3 µg/mL Triphala promoted the expression of p-Erk1/2, as well as p-p38 (see Figure 2(c)). As to the p-JNK1/2 content, upregulation of JNK protein was inhibited by Triphala preincubation (0.37, 1.1, and 3.3 µg/mL) in the SH-SY5Y cells exposed to H<sub>2</sub>O<sub>2</sub> and p-JNK1/2 expression was dramatically attenuated to the lowest level, which is similar to that expressed in blank control (see Figure 2(c)).

Significant upregulation of SOD1 was stimulated by 0.37, 1.1, and 3 µg/mL Triphala pretreatment in the H<sub>2</sub>O<sub>2</sub>-induced SH-SY5Y cells, relative to model control (see Figure 2(c)). Moreover, 3 µg/mL increased the SOD1 degree to the highest point that is even higher than blank control (see Figure 2(c)). Similarly, higher protein levels of catalase were stimulated by Triphala preincubation (0.37, 1.1, and 3.3 µg/mL) in SH-SY5Y cells exposed to H<sub>2</sub>O<sub>2</sub>, compared to both model and blank controls (see Figure 2(c)). Combined, the three concentrations (0.37, 1.1, and 3 µg/mL) of Triphala applied in the experiment were efficient in restoring the levels of neuroprotective-related proteins in the SH-SY5Y cells exposed to H<sub>2</sub>O<sub>2</sub>.

**3.6. MTC of Triphala in the Zebrafish Model.** In our study, the MTC of Triphala was determined firstly according to the fish (mammalian) toxicology [28]. The threshold of Triphala should be, on the one hand, high enough to maximize the neuroprotective effect. On the other hand, the preferred concentration would not be too high to induce neurotoxicity [17, 29]. As Table 1 showed, three engagements, 1.11 µM (1/9 MTC), 3.33 µM (1/3 MTC), and 10.0 µM (MTC), were selected as the preferred concentration of Triphala in the following experiment, which promoted better biological phenotypes of the zebrafishes, compared to the model fishes. Otherwise, Triphala of 30.0 and 90.0 µg/mL exerted toxicity and induced worse biological phenotypes of the zebrafishes, leading to a 3.33% (1/30th) mortality of the fishes. Zebrafishes treated with 0.123 and 0.370 µg/mL Triphala performed similarly to the model fishes. Thus, the MTC of Triphala *in vivo* was determined as 10.0 µg/mL.

**3.7. Triphala Suppressed Acrylamide-Induced Neurotoxicity in the Zebrafish Model.** According to the fluorescence intensity, Triphala's *in vivo* neuroprotective effects were observed in the zebrafish model injured by acrylamide. The fluorescence intensity of the control group (4153043 pixels) was significantly lower than that of the model group (10860891 pixels) ( $p < 0.05$ ) (see Figures 3 and 4(a)), indicating that the zebrafish model was successfully established. Also, the fluorescence intensity of the GSH-treated-positive group (4517110 pixels) was significantly lower than that of the model group ( $p < 0.05$ ) (see Figures 3 and 4(a)), suggesting the neuroprotective effects of the GSH on acrylamide. The fluorescence intensity rates of the increasing concentration (0.123, 0.370, 1.11, 3.33, and 10.0 µg/mL) of Triphala were 8611230, 6392234, 4382534, 4313911, and 4155579, respectively. Triphala of 0.123 and 0.370 µg/mL exerted no significant protective effects on zebrafishes exposed to acrylamide ( $p > 0.05$ ) (see Figures 3 and 4(a)). However, decreasing pixels of 1.11, 3.33, and 10.0 µg/mL Triphala were detected, compared to the model group ( $p < 0.05$ ) (see Figures 3 and 4(a)). The findings supported that Triphala, a comparable neuroprotective agent as GSH, inhibited the acrylamide-induced neuroapoptosis in zebrafishes.

**3.8. Triphala Scavenged Free Radicals in the Zebrafish Model Exposed to Acrylamide.** Based on the fluorescence value, the antioxidative effects of Triphala *in vivo* were evaluated in

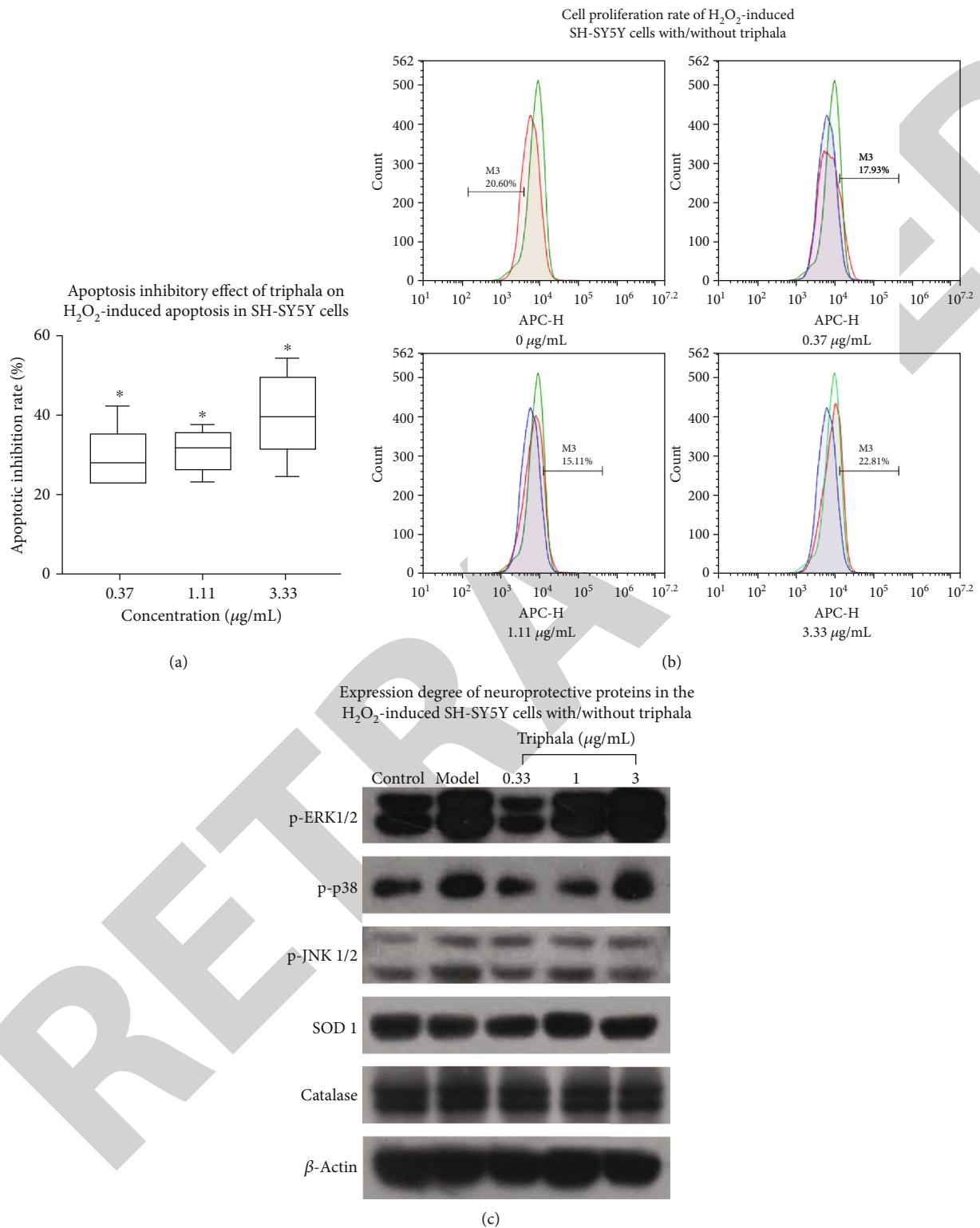


FIGURE 2: Effect of Triphala on hydrogen peroxide (H<sub>2</sub>O<sub>2</sub>)-induced apoptosis in human neuroblastoma SH-SY5Y cells. SH-SY5Y cells were preincubated by 0.37, 1.11, and 3.33 µg/mL Triphala for 24 h and then exposed to 400 µM H<sub>2</sub>O<sub>2</sub> for 20 h. In the control group, cells were not treated with either H<sub>2</sub>O<sub>2</sub> or Triphala. In the model group, only H<sub>2</sub>O<sub>2</sub> was added into cells, without Triphala incubation. (a) ELISA kit was used to determine the apoptosis inhibitory effect of Triphala on H<sub>2</sub>O<sub>2</sub>-induced SH-SY5Y cells. (b) Flow cytometry analysis was applied to evaluate the cell proliferation rate. (c) Western blotting was performed to determine the degrees of the neuroprotective proteins (p-Erk1/2, p-p38, p-JNK1/2, SOD, and catalase) in the H<sub>2</sub>O<sub>2</sub>-induced SH-SY5Y cells with/without Triphala pretreatment. The blots shown are representative of three independent experiments. β-Actin was used as a loading control. Data are expressed as mean ± SD (n = 3). \*p < 0.05 as compared to control.



TABLE 1: MTC exploration of *Triphala in vivo*.

Group ( $n = 30$ )	Triphala concentration ( $\mu\text{g/mL}$ )	Number of deaths (tails)	Mortality (%)	Biological phenotypes
Control	/	0	0.00	Normal
Model	/	0	0.00	Pericardial oedema; slight bending of the bodies
	0.123	0	0.00	Similar to the model
	0.370	0	0.00	Similar to the model
	1.11	0	0.00	Better than the model
Triphala+acrylamide	3.33	0	0.00	Better than the model
	10.0	0	0.00	Better than the model
	30.0	1	3.33	Worse than the model
	90.0	1	3.33	Worse than the model

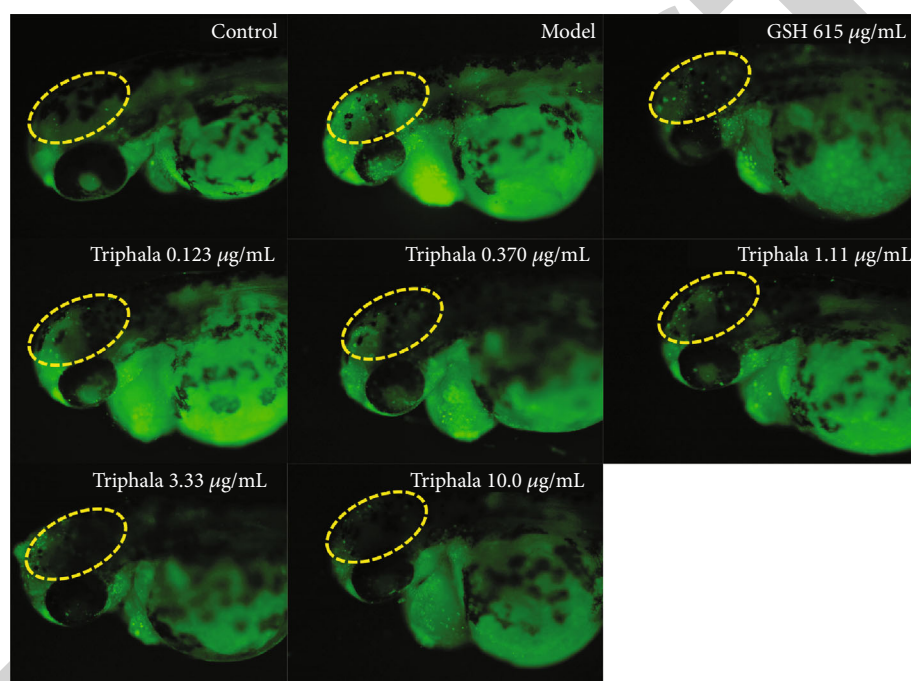


FIGURE 3: Representative photographs of the brain area (central nervous system) of the zebrafish model. The control group was incubated with neither *Triphala* nor acrylamide. The model group was only exposed to 10 mM acrylamide for 24 h. Glutathione (GSH) of 615  $\mu\text{g/mL}$  was applied to treat the acrylamide-induced zebrafishes together for 24 h (positive control group). Increasing concentrations (0.123, 0.370, 1.11, 3.33, and 10.0  $\mu\text{g/mL}$ ) of *Triphala* were applied to treat the acrylamide-induced fishes for 24 h at the same time (experiment group). The *in vivo* neuroapoptosis is stained in green and detected with the fluorescence microscope.

the zebrafish model exposed to acrylamide. The fluorescence value of the control group was 1667, which was significantly lower than that of the model group (2363) ( $p < 0.05$ ) (see Figure 4(b)), supporting the practicability of the zebrafish model. Besides, compared to that of the model group, the reduced fluorescence value of the GSH-treated-positive group (124) was measured ( $p < 0.05$ ) (see Figure 4(b)), indicating that GSH is an efficient antioxidant agent in scavenging the free radicals produced by acrylamide. The fluorescence intensity rates of the increasing concentration (0.123, 0.370, 1.11, 3.33, and 10.0  $\mu\text{g/mL}$ ) of *Triphala* were 858, 816, 716, 746, and 1168, respectively. Except for 10.0  $\mu\text{g/mL}$  *Triphala*, other concentrations of *Triphala* (0.123, 0.370, 1.11, and 3.33  $\mu\text{g/mL}$ ) significantly decreased the level of free

radical, relative to that of the model group ( $p < 0.05$ ) (see Figure 4(b)). The findings suggested *Triphala*'s comparable antioxidant efficiency as GSH in scavenging the free radicals in zebrafish exposed to acrylamide.

#### 4. Discussion

Herewith, we investigated the antioxidant and neuroprotective aspects of *Triphala* using an *in vitro*  $\text{H}_2\text{O}_2$ -induced SH-SY5Y cell model and an *in vivo* acrylamide-induced zebrafish model. Our MTT, ELISA, and flow cytometric results indicated that *Triphala* could attenuate the cytotoxic effects of  $\text{H}_2\text{O}_2$  by promoting cell proliferation and inhibiting cell apoptosis. Moreover, the underlying mechanisms were analyzed

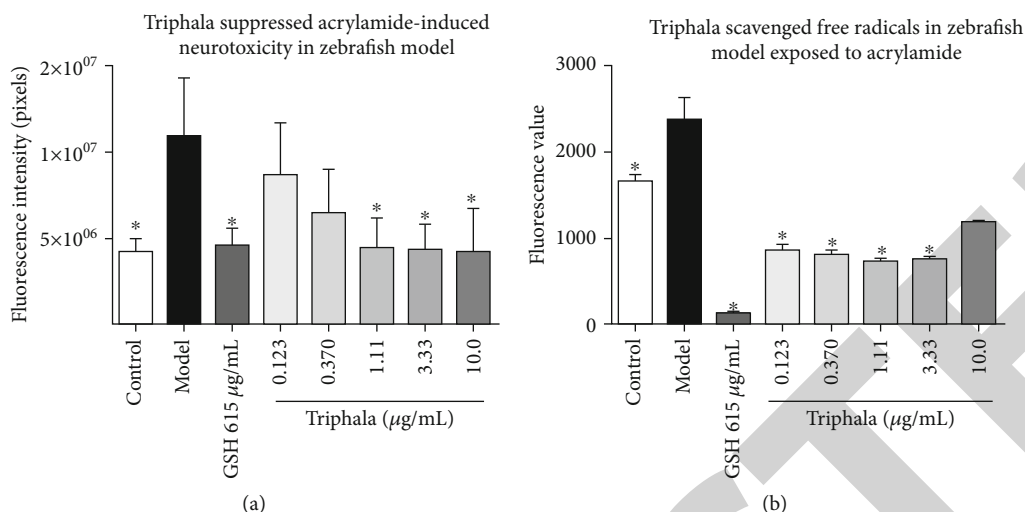


FIGURE 4: Effects of Triphala and acrylamide on zebrafishes *in vivo*. (a) The neuroprotective effects of Triphala *in vivo* were evaluated in the zebrafish model injured by acrylamide, according to the fluorescence intensity. Increasing concentrations (0.123, 0.370, 1.11, 3.33, and 10.0  $\mu\text{g/mL}$ ) of Triphala, as well as 615  $\mu\text{g/mL}$  glutathione (GSH), were applied to treat the acrylamide-induced zebrafishes together for 24 h. (b) The antioxidative effects of Triphala *in vivo* were evaluated in the zebrafish model exposed to acrylamide, according to the fluorescence value. Increasing concentrations (0.123, 0.370, 1.11, 3.33, and 10.0  $\mu\text{g/mL}$ ) of Triphala, as well as 615  $\mu\text{g/mL}$  glutathione (GSH), were applied to treat the acrylamide-induced zebrafishes together for 20 h. Control: zebrafishes incubated with fish water; model: zebrafishes only exposed to acrylamide. The data are expressed as mean  $\pm$  SD ( $n = 3$ ). \* $p < 0.05$  as compared to control.

by Western blotting, demonstrating that pretreatment of Triphala upregulated antioxidant enzymes (SOD1 and catalase) and suppressed MAPK (p-Erk1/2, p-JNK1/2, and p-p38) activation, which in turn exerted its neuroprotective effects on inhibiting cellular apoptosis against oxidative damage. Consistently, *in vivo* immunofluorescence staining evidenced the neuroprotective role of Triphala against the neurotoxicity induced by acrylamide in zebrafishes.

The cell viability level and proliferation rate are recognized as good indicators of cell health [30]. In our study,  $\text{H}_2\text{O}_2$  exposure induced apoptosis of SH-SY5Y cells by decreasing cell viability and inhibiting cell proliferation, consistent with previous reports [14, 31]. Possessing antioxidant properties, our previous study suggested the antitumor effect of Triphala on inhibiting the proliferation and increasing the apoptosis in many cancer cell lines [23]. In contrast, one fruit of Triphala (*Terminalia chebula* extract) was investigated by another two studies, suggesting its neuroprotective effects on enhancing cell viability in  $\text{H}_2\text{O}_2$ -treated PC12 cells [25, 26]. Our experiment first evaluated Triphala's neuroprotective effect on  $\text{H}_2\text{O}_2$ -induced SH-SY5Y cells to the best of our knowledge. Triphala dose-dependently increased the proliferative and protective rates of SH-SY5Y cells exposed to  $\text{H}_2\text{O}_2$ , while Triphala markedly attenuated the  $\text{H}_2\text{O}_2$ -induced increase in apoptosis. Consistently, Triphala's protective activity is similar to the neuroprotective peptide Orexin-A in increased proliferation in SH-SY5Y cells induced by  $\text{H}_2\text{O}_2$  [14]. In general, the findings overall indicated that Triphala plays a neuroprotective role in alleviating the  $\text{H}_2\text{O}_2$ -induced neurotoxicity.

Notably, based on immunofluorescence staining results, Triphala was evidenced as a comparable neuroprotective potent as GSH, decreasing the acrylamide-induced toxicity

in the central neural system of zebrafish. In line with the previous reports, our study confirmed that acrylamide could contribute to neuroapoptosis [32] and promote the free radicals in zebrafishes. GSH is determined as a known antioxidant that plays an essential role in balancing the oxidative stress in brain cells [32]. Besides, reduced GSH has been implicated in many neurological diseases, such as Parkinson's disease [33], Alzheimer's disease [34], epilepsy [35], and Huntington's disease [36]. In consistent with these reports, GSH application in the current study inhibited the neuroapoptosis and production of free radicals in zebrafish exposed to acrylamide. Similarly, Triphala possessed equivalent neuroprotective and antioxidant effects as GSH. Our findings first demonstrated that Triphala (especially 1.11 and 3.33  $\mu\text{g/mL}$ ) could decline neuroinjury and scavenge the free radicals in the zebrafish central neural system, exerting a critical neuroprotective property against acrylamide-induced oxidative stress.

Additionally, Triphala's underlying antioxidant mechanisms were also determined in a dose-dependent experiment by Western blotting through measuring neuroprotective-related proteins' expressions. Two major cellular antioxidant enzymes, SOD1 and catalase, can scavenge the ROS products to control the antioxidant system [37]. Recent studies reported that Triphala effectively attenuated oxidative stress via SOD1/catalase restoration both *in vitro* and *in vivo* [38]. For instance, Triphala extracts were able to quench free radicals by inducing SOD and catalase against bacteria [39]. Meanwhile, Triphala could increase the SOD and catalase expressions in the selenite-induced cataract model [40]. Furthermore, due to its antioxidant potential, Triphala restored the levels of SOD and CAT in a rat model of colitis [41] and arthritis [42]. In line with the above evidence, our finding

revealed that H<sub>2</sub>O<sub>2</sub> exposure decreased expressions of SOD and catalase in SH-SY5Y cells, whereas the reductions were enhanced by Triphala (0.37, 1.1, and 3 µg/mL) pretreatment. Moreover, higher concentrations of Triphala tend to be more efficient as it promoted the expression to a level even higher than the blank control. The restoring activities of SOD and catalase in the H<sub>2</sub>O<sub>2</sub> injury model indicated the neuroprotective role of Triphala in antioxidant processes via activating the SOD1/catalase clearance pathway.

Furthermore, ERKs, p38 MAPKs (p38), and JNKs the three well-known MAPK signal pathways, were investigated in the Triphala-induced antioxidant activities [43]. Recognized as the essential mediators, MAPK signaling pathways underlining the neural diseases are attracting more and more attention. Several studies have validated oxidative stress results in neural damage via MAPK signal cascades [43, 44]. For example, a significant increase in the phosphorylation of ERK1/2, JNK1/2, and p38 MAPK protein was detected in the ischemic penumbra rat model with middle cerebral artery occlusion and reperfusion [45]. Consistent with the previous findings, the present study has proven that H<sub>2</sub>O<sub>2</sub> promoted apoptosis through upregulating the phosphorylation of p-Erk1/2, p-JNK1/2, and p-p38 in SH-SY5Y cells. More importantly, our finding firstly demonstrated that Triphala attenuated the levels of p-Erk1/2, p-JNK1/2, and p-p38 in the H<sub>2</sub>O<sub>2</sub>-induced SH-SY5Y cells, indicating its antioxidant and neuroprotective properties against oxidative stress. Interestingly, in a dose-dependent experiment, unlike the fact that 0.37 and 1.1 µg/mL Triphala significantly suppressed the activation of p-Erk1/2, p-JNK1/2, and p-p38, 3 µg/mL Triphala downregulated the p-JNK1/2 level. In contrast, it upregulated the contents of p-Erk1/2 and p-p38. As mentioned, it is worth noting that Triphala is meanwhile proposed to be prooxidant in promoting the apoptosis of cancer cells by releasing ROS productions [38]. Oral administration of 50/100 mg/kg Triphala significantly induced apoptosis in Capan-2 cancer cells through ROS generation, associated with increased expression of p53 and ERK [21]. In the normal cells, ROS usually is low; however, the level rises in the cancer cells, which crosses the threshold and forces the cell into apoptosis [46]. Considering that SH-SY5Y cell is a human neuroblastoma cell line, Triphala's prooxidant activity in our experiment is a possibility, being supported by our investigation indicating that 50 and 250 µg/mL Triphala suppressed cell proliferation.

However, some limitations still existed in this study. First, the major focus is put on the antioxidant activities of Triphala, whereas, as mentioned above, the application of high or low concentrations of Triphala is likely to exert opposite effects on the proliferation rate of cancer cells, accounting for its prooxidant ability in combating tumors. These observations led to the hypothesis that the pleiotropic functions of Triphala on regulating oxidative stress may depend on various conditions. Furthermore, as a multi-ingredient formulation, Triphala consists of three fruit herbal medicines and hundreds of components, the majority of which are polyphenols and their bioactive metabolites, such as gallic acid, quinic acid, teresautalic acid, chebulinic acid, corilagin, salicin, ethyl gallate, and methyl gallate [47–50]. Therefore, one

point of further study should explore pharmacological mechanisms of the critical compounds with various concentrations in regulating antioxidant activities using different cell models. Second, few reports on the neuroprotective effects of Triphala are cognitive and only major antioxidant genes and vital signaling pathways were investigated in this study. Thus, the identification of the compound-target gene network is of great importance. Bioinformatics analysis, such as gene ontology enrichment analysis, functional pathways analysis, and target protein/miRNA interaction analysis, could facilitate a better understanding of the possible ingredients, targets, and mechanisms. Third, up to now, although a few clinical trials on Triphala have been done, such as gingivitis (NCT01898000) and periodontal disease (NCT01900535), most of the studies are done in animals and *in vitro* models; thus, more *in vivo* and clinical studies are needed in multiple conditions prior to its applicability.

It is important to note that this present research's findings also have a transfer value for future clinical use. Recently, there is an upsurge in the areas related to applying Triphala as an alternative therapy in various diseases due to its gifted therapeutic activity and minimal or no side effects. Neutralizing oxidative stress is core in the treatment of both neurodegenerative diseases and oral disorders. By that, Triphala's antioxidant and protective effects revealed in this study will also be pertinent to examine how Triphala plays a vital role in dentistry. For instance, Triphala was identified as an antibacterial and anti-inflammatory agent in treating periodontal diseases, with comparable chlorhexidine efficacy but without any detected side effect [24]. Moreover, Triphala could be applied as a root canal irrigant in treating primary endodontic infections, considering the high toxicity of the efficient irrigant (sodium hypochlorite). In addition, possessing the inhibitory activity against PMN-type collagenase, Triphala could be an alternative medicine of doxycycline in healing periodontal destruction, without side effects. Furthermore, other potential applications of Triphala in the oral cavity are noteworthy, such as wound healing of oral mucosa and regeneration in hard and soft tissues. Nevertheless, the detailed molecule mechanisms under these benefits of Triphala also necessitate investigations in the context of dentistry in well-designed preclinical studies.

## 5. Conclusion

In summary, the current *in vitro* study firstly indicated the neuroprotective effect of Triphala on attenuating H<sub>2</sub>O<sub>2</sub>-induced apoptosis in SH-SY5Y cells via restoration of the antioxidant enzymes (SOD1 and catalase) and suppression of the MAPK (p-Erk1/2, p-JNK1/2, and p-p38) activation. Furthermore, Triphala was evidenced as a comparable neuroprotective potent as GSH *in vivo*, which declined neuroapoptosis and scavenged free radicals in the zebrafish central neural system, possessing a critical neuroprotective property against acrylamide-induced oxidative stress. Consequently, Triphala might be a potential therapeutic agent to treat neurodegenerative diseases associated with oxidative stress.



## Data Availability

The data used to support the findings of this study are available from the corresponding author upon request.

## Conflicts of Interest

The authors declare that they have no conflicts of interest.

## Authors' Contributions

Wanchen Ning (wanchenning0627@gmail.com) and Simin Li (simin.li.dentist@gmail.com) are equally the co-first authors. Prof. Dr. Xianda Hu is the senior author of this research work. Dr. Jianlin Zhang (zhangjl2979@sina.com) and Prof. Dr. Xianda Hu (hellocean@hotmail.com) are equally the corresponding authors.

## Acknowledgments

This work was funded by the National Natural Science Foundation of China (Grant no. 81801635), which was provided to support the research work supervised by Prof. Min Wang at the Chinese Academy of Medical Sciences & Peking Union Medical College (CAMS & PUMC).

## References

- [1] A. M. Swomley and D. A. Butterfield, "Oxidative stress in Alzheimer disease and mild cognitive impairment: evidence from human data provided by redox proteomics," *Archives of Toxicology*, vol. 89, no. 10, pp. 1669–1680, 2015.
- [2] E. Deas, N. Cremades, P. R. Angelova et al., "Alpha-synuclein oligomers interact with metal ions to induce oxidative stress and neuronal death in Parkinson's disease," *Antioxidants & Redox Signaling*, vol. 24, no. 7, pp. 376–391, 2016.
- [3] S. I. Mota, R. O. Costa, I. L. Ferreira et al., "Oxidative stress involving changes in Nrf2 and ER stress in early stages of Alzheimer's disease," *Biochimica et Biophysica Acta (BBA) - Molecular Basis of Disease*, vol. 1852, no. 7, pp. 1428–1441, 2015.
- [4] Y. Xu, Q. Wang, Z. Wu et al., "The effect of lithium chloride on the attenuation of cognitive impairment in experimental hypoglycemic rats," *Brain Research Bulletin*, vol. 149, pp. 168–174, 2019.
- [5] Q. Wang, W. Yang, J. Zhang, Y. Zhao, and Y. Xu, "TREM2 overexpression attenuates cognitive deficits in experimental models of vascular dementia," *Neural Plasticity*, vol. 2020, 10 pages, 2020.
- [6] J. Kumar, S. L. Teoh, S. Das, and P. Mahaknaukrah, "Oxidative stress in oral diseases: understanding its relation with other systemic diseases," *Frontiers in Physiology*, vol. 8, p. 693, 2017.
- [7] Y. Wang, O. Andrukhov, and X. Rausch-Fan, "Oxidative stress and antioxidant system in periodontitis," *Frontiers in Physiology*, vol. 8, p. 910, 2017.
- [8] N. Sardaro, F. Della Vella, M. A. Incalza, D. Di Stasio, and A. Lucchese, "Oxidative stress and oral mucosal diseases: an overview," *In Vivo*, vol. 33, no. 2, pp. 289–296, 2019.
- [9] B.-J. Lee, M.-Y. Chan, H.-Y. Hsiao, C.-H. Chang, L.-P. Hsu, and P.-T. Lin, "Relationship of oxidative stress, inflammation, and the risk of metabolic syndrome in patients with oral cancer," *Oxidative Medicine and Cellular Longevity*, vol. 2018, 7 pages, 2018.
- [10] B. Uttara, A. Singh, P. Zamboni, and R. Mahajan, "Oxidative stress and neurodegenerative diseases: a review of upstream and downstream antioxidant therapeutic options," *Current Neuropharmacology*, vol. 7, no. 1, pp. 65–74, 2009.
- [11] Y. Xu, Q. Wang, D. Li et al., "Protective effect of lithium chloride against hypoglycemia-induced apoptosis in neuronal PC12 cell," *Neuroscience*, vol. 330, pp. 100–108, 2016.
- [12] G. Aliev, M. A. Smith, D. Seyidova et al., "The role of oxidative stress in the pathophysiology of cerebrovascular lesions in Alzheimer's disease," *Brain Pathology*, vol. 12, no. 1, pp. 21–35, 2002.
- [13] J.-F. Pei, X.-K. Li, W.-Q. Li et al., "Diurnal oscillations of endogenous H<sub>2</sub>O<sub>2</sub> sustained by p66<sup>Shc</sup> regulate circadian clocks," *Nature Cell Biology*, vol. 21, no. 12, pp. 1553–1564, 2019.
- [14] C.-M. Wang, C.-Q. Yang, B.-H. Cheng, J. Chen, and B. Bai, "Orexin-A protects SH-SY5Y cells against H<sub>2</sub>O<sub>2</sub>-induced oxidative damage via the PI3K/MEK1/2/ERK1/2 signaling pathway," *International Journal of Immunopathology and Pharmacology*, vol. 32, 2018.
- [15] Y. Li, A. Zhou, X. Cui, Y. Zhang, and J. Xie, "6'-p-Coumaroylspinosin protects PC12 neuronal cells from acrylamide-induced oxidative stress and apoptosis," *Journal of Food Biochemistry*, vol. 44, no. 9, article e13321, 2020.
- [16] T. Sumizawa and H. Igisu, "Apoptosis induced by acrylamide in SH-SY5Y cells," *Archives of Toxicology*, vol. 81, no. 4, pp. 279–282, 2007.
- [17] M. Faria, T. Ziv, C. Gómez-Canela et al., "Acrylamide acute neurotoxicity in adult zebrafish," *Scientific Reports*, vol. 8, no. 1, p. 7918, 2018.
- [18] C. T. Peterson, K. Denniston, and D. Chopra, "Therapeutic uses of Triphala in Ayurvedic medicine," *The Journal of Alternative and Complementary Medicine*, vol. 23, no. 8, pp. 607–614, 2017.
- [19] M. S. Baliga, S. Meera, B. Mathai, M. P. Rai, V. Pawar, and P. L. Palatty, "Scientific validation of the ethnomedicinal properties of the Ayurvedic drug Triphala: a review," *Chinese Journal of Integrative Medicine*, vol. 18, no. 12, pp. 946–954, 2012.
- [20] L. H. Russell, E. Mazzi, R. B. Badisa et al., "Differential cytotoxicity of Triphala and its phenolic constituent gallic acid on human prostate cancer LNCap and normal cells," *Anticancer Research*, vol. 31, no. 11, pp. 3739–3745, 2011.
- [21] Y. Shi, R. P. Sahu, and S. K. Srivastava, "Triphala inhibits both in vitro and in vivo xenograft growth of pancreatic tumor cells by inducing apoptosis," *BMC Cancer*, vol. 8, no. 1, p. 294, 2008.
- [22] R. Vadde, S. Radhakrishnan, L. Reddivari, and J. K. P. Vanamala, "Triphala extract suppresses proliferation and induces apoptosis in human colon cancer stem cells via suppressing c-Myc/cyclin D1 and elevation of Bax/Bcl-2 ratio," *BioMed Research International*, vol. 2015, Article ID 649263, 12 pages, 2015.
- [23] Y. Zhao, M. Wang, J. Tsering et al., "An integrated study on the antitumor effect and mechanism of Triphala against gynecological cancers based on network pharmacological prediction and in vitro experimental validation," *Integrative Cancer Therapies*, vol. 17, no. 3, pp. 894–901, 2018.
- [24] S. Prakash and A. U. Shelke, "Role of Triphala in dentistry," *Journal of Indian Society of Periodontology*, vol. 18, no. 2, pp. 132–135, 2014.

## Research Article

# Shared Molecular Mechanisms between Alzheimer's Disease and Periodontitis Revealed by Transcriptomic Analysis

Jieqi Jin <sup>1</sup>, Mengkai Guang <sup>2</sup>, Anthony Chukwunonso Ogbuehi <sup>3</sup>, Simin Li <sup>4</sup>, Kai Zhang <sup>2</sup>, Yihong Ma <sup>5</sup>, Aneesha Acharya <sup>6</sup>, Bihan Guo <sup>7</sup>, Zongwu Peng <sup>7</sup>, Xiangqiong Liu <sup>8</sup>, Yupei Deng <sup>8</sup>, Zhaobi Fang <sup>9</sup>, Xiongjie Zhu <sup>9</sup>, Shiting Hua <sup>9</sup>, Cong Li <sup>9</sup>, Rainer Haak <sup>4</sup>, Dirk Ziebolz <sup>4</sup>, Gerhard Schmalz <sup>4</sup>, Lei Liu <sup>10</sup>, Baohua Xu <sup>2</sup> and Xiaofeng Huang <sup>1</sup>

<sup>1</sup>Department of Stomatology, Beijing Friendship Hospital, Capital Medical University, Beijing 100050, China

<sup>2</sup>Department of Stomatology, China-Japan Friendship Hospital, Beijing 100029, China

<sup>3</sup>Department of Physics, University of Münster, Wilhelm-Klemm-Str. 9, 48149 Münster, Germany

<sup>4</sup>Department of Cariology, Endodontology and Periodontology, University Leipzig, Liebigstr. 12, Leipzig 04103, Germany

<sup>5</sup>Department of Neurology, Graduate School of Medical Sciences, Faculty of Life Sciences, Kumamoto University, Kumamoto, Japan

<sup>6</sup>Dr. D Y Patil Dental College and Hospital, Dr D Y Patil Vidyapeeth, Pimpri, Pune, India

<sup>7</sup>Faculty of Electrical Engineering, Information Technology, and Physics, University Braunschweig, Hans-Sommer-Str. 66, Braunschweig 38106, Germany

<sup>8</sup>Laboratory of Molecular Cell Biology, Beijing Tibetan Hospital, China Tibetology Research Center, 218 Anwaixiaoguanbeili Street, Chaoyang, Beijing 100029, China

<sup>9</sup>Zhujiang Hospital, Southern Medical University, Guangzhou 510282, China

<sup>10</sup>Department of Neurology, Shandong Provincial Third Hospital, Cheeloo College of Medicine, Shandong University, Jinan, 10091 Shandong Province, China

Correspondence should be addressed to Baohua Xu; [zrkqxbh@163.com](mailto:zrkqxbh@163.com)

Received 18 December 2020; Revised 20 February 2021; Accepted 9 March 2021; Published 1 April 2021

Academic Editor: Juan Yang

Copyright © 2021 Jieqi Jin et al. This is an open access article distributed under the Creative Commons Attribution License, which permits unrestricted use, distribution, and reproduction in any medium, provided the original work is properly cited.

**Objective.** To investigate the genetic crosstalk mechanisms that link periodontitis and Alzheimer's disease (AD). **Background.** Periodontitis, a common oral infectious disease, is associated with Alzheimer's disease (AD) and considered a putative contributory factor to its progression. However, a comprehensive investigation of potential shared genetic mechanisms between these diseases has not yet been reported. **Methods.** Gene expression datasets related to periodontitis were downloaded from the Gene Expression Omnibus (GEO) database, and differential expression analysis was performed to identify differentially expressed genes (DEGs). Genes associated with AD were downloaded from the DisGeNET database. Overlapping genes among the DEGs in periodontitis and the AD-related genes were defined as crosstalk genes between periodontitis and AD. The Boruta algorithm was applied to perform feature selection from these crosstalk genes, and representative crosstalk genes were thus obtained. In addition, a support vector machine (SVM) model was constructed by using the scikit-learn algorithm in Python. Next, the crosstalk gene-TF network and crosstalk gene-DEP (differentially expressed pathway) network were each constructed. As a final step, shared genes among the crosstalk genes and periodontitis-related genes in DisGeNET were identified and denoted as the core crosstalk genes. **Results.** Four datasets (GSE23586, GSE16134, GSE10334, and GSE79705) pertaining to periodontitis were included in the analysis. A total of 48 representative crosstalk genes were identified by using the Boruta algorithm. Three TFs (FOS, MEF2C, and USF2) and several pathways (i.e., JAK-STAT, MAPK, NF-kappa B, and natural killer cell-mediated cytotoxicity) were identified as regulators of these crosstalk genes. Among these 48 crosstalk genes and the chronic periodontitis-related genes in DisGeNET, C4A, C4B, CXCL12, FCGR3A, IL1B, and MMP3 were shared and identified as the most pivotal candidate links between periodontitis and AD. **Conclusions.** Exploration of available transcriptomic datasets revealed C4A, C4B, CXCL12, FCGR3A, IL1B, and MMP3 as the top candidate molecular linkage genes between periodontitis and AD.



## 1. Introduction

An association between periodontitis and Alzheimer's disease (AD) has been demonstrated, and periodontitis reportedly confers risk for the incidence and progression of Alzheimer's disease (AD) [1, 2]. Alzheimer's disease is a neurodegenerative disease characterized by the formation of amyloid- $\beta$  peptide (A $\beta$ P) plaques and intraneuronal neurofibrillary tangles (NFTs), which drives neuroinflammation in the brain [3]. Periodontitis, a chronic, immunoinflammatory disease affecting supporting structures of teeth, is multifactorial in nature, driven by polymicrobial dysbiosis and unfavorable shifts in the plaque biofilm composition, which disrupts the host-microbial homeostasis [4, 5]. Inflammation is considered the key connecting link between both these diseases [6]. Two purported mechanistic links have been highlighted. First, proinflammatory mediators including specific cytokines or chemokines in the periodontal milieu that enter systemic circulation impose a systemic inflammatory burden, propagating inflammatory responses by microglial cells in the brain [6]. Second, periodontal pathogens may directly enter the brain via blood circulation or peripheral nerves, as evidenced by the discovery of the keystone periodontal pathogen *Porphyromonas gingivalis* (Pg) in AD patients' brains [7, 8].

At the same time, genetic susceptibility and gene dysregulation have been identified in the context of both AD and periodontitis. In AD, frequently reported dysregulated genes include amyloid-beta precursor protein (APP), presenilin 1 (PSEN1), and presenilin 2 (PSEN2), apolipoproteins, and lipid homeostasis, genes involved in endocytosis, and membrane-spanning 4 (MS4) family [9]. In periodontitis, aberrant genes highlighted include interleukin-1, interleukin-6, interleukin-10, transforming growth factor-beta (TGF- $\beta$ ), tumor necrosis factor- $\alpha$  (TNF- $\alpha$ ), interferon-gamma (IFN- $\gamma$ ), and matrix metalloproteinases (MMPs) among others [10]. It is plausible that gene dysregulation in periodontitis could contribute to its association with AD, and crosstalk genes may biologically link AD and periodontitis serving as either shared susceptibility factors or molecular links.

Here, we designed a bioinformatic study of existing experimental datasets to understand putative molecular links between periodontitis and Alzheimer's disease by identifying crosstalk genes, transcription factors, and signaling pathways involved in both disorders. The molecular mechanisms identified through this approach could suggest potential therapeutic targets particularly relevant to drug development and personalized medicine approaches.

## 2. Materials and Methods

**2.1. Study Design.** Figure 1 depicts a flowchart outlining the study workflow. DEGs dysregulated in periodontitis- and AD-related genes were obtained from the GEO database and DisGeNET database, respectively. Crosstalk genes linking periodontitis and AD were identified as the AD-related genes that overlapped with significantly up- or downregulated DEGs in periodontitis. Thereafter, feature selection

from the crosstalk genes was performed using a conventional recursive feature elimination (RFE) algorithm and the Boruta algorithm. The crosstalk genes obtained by feature selection were used to construct two networks to identify the transcription factors and the differentially expressed pathways that target these crosstalk genes. In the next step, "core" crosstalk genes were identified as the crosstalk genes obtained by feature selection that were overlapping with chronic periodontitis-related genes in the DisGeNET database.

**2.2. Procurement of Periodontitis-Related Datasets.** Sample-matched whole-genome gene expression datasets from periodontitis were sourced and downloaded from the NCBI Gene Expression Omnibus (GEO). The eligibility criteria for these datasets were as follows: datasets that included established periodontitis samples as the experimental group and healthy gingival samples as the control group, where periodontitis was defined based in accordance with the case definition presented in the 2017 World Workshop: (1) interdental CAL detectable at  $\geq 2$  nonadjacent teeth or (2) buccal or oral CAL  $\geq 3$  mm with pocketing  $>3$  mm detectable at  $\geq 2$  teeth [11].

**2.3. Differential Gene Expression Analysis.** Differential gene expression analysis of periodontitis-related datasets was carried out using the Linear Models for Microarray (limma) package [12] in the R project (version 3.0.1, <http://www.r-project.org/>) [13]. Three such datasets, GSE23586, GSE16134, and GSE10334, were sourced and analyzed. Genes with  $p$  value  $< 0.05$  and  $|\log_{2}FC$  (fold change)  $|\geq 1$  were regarded as significant differentially expressed genes (DEGs). For another dataset, GSE79705, the screening range of DEGs was broadened by extending the thresholds and settings to  $p$  value  $< 0.05$  and  $|\log_{2}FC| > 0$  as DEGs.

Next, a Venn diagram (<http://bioinformatics.psb.ugent.be/webtools/Venn/>) was drawn to identify shared genes within the DEGs identified from the four datasets. The common up/downregulated DEGs in four datasets were used for the following analyses, and DEGs that were not common to all the datasets were excluded.

**2.4. Functional Enrichment Analysis.** Functional enrichment analysis of up/downregulated periodontitis-related DEGs was performed with DAVID (Database for Annotation, Visualization and Integrated Discovery, v6.8) [14, 15].  $p < 0.05$  was set as the threshold. GO (Gene Ontology) and pathway enrichment analysis of the identified DEGs was performed [16, 17].

**2.5. Construction of the Protein-Protein Interaction Network of Periodontitis-Related DEGs.** 280,826 PPI (protein-protein interaction) pairs including 19,610 genes were downloaded from HPRD (Human Protein Reference Database) [18], BioGRID (Biological General Repository for Interaction Datasets) [19], DIP (Database of Interacting Proteins) [20], MINT (Molecular INTeraction database) [21], PINA (Protein Interaction Network Analysis) [22], InnateDB (a knowledge resource for innate immunity interactions and pathways) [23], and INstruct (3D protein interactome networks with structural resolution) [24]. The Cytoscape

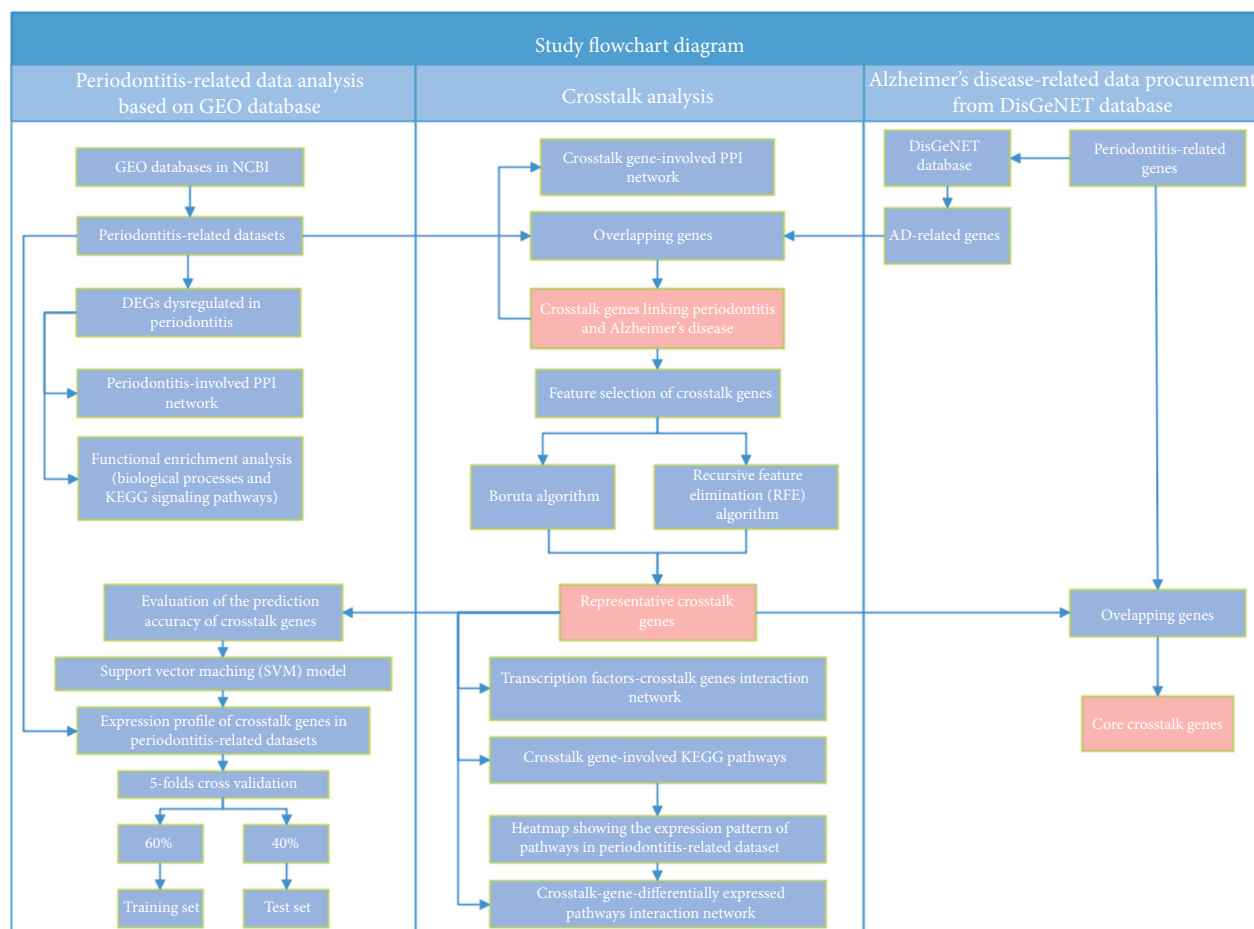


FIGURE 1: Flowchart depicting study workflow.

platform was used to visualize the network derived from PPI pairs of DEGs and conduct a topological analysis [25].

**2.6. Identification of Crosstalk Genes and Construction of the Crosstalk Gene-Related PPI Network.** AD-related genes were downloaded from the DisGeNET database [26]. The AD-related genes that overlapped with the up- and downregulated periodontitis-related DEGs were identified. These overlapping genes were regarded as “crosstalk” genes linking AD and periodontitis and further used for constructing a crosstalk gene-related PPI network. The crosstalk gene-related PPI network consisted of four types of nodes, namely, (1) DEGs dysregulated in periodontitis (not related to AD), (2) crosstalk genes or AD-related genes which were also DEGs dysregulated in periodontitis, (3) AD-related genes (not dysregulated in periodontitis), and (4) other genes (neither related to AD nor dysregulated in periodontitis).

**2.7. Feature Selection from Crosstalk Genes.** Since GSE16134 had the largest sample size among the periodontitis-related datasets, it was used as the test set. The other three datasets (GSE23586, GSE10334, and GSE79705) were used as validation sets. Firstly, expression values of the crosstalk genes (identified in the previous step) from GSE16134 were used as input for the Boruta algorithm in the R project [27] and

the conventional recursive feature elimination (RFE) algorithm [28] and feature selection was performed. Each gene was regarded as a feature.

**2.8. Support Vector Machine (SVM) Modeling Using Feature-Selected Crosstalk Genes.** The expression values in GSE16134 and GSE10334 were scale-standardized. Next, it was examined if the crosstalk genes obtained by feature selection were found in the four periodontitis-related datasets (i.e., GSE23586, GSE16134, GSE10334, and GSE79705). The gene expression values of these feature selection-obtained crosstalk genes were extracted from these datasets. If the number of expression profile genes in a certain dataset after extraction was lower than the number of feature selection-obtained crosstalk genes, the expression values of the missing genes were considered missing values and represented by the NA symbol. The missing values were processed by using the DMwR package [29] in R, and the K-Nearest Neighbors (KNN) algorithm was used to impute these missing values (NA) in that dataset. By imputing these missing values, all the four periodontitis-related datasets presented all the feature selection-obtained crosstalk genes. Thereafter, the scikit-learn package [30] was used to perform a grid search, and the best hyperparameters of a support vector machine (SVM) model were found by using 5-fold cross-validation

TABLE 1: Details of the included periodontitis-related GEO datasets.

Included four datasets	Type of periodontitis	Experimental platform	Number of examined genes	Number of inflamed gingival tissue samples	Number of healthy control samples	Number of total samples
GSE23586	3 patients with severe chronic periodontitis	GPL570	23,518	3	3	6
GSE16134	120 patients (65 with chronic periodontitis and 55 with aggressive periodontitis)	GPL570	24,441	241	69	310
GSE10334	63 with chronic periodontitis and 27 with aggressive periodontitis	GPL570	24,441	183	64	247
GSE79705	Generalized aggressive periodontitis (GAgP): $n = 4$ ; chronic periodontitis (CP): $n = 4$	GPL18734	19,305	8	4	12

TABLE 2: The number of up/downregulated DEGs identified in the four periodontitis-related datasets GSE23586, GSE16134, GSE10334, and GSE79705 at thresholds set for defining DEGs.

Data	Number of upregulated DEGs	Number of downregulated DEGs	Number of total DEGs	$ \log_2 FC $	$p$ value	Expression scale (if the data normalization was performed)
GSE23586	7	69	76	$>1$	$<0.05$	True
GSE16134	188	48	236	$>1$	$<0.05$	False
GSE10334	152	42	194	$>1$	$<0.05$	False
GSE79705	219	291	510	$>0$	$<0.05$	True

(CV) [31]. A SVM classifier model was established by using data from GSE16134 as the training set and test set, where the samples of the GSE16134 dataset were split into 60%:40% for the training set and test set, respectively. Data from the other three datasets (GSE23586, GSE10334, and GSE79705) were used as the validation set. The decision function method was used to obtain the score for each sample. Next, receiver operating characteristic (ROC) curves for the four datasets were generated by using the pROC package and displayed using the ggplot2 package in R.

**2.9. Targeting Relationships between Transcription Factors (TFs) and Crosstalk Genes.** Transcription factor- (TF-) target gene regulation pairs were obtained and downloaded from TRRUST [32], cGRNB [33], HTRIdb [34], ORTI [35], and TRANSFAC [36] databases. The TF-target gene interaction pairs corresponding to the feature selection-obtained crosstalk genes were extracted and used for constructing a TF-target gene interaction network with visualization using Cytoscape software [37].

**2.10. Pathway Analysis of the Crosstalk Genes.** Human data describing relationships between signaling pathways and genes were downloaded from the KEGG database, and all pathways related to the feature selection-obtained crosstalk genes were extracted. The expression levels of these crosstalk gene-related pathways were plotted as a heatmap, and differential expression analysis was performed and applied to the

four periodontitis-related datasets to identify the DEPs (differentially expressed pathways) using the R package limma. For the three datasets (GSE23586, GSE16134, and GSE79705), the pathways with  $p$  value  $< 0.05$  and  $|\log FC| \geq 1$  were regarded as differentially expressed pathways (DEPs), while for the dataset GSE79705, the pathways with  $p$  value  $< 0.05$  and  $|\log FC| > 0$  were regarded as DEPs.

**2.11. Classification Performance of the Core Crosstalk Genes.** The genes related to periodontitis were downloaded from the DisGeNET database [26]. The overlap between the periodontitis-related genes obtained from the DisGeNET database and the feature selection-obtained crosstalk genes was analyzed, and the overlapping genes were termed core crosstalk genes. The corresponding expression values of these overlapping genes in the four periodontitis-related datasets were obtained, and ROC curves were drawn.

### 3. Results

**3.1. Included Periodontitis-Related Datasets.** Four datasets pertaining to periodontitis (i.e., GSE23586, GSE16134, GSE10334, and GSE79705) were included and analyzed. Table 1 provides key details regarding the included datasets.

**3.2. Identification of Periodontitis-Related DEGs and Their Functions.** Table 2 shows the number of up- and downregulated DEGs that were identified in each of the four datasets.

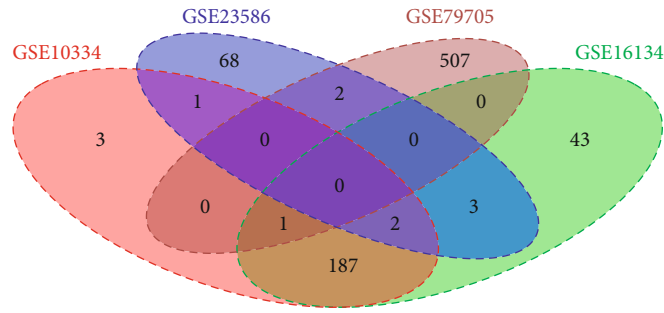


FIGURE 2: Venn diagram showing the overlap between DEGs identified in the four periodontitis-related datasets.

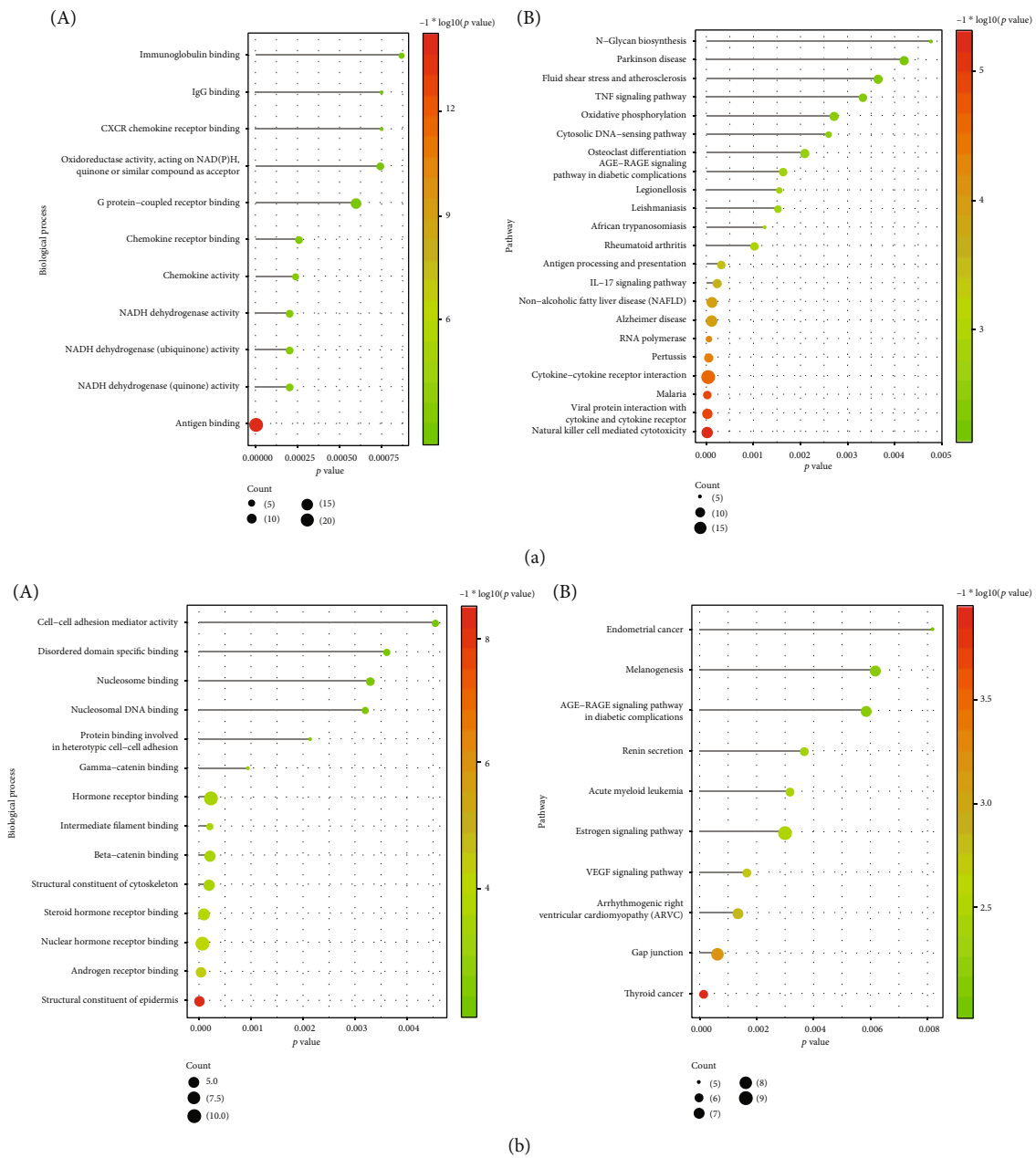


FIGURE 3: Functional enrichment analysis of up- and downregulated periodontitis-related DEGs. (a) The functional terms (the biological processes (A) and KEGG pathways (B)) enriched by upregulated periodontitis-related DEGs. (b) The functional terms (the biological processes (A) and KEGG pathways (B)) enriched by downregulated periodontitis-related DEGs.

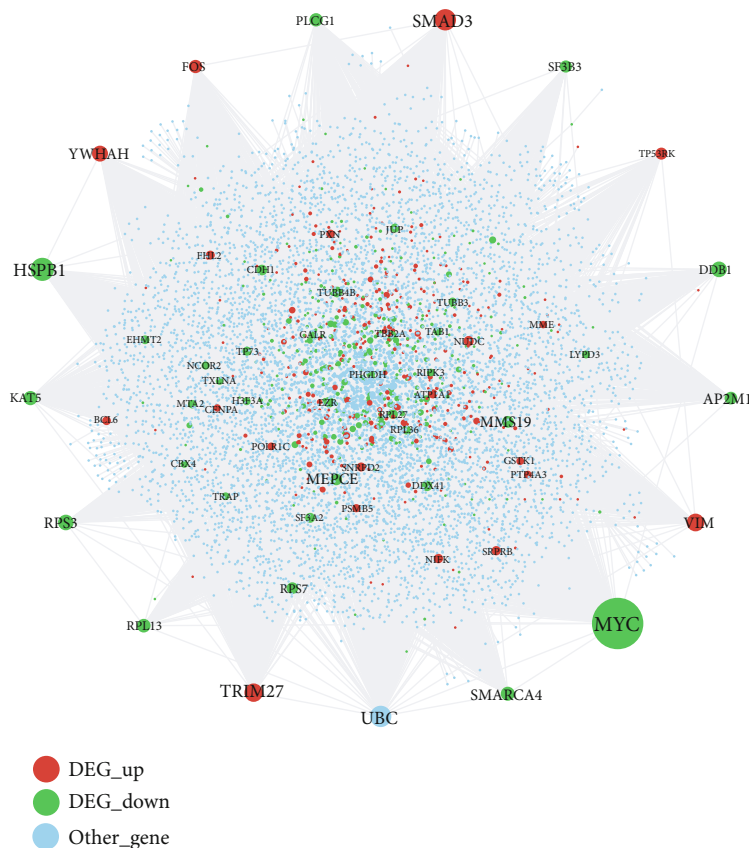


FIGURE 4: Protein-protein interaction (PPI) network associated with periodontitis. Red nodes represent the DEGs which were upregulated in periodontitis, green nodes represent the DEGs which were downregulated in periodontitis, and blue nodes represent other genes which were not DEGs but interacted with DEGs.

Figure 2 depicts a Venn diagram showing the overlap of DEGs identified from the four datasets. A total of 816 DEGs including 405 upregulated genes and 411 downregulated genes were used for the following analyses. Figure 3 shows the biological processes and signaling pathways in which the up- and downregulated DEGs were significantly enriched.

**3.3. The Hub Genes Identified by the Periodontitis-Related PPI Network.** Figure 4 depicts a PPI network based on the periodontitis-related DEGs, and Table 3 shows the topological characteristics of the top 30 nodes in the PPI network. As seen in Table 3, several genes with the highest degree were identified as hub genes. These upregulated DEGs included SMAD3, TRIM27, VIM, YWHAH, and FOS, and downregulated DEGs included MYC, HSPB1, DDB1, RPS3, KAT5, SMARCA4, RPL13, and PLCG1.

**3.4. Crosstalk Genes Bridging Alzheimer's Disease and Periodontitis.** In total, 51 upregulated crosstalk genes and 41 downregulated crosstalk genes were identified and are listed in Table 4. The crosstalk gene-related PPI network as shown in Figure 5 consisted of 3496 nodes and 5141 edges. The topological characteristics of the top 30 nodes in this network are presented in Table 5. Hub crosstalk genes with the highest degree included MYC, HSPB1, VIM, KAT5, RPL13, FOS, and CDH1.

**3.5. Crosstalk Genes Obtained by Feature Selection.** A total of 48 crosstalk genes were selected by using the Boruta algorithm (Figure 6(a)). In addition, 62 crosstalk genes were selected by using the RFE algorithm (Figure 6(b)). All 48 genes obtained by using the Boruta algorithm were included in the 62 genes obtained by the RFE algorithm, indicating that this 48-gene set was representative of the characteristics of all 92 crosstalk genes.

**3.6. Classification Accuracy Using the Feature Selection-Obtained Crosstalk Genes.** The 48 genes obtained by SVM feature selection were not shown in all of the four periodontitis-related datasets. The gene expression profiles of GSE16134 and GSE10334 included all of the 48 crosstalk genes, whereas GSE23586 included 44 crosstalk genes and GSE79705 included 45 crosstalk genes. The classification performance of these 48 crosstalk genes for the four datasets is shown in Table 6. For the test set GSE16134 and the validation set GSE10334, the accuracy performance was high at 91.94% and 88.26%, respectively. By comparison, the performance for the other two datasets GSE23586 and GSE79705 was low at 50% and 66.66%, respectively.

**3.7. ROC Curves for the Four Periodontitis-Related Datasets.** As shown in Figure 7, the AUC (area under the curve) values for the GSE16134 test set and the GSE10334 validation set



TABLE 3: Topological characteristics of the top 30 nodes in the periodontitis-related PPI network, ranked in descending order of degree.

Node	Label	Degree	Average shortest path length	Betweenness centrality	Closeness centrality	Clustering coefficient	Topological coefficient
MYC	DEG_down	1027	2.432727	0.177217	0.411061	0.001896	0.002805
HSPB1	DEG_down	433	2.638061	0.059908	0.379066	0.00278	0.005213
SMAD3	DEG_up	396	2.667636	0.052167	0.374864	0.004283	0.005425
UBC		395	2.112	0.241673	0.473485	0.004524	0.007004
TRIM27	DEG_up	334	2.864727	0.046792	0.349073	0.000791	0.006306
VIM	DEG_up	320	2.705212	0.037607	0.369657	0.005251	0.007619
YWHAH	DEG_up	282	2.838788	0.034115	0.352263	0.001868	0.00865
DDB1	DEG_down	276	2.76497	0.029677	0.361668	0.003531	0.008012
RPS3	DEG_down	275	2.844848	0.015036	0.351513	0.019323	0.014779
KAT5	DEG_down	245	2.717697	0.028224	0.367959	0.00716	0.007732
SMARCA4	DEG_down	242	2.715758	0.021646	0.368221	0.010116	0.008636
RPL13	DEG_down	234	2.755152	0.015773	0.362956	0.024541	0.011238
PLCG1	DEG_down	227	2.885091	0.030011	0.34661	0.002144	0.009614
FOS	DEG_up	226	2.880727	0.024538	0.347135	0.003265	0.009974
AP2M1	DEG_down	214	2.850182	0.025582	0.350855	0.007635	0.010848
SF3B3	DEG_down	203	2.765576	0.015188	0.361588	0.014583	0.010661
TP53RK	DEG_up	200	2.871394	0.013972	0.348263	0.01608	0.012798
MMS19	DEG_down	195	2.806909	0.022335	0.356264	0.004705	0.008763
RPS7	DEG_down	193	2.88303	0.008126	0.346857	0.028335	0.016367
MEPCE	DEG_down	189	2.905212	0.0145	0.344209	0.005066	0.012337
TUBB4B	DEG_down	173	2.880364	0.008167	0.347178	0.007595	0.019412
CDH1	DEG_down	171	2.888485	0.016186	0.346202	0.005848	0.011775
EZR	DEG_down	170	2.906667	0.016295	0.344037	0.004107	0.01554
DDX41	DEG_down	168	2.950061	0.009545	0.338976	0.007057	0.017509
NUDC	DEG_up	160	2.943758	0.016886	0.339702	0.00283	0.013954
SF3A2	DEG_down	156	2.949818	0.009075	0.339004	0.009926	0.01593
RPL27	DEG_down	147	2.912727	0.003949	0.343321	0.043985	0.020057
NIFK	DEG_up	145	3.107879	0.011111	0.321763	0.010345	0.016053
SRPRB	DEG_up	143	2.945333	0.017545	0.33952	0.001674	0.015983
ATP1A1	DEG_up	140	2.816606	0.011269	0.355037	0.009147	0.013032

were high at 95.77% and 90.53%, respectively, congruent with the results in Table 6. It was thus inferred that the classifier performance was adequate only when the sample sizes of the validation sets were similar to those of the training and test datasets, and therefore, poor performance was noted for GSE23586 and GSE79705 having much lower sample numbers.

**3.8. The Identification of Transcription Factors Regulating the Crosstalk Genes.** As shown in Figure 8, the TF-crosstalk gene target network consisted of 388 nodes and 1178 edges. Several transcription factors which were also DEGs played critical roles by regulating the most number of crosstalk genes, for example, FOS, MEF2C, and USF2 (Table 7).

**3.9. Signaling Pathways Enriched in the Crosstalk Genes.** From the 48 feature selection-obtained crosstalk genes, 37 crosstalk genes were found among gene-pathway interaction pair data in the KEGG database. 137 KEGG pathways corre-

sponded to these 37 crosstalk genes. Figure 9 shows the expression values of these 137 pathways in the four periodontitis-related datasets.

The numbers of crosstalk gene-related DEPs obtained from each of the four periodontitis-related datasets are listed in Table 8. The interaction relationships between crosstalk genes and DEPs are depicted in Figure 10, showing that several DEPs were dysregulated in at least two datasets, including cytokine-related pathways (cytokine-cytokine receptor interaction, chemokine, and IL-17), immune cell-related pathways (T cell receptor, B cell receptor, Th1 and Th2 cell differentiation, Th17 cell differentiation, natural killer cell-mediated cytotoxicity, and osteoclast differentiation), JAK-STAT signaling, NOD-like receptor signaling, MAPK signaling, Toll-like receptor signaling, NF-kappa B signaling, and C-type lectin receptor signaling.

**3.10. The Identification of Core Crosstalk Genes.** Among the 48 feature selection-obtained crosstalk genes and

TABLE 4: The 51 crosstalk genes that were upregulated and 41 crosstalk genes which were downregulated in periodontitis.

Regulation pattern in periodontitis	Crosstalk genes linking periodontitis and Alzheimer's disease
Upregulated	AMIGO1 (adhesion molecule with Ig-like domain 1; gene ID: 57463)
	ARG2 (arginase 2; gene ID: 384)
	BDKRB2 (bradykinin receptor B2; gene ID: 624)
	BRI3 (brain protein I3; gene ID: 25798)
	C1D (C1D nuclear receptor corepressor; gene ID: 10438)
	C3 (complement C3; gene ID: 718)
	C4A (complement C4A (Rodgers blood group); gene ID: 720)
	C4B (complement C4B; gene ID: 721)
	C4B_2 (complement component 4B (Chido blood group), copy 2; gene ID: 100293534)
	CASP7 (caspase 7; gene ID: 840)
	CD177 (CD177 molecule; gene ID: 57126)
	CD38 (CD38 molecule; gene ID: 952)
	CHCHD10 (coiled-coil-helix-coiled-coil-helix domain containing 10; gene ID: 400916)
	COX8A (cytochrome c oxidase subunit 8A; gene ID: 1351)
	CSF3 (colony-stimulating factor 3; gene ID: 1440)
	CTGF (cellular communication network factor 2; gene ID: 1490)
	CTSS (cathepsin S; gene ID: 1520)
	CXCL1 (C-X-C motif chemokine ligand 1; gene ID: 2919)
	CXCL12 (C-X-C motif chemokine ligand 12; gene ID: 6387)
	CXCL8 (C-X-C motif chemokine ligand 8; gene ID: 3576)
	CXCR4 (C-X-C motif chemokine receptor 4; gene ID: 7842)
	ENPP2 (ectonucleotide pyrophosphatase/phosphodiesterase 2; gene ID: 5168)
	FCGR3A (Fc fragment of IgG receptor IIIa; gene ID: 2214)
	FCGR3B (Fc fragment of IgG receptor IIIb; gene ID: 2215)
	FHL2 (four and a half LIM domains 2; gene ID: 2274)
	FOS (Fos proto-oncogene, AP-1 transcription factor subunit; gene ID: 2353)
	FOXO1 (forkhead box O1; gene ID: 2308)
	GSTK1 (glutathione S-transferase kappa 1; gene ID: 373156)
	GSTO1 (glutathione S-transferase omega 1; gene ID: 9446)
	HCLS1 (hematopoietic cell-specific Lyn substrate 1; gene ID: 3059)
	IGFBP7 (insulin-like growth factor binding protein 7; gene ID: 3490)
	IL1B (interleukin-1 beta; gene ID: 3553)
	LYZ (lysozyme; gene ID: 4069)
	MAK16 (MAK16 homolog; gene ID: 84549)
	MEF2C (myocyte-specific enhancer factor 2C; gene ID: 4208)
	MME (membrane metalloendopeptidase; gene ID: 4311)
	MMP1 (matrix metallopeptidase 1; gene ID: 4312)
	MMP3 (matrix metallopeptidase 3; gene ID: 4314)
	MS4A1 (membrane-spanning 4-domains A1; gene ID: 931)
	MSRA (methionine sulfoxide reductase A; gene ID: 4482)
	MZB1 (marginal zone B and B1 cell-specific protein; gene ID: 51237)
	NDUFB8 (NADH:ubiquinone oxidoreductase subunit B8; gene ID: 4714)
	PECAM1 (platelet endothelial cell adhesion molecule 1; gene ID: 5175)
	PLAT (plasminogen activator, tissue type; gene ID: 5327)
	PSENEN (presenilin enhancer, gamma-secretase subunit; gene ID: 55851)
	SEL1L (SEL1L adaptor subunit of ERAD E3 ubiquitin ligase; gene ID: 6400)
	SERPINI1 (serpin family I member 1; gene ID: 5274)
	ST6GAL1 (ST6 beta-galactoside alpha-2,6-sialyltransferase 1; gene ID: 6480)
	VCAN (versican; gene ID: 1462)
	VIM (vimentin; gene ID: 7431)
	WARS2 (tryptophanyl tRNA synthetase 2, mitochondrial; gene ID: 10352)
Downregulated	ABCA12 (ATP binding cassette subfamily A member 12; gene ID: 26154)
	ACE (angiotensin I converting enzyme; gene ID: 1636)
	ADRB1 (adrenoceptor beta 1; gene ID: 153)
	BCL2L2 (BCL2-like 2; gene ID: 599)
	BRSK1 (BR serine/threonine kinase 1; gene ID: 84446)
	CALML5 (calmodulin-like 5; gene ID: 51806)
	CALR (calreticulin; gene ID: 811)
	CD36 (CD36 molecule; gene ID: 948)
	CDH1 (cadherin 1; gene ID: 999)
	CDK5R1 (cyclin-dependent kinase 5 regulatory subunit 1; gene ID: 8851)
	CTDSP2 (CTD small phosphatase 2; gene ID: 10106)

TABLE 4: Continued.

Regulation pattern in periodontitis	Crosstalk genes linking periodontitis and Alzheimer's disease
	DNM1 (dynamin 1; gene ID: 1759)
	DSG1 (desmoglein 1; gene ID: 1828)
	FLG (filaggrin; gene ID: 2312)
	GJA1 (gap junction protein alpha 1; gene ID: 2697)
	GRHL3 (grainyhead-like transcription factor 3; gene ID: 57822)
	GRIN3B (glutamate ionotropic receptor NMDA type subunit 3B; gene ID: 116444)
	HM13 (histocompatibility minor 13; gene ID: 81502)
	HMGCR (3-hydroxy-3-methylglutaryl-CoA reductase; gene ID: 3156)
	HSPB1 (heat shock protein family B (small) member 1; gene ID: 3315)
	KAT5 (lysine acetyltransferase 5; gene ID: 10524)
	MAP3K12 (mitogen-activated protein kinase kinase kinase 12; gene ID: 7786)
	MED12 (mediator complex subunit 12; gene ID: 9968)
	MFN2 (mitofusin 2; gene ID: 9927)
	MYC (MYC proto-oncogene, bHLH transcription factor; gene ID: 4609)
	NEFL (neurofilament light; gene ID: 4747)
	NES (exportin 1; gene ID: 7514)
	NGF (nerve growth factor; gene ID: 4803)
	NOS3 (nitric oxide synthase 3; gene ID: 4846)
	NPTXR (neuronal pentraxin receptor; gene ID: 23467)
	PLXNA3 (plexin A3; gene ID: 55558)
	PPIL2 (peptidylprolyl isomerase-like 2; gene ID: 23759)
	PTGS1 (prostaglandin-endoperoxide synthase 1; gene ID: 5742)
	RPL13 (ribosomal protein L13; gene ID: 6137)
	SCIMP (SLP adaptor and CSK interacting membrane protein; gene ID: 388325)
	SPPL2B (signal peptide peptidase-like 2B; gene ID: 56928)
	TIAF1 (TGFB1-induced antiapoptotic factor 1; gene ID: 9220)
	TP73 (tumor protein P73; gene ID: 7161)
	TYRP1 (tyrosinase-related protein 1; gene ID: 7306)
	USF2 (upstream transcription factor 2, C-Fos interacting; gene ID: 7392)
	VEGFA (vascular endothelial growth factor A; gene ID: 7422)

periodontitis-related genes in the DisGeNET database, 12 common genes were identified as core crosstalk genes including C3, C4A, C4B, CXCL12, FCGR3A, FCGR3B, HSPB1, IL1B, MME, MMP3, PLAT, and VEGFA (Table 9). Among these 12 genes, 6 genes, C4A, C4B, CXCL12, FCGR3A, IL1B, and MMP3, were found associated with chronic periodontitis.

Figure 11 shows ROC curves for the 6 chronic periodontitis-related genes for each of the four datasets. An AUC value of more than 80% was presented by three genes, C4A, C4B, and CXCL12, for the dataset GSE10334, 5 genes, C4A, C4B, CXCL12, FCGR3A, and IL1B, for GSE16134, 3 genes, CXCL12, IL1B, and MMP3, for GSE23586, and all 6 genes for GSE79705. The 3 genes, C4A, C4B, and CXCL1, had the highest classification accuracy when the datasets with small samples (GSE23586 and GSE79705) were not considered.

#### 4. Discussion

The present study addressed shared genetic mechanisms and molecular links between periodontitis and Alzheimer's diseases by identifying gene expression, signaling pathways, and TFs that were most robustly associated with both these diseases. These findings are largely substantiated by preexisting experimental data.

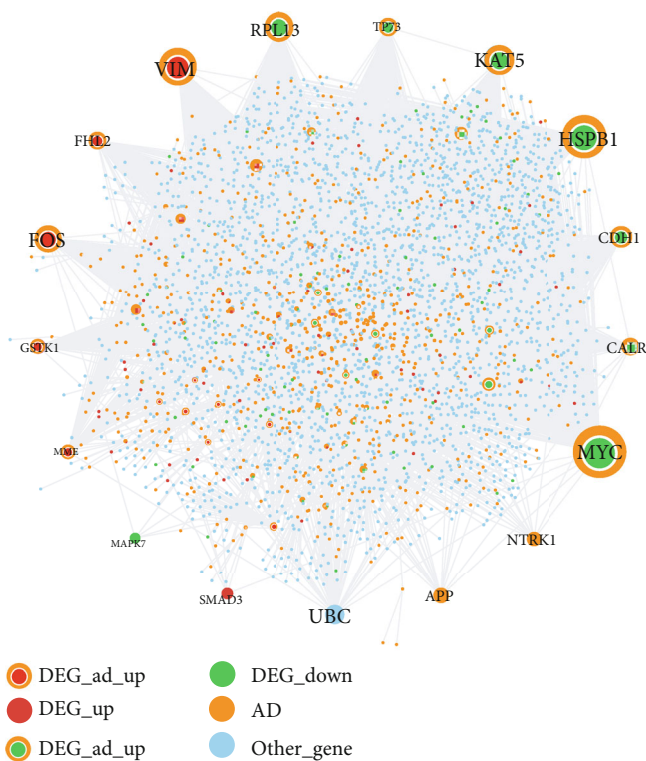


FIGURE 5: The crosstalk gene-related PPI network.

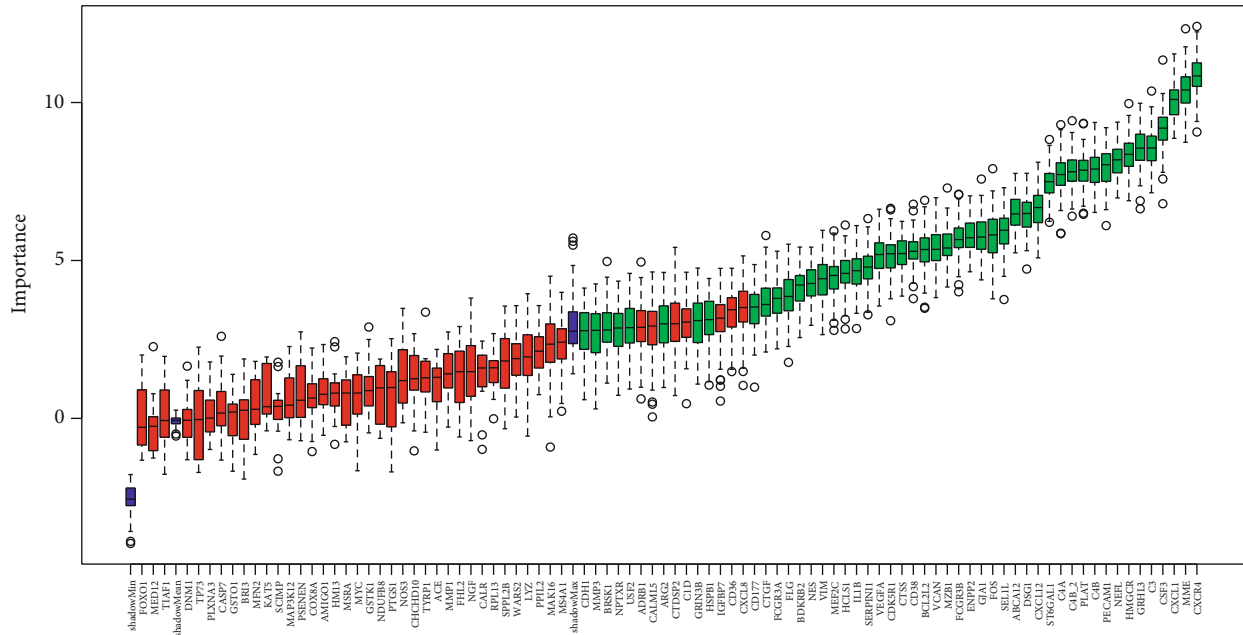
TABLE 5: Topological characteristics of the top 30 nodes in the crosstalk gene-related PPI network, ranked in descending order of degree.

Node	Label	Degree	Average shortest path length	Betweenness centrality	Closeness centrality	Clustering coefficient	Topological coefficient
MYC	DEG_AD_down	1027	2.127525	0.466698	0.47003	5.03E - 04	0.001842
HSPB1	DEG_AD_down	433	2.36959	0.184598	0.422014	0.001636	0.003351
VIM	DEG_AD_up	320	2.663301	0.116611	0.375474	0.001763	0.005783
KAT5	DEG_AD_down	245	2.566359	0.089476	0.389657	0.003011	0.005621
RPL13	DEG_AD_down	234	2.589729	0.089708	0.386141	0.001394	0.005672
FOS	DEG_AD_up	226	2.883151	0.083642	0.346843	1.97E - 04	0.017606
CDH1	DEG_AD_down	171	2.93191	0.058428	0.341075	0	0.025911
TP73	DEG_AD_down	137	2.61483	0.046781	0.382434	0.006333	0.009173
FHL2	DEG_AD_up	136	2.641085	0.057192	0.378632	0.004031	0.00889
CALR	DEG_AD_down	135	2.812464	0.046142	0.35556	0.002764	0.010949
GSTK1	DEG_AD_up	111	2.988459	0.035152	0.334621	0	0.026289
MME	DEG_AD_up	104	2.836988	0.040386	0.352487	0.001307	0.011694
MED12	DEG_AD_down	91	2.695615	0.030682	0.370973	0.006105	0.012517
CASP7	DEG_AD_up	90	2.901039	0.027131	0.344704	0.005243	0.015603
DNM1	DEG_AD_down	84	2.960185	0.029086	0.337817	0.001147	0.023716
FOXO1	DEG_AD_up	67	2.977784	0.017403	0.33582	0.004071	0.026586
CXCR4	DEG_AD_up	65	2.998557	0.020851	0.333494	0.003846	0.028808
NOS3	DEG_AD_down	62	2.963647	0.018786	0.337422	0.002644	0.027957
NDUFB8	DEG_AD_up	56	3.042412	0.02136	0.328687	0	0.027447
UBC	Other gene	53	2.084824	0.149265	0.479657	0.015965	0.027336
NES	DEG_AD_down	53	2.920946	0.017012	0.342355	0.007983	0.022954
CDK5R1	DEG_AD_down	50	3.0176	0.0133	0.331389	0.002449	0.037222
NEFL	DEG_AD_down	49	2.913445	0.014886	0.343236	0.008503	0.024673
C3	DEG_AD_up	43	3.043278	0.01705	0.328593	0	0.042101
SEL1L	DEG_AD_up	42	3.036065	0.013066	0.329374	0	0.045635
DSG1	DEG_AD_down	41	3.046163	0.00857	0.328282	0	0.068464
GJA1	DEG_AD_down	41	3.035199	0.015703	0.329468	0	0.04037
MEF2C	DEG_AD_up	41	3.039238	0.008676	0.32903	0	0.068892
LYZ	DEG_AD_up	40	3.042123	0.008578	0.328718	0	0.065086
GSTO1	DEG_AD_up	38	2.820254	0.010905	0.354578	0.019915	0.030356

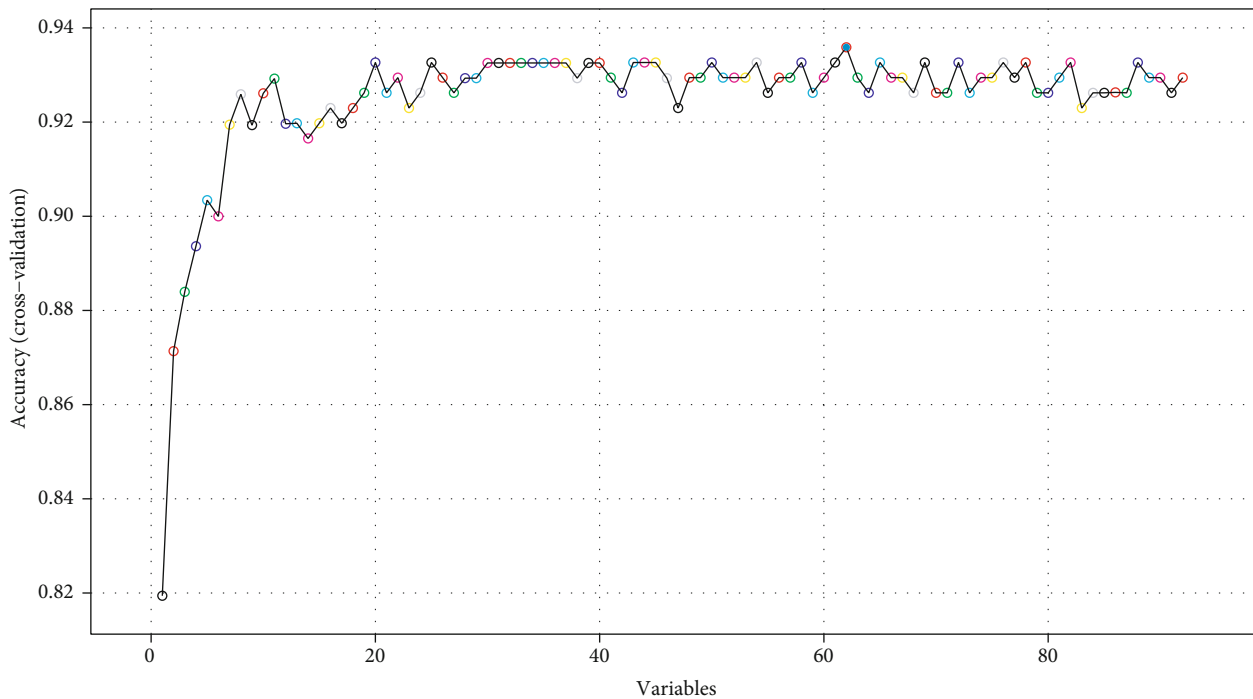
Six genes C4A, C4B, CXCL12, FCGR3A, IL1B, and MMP3 were identified as the most significant crosstalk genes linking chronic periodontitis and Alzheimer's disease. C4B and C4A, respectively, encode the basic and acidic forms of the complement factor 4, and C4 gene deficiency has been noted to predispose the development of severe chronic periodontitis [38]. In AD, the expression levels of C4 mRNA were shown to be 3.27-fold increased in temporal cortex samples as compared to controls [39]. The CXCL12 (C-X-C motif chemokine ligand 12) gene is the ligand of the C-X-C motif chemokine receptor 4 (CXCR4). CXCL12 expression in the gingival crevicular fluid of periodontitis patients was shown to be significantly higher than that of healthy subjects, suggesting that it might play a role in enhancing neutrophil migration and further the progression of periodontitis [40]. A decreased level of CXCL12 in Alzheimer's disease has been documented as affecting cognitive function, impairing learning and memory [41]. FCGR3A (Fc fragment of IgG receptor IIIa) encodes a receptor for the Fc portion of immunoglobu-

lin G, and FCGR3A polymorphisms are shown to confer susceptibility to periodontitis in Caucasians [42]. In AD, the Fc gamma receptor (FcγR) was recently found to exacerbate neurodegeneration [43]. Cytokines are considered a primary link between chronic periodontitis and Alzheimer's disease as they can enter systemic circulation through periodontal pockets [6]. The classical proinflammatory cytokine, IL1B, is elevated in periodontitis and can induce resorption of alveolar bone [44]. In AD, IL1B gene polymorphisms are linked to disease susceptibility [45]. MMP3 (matrix metalloproteinase 3) is implicated in the progression of chronic periodontitis and can degrade the periodontal tissue matrix [46]. Elevated brain levels of MMP3 have been associated with the duration of Alzheimer's disease, and it has been found to increase the activity of MMP9, thereby indirectly promoting aggregation and cerebral accumulation of tau deposits [47].

More interestingly, the six genes discussed in the last paragraph were also found to be the molecular crosstalks in



(a) Boruta algorithm to obtain genes



(b) RFE algorithm to obtain genes

FIGURE 6: 48 crosstalk genes selected by using the Boruta algorithm (a) and 62 crosstalk genes selected by using the RFE algorithm (b).

linking the peripheral immune system and central nervous system (CNS). It has been well demonstrated that the periodontal disease-evoked peripheral systemic host immune response can aggravate the progression of neuroinflammation and neurodegeneration in Alzheimer’s disease by switching the microglia from the primed phenotype to an aggressive proinflammatory phenotype [48, 49]. The immune-inflammatory mediators (e.g., cytokines and chemokines) abundantly expressed during periodontal inflam-

mation can circulate into the bloodstream and travel into the brain by crossing the blood-brain barrier (BBB) and impact the function of CNS [50]. Therefore, the crosstalk between the peripheral immune system and the CNS might be an important mechanism underlying periodontitis, increasing the risk of AD. This paragraph will provide a description regarding the potential role of the six crosstalk genes in linking periodontal disease and AD, especially by means of neuroimmune interaction. For example, the



TABLE 6: Classification performance of the 48 feature selection-obtained crosstalk genes in the four periodontitis-related datasets.

	GSE16134			GSE10334			GSE23586			GSE79705		
	Samples: test set	Samples: SVM model predicts accurately	Accuracy	Samples: validation set	Samples: SVM model predicts accurately	Accuracy	Samples: validation set	Samples: SVM model predicts accurately	Accuracy	Samples: validation set	Samples: SVM model predicts accurately	Accuracy
Case	93	92		183	177		3	3		8	8	
Control	31	22	91.94%	64	41	88.26%	3	0	50%	4	0	66.66%
Total	124	114		247	218		6	3		12	8	

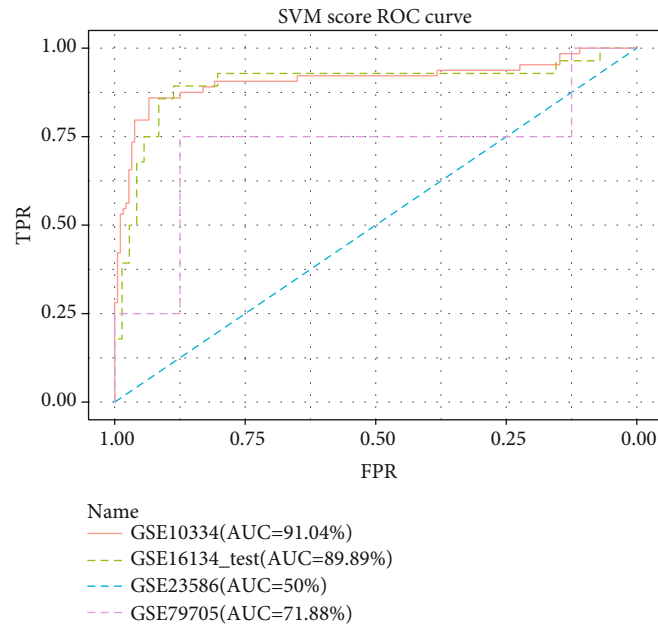


FIGURE 7: The ROC curves of four periodontitis-related datasets.

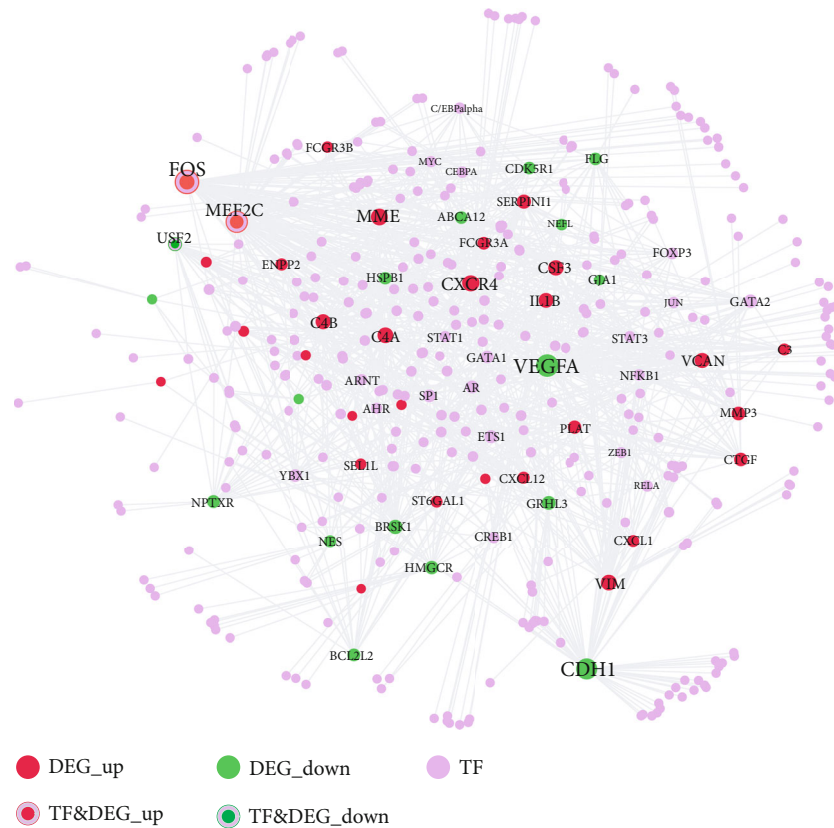


FIGURE 8: The transcription factor-crosstalk gene target network.

complement components C4A and C4B highly expressed in periodontal disease were found to modulate T cell immune response by stimulating the activation and migration of T cells [51–53]. The migration of T cells enhanced by C4A and C4B might allow T cells to traffic across the BBB and

enter the brain. For another example, the chemokine and its receptor-composed system CXCL12/CXCR4-7 system were found to be a significant player of the neuroimmune interface [54]. On the one hand, the chemokine CXCL12 mediated the immune-inflammatory response in CNS by

TABLE 7: Topological characteristics of the top 30 nodes in the TF-crosstalk gene target network, ranking in descending order.

Node	Label	Degree	Average shortest path length	Betweenness centrality	Closeness centrality	Clustering coefficient	Topological coefficient
FOS	DEG_up&TF	89	2.178295	0.206101	0.459075	0.020429	0.03825
VEGFA	DEG_down	77	2.211886	0.197219	0.452103	0.010936	0.038456
MEF2C	DEG_up&TF	76	2.328165	0.159945	0.429523	0.004211	0.044258
CDH1	DEG_down	69	2.540052	0.159392	0.393693	0	0.086634
CXCR4	DEG_up	47	2.596899	0.075105	0.385075	9.25E - 04	0.083836
MME	DEG_up	44	2.664083	0.04365	0.375364	0	0.131313
C4A	DEG_up	38	2.661499	0.029742	0.375728	0.01138	0.118617
VIM	DEG_up	38	2.521964	0.060293	0.396516	0.012802	0.065789
CSF3	DEG_up	36	2.550388	0.031734	0.392097	0.019048	0.075137
C4B	DEG_up	34	2.679587	0.018887	0.373192	0.012478	0.122037
VCAN	DEG_up	34	2.726098	0.030567	0.366825	0	0.143717
IL1B	DEG_up	33	2.741602	0.05746	0.36475	0	0.134602
BRSK1	DEG_down	30	2.741602	0.030404	0.36475	0	0.153788
SERPINI1	DEG_up	29	2.793282	0.019014	0.358002	0	0.127586
USF2	DEG_down&TF	27	2.591731	0.027575	0.385842	0.045584	0.081607
GRHL3	DEG_down	27	2.775194	0.027067	0.360335	0	0.150732
HSPB1	DEG_down	26	2.780362	0.017981	0.359665	0	0.155678
MMP3	DEG_up	26	2.607235	0.024377	0.383548	0.036923	0.074984
CTGF	DEG_up	25	2.788114	0.020669	0.358665	0	0.161905
HMGCR	DEG_down	25	2.767442	0.041119	0.361345	0	0.16
GATA2	TF	24	2.095607	0.052687	0.477189	0.018116	0.104678
PLAT	DEG_up	24	2.762274	0.028075	0.362021	0	0.173148
ETS1	TF	22	2.273902	0.03767	0.439773	0.012987	0.092022
NPTXR	DEG_down	22	2.826873	0.020478	0.353748	0	0.154545
AR	TF	21	2.24031	0.040698	0.446367	0.02381	0.105465
YBX1	TF	21	2.315245	0.037801	0.43192	0.004762	0.098928
BCL2L2	DEG_down	21	2.813953	0.018179	0.355372	0	0.144048
FCGR3A	DEG_up	21	2.81137	0.020521	0.355699	0	0.192799
ABCA12	DEG_down	20	2.79845	0.010961	0.357341	0	0.2
SP1	TF	20	2.191214	0.037362	0.456368	0.026316	0.109167
CDK5R1	DEG_down	20	2.824289	0.017878	0.354071	0	0.156098
FLG	DEG_down	20	2.653747	0.012281	0.376826	0.042105	0.093043

recruiting lymphocytes and macrophages [55]. On the other hand, CXCL12 can lead to neurotoxicity and neurodegeneration by activating the neuronal survival-associated G protein-activated inward rectifier K(+) (GIRK) [54]. FCGR3A (also named CD16) is essential for the antibody-dependent cellular cytotoxicity (ADCC) mediated by natural killer (NK) cells [56]. The increased cytotoxic activity of NK cells was found to cause the dysregulation of protein kinase C and further led to the cognitive deficits in Alzheimer's disease, indicating the contribution of immunological factors to the dysfunction of CNS [57]. IL1B, which was upregulated in periodontitis and transported through the vascular circulation into the brain, was found to play promoting roles in neuroinflammation by enhancing the expression of leukocyte chemotactic chemokines, cell surface adhesion molecules, cyclooxygenases, and MMPs within the brain parenchyma

[58]. Likewise, MMP3 abundantly produced in periodontitis was also found to be associated with neuroinflammation via activating microglial cells, as well as participating in the BBB breakdown through the proteolysis of fibronectin and type IV collagen [59]. Taken together, the six crosstalk genes identified in the present research were well evidenced to be involved in periodontitis-triggered peripheral systemic host immune response caused CNS dysfunction in Alzheimer's disease.

Three transcription factors, FOS, MEF2C, and USF2, were identified as related to the regulation of the crosstalk genes and were also found to be dysregulated in chronic periodontitis. The proto-oncogene FOS (also named C-Fos) was found to be involved in the transcriptional regulation of collagenase and cell proliferation genes in periodontal gingival fibroblasts [60]. In AD, FOS is reported to initiate amyloid-

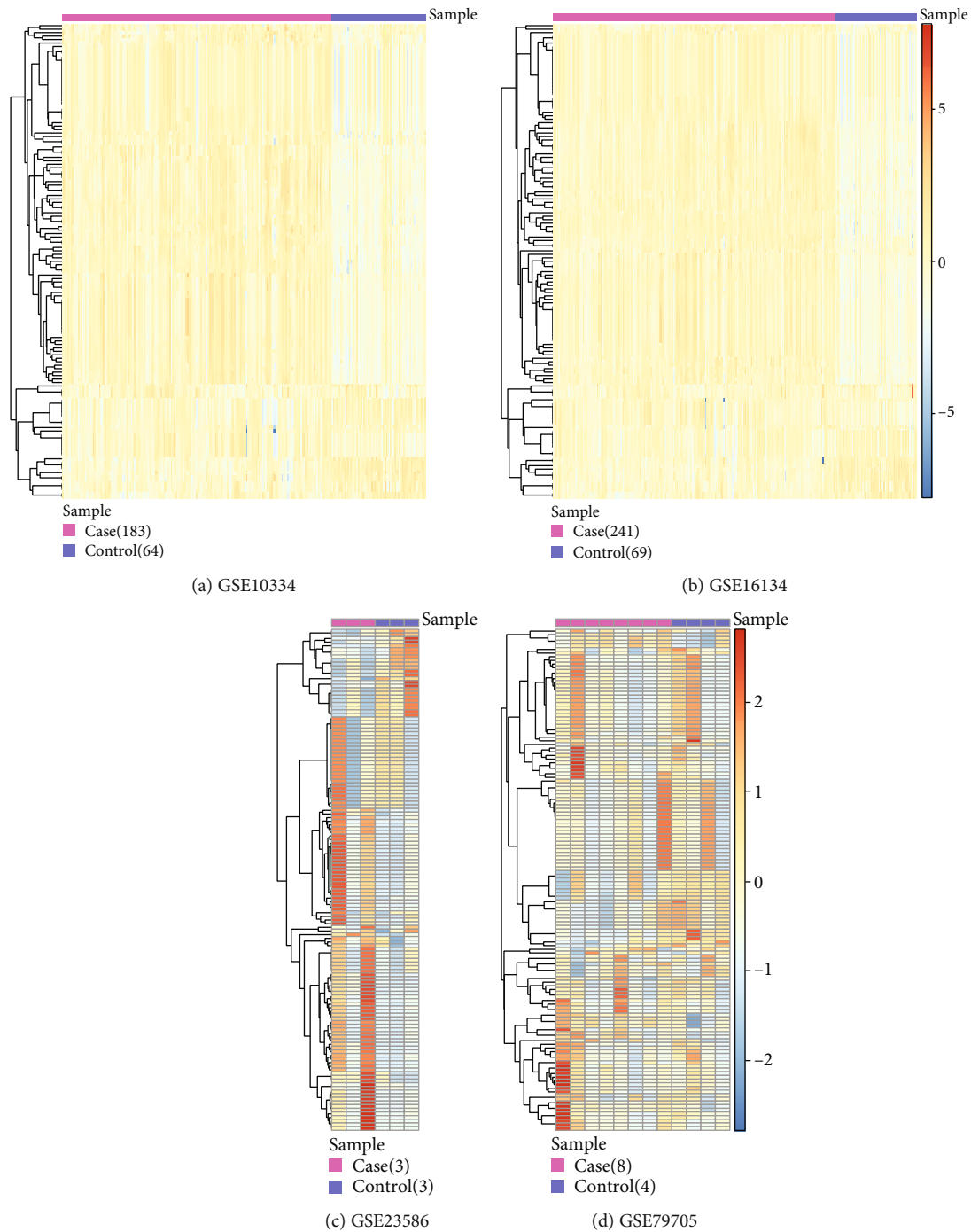


FIGURE 9: Heatmaps depicting 137 signaling pathways enriched in the crosstalk genes in the four periodontitis-related datasets.

$\beta$ -mediated apoptosis and found to be increased in the hippocampal regions of AD patients [61]. Myocyte-specific enhancer factor 2C (MEF2C) was identified as a critical transcription factor involved in the coexpression network of chronic periodontitis [62]. Genome-wide association studies (GWAS) have shown the linkage between mutation of MEF2C and aging-associated late-onset Alzheimer’s disease [63, 64]. Experimentally, a lack of MEF2C expression was shown to exaggerate microglial response and negatively affect brain function [65]. The USF2 (upstream transcription

TABLE 8: The number of crosstalk gene-related DEPs within the four periodontitis-related datasets.

Data	Sample	DEP Up	DEP Down	DEP Total	Log FC Abs	p value
GSE23586	6	1	12	13	>1	<0.05
GSE16134	310	84	2	86	>1	<0.05
GSE10334	247	77	2	79	>1	<0.05
GSE79705	12	4	4	8	>0	<0.05

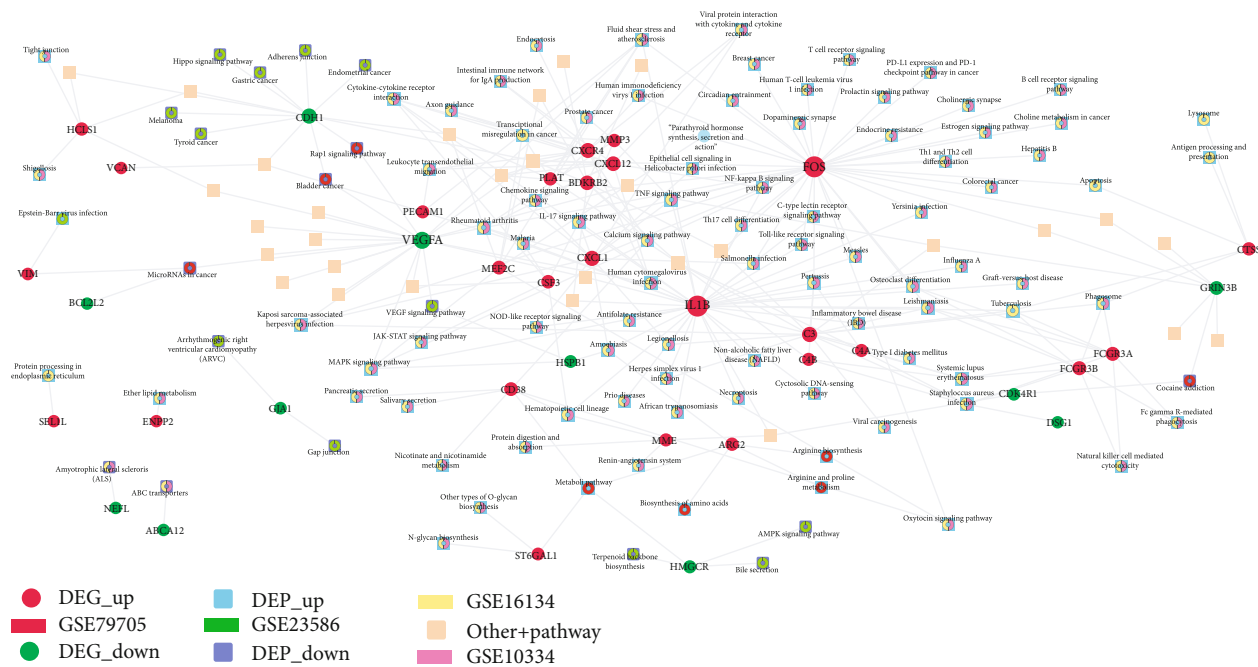
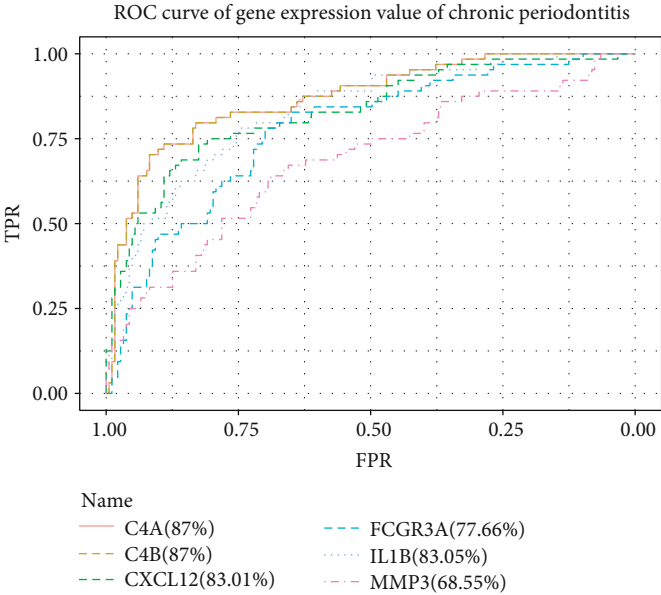


FIGURE 10: The crosstalk gene-differentially expressed pathway interaction network.

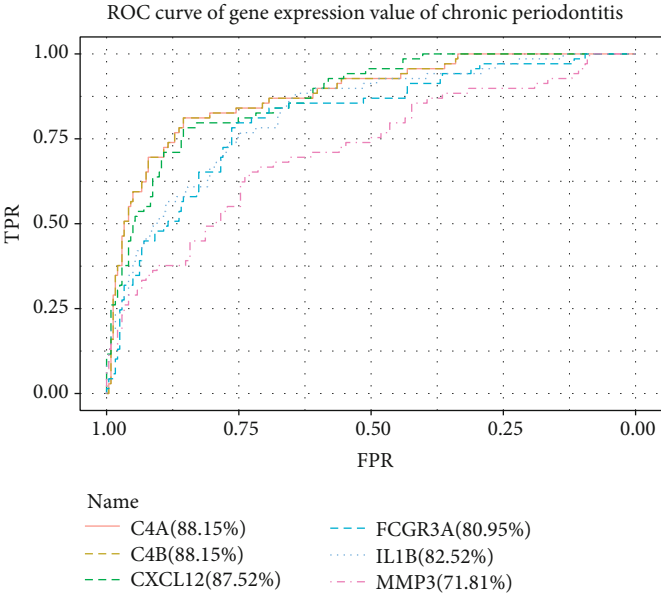
TABLE 9: The 12 overlapping genes between 48 feature selection-obtained crosstalk genes and periodontitis-related genes in the DisGeNET database. Among the 12 genes, 6 genes, C4A, C4B, CXCL12, FCGR3A, IL1B, and MMP3, were associated with chronic periodontitis.

Gene symbol	Gene ID	Disease ID	Disease name
C3	718	C0031099	Periodontitis
C4A	720	C0266929	Chronic periodontitis
C4B	721	C0266929	Chronic periodontitis
CXCL12	6387	C0266929	Chronic periodontitis
FCGR3A	2214	C0266929	Chronic periodontitis
FCGR3A	2214	C0031099	Periodontitis
FCGR3A	2214	C0031106	Periodontitis, juvenile
FCGR3A	2214	C0399447	Early-onset periodontitis
FCGR3A	2214	C0031030	Periapical periodontitis
FCGR3B	2215	C0399447	Early-onset periodontitis
FCGR3B	2215	C0031106	Periodontitis, juvenile
HSPB1	3315	C0031030	Periapical periodontitis
IL1B	3553	C1719494	Periodontitis, localized aggressive
IL1B	3553	C1719495	Aggressive periodontitis, generalized
IL1B	3553	C0399447	Early-onset periodontitis
IL1B	3553	C0001342	Acute periodontitis
IL1B	3553	C0031106	Periodontitis, juvenile
IL1B	3553	C0031030	Periapical periodontitis
IL1B	3553	C4025886	Severe periodontitis
IL1B	3553	C0031099	Periodontitis
IL1B	3553	C0266929	Chronic periodontitis
MME	4311	C0031099	Periodontitis
MMP3	4314	C0031106	Periodontitis, juvenile
MMP3	4314	C0001342	Acute periodontitis
MMP3	4314	C0266929	Chronic periodontitis
MMP3	4314	C0031099	Periodontitis
PLAT	5327	C1719495	Aggressive periodontitis, generalized
VEGFA	7422	C0031099	Periodontitis



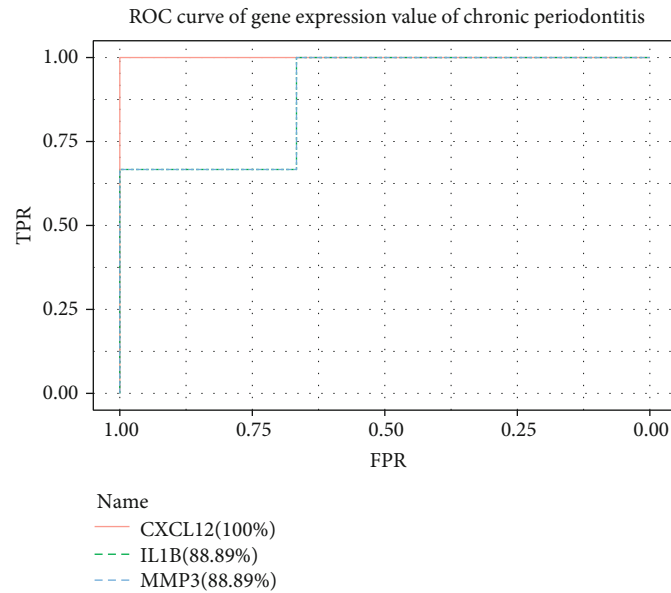


(a) GSE10334

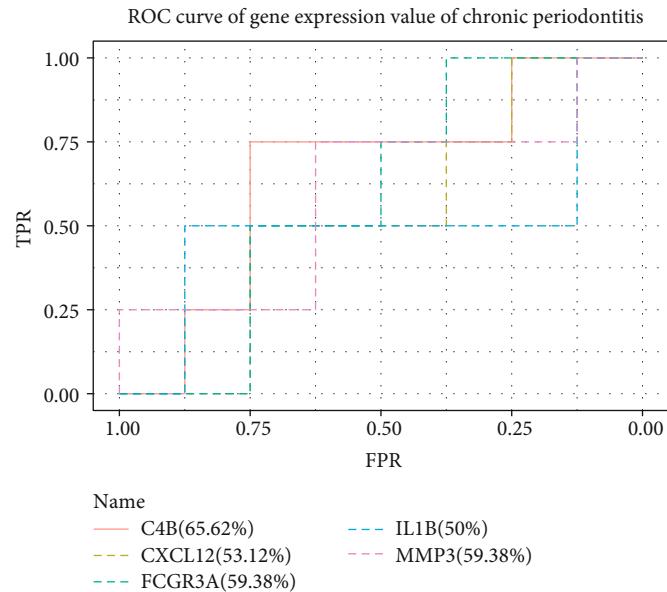


(b) GSE16134

FIGURE 11: Continued.



(c) GSE23586



(d) GSE79705

FIGURE 11: The ROC curves for 6 chronic periodontitis-related genes, C4A, C4B, CXCL12, FCGR3A, IL1B, and MMP3, in the four periodontitis-related datasets.

factor 2, C-Fos interacting) transcription factor is reported to enhance osteogenic differentiation of periodontal ligament cells (PDLs) [66]; however, its involvement in periodontal inflammation has not been reported. In the context of AD, the USF2 gene was shown to regulate the expression of genes *Dhcr24*, *Aplp2*, *Tia1*, *Pdrx1*, *Vdac1*, and *Syn2*, which drive the neuropathological mechanisms [67]. However, a study of Japanese participants found that the single nucleotide polymorphisms of the USF2 gene were not significantly related to the onset of AD [68].

Differentially expressed pathways were identified from the crosstalk gene-pathway network, and several pathways

including JAK-STAT, MAPK, NF-kappa B, and natural killer cell-mediated cytotoxicity were found as the most robust differentially expressed pathways in at least two periodontitis datasets. Overall, experimental evidence supports these as linkage mechanisms between periodontitis and AD. The activation of the JAK-STAT pathway induced by the *Porphyromonas gingivalis* lipopolysaccharide (LPS) and nicotine was shown to increase the expression of cyclooxygenase-2 (COX-2), prostaglandin E2 (PGE2), and proinflammatory cytokines in osteoblasts, thus further accelerating periodontitis progression [69, 70]. In AD, the inhibitor of the JAK-STAT pathway is reported as a therapeutic target, and

blocking this pathway can protect against neuroinflammation and dopaminergic neurodegeneration [71]. The MAPK pathway is the upstream signaling intermediate to many inflammatory cytokines such as TNF- $\alpha$ , IL-1 $\beta$ , IL-6, and prostaglandin E2 [72], and the blockage of this pathway could be beneficial for treating inflammatory diseases like chronic periodontitis and AD [73, 74]. The activation of MAPK signaling is noted to promote the production of MMPs and RANKL, leading to osteoclastogenesis and the acceleration of alveolar bone loss [73]. MAPK signaling is also implicated in multiple aspects of the neuropathology of AD, such as promoting neuroinflammation, amyloid-beta toxicity and aggregation, autophagy, and apoptosis [75]. The overexpression of NF- $\kappa$ B signaling plays a pivotal role in periodontitis-associated bone destruction by promoting the differentiation and activation of osteoclasts [76]. The blockade of NF- $\kappa$ B signaling is found to trigger detrimental neural alterations including neuroinflammation, activation of microglia, oxidative stress-related complications, and apoptosis [77]. Natural killer (NK) cells are important regulators of innate and adaptive immunity and are closely linked to the regulation of cytotoxicity [78]. Experimental data shows NK cells can directly recognize the *Fusobacterium nucleatum* pathogen, leading to alveolar bone resorption and periodontitis [79]. The overactivity of NK is also purported to play a driving role in the progression of AD by producing a series of proinflammatory cytokines [80].

The findings of this *in silico* analysis must be considered in light of the strengths and limitations of this work. By using a machine learning-based feature selection method as the core technique, the most putatively robust crosstalk genes could be identified. Furthermore, functional molecular links were also analyzed in terms of differentially expressed pathways. The integrated analysis of multiple periodontitis-related GEO datasets enabled a larger sample size for improved accuracy of our computational prediction in the present study. The major limitation of the current approach is that no experimental validation of the identified pivotal genetic molecular linkage candidates was performed. This work has multiple implications for future research. Experimental and clinical studies focused on these candidates could be valuable from the perspectives of identification of shared susceptibility, exaggerating pathogenic mechanisms, biomarkers, and therapeutic targets relevant to precision medicine and drug development or repurposing.

## 5. Conclusion

Bioinformatic analysis integrating experimental transcriptomic data from Alzheimer's disease and periodontitis revealed the most robust potentially shared molecular linkages. Six crosstalk genes, C4A, C4B, CXCL12, FCGR3A, IL1B, and MMP3, three transcription factors, FOS, MEF2C, and USF2, and several pathways, JAK-STAT, MAPK, NF- $\kappa$ B, and natural killer cell-mediated cytotoxicity, emerged as top candidate shared molecular linkage entities and merit future research in experimental and clinical studies.

## Data Availability

The data used to support the findings of this study are available from the corresponding author upon request.

## Ethical Approval

As this study only applied bioinformatic techniques based on computational analyses of publicly available datasets, therefore, this study did not require ethical approval.

## Consent

Consent for publication is not applicable in this study because no individual person's data was used.

## Conflicts of Interest

The authors declare no potential conflict of interest with respect to the authorship and publication of this paper.

## Authors' Contributions

Lei Liu (Email: law1984@126.com), Baohua Xu (Email: zrkqxbh@163.com), and Xiaofeng Huang (Email: huangxf1998@163.com) contributed equally to this work as the corresponding author. Jieqi Jin (Email: jjq007@126.com), Mengkai Guang (Email: tygmk@qq.com), and Anthony Chukwunonso Ogbuehi (Email: treasurerite@yahoo.com) contributed equally as the first author. Dirk Ziebolz (Email: dirk.ziebolz@medizin.uni-leipzig.de) and Gerhard Schmalz (Email: gerhard.schmalz@medizin.uni-leipzig.de) contributed equally as the senior author.

## References

- [1] T. L. Cerajewska, M. Davies, and N. X. West, "Periodontitis: a potential risk factor for Alzheimer's disease," *BDJ Team*, vol. 3, no. 4, p. 16062, 2016.
- [2] F. B. Teixeira, M. T. Saito, F. C. Matheus et al., "Periodontitis and Alzheimer's disease: a possible comorbidity between oral chronic inflammatory condition and neuroinflammation," *Frontiers in Aging Neuroscience*, vol. 9, p. 327, 2017.
- [3] K. Hensley, "Neuroinflammation in Alzheimer's disease: mechanisms, pathologic consequences, and potential for therapeutic manipulation," *Journal of Alzheimer's Disease*, vol. 21, no. 1, pp. 1–14, 2010.
- [4] D. F. Kinane, P. G. Stathopoulou, and P. N. Papapanou, "Periodontal diseases," *Nature Reviews. Disease Primers*, vol. 3, no. 1, p. 17038, 2017.
- [5] J. Meyle and I. Chapple, "Molecular aspects of the pathogenesis of periodontitis," *Periodontology 2000*, vol. 69, no. 1, pp. 7–17, 2015.
- [6] K. Abbayya, N. Y. Puthanakar, S. Naduwinmani, and Y. Chidambar, "Association between periodontitis and Alzheimer's disease," *North American Journal of Medical Sciences*, vol. 7, no. 6, pp. 241–246, 2015.
- [7] S. S. Dominy, C. Lynch, F. Ermini et al., "Porphyromonas gingivalis in Alzheimer's disease brains: Evidence for disease causation and treatment with small-molecule inhibitors," *Science Advances*, vol. 5, no. 1, article eaau3333, 2019.

- [8] S. K. Singhrao, A. Harding, S. Poole, L. Kesavalu, and S. Crean, "Porphyromonas gingivalis periodontal infection and its putative links with Alzheimer's disease," *Mediators of Inflammation*, vol. 2015, Article ID 137357, 10 pages, 2015.
- [9] L. M. Bekris, C.-E. Yu, T. D. Bird, and D. W. Tsuang, "Genetics of Alzheimer disease," *Journal of Geriatric Psychiatry and Neurology*, vol. 23, no. 4, pp. 213–227, 2010.
- [10] G. Kaarthikeyan and S. Meenakshi, "Genetic biomarkers in periodontal disease diagnosis," in *Periodontal Disease-Diagnose Considerations*, IntechOpen, 2019.
- [11] M. S. Tonetti, H. Greenwell, and K. S. Kornman, "Staging and grading of periodontitis: framework and proposal of a new classification and case definition," *Journal of Clinical Periodontology*, vol. 45, Supplement 20, pp. S149–S161, 2018.
- [12] M. E. Ritchie, B. Phipson, Y. H. Di Wu, C. W. Law, W. Shi, and G. K. Smyth, "limma powers differential expression analyses for RNA-sequencing and microarray studies," *Nucleic Acids Research*, vol. 43, no. 7, article e47, 2015.
- [13] S. Li, X. Chen, X. Liu et al., "Complex integrated analysis of lncRNAs-miRNAs-mRNAs in oral squamous cell carcinoma," *Oral Oncology*, vol. 73, pp. 1–9, 2017.
- [14] G. Dennis, B. T. Sherman, D. A. Hosack et al., "DAVID: database for annotation, visualization, and integrated discovery," *Genome Biology*, vol. 4, no. 9, pp. 1–11, 2003.
- [15] J. Bai, Y. Li, T. Shao et al., "Integrating analysis reveals microRNA-mediated pathway crosstalk among Crohn's disease, ulcerative colitis and colorectal cancer," *Molecular BioSystems*, vol. 10, no. 9, pp. 2317–2328, 2014.
- [16] S. Li, X. Liu, H. Li et al., "Integrated analysis of long noncoding RNA-associated competing endogenous RNA network in periodontitis," *Journal of Periodontal Research*, vol. 53, no. 4, pp. 495–505, 2018.
- [17] Y. Dong, Y. Xiao, Q. Shi, and C. Jiang, "Dysregulated lncRNA-miRNA-mRNA network reveals patient survival-associated modules and RNA binding proteins in invasive breast carcinoma," *Frontiers in Genetics*, vol. 10, p. 1284, 2020.
- [18] T. S. K. Prasad, R. Goel, K. Kandasamy et al., "Human protein reference database—2009 update," *Nucleic Acids Research*, vol. 37, Supplement 1, pp. D767–D772, 2009.
- [19] R. Oughtred, J. Rust, C. Chang et al., "The BioGRID database: a comprehensive biomedical resource of curated protein, genetic and chemical interactions," *Protein Science*, vol. 30, pp. 187–200, 2021.
- [20] I. Xenarios, D. W. Rice, L. Salwinski, M. K. Baron, E. M. Marcotte, and D. Eisenberg, "DIP: the database of interacting proteins," *Nucleic Acids Research*, vol. 28, no. 1, pp. 289–291, 2000.
- [21] A. Zanzoni, L. Montecchi-Palazzi, M. Quondam, G. Ausiello, M. Helmer-Citterich, and G. Cesareni, "MINT: a Molecular INTeraction database," *FEBS Letters*, vol. 513, no. 1, pp. 135–140, 2002.
- [22] M. J. Cowley, M. Pinese, K. S. Kassahn et al., "PINA v2. 0: mining interactome modules," *Nucleic Acids Research*, vol. 40, no. D1, pp. D862–D865, 2012.
- [23] K. Breuer, A. K. Foroushani, M. R. Laird et al., "InnateDB: systems biology of innate immunity and beyond—recent updates and continuing curation," *Nucleic Acids Research*, vol. 41, no. D1, pp. D1228–D1233, 2013.
- [24] M. J. Meyer, J. Das, X. Wang, and H. Yu, "INstruct: a database of high-quality 3D structurally resolved protein interactome networks," *Bioinformatics*, vol. 29, no. 12, pp. 1577–1579, 2013.
- [25] Y. Li, J. Xu, H. Chen et al., "Characterizing genes with distinct methylation patterns in the context of protein-protein interaction network: application to human brain tissues," *PLoS One*, vol. 8, no. 6, article e65871, 2013.
- [26] J. Piñero, À. Bravo, N. Queralt-Rosinach et al., "DisGeNET: a comprehensive platform integrating information on human disease-associated genes and variants," *Nucleic Acids Research*, vol. 45, no. D1, pp. D833–D839, 2017.
- [27] M. B. Kursa and W. R. Rudnicki, "Feature selection with the Boruta package," *Journal of Statistical Software*, vol. 36, no. 11, pp. 1–13, 2010.
- [28] H. Sanz, C. Valim, E. Vegas, J. M. Oller, and F. Reverter, "SVM-RFE: selection and visualization of the most relevant features through non-linear kernels," *BMC Bioinformatics*, vol. 19, no. 1, pp. 1–18, 2018.
- [29] L. Torgo, *Data Mining with R: Learning with Case Studies*, Chapman & Hall/CRC Data Mining and Knowledge Discovery Series, 2010.
- [30] F. Pedregosa, G. Varoquaux, A. Gramfort et al., "Scikit-learn: machine learning in Python," *The Journal of Machine Learning Research*, vol. 12, pp. 2825–2830, 2011.
- [31] M. Qiu, Q. Fu, C. Jiang, and D. Liu, "Machine learning based network analysis determined clinically relevant miRNAs in breast cancer," *Frontiers in Genetics*, vol. 11, p. 1467, 2020.
- [32] H. Han, J.-W. Cho, S. Lee et al., "TRRUST v2: an expanded reference database of human and mouse transcriptional regulatory interactions," *Nucleic Acids Research*, vol. 46, no. D1, pp. D380–D386, 2018.
- [33] H. Xu, H. Yu, K. Tu et al., "cGRNB: a web server for building combinatorial gene regulatory networks through integrated engineering of seed-matching sequence information and gene expression datasets," *BMC Systems Biology*, vol. 7, no. S2, p. S7, 2013.
- [34] L. A. Bovolenta, M. L. Acencio, and N. Lemke, "HTRIdb: an open-access database for experimentally verified human transcriptional regulation interactions," *BMC Genomics*, vol. 13, no. 1, p. 405, 2012.
- [35] F. Vafaee, J. R. Krycer, X. Ma, T. Burykin, D. E. James, and Z. Kuncic, "ORTI: an open-access repository of transcriptional interactions for interrogating mammalian gene expression data," *PLoS One*, vol. 11, no. 10, article e0164535, 2016.
- [36] E. Wingender, P. Dietze, H. Karas, and R. Knüppel, "TRANSFAC: a database on transcription factors and their DNA binding sites," *Nucleic Acids Research*, vol. 24, no. 1, pp. 238–241, 1996.
- [37] Y. Li, T. Shao, C. Jiang et al., "Construction and analysis of dynamic transcription factor regulatory networks in the progression of glioma," *Scientific Reports*, vol. 5, no. 1, pp. 1–12, 2015.
- [38] M. Seppänen, M. L. Lokki, I. L. Notkola et al., "Complement and c4 null alleles in severe chronic adult periodontitis," *Scandinavian Journal of Immunology*, vol. 65, no. 2, pp. 176–181, 2007.
- [39] D. G. Walker and P. L. McGeer, "Complement gene expression in human brain: comparison between normal and Alzheimer disease cases," *Molecular Brain Research*, vol. 14, no. 1–2, pp. 109–116, 1992.
- [40] A. M. Havens, E. Chiu, M. Taba Jr. et al., "Stromal-derived factor-1 $\alpha$  (CXCL12) levels increase in periodontal disease," *Journal of Periodontology*, vol. 79, no. 5, pp. 845–853, 2008.

- [41] A. Parachikova and C. Cotman, "Reduced CXCL12/CXCR4 results in impaired learning and is downregulated in a mouse model of Alzheimer disease," *Neurobiology of Disease*, vol. 28, no. 2, pp. 143–153, 2007.
- [42] G. G. Song and Y. H. Lee, "Associations between FCGR2A rs1801274, FCGR3A rs396991, FCGR3B NA1/NA2 polymorphisms and periodontitis: a meta-analysis," *Molecular Biology Reports*, vol. 40, no. 8, pp. 4985–4993, 2013.
- [43] J. P. Fuller, J. B. Stavenhagen, and J. L. Teeling, "New roles for Fc receptors in neurodegeneration—the impact on immunotherapy for Alzheimer's disease," *Frontiers in Neuroscience*, vol. 8, p. 235, 2014.
- [44] R. Cheng, Z. Wu, M. Li, M. Shao, and T. Hu, "Interleukin-1 $\beta$  is a potential therapeutic target for periodontitis: a narrative review," *International Journal of Oral Science*, vol. 12, no. 1, pp. 1–9, 2020.
- [45] S. L. M. Payão, G. M. Gonçalves, R. W. de Labio et al., "Association of interleukin 1 $\beta$  polymorphisms and haplotypes with Alzheimer's disease," *Journal of Neuroimmunology*, vol. 247, no. 1–2, pp. 59–62, 2012.
- [46] C. Franco, H.-R. Patricia, S. Timo, B. Claudia, and H. Marcela, "Matrix metalloproteinases as regulators of periodontal inflammation," *International Journal of Molecular Sciences*, vol. 18, no. 2, p. 440, 2017.
- [47] X.-X. Wang, M.-S. Tan, J.-T. Yu, and L. Tan, "Matrix metalloproteinases and their multiple roles in Alzheimer's disease," *BioMed Research International*, vol. 2014, Article ID 908636, 8 pages, 2014.
- [48] C. Holmes, "Review: systemic inflammation and Alzheimer's disease," *Neuropathology and Applied Neurobiology*, vol. 39, no. 1, pp. 51–68, 2013.
- [49] V. H. Perry and J. Teeling, "Microglia and macrophages of the central nervous system: the contribution of microglia priming and systemic inflammation to chronic neurodegeneration," in *Seminars in immunopathology*, Springer, 2013.
- [50] G. Ramesh, A. G. MacLean, and M. T. Philipp, "Cytokines and chemokines at the crossroads of neuroinflammation, neurodegeneration, and neuropathic pain," *Mediators of Inflammation*, vol. 2013, Article ID 480739, 20 pages, 2013.
- [51] G. Hajishengallis, T. Maekawa, T. Abe, E. Hajishengallis, and J. D. Lambris, "Complement involvement in periodontitis: molecular mechanisms and rational therapeutic approaches," *Immune Responses to Biosurfaces*, vol. 865, pp. 57–74, 2015.
- [52] E. V. Clarke and A. J. Tenner, "Complement modulation of T cell immune responses during homeostasis and disease," *Journal of Leukocyte Biology*, vol. 96, no. 5, pp. 745–756, 2014.
- [53] K. W.-h, W. van der Touw, and P. S. Heeger, "Complement regulation of T cell immunity," *Immunologic Research*, vol. 54, no. 1–3, pp. 247–253, 2012.
- [54] A. Guyon, "CXCL12 chemokine and its receptors as major players in the interactions between immune and nervous systems," *Frontiers in Cellular Neuroscience*, vol. 8, p. 65, 2014.
- [55] R. Ransohoff, "The chemokine system in neuroinflammation: an update," *The Journal of Infectious Diseases*, vol. 186, Supplement 2, pp. S152–S156, 2002.
- [56] W. H. Yeap, K. L. Wong, N. Shimasaki et al., "CD16 is indispensable for antibody-dependent cellular cytotoxicity by human monocytes," *Scientific Reports*, vol. 6, no. 1, p. 34310, 2016.
- [57] S. Solerte, M. Fioravanti, A. Pascale, E. Ferrari, S. Govoni, and F. Battaini, "Increased natural killer cell cytotoxicity in Alzheimer's disease may involve protein kinase C dysregulation," *Neurobiology of Aging*, vol. 19, no. 3, pp. 191–199, 1998.
- [58] S. S. Shafiq, W. S. T. Griffin, and M. K. O'Banion, "The role of interleukin-1 in neuroinflammation and Alzheimer disease: an evolving perspective," *Journal of Neuroinflammation*, vol. 5, no. 1, pp. 1–12, 2008.
- [59] E. M. Kim and O. Hwang, "Role of matrix metalloproteinase-3 in neurodegeneration," *Journal of Neurochemistry*, vol. 116, no. 1, pp. 22–32, 2011.
- [60] A. Trabandt, R. Gay, V. Sukhatme, and S. Gay, "Expression of collagenase and potential transcriptional factors c-fos and egr-1 in periodontal gingival fibroblasts," *Journal of Oral Pathology & Medicine*, vol. 21, no. 5, pp. 232–240, 1992.
- [61] D. L. Marcus, J. A. Strafaci, D. C. Miller et al., "Quantitative neuronal c-fos and c-jun expression in Alzheimer's disease," *Neurobiology of Aging*, vol. 19, no. 5, pp. 393–400, 1998.
- [62] G. Sun, T. Jiang, P. Xie, and J. Lan, "Identification of the disease-associated genes in periodontitis using the co-expression network," *Molecular Biology*, vol. 50, no. 1, pp. 124–131, 2016.
- [63] S. L. Rosenthal and M. I. Kamboh, "Late-onset Alzheimer's disease genes and the potentially implicated pathways," *Current Genetic Medicine Reports*, vol. 2, no. 2, pp. 85–101, 2014.
- [64] J.-C. Lambert, European Alzheimer's Disease Initiative (EADI), C. A. Ibrahim-Verbaas et al., "Meta-analysis of 74,046 individuals identifies 11 new susceptibility loci for Alzheimer's disease," *Nature Genetics*, vol. 45, no. 12, pp. 1452–1458, 2013.
- [65] A. Deczkowska, O. Matcovitch-Natan, A. Tsitsou-Kampeli et al., "Mef2C restrains microglial inflammatory response and is lost in brain ageing in an IFN- $\gamma$ -dependent manner," *Nature Communications*, vol. 8, no. 1, pp. 1–13, 2017.
- [66] F. Liu, X. Wang, B. Zheng, D. Li, and C. Chen, "USF2 enhances the osteogenic differentiation of PDLs by promoting ATF4 transcriptional activities," *Journal of Periodontal Research*, vol. 55, no. 1, pp. 68–76, 2020.
- [67] G. K. Acquah-Mensah and R. C. Taylor, "Brain in situ hybridization maps as a source for reverse-engineering transcriptional regulatory networks: Alzheimer's disease insights," *Gene*, vol. 586, no. 1, pp. 77–86, 2016.
- [68] N. Shibata, T. Ohnuma, S. Higashi et al., "Genetic association between USF 1 and USF 2 gene polymorphisms and Japanese Alzheimer's disease," *The Journals of Gerontology Series A: Biological Sciences and Medical Sciences*, vol. 61, no. 7, pp. 660–662, 2006.
- [69] H. Y.-k and I. S. Lee, "JAK/STAT pathway modulates on Porphyromonas gingivalis lipopolysaccharide- and nicotine-induced inflammation in osteoblasts," *Journal of Dental Hygiene Science*, vol. 17, no. 1, pp. 81–86, 2017.
- [70] W. Wei, X. Xiao, J. Li et al., "Activation of the STAT1 pathway accelerates periodontitis in Nos3 $^{-/-}$  mice," *Journal of Dental Research*, vol. 98, no. 9, pp. 1027–1036, 2019.
- [71] H. Qin, J. A. Buckley, X. Li et al., "Inhibition of the JAK/STAT pathway protects against  $\alpha$ -synuclein-induced neuroinflammation and dopaminergic neurodegeneration," *Journal of Neuroscience*, vol. 36, no. 18, pp. 5144–5159, 2016.
- [72] H. Chi, S. P. Barry, R. J. Roth et al., "Dynamic regulation of pro- and anti-inflammatory cytokines by MAPK phosphatase 1 (MKP-1) in innate immune responses," *Proceedings of the National Academy of Sciences*, vol. 103, no. 7, pp. 2274–2279, 2006.



- [73] K. L. Kirkwood and C. Rossa Jr., "The potential of p38 MAPK inhibitors to modulate periodontal infections," *Current Drug Metabolism*, vol. 10, no. 1, pp. 55–67, 2009.
- [74] L. Munoz and A. J. Ammit, "Targeting p38 MAPK pathway for the treatment of Alzheimer's disease," *Neuropharmacology*, vol. 58, no. 3, pp. 561–568, 2010.
- [75] G. Kheiri, M. Dolatshahi, F. Rahmani, and N. Rezaei, "Role of p38/MAPKs in Alzheimer's disease: implications for amyloid beta toxicity targeted therapy," *Reviews in the Neurosciences*, vol. 30, no. 1, pp. 9–30, 2018.
- [76] R. Ambili and P. Janam, "A critique on nuclear factor-kappa B and signal transducer and activator of transcription 3: the key transcription factors in periodontal pathogenesis," *Journal of Indian Society of Periodontology*, vol. 21, no. 5, pp. 350–356, 2017.
- [77] N. K. Jha, S. K. Jha, R. Kar, P. Nand, K. Swati, and V. K. Goswami, "Nuclear factor-kappa  $\beta$  as a therapeutic target for Alzheimer's disease," *Journal of Neurochemistry*, vol. 150, no. 2, pp. 113–137, 2019.
- [78] L. Parisi, B. Bassani, M. Tremolati, E. Gini, G. Farronato, and A. Bruno, "Natural killer cells in the orchestration of chronic inflammatory diseases," *Journal of Immunology Research*, vol. 2017, Article ID 4218254, 13 pages, 2017.
- [79] S. Chaushu, A. Wilensky, C. Gur et al., "Direct recognition of *Fusobacterium nucleatum* by the NK cell natural cytotoxicity receptor NKp46 aggravates periodontal disease," *PLoS Pathogens*, vol. 8, no. 3, article e1002601, 2012.
- [80] F. Jadidi-Niaragh, H. Shegarfi, F. Naddafi, and A. Mirshafiey, "The role of natural killer cells in Alzheimer's disease," *Scandinavian Journal of Immunology*, vol. 76, no. 5, pp. 451–456, 2012.

## Retraction

# Retracted: Clinical Efficacy and Safety of “Three-Dimensional Balanced Manipulation” in the Treatment of Cervical Spondylotic Radiculopathy by Finite Element Analysis

### BioMed Research International

Received 12 March 2024; Accepted 12 March 2024; Published 20 March 2024

Copyright © 2024 BioMed Research International. This is an open access article distributed under the Creative Commons Attribution License, which permits unrestricted use, distribution, and reproduction in any medium, provided the original work is properly cited.

This article has been retracted by Hindawi following an investigation undertaken by the publisher [1]. This investigation has uncovered evidence of one or more of the following indicators of systematic manipulation of the publication process:

- (1) Discrepancies in scope
- (2) Discrepancies in the description of the research reported
- (3) Discrepancies between the availability of data and the research described
- (4) Inappropriate citations
- (5) Incoherent, meaningless and/or irrelevant content included in the article
- (6) Manipulated or compromised peer review

The presence of these indicators undermines our confidence in the integrity of the article’s content and we cannot, therefore, vouch for its reliability. Please note that this notice is intended solely to alert readers that the content of this article is unreliable. We have not investigated whether authors were aware of or involved in the systematic manipulation of the publication process.

Wiley and Hindawi regrets that the usual quality checks did not identify these issues before publication and have since put additional measures in place to safeguard research integrity.

We wish to credit our own Research Integrity and Research Publishing teams and anonymous and named

external researchers and research integrity experts for contributing to this investigation.

The corresponding author, as the representative of all authors, has been given the opportunity to register their agreement or disagreement to this retraction. We have kept a record of any response received.

### References

- [1] S. Cao, Y. Chen, F. Zhang et al., “Clinical Efficacy and Safety of “Three-Dimensional Balanced Manipulation” in the Treatment of Cervical Spondylotic Radiculopathy by Finite Element Analysis,” *BioMed Research International*, vol. 2021, Article ID 5563296, 8 pages, 2021.

## Research Article

# Clinical Efficacy and Safety of “Three-Dimensional Balanced Manipulation” in the Treatment of Cervical Spondylotic Radiculopathy by Finite Element Analysis

Shengnan Cao,<sup>1</sup> Yuanzhen Chen,<sup>2</sup> Feng Zhang,<sup>2</sup> Shifei Sun,<sup>2</sup> Congan Wang,<sup>2</sup> Guangjian Hou,<sup>2</sup> Dandan Wang ,<sup>2</sup> Guodong Sun ,<sup>3,4</sup> and Bin Shi <sup>1,2</sup>

<sup>1</sup>School of Acupuncture-Tuina, Shandong University of Traditional Chinese Medicine, Jinan 250014, China

<sup>2</sup>Bone Biomechanics Engineering Laboratory of Shandong Province, Neck-Shoulder and Lumbocrural Pain Hospital of Shandong First Medical University, Jinan 250062, China

<sup>3</sup>School of Precision Instrument and Optoelectronics Engineering, Institute of Medical Engineering and Translational Medicine, Tianjin University, Tianjin 300072, China

<sup>4</sup>Department of Rehabilitation Medicine, The Third Affiliated Hospital of Shandong First Medical University, Jinan 250031, China

Correspondence should be addressed to Dandan Wang; 158wdd@163.com, Guodong Sun; 317060920@qq.com, and Bin Shi; sdyky-shibin@163.com

Received 6 February 2021; Revised 6 March 2021; Accepted 10 March 2021; Published 1 April 2021

Academic Editor: Yuzhen Xu

Copyright © 2021 Shengnan Cao et al. This is an open access article distributed under the Creative Commons Attribution License, which permits unrestricted use, distribution, and reproduction in any medium, provided the original work is properly cited.

Cervical spondylotic radiculopathy (CSR) is the most commonly encountered cervical spine disorder. Cervical manipulation has been demonstrated as an effective therapy for patients. However, the mechanisms of manipulations have not been elucidated. A total of 120 cervical spondylotic radiculopathy patients were divided into the “three-dimensional balanced manipulation” treatment group (TBM group) and control group randomly. The control group was treated with traditional massage; the TBM treatment group was treated with “three-dimensional balanced manipulation” based on traditional massage. The symptoms and clinical efficacy of the patients were compared before and after treatment for one month. A three-dimensional finite element model was established. The mechanical parameters were imported to simulate TBM, and finite element analysis was performed. The results showed that the total effective rate was significantly higher in the TBM group compared with the control group. The biomechanical analysis showed the vertebral body stress was mainly distributed in the C3/4 spinous processes; the deformation mainly concentrated in the anterior processes of the C3 vertebral body. The intervertebral disc stress in the C3~C7 segment was mainly distributed in the anterior part of the C3/4 intervertebral disc, and the deformation extends to the posterior part of the C3/4 nucleus pulposus. In summary, these data are suggesting that TBM was effective in CSR treatment. The results of the finite element model and biomechanical analysis provide an important foundation for effectively avoiding iatrogenic injuries and improving the effect of TBM in the treatment of CSR patients.

## 1. Introduction

Cervical spondylotic radiculopathy (CSR) is the most commonly encountered cervical spine disorder among middle-aged and elderly people, accounting for 60% to 70% of cervical spondylosis cases in China [1]. Conservative therapy and surgical interventions are the most common treatment strategies for CSR. Manipulation therapy is considered an efficacious and cost-effective approach for the

management of CSR [2], which has the effect of releasing adhesions, relieving muscle spasms, and correcting the joint dislocation in the treatment of CSR and has been widely used in the clinic for treating CSR patients [3]. Based on traditional rotatory manipulation and comprehensive consideration of cervical anatomy, physiology, and biomechanics, we developed a manipulation therapy named “three-dimensional balanced manipulation” (TBM) and widely used this TBM in the treatment of CSR patients [4]. The most

prominent feature of TBM is to decompose the core operations of rotary thrust into a fixed rotary position, the forward thrust of the operator, the instantaneous rotational force, and the upward thrust of the operator.

During the treatment of manipulation, the stress distribution in different parts of the cervical spine is critical to the safety of the manipulation. If the stress exceeds the normal range, the manipulation may damage the articular process joints, resulting in excessive protrusion of the intervertebral disc. However, the biomechanical mechanism of manipulation therapy for the treatment of conditions involving the cervical vertebra has not yet been elucidated. This is because that there is a scarcity of specimens for in vitro investigations and the distribution of and changes in stress within the cervical vertebrae cannot be measured by traditional experimental methods [5]. Therefore, a new detection method is urgently needed.

Finite element analysis (FEA) has been used to investigate the biomechanics of the cervical spine [6, 7]. It can provide information about stress distribution, deformation, and strain on any part of the cervical vertebrae during simulated manipulations, containing flexion, extension, and torsion [8]. Recently, different finite element models (FEM) of the cervical spine were constructed to investigate the biomechanics of the cervical spine or intervertebral disc [9–11]. However, few studies have established a FEM based on CSR, and few studies have performed biomechanical analysis of stress distribution, deformation of the model when imitating manipulation therapy.

This study was aimed to determine the effectiveness of TBM on CSR, and FEA was used to study the stress distribution and changes in the cervical spine during TBM treatment to investigate the safety and effectiveness of the TBM. The results will provide important support for the clinical efficacy and safety of TBM in the treatment of CSR.

## 2. Methods

**2.1. CSR Patients.** This study was officially approved by the Ethics Committee of Shandong Academy of Medical Sciences. Written consent was obtained from each patient for participation in the study. A total of 122 CSR patients were selected from January 2019 to March 2020 from the Neck-Shoulder and Lumbocurral Pain Hospital of Shandong First Medical University. The patients were divided into the TBM treatment and control groups by using the random number table method according to the order of treatment.

**2.2. Treatment.** The control group was treated with traditional massage, and the TBM treatment group was treated with TBM based on traditional massage. Manipulative treatment included adjustment of the left and right sides.

TBM treatment: consider a C4/5 left lesion and the C5 spinous process with a relatively left displacement as an example. The patient was in a sitting position. An assistant physician fixed the patient's lower limbs. The doctor held the left thumb to the right side of the C5 spinous process, and the other four fingers reached the occiput. The patient

was advised to relax, the neck flexing  $10^{\circ}\sim 20^{\circ}$  with the jaw placed on the right elbow of the doctor. The doctor slowly pulled the patient's neck with light force for about 1~2 min and, then, slowly rotated the patient's head and neck to the right until a resistance was encountered. At this point, the doctor forced the patient's head and neck to the right side with the right elbow and pushed the C5 spinous process to the left with the left thumb, with a reset of C5 spinous process or an audible cracking sound during manipulation. The same manipulation was used to reverse adjust the C4 spinous process. The patient placed on the back for clinical observation for 20 min. The patient received TBM treatment once every other day and 10 treatments constituted a course and follow-up after 1 month.

Traditional massage: the patient was in a sitting position. The doctor pressed and kneaded the patient's acupoints of Tianzong (SI11), Dazhui (GV14), Fengfu (GV16), and Fengchi (GB20), with his/her thumb, each for 5 min. Massage therapy was performed once every other day, and 10 treatments constituted a course, and follow up after 1 month.

**2.3. Efficacy Evaluation.** Clinical efficacy was evaluated based on the Visual Analogue Scale (VAS) and clinical efficacy standard against CSR according to "Diagnostic and Efficacy Criteria for TCM Disorders" promulgated by National Chinese Medicine in 1994.

Visual Analogue Scale (VAS): the VAS table was supervised by the Chinese Medical Association Pain Society. Patients marked the points on the back of the ruler according to their sense of pain. The VAS score was determined by the centimeters from the left end of the ruler to the point marked by the patient. VAS scores ranging from 0 to 10 were defined as follows: 0 (indicated a lack of pain, 0 cm), 1~3 (mild pain and do not affect work and life, 1~3 cm), 4~6 (moderate pain affecting work but not life, 4~6 cm), and 7~10 (severe pain affecting work and life, 7~10 cm).

Evaluation of clinical efficacy: the condition was considered to have been cured if the original discomfort disappeared, normal muscle strength was gained, the function of the neck and affected limbs recovered, and if the patient could participate in laborious activities and work normally. The patient was considered to show an improvement if the original symptoms obviously resolved, neck and shoulder pain disappeared, and limb function obviously improved. The treatment was considered ineffective if the symptoms and signs did not show any improvement. The calculation of cure rate: cure number/total number  $\times 100\%$ ; the calculation of total efficiency rate: (cure number + improvement number)/total number  $\times 100\%$ .

**2.4. C3~C7 FEM Establish and Loading Conditions.** FEM was reconstructed based on axial Computed Tomography (CT) images of a 39-year-old male CSR patient; the data were recorded and stored in the Digital Imaging and Communications in Medicine (DICOM) format. A three-dimensional FE model of the C3~C7 segments of the CSR was extracted and established using the Mimics 20.0 (Materialise, Inc., Leuven, Belgium) software. The model was further optimized using

tools such as Grid Editing in the Geomagic Studio 2015 (Raindrop Geomagic, Inc., Morrisville, NC) software to obtain a high-quality, curved, smooth solid model similar to the cervical vertebrae of patients with actual radiculopathy. The abovesaved entity model was imported into the ANSYS Workbench 18.1 (ANSYS, Inc. Pennsylvania, America) software, and the ligament was created by the geometry concept modeling function. The ligament start and end points and cross-sectional area were determined according to published literature [12–15]. The cervical vertebrae consisting of cortical and cancellous bones were simulated using Solid187 solid element. The CPT217 void pressure unit was used to simulate the intervertebral disc (nucleus pulposus and annulus fibrosus). The five ligaments were simulated by a nonlinear spring and connected to the relevant nodes. The facet joint was considered to be a nonlinear three-dimensional contact, modeled by a face-to-surface contact element with a coefficient of friction of 0.1. The mechanical properties of the isotropic elastic biomaterials in this study were assumed to be homogeneous and continuous. When force was applied, the cut surfaces of the model did not slide against each other, and each unit had sufficient stability.

The boundary conditions and loading conditions were set as follows: constrained the lower surface of the C7 vertebral body, and all nodes on the lower surface were completely fixed. The uppermost C3 was free from any constraints and accepted the load vector. A compressive load was applied to the superior part of the model to represent the head weight. Other types of loading, including tension, compression, lateral bending, and axial rotation, can be applied on the superior part of the uppermost vertebra body. To validate the movement and flexibility of the model, by setting the boundary and loading conditions, the flexion and extension, and rotation of the cervical spine in physiological conditions were simulated, and the motion angle were recorded and compared with the research results [10] to verify the mobility of the C3~C7 three-dimensional FEM.

**2.5. Simulation of TBM.** Consider a C4/5 left lesion and the C5 spinous process with a relative left displacement as an example. The present study simulated the left lateral lesion of C4/5 and TBM of the C5 spinous process with a relatively left displacement. For TBM in the sitting position, the patient sat upright, and the bottom of the C7 vertebral body and the joint surface of the inferior articular process were fixed with fixed support constraint. A 5kg downward force was applied to the upper surface of the C3 vertebral body. Then, TBM was slightly lifted and vertical traction force of 4.2kg was applied to the top of the C3 vertebral body. The C5 spinous process was slowly rotated with 20° flexion and 1.0N.m torque.

**2.6. Statistical Analysis.** Statistical analyses were performed with the Statistical Package for the Social Sciences, version 24.0 (SPSS Inc., Chicago, IL, USA). Clinical efficacy was analyzed using the  $\chi^2$  test. The two-tailed unpaired Student's *t*-test was used to assess differences in VAS between different groups. A paired *t*-test was used to analyze intragroup differences. All data were described as mean  $\pm$  standard deviation

( $\bar{x} \pm S$ ) values, and a two-sided *P* value of less than 0.05 considered to be statistically significant.

### 3. Results

**3.1. The Efficacy of TBM in the Treatment of CSR Patients.** In a comparison of the changes in symptoms and signs before and after treatment in the control and TBM groups, the VAS scores in the two groups were obtained before treatment ( $P > 0.05$ ). After one course of treatment, the VAS scores in the two groups after treatment were significantly lower than those before treatment ( $P < 0.01$ ), and the VAS score in the TBM group was significantly lower than that in the control group ( $P < 0.01$ , Figure 1(a)) after treatment. The findings of clinical evaluation of CSR patients were statistically analyzed. The cure rate in the TBM group was significantly higher than that in the control group (50.00% and 33.33%, respectively,  $P < 0.05$ ). The total effectiveness rate in the TBM group was significantly higher than that in the control group (95.00% vs. 76.67%,  $P < 0.05$ , Figure 1(b)).

**3.2. Stress Distribution of the C3~C7 Vertebral Body.** The TBM in the sitting position was decomposed and simulated. When the model was loaded with a downward force of head gravity, the stress was mainly concentrated at the vertebral body and the articular process (Figure 2(a)). As the upward traction increased, the stress was mainly concentrated at the C4 spinous process and articular process, C5 vertebral arch, spinous process and articular process, C7 transverse process, and articular process (Figure 2(b)). When a 1.0-N.m rotating torque of 20° left anterior was loaded on the model, the stress distribution of the C5 spinous process gradually increased and extended to the posterior part of the spinous process and the vertebral arch. When the combined force reached the maximum level, the stress on the C3~C7 vertebral body reached the maximum value of 17.781 MPa. Stress was concentrated at the C3~C4 spinous processes, anterior region of the C5 spinous process, spinous process root, vertebral arch, and the combination of the C6~C7 joints (Figure 2(c)).

Deformation of the vertebral body corresponded to the stress distribution. When the model was loaded with a downward force of head gravity, the vertebral deformation showed that the maximum displacement was located at the front end of the C3 vertebral body and the transverse process and was gradually distributed around the posterior vertebral body, the vertebral arch, and the superior articular process (Figure 2(d)). As the upward traction increased, the model was in tension and the displacement was gradually reduced. The maximum displacement of the whole model was located at the front of the C3 transverse process and the upper articular process (Figure 2(e)). When the model was loaded with a rotating torque of 20° left anterior, the C3 to C7 segments also showed a rotation displacement. The displacement of the model was mainly concentrated at the C3~C4 segments, and the maximum displacement was located at the front of the articular process and transverse process of C3. In



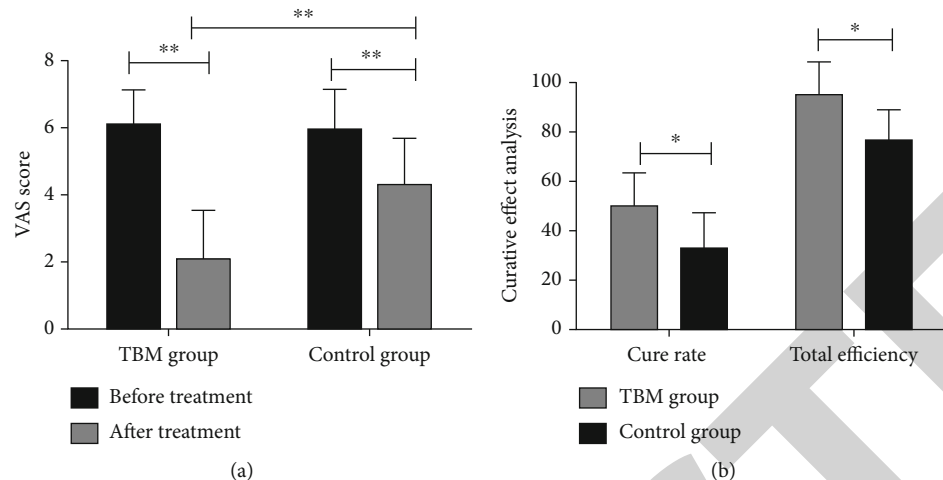


FIGURE 1: “Three-dimensional balanced manipulation” was effective in treating cervical spondylotic radiculopathy. (a) Visual Analogue Scale of “three-dimensional balanced manipulation” group and control group before and after treatment. (b) The clinical efficiency and total effective rate in “three-dimensional balanced manipulation” group and control group. \* $P < 0.05$ , \*\* $P < 0.01$ .

addition, the superior articular process and transverse process of C4 and the C5 superior articular process showed slight displacement (Figure 2(f)).

**3.3. Biomechanical Analysis of Intervertebral Disc of C3~C7.** When the model was loaded with a downward force of head gravity, the compressive stress mainly accumulated around the periphery of the nucleus pulposus (Figure 3(a)). When an upward traction was applied to the model, the C3 vertebral body was gradually pulled upward, and the tensile stress was mainly concentrated at the C4/5, C5/6 intervertebral disc (Figure 3(b)). When the rotational torque was loaded on the model, the changes in compressive stress were mainly concentrated at the nucleus pulposus of C4/5 with a value of 30.429 MPa, the anterior disc of C3/4, the nucleus of C5/6, and the posterior part of the C6/7 disc (Figure 3(c)).

Deformation analysis of the intervertebral discs showed that the compression displacement was mainly at the front end of the C3/4 intervertebral disc and the anterior half of the nucleus pulposus with a decreasing distribution to the posterior half (Figure 3(d)). As upward traction was applied to the C3 vertebral body, and the displacement decreased gradually as the tension increased. The stress was concentrated mainly at the anterior part of the annulus fibrosus and nucleus pulposus (Figure 3(e)). With a 1.0-N.m rotational torque loaded on the model, the displacement of the four intervertebral discs increased, and the displacement of the C3/4 intervertebral disc was the largest. The displacement extended to the middle and posterior parts of the C3/4 nucleus pulposus. The displacement of the nucleus pulposus and the anterior disc of the C4/5, C5/6 gradually expanded (Figure 3(f)).

#### 4. Discussion

Currently, in the absence of myelopathy or obvious muscle weakness, patients with cervical radicular pain should be

treated conservatively [16]. Complementary and alternative medicine interventions for CSR patients have shown a tendency to improve the associated symptoms and clinical signs [17]. Neck pain may be caused by the compression of the lesser and greater occipital nerves by posterior cervical muscles and their fascial attachments at the occipital ridge with subsequent local perineural inflammation. Traditional Chinese manipulation therapy is a frequently applied complementary and alternative medicine intervention to relieve the symptoms of CSR due to its immediate effects on pain and the absence of toxic and side effects [18].

A previous study proposed a TBM based on the traditional rotatory manipulation with comprehensive consideration of cervical anatomy, physiology, and biomechanics [19]. Another study revealed that TBM can relieve muscle spasm, adjusting the relationship between abnormal spine and bone, correcting spinal dislocation, and restoring the biomechanical balance of the spine [20]. In the present study, the clinical efficacy analysis of 120 CSR patients revealed that the cure rate and total effectiveness rate in the TBM group were significantly higher than those in the control group. None of the patients showed adverse reactions during treatment. In the study by Yang et al., the therapeutic effectiveness and safety of balance chiropractic therapy for CSR were investigated [17, 21]. These studies, together with ours, suggest that manipulation therapy has become a widely applied conservative intervention to relieve the symptoms of CSR.

In the present study, despite the widespread use of TBM in clinical practice, little is known about the biomechanical characteristics of TBM. Therefore, the FE analysis was used as a noninvasive approach to investigate stress distribution and displacement in CSR during simulated TBM, which has seldom been reported. Findings from our study would impart useful insight for the spinal manipulators and help to further understand the clinical efficacy of TBM.

A traditional viewpoint holds that decreasing of intradiscal pressure is thought to be helpful for prolapsed discs

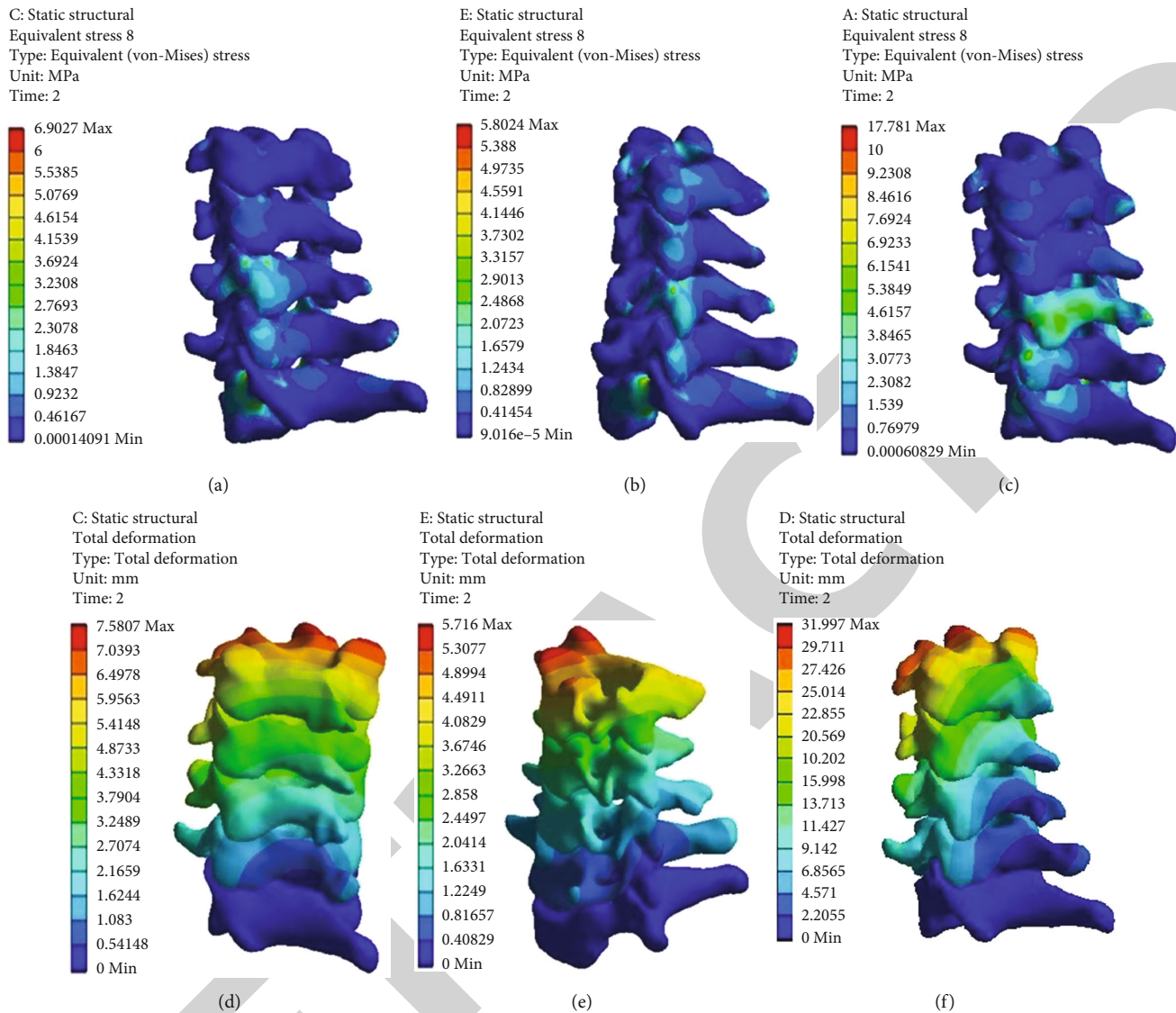


FIGURE 2: Biomechanical analysis of the C3~C7 segment vertebral body in the process of “three-dimensional balanced manipulation.” (a) Stress distribution when the model was only loaded with a downward force of head gravity. (b) Stress distribution during head loading and upward traction. (c) Side view of the stress distribution of the vertebral body during the complete manipulation. (d) The overall model deformation distribution diagram when only the head gravity is loaded. (e) Distribution map of overall deformation when loading head and upward traction. (f) Side view of the distribution of vertebral body deformation under complete manipulation. (a–c) The color represents stress variety, red represents maximum stress, blue represents minimum stress, and from red to blue represents decreasing stress. (d–f) The color represents deformation variety, red represents maximum deformation, blue represents minimum deformation, and from red to blue means represents decreasing deformation.

reabsorption, and intradiscal pressure can be reduced through spinal manipulation [21]. This opinion indicates that spinal manipulation, or TBM, might play a role in reducing intradiscal pressure for treating CSR. In the present study, when the manipulative force was completely loaded on the model, the deformation and displacement extended to the middle and posterior parts of the C3/4 nucleus pulposus, the periphery of the nucleus pulposus of C4/5 and C5/6, and the anterior part of the cervical disc. Since we found that TBM could increase vertebral body and intervertebral disc displacement in a FEM, which may be beneficial for increasing the intervertebral space, expanding the intervertebral foramen, relieving the mechanical compression of the nerve

roots by the upper and lower articular processes, and relieving the nerve root compression and stimulating symptoms. This suggested that the clinical efficacy of TBM was associated with the relative displacement between the intervertebral disc and the adjacent nerve root. These mechanisms of clinical efficacy of TBM in the treatment of CSR need to be further investigated in future studies.

When the rotational torque was loaded on the model, the maximum von Mises stress value increased to 17.781 MPa in the anterior region of the C5 spinous process, and the intervertebral disc of C4/5 with a value of 30.429 MPa. It is far less than the initial stress of vertebral fractures [22]. Therefore, the TBM used in the treatment with CSR is within the safe range and

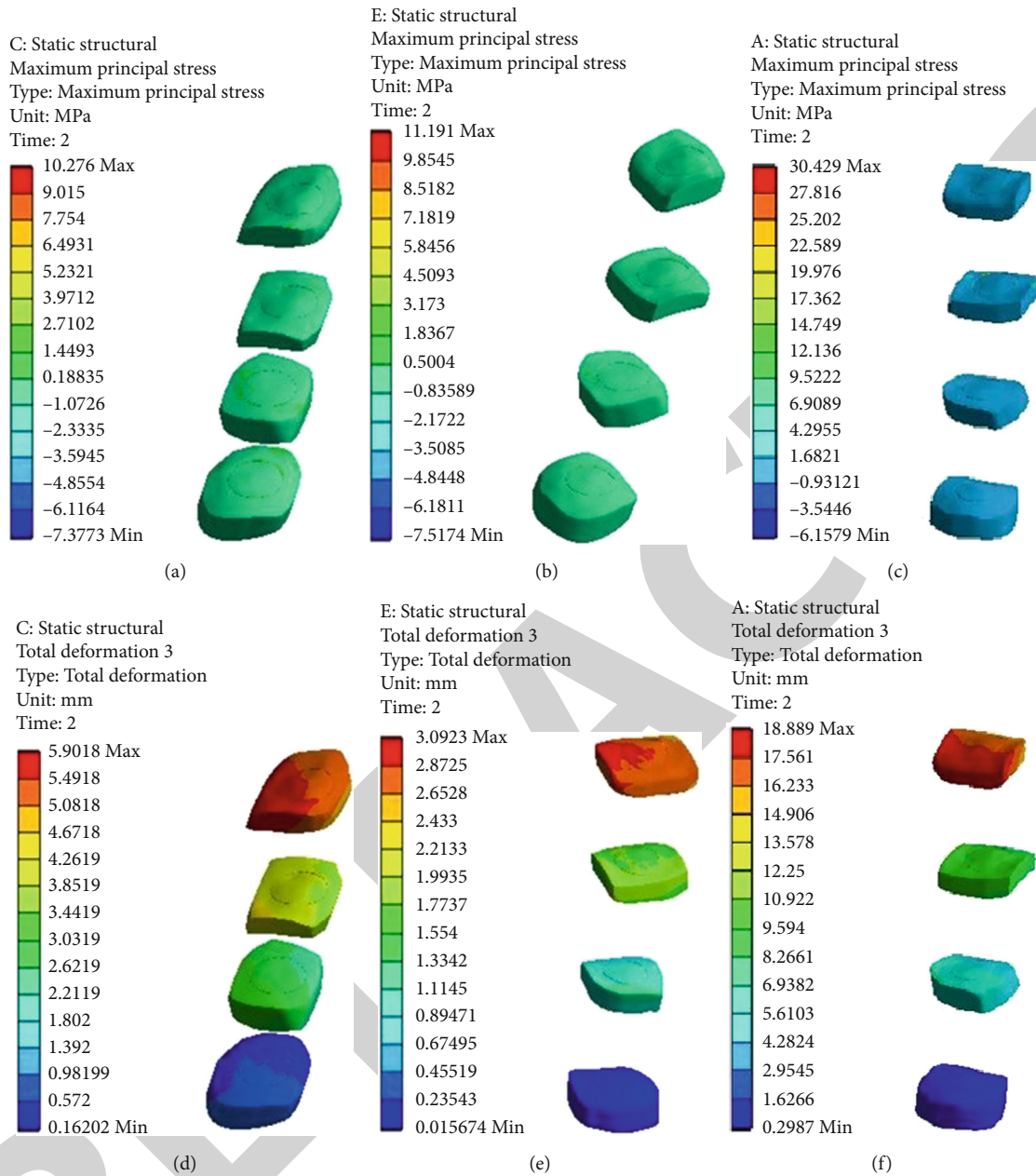


FIGURE 3: Biomechanical analysis of the intervertebral disc in C3~C7 segments during the process of “three-dimensional balanced manipulation.” (a) Stress distribution when the model was only loaded with a downward force of head gravity. (b) Stress distribution during head loading and upward traction. (c) Side view of the stress distribution of the vertebral body during the complete manipulation. (d) Distribution map of the overall intervertebral disc deformation when only the head gravity is loaded. (e) Distribution of the overall disc deformation when the head is loaded and upward traction. (f) Deformation distribution of intervertebral disc under complete manipulation. (a–c) The color represents stress variety, red represents maximum stress, blue represents minimum stress, and from red to blue represents decreasing stress. (d–f) The color represents deformation variety, red represents maximum deformation, blue represents minimum deformation, and from red to blue represents decreasing deformation.

will not cause normal cervical vertebrae, pedicles, spinous processes, facet joints, and other bone structural damage. The FEA results provide an important foundation for effectively avoiding iatrogenic injuries of TBM in the treatment of CSR.

The present study has several limitations. Although the experimental analysis approximated the clinical condition, the FEM of this study selected young people and the C4/5 segment. Future studies will expand the sample size for

patients of different ages and study the FEA of multisegment and multiage groups.

## 5. Conclusion

The present study found that TBM was effective in the treatment of CSR patients. The FE model and biomechanical analysis of the C3~C7 cervical segment revealed the stress



distribution and displacement of each part during TBM treatment. Our results clarify the stress distribution of different parts of the vertebral body and intervertebral disc during the manipulation process, which provide an important foundation for effectively avoiding iatrogenic injuries and improving the clinical efficacy of TBM in the treatment of CSR. Our study provides a new strategy for complementary and alternative medicine treatment of CSR. The findings of our study would further the understanding of the biomechanical characteristics and clinical efficacy of TBM in the treatment of CSR.

### Data Availability

The data used to support the findings of this study are available from the corresponding author upon request.

### Conflicts of Interest

All authors declare that they have no conflicts of interest.

### Authors' Contributions

All authors had access to the data and a role in writing the manuscript. All authors read and approved the final manuscript. Shengnan Cao and Yuanzhen Chen contributed equally to this work.

### Acknowledgments

This study was supported by the Natural Science Foundation of Shandong Province (grant number ZR2018LH019 and ZR2019MH134), Academic Promotion Project of Shandong First Medical University (grant number 2019QL003), Central government guides local science and technology development fund projects (grant number YDZX20203700002055), and TCM Technology Development Project of Shandong Province (grant number 2019-0543 and 2019-0545).

### References

- [1] X. Wei, S. Wang, L. Li, and L. Zhu, "Clinical evidence of Chinese massage therapy (Tui Na) for cervical radiculopathy: a systematic review and meta-analysis," *Evidence-based Complementary and Alternative Medicine*, vol. 2017, Article ID 9519285, 10 pages, 2017.
- [2] L. Zhu, X. Wei, and S. Wang, "Does cervical spine manipulation reduce pain in people with degenerative cervical radiculopathy? A systematic review of the evidence, and a meta-analysis," *Clinical Rehabilitation*, vol. 30, pp. 145–155, 2015.
- [3] F. Yang, W. X. Li, Z. Liu, and L. Liu, "Balance chiropractic therapy for cervical spondylotic radiculopathy: study protocol for a randomized controlled trial," *Trials*, vol. 17, no. 1, p. 513, 2016.
- [4] G. Sun, B. Shi, D. Wang, J. Wang, and H. Xu, "Application analysis of gesture motion capture technology and finite element analysis in the study of the mechanism of three-dimensional orthopedic manipulation of cervical spondylotic radiculopathy," *Sichuan Medicine*, vol. 39, pp. 223–225, 2018.
- [5] L. Li, T. Shen, and Y. K. Li, "A finite element analysis of stress distribution and disk displacement in response to lumbar rotation manipulation in the sitting and side-lying positions," *Journal of Manipulative and Physiological Therapeutics*, vol. 40, no. 8, pp. 580–586, 2017.
- [6] I. Zafarparandeh, D. U. Erbulut, I. Lazoglu, and A. F. Ozer, "Development of a finite element model of the human cervical spine," *Turkish Neurosurgery*, vol. 24, no. 3, pp. 312–318, 2014.
- [7] L. Fiorillo, M. Ciccù, C. D'Amico, R. Mauceri, G. Oteri, and G. Cervino, "Finite element method and Von Mises investigation on bone response to dynamic stress with a novel conical dental implant connection," *BioMed Research International*, vol. 2020, Article ID 2976067, 13 pages, 2020.
- [8] Y. Chen, E. Dall Ara, E. Sales et al., "Micro-CT based finite element models of cancellous bone predict accurately displacement once the boundary condition is well replicated: a validation study," *Journal of the Mechanical Behavior of Biomedical Materials*, vol. 65, pp. 644–651, 2017.
- [9] Z. Deng, K. Wang, H. Wang, T. Lan, H. Zhan, and W. Niu, "A finite element study of traditional Chinese cervical manipulation," *European Spine Journal*, vol. 26, no. 9, pp. 2308–2317, 2017.
- [10] K. Wang, H. Wang, Z. Deng, Z. Li, H. Zhan, and W. Niu, "Cervical traction therapy with and without neck support: a finite element analysis," *Musculoskeletal Science & Practice*, vol. 28, pp. 1–9, 2017.
- [11] X. D. Wang, M. S. Feng, and Y. C. Hu, "Establishment and finite element analysis of a three-dimensional dynamic model of upper cervical spine instability," *Orthopaedic Surgery*, vol. 11, no. 3, pp. 500–509, 2019.
- [12] K. Brodin and P. Halldin, "Development of a finite element model of the upper cervical spine and a parameter study of ligament characteristics," *Spine (Phila Pa 1976)*, vol. 29, no. 4, pp. 376–385, 2004.
- [13] Y. Qi and G. Lewis, "Influence of assigned material combination in a simulated total cervical disc replacement design on kinematics of a model of the full cervical spine: a finite element analysis study," *Bio-medical Materials and Engineering*, vol. 27, no. 6, pp. 633–646, 2016.
- [14] N. Kallemeyn, A. Gandhi, S. Kode, K. Shivanna, J. Smucker, and N. Grosland, "Validation of a C2-C7 cervical spine finite element model using specimen-specific flexibility data," *Medical Engineering & Physics*, vol. 32, no. 5, pp. 482–489, 2010.
- [15] S. K. Ha, "Finite element modeling of multi-level cervical spinal segments (C3-C6) and biomechanical analysis of an elastomer-type prosthetic disc," *Medical Engineering & Physics*, vol. 28, no. 6, pp. 534–541, 2006.
- [16] B. I. Woods and A. S. Hilibrand, "Cervical radiculopathy: epidemiology, etiology, diagnosis, and treatment," *Journal of Spinal Disorders & Techniques*, vol. 28, no. 5, pp. E251–E259, 2015.
- [17] X. Wei, S. Wang, J. Li et al., "Complementary and alternative medicine for the management of cervical radiculopathy: an overview of systematic reviews," *Evidence-based Complementary and Alternative Medicine*, vol. 2015, Article ID 793649, 10 pages, 2015.
- [18] M. A. Childress and B. A. Becker, "Nonoperative management of cervical radiculopathy," *American Family Physician*, vol. 93, no. 9, pp. 746–754, 2016.
- [19] H. Yu and B. Shi, "Treatment of 48 cases of knee osteoarthritis of Yang deficiency and cold coagulation type with herbal ginger moxibustion journal of external therapy of traditional," *Chinese Medicine*, vol. 27, pp. 18–19, 2018.

## *Retraction*

# **Retracted: Experimental Study of lncRNA RP11-815M8.1 Promoting Osteogenic Differentiation of Human Bone Marrow Mesenchymal Stem Cells**

### **BioMed Research International**

Received 12 March 2024; Accepted 12 March 2024; Published 20 March 2024

Copyright © 2024 BioMed Research International. This is an open access article distributed under the Creative Commons Attribution License, which permits unrestricted use, distribution, and reproduction in any medium, provided the original work is properly cited.

This article has been retracted by Hindawi following an investigation undertaken by the publisher [1]. This investigation has uncovered evidence of one or more of the following indicators of systematic manipulation of the publication process:

- (1) Discrepancies in scope
- (2) Discrepancies in the description of the research reported
- (3) Discrepancies between the availability of data and the research described
- (4) Inappropriate citations
- (5) Incoherent, meaningless and/or irrelevant content included in the article
- (6) Manipulated or compromised peer review

The presence of these indicators undermines our confidence in the integrity of the article's content and we cannot, therefore, vouch for its reliability. Please note that this notice is intended solely to alert readers that the content of this article is unreliable. We have not investigated whether authors were aware of or involved in the systematic manipulation of the publication process.

Wiley and Hindawi regrets that the usual quality checks did not identify these issues before publication and have since put additional measures in place to safeguard research integrity.

We wish to credit our own Research Integrity and Research Publishing teams and anonymous and named

external researchers and research integrity experts for contributing to this investigation.

The corresponding author, as the representative of all authors, has been given the opportunity to register their agreement or disagreement to this retraction. We have kept a record of any response received.

### **References**

- [1] X. Sun, J. Cao, J. Han et al., "Experimental Study of lncRNA RP11-815M8.1 Promoting Osteogenic Differentiation of Human Bone Marrow Mesenchymal Stem Cells," *BioMed Research International*, vol. 2021, Article ID 5512370, 8 pages, 2021.



## Research Article

# Experimental Study of lncRNA RP11-815M8.1 Promoting Osteogenic Differentiation of Human Bone Marrow Mesenchymal Stem Cells

Xiang Sun <sup>1</sup>, Junchuan Cao <sup>2</sup>, Jiusong Han <sup>1</sup>, Bo Jia <sup>1</sup>, Jing Wang <sup>1</sup>, Junxiang Lian <sup>1</sup>, Jianwei Gao <sup>3</sup>, Shuguang Liu <sup>1</sup> and Hui Xiao <sup>4</sup>

<sup>1</sup>Department of Oral and Maxillofacial Surgery, Stomatological Hospital, Southern Medical University (Guangdong Provincial Stomatological Hospital), Guangzhou, Guangdong 510280, China

<sup>2</sup>Department of Stomatology, Chengdu Women's and Children's Hospital, School of Medicine, University of Electronic Science and Technology of China, Chengdu, Sichuan 611731, China

<sup>3</sup>Department of Orthopedics, Taian City Central Hospital, Taian, Shandong 271000, China

<sup>4</sup>Department of Orthodontics, Stomatological Hospital, Southern Medical University (Guangdong Provincial Stomatological Hospital), Guangzhou, Guangdong 510280, China

Correspondence should be addressed to Jianwei Gao; [gaojianwei6789@163.com](mailto:gaojianwei6789@163.com), Shuguang Liu; [dr.liusg@163.com](mailto:dr.liusg@163.com), and Hui Xiao; [zzmmxh@126.com](mailto:zzmmxh@126.com)

Received 6 February 2021; Revised 25 February 2021; Accepted 9 March 2021; Published 27 March 2021

Academic Editor: Yuzhen Xu

Copyright © 2021 Xiang Sun et al. This is an open access article distributed under the Creative Commons Attribution License, which permits unrestricted use, distribution, and reproduction in any medium, provided the original work is properly cited.

**Objective.** This study is aimed at investigating the role of long noncoding RNA (lncRNA) RP11-815M8.1 in the osteogenic differentiation of human bone marrow mesenchymal stem cells (hBMSCs). **Methods.** RT-PCR was used to detect the expression of lncRNA RP11-815M8.1 before and after osteogenic differentiation of hBMSCs. The lncRNA RP11-815M8.1 in hBMSCs was overexpressed or silenced via lentiviral transfection. The transfection efficiency was detected by RT-PCR, and the proliferation of hBMSCs was determined by CCK-8. After 14 days of osteogenic differentiation of transfected hBMSCs, the expression of osteogenic transcription factors (ALP, OCN, OPN, Runx2, and Osterix) was detected by alizarin red staining and RT-PCR. The mRNAs directly regulated by lncRNA RP11-815M8.1 and targeted miRNAs were analyzed according to the positional relationship between lncRNA and mRNA in the genome and miRanda software. **Results.** The expression of lncRNA RP11-815M8.1 enhanced with increasing osteogenic differentiation time of hBMSCs. Two days after the transfection of hBMSCs, lncRNA RP11-815M8.1 expression was significantly increased in the overexpression group and significantly decreased in the knockdown group, compared to control cells. The CCK-8 assay showed that overexpression and knockdown of lncRNA RP11-815M8.1 did not affect the proliferation of hBMSCs. After 14 days of differentiation of hBMSCs, stronger alizarin red staining was observed in the overexpression groups, and the expression of osteogenic transcription factors was increased in the overexpression group compared to the control. In the knockdown group, alizarin red staining and the expression of osteogenic transcription factors were decreased. Bioinformatics analysis showed that lncRNA RP11-815M8.1 was directly associated with one mRNA, 27 interacting miRNAs, and 20 miRNA-targeted mRNAs. **Conclusion.** The osteogenic differentiation of hBMSCs can be promoted by lncRNA RP11-815M8.1 in vitro.

## 1. Introduction

The oral and maxillofacial bone structure is an important basis to support the face, and the repair of maxillofacial bone tissue defects, caused by trauma, tumors, and congenital

deformity, is an urgent and difficult issue in oral and maxillofacial surgery [1]. The conventional repair methods like autologous and allogeneic bone grafts have their own disadvantages, for example, the source of autogenous bone is limited and the immune rejection of allogeneic bone was large

[2]. However, the recent development of bone tissue engineering has opened up a new opportunity for bone defect repair. The repair process of bone defect includes changes in the balance between osteoclasts and osteoblasts, decreased bone resorption by osteoclasts, concurrent osteoblast chemotaxis in the defect site, activation and differentiation, and coordination, restoration, and repair of the bone defect site with osteoblasts, which mainly originate from bone marrow mesenchymal stem cells (BMSCs) [3, 4]. Human BMSCs (hBMSCs), as important seed cells in bone tissue engineering, have high self-renewal and multidirectional differentiation potential and can be differentiated into osteoblasts under appropriate conditions [5]. Other advantages of hBMSCs include convenient sources, limited damage to the body, and minimized immune rejection after transplantation [6]. Therefore, the mechanism investigation of osteogenic differentiation of hBMSCs will contribute to the clinical application of hBMSCs in bone tissue engineering.

Long noncoding RNAs (lncRNAs) are a series of RNA molecules longer than 200 nucleotides that are not translated into proteins and were initially considered byproducts of the transcription process with no biological function [7]. It has been reported that the complex network regulated by lncRNAs plays an important role in the process of cell and tissue differentiation. For example, studies have shown that lncRNAs are related to differentiation of neuronal [8], muscle [9], epidermal [10], and adipogenic [11]. Recent studies have also found that lncRNAs are involved in the regulation of osteoblastic differentiation of mesenchymal stem cells (MSCs) [12, 13]. However, the potential functions and regulatory mechanisms of lncRNAs in the osteogenic differentiation of hBMSCs remain unclear.

In a previous study using high-throughput sequencing of lncRNAs, we found that lncRNA RP11-815M8.1 was differentially expressed in the osteogenic differentiation process of hBMSCs. This study was conducted to explore the role of lncRNA RP11-815M8.1 in the process of osteogenic differentiation of hBMSCs by RT-PCR detection and lentiviral vector transfection and predict the potential targets of lncRNA RP11-815M8.1 by bioinformatics analysis. Thus, this study provides a new lncRNA target in the mechanism of osteogenic differentiation of hBMSCs and a new strategy for the construction of improved tissue-engineered bone grafts.

## 2. Materials and Methods

**2.1. Cell Culture and Osteogenic Differentiation.** Frozen primary hBMSCs (ScienCell-7500, USA) were placed in a water bath at 37°C until completely thawed and seeded at a density of  $5 \times 10^3/\text{cm}^2$  in a T-75 culture flask coated with polylysine. Cells were cultured in mesenchymal stem cell growth medium (ScienCell-7501, USA) and incubated at 37°C with 5% CO<sub>2</sub> and 95% relative humidity. The next day, the medium was changed to remove residual DMSO and the nonadherent cells. After that, the medium was changed every 3 days. When the cells reached 90% confluence, they were trypsinized with 0.25% trypsin/0.02% EDTA, and subculturing was carried out to generate P3 cells. P3 hBMSCs were

TABLE 1: Gene sequences of lncRNA RP11-815M8.1.

Gene name	Official symbol	Gene sequences
RP11-815M8.1	LINC02257	AGATGCACATGAAATTTGG
		TGCCGTGACTCGGATTG
		GGGGACCTCCCTTGGGAG
		ATCAATCCCCTGTACTC
		CTGTTCTTTGCTCCGTGA
		GAAAGATCCACCTATGA
		CCCTCAGGTCCTCAGACC
		GACTAGCCCAAGGAACA
		TCTACCAATTTTAAATC
		AGGTGGAGTCTCGCACT
		GTCATCCTGGCTGGAATG
		CAGTGGTGCAAGCCGAC
		TCACTGCAACCTCTGCCT
		CTTGGGTTCAAGTGATT
		CTCCTGCTTCAGCCTCCT
		GATTTGCTGGGATTGCA
		GAGCAAACCAGTGAAAAA
		ATGGCCTTCGCACTCCT
		GAGAGACCTTTCACCGGG
		CTTTCTACTTTTGAATTCTC
		TCCATAGCTGGTTTCTCTT
		AGGCCTCGATAGAGCAG
		TCCCTGAATCACACAGGT
		ATGCTGACTACGTCTTT
		TCCTGGTACAAACCATCA
		TGGGGGAAACACACAGC
		AAGAAGCATCTTCAGGTC
ACAAGATAGGTAATACC		
ATCTACCTGAATTTTTTTC		
AAAAGCAGCAGAATATT		
TAGTTTTCTATTTTCAGTG		
GCTTCTAACAGAGATCA		
TGTTTGCACAAGATTA		
ATGTCTGCAGTGGTCGT		
CTTAAAAA		

seeded in 6-well plates at a density of  $2 \times 10^4/\text{cm}^2$  per well. When the confluence was over 80%, the medium was replaced with MSC osteogenic differentiation medium (ScienCell-7531, USA). The medium was completely changed with fresh osteogenic differentiation medium every 3 days, and the cells were harvested and collected after 7, 14, and 21 days of osteogenic differentiation. RNA was extracted, and the expression of lncRNA RP11-815M8.1 was detected by RT-PCR.

**2.2. Cell Transfection.** The full-length sequence of lncRNA RP11-815M8.1 was obtained from the NCBI database (Table 1). The lncRNA RP11-815M8.1-overexpressing lentiviral vector (OE-RP11-815M8.1) was constructed with the pBABE vector, and the lncRNA RP11-815M8.1-knockdown lentiviral vector (sh-RP11-815M8.1) was constructed with the PLKO.1 vector. All of the above viral vectors were purchased from Anhui General Biotechnology Co., Ltd. Cells at a density of  $1.2 \times 10^6$  cells/well were seeded in a 6-well plate. After 16 h, the constructed vector was transferred into 293FT cells according to the instruction of the Lipofectamine 2000 (Promega, USA) transfection kit. The medium was changed

8 h after transfection, and the supernatant was collected and stored at 4°C in 48 h. Next, 0.3 mL of the collected supernatant was mixed with MSC culture medium and then added 0.7 mL of cell culture medium and 1.0  $\mu$ L of polybrene (final concentration was 8 ng/mL). Then, the solution was mixed in hBMSCs cultured Petri dishes with a cell density of less than 60%. One day after MSC culture, the medium was changed to obtain hBMSCs transfected with the lncRNA RP11-815M8.1-overexpressing lentiviral vector (OE-RP11-815M8.1 group), lncRNA RP11-815M8.1-knockdown lentiviral vector (sh-RP11-815M8.1 group), and the corresponding empty transfection vector controls (pBABE group, PLKO.1 group). After 2 days, the cells were collected for extraction of RNA.

**2.3. CCK-8 Assay.** A CCK-8 assay was used to verify the effect of lentiviral vector transfection on the proliferation of hBMSCs. According to the instructions of the CCK-8 Kit (Biyuntian, China), the cells were seeded into 96-well plates at a density of  $1 \times 10^4$  cells/well, and 10  $\mu$ L CCK-8 solution was added. The cells were cultured at 37°C, 5% CO<sub>2</sub>, and 95% air humidity. Cell proliferation was detected by the CCK-8 method using a plate reader (Delang, China) at a wavelength of 450 nm on days 2, 5, 8, and 11.

**2.4. Alkaline Phosphatase (ALP) Staining.** The culture medium was removed after osteogenic differentiation; alkaline phosphatase (ALP) staining was performed to identify MSCs according to the instructions of the ALP staining kit (Sigma, USA). The cells were washed twice with phosphate-buffered saline (PBS) and fixed at room temperature with 4% paraformaldehyde for 10 minutes. After fixation, the cells were rinsed again with PBS. An appropriate amount of ALP dye solution was added to the fixed cells in a 6-well plate in the dark and incubated at room temperature for approximately 15-30 minutes. The staining was monitored under a fluorescence microscope every 5 minutes. After the staining was stable, the plate was rinsed with PBS again for final observation. Osteogenic differentiation was confirmed by deepening cytoplasmic staining.

**2.5. Alizarin Red Staining.** To investigate the osteogenic differentiation, alizarin red staining was performed according to the alizarin red kit (Sigma, USA) instruction. The cells were rinsed with PBS and fixed with ethanol for 30 minutes. Next, the liquid was removed, the cells were rinsed twice with PBS, and 2% alizarin red S staining solution was slowly added to the samples, and after incubation at room temperature for 5-10 minutes, the alizarin red solution was removed, after which the cells were rinsed with PBS twice and observed under an inverted microscope. Osteogenic differentiation was validated by increased red calcium salt deposition.

**2.6. RNA Extraction and RT-PCR Assay.** Total RNA was extracted from the cells according to the instructions of the TRIzol Kit (Invitrogen, California, USA) and then reverse transcribed into cDNA using the cDNA reverse transcription kit (TaKaRa, Tokyo, Japan). The cDNA was mixed with the reagents according to the instructions of the SuperReal Fluorescence Quantitative PreMix Color (SYBR Green-FP215) kit

TABLE 2: Sequences of primers for RT-PCR.

Primer	Primer sequence (5'-3')
h-lncRNA RP11-815M8.1 qF	CTAGCCAAGGAACATCTCAC
h-lncRNA RP11-815M8.1 qR	AGCAGGAGAATCACTTGAACC
h-ALP qF	AGAATCTGGTGCAGGAATGG
h-ALP qR	TCGTATTTTCATGTCTCCAGGC
h-OCN qF	TGCAGCCTTTGTGTCCAAG
h-OCN qR	CCCAGCCATTGATACAGGTAG
h-OPN qF	AGGCTGATTCTGGAAGTTCTG
h-OPN qR	CTTACTTGGGAAGGGTCTGTGG
h-Runx2 qF	TTCACCTTGACCATAACCGTC
h-Runx2 qR	GGCGGTCAGAGAACAACTAG
h-Osterix qF	CCACCTACCCATCTGACTTTG
h-Osterix qR	CCACTATTTCCCACTGCCTT
h-GAPDH qF	TGTTGCCATCAATGACCCCTT
h-GAPDH qR	CTCCACGACGTACTCAGCG

(TIANGEN BIOTECH (BEIJING) CO., LTD), and the assay was performed using a real-time quantitative PCR apparatus (Roche LC96, Switzerland). The hBMSCs transfected with the lncRNA RP11-815M8.1-overexpressing lentiviral vector (OE-RP11-815M8.1 group), the RP11-815M8.1-knockdown lentiviral vector (sh-RP11-815M8.1 group), and the corresponding empty control vectors (pBABE group, PLKO.1 group) were incubated with osteogenic induction and differentiation medium for 14 days, and the expression of osteogenic transcription factors (ALP, OCN, OPN, Runx2, and Osterix) was detected by RT-PCR. Osteogenic differentiation was verified by the expression of osteogenic transcription factors. The primer sequences are shown in Table 2.

**2.7. Prediction of Targeted miRNAs and mRNAs Directly Regulated by lncRNA RP11-815M8.1.** According to the positional relationship between lncRNAs and mRNAs in the genome, upstream and downstream transcripts of lncRNAs were found within 100 kb, and these genes and their corresponding transcripts were identified. Since miRNAs play a crucial role in the process of transcriptional regulation, and lncRNAs play an important role in regulating protein-coding genes by binding to miRNAs, the targeting miRNAs of lncRNA RP11-815M8.1 were further predicted by miRanda software.

**2.8. Statistical Analysis.** Statistical graphs were generated by GraphPad Prism 8, and SPSS 22.0 software was used for the statistical analysis. Measurement data are expressed as the mean  $\pm$  standard deviation. A paired sample *t*-test was used to compare the expression levels between each group and the control group, and  $p < 0.05$  indicated a statistically significant difference between groups.

### 3. Results

**3.1. The Expression of lncRNA RP11-815M8.1 Was Increased during the Osteogenic Differentiation of hBMSCs.** After 21 days of osteogenic differentiation of P3 hBMSCs, the



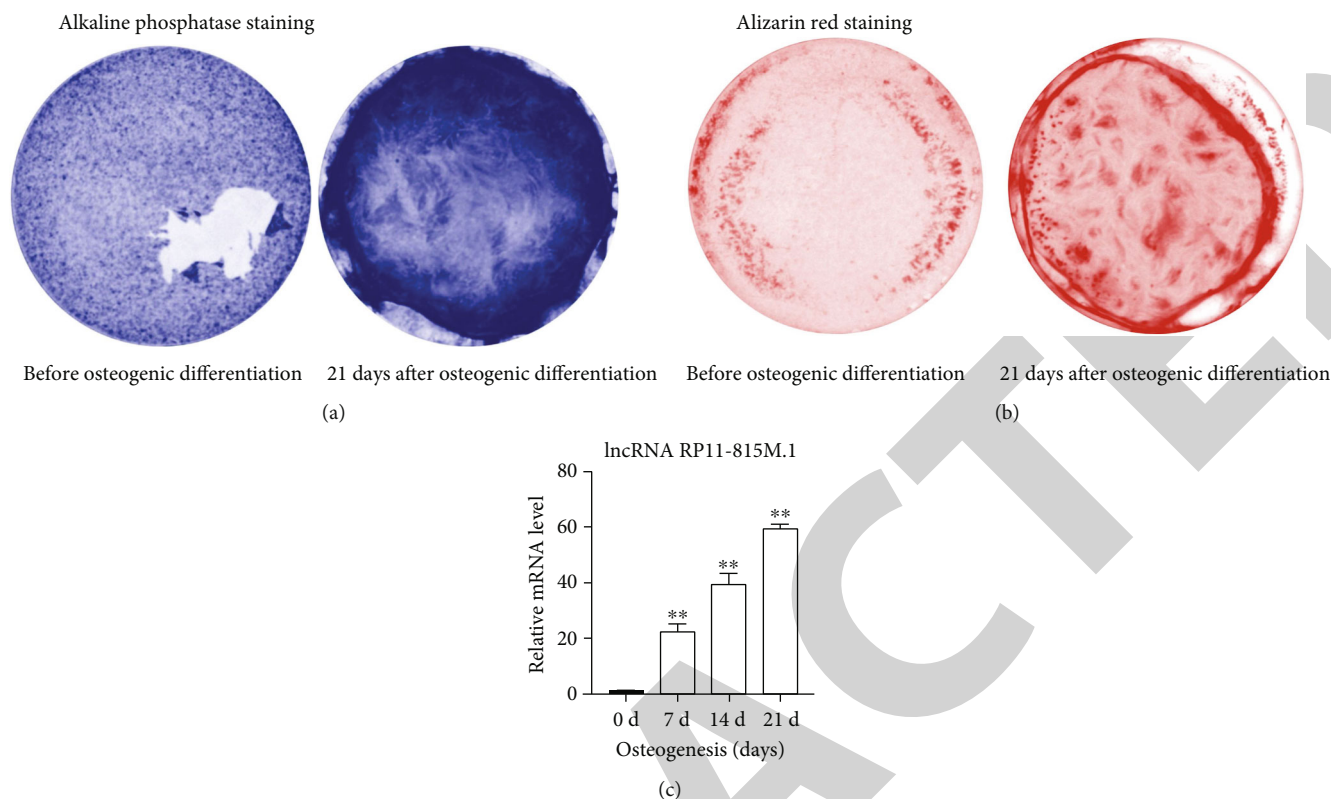


FIGURE 1: Osteogenic differentiation of hBMSCs: (a) ALP staining; (b) alizarin red staining; (c) changes in the expression level of lncRNA RP11-815M8.1 (\*\* $p < 0.01$ ); the data was normalized to the D0 group which was set as 100%.

TABLE 3: Changes in the expression level of lncRNA RP11-815M8.1 before and after osteogenic differentiation of hBMSCs.

lncRNA	D0	D7	D14	D21
RP11-815M8.1	1.01 ± 0.20	22.31 ± 2.74	39.51 ± 3.72	59.39 ± 1.67

cytoplasmic staining was deepened indicating positive ALP staining (Figure 1(a)). Positive alizarin red staining showed red calcium salt deposition (Figure 1(b)). These results indicated the osteogenic differentiation of hBMSCs. The expression of lncRNA RP11-815M8.1 before and after osteogenic differentiation of hBMSCs was detected by RT-PCR, and the results showed that the expression of lncRNA RP11-815M8.1 gradually increased by time (Figure 1(c), Table 3).

**3.2. Efficiency of Overexpression and Interference of lncRNA RP11-815M8.1 through Lentiviral Vector Transfection and the Effect on hBMSC Proliferation.** The lncRNA RP11-815M8.1-overexpressed lentiviral vector, knockdown lentiviral vector, and the corresponding empty vectors were transfected into hBMSCs, and the changes in the expression level of lncRNA RP11-815M8.1 were detected by RT-PCR 2 days later. The results showed that the expression of lncRNA RP11-815M8.1 was significantly increased in the OE-RP11-815M8.1 group (Figure 2(a)) and significantly decreased in the sh-RP11-815M8.1 group compared with the pBABE group and PLKO.1 group (Figure 2(b)), respectively (Table 4).

A CCK-8 assay was used to detect cell proliferation via measurement of cell culture density using a plate reader at the wavelength of 450 nm at 2, 5, 8, and 11 days after hBMSC transfection. The results showed that the overexpression and knockdown of lncRNA RP11-815M8.1 did not affect the proliferation of hBMSCs (Figure 3).

**3.3. Functional Validation of the Role of lncRNA RP11-815M8.1 in the Process of Osteogenic Differentiation of hBMSCs.** The hBMSCs in the OE-RP11-815M8.1 group, the sh-RP11-815M8.1 group, and corresponding control groups (pBABE group, PLKO.1 group) were differentiated in 14 days after induction of osteogenic differentiation, and the effect of osteogenic differentiation was analyzed by alizarin red staining. The results showed that the red calcium salt deposition in the OE-RP11-815M8.1 group was increased compared to the pBABE group. Compared with the PLKO.1 group, the sh-RP11-815M8.1 group had less red calcium salt deposition (Figure 4). The expression of osteogenic transcription factors (ALP, OCN, OPN, Runx2, and Osterix) was detected by RT-PCR, and the results showed that the expression of ALP, OCN, OPN, Runx2, and Osterix increased in the OE-RP11-

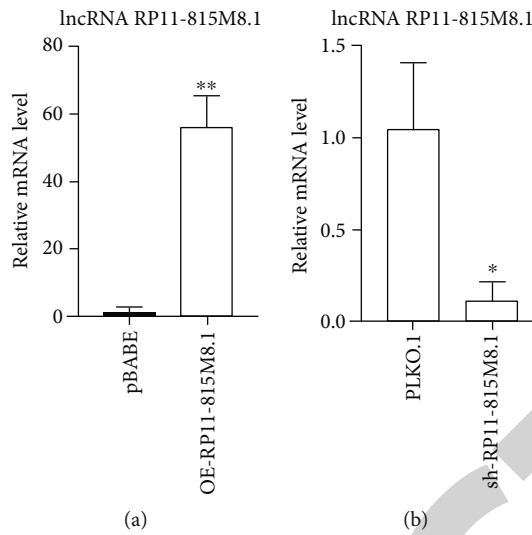


FIGURE 2: Transfection efficiency of the overexpression and knockdown of lncRNA RP11-815M8.1. (a) lncRNA RP11-815M8.1 expression was significantly increased in the OE-RP11-815M8.1 group compared with the pBABE group. (b) The expression of lncRNA RP11-815M8.1 in the sh-RP11-815M8.1 group was significantly decreased compared with that in the PLKO.1 group (\* $p < 0.05$ , \*\* $p < 0.01$ ).

TABLE 4: Efficiency of lentiviral vector transfection for the overexpression and knockdown of lncRNA RP11-815M8.1.

lncRNA	pBABE	OE-RP11-815M8.1	PLKO.1	sh-RP11-815M8.1
RP11-815M8.1	1.39 ± 1.41	55.90 ± 9.40	1.05 ± 0.36	0.11 ± 0.10

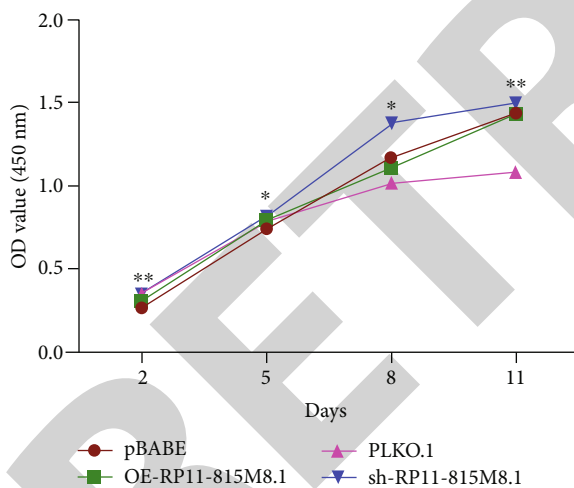


FIGURE 3: Effects of the overexpression and knockdown of lncRNA RP11-815M8.1 on hBMSC growth (\* $p < 0.05$ , \*\* $p < 0.01$ ).

815M8.1 group in comparison to the pBABE group (Figure 5(a), Table 5). The expression of ALP, OCN, OPN, Runx2, and Osterix in the sh-RP11-815M8.1 group was decreased compared to the PLKO.1 group (Figure 5(b), Table 6).

3.4. *lncRNA RP11-815M8.1 Directly Regulates mRNAs and Binds to miRNAs.* According to the positional relationship between lncRNA and mRNA in the genome, only one mRNA, DUSP10-204, was found within the range of 100 kb upstream and downstream of lncRNA RP11-815M8.1. The

targeting miRNAs of lncRNA RP11-815M8.1 were predicted by using miRanda software, and a total of 27 miRNAs related to lncRNA RP11-815M8.1 were found. The mRNAs targeted by the 27 miRNAs were identified in the miRDB database, and 20 of them had score values over 99. The result is shown in Figure 6.

#### 4. Discussion and Conclusions

BMSCs have multidirectional differentiation potential and high self-renewal and proliferation abilities. They can differentiate not only into osteoblasts under specific culture conditions *in vitro* but also into osteoblasts *in vivo* by attaching to certain vectors and are considered to be an important choice of seed cells in bone tissue engineering [14]. Therefore, the mechanism investigation of osteogenic differentiation of hBMSCs may contribute to the clinical application in bone tissue engineering.

Initially, lncRNAs were considered to be transcriptional noise of the genome without biological function. However, protein-coding mRNAs account for only 1.5% of RNA transcripts in the mammalian genome; most of the genome consists of noncoding RNAs, such as miRNAs, more than 80% of which are lncRNAs [15]. Studies have shown that lncRNA has a stable secondary structure, different subcellular localization, and higher expression in specific cells and tissues, all of which indicate that lncRNAs are functional [16]. On the other hand, studies in recent years have also found that lncRNAs can regulate gene expression at the epigenetic, transcriptional, and posttranscriptional levels and participate in various essential cellular regulatory processes [17].



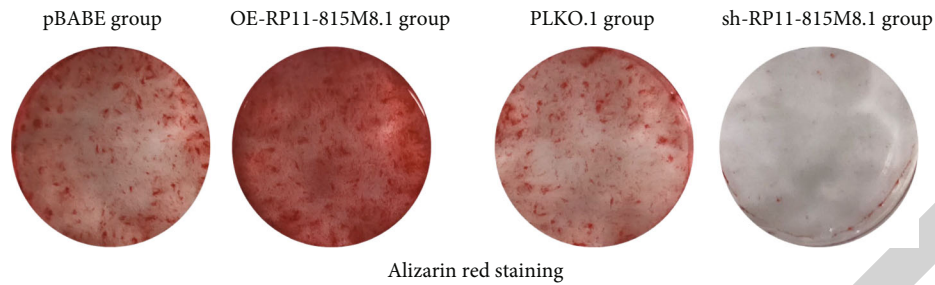


FIGURE 4: Alizarin red staining results 14 days after osteogenic differentiation of hBMSCs transfected with lentiviral vectors for the overexpression and knockdown of lncRNA RP11-815M8.1. hBMSCs transfected with the lncRNA RP11-815M8.1-overexpressing lentiviral vector (OE-RP11-815M8.1 group), lncRNA RP11-815M8.1-knockdown lentiviral vector (sh-RP11-815M8.1 group), and the corresponding empty transfection vector controls (pBABA group, PLKO.1 group).

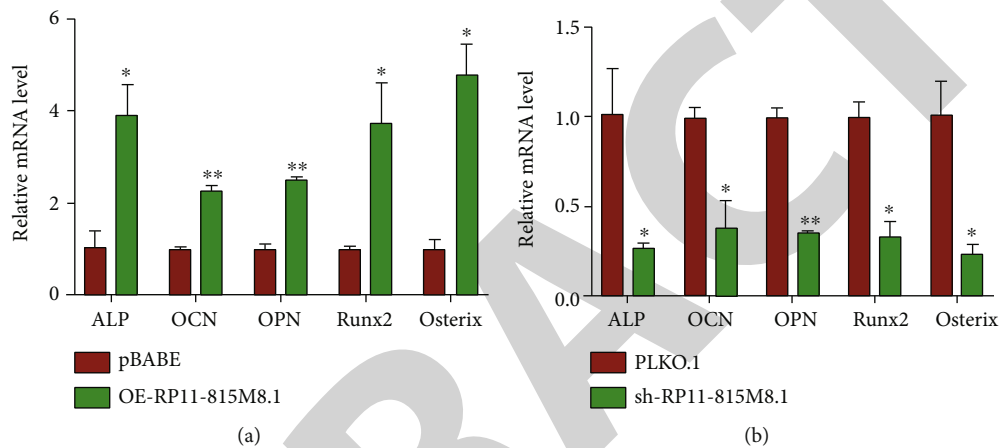


FIGURE 5: Expression of osteogenic transcription factors. (a) Expression of osteogenic transcription factors in hBMSCs transfected with the lncRNA RP11-815M8.1-overexpressing lentiviral vector 14 days after osteogenic differentiation. (b) Expression of osteoblastic-specific transcription factors in hBMSCs transfected with lncRNA RP11-815M8.1-knockdown lentiviral vectors 14 days after osteogenic differentiation (\* $p < 0.05$ , \*\* $p < 0.01$ ).

TABLE 5: Expression of osteogenic transcription factors in hBMSCs transfected with the lncRNA RP11-815M8.1-overexpressing lentiviral vector 14 days after osteogenic differentiation.

Osteogenic transcription factors	D0	D14
ALP	1.04 ± 0.35	3.89 ± 0.67
OCN	1.00 ± 0.04	2.27 ± 0.10
OPN	1.00 ± 0.11	2.51 ± 0.06
Runx2	1.00 ± 0.06	3.74 ± 0.87
Osterix	1.01 ± 0.19	4.79 ± 0.66

Moreover, an increasing number of studies have demonstrated that lncRNAs are closely related to BMSC osteogenic differentiation in recent years. Cao et al. [18] reported that high glucose inhibited the osteogenic differentiation of BMSCs in mice by inhibiting the expression of lncRNA AK028326 and CXCL13. Liang et al. [19] found that miR-141 and miR-22 did target H19 by inducing transcriptional suppression and regulate gene expression in hBMSCs through the classical Wnt/ $\beta$ -catenin pathway. Shang et al. [20] showed that TCONS\_00041960 regulated osteogenic differentiation of BMSCs in rats by competing as endogenous

TABLE 6: Expression of osteogenic transcription factors in hBMSCs transfected with the lncRNA RP11-815M8.1-knockdown lentiviral vector 14 days after osteogenic differentiation.

Osteogenic transcription factors	D0	D14
ALP	1.02 ± 0.25	0.27 ± 0.02
OCN	1.00 ± 0.05	0.38 ± 0.15
OPN	1.00 ± 0.05	0.36 ± 0.01
Runx2	1.00 ± 0.09	0.33 ± 0.09
Osterix	1.01 ± 0.19	0.24 ± 0.05

RNA of miR-204-5p and miR-125a-3p. Wang et al. [21] found that lncRNA MEG3 inhibited the osteogenic differentiation of BMSCs by enhancing the expression of miR-133a-3p and accelerated the occurrence of osteoporosis in postmenopausal osteoporosis patients.

Thus, we screened the differentially expressed lncRNAs before and after osteogenic differentiation of hBMSCs using high-throughput sequencing of lncRNAs in the previous study, including 7 known lncRNAs, 57 unknown lncRNAs, and 409 mRNAs. The lncRNA RP11-815M8.1 was selected due to the large differential expression ratio identified by



## Research Article

# Sirt-1 Regulates Physiological Process and Exerts Protective Effects against Oxidative Stress

Lei Liu <sup>1,2,3</sup>, Guangyuan Xia,<sup>2,4</sup> Peifan Li,<sup>2</sup> Yiming Wang <sup>2,4</sup> and Qian Zhao <sup>5</sup>

<sup>1</sup>Department of Mental Health and Psychiatry, The Second Affiliated Hospital of Soochow University, Suzhou, Jiangsu, China 215006

<sup>2</sup>Department of Psychiatry, Affiliated Hospital of Guizhou Medical University, Guiyang, Guizhou, China 550025

<sup>3</sup>Department of Psychiatry, Zaozhuang Mental Health Center, Zaozhuang, Shandong, China 277103

<sup>4</sup>College Students' Mental Health Education and Counseling Center, Guizhou Medical University, Guiyang, Guizhou, China 550004

<sup>5</sup>Department of Nuclear Medicine, General Hospital of Ningxia Medical University, Ningxia, Ningxia Hui Autonomous Region, China 750004

Correspondence should be addressed to Yiming Wang; 754603457@qq.com and Qian Zhao; cecilia\_hh@126.com

Received 20 February 2021; Revised 5 March 2021; Accepted 10 March 2021; Published 24 March 2021

Academic Editor: Yuzhen Xu

Copyright © 2021 Lei Liu et al. This is an open access article distributed under the Creative Commons Attribution License, which permits unrestricted use, distribution, and reproduction in any medium, provided the original work is properly cited.

**Background.** Recent studies suggest a correlation between the reduced Sirt-1 expression with Alzheimer's diseases (AD) and depression, respectively, suggesting a possible pathogenic role of the altered Sirt-1 expression in neuronal degenerative diseases, such as AD and depression. However, the molecular mechanisms underlying how Sirt-1 reduction impairs neuronal functions remain unknown. **Methods.** We used the SK-N-SH neuroblastoma cells to study the role of Sirt-1 expression on physiological roles in neuronal cells. Gain of Sirt-1 was achieved by transiently transfecting Sirt-1 expression plasmid. Sirt-1-specific shRNA was used to elucidate the role of Sirt-1 loss of function. CCK-8 (Cell Counting Kit-8) assay and flow cytometry were used to evaluate cell proliferation. Semiquantitative western blotting was used to detect relative protein levels. A further luciferase reporter gene assay was employed to examine the effect of Sirt-1 expression on the transcriptional activity of p53. RT-qPCR was used to determine the mRNA levels of p21, Bax, and Bcl-2, which were the downstream target genes of p53. **Results.** Sirt-1 suppressed the p53 downstream gene p21 transcription, while shRNA-mediated Sirt-1 knockdown resulted in a significant increase in p21 expression, implying a possibility that Sirt-1 promotes neuron proliferation through suppressing p53 transcriptional activity. The mRNA and protein levels of p53 were not affected by the altered Sirt-1 expression, suggesting that Sirt-1 regulates the transcriptional regulatory activity of p53 rather than p53 expression. Indeed, we further confirmed that Sirt-1 appeared to inhibit p53 transcriptional activity by attenuating its acetylation and resulted in a decrease of p53's binding to the p21 promoter. Overexpressed Sirt-1 scavenged reactive oxygen species (ROS) production in SK-N-SH with H<sub>2</sub>O<sub>2</sub>. Knockdown of Sirt-1 presented opposite effect; the addition of EX527 (Sirt-1 inhibitor) increased ROS accumulation. **Conclusions.** Oxidative stress induces Sirt-1 in neuron cells, and Sirt-1 promotes proliferation in SK-N-SH cells, which protects them from oxidative stress-induced cell death, potentially via suppressing the transcriptional activity of p53. These results provide a molecular explanation underlying how the reduced Sirt-1 potentially causes the AD and depression-related diseases, supporting the idea that Sirt-1 can possibly be used as a diagnostic biomarker and/or therapeutic drug target for the AD and depression-related diseases.

## 1. Introduction

Silent mating type information regulation 2 homolog 1 (Sirt-1), which is a member of the sirtuin family, exerts stress-protecting effects against inhibition of cell cycle entry and induction of apoptotic cell death via transcriptionally regu-

lating gene expression [1]. Sirt-1 is one of the nicotinamide adenine dinucleotide- (NAD<sup>+</sup>-) dependent histone deacetylases and is discovered to be a critical component of seven homologous proteins regulating cell functions through chromatin remodeling/histone deacetylation [2–4]. In these manners, Sirt-1 plays critical roles in many human physiological

functions, including DNA repair, aging, gene expression, and apoptosis [5]. In mouse C2C12 myoblasts, Sirt-1 was found to inhibit the differentiating processes and expression of myogenin, which resulted in the proliferating inhibition and immaturation of satellite cells [6, 7]. Oberdoerffer and colleagues reported that, in mammalian cells, including in neurons, Sirt-1 was triggered by DNA damage and then redistributed to DNA breaks for repairmen, functioning as a transcriptional factor [8]. Notably, Sirt-1 was also found to be a neuroprotective molecule, which protected neurons against oxidative stress-induced cellular damage and stressful perturbations in both acute and chronic neurological diseases, including AD [9, 10]. In animal models of AD and Huntington's disease, overexpression of Sirt-1 abrogated neuronal degeneration and nonapoptotic and apoptotic cell death and indicated the tight association of Sirt-1 to physiological processes in neurons.

Sirt-1 interacts with several target substrates, including forkhead box O (FOXO) family members and p53 [11–13]. It was shown that in mammalian cells, Sirt-1 appeared to control the cellular response to stress by interacting with the FOXO family of forkhead transcription factors and thus exerting protective effects against oxidative stress-induced cellular damage [14]. By exerting deacetylating activity, Sirt-1 inactivates p53 and thus regulates cell survival and proliferation [13]. Suppression of Sirt-1 resulted in hyperacetylation of p53, which prevented its binding to Mdm2, resulting in cell cycle arrest and apoptosis [13]. The cyclin-dependent kinase (CDK) inhibitor p21 is a critical regulator in the cell cycle checkpoint resulting in the inhibition of G<sub>1</sub> progression and induction of senescence by blocking the activity of CDKs, without knowing how cell cycle is blocked [15, 16]. p21, which is one of the most well-known p53 target genes, is tightly transcriptionally regulated by deacetylated p53 and results in p53-dependent G<sub>1</sub> arrest after DNA damage [17]. By considering the regulation of Sirt-1 on FOXO and p53, we hypothesized that Sirt-1 might exert protective effects in neurons by deacetylating FOXO and p53.

Oxidative stress is a state which might either generates or accumulates the levels of cellular reactive oxygen species (ROS) [18]. Increasing ROS may dysfunction mitochondrial, damaging lipids, proteins, and DNA, which are consistently observed in AD subject autopsy brains [19]. In recent years, oxidative stress is recognized as a central factor in major depressive disorder (MDD) and AD. Oxidative stress-induced ROS accumulation causes brain damage and triggers specific antioxidant defense, including increasing the expressing level of amyloid- $\beta$  and accumulation of hyperphosphorylated tau, leading to complex pathological cascades culminating in AD [20–22]. In the rat brain, activation of Sirt-1 inhibited p53 acetylation and ROS production, which was further promoted by the addition of EX527, a Sirt-1 inhibition, which indicated that Sirt-1 might exert a protective effect against oxidative stress-related AD, by deacetylating p53 and thus scavenged ROS accumulation [23].

Here, we aimed to investigate whether Sirt-1 might protect neuronal cells against oxidative stress by regulating FOXO or p53. SK-N-SH neuroblastoma cells were employed

to figure out the roles of Sirt-1 expression on physiological roles in neuronal cells. This study determined for the first time that Sirt-1 might regulate p53 depending on its deacetylation activity and scavenge ROS induced by oxidative stress, demonstrating the importance of Sirt-1 and oxidative-induced ROS in the progression of AD and relative diseases.

## 2. Material and Methods

**2.1. Cell Culture and Treatment.** SK-N-SH cells (human neuroblastoma cell line) and SK-N-AS (p53-null cell line) were purchased from the Chinese Academy of Sciences (Beijing, China). As described by Huang et al. [24], SK-N-SH cells were cultured in Dulbecco's modified Eagle's medium (DMEM, Gibco, USA) at 37°C in a 5% CO<sub>2</sub> humidified atmosphere, with 10% fetal bovine serum (FBS, Gibco, USA) and 1% penicillin. When cells were 70–80% confluent, Opti-MEM was used with 2 h prior to transfection.

**2.2. siRNA Transfection.** We followed the methods of Kobayashi et al. [25]. The Sirt-1-specific si-Sirt-1 (GenePharma, China) was synthesized to knockdown the expression of Sirt-1 in cells. The sequence of si-Sirt-1 and siRNA-NC were provided by GenePharma (China). siRNA transfection was conducted according to the manufacturer's instructions. After transfection for 72 h, total protein and RNAs were prepared for western blotting analysis and qPCR, respectively.

**2.3. Western Blotting.** Cells were lysed, and BCA assay (Beyotime Biotechnology, China) was used for detecting the protein concentration. Western blotting was conducted by the methods of Xu et al. [26]. Primary antibodies were as follows: Sirt-1, Abcam, #ab220807; FOXO1, Abcam, #ab39670; p53, Abcam, #ab26; p21, Abcam, #ab109520; p53 (acetyl K382), Abcam, #ab75754; p53 (acetyl K120), Abcam, #ab78316.  $\beta$ -Actin was used as an internal control. The chemiluminescence detection kit ECL (Millipore, USA) was used to detect the bound antibodies.

**2.4. Luciferase Reporter Assay.** To evaluate the interaction between Sirt-1 and the Nanog 3'-UTR, the dual-luciferase reporter assay (Promega, USA) was conducted. The Nanog 3'-UTR and the mutant Nanog 3'-UTR were cloned and sequenced. We followed the methods of Xu et al. [26]. After transfection for 48 h, luciferase activity was detected and normalized with the Dual-Luciferase Reporter Assay System (Beyotime Biotechnology, Haimen, China).

**2.5. CCK-8 Assay.** We followed the methods of Wang et al. [27]. CCK-8 assay was conducted by using Cell Counting Kit-8 (AbMole Bioscience, USA). Cells were seeded into a 96-well plate ( $5.0 \times 10^3$ /well) and exposed to si-RNA or not for 1 to 5 days. Then, 10  $\mu$ L CCK-8 was added and cells were further incubated for 4 h. A microplate absorbance reader (Bio-Rad) was used to detect cell viability at 490 nm.

**2.6. Apoptosis Analysis.** Apoptosis analysis was conducted with the annexin V-FITC apoptosis assay kit (Abcam, Britain) according to kit instruction, as described by Qi et al. [28]. Cells ( $5 \times 10^5$ – $1 \times 10^6$ /mL) were suspended in 200  $\mu$ L



binding buffer; 10  $\mu$ L annexin V-FITC were added, and cells were incubated in the dark, 4°C for 30 minutes. Then, 300  $\mu$ L binding buffer and 5  $\mu$ L PI were added and cell apoptosis was tested on the machine within 1 hour.

**2.7. Colony Formation in Soft Agar.** As described by Xu et al. [26],  $1 \times 10^3$  cells were mixed with 0.3% low melting agar, supplemented with DMEM (including 10% FBS). Then, cells were plated on a low melting agar-coated 6-well plate (0.6%) and incubated at 37°C for 15 days. Cells were stained with crystal violet (0.05%, 0.2 mL/well) for 30 min, at 37°C. The numbers of positive colonies (>8 cells/colony) were counted. The test was repeated twice.

**2.8. EdU (5-Ethynyl-2'-Deoxyuridine) Staining.** We followed the methods of Zeng et al. [29]. Cells ( $2 \times 10^5$ /well) in a 6-well plate were supplemented with DMEM containing 50 mM EdU (RiboBio, Guangzhou, China) for 2 hours. The cells were washed (4°C) and fixed with 4% paraformaldehyde (at room temperature) for 10 min. EdU immunostaining was conducted with Apollo staining reaction buffer. Stained cells were observed under the fluorescence microscope (Olympus, Melville, NY).

**2.9. Cell Cycle Analysis.** As described by Qi et al. [28], cell cycle analysis was conducted with the Cell Cycle Analysis Kit (BioVision, USA) according to kit instruction. Cells were suspended and washed with PBS three times. Then, a cell pellet was fixed with 70% alcohol (ice-cold) at 4°C overnight. Then, cells were washed with PBS (ice-cold). 400  $\mu$ L PI solution (5  $\mu$ g/mL) was added to the cells for 0.5 h in the dark. Then, cell cycle was analyzed by flow cytometers (Beckman Coulter, Brea, CA, USA).

**2.10. Chromatin Immunoprecipitation.** As described by Zhang et al. [30, 31], chromatin from cell cultures at 0 and 24 h was prepared. Chromatin was immunoprecipitated with 4  $\mu$ g of Sp1 antibody (Abcam, Britain). In parallel immunoprecipitation procedures, 4  $\mu$ g of G<sub>aq</sub> antibody (Santa Cruz Biotechnology, USA) was used as a control. Precipitated DNA was amplified for 25 cycles. The promoter-specific forward primer is CTGTTTTTCAGTGCCAACT, and the reverse primer is CATGGGGCCCCGTCGGCCGCTG.

**2.11. Invasion Assay.** Cells were suspended with a serum-free medium with the concentration of  $2 \times 10^5$ /mL. We followed the methods of Wang et al. [32]. Nine random fields were counted under the microscope, and the statistical results were obtained.

**2.12. ROS Analysis.** Cells were suspended with a serum-free medium with the concentration of  $2 \times 10^5$ /mL. We followed the methods of Schieber and Chandel [19]. Nine random fields were counted under laser scanning confocal microscopy, and the statistical results were obtained.

**2.13. Statistical Analysis.** Statistical analysis was conducted by SPSS 20.0 software (IBM). The data was presented as  $-x \pm s$ . *t*-test was used for comparison between two

groups. ANOVA was used for comparison among multiple groups. *P* < 0.05 were considered statistically significant.

### 3. Results

**3.1. Sirt-1 Promotes Cell Proliferation of SK-N-SH Neuronal Precursor Cells.** In order to study the possible functions of Sirt-1 protein in nerve cells/neural precursor cells, SK-N-SH cells were used. We tested the impact of altered Sirt-1 expression either by transient overexpression or by small RNA interference. Western blotting analysis validated that siRNA largely diminished Sirt-1 expression in SK-N-SH cells in a dose-dependent manner; in contrast, transient transfection resulted in a 2- to 3-fold increase in Sirt-1 protein expression (Figures 1(a) and 1(b)). Importantly, suppression of Sirt-1 expression resulted in a significant reduction in SK-N-SH cell proliferation as analyzed by the CCK-8 method (Figure 1(c)). Conversely, overexpressing Sirt-1 dramatically enhanced the cell growth. When cell viability was significantly enhanced, proliferation-positive cells were increased, and Sirt-1 appears to promote SK-N-SH cell growth through facilitating their cell cycle progression because cells at G<sub>1</sub>/G<sub>0</sub> were significantly reduced and those at the S or M phase were increased (Figure 1(e)), indicating that Sirt-1 affected the level of cell proliferation by regulating cell cycle. These results demonstrate that Sirt-1 is a positive regulator for neuronal cell proliferation and promotes cell growth through either enhancing cell cycle progression or inhibiting cell apoptosis or both.

**3.2. Sirt-1 Selectively Inhibits the p53-p21 Pathway in SK-N-SH Cells.** It has been shown that Sirt-1 regulates cell growth and survival through targeting p53 and FOXO1 [17]. We then speculated which pathway is regulated by Sirt-1 to promote SK-N-SH cell growth. The protein expression levels of p53 and FOXO1 were unaltered neither by Sirt-1 knockdown nor by its overexpression (Figure 2(a)). We then reasoned whether Sirt-1 regulates the transcription of p53 and FOXO1. Indeed, Sirt-1 expression inhibited, which its knockdown enhanced the luciferase activity driven by p53 (Figure 2(b)). As a control, the p53-specific inhibitor largely abolished p53 reporter activity (Figure 2(b)). Those results clearly indicate that Sirt-1 is a negative regulator of p53 transcriptional activity.

**3.3. Sirt-1 Suppresses p53 Binding to p21 Promoter.** To determine whether Sirt-1 attenuates p21 mRNA transcription in a p53-dependent manner, we tested the effects of p53 inhibitor pifithrin- $\alpha$  pretreatment on Sirt-1-mediated p21 suppression. As expected, pifithrin- $\alpha$  pretreatment totally abolished the increase in p21 expression by Sirt-1 knockdown (Figures 3(a) and 3(b)). Together with the fact that neither p53 mRNA nor its protein expression levels were altered by Sirt-1, these results suggest that Sirt-1 inhibits p21 transcription possibly through a p53-dependent manner.

We then used chromatin immunoprecipitation to detect changes in the binding activity of p53 to the p21 promoter region after Sirt-1 overexpression/interference. 3'-UTR of DHFR was used as a target negative control. As was shown



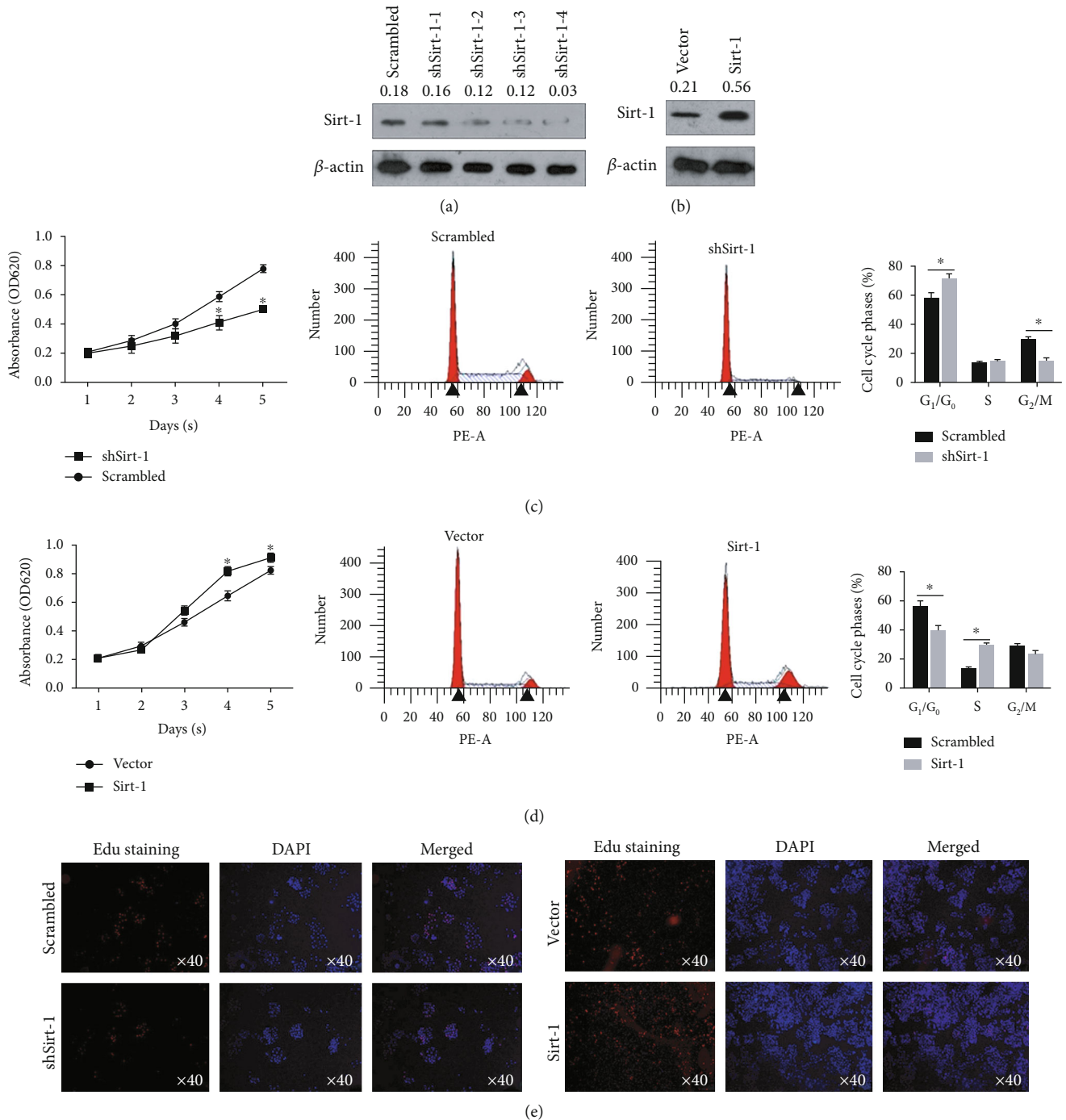


FIGURE 1: Sirt-1 positively promotes cell proliferation in SK-N-SH cells. (a) Stable knockdown of Sirt-1 by introducing shRNA targeting to Sirt-1 mRNA was performed, and knockdown efficacy was confirmed in four individual clones. (b) Stable overexpression of Sirt-1 was measured by semiquantitative western blot analysis to confirm the Sirt-1 protein level. After knockdown (c) or overexpression (d) of Sirt-1, cell viability from days 1-5 and cell cycle distribution were analyzed. \* $P < 0.05$ , vs. scrambled group. (e) EdU staining was then performed to further confirm the effect of Sirt-1 on the proportion of proliferating cells.

in Figure 3(c), the binding activity of p53 to p21 was decreased when interfered with Sirt-1 and increased when overexpression of Sirt-1.

**3.4. Sirt-1 Exerts Its Deacetylation Activity on p53's Lysine 382 and Thus Regulates Cell Proliferation.** First, we examined

whether the acetylation of p53 was regulated by Sirt-1, which had been known critical for p53 transcriptional activation [33]. The results showed that (Figure 4(a)), the expression of Sirt-1 had no effect on the total protein level of p53, but p53 deacetylation at 382 lysine was significantly inhibited (Figure 4(b)).

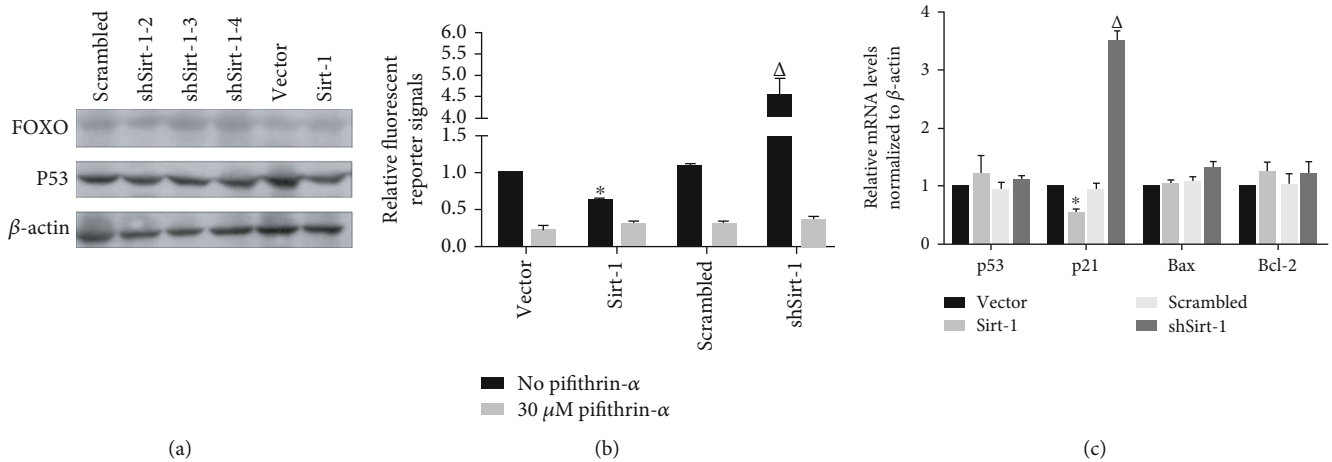


FIGURE 2: Sirt-1 regulates p53's transcriptional activity and its downstream gene. (a) After stable knockdown or overexpression of Sirt-1, FOXO and p53 levels were analyzed by performing western blot. (b) By performing fluorescent reporter assay, the effect of Sirt-1 on p53's transcriptional activity was measured. \* $P < 0.05$ , vs. vector group;  $\Delta P < 0.05$ , vs. scrambled group. (c) RT-qPCR was performed to detect mRNA levels of p53's downstream target genes, including p21, Bax, and Bcl-2. \* $P < 0.05$ , vs. vector group;  $\Delta P < 0.05$ , vs. scrambled group.

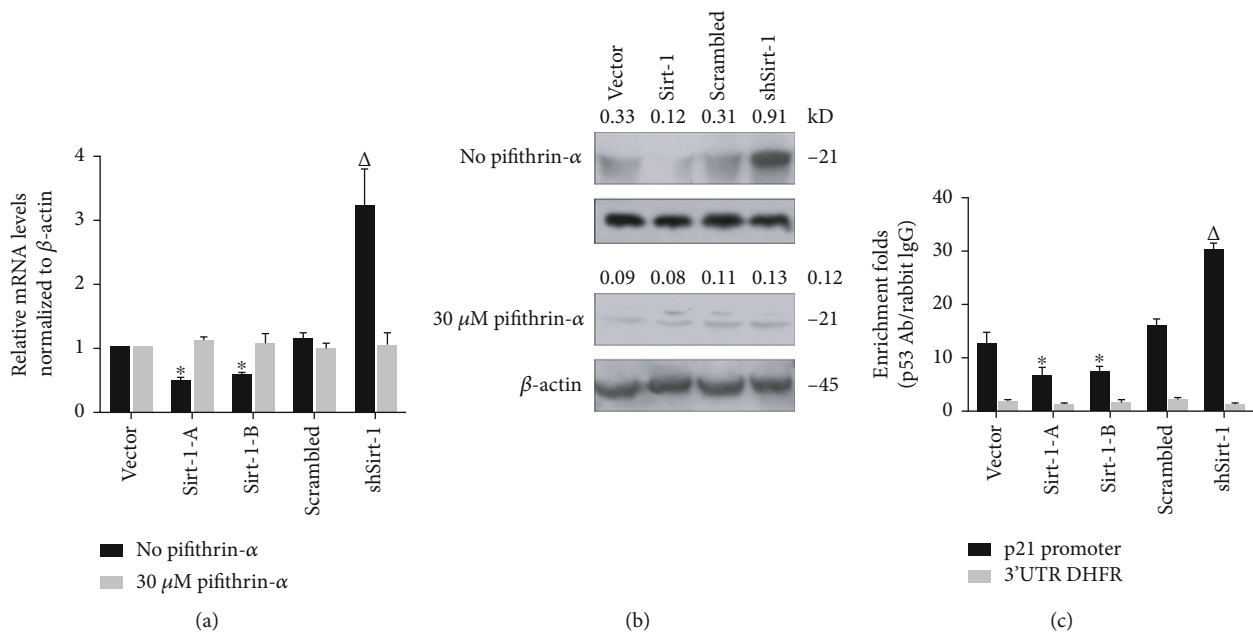


FIGURE 3: Sirt-1 indirectly regulates p21 depending on p53's transcriptional activity. p21 mRNA (a) and protein levels (b) were measured with or without the presence of 30  $\mu$ M pifithrin- $\alpha$ , an inhibitor of p53 transcriptional activity. \* $P < 0.05$ , vs. vector group;  $\Delta P < 0.05$ , vs. scrambled group. (c) Chromatin immunoprecipitation was performed to further confirm the effect of Sirt-1 on the binding of p53 to p21 promoter region. \* $P < 0.05$ , vs. vector group;  $\Delta P < 0.05$ , vs. scrambled group.

To determine how Sirt-1 regulates the binding of p53 to the promoter region of downstream target genes, we performed western blot to detect the acetylation level of p53 on 382 aa. p53 was highly acetylated at the lysine residue 382, which was largely inhibited by transient transfection of Sirt-1. Conversely, shRNA-mediated Sirt-1 knockdown resulted in a significant increase in p53 acetylation (Figure 4(a)). Since acetylation of p53 is required for its promoter binding activity, we then tested whether Sirt-1-mediated p53 deacetylation inhibited its promoter binding.

Indeed, ChIP analysis detected a reduction in p53 promoter binding, which was reversed by Sirt-1-specific inhibitor EX7 (Figure 4(b)). In addition, Sirt-1 knockdown enhanced p53 promoter binding activity, further addition of Sirt-1 inhibitor, while slightly increased, but not statistically significantly enhanced p53 recruitment to the promoter (Figure 4(b)). Further analysis revealed similar changes of Sirt-1 catalytic activity in the cell lysate parallelly prepared as in Figure 4(b), suggesting regulation of p53 transcriptional activity relies on its deacetylative activity

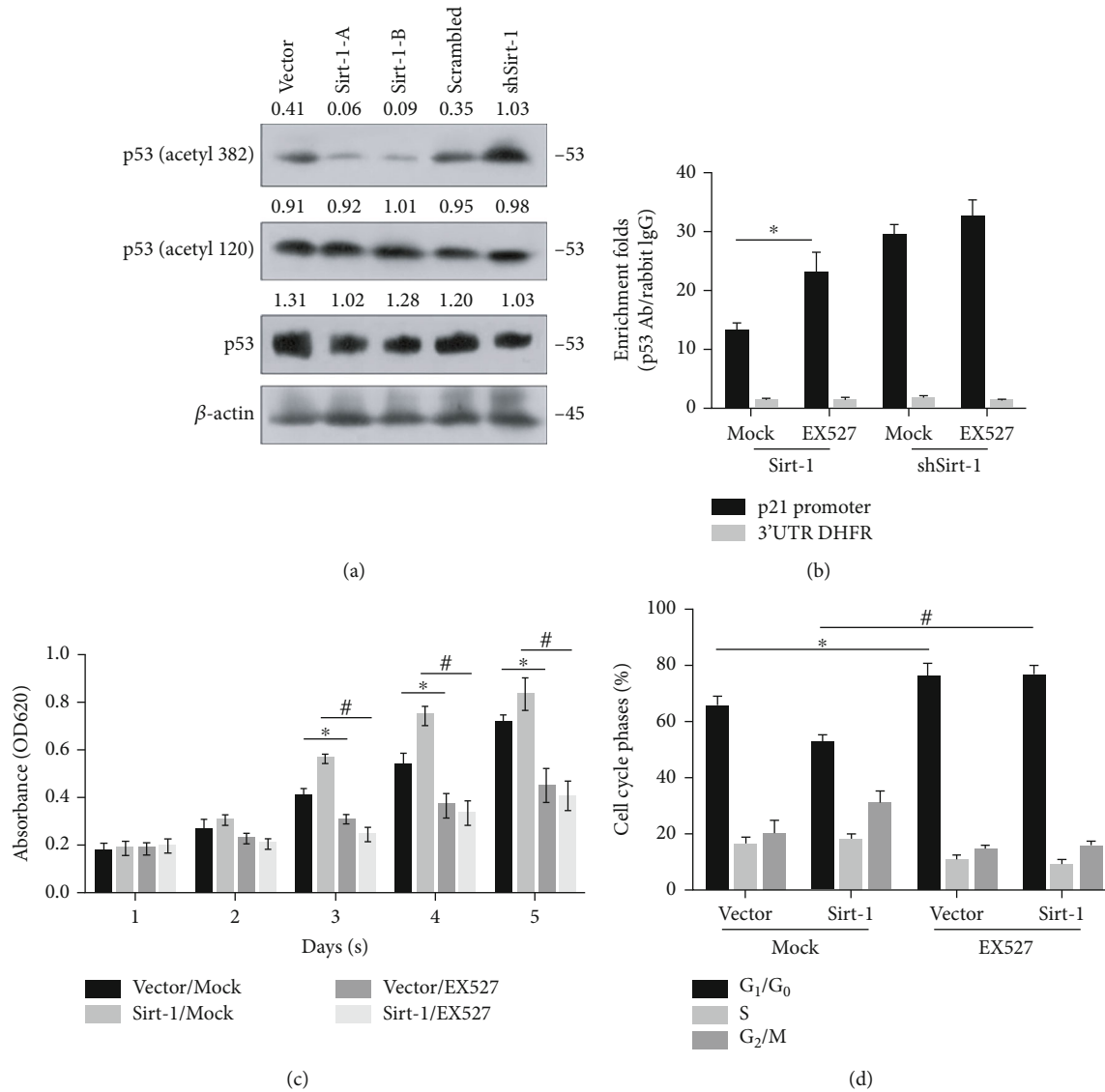


FIGURE 4: Sirt-1 regulates p53 acetylation at 382 amino acids (aa) and thus transcriptionally regulates p21. (a) Acetylation at 120 aa and 382 aa was detected by western blot. (b) Chromatin immunoprecipitation was performed after inhibiting acetylation by adding EX527. (c) Cell viability from days 1-5 was measured to access the effect of Sirt-1 via its acetylation activity. \* $P < 0.05$ , vs. vector group; # $P < 0.05$ , vs. scrambled group. (d) Cell cycle distribution was then measured by performing PI staining followed by flow cytometry. \* $P < 0.05$ , vs. vector group; # $P < 0.05$ , vs. scrambled group.

(Figure 4(c)). More importantly, Sirt-1 enhanced, but its knockdown resulted in an inhibition of the cell cycle progression (Figure 4(d)). Collectively, these results suggest that Sirt-1 regulates cell cycle progression through deacetylating p53 to attenuate its transcriptional activity.

**3.5. Sirt-1 Failed to Affect Cell Proliferation in SK-N-AS Cells.** To further confirm whether Sirt-1 affects cell proliferation via regulating p53, SK-N-AS, a p53-null cell line was employed. Sirt-1 was overexpressed or knocked down in SK-N-AS. By performing western blot, the efficient overexpression of Sirt-1 and knockdown of endogenous Sirt-1 were confirmed (Figure 5(a)). Opposite to the effects of overexpressed or knockdown Sirt-1 in SK-N-SH, modification of Sirt-1 failed

to obviously affect cell proliferation (Figures 5(b) and 5(c)) and cell cycle distribution (Figure 5(d)). Taken together, Sirt-1 affects cell proliferation and distribution of cell cycle mainly via the presence of p53.

**3.6. Sirt-1 Affects Cell Migration and Invasion.** Knockdown or overexpression of Sirt-1, migration, and invasion were measured. Migration results validated that siRNA largely diminished Sirt-1 expression, which dramatically weakened the migration (Figure 6(a)) and invasion (Figure 6(b)) of SK-N-SH cells. In contrast, transient transfection resulted in the increase in Sirt-1 protein expression, which dramatically enhanced the migration (Figure 6(a)) and invasion (Figure 6(b)) of SK-N-SH cells.

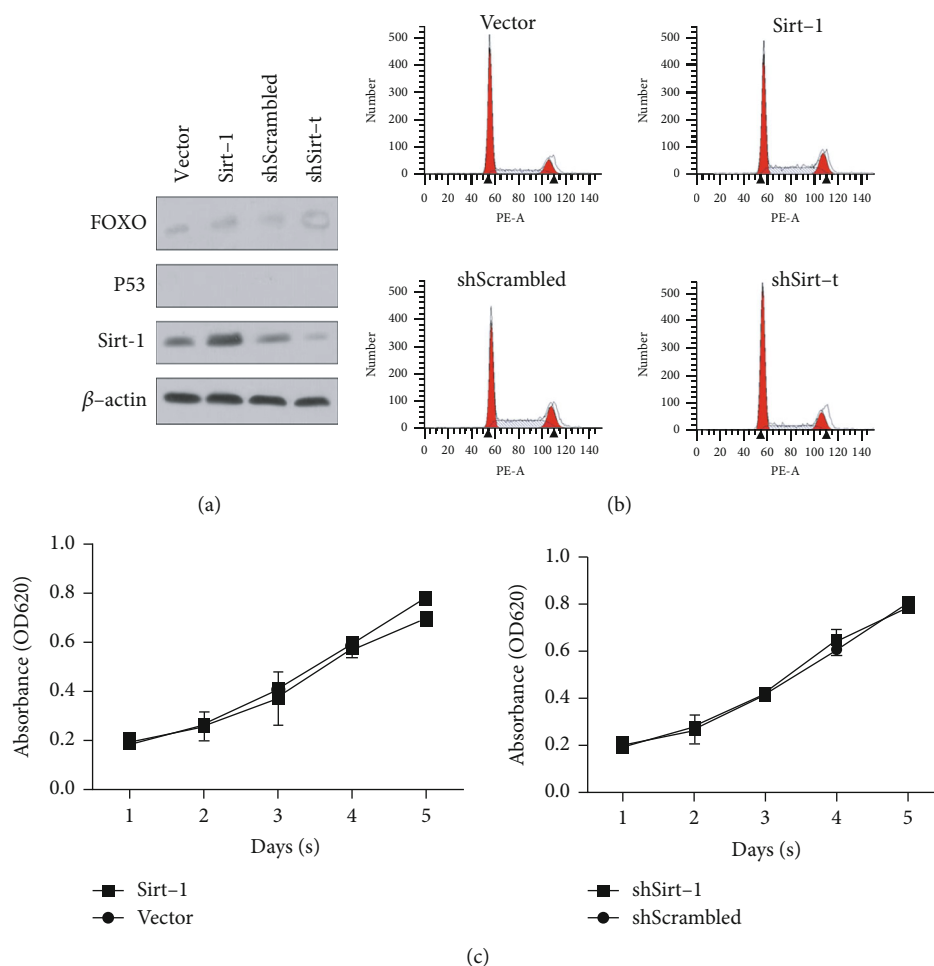


FIGURE 5: Sirt-1 failed to affect cell proliferation in SK-N-AS cells. (a) After overexpression or knockdown of Sirt-1, the protein levels of  $\beta$ -actin, Sirt-1, and FOXO were measured by western blot. (b) Cell viability from days 1-5 was measured to access the effect of Sirt-1 on SK-N-AS cells. (c) Cell cycle distribution was then measured by performing PI staining followed by flow cytometry. \* $P < 0.05$ , vs. vector group.

**3.7. Sirt-1 Inhibits  $H_2O_2$ -Induced Neuronal Cell Death.** In addition to p53, it has been shown that Sirt-1 functions as a negative regulator for ROS production, implying a possibility that Sirt-1 may protect neurons from oxidative stress-induced cell death. After 24h treatment with 50-250 mM  $H_2O_2$ , reactive oxygen species (ROS) was obviously increased and scavenged by adding 10mM of NAC (Figures 7(a) and 7(b)), and thus, 200 mM of  $H_2O_2$  was added to induce oxidative stress. Overexpressed Sirt-1 scavenged ROS production in SK-N-SH with  $H_2O_2$ , and knockdown of Sirt-1 presented opposite effect (Figures 8(a) and 8(b)). Similarly, the addition of 10 mM EX527 increased ROS accumulation, which indicated that the deacetylation activity of Sirt-1 is critical for its ROS suppressive activity (Figure 8(c)). Notably,  $H_2O_2$  treatment obviously increased the Sirt-1 protein level without affecting p53 protein (Figure 8(d)) and decreased p53's transcriptional activity (Figure 8(e)). Our results demonstrated that oxidative stress induced Sirt-1 in neuron cells, possibly to protect them from oxidative stress-induced cell death, through suppressing p53 transcriptional activity (Figure 8(f)).

To evaluate the protective effect of Sirt-1 from oxidative stress-induced SK-N-SH cell death, we first detect cell viability after 48-hour incubation in 200 mM  $H_2O_2$ . As it is shown in Figure 9(a), overexpressed Sirt-1 significantly improved cell viability under oxidative stress. Notably, knockdown of Sirt-1 failed to affect cell viability, possibly due to the endogenous Sirt-1 expression that remains at a low level and barely affected cell injury induced by oxidative stress. Consistent with this, inhibition of deacetylation activity of endogenous Sirt-1 by EX527 did not show any effects (Figure 9(b)). Taken together, our results show that overexpressed Sirt-1 inhibits oxidative stress-induced apoptotic cell death depending on its deacetylation activity (Figure 9(c)).

#### 4. Discussion

Sirt-1 has been widely studied as a regulator of many cellular physiological and pathological processes [34, 35] It was also observed that Sirt-1 was associated with cognitive impairment in AD, and similar results were obtained in depression studies [36, 37]. However, how Sirt-1 affected AD or



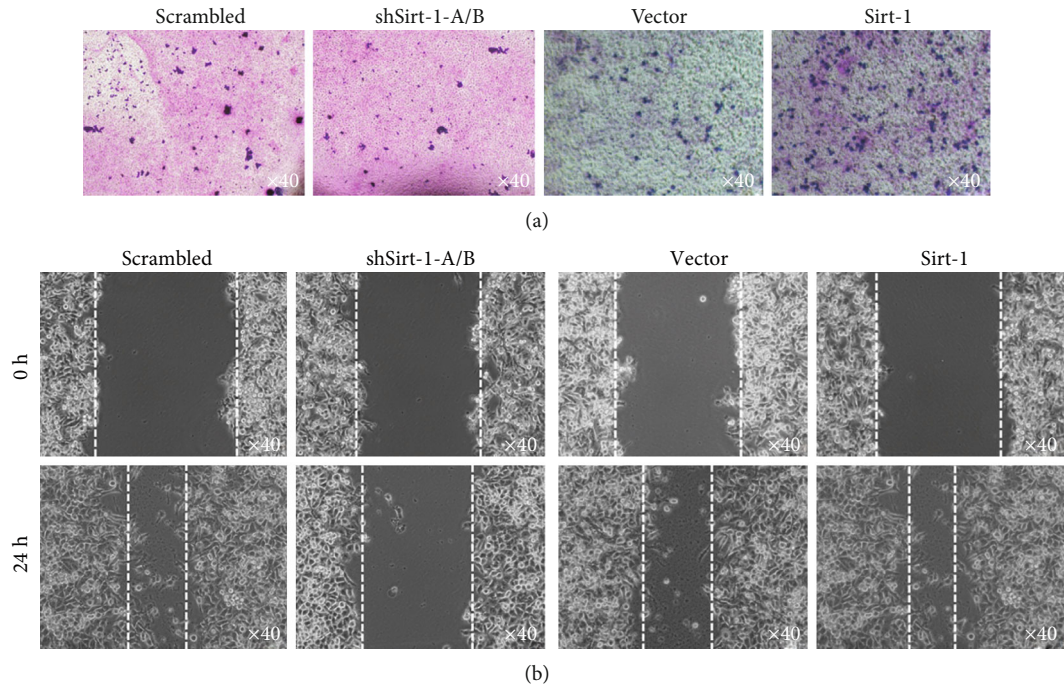


FIGURE 6: Sirt-1 affects cell migration and invasion. Knockdown or overexpression of Sirt-1, migration (a), and invasion (b) were measured.

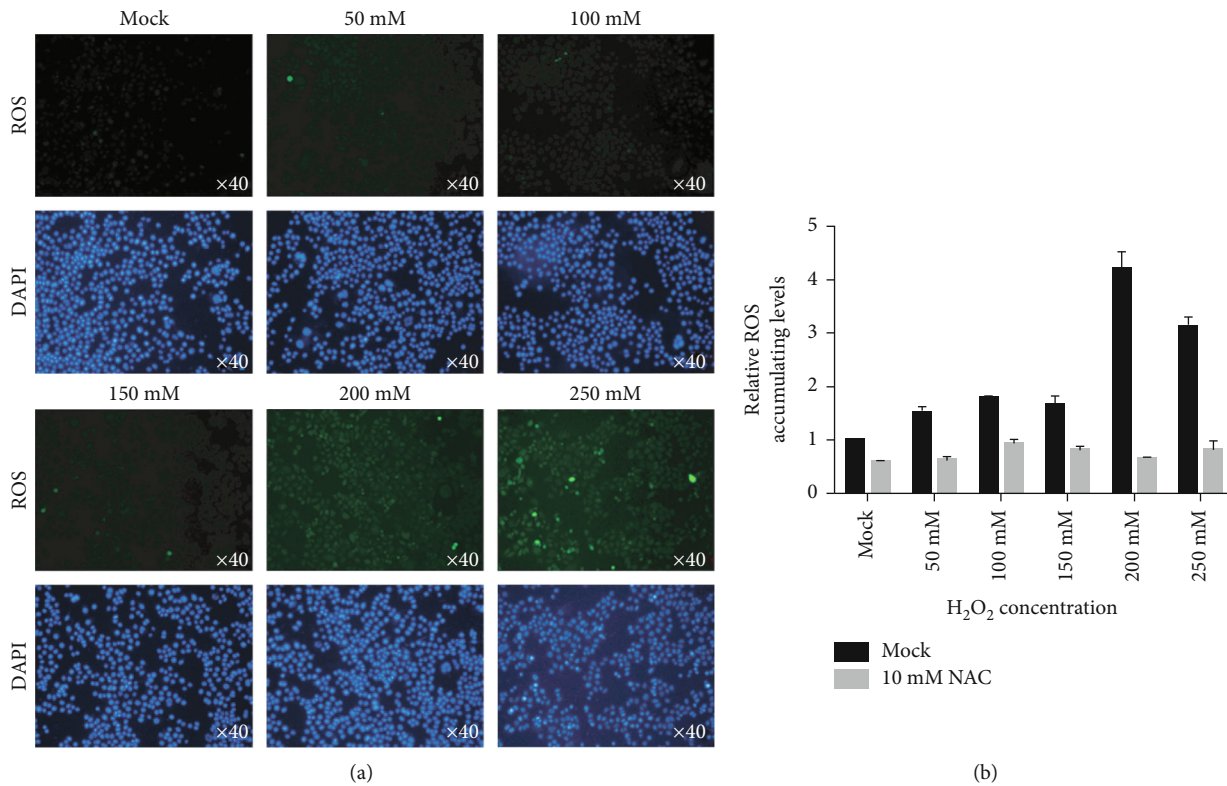


FIGURE 7: ROS level was induced after H<sub>2</sub>O<sub>2</sub> treatment. (a) ROS staining was imaged after 24 h exposure to different concentrations of H<sub>2</sub>O<sub>2</sub>. (b) ROS level was quantitatively measured.

depression is still unknown, especially the association among Sirt-1, AD, and depression. In this study, we investigated the regulation of Sirt-1 on the proliferation in SK-N-SH cells and

found that Sirt-1 affected physiological processes. Modified Sirt-1 by overexpression and knockdown transcriptionally regulated p53's downstream target gene, p21, in a p53-



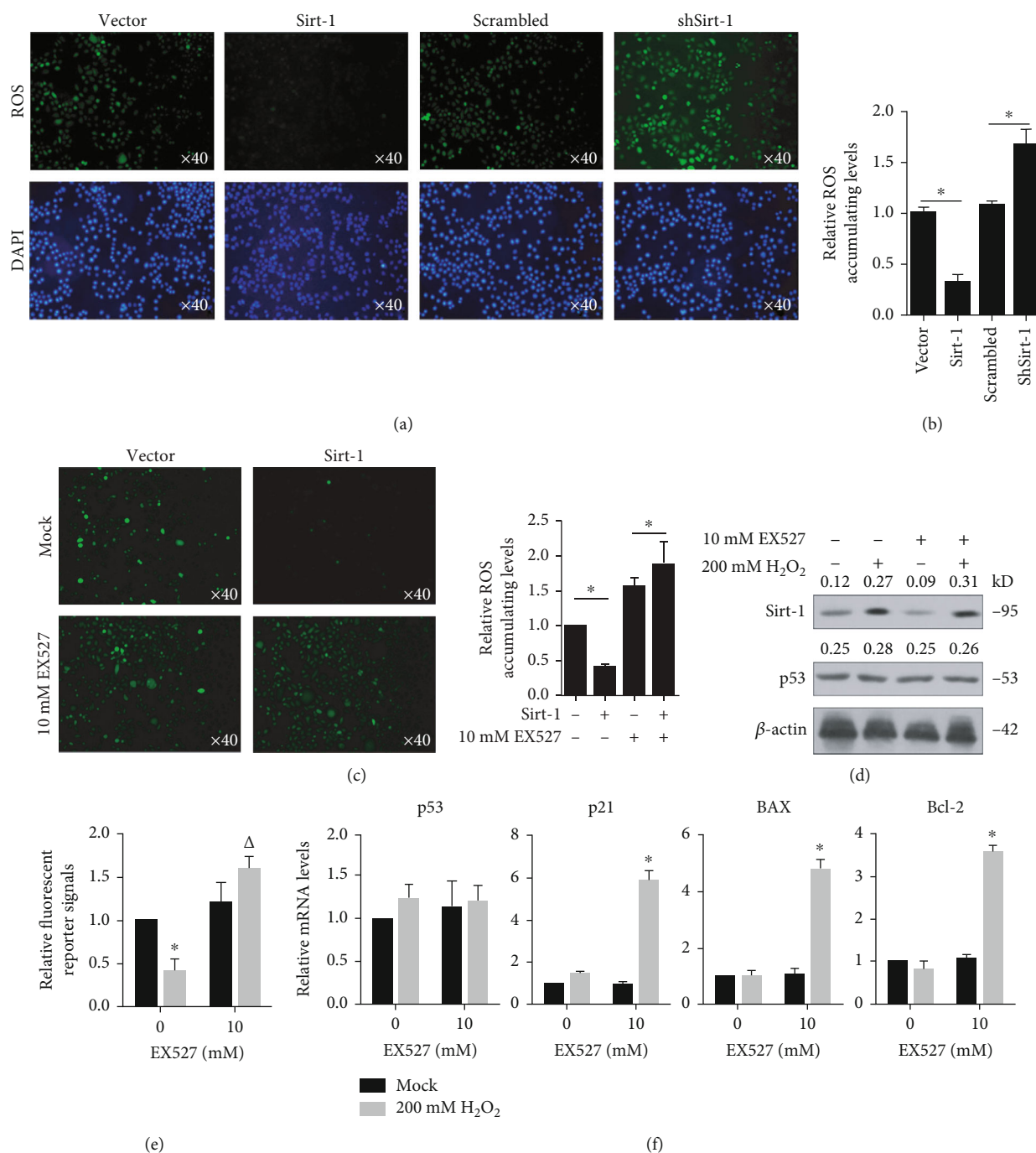


FIGURE 8: Sirt-1 abolished ROS accumulation after oxidative stress. (a, b) ROS accumulation of Sirt-1 was measured by the Reactive Oxygen Species Assay Kit under laser scanning confocal microscopy. The presence of Sirt-1 decreased ROS accumulation under oxidative stress. (c) The effect of Sirt-1 on the ROS level was measured. The results show that Sirt-1 affects the ROS level depending on the presence of its deacetylation activity. \* $P < 0.05$ . (d) The effects of adding EX527 on Sirt-1 and p53 expression were measured. Oxidative stress induced by  $H_2O_2$  obviously increased Sirt-1 protein. (e) Transcriptional activity of p53 was measured after  $H_2O_2$  treatment. \* $P < 0.05$ , vs. mock group;  $\Delta P < 0.05$ , vs. mock/EX527 group. (f) The effects of Sirt-1 to p53, p21, Bax, and Bcl-2 expression were measured. p53 and its downstream target gene expressions were measured by RT-qPCR. \* $P < 0.05$ , vs. mock/EX527 group.

dependent manner. Sirt-1 regulates the transcriptional activity of p53 by inhibition of the acetylation of p53. By employing human neuroblastoma cell line SK-N-AS, which is a p53-null cell line, upregulation or downregulation of Sirt-1 failed to affect p21 and cell cycle distribution, which further con-

firmed the necessity of p53 on Sirt-1's regulatory roles in Figure 2(b). The deacetylation activity of Sirt-1 is necessary to regulate physiological processes, including cell proliferation via regulating the transcriptional activity of p53, and thus regulates its downstream target genes. The above results

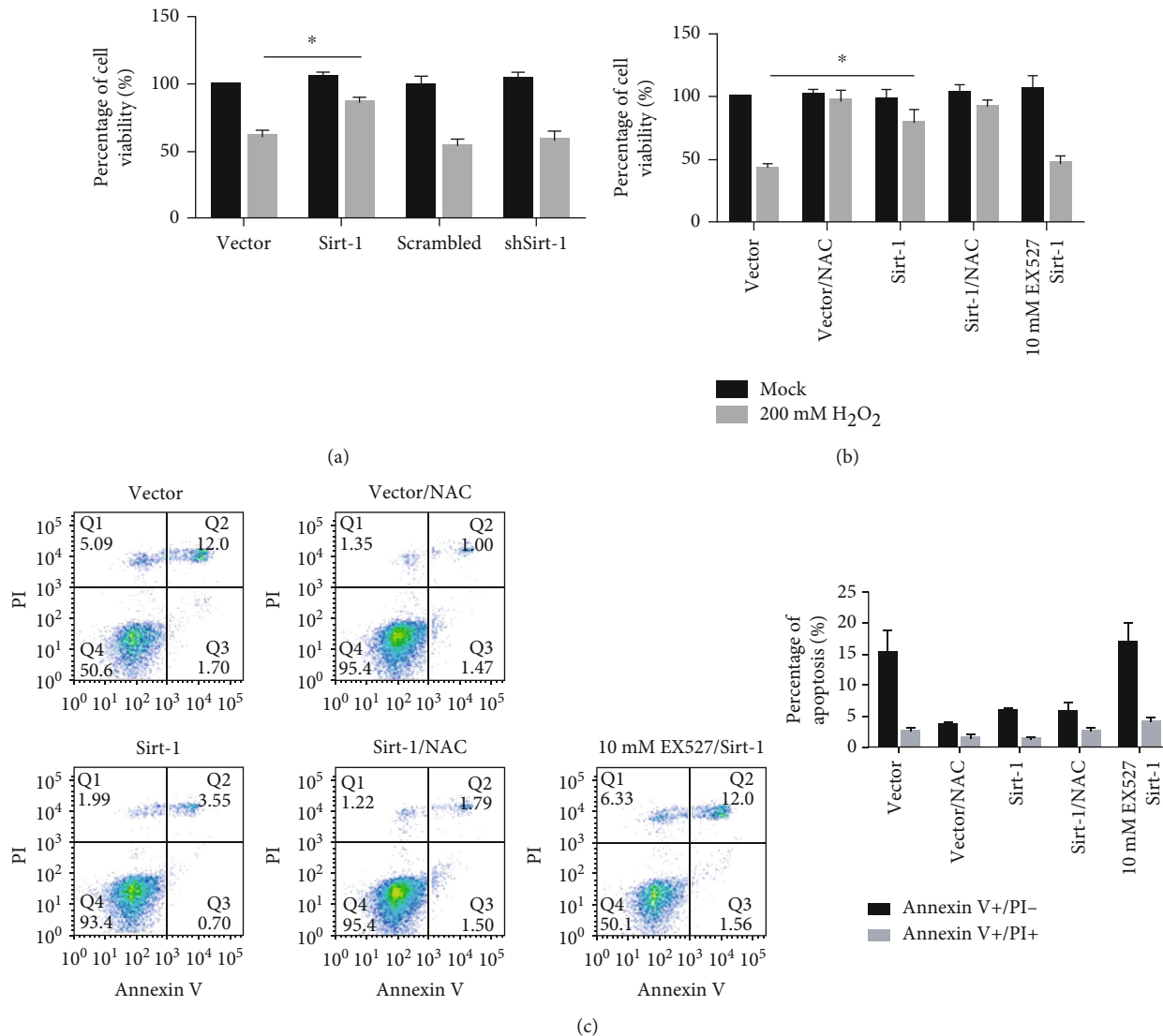


FIGURE 9: Sirt-1 protects cells from oxidative stress induced by H<sub>2</sub>O<sub>2</sub> via its deacetylation activity. (a) Adding 200 mM H<sub>2</sub>O<sub>2</sub>, the percentage of cell viabilities in the vector group, Sirt-1 group, scrambled group, and shSirt-1 group were measured. Sirt-1 presence protects cells from H<sub>2</sub>O<sub>2</sub>-induced decrease in cell viability. \**P* < 0.05, vs. vector group. (b, c) The percentage of apoptosis in the vector group, Sirt-1 group, scrambled group, shSirt-1 group, and EX527 group was measured. Sirt-1 exerts protective effects on cell viability and cell survival from apoptotic cell death depending on its deacetylation activity.

suggest that Sirt-1 may be closely related to the raising of AD by exerting protective effects on neuronal cells.

We also found that Sirt-1 promotes cell proliferation via regulating cell cycle progression. Overexpression of Sirt-1 enhanced cell viability and cell proliferation by promoting the entry of cell cycle from the G<sub>1</sub> phase to the G<sub>0</sub> phase, which is consistent with previous studies [38, 39]. As an important member of the sirtuin family, Sirt-1 is involved in regulating cell proliferation in many human cells. In AD model animals, overexpression of Sirt-1 slowed cell death, neurodegeneration, and cognitive decline [40, 41]. Acetylshikonin, which upregulates Sirt-1, can reduce cognitive dysfunction [42]. In contrast, inhibition of Sirt-1 expression can prevent oligodendrocyte progenitor cell proliferation [43]. Downregulation of Sirt-1 in

senescent microglia plays a key role in aggravating senescence in mice, while overexpression of Sirt-1 significantly prolongs life [44].

We observed that in SK-N-NH, but not in SK-N-AS, inhibition of Sirt-1 promoted the transcriptional activity of p53, but not that of FOXO1, which indicated that Sirt-1 specifically regulates p53 in SK-N-NH with wild-type p53. p53 is one of the most critical transcriptional factors to regulate nonhistone proteins [45, 46]. Acetylation of p53 increases the stability of the p53 protein and its antiviral to DNA damage, which is necessary for the detection of DNA damage and the activation of oncogenes [47, 48]. Previous literature studies have shown that Sirt-1 regulates the transcriptional regulatory activity of p53 by deacetylation of p53, which is similar to our results [20].

Under oxidative stress, p53 promotes cell death after the failure of DNA repair [17]. Sirt-1 was reported to exert protective effects on rat neuronal cells in vivo by inhibiting p53 transcriptional activity. EX527, a Sirt-1 inhibitor, exerted similar effects to that of Sirt-1 knockdown. EX527 treatment potentially due to the induction of ROS by oxidative stress could be scavenged by activation of Sirt-1 and inhibition of p53 [19]. By considering that oxidative stress is recognized as a central stress factor in major depressive disorder (MDD) and AD, activation of Sirt-1 may prevent from MDD and AD via protecting neuronal cells from oxidative stress.

In summary, we demonstrated the important role of Sirt-1 in maintaining the proliferation and suppressing the oxidative stress-induced neuronal cell death. At the molecular level, Sirt-1 inhibits p53 transcription activation through directly deacetylating p53 and thus reduces p21 gene expression. On the other hand, Sirt-1 protects neuronal cells from oxidative stress-induced apoptosis via suppressing ROS production. These results provide a molecular explanation of the protective effect of Sirt-1 on AD and depression-related diseases and provide a rationale for Sirt-1 as a biomarker and therapeutic target for the diagnosis, treatment, and prevention of AD and depression-related diseases.

### Data Availability

The data used to support the findings of this study are available from the corresponding author upon request.

### Conflicts of Interest

The authors declare that they have no conflicts of interest.

### Authors' Contributions

Lei Liu, Guangyuan Xia, and Peifan Li are joint first authors.

### Acknowledgments

The authors thank Dr. Li Jia for her generous assistance to the manuscript. This study had support from the National Natural Science Foundation of China (Nos. 81761128036, 81960262, and 31760294), as well as supports from the High-Level Innovative Talents Cultivation Program of Guizhou Province (Qian Ke He SY[2018]5802 and [2016]5679), Guizhou Science and Technology Cooperation Support [2020] No. 4Y198, and Guiyang City Science and Technology Projects, Zhu Subjects Contract ([2018]1-94).

### References

- [1] W. Duan, "Sirtuins: from metabolic regulation to brain aging," *Frontiers in Aging Neuroscience*, vol. 5, 2013.
- [2] T. Finkel, C. X. Deng, and R. Mostoslavsky, "Recent progress in the biology and physiology of sirtuins," *Nature*, vol. 460, no. 7255, pp. 587–591, 2009.
- [3] M. C. Haigis and D. A. Sinclair, "Mammalian sirtuins: biological insights and disease relevance," *Annual Review of Pathology*, vol. 5, no. 1, pp. 253–295, 2010.
- [4] L. Guarente and H. Franklin, "Epstein lecture: sirtuins, aging, and medicine," *Journal of Medicine*, vol. 364, no. 23, pp. 2235–2244, 2011.
- [5] O. Grubisha, B. C. Smith, and J. M. Denu, "Small molecule regulation of Sir2 protein deacetylases," *The FEBS Journal*, vol. 272, no. 18, pp. 4607–4616, 2005.
- [6] M. Vinciguerra, M. Fulco, A. Ladurner, V. Sartorelli, and N. Rosenthal, "Sirt1 in muscle physiology and disease: lessons from mouse models," *Disease Models & Mechanisms*, vol. 3, no. 5-6, pp. 298–303, 2010.
- [7] M. Fulco, R. L. Schiltz, S. Iezzi et al., "Sir2 regulates skeletal muscle differentiation as a potential sensor of the redox state," *Molecular Cell*, vol. 12, no. 1, pp. 51–62, 2003.
- [8] P. Oberdoerffer, S. Michan, M. McVay et al., "SIRT1 redistribution on chromatin promotes genomic stability but alters gene expression during aging," *Cell*, vol. 135, no. 5, pp. 907–918, 2008.
- [9] S. W. Min, S. H. Cho, Y. Zhou et al., "Acetylation of tau inhibits its degradation and contributes to tauopathy," *Neuron*, vol. 67, no. 6, pp. 953–966, 2010.
- [10] G. Donmez, "The neurobiology of sirtuins and their role in neurodegeneration," *Trends in Pharmacological Sciences*, vol. 33, no. 9, pp. 494–501, 2012.
- [11] J. Ji, P. Tao, Q. Wang, L. Li, and Y. Xu, "SIRT1: mechanism and protective in diabetic nephropathy," *Endocrine, Metabolic & Immune Disorders - Drug Targets*, vol. 20, 2020.
- [12] D. Frescas, L. Valenti, and D. Accili, "Nuclear trapping of the forkhead transcription factor FoxO1 via Sirt-dependent deacetylation promotes expression of glucogenetic genes," *The Journal of Biological Chemistry*, vol. 280, no. 21, pp. 20589–20595, 2005.
- [13] J. Yi and J. Luo, "SIRT1 and p53, effect on cancer, senescence and beyond," *Biochimica et Biophysica Acta (BBA) - Proteins and Proteomics*, vol. 1804, no. 8, pp. 1684–1689, 2010.
- [14] A. Brunet, L. B. Sweeney, J. F. Sturgill et al., "Stress-dependent regulation of FOXO transcription factors by the SIRT1 deacetylase," *Science*, vol. 303, no. 5666, pp. 2011–2015, 2004.
- [15] J. G. Jackson and O. M. Pereira-Smith, "p53 is preferentially recruited to the promoters of growth arrest genes p21 and GADD45 during replicative senescence of normal human fibroblasts," *Cancer Research*, vol. 66, no. 17, pp. 8356–8360, 2006.
- [16] W. Wei, R. M. Hemmer, and J. M. Sedivy, "Role of p14 (ARF) in replicative and induced senescence of human fibroblasts," *Molecular and Cellular Biology*, vol. 21, no. 20, pp. 6748–6757, 2001.
- [17] H. Xu, Y. Zhou, K. A. Coughlan et al., "AMPK $\alpha$ 1 deficiency promotes cellular proliferation and DNA damage via p21 reduction in mouse embryonic fibroblasts," *Biochim Biophys Acta*, vol. 1853, no. 1, pp. 65–73, 2015.
- [18] M. P. Mattson, "Pathways towards and away from Alzheimer's disease," *Nature*, vol. 430, no. 7000, pp. 631–639, 2004.
- [19] M. Schieber and N. S. Chandel, "Corrigendum to Ameliorative effect of saffron aqueous extract on hyperglycemia, hyperlipidemia, and oxidative stress on diabetic encephalopathy in streptozotocin induced experimental diabetes mellitus," *BioMed Research International*, vol. 2020, 2020.
- [20] C. Matrone, M. T. Ciotti, D. Mercanti, R. Marolda, and P. Calissano, "NGF and BDNF signaling control amyloidogenic route and Abeta production in hippocampal neurons,"

- Proc Natl Acad Sci USA*, vol. 105, no. 35, pp. 13139–13144, 2008.
- [21] S. Kaptoge, E. D. Angelantonio, C. Moore et al., “Longer-term efficiency and safety of increasing the frequency of whole blood donation (INTERVAL): extension study of a randomised trial of 20 757 blood donors,” *Lancet Haematol*, vol. 6, no. 10, pp. e510–e520, 2019.
- [22] X. Huang, C. S. Atwood, M. A. Hartshorn et al., “The A beta peptide of Alzheimer’s disease directly produces hydrogen peroxide through metal ion reduction,” *Biochemistry*, vol. 38, no. 24, pp. 7609–7616, 1999.
- [23] M. Khan, S. A. Shah, and M. O. Kim, “17 $\beta$ -Estradiol via SIRT1/acetyl-p53/NF-kB signaling pathway rescued postnatal rat brain against Acute ethanol intoxication,” *Molecular Neurobiology*, vol. 55, no. 4, pp. 3067–3078, 2018.
- [24] T. C. Huang, H. Y. Chang, C. Y. Chen et al., “Silencing of miR-124 induces neuroblastoma SK-N-SH cell differentiation, cell cycle arrest and apoptosis through promoting AHR,” *FEBS Letters*, vol. 585, no. 22, pp. 3582–3586, 2011.
- [25] Y. Kobayashi, Y. Furukawa-Hibi, C. Chen et al., “Sirt1 is critical regulator of FOXO-mediated transcription in response to oxidative stress,” *International Journal of Molecular Medicine*, vol. 16, no. 2, pp. 237–243, 2005.
- [26] D. D. Xu, P. J. Zhou, Y. Wang et al., “miR-150 suppresses the proliferation and tumorigenicity of leukemia stem cells by targeting the Nanog signaling pathway,” *Frontiers in Pharmacology*, vol. 7, no. 439, 2016.
- [27] H. Wang, L. Wang, S. Zhang, Z. Xu, and G. Zhang, “Downregulation of LINC00665 confers decreased cell proliferation and invasion via the miR-138-5p/E2F3 signaling pathway in NSCLC,” *Biomedicine & Pharmacotherapy*, vol. 127, no. 110214, p. 110214, 2020.
- [28] K. Qi, Y. Li, K. Huang et al., “Pre-application of arsenic trioxide may potentiate cytotoxic effect of vinorelbine/docetaxel on neuroblastoma SK-N-SH cells,” *Biomedicine & Pharmacotherapy*, vol. 113, no. 108665, 2019.
- [29] C. Zeng, F. Pan, and L. A. Jones, “Evaluation of 5-ethynyl-2'-deoxyuridine staining as a sensitive and reliable method for studying cell proliferation in the adult nervous system,” *Brain Research*, vol. 1319, no. 11, pp. 21–32, 2010.
- [30] X. W. Zhang, W. Qin, W. J. Gou, J. F. Li, B. Y. Liu, and F. C. Zhang, “Effect of Bmi-1 gene on the proliferation of gastric cancer cells and its mechanism,” *World Chinese Journal of Digestology*, vol. 17, no. 14, pp. 1390–1393, 2009.
- [31] Y. Zhang, W. W. Luo, K. Wang, and J. Shi, “Overexpression of histone deacetylase 11 suppresses basal-like breast cancer cell invasion and metastasis,” *J South Med Univ*, vol. 39, no. 7, pp. 751–759, 2019.
- [32] Q. S. Wang, Y. Xia, and H. X. Chen, “LINC01296 regulates Wnt/ $\beta$ -catenin signaling pathway and affects SK-N-SH cell proliferation, apoptosis, migration and invasion,” *Chinese Journal of Cell Biology*, vol. 42, no. 12, pp. 2116–2125, 2020.
- [33] Z. Lin, H. Yang, Q. Kong et al., “USP22 antagonizes p53 transcriptional activation by deubiquitinating Sirt1 to suppress cell apoptosis and is required for mouse embryonic development,” *Molecular Cell*, vol. 46, no. 4, pp. 484–494, 2012.
- [34] X. Bi, Q. Ye, D. Li et al., “Inhibition of nucleolar stress response by Sirt1: a potential mechanism of acetylation-independent regulation of p53 accumulation,” *Aging Cell*, vol. 18, no. 2, p. e12900, 2019.
- [35] S. Libert and L. Guarente, “Metabolic and neuropsychiatric effects of calorie restriction and sirtuins,” *Annual Review of Physiology*, vol. 75, no. 1, pp. 669–684, 2013.
- [36] M. Schott and C. Petersen, “New criteria for Alzheimer’s disease: which, when and why?,” *Brain*, vol. 138, no. 5, pp. 1134–1137, 2015.
- [37] J. Shen, Y. Li, C. Qu, L. Xu, H. Sun, and J. Zhang, “The enriched environment ameliorates chronic unpredictable mild stress-induced depressive-like behaviors and cognitive impairment by activating the SIRT1/miR-134 signaling pathway in hippocampus,” *Journal of Affective Disorders*, vol. 248, pp. 81–90, 2019.
- [38] D. Kim, M. D. Nguyen, M. M. Dobbin et al., “SIRT1 deacetylase protects against neurodegeneration in models for Alzheimer’s disease and amyotrophic lateral sclerosis,” *EMBO JOURNAL*, vol. 26, no. 13, pp. 3169–3179, 2007.
- [39] B. Gomes, J. Silva, C. Romeiro et al., “Neuroprotective mechanisms of resveratrol in Alzheimer’s disease: role of SIRT1,” *Oxidative Medicine and Cellular Longevity*, vol. 2018, Article ID 8152373, 15 pages, 2018.
- [40] Q. Li, J. Zeng, M. Su, Y. He, and B. Zhu, “Acetylshikonin from *Zicao* attenuates cognitive impairment and hippocampus senescence in d-galactose-induced aging mouse model via upregulating the expression of SIRT1,” *Brain Research Bulletin*, vol. 137, pp. 311–318, 2018.
- [41] B. Jablonska, M. Gierdalski, L. J. Chew et al., “Sirt1 regulates glial progenitor proliferation and regeneration in white matter after neonatal brain injury,” *Nature Communications*, vol. 7, no. 1, 2016.
- [42] S. H. Cho, J. A. Chen, F. Sayed et al., “SIRT1 deficiency in microglia contributes to cognitive decline in aging and neurodegeneration via epigenetic regulation of IL-1 $\beta$ ,” *The Journal of Neuroscience*, vol. 35, no. 2, pp. 807–818, 2015.
- [43] J. Yuan, K. Minter-Dykhouse, and Z. K. Lou, “A c-Myc-SIRT1 feedback loop regulates cell growth and transformation,” *The Journal of Cell Biology*, vol. 185, no. 2, pp. 203–211, 2009.
- [44] E. Conrad, T. Polonio-Vallon, M. Meister et al., “HIPK2 restricts SIRT1 activity upon severe DNA damage by a phosphorylation-controlled mechanism,” *Cell Death & Differentiation*, vol. 23, no. 1, pp. 110–122, 2016.
- [45] J. Zhang, L. Shen, and L. Q. Sun, “The regulation of radiosensitivity by p53 and its acetylation,” *Cancer Letters*, vol. 363, no. 2, pp. 108–118, 2015.
- [46] D. Wang, N. Kon, G. Lasso et al., “Acetylation-regulated interaction between p53 and SET reveals a widespread regulatory mode,” *Nature*, vol. 538, no. 7623, pp. 118–122, 2016.
- [47] M. Hernandez-Jimenez, O. Hurtado, M. I. Cuartero et al., “Silent information regulator 1 protects the brain against cerebral ischemic damage,” *Stroke*, vol. 44, no. 8, pp. 2333–2337, 2013.
- [48] Y. Feng, T. Liu, S. Y. Dong et al., “Rotenone affects p53 transcriptional activity and apoptosis via targeting SIRT1 and H3K9 acetylation in SH-SY5Y cells,” *Journal of Neurochemistry*, vol. 134, no. 4, pp. 668–676, 2015.



## Research Article

# Serum ICAM-1 as a Predictor of Prognosis in Patients with Acute Ischemic Stroke

Lei Wang,<sup>1</sup> Yan Chen,<sup>2</sup> Depeng Feng,<sup>3</sup> and Xiaoling Wang<sup>3</sup> 

<sup>1</sup>Department of Infectious Disease, Beijing Tiantan Hospital, Capital Medical University, Beijing, China

<sup>2</sup>Department of Geriatric Medicine, Shandong Provincial Third Hospital, Cheeloo College of Medicine, Shandong University, Jinan, Shandong Province, China

<sup>3</sup>Department of Neurology, Liaocheng People's Hospital, Liaocheng, Shandong Province, China

Correspondence should be addressed to Xiaoling Wang; haiyun900@163.com

Received 17 February 2021; Revised 9 March 2021; Accepted 11 March 2021; Published 19 March 2021

Academic Editor: Yuzhen Xu

Copyright © 2021 Lei Wang et al. This is an open access article distributed under the Creative Commons Attribution License, which permits unrestricted use, distribution, and reproduction in any medium, provided the original work is properly cited.

**Objective.** Inflammation is one of the key mechanisms involved in functional impairment after stroke. Intercellular adhesion molecule-1 (ICAM-1) is an important inflammatory molecule in the body. The purpose of our study was to determine the correlation between ICAM-1 and the prognosis of acute ischemic stroke (AIS). **Methods.** 286 AIS patients treated at Beijing Tiantan Hospital were continuously included in the study. The demographic data of the patients were collected, and the fasting blood within 24 hours of admission was collected to detect the clinical indicators. The functional prognosis was measured using the modified Rankin Scale (mRS) 3 months after stroke. The poor prognosis is defined as mRS  $\geq 3$ . The enzyme-linked immunosorbent assay (ELISA) was used to determine the serum ICAM-1 levels. **Results.** The serum ICAM-1 levels of patients with poor prognosis were significantly higher than that of patients with good prognosis ( $144.2 \pm 14.8$  vs  $117.5 \pm 12.1$  pg/ml). Receiver operating characteristic curve (ROC) analysis showed that the sensitivity and specificity of serum ICAM-1 for predicting the prognosis of AIS were 74% and 76%, respectively. In logistic regression analysis, the serum ICAM-1 level is still an independent predictor of poor prognosis (odds ratio [OR]: 0.52; 95% confidence interval [CI]: 0.318-0.839). **Conclusions.** Higher serum ICAM-1 levels on admission in AIS patients might increase the risk of poor prognosis.

## 1. Introduction

The definition of stroke is a neurological impairment syndrome caused by the permanent brain, spinal cord, or retinal cell death caused by vascular etiology [1]. The morbidity and disability rate of stroke are relatively high, with 13.7 million new stroke patients every year, and 5.8 million deaths due to stroke [2]. In the world, more than 80 million people have survived strokes, of which about 70% are ischemic strokes, and the rest are cerebral hemorrhage (ICH) or subarachnoid hemorrhage (SAH). Stroke is the second leading cause of death in the world, while it ranks first in China. China's national research and regular government reports show that the burden of stroke is high and is gradually increasing [3]. The pathogenic mechanism

of AIS is complicated, and there is no cure [4, 5]. Therefore, finding the pathogenic target of AIS and developing targeted treatment are urgent problems to be solved.

Intercellular adhesion molecule-1 (ICAM-1), also named CD54, is a type I transmembrane protein with a molecular weight between 80 and 114 kDa, and its molecular weight varies depending on the level of glycosylation [6]. The full length of ICAM-1 consists of five immunoglobulin (Ig) domains, a short cytoplasmic tail with multiple threonine residues, and a transmembrane domain [7]. Alternative splicing is a common post transcriptional mechanism that is widely used to regulate the gene expression [8]. ICAM-1 can produce soluble ICAM-1 through alternative splicing, which can be measured in various body fluids [9]. Studies have shown that ICAM-1 levels are elevated in atherosclerosis, cardiovascular



disease, and metabolic vascular neuropathy [10–13]. However, there are still few studies on the correlation between ICAM-1 and AIS.

Neurons, microglia, astrocytes, and vascular components together form a functional neurovascular unit, which is the anatomical basis for the pathogenesis of AIS [14, 15]. Microglia are important innate immune cells in the body, and their different activation states exert different inflammatory effects [16–18]. More and more evidences show that inflammation plays a key role in the pathogenesis of AIS and may become a potential target for treatment [19, 20]. In this study, we explored the predictive effect of the inflammatory molecule ICAM-1 on the prognosis of AIS, which may provide an important target for the therapeutic intervention of stroke.

## 2. Methods

**2.1. Study Population.** From January 2020 to December 2020, AIS patients who were treated at Beijing Tiantan Hospital were included in the study. After screening, a total of 286 patients were included in the study. An AIS attack is defined as the patient's first neurological deficit, which is confirmed by brain CT or MRI. The exclusion criteria include (1) past history of stroke, (2) combined with tumor, (3) combined with infectious disease or autoimmune disease, (4) intravenous thrombolysis or arterial thrombectomy, and (5) combined with cerebral hemorrhage. The study complied with the Declaration of Helsinki and was approved by the local medical ethics committee. Research subjects or guardians agree to participate in the research and sign an informed consent form.

**2.2. Characteristics of AIS Patients.** All subjects underwent the National Institute of Health Stroke Scale immediately after enrollment to evaluate the patients' neurological function. Their demographic data (age and gender) were collected. At the same time, the past medical history (hypertension, diabetes, coronary heart disease, and atrial fibrillation) was asked and recorded. An electronic sphygmomanometer is used to measure the patient's blood pressure in a quiet state. The patient's fasting blood glucose and total cholesterol were measured in the biochemical laboratory.

**2.3. Serum ICAM-1 Determination.** Fasting blood of all patients was collected within 24 hours of admission. Peripheral blood was allowed to stand for half an hour at room temperature and then centrifuged at low temperature and high speed. Separate and pack the serum and store it in a refrigerator at  $-80^{\circ}\text{C}$  for later use. The concentration of serum ICAM-1 was determined by the enzyme-linked immunosorbent assay (ELISA). All ICAM-1 antibodies for the experiment were purchased from Abcam Co., Ltd. (Abcam, Cambridge, MA). The ELISA test method refers to the previous literature and product instructions [21–23].

**2.4. Prognosis Assessment and Grouping.** The modified Rankin Scale (mRS) is a commonly used neuroevaluation scale, mainly used to evaluate the degree of disability in patients with neurological dysfunction. The scale was first proposed

by Dr. John Rankin of Scotland in 1957, and it has become the most widely used clinical outcome tool in stroke clinical trials [24–26]. In this study, the modified Rankin Score (mRS) was used to measure the functional prognosis 3 months after stroke. A good prognosis is defined as  $\text{mRS} < 3$ , and a poor prognosis is defined as  $\text{mRS} \geq 3$ . According to the difference of mRS scores, AIS patients were divided into the good outcome group and poor outcome group.

**2.5. Statistical Analysis.** Continuous variables were described as mean  $\pm$  standard deviation or median and interquartile range and compared with Student's *t*-test. Categorical variables are described as *n* (%) and compared with the chi-square test. The receiver operating characteristic curve is applied to determine the cut point of ICAM-1 to distinguish between good and poor outcomes. Logistic regression analysis was used to evaluate the independent contribution of different variables to prognosis prediction. Statistical analysis was performed using SPSS22.0 software (SPSS Inc., Chicago, Illinois, USA), and *p* value  $< 0.05$  was considered statistically significant.

## 3. Results

**3.1. Characteristics of AIS Patients.** A total of 286 AIS patients were included in this study. According to the mRS score, they were divided into a good outcome group ( $n = 181$ ) and a poor outcome group ( $n = 105$ ). The ages of AIS patients in the good outcome group and poor outcome group were ( $61.4 \pm 8.9$ ) and ( $61.7 \pm 9.6$ ) years, respectively. The proportion of men with AIS in the good outcome group and poor outcome group was 60.8% and 59.0%, respectively. There was no significant statistical difference in age and gender between the two groups ( $p > 0.05$ ). We further compared the past medical history of the two groups of AIS patients, and we found that their incidence of hypertension, diabetes, coronary heart disease, and atrial fibrillation was not significantly different ( $p > 0.05$ ). Regarding clinical indicators, such as systolic blood pressure, diastolic blood pressure, fasting blood glucose, and total cholesterol, there was also no significant statistical difference between the two groups ( $p > 0.05$ ). However, the serum ICAM-1 concentrations of AIS patients in the good outcome group and the poor outcome group were ( $117.5 \pm 12.1$ ) and ( $144.2 \pm 14.8$ ) pg/ml, respectively, and the serum ICAM-2 levels of AIS patients in the poor outcome group were significantly higher in the good outcome group ( $p < 0.001$ ). The characteristics of all AIS patients are shown in Table 1.

**3.2. ROC Analysis for the Serum ICAM-1 Level in the AIS Patients.** As shown in Figure 1, in order to evaluate the diagnostic value of serum ICAM-1 as a potential prognostic marker of AIS, we performed ROC curve analysis. For serum ICAM-1, the sensitivity is 74%, the specificity is 76%, and the area under the curve (AUC) is 0.772. The best cutoff value of the ROC curve for distinguishing good outcomes from poor outcomes is 129.5 pg/ml. When the baseline serum ICAM-1 concentration is higher than 129.5 pg/ml, it indicates that the prognosis of AIS patients is poor. However, when the

TABLE 1: Characteristics of AIS patients with poor outcome and good outcome.

	Good outcome (n = 181)	Poor outcome (n = 105)	p value
Age, years	61.4 ± 8.9	61.7 ± 9.6	0.790
Male, n (%)	110 (60.8)	62 (59.0)	0.774
NHSS on admission	5 (2-7)	10 (8-14)	<0.001
Hypertension, n (%)	89 (49.2)	53 (50.5)	0.832
Diabetes mellitus, n (%)	54 (29.8)	32 (30.5)	0.909
Coronary heart disease, n (%)	19 (10.5)	12 (11.4)	0.807
Atrial fibrillation, n (%)	10 (5.5)	6 (5.7)	0.946
Systolic blood pressure, mmHg	148.3 ± 10.2	148.5 ± 10.7	0.875
Diastolic blood pressure, mmHg	92.6 ± 7.9	92.8 ± 8.3	0.840
Fasting blood-glucose, mmol/l	6.2 ± 0.8	6.3 ± 0.9	0.332
Total cholesterol, mmol/l	4.7 ± 1.2	4.8 ± 1.1	0.484
ICAM-1, pg/ml	117.5 ± 12.1	144.2 ± 14.8	<0.001

AIS: acute ischemic stroke; NIHSS: National Institute of Health Stroke Scale; ICAM-1: intercellular adhesion molecule-1.

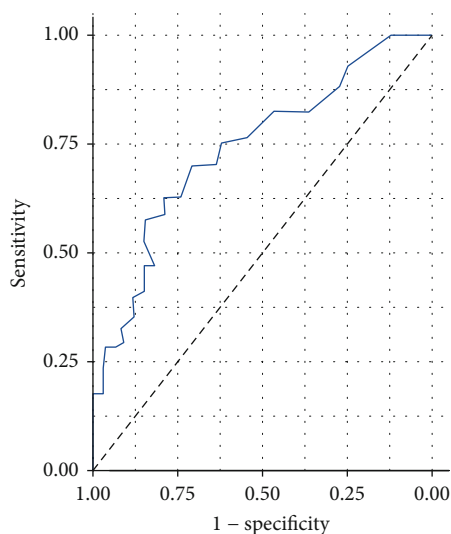


FIGURE 1: ROC analysis for the serum ICAM-1 level in the AIS patients.

baseline serum ICAM-1 concentration is lower than 129.5 pg/ml, it indicates that AIS patients have a good prognosis.

**3.3. Logistic Regression Analysis.** The clinical baseline characteristics were incorporated into logistic regression to analyze the predictive value of different variables on the prognosis of AIS. Clinical baseline characteristics include age, gender, NIHSS score, hypertension, coronary heart disease, diabetes, atrial fibrillation, systolic blood pressure, diastolic blood pressure, fasting blood glucose, total cholesterol, and serum ICAM-1 concentration. The results of the logistic regression analysis are shown in Table 2. The results showed that after adjusting for age, gender, NIHSS score, hypertension, coronary heart disease, diabetes, atrial fibrillation, systolic blood pressure, diastolic blood pressure, fasting blood glucose,

TABLE 2: Risks variables for poor outcome at 3 months in AIS patients.

	OR	95% CI	p value
Age, years	1.35	0.843-1.418	0.231
Male, n (%)	1.16	0.902-1.194	0.365
NHSS on admission	0.65	0.436-0.803	0.058
Hypertension, n (%)	1.33	0.887-1.379	0.272
Diabetes mellitus, n (%)	1.31	0.835-1.352	0.107
Coronary heart disease, n (%)	1.18	0.891-1.205	0.329
Atrial fibrillation, n (%)	1.24	0.858-1.287	0.353
Systolic blood pressure, mmHg	1.35	0.774-1.386	0.432
Diastolic blood pressure, mmHg	1.31	0.970-1.361	0.504
Fasting blood-glucose, mmol/l	1.27	0.859-1.304	0.766
Total cholesterol, mmol/l	1.20	0.831-1.275	0.520
ICAM-1, pg/ml	0.52	0.318-0.839	0.007

AIS: acute ischemic stroke; NIHSS: National Institute of Health Stroke Scale; ICAM-1: intercellular adhesion molecule-1.

and total cholesterol, the serum ICAM-1 level is still the prognosis of AIS patients' independent predictor ( $p = 0.007$ ).

#### 4. Discussion

The main finding of our current study is that the serum ICAM-1 levels of patients with poor AIS outcomes are significantly higher than those with good outcomes. Our further ROC analysis indicated that the cut-off value of serum ICAM-1 as a diagnostic target for predicting the prognosis of AIS was 129.5 pg/ml, and its sensitivity and specificity were 74% and 76%, respectively. After adjusting the clinical baseline data, the serum ICAM-1 level can still be used as an independent biomarker for predicting the prognosis of AIS patients.

Inflammation is the main factor affecting the pathobiology and prognosis of AIS [27]. Although the inflammatory response begins with local occlusion and hypoperfusion of blood vessels and ischemic brain parenchyma, the inflammatory mediators generated in situ spread throughout the organism, leading to systemic inflammation [28]. Increased blood levels of systemic inflammatory markers are associated with adverse outcomes after AIS. Animal studies have demonstrated the causal relationship between systemic inflammation and AIS neurological damage and poor prognosis [29]. The underlying mechanisms of systemic inflammation affecting the poor prognosis of AIS include neutrophil infiltration, blood-brain barrier (BBB) destruction, and cerebral ischemia-reperfusion injury [30, 31]. Animal experiments showed that reducing leukocyte infiltration could reduce the neurological damage of AIS and delay disease progression [32]. However, clinical trials of antileukocyte therapy have not reached a consistent conclusion with animal experiments.

ICAM-1 is a glycoprotein adhesion receptor mainly expressed on the surface of endothelial cells [33, 34]. Its main function is similar to chemokines and can induce the recruitment of leukocytes from the circulation to the inflammation site [35]. The unique domain of ICAM-1 allows it to be used as a biosensor, which can associate with the actin cytoskeleton after binding to a ligand to achieve signal transduction [36]. sICAM-1 is produced as a splice isoform of ICAM-1 or as a result of proteolytic cleavage. sICAM-1 retains all 5 extracellular Ig domains, and the molecular composition of the Ig domain of sICAM-1 varies depending on the protease that catalyzes the cleavage [9]. Studies have found that sICAM-1 has the dual effects of proinflammatory and anti-inflammatory [37], which suggests the complexity of its involvement in pathogenic mechanisms.

The mechanism of ICAM-1 involved in neuroinflammatory injury after stroke has been reported. Research by Zhang et al. showed that anti-ICAM-1 antibody could significantly reduce ischemic brain damage after focal cerebral ischemia in rats, while reducing polymorphonuclear leukocytes in the injured area [38]. Consistent with the above results, Bowes et al. further verified that anti-ICAM-1 could reduce neurological damage after stroke in a rabbit cerebral ischemia model, but it had no synergistic effect with tissue plasminogen activator (tPA) [39]. However, there are also different conclusions in animal experiments. Studies have shown that ICAM-1 knockout mice can neither inhibit the recruitment of neutrophils after cerebral ischemia nor can they provide protection for neurons after ischemia and reperfusion [40]. These different conclusions precisely suggest that ICAM-1 is involved in the complexity of inflammatory damage after stroke.

Not only in animal experiments but also in clinical studies, ICAM-1 has also been shown to be associated with ischemic stroke. A study in Finland showed that the expression of ICAM-1 was significantly upregulated after AIS, and it worked in concert with chemokines to cause granulocyte infiltration. This may be one of the potential mechanisms of ICAM-1 aggravating the neurological damage in stroke [41]. Unlike the above study, a clinical study in Croatia

showed that serum ICAM-1 levels have nothing to do with the severity of stroke [42]. The explanation for this completely different conclusions may be as follows: first, the difference of race and second, the Croatian study is grouped according to different stroke subtypes, which may be the main reason for the different conclusions from the Finnish study. The results of Enlimomab Acute Stroke Trial Investigators showed that anti-ICAM-1 treatment not only failed to reduce the neurological damage of ischemic stroke but also significantly worsened the stroke outcome [43]. Interestingly, a recent study from China showed that serum ICAM-1 levels in AIS patients were elevated, and it was related to the increased risk of hemorrhage conversion after AIS [44].

Our research has some limitations. Firstly, our AIS patients come from a single center, and the sample size is small. Secondly, we have not dynamically monitored the changes in serum ICAM-1 nor have we conducted long-term follow-up of AIS patients. Thirdly, our AIS patients do not include patients treated with recombinant plasminogen activator (rtPA) and healthy volunteers. Therefore, we cannot evaluate the correlation between ICAM-1 and prognosis in patients with AIS after intravenous thrombolysis. Fourthly, we did not detect the levels of serum traditional inflammation markers nor did we explore their correlation with ICAM-1. Finally, we did not perform subgroup analysis of AIS patients with different causes. However, our research still has obvious advantages. Our study reported for the first time the correlation between serum ICAM-1 levels and the short-term prognosis of AIS stroke.

## 5. Conclusions

The level of serum ICAM-1 in AIS patients with poor prognosis was significantly higher than that in the good prognosis group. The baseline serum ICAM-1 level predicts the prognosis of AIS with high sensitivity and specificity. And after adjusting for multivariate, the serum ICAM-1 level is still an independent predictor of AIS functional outcome. The study of stroke targeting ICAM-1 is currently controversial, and more studies are still needed in the future to clarify this complex pathological mechanism.

## Data Availability

The data used to support the findings of this study are available from the corresponding author upon request.

## Conflicts of Interest

All the authors declare no conflict of interests.

## References

- [1] Y. Xu, K. Wang, Q. Wang, Y. Ma, and X. Liu, "The antioxidant enzyme PON1: a potential prognostic predictor of acute ischemic stroke," *Oxidative Medicine and Cellular Longevity*, vol. 2021, Article ID 6677111, 8 pages, 2021.
- [2] M. S. Phipps and C. A. Cronin, "Management of acute ischemic stroke," *BMJ*, vol. 368, p. l6983, 2020.

- [3] S. Wu, B. Wu, M. Liu et al., "Stroke in China: advances and challenges in epidemiology, prevention, and management," *Lancet Neurology*, vol. 18, no. 4, pp. 394–405, 2019.
- [4] Y. Xu, Q. Wang, J. Chen, Y. Ma, and X. Liu, "Updating a strategy for histone deacetylases and its inhibitors in the potential treatment of cerebral ischemic stroke," *Disease Markers*, vol. 2020, Article ID 8820803, 8 pages, 2020.
- [5] T. Leng and Z. G. Xiong, "Treatment for ischemic stroke: from thrombolysis to thrombectomy and remaining challenges," *Brain Circ*, vol. 5, no. 1, pp. 8–11, 2019.
- [6] C. Lawson and S. Wolf, "ICAM-1 signaling in endothelial cells," *Pharmacological Reports*, vol. 61, no. 1, pp. 22–32, 2009.
- [7] T. N. Ramos, D. C. Bullard, and S. R. Barnum, "ICAM-1: isoforms and phenotypes," *Journal of Immunology*, vol. 192, no. 10, pp. 4469–4474, 2014.
- [8] T. M. Bui, H. L. Wiesolek, and R. Sumagin, "ICAM-1: a master regulator of cellular responses in inflammation, injury resolution, and tumorigenesis," *Journal of Leukocyte Biology*, vol. 108, no. 3, pp. 787–799, 2020.
- [9] R. Rothlein, E. A. Mainolfi, M. Czajkowski, and S. D. Marlin, "A form of circulating ICAM-1 in human serum," *The Journal of Immunology*, vol. 147, no. 11, pp. 3788–3793, 1991.
- [10] V. Marzolla, A. Armani, C. Mammi et al., "Essential role of ICAM-1 in aldosterone-induced atherosclerosis," *International Journal of Cardiology*, vol. 232, pp. 233–242, 2017.
- [11] H. R. Mohammadi, M. S. Khoshnam, and E. Khoshnam, "Effects of different modes of exercise training on body composition and risk factors for cardiovascular disease in middle-aged men," *International Journal of Preventive Medicine*, vol. 9, no. 1, p. 9, 2018.
- [12] H. Y. Jin and T. S. Park, "Role of inflammatory biomarkers in diabetic peripheral neuropathy," *Journal of diabetes investigation*, vol. 9, no. 5, pp. 1016–1018, 2018.
- [13] A.-M. L. Wegeberg, T. Okdahl, T. Fløyel et al., "Circulating inflammatory markers are inversely associated with heart rate variability measures in type 1 diabetes," *Mediators of Inflammation*, vol. 2020, 10 pages, 2020.
- [14] W. Cai, K. Zhang, P. Li et al., "Dysfunction of the neurovascular unit in ischemic stroke and neurodegenerative diseases: an aging effect," *Ageing Research Reviews*, vol. 34, pp. 77–87, 2017.
- [15] W. Eldahshan, S. C. Fagan, and A. Ergul, "Inflammation within the neurovascular unit: focus on microglia for stroke injury and recovery," *Pharmacological Research*, vol. 147, p. 104349, 2019.
- [16] Q. Wang, W. Yang, J. Zhang, Y. Zhao, and Y. Xu, "TREM2 overexpression attenuates cognitive deficits in experimental models of vascular dementia," *Neural Plasticity*, vol. 2020, Article ID 8834275, 10 pages, 2020.
- [17] Q. Wang, Y. Xu, C. Qi, A. Liu, and Y. Zhao, "Association study of serum soluble TREM2 with vascular dementia in Chinese Han population," *The International Journal of Neuroscience*, vol. 130, no. 7, pp. 708–712, 2020.
- [18] T. Yu, Y. Lin, Y. Xu et al., "Repressor Element 1 Silencing Transcription Factor (REST) Governs Microglia-Like BV2 Cell Migration via Progranulin (PGRN)," *Neural Plasticity*, vol. 2020, Article ID 8855822, 9 pages, 2020.
- [19] X. Du, Y. Xu, S. Chen, and M. Fang, "Inhibited CSF1R alleviates ischemia injury via inhibition of microglia M1 polarization and NLRP3 pathway," *Neural Plasticity*, vol. 2020, Article ID 8825954, 11 pages, 2020.
- [20] W. J. Tu, X. Dong, S. J. Zhao, D. G. Yang, and H. Chen, "Prognostic value of plasma neuroendocrine biomarkers in patients with acute ischaemic stroke," *Journal of Neuroendocrinology*, vol. 25, no. 9, pp. 771–778, 2013.
- [21] X. Wang, F. Zhang, W. Ma, D. Feng, J. Zhang, and J. Xu, "Increased levels of serum neuregulin 1 associated with cognitive impairment in vascular dementia," *BioMed Research International*, vol. 2020, Article ID 6683747, 5 pages, 2020.
- [22] Y. Xu, Q. Wang, Z. Qu, J. Yang, X. Zhang, and Y. Zhao, "Protective effect of hyperbaric oxygen therapy on cognitive function in patients with vascular dementia," *Cell Transplantation*, vol. 28, no. 8, pp. 1071–1075, 2019.
- [23] J. Zhang, L. Tang, J. Hu, Y. Wang, and Y. Xu, "Uric acid is associated with cognitive impairment in the elderly patients receiving maintenance hemodialysis—a two-center study," *Brain and Behavior: A Cognitive Neuroscience Perspective*, vol. 10, no. 3, p. e01542, 2020.
- [24] J. L. Banks and C. A. Marotta, "Outcomes validity and reliability of the modified Rankin scale: implications for stroke clinical trials: a literature review and synthesis," *Stroke*, vol. 38, no. 3, pp. 1091–1096, 2007.
- [25] T. Quinn, J. Dawson, and M. Walters, "Dr John Rankin; his life, legacy and the 50th anniversary of the Rankin stroke scale," *Scottish Medical Journal*, vol. 53, no. 1, pp. 44–47, 2008.
- [26] J. P. Broderick, O. Adeoye, and J. Elm, "Evolution of the modified Rankin scale and its use in future stroke trials," *Stroke*, vol. 48, no. 7, pp. 2007–2012, 2017.
- [27] A. Tuttolomondo, D. Di Raimondo, R. di Sciacca, A. Pinto, and G. Licata, "Inflammatory cytokines in acute ischemic stroke," *Current Pharmaceutical Design*, vol. 14, no. 33, pp. 3574–3589, 2008.
- [28] B. W. McColl, S. M. Allan, and N. J. Rothwell, "Systemic infection, inflammation and acute ischemic stroke," *Neuroscience*, vol. 158, no. 3, pp. 1049–1061, 2009.
- [29] T. Dziedzic, "Systemic inflammation as a therapeutic target in acute ischemic stroke," *Expert Review of Neurotherapeutics*, vol. 15, no. 5, pp. 523–531, 2015.
- [30] S. Amaro, F. Jiménez-Altayó, and Á. Chamorro, "Uric acid therapy for vasculoprotection in acute ischemic stroke," *Brain Circulation*, vol. 5, no. 2, pp. 55–61, 2019.
- [31] A. Chamorro, A. Meisel, A. M. Planas, X. Urra, D. Van De Beek, and R. Veltkamp, "The immunology of acute stroke," *Nature Reviews Neurology*, vol. 8, no. 7, pp. 401–410, 2012.
- [32] L. Kang, H. Yu, X. Yang et al., "Neutrophil extracellular traps released by neutrophils impair revascularization and vascular remodeling after stroke," *Nature Communications*, vol. 11, no. 1, p. 2488, 2020.
- [33] M. Ucci, P. Di Tomo, F. Tritschler et al., "Anti-inflammatory role of carotenoids in endothelial cells derived from umbilical cord of women affected by gestational diabetes mellitus," *Oxidative Medicine and Cellular Longevity*, vol. 2019, 11 pages, 2019.
- [34] J. Wang, V. Polaki, S. Chen, and J. C. Bihl, "Exercise improves endothelial function associated with alleviated inflammation and oxidative stress of perivascular adipose tissue in type 2 diabetic mice," *Oxidative Medicine and Cellular Longevity*, vol. 2020, 12 pages, 2020.
- [35] R. Lyck and G. Enzmann, "The physiological roles of ICAM-1 and ICAM-2 in neutrophil migration into tissues," *Current Opinion in Hematology*, vol. 22, no. 1, pp. 53–59, 2015.



- [36] H. Cung, M. J. Aragon, K. Zychowski et al., "Characterization of a novel endothelial biosensor assay reveals increased cumulative serum inflammatory potential in stabilized coronary artery disease patients," *Journal of Translational Medicine*, vol. 13, no. 1, 2015.
- [37] J. Janowska, J. Chudek, M. Olszanecka-Glinianowicz, E. Semik-Grabarczyk, and B. Zahorska-Markiewicz, "Interdependencies among selected pro-inflammatory markers of endothelial dysfunction, C-peptide, anti-inflammatory interleukin-10 and glucose metabolism disturbance in obese women," *International Journal of Medical Sciences*, vol. 13, no. 7, pp. 490–499, 2016.
- [38] R. L. Zhang, M. Chopp, Y. Li et al., "Anti-ICAM-1 antibody reduces ischemic cell damage after transient middle cerebral artery occlusion in the rat," *Neurology*, vol. 44, no. 9, pp. 1747–1751, 1994.
- [39] M. P. Bowes, J. A. Zivin, and R. Rothlein, "Monoclonal antibody to the ICAM-1 adhesion site reduces neurological damage in a rabbit cerebral embolism stroke model," *Experimental Neurology*, vol. 119, no. 2, pp. 215–219, 1993.
- [40] G. U. Enzmann, S. Pavlidou, M. Vaas, J. Klohs, and B. Engelhardt, "ICAM-1null C57BL/6 mice are not protected from experimental ischemic stroke," *Translational Stroke Research*, vol. 9, no. 6, pp. 608–621, 2018.
- [41] P. J. Lindsberg, O. Carpen, A. Paetau, M.-L. Karjalainen-Lindsberg, and M. Kaste, "Endothelial ICAM-1 expression associated with inflammatory cell response in human ischemic stroke," *Circulation*, vol. 94, no. 5, pp. 939–945, 1996.
- [42] V. Supanc, Z. Biloglav, V. B. Kes, and V. Demarin, "Role of cell adhesion molecules in acute ischemic stroke," *Annals of Saudi Medicine*, vol. 31, no. 4, pp. 365–370, 2011.
- [43] Enlimomab Acute Stroke Trial Investigators, "Use of anti-ICAM-1 therapy in ischemic stroke: Results of the Enlimomab Acute Stroke Trial," *Neurology*, vol. 57, no. 8, pp. 1428–1434, 2001.
- [44] B. N. Wu, J. Wu, D. L. Hao, L. L. Mao, J. Zhang, and T. T. Huang, "High serum sICAM-1 is correlated with cerebral microbleeds and hemorrhagic transformation in ischemic stroke patients," *British Journal of Neurosurgery*, vol. 32, no. 6, pp. 631–636, 2018.



## Retraction

# Retracted: Applicability of High-Frequency Ultrasound to the Early Diagnosis of Diabetic Peripheral Neuropathy

### BioMed Research International

Received 12 March 2024; Accepted 12 March 2024; Published 20 March 2024

Copyright © 2024 BioMed Research International. This is an open access article distributed under the Creative Commons Attribution License, which permits unrestricted use, distribution, and reproduction in any medium, provided the original work is properly cited.

This article has been retracted by Hindawi following an investigation undertaken by the publisher [1]. This investigation has uncovered evidence of one or more of the following indicators of systematic manipulation of the publication process:

- (1) Discrepancies in scope
- (2) Discrepancies in the description of the research reported
- (3) Discrepancies between the availability of data and the research described
- (4) Inappropriate citations
- (5) Incoherent, meaningless and/or irrelevant content included in the article
- (6) Manipulated or compromised peer review

The presence of these indicators undermines our confidence in the integrity of the article's content and we cannot, therefore, vouch for its reliability. Please note that this notice is intended solely to alert readers that the content of this article is unreliable. We have not investigated whether authors were aware of or involved in the systematic manipulation of the publication process.

Wiley and Hindawi regrets that the usual quality checks did not identify these issues before publication and have since put additional measures in place to safeguard research integrity.

We wish to credit our own Research Integrity and Research Publishing teams and anonymous and named external researchers and research integrity experts for contributing to this investigation.

The corresponding author, as the representative of all authors, has been given the opportunity to register their agreement or disagreement to this retraction. We have kept a record of any response received.

### References

- [1] X. Ma, T. Li, L. Du, G. Liu, T. Sun, and T. Han, "Applicability of High-Frequency Ultrasound to the Early Diagnosis of Diabetic Peripheral Neuropathy," *BioMed Research International*, vol. 2021, Article ID 5529063, 6 pages, 2021.

## Research Article

# Applicability of High-Frequency Ultrasound to the Early Diagnosis of Diabetic Peripheral Neuropathy

Xishun Ma <sup>1</sup>, Tongxia Li,<sup>2</sup> Lizhen Du <sup>1</sup>, Gang Liu,<sup>1</sup> Ting Sun,<sup>1</sup> and Tongliang Han <sup>1</sup>

<sup>1</sup>Department of Ultrasound, Qingdao Municipal Hospital, Qingdao, Shandong 266071, China

<sup>2</sup>Department of Tuberculosis, Qingdao Chest Hospital, Qingdao Central Medical Group, Qingdao, Shandong 266043, China

Correspondence should be addressed to Lizhen Du; 78775272@qq.com and Tongliang Han; hantongliang\_qd@sina.com

Received 6 February 2021; Revised 24 February 2021; Accepted 2 March 2021; Published 18 March 2021

Academic Editor: Yuzhen Xu

Copyright © 2021 Xishun Ma et al. This is an open access article distributed under the Creative Commons Attribution License, which permits unrestricted use, distribution, and reproduction in any medium, provided the original work is properly cited.

This study investigated the applicability of high-frequency ultrasound (HFU) to the early diagnosis of diabetic peripheral neuropathy (DPN). Patients with type 2 diabetes ( $N = 60$ ) were divided into diabetic nonperipheral neuropathy and DPN groups (group A and group B, respectively;  $n = 30$  each) based on electroneurophysiologic findings. Additionally, 30 nondiabetic patients were included as the healthy control group (group C). We calculated the cross-sectional area (CSA) of the median nerve (MN) of the right upper limb at 7 different sites (MN1–7) based on measured width ( $W$ ) and thickness ( $T$ ). Ultrasound imaging characteristics of the MN including internal echo, internal structure, boundary, epineurium, and blood flow were recorded. The 90 subjects (51 male and 39 female) had an average age of  $56.09 \pm 12.66$  years.  $W$ ,  $T$ , and CSA of the MN were increased in group A compared to group C (with significant differences at MN1, MN4, and MN7 ( $P < 0.05$ )) and in group B compared to group C (with significant differences at all 7 levels, especially MN6 and MN7 ( $P < 0.05$ )). Receiver operating characteristic curve analysis showed that CSA at the MN7 level had the highest diagnostic accuracy for DPN in group B, with a threshold value of  $12.42 \text{ mm}^2$ . Ultrasound examination revealed that the MN had lost the internal sieve mesh structure and showed reduced echo, a partial blood flow signal, and thickened epineurium in patients with DPN; these findings were particularly obvious at MN6 and MN7, corresponding to the carpal tunnel. CSA was positively correlated with motor latency and F wave average latency and negatively correlated with motor conduction velocity, motor amplitude, and sensory conduction velocity in group B. Thus, HFU may be useful for the early diagnosis of DPN, which can improve clinical outcomes.

## 1. Introduction

Diabetic peripheral neuropathy (DPN) is one of the most common chronic complications of diabetes. At present, the diagnosis of DPN mainly depends on electroneurophysiologic examination, but this has drawbacks such as invasiveness and high costs in terms of time and resources. The development of high-frequency ultrasound (HFU) has permitted the analysis of the morphologic features of peripheral nerves, thus enabling early detection of lesions. In the present study, we examined the applicability of HFU to the early diagnosis of DPN by retrospective analysis of data from patients with DPN and diabetic nonperipheral neuropathy (DNPN).

## 2. Materials and Methods

**2.1. Participants.** We analyzed data for 60 patients with type 2 diabetes who were admitted to the Endocrinology Department of Qingdao Municipal Hospital from October 2019 to October 2020 along with data for 30 healthy subjects collected during the same period. PASS software was used to calculate sample size. The ethics committee of the hospital approved the study, and informed consent was acquired from patients or families. The right upper limb median nerve was selected as the specific study object for the following reasons: no significant difference between unilateral and bilateral upper limbs and electrophysiological examination of the right upper limb. All patients met the 1999 World Health

TABLE 1:  $W$ ,  $T$ , and CSA of the median nerve at different levels in the 3groups.

MN level	Group A			Group B			Group C		
	$W$	$T$	CSA	$W$	$T$	CSA	$W$	$T$	CSA
MN1	4.91 ± 0.70	2.93 ± 0.39	11.31 ± 2.33	5.00 ± 0.46	3.09 ± 0.51	12.19 ± 2.52	4.51 ± 0.49	2.80 ± 0.33	9.88 ± 1.33
MN2	4.91 ± 0.65	2.71 ± 0.35	10.49 ± 1.98	5.26 ± 0.68	2.92 ± 0.48	11.99 ± 2.42	4.60 ± 0.57	2.68 ± 0.39	9.66 ± 1.72
MN3	4.42 ± 0.69	2.23 ± 0.39	7.75 ± 1.92	4.81 ± 0.68	2.29 ± 0.44	8.66 ± 2.05	4.30 ± 0.65	2.08 ± 0.32	7.05 ± 1.63
MN4	4.20 ± 0.57	2.61 ± 0.52	8.61 ± 2.03	4.38 ± 0.69	2.65 ± 0.37	9.11 ± 1.91	3.90 ± 0.54	2.40 ± 0.34	7.36 ± 1.59
MN5	5.96 ± 1.02	2.21 ± 0.30	10.36 ± 2.33	6.44 ± 0.70	2.35 ± 0.31	11.91 ± 2.20	5.70 ± 0.64	2.11 ± 0.25	9.45 ± 1.76
MN6	5.68 ± 0.75	2.33 ± 0.23	10.37 ± 1.64	6.64 ± 0.66	2.50 ± 0.30	13.09 ± 2.04	5.79 ± 0.72	2.11 ± 0.30	9.62 ± 1.96
MN7	6.01 ± 0.76	2.47 ± 0.28	11.48 ± 1.71	6.77 ± 0.60	2.55 ± 0.25	13.57 ± 1.71	5.44 ± 0.90	2.08 ± 0.42	8.87 ± 2.28

CSA: cross-sectional area (mm<sup>2</sup>); MN: median nerve;  $T$ : thickness (mm);  $W$ : width (mm).

Organization diagnostic criteria for diabetes. Based on findings from the electroneurophysiologic examination, the patients were divided into DNPN and DPN groups (groups A and B, respectively); the 30 healthy subjects served as the control group (group C). Group A had 20 males and 10 females; group B had 19 males and 11 females; and group C had 12 males and 18 females. Patients with neuropathy caused by type 1 diabetes, lumbar spine disease, cerebrovascular disease, trauma, etc. were excluded. There were no statistically significant differences in age and sex ratios among the groups.

**2.2. HFU Scan.** The HFU linear array probe of a LOGIQ E8 (GE Healthcare, Little Chalfont, UK) or EPIQ 7 (Philips, Amsterdam, the Netherlands) ultrasound system was used for HFU scanning. The subject was in a supine position with right upper extremity abduction. The probe was placed vertically near the ulnar brachial artery of the subject's right upper limb to locate the median nerve (MN), which was measured at 7 different sites including 4–5 cm above the elbow (MN1), at the elbow joint (MN2), at the pronator teres entrance level (MN3), 4–5 cm above the transverse wrist stripes (MN4), at the transverse wrist stripes (MN5), at the pea bone level (MN6), and at the hook bone level (MN7). Vertical and cross-sectional scanning was performed. The width ( $W$ ) and thickness ( $T$ ) of the MN were measured and used to calculate the cross-sectional area (CSA). Additionally, changes in internal structure, echo, blood flow, and the epineurium at the 7 sites were recorded.

**2.3. Electroneurophysiologic Examination.** For neuroelectro-physiologic recordings, the patient was relaxed and in a supine position under constant temperature and quiet conditions. The following motor and sensory nerve conduction and F wave parameters were measured: distal motor latency (DML), mixed nerve action potential, motor conduction velocity (MCV), sensory nerve action potential, sensory conduction velocity (SCV), and F-wave average latency (F-AL).

All operators were experienced doctors, and all measurements were obtained under double-blind test.

**2.4. Statistical Analysis.** Data are presented as mean ± standard deviation and were analyzed using SPSS v22.0 software (SPSS Inc., Chicago, IL, USA). Single-factor analysis of

variance and the  $t$ -test were used to compare quantitative data, and the chi-squared test was used for categorical variables. Receiver operating characteristic (ROC) curve analysis was carried out to determine the optimal threshold value for accurate diagnosis of DPN. Correlation analysis was performed by linear regression. Differences with  $P < 0.05$  were considered statistically significant.

### 3. Results

**3.1. Comparison of MN Ultrasound Measurements between Groups.** The size of the MN in group C decreased from the proximal part to the distal end.  $W$ ,  $T$ , and CSA of the MN were increased in group A compared to group C, with significant differences at MN1, MN4, and MN7 ( $P < 0.05$ ). Similarly,  $W$ ,  $T$ , and CSA of the MN were increased in group B compared to groups C and A, with significant differences at all 7 levels but especially at MN6 and MN7 ( $P < 0.05$ ) (Tables 1 and 2).

**3.2. ROC Curve Analysis of CSA at Different Sites along the MN in DPN Patients.** Patients with DPN had larger area under the ROC curve (AUC) for CSA of the MN than the other groups, with higher specificity and sensitivity at MN6 and MN7 than at other levels. MN6 and MN7 corresponded to the carpal tunnel. MN7 had the highest AUC at 0.88, with a sensitivity and specificity of 0.73 and 0.88, respectively; thus, the diagnostic accuracy was the highest at the MN7 level. The optimal threshold value of CSA was 12.42 mm<sup>2</sup> (Figure 1 and Table 3).

**3.3. HFU Features of the MN.** The results of HFU scans showed that the MN in group C had a mesh-like structure in cross section, with a clear internal structure and boundary, uniform thickness of the epineurium, and parallel bands of high and low echoes in vertical sections (Figure 2). There was no obvious blood flow in the nerve. Compared to group C, in groups A and B, the internal sieve mesh structure of the MN was lost (group A, 76.7%; group B, 96.7%; and group C, 36.7%); moreover, the echo was reduced (group A, 66.7%; group B, 96.7%; group C, 36.7%) and there was a partial blood flow signal (group A, 26.7%; group B, 40%; and group C, 6.7%), accompanied by a thickened epineurium. These HFU findings were especially obvious at MN6 and MN7

TABLE 2: Comparisons of  $W$ ,  $T$ , and CSA at different levels of the median nerve between groups ( $t$ -test).

MN level	$W$		$T$		CSA	
	$t$ statistic	$P$	$t$ statistic	$P$	$t$ statistic	$P$
Group A vs. group C						
MN1	2.53	0.010	1.41	0.170	2.93	$\leq 0.001$
MN2	1.99	0.050	0.32	0.750	1.73	0.080
MN3	0.71	0.480	1.58	0.120	1.53	0.130
MN4	2.13	0.030	1.84	0.070	2.65	0.010
MN5	1.19	0.230	1.41	0.160	1.72	0.090
MN6	-0.57	0.570	3.17	$\leq 0.001$	1.60	0.110
MN7	2.65	0.010	4.14	$\leq 0.001$	5.01	$\leq 0.001$
Group B vs. group C						
MN1	3.95	$\leq 0.001$	2.66	0.010	4.43	$\leq 0.001$
MN2	4.07	$\leq 0.001$	2.11	0.040	4.29	$\leq 0.001$
MN3	2.98	$\leq 0.001$	2.08	0.040	3.38	$\leq 0.001$
MN4	2.97	$\leq 0.001$	2.78	$\leq 0.001$	3.84	$\leq 0.001$
MN5	4.29	$\leq 0.001$	3.39	$\leq 0.001$	4.79	$\leq 0.001$
MN6	4.75	$\leq 0.001$	5.04	$\leq 0.001$	6.71	$\leq 0.001$
MN7	6.80	$\leq 0.001$	5.21	$\leq 0.001$	9.05	$\leq 0.001$
Group A vs. group B						
MN1	0.60	0.550	1.39	0.170	1.40	0.170
MN2	2.03	0.040	1.91	0.060	2.62	0.010
MN3	2.22	0.030	0.58	0.570	1.77	0.080
MN4	1.06	0.290	0.42	0.680	0.97	0.330
MN5	2.13	0.030	1.83	0.070	2.64	0.010
MN6	5.23	$\leq 0.001$	2.46	0.020	5.68	$\leq 0.001$
MN7	4.33	$\leq 0.001$	1.17	0.250	4.75	$\leq 0.001$

CSA: cross-sectional area ( $\text{mm}^2$ ); MN: median nerve;  $T$ : thickness (mm);  $W$ : width (mm).

(hook bone level). The MN in groups A and B showed significant reductions in the internal sieve mesh structure, echo, and blood flow compared to group C ( $P < 0.05$ ); and between groups A and B, the differences in the decreased internal echo and loss of mesh structure were significant ( $P < 0.05$ ), whereas blood flow signals were comparable ( $P > 0.05$ ) (Table 4).

3.4. Correlation Analysis between HFU Measurements and Electroneurophysiologic Parameters in DPN Patients. The CSA of the MN in the DPN group was positively correlated with DML and F-AL and negatively correlated with MNAP, MCV, and SCV (Table 5).

#### 4. Discussion

DPN is one of the most common chronic complications of diabetes, developing in more than half of patients [1]. The main clinical manifestations are symmetric pain, numbness, loss or disappearance of pain and temperature sensitivity, muscle weakness, and muscle atrophy of bilateral extremities

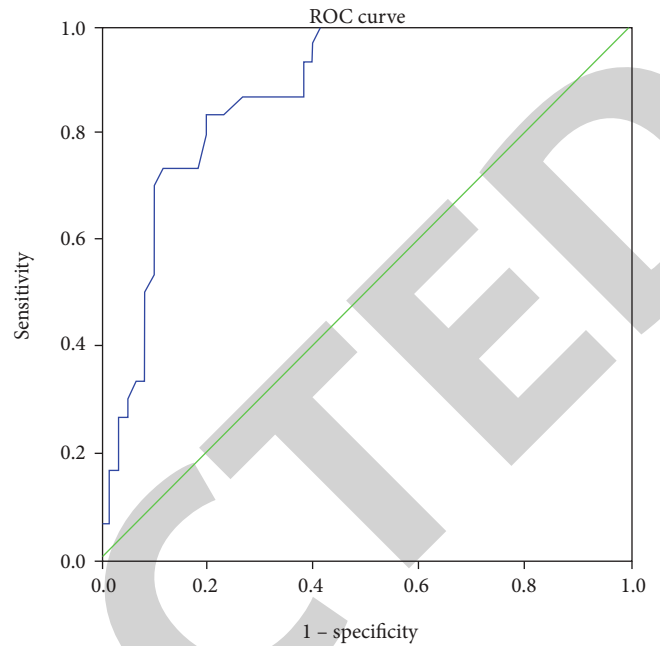


FIGURE 1: ROC curve for CSA of the MN at MN7 in DPN patients.

TABLE 3: Receiver operating characteristic curve analysis for the cross-sectional area at different levels of the median nerve in diabetic peripheral neuropathy patients.

MN level	AUC	Sensitivity	Specificity	Optimal threshold for CSA
MN1	0.69	0.53	0.80	12.05
MN2	0.72	0.50	0.82	11.79
MN3	0.70	0.67	0.67	7.85
MN4	0.67	0.77	0.57	7.62
MN5	0.75	0.90	0.57	9.86
MN6	0.87	0.93	0.70	10.71
MN7	0.88	0.73	0.88	12.42

AUC, area under the receiver operating characteristic curve; CSA: cross-sectional area ( $\text{mm}^2$ ); MN: median nerve;  $T$ : thickness (mm);  $W$ : width (mm).

as well as typical glove- and sock-like sensory disorders [2, 3]. DPN has an insidious onset and high incidence, and its pathologic severity is not proportional to clinical symptoms, as many patients are asymptomatic for a long time. It has been reported that 10% of newly diagnosed type 2 diabetes patients already have peripheral neuropathy when the disease course is  $>10$  years [4], and more than 50% of patients develop varying degrees of DPN, which is associated with serious complications such as foot gangrene and ulcers that can seriously affect the quality of life of patients. Therefore, early diagnosis of DPN is critical to ensure a good clinical outcome.

The pathogenesis of DPN is unclear; because of the existence of many types of peripheral neuropathy, it is difficult to explain all of the pathologic features by a single mechanism. Long-term hyperglycemia metabolic disorder and



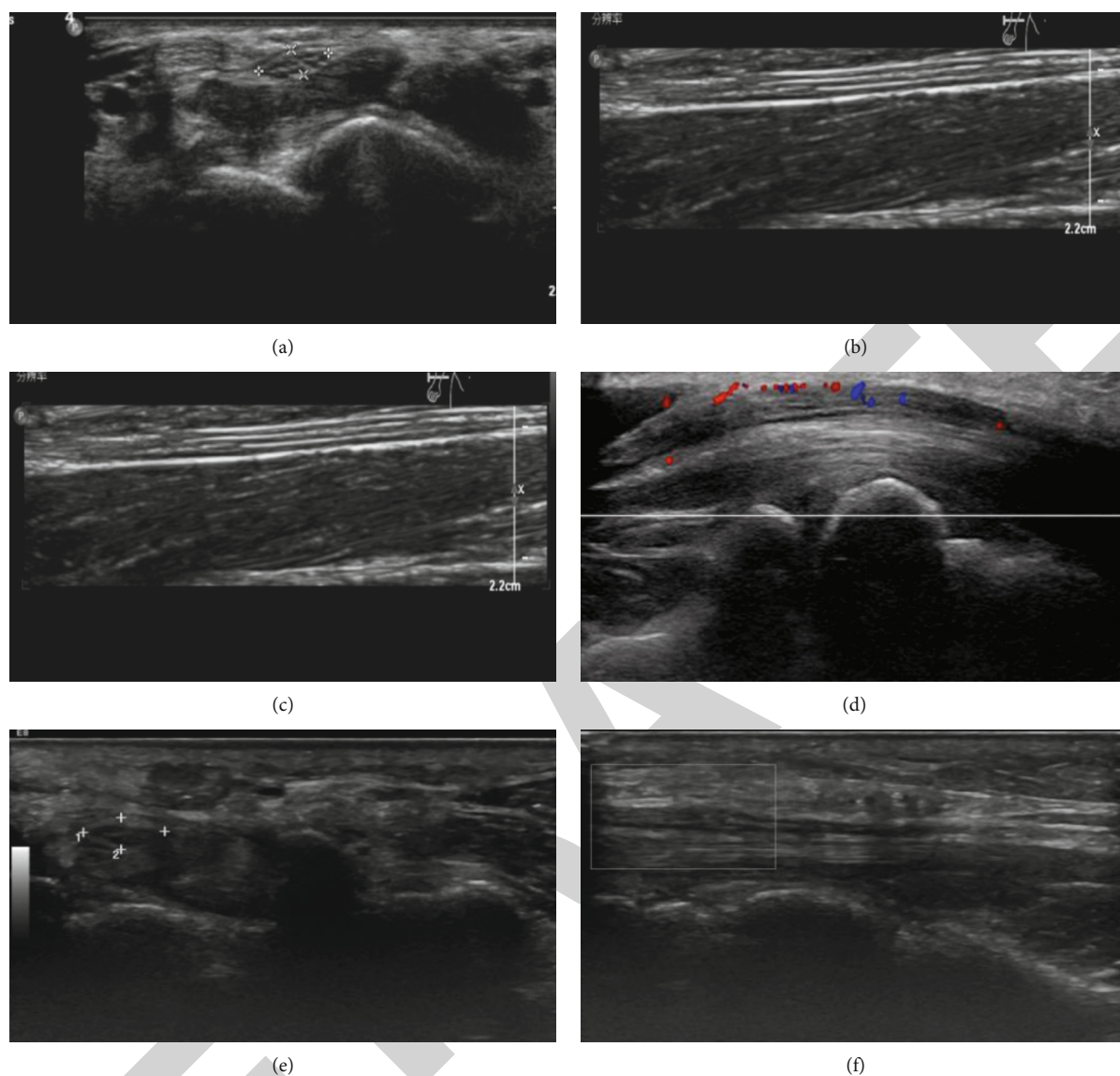


FIGURE 2: Representative HFU images of the MN. (a, b) In group C, the MN showed a sieve mesh structure in cross section (a) and parallel bands of high and low echoes (b). (c, d) In a 68-year-old male patient in group B, the sieve mesh structure of the MN was lost and the internal echo was decreased at the level of MN6 in cross section (c); the MN showed increased blood flow at MN6 and MN7 in vertical sections (d). (e, f) In a 60-year-old male patient in group B, the MN had a thickened epineurium at the level of MN7 in cross section (e) and there was no blood flow in vertical sections (f).

microvascular disease are the major risk factors; others include changes in nerve growth factor level, peroxide- and free radical-induced damage, and abnormal metabolism of essential fatty acids [5].

At present, the diagnosis of DPN mainly relies on clinical manifestations and electroneurophysiologic findings. However, by the time the patient shows clinical symptoms, there are already obvious lesions in the peripheral nerves and early intervention is not possible. Electroneurophysiologic examination is the gold standard for DPN diagnosis, but it is time-consuming, laborious, costly, and invasive and is thus unsuitable for routine DPN screening [6]. With advances in ultrasound technology in recent years including probes with higher frequency and better resolution, it has become possible to visualize internal structures such as the epineurium,

perineurium, and nerve bundles with a diameter of  $\leq 0.5$  mm as well as some small nerves and cutaneous nerves. Thus, HFU provides valuable morphologic information that can complement electrophysiologic data [7, 8].

In this study, we compared the features of the MN of the right upper limb in patients with DPN or DNPN and healthy control subjects, including changes in size, internal echo, structure, and blood flow. In healthy subjects, CSA and anteroposterior diameter of the MN were reduced compared to the elbow joint, especially at the level of the carpal tunnel; and the shape was also changed from round or oval to flat oval. The  $W$ ,  $T$ , and CSA at the 7 measured sites along the MN were increased in DNPN and DPN patients compared to controls; the differences were statistically significant. The level of aldose reductase was shown to be elevated in DPN,



TABLE 4: Analysis of ultrasonographic features at the MN7 level of the median nerve.

	Blood flow		Mesh structure		Internal echo Reduction	No change
	With	Without	With	Without		
Group C vs. group A						
Group C	2	28	19	11	11	19
Group A	8	22	7	23	20	10
$\chi^2$	4.32		9.77		5.41	
P	0.040		$\leq 0.001$		0.020	
Group C vs. group B						
Group C	2	28	19	11	11	19
Group B	12	18	1	29	29	1
$\chi^2$	9.32		24.30		24.30	
P	$\leq 0.001$		$\leq 0.001$		0.010	
Group B vs. group A						
Group A	8	22	7	23	20	10
Group B	12	18	1	29	29	1
$\chi^2$	1.20		5.19		9.02	
P	0.210		0.030		$\leq 0.001$	

TABLE 5: Correlation analysis between the cross-sectional area of the median nerve and neurophysiologic parameters at MN7 in diabetic peripheral neuropathy patients.

	DML	MNAP	MCV	F-AL	SNAP	SCV
R	0.61	-0.78	-0.56	0.51	-0.17	-0.54
P	$\leq 0.001$	$\leq 0.001$	$\leq 0.001$	$\leq 0.001$	0.380	$\leq 0.001$

DML: distal motor latency; F-AL: F-wave average latency; MCV: motion conduction velocity; MNAP: mixed nerve action potential; SCV: sensory conduction velocity; SNAP: sensory nerve action potential.

resulting in excessive conversion of glucose to sorbitol and fructose accumulation [9]. Sorbitol and fructose are hypertonic molecules that can increase osmotic pressure in nerve cells and cause water and sodium retention and nerve swelling and thickening, which are all pathophysiological effects.

Comparing group B with group A, the differences were only statistically significant at the level of the carpal tunnel (MN6, MN7). In our ROC curve analysis, the AUC was largest at the level of MN7 (hook bone), and the optimal threshold value for CSA was 12.42 mm<sup>2</sup>. The MN exits the carpal tunnel at the level of the hook bone. The carpal tunnel contains abundant flexor tendons that can easily compress the nerve. When the MN is lesioned and degenerates in patients with DPN, it can be vulnerable to compression and edematous or thickened. Additionally, in patients with DPN, the internal sieve-like structure of the MN was lost and echo

was reduced by HFU. The pathologic basis for these effects may be the hyperglycemic state of DPN patients, which resulted in a decreased blood supply to the nerve and hypoxia. The blood supply and nutrition of nerve fiber bundles depend on the tunica intima, which was the most affected structure. When complicated with peripheral neuropathy, hyperglycemia can cause nerve cells to swell, disintegrate, and demyelinate [10].

The ultrasound findings were more prominent at the level of the carpal tunnel because under normal circumstances, this area is affected by the carpal bone; thus, the probe was unable to remain in a vertical position relative to the cut nerve surface at all times, causing the echo of the MN to be lower at the carpal tunnel than at the upper arm. Moreover, the internal mesh-like structure was less clear in the former than in the latter, which was further aggravated under pathologic conditions. We also found that the peripheral and internal blood flow rates of the MN were relatively low. Blood flow in the MN was observed in 40% of DPN patients, which was higher than the rate in the other two groups. This may be attributable to the fact that blood flow in the endoneurium and perineurium is increased due to the enhancement of vascular reactivity in the early stage of diabetes but is decreased as a result of vascular sclerosis in the late stage [11].

The CSA of the MN showed positive and negative correlations with electroneurophysiologic parameters in patients with DPN, indicating that HFU can to some extent reveal changes in the functional properties of nerves. Moreover, it can clearly display the anatomic position of nerves and their relationship to adjacent structures as well as morphologic changes. Thus, HFU can aid in the early diagnosis of DPN by allowing lesions to be detected at an early stage, which can improve clinical outcomes.

Because the gold standard for diagnosing DPN is neurophysiological examination, our diagnosis of DPN may be not accurate enough because of small samples. Therefore, large samples are needed for further confirmation.

## Data Availability

All data generated or used in this study can be found in the article.

## Conflicts of Interest

The authors declare that there is no conflict of interest regarding the publication of this paper.

## Authors' Contributions

Xishun Ma and Tongxia Li are co-first authors. Lizhen Du and Tongliang Han are cocorrespondence authors.

## Acknowledgments

The authors thank all study participants. This work was supported by grants from Qingdao Medical Research Guidance Plan of 2020 (no. WJZD018).

## Retraction

# Retracted: Agomelatine Softens Depressive-Like Behavior through the Regulation of Autophagy and Apoptosis

### BioMed Research International

Received 12 March 2024; Accepted 12 March 2024; Published 20 March 2024

Copyright © 2024 BioMed Research International. This is an open access article distributed under the Creative Commons Attribution License, which permits unrestricted use, distribution, and reproduction in any medium, provided the original work is properly cited.

This article has been retracted by Hindawi following an investigation undertaken by the publisher [1]. This investigation has uncovered evidence of one or more of the following indicators of systematic manipulation of the publication process:

- (1) Discrepancies in scope
- (2) Discrepancies in the description of the research reported
- (3) Discrepancies between the availability of data and the research described
- (4) Inappropriate citations
- (5) Incoherent, meaningless and/or irrelevant content included in the article
- (6) Manipulated or compromised peer review

The presence of these indicators undermines our confidence in the integrity of the article's content and we cannot, therefore, vouch for its reliability. Please note that this notice is intended solely to alert readers that the content of this article is unreliable. We have not investigated whether authors were aware of or involved in the systematic manipulation of the publication process.

Wiley and Hindawi regrets that the usual quality checks did not identify these issues before publication and have since put additional measures in place to safeguard research integrity.

We wish to credit our own Research Integrity and Research Publishing teams and anonymous and named external researchers and research integrity experts for contributing to this investigation.




The corresponding author, as the representative of all authors, has been given the opportunity to register their agreement or disagreement to this retraction. We have kept a record of any response received.

### References

- [1] F. Chen, S. Chen, J. Liu, N. Amin, W. Jin, and M. Fang, "Agomelatine Softens Depressive-Like Behavior through the Regulation of Autophagy and Apoptosis," *BioMed Research International*, vol. 2021, Article ID 6664591, 10 pages, 2021.

## Research Article

# Agomelatine Softens Depressive-Like Behavior through the Regulation of Autophagy and Apoptosis

Fengpei Chen,<sup>1</sup> Shijia Chen ,<sup>2</sup> Jie Liu,<sup>1</sup> Nashwa Amin,<sup>2,3</sup> Weidong Jin ,<sup>1,4</sup> and Marong Fang <sup>2</sup>

<sup>1</sup>The Second Clinical Medical College of Zhejiang Chinese Medical University, Hangzhou 310053, China

<sup>2</sup>Institute of Neuroscience, Zhejiang University School of Medicine, Hangzhou 310058, China

<sup>3</sup>Department of Zoology, Faculty of Science, Aswan University, Egypt

<sup>4</sup>Zhejiang Mental Health Center, Tongde Hospital of Zhejiang province, Hangzhou 310012, China

Correspondence should be addressed to Weidong Jin; [wjjin@163.com](mailto:wjjin@163.com) and Marong Fang; [fangmaro@zju.edu.cn](mailto:fangmaro@zju.edu.cn)

Received 12 December 2020; Revised 11 January 2021; Accepted 26 February 2021; Published 18 March 2021

Academic Editor: Andrea Scribante

Copyright © 2021 Fengpei Chen et al. This is an open access article distributed under the Creative Commons Attribution License, which permits unrestricted use, distribution, and reproduction in any medium, provided the original work is properly cited.

Depression is a common and disabling mental disorder with high recurrence rate. Searching for more effective treatments for depression is a long-standing primary objective in neuroscience. Agomelatine (AGO) was reported as an antidepressant with unique pharmacological effects. However, its effects and the underlying mechanism are still unclear. In this study, we sought to evaluate the antidepressant effects of AGO on the chronic restraint stress (CRS) mouse model and preliminarily investigate its effects on the gut microbial metabolites. The CRS model mice were established in 28 days with AGO (60 mg/kg/day, by oral) or fluoxetine (15 mg/kg/day, by oral) administration. The number of behavioral tests was conducted to evaluate the effect of AGO on depression-like behavior alleviation. Meanwhile, the expression of the BDNF/TrkB/pERK signaling pathway, apoptosis, autophagy, and inflammatory protein markers were assessed using western blot and immunofluorescence. Our findings show that AGO can attenuate the depressive-like behavior that significantly appeared in both sucrose preference and forced swimming tests. Additionally, a noticeable upregulation of autophagy including Beclin1 and LC3II, microglial activity marker Iba-1, and BDNF/TrkB/pERK signaling pathways are indicated. An obvious decreased expression of NF- $\kappa$ B, iNOS, and nNOS as well as apoptosis including Bax is observed in AGO administration mice. On the other hand, we found that AGO impacted the rebalancing of short-chain fatty acids (SCFAs) in mouse feces. Altogether, these findings suggest that AGO can exert antidepressant effects in a different molecular mechanism.

## 1. Introduction

Depression is characterized by sadness, anhedonia, low self-esteem, loss of motivation, sleep disruption, loss of appetite, and other cognitive symptoms [1]. Symptoms of depression are highly prevalent, affecting up to 27% of the general population according to recent meta-analytic data [2]. However, the exact biological, psychological, and social mechanisms underlying the pathogenesis of depression remain largely unknown. Currently, most patients with depression are treated with synthetic drugs including selective serotonin reuptake inhibitors (SSRI) that act on the monoaminergic system, serotonin-norepinephrine reuptake inhibitors (SNRIs),

tricyclic antidepressants (TCAs), norepinephrine and dopamine reuptake blockers, and monoamine oxidase inhibitors which exhibit little or no improvement on depression and have side effects such as fatigue, sleep disorders, cognitive disorders, and sexual dysfunctions [3–5].

AGO is an antidepressant with unique pharmacological actions. Previous studies reported AGO to act as both a melatonin agonist and a selective serotonin antagonist [6]. In the previous decade, AGO was reported to have at least comparable efficacy to other antidepressants in terms of response and remission rates and to confer better tolerability and be associated with fewer side effects [7–9]. In vertebrates, the pineal gland is the main source of melatonin production.

Of the many substances identified, recent studies suggest that melatonin and its metabolites are highly effective physiological antioxidants and can also exert direct, non-receptor-mediated actions, such as the scavenging of a number of free radicals including both reactive oxygen and nitrogen species (ROS and RNS, respectively) [10–13].

BDNF is associated with neuropsychiatric disorders, such as depression [14] and schizophrenia [15]. BDNF and its mechanisms are also therapeutic targets of pharmacological agents that are currently used to treat mice with depression [16]. Previous studies have shown that fluoxetine can improve depression-like behaviors by regulating the BDNF signaling pathway [17]. However, the role of BDNF in the antidepressant process of AGO still requires in-depth research. Ample preclinical evidence suggested that exposure to acute or chronic stress agents triggers the production of cytokines, which may be related to the physiological processes mediated by autophagy [18]. The induction of autophagy protects neurons and glial cells under stress through the deregulation of various DAMPs and suppression of stress reaction, which will contribute to the alleviation of depression [18, 19]. The observation that the increase in autophagic markers goes along with the reversal of the behavioral effects argues in favor of autophagy being a beneficial component of the stress response in general [20]. Existing research shows that fluoxetine could promote the autophagic flux unblocked in the way of enhancing fusion of autophagosomes with lysosomes in primary astrocytes and finally ameliorates depression [21]. Similarly, apoptosis, another molecular mechanism that maintains cellular homeostasis, has recently been shown to be closely related to the development of depression [22]. Moreover, autophagy is important in cell death decisions and can protect cells by preventing them from undergoing apoptosis [23]. All of these indicate that autophagy and apoptosis may act as key mediators in antidepressant and stress-induced behavioral action.

However, whether AGO can alleviate depression by regulating autophagy or apoptosis is currently not clearly understood. In the current study, we aimed to investigate (i) the underlying mechanisms of AGO administration in CRS-induced depression, (ii) the changes in the hippocampus and subsequent anxiety behavior, and (iii) the impact of the AGO regimen on brain inflammation factors and microbial metabolites such as SCFAs.

## 2. Materials and Methods

**2.1. Animals.** Male C57BL/6N mice (weighing  $20 \pm 2$  g, 8 weeks old) were used in this study. The mice were maintained in a room at  $24 \pm 1^\circ\text{C}$  with 50%–60% relative humidity under a 12 h light/dark cycle (lights on at 09:00) with free access to food and water. All experimental procedures were approved and performed according to the Animal Care and Use Committee of the Institute of Zhejiang University, China. The animal ethics number is ZJU20160267.

**2.2. Study Design and Drug Administration.** After 2 weeks of adaptation, the mice were randomly assigned to 4 groups of 8 mice each: control (CON), chronic restraint stress (CRS), flu-

oxetine (FLX), and agomelatine (AGO). All groups were subjected to CRS except the control group. Fluoxetine (Patheon, France) and agomelatine (Lianyungang, China) were dissolved in physiological saline (NaCl, 0.9%). Dose and administration schedules of AGO and FLX were based on previous results [24]. Specifically, mice in the CRS group were subjected to CRS and intragastric administration of 8.0 mL/kg saline daily, and AGO and FLX were administered to mice at doses of 60 mg/kg body weight/day and 15 mg/kg body weight/day, respectively. Drugs were administered half an hour before the CRS regimen. The specific experimental procedure is shown in Scheme 1.

**2.3. The Chronic Restraint Stress Model.** The CRS model was based on the Chiba method [25], with slight modification. Briefly, mice were individually restricted in a modified, well-ventilated tube for 6 h without water and food, and mice were exposed to CRS for 28 consecutive days.

### 2.4. Behavioral Test

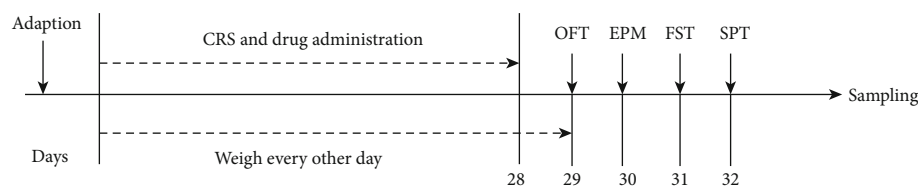
**2.4.1. Open Field Test (OFT).** The apparatus consisted of a white Plexiglas box ( $45\text{ cm} \times 45\text{ cm} \times 45\text{ cm}$ ) divided into two zones: outer square (periphery) and inner square (center:  $25\text{ cm} \times 25\text{ cm}$ ). Each mouse was placed in the center of the box and allowed to freely explore the environment in a room with dim light for 5 min. The movement of the mouse was recorded by a video camera (VideoTrack, Viewpoint Inc., France). The total distance covered in the box and the time spent in the central zone were calculated.

**2.4.2. Elevated Plus Maze (EPM).** The elevated plus maze apparatus consisted of two opposite-facing closed arms ( $30\text{ cm} \times 5\text{ cm} \times 15\text{ cm}$ ), two opposite-facing open arms ( $30\text{ cm} \times 5\text{ cm}$ ), and a central area ( $5\text{ cm} \times 5\text{ cm}$ ), and the maze was 50 cm above the ground. For the elevated plus maze, the mouse was placed in the center of the maze facing one of the two closed arms. A 5-minute test was recorded using an automatic analyzing system (ANY-maze, Stoelting, USA). The number of entries and the time spent in the open arms were recorded using an automatic analyzing system.

**2.4.3. Forced Swimming Test (FST).** Mice were placed into a cylinder (12 cm diameter, 25 cm height) filled with  $24 \pm 1^\circ\text{C}$  water. Water depth was adjusted so that the mice can neither touch the bottom nor jump out. Two mice at a time were videotaped from the side. A cardboard divider separated the cylinders so that the mice could not see each other during the trials. The mouse activity was video recorded for 6 min, and the duration of immobility was recorded during the last 4 min of the 6 min test. After the test session, mice were placed in a clean cage containing paper towels under a heat lamp until dry. Immobility was defined according to criteria described [26].

**2.4.4. Sucrose Preference Test (SPT).** The SPT was performed as previously reported [17] with slight modification. Briefly, mice were single housed and were accustomed to two bottles of water after two bottles of 2% sucrose for a day. After being deprived of water and food for 24 h, the mice were exposed to





SCHEME 1: Experimental schedule. Mice were treated for a total of 4 weeks with agomelatine, fluoxetine, or saline. After 4 weeks of treatment, animals underwent a battery of tests relevant to depression. All groups were sacrificed on the same day. Tissues were harvested for further analysis. CRS: chronic restraint stress; OFT: open field test; FST: forced swimming test; SPT: sucrose preference test.

one bottle of 2% sucrose and one bottle of water for 2 h during the dark phase. Bottle positions were switched after 1 h (for a 2 h test). After 2 hours of testing, water and sucrose consumption was measured.

**2.5. Western Blot.** Mice were sacrificed by cervical dislocation. The hippocampus was extracted for the evaluation of protein level and stored at  $-80^{\circ}\text{C}$  until use. Total protein of the hippocampus was prepared from each group using 1 mL ice-cold RIPA buffer, supplemented with 1% PMSF (phenylmethanesulfonyl fluoride, Beyotime ST505), protease inhibitors, and phosphatase inhibitors. Probes were ground and then centrifuged at 12,000 rpm for 30 min at  $4^{\circ}\text{C}$  before protein supernatants were obtained. The protein concentration was determined by using the BCA assay.  $20\ \mu\text{g}$  protein was electrophoresed on a 10% SDS-PAGE gel and transferred onto a polyvinylidene difluoride (PVDF) membrane. After blocking with 5% nonfat milk in TBS-Tween 20, membranes were incubated with primary antibodies overnight at  $4^{\circ}\text{C}$  as follows: rabbit anti-NF- $\kappa\text{B}/\text{p65}$  (Cell Signaling Technology, 1:1,000), rabbit anti-nNOS (Omnimabs, 1:500), rabbit anti-iNOS (Boster, 1:500), rabbit anti-LC3B (Novus, 1:1000), rabbit anti-p62 (Cell Signaling Technology, 1:1000), rabbit anti-Beclin (Cell Signaling Technology, 1:1000), rabbit anti-Bax (Boster, 1:500), rabbit anti-Bcl2 (ABclonal, 1:500), rabbit anti-BDNF (Boster, 1:500), rabbit anti-TrkB (Abcam, 1:1000), rabbit anti-pERK (Cell Signaling Technology, 1:1000), and mouse anti-GAPDH (ABclonal, 1:10000). Then, the membranes were subjected to three washing steps with TBS-Tween 20 (each 5 minutes) before incubation with the secondary antibody goat anti-rabbit IgG antibody (Bioker, 1:5000) and goat anti-mouse IgG antibody (Bioker, 1:5000) at room temperature for 2 h. After the final washing steps, membranes were subjected to enhanced chemiluminescence reaction and bands were quantified by densitometry (Quantity One 4.2, Bio-Rad, Hercules, CA). Densitometric values of markers were normalized to GAPDH levels. Each experiment was performed at least three times. The detection and quantification of each band were performed using Image Lab software.

**2.6. Immunofluorescent Staining.** Mice were perfused with 4% paraformaldehyde (PFA) after being perfused through the heart with 50 mL ( $\pm$ ) of saline. Brain tissue sections were subjected to immunohistochemistry analysis. Frozen sections, about  $16\ \mu\text{m}$  thick, were rinsed in 0.01 M PBS for 5 min and then moved to room temperature for 1 h and blocked with 5% normal goat serum. Incubation with primary antibodies

occurred overnight at  $4^{\circ}\text{C}$ : Iba1 (Abcam, 1:100). The sections were washed with 0.01 M PBST for 5 min three times on the following day and then incubated with secondary antibodies containing FITC goat anti-rabbit IgG (1:100, Boster, BA1105) and Alexa Fluor<sup>®</sup> anti-rabbit 488 for 3 h in the dark at room temperature. After washing, probes were mounted in medium containing DAPI (VECTASHIELD, USA). A fluorescence microscope (Olympus BX61, NIKON, Japan) was used for taking images. Iba1 staining was obtained with the NIH ImageJ software (<https://imagej.net/welcome>).

**2.7. Fecal SCFA Detection: Gas Chromatographic Analysis.** The fecal samples were frozen immediately after collection and stored  $-80^{\circ}\text{C}$  until analysis. Specifically, 80 mg of each fresh stool sample was weighed, suspended in 500  $\mu\text{L}$  anhydrous alcohol, and homogenized for approximately 5 min. Then, the sample was incubated at room temperature for 10 min with occasional shaking and centrifuged for 10 min at 12,000 rpm. The supernatant was transferred into 2 mL screw top vials (Agilent, United States). The concentration of SCFAs (including acetate, propionate, butyrate, isobutyrate, and valeric acid) in mouse fecal samples was determined using an Agilent 7890A gas chromatography unit, fitted with a high-resolution gas chromatography DB-624 column ( $30\ \text{m} \times 0.32\ \text{mm} \times 1.8\ \mu\text{m}$ , Agilent, United States). Nitrogen was supplied as a carrier gas at a flow rate of 1.2 mL/min. The initial oven temperature was  $100^{\circ}\text{C}$ , maintained for 5.0 min, raised to  $200^{\circ}\text{C}$  at  $20^{\circ}\text{C}/\text{min}$ , and finally held at  $200^{\circ}\text{C}$  for 5 min.

**2.8. Statistical Analysis.** Normalization and equal variances between group samples were assessed using the normal Q-Q plot and homogeneity test for variance, respectively. When normalization and equal variance between sample groups were achieved, one-way ANOVA with LSD was used. Where normalization or equal variance of samples failed, Mann-Whitney U tests were performed. Each value was presented as a mean  $\pm$  SEM and analyzed with one-way ANOVA using SPSS 22.0 software. A value of  $P < 0.05$  was considered significant.

### 3. Results

**3.1. AGO Ameliorates CRS-Induced Depressive-Like Behavior.** In order to investigate the effect of AGO in the depressive-like behavior, we sought to first analyze the body weight during CRS and drug treatment. No significant differences were found in the baseline body weight among the four groups. Then, statistical analysis revealed that CRS resulted



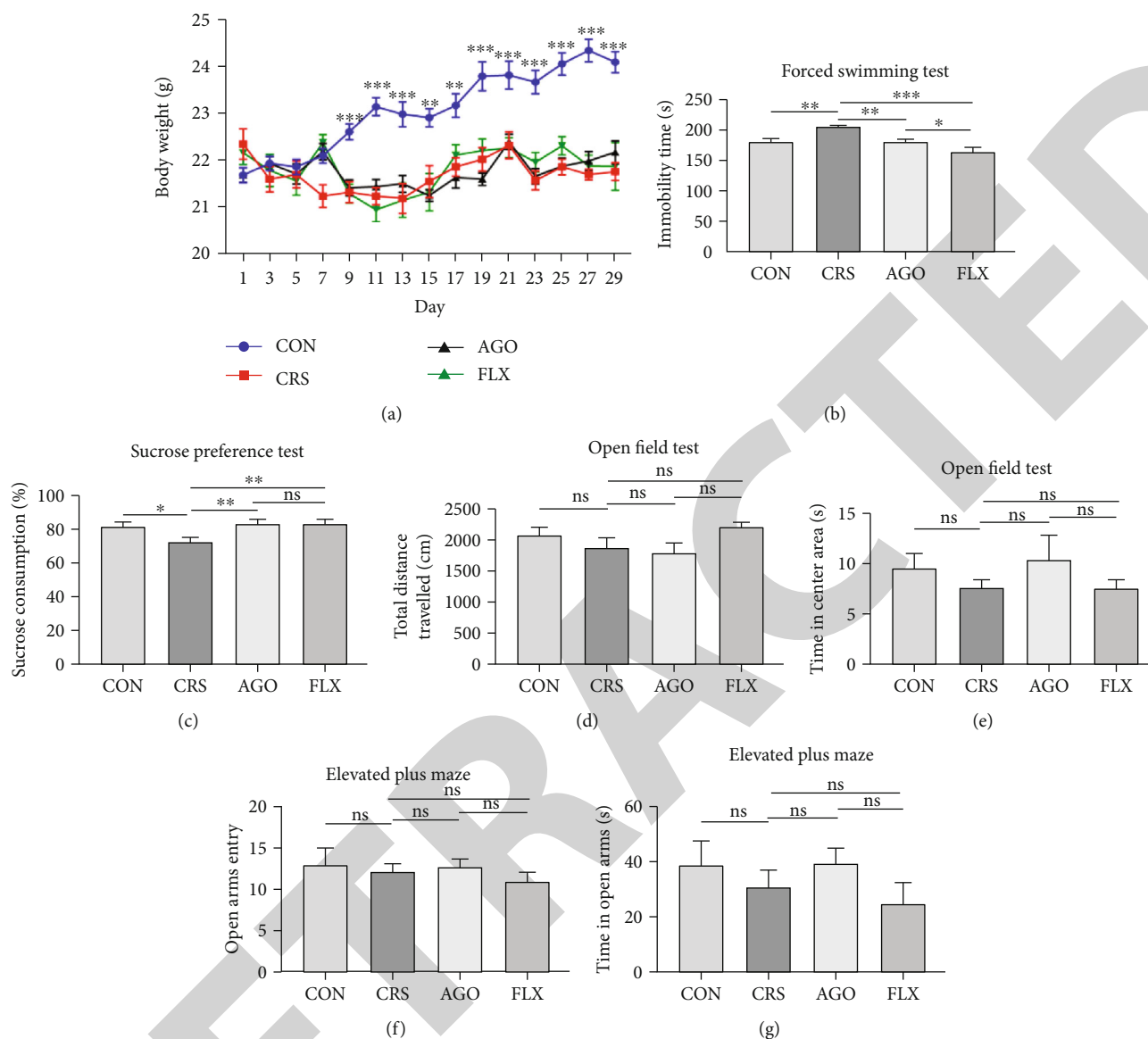


FIGURE 1: CRS-induced depression-like behaviors in mice. (a) Effects of CRS and drug treatment on body weight are presented. (b) The immobility time in FST after CRS, AGO, and FLX treatment is shown. (c) SPT after CRS and drug treatment is depicted. (d) Total distance traveled in the OFT after CRS and drug treatment is presented. (e) Time spent in the center area in OFT after CRS and drug treatment is presented. (f) Open arms entry in the EPM is shown. (g) Time in open arms in the EPM after CRS and drug treatment is shown. \* $P < 0.05$ ; \*\* $P < 0.01$ ; \*\*\* $P < 0.001$ ; ns = not significant. The values represent mean  $\pm$  SEM.  $n = 8$ .

in retardation of the body weight gain starting with day 9 compared to the control group, while AGO and FLX treatment did not counteract the effect (Figure 1(a)). At the end of the chronic stress period, a battery of well-established behavioral tests aimed at measuring anxiety-like behavior (OFT, EPM) and depression-like behaviors (SPT, FST) were conducted. Mice in the CRS group showed significant longer freezing time in FST (Figure 1(b)) and lower sucrose preference (Figure 1(c)) compared with the control mice. AGO and FLX significantly restored the above changes. Unfortunately, no significant effect was observed in the locomotor activity and the time spent in the central area (Figures 1(d) and 1(e)). In addition, the CRS procedure did not alter entries

into and time spent in the open arms (Figures 1(f) and 1(g)). These experiments suggest that AGO restores the depressive-like behavior after CRS.

**3.2. Effect of AGO Treatment on BDNF/TrkB and ERK1/2 Activity.** Recent studies demonstrate that BDNF-TrkB signaling is required for promoting proliferation [27] of newborn neurons in the adult hippocampus in response to antidepressant administration. Previous studies were conducted in order to determine if AGO administration alters the level of BDNF in the hippocampus [14], a region implicated in the actions of antidepressants. Indeed, expression of BDNF and TrkB declined in the hippocampus of mice subjected to CRS as depicted in Figures 2(a)–2(c). This

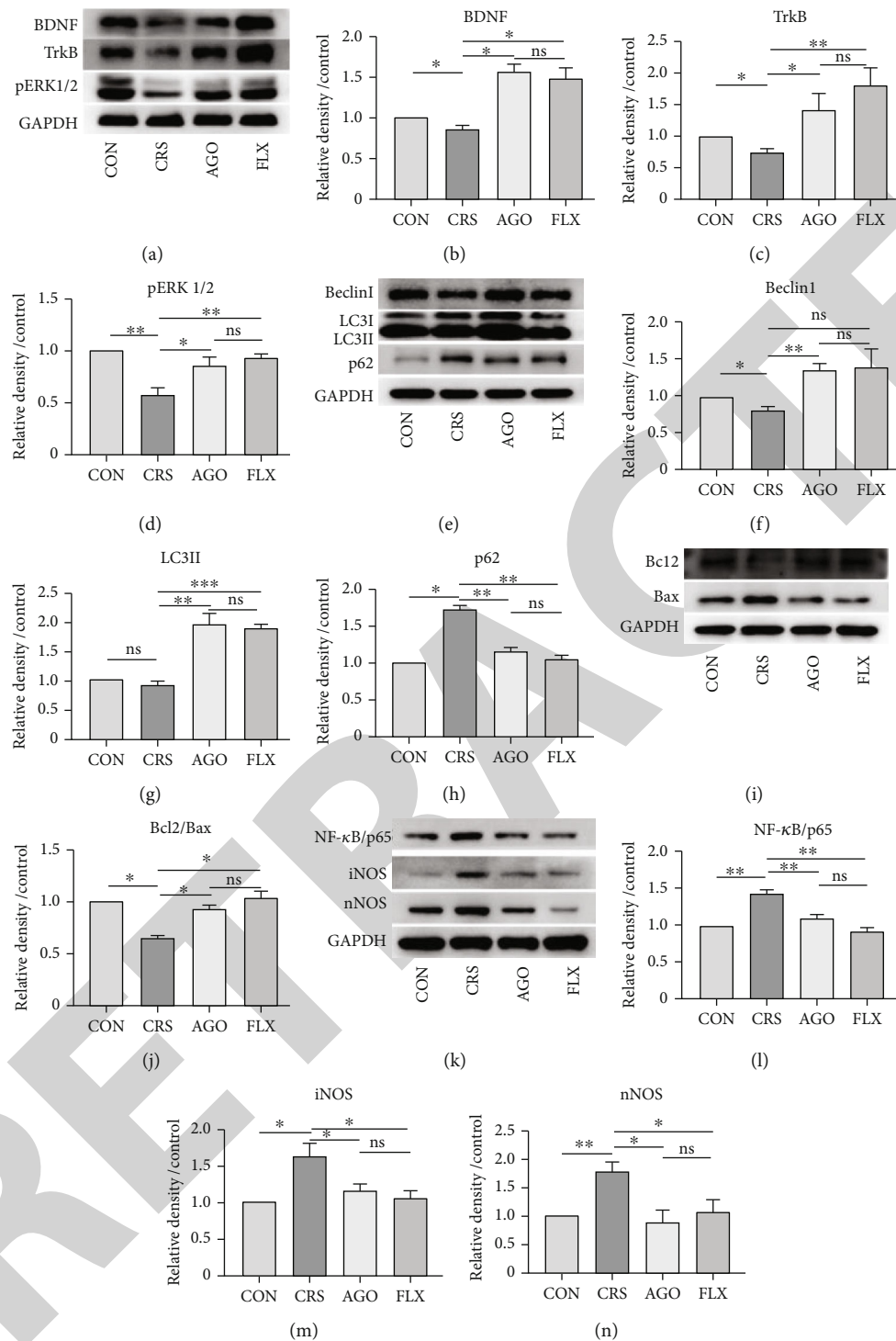


FIGURE 2: Effect of AGO treatment on BDNF/TrkB and pERK1/2 in autophagy, apoptosis, and inflammation in CRS mice. (a) Representative western blot results of BDNF, TrkB, and pERK1/2 are shown; densitometry analysis of BDNF (b), TrkB (c), and pERK1/2 (d) in the hippocampus is presented. (e) Representative western blot results of LC3II, Beclin1, and p62 are shown; densitometry analysis of Beclin1 (f), LC3II (g), and p62 (h) in the hippocampus. (i) Representative western blot results of Bcl2 and Bax are shown; (j) densitometry analysis of the Bcl2/Bax ratio in the hippocampus. (k) Representative western blot results of NF-κB/p65, iNOS, and nNOS; densitometry analysis of NF-κB/p65 (l), iNOS (m), and nNOS (n) in the hippocampus. \* $P < 0.05$ ; \*\* $P < 0.01$ ; \*\*\* $P < 0.001$ ; ns = not significant. The values represent mean  $\pm$  SEM.  $n = 3-5$ .

was corroborated with decreased levels of active ERK1/2 (Figures 2(a) and 2(d)). Interestingly, AGO restored the CRS-induced decrease to levels achieved by FLX regimens.

Moreover, there was no significant change between the AGO and FLX groups, indicating that these two drugs protect similarly against CRS-induced depressive

symptoms by interfering with BDNF and TrkB expression and ERK activity in the hippocampus.

**3.3. AGO Promotes CRS-Induced Autophagy in the Hippocampus.** To confirm the protective effect of AGO on hippocampal autophagy in the CRS model, we sought to investigate the putative protective mechanisms of AGO. Therefore, the expression level of autophagy markers LC3II, p62, and Beclin1 was analyzed by western blotting. Our experiments showed that Beclin1 was downregulated in the CRS group (Figures 2(e) and 2(f)), which was restored in AGO-treated mice comparable to the levels found in animals subjected to FLX regimens. Similarly, LC3 II expression in the hippocampus increased in mice subjected to AGO and FLX treatment after CRS (Figures 2(e) and 2(g)). Given that LC3II and Beclin1 can only reflect the initialization of autophagy, we also detected the protein level of p62, which is the best-characterized molecule and degradation product of autophagy. As shown in Figures 2(e) and 2(h), hippocampal p62 levels were increased in CRS mice but significantly decreased after treatment with AGO and FLX. The results suggest that stress led to lower levels of autophagy after the chronic restraint stress; this was ameliorated by AGO treatment having higher levels than stressed animal.

**3.4. AGO Decreases CRS-Induced Apoptosis in the Hippocampus.** To confirm the role of AGO treatment in the apoptosis mechanism, we investigated the hippocampal Bax and Bcl-2 protein levels to evaluate apoptosis. As shown in Figures 2(i) and 2(j), CRS resulted in a decrease in the Bcl2/Bax ratio in the hippocampus. Administration of AGO was associated with a significantly increased Bcl2/Bax ratio in the hippocampus. Altogether, these findings suggest that AGO might improve depressive symptoms in the CRS mouse model by maintaining essential autophagy and inhibiting excessive apoptosis.

**3.5. AGO Treatment Alleviates CRS-Induced Inflammation in the Hippocampus.** Ample preclinical and clinical evidence showed that external stress is accompanied by an increased production of proinflammatory cytokines and their upstream regulators. NF- $\kappa$ B is a transcription factor reported to regulate a plethora of proinflammatory cytokines, such as iNOS [28]. Our experiments show that NF- $\kappa$ B subunit p65/RelA is elevated after CRS in the hippocampus (Figures 2(k) and 2(l)). Furthermore, our data show that iNOS and nNOS are also elevated after CRS (Figures 2(k), 2(m), and 2(n)). Most importantly, administration of AGO partially restored both p65 and iNOS/nNOS levels, which were comparable with FLX treatment (Figures 2(k), 2(m), and 2(n)). Altogether, these findings implicate NF- $\kappa$ B in CRS-induced inflammation.

**3.6. Effect of AGO Treatment on Alterations of Microglia in the Mouse Hippocampus.** To investigate the effect of AGO and FLX on microglia in the hippocampus, immunofluorescence staining for hippocampal sections was performed. IBA1 was used as a specific marker for microglia. CRS admin-

istration resulted in a decrease in IBA1 expression in the hippocampal region (Figures 3(a) and 3(b)). Importantly, AGO treatment ameliorated IBA1 expression compared with that of CRS mice (Figures 3(a) and 3(b)) in line with data presented in Figure 2.

**3.7. Changes in SCFA Concentrations.** Based on the “microbiota-gut-brain” axis, we determined the effects of AGO administration on short-chain fatty acids. The SCFA (acetate, propionate, isobutyrate, butyrate, and valeric acid) concentration in mouse fecal samples was analyzed by GC and is shown in Figure 4. Of all investigated fatty acids, only isobutyrate showed a difference between CRS and control. Administration of AGO mainly decreased the concentration of acetate, valeric acid, and total SCFAs and not isobutyrate. On the other hand, high levels of isobutyric acid induced by CRS were relieved by drug treatment indicating that established AGO or FLX regimens can attenuate depressive-like behaviors via the modulation of microbiota-driven SCFA levels.

## 4. Discussion

In our present study, we found that AGO treatment for 4 weeks alleviated depression-like behaviors via activating autophagy and the BDNF-TrkB pathway in the hippocampus of CRS mice. Moreover, an obvious decrease in inflammation including NF- $\kappa$ B, iNOS, and nNOS as well as apoptosis including Bax is confirmed. It implies the possibility that regulating autophagy and the BDNF-TrkB pathway may be an alternative mode of action for AGO besides its role in modulating melatonin.

CRS is a noninvasive protocol, which is very similar to human psychological stress [29] and therefore renders as a reliable animal model of studying the depression with good replicability. Our findings revealing lower body weight gain and depressive-like behaviors (FST and SPT) after CRS are consistent with previous studies [30]. Contradicting literature reported either the failure of CRS to generate an anxiety-like behavior or an important role of CRS in inflicting such behavioral changes [31–33]. Reasons for this discrepancy might be attributed to the parameters of the applied restraint stress (e.g., frequency and duration) [34]. In short, the successful establishment of depression model mice allowed us to study the antidepressant mechanism of AGO.

BDNF-related signaling pathways have been reported to play an essential role in the pathogenesis of stress-induced depression-like behaviors [35]. In the present study, we found that expression levels of BDNF/TrkB in the hippocampus of the CRS group were significantly downregulated. This is consistent with the current clinical research results [36]. Such BDNF/TrkB [37] integration leads to the activation of some signaling pathways including extracellular signal-regulated kinase 1/2 (ERK1/2) which is consistent with our findings that CRS-induced depressive-like behaviors and the consequent downregulation of BDNF/TrkB and ERK1/2 activity could be reversed by AGO administration.

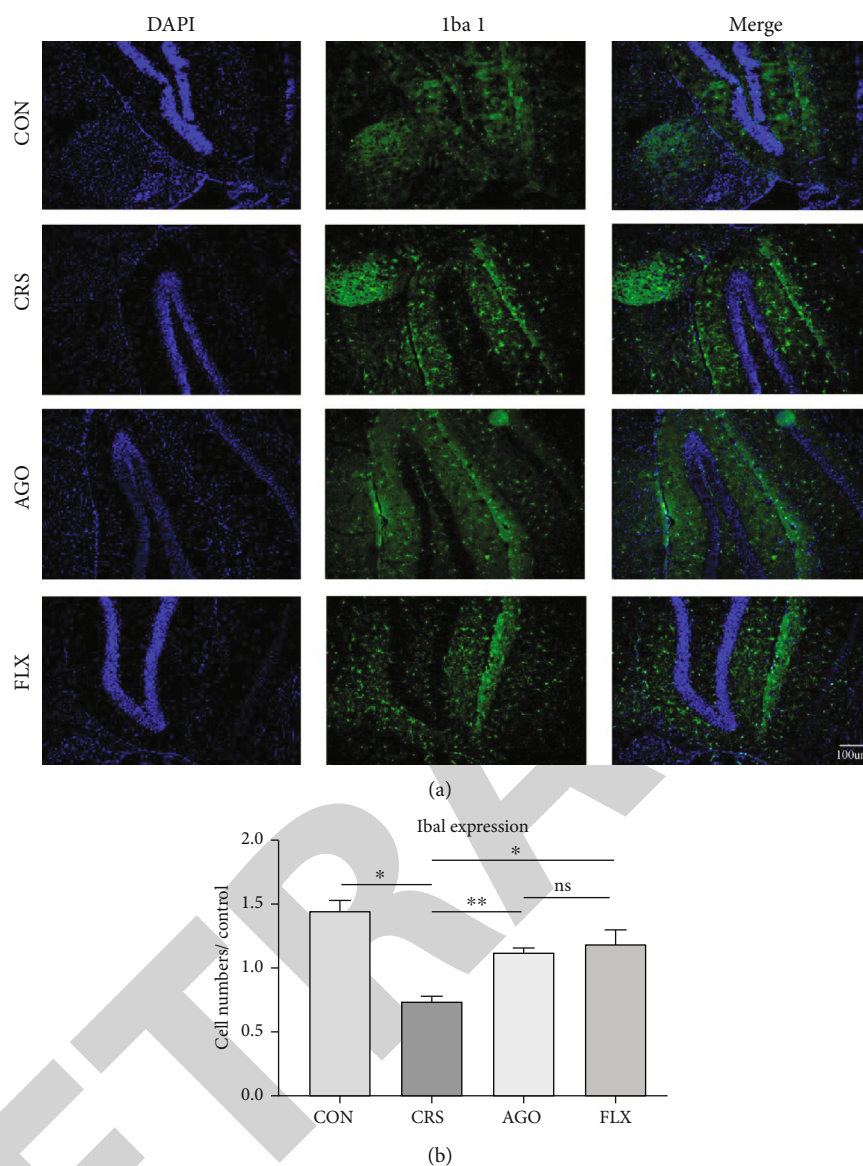


FIGURE 3: Immunofluorescence results indicated variation of microglial activation after CRS and AGO treatment. (a) Representative images of Iba1 (green) and DAPI (blue). Merged images are shown in the right panel. Scale bar = 100 μm. (b) Quantification analysis of Iba1-positive cells in the DG of the hippocampus. \* $P < 0.05$ ; \*\* $P < 0.01$ ; ns = not significant. Values are expressed as mean  $\pm$  SEM.  $n = 3$ .

In fact, autophagy and apoptosis constitute a strategy to adapt to and cope with the stress. The two affect each other and form a complex molecular regulatory network [38]. Stress is known to predispose rodents to depressive-like behaviors via inducing apoptosis in the hippocampus of mice [39]. Studies have shown that knocking out the proapoptotic factor Bax can reduce anxiety and depression-like behaviors in a mouse model of stress [40]. Analogously, enhanced apoptosis was detected in the hippocampus of rats tested in a repeated unpredictable stress model of depression [22]. The results of the present study indicate that AGO acts as an antidepressant partly through its role in improving the ratio of Bcl2/Bax. In many cases, autophagy usually manifests well before apoptosis “dismantles”

the cell. Preclinical experiments have found that signs of decreased autophagy appeared in both chronic unpredictable stress and LPS-related depression model [41, 42]. Our results confirmed that CRS does cause differences in the expression of autophagy and apoptotic factors in the hippocampus; i.e., CRS results in increased p62 and decreased Beclin1. Unfortunately, we did not find any differences upon LC3II expression. However, the features of depression could be prevented through increased autophagy and antiapoptosis activity as a result of AGO or FLX administration. This is consistent with our previous research on the antidepressant mechanism of FLX [43]. Therefore, we think that this might represent a potential antidepressant mechanism orchestrated by AGO.



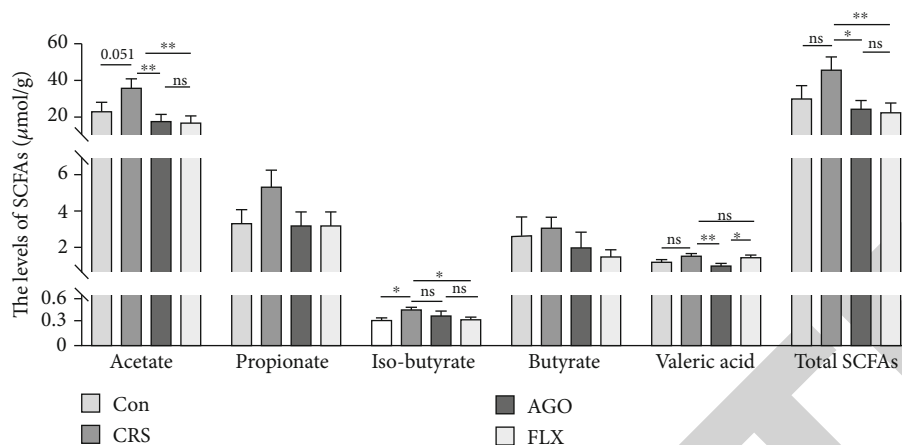


FIGURE 4: Effects of AGO on CRS-induced SCFA changes in fecal samples. \* $P < 0.05$ ; \*\* $P < 0.01$ ; \*\*\* $P < 0.001$ ; ns = not significant. The values represent mean  $\pm$  SEM.  $n = 8$ .

SCFAs are the key molecules that modulate microglial maturation and function, as well as depression [44–46]. In other studies, the mechanism of melatonin receptor expression may involve the action of SCFAs [47], and this effect does not necessarily affect the signals of brain neurons. It may be manifested by altering brain inflammation, affecting neuronal BDNF or autophagy pathways. Results from this study indicate that the CRS procedure can significantly increase isobutyrate level in feces and decrease IBA1 expression in the hippocampus indicating that isobutyrate plays an important role in the CRS procedure and may be involved in regulating the expression of IBA1. As microglia are the resident immune cells in the brain, they normally respond to various neuropathological stimuli, including stress, injury, and infection [48]. Once activated, a rapid proliferation in microglial densities and morphological changes result, followed by the release of proinflammatory and anti-inflammatory cytokines [49]. In this study, we found that CRS-induced depression is accompanied by elevated proinflammatory cytokine regulators such as transcription factor NF- $\kappa$ B or increased iNOS, in line with previous studies [50]. As a novel antidepressant, AGO can rebalance the above changes to exert an antidepressant effect. In other words, AGO can exert antidepressant effects through immune pathways. More importantly, for the changes in the content of isobutyric acid induced by CRS, we found that AGO could not reverse the disordered concentration but FLX did. The possible reasons might be related to the different molecular mechanisms of the two drugs.

## 5. Conclusion

Taken together, these data provide further evidence for a beneficial role of AGO and its effects in the hippocampus under stressful conditions and confirmed that AGO can protect the CRS mice from depression. AGO may funnel its antidepressant effect through part of the molecular pathways delineated in the above, further confirming the

important role of these cellular events in depression, and therefore might be used as an antidepressant drug in CRS.

## Data Availability

The data used to support the findings of this study are available from the corresponding author upon request.

## Conflicts of Interest

All authors have no conflicts of interest to disclose.

## Acknowledgments

The National Natural Science Foundation of China (grant numbers 81871063 and 81971769) supported this study. We are grateful to the Core Facilities of Zhejiang University and Institute of Neuroscience and Institute of Agrobiological and Environmental Sciences, Zhejiang University, for providing technical assistance.

## References

- [1] E. Falkum, G. Pedersen, and S. Karterud, "Diagnostic and Statistical Manual of Mental Disorders, Fourth Edition, paranoid personality disorder diagnosis: a unitary or a two-dimensional construct?," *Comprehensive Psychiatry*, vol. 50, no. 6, pp. 533–541, 2009.
- [2] J. Wang, X. Wu, W. Lai et al., "Prevalence of depression and depressive symptoms among outpatients: a systematic review and meta-analysis," *BMJ Open*, vol. 7, no. 8, article e017173, 2017.
- [3] Z. Aszalos, "Effects of antidepressants on sleep," *Orvosi Hetilap*, vol. 147, no. 17, pp. 773–783, 2006.
- [4] S. S. Morimoto, D. Kanellopoulos, K. J. Manning, and G. S. Alexopoulos, "Diagnosis and treatment of depression and cognitive impairment in late life," *Annals of the New York Academy of Sciences*, vol. 1345, no. 1, pp. 36–46, 2015.



- [5] J. Rothmore, "Antidepressant-induced sexual dysfunction," *The Medical Journal of Australia*, vol. 212, no. 7, pp. 329–334, 2020.
- [6] C. de Bodinat, B. Guardiola-Lemaitre, E. Mocaer, P. Renard, C. Munoz, and M. J. Millan, "Agomelatine, the first melatonergic antidepressant: discovery, characterization and development," *Nature Reviews Drug Discovery*, vol. 9, no. 8, pp. 628–642, 2010.
- [7] I. B. Hickie and N. L. Rogers, "Novel melatonin-based therapies: potential advances in the treatment of major depression," *Lancet*, vol. 378, no. 9791, pp. 621–631, 2011.
- [8] S. P. Singh, V. Singh, and N. Kar, "Efficacy of agomelatine in major depressive disorder: meta-analysis and appraisal," *The International Journal of Neuropsychopharmacology*, vol. 15, no. 3, pp. 417–428, 2012.
- [9] D. Taylor, A. Sparshatt, S. Varma, and O. Olofinjana, "Antidepressant efficacy of agomelatine: meta-analysis of published and unpublished studies," *BMJ*, vol. 348, no. mar19 5, p. g1888, 2014.
- [10] A. Gonzalez-Candia, M. Veliz, C. Carrasco-Pozo et al., "Antenatal melatonin modulates an enhanced antioxidant/pro-oxidant ratio in pulmonary hypertensive newborn sheep," *Redox Biology*, vol. 22, article 101128, 2019.
- [11] P. Jumnonprakhon, P. Govitrapong, C. Tocharus, and J. Tocharus, "Inhibitory effect of melatonin on cerebral endothelial cells dysfunction induced by methamphetamine via NADPH oxidase-2," *Brain Research*, vol. 1650, pp. 84–92, 2016.
- [12] A. W. Siu, M. Maldonado, M. Sanchez-Hidalgo, D. X. Tan, and R. J. Reiter, "Protective effects of melatonin in experimental free radical-related ocular diseases," *Journal of Pineal Research*, vol. 40, no. 2, pp. 101–109, 2006.
- [13] D. Zhao, H. Wang, S. Chen, D. Yu, and R. J. Reiter, "Phytomelatonin: an emerging regulator of plant biotic stress resistance," *Trends in Plant Science*, vol. 26, no. 1, pp. 70–82, 2021.
- [14] C. Bjorkholm and L. M. Monteggia, "BDNF - a key transducer of antidepressant effects," *Neuropharmacology*, vol. 102, pp. 72–79, 2016.
- [15] S. Y. Peng, W. Q. Li, L. X. Lv, Z. J. Zhang, and X. P. Zhan, "BDNF as a biomarker in diagnosis and evaluation of treatment for schizophrenia and depression," *Discovery Medicine*, vol. 26, no. 143, pp. 127–136, 2018.
- [16] J. C. Zhang, W. Yao, and K. Hashimoto, "Brain-derived neurotrophic factor (BDNF)-TrkB signaling in inflammation-related depression and potential therapeutic targets," *Current Neuropharmacology*, vol. 14, no. 7, pp. 721–731, 2016.
- [17] X. Tan, X. Du, Y. Jiang, B. O. A. Botchway, Z. Hu, and M. Fang, "Inhibition of autophagy in microglia alters depressive-like behavior via BDNF pathway in postpartum depression," *Frontiers in Psychiatry*, vol. 9, p. 434, 2018.
- [18] Y. Zhu, J. Deng, M. L. Nan et al., "The interplay between pattern recognition receptors and autophagy in inflammation," *Advances in Experimental Medicine and Biology*, vol. 1209, pp. 79–108, 2019.
- [19] N. C. Gassen and T. Rein, "Is there a role of autophagy in depression and antidepressant action?," *Frontiers in Psychiatry*, vol. 10, p. 337, 2019.
- [20] G. Kroemer, G. Marino, and B. Levine, "Autophagy and the integrated stress response," *Molecular Cell*, vol. 40, no. 2, pp. 280–293, 2010.
- [21] X. Shu, Y. Sun, X. Sun et al., "The effect of fluoxetine on astrocyte autophagy flux and injured mitochondria clearance in a mouse model of depression," *Cell Death & Disease*, vol. 10, no. 8, p. 577, 2019.
- [22] T. A. Kosten, M. P. Galloway, R. S. Duman, D. S. Russell, and C. D'Sa, "Repeated unpredictable stress and antidepressants differentially regulate expression of the bcl-2 family of apoptotic genes in rat cortical, hippocampal, and limbic brain structures," *Neuropsychopharmacology*, vol. 33, no. 7, pp. 1545–1558, 2008.
- [23] P. Boya, R. A. González-Polo, N. Casares et al., "Inhibition of macroautophagy triggers apoptosis," *Molecular and Cellular Biology*, vol. 25, no. 3, pp. 1025–1040, 2005.
- [24] P. Patrício, A. Mateus-Pinheiro, M. Irmeler et al., "Differential and converging molecular mechanisms of antidepressants' action in the hippocampal dentate gyrus," *Neuropsychopharmacology*, vol. 40, no. 2, pp. 338–349, 2015.
- [25] N. L. Schramm, M. P. McDonald, and L. E. Limbird, "The alpha(2a)-adrenergic receptor plays a protective role in mouse behavioral models of depression and anxiety," *The Journal of Neuroscience*, vol. 21, no. 13, pp. 4875–4882, 2001.
- [26] E. Falcon, K. Maier, S. A. Robinson, T. E. Hill-Smith, and I. Lucki, "Effects of buprenorphine on behavioral tests for antidepressant and anxiolytic drugs in mice," *Psychopharmacology*, vol. 232, no. 5, pp. 907–915, 2015.
- [27] Y. Li, B. W. Luikart, S. Birnbaum et al., "TrkB regulates hippocampal neurogenesis and governs sensitivity to antidepressive treatment," *Neuron*, vol. 59, no. 3, pp. 399–412, 2008.
- [28] M. Napolitano, D. Zei, D. Centonze et al., "NF- $\kappa$ B/NOS crosstalk induced by mitochondrial complex II inhibition: implications for Huntington's disease," *Neuroscience Letters*, vol. 434, no. 3, pp. 241–246, 2008.
- [29] M. Hinwood, J. Morandini, T. A. Day, and F. R. Walker, "Evidence that microglia mediate the neurobiological effects of chronic psychological stress on the medial prefrontal cortex," *Cerebral Cortex*, vol. 22, no. 6, pp. 1442–1454, 2012.
- [30] S. H. Yoon, B. H. Kim, S. K. Ye, and M. H. Kim, "Chronic non-social stress affects depressive behaviors but not anxiety in mice," *The Korean journal of physiology & pharmacology : official journal of the Korean Physiological Society and the Korean Society of Pharmacology*, vol. 18, no. 3, pp. 263–268, 2014.
- [31] H. Y. Liu, J. Yue, L. N. Hu et al., "Chronic minocycline treatment reduces the anxiety-like behaviors induced by repeated restraint stress through modulating neuroinflammation," *Brain Research Bulletin*, vol. 143, pp. 19–26, 2018.
- [32] V. K. Parihar, B. Hattiangady, R. Kuruba, B. Shuai, and A. K. Shetty, "Predictable chronic mild stress improves mood, hippocampal neurogenesis and memory," *Molecular Psychiatry*, vol. 16, no. 2, pp. 171–183, 2011.
- [33] J. Y. Zhang, T. H. Liu, Y. He et al., "Chronic stress remodels synapses in an amygdala circuit-specific manner," *Biological Psychiatry*, vol. 85, no. 3, pp. 189–201, 2019.
- [34] T. Buynitsky and D. I. Mostofsky, "Restraint stress in biobehavioral research: recent developments," *Neuroscience and Biobehavioral Reviews*, vol. 33, no. 7, pp. 1089–1098, 2009.
- [35] B. A. Bus, M. L. Molendijk, I. Tendolkar et al., "Chronic depression is associated with a pronounced decrease in serum brain-derived neurotrophic factor over time," *Molecular Psychiatry*, vol. 20, no. 5, pp. 602–608, 2015.
- [36] M. M. Youssef, M. D. Underwood, Y. Y. Huang et al., "Association of BDNF Val66Met polymorphism and brain BDNF levels with major depression and suicide," *The International*

## Retraction

# Retracted: A Network Pharmacology to Explore the Mechanism of *Calculus Bovis* in the Treatment of Ischemic Stroke

### BioMed Research International

Received 12 March 2024; Accepted 12 March 2024; Published 20 March 2024

Copyright © 2024 BioMed Research International. This is an open access article distributed under the Creative Commons Attribution License, which permits unrestricted use, distribution, and reproduction in any medium, provided the original work is properly cited.

This article has been retracted by Hindawi following an investigation undertaken by the publisher [1]. This investigation has uncovered evidence of one or more of the following indicators of systematic manipulation of the publication process:

- (1) Discrepancies in scope
- (2) Discrepancies in the description of the research reported
- (3) Discrepancies between the availability of data and the research described
- (4) Inappropriate citations
- (5) Incoherent, meaningless and/or irrelevant content included in the article
- (6) Manipulated or compromised peer review

The presence of these indicators undermines our confidence in the integrity of the article's content and we cannot, therefore, vouch for its reliability. Please note that this notice is intended solely to alert readers that the content of this article is unreliable. We have not investigated whether authors were aware of or involved in the systematic manipulation of the publication process.

Wiley and Hindawi regrets that the usual quality checks did not identify these issues before publication and have since put additional measures in place to safeguard research integrity.

We wish to credit our own Research Integrity and Research Publishing teams and anonymous and named external researchers and research integrity experts for contributing to this investigation.

The corresponding author, as the representative of all authors, has been given the opportunity to register their agreement or disagreement to this retraction. We have kept a record of any response received.

### References

- [1] F. Liu, L. Li, J. Chen, Y. Wu, Y. Cao, and P. Zhong, "A Network Pharmacology to Explore the Mechanism of *Calculus Bovis* in the Treatment of Ischemic Stroke," *BioMed Research International*, vol. 2021, Article ID 6611018, 20 pages, 2021.

## Research Article

# A Network Pharmacology to Explore the Mechanism of *Calculus Bovis* in the Treatment of Ischemic Stroke

Fangchen Liu <sup>1,2</sup>, Ling Li <sup>3</sup>, Jian Chen <sup>3</sup>, Ying Wu <sup>1</sup>, Yongbing Cao <sup>3</sup>  
and Ping Zhong <sup>1,4</sup>

<sup>1</sup>Department of Neurology, Shanghai TCM-Integrated Hospital, Shanghai University of Traditional Chinese Medicine, Shanghai 200082, China

<sup>2</sup>Shanghai University of Traditional Chinese Medicine, Shanghai 201203, China

<sup>3</sup>Institute of Vascular Disease, Shanghai TCM-Integrated Hospital, Shanghai University of Traditional Chinese Medicine, Shanghai 200082, China

<sup>4</sup>Department of Neurology, Shidong Hospital of Yangpu District, Shanghai 200090, China

Correspondence should be addressed to Yongbing Cao; [ybcao@vip.sina.com](mailto:ybcao@vip.sina.com) and Ping Zhong; [zphgl@163.com](mailto:zphgl@163.com)

Received 17 December 2020; Revised 15 February 2021; Accepted 20 February 2021; Published 11 March 2021

Academic Editor: Yuzhen Xu

Copyright © 2021 Fangchen Liu et al. This is an open access article distributed under the Creative Commons Attribution License, which permits unrestricted use, distribution, and reproduction in any medium, provided the original work is properly cited.

**Background.** *Calculus Bovis* is a valuable Chinese medicine, which is widely used in the clinical treatment of ischemic stroke. The present study is aimed at investigating its target and the mechanism involved in ischemic stroke treatment by network pharmacology. **Methods.** Effective compounds of *Calculus Bovis* were collected using methods of network pharmacology and using the Bioinformatics Analysis Tool for Molecular Mechanism of Traditional Chinese Medicine (BATMAN-TCM) and the Traditional Chinese Medicine Systems Pharmacology Database and Analysis Platform (TCMSP). Potential compound targets were searched in the TCMSP and SwissTargetPrediction databases. Ischemic stroke-related disease targets were searched in the Drugbank, DisGeNet, OMIM, and TTD databases. These two types of targets were uploaded to the STRING database, and a network of their interaction (PPI) was built with its characteristics calculated, aiming to reveal a number of key targets. Hub genes were selected using a plug-in of the Cytoscape software, and Gene Ontology (GO) biological processes and pathway enrichment analyses of Kyoto Encyclopedia of Genes and Genomes (KEGG) were conducted using the clusterProfiler package of R language. **Results.** Among 12 compounds, deoxycorticosterone, methyl cholate, and biliverdin were potentially effective components. A total of 344 *Calculus Bovis* compound targets and 590 ischemic stroke targets were found with 92 overlapping targets, including hub genes such as TP53, AKT, PIK2CA, MAPK3, MMP9, and MMP2. Biological functions of *Calculus Bovis* are associated with protein hydrolyzation, phosphorylation of serine/threonine residues of protein substrates, peptide bond hydrolyzation of peptides and proteins, hydrolyzation of intracellular second messengers, antioxidation and reduction, RNA transcription, and other biological processes. **Conclusion.** *Calculus Bovis* may play a role in ischemic stroke by activating PI3K-AKT and MAPK signaling pathways, which are involved in regulating inflammatory response, cell apoptosis, and proliferation.

## 1. Introduction

Stroke is an acute cerebrovascular disease with typical clinical manifestations of sudden weakness in one side of the face, arms, or legs; sudden faintness; and unconsciousness. Ischemic stroke, the most common form of stroke, accounts for 70-80% of the total number of cases among stroke patients

[1]. In China, deaths due to cerebrovascular diseases accounted for more than 20% of the total deaths in 2018 [2]. The rehabilitation of patients with ischemic stroke is often ineffective which brings a heavy burden to society and families. Currently, tissue-type plasminogen activator (tPA) is the only approved treatment for acute ischemic stroke [3-5]. However, its clinical application is greatly

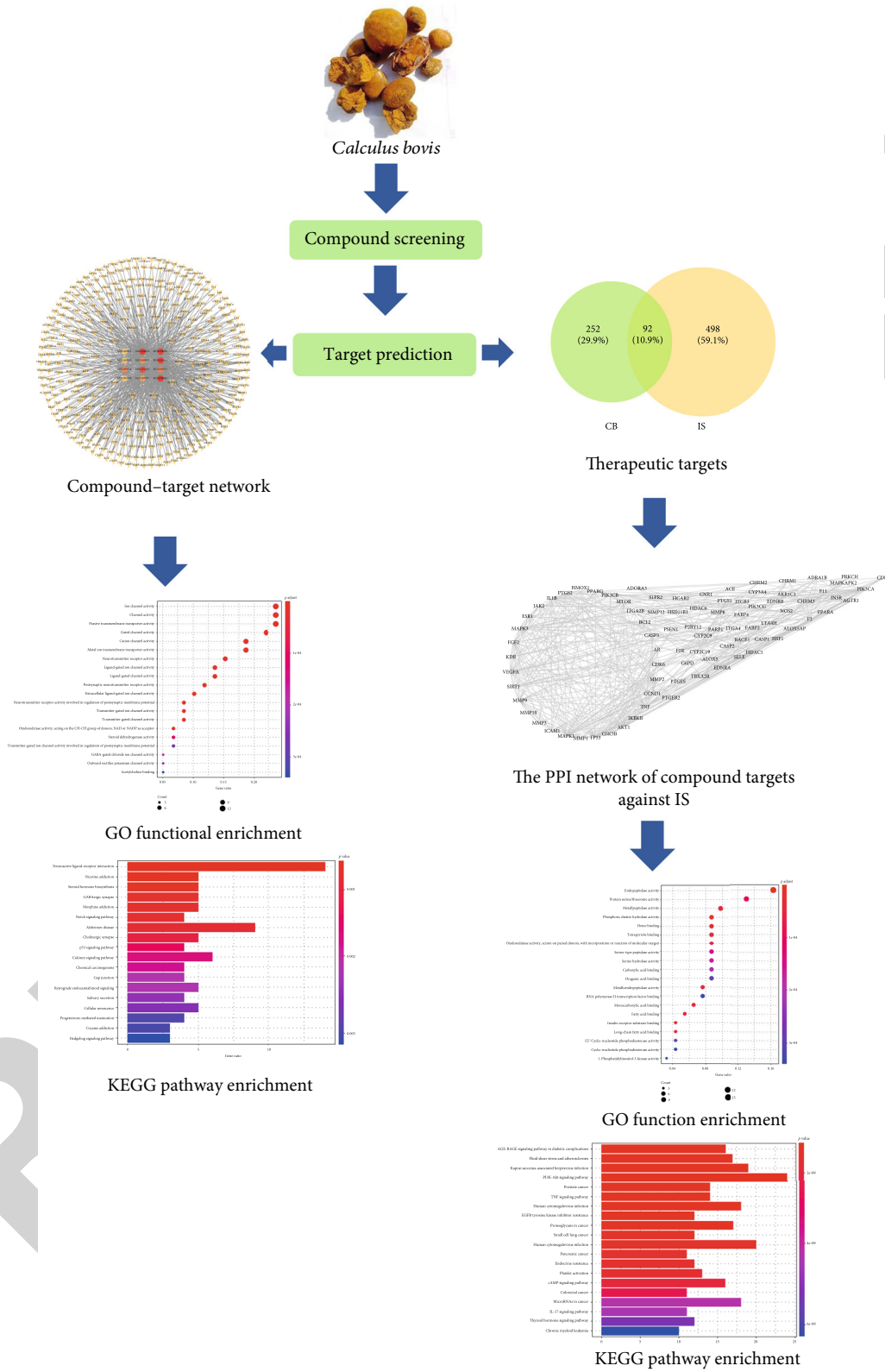


FIGURE 1: The schematic map of the present study.

limited due to the narrow treatment time window, high bleeding risk, and many contraindications [6]. In China, stroke has been managed with herbs or other Chinese methods for thousands of years. Chinese herbal medicine

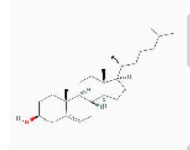
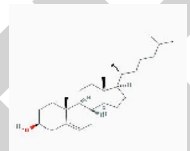
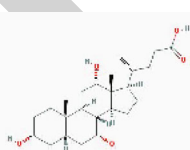
are now widely accepted as the main complementary treatment in East Asia, North America, and Europe because of their good therapeutic effect, low toxicity, and low cost [7–9].

TABLE 1: Active ingredients of *Calculus Bovis*.

Mol ID	Mol name	2D structure	OB (%)	DL
MOL000263	Oleanolic acid		29.02	0.76
MOL000298	Ergosterol		14.29	0.72
MOL000511	Ursolic acid		16.77	0.75
MOL008834	Bilicerdin		23.79	0.75
MOL008835	3-[2-[[3-(2-Carboxyethyl)-4-methyl-5-[(E)-(4-methyl-5-oxo-3-vinyl-2-pyrrolylidene)methyl]-1H-pyrrol-2-yl)methyl]-4-methyl-5-[(Z)-(3-methyl-5-oxo-4-vinyl-2-pyrrolylidene)methyl]-1H-pyrrol-3-yl]propanoic acid		16.53	0.75
MOL008838	Methyl (4R)-4-[(3R,5S,7S,8R,9S,10S,12S,13R,14S,17R)-3,7,12-trihydroxy-10,13-dimethyl-2,3,4,5,6,7,8,9,11,12,14,15,16,17-tetradecahydro-1H-cyclopenta[a]phenanthren-17-yl]pentanoate		32.32	0.76
MOL008839	Methyl desoxycholate		34.63	0.73
MOL008840	2-[(3alpha,12alpha-Dihydroxy-24-oxo-5beta-cholan-24-yl)amino]ethanesulfonic acid		15.92	0.87
MOL008843	Cherianoine		27.32	0.12



TABLE 1: Continued.

Mol ID	Mol name	2D structure	OB (%)	DL
MOL008846	ZINC01280365		46.38	0.49
MOL000953	CLR		37.87	0.68
MOL009807	CHD		22.17	0.72

Abbreviations: OB = oral bioavailability; DL = drug likeness; Mol = molecular.

*Calculus Bovis*, one of the most commonly used Chinese herbs for stroke, has been used for over 2,000 years in China. It was first described in “Shen Nong Ben Cao Jing” as a medication with a bitter taste and cooling nature [10]. And it has been applied in conditions like loss of consciousness due to stroke, epilepsy, mania, and other mental disorders. It was shown that *Calculus Bovis* protects the brain through its anti-inflammatory, antiapoptosis [11], antilipid peroxidation [12], and antioxidative stress effects [13]. It is well known that herbs have multiple ingredients targeting multiple sites and multiple pathways [14, 15]. Currently, *Calculus Bovis* and its formulas are widely used to treat ischemic stroke, but the mechanisms underlying its therapeutic effect have not been studied intensively.

Network pharmacology for Chinese herbs is developed to decipher interactions between herbs and diseases at a system level by analysing the network between herbs, compounds, targets, diseases, and genes [16–19]. In the present study, our aim is to reveal the underlying mechanisms of *Calculus Bovis* in managing ischemic stroke by network pharmacology methods, which will lay the foundation for future pharmacological and clinical studies on ischemic stroke. The protocol of our experimental procedures is shown in Figure 1.

## 2. Materials and Methods

### 2.1. Data Acquisition

**2.1.1. Prediction of Compounds of *Calculus Bovis* and Their Targets.** Compounds of *Calculus Bovis* were collected from the herbal platform TCMSP and BATMAN-TCM. The TCMSP (<https://tcmsp.com/tcmsp.php>) is a systems pharmacology platform for herbs providing information about compounds and their targets [20]. The BATMAN-TCM (<http://bionet.ncpsb.org/batman-tcm/>) is an online bioinformatics analysis tool comprised of functions like target predic-

tion for herbs and target analysis [21]. When “NIU HUANG (*Calculus Bovis*)” was typed in the “Cluster name,” “Score cutoff” value was set at 20, and “Adjusted *p* value” was set at 0.05, compounds of *Calculus Bovis* and their targets would be displayed. In addition, potential targets could be searched in the TCMSP and SwissTargetPrediction (<http://www.swisstargetprediction.ch/>) databases [22] to further confirm the targets of compounds derived from *Calculus Bovis*. Names of target proteins were translated into gene names in the UniProt (<http://www.uniprot.org/>) database. If there was overlap in their target genes, the duplicates were deleted. Similarly, when the gene names of the protein targets were not found in the Uniprot database, they were deleted. SMILES IDs of compounds contained in *Calculus Bovis* were searched in the PubChem (<https://pubchem.ncbi.nlm.nih.gov/>) database, and their targets were predicted using SwissTargetPrediction after setting “*Homo sapiens*.” After collecting targets from the TCMSP, BATMAN-TCM, and SwissTargetPrediction databases, the duplicates were deleted.

**2.1.2. Prediction of Pharmacodynamics.** In pharmacological studies, absorption, distribution, metabolism, and excretion (ADME) are key indices for identifying specific drugs [23]. Herein, 2 key parameters related to ADME, namely, oral bioavailability (OB) and drug-like activities (DL), were analyzed to explore potential bioactive compounds in *Calculus Bovis*. Based on the content of known compounds, OB and DL were set at  $\geq 15\%$  and  $\geq 0.1$ , respectively. It has been reported that ergosterol (MOL000298; OB: 14.29%; DL: 0.72) is an indispensable compound of *Calculus Bovis* [24, 25] and was included in the present study. All compounds included in the present study were supported by the literature.

**2.1.3. Collection of Disease Targets of Ischemic Stroke.** Key words such as “ischemic stroke,” “cerebral ischemic stroke,” and “brain ischemia” were used, and “*Homo sapiens*” was

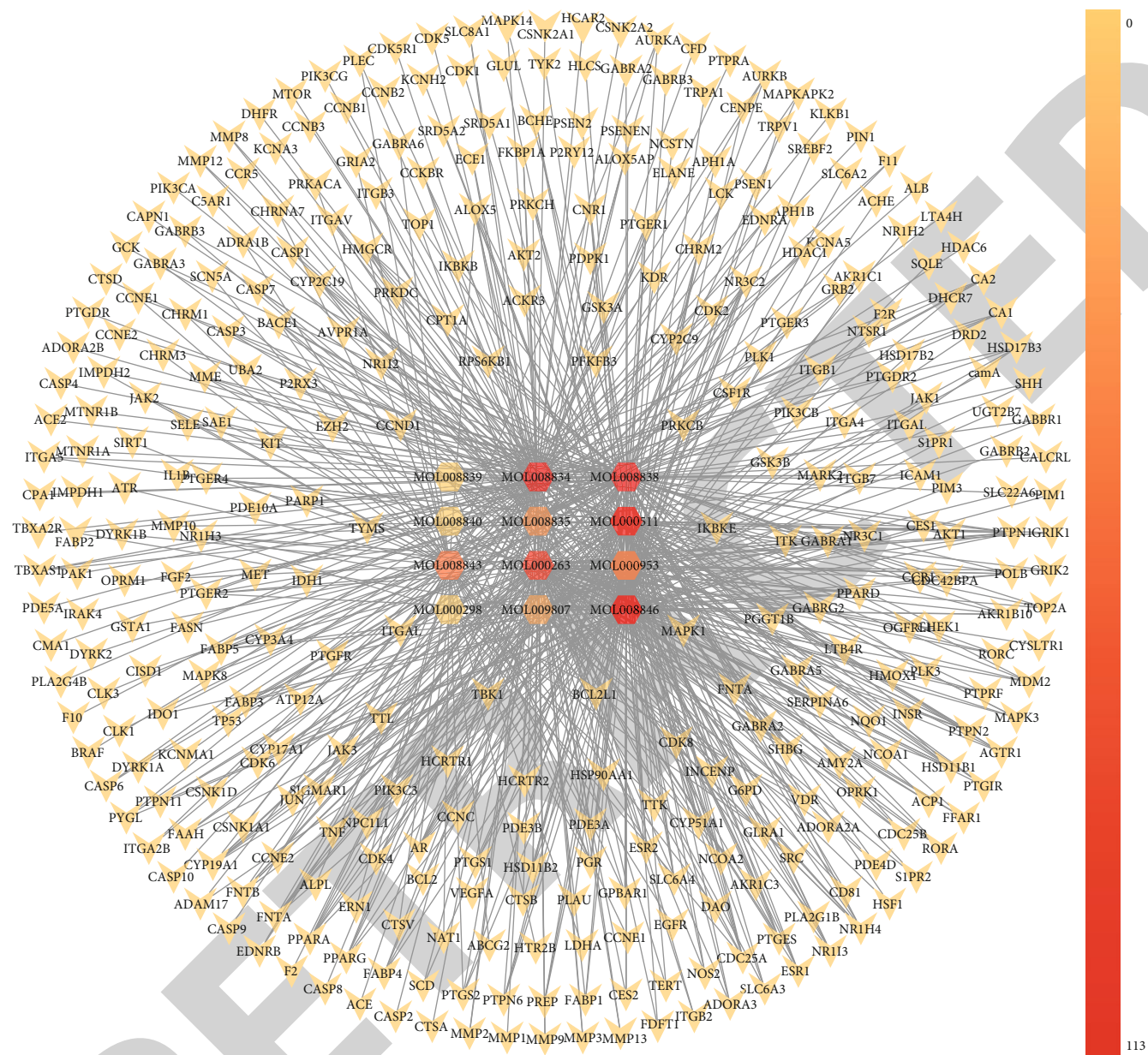


FIGURE 2: *Calculus Bovis* compound-target network. Note: circles represent compounds, triangles represent targets, and their colors darken as their degrees of freedom increase.

TABLE 2: *Calculus Bovis* compound-candidate target network parameters.

Network parameters	Values
Number of nodes	362
Network density	0.011
Network diameter	5
Network heterogeneity	3.212
Average number of neighbors	3.901
Characteristic path length	3.236
Shortest paths	130682 (100%)
Network centralization	0.304

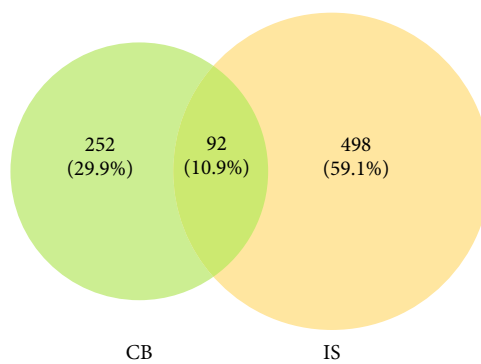


FIGURE 3: Venny diagram of *Calculus Bovis* targets and ischemic stroke disease targets. CB: *Calculus Bovis* target; IS: ischemic stroke disease target.



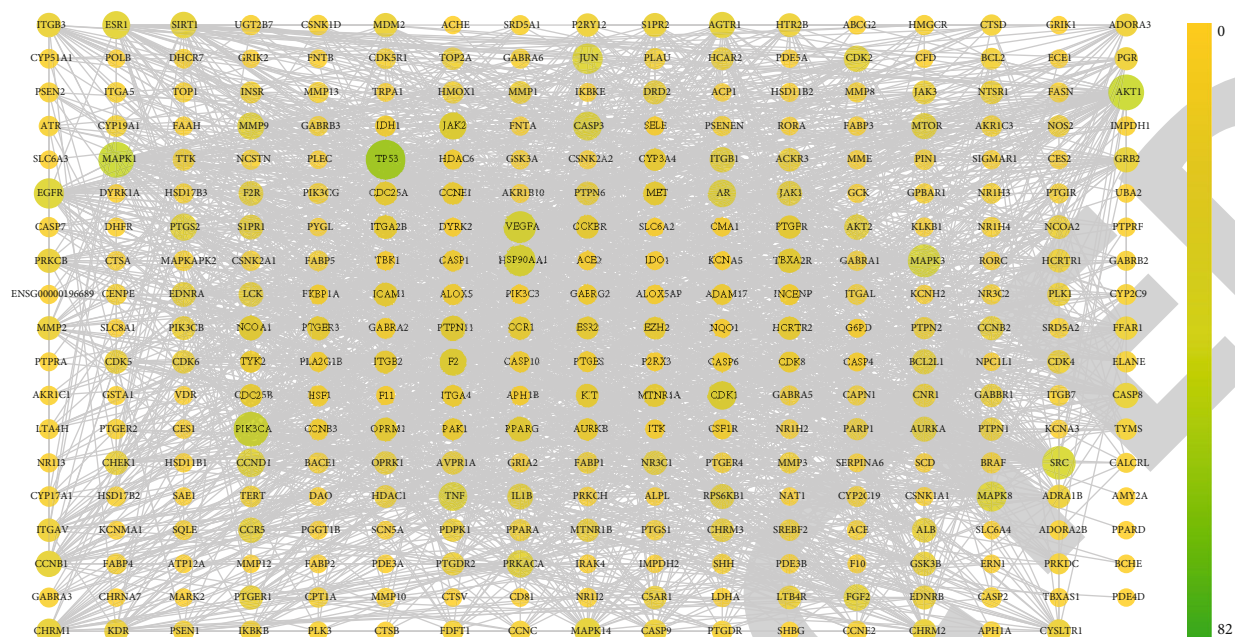


FIGURE 4: Protein-protein interaction (PPI) network of *Calculus Bovis* compound targets. Darkness of colors and sizes of circles represent the degree of freedom as the scale indicates.

selected for species. They were searched in the Drugbank [26], DisGeNet [27], OMIM [28], and TTD databases [29], and duplicate genes were deleted.

**2.1.4. Venny Plotting.** Both compound targets and disease targets were uploaded to the website of Venny 2.1.0 (<https://bioinfogp.cnb.csic.es/tools/venny/>); overlapping genes were the potential targets of bioactive compounds, and they interact with the body in ischemic stroke.

**2.1.5. Protein-Protein Interaction (PPI).** The STRING (<https://string-db.org>) database has collected a large number of well-known or predicted protein-protein interaction results [30]. Overlapping genes from Venny plots were uploaded to the database and “*Homo sapiens*” was selected for species, high confidence (0.700) was set for the minimum required interaction score, and irrelevant targets were concealed. As a result, a network map showing interactions between individual targets was rendered.

**2.2. Network Construction and Hub Gene Selection.** Network analysis facilitates interpretation of relationships between herbs, compounds, diseases, and genes. In the present study, two networks were constructed using Cytoscape 3.7.0 (<https://cytoscape.org/>) [31]: (1) a network of *Calculus Bovis* compounds and compound targets and (2) a PPI network of *Calculus Bovis* compound targets and a PPI network of *Calculus Bovis* treating ischemic stroke targets after connecting *Calculus Bovis* compound targets and disease targets. Topographical analysis for networks was completed using the NetworkAnalyzer tool in Cytoscape. Overlapping genes, also named Hub genes, were selected from the PPI networks using the cytoHubba plug-in in Cytoscape and 3 algorithms were used in the calculations. The latter included degree of

freedom, Maximum Neighborhood Component (MNC), and Maximal Clique Centrality (MCC).

**2.3. Gene Functions and Pathway Enrichment Analysis.** Gene Ontology (GO) enrichment analysis and Kyoto Encyclopedia of Genes and Genomes (KEGG) pathway analysis were conducted using the clusterProfiler package of R (R 4.0.2 for Windows) to identify biological processes and pathways with systemic involvement. Biological processes and pathways with a significant difference were selected, and their numbers of enrichment as well their  $p$  values were ranked. The top 20 results from the GO enrichment and KEGG pathway enrichment analyses were presented. Visualization of these pathways with a  $p$  value < 0.05 was completed using the R software package.

### 3. Results and Analysis

A total of 12 bioactive compounds were found after ADME screening, and all of them have been verified in other studies.

**3.1. *Calculus Bovis* Compound-Target Network.** A total of 344 targets were found by 12 bioactive compounds of *Calculus Bovis*. Details of these ingredients are listed in Table 1, and the map of the compound-target network is shown in Figure 2. Circles represent compounds of *Calculus Bovis*, and triangles represent the targets; their colors are darkened as their degrees of freedom increased. There were 362 nodes and 706 edges with a network density of 0.011 and a network diameter of 5. Details of these parameters are listed in Table 2.

**3.2. Disease Targets of Ischemic Stroke.** Using key words listed in Section 2.1.3, 74 disease targets were found in the Drugbank database, 313 were found in the DisGeNet database



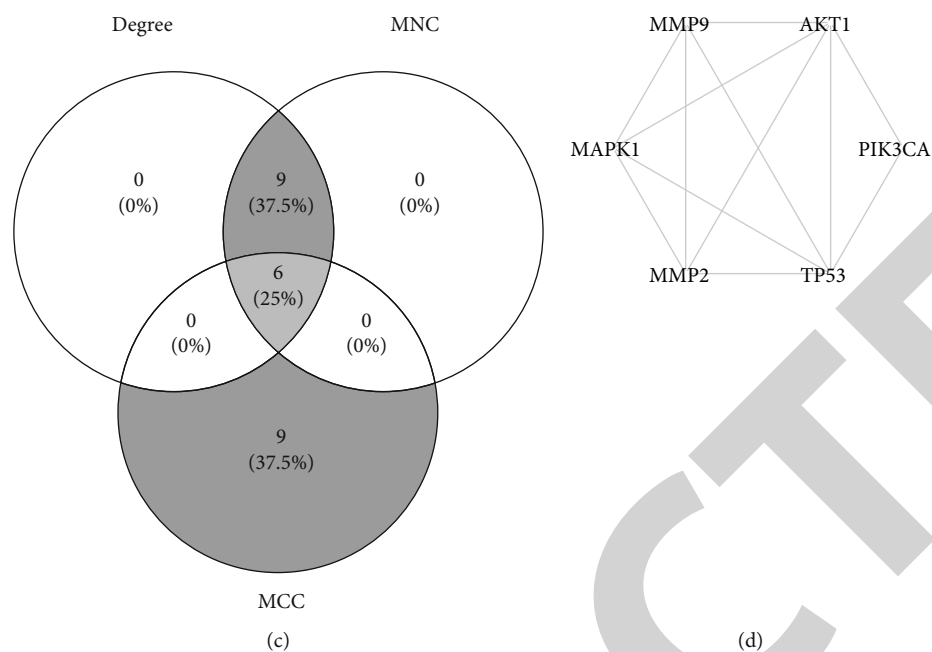


FIGURE 5: The PPI network of *Calculus Bovis* compound targets against ischemic stroke (IS): (a) the original PPI data generated from the STRING database showing detailed interactions of the targets; (b) the PPI network constructed using Cytoscape (version 3.7.0); (c) the top 15 genes were calculated from the PPI network by the degree of freedom, MNC, and MCC, and the overlapping genes were then screened by Venn diagrams; (d) the PPI network of hub genes.

TABLE 3: GO enrichment analysis results of *Calculus Bovis* targets.

No.	ID	Description	Count	<i>p</i> value
1	GO:0005216	Ion channel activity	14	$1.15918 \times 10^{-10}$
2	GO:0015267	Channel activity	14	$3.57104 \times 10^{-10}$
3	GO:0022803	Passive transmembrane transporter activity	14	$3.67058 \times 10^{-10}$
4	GO:0022836	Gated channel activity	13	$7.88226 \times 10^{-11}$
5	GO:0005261	Cation channel activity	11	$1.25701 \times 10^{-8}$
6	GO:0046873	Metal ion transmembrane transporter activity	11	$1.85161 \times 10^{-7}$
7	GO:0030594	Neurotransmitter receptor activity	9	$1.68357 \times 10^{-10}$
8	GO:0015276	Ligand-gated ion channel activity	8	$1.76915 \times 10^{-8}$
9	GO:0022834	Ligand-gated channel activity	8	$1.76915 \times 10^{-8}$
10	GO:0098960	Postsynaptic neurotransmitter receptor activity	7	$3.22861 \times 10^{-9}$
11	GO:0005230	Extracellular ligand-gated ion channel activity	6	$1.78299 \times 10^{-7}$
12	GO:0099529	Neurotransmitter receptor activity involved in regulation of postsynaptic membrane potential	5	$6.54501 \times 10^{-7}$
13	GO:0022824	Transmitter-gated ion channel activity	5	$1.78703 \times 10^{-6}$
14	GO:0022835	Transmitter-gated channel activity	5	$1.78703 \times 10^{-6}$
15	GO:0016229	Steroid dehydrogenase activity	4	$5.40 \times 10^{-6}$
16	GO:0016628	Oxidoreductase activity, acting on the CH-CH group of donors, NAD or NADP as acceptor	4	$1.58 \times 10^{-6}$
17	GO:1904315	Transmitter-gated ion channel activity involved in regulation of postsynaptic membrane potential	4	$1.78589 \times 10^{-5}$
18	GO:0022851	GABA-gated chloride ion channel activity	3	$9.83 \times 10^{-6}$
19	GO:0042166	Acetylcholine binding	3	$2.32 \times 10^{-5}$
20	GO:0015271	Outward rectifier potassium channel activity	3	$1.56 \times 10^{-5}$



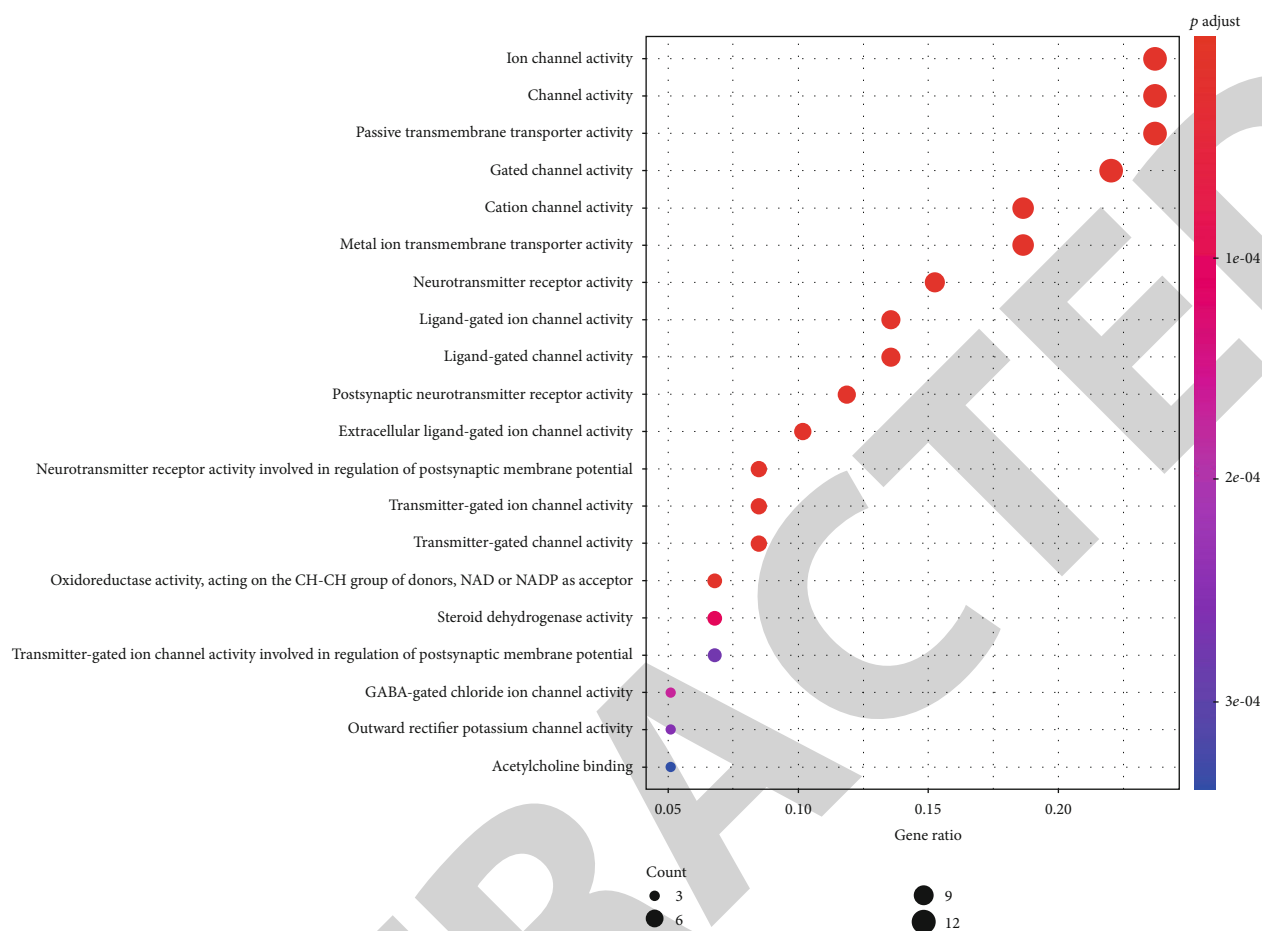


FIGURE 6: Bubble plot of GO enrichment analysis of *Calculus Bovis* targets. Bubble plot: letters on the left are GO names, numbers on the bottom are the proportions of genes, sizes of the circles indicate the numbers of enriched genes, and colors reflect  $p$  values. The redder the colors are, the more enriched the genes are, and the smaller the  $p$  values are.

after screening for values above the average, 322 were found in the OMIM database, and 10 were found in the TTD database. A total of 590 targets were found after deleting gene duplicates.

### 3.3. Prediction of *Calculus Bovis* Targets in Ischemic Stroke.

After entering compound targets and disease targets to Venny 2.1.0 in the form of gene names, 92 overlapping genes were found (see Figure 3). These genes were the shared targets of the bioactive compounds and disease targets in ischemic stroke.

### 3.4. Construction of PPI Networks

**3.4.1. The PPI Network of *Calculus Bovis* Targets.** PPI networks have been widely used in studying protein-protein interactions in different diseases. To construct the PPI network of *Calculus Bovis* targets, 12 compounds were connected with 344 targets in the TCMSP and the SwissTargetPrediction databases, and they were imported into the STRING database (species: *Homo sapiens*; minimum required interaction score: high confidence (0.700)), and the PPI network was visualized after reconstructing it with Cytoscape (version 3.7.0). As shown in Figure 4, colors dark-

ened as the degree of freedom increased. This PPI network contained 322 nodes and 2195 edges with a diameter of 8 and an average number of neighbors of 13.634. It showed that TP53 (degree = 82), AKT1 (degree = 67), MAPK1 (degree = 67), PIK3CA (degree = 63), SRC (degree = 58), MAPK3 (degree = 56), VEGFA (degree = 52), HSP90AA1 (degree = 48), JUN (degree = 46), EGFR (degree = 46), MAPK8 (degree = 45), TNF (degree = 40), and CASP3 (degree = 40) were the key nodes of this PPI network.

### 3.4.2. The PPI Network of *Calculus Bovis*-Ischemic Stroke Targets and Hub Genes.

To explore the potential therapeutic mechanisms of *Calculus Bovis* in managing ischemic stroke, 92 shared targets by *Calculus Bovis* compounds and ischemic stroke were connected and imported into the STRING database as shown in Figure 5(a). The PPI network of *Calculus Bovis*-ischemic stroke targets were constructed by visualizing the results using Cytoscape (Figure 5(b)). This PPI network had 83 nodes and 403 edges with a network diameter of 6 and an average number of neighbors of 9.711. The top 10 targets with the highest degree of freedom were TP53 (degree = 33), AKT1 (degree = 30), MAPK1 (degree = 29), VEGFA (degree = 27), TNF (degree = 25), PIK3CA (degree = 25), MAPK3 (degree = 24), MMP9 (degree = 22),

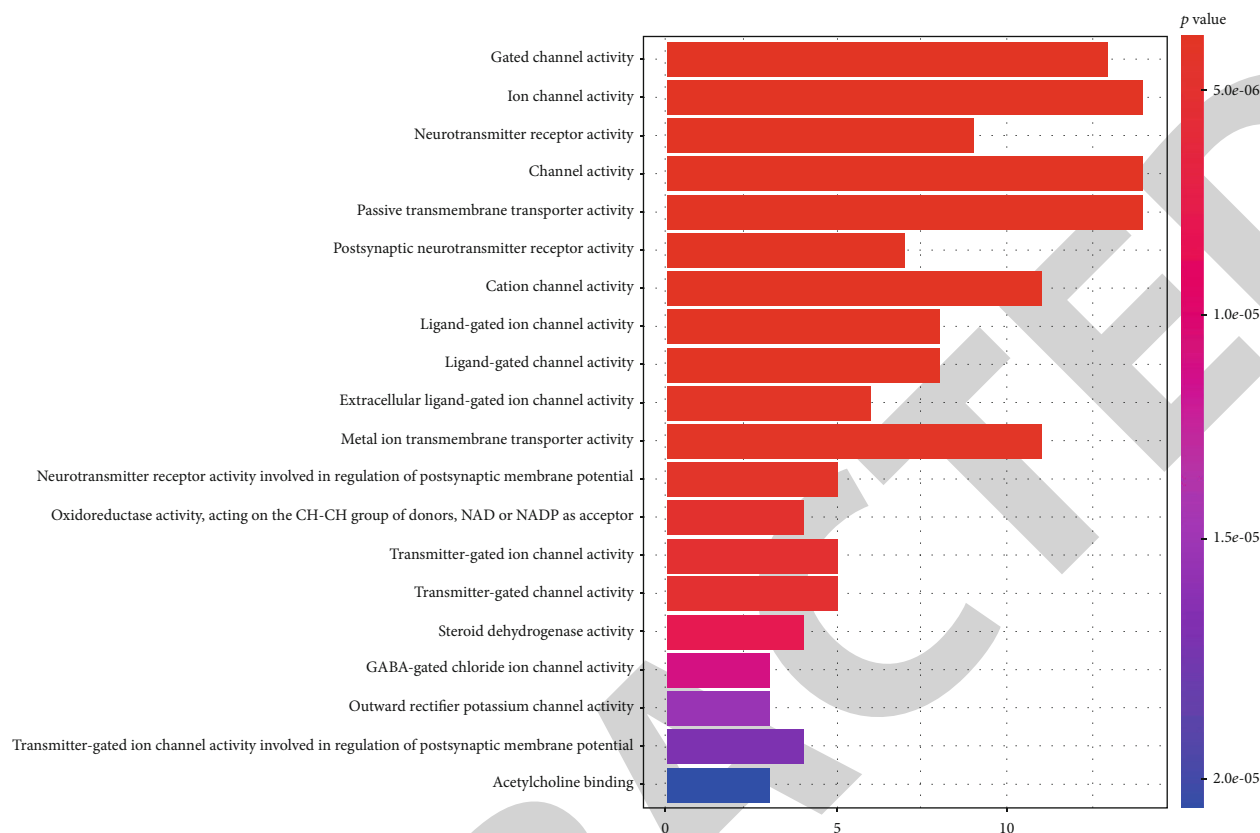


FIGURE 7: Column chart of GO functional enrichment analysis of *Calculus Bovis* targets. Column chart: letters on the left are GO names, numbers on the bottom are the numbers of genes enriched on GO, and  $p$  reflects the significance of enrichment. The redder the colors are, the more enriched the genes are, and the smaller the  $p$  values are.

PTGS2 (degree = 22), and IL-1B (degree = 20). A total of 6 Hub genes were found using 3 algorithms: degree of freedom, Maximum Neighborhood Component (MNC), and Maximal Clique Centrality (MCC) (Figure 5(c)). These genes were TP53, AKT1, PIK3CA, MAPK3, MMP9, and MMP2. Their network of interactions is shown in Figure 5(d). In addition, TP53, AKT1, MAPK1, VEGFA, PIK3CA, and MAPK3 were among the top 10 candidates ranked by degree of freedom.

**3.5. GO Enrichment Analysis.** To further investigate the underlying mechanism of *Calculus Bovis* in managing ischemic stroke, 344 targets and 92 shared targets were collected for GO enrichment analysis.

**3.5.1. GO Enrichment Analysis for *Calculus Bovis* Targets.** Twenty results were selected based on their  $p$  values and their numbers of enrichment. They were primarily involved in ion channel activity (GO:0005216), channel activity (GO:0015267), passive transmembrane transporter activity (GO:0022803), gated channel activity (GO:0022836), cation channel activity (GO:0005261), metal ion transmembrane transporter activity (GO:0046873), neurotransmitter receptor activity (GO:0030594), ligand-gated ion channel activity (GO:0015276), ligand-gated channel activity (GO:0022834), postsynaptic neurotransmitter receptor activity (GO:0098960), extracellular ligand-gated ion channel activity (GO:0005230), neurotransmitter receptor activity involved

in regulation of postsynaptic membrane potential (GO:0099529), transmitter-gated ion channel activity (GO:0022824), transmitter-gated channel activity (GO:0022835), and steroid dehydrogenase activity (GO:0016229). Details are listed in Table 3. Results are presented using a bubble plot and a column chart using the R package.

(1) *Bubble Plot.* In the bubble plot, letters on the left are GO names, numbers on the bottom are the proportions of genes, sizes of circles indicate the numbers of enriched genes, and colors reflect  $p$  values. The redder the colors are, the more enriched the genes are, and the smaller the  $p$  values are (Figure 6).

(2) *Column Chart.* In the column chart, letters on the left are GO names, numbers on the bottom are the numbers of genes enriched on GO, and  $p$  reflects significance of enrichment. The redder the colors are, the more enriched the genes are, and the smaller the  $p$  values are (Figure 7).

**3.5.2. GO Enrichment Analysis of Shared Targets of *Calculus Bovis* and Ischemic Stroke.** GO enrichment analysis was performed against the 92 shared targets. The top 20 were selected based on their  $p$  values and numbers of enrichment, including endopeptidase activity (GO:0004175); protein serine/threonine kinase activity (GO:0004674);

TABLE 4: GO enrichment analysis results of shared targets by *Calculus Bovis* and ischemic stroke.

No.	ID	Description	Count	<i>p</i> value
1	GO:0004175	Endopeptidase activity	15	$5.14505 \times 10^{-9}$
2	GO:0004674	Protein serine/threonine kinase activity	12	$2.81896 \times 10^{-6}$
3	GO:0008237	Metallopeptidase activity	9	$4.20451 \times 10^{-7}$
4	GO:0008081	Phosphoric diester hydrolase activity	8	$3.02315 \times 10^{-8}$
5	GO:0020037	Heme binding	8	$5.05803 \times 10^{-7}$
6	GO:0046906	Tetrapyrrole binding	8	$8.71647 \times 10^{-7}$
7	GO:0016705	Oxidoreductase activity, acting on paired donors, with incorporation or reduction of molecular oxygen	8	$1.74788 \times 10^{-6}$
8	GO:0008236	Serine-type peptidase activity	8	$4.78249 \times 10^{-6}$
9	GO:0017171	Serine hydrolase activity	8	$5.61466 \times 10^{-6}$
10	GO:0031406	Carboxylic acid binding	8	$7.36664 \times 10^{-6}$
11	GO:0043177	Organic acid binding	8	$1.14448 \times 10^{-5}$
12	GO:0004222	Metalloendopeptidase activity	7	$1.07557 \times 10^{-6}$
13	GO:0001085	RNA polymerase II transcription factor binding	7	$1.62174 \times 10^{-5}$
14	GO:0033293	Monocarboxylic acid binding	6	$9.84665 \times 10^{-7}$
15	GO:0005504	Fatty acid binding	5	$8.40369 \times 10^{-7}$
16	GO:0043560	Insulin receptor substrate binding	4	$2.19487 \times 10^{-7}$
17	GO:0036041	Long-chain fatty acid binding	4	$6.57868 \times 10^{-7}$
18	GO:0004114	3',5'-Cyclic-nucleotide phosphodiesterase activity	4	$1.27273 \times 10^{-5}$
19	GO:0004112	Cyclic-nucleotide phosphodiesterase activity	4	$1.47051 \times 10^{-5}$
20	GO:0016303	1-Phosphatidylinositol-3-kinase activity	3	$1.58908 \times 10^{-5}$

metallopeptidase activity (GO:0008237); phosphoric diester hydrolase activity (GO:0008081); heme binding (GO:0020037); tetrapyrrole binding (GO:0046906); oxidoreductase activity, acting on paired donors, with incorporation or reduction of molecular oxygen (GO:0016705); serine-type peptidase activity (GO:0008236); serine hydrolase activity (GO:0017171); carboxylic acid binding (GO:0031406); organic acid binding (GO:0043177); metalloendopeptidase activity (GO:0004222); RNA polymerase II transcription factor binding (GO:0001085); monocarboxylic acid binding (GO:0033293); and fatty acid binding (GO:0005504) (see Table 4). Results were visualized as a bubble plot (Figure 8) and a column chart (Figure 9) using the R package.

**3.6. KEGG Pathway Enrichment Analysis.** KEGG pathway enrichment analysis was performed for 344 *Calculus Bovis* targets and 92 shared targets.

**3.6.1. KEGG Pathway Enrichment Analysis for *Calculus Bovis* Targets.** Eighteen results were selected based on their *p* values and their numbers of enrichment. They were mainly involved in neuroactive ligand-receptor interaction (hsa04080), Alzheimer disease (hsa05010), calcium signaling pathway (hsa04020), nicotine addiction (hsa05033), steroid hormone biosynthesis (hsa00140), GABAergic synapse (hsa04727), morphine addiction (hsa05032), cholinergic syn-

apse (hsa04725), retrograde endocannabinoid signaling (hsa04723), and cellular senescence (hsa04218) (see Table 5).

(1) *Bubble Plot.* In the bubble plot, letters on the left are KEGG names, numbers on the bottom are the proportions of genes, sizes of circles indicate the numbers of enriched genes, and colors reflect *p* values. The redder the colors are, the more enriched the genes are, and the smaller the *p* values are (Figure 10).

(2) *Column Chart.* In the column chart, letters on the left are KEGG names, numbers on the bottom are the numbers of genes enriched on KEGG, columns represent genes enriched on KEGG, and *p* reflects significance of enrichment. The redder the colors are, the more enriched the genes are, and the smaller the *p* values are (Figure 11).

**3.6.2. KEGG Pathway Enrichment Analysis for Shared Targets.** KEGG pathway enrichment analysis was performed on 92 shared targets, and 145 pathways were found. The top 20 candidates were selected based on their *p* values and numbers of enrichment, and they were involved in the PI3K-AKT signaling pathway (hsa04151), human papillomavirus infection (hsa05165), Kaposi sarcoma-associated herpesvirus infection (hsa05167), human cytomegalovirus infection (hsa05163), microRNAs in cancer (hsa05206), fluid shear stress and atherosclerosis (hsa05418), proteoglycans in

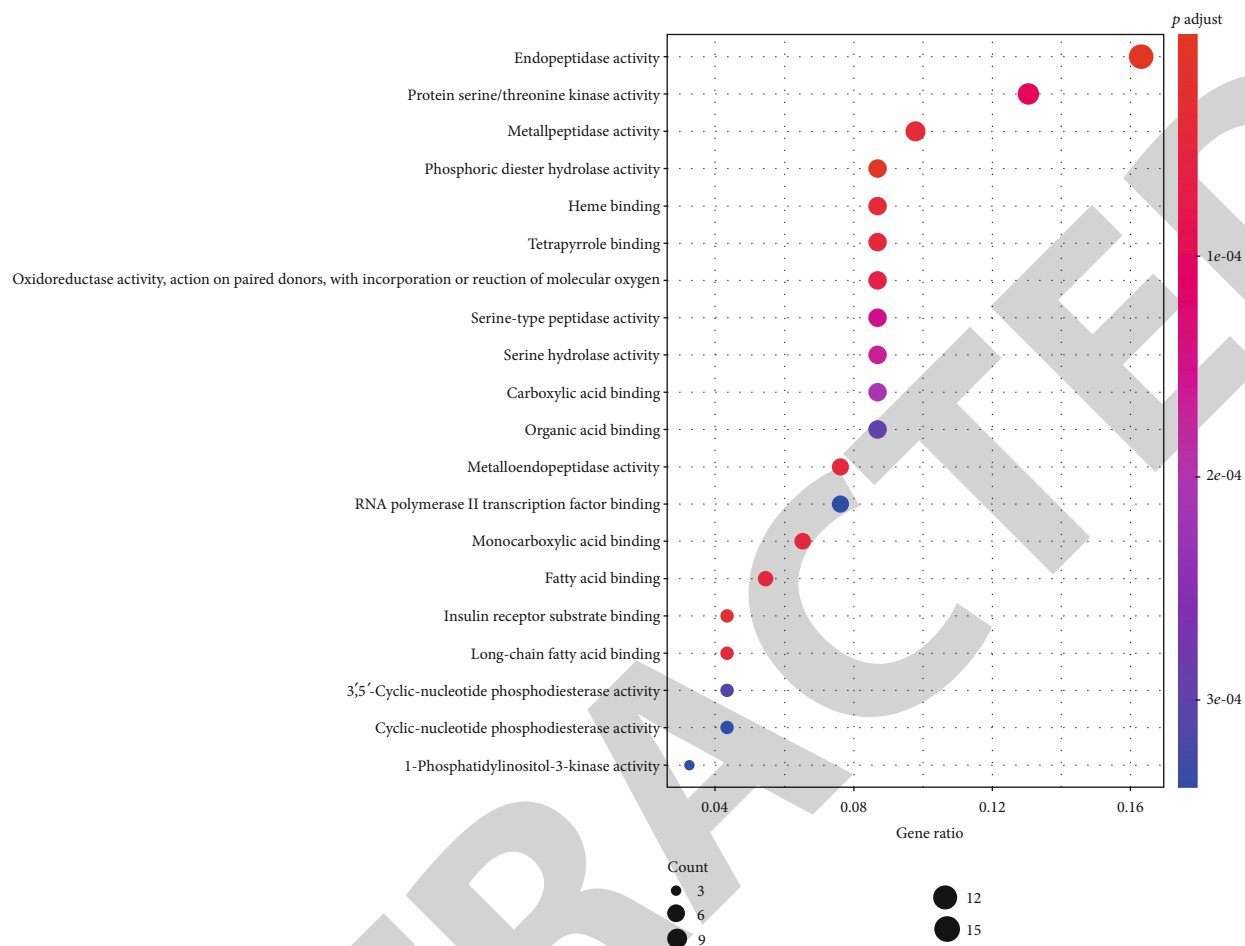


FIGURE 8: Bubble plot of GO enrichment analysis of shared targets by *Calculus Bovis* and ischemic stroke.

cancer (hsa05205), AGE-RAGE signaling pathway in diabetic complications (hsa04933), cAMP signaling pathway (hsa04024), prostate cancer (hsa05215), TNF signaling pathway (hsa04668), platelet activation (hsa04611), EGFR tyrosine kinase inhibitor resistance (hsa01521), small cell lung cancer (hsa05222), and endocrine resistance (hsa01522) (Table 6). Results were visualized as a bubble plot (Figure 12) and a column chart (Figure 13) using the R package.

#### 4. Discussion

Network pharmacology was used in this study to investigate *Calculus Bovis* itself and its potential mechanism for the treatment of ischemic stroke through compound target network construction, PPI network analysis, GO enrichment analysis, and KEGG pathway analysis.

Network analysis of compound targets showed that deoxycorticosterone (MOL008846), methyl cholate (MOL008838), and biliverdin (MOL008834) had the most connections with these targets, suggesting that these 3 compounds might be the key compounds of *Calculus Bovis*.

Deoxycorticosterone is a type of steroid hormone possessing activities of the mineralocorticoid and serves as the precursor of aldosterone. It is involved in water and salt

metabolism, playing an important role in electrolyte balance and in the volume of body fluid [32]. It has been reported that deoxycorticosterone and its derivatives—neurosteroids transformed in the fetal brain—protect the central nervous system. Inhibiting the production of neurosteroids increases basal cell death [33]. Neuroactive steroid hormones are involved in the regulation of diverse physiological functions, such as cell differentiation, neuroprotection, memory reinforcement, and amelioration of anxiety and pressure [34]. Methyl cholate is the methyl ester form of cholic acid, inhibiting the synthesis of cholesterol [35]. It has been reported that methyl cholate suppresses the growth of certain Gram-positive and Gram-negative bacteria [36] and has a good anti-inflammatory effect [37]. Biliverdin is a type of bile pigment, an oxidized product of heme. Emerging evidence has shown that biliverdin is an endogenous antioxidant facilitating the restoration of the tissue oxidation-reduction environment [38]. In the middle cerebral artery occlusion (MCAO) model, it significantly decreased the infarct area and the production of peroxides in the cortex [39]. These indicate that biliverdin plays a pivotal role in mitigating ischemic brain injury through its antioxidative stress effect. In addition, a single target was regulated by multiple compounds as shown in our network. Protein-tyrosine phosphatase 1B (PTPN1) was subject to the regulation of deoxycorticosterone,

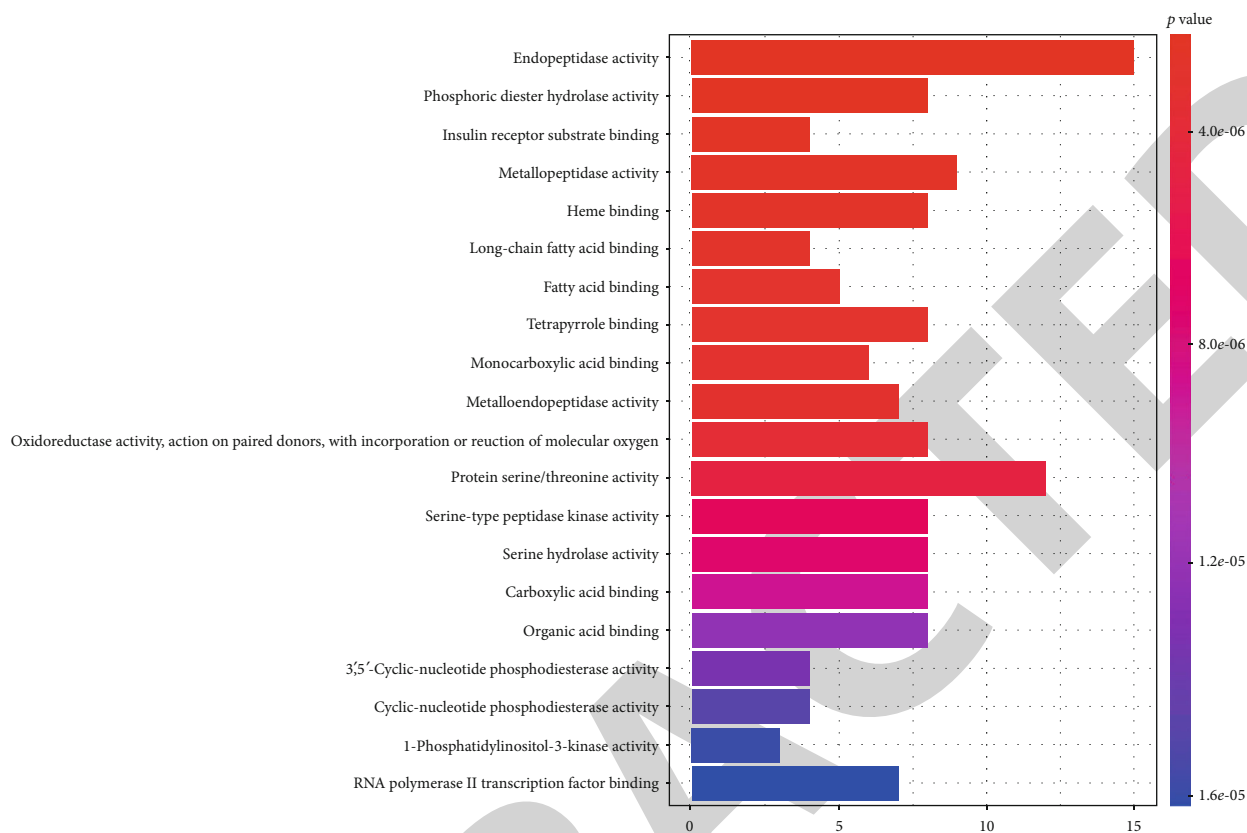


FIGURE 9: Column chart of GO enrichment analysis of shared targets by *Calculus Bovis* and ischemic stroke.

TABLE 5: KEGG pathway enrichment analysis results of *Calculus Bovis* targets.

No.	ID	Description	Count	p value
1	hsa04080	Neuroactive ligand-receptor interaction	14	$1.03 \times 10^{-8}$
2	hsa05010	Alzheimer disease	9	$4.14 \times 10^{-6}$
3	hsa04020	Calcium signaling pathway	6	$3.4 \times 10^{-5}$
4	hsa05033	Nicotine addiction	5	$2.08104 \times 10^{-4}$
5	hsa00140	Steroid hormone biosynthesis	5	$2.31001 \times 10^{-4}$
6	hsa04727	GABAergic synapse	5	$3.04528 \times 10^{-4}$
7	hsa05032	Morphine addiction	5	$3.73161 \times 10^{-4}$
8	hsa04725	Cholinergic synapse	5	$6.29559 \times 10^{-4}$
9	hsa04723	Retrograde endocannabinoid signaling	5	$1.033601 \times 10^{-3}$
10	hsa04218	Cellular senescence	5	$1.40748 \times 10^{-3}$
11	hsa04330	Notch signaling pathway	4	$1.594499 \times 10^{-3}$
12	hsa04115	p53 signaling pathway	4	$2.068787 \times 10^{-3}$
13	hsa05204	Chemical carcinogenesis	4	$2.107734 \times 10^{-3}$
14	hsa04540	Gap junction	4	$2.532292 \times 10^{-3}$
15	hsa04970	Salivary secretion	4	$2.652055 \times 10^{-3}$
16	hsa04914	Progesterone-mediated oocyte maturation	4	$3.294802 \times 10^{-3}$
17	hsa05030	Cocaine addiction	3	$3.367718 \times 10^{-3}$
18	hsa04340	Hedgehog signaling pathway	3	$3.567181 \times 10^{-3}$



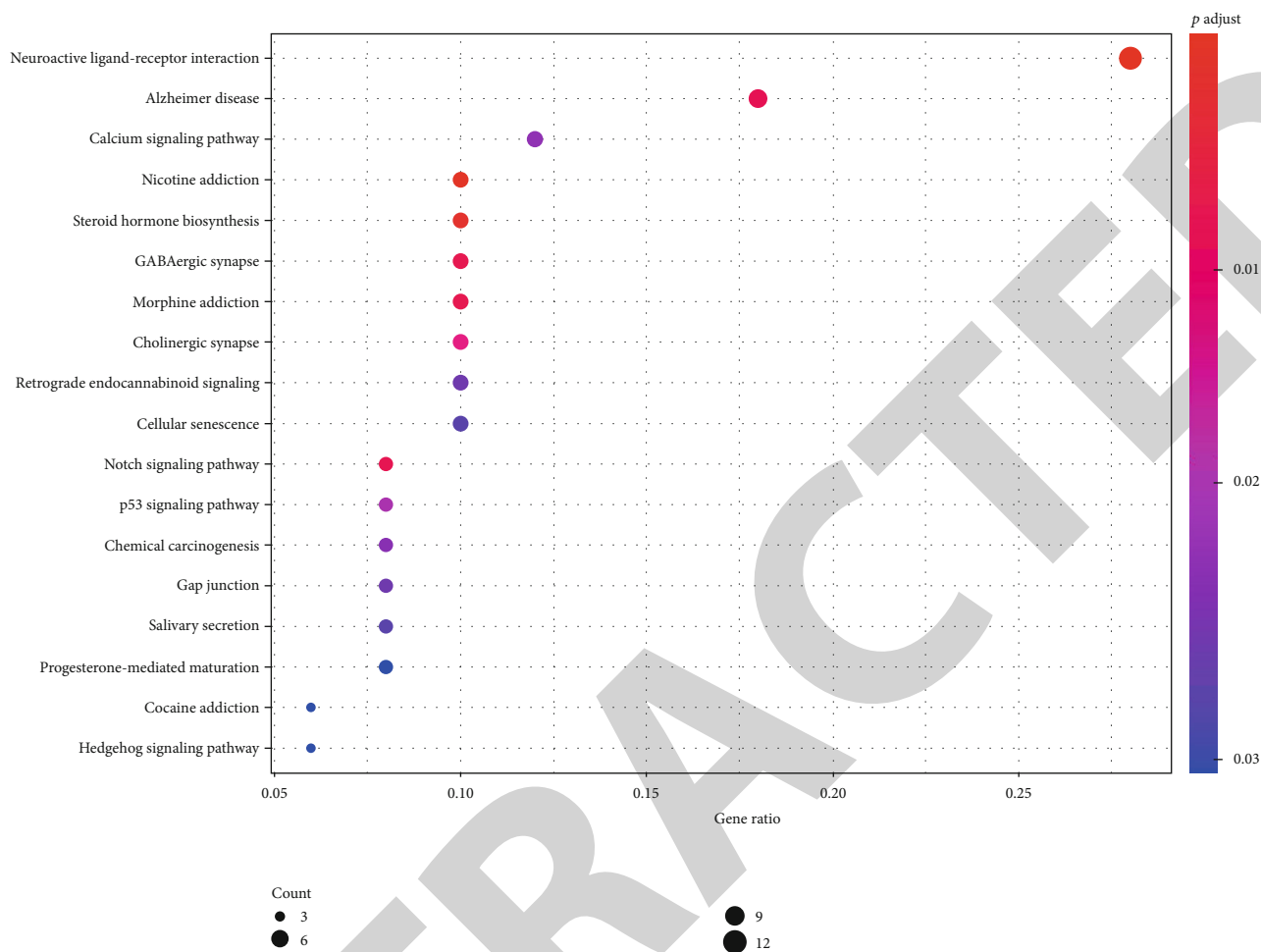


FIGURE 10: Bubble plot of KEGG pathway enrichment analysis of *Calculus Bovis* targets. Bubble plot: letters on the left are KEGG names, numbers on the bottom are the proportions of genes, sizes of the circles indicate the numbers of enriched genes, and colors reflect  $p$  values. The redder the colors are, the more enriched the genes are, and the smaller the  $p$  values are.

oleanolic acid, ergosterol, ursolic acid, biliverdin, bilirubin, methyl cholate, methyl desoxycholate, taurodeoxycholic acid, and others. PTPs are involved in regulating differentiation and survival of neurons and have also been reported to be a new target of antiplatelet therapy [40]. PTPN1 is a negative regulator of the leptin and insulin signaling pathways, and PTP1B knockout mice are exempt from obesity and diabetes, both of which are risk factors of ischemic stroke [41].

Similarly, other targets like 11-beta-hydroxysteroid dehydrogenase 1 (HSD11B1), dual-specificity phosphatase Cdc25A (CDC25A), cytochrome P450 19A1 (CYP19A1), progesterone receptor (PGR), and androgen receptor (AR) were also regulated by two or more compounds. The present study revealed not only relationships between *Calculus Bovis* compounds and their targets but also the potential pharmacological effects of *Calculus Bovis*, which reflects the multi-compound and multitarget theory of modern drugs.

Furthermore, the PPI network demonstrated information not only about protein homology and coexpression but also about protein-protein interactions. Our PPI analysis showed that *Calculus Bovis* influences ischemic stroke through its impact on a complex biological network, includ-

ing TP53, AKT1, MAPK1, VEGFA, TNF, PIK3CA, MAPK3, MMP9, PTGS2, and IL1B. Hub gene screening revealed that TP53, AKT1, PIK3CA, MAPK3, MMP9, and MMP2 were essential in this process. The above potential targets for the action of *Calculus Bovis* in the treatment of ischemic stroke are our first discoveries.

TP53, cellular tumor antigen p53, is a tumor suppressing gene. It promotes cell apoptosis, increases gene stability, and suppresses tumorigenesis [42]. It has been reported that methylation of the TP53 promoter was increased in ischemic stroke, and this increase was associated with the thickness of the intima of the carotid artery, degree of atherosclerosis of the carotid artery, and levels of homocysteine in the peripheral blood [43]. More evidence showed that TP53 induced glycolysis, and apoptosis regulator (TIGAR) suppressed glycolysis, increased pentose-phosphate pathway flux, and maintained the function of mitochondria. As a result, it protected the brain from ischemic injury [44]. The Tp53 Arg/Arg genotype has been considered a genetic marker for predicting poor prognosis after ischemic stroke [45]. AKT1 (serine/threonine-protein kinase AKT) codes for the serine/threonine-protein kinase which regulates apoptosis proteins

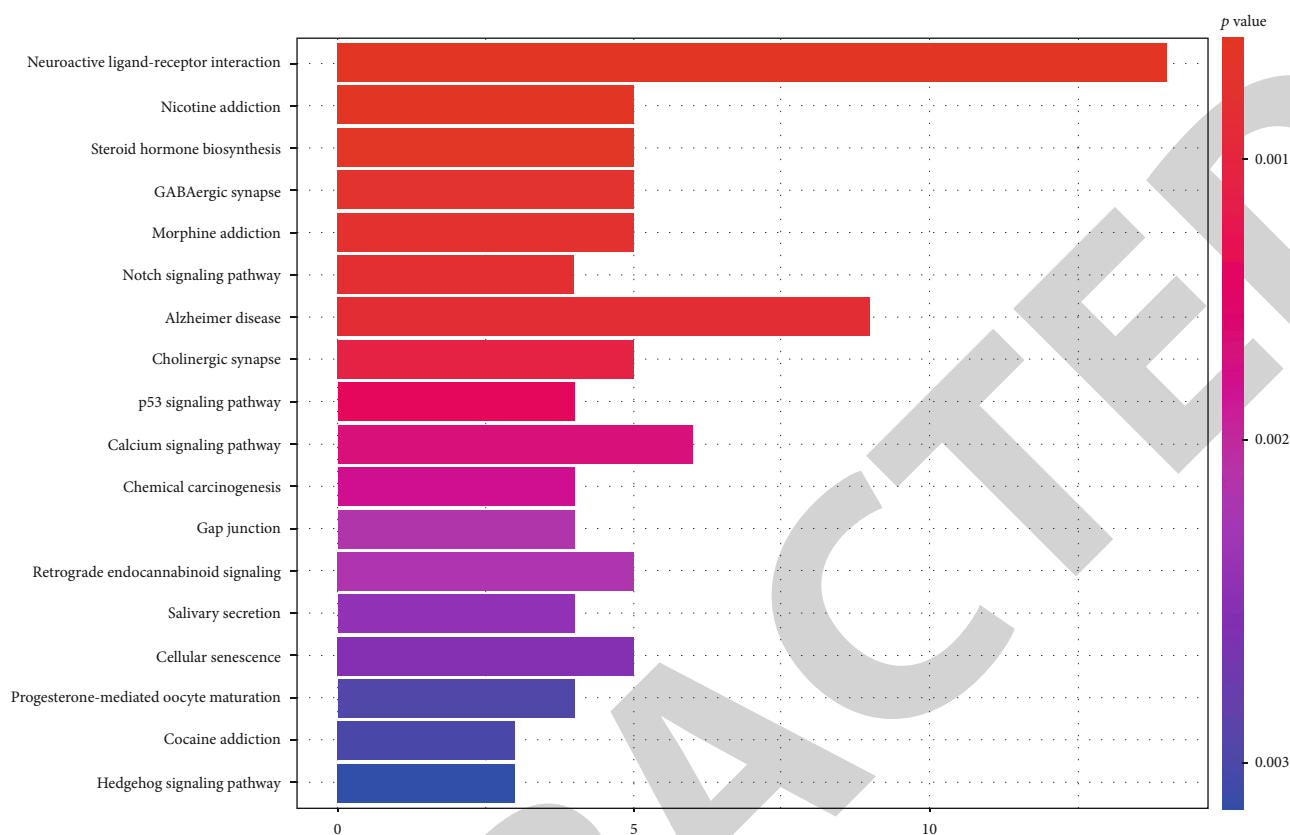


FIGURE 11: Column chart of KEGG pathway enrichment analysis of *Calculus Bovis* targets. Column chart: letters on the left are KEGG names, numbers on the bottom are the numbers of genes enriched on KEGG, columns represent genes enriched on KEGG, and  $p$  reflects the significance of enrichment. The redder the colors are, the more enriched the genes are, and the smaller the  $p$  values are.

and transcription factors. It is the key player in regulating cell survival, growth, apoptosis, and proliferation in the presence of growth factors and external stimuli, especially brain ischemia and reperfusion injury. AKT1 gene variance is closely related to metabolic syndrome, a risk factor of stroke [46].

AKT/PKB was involved in brain ischemia, and its activity was related to the extent of ischemic injury. Activation of AKT was the key factor in determining survival of neurons after ischemic injury [47]. PIK3CA codes for the p110 subunit of the phosphatidylinositol 3-kinases (PI3Ks), and its mutations decrease cell apoptosis and increase the activity of downstream PI3Ks. It is known that activation of PI3K/AKT promotes repair of neural injury due to ischemic stroke [48, 49] and angiogenesis in the hypoxic environment in vitro [50]. Consequently, it protects the rat brain from inflammation resulting from ischemia-reperfusion injury [51]. Activation of the TrkB/PI3K/AKT pathway also increases activation of Nrf2 and its translocation to the nucleus, which plays a pivotal role in protecting the central nervous system from oxidative stress [52].

MAPK (mitogen-activated protein kinase) is involved in reaction to physiological and pathological stimuli, such as cytokines, neurotransmitters, hypoxia, and hypoglycemia [53]. MAPK3 (MAP kinase ERK1) and MAPK1 (MAP kinase ERK2) form ERK1/2, a subfamily of MAPK. They play important roles in cell proliferation, differentiation, migration, invasion, apoptosis, and other biological processes. In

the  $H_2O_2$  induced PC12 cell injury model, activation of the AKT and ERK1/2 pathways leads to an antioxidation effect [54]. Levels of ERK1 and ERK2 were increased after ischemic stroke onset. In vitro research further revealed that activation of ERK1/2 increased neuronal apoptosis, indicating that they are important targets for ischemic stroke treatment [55].

GO and KEGG pathway enrichment analyses for *Calculus Bovis* targets showed that *Calculus Bovis* was closely related to ion channel activity, neurotransmitter receptor activity, and other physiological functions. Pathway enrichment analysis demonstrated its involvement in a number of pathways in the central nervous system, calcium-related signaling, and so on. These were consistent with the analgesic and antiepilepsy effects of *Calculus Bovis* and its clinical application in these fields, which lays the theoretical foundation for managing ischemic stroke using *Calculus Bovis*.

GO enrichment and KEGG pathway analyses against the shared 92 targets showed that *Calculus Bovis* was closely related to hydrolyzation of proteins, phosphorylation of serine/threonine residues of protein substrates, peptide bond hydrolyzation of peptides and proteins, hydrolyzation of second intracellular messengers, antioxidation and reduction, RNA transcription, and other biological processes. Among them, 15 (16.3%) were related to endopeptidase activities of the matrix metalloproteinase (MMPs) family (MMP1, MMP2, MMP3, MMP8, MMP9, MMP10, and MMP12) and the cysteine-containing aspartate-specific peptidase

TABLE 6: KEGG pathway enrichment analysis for shared targets.

No.	ID	Description	Count	p value
1	hsa04151	PI3K-AKT signaling pathway	24	$2.12708 \times 10^{-13}$
2	hsa05165	Human papillomavirus infection	20	$2.45479 \times 10^{-10}$
3	hsa05167	Kaposi sarcoma-associated herpesvirus infection	19	$1.3448 \times 10^{-13}$
4	hsa05163	Human cytomegalovirus infection	18	$2.23341 \times 10^{-11}$
5	hsa05206	MicroRNAs in cancer	18	$4.23388 \times 10^{-9}$
6	hsa05418	Fluid shear stress and atherosclerosis	17	$8.25476 \times 10^{-14}$
7	hsa05205	Proteoglycans in cancer	17	$4.88669 \times 10^{-11}$
8	hsa04933	AGE-RAGE signaling pathway in diabetic complications	16	$6.21323 \times 10^{-15}$
9	hsa04024	cAMP signaling pathway	16	$1.04013 \times 10^{-9}$
10	hsa05215	Prostate cancer	14	$1.54571 \times 10^{-12}$
11	hsa04668	TNF signaling pathway	14	$1.16611 \times 10^{-11}$
12	hsa04611	Platelet activation	13	$6.34665 \times 10^{-10}$
13	hsa01521	EGFR tyrosine kinase inhibitor resistance	12	$3.67514 \times 10^{-11}$
14	hsa05222	Small cell lung cancer	12	$2.32309 \times 10^{-10}$
15	hsa01522	Endocrine resistance	12	$4.93414 \times 10^{-10}$
16	hsa04919	Thyroid hormone signaling pathway	12	$5.80768 \times 10^{-9}$
17	hsa05212	Pancreatic cancer	11	$4.36655 \times 10^{-10}$
18	hsa05210	Colorectal cancer	11	$1.70773 \times 10^{-9}$
19	hsa04657	IL-17 signaling pathway	11	$4.49095 \times 10^{-9}$
20	hsa05220	Chronic myeloid leukemia	10	$7.44115 \times 10^{-9}$

family (CASP1, CASP2, and CASP3). MMPs are a type of highly conserved proteinase in nature, belonging to the family of zinc-dependent endopeptidases. They are capable of degrading extracellular matrix, growth factors, cytokines, and cell adhesion molecules. They are indispensable in ECM and tissue remodeling, angiogenesis, immune reactions, inflammation, cell migration, proliferation, cell apoptosis, and other physiological and pathological processes [56]. Their mRNAs were dramatically increased in the cortex of the mouse ischemia model in which thrombus was induced [57]. Decreasing levels of MMPs significantly ameliorated transgression of neutrophils, which resulted in neuroprotection against ischemic stroke [58]. Targeted inhibition of the PI3K/AKT/MMP-9 signaling pathway suppressed tumor invasion and metastasis [59], but this has not been tested in neuronal cells. Caspases are closely related to apoptosis of eukaryocytes and regulation of cell proliferation as well as differentiation. Caspase 3 is the most important and indispensable one in the cascade of cell apoptosis. In brain ischemia, levels of CASP3 mRNA and protein were increased, and its activity was significantly reversed by a CASP3 inhibitor, preventing the hydrolyzation of poly(-ADP-ribose) polymerase. Consequently, apoptosis was suppressed and neurological functions improved [60]. Neuroinflammation is a key pathological process, in which CASP1-activated inflammasomes play an essential role. It has been reported that CASP1 was increased in the mouse brain after cerebral ischemia, which was suppressed by a

CASP1 inhibitor through decreasing the activation of microglial cells, protecting the brain from ischemic injury. These indicate that CASP1 is a potential drug target for ischemic stroke management [61]. Both in vitro and in vivo experiments have shown that activation of the PI3K/AKT pathway increases the phosphorylation of Bad and decreases the level of caspase-3, through which apoptosis is suppressed [62].

Another 12 genes (13.0%) are related to activities of protein serine/threonine kinases, consistent with the findings of the PI3K-AKT signaling pathway (24 enriched genes, 27.2%) in the KEGG pathway analysis. AKT is also named serine/threonine kinase, whose activation is key for neuronal survival [63]. It is known that phosphorylated AKT was decreased in the infarct area after ischemia-reperfusion injury and increased in the penumbra after reperfusion. An inhibitor of PI3K decreased the level of phosphorylated AKT and increased the infarct area, indicating that PI3K/AKT is involved in the pathogenesis of brain ischemia and activation of AKT increases neuronal survival [64]. Among them, MAPK3 (ERK1) is not only a Hub gene involved in regulating the activity of protein serine/threonine kinases as shown by GO analysis but is also enriched in the PI3K-AKT signaling pathway. These suggest that MAPK3 is an important component of this network. Therefore, *Calculus Bovis* might protect the brain from ischemic stroke through its anti-inflammatory and antiapoptosis effects which are accomplished by interacting with the abovementioned key genes and pathways.

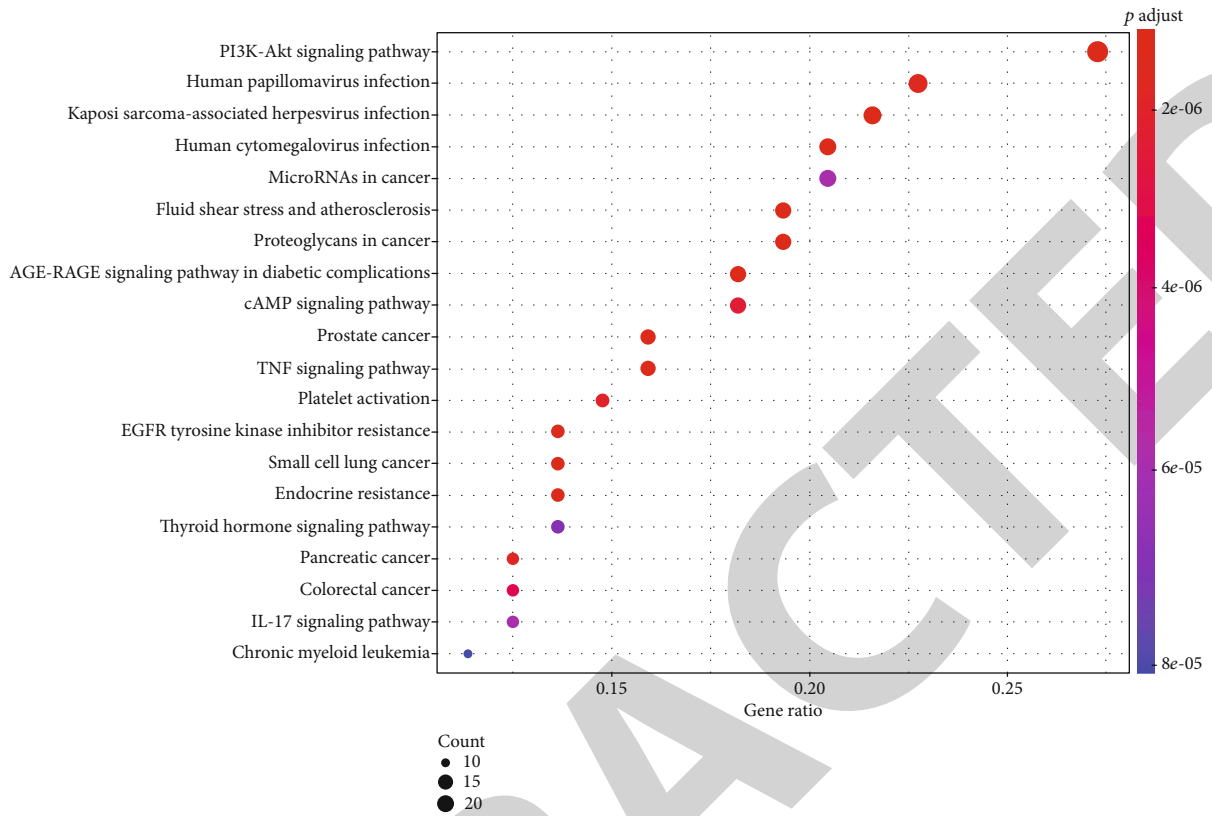


FIGURE 12: Bubble plot of KEGG pathway enrichment analysis of shared targets.

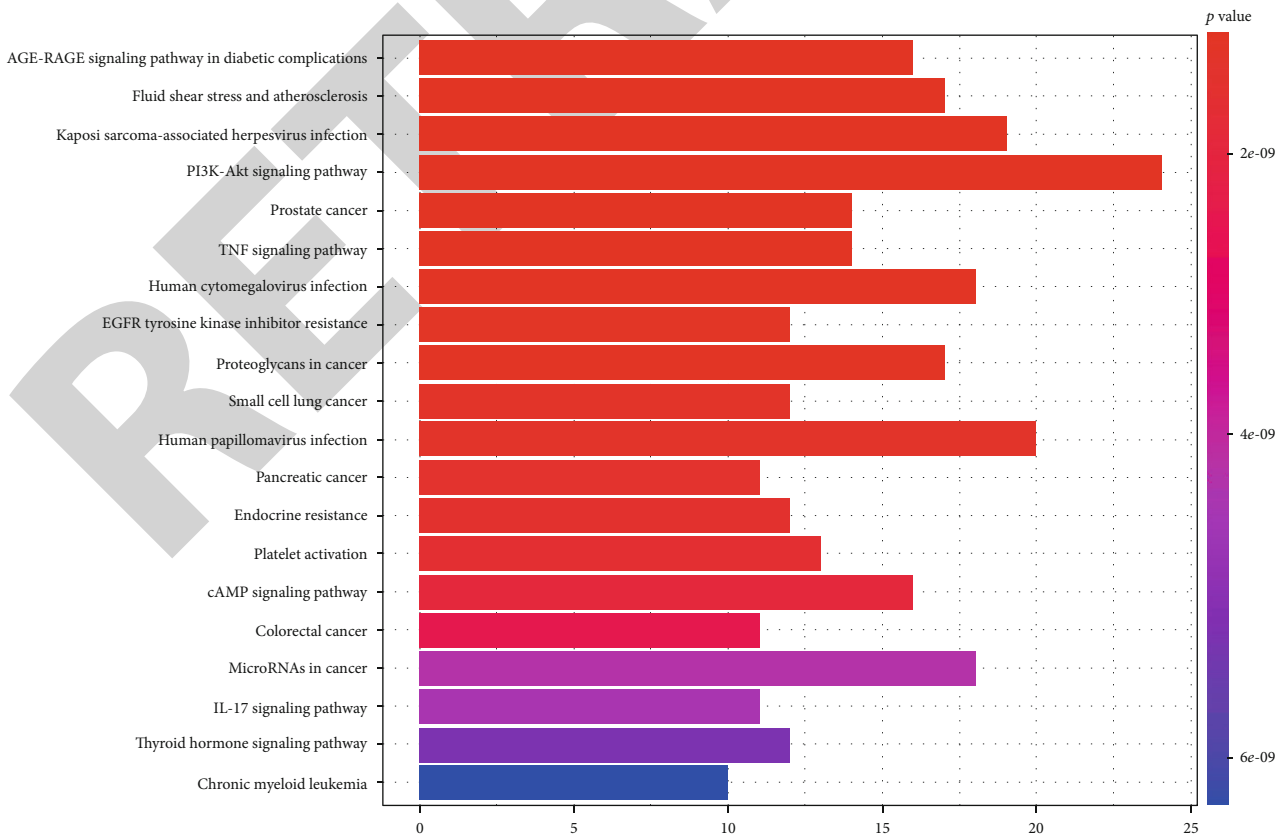


FIGURE 13: Column chart of KEGG pathway enrichment analysis of shared targets.

However, there are some limitations in this study. Access to databases of Chinese herbal medicines and disease targets is relatively limited, and there may be some data selection bias. Meanwhile, due to the fact that this study was based on data analysis, the conclusion needs to be confirmed by further research.

## 5. Conclusion

Bioactive compounds, potential targets, and underlying mechanisms of *Calculus Bovis* were examined using network pharmacology methods. KEGG pathway analysis showed that the PI3K/AKT and the MAPK signaling pathways were the key targets for ischemic stroke treatment. The effect of *Calculus Bovis* was achieved through directly or indirectly regulating the above targets and pathways. Our results confirmed that *Calculus Bovis* was a multicomponent and multi-target drug with a multisystem character in the treatment of ischemic stroke, which laid the theoretical foundation for the development of drugs and therapeutic methods based on the results of *Calculus Bovis* in the future.

## Data Availability

The data used to support the findings of this study are included within the article.

## Conflicts of Interest

The authors declare that there is no conflict of interests.

## Acknowledgments

The present study was supported by the Shanghai Municipal Committee of Science and Technology (through grant no. 19401935700 to Ping Zhong), the National Science and Technology Major Projects for “Major New Drugs Innovation and Development” (through grant no. 2018ZX09201008-002-092), and the Three-Year Action Plan of “Strong and Excellent Chinese Medicine” in Hongkou District (through grant no. HGY-MGB-2018-01-07 to Yongbing Cao).

## Supplementary Materials

Supplementary 1. Table S1: all ingredients of *Calculus Bovis*.  
Supplementary 2. Table S2: targets of active ingredients of *Calculus Bovis*. (*Supplementary Materials*)

## References

- [1] S. I. Hay, A. A. Abajobir, K. H. Abate et al., “Global, regional, and national disability-adjusted life-years (DALYs) for 333 diseases and injuries and healthy life expectancy (HALE) for 195 countries and territories, 1990-2016: a systematic analysis for the Global Burden of Disease Study 2016,” *Lancet*, vol. 390, no. 10100, pp. 1260–1344, 2017.
- [2] L. D. Wang, J. H. Wang, B. Peng, and Y. M. Xu, “Brief report on stroke prevention and treatment in China, 2019,” *Chinese Journal of Cerebrovascular Diseases*, vol. 17, no. 5, pp. 272–281, 2020.
- [3] D. Keizman, P. Huang, M. A. Eisenberger et al., “Angiotensin system inhibitors and outcome of sunitinib treatment in patients with metastatic renal cell carcinoma: a retrospective examination,” *European Journal of Cancer*, vol. 47, no. 13, pp. 1955–1961, 2011.
- [4] A. P. Jadhav and T. G. Jovin, “Endovascular therapy for acute ischemic stroke: the standard of care,” *Brain circulation*, vol. 2, no. 4, pp. 178–182, 2016.
- [5] S. Yoshimura, N. Sakai, K. Uchida et al., “Endovascular therapy in ischemic stroke with acute large-vessel occlusion: Recovery by Endovascular Salvage for Cerebral Ultra-Acute Embolism Japan Registry 2,” *Journal of the American Heart Association*, vol. 7, no. 9, 2018.
- [6] J. F. Meschia, C. Bushnell, B. Boden-Albala et al., “Guidelines for the primary prevention of stroke,” *Stroke*, vol. 45, no. 12, pp. 3754–3832, 2014.
- [7] T.-T. Sham, C.-O. Chan, Y.-H. Wang, J.-M. Yang, D. K.-W. Mok, and S.-W. Chan, “A review on the traditional Chinese medicinal herbs and formulae with hypolipidemic effect,” *BioMed Research International*, vol. 2014, Article ID 925302, 21 pages, 2014.
- [8] L. J. Xiao and R. Tao, “Traditional Chinese medicine (TCM) therapy,” *Advances in Experimental Medicine and Biology*, vol. 1010, pp. 261–280, 2017.
- [9] W. Xu, A. D. Towers, P. Li, and C. JP, “Traditional Chinese medicine in cancer care: perspectives and experiences of patients and professionals in China,” *European journal of cancer care*, vol. 15, no. 4, pp. 397–403, 2006.
- [10] W. J. Kong, X. Y. Xing, X. H. Xiao, J. B. Wang, Y. L. Zhao, and M. H. Yang, “Multi-component analysis of bile acids in natural *Calculus bovis* and its substitutes by ultrasound-assisted solid-liquid extraction and UPLC-ELSD,” *Analyst*, vol. 137, no. 24, pp. 5845–5853, 2012.
- [11] X. L. Xu, *Comparative Study on the Effects of Effective Components of Bezoar on Anti-Cerebral Infarction and Regulating Endoplasmic Reticulum Stress*, Beijing University Of Chinese Medicine, 2016.
- [12] C. Y. Li, P. T. Li, Y. S. Pan, X. Jia, and K. L. Li, “Effects of compatibility of bezoar and gardenia on lipid peroxidation injury at different time of focal cerebral ischemia and reperfusion in rats,” *China Journal of Traditional Chinese Medicine and Pharmacy*, vol. 9, pp. 528–530, 2004.
- [13] D. Shifen, L. Liming, Z. Shuofeng, and S. Jianning, “Protective effect of An-Gong-Niu-Huang-Wan (containing natural or artificial Moschus) on experimental cerebral ischemia in rats,” *Modernization of Traditional Chinese Medicine and Materia Medica-World Science and Technology*, vol. 15, no. 1, pp. 85–90, 2013.
- [14] X. Liu, J. Wu, D. Zhang, K. Wang, X. Duan, and X. Zhang, “A network pharmacology approach to uncover the multiple mechanisms of *Hedyotis diffusa* Willd. on colorectal cancer,” *Evidence-based Complementary and Alternative Medicine*, vol. 2018, Article ID 6517034, 12 pages, 2018.
- [15] L. Gao, J. Hao, Y. Y. Niu et al., “Network pharmacology dissection of multiscale mechanisms of herbal medicines in stage IV gastric adenocarcinoma treatment,” *Medicine (Baltimore)*, vol. 95, no. 35, article e4389, 2016.
- [16] S. Li, B. Zhang, D. Jiang, Y. Wei, and N. Zhang, “Herb network construction and co-module analysis for uncovering the



- combination rule of traditional Chinese herbal formulae," *BMC Bioinformatics*, vol. 11, Suppl 11, p. S6, 2010.
- [17] M. Wang, Y. Qi, and Y. Sun, "Exploring the antitumor mechanisms of Zingiberis Rhizoma combined with Coptidis Rhizoma using a network pharmacology approach," *BioMed Research International*, vol. 2020, Article ID 8887982, 18 pages, 2020.
- [18] L. Wang, Y. Zhi, Y. Ye et al., "Identify molecular mechanisms of Jiangzhi decoction on nonalcoholic fatty liver disease by network pharmacology analysis and experimental validation," *BioMed Research International*, vol. 2020, Article ID 8829346, 16 pages, 2020.
- [19] L. Yang, H. Li, M. Yang et al., "Exploration in the mechanism of kaempferol for the treatment of gastric cancer based on network pharmacology," *BioMed Research International*, vol. 2020, Article ID 5891016, 11 pages, 2020.
- [20] J. Ru, P. Li, J. Wang et al., "TCMSP: a database of systems pharmacology for drug discovery from herbal medicines," *Journal of Cheminformatics*, vol. 6, no. 1, p. 13, 2014.
- [21] Z. Liu, F. Guo, Y. Wang et al., "BATMAN-TCM: a bioinformatics analysis tool for molecular mechanism of traditional Chinese medicine," *Scientific Reports*, vol. 6, no. 1, p. 21146, 2016.
- [22] A. Daina, O. Michielin, and V. Zoete, "SwissTargetPrediction: updated data and new features for efficient prediction of protein targets of small molecules," *Nucleic Acids Research*, vol. 47, no. W1, pp. W357–W364, 2019.
- [23] H. A. Barton, T. P. Pastoor, K. Baetcke et al., "The acquisition and application of absorption, distribution, metabolism, and excretion (ADME) data in agricultural chemical safety assessments," *Critical Reviews in Toxicology*, vol. 36, no. 1, pp. 9–35, 2008.
- [24] J. Jia, J. M. Sun, H. Zang, and H. Zhang, "Research progress on the chemical constituents and pharmacological activities of natural bezoar," *Journal of Chinese Medicine*, vol. 33, no. 3, pp. 271–274, 2013.
- [25] Z. L. Huang, "Pharmacological research and clinical application of bezoar and some of its components," *Chinese Traditional Patent Medicine*, vol. 10, pp. 26–28, 1985.
- [26] D. S. Wishart, Y. D. Feunang, A. C. Guo et al., "DrugBank 5.0: a major update to the DrugBank database for 2018," *Nucleic Acids Research*, vol. 46, no. D1, pp. D1074–D1082, 2018.
- [27] J. Piñero, N. Queralt-Rosinach, À. Bravo et al., "DisGeNET: a discovery platform for the dynamical exploration of human diseases and their genes," *Database: The Journal of Biological Databases and Curation*, vol. 2015, 2015.
- [28] A. Hamosh, A. F. Scott, J. S. Amberger, C. A. Bocchini, and V. McKusick, "Online Mendelian Inheritance in Man (OMIM), a knowledgebase of human genes and genetic disorders," *Nucleic Acids Research*, vol. 33, no. Database issue, pp. D514–D517, 2005.
- [29] Y. Wang, S. Zhang, F. Li et al., "Therapeutic target database 2020: enriched resource for facilitating research and early development of targeted therapeutics," *Nucleic Acids Research*, vol. 48, no. D1, pp. D1031–D1041, 2020.
- [30] D. Szklarczyk, A. L. Gable, D. Lyon et al., "STRING v11: protein-protein association networks with increased coverage, supporting functional discovery in genome-wide experimental datasets," *Nucleic Acids Research*, vol. 47, no. D1, pp. D607–D613, 2019.
- [31] P. Shannon, A. Markiel, O. Ozier et al., "Cytoscape: a software environment for integrated models of biomolecular interaction networks," *Genome Research*, vol. 13, no. 11, pp. 2498–2504, 2003.
- [32] C. A. Shaughnessy, A. Barany, and S. D. McCormick, "11-Deoxycortisol controls hydromineral balance in the most basal osmoregulating vertebrate, sea lamprey (*Petromyzon marinus*)," *Scientific Reports*, vol. 10, no. 1, p. 12148, 2020.
- [33] J. J. Hirst, H. K. Palliser, D. M. Yates, T. Yawno, and D. W. Walker, "Neurosteroids in the fetus and neonate: potential protective role in compromised pregnancies," *Neurochemistry International*, vol. 52, no. 4–5, pp. 602–610, 2008.
- [34] A. M. Traish, "5 $\alpha$ -Reductases in human physiology: an unfolding story," *Endocrine Practice*, vol. 18, no. 6, pp. 965–975, 2012.
- [35] H. J. Kim, S. H. Yim, and I. S. Lee, "A cholesterol biosynthesis inhibitor from *Rhizopus oryzae*," *Archives of Pharmacological Research*, vol. 27, no. 6, pp. 624–627, 2004.
- [36] T. Sugai, M. Takizawa, M. Bakke, Y. Ohtsuka, and H. Ohta, "Efficient lipase-catalyzed preparation of long-chain fatty acid esters of bile acids: biological activity and synthetic application of the products," *Bioscience, Biotechnology, and Biochemistry*, vol. 60, no. 12, pp. 2059–2063, 2014.
- [37] Y. J. Tan, "Study on preparation of cholic acid-baicalin nasal liposome and its protective effect on cerebral ischemia reperfusion injury in rats," *Chengdu University of Traditional Chinese Medicine*, 2019.
- [38] H. M. Schipper, W. Song, A. Tavitian, and M. Cressatti, "The sinister face of heme oxygenase-1 in brain aging and disease," *Progress in Neurobiology*, vol. 172, pp. 40–70, 2019.
- [39] T. Yamashita, K. Deguchi, S. Nagotani, T. Kamiya, and K. Abe, "Gene and stem cell therapy in ischemic stroke," *Cell Transplantation*, vol. 18, no. 9, pp. 999–1002, 2009.
- [40] L. Tautz, Y. A. Senis, C. Oury, and S. Rahmouni, "Perspective: tyrosine phosphatases as novel targets for antiplatelet therapy," *Bioorganic & Medicinal Chemistry*, vol. 23, no. 12, pp. 2786–2797, 2015.
- [41] E. Reimer, M. Stempel, B. Chan, H. Bley, and M. M. Brinkmann, "Protein tyrosine phosphatase 1B is involved in efficient type I interferon secretion upon viral infection," *Journal of Cell Science*, vol. 134, no. 5, 2020.
- [42] V. J. Bykov, S. E. Eriksson, J. Bianchi, and K. G. Wiman, "Targeting mutant p53 for efficient cancer therapy," *Nature Reviews. Cancer*, vol. 18, no. 2, pp. 89–102, 2018.
- [43] Y. Wei, Z. Sun, Y. Wang et al., "Methylation in the TP53 promoter is associated with ischemic stroke," *Molecular Medicine Reports*, vol. 20, no. 2, pp. 1404–1410, 2019.
- [44] M. Li, M. Sun, L. Cao et al., "A TIGAR-regulated metabolic pathway is critical for protection of brain ischemia," *The Journal of Neuroscience*, vol. 34, no. 22, pp. 7458–7471, 2014.
- [45] J. C. Gomez-Sanchez, M. Delgado-Esteban, I. Rodriguez-Hernandez et al., "The human Tp53 Arg72Pro polymorphism explains different functional prognosis in stroke," *The Journal of Experimental Medicine*, vol. 208, no. 3, pp. 429–437, 2011.
- [46] F. S. Eshaghi, H. Ghazizadeh, S. Kazami-Nooreini et al., "Association of a genetic variant in AKT1 gene with features of the metabolic syndrome," *Genes & diseases*, vol. 6, no. 3, pp. 290–295, 2019.
- [47] Y. G. Chen, B. Yin, and B. Y. Luo, "Research progress of Akt signaling pathway and cell survival," *Journal of International Neurology and Neurosurgery*, vol. 39, no. 4, pp. 362–365, 2012.

## Research Article

# Plasma Resolvin D2 to Leukotriene B<sub>4</sub> Ratio Is Reduced in Diabetic Patients with Ischemic Stroke and Related to Prognosis

Zhijuan Miao <sup>1</sup>, Xin Tang,<sup>1</sup> Marianne Schultzberg,<sup>2</sup> Yuwu Zhao <sup>1</sup> and Xiuzhe Wang <sup>1</sup>

<sup>1</sup>Department of Neurology, Shanghai Jiao Tong University Affiliated Sixth People's Hospital, Shanghai, China

<sup>2</sup>Department of Neurobiology, Care Sciences and Society, Center for Alzheimer Research, Karolinska Institutet, Stockholm, Sweden

Correspondence should be addressed to Yuwu Zhao; zhaoyuwu2005@126.com and Xiuzhe Wang; xiuzhewang@hotmail.com

Received 25 December 2020; Revised 5 February 2021; Accepted 18 February 2021; Published 26 February 2021

Academic Editor: Andrea Scribante

Copyright © 2021 Zhijuan Miao et al. This is an open access article distributed under the Creative Commons Attribution License, which permits unrestricted use, distribution, and reproduction in any medium, provided the original work is properly cited.

**Background.** Diabetes mellitus (DM) aggravates symptoms and prognosis of acute ischemic stroke (AIS), and inflammation plays an important role therein. Resolvin D2 (RvD2) is one of the specialized pro-resolving mediators (SPMs), while leukotriene B<sub>4</sub> (LTB<sub>4</sub>) is a classic proinflammatory mediator. The ratio of RvD2 to LTB<sub>4</sub> is an index of pro-resolving/proinflammatory balance. We aim to explore the role of RvD2/LTB<sub>4</sub> ratio in ischemic stroke complicated with DM. **Methods.** The plasma levels of RvD2 and LTB<sub>4</sub> were analyzed by enzyme immunoassay in stroke patients with DM (DM + AIS group) or without DM (nonDM+AIS group). Patients were followed up at 90 days after stroke onset, and modified Rankin Score (mRS) was assessed. The association of RvD2/LTB<sub>4</sub> ratio with stroke severity and prognosis was also analyzed. **Results.** The plasma levels of RvD2 were positively correlated to LTB<sub>4</sub>. The RvD2/LTB<sub>4</sub> ratio in DM + AIS group was lower than that in the nonDM+AIS group. No correlation was found between the RvD2/LTB<sub>4</sub> ratio and infarct size or NIHSS score. The RvD2/LTB<sub>4</sub> ratio at baseline was significantly lower in the poor prognosis group (mRS ≥ 3) than that in the good prognosis group (mRS ≤ 2). **Conclusions.** Our study indicated that the balance between pro-resolving and proinflammatory mediators was impaired by diabetes in ischemic stroke. The RvD2/LTB<sub>4</sub> ratio may serve as a biomarker of prognosis for ischemic stroke.

## 1. Introduction

Diabetes mellitus (DM) is an independent risk factor for ischemic stroke and can treble the risk of cardiovascular and cerebrovascular diseases [1]. Inflammation plays an important role in the pathogenesis of diabetes. Pickup showed that cytokines mediate inflammatory response in type 2 diabetes and are directly involved in the development of DM and its vascular complications [2]. The use of salicylic acid or interleukin (IL-) 1 receptor antagonists in DM patients can lower blood glucose levels, further supporting the hypothesis that DM is an inflammatory disease [3]. Inflammation also plays a key role in the pathophysiology of ischemic stroke complicated with DM [4]. For example, matrix metalloproteinase-2 (MMP-2) activity, cyclooxygenase-2 (COX-2), IL-1 $\beta$ , and IL-6 were increased in the diabetic mouse brain after stroke [5–7].

Resolution of inflammation is the key program that regulates inflammation and ensures proinflammatory responses are not overactive. Uncontrolled inflammatory response and impaired resolution contribute to the pathological process of many diseases. In the past decade, specialized pro-resolving mediators (SPMs) have been identified as the central controllers of inflammation resolution. These small lipid molecules, including, e.g., lipoxins (LXs), resolvins (Rvs), protectins (PDs), and maresins (MaRs), monitor inflammation of resolution in a receptor-dependent manner [8]. The balance between proinflammatory mediators and SPMs regulates the duration of inflammatory response and the time course of homeostasis recovery. Imbalance between these two forces leads to the occurrence of inflammatory diseases. Leukotriene B<sub>4</sub> (LTB<sub>4</sub>) is a classical proinflammatory lipid mediator derived from arachidonic acid (AA). The ratio of SPMs to LTB<sub>4</sub> reflects the degree of the resolving-

proinflammatory balance and has been studied in a variety of disease models. For example, it has been reported that the  $LXA_4/LTB_4$  ratio decreased in alveolar lavage fluid of patients with cystic fibrosis, suggesting that disturbed resolution of inflammation contributes to the pathological changes of cystic fibrosis in the airway [9]. The ratio of  $RvD1/LTB_4$  and  $MaR1/LTB_4$  was reduced in preeclampsia compared to normal pregnancy, indicating that insufficient production of SPMs may be involved in the occurrence of preeclampsia [10]. Resolvin D2 ( $RvD2$ ) is derived from docosahexaenoic acid (DHA). It has been shown that  $RvD2$  can reduce infarct volume and dampen inflammation in experimental models of stroke [11, 12].

The  $RvD2/LTB_4$  ratio has been used as a biomarker for carotid intima thickness and plaque stability in cardiovascular disease [13, 14].

The aim of this study is to characterize the changes of  $RvD2/LTB_4$  ratio in DM patients with acute ischemic stroke. We also explored possible associations between the  $RvD2/LTB_4$  ratio and clinical characteristics of the patients, as well as the relationship of  $RvD2/LTB_4$  ratio and stroke prognosis.

## 2. Methods

**2.1. Study Population and Clinical Data Collection.** We enrolled 57 patients with acute ischemic stroke from the Department of Neurology, Shanghai Jiao Tong University Affiliated Sixth People's Hospital. According to the combination of DM, the patients were divided into two groups: non-DM patients with acute ischemic stroke (nonDM+AIS group) and DM patients with acute ischemic stroke (DM+ AIS group). Patients with coma, severe cardiac/hepatic/renal dysfunction, mental illness, history of other endocrine diseases, tumor, or autoimmune disease were excluded from the study. Patients who had acute systematic inflammatory disease within 1 month or received fibrinolytic thrombolysis were also excluded. All stroke patients met the diagnostic criteria of Chinese guidelines for the diagnosis and treatment of acute ischemic stroke 2014 [15] and were confirmed by computed tomography (CT) or magnetic resonance imaging (MRI). All DM patients met the diagnostic criteria made by the European Diabetes Policy Group for type 2 diabetes [16]. The patients were followed up at 90 days after stroke onset, and the modified Rankin Score (mRS) was assessed.

General information was collected covering age, gender, smoking/drinking history, and medical history. Routine laboratory analyses including glycated hemoglobin (HbA1c), fasting blood glucose, triglyceride, cholesterol, high-density lipoprotein (HDL), low-density lipoprotein (LDL), serum uric acid, white blood cell count, and neutrophil count were performed following routine procedures in the Department of Laboratory Medicine of Shanghai Jiao Tong University Affiliated Sixth People's Hospital. All participants or their authorized caregivers signed an informed consent. The study was approved by the ethical committee of Shanghai Jiao Tong University Affiliated Sixth People's Hospital.

**2.2. Blood Sampling and Enzyme Immunoassay Analysis.** Fasting blood samples were collected in EDTA anticoagulant tubes by venipuncture from all participants. All samples were taken within 72 h after disease onset. The samples were then centrifuged immediately, and the resulting plasma was stored at  $-80^{\circ}\text{C}$  until further processing. Endogenous concentrations of  $RvD2$  and  $LTB_4$  in plasma were determined by enzyme immunoassay (EIA) kits (Cayman Chemical, MI, USA). The collected plasma samples underwent a purification procedure according to the instructions of the EIA kits. Briefly, C18 Sep-Pak<sup>®</sup> light columns (Waters Corporation, MA, USA) were conditioned by methanol and water. The plasma samples were acidified to pH 4.0 (for  $LTB_4$ ) or pH 5.0 (for  $RvD2$ ) and injected into the preconditioned C18 column. Subsequently, the columns were washed with distilled water, and the purified samples were eluted with 1% methanol in ethyl acetate (for  $LTB_4$ ) or methanol (for  $RvD2$ ). The samples were then dried by  $N_2$  gas and resuspended in EIA buffer for assessment of  $RvD2$  and  $LTB_4$  according to the specific instructions for the kits.

**2.3. Statistical Analysis.** All statistical analyses were performed using the IBM SPSS software (version 22, SPSS Inc., USA). Continuous and parametric variables were expressed as mean  $\pm$  standard deviation (SD), and nonparametric distributed variables were expressed as median (IQR) and 25th-75th percentiles. Categorical variables were expressed as percentages. Differences between the two groups were compared by Mann-Whitney  $U$  test for nonparametric variables, and  $\chi^2$  or Fisher's exact test was used for categorical variables. Spearman correlation analysis was performed to evaluate the possible associations of lipid mediator with clinical or laboratory parameters. Receiver operating characteristic (ROC) curves and area under the curves (AUC) were calculated to evaluate the predictive power of the  $RvD2/LTB_4$  ratio for stroke outcome.  $p < 0.05$  was considered as significant in all statistical analyses.

## 3. Results

**3.1. Clinical Characteristics.** A total of 57 cases were enrolled, including 25 nondiabetic patients with acute ischemic stroke (nonDM+AIS group) and 32 diabetic patients with acute ischemic stroke (DM+ AIS group). There was no significant difference in age, history of smoking, drinking, hypertension, and atrial fibrillation between the two groups. The levels of HbA1c and fasting blood glucose were higher in the diabetic group than in the nondiabetic group (Table 1). There was no significant difference with regard to other laboratory tests, including triglycerides, cholesterol, HDL, LDL, serum uric acid, white blood cell count, and neutrophil count.

**3.2. Plasma Levels of  $RvD2$ ,  $LTB_4$ , and Their Ratio in DM+ AIS and nonDM+ AIS Groups.** There was no significant difference between the two groups with regard to plasma  $RvD2$  concentration (Figure 1(a)).  $LTB_4$  levels in the DM+ AIS group were higher than that in the nonDM+ AIS group (Figure 1(b)). To evaluate the balance of pro-resolving lipid mediators and pro-inflammation lipid

TABLE 1: Baseline characteristics of the patients.

	nonDM+AIS ( <i>n</i> = 25)	DM + AIS ( <i>n</i> = 32)	<i>p</i>
Age	66.36 ± 9.50	69.31 ± 9.89	0.260
Gender (male)	19 (76)	24 (75)	0.931
Smoking	8 (32)	6 (18.8)	0.249
Alcohol use	4 (16)	4 (12.5)	0.706
Hypertension	17 (68)	26 (81.3)	0.249
Atrial fibrillation	3 (12)	5 (15.6)	0.995
HbA1c	5.80 (5.50-6.05)	7.55 (6.90-9.23)	<0.01
Fasting blood glucose/mmol/L	5.31 (4.88-6.31)	7.82 (6.67-9.58)	<0.01
Triglyceride/mmol/L	4.63 (3.48-5.58)	4.50 (3.44-5.75)	0.803
Cholesterol/mmol/L	1.63 (1.21-2.17)	1.59 (1.02-3.08)	0.923
HDL/mmol/L	1.13 (0.81-1.31)	0.98 (0.87-1.20)	0.705
LDL/mmol/L	3.08 ± 1.01	3.09 ± 0.86	0.975
Uric acid/umol/L	346 (326-361)	321 (259-354)	0.061
White blood cell count × 10 <sup>9</sup> /L	7.20 (5.75-9.05)	6.95 (5.95-8.68)	0.994
Neutrophils cell count × 10 <sup>9</sup> /L	4.20 (3.10-5.90)	4.90 (3.83-6.88)	0.228

Data are presented as mean ± SD or median ± IQR or *n* (%). DM: diabetes mellitus group; HDL: high-density lipoprotein; AIS: acute ischemic stroke; LDL: low-density lipoprotein.

mediators, we calculated the RvD2/LTB<sub>4</sub> ratio. The DM + AIS group had a lower RvD2/LTB<sub>4</sub> ratio than the non-DM+AIS group (Figure 1(c)). A positive correlation was found between RvD2 and LTB<sub>4</sub> levels ( $r = 0.262$ ,  $p = 0.049$ ) (Figure 1(d)).

**3.3. Association of Infarct Volume/NIHSS Score with RvD2/LTB<sub>4</sub> Ratio.** Diffusion-weighted MRI was used to assess infarct volume. The volume of cerebral infarction was calculated according to the Pullicino formula (length × width × layer/2, cm<sup>3</sup>) [17]. The stroke patients were divided into small infarct (<5 cm<sup>3</sup>,  $n = 29$ ), medium infarct (5-10 cm<sup>3</sup>,  $n = 7$ ), and large infarct (>10 cm<sup>3</sup>,  $n = 19$ ). There was no significant difference in RvD2/LTB<sub>4</sub> ratio between the three groups (Figure 2(a)). The NIHSS score was used to evaluate the degree of neurological impairment on the first day of admission. The patients were divided into three groups, including mild neurological impairment (NIHSS score < 4,  $n = 28$ ), moderate neurological impairment (NIHSS score 4-15,  $n = 25$ ), and severe neurological impairment (NIHSS score > 15,  $n = 4$ ). We found that there was a gradient trend of decrease of RvD2/LTB<sub>4</sub> ratio from mild to severe neurological impairment, though not statistically significant (Figure 2(b)).

**3.4. Relationship between the Ratio of RvD2/LTB<sub>4</sub> and Stroke Prognosis.** According to the 90-day mRS score, the patients were divided into the good prognosis group (mRS ≤ 2,  $n = 36$ ) and poor prognosis group (mRS ≥ 3,  $n = 21$ ). We found that baseline RvD2/LTB<sub>4</sub> ratio in the good prognosis group was higher than that in the poor prognosis (0.85[0.42-1.17] vs. 0.58 [0.28-0.77],  $p = 0.040$ ) (Figure 2(c)). Correlation analysis showed that the RvD2/LTB<sub>4</sub> ratio was negatively correlated with the mRS score (Spearman's rho test,  $r = -$

0.291,  $p = 0.028$ ) (Figure 2(d)). ROC curve analysis revealed that RvD2/LTB<sub>4</sub> produced an unsatisfactory area under the curve (AUC = 0.664) for predicting stroke prognosis with a 95% confidence interval of 0.527-0.784,  $p = 0.025$ . The associated criterion was 0.63 with 76.2% specificity and 58.3% sensitivity (Figure 3).

## 4. Discussion

In the present study, the RvD2/LTB<sub>4</sub> ratio was significantly reduced in DM stroke patients compared to non-DM stroke diabetic patients, indicating that DM impairs the balance between pro-resolving and proinflammatory signals in ischemic stroke. Furthermore, the RvD2/LTB<sub>4</sub> ratio in the acute stage of ischemic stroke was correlated with patient prognosis. These results provided novel potential mechanisms in excessive inflammation in DM patients with ischemic stroke.

Inflammation is a key program that mediates pathogenic and pathological effects of DM on ischemic stroke [4, 18]. The levels of circulating proinflammatory cytokines, such as tumor necrosis factor- $\alpha$  (TNF- $\alpha$ ) and IL-1, are increased in DM patients [19]. Sitagliptin was applied in the treatment of diabetes mellitus type 2. Studies have shown that sitagliptin has a neuroprotective effect by reducing neuroinflammation [20]. Atorvastatin could decrease the concentration of IL-6 and TNF- $\alpha$  and improved the outcome of ventilator-associated pneumonia in patients with ischemic stroke [21]. Herrera et al. demonstrated that RvE1 increased the neutrophil phagocytosis of *P. gingivalis* in WT animals but had no impact in diabetes animals. In RvE1 receptor-transgenic diabetic mice, the impaired neutrophil phagocytosis ability was rescued by RvE1 [22]. Above all, the proresolution system appears to be



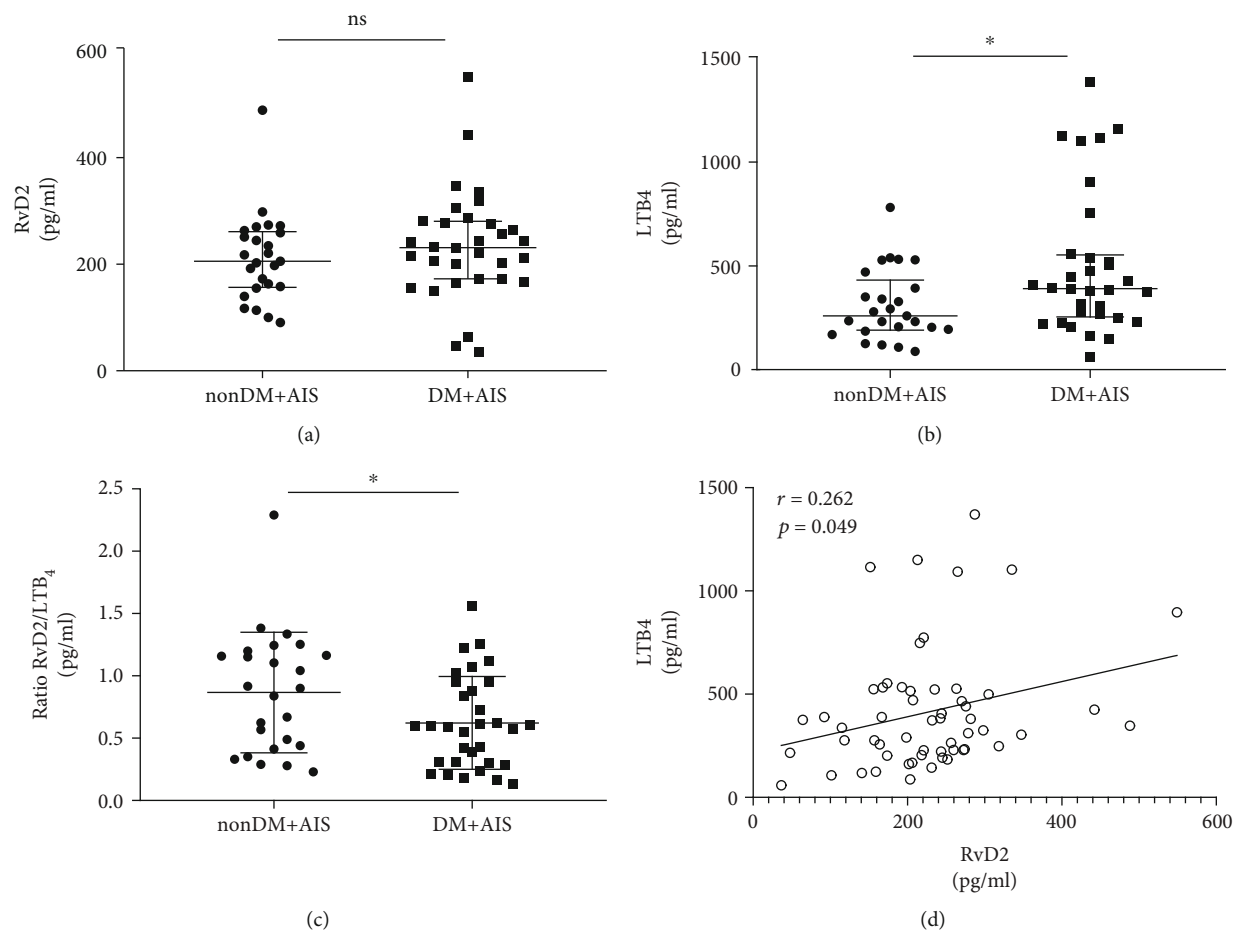


FIGURE 1: Plasma levels of RvD2, LTB<sub>4</sub>, and RvD2/LTB<sub>4</sub> ratio in acute ischemic stroke. (a) Comparison of the plasma concentrations of RvD2 shows no difference in the nonDM+AIS group and DM + AIS group. (b) Plasma concentrations of LTB<sub>4</sub> were increased in the nonDM+AIS group and nonDM+AIS group. (c) The RvD2/LTB<sub>4</sub> ratio of the DM + AIS group was lower compared to that in the nonDM+AIS group. (d) Correlation analysis shows a positive association between RvD2 and LTB<sub>4</sub> (Spearman rho test,  $r = 0.262$ ,  $p = 0.049$ ). Error bars represent IQR. ns: none significant. \*  $p < 0.05$ . DM: diabetes mellitus; AIS: acute ischemic stroke; LTB<sub>4</sub>: leukotriene B<sub>4</sub>; RvD2: resolvin D2.

compromised in DM. This may explain why diabetic patients with ischemic stroke have more severe symptoms and prognosis. Parlapiano et al. demonstrated that diabetic patients have increased levels of LTB<sub>4</sub> and activity of polymorphonuclear leukocyte, and this activation is correlated to glycated hemoglobin level [23].

Overactivated inflammation has been reported in the etiology of exaggerated brain damage in diabetic stroke models [24, 25]. Effective resolution of inflammation is essential for balancing poststroke inflammation to restore homeostasis of the brain. SPMs promote the resolution of inflammation and the recovery of tissue homeostasis [8]. RvD2 has been shown to exert anti-inflammatory and pro-resolving properties in various disease models [12, 26, 27]. The levels of endogenous RvD2 were inconsistent in different disease models and at different stages of the disease. Zuo et al. reported that the experimental stroke led to a decrease of RvD2 in the brain [12]. In epilepsy, the levels of brain RvD2 were reduced after seizure [28]. Conversely, in a mouse model of acute lung injury,

the levels of RvD2 were increased within 24h of LPS-induced lung inflammation [29]. In a murine model of hind limb ischemia, RvD2 and 17-HDHA were generated robustly in the bone marrow as early as 24h postsurgery [27]. Thus, it is valuable to evaluate the balance of pro-resolving and proinflammatory signals in a comprehensive way. LTB<sub>4</sub> is a classic inflammatory lipid mediator and has been implicated in ischemic stroke pathology [30, 31]. The levels of LTB<sub>4</sub> in plasma increased rapidly after stroke in humans [30]. Early and sustained increase of LTB<sub>4</sub> is associated with poor functional recovery of stroke [30]. High LTB<sub>4</sub> levels were also associated with larger nonhealing lesion areas and increased bacterial load in skin wound of diabetic mice [32]. The ratio of SPMs/LTB<sub>4</sub> has been considered as an index of the balance between pro-resolving and proinflammatory signals. For example, the ratios of plasma RvD1/LTB<sub>4</sub> and MaR1/LTB<sub>4</sub> were associated with inflammation status in preeclampsia [10]. In atherosclerosis, reduced salivary RvD1/LTB<sub>4</sub> ratio was found to reflect an imbalance of pro-resolving and



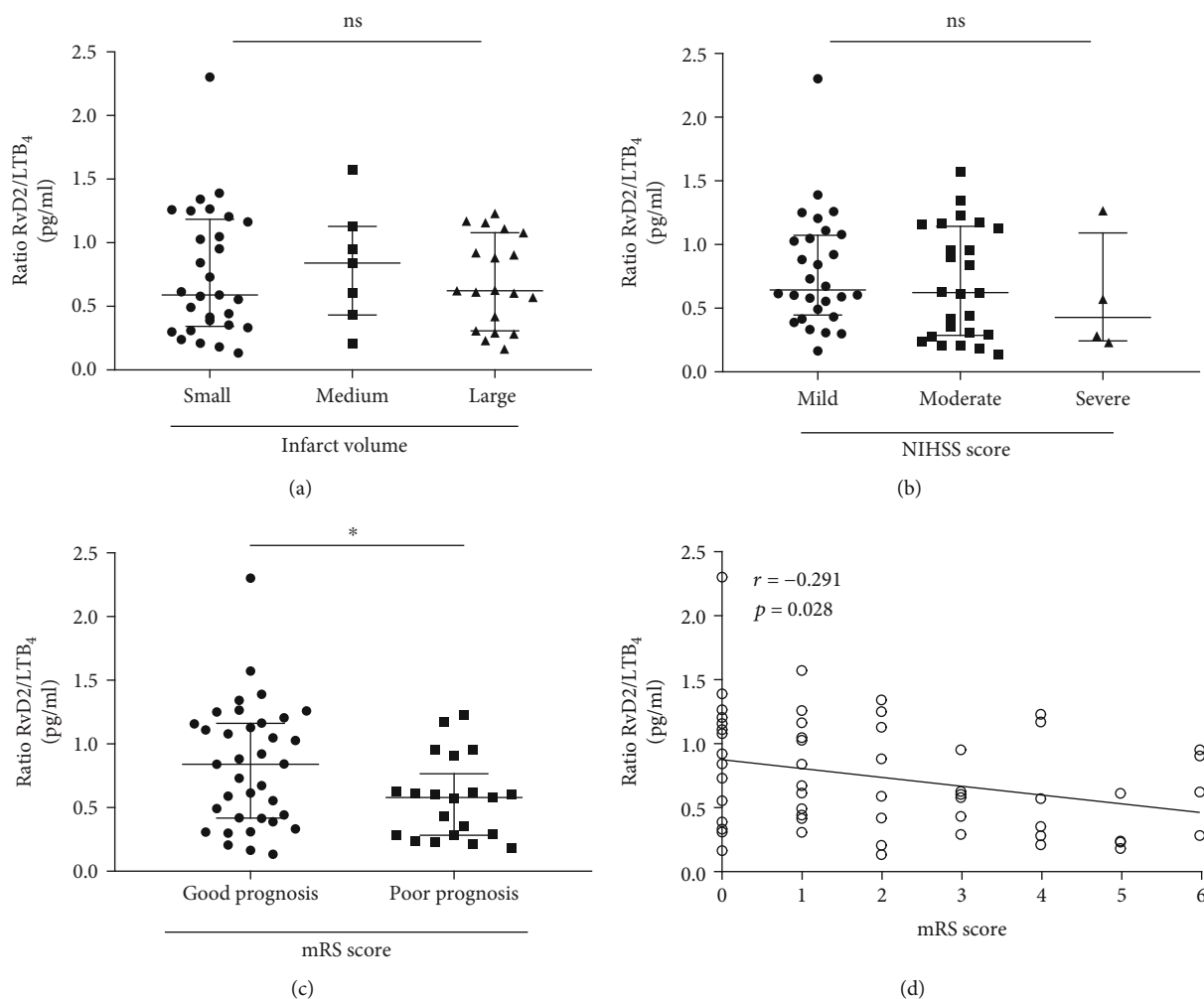


FIGURE 2: The association of RvD2/LTB<sub>4</sub> ratio with infarct volume, NIHSS score, and 90-day prognosis. (a) Ratios of plasma RvD2/LTB<sub>4</sub> were not different in the small, medium, and large infarct volume group. (b) Ratios of plasma RvD2/LTB<sub>4</sub> were not different in mild, moderate, and severe neurological deficit groups. (c) Ratios of plasma RvD2/LTB<sub>4</sub> in good prognosis were higher compared with that in the poor prognosis group. (d) There was a negative association of RvD2/LTB<sub>4</sub> ratio with 90-day mRS (Spearman rho test,  $r = -0.291$ ,  $p = 0.028$ ). Error bars represent IQR. ns: none significant. \*  $p < 0.05$ . LTB<sub>4</sub>: leukotriene B<sub>4</sub>; mRS: modified Rankin Scale; NIHSS: National Institutes of Health Stroke Scale; RvD2: resolvin D2.

proinflammatory forces and could predict thicker carotid intima [13]. Moreover, an abnormal ratio of SPM/LTB<sub>4</sub> was observed in the instable plaques derived from atherosclerosis patients [14].

In the present study, we utilized the plasma RvD2/LTB<sub>4</sub> ratio as a possible indicator for poststroke inflammation. We found lower RvD2/LTB<sub>4</sub> ratio in DM patients compared to non-DM patients. With ischemic stroke compared to non-diabetic patients. This may indicate that DM impairs the resolution of inflammation in acute ischemic stroke. Such an effect of DM in the resolution of inflammation has been shown in other diseases. For example, an imbalance of proinflammatory and pro-resolving mediators was observed in DM patients with tuberculosis [33]. A study on DM-associated retina damage showed that hyperglycemia may decrease RvD1 in the retina [34]. Furthermore, DM has been shown to impair the biosynthesis of PD1 and thus result in

the overactivation of macrophages in wound healing [35]. These studies supported our finding that DM may disturb the resolution of inflammation in ischemic stroke.

We also explored the association of RvD2/LTB<sub>4</sub> ratio with stroke severity and prognosis. We found no correlation between the RvD2/LTB<sub>4</sub> ratio and infarct volume nor NIHSS score. This finding is consistent with previous publications showing that inflammation is not linearly associated with the degree of brain damage in stroke [31, 36, 37].

On the other hand, it has been shown that neuroendocrine biomarkers, such as copeptin and cortisol, are correlated with short-term outcome and mortality of ischemic stroke [38]. We found an association between plasma RvD2/LTB<sub>4</sub> ratio and 90-day prognosis. Patients with poor prognosis had lower levels of RvD2/LTB<sub>4</sub> ratio at baseline. The levels of pro-resolving activities at the acute phase may represent an overall capacity of the body to restore

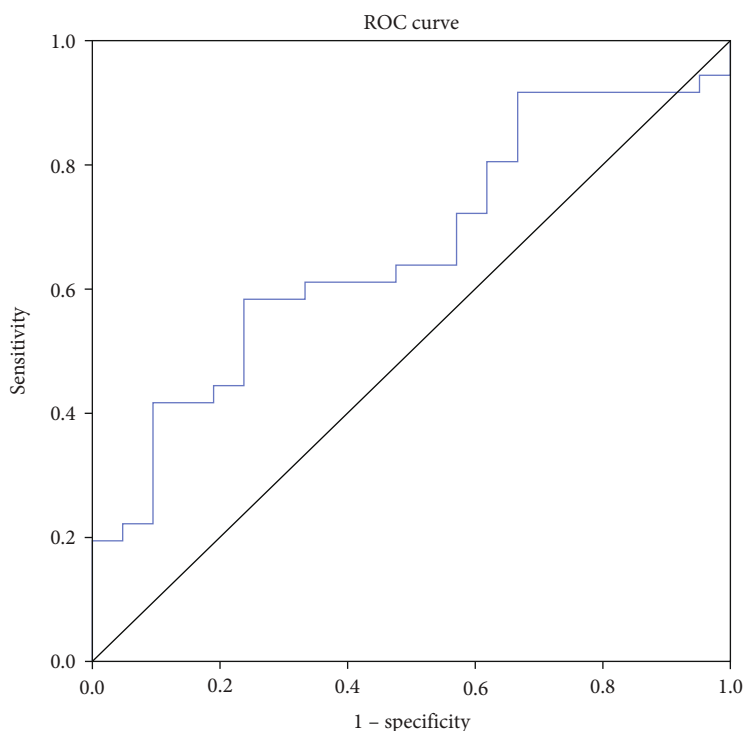


FIGURE 3: Possible predictive role of RvD2/LTB<sub>4</sub> in stroke prognosis. ROC curve analysis showed AUC = 0.664 with a 95% confidence interval of 0.527–0.784,  $p = 0.025$ . The associated criterion was 0.63 with 76.2% specificity and 58.3% sensitivity. AUC: area under the curve; LTB<sub>4</sub>: leukotriene B<sub>4</sub>; ROC: receiver operating characteristic curves; RvD2: resolvin D2.

homeostasis after stroke. This is consistent with the previous report that high levels of circulating TNF- $\alpha$ , IL-6, and MMP-9 were associated with a poor prognosis in acute ischemic stroke [39–41]. The ROC curve analysis of the RvD2/LTB<sub>4</sub> ratio for prognosis revealed an AUC of 0.664. Although the RvD2/LTB<sub>4</sub> ratio may serve as a biomarker of stroke prognosis, the predictive power, specificity, and sensitivity are relatively low.

In summary, our data indicate that DM may disturb the balance between pro-resolving and proinflammatory mediators in ischemic stroke. Moreover, the reduced RvD2/LTB<sub>4</sub> ratio in the acute phase of stroke may predict a poor prognosis. These findings provide new insights into the failure of resolution of inflammation in DM patients with ischemic stroke. Limitation of this study includes the small sample size, single center design, and no validation cohort. Larger sample sizes of patients from multiple centers are needed to validate our findings in future studies. In addition, studies involving animal and cellular models are essential to further elucidate the intrinsic mechanisms of resolution failure in DM patients with acute ischemic stroke.

### Data Availability

The data used to support the findings of this study are available from the corresponding authors upon request.

### Ethical Approval

The study protocols were approved by local ethics committee boards.

### Conflicts of Interest

The authors declare no conflicts of interest.

### Authors' Contributions

ZM and XT performed the experiment and analyzed the data. MS gave important suggestion in methodology and was involved in manuscript preparation. YZ and XW designed and monitored the study. All the authors read through the manuscript and approved the final version.

### Acknowledgments

We thank all the patients who participated in this study and the staff of our stroke unit. The authors received the following financial support for the research, authorship, and/or publication of this article: the National Nature Science Foundation of China (grant numbers 31771185, 81974158, and 31811530007) and the Swedish Foundation for International Cooperation in Research and Higher Education (Grant No. CH2017-7308).

## References

- [1] Emerging Risk Factors Collaboration, N. Sarwar, P. Gao et al., "Diabetes mellitus, fasting blood glucose concentration, and risk of vascular disease: a collaborative meta-analysis of 102 prospective studies," *The Lancet*, vol. 375, no. 9733, pp. 2215–2222, 2010.
- [2] J. C. Pickup, "Inflammation and activated innate immunity in the pathogenesis of type 2 diabetes," *Diabetes Care*, vol. 27, no. 3, pp. 813–823, 2004.
- [3] M. Y. Donath and S. E. Shoelson, "Type 2 diabetes as an inflammatory disease," *Nature Reviews Immunology*, vol. 11, no. 2, pp. 98–107, 2011.
- [4] D. Y. Fann, S. Y. Lee, S. Manzanero, P. Chunduri, C. G. Sobey, and T. V. Arumugam, "Pathogenesis of acute stroke and the role of inflammasomes," *Ageing Research Reviews*, vol. 12, no. 4, pp. 941–966, 2013.
- [5] A. Ergul, M. M. Elgebaly, M. L. Middlemore et al., "Increased hemorrhagic transformation and altered infarct size and localization after experimental stroke in a rat model type 2 diabetes," *BMC Neurology*, vol. 7, no. 1, p. 33, 2007.
- [6] K. Tureyen, K. Bowen, J. Liang, R. J. Dempsey, and R. Vemuganti, "Exacerbated brain damage, edema and inflammation in type-2 diabetic mice subjected to focal ischemia," *Journal of Neurochemistry*, vol. 116, no. 4, pp. 499–507, 2011.
- [7] C. Bémeur, L. Ste-Marie, P. Desjardins et al., "Dehydroascorbic acid normalizes several markers of oxidative stress and inflammation in acute hyperglycemic focal cerebral ischemia in the rat," *Neurochemistry International*, vol. 46, no. 5, pp. 399–407, 2005.
- [8] C. N. Serhan, "Pro-resolving lipid mediators are leads for resolution physiology," *Nature*, vol. 510, no. 7503, pp. 92–101, 2014.
- [9] F. C. Ringholz, P. J. Buchanan, D. T. Clarke et al., "Reduced 15-lipoxygenase 2 and lipoxin A4/leukotriene B4 ratio in children with cystic fibrosis," *The European Respiratory Journal*, vol. 44, no. 2, pp. 394–404, 2014.
- [10] L. Oliveira Perucci, T. A. P. Santos, and P. C. Santos, "Pre-eclampsia is associated with reduced resolvin D1 and maresin 1 to leukotriene B4 ratios in the plasma," *American Journal of Reproductive Immunology*, vol. 83, no. 2, article e13206, 2020.
- [11] X. Dong, J. Gao, C. Y. Zhang, C. Hayworth, M. Frank, and Z. Wang, "Neutrophil membrane-derived nanovesicles alleviate inflammation to protect mouse brain injury from ischemic stroke," *ACS Nano*, vol. 13, no. 2, pp. 1272–1283, 2019.
- [12] G. Zuo, D. Zhang, R. Mu et al., "Resolvin D2 protects against cerebral ischemia/reperfusion injury in rats," *Molecular Brain*, vol. 11, no. 1, p. 9, 2018.
- [13] S. Thul, C. Labat, M. Temmar, A. Benetos, and M. Bäck, "Low salivary resolvin D1 to leukotriene B4 ratio predicts carotid intima media thickness: a novel biomarker of non-resolving vascular inflammation," *European Journal of Preventive Cardiology*, vol. 24, no. 9, pp. 903–906, 2017.
- [14] G. Fredman, J. Hellmann, J. D. Proto et al., "An imbalance between specialized pro-resolving lipid mediators and pro-inflammatory leukotrienes promotes instability of atherosclerotic plaques," *Nature Communications*, vol. 7, no. 1, article 12859, 2016.
- [15] M. Liu and M. L. He, "Chinese guidelines for the diagnosis and treatment of acute ischemic stroke 2014," *Zhong Hua Shen Jing Ke Za Zhi*, vol. 48, no. 4, pp. 246–257, 2015.
- [16] 1999 European Diabetes Policy Group, "A desktop guide to Type 2 diabetes mellitus," *Diabetic Medicine*, vol. 16, no. 9, pp. 716–730, 1999.
- [17] J. R. Sims, L. R. Gharai, P. W. Schaefer et al., "ABC/2 for rapid clinical estimate of infarct, perfusion, and mismatch volumes," *Neurology*, vol. 72, no. 24, pp. 2104–2110, 2009.
- [18] V. Shukla, A. K. Shakya, M. A. Perez-Pinzon, and K. R. Dave, "Cerebral ischemic damage in diabetes: an inflammatory perspective," *Journal of Neuroinflammation*, vol. 14, no. 1, p. 21, 2017.
- [19] T. Temelkova-Kurktschiev, E. Henkel, C. Koehler, K. Karrei, and M. Hanefeld, "Subclinical inflammation in newly detected type II diabetes and impaired glucose tolerance," *Diabetologia*, vol. 45, no. 1, p. 151, 2002.
- [20] M. Wiciński, E. Wódkiewicz, M. Słupski et al., "Neuroprotective activity of sitagliptin via reduction of neuroinflammation beyond the incretin effect: focus on alzheimer's disease," *BioMed Research International*, vol. 2018, Article ID 6091014, 9 pages, 2018.
- [21] Y. Yu, C. Zhu, C. Liu, and Y. Gao, "Effect of prior atorvastatin treatment on the frequency of hospital acquired pneumonia and evolution of biomarkers in patients with acute ischemic stroke: a multicenter prospective study," *BioMed Research International*, vol. 2017, Article ID 5642704, 8 pages, 2017.
- [22] B. S. Herrera, H. Hasturk, A. Kantarci et al., "Impact of resolvin E1 on murine neutrophil phagocytosis in type 2 diabetes," *Infection and Immunity*, vol. 83, no. 2, pp. 792–801, 2015.
- [23] C. Parlapiano, C. Danese, M. Marangi et al., "The relationship between glycated hemoglobin and polymorphonuclear leukocyte leukotriene B4 release in people with diabetes mellitus," *Diabetes Research and Clinical Practice*, vol. 46, no. 1, pp. 43–45, 1999.
- [24] R. Kumari, L. B. Willing, J. K. Krady, S. J. Vannucci, and I. A. Simpson, "Impaired wound healing after cerebral hypoxia—ischemia in the diabetic mouse," *Journal of Cerebral Blood Flow and Metabolism*, vol. 27, no. 4, pp. 710–718, 2007.
- [25] R. Kumari, L. B. Willing, S. D. Patel et al., "The PPAR-gamma agonist, darglitazone, restores acute inflammatory responses to cerebral hypoxia-ischemia in the diabetic Ob/Ob mouse," *Journal of Cerebral Blood Flow and Metabolism*, vol. 30, no. 2, pp. 352–360, 2010.
- [26] L. B. Pascoal, B. Bombassaro, A. F. Ramalho et al., "Resolvin RvD2 reduces hypothalamic inflammation and rescues mice from diet-induced obesity," *Journal of Neuroinflammation*, vol. 14, no. 1, p. 5, 2017.
- [27] M. J. Zhang, B. E. Sansbury, J. Hellmann et al., "Resolvin D2 enhances postischemic revascularization while resolving inflammation," *Circulation*, vol. 134, no. 9, pp. 666–680, 2016.
- [28] F. Frigerio, G. Pasqualini, I. Craparotta et al., "n-3 Docosapentaenoic acid-derived protectin D1 promotes resolution of neuroinflammation and arrests epileptogenesis," *Brain*, vol. 141, no. 11, pp. 3130–3143, 2018.
- [29] H. P. Sham, K. H. Walker, R. E. Abdunour et al., "15-epi-Lipoxin A<sub>4</sub>, resolvin D2, and resolvin D3 induce NF- $\kappa$ B regulators in bacterial pneumonia," *The Journal of Immunology*, vol. 200, no. 8, pp. 2757–2766, 2018.
- [30] S. J. Chan, M. P. E. Ng, H. Zhao et al., "Early and sustained increases in leukotriene B4 levels are associated with poor clinical outcome in ischemic stroke patients," *Neurotherapeutics*, vol. 17, no. 1, pp. 282–293, 2020.

- [31] X. Liu, J. Liu, S. Zhao et al., "Interleukin-4 is essential for microglia/macrophage M2 polarization and long-term recovery after cerebral ischemia," *Stroke*, vol. 47, no. 2, pp. 498–504, 2016.
- [32] S. L. Brandt, S. Wang, N. N. DeJani et al., "Excessive localized leukotriene B4 levels dictate poor skin host defense in diabetic mice," *JCI Insight*, vol. 3, no. 17, 2018.
- [33] R. Shivakoti, J. Dalli, D. Kadam et al., "Lipid mediators of inflammation and resolution in individuals with tuberculosis and tuberculosis-diabetes," *Prostaglandins & Other Lipid Mediators*, vol. 147, article 106398, 2020.
- [34] H. Shi, T. W. Carion, Y. Jiang, A. Chahine, J. J. Steinle, and E. A. Berger, "A regulatory role for  $\beta$ -adrenergic receptors regarding the resolvin D1 (RvD1) pathway in the diabetic retina," *PLoS One*, vol. 12, no. 11, article e0185383, 2017.
- [35] S. Hong, H. Tian, Y. Lu et al., "Neuroprotectin/protectin D1: endogenous biosynthesis and actions on diabetic macrophages in promoting wound healing and innervation impaired by diabetes," *American Journal of Physiology Cell Physiology*, vol. 307, no. 11, pp. C1058–C1067, 2014.
- [36] M. H. Grønhoj, B. H. Clausen, C. D. Fenger, K. L. Lambertsen, and B. Finsen, "Beneficial potential of intravenously administered IL-6 in improving outcome after murine experimental stroke," *Brain, Behavior, and Immunity*, vol. 65, pp. 296–311, 2017.
- [37] J. Montaner, J. Alvarez-Sabín, C. Molina et al., "Matrix metalloproteinase expression after human cardioembolic stroke: temporal profile and relation to neurological impairment," *Stroke*, vol. 32, no. 8, pp. 1759–1766, 2001.
- [38] W.-J. Tu, X. Dong, S.-J. Zhao, D.-G. Yang, and H. Chen, "Prognostic value of plasma neuroendocrine biomarkers in patients with acute ischaemic stroke," *Journal of Neuroendocrinology*, vol. 25, no. 9, pp. 771–778, 2013.
- [39] L. Ramiro, A. Simats, T. García-Berrocso, and J. Montaner, "Inflammatory molecules might become both biomarkers and therapeutic targets for stroke management," *Therapeutic Advances in Neurological Disorders*, vol. 11, 2018.
- [40] A. Bustamante, T. Sobrino, D. Giralt et al., "Prognostic value of blood interleukin-6 in the prediction of functional outcome after stroke: a systematic review and meta-analysis," *Journal of Neuroimmunology*, vol. 274, no. 1-2, pp. 215–224, 2014.
- [41] G. Mazzotta, P. Sarchielli, V. Caso et al., "Different cytokine levels in thrombolysis patients as predictors for clinical outcome," *European Journal of Neurology*, vol. 11, no. 6, pp. 377–381, 2004.

## Retraction

# Retracted: Measuring Subthalamic Nucleus Volume of Parkinson's Patients and Evaluating Its Relationship with Clinical Scales at Pre- and Postdeep Brain Stimulation Treatment: A Magnetic Resonance Imaging Study

### BioMed Research International

Received 12 March 2024; Accepted 12 March 2024; Published 20 March 2024

Copyright © 2024 BioMed Research International. This is an open access article distributed under the Creative Commons Attribution License, which permits unrestricted use, distribution, and reproduction in any medium, provided the original work is properly cited.

This article has been retracted by Hindawi following an investigation undertaken by the publisher [1]. This investigation has uncovered evidence of one or more of the following indicators of systematic manipulation of the publication process:

- (1) Discrepancies in scope
- (2) Discrepancies in the description of the research reported
- (3) Discrepancies between the availability of data and the research described
- (4) Inappropriate citations
- (5) Incoherent, meaningless and/or irrelevant content included in the article
- (6) Manipulated or compromised peer review

The presence of these indicators undermines our confidence in the integrity of the article's content and we cannot, therefore, vouch for its reliability. Please note that this notice is intended solely to alert readers that the content of this article is unreliable. We have not investigated whether authors were aware of or involved in the systematic manipulation of the publication process.

Wiley and Hindawi regrets that the usual quality checks did not identify these issues before publication and have since put additional measures in place to safeguard research integrity.

We wish to credit our own Research Integrity and Research Publishing teams and anonymous and named external researchers and research integrity experts for contributing to this investigation.

The corresponding author, as the representative of all authors, has been given the opportunity to register their agreement or disagreement to this retraction. We have kept a record of any response received.

### References

- [1] L. Lu, K. Xu, L. Shi et al., "Measuring Subthalamic Nucleus Volume of Parkinson's Patients and Evaluating Its Relationship with Clinical Scales at Pre- and Postdeep Brain Stimulation Treatment: A Magnetic Resonance Imaging Study," *BioMed Research International*, vol. 2021, Article ID 6646416, 7 pages, 2021.



## Research Article

# Measuring Subthalamic Nucleus Volume of Parkinson's Patients and Evaluating Its Relationship with Clinical Scales at Pre- and Postdeep Brain Stimulation Treatment: A Magnetic Resonance Imaging Study

Li Lu,<sup>1</sup> Kai Xu ,<sup>1</sup> Lin Shi,<sup>1</sup> Weiqiang Dou,<sup>2</sup> Kai Liu ,<sup>1</sup> Hong Ma,<sup>1</sup> Lixiang Xie,<sup>1</sup> Chao Zhang,<sup>1</sup> and Cailuan Lu<sup>1</sup>

<sup>1</sup>Department of Radiology, Affiliated Hospital of Xuzhou Medical University, Xuzhou, Jiangsu Province, China

<sup>2</sup>GE Healthcare, MR Research China, Beijing, China

Correspondence should be addressed to Kai Xu; [xkpaper@163.com](mailto:xkpaper@163.com)

Received 11 December 2020; Revised 9 February 2021; Accepted 19 February 2021; Published 25 February 2021

Academic Editor: Yuzhen Xu

Copyright © 2021 Li Lu et al. This is an open access article distributed under the Creative Commons Attribution License, which permits unrestricted use, distribution, and reproduction in any medium, provided the original work is properly cited.

This study investigated potential imaging biomarkers for predicting the efficacy of deep brain stimulation (DBS) of the subthalamic nucleus (STN) in patients with Parkinson's disease (PD). A total of 59 PD patients and 50 healthy control subjects underwent high-resolution 3-dimensional T1-weighted brain magnetic resonance imaging. Bilateral STN volumes were compared between the 2 groups, and a correlation analysis was performed to assess the relationship between bilateral STN volumes or intracranial volume (ICV) and pre- or postoperative clinical scale scores. The results showed that the left STN volume differed significantly between PD patients and controls. In patients, the left STN volume was negatively correlated with pre- and postoperative quality of life scores and positively correlated with Mini-mental State Examination (MMSE) and Montreal Cognitive Assessment scores; ICV was also positively correlated with the MMSE score. These findings indicate that changes in the left STN volume are a useful biomarker for evaluating the clinical outcome of PD patients following DBS.

## 1. Introduction

Parkinson's disease (PD) is a common movement disorder and neurodegenerative disease [1] characterized by the loss of dopaminergic neurons [2–5] mainly in the substantia nigra (SN). Drugs and invasive treatments are the main therapeutic options for PD. Given the limited efficacy of pharmacotherapy, stereotactic surgery is increasingly being considered for PD treatment in terms of the potential risks and benefits [6–10].

Deep brain stimulation (DBS) is a widely used invasive procedure that has been considered as an effective surgical treatment for movement disorders [11, 12]. The method involves implantation of electrodes into specific brain regions to stimulate neural circuits [13]. DBS has been used to treat various neurologic diseases including PD, dystonia, and essential tremor [14]. The target area for DBS in PD is usually the sub-

thalamic nucleus (STN), which is an important node in the cortical–basal ganglia–thalamocortical loop [15–18]. Low-frequency DBS of the STN was shown to reduce gait freezing in PD patients [19]. DBS is thought to relieve motor symptoms by selectively activating white matter tracts or by normalizing aberrantly activated neural networks [20]. Although DBS has yielded promising results in PD treatment, the mechanisms underlying the observed effects are not fully understood [21, 22], especially in terms of how impaired neural circuitry is restored [23, 24].

Changes in the regional brain volume can alter electrode targeting, reflect postoperative progression of subclinical dementia, or directly interfere with the therapeutic action of DBS [25]. Magnetic resonance imaging (MRI) is a noninvasive method that has been used to investigate structural and functional changes in PD [26–29] and predict motor outcomes following DBS based on thalamic and ventricular

volumes [25]. However, few studies have focused on the relationship between STN volume and PD symptoms before and after DBS. The aim of the present study was to identify imaging biomarkers for predicting clinical outcome in PD patients treated by DBS by analyzing the relationship between STN volume and disease duration as well as pre-/postoperative clinical measures.

## 2. Materials and Methods

**2.1. Subjects.** This study was approved by the Ethics Committee of the Affiliated Hospital of Xuzhou Medical University. A total of 200 patients with clinically confirmed primary PD were recruited between April 2016 and November 2017. Written consent was obtained from each patient prior to their participation in the study. All patients were evaluated for nonmotor symptoms and with the Geriatric Depression Scale, Beck self-rating form, rapid eye movement sleep behavior disorder self-rating form, sleepiness scale, 39-item Parkinson's Disease Questionnaire scale, end-of-agent questionnaire, dyskinesia questionnaire, new frozen gait questionnaire, Mini-mental State Examination (MMSE), Montreal Cognitive Assessment (MoCA), Hamilton Anxiety Scale, and Hamilton Depression Scale (HAMD). According to the 2012 China DBS expert consensus, 2 neurologists with 15 and 10 years of experience collected patient information and assessed disease course, levodopa response, and comorbidities. The preoperative inclusion criteria were as follows [30, 31]. (1) The patient met the United Kingdom Parkinson's Disease Society brain bank or Chinese diagnostic criteria for primary PD, had hereditary or one of the many genotypes of PD, and showed good response to levodopa. (2) The patient had PD for >5 years, with tremor as the main symptom that was not alleviated by standard drug treatment and seriously affected the patient's quality of life; if the patient strongly requested symptom alleviation through early surgery, the postoperative evaluation was extended to 3 years. (3) The patient was  $\leq 75$  years old; for older patients with severe tremor, the age limit was appropriately extended. (4) The patient responded to levodopa but the symptoms were not completely abolished, and quality of life remained low, or the patient was intolerant to the drug. (5) Disease severity was determined as a Hoehn and Yahr (HY) scale score of 2.5–4 in the "off" period of the drug (i.e., med-off). (6) Patients were not suitable for surgery because of the following conditions: severe cognitive dysfunction that could affect activities of daily living, severe refractory depression, anxiety, or schizophrenia, or other illnesses that could affect surgery or survival. Based on these criteria, 62 patients were included in the study and underwent DBS surgery. None of the patients had contraindications for MRI examination. However, because of head motion artifacts and incomplete MRI measurements, data for 3 patients were excluded (Figure 1).

Ultimately, 59 PD patients (33 males and 26 females, mean age:  $65.72 \pm 7.53$  years, age range: 43–77 years) were included in the study. Each patient underwent pre- and postoperative assessment with the Unified Parkinson's Disease Rating Scale (UPDRS) III and HY staging. The HY stage of the 59 patients was between 2.5 and 5. Preoperative med-on

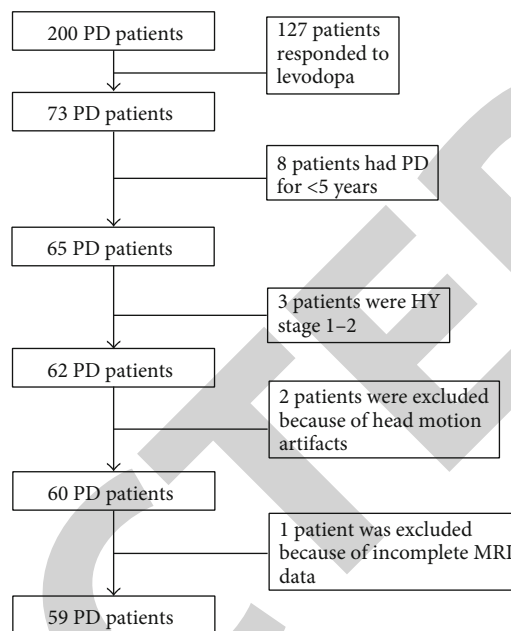


FIGURE 1: Flow chat of patient selection. 200 patients, clinically confirmed with primary PD, were recruited, and 141 patients were excluded due to different reasons including treatment with medication, PD history less than five years, 1-2 HY stage, head motion artifacts, or incomplete MRI data.

and med-off UPDRS III scores, postoperative med-on/DBS-on, postoperative med-off/DBS-off, and postoperative med-off/DBS-on UPDRS III scores were assessed. The control group comprised 50 healthy volunteers (23 males, 27 females, mean age:  $59.84 \pm 7.14$  years). There were no significant differences in the age or sex ratio between the 2 groups. All study participants were right-handed.

**2.2. MRI Examination.** A 3.0 T whole-body scanner (750w; GE Healthcare, Cleveland, OH, USA) with a standard bird-cage head transmitter and receiver coil was used for MRI. All subjects were scanned in the supine position. A foam material was placed on both sides of the subject's head to prevent head movement. The scan consisted of a high-resolution 3-dimensional T1-weighted (T1w) gradient echo-based sequence with the following parameters: repetition time = 7.0 ms, echo time = 3.0 ms, flip angle =  $12^\circ$ , field of view =  $256 \times 256$  mm<sup>2</sup>, matrix size =  $256 \times 256$ , slice thickness = 1 mm, and number of slices = 192; the scanning time was 4 min 15 s.

**2.3. STN Volume Measurement.** FreeSurfer v5.1.0 software (<http://surfer.nmr.mgh.harvard.edu>) [32] was used for sub-cortical volume segmentation. Preprocessing consisted of the following steps: (1) removal of nonbrain tissues, (2) automatic Talairach conversion, (3) separation of white and gray matter volumes, (4) signal normalization and registration to outline gray/white matter boundaries, (6) automatic topologic correction, (7) surface deformation, and (8) registration of the subject's brain to a standard template. All of the steps were performed in FreeSurfer and manually adjusted as

TABLE 1: Clinical information of PD patients and control subjects.

	PD	Control	Test statistic	<i>p</i> value
Age, years (mean $\pm$ SD)	65.72 $\pm$ 7.53	59.84 $\pm$ 7.14	0.026	0.872
Sex			1.936	0.586
Male	33	23		
Female	26	27		
Disease duration, years				
$\geq 10$	19	—		
5–10	22	—		
$\leq 5$	18	—		
Onset (affected area)				
Left limb	15	—		
Right limb	44	—		
Electrode implantation				
Bilateral STN	57	—		
Bilateral GPi	2	—		

GPi: internal globus pallidus; PD: Parkinson's disease; SD: standard deviation; STN: subthalamic nucleus.

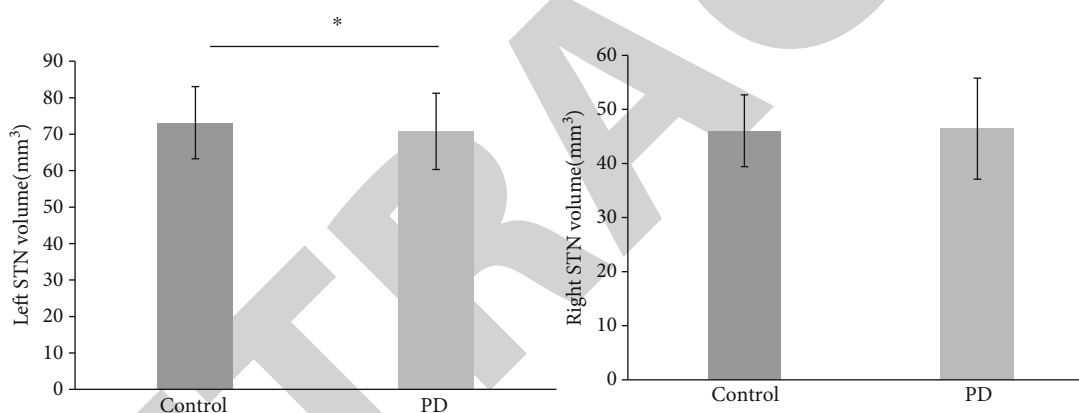


FIGURE 2: STN volumes in PD patients and controls. The Left STN volume was significantly lower in PD patients than in control subjects. The error bars represent mean  $\pm$  standard deviation.

necessary. The STN was identified based on the DBS Intrinsic Template Atlas [33] (<http://www.lead-dbs.org/>). The mask of the bilateral STN standard space was extracted from the automated anatomic atlas template and binarized. Individual T1W images were registered into the standard space MNI152 template to obtain a registered parameter matrix. The resultant matrix was then inverted from the standard into the individual space to obtain the transformation parameters. The STN in the standard space was transformed accordingly into the individual space, and the voxel number was calculated and used to calculate the volume of each STN. Intracranial volume (ICV) was determined in the same manner and used as a covariate in STN volume comparisons. A general linear model was used to analyze bilateral STN volumes, with the group as a fixed factor, ICV as a covariate, and bilateral STN volumes as a dependent variable.

**2.4. Statistical Analysis.** Data were analyzed using SPSS v20.0 software (IBM, Armonk, NY, USA). Bilateral STN volumes

were compared between patients and controls with the 2-tailed *t* test at a significance level of  $p < 0.025$  ( $[0.05/2]$ ). Pearson correlation analysis was performed to evaluate the relationship between bilateral STN volumes and UPDRS III or 39-item Parkinson's Disease Questionnaire (PDQ-39) score. Bonferroni correction ( $p < 0.025$ ,  $[0.05/2]$ ) was applied to multiple comparisons in the correlation analysis.

**2.5. Postoperative DBS Programming.** For all patients, interventions were programmed 1 month after the operation by a neurologist experienced in movement disorders. Monopolar stimulation was used for programming at each contact under the state of drug withdrawal. Initial stimulus parameters were a pulse width of 60  $\mu$ s and frequency of 130 Hz. All DBS electrodes in the ventral to dorsal direction were first tested with a voltage of 2.5 V. The motor function was evaluated based on the postoperative UPDRS III score. Stimulus parameters were then modified for each patient according to the medication and fluctuation of symptoms. The optimal

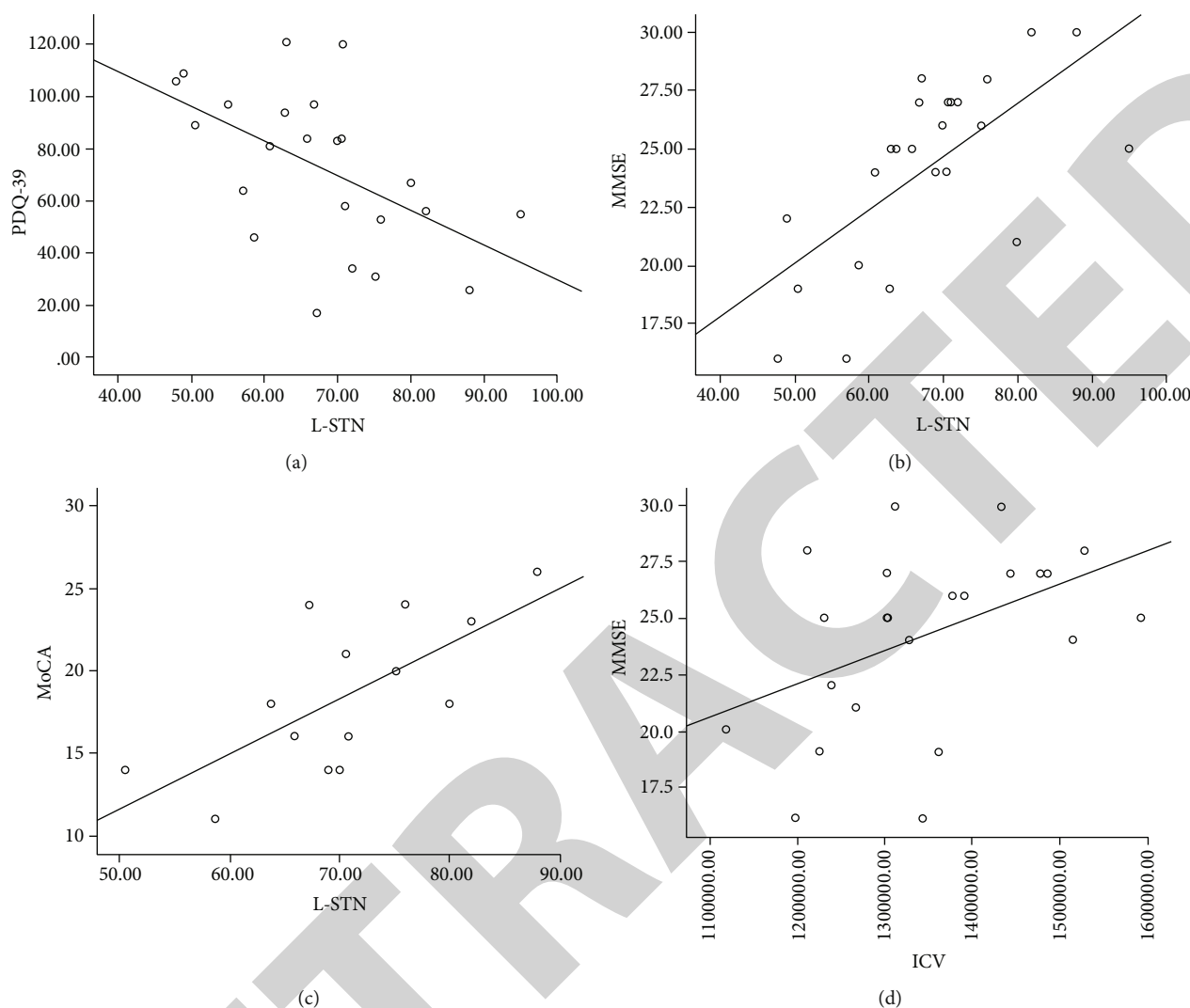


FIGURE 3: Correlation analysis between the STN volume and preoperative clinical measures in PD patients. The left STN volume was negatively correlated with preoperative PDQ-39 (a) and positively correlated with MMSE (b) and MoCA (c) scores. ICV was positively correlated with the MMSE score (d).

stimulation site was programmed with the lowest threshold for symptom reduction and highest threshold for side effects. All patients were evaluated with clinical scales 6 months after the operation.

### 3. Results

**3.1. Clinical Information of the Subjects.** Of the 59 patients, electrodes were implanted into bilateral STN in 57 patients and in bilateral internal globus pallidus (GPi) in 2 patients (Table 1). The history of PD in the patients ranged from 1 to 23 years, with a mean duration of  $8.16 \pm 4.32$  years. In 15 patients, tremors first manifested in the left limb and gradually spread to the right limb, while in 44 patients, the pattern was reversed. All patients underwent follow-up assessment with clinical scales at 6 months postsurgery.

**3.2. Comparison of STN Volumes between PD Patients and Control Subjects.** PD patients had a smaller left STN volume

than control subjects ( $70.757 \pm 10.448$  vs  $73.162 \pm 9.883$  mm<sup>3</sup>;  $F = 5.624$ ,  $p = 0.02$  with Bonferroni correction), but a comparable right STN volume ( $46.448 \pm 9.358$  vs  $46.041 \pm 6.636$  mm<sup>3</sup>;  $F = 0.007$ ,  $p = 0.932$ ) (Figure 2). There was no significant difference in ICV between PD patients and controls ( $1388.1 \pm 164.9$  vs  $1323.9 \pm 156.6$  cm<sup>3</sup>;  $p > 0.05$ ).

**3.3. Correlation between STN Volume/ICV and Disease Duration.** We performed a correlation analysis between the STN volume or ICV and duration of PD. Neither STN volume nor ICV was correlated with disease duration ( $p > 0.05$ ).

**3.4. Correlation between STN Volume and Pre-/Postoperative Clinical Scores.** The correlation between the STN volume and pre- or postoperative clinical measures was also evaluated. In the preoperative assessment, the left STN volume was negatively correlated with quality of life score ( $r = -0.532$ ,  $p = 0.009$ ) and positively correlated with the MMSE and MoCA scores ( $r = 0.665$  and  $0.695$ , respectively;  $p < 0.05$ ) in PD

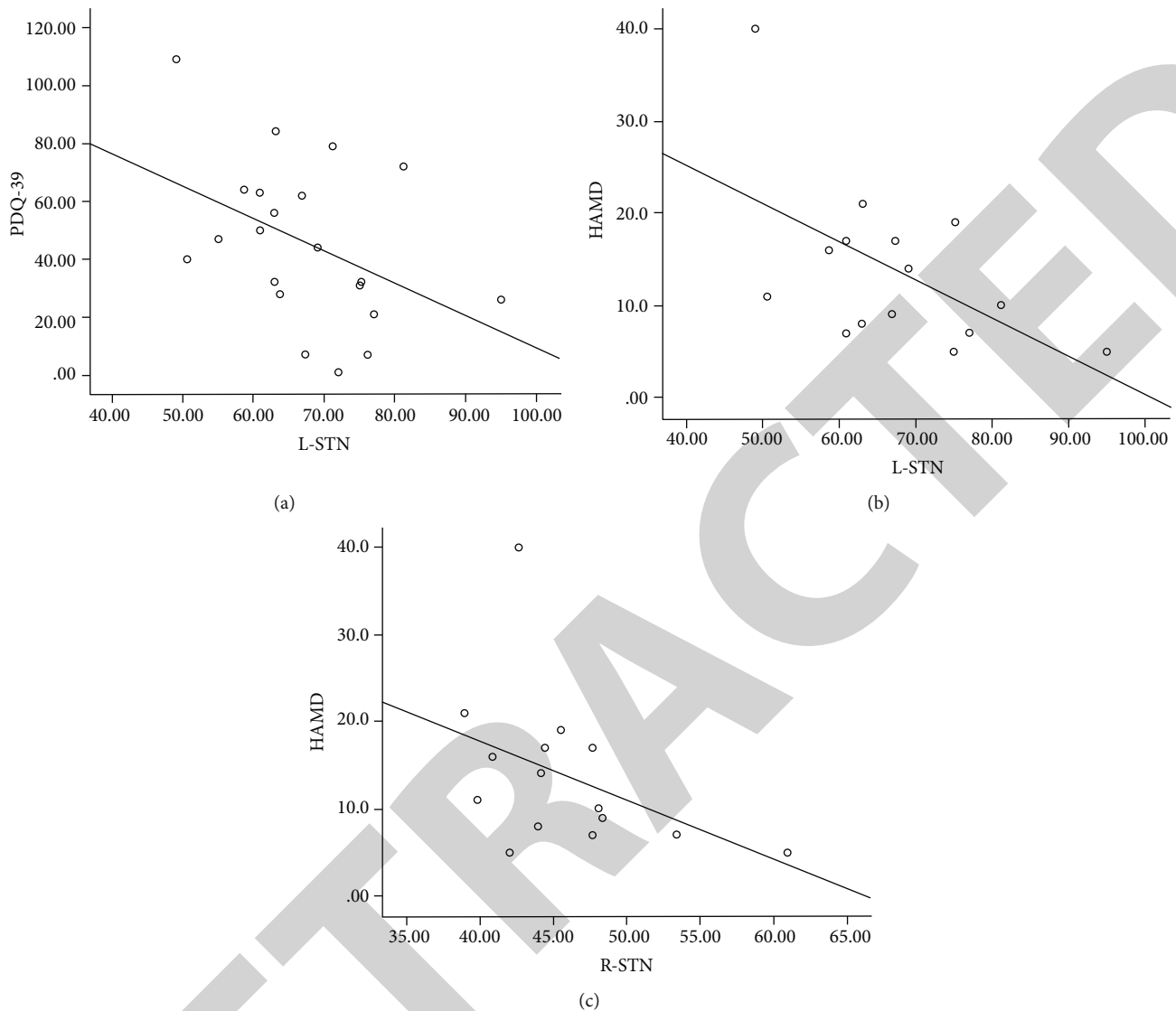


FIGURE 4: Correlation analysis between the STN volume and postoperative clinical measures in PD patients. The left STN (L-STN) volume was negatively correlated with postoperative PDQ-39 (a) and HAMD (b) scores, and the right STN (R-STN) volume was negatively correlated with the HAMD score (c).

patients. Moreover, ICV was positively correlated with the MMSE score ( $r = 0.443$ ,  $p = 0.030$ ). No significant correlations were observed between the left or right STN volume or ICV and med-on/med-off UPDRS III scores (all  $p > 0.05$ ; Figure 3).

In the postoperative assessment, the left STN volume was negatively correlated with quality of life score ( $r = -0.480$ ,  $p = 0.028$ ) and HAMD score ( $r = -0.570$ ,  $p = 0.021$ ); the right STN volume was also negatively correlated with the HAMD score ( $r = -0.534$ ,  $p = 0.033$ ) (Figure 4). There was no significant correlation between the left or right STN volume, ICV, and med-on/DBS-on, med-off/DBS-on, or med-off/DBS-off UPDRS III scores (all  $p > 0.05$ ).

#### 4. Discussion

This study investigated the relationship between the STN volume and duration of PD and pre-/postoperative clinical

measures in order to evaluate the clinical utility of MRI findings in PD patients. We found that the left STN volume was reduced in PD patients, and that the STN volume was negatively correlated with pre- and postoperative quality of life scores. The left STN volume of PD patients in our study was  $70.757 \pm 10.448 \text{ mm}^3$ . A previous study found no statistically significant difference between males and females in terms of the size of the STN, which was determined from length and width measurements [34]; meanwhile, another reported an STN volume of about  $150 \text{ mm}^3$  that was calculated from front-to-back, inside-to-outside, and ventral-to-dorsal distances to the anterior-posterior commissure line [35]. As the STN has a double-lens shape, we think that its volume cannot be accurately determined by applying a geometric algorithm. Additionally, differences in left and right STN volumes have not been previously reported. In the present study, we separately measured left and right STN



volumes as well as the whole brain volume and examined their correlations with clinical measures of PD. The lower left STN volume in PD patients compared to controls may be explained by the fact that 77.9% of our patients (46/59) had disease onset in the right limb, with progressive left limb involvement; moreover, most patients exhibited more severe right limb symptoms.

PD motor symptoms typically manifest on one side of the body and gradually spread to the opposite side, with asymmetric symptom presentation over the course of the disease. Damage to subnuclei of the SN pars compacta is the most important hallmark of PD and leads to dopamine deficiency in the striatum. The loss of dopaminergic input into the striatum results in changes in basal ganglia circuitry; for example, direct inhibitory input to the GPi—the main output nucleus—is decreased while indirect excitatory input is increased, resulting in an overall reduction in thalamic activity and attenuation of cortical excitability. Histopathologic studies have shown that 50%–70% of SN neurons have undergone apoptosis by the time motor symptoms appear. Asymmetric loss of dopaminergic neurons in bilateral SN may explain the symptom asymmetry [5, 36]. Over half of PD patients show obvious differences in UPDRS III scores between the left and right limbs. Studies using fluorine-18-labeled fluorodopa (18F-dopa) positron emission tomography and single-photon emission computed tomography have demonstrated that uptake of the tracer was decreased in the striatum corresponding to the side of the body more severely affected by PD symptoms [37]. A pathologic analysis of 21 cases of PD asymmetry found that neurodegeneration in the SN occurred asymmetrically, with greater neuronal loss on the side contralateral to the initially affected side [36]. It has been suggested that the reduced duration of levodopa response in PD patients with dyskinesia is attributable to decreases in the number of nigrostriatal dopaminergic neuron terminals and in the dopamine storage capacity of the striatum, specifically on the contralateral side. As most patients in our study had right-limb symptom onset, we speculate that there was greater loss of neurons and decreased dopamine storage capacity in the SN and STN on the left side, with a corresponding reduction in the left STN volume [24].

The left STN volume in PD patients was also negatively correlated with pre-/postoperative PDQ-39 scores. The STN is an important structure in the surgical treatment of PD [15, 16]; both the STN and GPi are part of a neural network that includes the frontal striatum and cortical (motor cortex) and subcortical (basal ganglia/thalamus) regions and are part of the indirect and direct pathways, respectively, through the basal ganglia. Stimulation of both regions has been shown to improve PD symptoms [38, 39]. We found that increased neurodegeneration in the left STN of PD patients—as reflected by lower left STN volume—was associated with lower pre- and postoperative quality of life and higher neurocognitive assessment scores. Thus, with progressive disease, patients experienced a decline in life quality and corresponding increase in symptoms of depression; postoperatively, neuropsychological symptoms improved while no change was observed in patient's quality of life.

There were some limitations to this study. Firstly, we did not perform manual segmentation in calculating STN volume from T2W images. In future studies, high-resolution MR images will be acquired for a thinner STN layer (<2 mm), and the accuracy of automatic vs manual segmentation of STN measurements will be compared. Secondly, as each patient had undergone DBS surgery, the HY stage was relatively high in our cohort, and the patients were in the mid-to-late stage of disease; therefore, we did not examine the correlation between HY stage and STN volume.

## 5. Conclusions

In conclusion, the results of this study demonstrate that the left STN volume was reduced in PD patients compared to healthy control subjects. Moreover, the STN volume was negatively correlated with pre- and postoperative PDQ-39 scores. These results indicate that the STN volume is closely associated with the clinical status of PD patients and can serve as a biomarker for evaluating clinical outcome following DBS surgery.

## Data Availability

The data used to support the findings of this study are available from the corresponding author upon request.

## Conflicts of Interest

The authors declare that there is no conflict of interest regarding the publication of this paper.

## References

- [1] M. Gandolfi, C. Geroin, E. Dimitrova et al., “Virtual reality telerehabilitation for postural instability in Parkinson's disease: a multicenter, single-blind, randomized, controlled trial,” *BioMed Research International*, vol. 2017, Article ID 7962826, 11 pages, 2017.
- [2] J. C. Corona, “Natural Compounds for the Management of Parkinson's Disease and Attention- Deficit/Hyperactivity Disorder,” *BioMed research international*, vol. 2018, Article ID 4067597, 12 pages, 2018.
- [3] B. D. Wissel, A. K. Dwivedi, A. Merola et al., “Functional neurological disorders in Parkinson disease,” *Journal of Neurology, Neurosurgery, and Psychiatry*, vol. 89, no. 6, pp. 566–571, 2018.
- [4] W. Deeb, M. S. Okun, and L. Almeida, “Deep brain stimulation for Parkinson disease dementia: a new frontier?,” *JAMA Neurology*, vol. 75, no. 2, pp. 152–153, 2018.
- [5] Z. Zhong, D. Merkitich, M. M. Karaman et al., “High-spatial-resolution diffusion MRI in Parkinson disease: lateral asymmetry of the substantia nigra,” *Radiology*, vol. 291, no. 1, pp. 149–157, 2019.
- [6] R. Martínez-Fernández, A. Kibleur, S. Chabardès et al., “Different effects of levodopa and subthalamic stimulation on emotional conflict in Parkinson's disease,” *Human Brain Mapping*, vol. 39, no. 12, pp. 5014–5027, 2018.
- [7] L. Kahn, M. Mathkour, S. X. Lee et al., “Long-term outcomes of deep brain stimulation in severe Parkinson's disease utilizing UPDRS III and modified Hoehn and Yahr as a severity scale,”

## Retraction

# Retracted: A Prediction Model for Cognitive Impairment Risk in Colorectal Cancer after Chemotherapy Treatment

### BioMed Research International

Received 12 March 2024; Accepted 12 March 2024; Published 20 March 2024

Copyright © 2024 BioMed Research International. This is an open access article distributed under the Creative Commons Attribution License, which permits unrestricted use, distribution, and reproduction in any medium, provided the original work is properly cited.

This article has been retracted by Hindawi following an investigation undertaken by the publisher [1]. This investigation has uncovered evidence of one or more of the following indicators of systematic manipulation of the publication process:

- (1) Discrepancies in scope
- (2) Discrepancies in the description of the research reported
- (3) Discrepancies between the availability of data and the research described
- (4) Inappropriate citations
- (5) Incoherent, meaningless and/or irrelevant content included in the article
- (6) Manipulated or compromised peer review

The presence of these indicators undermines our confidence in the integrity of the article's content and we cannot, therefore, vouch for its reliability. Please note that this notice is intended solely to alert readers that the content of this article is unreliable. We have not investigated whether authors were aware of or involved in the systematic manipulation of the publication process.

Wiley and Hindawi regrets that the usual quality checks did not identify these issues before publication and have since put additional measures in place to safeguard research integrity.

We wish to credit our own Research Integrity and Research Publishing teams and anonymous and named external researchers and research integrity experts for contributing to this investigation.

The corresponding author, as the representative of all authors, has been given the opportunity to register their agreement or disagreement to this retraction. We have kept a record of any response received.

### References

- [1] S.-P. Zhou, S.-D. Fei, H.-H. Han, J.-J. Li, S. Yang, and C.-Y. Zhao, "A Prediction Model for Cognitive Impairment Risk in Colorectal Cancer after Chemotherapy Treatment," *BioMed Research International*, vol. 2021, Article ID 6666453, 13 pages, 2021.

## Research Article

# A Prediction Model for Cognitive Impairment Risk in Colorectal Cancer after Chemotherapy Treatment

Shu-Ping Zhou, Su-Ding Fei , Hui-Hui Han, Jing-Jing Li, Shuang Yang, and Chun-Yang Zhao

Ningbo College of Health Sciences, No. 51, Xuefu Road, Yinzhou, Ningbo 315100, China

Correspondence should be addressed to Su-Ding Fei; [sfdmedicald@126.com](mailto:sfdmedicald@126.com)

Received 30 December 2020; Revised 1 February 2021; Accepted 10 February 2021; Published 20 February 2021

Academic Editor: Yuzhen Xu

Copyright © 2021 Shu-Ping Zhou et al. This is an open access article distributed under the Creative Commons Attribution License, which permits unrestricted use, distribution, and reproduction in any medium, provided the original work is properly cited.

**Background.** A prediction model can be developed to predict the risk of cancer-related cognitive impairment in colorectal cancer patients after chemotherapy. **Methods.** A regression analysis was performed on 386 colorectal cancer patients who had undergone chemotherapy. Three prediction models (random forest, logistic regression, and support vector machine models) were constructed using collected clinical and pathological data of the patients. Calibration and ROC curves and C-indexes were used to evaluate the selected models. A decision curve analysis (DCA) was used to determine the clinical utility of the line graph. **Results.** Three prediction models including a random forest, a logistic regression, and a support vector machine were constructed. The logistic regression model had the strongest predictive power with an area under the curve (AUC) of 0.799. Age, BMI, colostomy, complications, CRA, depression, diabetes, QLQ-C30 score, exercise, hypercholesterolemia, diet, marital status, education level, and pathological stage were included in the nomogram. The C-index (0.826) and calibration curve showed that the nomogram had good predictive ability and the DCA curves indicated that the model had strong clinical utility. **Conclusions.** A prediction model with good predictive ability and practical clinical value can be developed for predicting the risk of cognitive impairment in colorectal cancer after chemotherapy.

## 1. Introduction

Chemotherapy is a common complementary treatment for colorectal cancer. Cancer-related cognitive impairment (CRCI) occurs in cancer patients after chemotherapy [1–5].

The new treatment prolongs the life expectancy of cancer patients while it increases the incidence of CRCI. The National Cancer Institute (NCI) has indicated that CRCI should be thoroughly studied. CRCI has a substantial impact on the postoperative quality of life and the overall prognosis of patients [6, 7]. CRCI makes daily life and rehabilitation care difficult for cancer patients, leading to a reduced quality of life and a shorter life span [8, 9]. Therefore, it is important to explore the potential risk factors associated with the development of CRCI in colon cancer patients after chemotherapy. The knowledge of these potential risk factors can help to improve the overall prognosis of patients.

The development of cognitive impairment in cancer patients is linked to various psychosocial or tumor-related factors [10]. However, there are no systematic assessment tools to predict the risk for CRCI complications in colon cancer patients after chemotherapy [11]. CRCI risk prediction is now possible because of the advancements in computer science and technology [12, 13]. A validated model can be developed to predict the CRCI risk in colorectal patients after chemotherapy. This is based on the existing clinical and epidemiological characteristics of patients who developed cognitive impairment after chemotherapy.

In this study, a predictive model was developed to predict the CRCI risk in colorectal cancer patients after chemotherapy to improve life quality. This model provides a clinical basis for individualized treatment options, especially for individuals at high CRCI risk. In conclusion, this study provides new ideas for improving the quality of life of colorectal cancer patients.

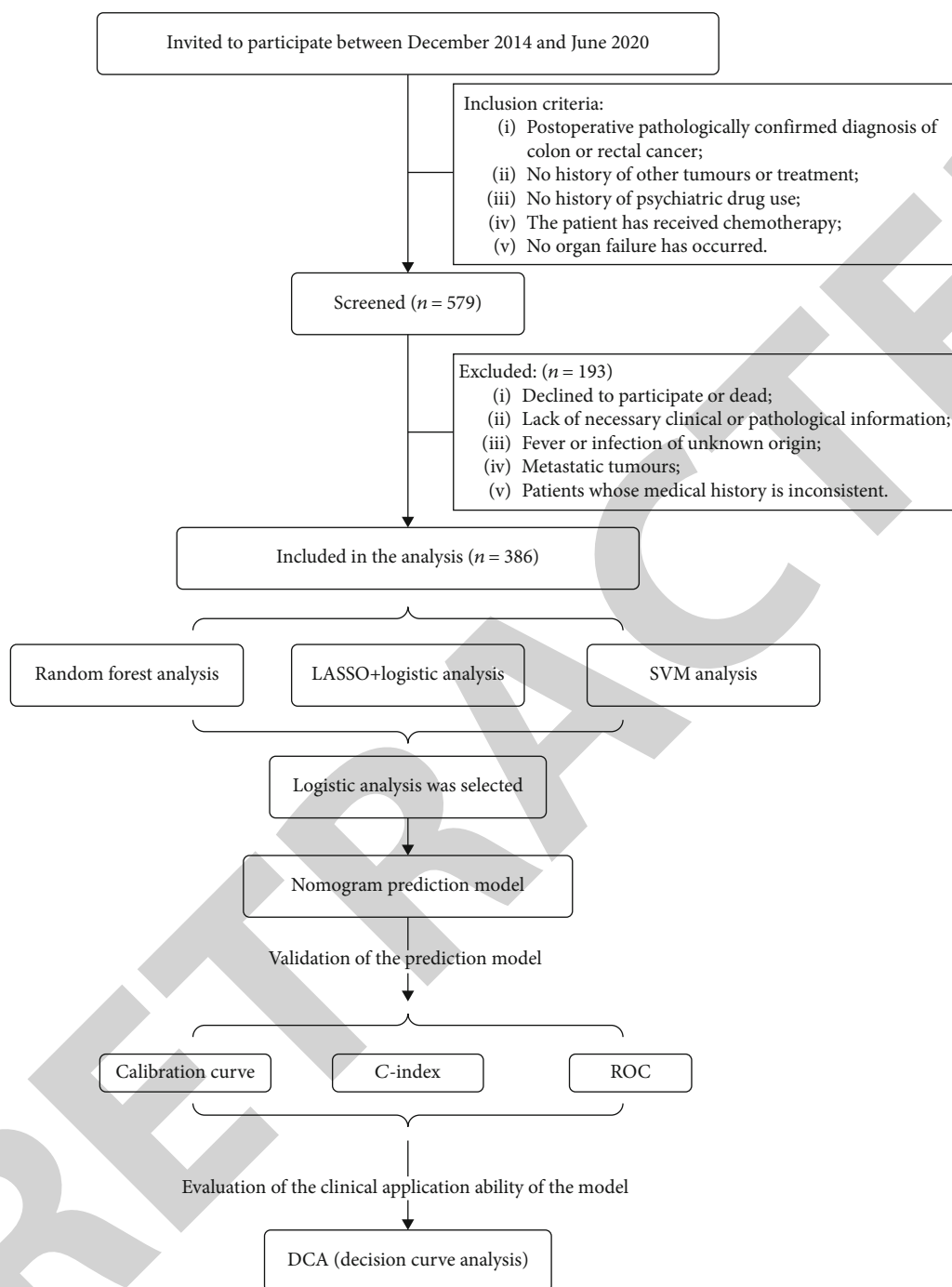


FIGURE 1: Flow chart of the study population.

## 2. Materials and Methods

**2.1. Patients.** Data was collected from 386 patients who underwent surgery and postoperative chemotherapy between June 2016 and August 2020 at Ningbo Medical Center Lihuili Eastern Hospital. A retrospective analysis was then performed, and further questionnaires and follow-ups were conducted using telephone appointments and community follow-ups. The ethics committee of the hospital approved this study, and informed consent was obtained from patients or their families. Inclusion criteria were (1) postoperative

pathologically confirmed diagnosis of colon or rectal cancer, (2) no history of other tumors or treatment, (3) no history of psychiatric drug use, (4) chemotherapy treatment, and (5) no organ failure occurrence. Exclusion criteria were (1) refusal to participate, (2) death during the study, (3) inadequate clinical or pathological information, (4) fever or infection of unknown origin, (5) metastatic tumors, and (6) inconsistent medical history with follow-up information.

**2.2. CRCI or Depression Diagnosis.** Experienced neuropsychologists examined the cognitive function using the Mini-

TABLE 1: Differences of demographic and clinical characteristics between patients with and without CRCL.

Variables	Normal (n = 269)	CRCL (n = 117)	p value
Age	63.30 ± 9.59	68.03 ± 10.44	≤0.001**
BMI	25.76 ± 3.44	24.95 ± 3.04	0.029*
Waist	87.47 ± 9.14	87.32 ± 9.74	0.883
Heart rate	72.78 ± 8.63	73.19 ± 9.72	0.693
Depression			≤0.001**
No	177 (65.80)	55 (47.01)	
Yes	92 (34.20)	62 (52.99)	
Gender			0.088
Female	124 (46.10)	65 (55.56)	
Male	145 (53.90)	52 (44.44)	
Smoking history			0.137
No	192 (71.38)	92 (78.63)	
Yes	77 (28.62)	25 (21.37)	
Education level			0.68
Higher education	66 (24.54)	27 (23.08)	
Primary education or below	100 (37.17)	49 (41.88)	
Secondary education	103 (38.29)	41 (35.04)	
Marital status			0.242
Single or divorce	76 (28.25)	40 (34.18)	
Married	193 (71.75)	77 (65.82)	
Medical insurance			0.701
Commercial insurance payment	46 (17.10)	16 (13.68)	
Social security payments	205 (76.21)	93 (79.49)	
Self-paying	18 (6.69)	8 (6.84)	
Homeplace			0.573
Rural areas	93 (34.57)	37 (31.62)	
Urban areas	176 (65.43)	80 (68.38)	
Per capita monthly household income			0.194
2001-5000 yuan per month	133 (49.44)	60 (51.28)	
<2000 yuan per month	48 (17.84)	28 (23.93)	
>5000 yuan per month	88 (32.71)	29 (24.79)	
Drinking			0.012*
No	196 (72.86)	99 (84.62)	
Yes	73 (27.14)	18 (15.38)	
Diet			0.397
Balanced diet	82 (30.48)	42 (35.90)	
Carnivorous	101 (37.55)	36 (30.77)	
Vegetarian	86 (31.97)	39 (33.33)	
Exercise			≤0.001**
Less than 3 times a week	131 (48.70)	52 (44.44)	
More than 3 times a week	64 (23.79)	6 (5.13)	
No	74 (27.51)	59 (50.43)	
Hypertension			0.733
No	175 (65.06)	74 (63.25)	
Yes	94 (34.94)	43 (36.75)	



TABLE 1: Continued.

Variables	Normal (n = 269)	CRCI (n = 117)	p value
Diabetes			0.043*
No	212 (78.81)	81 (69.23)	
Yes	57 (21.19)	36 (30.77)	
Hypercholesterolemia			0.758
No	154 (57.25)	65 (55.56)	
Yes	115 (42.75)	52 (44.44)	
Pathological stage			0.239
No	125 (46.47)	62 (52.99)	
Yes	144 (53.53)	55 (47.01)	
Colostomy			0.010**
No	235 (87.36)	90 (76.92)	
Yes	34 (12.64)	27 (23.08)	
Tumor location			0.039*
Left hemicolon	67 (24.91)	23 (19.66)	
Rectum	103 (38.29)	50 (42.74)	
Right hemicolon	70 (26.02)	21 (17.95)	
Transverse colon	29 (10.78)	23 (19.66)	
Complications			≤0.001**
No	244 (90.71)	92 (78.63)	
Yes	25 (9.29)	25 (21.37)	
CRA			0.012*
No	53 (19.70)	11 (9.40)	
Yes	216 (80.30)	106 (90.60)	
PSQI	6.65 ± 3.74	7.26 ± 3.22	0.107
Social Impact Scale	62.43 ± 8.25	62.41 ± 7.62	0.985
Total score QLQ-C30	56.67 ± 11.98	55.09 ± 11.98	0.235

Mental State Examination (MMSE) described in previous studies [14, 15]. The MMSE cut-off point for CRCI was similar to those in previous studies [16, 17]. An experienced psychiatrist assessed the depression diagnosis using the HAMD-17 (with good internal consistency and validity) [18, 19]. Depression diagnosis was made when HAMD-17 ≥ 8, and its total score was between 0 and 54 [20, 21].

**2.3. Patient and Clinical Statistical Characteristics.** Clinical information (clinicopathological stage, tumor site origin, colostomy, basal heart rate, history of hypertension and diabetes mellitus, tumor-related anemia, and treatment complications) was collected and confirmed from the patient's medical history and follow-up survey one year after treatment. Patient demographic information including age, gender, height, weight, grip strength, smoking history, education level, marital status, alcohol consumption history, dietary preferences, and exercise frequency was also collected. The anemia status was evaluated using the WHO and American Cancer Institute (NCI) anemia grading criteria. Patients were diagnosed with CRA when their hemoglobin (Hb) was <120 g/L in men and <110 g/L in women.

**2.4. Rating Scale Collection.** The Pittsburgh Sleep Quality Index (PSQI) with a Cronbach factor of 0.805 was used to assess the quality of a patient's sleep [22, 23]. The PSQI scores between 0 and 21 with higher scores indicate poor sleep quality. The Social Impact Scale including social exclusion, economic discrimination, inherent shame, and social isolation measures the patient's stigma [24]. The Chinese EORTC QLQ-C30 consists of 30 items divided into 15 sections. The scale scores range between 30 and 126. The higher the score, the poorer the patient's quality of life. The Chinese EORTC QLQ-C30 had good reliability and validity [25].

**2.5. Statistical Analysis.** All statistical analyses were determined using the R software (version 3.5.3). Patients were randomly divided into the training and validation groups (group ratio 7:3), and three models were selected. The model with the strongest predictive power was selected by calculating their respective AUC values. The stochastic forest model was effective at high latitudes and could quantify the importance of each feature and balance errors in the unbalanced data [26]. Support vector machines were effective in feature selection and the removal of redundant features, especially when dealing with small data [27]. Multiple logistic regression models

TABLE 2: Differences of demographic and clinical characteristics between the training and testing sets.

Variables	Entire cohort (n = 386)	Training set (n = 114)	Testing set (n = 272)	p value
CRCI				
No	269 (69.69)	79 (69.30)	190 (69.85)	0.994
Yes	117 (30.31)	35 (30.70)	82 (30.15)	
Age	64.73 ± 10.8	63.78 ± 9.11	65.13 ± 10.45	0.23
Gender				0.051
Female	189 (48.96)	44 (38.60)	145 (53.31)	
Male	197 (51.04)	70 (61.40)	127 (46.69)	
BMI	25.52 ± 3.34	25.70 ± 3.43	25.44 ± 3.31	0.49
Waist	87.42 ± 9.31	87.13 ± 9.94	87.54 ± 9.05	0.692
Heart rate	72.90 ± 8.96	71.91 ± 9.08	73.32 ± 8.90	0.161
Smoking history				0.08
No	284 (73.58)	75 (65.79)	209 (76.84)	
Yes	102 (26.42)	39 (34.21)	63 (23.16)	
Education level				0.465
Higher education	93 (24.09)	29 (25.44)	64 (23.53)	
Primary education or below	149 (38.60)	36 (31.58)	113 (41.54)	
Secondary education	144 (37.31)	49 (42.98)	95 (34.93)	
Marital status				0.73
Single or divorce	116 (30.05)	31 (27.19)	85 (31.25)	
Married	270 (69.95)	83 (72.81)	187 (68.75)	
Medical insurance				0.444
Commercial insurance payment	62 (16.06)	17 (14.91)	45 (16.54)	
Social security payments	298 (77.20)	85 (74.56)	213 (78.31)	
Self-paying	26 (6.74)	12 (10.53)	14 (5.15)	
Homeplace				0.947
Rural areas	130 (33.68)	37 (32.46)	93 (34.19)	
Urban areas	256 (66.32)	77 (67.54)	179 (65.81)	
Per capita monthly household income				0.961
2001-5000 yuan per month	193 (50.00)	60 (52.63)	133 (48.90)	
<2000 yuan per month	76 (19.69)	20 (17.54)	56 (20.59)	
>5000 yuan per month	117 (30.31)	34 (29.82)	83 (30.51)	
Depression				0.945
No	232 (60.10)	70 (61.40)	162 (59.56)	
Yes	154 (39.90)	44 (38.60)	110 (40.44)	
Drinking				0.556
No	295 (76.42)	83 (72.81)	212 (77.94)	
Yes	91 (23.58)	31 (27.19)	60 (22.06)	
Diet				0.576
Balanced diet	124 (32.12)	37 (32.46)	87 (31.99)	
Carnivorous	137 (35.49)	34 (29.82)	103 (37.87)	
Vegetarian	125 (32.38)	43 (37.72)	82 (30.15)	
Exercise				0.27
Less than 3 times a week	183 (47.41)	44 (38.60)	139 (51.10)	
More than 3 times a week	70 (18.13)	23 (20.18)	47 (17.28)	
No	133 (34.46)	47 (41.23)	86 (31.62)	

TABLE 2: Continued.

Variables	Entire cohort (n = 386)	Training set (n = 114)	Testing set (n = 272)	p value
Diabetes				0.507
No	293 (75.91)	91 (79.82)	202 (74.26)	
Yes	93 (24.09)	23 (20.18)	70 (25.74)	
Hypertension				0.992
No	249 (64.51)	73 (64.04)	176 (64.71)	
Yes	137 (35.49)	41 (35.96)	96 (35.29)	
Hypercholesterolemia				0.441
No	219 (56.74)	59 (51.75)	160 (58.82)	
Yes	167 (43.26)	55 (48.25)	112 (41.18)	
Pathological stage				0.771
No	187 (48.45)	52 (45.61)	135 (49.63)	
Yes	199 (51.55)	62 (54.39)	137 (50.37)	
Colostomy				0.953
No	325 (84.20)	97 (85.09)	228 (83.82)	
Yes	61 (15.80)	17 (14.91)	44 (16.18)	
CRA				0.649
No	64 (16.58)	22 (19.30)	42 (15.44)	
Yes	322 (83.42)	92 (80.70)	230 (84.56)	
Complications				0.655
No	336 (87.05)	102 (89.47)	234 (86.03)	
Yes	50 (12.95)	12 (10.53)	38 (13.97)	
Tumor location				1
Left hemicolon	90 (23.32)	27 (23.68)	63 (23.16)	
Rectum	153 (39.64)	44 (38.60)	109 (40.07)	
Right hemicolon	91 (23.58)	27 (23.68)	64 (23.53)	
Transverse colon	52 (13.47)	16 (14.04)	36 (13.24)	
PSQI	6.83 ± 3.60	6.65 ± 3.64	6.91 ± 3.58	0.514
Social Impact Scale	62.42 ± 8.06	63.61 ± 8.53	61.92 ± 7.81	0.06
Total score QLQ-C30	56.20 ± 11.98	55.61 ± 12.19	56.44 ± 11.91	0.533

are common and were also included. LASSO analysis was incorporated for dimensional reduction to filter the most suitable predictors to prevent overfitting [28]. The aim of this step was to select the core variables. LASSO regression has more advantages than ridge regression in terms of variable selection. Therefore, we choose LASSO regression to filter the variables as reported in a previous study [29]. ROC curves were used for visualization of AUC values to assess the accuracy of the model [30]. For models with high AUC values, the calibration curve and C-index were used to assess their predictive power further [31, 32]. Finally, the DCA curve was used to assess the clinical applicability of the model [33]. A *p* value less than 0.05 was considered statistically significant. A one-way ANOVA or two-tailed *t*-test was used to determine the significance between groups.

### 3. Result

**3.1. Demographic and Clinical Characteristics.** Figure 1 illustrates the study flow. Clinical information of 386 colorectal

cancer patients (189 women and 269 men) after chemotherapy treatment followed up between December 2014 and June 2020 was assessed. Patients were grouped into either the normal group (*n* = 269) or the CRCI group (*n* = 117). The differences in demographic and clinical characteristics between the CRCI and non-CRCI patients are shown in Table 1. Age, BMI, depression, alcohol consumption history, exercise frequency, diabetes history, colostomy, primary tumor focus, comorbidities, and CRA occurrence were statistically different between the CRCI and normal groups (*p* > 0.05).

**3.2. Predictive Model Selection and Predictor Screening.** Patients were randomly divided into the training and validation groups (group ratio 7:3), as shown in Table 2. Three models were selected, and the model with the strongest predictive power was finally obtained by calculating their respective AUC values. The stochastic forest model was constructed using important values for each factor (Figure 2(a)). The random forest model had an AUC value of 0.73 indicating that its predictive power should be improved. Model overfitting

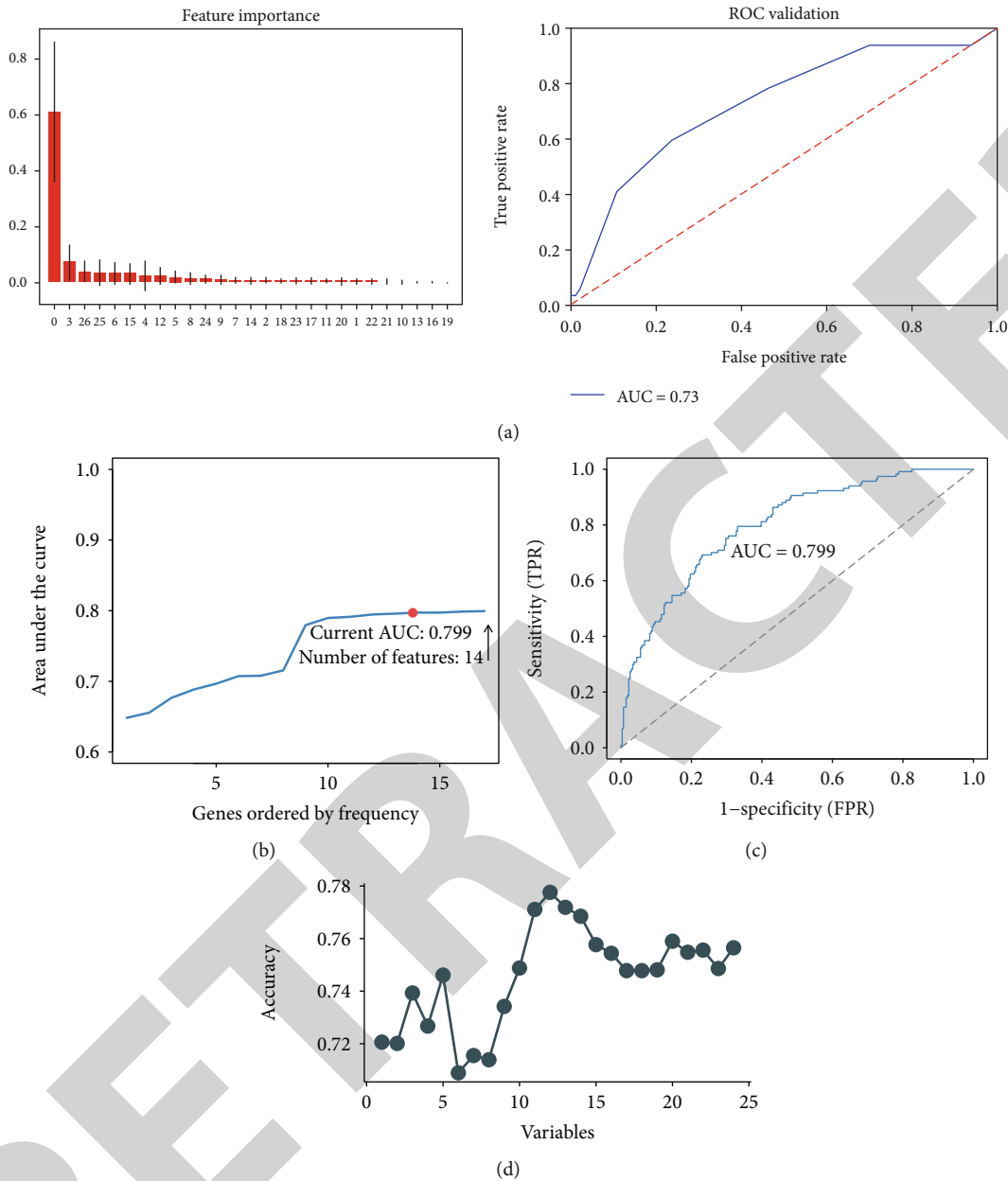


FIGURE 2: Predictive model selection and predictor screening. (a) The random forest model. The graph on the left shows the importance of each factor in the random forest model, and the ROC curve demonstrates the accuracy of the random forest model (AUC = 0.730). (b, c) LASSO analysis conducted 1000 times. The factors were included in the logistic regression model to obtain a pattern diagram of the AUC for the number of occurrences. The model with 14 predictors had good predictive power (AUC = 0.799). (d) A prediction model developed using the SVM method with the highest prediction accuracy when 13 predictive factors are included (AUC = 0.7719).

occurs in machine learning. The least absolute shrinkage and selection operator (LASSO) was used to reduce the number of features further to prevent model overfitting. The LASSO method is not effective in providing the same predictors each time. In this study, 1000 random LASSO regression analyses were conducted. These predictors were sequentially included in the logistic model according to the number of occurrences of the predictor. The final results suggested that the model had the most effective predictive ability when 14 predictors were included (AUC = 0.799) (Figure 2(b)). Support vector machine (SVM) models were more effective in selecting rele-

vant features and removing redundant features than linear analysis. SVM models were also used to construct predictive models (Figure 2(c)) and had the strongest predictive accuracy (AUC = 0.7719) with 13 predictive factors. In summary, the LASSO-based logistic prediction model has the strongest predictive power for the CRCI risk in colorectal cancer patients after chemotherapy.

3.3. *Building Visual Predictive Models.* A visual nomogram prediction model based on a logistic model was developed to predict the CRCI risk in colorectal cancer patients after

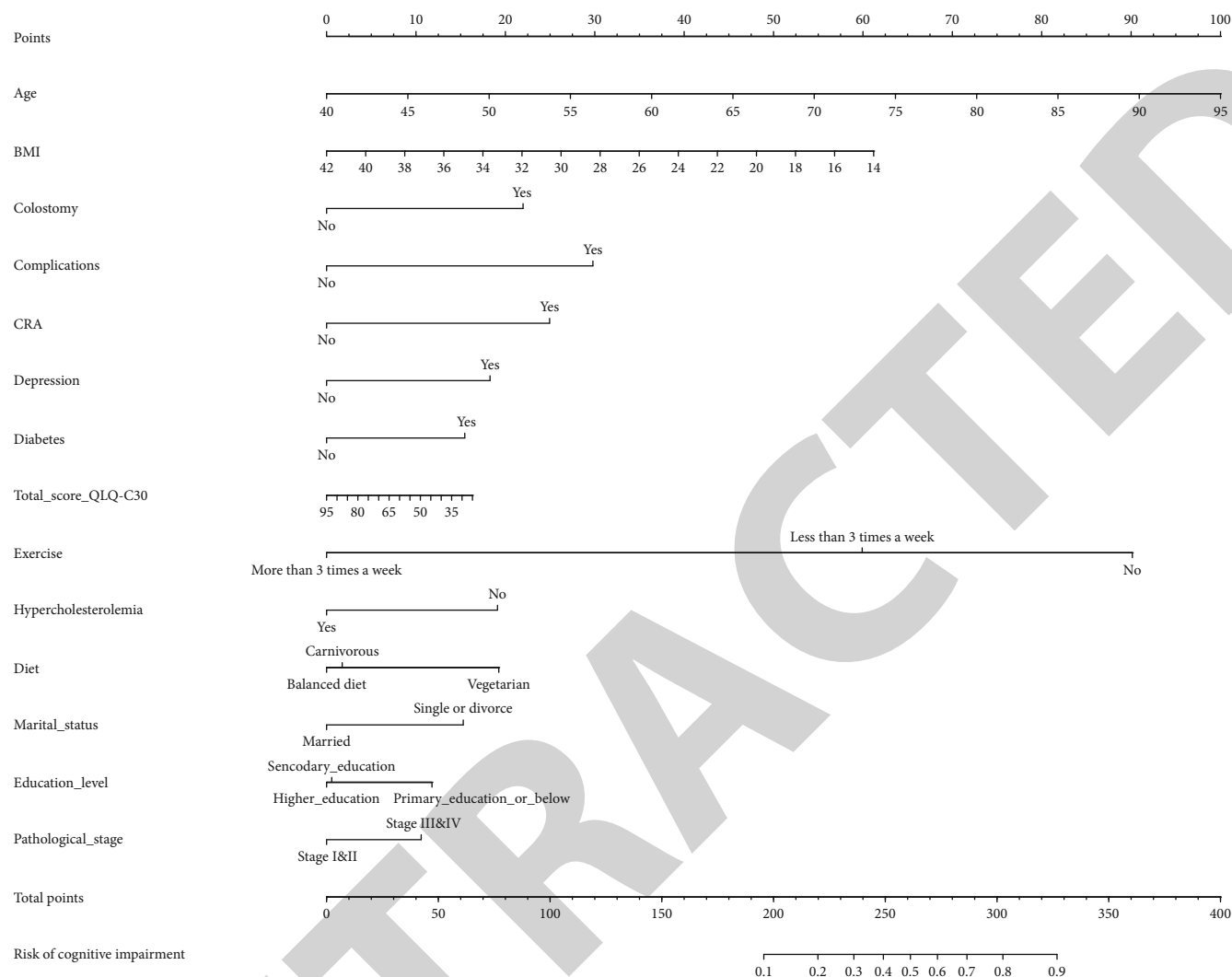


FIGURE 3: Building visual predictive models. Nomogram prediction model for CRCI risk in colorectal cancer patients after chemotherapy. Note the 14 factors including age, BMI, colostomy, complications, CRA, depression, diabetes, QLQ-C30 score, exercise, hypercholesterolemia, diet, marital status, education level, and pathological stage.

chemotherapy (Figure 3, Table 3). Age, BMI, colostomy, complications, CRA, depression, diabetes, QLQ-C30 score, exercise, hypercholesterolemia, diet, marital status, education level, and pathological stage were the 14 predictive factors.

**3.4. Nomogram Prediction Model Validation.** The nomogram calibration curves showed good concordance, indicating that the model can be used to predict CRCI risk in colorectal cancer patients after chemotherapy (Figure 4(a)). Furthermore, the *C*-index was high in both the training and test groups, scoring 0.826 (95% CI, 0.774-0.877), 0.734 (95% CI, 0.633-0.835), and 0.796 (95% CI, 0.750-0.842), respectively (Table 4). An AUC value of 0.796 was achieved in the overall sample, 0.826 in the training group, and 0.734 in the test group (Figure 4(b)).

**3.5. Clinical Application Evaluation.** The nomogram results are shown in Figure 5. Findings showed that the decision curve using the nomogram prediction model had better clin-

ical decision-making. The DCA revealed that when the threshold probability of a patient and doctor is 0% and 78%, respectively, in the entire cohort, using this nomogram provides additional benefits as reported previously [34]. Therefore, the model can predict CRCI risk in colorectal cancer patients after chemotherapy at an early stage. This can promote early clinical intervention, thus supporting personalized postoperative cancer rehabilitation.

## 4. Discussion

In this study, a LASSO regression model was used to obtain the most dominant factors influencing prognosis. The LASSO regression model had the most effective predictive power when the number of major predictors was screened down from 28 to 14. The predictive factors included age, BMI, colostomy, complications, CRA, depression, diabetes, QLQ-C30 score, exercise, hypercholesterolemia, diet, marital status, education level, and pathological stage. A risk



TABLE 3: Prediction factors for CRCI.

Variables	$\beta$	Prediction model Odds ratio (95% CI)	<i>p</i> value
Intercept	-2.316	0.099 (0.003-2.904)	0.181
Age	0.061	1.063 (1.034-1.094)	$\leq 0.001$
BMI	-0.073	0.929 (0.857-1.005)	0.072
Colostomy (yes)	0.736	2.088 (1.026-4.262)	0.042
Complications (yes)	0.998	2.712 (1.273-5.838)	0.010
CRA (yes)	0.835	2.306 (1.108-5.182)	0.032
Depression (yes)	0.612	1.845 (1.026-3.34)	0.041
Diabetes (yes)	0.518	1.678 (0.92-3.054)	0.090
Total score QLQ-C30	-0.008	0.992 (0.969-1.016)	0.517
Exercise			
Less than 3 times a week	-1.012	0.363 (0.202-0.643)	$\leq 0.001$
More than 3 times a week	-3.019	0.049 (0.015-0.132)	$\leq 0.001$
Hypercholesterolemia (yes)	-0.640	0.527 (0.285-0.955)	0.038
Diet			
Balanced	-0.645	0.525 (0.268-1.015)	0.057
Carnivorous	-0.587	0.556 (0.265-1.148)	0.116
Marital status (single or divorce)	0.512	1.669 (0.933-3.044)	0.089
Education level			
Secondary education	-0.375	0.687 (0.374-1.25)	0.221
Higher education	-0.395	0.674 (0.336-1.331)	0.259
Pathological stage (stage I&II)	-0.354	0.702 (0.416-1.176)	0.180

Note:  $\beta$  is the regression coefficient.

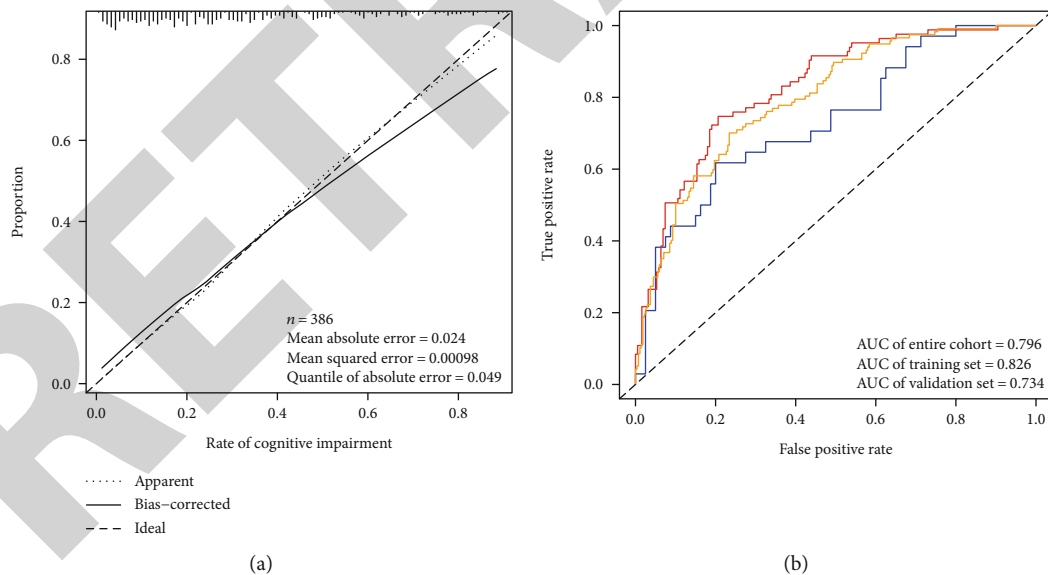


FIGURE 4: Nomogram prediction model validation. (a) Calibration curve of a model for predicting CRCI risk in colorectal cancer patients after chemotherapy. The closer combination of the solid and dashed lines indicates better predictive power. The predictive power of the model is shown using the ROC curve. (b) The AUC values for the training group (red), the test group (blue), and the encore cohort (orange) were 0.826, 0.734, and 0.796, respectively.

prediction model was developed using these predictors to predict CRCI occurrence in colorectal cancer patients after chemotherapy. The test group was used to further evaluate the predictive model, and it was found to have good predictive ability and excellent performance in clinical

decision-making. Therefore, this model can predict CRCI risk in colorectal cancer patients after chemotherapy at an early stage. This can facilitate early clinical intervention, thus improving the long-term prognosis of colorectal cancer patients.

TABLE 4: C-index of the nomogram prediction model.

Dataset group	C-index of the prediction model	
	C-index	The C-index (95% CI)
Training set	0.826	0.774-0.877
Validation set	0.734	0.633-0.835
Entire cohort	0.796	0.750-0.842

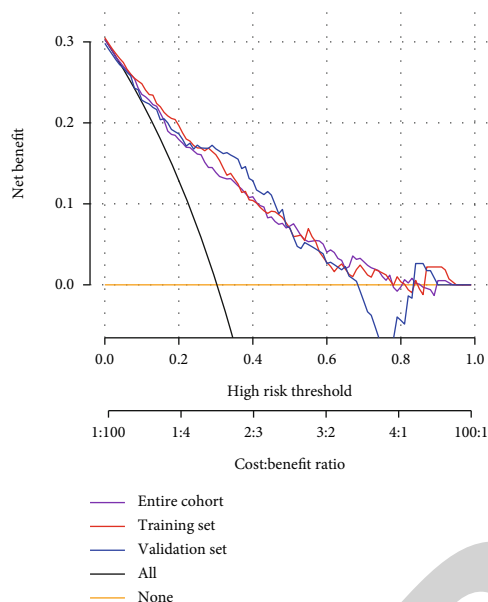


FIGURE 5: Clinical application evaluation. The DCA curve for this predictive model shows the decision analysis for the entire cohort, the training set, and the validation set.

Cognitive impairment is a transitional state from normal aging to dementia with 80% having dementia after six years [35]. The onset of Alzheimer's disease can be delayed if patients are intervened in the early cognitive impairment stages [36]. Therefore, research is necessary for efficiently diagnosing early AD patients and identifying prodromal AD stages. Nomogram prediction models have been widely used for disease-related prognostic analysis. The analytical results are visualized, greatly increasing the prediction accuracy and making them more suitable for clinical decision-making [37]. A nomogram prediction model was used to predict CRCI risk in colorectal cancer patients after chemotherapy. Three models were selected, and a nomogram prediction model based on logistic analysis was finally obtained by calculating their respective AUC values. In conclusion, this study establishes and validates a predictive model for predicting CRCI risk in colorectal cancer patients after chemotherapy. Some predictors in this study are related to CRCI risk in cancer patients. Cancer and cognitive impairment often coexist in old age. The burden of cancer and its treatment can lead to cognitive impairment [11]. There is a significant correlation between age and CRCI occurrence. Studies have found that overweight and high BMI are associated with a reduced risk of cognitive impairment in Chinese elderly people [38, 39]. Diabetes has also been identified as a possible

risk factor for CIRC [40]. Previous studies have identified hypercholesterolemia as a vascular risk marker for injury recognition, and it has also been incorporated into the CRCI risk prediction model [41]. Patients with familial hypercholesterolemia (who experience cognitive impairment between 14 and 40 years) tend to develop mild cognitive impairment at 50 years [42]. A recent meta-analysis suggested that physical activity improves cognition in patients with mild cognitive impairment or dementia [43]. Several studies have also identified the positive impact of the Mediterranean diet on patients with cognitive impairment [44]. Therefore, physical exercise and a balanced diet are essential for early cancer recovery. Patients with a higher level of education show better compliance and recognize the importance of a healthy lifestyle in their recovery. Therefore, clinical education improves patients' perceptions of the disease [45]. Intensive clinical education can reduce CRCI risk in patients.

Colostomies are also associated with cognitive impairment. Many patients require a colostomy after colon surgery. However, a stoma can have a serious impact on a colon cancer patient's diet, quality of life, and physical and mental well-being [46]. Surgical injury and treatment-related complications are key risk factors for cognitive impairment. Systemic inflammatory response activation damages the central nervous system [47]. Colorectal cancer and disease-related treatments (surgery, chemotherapy, etc.) contribute to cancer-related anemia. Studies have demonstrated that chronic anemia causes cognitive impairment regardless of age, kidney function, and HbA1c levels [48].

A good marriage can prevent cognitive impairment but is easily overlooked. Older people who are divorced or widowed are vulnerable to symptoms associated with cognitive impairment [49]. Therefore, postchemotherapy cancer patients' mental health should be taken into account, helping them face their new life with a more positive and optimistic attitude and increase their awareness of the disease and treatment [50]. The patient's family and friends should also provide social support, thus improving their psychological condition [51].

This nomogram prediction model provides a basis for further research on CRCI risk in colorectal cancer patients after chemotherapy. Moreover, cognitive impairment biomarkers, cognitive evaluation, demographic data, clinicopathological characteristics, positron emission tomography data, functional magnetic resonance imaging, cerebrospinal fluid examination, and other data components should be added to the multimodal database for future studies. With the increase of sample size, the model would be further optimized. Further multicenter research should be supplemented to expand cooperation. The sample size of the study data should be increased to obtain a more accurate and stable predictive model for CRCI risk. Finally, further application of this predictive model may need to be adapted to clinical reality. In summary, a new predictive model has been developed to predict CRCI risk in colorectal cancer patients after chemotherapy. The model suggests that advanced age, colostomy, postoperative complications, diabetes, hyperlipidemia, divorce status, lower education, and the later pathological stage could be the risk factors for

CRCI in colorectal cancer patients after chemotherapy. This study suggests that a balanced diet, adequate physical activity, and well-controlled diabetes are essential for cognitive maintenance in elderly patients. Mental health during the patient's illness should also be taken into account. The patient's social identity also needs to be promoted to reduce the risk of depression and CRCI.

## 5. Conclusion

In conclusion, a predictive model with a high degree of accuracy can be developed and validated to predict the CRCI risk in colorectal cancer patients after chemotherapy. The model provides a clinical rationale for individualized treatment options by identifying individuals' CRCI risk. It also provides new ideas for improving the quality of life of colorectal cancer patients.

## Abbreviations

CRA:	Cancer-related anemia
CRCI:	Cancer-related cognitive impairment
DCA:	Decision curve analysis
LASSO:	Least absolute shrinkage and selection operator
ROC:	Receiver operating characteristic curve
HAMD-17:	The 17-item HAMD
PCA:	Principal component analysis
PSQI:	Pittsburgh Sleep Quality Index
QLQ-C30:	European Organization for Research and Treatment Cancer Quality of Life Department C30
SIS:	Social Impact Scale
SVM:	Support vector machine
SSRS:	Social Support Rate Scale.

## Data Availability

The datasets generated and analyzed during the present study are available from the corresponding author on reasonable request.

## Conflicts of Interest

The authors declare that they have no conflict of interest.

## References

- [1] M. Lange, F. Joly, J. Vardy et al., "Cancer-related cognitive impairment: an update on state of the art, detection, and management strategies in cancer survivors," *Annals of Oncology*, vol. 30, no. 12, pp. 1925–1940, 2019.
- [2] F. Joly, B. Giffard, O. Rigal et al., "Impact of cancer and its treatments on cognitive function: advances in research from the Paris International Cognition and Cancer Task Force symposium and update since 2012," *Journal of Pain and Symptom Management*, vol. 50, no. 6, pp. 830–841, 2015.
- [3] T. A. Ahles, J. C. Root, and E. L. Ryan, "Cancer- and cancer treatment-associated cognitive change: an update on the state of the science," *Journal of Clinical Oncology*, vol. 30, no. 30, pp. 3675–3686, 2012.
- [4] S. Deprez, S. R. Kesler, A. J. Saykin, D. H. S. Silverman, M. B. de Ruyter, and B. C. McDonald, "International Cognition and Cancer Task Force recommendations for neuroimaging methods in the study of cognitive impairment in non-CNS cancer patients," *Journal of the National Cancer Institute*, vol. 110, no. 3, pp. 223–231, 2018.
- [5] J. S. Wefel, J. Vardy, T. Ahles, and S. B. Schagen, "International Cognition and Cancer Task Force recommendations to harmonise studies of cognitive function in patients with cancer," *The Lancet Oncology*, vol. 12, no. 7, pp. 703–708, 2011.
- [6] C. J. Nelson, J. S. Lee, M. C. Gamboa, and A. J. Roth, "Cognitive effects of hormone therapy in men with prostate cancer: a review," *Cancer*, vol. 113, no. 5, pp. 1097–1106, 2008.
- [7] L. M. Wu, M. A. Diefenbach, W. A. Gordon, J. B. Cantor, and M. M. Cherrier, "Cognitive problems in patients on androgen deprivation therapy: a qualitative pilot study," *Urologic Oncology*, vol. 31, no. 8, pp. 1533–1538, 2013.
- [8] K. P. Loh, M. C. Janelins, S. G. Mohile et al., "Chemotherapy-related cognitive impairment in older patients with cancer," *Journal of Geriatric Oncology*, vol. 7, no. 4, pp. 270–280, 2016.
- [9] J. Steinmetz, K. B. Christensen, T. Lund, N. Lohse, L. S. Rasmussen, and the ISPOCD Group, "Long-term consequences of postoperative cognitive dysfunction," *Anesthesiology*, vol. 110, no. 3, pp. 548–555, 2009.
- [10] C. J. Treanor, J. Li, and M. Donnelly, "Cognitive impairment among prostate cancer patients: an overview of reviews," *European Journal of Cancer Care*, vol. 26, no. 6, 2017.
- [11] J. Snaedal, "Does my older cancer patient have cognitive impairment?," *Journal of Geriatric Oncology*, vol. 9, no. 3, pp. 183–185, 2018.
- [12] N. Yamanakkanavar, J. Y. Choi, and B. Lee, "MRI segmentation and classification of human brain using deep learning for diagnosis of Alzheimer's disease: a survey," *Sensors*, vol. 20, no. 11, p. 3243, 2020.
- [13] Y. S. Chen, Y. X. Cai, X. R. Kang et al., "Predicting the risk of sarcopenia in elderly patients with patellar fracture: development and assessment of a new predictive nomogram," *PeerJ*, vol. 8, article e8793, 2020.
- [14] R. W. Elwood, "The Wechsler Memory Scale-Revised: psychometric characteristics and clinical application," *Neuropsychology Review*, vol. 2, no. 2, pp. 179–201, 1991.
- [15] C. P. Hughes, L. Berg, W. L. Danziger, L. A. Coben, and R. L. Martin, "A new clinical scale for the staging of dementia," *The British Journal of Psychiatry*, vol. 140, no. 6, pp. 566–572, 1982.
- [16] Y. Shimizu, N. Sawada, M. Iwasaki et al., "Reproductive history and risk of cognitive impairment in Japanese women," *Maturitas*, vol. 128, pp. 22–28, 2019.
- [17] M. Sugishita, Y. Koshizuka, S. Sudou et al., "The validity and reliability of the Japanese version of the Mini-Mental State Examination (MMSE-J) with the original procedure of the attention and calculation task (2000)," *Japanese Journal of Cognitive Neuroscience*, vol. 20, pp. 91–110, 2018.
- [18] M. Hamilton, "Development of a rating scale for primary depressive illness," *The British Journal of Social and Clinical Psychology*, vol. 6, no. 4, pp. 278–296, 1967.
- [19] A. J. Rush, M. H. Trivedi, H. M. Ibrahim et al., "The 16-item Quick Inventory of Depressive Symptomatology (QIDS), clinician rating (QIDS-C), and self-report (QIDS-SR): a psychometric evaluation in patients with chronic major depression," *Biological Psychiatry*, vol. 54, no. 5, pp. 573–583, 2003.

- [20] E. Frank, R. F. Prien, R. B. Jarrett et al., "Conceptualization and rationale for consensus definitions of terms in major depressive disorder. Remission, recovery, relapse, and recurrence," *Archives of General Psychiatry*, vol. 48, no. 9, pp. 851–855, 1991.
- [21] Y. Jia, W. Zhang, S. You, M. Li, L. Lei, and L. Chen, "A nomogram for predicting depression in patients with hepatocellular carcinoma: an observational cross-sectional study," *International Journal of Psychiatry in Clinical Practice*, vol. 23, no. 4, pp. 273–280, 2019.
- [22] D. J. Buysse, C. F. Reynolds 3rd, T. H. Monk, S. R. Berman, and D. J. Kupfer, "The Pittsburgh Sleep Quality Index: a new instrument for psychiatric practice and research," *Psychiatry Research*, vol. 28, no. 2, pp. 193–213, 1989.
- [23] F. Hita-Contreras, E. Martínez-López, P. A. Latorre-Román, F. Garrido, M. A. Santos, and A. Martínez-Amat, "Reliability and validity of the Spanish version of the Pittsburgh Sleep Quality Index (PSQI) in patients with fibromyalgia," *Rheumatology International*, vol. 34, no. 7, pp. 929–936, 2014.
- [24] A. W. Pan, L. Chung, B. L. Fife, and P. C. Hsiung, "Evaluation of the psychometrics of the Social Impact Scale: a measure of stigmatization," *International Journal of Rehabilitation Research*, vol. 30, no. 3, pp. 235–238, 2007.
- [25] T. J. GY, C. Pan, Z. Kai, and Z. Lei, "Evaluation of the Chinese version of EORTCQLQ-C30, QLQ-BN20 for brain tumor patients," *Journal of Nurses Training*, vol. 35, pp. 90–94, 2020.
- [26] R. T. Buxton, M. F. McKenna, M. Clapp et al., "Efficacy of extracting indices from large-scale acoustic recordings to monitor biodiversity," *Conservation Biology*, vol. 32, no. 5, pp. 1174–1184, 2018.
- [27] M. L. Huang, Y. H. Hung, W. M. Lee, R. K. Li, and B. R. Jiang, "SVM-RFE based feature selection and Taguchi parameters optimization for multiclass SVM classifier," *ScientificWorldJournal*, vol. 2014, article 795624, 2014.
- [28] A. C. Kidd, M. McGettrick, S. Tsim, D. L. Halligan, M. Bylesjo, and K. G. Blyth, "Survival prediction in mesothelioma using a scalable Lasso regression model: instructions for use and initial performance using clinical predictors," *BMJ Open Respiratory Research*, vol. 5, no. 1, article e000240, 2018.
- [29] Y. Wang, Z. J. Zhao, X. R. Kang et al., "lncRNA DLEU2 acts as a miR-181a sponge to regulate SEPP1 and inhibit skeletal muscle differentiation and regeneration," *Aging*, vol. 12, no. 23, pp. 24033–24056, 2020.
- [30] F. E. Harrell Jr., K. L. Lee, R. M. Califf, D. B. Pryor, and R. A. Rosati, "Regression modelling strategies for improved prognostic prediction," *Statistics in Medicine*, vol. 3, no. 2, pp. 143–152, 1984.
- [31] A. A. Kramer and J. E. Zimmerman, "Assessing the calibration of mortality benchmarks in critical care: the Hosmer-Lemeshow test revisited," *Critical Care Medicine*, vol. 35, no. 9, pp. 2052–2056, 2007.
- [32] M. J. Pencina and R. B. D'Agostino, "Overall C as a measure of discrimination in survival analysis: model specific population value and confidence interval estimation," *Statistics in Medicine*, vol. 23, no. 13, pp. 2109–2123, 2004.
- [33] E. W. Steyerberg and Y. Vergouwe, "Towards better clinical prediction models: seven steps for development and an ABCD for validation," *European Heart Journal*, vol. 35, no. 29, pp. 1925–1931, 2014.
- [34] H. Wang, L. Zhang, Z. Liu et al., "Predicting medication non-adherence risk in a Chinese inflammatory rheumatic disease population: development and assessment of a new predictive nomogram," *Patient Preference and Adherence*, vol. 12, pp. 1757–1765, 2018.
- [35] "2015 Alzheimer's disease facts and figures," *Alzheimer's & Dementia*, vol. 11, no. 3, pp. 332–384, 2015.
- [36] "2014 Alzheimer's disease facts and figures," *Alzheimer's Dementia*, vol. 10, no. 2, pp. e47–e92, 2014.
- [37] L. Wei, S. Champman, X. Li et al., "Beliefs about medicines and non-adherence in patients with stroke, diabetes mellitus and rheumatoid arthritis: a cross-sectional study in China," *BMJ Open*, vol. 7, no. 10, article e017293, 2017.
- [38] Q. Hou, Y. Guan, W. Yu et al., "Associations between obesity and cognitive impairment in the Chinese elderly: an observational study," *Clinical Interventions in Aging*, vol. 14, pp. 367–373, 2019.
- [39] T. Santos, L. C. Fonseca, G. Tedrus, and J. L. Delbue, "Alzheimer's disease: nutritional status and cognitive aspects associated with disease severity," *Nutrición Hospitalaria*, vol. 35, no. 6, pp. 1298–1304, 2018.
- [40] N. Mallorquí-Bagué, M. Lozano-Madrid, E. Toledo et al., "Type 2 diabetes and cognitive impairment in an older population with overweight or obesity and metabolic syndrome: baseline cross-sectional analysis of the PREDIMED-plus study," *Scientific Reports*, vol. 8, no. 1, p. 16128, 2018.
- [41] P. B. Gorelick, A. Scuteri, S. E. Black et al., "Vascular contributions to cognitive impairment and dementia: a statement for healthcare professionals from the American Heart Association/American Stroke Association," *Stroke*, vol. 42, no. 9, pp. 2672–2713, 2011.
- [42] B. M. Suárez, "Psychological issues and cognitive impairment in adults with familial hypercholesterolemia," *Family Practice*, vol. 34, no. 5, pp. 520–524, 2017.
- [43] E. G. A. Karssemeijer, J. A. Aaronson, W. J. Bossers, T. Smits, M. G. M. Olde Rikkert, and R. P. C. Kessels, "Positive effects of combined cognitive and physical exercise training on cognitive function in older adults with mild cognitive impairment or dementia: a meta-analysis," *Ageing Research Reviews*, vol. 40, pp. 75–83, 2017.
- [44] B. Singh, A. K. Parsaik, M. M. Mielke et al., "Association of Mediterranean diet with mild cognitive impairment and Alzheimer's disease: a systematic review and meta-analysis," *Journal of Alzheimer's Disease*, vol. 39, no. 2, pp. 271–282, 2014.
- [45] N. Matyas, F. Keser Aschenberger, G. Wagner et al., "Continuing education for the prevention of mild cognitive impairment and Alzheimer's-type dementia: a systematic review and overview of systematic reviews," *BMJ Open*, vol. 9, no. 7, article e027719, 2019.
- [46] C. XJ and F. TS, "The difference of curative effect between laparoscopic radical mastectomy and traditional open radical mastectomy for colon cancer," *World Journal of Complex Medicine*, vol. 11, 2020.
- [47] A. Alam, Z. Hana, Z. Jin, K. C. Suen, and D. Ma, "Surgery, neuroinflammation and cognitive impairment," *eBioMedicine*, vol. 37, pp. 547–556, 2018.
- [48] A. Andreev, B. Erdinc, K. Shivaraj et al., "The association between anemia of chronic inflammation and Alzheimer's disease and related dementias," *Journal of Alzheimer's Disease Reports*, vol. 4, no. 1, pp. 379–391, 2020.
- [49] H. Liu, Y. Zhang, S. A. Burgard, and B. L. Needham, "Marital status and cognitive impairment in the United States: evidence



## Research Article

# The Relationship between Serum Amyloid A Level and Cognitive Dysfunction in Patients with Vascular Dementia: Preliminary Findings

Min Xu <sup>1</sup>, Xiao-ying He <sup>2</sup>, and Pan Huang <sup>3</sup>

<sup>1</sup>Department of Neurology, The Second People's Hospital of Deyang City, No. 340 Minjiang West Road, Deyang, Sichuan 618000, China

<sup>2</sup>Department of Neurology, The Affiliated Hospital of Southwest Medical University, No. 25 Taiping Street, Luzhou, Sichuan 646000, China

<sup>3</sup>Department of Neurology, People's Hospital of Deyang City, No. 173 TaiShan North Road, Deyang, Sichuan 618000, China

Correspondence should be addressed to Pan Huang; 1032857970@qq.com

Received 2 January 2021; Revised 25 January 2021; Accepted 3 February 2021; Published 16 February 2021

Academic Editor: Yuzhen Xu

Copyright © 2021 Min Xu et al. This is an open access article distributed under the Creative Commons Attribution License, which permits unrestricted use, distribution, and reproduction in any medium, provided the original work is properly cited.

**Objective.** This study was aimed at investigating the relationship between serum amyloid A (SAA) levels and cognitive dysfunction in patients with vascular dementia (VAD). **Methods.** Using cross-sectional research methods, 146 patients with VAD were selected as the VAD group and 70 normal people were selected as the NC group. Upon admission, the clinical and biochemical characteristics of the two groups of study subjects were collected, and the MMSE scale was used to assess cognitive function. A sandwich enzyme-linked immunosorbent assay was used to detect SAA levels. **Results.** There was no significant difference in clinical data and biochemical characteristics in the VAD group ( $p > 0.05$ ). Compared with the VAD group, the NC group has a higher level of education ( $p < 0.05$ ). The SAA level of the VAD group was higher than that of the NC group, and there was a significant difference ( $p < 0.05$ ). Spearman correlation analysis showed that SAA and MMSE in the VAD group were negatively correlated. Further multiple regression analysis showed that the serum amyloid A level is an independent risk factor for cognitive dysfunction in VAD patients. **Conclusion.** The level of SAA in VAD patients is significantly increased, which can be used as a potential peripheral blood marker to predict cognitive impairment in VAD patients.

## 1. Introduction

Vascular dementia (VAD) refers to a syndrome with a clinical stroke or subclinical cerebrovascular injury that affects at least one cognitive dysfunction. The disease is a heterogeneous brain disease, accounting for more than 20% of dementia, and the prevalence of VAD is 1.0%-8.8% [1]. Studies have speculated that by 2030, VAD patients will reach 66 million, and by 2050, it will reach 120 million [2, 3]. However, in the face of such a large patient population, there is no specific treatment plan for the disease so far, and there is no specific and sensitive molecular marker [4]. Unlike Alzheimer's disease, VAD is potentially preventable. Finding specific markers that can be detected and diagnosed early is conducive to early intervention, delaying the progression of

the disease, and reducing the social burden caused by cerebrovascular disease.

SAA is known for its role in secondary amyloidosis. It was isolated and identified from serum in 1976 and is a highly conserved member of the acute phase protein family [5]. The SAA-encoded protein is located in the p15.1 region of chromosome 11, with a size of 150 kb. Human SAA is synthesized in the liver by the cytokines IL-1 $\beta$ , IL-6, and tumor necrosis factor- $\alpha$  (TNF- $\alpha$ ) [6]. SAA is the precursor substance of tissue amyloid A and one of the acute phase response proteins. After the body is infected, wounded, or inflamed, the level of SAA rises rapidly [7, 8]. In recent years, with the in-depth study of SAA's gene regulation, protein structure, and biological function, it has been discovered that SAA is also involved in the pathogenesis of many chronic



diseases, but the relationship between SAA and VAD is lacking. The main purpose of this study is to detect SAA levels and further clarify whether SAA can be used as a potential biomarker for the prevention and treatment of VAD.

## 2. Materials and Methods

**2.1. Research Object.** We followed the methods of Dr. Juan Li et al. [9]. A total of 146 VAD patients admitted to our hospital from February 2015 to February 2020 were selected as the VAD group, including 70 females and 76 males, aged 40-75 years, with an average of  $69.75 \pm 7.23$  years old. In addition, 70 normal people were selected as the NC group, including 32 females and 38 males, aged 41-78 years old, with an average of  $70.31 \pm 6.74$  years old. The diagnosis of VAD refers to the diagnostic criteria established by the National Institute of Neurological Diseases and Stroke (NINDS-AIREN) and the Diagnostic and Statistical Manual of Mental Disorders (DSM-V) and is determined by two neurologists as the diagnosis of VAD [10, 11]. All VAD patients are diagnosed for the first time and have not been treated. Exclusion criteria are as follows: (1) suffering from other types of dementia; (2) suffering from inflammatory and infectious diseases; (3) suffering from immunological diseases or receiving immunosuppressive treatment; (4) suffering from mental illness; (5) dementia caused by acute cerebrovascular disease or infectious disease; (6) suffering from malignant tumor; (7) operation history or other severe trauma within 3 months; (8) suffering from severe heart, liver, or kidney insufficiency; and (9) used drugs to treat dementia. This study complied with the "Declaration of Helsinki." We obtained the written consent of all subjects and the approval of the Ethics Committee of Deyang People's Hospital.

**2.2. Clinical and Biochemical Characteristics.** When admitted to the hospital, the investigators collected the clinical and biochemical characteristics of all patients, including years of education, smoking, drinking, high blood pressure (HBP), diabetes (DM), hyperlipidemia (HLP), body mass index (BMI), systolic blood pressure (SBP), diastolic blood pressure (DBP), total cholesterol (TC), triglycerides (TG), high density lipoprotein cholesterol (HDL-C), low density lipoprotein cholesterol (LDL-C), serum creatinine (Scr), and aspartate aminotransferase/alanine aminotransferase (AST/ALT) (Figure 1).

**2.3. SAA Determination.** In the morning, 5 ml of fasting peripheral venous blood sample was taken from the patient and placed at room temperature to allow it to coagulate naturally for 10-20 minutes. Then, the coagulated blood sample was centrifuged for 30 minutes at 3000 rpm. After centrifugation, the upper serum was carefully separated, collected, and stored in a  $-80^{\circ}\text{C}$  ultralow temperature refrigerator. SAA was measured from the stored serum using Invitrogen (Waltham, MA, USA) Sandwich ELISA kit according to the manufacturer's instructions.

**2.4. Cognitive Function Assessment.** The Chinese version of the MMSE scale (Chinese version) was used to evaluate the cognitive function of all patients [12]. The MMSE scale includes six cognitive domains: orientation (time, place),

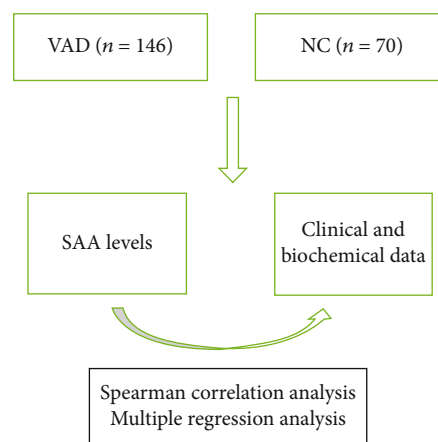


FIGURE 1: Flow chart.

timely memory, delayed memory, attention and calculation, language ability, and visual space perception. The total score of the scale ranges from 0 to 30 points. 24-30 is divided into normal, and  $<24$  is divided into cognitive dysfunction.

**2.5. Statistical Analysis.** The concentration of SAA showed a normal distribution. In this study, categorical variables are recorded by numbers (percentage, %), while continuous variables are recorded by mean  $\pm$  standard deviation (mean  $\pm$  SD). The *t*-test was applied for the comparison of continuous variables, and the chi-square test was applied for the comparison of categorical variables. Spearman's correlation analysis is used to assess the binary correlation. Multivariate regression analysis was applied to assess the predictive value of clinical and biochemical characteristics on the cognitive function in patients with VAD. The SPSS17.0 statistical software (SPSS Inc., IL, USA) was used in the study, and a *p* value of 0.05 was considered significant.

## 3. Result

**3.1. Clinical and Biochemical Characteristics.** The study included a total of 216 patients in the Department of Neurology of our hospital from February 2015 to February 2020, including 146 VAD patients and 70 normal controls. The clinical and biochemical characteristics of all subjects are shown in Table 1. In age, gender, smoke and drinking habits, chronic medical history (HBP, DM, and HLP), and biochemical characteristics (BMI, SBP, DBP, TC, TG, HDL-C, LDL-C, BUA, Scr, and AST/ALT), no significant difference was found between the VAD group and the NC group ( $p > 0.05$ ). However, as shown in Figure 2, there are significant differences between the two groups in terms of years of education, MMSE scores, and SAA levels ( $p < 0.05$ ).

**3.2. Spearman Correlation Analysis.** Spearman correlation analysis was used to analyze the correlation between clinical and biochemical characteristics and the MMSE score of VAD patients. The results are shown in Table 2 and Figure 3. Spearman correlation analysis showed that the SAA level of VAD patients was negatively correlated with

TABLE 1: Clinical and biochemical characteristics of all subjects.

Item	VAD group (n = 146)	Normal group (n = 70)	p
Age (years)	69.75 ± 7.23	70.31 ± 6.74	>0.05
Sex (M/F)	76/70	38/32	>0.05
Smoke (n, %)	34 (23.28%)	17 (24.28%)	>0.05
Hypertension (n,%)	51 (19.02%)	15 (18.75%)	>0.05
DM (n,%)	25 (17.12%)	11 (15.71%)	>0.05
Drinking habit (n,%)	49 (33.75%)	22 (31.43%)	>0.05
BUA (μmol/l)	353.85 ± 34.23	358.21 ± 35.36	>0.05
TC (mmol/l)	4.79 ± 0.38	4.82 ± 0.41	>0.05
TG (mmol/l)	1.25 ± 0.22	1.28 ± 0.26	>0.05
HDL-C (mmol/l)	0.92 ± 0.21	0.94 ± 0.22	>0.05
LDL-C (mmol/l)	2.91 ± 0.42	2.88 ± 0.43	>0.05
AST/ALT	0.73 ± 0.21	0.74 ± 0.22	>0.05
BMI (kg/m <sup>2</sup> )	23.54 ± 1.28	23.74 ± 1.25	>0.05
Scr (μmol/l)	53.25 ± 6.47	52.87 ± 6.35	>0.05
SBP (mmHg)	135.62 ± 15.36	134.82 ± 15.13	>0.05
DBP (mmHg)	88.46 ± 12.85	87.68 ± 13.36	>0.05
HLP (n, %)	30 (20.54%)	14 (20.00%)	>0.05
Education (years)	10.28 ± 2.21	14.63 ± 3.12	<0.05
MMSE (points)	28.53 ± 3.73	21.93 ± 2.78	<0.05
SAA (mg/l)	99.49 ± 12.47	17.97 ± 3.28	<0.05

NC: normal controls; VAD: vascular dementia; SAA: serum amyloid A; HBP: high blood pressure; SBP: systolic blood pressure; DBP: diastolic blood pressure; HLP: hyperlipidemia; TC: total cholesterol; TG: triglycerides; HDL-C: high-density lipoprotein cholesterol; LDL-C: low-density lipoprotein cholesterol; DM: diabetes mellitus; MMSE: Mini-Mental State Examination; Scr: serum creatinine; BUA: blood urea nitrogen.

the MMSE score, and the correlation coefficient was significant ( $r = -0.424$ ,  $p < 0.05$ ). However, in our current study, SAA levels are not significantly correlated with the demographic characteristics of VAD patients such as age, gender, education level, smoking habit, drinking habit, HLP, HBP, DM, SBP, DBP, BMI, TC, TG, HDL-C, LDL-C, Scr, BUA, and AST/ALT ( $p > 0.05$ ).

**3.3. Multiple Regression Analysis.** The results of multiple regression analysis of the MMSE score and SAA level of VAD patients are shown in Table 3. The results show that the SAA level can be used as an independent predictive risk factor for cognitive decline in VAD patients. After adjusting for age, gender, years of education, smoking habit, drinking habit, SBP, DBP, TC, TG, HDL-C, LDL-C, FBG, and other clinical and biochemical characteristics, SAA levels are still important for the independent value of VAD cognitive function significance ( $\beta = 0.427$ ,  $p = 0.024$ ).

#### 4. Discussion

The current diagnosis of VAD must meet the following conditions: (1) there must be clinical symptoms of dementia, (2)

there must be sufficient evidence of cerebrovascular disease at the same time (including evidence of medical history, physical examination, and radiographic imaging), and (3) the two must be related to each other. In the early 1990s, the diagnostic criteria for VAD were mainly based on AD, emphasizing irreversible cognitive dysfunction and impaired ability of daily living [13]. However, as research progresses, the definition of VAD is considered to be limited because it does not take into account the more common cognitive impairments associated with cerebrovascular diseases, such as executive dysfunction and psychomotor retardation. Therefore, vascular cognitive impairment (VCI) is introduced; VCI refers to a syndrome with a clinical stroke or subclinical cerebrovascular injury that affects at least one cognitive dysfunction, and VAD is the most serious form of VCI [14]. The main purpose of introducing VCI is to better reflect all cognitive changes caused by vascular factors. It is hoped that the vascular factors of cognitive impairment can be identified early and the vascular risk factors can be controlled to slow down the progression of the disease.

This study investigated the relationship between cognitive function and SAA levels in VAD patients and found that compared with normal controls, VAD patients had higher SAA levels and lower MMSE scores. At the same time, it was also found that the SAA level and MMSE score were significantly negatively correlated in VAD patients, but this correlation was not affected by interfering factors such as age, gender, education level, SBP, DBP, BMI, TG, TC, HDL-C, and LDL-C impact. To our knowledge, this is the first time that SAA is an independent risk factor for cognitive impairment in VAD patients. The pathogenesis of VAD is not clear. Vascular mechanisms, decreased cerebral perfusion, small vessel disease, microinfarction, and microhemorrhage are all related to it. Therefore, the factors that can affect the above links may cause the occurrence of VAD [15–18]. The SAA coding genes include SAA1, SAA2, SAA3, and SAA4, mainly SAA1 and SAA2; both genes are 15–20 kb in size, and their promoter region contains nuclear factor- $\kappa$ B (NF- $\kappa$ B) and interleukin-6 (IL-6). Transcription factor recognition sequence, which is the binding site of RAS activator, can be activated by interleukin-1 $\beta$  (IL-1 $\beta$ ), IL-6, and tumor necrosis factor (TNF). From the two coding genes, it can be speculated that the biological function of SAA is related to inflammation. Studies have shown that when the concentration of SAA is as low as 10 mg/l, it has the ability to induce chemokines and chemotactic leukocyte migration. When the concentration of SAA is greater than 10–60 mg/l, it can stimulate endothelial cell proliferation, adhesion, invasion, and formation of a capillary-like structure that stimulates the formation of new blood vessels in the body [19, 20]. In addition, SAA also regulates the outflow or inflow of cholesterol from cells [21]. Current research shows that SAA is related to various pathophysiological processes of atherosclerosis. SAA can stimulate the proliferation and migration of smooth muscle cells, chemoattract neutrophils and monocytes, promote local inflammation, and induce endothelial dysfunction [22]. SAA also increases the synthesis of proteoglycans in vitro and in vivo by inducing transforming growth factor- $\beta$  (TGF- $\beta$ ), leading to increased LDL retention in

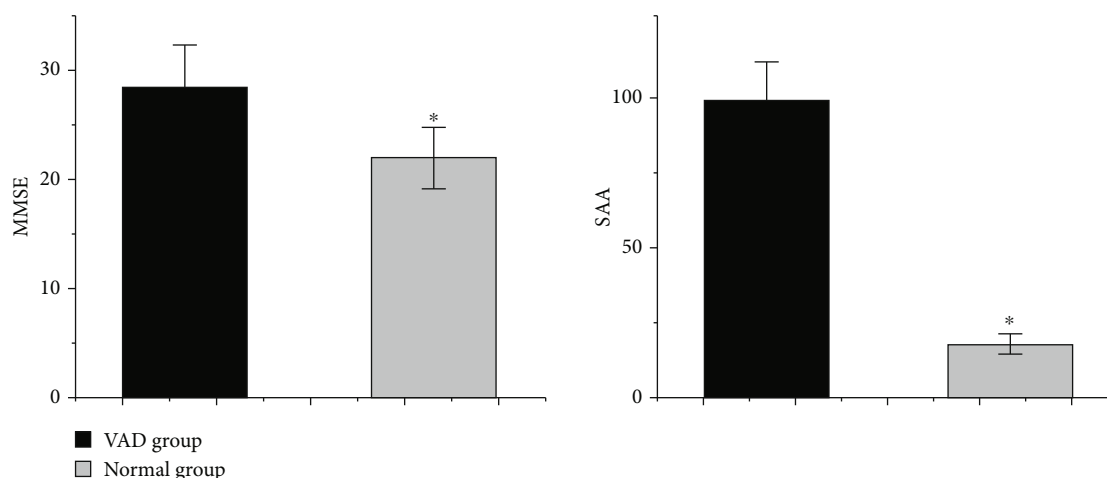


FIGURE 2: Comparison of MMSE and SAA between VAD group and NC group \* $p < 0.05$ .

TABLE 2: Correlation analysis of MMSE score and various parameters in VAD patients.

	<i>r</i>	SAA	<i>p</i>
MMSE	-0.67		<0.05

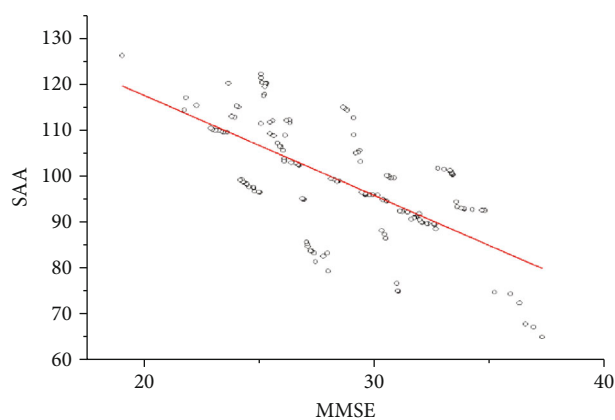


FIGURE 3: Correlation analysis of MMSE score and various parameters in VAD patients.

atherosclerotic lesions [23]. In addition, SAA stimulates the formation of foam cells by inducing the endothelial receptors of oxidized low-density lipoproteins and produces a large amount of lipid peroxides. It can also compete with apolipoprotein A1 to bind to HDL, reducing cholesterol transport to the liver and causing lipid deposition [24]. In addition to being related to atherosclerosis, SAA is also related to obesity and type 2 diabetes. There is a large amount of SAA-mRNA expression in liver fat cells of obese patients, and its expression is related to BMI [25]. In type 2 diabetes, the level of SAA is significantly higher than normal, which is mainly related to the fact that SAA can cause insulin resistance, affect the reverse transport of cholesterol, and stimulate mononuclear

TABLE 3: Relationship between MMSE score and various parameters in VAD.

	Regression coefficient	<i>p</i>	95% CI
Age (years)	0.139	0.176	0.724-1.205
Sex (M/F)	0.256	0.195	0.785-1.189
SBP (mmHg)	0.384	0.433	0.782-1.089
DBP (mmHg)	0.376	0.335	0.551-1.231
BUA ( $\mu\text{mol/l}$ )	0.213	0.186	0.736-1.154
TC (mmol/l)	0.271	0.178	0.826-1.214
TG (mmol/l)	0.312	0.569	0.482-1.332
HDL-C (mmol/l)	0.406	0.226	0.779-1.165
LDL-C (mmol/l)	0.263	0.185	0.825-1.127
AST/ALT	0.446	0.202	0.694-1.098
BMI ( $\text{kg/m}^2$ )	0.341	0.527	0.476-1.128
Scr ( $\mu\text{mol/l}$ )	0.336	0.428	0.628-1.257
Education (years)	0.224	0.076	0.652-1.183
SAA (mg/l)	0.427	0.024	1.635-2.854

macrophages to damage vascular endothelium [26–30]. As we all know, atherosclerosis, obesity, and type 2 diabetes are all risk factors for VAD.

Our study found the differential expression of SSA levels in VAD patients for the first time and confirmed that SAA levels are negatively correlated with the cognitive function of VAD patients, which has important clinical potential application value in VAD. But our research also has some limitations. First, the current study is a single-center study with a small sample. Secondly, we did not monitor SAA levels longitudinally nor did we dynamically follow-up patients' cognitive function and prognosis. Third, because the gold standard for diagnosing VAD is biopsy, our diagnosis of VAD may not be accurate enough, and VAD patients may also be accompanied by other types of cognitive impairment. Therefore, larger samples of clinical and basic research are needed for further verification.

## Data Availability

All data, models, and codes generated or used during the study appear in the submitted article.

## Ethical Approval

The study was approved by the Ethics Committee of Deyang People's Hospital, ethics approval number 2014-12-03.

## Conflicts of Interest

The authors declare that they have no any conflict of interests.

## Authors' Contributions

Pan Huang and Xiao Ying He are co-first authors, and they contributed equally to this work.

## Acknowledgments

All the authors are grateful to the Department of Neurology, People's Hospital of Deyang City.

## References

- [1] P. B. Gorelick, A. Scuteri, S. E. Black et al., "Vascular contributions to cognitive impairment and dementia," *Stroke*, vol. 42, no. 9, pp. 2672–2713, 2011.
- [2] Q. Wang, Y. Xu, C. Qi, A. Liu, and Y. Zhao, "Association study of serum soluble TREM2 with vascular dementia in Chinese Han population," *The International Journal of Neuroscience*, vol. 130, no. 7, pp. 708–712, 2020.
- [3] Y. Xu, Q. Wang, R. Cui, K. Lu, Y. Liu, and Y. Zhao, "Uric acid is associated with vascular dementia in Chinese population," *Brain and Behavior*, vol. 7, no. 2, p. e00617, 2017.
- [4] J. B. Toledo, S. E. Arnold, K. Raible et al., "Contribution of cerebrovascular disease in autopsy confirmed neurodegenerative disease cases in the National Alzheimer's Coordinating Centre[J]," *Brain A Journal of Neurology*, vol. 136, no. 9, pp. 2697–2706, 2013.
- [5] P. Woo, J. Sipe, C. A. Dinarello, and H. R. Colten, "Structure of a human serum amyloid A gene and modulation of its expression in transfected L cells," *The Journal of Biological Chemistry*, vol. 262, no. 32, pp. 15790–15795, 1987.
- [6] I. N. Baranova, A. C. P. Souza, A. V. Bocharov et al., "Human SR-BII mediates SAA uptake and contributes to SAA pro-inflammatory signaling in vitro and in vivo," *PLoS One*, vol. 12, no. 4, article e0175824, 2017.
- [7] M. Buck, M. Gouwy, J. Wang et al., "Structure and expression of different serum amyloid A (SAA) variants and their concentration dependent functions during host insults," *Current Medicinal Chemistry*, vol. 23, no. 17, pp. 1725–1755, 2016.
- [8] L. Sun and R. D. Ye, "Serum amyloid A1: structure, function and gene polymorphism," *Gene*, vol. 583, no. 1, pp. 48–57, 2016.
- [9] J. Li, S. Li, Y. Song et al., "Association of serum FAM19A5 with cognitive impairment in vascular dementia," *Disease Markers*, vol. 2020, no. 8, 2020.
- [10] T. Erkinjuntt, "Clinical criteria for vascular dementia: the NINDS-AIREN criteria," *Dementia and Geriatric Cognitive Disorders*, vol. 5, no. 1, pp. 189–192, 2004.
- [11] M. Heyck and A. Ibarra, "Microbiota and memory: a symbiotic therapy to counter cognitive decline?," *Brain Circulation*, vol. 5, no. 3, pp. 124–129, 2019.
- [12] R. Cassani, M. Estarellas, R. San-Martin, F. J. Fraga, and T. H. Falk, "Systematic review on resting-state EEG for Alzheimer's disease diagnosis and progression assessment," *DiseaseMarkers*, vol. 5174815, 2018.
- [13] G. C. Roman, T. K. Tatemichi, T. Erkinjuntti et al., "Vascular dementia: diagnostic criteria for research studies: report of the NINDS-AIREN International Workshop," *Neurology*, vol. 43, no. 2, pp. 250–260, 1993.
- [14] V. Hachinski, D. Ganten, D. Lackland, R. Kreutz, K. Tsioufis, and W. Hacke, "Implementing the proclamation of stroke and potentially preventable dementias," *International Journal of Stroke*, vol. 13, no. 8, pp. 780–786, 2018.
- [15] A. H. Hainsworth, A. T. Oommen, and L. R. Bridges, "Endothelial cells and human cerebral small vessel disease," *Brain Pathology*, vol. 25, no. 1, pp. 44–50, 2015.
- [16] R. G. de Eulate, I. Goñi, A. Galiano et al., "Reduced cerebral blood flow in mild cognitive impairment assessed using phase-contrast MRI," *Journal of Alzheimer's Disease*, vol. 58, no. 2, pp. 585–595, 2017.
- [17] M. I. Bergkamp, J. G. J. Wissink, E. M. C. van Leijssen et al., "Risk of nursing home admission in cerebral small vessel disease," *Stroke*, vol. 49, no. 11, pp. 2659–2665, 2018.
- [18] J. H. Park, S. W. Seo, C. Kim et al., "Pathogenesis of cerebral microbleeds: in vivo imaging of amyloid and subcortical ischemic small vessel disease in 226 individuals with cognitive impairment," *Annals of Neurology*, vol. 73, no. 5, pp. 584–593, 2013.
- [19] M. Connolly, P. R. Rooney, T. McGarry et al., "Acute serum amyloid A is an endogenous TLR2 ligand that mediates inflammatory and angiogenic mechanisms," *Annals of the Rheumatic Diseases*, vol. 75, no. 7, pp. 1392–1398, 2016.
- [20] C. Hong, C. Shen, H. Ding et al., "An involvement of SR-B1 mediated p38 MAPK signaling pathway in serum amyloid A-induced angiogenesis in rheumatoid arthritis," *Molecular Immunology*, vol. 66, no. 2, pp. 340–345, 2015.
- [21] R. Kisilevsky and P. N. Manley, "Acute-phase serum amyloid A: perspectives on its physiological and pathological roles," *Amyloid*, vol. 19, no. 1, pp. 5–14, 2012.
- [22] M. De Buck, N. Berghmans, N. Pörtner et al., "Serum amyloid A1 $\alpha$  induces paracrine IL-8/CXCL8 via TLR2 and directly synergizes with this chemokine via CXCR2 and formyl peptide receptor 2 to recruit neutrophils," *Journal of Leukocyte Biology*, vol. 98, no. 6, pp. 1049–1060, 2015.
- [23] J. C. Thompson, C. Jayne, J. Thompson et al., "A brief elevation of serum amyloid A is sufficient to increase atherosclerosis[S]," *Journal of Lipid Research*, vol. 56, no. 2, pp. 286–293, 2015.
- [24] J. M. Wroblewski and A. Jahangiri, "Nascent HDL formation by hepatocytes is reduced by the concerted action of serum amyloid A and endothelial lipase," *Journal of Lipid Research*, vol. 52, no. 12, pp. 2255–2261, 2011.
- [25] R. Z. Yang, M. J. Lee, H. Hu et al., "Acute-phase serum amyloid A: an inflammatory adipokine and potential link between obesity and its metabolic complications," *PLoS Medicine*, vol. 3, no. 6, article e287, 2006.

- [26] E. Hatanaka, P. T. Monteagudo, M. S. M. Marrocos, and A. Campa, "Interaction between serum amyloid A and leukocytes—a possible role in the progression of vascular complications in diabetes," *Immunology Letters*, vol. 108, no. 2, pp. 160–166, 2007.
- [27] L. Cai, M. C. de Beer, F. C. de Beer, and D. R. van der Westhuyzen, "Serum amyloid A is a ligand for scavenger receptor class B type I and inhibits high density lipoprotein binding and selective lipid uptake\*," *The Journal of Biological Chemistry*, vol. 280, no. 4, pp. 2954–2961, 2005.
- [28] J. Y. Mao, J. T. Sun, K. Yang et al., "Serum amyloid A enrichment impairs the anti-inflammatory ability of HDL from diabetic nephropathy patients," *Journal of Diabetes and its Complications*, vol. 31, no. 10, pp. 1538–1543, 2017.
- [29] S. Yuan, K. J. Liu, and Z. Qi, "Occludin regulation of blood–brain barrier and potential therapeutic target in ischemic stroke," *Brain Circulation*, vol. 6, no. 3, pp. 152–162, 2020.
- [30] Q. Wang, W. Yang, J. Zhang, Y. Zhao, and Y. Xu, "TREM2 overexpression attenuates cognitive deficits in experiment models of vascular dementia," *Neural Plasticity*, vol. 7, no. 12, 2020.



## Retraction

# Retracted: Identification of the Potential Biomarkers Involved in the Human Oral Mucosal Wound Healing: A Bioinformatic Study

### BioMed Research International

Received 12 March 2024; Accepted 12 March 2024; Published 20 March 2024

Copyright © 2024 BioMed Research International. This is an open access article distributed under the Creative Commons Attribution License, which permits unrestricted use, distribution, and reproduction in any medium, provided the original work is properly cited.

This article has been retracted by Hindawi following an investigation undertaken by the publisher [1]. This investigation has uncovered evidence of one or more of the following indicators of systematic manipulation of the publication process:

- (1) Discrepancies in scope
- (2) Discrepancies in the description of the research reported
- (3) Discrepancies between the availability of data and the research described
- (4) Inappropriate citations
- (5) Incoherent, meaningless and/or irrelevant content included in the article
- (6) Manipulated or compromised peer review

The presence of these indicators undermines our confidence in the integrity of the article's content and we cannot, therefore, vouch for its reliability. Please note that this notice is intended solely to alert readers that the content of this article is unreliable. We have not investigated whether authors were aware of or involved in the systematic manipulation of the publication process.

Wiley and Hindawi regrets that the usual quality checks did not identify these issues before publication and have since put additional measures in place to safeguard research integrity.

We wish to credit our own Research Integrity and Research Publishing teams and anonymous and named external researchers and research integrity experts for contributing to this investigation.




















The corresponding author, as the representative of all authors, has been given the opportunity to register their agreement or disagreement to this retraction. We have kept a record of any response received.

### References

- [1] W. Ning, X. Jiang, Z. Sun et al., "Identification of the Potential Biomarkers Involved in the Human Oral Mucosal Wound Healing: A Bioinformatic Study," *BioMed Research International*, vol. 2021, Article ID 6695245, 16 pages, 2021.

## Research Article

# Identification of the Potential Biomarkers Involved in the Human Oral Mucosal Wound Healing: A Bioinformatic Study

Wanchen Ning <sup>1</sup>, Xiao Jiang <sup>2</sup>, Zhengyang Sun <sup>3</sup>, Anthony Chukwunonso Ogbuehi <sup>4</sup>, Wenli Gu <sup>2</sup>, Aneesha Acharya <sup>5</sup>, Zhaobi Fang <sup>6</sup>, Xiongjie Zhu <sup>6</sup>, Qianhua Ou <sup>6</sup>, Muhui Zeng <sup>6</sup>, Cong Li <sup>6</sup>, Shiting Hua <sup>6</sup>, Prabhakar Mujagond <sup>6</sup>, Xiangqiong Liu <sup>7</sup>, Yupei Deng <sup>7</sup>, Hongying Pan <sup>8</sup>, Shaonan Hu <sup>9</sup>, Xianda Hu <sup>7</sup>, and Simin Li <sup>2</sup>

<sup>1</sup>Department of Conservative Dentistry and Periodontology, Ludwig-Maximilians-University of Munich, Goethestrasse 70, 80336 Munich, Germany

<sup>2</sup>Stomatological Hospital, Southern Medical University, 366 South Jiangnan Ave, Haizhu district, 510280 Guangzhou, China

<sup>3</sup>Faculty of Mechanical Engineering, Chemnitz University of Technology, Reichenhainer Str. 70, 09126 Chemnitz, Germany

<sup>4</sup>Faculty of Physics, University of Münster, Wilhelm-Klemm-Straße 9, 48149 Münster, Germany

<sup>5</sup>Dr. D.Y. Patil Dental College and Hospital, Dr. D.Y. Patil Vidyapeeth, Pimpri, Pune, India

<sup>6</sup>Zhujiang Hospital, Southern Medical University, Guangzhou 510282, China

<sup>7</sup>Beijing Tibetan Hospital, China Tibetology Research Center, 218 Anwaixiaoguanbeili Street, Chaoyang, Beijing 100029, China

<sup>8</sup>School of Dentistry, University of Michigan, 1011 N University Ave, Ann Arbor, MI 48109, USA

<sup>9</sup>Innovation Center Computer Assisted Surgery (ICCAS), University Leipzig, Semmelweisstraße 14, 04103 Leipzig, Germany

Correspondence should be addressed to Simin Li; [simin.li.dentist@gmail.com](mailto:simin.li.dentist@gmail.com)

Received 7 December 2020; Revised 16 December 2020; Accepted 25 January 2021; Published 12 February 2021

Academic Editor: Burak Durmaz

Copyright © 2021 Wanchen Ning et al. This is an open access article distributed under the Creative Commons Attribution License, which permits unrestricted use, distribution, and reproduction in any medium, provided the original work is properly cited.

**Objective.** To identify the key genetic and epigenetic mechanisms involved in the wound healing process after injury of the oral mucosa. **Materials and Methods.** Gene expression profiling datasets pertaining to rapid wound healing of oral mucosa were identified using the Gene Expression Omnibus (GEO) database. Differential gene expression analysis was performed to identify differentially expressed genes (DEGs) during oral mucosal wound healing. Next, functional enrichment analysis was performed to identify the biological processes (BPs) and signaling pathways relevant to these DEGs. A protein-protein interaction (PPI) network was constructed to identify hub DEGs. Interaction networks were constructed for both miRNA-target DEGs and DEGs-transcription factors. A DEGs-chemical compound interaction network and a miRNA-small molecular interaction network were also constructed. **Results.** DEGs were found significantly enriched in several signaling pathways including arachidonic acid metabolism, cell cycle, p53, and ECM-receptor interaction. Hub genes, GABARAPL1, GABARAPL2, HDAC5, MAP1LC3A, AURKA, and PLK1, were identified via PPI network analysis. Two miRNAs, miR-34a-5p and miR-335-5p, were identified as pivotal players in the miRNA-target DEGs network. Four transcription factors FOS, PLAU, BCL6, and RORA were found to play key roles in the TFs-DEGs interaction network. Several chemical compounds including Valproic acid, Doxorubicin, Nickel, and tretinoin and small molecular drugs including atorvastatin, 17 $\beta$ -estradiol, curcumin, and vitamin D3 were noted to influence oral mucosa regeneration by regulating the expression of healing-associated DEGs/miRNAs. **Conclusion.** Genetic and epigenetic mechanisms and specific drugs were identified as significant molecular mechanisms and entities relevant to oral mucosal healing. These may be valuable potential targets for experimental research.

## 1. Introduction

Oral mucosal injury is inherent to several disorders and conditions such as trauma, periodontal disease, cancer, and

dental implant surgery [1]. Oral mucosal regeneration is an area of increasing research focus and includes the application of regenerative modalities such as 3D cell sheets consisting of oral mucosal cells (keratinocytes, fibroblasts, and endothelial

cells) [2, 3]. Genetic modification of such cell-based constructs may potentially further accelerate their healing capacity [4, 5] and provide a novel strategy to promote wound healing in oral mucosa injury. Therefore, investigating the genetic mechanisms involved in the wound healing process of oral mucosa injury could be of significant translational value.

Wound healing of oral mucosa is unique because it is typically faster and shows a low tendency for scarring [6]. The superior healing characteristics of the oral mucosa might be owing to various factors including the specific anatomy of the oral cavity and environmental factors such as microbial flora, saliva secretion, and pH balance. Some other or reasons plausible causes include growth factor production, stem cell levels, cellular proliferation capacity, and genetic and epigenetic factors [7, 8]. As genetic and epigenetic regulation plays a pivotal role in the unique healing characteristics of the oral mucosa, significant research attention [9–12] has focused on the involvement of genetic and epigenetic factors (e.g., genes, signaling pathways, transcription factors, and miRNAs) in the wound healing process of oral mucosa injury. In this context, vascular endothelial growth factor (VEGF) has been found to promote palatal mucosal wound healing by accelerating neovascularization and reepithelialization [9]. In another report, intrinsic apoptosis pathways Casp2 and Trp53 were found activated during oral mucosal wound healing [10]. The transcription factor forkhead box O1 (FOXO1) has been found as increased in the nucleus of keratinocytes and promote reepithelialization during wound healing of oral mucosa [11]. The overexpression of miR-31 has been found to promote oral mucosal wound closure by enhancing the proliferation and migration of keratinocytes [12].

Apart from these experimental studies, high-throughput sequencing investigations have shown alterations of mRNAs or noncoding RNA expression profiles during oral mucosa healing by establishing paired injury models in rats (GSE23006 [7] and GSE121996 [13]) and humans (GSE97615 [14]). To the authors' knowledge, there is no comprehensive bioinformatic investigation leveraging the publicly available datasets pertaining to genetic and epigenetic mechanisms involved in oral mucosa regeneration. Bioinformatics can enable the interpretation and visualization of large datasets through network construction [15]. Plausibly, the important factors critical to a specific pathophysiological process can be identified through bioinformatic analysis of relevant gene expression datasets. The present study is aimed at analyzing the data in the GSE97615 [14] using multiple bioinformatic techniques in order to identify specific molecular mechanisms that are key to the regulation of the wound healing processes in human oral mucosa injury.

## 2. Materials and Methods

**2.1. Sourcing of Gene Expression Data.** Datasets investigating genetic alterations using paired models of rapid wound healing of oral mucosa were searched for in the Gene Expression Omnibus (GEO) database in NCBI [16]. The study design of the included datasets consisted of two groups, the control

group where oral mucosal injury was created and the experimental group where wound healing was complete. The model of oral mucosa injury was created by a sterile uniform punch biopsy (McKesson) in the mucosa of the cheek [14]. The inclusion criteria pertaining to this dataset were as follows: [1] all participants being nonsmokers without any systemic diseases; [2] uniform biopsy at less than 5 mm, which was within self-regenerative capacity of the human oral mucosa; and [3] datasets with at least 3 pairs of samples (3 controls and 3 experimental samples).

**2.2. Differential Gene Expression Analysis.** RNAseq data were processed using TopHat software [17], and RPKM (Reads Per Kilobase Million) was calculated by using Partek software [18]. Differential expression analysis was conducted by using the “DESeq” package in R environment [19]. The differentially expressed mRNAs (genes) with  $p$  value  $< 0.05$  and  $|\log FC| \geq 1$  were selected as DEGs. The DEGs with  $\log FC \geq 1$  were considered upregulated DEGs, while DEGs with  $\log FC \leq -1$  were considered downregulated DEGs.

**2.3. Functional Enrichment Analysis.** Functional enrichment analysis of the DEGs involved in the wound healing process of oral mucosa injury was performed using the “clusterProfiler” package in R [20]. The functions of the DEGs were explored by investigating their enriched Gene Ontology (GO) terms, in particular, biological processes (BPs) and Kyoto Encyclopedia of Genes and Genomes (KEGG) pathways. The GO terms and KEGG pathways with  $p$  value  $< 0.05$  were regarded as significant functions. If the number of enriched BPs and pathways was more than 30, the top 30 were chosen to be visualized in the bar plot. If the number of enriched BPs and pathways was less than 30, then all of the BPs and pathways were visualized in the bar plot.

**2.4. Construction of Protein-Protein Interaction (PPI) Network.** Experimentally validated PPI pairs were downloaded from a variety of databases including HPRD [21], BIOGRID [22], DIP [23], MINT [24], mentha [25], PINA [26], InnateDB [27], and Instruct [28]. PPI pairs of DEGs were extracted from these databases and further used for constructing the PPI network. The constructed PPI network was plotted using Cytoscape Version 3.7.2 [29]. The topological characteristics of the nodes in the PPI network were determined.

**2.5. Construction of miRNA-Target DEGs Interaction Network.** Experimentally validated miRNA-target interaction pairs were downloaded from three databases, including “miRTarBase” [30], “miRecords” [31], and “TarBase” v.8 [32]. miRNAs targeting DEGs were extracted from these databases and used for constructing a miRNA-target DEGs interaction network using the Cytoscape platform [29]. The topological characteristics of the nodes in the miRNA-target DEGs network were determined.

**2.6. Construction of Transcription Factor- (TF-) Target DEGs Interaction Network.** The TF-target gene interaction pairs were downloaded from many databases, including “TRANSFAC” [33], “HTRIdb” [34], “TRRUST” [35], “ORTI” [36],

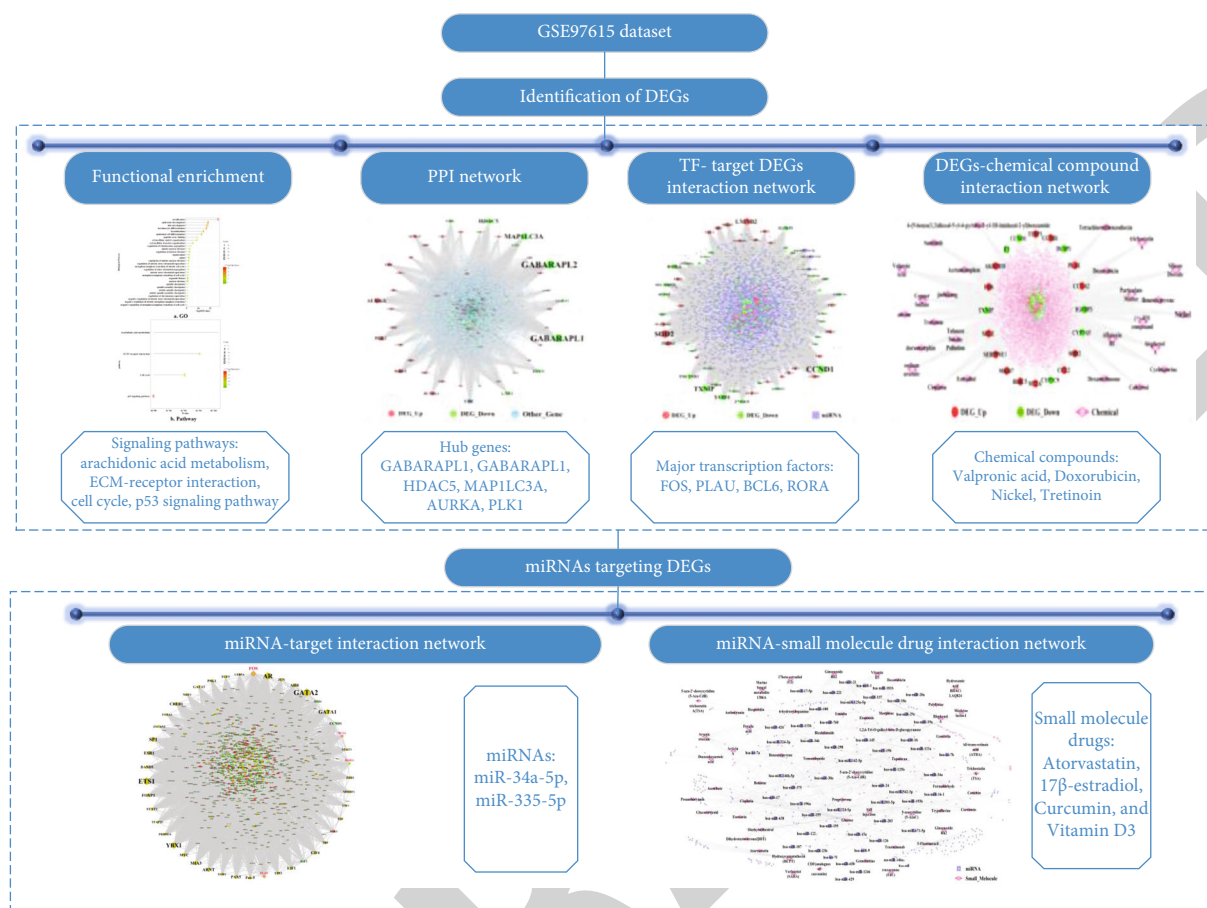


FIGURE 1: Study flowchart. The GSE97615 dataset was analyzed using a series of bioinformatic analyses: differential expression analysis; functional enrichment analysis; and construction of networks including PPI network, TF-target DEGs network, DEGs-chemical compound interaction network, miRNA-target interaction network, and miRNA-small molecular drug interaction network.

and “cGRNB” [37]. The TFs targeting DEGs were extracted and used for constructing the TFs-target DEGs interaction network using Cytoscape [29]. The topological characteristics of the nodes in the TFs-target DEGs network were determined.

**2.7. Construction of the DEGs-Chemical Compound Interaction Network.** Data pertaining to the interactions between genes and chemical compounds were downloaded from CTD (Comparative Toxicogenomics Database) [38]. Only the data regarding the human species were extracted. 858,086 interaction pairs between genes and chemical compounds were obtained. Among these interaction pairs, chemical compounds that correspond to DEGs were extracted, and thus, 41,634 interaction pairs between DEGs and chemical compounds were derived. Thereafter, Cytoscape [29] was employed to visualize the interaction relationships between DEGs and their interacting chemical compounds. Following the construction of the DEGs-chemical compound interaction network, a topological analysis was performed to calculate the characteristics of the nodes in the network.

**2.8. Construction of the miRNA-Small Molecule Drug Interaction Network.** The data regarding known miRNAs and small molecular drugs were downloaded from the

SM2miR database [39]. Only data associated with human species were extracted, and 2,756 interaction pairs between known miRNAs and small molecular drugs were obtained. Among these pairs, miRNAs that target DEGs were extracted, and the small molecule drugs that impact the expression levels of these miRNAs were further obtained. Therefore, 1,074 interaction pairs between small molecular drugs and miRNAs that target DEGs were studied. In order to visualize these interaction pairs, Cytoscape [29] was used to construct the miRNA-small molecule drug interaction network.

### 3. Results

**3.1. Included Gene Expression Dataset.** The dataset GSE97615 was included in this analysis [14]. This dataset examined gene expression profiles using high-throughput sequencing technology on the GPL11154 platform of Illumina HiSeq 2000. In the experimental group, oral buccal mucosal injury was generated on day 1, and wound healing was found to be almost complete on day 3. As nonsignificant differences in gene expression were noted between biopsies obtained on day 1 versus day 6, the oral biopsy samples of day 1 (GSM2573167, GSM2573168, GSM2573169, and GSM2573170) and day 3 (GSM2573171, GSM2573172,



TABLE 1: The top 30 DEGs involved in the process of oral mucosa regeneration, ranked by the ascending order of  $p$  value.

Name	Base mean	Base meanA	Base meanB	Fold change	$\log_2$ fold change	$p$ val	$p$ adj
DEFB4A	40.12592	2.388343	77.8635	32.60148	5.026865	$1.05E-25$	$7.32E-22$
S100A7	310.8578	17.06716	604.6484	35.42758	5.146801	$1.33E-23$	$6.19E-20$
DEFB4B	13.92444	0.57421	27.27467	47.49947	5.56984	$3.75E-23$	$1.31E-19$
FLG	21.40743	40.1873	2.627564	0.065383	-3.93494	$3.94E-22$	$1.10E-18$
KRT76	8.60035	16.71021	0.490492	0.029353	-5.09036	$4.74E-19$	$1.10E-15$
CES1	9.660384	18.36781	0.952953	0.051882	-4.26863	$7.36E-19$	$1.47E-15$
CCL19	11.84998	1.619644	22.08032	13.63283	3.769013	$2.64E-18$	$4.61E-15$
ALOX12	101.6108	186.2771	16.94443	0.090964	-3.45857	$5.61E-17$	$8.69E-14$
CYP4F35P	13.31745	24.28438	2.350513	0.096791	-3.36898	$8.10E-17$	$1.03E-13$
ETNK2	25.88451	47.104	4.665033	0.099037	-3.33589	$8.10E-17$	$1.03E-13$
TUBB3	9.802023	1.010702	18.59334	18.39647	4.201357	$8.86E-17$	$1.03E-13$
DPT	13.10894	23.69376	2.524124	0.106531	-3.23065	$1.35E-16$	$1.45E-13$
KPRP	12.68058	23.2699	2.091252	0.089869	-3.47603	$2.49E-16$	$2.48E-13$
CLEC3B	16.77294	29.85829	3.68758	0.123503	-3.01739	$7.10E-16$	$6.60E-13$
ANKRD37	55.14818	100.8559	9.44044	0.093603	-3.4173	$9.28E-16$	$8.09E-13$
CYP4F29P	22.09975	39.23028	4.969215	0.126668	-2.98088	$2.17E-15$	$1.78E-12$
KRT3	46.56198	82.43067	10.6933	0.129725	-2.94647	$8.72E-15$	$6.76E-12$
CRISP3	47.9651	84.80899	11.12121	0.131132	-2.9309	$6.57E-14$	$4.83E-11$
PPP1R3C	50.11791	89.58462	10.65119	0.118895	-3.07224	$9.76E-14$	$6.80E-11$
SOCS3	7.850827	1.029401	14.67225	14.2532	3.833214	$7.74E-13$	$5.14E-10$
KRT16P2	25.30934	6.520768	44.09791	6.762687	2.757597	$8.42E-13$	$5.34E-10$
KLK6	49.11907	12.67537	85.56277	6.750319	2.754956	$9.84E-13$	$5.97E-10$
MFAP4	14.13919	23.95185	4.326524	0.180634	-2.46886	$3.25E-12$	$1.89E-09$
CD177	6.239805	0.532066	11.94754	22.45498	4.488964	$6.07E-12$	$3.38E-09$
CDH3	20.64668	5.975959	35.3174	5.909913	2.563137	$7.13E-12$	$3.82E-09$
ANKRD20A5P	6.083548	11.44316	0.723938	0.063264	-3.98248	$4.05E-11$	$2.02E-08$
PSCA	36.97691	63.83741	10.11641	0.158471	-2.65771	$4.88E-11$	$2.35E-08$
SFRP2	27.36962	45.66674	9.072498	0.198668	-2.33157	$5.22E-11$	$2.43E-08$
DUSP5	32.6366	55.26694	10.00626	0.181053	-2.46551	$5.51E-11$	$2.48E-08$
CLDN17	30.11305	49.5288	10.69729	0.215981	-2.21102	$2.50E-10$	$1.09E-07$

GSM2573173, and GSM2573174) were selected as representatives of injured versus healed oral mucosal tissue for comparative analysis in this study.

**3.2. Analytical Approaches.** A series of bioinformatic analyses were performed and are depicted as a flowchart (Figure 1). Firstly, differential gene expression analysis was performed to identify DEGs during the healing process of oral mucosa injury. Subsequently, functional enrichment analysis was performed to explore the signaling pathways in which DEGs were enriched. In addition, a protein-protein interaction (PPI) network was constructed to identify the hub proteins that are likely to play critical roles in the healing process. Additionally, a transcription factor- (TF-) target DEGs interaction network was constructed to identify the transcription factors that might be key to regulation of the healing process

by targeting the greatest number of DEGs. Thereafter, a miRNA-target interaction network was constructed based on DEGs and miRNAs which target these DEGs. Finally, in order to explore the chemical compounds and small molecular drugs that can regulate the healing process of oral mucosa injury, a DEGs-chemical compound interaction network and miRNA-small molecular drug interaction network were each constructed.

**3.3. Identification of DEGs Involved in the Oral Mucosa Regeneration.** By performing differential expression analysis, a total of 650 DEGs consisting of 448 downregulated DEGs and 202 upregulated DEGs were identified as significantly involved in the oral mucosa regeneration (File S1). Table 1 shows the top 30 DEGs with the most significant  $p$  values, including defensin beta 4A (DEFB4A), C-C motif chemokine



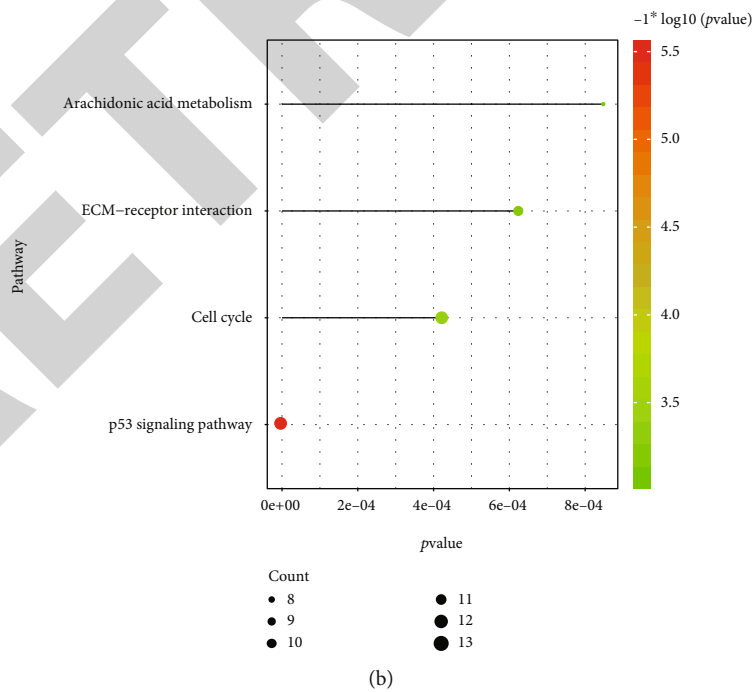
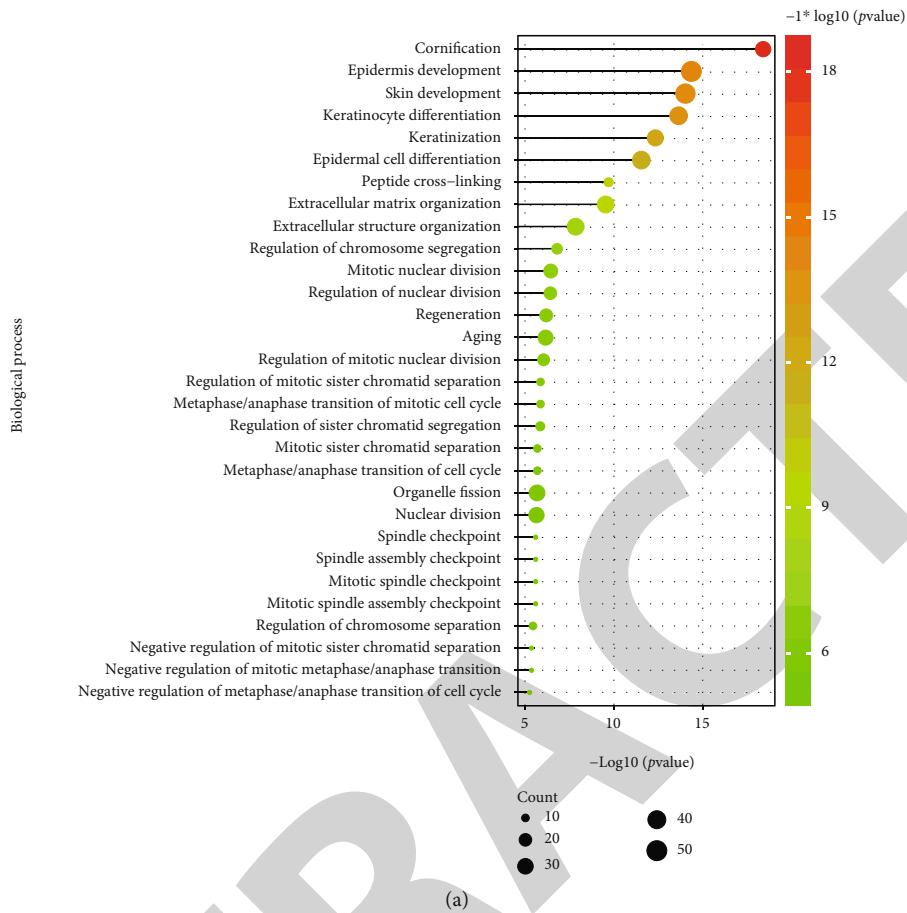


FIGURE 2: The enriched functions of DEGs involved in the oral mucosa regeneration process: (a) GO terms-biological processes; (b) signaling pathways. The count represents the number of genes enriched in a BP term, and  $-\log_{10}(p\text{ value})$  represents the enrichment score. The bigger size of the dots corresponding to a BP term means more genes were enriched in this term. The coloured dots represent the term enrichment: green indicates low enrichment, and red indicates high enrichment.

ligand 19 (CCL19), filaggrin (FLG), cysteine-rich secretory protein 3 (CRISP3), and suppressor of cytokine signaling 3 (SOCS3).

**3.4. Functional Terms Enriched by DEGs.** File S2 and S3 show the significantly enriched biological processes and signaling pathways associated with DEGs, respectively. Figure 2(a) shows that DEGs involved in oral wound healing were implicated in many biological processes such as epidermis development, keratinocyte differentiation, keratinization, epidermal cell differentiation, extracellular matrix organization, biological processes related to cell cycle, and spindle checkpoint. Figure 2(b) shows that DEGs involved in oral wound healing were implicated in arachidonic acid metabolism, ECM-receptor interaction, cell cycle, and the p53 signaling pathway.

**3.5. Identification of Hub Genes in the PPI Network.** The PPI network (shown in Figure 3) consisted of 7,055 nodes and 16,851 edges (File S4). As shown in Table 2, the top 30 nodes with the highest degree were listed, such as GABA type A receptor-associated protein-like 1 (GABARAPL1), GABA type A receptor-associated protein-like 2 (GABARAPL2), microtubule-associated protein 1 light chain 3 alpha (MAP1LC3A), histone deacetylase 5 (HDAC5), aurora kinase A (AURKA), and polo-like kinase 1 (PLK1). These genes with the highest degree were deemed to be of the highest significance in the PPI network by interacting with the greatest number of genes.

**3.6. Identification of the Significant miRNAs Targeting DEGs.** The miRNA-target DEGs interaction network shown in Figure 4 consisted of 2,995 nodes and 20,362 edges (File S5). Table 3 shows the topological characteristics of the top 30 nodes in the network. Two miRNAs (miR-34a-5p and miR-335-5p) played the most significant roles in this network by targeting the greatest number of DEGs. By tracking the target relationship between a certain miRNA and its target DEGs within the top 30 nodes, it was determined that miR-34a-5p targets several DEGs including AMOTL2, CCNB1, CCND1, DDX21, FSCN1, HBP1, ID4, KPNA2, MKI67, MSN, NAV1, RRM2, SECISBP2L, SESN2, THBS1, and TXNIP. miR-335-5p was found to target several DEGs including DDX21, HBP1, RMND5A, RORA, SECISBP2L, SESN2, TXNIP, and YOD1.

**3.7. Identification of Hub Transcription Factors That Target DEGs.** The TFs-target DEGs interaction network shown in Figure 5 consisted of 1,054 nodes and 946 edges (File S6). Table 4 shows the top TFs with the highest degree that are pivotal to this network. Protooncogene c-Fos (FOS), B-cell lymphoma 5 protein (BCL6), and urokinase-type plasminogen activator (PLAU) were not only TFs but also upregulated DEGs. RAR-related orphan receptor A (RORA) was TF and a downregulated DEGs.

**3.8. Identification of Chemical Compounds That Regulate the Expression of DEGs.** A DEGs-chemical compound interaction network was constructed and is shown in Figure 6. This network is comprised of 3,612 nodes and 27,426 edges (File

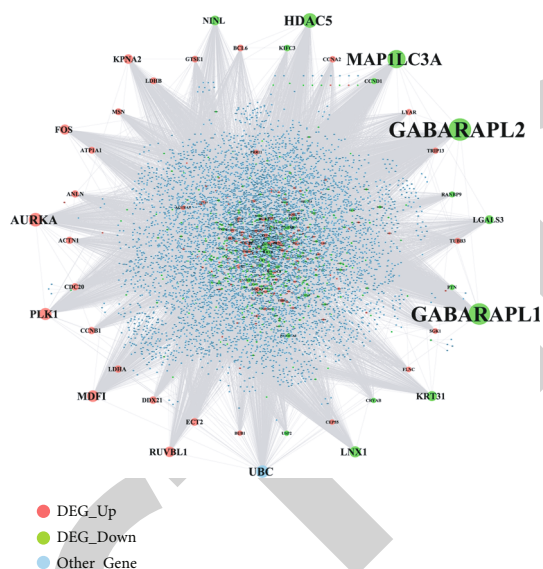


FIGURE 3: The PPI network of DEGs involved in the oral mucosa regeneration process. The nodes with different colours represent the upregulated and downregulated DEGs and other genes that are not DEGs.

S7. Specific chemical compounds targeting the DEGs that were dysregulated in the healing process of oral mucosa injury included Valproic acid, Doxorubicin, Nickel, and tretinoin.

**3.9. Identification of Small Molecular Drugs That Regulate the Expression of miRNAs.** A miRNA-small molecular drug interaction network was constructed and is shown in Figure 7. This network is comprised of 522 nodes and 1,074 edges (File S8). Several small molecular drugs were found to regulate the expression of miRNAs targeting the DEGs dysregulated during healing of oral mucosa injury including atorvastatin, 17 $\beta$ -estradiol, curcumin, and vitamin D3.

## 4. Discussion

Bioinformatic analysis revealed several genetic and epigenetic regulatory mechanisms implicated in oral mucosa wound healing including specific mRNAs, miRNAs, pathways, TFs, and targeted drugs.

Hub genes identified as central to the PPI network that interacted with the greatest number of genes included GABARAPL1, GABARAPL2, HDAC5, MAP1LC3A, AURKA, and PLK1. Gamma-aminobutyric acid receptor-associated protein-like 1 (GABARAPL1) and GABARAPL2 are proteins associated with gamma-aminobutyric acid (GABA), a non-protein amino acid, and the overexpression of GABA has been shown to suppress inflammation by inhibiting inflammatory mediators (iNOS, IL-1beta, and TNF-alpha), promoting fibroblast cell proliferation, and stimulating reepithelialization, suggesting that GABA could accelerate the healing process at the early stage of cutaneous wound healing [40]. Histone deacetylase 5 (HDAC5) belongs to class IIa HDACs and plays a key role in angiogenesis, inflammation, and immunity [41]. HDAC was shown to inhibit fibroblast proliferation by

TABLE 2: The topological characteristics of the top 30 hub genes in the PPI network.

Name	Label	Degree	Average shortest path length	Betweenness centrality	Closeness centrality	Clustering coefficient	Topological coefficient
GABARAPL2	Down	583	2.689935	0.071254	0.371756	0.005399	0.005164
GABARAPL1	Down	559	2.711402	0.057754	0.368813	0.006036	0.005542
MAP1LC3A	Down	463	2.683537	0.053743	0.372643	0.007429	0.005812
HDAC5	Down	363	2.837504	0.045007	0.352422	0.001614	0.007383
AURKA	Up	332	2.768126	0.049883	0.361255	0.003904	0.007122
UBC	Other	302	2.217088	0.270483	0.451042	0.005258	0.007895
PLK1	Up	288	2.75462	0.047684	0.363026	0.006259	0.0075
MDFI	Up	277	2.965596	0.057747	0.3372	1.91E-04	0.005234
LNX1	Down	265	3.016776	0.047711	0.33148	1.50E-04	0.006827
RUVBL1	Up	243	2.846034	0.034842	0.351366	0.002092	0.010082
KRT31	Down	235	2.960904	0.039526	0.337735	0.002633	0.006649
FOS	Up	232	2.932897	0.035432	0.34096	0.001416	0.010324
NINL	Down	226	2.914984	0.038519	0.343055	0.002989	0.007416
KPNA2	Up	216	2.815326	0.032401	0.355199	0.003874	0.009379
LGALS3	Down	201	2.922377	0.033476	0.342187	0.002459	0.007997
ECT2	Up	168	2.89238	0.025887	0.345736	0.003302	0.010711
DDX21	Up	161	2.89437	0.0152	0.345498	0.008063	0.014814
LDHA	Up	156	2.850299	0.0153	0.35084	0.013245	0.013064
ACTN1	Up	155	2.871908	0.021745	0.348201	0.003848	0.011807
CDC20	Up	155	2.823003	0.017314	0.354233	0.018812	0.012271
CCNB1	Up	155	2.90816	0.014414	0.34386	0.017677	0.014428
ANLN	Up	153	2.993034	0.02056	0.334109	0.00517	0.012216
ATP1A1	Up	144	2.873472	0.018625	0.348011	0.00483	0.012658
LDHB	Up	142	2.954933	0.010182	0.338417	0.012589	0.016739
MSN	Up	142	2.969719	0.015946	0.336732	0.00402	0.015602
BCL6	Up	138	2.938442	0.022118	0.340316	0.004055	0.011744
GTSE1	Up	138	2.953512	0.017776	0.33858	0.007634	0.012333
KIFC3	Down	136	2.949957	0.018258	0.338988	0.006904	0.012187
CCNA2	Up	132	2.961189	0.013698	0.337702	0.011937	0.016085
CCND1	Down	128	2.925931	0.013883	0.341772	0.00427	0.016102

repressing the PDGF-receptor (R)- $\alpha$  [42], which aligns with our finding implicating downregulation of HDAC in the oral mucosal wound healing processes. Microtubule-associated protein 1 light chain 3 alpha (MAP1LC3A), also named LC3, encodes a central protein in the autophagy pathway and is therefore widely used as a marker for detecting autophagy and autophagic cell death [43]. As the activation of the autophagy pathway is reported as essential for myofibroblast differentiation and collagen deposition during wound healing [44], the MAP1LC3A gene as an autophagy-related marker is plausible as integral to oral mucosal wound healing. Besides, another family member of microtubule-associated protein-microtubule-associated protein 4 (MAP4) has been shown to regulate the migration and proliferation of epidermal keratinocytes and further influence epidermal wound healing by activating the p38/MAPK pathway. However, the function of the microtubule-associated protein family has not been investigated in the context of oral mucosal injury healing. Aurora kinase A (AURKA) encodes a cell cycle-regulated kinase that

is involved in the formation and/or stabilization of microtubules [45]. Targeting microtubules could potentially enhance the wound healing process by promoting cell migration [46]; thus, AURKA might impact oral mucosa wound repair by influencing cell migration. PLK1 is a family member of the polo-like kinase (Plks) family, which has been demonstrated to be a key regulator of the cell cycle [47]. PLK1 plays a role in regulating mitotic entry, spindle assembly, anaphase entry, and cytokinesis in the mitotic phase and DNA checkpoints [48]. Since cell cycle regulatory genes are important for the reepithelialization of oral mucosal wounds by influencing cellular proliferation [49], the overexpression of PLK1 possibly enhances the oral mucosal wound healing by promoting cell proliferation. While existing evidence supports the role of most of the hub genes' involvement in oral mucosal wound healing, their specific functions have not yet been verified by previous research. Future experimental studies should be designed to validate their roles during the healing of oral mucosal injury.

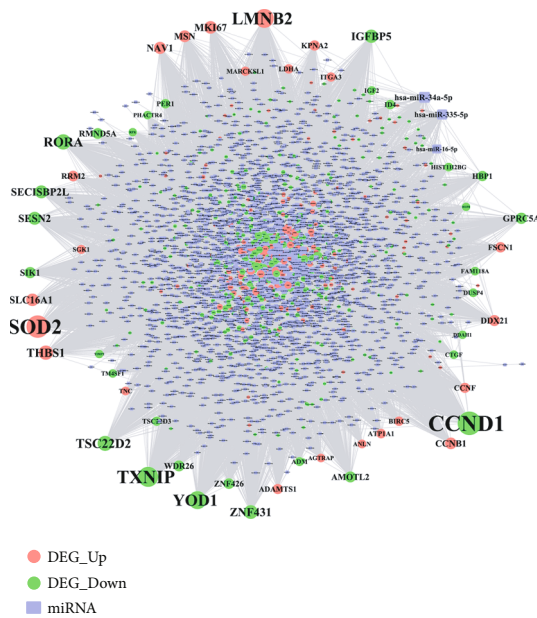


FIGURE 4: The miRNA-target interaction network involved in oral mucosa regeneration. The round nodes with different colours, respectively, represent the upregulated and downregulated DEGs, while the square nodes represent the miRNAs that target DEGs.

Two miRNAs, miR-34a-5p and miR-335-5p, were identified as pivotal in the miRNA-target DEGs network, by targeting the greatest number of DEGs. miR-34a-5p, derived from 5' ends of pre-miR-34a, is a member of the miR-34 family, and miR-34a is a well-known tumor suppressor [50], shown to mediate endothelial progenitor cell-mediated angiogenesis [51]. The knockout of miR-34a has been shown to impair wound healing by augmenting inflammatory response and delaying reepithelialization [52], implying that miR-34a upregulation could be a potential novel strategy for enhancing mucosal regeneration. As shown in Figure 4, miR-34a-5p was noted to target several DEGs including AMOTL2, THBS1, and FSCN1. Among these, Angiotensin-Like 2 (AMOTL2) has been previously reported as downregulated during wound healing after oral mucosal injury. The AMOTL2 gene has also been found to regulate the polarity, migration, and proliferation of endothelial cells [53]. Thus, it may be considered a potential target for gene therapy in cell-based regenerative strategies, as its upregulation in oral mucosa endothelial cells could facilitate angiogenesis during wound healing. Thrombospondin 1 (THBS1), also named TSP1, is documented to be a major activator of transforming growth factor- (TGF-)  $\beta$ 1 [54]. Previous studies have shown that the knockdown of TSP1 could decrease the rate of reepithelialization, wound neovascularization, and migration of fibroblast and endothelial cells, thereby impairing the wound healing process [55–57]. Our results indicated that TSP1 was upregulated during oral mucosal wound healing, which corroborates previous observations. The fascin actin-bundling protein 1 (FSCN1), also called fascin, encodes an actin-bundling protein that regulates the focal adhesion dynamics of cytoskeletal structures during cell migration [58]. The overexpression of FSCN1 is reported to promote

the cell migration of dendritic cells [59], which is in agreement with the expression pattern of FSCN1 noted in the present study. These genes may be considered targets of further research focused on gene modulation to enhance oral mucosal wound healing.

miR-335-5p was also identified as an important factor. The overexpression of miR-335 has been reported to promote diabetic wound healing by repressing the Sp1 transcription factor (Sp1) and downregulating matrix metalloproteinase- (MMP-) 9 [60]. Figure 3 in this study shows the DEGs targeted by miR-335-5p, including YOD1, TXNIP, and HBP1. Their relevance to wound healing is supported by earlier reports. For example, YOD1 (also known as OTUD2) is known to encode a protein that belongs to the ovarian tumor (OUT) family of deubiquitinating enzymes (DUBs) [61]. The overexpression of YOD1 was shown to promote the migration of oral keratinocytes by activating the TGF- $\beta$ 3 signaling pathway [62]. Contradictory to this observation, the present study indicated a downregulation of YOD1 during the mucosal healing process. Another identified gene, thioredoxin interacting protein (TXNIP), also known as vitamin D3 upregulated protein, is a major regulator of redox signaling and endoplasmic reticulum (ER) stress [63]. A recent study showed that the supplementation of vitamin D could significantly accelerate wound healing by suppressing ER stress [64]; however, the present study noted a downregulation of TXNIP in mucosal regeneration. Another gene targeted by miR-335-5p, HMG-box transcription factor 1 (HBP1), is a repressor of the cyclin D1 gene and can inhibit the Wnt-mediated beta-catenin signaling pathway. The activation of Wnt signaling has been shown to promote mucosal repair [65]. Our results indicated the downregulation of HBP1 during oral mucosal repair, suggesting that downregulating HBP1 might promote Wnt signaling and thereby augment oral mucosal repair.

Four signaling pathways (arachidonic acid metabolism, cell cycle, p53, and extracellular matrix- (ECM-) receptor interaction) were found significantly enriched during the healing of oral mucosa. Arachidonic acid (AA) is a fatty acid that is abundantly expressed after tissue injury [66]. AA and its metabolites have been demonstrated to facilitate wound healing by inducing the adhesion and migration of endothelial cells, as well as angiogenesis [66]. The effects of induction of AA on cell motility were found regulated by membrane type 3-matrix metalloproteinase- (MT3-MMP-) dependent fibronectin degradation [67]. The arrest of the cell cycle has been shown to impair wound healing, which is characterized by a significant number of senescent fibroblasts that are irreversible and refractory to growth factor stimulation, unless genetically modified [68]. In addition, it has been shown that periodontal pathogens (*Fusobacterium nucleatum* and *Porphyromonas gingivalis*) reduce wound healing by downregulating the cell cycle genes cyclin1, cyclin-dependent kinase 1 (CDK1), and CDK4 that are critical for G1/S transition and initiating the further process of DNA replication in S phase [69]. Concerning the cell cycle, the tumor suppressor gene p53 is of importance, being a master cell cycle regulator [70] and linked to the intrinsic apoptosis pathway, which is predominantly involved in the wound



TABLE 3: The topological characteristics of the top 30 nodes of the miRNA-target network involved in the oral mucosa regeneration.

Name	Label	Degree	Average shortest path length	Betweenness centrality	Closeness centrality	Topological coefficient
CCND1	Down	388	2.593186	0.081676	0.385626	0.035366
SOD2	Up	363	2.631931	0.071979	0.379949	0.032418
TXNIP	Down	322	2.646627	0.053959	0.377839	0.033412
LMNB2	Up	297	2.706747	0.049038	0.369447	0.029849
YOD1	Down	282	2.674015	0.046754	0.37397	0.04023
RORA	Down	231	2.725451	0.028034	0.366912	0.043835
TSC22D2	Down	225	2.752171	0.030429	0.36335	0.04615
THBS1	Up	209	2.738811	0.02335	0.365122	0.047046
ZNF431	Down	203	2.790247	0.028431	0.358391	0.040197
IGFBP5	Down	193	2.775551	0.023039	0.360289	0.042372
SECISBP2L	Down	186	2.755511	0.022275	0.362909	0.048889
SESN2	Down	186	2.738811	0.023606	0.365122	0.04734
MKI67	Up	178	2.782231	0.016852	0.359424	0.051973
SLC16A1	Up	176	2.834335	0.020942	0.352816	0.037253
NAV1	Up	168	2.784903	0.019746	0.359079	0.045105
MSN	Up	162	2.804275	0.020327	0.356598	0.042947
CCNB1	Up	159	2.798931	0.0135	0.357279	0.0552
GPRC5A	Down	155	2.818303	0.018532	0.354823	0.052165
SIK1	Down	153	2.806947	0.012722	0.356259	0.061204
AMOTL2	Down	149	2.815631	0.015657	0.35516	0.042484
WDR26	Down	148	2.814295	0.01461	0.355329	0.053959
DDX21	Up	147	2.765531	0.012253	0.361594	0.057614
RMND5A	Down	146	2.777555	0.012082	0.360029	0.054446
hsa-miR-34a-5p miRNA		144	2.359051	0.030631	0.423899	0.028501
ZNF426	Down	142	2.831663	0.016397	0.353149	0.041514
RRM2	Up	139	2.812291	0.013288	0.355582	0.058531
FSCN1	Up	136	2.843687	0.015655	0.351656	0.042006
HBP1	Down	135	2.795591	0.01225	0.357706	0.06161
KPNA2	Up	135	2.817635	0.010852	0.354908	0.062084
hsa-miR-335-5p miRNA		130	2.58016	0.032712	0.387573	0.022844

healing of oral mucosa, in contrast to that of skin [10]. The inhibition of p53 was reported to accelerate the early epithelization and neovascularization during wound healing [71], which supports a previous report showing that the expression level of p53 on the 3rd-day postwounding was close to that with prewounding levels and very low [10]. Furthermore, the interaction between ECM and cellular adhesion receptors (e.g., integrin and growth factor receptors) has been shown to regulate cellular activities of progenitor stem cells, including migration, differentiation, proliferation, and survival, during all phases of cutaneous wound healing [72]. In addition, fibronectin (FN) and chondroitin sulphate (CS), two components of ECM, are found as significantly elevated in oral mucosa as compared with skin [73], which could account for the faster healing of oral mucosa wounds than skin wounds [14]. These findings, together with our results, suggest that p53 signaling and ECM (especially FN and CS) interaction signaling can be regarded as specific characteris-

tics of oral mucosa wound healing that are distinct from skin wound healing.

Four transcription factors, FOS, PLAU, BCL6, and RORA, were identified as highly crucial to oral mucosa wound healing and as differentially expressed during the healing process. The transcription factor FOS (also called c-Fos) has been found to stimulate cell proliferation and regulate cell growth by interacting with c-Jun and further activating the activator protein- (AP-) 1 complex [74]. FOS was also found to be rapidly and specifically expressed by epidermal cells at the margin of the wound, thereby acting as an early molecular component during the wound healing process [75]. Another identified factor, plasminogen activator, urokinase (PLAU), encodes a secreted serine protease that can convert plasminogen to plasmin. The plasminogen activator/plasmin system has been shown to modulate cell adhesion and cellular migration by activating MMPs and TGF- $\beta$ , thereby providing the important link between PLAU



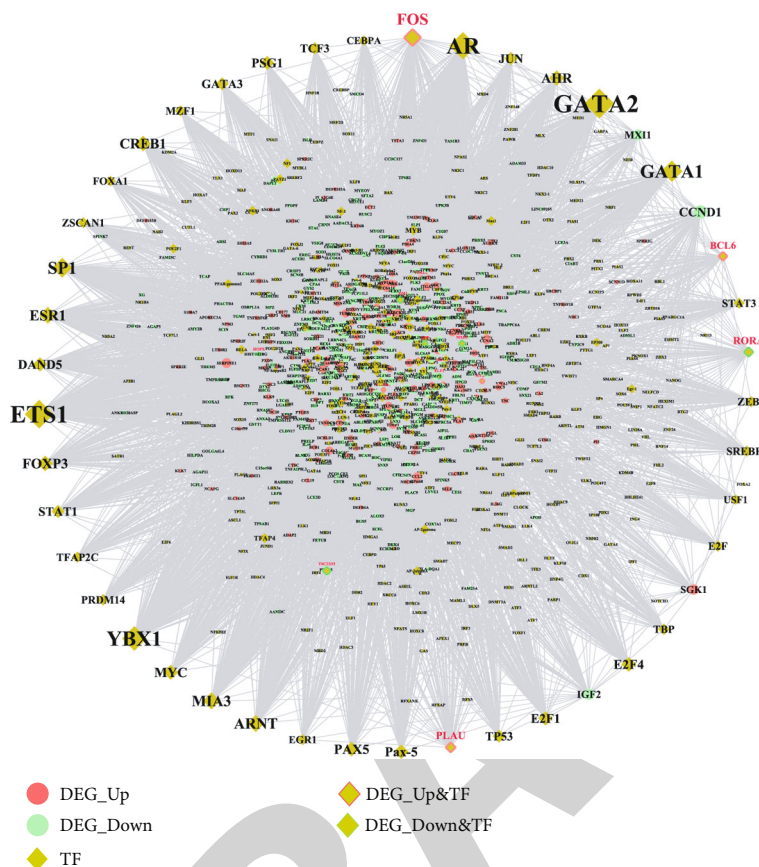


FIGURE 5: The transcription factor-target interaction network involved in oral mucosa regeneration. The round nodes with different colours represent the up- and downregulated DEGs; the diamond nodes with no-colour edges represent TFs; the diamond nodes with red-edges represent that these nodes are not only upregulated DEGs but also TFs; the diamond nodes with emerald colour represent that these nodes are not only downregulated DEGs but also TFs.

expression and wound healing [76]. B-cell lymphoma 6 protein (BCL6) (also named zinc finger protein 51 (ZNF51)) has been validated as a target of miR-155 [77]. The downregulation of BCL6 mRNA expression induced by the depletion of miR-155 has been noted to enhance dermal wound healing [77]. Retinoid-related orphan receptor alpha (RORA) is a transcription factor demonstrated to regulate the differentiation/survival of keratinocytes under hypoxic conditions [78]. Since oral mucosa wounds heal under significantly lower hypoxic conditions than skin wounds [79], the overexpression of RORA might be considered a specific feature of oral mucosa wound healing.

Four significant chemical compounds, Valproic acid, Doxorubicin, Nickel, and tretinoin, were identified to regulate the expression of DEGs that were dysregulated during oral mucosal wound healing. Valproic acid (VPA) has been commonly prescribed to treat neurological disorders for several decades owing to its neuroprotective effects [80]. VPA has the potential to enhance cutaneous wound healing as it exerts differential effects on cell proliferation and migration, via activating Wnt/ $\beta$ -catenin, extracellular signal-regulated kinase (ERK), and phosphatidylinositol 3-kinase (PI3K)/Akt signaling pathways [81]. Doxorubicin (DXR) is a typical chemotherapeutic agent that is widely used in cancer treatment and can act as an inhibitor of wound healing processes. For-

mer research suggested that DXR significantly delayed the restoration of tensile strength, resulting in skin thinning and degeneration of skin appendage after surgery [82]. Nickel (Ni), a metallic element routinely utilized for orthodontic and prosthetic device construction, improves chemical stabilization, corrosion resistance, and durability [83]. However, Ni can cause side effects under inflammatory conditions [84] and in turn induce immune responses along with exacerbating inflammation, thus impairing oral wound healing [85]. A high concentration of Ni was noted to promote inflammatory processes and proliferation via toll-like receptor- (TLR-) 4/nuclear factor-kappa B (NF- $\kappa$ B) activation in Interleukin- (IL-) 1 $\beta$ -induced human gingival fibroblasts (HGFs) [85]. Tretinoin, also known as all-trans retinoic acid (ATRA), has been applied as a useful treatment for epithelial wound healing and keratinization disorders, because of its role in stimulating angiogenesis and collagen production [86]. However, a previous study demonstrated that tretinoin retarded reepithelialization in open wounds [87]. In contrast, collagen production was found increased by tretinoin [88] in recent experimental research [89]. Therefore, the impact of tretinoin on wound healing remains controversial.

Four small molecules, atorvastatin, 17 $\beta$ -estradiol, curcumin, and vitamin D3, were identified as primary drug candidates relevant to oral mucosa regeneration. Statins are

TABLE 4: The topological characteristics of the top 30 nodes in the TF-target interaction network.

Name	Label	Degree	Average shortest path length	Betweenness centrality	Closeness centrality	Clustering coefficient	Topological coefficient
GATA2	TF	253	2.191833	0.082064	0.456239	0.001663	0.04192
ETS1	TF	241	2.178538	0.08846	0.459024	0.001729	0.040046
AR	TF	227	2.194682	0.07873	0.455647	0.00191	0.041171
YBX1	TF	202	2.298196	0.068148	0.435124	7.88E-04	0.044113
GATA1	TF	168	2.426401	0.030482	0.412133	0.001853	0.055186
SP1	TF	154	2.312441	0.036965	0.432444	0.00365	0.050859
FOS	Up_TF	139	2.025641	0.069117	0.493671	0.060369	0.045021
ARNT	TF	128	2.417854	0.018538	0.41359	0.002338	0.06006
MIA3	TF	127	2.48433	0.017272	0.402523	3.75E-04	0.068054
ESR1	TF	124	2.458689	0.021245	0.406721	0.001967	0.053796
CREB1	TF	113	2.439696	0.016546	0.409887	0.006637	0.059282
FOXP3	TF	113	2.603039	0.021352	0.384166	6.32E-04	0.065569
AHR	TF	109	2.504274	0.012008	0.399317	0.003058	0.068831
MYC	TF	108	2.5717	0.018731	0.388848	6.92E-04	0.068219
PAX5	TF	105	2.623932	0.011361	0.381107	1.83E-04	0.080365
E2F4	TF	104	2.518519	0.024369	0.397059	0.002801	0.052057
Pax-5	TF	102	2.683761	0.009227	0.372611	0	0.091831
E2F1	TF	99	2.477683	0.015085	0.403603	0.00268	0.062549
DAND5	TF	98	2.622982	0.007305	0.381245	0.002525	0.078717
PSG1	TF	97	2.645774	0.006395	0.377961	0.002577	0.081277
JUN	TF	91	2.509972	0.014222	0.398411	0.016361	0.063318
CCND1	Down	91	2.195632	0.057784	0.45545	0.01514	0.05193
STAT1	TF	89	2.51377	0.012112	0.397809	0.006639	0.062582
GATA3	TF	87	2.593542	0.009757	0.385573	0.002673	0.062089
TP53	TF	87	2.60019	0.015924	0.384587	0.001069	0.059128
Delta-CREB	TF	85	2.717949	0.005681	0.367925	0	0.096063
TCF3	TF	82	2.630579	0.009266	0.380144	0.002409	0.071966
PRDM14	TF	73	2.65812	0.006654	0.376206	0.003044	0.059795
PLAU	Up_TF	73	2.189934	0.029773	0.456635	0.082572	0.056671
TBP	TF	72	2.595442	0.016121	0.385291	0.003912	0.058185

recognized as therapeutic agents for treating different inflammatory conditions and wound healing and display diverse pleiotropic effects including anti-inflammatory, antioxidant, immunomodulation, antibacterial, and neangiogenesis effects [90]. Both oral and topical administration of atorvastatin produced a significant enhancement in wound healing [91, 92], which accelerated tissue repair by modulating inflammatory cytokines and cell growth-associated proteins. The female sex hormone  $17\beta$ -estradiol (estrogen/E2) is found to exert differential effects on females and males during wound healing [93].  $17\beta$ -Estradiol treatments are well established to have a beneficial influence on female cutaneous physiology:  $17\beta$ -estradiol promotes anti-inflammatory (M2) macrophage actions and the migration of keratinocytes and fibroblasts while decreasing the expression of proinflammatory cytokines and wound protease [93]. However,  $17\beta$ -estradiol is found to delay wound repair in male mice, since it retards reepithelialization and inhibits collagen secretion [94]. Curcumin, a highly pleiotropic molecule, is considered

a novel therapeutic for improving wound regeneration and is characterized by its anti-infectious, anti-inflammatory, and antioxidant properties [95]. Different topical formulations of curcumin, including nanoformulations, have been applied for wound healing activities (e.g., inflammation, proliferation, and remodelling) and play a vital role in scavenging free radicals, alleviating proinflammatory activities, improving neovascularization and extracellular matrix (ECM) synthesis, and inhibiting apoptosis and scar maturation [96]. Vitamin D3 is a fat-soluble secosteroid and exerts various effects on biological activities, including immunomodulation, antiaging, anticarcinogenesis, and anti-infection effects [97]. Previous studies have suggested that vitamin D has a potent anti-inflammatory and immunomodulating effect on dental caries [98] and oral candidiasis [99]. Specifically, vitamin D is shown to promote oral mucosal wound healing in many autoimmune oral diseases such as recurrent aphthous stomatitis, Behcet syndrome, and Sjögren syndrome [97].





larger sample sizes is essential to replicate these preliminary results. Furthermore, datasets examining the noncoding RNA (e.g., miRNAs, lncRNAs, and circRNAs) expression profiles were not found in public databases; therefore, the identification of the miRNAs in this study was through prediction based on the targeting interactions between DEGs and miRNAs. Studies investigating the epigenetic mechanisms involved in oral mucosa wound healing by examining noncoding RNA expression profiles would be valuable in this context.

Despite these limitations, the findings of our study may serve as the theoretical basis directing future experiments concerning oral wound healing models and related target genes. They also provide insights into potential therapeutic targets and strategies for treating chronic and nonhealing oral mucosa wounds. These results could also plausibly be applied to genetic and epigenetic modification of stem cells utilized for tissue regeneration and optimize the design of the tissue-engineered 3-dimensional (3D) culture models of oral mucosa regeneration. Further, these findings could advance the development of topical drugs targeting relevant gene targets for treating oral mucosa lesions. Challenges in clinical translation include that of synergistic application with conventionally used topical drugs accruing anti-inflammatory, analgesic, anesthetic, and antimicrobial effects. As such, these results should be considered preliminary and a directive for future research design.

## 5. Conclusion

This study identified several genes (GABARAPL1, GABARAPL2, HDAC5, MAP1LC3A, AURKA, and PLK1), two miRNAs (miR-34a-5p and miR-335-5p), four transcription factors (FOS, PLAU, BCL6, and RORA), and signaling pathways (arachidonic acid metabolism, cell cycle, p53, and extracellular matrix- (ECM-) receptor interaction) to be the most significant biomarkers in the wound repair process of oral mucosa injury. This study also identified significant chemical compounds (Valproic acid, Doxorubicin, Nickel, and tretinoin), as well as small molecular drugs (atorvastatin, 17 $\beta$ -estradiol, curcumin, and vitamin D3), which could influence the oral mucosal wound healing by regulating the expression of healing-associated DEGs/miRNAs. These entities could be important targets for genetic and epigenetic modification of oral mucosa-derived cells for tissue engineering and other treatment approaches for promoting oral mucosal wound healing.

## Data Availability

The data used to support the findings of this study are available from the corresponding author upon request.

## Ethical Approval

As this study only applied bioinformatic techniques based on computational analyses, all of the data from oral buccal mucosa biopsies were obtained from the public datasets, and original samples were not obtained. Therefore, this study did not require ethical approval.

## Conflicts of Interest

The authors declare that they have no conflicts of interest.

## Authors' Contributions

Wanchen Ning (Email: wanchen.ning@campus.lmu.de) is the first author and senior author. Dr. Shaonan Hu (Email: shaonan.hu@medizin.uni-leipzig.de), Prof. Dr. Xianda Hu (Email: hellocean@hotmail.com), and Dr. rer. med. Simin Li (Email: simin.li.dentist@gmail.com) are equal to the corresponding author.

## Acknowledgments

Dr. Wanchen Ning received doctoral study support from the China Scholarship Council (CSC) for Wanchen Ning (CSC No: 201608080112) at Ludwig-Maximilians-Universität München. Dr. Simin Li was funded by the Science Research Cultivation Program of Stomatological Hospital, Southern Medical University (Guangdong Provincial Stomatological Hospital) (No. PY2020004).

## Supplementary Materials

*Supplementary 1.* File S1. The DEGs dysregulated in the self-healing process of human oral mucosa injury.

*Supplementary 2.* File S2. The GO terms enriched by DEGs.

*Supplementary 3.* File S3. The KEGG pathways enriched by DEGs.

*Supplementary 4.* File S4. The topological characteristics of the nodes in the PPI network.

*Supplementary 5.* File S5. The topological characteristics of the nodes in the miRNA-target network.

*Supplementary 6.* File S6. The topological characteristics of the nodes in the TF-target network.

*Supplementary 7.* File S7. The topological characteristics of the nodes in the DEGs-chemical compound interaction network.

*Supplementary 8.* File S8. The topological characteristics of the nodes in the miRNA-small molecular drug interaction network.

## References

- [1] M. Koray and T. Tosun, "Oral mucosal trauma and injuries," in *Trauma in Dentistry*, IntechOpen, London, UK, 2019.
- [2] J. Lee, D. Shin, and J.-L. Roh, "Use of a pre-vascularised oral mucosal cell sheet for promoting cutaneous burn wound healing," *Theranostics*, vol. 8, no. 20, pp. 5703–5712, 2018.
- [3] J. L. Roh, J. Lee, H. Jang, E. H. Kim, and D. Shin, "Use of oral mucosal cell sheets for accelerated oral surgical wound healing," *Head & neck*, vol. 40, no. 2, pp. 394–401, 2018.
- [4] J. W. Sessions, D. G. Armstrong, S. Hope, and B. D. Jensen, "A review of genetic engineering biotechnologies for enhanced chronic wound healing," *Experimental Dermatology*, vol. 26, no. 2, pp. 179–185, 2017.

- [5] S.-B. Yong, J. Y. Chung, Y. Song, and Y.-H. Kim, "Recent challenges and advances in genetically-engineered cell therapy," *Journal of Pharmaceutical Investigation*, vol. 48, no. 2, pp. 199–208, 2018.
- [6] K. Mak, A. Manji, C. Gallant-Behm et al., "Scarless healing of oral mucosa is characterized by faster resolution of inflammation and control of myfibroblast action compared to skin wounds in the red Duroc pig model," *Journal of dermatological science*, vol. 56, no. 3, pp. 168–180, 2009.
- [7] L. Chen, Z. H. Arbieva, S. Guo, P. T. Marucha, T. A. Mustoe, and L. A. DiPietro, "Positional differences in the wound transcriptome of skin and oral mucosa," *BMC Genomics*, vol. 11, no. 1, p. 471, 2010.
- [8] A. Turabelidze, S. Guo, A. Y. Chung et al., "Intrinsic differences between oral and skin keratinocytes," *PLoS One*, vol. 9, no. 9, article e101480, 2014.
- [9] S. G. Keswani, S. Balaji, L. D. Le et al., "Role of salivary vascular endothelial growth factor (VEGF) in palatal mucosal wound healing," *Wound Repair and Regeneration*, vol. 21, no. 4, pp. 554–562, 2013.
- [10] A. Johnson, M. Francis, and L. A. DiPietro, "Differential apoptosis in mucosal and dermal wound healing," *Advances in wound care*, vol. 3, no. 12, pp. 751–761, 2014.
- [11] D. T. Graves and T. N. Milovanova, "Mucosal immunity and the FOXO1 transcription factors," *Frontiers in Immunology*, vol. 10, p. 2530, 2019.
- [12] L. Chen, A. Simões, Z. Chen et al., "Overexpression of the oral mucosa-specific microRNA-31 promotes skin wound closure," *International journal of molecular sciences*, vol. 20, no. 15, p. 3679, 2019.
- [13] A. Simões, L. Chen, Z. Chen et al., "Differential microRNA profile underlies the divergent healing responses in skin and oral mucosal wounds," *Scientific Reports*, vol. 9, no. 1, 2019.
- [14] R. Iglesias-Bartolome, A. Uchiyama, A. A. Molinolo et al., "Transcriptional signature primes human oral mucosa for rapid wound healing," *Science translational medicine*, vol. 10, no. 451, 2018.
- [15] Y. Tao, Y. Liu, C. Friedman, and Y. A. Lussier, "Information visualization techniques in bioinformatics during the postgenomic era," *Drug Discovery Today: BIOSILICO*, vol. 2, no. 6, pp. 237–245, 2004.
- [16] E. Clough and T. Barrett, "The Gene Expression Omnibus Database," in *Statistical genomics*, pp. 93–110, Springer, 2016.
- [17] C. Trapnell, L. Pachter, and S. L. Salzberg, "TopHat: discovering splice junctions with RNA-Seq," *Bioinformatics*, vol. 25, no. 9, pp. 1105–1111, 2009.
- [18] T. Downey, "[13] Analysis of a multifactor microarray study using Partek genomics solution," *Methods in enzymology*, vol. 411, pp. 256–270, 2006.
- [19] S. Anders and W. Huber, "Differential expression analysis for sequence count data," *Genome Biology*, vol. 11, no. 10, 2010.
- [20] G. Yu, L.-G. Wang, Y. Han, and Q.-Y. He, "clusterProfiler: an R package for comparing biological themes among gene clusters," *OmicS: a journal of integrative biology*, vol. 16, no. 5, pp. 284–287, 2012.
- [21] S. Peri, J. D. Navarro, R. Amanchy et al., "Development of human protein reference database as an initial platform for approaching systems biology in humans," *Genome Research*, vol. 13, no. 10, pp. 2363–2371, 2003.
- [22] R. Oughtred, C. Stark, B.-J. Breitkreutz et al., "The BioGRID interaction database: 2019 update," *Nucleic acids research*, vol. 47, no. D1, pp. D529–D541, 2019.
- [23] I. Xenarios, D. W. Rice, L. Salwinski, M. K. Baron, E. M. Marcotte, and D. Eisenberg, "DIP: the database of interacting proteins," *Nucleic acids research*, vol. 28, no. 1, pp. 289–291, 2000.
- [24] A. Chatr-aryamontri, A. Ceol, L. M. Palazzi et al., "MINT: the Molecular INTeraction database," *Nucleic acids research*, vol. 35, Supplement 1, pp. D572–D574, 2007.
- [25] A. Calderone and G. Cesareni, "Mentha: the interactome browser," *EMBNet.journal*, vol. 18, no. A, p. 128, 2012.
- [26] M. J. Cowley, M. Pinese, K. S. Kassahn et al., "PINA v2.0: mining interactome modules," *Nucleic acids research*, vol. 40, no. D1, pp. D862–D865, 2012.
- [27] K. Breuer, A. K. Foroushani, M. R. Laird et al., "InnateDB: systems biology of innate immunity and beyond—recent updates and continuing curation," *Nucleic acids research*, vol. 41, no. D1, pp. D1228–D1233, 2013.
- [28] M. J. Meyer, J. Das, X. Wang, and H. Yu, "INstruct: a database of high-quality 3D structurally resolved protein interactome networks," *Bioinformatics*, vol. 29, no. 12, pp. 1577–1579, 2013.
- [29] P. Shannon, A. Markiel, O. Ozier et al., "Cytoscape: a software environment for integrated models of biomolecular interaction networks," *Genome Research*, vol. 13, no. 11, pp. 2498–2504, 2003.
- [30] H.-Y. Huang, Y.-C.-D. Lin, J. Li et al., "miRTarBase 2020: updates to the experimentally validated microRNA–target interaction database," *Nucleic acids research*, vol. 48, no. D1, pp. D148–DD54, 2020.
- [31] F. Xiao, Z. Zuo, G. Cai, S. Kang, X. Gao, and T. Li, "miRecords: an integrated resource for microRNA–target interactions," *Nucleic acids research*, vol. 37, Supplement 1, pp. D105–D110, 2009.
- [32] D. Karagkouni, M. D. Paraskevopoulou, S. Chatzopoulos et al., "DIANA-TarBase v8: a decade-long collection of experimentally supported miRNA–gene interactions," *Nucleic acids research*, vol. 46, no. D1, pp. D239–D245, 2018.
- [33] E. Wingender, P. Dietze, H. Karas, and R. Knüppel, "TRANSFAC: a database on transcription factors and their DNA binding sites," *Nucleic acids research*, vol. 24, no. 1, pp. 238–241, 1996.
- [34] L. A. Bovolenta, M. L. Acencio, and N. Lemke, "HTRIdb: an open-access database for experimentally verified human transcriptional regulation interactions," *BMC Genomics*, vol. 13, no. 1, p. 405, 2012.
- [35] H. Han, J. W. Cho, S. Lee et al., "TRRUST v2: an expanded reference database of human and mouse transcriptional regulatory interactions," *Nucleic Acids Research*, vol. 46, no. D1, pp. D380–D386, 2018.
- [36] F. Vafaei, J. R. Krycer, X. Ma, T. Burykin, D. E. James, and Z. Kuncic, "ORTI: an open-access repository of transcriptional interactions for interrogating mammalian gene expression data," *PLoS One*, vol. 11, no. 10, article e0164535, 2016.
- [37] H. Xu, H. Yu, K. Tu et al., "cGRNB: a web server for building combinatorial gene regulatory networks through integrated engineering of seed-matching sequence information and gene expression datasets," *BMC Systems Biology*, vol. 7, Supplement 2, 2013.
- [38] C. J. Mattingly, M. C. Rosenstein, G. T. Colby, J. N. Forrest Jr., and J. L. Boyer, "The Comparative Toxicogenomics Database



- (CTD): a resource for comparative toxicological studies," *Journal of Experimental Zoology Part A: Comparative Experimental Biology*, vol. 305A, no. 9, pp. 689–692, 2006.
- [39] X. Liu, S. Wang, F. Meng et al., "SM2miR: a database of the experimentally validated small molecules' effects on micro-RNA expression," *Bioinformatics*, vol. 29, no. 3, pp. 409–411, 2013.
- [40] D. Han, H. Y. Kim, H. J. Lee, I. Shim, and D. H. Hahm, "Wound healing activity of gamma-aminobutyric acid (GABA) in rats," *Journal of Microbiology and Biotechnology*, vol. 17, no. 10, pp. 1661–1669, 2007.
- [41] C. Urbich, L. Rössig, D. Kaluza et al., "HDAC5 is a repressor of angiogenesis and determines the angiogenic gene expression pattern of endothelial cells," *Blood*, vol. 113, no. 22, pp. 5669–5679, 2009.
- [42] N. Zhang, C. W. Chan, E. Sanchez-Guerrero, and L. M. Khachigian, "Repression of PDGF-R- $\alpha$  after cellular injury involves TNF- $\alpha$ , formation of a c-Fos-YY1 complex, and negative regulation by HDAC," *American Journal of Physiology. Cell Physiology*, vol. 302, no. 11, pp. C1590–C1598, 2012.
- [43] I. Tanida, T. Ueno, and E. Kominami, "LC3 and autophagy," *Methods in Molecular Biology*, vol. 445, pp. 77–88, 2008.
- [44] E. Vescarelli, A. Pilloni, F. Dominici et al., "Autophagy activation is required for myofibroblast differentiation during healing of oral mucosa," *Journal of Clinical Periodontology*, vol. 44, no. 10, pp. 1039–1050, 2017.
- [45] A. S. Nikonova, I. Atsaturov, I. G. Serebriiskii, R. L. Dunbrack Jr., and E. A. Golemis, "Aurora A kinase (AURKA) in normal and pathological cell division," *Cellular and Molecular Life Sciences*, vol. 70, no. 4, pp. 661–687, 2013.
- [46] R. A. Charafeddine, J. D. Nosanchuk, and D. J. Sharp, "Targeting microtubules for wound repair," *Adv Wound Care*, vol. 5, no. 10, pp. 444–454, 2016.
- [47] S. Y. Lee, C. Jang, and K. A. Lee, "Polo-like kinases (plks), a key regulator of cell cycle and new potential target for cancer therapy," *Development & Reproduction*, vol. 18, no. 1, pp. 65–71, 2014.
- [48] S. Schmucker and I. Sumara, "Molecular dynamics of PLK1 during mitosis," *Molecular & Cellular Oncology*, vol. 1, no. 2, article e954507, 2014.
- [49] J. Bartkova, B. Grøn, E. Dabelsteen, and J. Bartek, "Cell-cycle regulatory proteins in human wound healing," *Archives of Oral Biology*, vol. 48, no. 2, pp. 125–132, 2003.
- [50] L. Zhang, Y. Liao, and L. Tang, "MicroRNA-34 family: a potential tumor suppressor and therapeutic candidate in cancer," *Journal of Experimental & Clinical Cancer Research*, vol. 38, no. 1, p. 53, 2019.
- [51] T. Zhao, J. Li, and A. F. Chen, "MicroRNA-34a induces endothelial progenitor cell senescence and impedes its angiogenesis via suppressing silent information regulator 1," *American Journal of Physiology. Endocrinology and Metabolism*, vol. 299, no. 1, pp. E110–E116, 2010.
- [52] N. Zhao, G. Wang, S. Long et al., "MicroRNA-34a deficiency leads to impaired wound closure by augmented inflammation in mice," *Annals of Translational Medicine*, vol. 8, no. 7, p. 447, 2020.
- [53] Y. Wang, Z. Li, P. Xu et al., "Angiomotin-like2 gene (amotl2) is required for migration and proliferation of endothelial cells during angiogenesis," *The Journal of Biological Chemistry*, vol. 286, no. 47, pp. 41095–41104, 2011.
- [54] T. R. Kyriakides and S. Maclachlan, "The role of thrombospondins in wound healing, ischemia, and the foreign body reaction," *Journal of cell communication and signaling*, vol. 3, no. 3-4, pp. 215–225, 2009.
- [55] A. Agah, T. R. Kyriakides, J. Lawler, and P. Bornstein, "The lack of thrombospondin-1 (TSP1) dictates the course of wound healing in double-TSP1/TSP2-null mice," *The American journal of pathology*, vol. 161, no. 3, pp. 831–839, 2002.
- [56] L. A. DiPietro, N. N. Nissen, R. L. Gamelli, A. E. Koch, J. M. Pyle, and P. J. Polverini, "Thrombospondin 1 synthesis and function in wound repair," *The American journal of pathology*, vol. 148, no. 6, pp. 1851–1860, 1996.
- [57] M. Streit, P. Velasco, L. Riccardi et al., "Thrombospondin-1 suppresses wound healing and granulation tissue formation in the skin of transgenic mice," *The EMBO journal*, vol. 19, no. 13, pp. 3272–3282, 2000.
- [58] M. Lamb and T. Tootle, "Investigating the roles of Fascin in collective cell migration using *Drosophila* border cell migration," *The FASEB Journal*, vol. 31, no. S1, 2017.
- [59] Y. Yamakita, F. Matsumura, M. W. Lipscomb et al., "Fascin1 promotes cell migration of mature dendritic cells," *Journal of immunology*, vol. 186, no. 5, pp. 2850–2859, 2011.
- [60] W. Wang, C. Yang, X. Y. Wang et al., "MicroRNA-129 and -335 promote diabetic wound healing by inhibiting Sp1-mediated MMP-9 expression," *Diabetes*, vol. 67, no. 8, pp. 1627–1638, 2018.
- [61] R. Ernst, B. Mueller, H. L. Ploegh, and C. Schlieker, "The otubain YOD1 is a deubiquitinating enzyme that associates with p97 to facilitate protein dislocation from the ER," *Molecular Cell*, vol. 36, no. 1, pp. 28–38, 2009.
- [62] Q. Ju, M. X. Li, G. Chen et al., "Overexpression of YOD1 promotes the migration of human oral keratinocytes by enhancing TGF- $\beta$ 3 signaling," *Biomedical and Environmental Sciences*, vol. 31, no. 7, pp. 499–506, 2018.
- [63] J. W. Chung, J. H. Jeon, S. R. Yoon, and I. Choi, "Vitamin D3 upregulated protein 1 (VDUP1) is a regulator for redox signaling and stress-mediated diseases," *The Journal of dermatology*, vol. 33, no. 10, pp. 662–669, 2006.
- [64] Y. F. Yuan, S. K. Das, and M. Q. Li, "Vitamin D ameliorates impaired wound healing in streptozotocin-induced diabetic mice by suppressing endoplasmic reticulum stress," *Journal of diabetes research*, vol. 2018, 10 pages, 2018.
- [65] J. Cosín-Roger, D. Ortiz-Masiá, S. Calatayud, C. Hernández, J. V. Esplugues, and M. D. Barrachina, "The activation of Wnt signaling by a STAT6-dependent macrophage phenotype promotes mucosal repair in murine IBD," *Mucosal immunology*, vol. 9, no. 4, pp. 986–998, 2016.
- [66] J. R. Silva, B. Burger, C. M. C. Kühn, T. Candreva, M. B. P. dos Anjos, and H. G. Rodrigues, "Wound healing and omega-6 fatty acids: from inflammation to repair," *Mediators of Inflammation*, vol. 2018, Article ID 2503950, 17 pages, 2018.
- [67] S. Oh, S. Lee, Y. Jung, H. Lee, and H. Han, "Arachidonic acid promotes skin wound healing through induction of human MSC migration by MT3-MMP-mediated fibronectin degradation," *Cell death & disease*, vol. 6, no. 5, article e1750, 2015.
- [68] J. S. V. Berg and M. C. Robson, "Arresting cell cycles and the effect on wound healing," *Surgical Clinics of North America*, vol. 83, no. 3, pp. 509–520, 2003.
- [69] R. Bhattacharya, F. Xu, G. Dong et al., "Effect of bacteria on the wound healing behavior of oral epithelial cells," *PLoS One*, vol. 9, no. 2, article e89475, 2014.

## Retraction

# Retracted: Potential Factors for Psychological Symptoms at Three Months in Patients with Young Ischemic Stroke

### BioMed Research International

Received 12 March 2024; Accepted 12 March 2024; Published 20 March 2024

Copyright © 2024 BioMed Research International. This is an open access article distributed under the Creative Commons Attribution License, which permits unrestricted use, distribution, and reproduction in any medium, provided the original work is properly cited.

This article has been retracted by Hindawi following an investigation undertaken by the publisher [1]. This investigation has uncovered evidence of one or more of the following indicators of systematic manipulation of the publication process:

- (1) Discrepancies in scope
- (2) Discrepancies in the description of the research reported
- (3) Discrepancies between the availability of data and the research described
- (4) Inappropriate citations
- (5) Incoherent, meaningless and/or irrelevant content included in the article
- (6) Manipulated or compromised peer review

The presence of these indicators undermines our confidence in the integrity of the article's content and we cannot, therefore, vouch for its reliability. Please note that this notice is intended solely to alert readers that the content of this article is unreliable. We have not investigated whether authors were aware of or involved in the systematic manipulation of the publication process.

Wiley and Hindawi regrets that the usual quality checks did not identify these issues before publication and have since put additional measures in place to safeguard research integrity.

We wish to credit our own Research Integrity and Research Publishing teams and anonymous and named external researchers and research integrity experts for contributing to this investigation.

The corresponding author, as the representative of all authors, has been given the opportunity to register their agreement or disagreement to this retraction. We have kept a record of any response received.

### References

- [1] D. Xu, X. Chu, K. Wang et al., "Potential Factors for Psychological Symptoms at Three Months in Patients with Young Ischemic Stroke," *BioMed Research International*, vol. 2021, Article ID 5545078, 7 pages, 2021.

## Research Article

# Potential Factors for Psychological Symptoms at Three Months in Patients with Young Ischemic Stroke

Dongjuan Xu,<sup>1</sup> Xi Chu,<sup>2</sup> Kun Wang,<sup>3,4</sup> Liyan Wei,<sup>1</sup> Yunyun Xu,<sup>1</sup> Xiaomin Huang,<sup>5</sup> Jinna Li,<sup>6</sup> Lina Xu,<sup>6</sup> Lu Yin,<sup>7</sup> Hong Liu,<sup>8</sup> Xiaolei Liu,<sup>9</sup> Haixia Leng,<sup>4</sup> Qing Xue,<sup>4</sup> Mao Peng,<sup>4</sup> Longbin Jia,<sup>6</sup> and Hongxing Wang<sup>4,10,11</sup>

<sup>1</sup>Department of Neurology, Dongyang People's Hospital, Wenzhou Medical University, Zhejiang, China 322100

<sup>2</sup>Health Management Department, Xuanwu Hospital, Capital Medical University, Beijing, China 100053

<sup>3</sup>Department of Neurology, Beijing Puren Hospital, Beijing, China 100062

<sup>4</sup>Department of Neurology, Xuanwu Hospital, Capital Medical University, Beijing, China 100053

<sup>5</sup>Department of Neurology, Ningcheng Center Hospital, Inner Mongolia, China 024200

<sup>6</sup>Department of Neurology, Jincheng People's Hospital, Shanxi, China 048026

<sup>7</sup>Medical Research & Biometrics Centre, National Centre for Cardiovascular Diseases, Fuwai Hospital, Peking Union Medical College & Chinese Academy of Medical Sciences, Beijing, China Beijing, China 102300

<sup>8</sup>Department of Neurology, Heping Hospital Affiliated to Changzhi Medical College, Shanxi, China 046000

<sup>9</sup>Department of Neurology, The First Affiliated Hospital of Kunming Medical University, Yunnan, China 650032

<sup>10</sup>Beijing Psychosomatic Disease Consultation Center, Xuanwu Hospital, Capital Medical University, Beijing, China 100053

<sup>11</sup>Institute of Sleep and Consciousness Disorders, Beijing Institute for Brain Disorders, Capital Medical University, Beijing, China 100053

Correspondence should be addressed to Hongxing Wang; wanghongxing@xwh.ccmu.edu.cn

Received 8 January 2021; Revised 13 January 2021; Accepted 20 January 2021; Published 9 February 2021

Academic Editor: Yuzhen Xu

Copyright © 2021 Dongjuan Xu et al. This is an open access article distributed under the Creative Commons Attribution License, which permits unrestricted use, distribution, and reproduction in any medium, provided the original work is properly cited.

**Objective.** Psychological status plays a vital role in the recovery in young ischemic stroke patients. However, few reports on the psychological symptoms in Chinese young ischemic stroke patients have been published. In the present study, we aimed to outline the psychological status of young ischemic stroke patients and its risk factors at three months after their stroke. **Methods.** 364 patients with young ischemic stroke and 384 age-matched healthy controls were consecutively recruited from our study hospitals of the mainland of China between June 2018 and November 2020. Social demographic and clinical data were collected from all enrolled participants in the acute stage of their stroke, and their psychological variables were assessed via the Symptom Checklist 90 Revised (SCL-90-R) at three-month timepoint after their stroke. Multivariable logistic regression analyses were run to identify the independent factors for psychological variables in patients. **Results.** Compared with healthy controls, patients with young ischemic stroke had significantly higher total score of SCL-90-R and all subscale total scores ( $p < 0.01$  or  $0.05$ ). 22.3% (81/364 cases) in young ischemic stroke patients had psychological abnormalities. Compared with young ischemic stroke patients without psychological symptoms ( $n = 283$ ), patients with psychological symptoms ( $n = 81$ ) had higher rate of married status ( $p = 0.03$ ), rate of hypertension ( $p = 0.01$ ), infarct size ( $p = 0.01$ ), and the family dysfunction ( $p < 0.01$ ). Multivariate logistic regression analyses revealed that the family dysfunction (odds ratio [OR], 2.50, 95% confidence interval [CI]: 1.71 to 3.54,  $p < 0.01$ ), having hypertension (OR, 3.27, 95% CI: 1.92 to 4.27,  $p = 0.02$ ), and  $\geq 20\text{mm}^3$  infarct size (OR, 2.39, 95% CI: 1.53 to 3.45,  $p < 0.01$ ) were independent factors for having psychological abnormalities in patients with young ischemic stroke at three months after their stroke. Single (OR, 1.23, 95% CI: 1.03 to 1.54,  $p = 0.01$ ), poor family function (OR, 1.21, 95% CI: 1.05 to 1.45,  $p = 0.03$ ), and  $\geq 20\text{mm}^3$  infarct size (OR, 1.74, 95% CI: 1.14 to 3.13,  $p = 0.02$ ) were independent factors for having depression in patients with psychological symptoms. The family dysfunction (OR, 2.32, 95% CI: 1.51 to 2.80,  $p < 0.01$ ) and hypertension (OR, 2.41, 95% CI: 1.54 to 3.46,  $p = 0.03$ ) were independent factors for emerging somatization and anxiety in patients with psychological symptoms, respectively. **Conclusions.** At three months after their stroke, young ischemic stroke patients had psychological problems and risk factors for developing them.

## 1. Introduction

Stroke is one leading cause of death in adults worldwide [1, 2] and is one of the main causes of death and a significant contributor to disability in adults in China, characterized by high rates of morbidity, fatality, and disability, bringing a severe economic burden [3–5]. Among the stroke population, the incidence of stroke in older adults decreases while the incidence of young adult stroke is increasing, around 1 in 10 about a young adult [1]. Youth adult stroke often occurs in adults aged 18 to 60 years, especially 18 to 45 years [6]. Moreover, there is a trend that stroke occurs in individuals at a younger age [6, 7]. Most importantly, stroke in young adults has a considerable socioeconomic influence associated with high health-care costs and tremendous loss of labor productivity [4, 6, 8, 9]. Therefore, any potential characteristics of the young adults' stroke still need to be further emphasized [10].

The negative emotion is one of the most symptoms emerging in patients with stroke [10, 11]. Unfortunately, the current optimal management of young adult patients with stroke, unlike treatment for older adults, is unknown [1, 12]. The available recovery strategy for young stroke patients does not provide psychological intervention [10]. The related risk factors on young adult patients have been summarized in the recent review [1], as there is no report on the psychological symptoms and its risk factors in young ischemic stroke patients.

The recovery for young ischemic stroke patients relies on not only physical rehabilitation but also psychological situation [1, 10, 13, 14]. Recent studies have shown that the post-stroke psychological status plays a role in the recovery of young ischemic stroke patients in the clinical practice setting [10, 15], while family support and social support are important factors associated with psychological status for persons who can find assistance from outside when they need help [16–18]. These aforementioned studies suggest that the post-stroke psychological level is necessarily explored in young ischemic stroke patients for their recovery. Here, we conducted a prospective study to investigate the psychological status and its risk factors in these populations.

## 2. Methods

**2.1. Clinic Setting.** All 364 patients and 384 age-matched healthy controls were consecutively recruited from our study hospitals and their health management departments, including 5 comprehensive hospitals of the mainland of China between June 2018 and November 2020. The study protocols were approved by the Local Ethics Committees of Xuanwu Hospital, Capital Medical University (LYS2018008) and Dongyang People's Hospital, Wenzhou Medical University (2017-KY-036 and 2018-YX-051). All subjects provided written informed consent. This research was conducted by the Helsinki Declaration.

**2.2. Participants.** Patients were consecutively enrolled the study if they met the following criteria: (a) aged 18 to 45 years, (b) satisfied the stroke diagnostic criteria formulated by the Chinese cerebrovascular disease classification and

were confirmed by magnetic resonance imaging or computed tomography scan [19], (c) could answer questionnaires independently, and (d) knew his/her illness. The exclusion criteria were (a) presence of the other nonvascular causes (such as primary brain tumor, brain metastases, subdural hematoma, postictal paralysis, and brain trauma) related to brain dysfunction; (b) a previous history of depression, psychosis, and dementia; (c) could not understand and complete the examination; and (d) refused to provide written consent.

**2.3. Measures.** At the baseline (i.e., in the acute stage of stroke), the following basic data were collected. Social-demographic and clinical data were collected from all enrolled participants in the acute stage of their stroke, including age, sex, living area (i.e., urban and rural), education status (i.e., junior high school and lower, senior high school and higher), marital status (i.e., married, unmarried, divorced, and widowed), having medical insurance (yes or no), monthly income (>6,000 Yuan, ≤6,000 Yuan), smoke and drink dependence (yes or no), hypertension (yes or no), diabetes (yes or no), atrial fibrillation (yes or no), the National Institute of Health Stroke Scale (NIHSS) [20], the modified Rankin Scale (mRS) [21], the Barthel Index (BI), infarct location (i.e., cortex, white matter lesions, basal ganglia + thalamus, brain stem, and cerebellum) [22, 23], and infarct size (≥20 vs. <20 mm<sup>3</sup>) calculated in three days after stroke onset by manually delineating the hypodense infarcted area(s) on hyperintense area(s) on axial diffusion weighted imaging slices on magnetic resonance imaging (MRI) [24, 25].

At three-month time after their stroke, all participants' psychological state was evaluated. In details, the psychological status, family function, and social support were assessed via the Symptom Checklist 90 Revised (SCL-90-R), the family function assessment scale (FFAS), and the social support rating scale (SSRS) at three months after stroke, respectively. After obtaining written informed consent, as explained by our study alliance doctors, all participants were administered via the questionnaires for their clinical assessment. The qualified raters were trained to give information about the questionnaire to the participants, who were permitted to complete the questionnaire by themselves without time restriction and in a state where patients were willing to cooperate.

The SCL-90-R is a 5-point scale, 90-item self-report tool that measures the degree of symptoms on different dimensions such as somatization, obsessive-compulsive, depression, anxiety, phobic anxiety, hostility, interpersonal sensitivity, paranoid ideation, and psychoticism [26]. It is widely used to screen psychological symptoms, and the Chinese version of the SCL-90-R is reported [27] with favorable validity and reliability [28]. Higher scores indicate more significant psychological symptoms. For Chinese, the total score of SCL-90-R is over 160, which is regarded as the criteria of an individual who has abnormal psychological status [29]. The results on SCL-90-R of the study were compared with the previously reported standard models of 1986 [30] and 2006 [31].

FFAS is a 3-point scale (0-not at all, 1-sometimes, 2-often), 5 items self-report instrument to evaluate family functioning via five dimensions, including adaption, cooperation, growth, affection, and intimacy. The total score of FFAS is 10



TABLE 1: Comparisons of SCL-90-R between young ischemic stroke patients and age-matched young healthy controls.

Features	Healthy ( $n = 384$ )	Patients ( $n = 364$ )	$p^1$
Age (years), mean $\pm$ SD	31.9 $\pm$ 6.1	31.8 $\pm$ 6.3	0.85
Male sex, % ( $n$ )	33.8 (130)	36.5 (133)	0.44
Urban residents, % ( $n$ )	92.4 (355)	97.2 (354)	0.52
Senior high school or higher, % ( $n$ )	93.5 (359)	93.1 (339)	0.84
Married, % ( $n$ )	42.2 (162)	70.3 (256)	<0.01
Had medical insurance, % ( $n$ )	98.7 (379)	98.6 (359)	1.00
Monthly income >6000 yuan, % ( $n$ )	57.3 (220)	56.9 (207)	0.91
Total SCL-90-R scores, mean $\pm$ SD	98.6 $\pm$ 16.9	147.4 $\pm$ 26.1	<0.01
Subscales of SCL-90-R			
Somatization, mean $\pm$ SD	1.1 $\pm$ 0.4	1.8 $\pm$ 0.5	<0.01
Obsessive-compulsive, mean $\pm$ SD	1.2 $\pm$ 0.3	1.7 $\pm$ 0.3	<0.01
Interpersonal sensitivity, mean $\pm$ SD	1.2 $\pm$ 0.3	1.5 $\pm$ 0.2	<0.01
Depression, mean $\pm$ SD	1.1 $\pm$ 0.3	1.7 $\pm$ 0.3	<0.01
Anxiety, mean $\pm$ SD	1.1 $\pm$ 0.3	1.8 $\pm$ 0.5	<0.01
Hostility, mean $\pm$ SD	1.0 $\pm$ 0.3	1.8 $\pm$ 0.4	<0.01
Phobic anxiety, mean $\pm$ SD	1.0 $\pm$ 0.4	1.8 $\pm$ 0.4	<0.01
Paranoid ideation, mean $\pm$ SD	1.0 $\pm$ 0.4	1.1 $\pm$ 0.1	0.02
Psychoticism, mean $\pm$ SD	0.9 $\pm$ 0.2	1.4 $\pm$ 0.1	<0.01

Abbreviations: SCL-90-R: Symptom Checklist 90 Revised; SD: standard deviance; <sup>1</sup> $p$  value was obtained using chi-square tests or Fisher's exact tests for categorical variables and Mann-Whitney  $U$  tests for continuous variables.

points, and the higher total score indicates better family function. The criteria for a good family function, moderate impairment in family function, and severe impairment in family function are 7-10 points, 4-6 points, and 0-3 points of the FFAS total score, respectively [16].

SSRS is a 10-item self-reported tool that evaluates the degree of an individual's social support over the past year. The tool comprises three subscales: subjective support, objective support, and utilization of support [17]. Subjective support means perceived social support that individual feel supported, cared, and helped by his/her family members, friends, and colleagues (e.g., how many close friends do you have? (1) None, (2) 1-2, (3) 3-5, and (4) 6). Objective support refers to visible, practical, and direct support (e.g., the recourses where you got financial and reliable support when you needed help?). The employment of support means the level of social support applied (how do you get help when in need? (1) I am self-dependent. (2) I seldom ask for help from others. (3) I sometimes ask for help from others. (4) I often ask for help from my relatives and friends.). The SSRS total score ranges from 12 to 66 points, and higher scores on this tool indicate a higher degree of social support. The SSRS has been shown to have good reliability and validity, with Cronbach's  $\alpha$  ranging from 0.825 to 0.896 [18]. The results of SSRS are classified into three different levels in our study. It is generally considered <20 points that indicate that the individual has obtained less social support, 20-30 points suggest that the individual has accepted general social support, and >30 points indicate that the individual has received satisfactory social support [18].

**2.4. Statistical Analysis.** In this study, a two-tailed significance level of overall  $p < 0.05$  was considered statistically significant. SAS, version 9.4 (SAS Institute Inc.), was used. Continuous data are shown as the means  $\pm$  standard deviation. Two-sample Wilcoxon tests for two groups were applied to evaluate different across groups according to various variables, such as sex, living in rural areas, educational level, marital status, medical insurance, monthly income, substance dependence (smoke, alcohol drink), hypertension, diabetes, atrial fibrillation, infarct location, family function, and social support and subscales of SCL-90-R. Subgroup analyses were performed for young adult stroke patients with and without psychological symptoms. We performed multi-variable logistic regression analyses using stepwise variable selection, and all variables were entered into the model to explore independent impact factors for psychological status.  $p < 0.15$  was used for variable selection.

### 3. Results

**3.1. Comparisons between Young Ischemic Stroke Patients and Age-Matched Young Healthy Controls.** In this sample, a total of 364 young adult stroke patients were included, with an age of  $31.8 \pm 6.3$  years (from 20 to 44 years). The positive detection rate of psychological abnormalities in young stroke patients was 22.3% (81/364 cases), with the reference of 160 as the cut-off value in China [28]. The SCL-90-R total score and subfactors were presented in Table 1. In comparison with the age-matched healthy controls during the same study period, the young patients in our study had higher scores on



TABLE 2: Comparisons on clinical characteristics between young ischemic stroke patients with and without psychological symptoms.

Characteristics	Patients without psychological symptoms (n = 283)	Patients with psychological symptoms (n = 81)	P <sup>1</sup>
Age (years), mean ± SD	31.8 ± 6.3	31.9 ± 6.2	0.46
Male sex, % (n)	37.1 (105)	34.6 (28)	0.68
Urban residents, % (n)	97.2 (275)	97.5 (79)	1.00
Senior high school or higher, % (n)	93.6 (265)	91.4 (74)	0.47
Married, % (n)	67.5 (191)	80.2 (65)	0.03
Had medical insurance, % (n)	98.9 (280)	97.5 (79)	0.34
Monthly income > 6000 yuan, % (n)	55.8 (158)	60.5 (49)	0.45
Smoker, % (n)	23.3 (66)	14.8 (12)	0.10
Drinker, % (n)	24.4 (69)	29.6 (24)	0.34
Hypertension, % (n)	10.2 (29)	21.0 (17)	0.01
Diabetes, % (n)	12.4 (35)	12.4 (10)	1.00
Atrial fibrillation, % (n)	20.1 (57)	18.5 (15)	0.75
Infarct location, % (n)			0.06
Cortex	32.5 (92)	21.0 (17)	
White matter lesions	4.6 (13)	0.0 (0)	
Basal ganglia + thalamus	32.5 (92)	39.5 (32)	
Brain stem	23.3 (66)	29.6 (24)	
Cerebellum	7.1 (20)	9.9 (8)	
Infarct size mm <sup>3</sup> , mean ± SD	20.63 ± 30.48	31.87 ± 43.71	0.01
NHSS score, mean ± SD	2.8 ± 3.3	2.6 ± 3.2	0.61
mRS score, mean ± SD	2.5 ± 0.8	2.5 ± 0.7	0.78
BI score, mean ± SD	82.9 ± 24	81.7 ± 27.6	0.70
Total SCL-90, mean ± SD	134.8 ± 7.6	191.6 ± 18.5	<0.01
FFAS total score, mean ± SD	4.5 ± 1.5	4.4 ± 2.2	0.75
7-10	15.6 (44)	24.7 (20)	<0.01
4-6	52.3 (148)	30.7 (25)	
0-3	32.2 (91)	44.4 (36)	
SSRS total score, mean ± SD	34.7 ± 10.2	33.2 ± 11.3	0.27
<20	9.2 (26)	7.4 (6)	0.09
20-30	22.6 (64)	34.6 (28)	
>30	68.2 (193)	28.0 (47)	
Subjective support, mean ± SD	20.1 ± 5.2	19.3 ± 5.8	0.22
Objective support, mean ± SD	8.1 ± 3.3	7.5 ± 3.6	0.16
Utilization of support, mean ± SD	6.5 ± 2.0	6.4 ± 2.3	0.85

Abbreviations: SD: standard deviance; NIHSS: National Institute of Health Stroke Scale; mRS: the modified Rankin Scale; BI: Barthel Index; FFAS: the Family function assessment scale; SSRS: the Social support rating scale; <sup>1</sup>p was obtained using chi-square tests or Fisher's exact tests for categorical variables and Mann-Whitney U tests for continuous variables.

psychological variables, including somatization, obsessive-compulsive, interpersonal sensitivity, depression, anxiety, hostility, phobic anxiety, paranoid ideation, and psychotism ( $p < 0.01$  or  $0.05$ ).

**3.2. Clinical Characteristics between Young Ischemic Stroke Patients with and without Psychological Symptoms.** Based on the SCL-90-R total score of 160 as a cut-off, all patients were classified into two subgroups as patients with and without psychological symptoms showing in Table 2. Marital status ( $p = 0.03$ ), hypertension ( $p = 0.01$ ), infarct size ( $p = 0.01$ ),

and percentage of patients with different levels of FFAS scores ( $p < 0.01$ ) were found significantly different between two subgroups.

**3.3. Multivariate Regression Analysis.** The multivariate logistic regression analyses (Table 3) showed that the family dysfunction (odds ratio [OR], 2.50, 95% confidence interval [CI], 1.71 to 3.54;  $p < 0.01$ ), having hypertension (OR, 3.27; 95% CI, 1.92 to 4.27;  $p = 0.02$ ), and  $\geq 20\text{mm}^3$  infarct size (OR, 2.39, 95% CI: 1.53 to 3.45,  $p < 0.01$ ) were risk factors for psychological symptoms among young ischemic patients.

TABLE 3: Outcomes of psychological manifestations via multivariate logistic regression analyses using stepwise variable selection.

Variables	OR (95% CI)	<i>p</i>
Model for SCL-90-R		
Family function (moderate and serious dysfunction vs. good)	2.50 (1.71, 3.54)	<0.01
Hypertension (yes vs. no)	3.27 (1.92, 4.27)	0.02
Infarct size ( $\geq 20$ vs. $< 20$ cm <sup>3</sup> )	2.39 (1.53, 3.45)	<0.01
Model for depression		
Marital status (single vs. married)	1.23 (1.03, 1.54)	0.01
Family function (moderate and serious dysfunction vs. good)	1.21 (1.05, 1.45)	0.03
Infarct size ( $\geq 20$ vs. $< 20$ cm <sup>3</sup> )	1.74 (1.14, 3.13)	0.02
Model for somatization		
Family function (moderate and serious dysfunction vs. good)	2.32 (1.51, 2.80)	<0.01
Model for anxiety		
Hypertension (yes vs. no)	2.41 (1.54, 3.46)	0.03

Abbreviations: OR: odds ratio; CI: confidence interval; SCL-90-R: Symptom Checklist 90 Revised.

In depression models, being single (OR, 1.23, 95% CI: 1.03 to 1.54,  $p = 0.01$ ), the family dysfunction (OR, 1.21, 95% CI: 1.05 to 1.45,  $p = 0.03$ ), and  $\geq 20$  mm<sup>3</sup> infarct size (OR, 1.74, 95% CI: 1.14 to 3.13,  $p = 0.02$ ) were selected as independent factors for patients with psychological symptoms. For somatization and anxiety, the family dysfunction (OR, 2.32, 95% CI: 1.51 to 2.80,  $p < 0.01$ ) and hypertension (OR, 2.41, 95% CI: 1.54 to 3.46,  $p = 0.03$ ) were predictors among patients with psychological symptoms, respectively.

#### 4. Discussion

The study showed that young ischemic adult stroke patients at three-month timepoint after their stroke had obvious psychological symptoms with an incidence of 22.3%, and the patients with psychological symptoms had higher percentages of married status, hypertension, family dysfunction, and large infarct size. The family dysfunction, having hypertension, and larger infarct size were prominently risk factors for those young patients developing psychological symptoms at three months after stroke.

Around one-fifth of patients with young ischemic stroke had psychological symptoms after three months of onset. This means that those young stroke patients are commonly comorbid with psychological abnormalities, which may negatively affect their quality of life and recovery outcome [5, 32] and might develop into various mental disorders after stroke [1]. Unlike older adults, as a particular social group, young people bear greater social responsibility. Therefore, it is of great significance to formulate strategies for youth stroke health care, which needs physical rehabilitation and psychological support. This concept of mixture intervention and rehabilitation needs to be gradually established for young stroke patients.

Our study found that young adult stroke patients with psychological symptoms had larger infarct size and higher percentages of having hypertension and family dysfunction than those in patients without psychological symptoms. There are no differences on clinical features, including infarct locations, NIHSS score, mRS score, BI score, diabetes, atrial

fibrillation, smoking, and drinking, and social supports, including subjective support, objective support, and utilization of support. These results indicated that two groups with and without psychological symptoms had similar disease features when their acute stages of stroke and the same social supports around them after three months. We further revealed that large infarct size, hypertension, and family dysfunction at the onset of stroke were risk factors for having psychological abnormalities among patients. Being single, the family dysfunction, and large infarct size were risk predictors for patients with psychological symptoms to have depressive symptoms. And the family dysfunction was a risk of emerging somatization and hypertension for anxiety in patients with psychological symptoms. These findings implied that the aforementioned variables might be associated with future intervention targets for young stroke patients.

Our results were consistent with the previous reports that a good family function is a crucial protector for family members to cope with emergencies and alleviate their psychological stressors [33, 34]. Importantly, the family function is closely related to individual health status, disease occurrence, and recovery [34]. The possible reasons for family function's role in an individual psychological situation may involve that family members have close relationships with each other and have subjective satisfaction with family functions. The close relations among family members do benefit to reduce the psychological stress and avoid the occurrence of negative emotions. Furthermore, the patient in good family function can obtain other family members' immediate assistance and relieve his/her psychological stress associated with stroke.

Our study did not find that social support was different among two groups in young adult stroke patients. This may indicate that subjects in our study have necessary social support for their daily life. Indeed, satisfactory social support means that individuals could obtain social support from the outside when they need help [35] and avoid the occurrence of adverse psychological problems [36, 37]. In addition, social support theory holds that social support can alleviate individual stress in adverse events and is a protective factor

for individuals' physical and mental development [36–38]. Moreover, social support is closely related to the individual's ability to respond to adverse events [39].

The study had some limitations. First, the study was a cross-sectional design, which is hard to verify the causal relationships of hypertension, infarct size, family functioning, and psychological status in young stroke patients. Second, abnormal psychological status may cause poor family function. Therefore, longitudinal studies are needed to clarify the causality in young stroke patients. Third, the study had an uneven number of samples in subgroups divided by clinical variables, especially marital status. Therefore, the results of the spousal situation in this study will need to be further verified. These limitations need to be further explained for developing effective strategies for young stroke patients.

The study provided meaningful evidence for young stroke patients for their further intervention, and some strengths should be emphasized. Our study is the first report on young Chinese stroke patients who had abnormal psychological status at three months after their stroke. The results benefit these patients' recovery after stroke via caring for psychological status. In addition, our study was conducted in outpatient clinic settings. The results had general application into other common outpatient settings.

## 5. Conclusions

In conclusion, young Chinese adult stroke patients had obvious psychological symptoms at three-month timepoint after their stroke, severe family dysfunction, hypertension, and large infarct size were risk predictors of emerging psychological abnormalities in Chinese young adult stroke patients three months later after their stroke. Therefore, further prevention and intervention strategies on psychological symptoms should focus on bettering family function, controlling hypertension, and positively intervening in primary vascular diseases associated with young ischemic stroke, to enhance their recovery after stroke.

## Data Availability

The materials in this manuscript are available from the corresponding author on reasonable request.

## Conflicts of Interest

All authors declare that they have no conflict of interest.

## Authors' Contributions

Dongjuan Xu, Xi Chu, Kun Wang, Lianyan Wei, Yunyun Xu, Xiaomin Huang, Jinna Li, Lina Xu, Hong Liu, Xiaolei Liu, Haixia Leng, Qing Xue, Mao Peng, and Longbin Jia carried out the data collection, data analysis, and revised the paper. Lu Yin analyzed the experiments. Hongxing Wang conceived and designed the experiments.

## Acknowledgments





This work was funded by the Zhejiang Provincial Natural Science Foundation of China (LGF18H090001), the National Key Technology R & D Program of China (2017YFC1310001), and Jinhua Science and Technology Plan Key Projects under Grant (2019-3-024).

## References

- [1] M. S. Ekker, E. M. Boot, A. B. Singhal et al., "Epidemiology, aetiology, and management of ischaemic stroke in young adults," *The Lancet Neurology*, vol. 17, no. 9, pp. 790–801, 2018.
- [2] Y. J. Jang, D. Park, H. S. Kim et al., "Assessment of the implementation of critical pathway in stroke patients: a 10-year follow-up study," *BioMed Research International*, vol. 2020, Article ID 3265950, 9 pages, 2020.
- [3] L. P. Liu, L. K. Wong, D. Z. Wang, and Z. R. Miao, "Current status of endovascular procedures in management of ischemic stroke in China," *CNS neuroscience & therapeutics*, vol. 20, no. 6, pp. 483–484, 2014.
- [4] V. L. Feigin, G. A. Roth, M. Naghavi et al., "Global burden of stroke and risk factors in 188 countries, during 1990–2013: a systematic analysis for the Global Burden of Disease Study 2013," *Lancet Neurology*, vol. 15, no. 9, pp. 913–924, 2016.
- [5] W. Wang, B. Jiang, H. Sun et al., "Prevalence, incidence, and mortality of stroke in China: results from a nationwide population-based survey of 480 687 adults," *Circulation*, vol. 135, no. 8, pp. 759–771, 2017.
- [6] W. W. Zhang, Z. Zhang, and Q. Bi, "A nation-wide multicenter related factor investigation in 2359 cases of young stroke," *Chinese journal of clinical rehabilitation*, vol. 7, pp. 2694–2695, 2003.
- [7] B. Nawaz, G. E. Eide, A. Fromm et al., "Young ischaemic stroke incidence and demographic characteristics - the Norwegian stroke in the young study - a three-generation research program," *European Stroke Journal*, vol. 4, pp. 347–354, 2019.
- [8] N. A. Maaijwee, L. C. Rutten-Jacobs, R. M. Arntz et al., "Long-term increased risk of unemployment after young stroke: a long-term follow-up study," *Neurology*, vol. 83, pp. 1132–1138, 2014.
- [9] Z. Chen, B. Jiang, X. Ru et al., "Mortality of stroke and its subtypes in China: results from a nationwide population-based survey," *Neuroepidemiology*, vol. 48, pp. 95–102, 2017.
- [10] H. Wang, W. Zhang, X. Yang et al., "Deeply understanding clinic status of post-stroke depression: a clinic syndrome following brain injury," *Zhonghua Yi Xue Za Zhi*, vol. 99, pp. 1611–1614, 2019.
- [11] M. L. Hackett, S. Kohler, J. T. O'Brien, and G. E. Mead, "Neuropsychiatric outcomes of stroke," *The Lancet Neurology*, vol. 13, no. 5, pp. 525–534, 2014.
- [12] L. L. Liu, Z. F. Mou, H. X. Yang, M. SHI, H. WAN, and Y. WANG, "Relevant study of mental health and coping style in patients with cerebral stroke," *China Medical Herald*, vol. 12, pp. 51–54, 2015.
- [13] N. A. Maaijwee, L. C. Rutten-Jacobs, P. Schaapsmeeders, E. J. Van Dijk, and F. E. de Leeuw, "Ischaemic stroke in young adults: risk factors and long-term consequences," *Nature Reviews Neurology*, vol. 10, pp. 315–325, 2014.

## Research Article

# The Hsp90 Inhibitor 17-DMAG Attenuates Hyperglycemia-Enhanced Hemorrhagic Transformation in Experimental Stroke

Jiaming Zhang <sup>1</sup>, Kai Wang <sup>2</sup>, Jia Qi,<sup>3</sup> Xiaodong Cao <sup>1</sup>, and Feng Wang <sup>4</sup>

<sup>1</sup>Department of Emergency, Wuxi People's Hospital Affiliated to Nanjing Medical University, Wuxi, China 214023

<sup>2</sup>Department of Neurology, Second Affiliated Hospital of Xuzhou Medical University, Xuzhou City, Jiangsu Province, China

<sup>3</sup>Department of Pharmacy, Xinhua Hospital Affiliated to Shanghai Jiaotong University School of Medicine, Shanghai, China

<sup>4</sup>Department of Neurology, Shanghai 7th Hospital Affiliated to Shanghai Traditional Chinese Medical University, Shanghai, China 200000

Correspondence should be addressed to Feng Wang; [wfwangfeng@yahoo.com](mailto:wfwangfeng@yahoo.com)

Received 14 December 2020; Revised 7 January 2021; Accepted 17 January 2021; Published 4 February 2021

Academic Editor: Yuzhen Xu

Copyright © 2021 Jiaming Zhang et al. This is an open access article distributed under the Creative Commons Attribution License, which permits unrestricted use, distribution, and reproduction in any medium, provided the original work is properly cited.

**Introduction.** Hemorrhagic transformation (HT) is one of the most common complications of ischemic stroke which is exacerbated by hyperglycemia. Oxidative stress, inflammatory response, and matrix metalloproteinases (MMPs) have been evidenced to play a vital role in the pathophysiology of HT. Our previous study has reported that 17-DMAG, an Hsp90 inhibitor, protects the brain against ischemic injury via inhibiting inflammation and reducing MMP-9 after ischemia. However, whether 17-DMAG would attenuate HT in hyperglycemic middle cerebral artery occlusion (MCAO) rats is still unknown. **Methods.** Acute hyperglycemia was induced by an injection of 50% dextrose. Rats were pretreated with 17-DMAG before MCAO. Infarction volume, hemorrhagic volume neurological scores, expressions of inflammatory molecules and tight junction proteins, and activity of MMP-2 and MMP-9 were assessed 24h after MCAO. **Results.** 17-DMAG was found to reduce HT, improve neurological function, and inhibit expressions of inflammatory molecules and the activation of MMPs at 24h after MCAO. **Conclusion.** These results implicated that Hsp90 could be a novel therapeutic target in HT following ischemic stroke.

## 1. Introduction

Hemorrhagic transformation (HT) occurs in 10–4% of patients suffering from ischemic stroke, leading to significant morbidity and mortality in affected individuals [1, 2]. Previous studies have clearly demonstrated that hyperglycemia can increase HT incidence following ischemic stroke, potentially leading to more serious brain infarction in these patients [3]. This hyperglycemia-mediated enhancement of HT is known to be associated with increased oxidative stress and inflammatory activity, potentially leading to blood-brain barrier (BBB) disruption and the death of neurons [4]. This BBB disruption is thought to be primarily mediated by matrix metalloproteinases (MMP-2 and MMP-9) that are produced in response to inflammation and oxidative stress, thereby leading to the development of HT in ischemic stroke patients [5]. However, at present, the specific molecular mechanisms governing the onset of HT remain poorly

understood, and no effective treatments are available that are capable of preventing HT onset or curtailing HT-associated damage in patients after ischemic stroke.

The highly conserved chaperone protein Hsp90 (heat shock protein 90) is essential to guiding and stabilizing the folding of over 200 different proteins, including myriad transcription factors, kinases, and signaling regulators [6]. In the context of inflammation and oxidative stress as occurs during ischemic stroke, Hsp90 has further been shown to play an essential role in regulating the expression and activity of MMP proteins [7]. We have previously found that serum Hsp90 levels are significantly increased in patients following ischemic stroke and that these levels correlate with MMP-9 expression, thus raising the possibility that Hsp90 may play a key role in regulating MMP-9 expression and consequent disruption of the BBB after cerebral ischemia [8]. However, whether Hsp90 inhibition is effective for HT in hyperglycemia condition still requires further investigation. Several potent Hsp90



inhibitors have been developed to date, with some of these compounds having been tested in clinical trials aimed at exploring their utility as a means of treating cancer. The selective Hsp90 inhibitor 17-dimethyl-aminothylamino-17-demethoxy-geldanamycin (17-DMAG) has been found to function through its ability to block the Hsp90 ATP binding site, thereby facilitating the degradation of certain Hsp90 target proteins [9]. We have recently found that 17-DMAG is capable of decreasing oxidative stress and inflammation in mice, thereby leading to reduced MMP expression and decreased ischemic brain damage and abdominal aortic aneurysm-associated morbidity and mortality [7, 8]. As MMPs are known to be key mediators of hyperglycemia-enhanced HT development after ischemic stroke, we therefore hypothesized that inhibiting Hsp90 may represent an effective means of treating HT in this context. In the present study, we therefore tested the ability of 17-DMAG to suppress the development or severity of acute hyperglycemia-enhanced HT in an experimental stroke model and to explore the molecular mechanisms underlying such suppression.

## 2. Materials and Methods

**2.1. Statement of Ethics.** The research conforms to the Guide for the Care and Use of Laboratory Animals published by the US National Institutes of Health (NIH Publication No. 85-23, revised 1996), and the protocol was approved by the Institutional Animal Care Committee at Nanjing Medical University.

**2.2. Middle Cerebral Artery Occlusion (MCAO) Model.** Rats used for this study were randomized into three groups: sham, MCAO, or 17-DMAG+MCAO. The MCAO procedure was conducted in these rats as in past studies [10]. Briefly, a small incision was made in the external carotid artery through which a 4-0 nylon monofilament with a rounded tip was introduced. After 1.5 h, this suture was removed to permit the initiation of reperfusion. The surgical procedure in sham rats was identical, but the suture was not inserted. At 30 minutes prior to MCAO, rats in both the MCAO and 17-DMAG+MCAO groups were intraperitoneally injected with 50% dextrose (DX, 6 ml/kg) in order to induce acute hyperglycemia. Immediately following MCAO treatment, appropriate animals were intraperitoneally administered 17-DMAG (0.2 mg/kg) or vehicle control, with doses having been selected based on our previous analysis [8].

**2.3. Hemorrhagic Volume Measurement.** A spectrophotometric assay was used to assess the volume of cerebral hemorrhage in model animals, as in previous studies [11]. Briefly, a standard curve was generated using a mock-up hemorrhage model wherein specific volumes of blood were added to perfused brain tissue samples, after which hemispheric brain tissue underwent sonication-based homogenization. These homogenates were then spun for 30 minutes at 13,000 rpm, after which 400  $\mu$ l of the supernatant was collected and combined with 1.6 Drabkin reagent (Sigma). A spectrophotometer (Spectronics 3000; Milton-Roy) was then used to quantify sample absorbance at 540 nm. Hemoglobin content in exper-

imental animals was determined through comparison with the resultant standard curve, thus allowing for quantification of hemorrhage volume.

**2.4. 2,3,5-Triphenyltetrazolium Chloride (TTC) Staining.** TTC staining was used to measure infarct volume, as in previous reports [12]. Briefly, 24 h post-MCAO, rats underwent deep anesthetization using isoflurane and were then euthanized. Brain tissue was collected and separated into six total serial coronal sections at 2 mm thickness. These sections were then added to 2% TTC for 15 minutes prior to analysis. The relative infarct size was calculated with the following equation: relative infarct size = (contralateral area – ipsilateral noninfarct area)/contralateral area.

**2.5. Neurobehavioral Assessments.** A previously developed scoring system was used to gauge neurological deficits in study animals at 24 h post-MCAO [13]. A researcher who was blinded to animal group assignments made all neurobehavioral measurements. Six individual test scores (spontaneous activity, symmetry in the movement of four limbs, forepaw outstretching, climbing, body proprioception, and response to vibrissal touch) were added together to yield an overall score that was between 3 and 18. The cumulative score for each group was then calculated.

**2.6. Western Blotting.** Cortical tissue samples were collected, and total protein was then extracted and quantified with a BCA kit (Thermo Scientific). Equivalent protein amounts then underwent 10% SDS-PAGE separation and were transferred to PVDF membranes for 2 h at 300 mA, and blots were then blocked with 5% nonfat milk in TBST for 1 h. Next, blots were probed overnight with antibodies specific for the following: histidine adduct (1:1000; Abcam); nitrotyrosine (1:1000; Cell Signaling Technology [CST]), ZO-1 (1:500; CST), occludin (1:500; CST), TNF- $\alpha$  (1:1000; CST), IL- $\beta$  (1:1000; CST), and GAPDH (1:1000; CST). Next, an IRDye800CW-conjugated secondary antibody was used to probe blots, after which an Odyssey imaging system (LICOR) was used to detect protein bands.

**2.7. Gelatin Zymography.** MMP-2 and MMP-9 activity in brain tissue homogenates was quantified via gelatin zymography as in previous studies [14]. Briefly, a total of 50  $\mu$ g of a given lysate sample was added to a well holding 10% acrylamide gels containing 0.1% gelatin. Tris-glycine running buffer was then used for separation, after which gels were washed and added to renaturing buffer for 1 h at 37°C. Next, gels were added to the development buffer for 24 h at 37°C, after which they were stained for 1 h using 0.5% Coomassie Blue G-250. Destaining solution was then used to treat gels thrice, after which ImageJ was used to quantify MMP activity.

**2.8. Statistical Analyses.** Data are means  $\pm$  SEM. Samples were compared via two-way ANOVAs with Tukey's post hoc test, with  $p < 0.05$  as the significance threshold.



### 3. Results

**3.1. Blood Glucose Level Measurement.** At 2 h postdextrose injection, injected animals had significantly increased blood glucose levels relative to at baseline, and these levels remained elevated for up to 6 h. No impact on blood glucose levels was observed following 17-DMAG treatment (Figure 1(a)). Moreover, treatment of mice with 0.2 mg/kg 17-DMAG barely affected the body weight of the mice, suggesting the possible safety of 17-DMAG at this low dose.

**3.2. 17-DMAG Modulates Hyperglycemia-Enhanced HT following MCAO.** Consistent with past reports, we found that hyperglycemia led to extensive HT in ischemic areas of the brain in MCAO model rats at 24 h post-MCAO. Relative to animals injected with vehicle control, animals administered 17-DMAG exhibited significant reductions in both infarct size and hemorrhage volume at 24 h post-MCAO (Figures 1(b)–1(d)). There was also a clear correlation between infarct size and hemorrhage volume in these animals (Figures 1(b)–1(d)). Relative to sham controls, MCAO model animals exhibited clear neurological deficits that were partially reversed in MCAO model animals that had been treated with 17-DMAG (Figure 1(e)).

**3.3. 17-DMAG Treatment Suppresses MCAO-Mediated Changes in Tight Junction Protein Levels.** We next assessed whether 17-DMAG modulates BBB disruption in hyperglycemic MCAO model rats via measuring levels of the tight junction proteins occludin and ZO-1 via Western blotting. We observed significant reductions in occludin and ZO-1 levels in MCAO model animals, whereas 17-DMAG treatment significantly reduced these MCAO-associated changes (Figure 2).

**3.4. 17-DMAG Alters MMP Activity in Hyperglycemic MCAO Model Rats.** We next extended our analysis of how 17-DMAG impacts HT following MCAO in hyperglycemic rats through an assessment of MMP-2 and MMP-9 activity via a gelatin zymography approach. We observed significant increases in MMP-2 and MMP-9 activity at 24 h post-MCAO in hyperglycemic animals, whereas 17-DMAG treatment significantly reduced the activity of these MMPs (Figure 3). This thus suggests that 17-DMAG can suppress hyperglycemia-induced HT in part via inhibiting MMP-2 and MMP-9 following MCAO.

**3.5. 17-DMAG Modulates Oxidative Stress in Hyperglycemic MCAO Model Rats.** We observed significant increases in MDA content in ischemic brain tissues at 24 h post-MCAO, whereas these levels were significantly lower in animals treated with 17-DMAG. Consistent with this result, we similarly observed increased 4-hydroxy-2-nonenal and nitrotyrosine levels in MCAO model animals at 24 h post-MCAO, with 17-DMAG reducing these levels (Figure 4).

**3.6. 17-DMAG Suppresses Inflammation in Hyperglycemic MCAO Model Rats.** At 24 h post-MCAO, rats exhibited significant increases in TNF- $\alpha$  and IL-1 $\beta$  levels, whereas 17-

DMAG suppressed the upregulation of these inflammatory cytokines (Figure 5).

### 4. Discussion/Conclusion

The present report expands upon our previous study by demonstrating that the Hsp90 inhibitor 17-DMAG can both reduce brain infarction and suppress hyperglycemia-enhanced HT following MCAO in rats. Our results further suggest that 17-DMAG can prevent HT at least in part by decreasing inflammatory TNF- $\alpha$  and IL-1 $\beta$  production, suppressing oxidative stress, and inhibiting MMP-9 activity. As such, 17-DMAG may offer value as a therapeutic compound that can prevent HT in patients suffering from ischemic stroke.

Hsp90 functions as a key chaperone that supports the folding of many essential proteins within cells, including signaling proteins and transcription factors [15]. The Hsp90 inhibitor 17-DMAG reportedly suppresses inflammation and oxidative stress in many different disease models, including models of ischemic stroke and abdominal aortic aneurysm. We have previously shown that acute stroke patients exhibit increased expression of both serum Hsp90 and MMP-9, suggesting that Hsp90 may thus be related to BBB disruption in patients suffering from stroke. In an animal MCAO model, inhibition of Hsp90 has been shown to mediate neuroprotection that is associated with reduced inflammation and oxidative stress, as well as with reduced MMP activity and enhanced BBB integrity. Elevated MMP expression and activity has been shown to play a central role in stroke-associated breakdown of the BBB owing to the degradation of tight junctions [16]. Disruption of the BBB is associated with increased vascular permeability, resulting in more blood cells entering the parenchyma, thus driving hemorrhagic transformation. Up to 40% of ischemic stroke patients are hyperglycemic due to either acute stress or diabetes upon hospitalization. In the present study, we therefore explored the impact of the Hsp90 inhibitor 17-DMAG on hyperglycemia-induced HT in a rat MCAO model system. Consistent with previous reports, we found that 17-DMAG treatment enhanced neurological functionality and reduced HT in these animals, with improved tight junction integrity and MMP inhibition. In the mechanism, similar to our previous research in the bEnd.3 cell, it is speculated that 17-DMAG may inhibit MMP transcription and secretion by disrupting the binding of Hsp90 and IKK, which may lead to the degradation of IKK and subsequent inhibition of the binding of P65 to the promoter regions of MMP-9 [8]. Of note, 17-DMAG was also found to inhibit ANG II-induced expression of MMP-2 and MMP-9 via inhibition of AP-1 transcriptional activity [7].

HT is a serious event that occurs during reperfusion in hyperglycemic patients. Such injury is most often associated with oxidative stress and cell membrane lipid damage, resulting in cellular death. Hyperglycemia leads to increased production of reactive oxygen species (ROS) and associated ROS-mediated signaling, thus increasing levels of neuronal damage [17–19]. Importantly, there is substantial evidence suggesting that Hsp90 is a key regulator of ROS generation

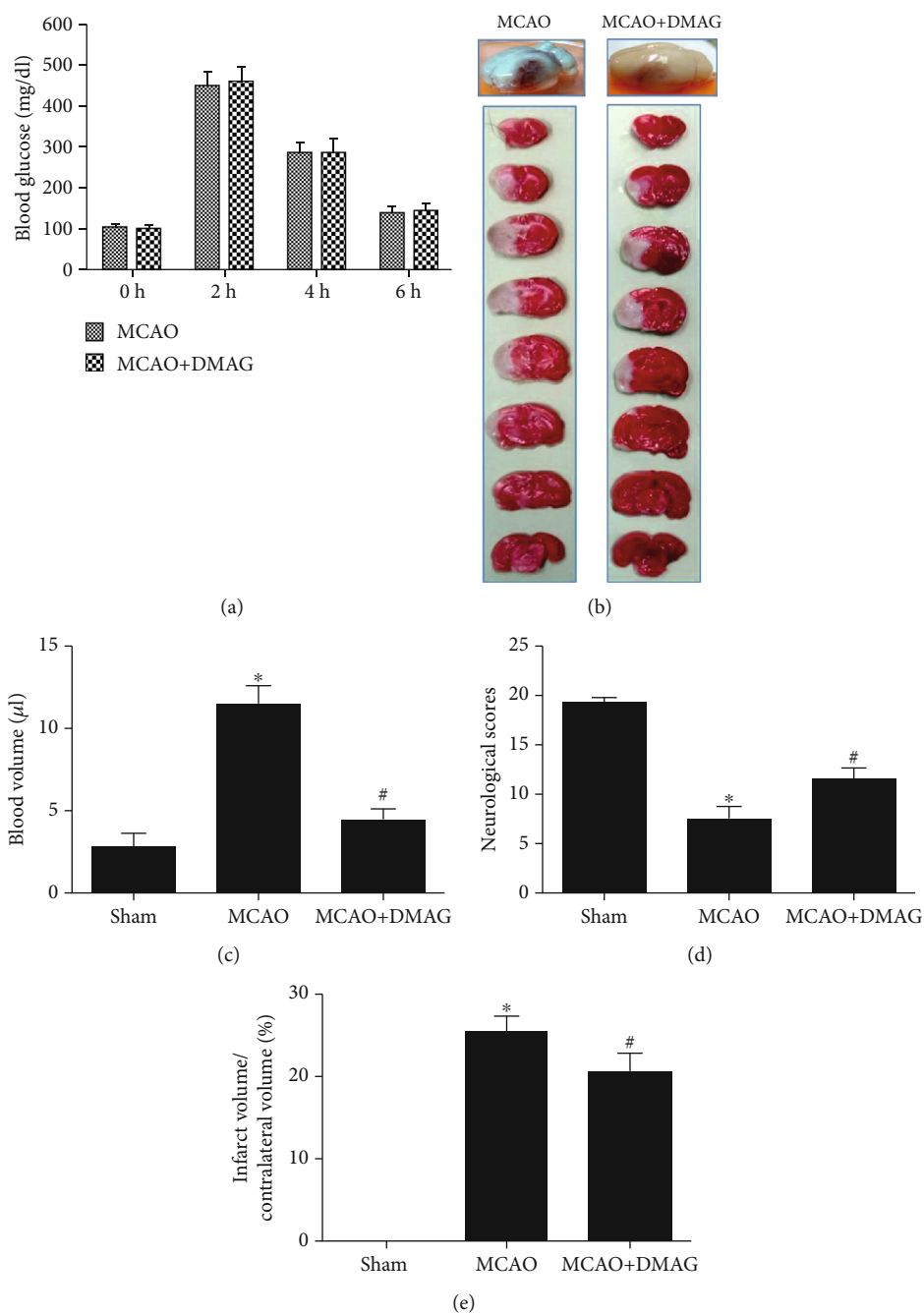


FIGURE 1: The effects of 17-DMAG on HT and neurological function in hyperglycemic MCAO rats. (a) 17-DMAG had no effects on blood glucose at the 4 time points. (b) Representative pictures of whole brain and TTC stained slices. 17-DMAG reduced hemorrhagic transformation following MCAO and decreased infarction volume. (c) Statistical analysis of blood volume in each group. 17-DMAG significantly reduced hyperglycemia-enhanced hemorrhagic volume at 24 h after MCAO. (d) Neurological function scoring at 24 h after MCAO. 17-DMAG significantly improved the neurological deficit at 24 h. \* $p < 0.05$  compared with sham group; # $p < 0.05$  compared with MCAO group.  $n = 5-8$  for each group.

owing to its ability to interact with enzymes in the nicotinamide adenine dinucleotide phosphate oxidase (Nox) family which mediates ROS production [19–20]. We have previously shown that 17-DMAG-mediated inhibition of Hsp90 can improve ROS scavenging and thereby improve ischemia/reperfusion injury outcomes. In this study, we determined that, consistent with previous findings, hyperglycemia and ischemia/reperfusion injury were associ-

ated with significant oxidative stress, potentially leading to BBB disruption and cerebral edema, with 17-DMAG being sufficient to suppress this damage associated with hyperglycemia-induced HT.

Inflammation is well-known to be closely associated with the pathogenesis of ischemic injuries. Hsp90 has also been shown to be a key regulator of inflammation, making it an important target of therapeutic intervention in patients

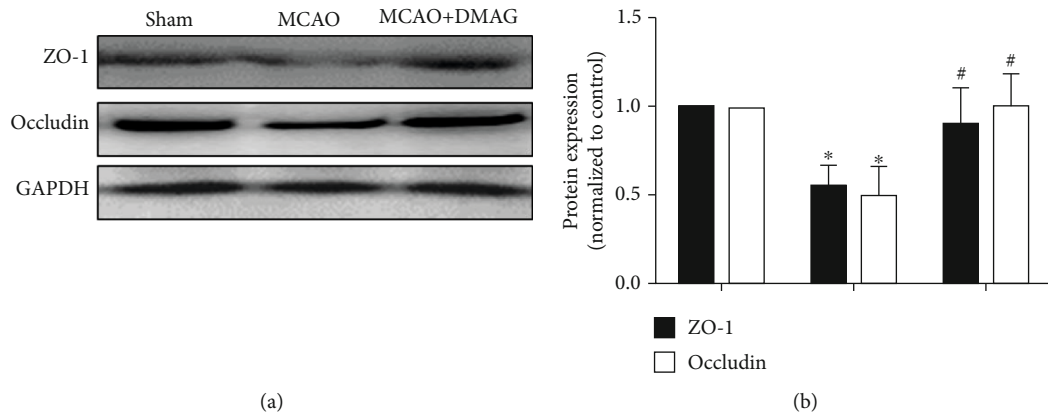


FIGURE 2: Effects of 17-DMAG on tight junction proteins in hyperglycemic MCAO rats. (a) Representative Western blots of ZO-1 and occludin. (b) 17-DMAG significantly restored occludin and ZO-1 downregulation. \* $p < 0.05$ , compared with the sham group; # $p < 0.05$ , compared with the MCAO group;  $n = 3$  for each group.

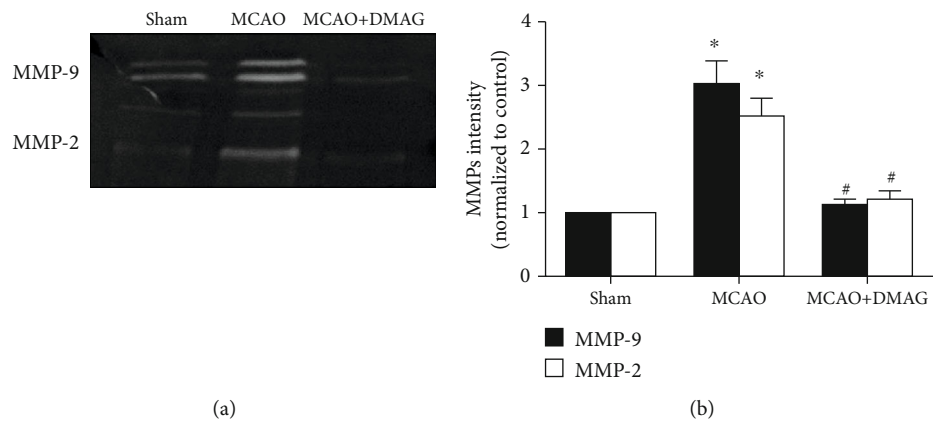


FIGURE 3: Effects of 17-DMAG on MMP activation in hyperglycemic rats after MCAO. (a) Representative bands for MMP-9 and MMP-2. (b) Statistical analysis for MMP-9 and MMP-2 activation. 17-DMAG remarkably decreased the activity of MMP-9 and MMP-2. \* $p < 0.05$ , compared with the sham group; # $p < 0.05$ , compared with the MCAO group;  $n = 3$  for each group.

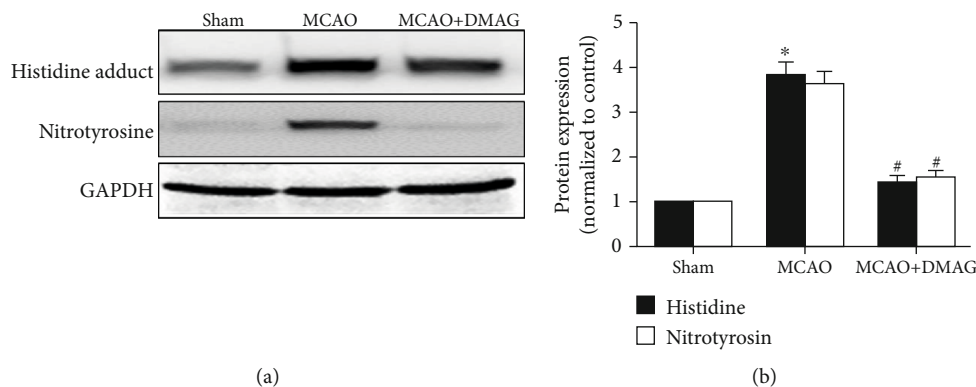


FIGURE 4: Effects of 17-DMAG on oxidative stress in hyperglycemic rats after MCAO. (a) Representative immunoblots of histidine adduct and nitrotyrosine at 24 h in the ischemic hemisphere. (b) Statistical analysis for the Western blot showed increased histidine adduct and nitrotyrosine levels in the MCAO group which were restored by 17-DMAG. \* $p < 0.05$ , compared with the sham group; # $p < 0.05$ , compared with the MCAO group;  $n = 3-4$  for each group.

suffering from ischemic stroke. We have previously shown that the Hsp90 inhibitor 17-DMAG can reduce damaging inflammation and oxidative stress in an animal model of

stroke, thus suggesting that 17-DMAG or other Hsp90 inhibitors may be ideal for achieving neuroprotection in the context of cerebral ischemia [8]. Other studies have shown that

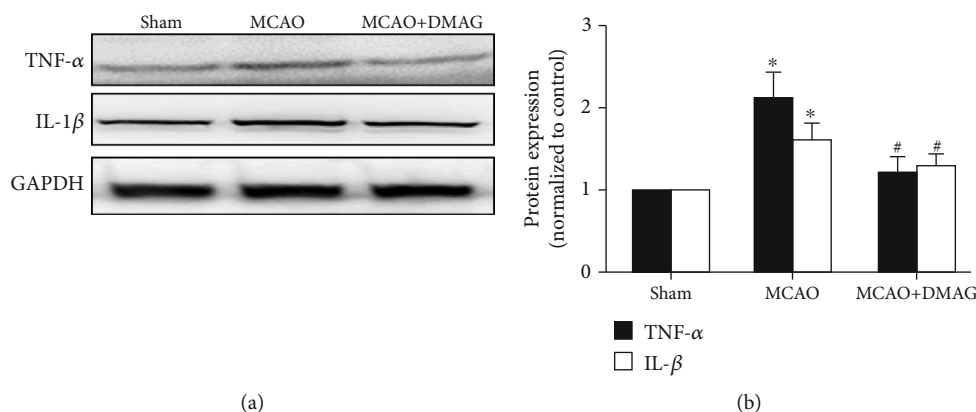


FIGURE 5: Effects of 17-DMAG on inflammation in hyperglycemic rats after MCAO. (a) Representative Western blots of TNF- $\alpha$  and IL-1 $\beta$ . (b) 17-DMAG effectively inhibited the increase of TNF- $\alpha$  and IL-1 $\beta$  in hyperglycemic rats after MCAO. \* $p < 0.05$ , compared with the sham group; # $p < 0.05$ , compared with the MCAO group;  $n = 3$  for each group.

Hsp90 inhibition can reduce the upregulation of inflammatory cytokines in ischemic brain tissue via disruption of IKK activity and associated NF- $\kappa$ B activation [21]. Consistent with these past findings, in the present report, we found that 17-DMAG suppressed inflammation and MMP-9 activity, thereby preventing BBB disruption and HT development in an animal model of ischemic stroke.

In conclusion, we demonstrated that 17-DMAG, an HSP90 inhibitor, markedly attenuated hyperglycemia-enhanced HT and improved neurological function after MCAO through simultaneously inhibiting ROS production, MMP expression, and inflammatory response. Although 17-DMAG has been withdrawn from the clinical trials for the treatment of cancer patients due to side effects, today, clinical trials of tens of Hsp90 inhibitors in oncological indications are underway [9]. Therefore, our findings may have direct translational implications for HT following ischemia stroke.

## Data Availability

The data used to support the findings of this study are available from Dr. Feng Wang upon request.

## Conflicts of Interest

The authors declare that they have no conflicts of interest.

## Authors' Contributions

Jiaming Zhang and Kai Wang are co-first authors and they contributed equally to this work.

## Acknowledgments

This study was supported by funds from the Shanghai Municipal Commission of Health and Family Planning (201540301), Scientific Research Project of Jiangsu Health Committee (No. H2019054), Xuzhou Science and Technology Planning Project (No. KC16SL121), and Natural Science Foundation of Shanghai (17ZR1418300).

## References

- [1] V. Terruso, M. D'Amelio, N. Di Benedetto et al., "Frequency and determinants for hemorrhagic transformation of cerebral infarction," *Neuroepidemiology*, vol. 33, no. 3, pp. 261–265, 2009.
- [2] J. A. Stone, J. Z. Willey, S. Keyrouz et al., "Therapies for hemorrhagic transformation in acute ischemic stroke," *Current Treatment Options in Neurology*, vol. 19, no. 1, p. 1, 2017.
- [3] D. Mi, P. Wang, B. Yang, Y. Pu, Z. Yang, and L. Liu, "Correlation of hyperglycemia with mortality after acute ischemic stroke," *Therapeutic Advances in Neurological Disorders*, vol. 11, 2017.
- [4] H. Kamada, F. Yu, C. Nito, and P. H. Chan, "Influence of hyperglycemia on oxidative stress and matrix metalloproteinase-9 activation after focal cerebral ischemia/reperfusion in rats: relation to blood-brain barrier dysfunction," *Stroke*, vol. 38, no. 3, pp. 1044–1049, 2007.
- [5] C. Lehner, R. Gehwolf, H. Tempfer et al., "Oxidative stress and blood-brain barrier dysfunction under particular consideration of matrix metalloproteinases," *Antioxidants & Redox Signaling*, vol. 15, no. 5, pp. 1305–1323, 2011.
- [6] C. Dello Russo, P. E. Polak, P. R. Mercado et al., "The heat-shock protein 90 inhibitor 17-allylamino-17-demethoxygeldanamycin suppresses glial inflammatory responses and ameliorates experimental autoimmune encephalomyelitis," *Journal of Neurochemistry*, vol. 99, no. 5, pp. 1351–1362, 2006.
- [7] J. Qi, P. Yang, B. Yi et al., "Heat shock protein 90 inhibition by 17-DMAG attenuates abdominal aortic aneurysm formation in mice," *American Journal of Physiology. Heart and Circulatory Physiology*, vol. 308, no. 8, pp. H841–H852, 2015.
- [8] J. Qi, Y. Liu, P. Yang et al., "Heat shock protein 90 inhibition by 17-dimethylaminoethylamino-17-demethoxygeldanamycin protects blood-brain barrier integrity in cerebral ischemic stroke," *American Journal of Translational Research*, vol. 7, no. 10, pp. 1826–1837, 2015.
- [9] T. Kim, G. Keum, and A. N. Pae, "Discovery and development of heat shock protein 90 inhibitors as anticancer agents: a review of patented potent geldanamycin derivatives," *Expert Opinion on Therapeutic Patents*, vol. 23, no. 8, pp. 919–943, 2013.
- [10] C. H. Chen, A. Manaenko, Y. Zhan et al., "Hydrogen gas reduced acute hyperglycemia-enhanced hemorrhagic

- transformation in a focal ischemia rat model,” *Neuroscience*, vol. 169, no. 1, pp. 402–414, 2010.
- [11] Q. Hu, C. Chen, J. Yan et al., “Therapeutic application of gene silencing MMP-9 in a middle cerebral artery occlusion-induced focal ischemia rat model,” *Experimental Neurology*, vol. 216, no. 1, pp. 35–46, 2009.
- [12] D. Gao, X. Zhang, X. Jiang et al., “Resveratrol reduces the elevated level of MMP-9 induced by cerebral ischemia-reperfusion in mice,” *Life Sciences*, vol. 78, no. 22, pp. 2564–2570, 2006.
- [13] J. H. Garcia, S. Wagner, K. F. Liu, and X. J. Hu, “Neurological deficit and extent of neuronal necrosis attributable to middle cerebral artery occlusion in rats. Statistical validation,” *Stroke*, vol. 26, no. 4, pp. 627–634, 1995.
- [14] Y.-X. Wang, B. Martin-McNulty, V. da Cunha et al., “Fasudil, a rho-kinase inhibitor, attenuates angiotensin II-induced abdominal aortic aneurysm in apolipoprotein E-deficient mice by inhibiting apoptosis and proteolysis,” *Circulation*, vol. 111, no. 17, pp. 2219–2226, 2005.
- [15] O. S. Kwon, T. J. Hong, S. K. Kim, J. H. Jeong, J. S. Hahn, and J. Jang, “Hsp90-functionalized polypyrrole nanotube FET sensor for anti-cancer agent detection,” *Biosensors & Bioelectronics*, vol. 25, no. 6, pp. 1307–1312, 2010.
- [16] S. Chen, J. Q. Luo, C. Reis, A. Manaenko, and J. M. Zhang, “Hydrocephalus after subarachnoid hemorrhage: pathophysiology, diagnosis, and treatment,” *BioMed Research International*, vol. 2017, Article ID 8584753, 8 pages, 2017.
- [17] P. A. Li, G. J. Liu, Q. P. He, R. A. Floyd, and B. K. Siesjo, “Production of hydroxyl free radical by brain tissues in hyperglycemic rats subjected to transient forebrain ischemia,” *Free Radical Biology & Medicine*, vol. 27, no. 9-10, pp. 1033–1040, 1999.
- [18] D. Bonnefont-Rousselot, “Glucose and reactive oxygen species,” *Current Opinion in Clinical Nutrition and Metabolic Care*, vol. 5, no. 5, pp. 561–568, 2002.
- [19] M. C. de Pinto, F. Tommasi, and L. De Gara, “Changes in the antioxidant systems as part of the signaling pathway responsible for the programmed cell death activated by nitric oxide and reactive oxygen species in tobacco bright-yellow 2 cells,” *Plant Physiology*, vol. 130, no. 2, pp. 698–708, 2002.
- [20] F. Chen, Y. Yu, J. Qian et al., “Opposing actions of heat shock protein 90 and 70 regulate nicotinamide adenine dinucleotide phosphate oxidase stability and reactive oxygen species production,” *Arteriosclerosis, Thrombosis, and Vascular Biology*, vol. 32, no. 12, pp. 2989–2999, 2012.
- [21] S. Shiraya, K. Miwa, M. Aoki et al., “Hypertension accelerated experimental abdominal aortic aneurysm through upregulation of nuclear factor kappaB and Ets,” *Hypertension*, vol. 48, no. 4, pp. 628–636, 2006.



## Research Article

# Imaging Hyperreflective Foci as an Inflammatory Biomarker after Anti-VEGF Treatment in Neovascular Age-Related Macular Degeneration Patients with Optical Coherence Tomography Angiography

Jing Wu <sup>1</sup>, Chaoyang Zhang <sup>2,3</sup>, Qian Yang <sup>4</sup>, Hai Xie <sup>4</sup>, Jingting Zhang <sup>2,3</sup>,  
Qinghua Qiu <sup>2,3</sup>, Kun Liu <sup>2,3</sup>, Dawei Luo <sup>2,3</sup>, Fang Liu <sup>1</sup> and Jingfa Zhang <sup>1,2,3,4</sup>

<sup>1</sup>Department of Ophthalmology, Shanghai Tenth People's Hospital, Tongji University School of Medicine, Shanghai, China

<sup>2</sup>Department of Ophthalmology, Shanghai General Hospital (Shanghai First People's Hospital), Shanghai Jiao Tong University, Shanghai, China

<sup>3</sup>National Clinical Research Center for Eye Diseases, Shanghai Key Laboratory of Ocular Fundus Diseases, Shanghai Engineering Center for Visual Science and Photomedicine, Shanghai Engineering Center for Precise Diagnosis and Treatment of Eye Diseases, Shanghai, China

<sup>4</sup>Tongji Eye Institute, Tongji University School of Medicine, Shanghai, China

Correspondence should be addressed to Fang Liu; [fangliu\\_2004@yahoo.com](mailto:fangliu_2004@yahoo.com) and Jingfa Zhang; [13917311571@139.com](mailto:13917311571@139.com)

Received 30 December 2020; Revised 20 January 2021; Accepted 27 January 2021; Published 4 February 2021

Academic Editor: Qian Wang

Copyright © 2021 Jing Wu et al. This is an open access article distributed under the Creative Commons Attribution License, which permits unrestricted use, distribution, and reproduction in any medium, provided the original work is properly cited.

**Purpose.** To investigate the hyperreflective foci (HRF) as an inflammatory biomarker using optical coherence tomography angiography (OCTA) in neovascular age-related macular degeneration (AMD) patients after anti-vascular endothelial growth factor (anti-VEGF) treatment and its association with the retinal microcapillary density. **Methods.** Twenty-five eyes from 25 patients with neovascular AMD were included in the study. All eyes were imaged with OCTA at baseline (M0) and after 3 consecutive injections (M3; injection performed each month) of anti-VEGF. The number of HRF in the superficial capillary plexus (SCP), deep capillary plexus (DCP), and outer retina was counted. The vascular density of the fovea, parafovea, and the whole macula, as well as the area of the foveal avascular zone (FAZ), was measured. **Results.** The mean interval between baseline and follow-up with OCTA was  $93.08 \pm 5.00$  (range, 85-101) days. Compared with the baseline, the number of HRF significantly decreased in DCP ( $7.52 \pm 3.06$  vs.  $3.76 \pm 1.48$ ,  $P < 0.01$ ) and outer retina ( $12.04 \pm 4.91$  vs.  $5.88 \pm 3.32$ ,  $P < 0.01$ ) after treatment. There was no significant difference for HRF number in the SCP, the vascular density (containing foveal, parafoveal, and whole macular), and FAZ area before and after treatments. **Conclusion.** The number of HRF in DCP and outer retina might serve as an inflammatory biomarker in patients with neovascular AMD. The reduced HRF possibly represents the alleviation of inflammation after anti-VEGF treatment in patients with AMD.

## 1. Introduction

Age-related macular degeneration (AMD) is the main cause of irreversible severe vision loss in elderly individuals, with a prevalence that exponentially increases with aging. It has been estimated that about 288 million people worldwide will suffer from AMD by 2040 [1]. AMD is subdivided into two

types, dry and wet form. The wet form is also called neovascular AMD, which largely benefits from anti-VEGF reagent intravitreal injection. Although the exact pathophysiological mechanism of AMD remains unclear, the prolonged inflammatory response has a crucial role in the onset and development of AMD [2]. During AMD progression, retinal inflammation can lead to the disturbance of the retinal

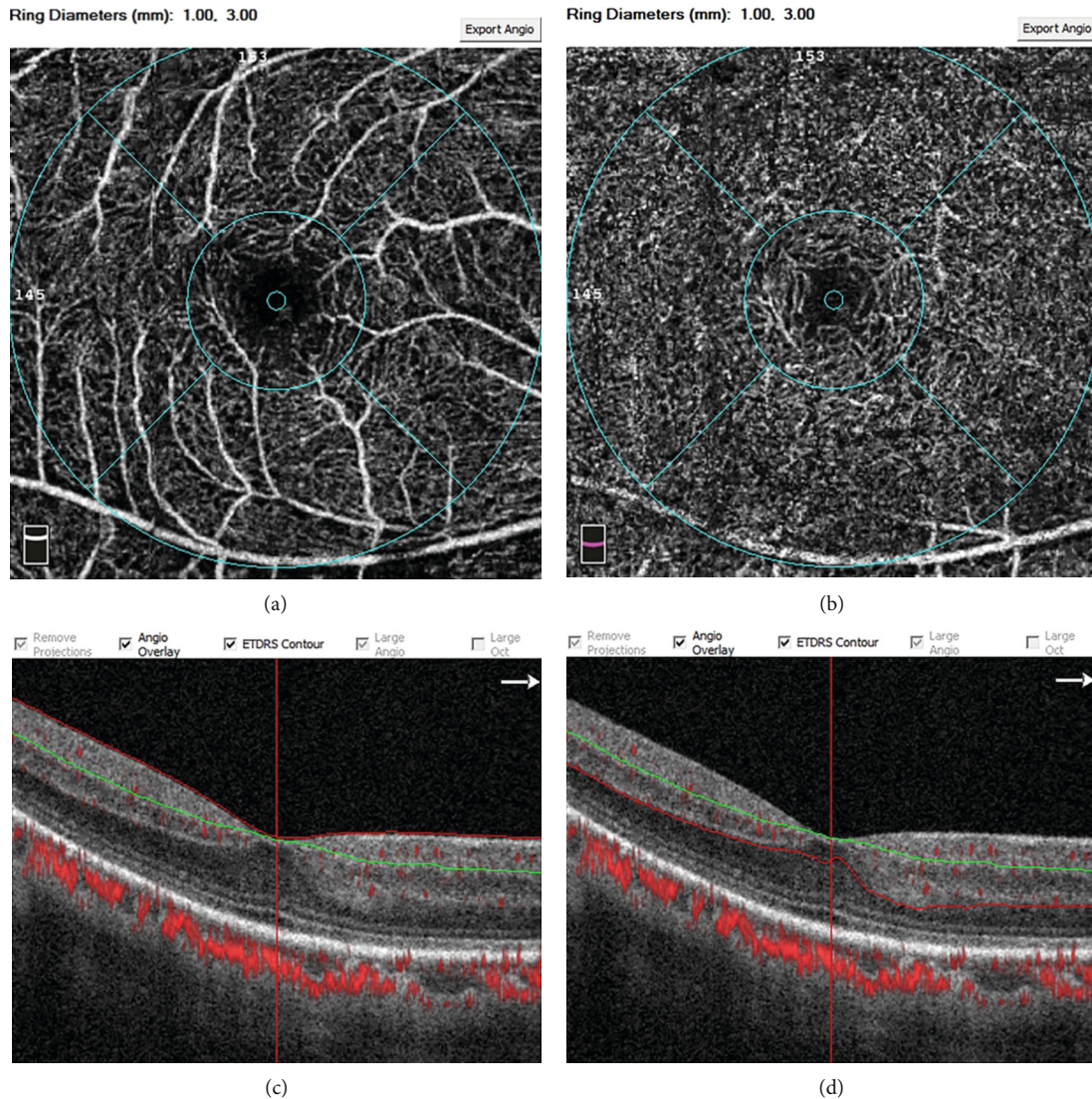


FIGURE 1: Representative OCT-A images at the  $3 \times 3 \text{ mm}^2$  sections centered on the fovea showing the segmentation of microvascular density analysis of the SCP (a, c) and DCP (b, d). As discussed in Section 2, segmentation in the OCT B-scan was set in OCTA automatically. SCP (c), the segmentation was between internal limiting membrane (red line) and  $15 \mu\text{m}$  below IPL (green line); DCP (d), the segmentation was between  $15 \mu\text{m}$  below IPL (green line) and  $70 \mu\text{m}$  below IPL (red line); the segmentation beneath the red line was outer retina (d). DCP: deep retinal capillary plexus; IPL: inner plexiform layer; SCP: superficial retinal capillary plexus.

microenvironment, resulting in retinal pigment epithelial (RPE) dysfunction, photoreceptor apoptosis, and choroidal neovascularization [3].

With the advancement of noninvasive retinal imaging technologies, such as optical coherence tomography (OCT), the hyperreflective foci (HRF) can be imaged, which attracted the researchers' attention [4, 5]. HRF in the retina detected with OCT were defined as a discrete and well-circumscribed dot-shaped lesion of equal or higher reflectivity than the RPE band, without back shadowing, and the maximum diameter between  $20$  and  $50 \mu\text{m}$  [6, 7]. HRF were first described by Coscas et al. in 2009 as the hyperreflective dots (HRD) using spectral-domain OCT in AMD patients [8]. Subsequently, HRF have been reported in many retinal diseases, including diabetic retinopathy, choroideremia, and retinal vein occlusion [9–11]. Although there is still no con-

sensus on its origin, HRF likely characterize a progressive state of the damaged retinal tissue within an inflammatory retinal microenvironment.

Nowadays, many studies that support the hypothesis that activated microglial cells induced by an inflammatory response in the retina are a pivotal origination of HRF [12, 13]. Microglial cells are the major resident immune cells in the retina, which have a critical role in the inflammatory response of neurodegenerative diseases, and are mainly scattered within the inner retina under physiological conditions. Once retinal homeostasis is disturbed, microglial cells proliferate and become activated, releasing proinflammatory cytokines and migrating from the inner retina to the outer retina, thus forming aggregates [14, 15]. These microglial aggregates have been identified as HRF within retinal layers in pathologic conditions, leading to microglia-mediated retinal

TABLE 1: Baseline characteristics of patients with neovascular AMD and comparison of HRF in the SCP, DCP, and outer retina using OCTA between baseline and after the intravitreal anti-VEGF injections.

	M0	M3	P
Eyes (no.)	25	—	—
Sex (male/female)	15/10	—	—
Ages (years)	71.4 ± 9.66	—	—
BCVA (logMAR)	0.84 ± 0.41	0.57 ± 0.37	<0.01*
HRF-SCP (no.)	5.80 ± 1.63	5.32 ± 1.95	0.12
HRF-DCP (no.)	7.52 ± 3.06	3.76 ± 1.48	<0.01*
HRF-outer retina (no.)	12.04 ± 4.91	5.88 ± 3.32	<0.01*

Data are shown as a number or mean ± standard deviation. \*Significant at  $P < 0.05$ . M0, baseline; M3, 3 consecutive monthly anti-VEGF injections. BCVA: best-corrected visual acuity; DCP: deep retinal capillary plexus; HRF: hyperreflective foci; Log MAR: the logarithm of the minimum angle of resolution; No.: number; SCP: superficial retinal capillary plexus; VEGF: vascular endothelial growth factor.

damage and neuroinflammation. Thus, HRF might reflect a dynamic process of retinal inflammation in different retinal diseases.

In this study, we investigated whether HRF could serve as a possible biomarker of retinal inflammation in patients with neovascular AMD and its possible association with retinal microcapillary density. The number of HRF, vascular density in different retinal layers, and the foveal avascular zone (FAZ) area was measured and quantified with OCT angiography (OCTA) in neovascular AMD patients before and after 3 consecutive anti-VEGF injections.

## 2. Materials and Methods

### 3. Patients

In this retrospective study, we enrolled 25 consecutive treatment-naïve eyes from 25 neovascular AMD patients who were diagnosed with comprehensive ophthalmologic examinations in the Department of Ophthalmology, Shanghai General Hospital affiliated to Shanghai Jiao Tong University, Shanghai, China, between January 1, 2020, and July 30, 2020. The participants with three consecutive monthly intravitreal injections of anti-VEGF agents were enrolled. This study was approved by the Clinical Research Ethical Committee of Shanghai General Hospital affiliated to Shanghai Jiao Tong University (Permits No. 2020KY205) and adhered to the principles of the Declaration of Helsinki. All individual participants provided written informed consent.

The exclusion criteria were as follows: (a) previous treatments for neovascular AMD (including other intravitreal anti-VEGF injections and laser photocoagulation); (b) other vitreoretinal diseases, including dry AMD, vitreous hemorrhage, subretinal fibrosis, and retinal vascular disease; (c) high myopia (refractive errors > 6 diopters of spherical equivalent refraction or >3 diopters of astigmatism); and (d) history of ocular surgery, uveitis, and apparent media opacification.

All participants underwent full ophthalmologic examinations, including best-corrected visual acuity (BCVA), intraocular pressure (IOP) measurement, and anterior segment evaluation using slit-lamp biomicroscopy, fundus photography, and OCTA imaging at the baseline (M0) and 1 week after treatment (M3).

**3.1. Intravitreal Injection of Anti-VEGF Agent.** One experienced surgeon performed all intravitreal injections. The intravitreal injection was performed at the temporal limbus through the eyeball's pars plana under aseptic conditions. All patients received three once-monthly intravitreal injections of aflibercept (2 mg/0.05 mL) using a 30-gauge needle. A 1-week variation was allowed for every injection interval.

**3.2. Optical Coherence Tomography Angiography (OCTA) Evaluation.** Retinal microvasculature was imaged using the RTVue XR Avanti OCT system (Optovue, Inc., Fremont, CA, USA), and measurements were acquired using the manufacturer's AngioVue software. The scan covered an area of  $3 \times 3 \text{ mm}^2$  sections centered on the fovea. Enface images of the superficial capillary plexus (SCP), deep capillary plexus (DCP), and FAZ area were automatically recorded and analyzed by the OCTA autosegmentation software. The SCP was segmented as  $3 \mu\text{m}$  below the internal limiting membrane and  $15 \mu\text{m}$  below the inner plexiform layer (IPL); the DCP was set between  $15 \mu\text{m}$  and  $70 \mu\text{m}$  beneath IPL, while the outer retina was located beneath the DCP. In the SCP and DCP, two central circles divided capillary plexus into the "fovea area" (a disc with a 0.6 mm diameter) and "parafovea area" (an internal annular zone, 0.3-1.5 mm from the fovea) as shown in Figure 1. The boundary of FAZ was set by a combination of a canny edge detection algorithm and a level set algorithm centered on the fovea in the whole retinal vasculature [16]. We further manually refined and adjusted the boundary in the case of imprecise segmentation.

The number of HRF was manually counted within a 3 mm diameter centered on the foveal area using a fovea-spanning horizontal B-scan. HRF were subdivided into 3 categories according to different retinal layers: the SCP, the DCP, and the outer retina, as described above. The maximal diameter of HRF was limited within the  $20 \mu\text{m}$  to  $50 \mu\text{m}$  range in order to exclude small counting noise signals as HRF noise signals and prevent large hyperreflective clumps, which are presented as typical hard exudates in fundus photography. Poor quality images with a signal strength index < 4/10 were excluded from further analysis. The quantification of HRF was carried out by two experienced physicians independently.

**3.3. Statistical Analyses.** The data were analyzed by using SPSS 22.0 software. All values are presented as a number or mean ± standard deviation. The visual acuity was presented as the logarithm of the minimum angle of resolution (logMAR). A paired *t*-test was used to compare the number of HRF, the vascular density of SCP and DCP, and the FAZ area between the baseline (M0) and after 3 consecutive monthly anti-VEGF injections (M3). *P* value <0.05 was considered as statistical significance.



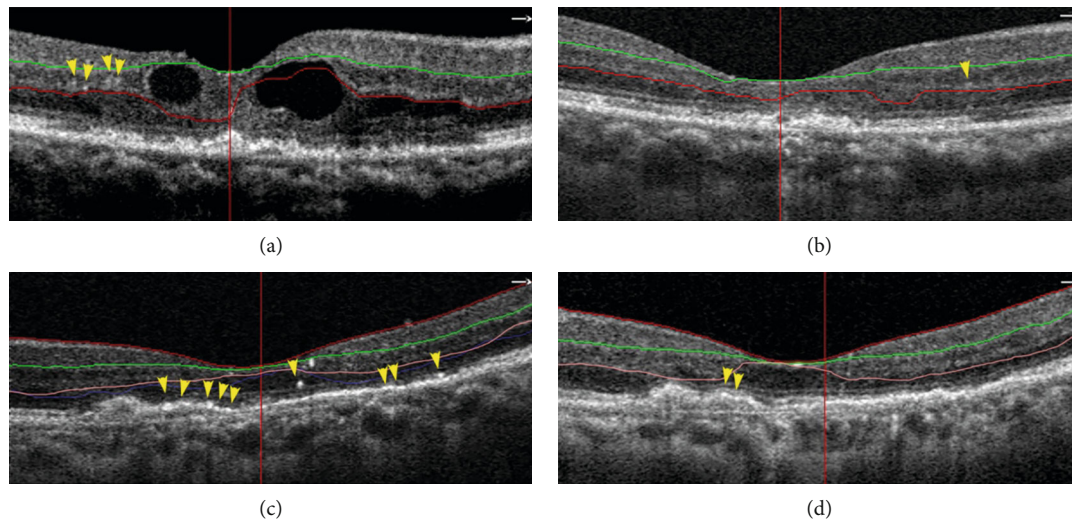


FIGURE 2: Representative images of two patients showing the HRF in the DCP and outer retina at baseline and after three monthly intravitreal anti-VEGF injections. Patient 1: 63-year-old man with neovascular AMD, HRF were observed in DCP (between red and green line) at the  $3 \times 3 \text{ mm}^2$  sections centered on the fovea at the baseline (a) and after anti-VEGF injections (b). The number of HRF was reduced in DCP, and his BCVA was improved from logMAR 1.0 (baseline) to logMAR 0.7 (after treatment). Patient 2: 74-year-old female with neovascular AMD, HRF were observed mainly in the outer retina (beneath the pink line) at the  $3 \times 3 \text{ mm}^2$  sections centered on the fovea at the baseline (c) and after anti-VEGF injections (d). The number of HRF was reduced in the outer retina, and the BCVA was improved from logMAR 0.8 (baseline) to logMAR 0.4 (after treatment). The yellow arrowhead indicates the HRF. The microstructures, including the outer limiting membrane, ellipsoid zone, and interdigital zone/retinal pigment epithelial layer, were partially restored in patients after 3 consecutive anti-VEGF treatments.

TABLE 2: Comparison of microvascular density in the SCP and DCP using OCTA between baseline and after the intravitreal anti-VEGF injections.

	M0	M3	P
SCP			
Fovea	17.22 ± 7.10	15.24 ± 7.78	0.10
Parafovea	43.02 ± 5.90	42.03 ± 5.78	0.32
Whole	40.40 ± 6.11	39.59 ± 5.94	0.44
DCP			
Fovea	26.85 ± 8.50	25.84 ± 8.24	0.58
Parafovea	44.42 ± 6.17	47.08 ± 5.99	0.08
Whole	42.96 ± 5.48	44.52 ± 4.58	0.24

Data are shown as mean ± standard deviation. \*Significant at  $P < 0.05$ . M0, baseline; M3, 3 consecutive monthly anti-VEGF injections. DCP: deep retinal capillary plexus; HRF: hyperreflective foci; SCP: superficial retinal capillary plexus; VEGF: vascular endothelial growth factor.

## 4. Results

**4.1. Patient Characteristics.** Twenty-five eyes from 25 patients (10 females and 15 males) with neovascular AMD were consecutively enrolled in the study, as shown in Table 1. All patients underwent 3 consecutive monthly injections (M3) of aflibercept. The mean age of patients was  $71.4 \pm 9.66$  years old. The mean interval between baseline and final follow-up was  $93.08 \pm 5.0$  (range, 85-101) days. There was a significant improvement of BCVA from baseline (M0,  $0.84 \pm 0.41$ ) to the final follow-up (M3,  $0.57 \pm 0.37$ ), and the mean change of BCVA was  $-0.25 \pm 0.23$ .

**4.2. Comparison of HRF in the SCP, DCP, and Outer Retina between Baseline and after the Intravitreal Anti-VEGF Injections.** Analysis of the OCTA parameters revealed that the HRF was distributed across all retinal layers, including SCP, DCP, and outer retina, in neovascular AMD patients. As shown in Table 1, the number of HRF was the highest in the outer retina ( $12.04 \pm 4.91$ ) and the lowest in SCP ( $5.80 \pm 1.63$ ) in the treatment-naïve patient. After the intravitreal anti-VEGF injections, the number of HRF was significantly reduced in the DCP ( $7.52 \pm 3.06$  vs.  $3.76 \pm 1.48$ ,  $P < 0.01$ ) and outer retina ( $12.04 \pm 4.91$  vs.  $5.88 \pm 3.32$ ,  $P < 0.01$ ), compared to baseline; the representative images of HRF were shown in Figure 2. The mean change of HRF in the DCP and outer retina was  $-3.76 \pm 2.71$  and  $-6.16 \pm 4.03$ , respectively. However, there was no significant difference for HRF number in the SCP before and after treatment ( $P = 0.12$ ).

**4.3. Comparison of Microvascular Density in the SCP and DCP between Baseline and after the Intravitreal Anti-VEGF Injections.** Regarding retinal microvascular density in the SCP and DCP analyzed with OCTA, no significant difference was found for the microvascular density in the foveal, parafoveal, and whole macular sectors before and after treatment as shown in Table 2.

**4.4. Comparison of FAZ Areas between Baseline and after the Intravitreal Anti-VEGF Injections.** The distribution of FAZ areas in the retina is depicted in Figure 3. The FAZ areas (mean ± SD) at baseline and after the intravitreal anti-VEGF injections were  $0.34 \pm 0.09 \text{ mm}^2$  (M0, baseline) and

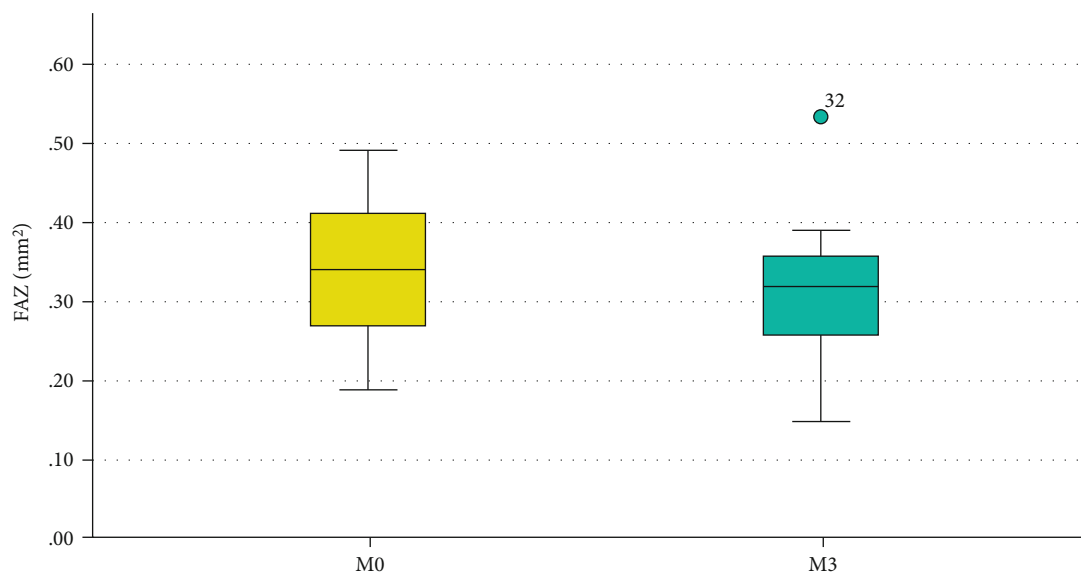


FIGURE 3: Comparison of FAZ areas between baseline and after the intravitreal anti-VEGF injections. The FAZ areas of the neovascular AMD patients were  $0.34 \pm 0.09 \text{ mm}^2$  (M0, baseline) and  $0.31 \pm 0.08 \text{ mm}^2$  (M3, after treatment) ( $P = 0.11$ ). Data are shown as mean  $\pm$  standard deviation.

$0.31 \pm 0.08 \text{ mm}^2$  (M3, after treatment), respectively, with no statistically significant differences ( $P = 0.11$ ).

## 5. Discussion

Microglial cells are considered to have a vital role in the inflammatory response in the pathogenesis of AMD [2, 17, 18]. However, whether microglia are affected by anti-VEGF treatment in AMD patients remains unclear. In this study, we compared the change of HRF numbers before and after anti-VEGF treatment. Our results revealed that the number of HRF in the retina was reduced in DCP and outer retina after 3 monthly consecutive anti-VEGF treatments in patients with neovascular AMD, while the microvascular densities and the FAZ area remained unchanged.

The introduction of high-resolution OCTA has facilitated the study of different capillary plexus in vivo. Previous studies have suggested that HRF may be used as a marker of inflammation in AMD patients [19, 20]. It has been hypothesized that HRF appear after microglial activation and inflammatory cytokines release. Microglial cells are the major resident immune cells in the central nervous system and retina. During physiological condition, the resting microglia are mainly scattered within the inner retinal layers, including the nerve fiber layer, ganglion cell layer, inner plexiform layer, and inner nuclear layer. However, under pathological conditions, activated microglia proliferate and migrate from the inner to the outer retina, secreting proinflammatory cytokines to damage the surrounding retinal neuronal cells [21]. At the same time, activated microglia undergo morphological changes and aggregate to form HRF as imaged with OCT or OCTA.

In our study, the HRF was localized in almost every retinal layer, especially the outer retina of patients with neovascular AMD, indicating the migration and aggregation of

microglia cells in the outer retina. Our results were consistent with the previous observations [10, 22], which suggested that HRF might serve as an inflammation OCTA biomarker in neovascular AMD. After aflibercept injections, the number of HRF in DCP and outer retina was significantly reduced, while visual acuity was improved, which might be due to the anti-inflammatory effect of aflibercept. Inflammation is involved in the pathogenesis of neurovascular AMD. This process involves inflammatory cells, such as microglia and monocyte/macrophage, and the related inflammatory cytokines, such as vascular endothelial growth factor A (VEGF-A), placental growth factor (PGF), and monocyte chemokine protein (MCP-1) [23]. PGF and VEGF contribute to the neovascularization by binding VEGF receptor 1 and 2 (VEGFR-1 and VEGFR-2) on endothelial cells, as well as the inflammatory process binding VEGFR-1 on microglia and monocyte/macrophage [24–26]. Besides having an antiangiogenesis function, aflibercept targets VEGF-A/B and PGF, deactivates the inflammatory cells, and reduces the release of corresponding inflammatory cytokines [27]. Therefore, the decreased HRF number and alleviation of inflammation might improve the retinal microstructure on OCTA and the visual function, as indicated by BCVA.

Previous experimental studies have demonstrated that microglia-induced retinal inflammation is a relatively early process during AMD development, which precedes neovascularization, microvascular dysfunction, and retinal neurodegeneration [28]. In this study, we detected the microvascular densities in the foveal, parafoveal, and whole macula of SCP and DCP with OCTA to explore the correlation between HRF number and macular microvascular densities. However, we found no significant differences in vascular densities of the SCP and DCP before and after treatments. The FAZ area represents the level of local retinal ischemia and atrophic changes in macular capillaries. We found no



difference in the FAZ area before and after treatments. Therefore, the HRF reduction in DCP and outer retina is likely to be more sensitive and more rapidly responding than the change of microvascular densities in the retina with neovascular AMD after anti-VEGF treatment.

Previous studies have also indicated that HRF could be an inflammatory hallmark, contributing to retinal dysfunction in many retinal diseases. For example, in neovascular diabetic retinopathy, HRF was significantly higher in diabetic patients compared with healthy controls [12]. Furthermore, as inflammatory cytokines could increase vascular permeability in patients with diabetic macular edema, Stela et al. found significant decreases in HRF and central retinal thickness in the retina after anti-VEGF treatment [29]. These studies suggested that HRF might have a pivotal role in retinal neuroinflammation diseases. Moreover, some preliminary studies have shown that HRF are correlated with cytokines levels in the vitreous and aqueous humor; yet, further studies are required to confirm these findings [7, 30].

Hsia et al. [31] compared the change of HRF in different retinal layers to predict visual outcomes after anti-VEGF therapy using spectral-domain optical coherence tomography (SD-OCT). They found a faster decrease of HRF in the subretinal fluid (SRF) after anti-VEGF therapy, which suggested that HRF might be used as a potential biomarker to predict the visual outcome. Our result was consistent with the above study. We found that the HRF was mainly distributed in the outer retina in patients with neovascular AMD, and the number of HRF was reduced after anti-VEGF treatment. However, there were some differences between these two studies. For example, different instruments were employed to study the HRF distribution and quantitation in different retinal layers. Hsia et al. used SD-OCT to quantify HRF in the inner retina, outer retina, and subretinal fluid layer, while we applied OCTA to characterize the HRF distribution in SCP, DCP, and outer retina. In addition, we compared the relationship between HRF change and the retinal microcapillary density, which is important for assessing the treatment outcome for AMD patients, as neovascular AMD is characterized by macular neovascularization. Hsia et al. found that the eyes with decreased HRF in the SRF after 3 consecutive anti-VEGF treatments might have better visual acuity at 12 months, suggesting that HRF might be used as a biomarker for predicting the effects of anti-VEGF treatment. In our study, we only observed the effect of anti-VEGF therapy after the three-month injections. The small sample size and relatively short-term observation are the major limitations of this study.

## 6. Conclusion

The present study suggested that HRF could be used as an indicator or sensitive biomarker for retinal inflammation in neovascular AMD. After anti-VEGF treatment, the reduced HRF number might indicate the alleviation of inflammation in the retina and, possibly, improvement in the visual function in patients with neovascular AMD. Yet, long-term observation and a study with a larger sample size should be

performed to compare the relationship among HRF, visual outcome, intraretinal cysts, and similar.

## Data Availability

The data used to support the findings of this study are available from the corresponding author upon request.

## Conflicts of Interest

The authors report no proprietary or commercial interest in any product mentioned or concept discussed in this article and no conflict outside the current study.

## Acknowledgments

This research was supported by the National Natural Science Foundation of China (81570852, 81870667, 81970810, 81970811), the Science and Technology Commission of Shanghai Municipality (19495800700), the Clinical Research and Cultivation Project of Shanghai Municipal Hospital, China (SHDC12019X30), and Science and Technology Commission of Shanghai Municipality (20142203200).

## References

- [1] W. L. Wong, X. Su, X. Li et al., "Global prevalence of age-related macular degeneration and disease burden projection for 2020 and 2040: a systematic review and meta-analysis," *The Lancet Global Health*, vol. 2, no. 2, pp. e106–e116, 2014.
- [2] A. Kauppinen, J. J. Paterno, J. Blasiak, A. Salminen, and K. Kaarniranta, "Inflammation and its role in age-related macular degeneration," *Cellular and Molecular Life Sciences*, vol. 73, no. 9, pp. 1765–1786, 2016.
- [3] C. R. Fisher and D. A. Ferrington, "Perspective on AMD pathobiology: a bioenergetic crisis in the RPE," *Investigative Ophthalmology & Visual Science*, vol. 59, no. 4, pp. Amd41–amd47, 2018.
- [4] S. G. Schuman, A. F. Koreishi, S. Farsiu, S. H. Jung, J. A. Izatt, and C. A. Toth, "Photoreceptor layer thinning over drusen in eyes with age-related macular degeneration imaged in vivo with spectral-domain optical coherence tomography," *Ophthalmology*, vol. 116, no. 3, pp. 488–496, 2009.
- [5] L. Altay, P. Scholz, T. Schick et al., "Association of hyperreflective foci present in early forms of age-related macular degeneration with known age-related macular degeneration risk polymorphisms," *Investigative Ophthalmology & Visual Science*, vol. 57, no. 10, pp. 4315–4320, 2016.
- [6] H. Lee, B. Ji, H. Chung, and H. C. Kim, "Correlation between optical coherence tomographic hyperreflective foci and visual outcomes after anti-VEGF treatment in neovascular age-related macular degeneration and polypoidal choroidal vasculopathy," *Retina*, vol. 36, no. 3, pp. 465–475, 2016.
- [7] H. Lee, H. Jang, Y. A. Choi, H. C. Kim, and H. Chung, "Association between soluble CD14 in the aqueous humor and hyperreflective foci on optical coherence tomography in patients with diabetic macular edema," *Investigative Ophthalmology & Visual Science*, vol. 59, no. 2, pp. 715–721, 2018.
- [8] G. Coscas, U. de Benedetto, F. Coscas et al., "Hyperreflective dots: a new spectral-domain optical coherence tomography entity for follow-up and prognosis in exudative age-related

- macular degeneration," *Ophthalmologica*, vol. 229, no. 1, pp. 32–37, 2013.
- [9] K. Ogino, T. Murakami, A. Tsujikawa et al., "Characteristics of optical coherence tomographic hyperreflective foci in retinal vein occlusion," *Retina*, vol. 32, no. 1, pp. 77–85, 2012.
- [10] S. Vujosevic, T. Torresin, S. Bini et al., "Imaging retinal inflammatory biomarkers after intravitreal steroid and anti-VEGF treatment in diabetic macular oedema," *Acta Ophthalmologica*, vol. 95, no. 5, pp. 464–471, 2017.
- [11] F. Romano, A. Arrigo, R. E. MacLaren et al., "Hyperreflective foci as a pathogenetic biomarker in choroideremia," *Retina*, vol. 40, no. 8, pp. 1634–1640, 2020.
- [12] S. Vujosevic, S. Bini, G. Midena, M. Berton, E. Pilotto, and E. Midena, "Hyperreflective intraretinal spots in diabetics without and with nonproliferative diabetic retinopathy: an in vivo study using spectral domain OCT," *Journal Diabetes Research*, vol. 2013, article 491835, pp. 1–5, 2013.
- [13] E. Pilotto, S. Mianta, T. Torresin et al., "Hyperreflective foci in the retina of active relapse-onset multiple sclerosis," *Ophthalmology*, vol. 127, no. 12, pp. 1774–1776, 2020.
- [14] M. Karlstetter, R. Scholz, M. Rutar, W. T. Wong, J. M. Provis, and T. Langmann, "Retinal microglia: just bystander or target for therapy?," *Progress in Retinal and Eye Research*, vol. 45, pp. 30–57, 2015.
- [15] Y. Sun, L. Gao, W. Hou, and J. Wu, " $\beta$ -Sitosterol alleviates inflammatory response via inhibiting the activation of ERK/p38 and NF- $\kappa$ B pathways in LPS-exposed BV2 cells," *BioMed Research International*, vol. 2020, Article ID 7532306, 2020.
- [16] J. Wu, X. Zhang, G. Azhati, T. Li, G. Xu, and F. Liu, "Retinal microvascular attenuation in mental cognitive impairment and Alzheimer's disease by optical coherence tomography angiography," *Acta Ophthalmologica*, vol. 98, no. 6, pp. e781–e787, 2020.
- [17] R. Natoli, N. Fernando, M. Madigan et al., "Microglia-derived IL-1 $\beta$  promotes chemokine expression by Müller cells and RPE in focal retinal degeneration," *Molecular Neurodegeneration*, vol. 12, no. 1, p. 31, 2017.
- [18] W. Ma, S. M. Silverman, L. Zhao et al., "Absence of TGF $\beta$  signaling in retinal microglia induces retinal degeneration and exacerbates choroidal neovascularization," *eLife*, vol. 8, 2019.
- [19] M. Nassisi, W. Fan, Y. Shi et al., "Quantity of intraretinal hyperreflective foci in patients with intermediate age-related macular degeneration correlates with 1-year progression," *Investigative Ophthalmology & Visual Science*, vol. 59, no. 8, pp. 3431–3439, 2018.
- [20] L. Tiosano, I. Byon, A. R. Alagorie, Y. S. Ji, and S. R. Sadda, "Choriocapillaris flow deficit associated with intraretinal hyperreflective foci in intermediate age-related macular degeneration," *Graefes Archive for Clinical and Experimental Ophthalmology*, vol. 258, no. 11, pp. 2353–2362, 2020.
- [21] V. H. Perry, J. A. R. Nicoll, and C. Holmes, "Microglia in neurodegenerative disease," *Nature Reviews Neurology*, vol. 6, no. 4, pp. 193–201, 2010.
- [22] E. Midena, E. Pilotto, and S. Bini, "Hyperreflective Intraretinal foci as an OCT biomarker of retinal inflammation in diabetic macular edema," *Investigative Ophthalmology & Visual Science*, vol. 59, no. 13, p. 5366, 2018.
- [23] S. A. Minaker, R. H. Mason, G. Lahaie Luna, P. Bapat, and R. H. Muni, "Changes in aqueous and vitreous inflammatory cytokine levels in neovascular age-related macular degeneration: a systematic review and meta-analysis," *Acta Ophthalmologica*, vol. 99, 2020.
- [24] F. Cunningham, T. Van Bergen, P. Canning, I. Lengyel, J. H. M. Feyen, and A. W. Stitt, "The placental growth factor pathway and its potential role in macular degenerative disease," *Current Eye Research*, vol. 44, no. 8, pp. 813–822, 2019.
- [25] T. van Bergen, I. Etienne, F. Cunningham et al., "The role of placental growth factor (PlGF) and its receptor system in retinal vascular diseases," *Progress in Retinal and Eye Research*, vol. 69, pp. 116–136, 2019.
- [26] D. Liu, H. Xu, C. Zhang et al., "Erythropoietin maintains VE-cadherin expression and barrier function in experimental diabetic retinopathy via inhibiting VEGF/VEGFR2/Src signaling pathway," *Life Sciences*, vol. 259, article 118273, 2020.
- [27] F. Lazzara, A. Fidilio, C. B. M. Platania et al., "Aflibercept regulates retinal inflammation elicited by high glucose via the PlGF/ERK pathway," *Biochemical Pharmacology*, vol. 168, pp. 341–351, 2019.
- [28] E. L. Fletcher, "Contribution of microglia and monocytes to the development and progression of age related macular degeneration," *Ophthalmic & physiological optics : the journal of the British College of Ophthalmic Opticians (Optometrists)*, vol. 40, no. 2, pp. 128–139, 2020.
- [29] S. Vujosevic, M. Berton, S. Bini, M. Casciano, F. Cavarzeran, and E. Midena, "Hyperreflective retinal spots and visual function after anti-vascular endothelial growth factor treatment in center-involving diabetic macular edema," *Retina*, vol. 36, no. 7, pp. 1298–1308, 2016.
- [30] V. Sitniska, P. Enders, C. Cursiefen, S. Fauser, and L. Altay, "Association of imaging biomarkers and local activation of complement in aqueous humor of patients with early forms of age-related macular degeneration," *Graefes Archive for Clinical and Experimental Ophthalmology*, vol. 259, 2020.
- [31] Y. Hsia, C. H. Yang, Y. T. Hsieh, C. M. Yang, T. C. Ho, and T. T. Lai, "Hyperreflective foci in predicting the treatment outcome of anti-vascular endothelial growth factor in neovascular age-related macular degeneration," *Graefes Archive for Clinical and Experimental Ophthalmology*, vol. 258, no. 2, pp. 273–280, 2020.

## Retraction

# Retracted: Genome Assembly and Analyses of the Macrofungus *Macrocybe gigantea*

### BioMed Research International

Received 12 March 2024; Accepted 12 March 2024; Published 20 March 2024

Copyright © 2024 BioMed Research International. This is an open access article distributed under the Creative Commons Attribution License, which permits unrestricted use, distribution, and reproduction in any medium, provided the original work is properly cited.

This article has been retracted by Hindawi following an investigation undertaken by the publisher [1]. This investigation has uncovered evidence of one or more of the following indicators of systematic manipulation of the publication process:

- (1) Discrepancies in scope
- (2) Discrepancies in the description of the research reported
- (3) Discrepancies between the availability of data and the research described
- (4) Inappropriate citations
- (5) Incoherent, meaningless and/or irrelevant content included in the article
- (6) Manipulated or compromised peer review

The presence of these indicators undermines our confidence in the integrity of the article's content and we cannot, therefore, vouch for its reliability. Please note that this notice is intended solely to alert readers that the content of this article is unreliable. We have not investigated whether authors were aware of or involved in the systematic manipulation of the publication process.

Wiley and Hindawi regrets that the usual quality checks did not identify these issues before publication and have since put additional measures in place to safeguard research integrity.

We wish to credit our own Research Integrity and Research Publishing teams and anonymous and named external researchers and research integrity experts for contributing to this investigation.




The corresponding author, as the representative of all authors, has been given the opportunity to register their agreement or disagreement to this retraction. We have kept a record of any response received.

### References

- [1] L. Kui, Z. Zhang, Y. Wang et al., "Genome Assembly and Analyses of the Macrofungus *Macrocybe gigantea*," *BioMed Research International*, vol. 2021, Article ID 6656365, 14 pages, 2021.

## Research Article

# Genome Assembly and Analyses of the Macrofungus *Macrocybe gigantea*

Ling Kui <sup>1,2</sup>, Zhe Zhang,<sup>1</sup> Yangzi Wang,<sup>1</sup> Yesheng Zhang,<sup>3</sup> Shiming Li,<sup>4</sup> Xiao Dong,<sup>4</sup> Qiujia Xia,<sup>5</sup> Jun Sheng <sup>6,7</sup>, Jian Wang,<sup>3,5</sup> and Yang Dong <sup>1,8,9</sup>

<sup>1</sup>College of Biological Big Data, Yunnan Agricultural University, Kunming 650201, China

<sup>2</sup>School of Pharmacy, Jiangsu University, Zhenjiang 212013, China

<sup>3</sup>BGI-Shenzhen, Shenzhen 518083, China

<sup>4</sup>BGI Institute of Applied Agriculture, BGI-Shenzhen, Shenzhen 518120, China

<sup>5</sup>BGI Education Center, University of Chinese Academy of Sciences, Shenzhen 518083, China

<sup>6</sup>Yunnan Plateau Characteristic Agricultural Industry Research Institute, Kunming, 650201 Yunnan, China

<sup>7</sup>Key Laboratory of Puer Tea Science, Ministry of Education, Yunnan Agricultural University, Kunming, 650201 Yunnan, China

<sup>8</sup>Guangxi Key Laboratory of Medicinal Resources Protection and Genetic Improvement, Guangxi Botanical Garden of Medicinal Plants, Nanning 530023, China

<sup>9</sup>State Key Laboratory for Conservation and Utilization of Bio-Resources in Yunnan, Yunnan Agricultural University, Kunming 650201, China

Correspondence should be addressed to Yang Dong; [loyalyang@163.com](mailto:loyalyang@163.com)

Received 2 December 2020; Revised 19 December 2020; Accepted 1 January 2021; Published 19 January 2021

Academic Editor: Yuzhen Xu

Copyright © 2021 Ling Kui et al. This is an open access article distributed under the Creative Commons Attribution License, which permits unrestricted use, distribution, and reproduction in any medium, provided the original work is properly cited.

*Macrocybe gigantea* (*M. gigantea*) is a macrofungus genus that contains a big number of fairly fleshy gilled mushrooms with white spores. This macrofungus produces diverse bioactive compounds, antioxidants, and water-soluble polysaccharides. However, the genomic resources of this species remain unknown. Here, we assembled the genome of *M. gigantea* (41.23 Mb) into 336 scaffolds with a N50 size of 374,455 bp and compared it with the genomes of eleven other macrofungi. Comparative genomics study confirmed that *M. gigantea* belonged to the *Macrocybe* genus, a stand-alone genus different from the *Tricholoma* genus. In addition, we found that glycosyl hydrolase family 28 (GH28) in *M. gigantea* shared conserved motifs that were significantly different from their counterparts in *Tricholoma*. The genomic resource uncovered by this study will enhance our understanding of fungi biology, especially the differences in their growth rates and energy metabolism.

## 1. Introduction

*Macrocybe gigantea* (*M. gigantea*), which is commonly named *Tricholoma giganteum*, belongs to a genus of fungi in the family of *Tricholomataceae*. *Macrocybe* fungi are widely distributed in tropical regions worldwide, and this genus is related to the genus *Calocybe* [1]. Since the end of the last century, *Macrocybe* has been treated under *Tricholoma* [2]. Pegler et al. separated *Macrocybe* out from *Tricholoma* and ranked it as a stand-alone genus according to morphological and molecular evidence. Previously, most studies of *M. gigantea* were focused on the analysis of anti-

bacterial activities of bioactive compounds, antioxidants, and water-soluble polysaccharides [3–6]. Generally, a single cluster weighs about 20 to 30 kilograms. The largest cluster of giant chanterelles, which was found very recently in Pu'er City of Yunnan Province in China, weighs about 150 kilograms.

Due to the lack of a reference genome, most of the macrofungi cannot be studied in the laboratory. However, the rapid development of sequencing methods and analytic tools, which is extensively utilized for the study of evolution, pathology, and molecular population genetics, has been promoting the generation, release, and update of draft data.



TABLE 1: Summary of the *M. gigantea* genome assembly features.

Type	Value
Genome size (Mb)	41.23 M
Pair-end libraries	Pacific Biosciences RSII and Sequel
Total reads (#)	1,135,758
Total base (Gb)	8.753(213X)
Genome N50 (kb)	374
Scaffold_reads	336
GC (%)	49.82
Complete Buscos (%)	80.7
Repeat size in genome (%)	9.0338
Gene numbers	11,722
Gene annotation statistics	Value
Total num of genes(glean result)	11,722
Average length gene(bp)	2,019.56
Average no. of cds (bp)	1,544.21
Average no. of exons per gene	6.72
Average exon size (bp)	6.72
Average intron length (bp)	38.23

Recently, several macrofungi genomes have been published, and a lot of large fungal genome projects are in progress [7]. Especially, the Human Microbiome Project [8], the microbial dark matter project, and the 1000 fungal genomes project (<http://1000.fungalgenomes.org>) [9] have given rise to thousands of microbial genome assemblies; more unprecedented findings are on the way in the short future. In 2018, we reported about 90 draft genome assemblies from different fungi, so far, which is the largest genomic dataset for macrofungi species [7]. As a typical representative of macrofungi, there are a lot of evolutionary and genetic problems to be explored in *M. gigantea*; however, the genome of this species has not been reported.

In this study, the genome of *M. gigantea* was sequenced, and a comparative genomics approach has been used to study it. The results show that different from the *Tricholoma* genus, *M. gigantea* belongs to the *Macrocybe* genus, which is a stand-alone genus. Furthermore, we found that glycosyl hydrolase family 28 (GH28) in *M. gigantea* shared conserved motifs that were significantly different from their counterparts in *Tricholoma*. The genomic data obtained in this study could be a useful resource for the investigation of these macrofungi in the future.

## 2. Materials and Methods

**2.1. Sequencing and Assembly of the Contig-Level Genome.** Sequencing libraries were prepared according to the standard protocol from Pacific Biosciences of California, Inc., and sequenced on the PacBio RS II platform with the P6 polymerase/C4 chemistry (Pacific Biosciences, USA). Then, about 8.7 Gb sequencing data (two times), including 1,135,758 reads, were produced, and the average read length is 7,707 bp (Table 1). We first made corrections on those reads by using the error correction module embedded in Canu

(<http://canu.readthedocs.org>) with a parameter-corrected error rate of 0.045 as the error rate of PacBio reads (15~20%) is high. Subsequently, the corrected PacBio sub-reads were imported to do genome assembly with Canu [10]. After aligning to the downloaded sequences from GenBank with length > 1 Kb with BWA, the contaminant contigs derived from other fungi, bacteria, or human genome were removed.

**2.2. Annotate Tandem Repeats.** Genome-wide tandem repeats (TEs) were identified by making use of the Tandem Repeats Finder program with the default settings [11]. A combination of homology-based and *de novo* approaches were used to define the TEs in the *M. gigantea* genome. In the field of homology-based prediction, *RepeatMasker* [12] was implemented to identify TEs against Repbase (Release 16.10; <http://www.girinst.org/repbase/index.html>) at the DNA level with the default settings. Besides, *Repeat Protein Mask* with the default settings was carried out to identify TEs via the RMBLAST search against the TE protein database at the protein level. For the *de novo* prediction, *Repeat Modeler* (<http://repeatmasker.org/>) [12] and *LTR FINDER* [13] were utilized to define the *de novo* evolved repeats from the above-assembled genome. Identification of the S-locus TEs in *M. gigantea* and *A. thaliana* was accomplished by the widely used *CENSOR* (<http://www.girinst.org/censor/>) with the default settings.

**2.3. Predict Protein-Coding Genes.** Both of the *de novo* and homology-based prediction methods were used here to annotate protein-coding genes in the *M. gigantea* genome. All of the coding sequences in the genes of *Laccaria bicolor* Orton, *T. matsutake*, and *Hypsizygus marmoratus* were captured by running the *Phytozome* v9.1 program (<http://www.phytozome.net/>) and then imported to the homology-



based gene annotation process. Subsequently, *TBLASTN* was performed to map the protein-coding sequences of the aforementioned species to the *M. gigantea* genome with the  $e^{-5}$  *E*-value and  $-F$  parameters. For each individual protein, all matched DNA sequences in the reference *M. gigantea* genome were concatenated by *Solar* after filtering the low-quality records. A long protein-coding region was packaged by extending a 2,000 bp fragment at both the upstream and downstream of the concatenated sequence. After that, *GeneWise* [14] was used to predict gene structures one by one with the “new” protein-coding regions. Two *de novo* prediction programs, *AUGUSTUS* [15] and *Genemark*, were successively used to annotate the protein-coding genes. The protein-coding gene sets in *M. gigantea* predicted by *de novo* and homology-based methods were merged to form a comprehensive and nonredundant reference gene list using *EvidenceModeler* [16]. Again, all programs above were executed with the default settings unless independent indications were given.

**2.4. Gene Family Cluster.** All of the coding sequences in the protein-coding genes in *A. ostoyae* C18/9, *P. eryngii*, *C. cinerea*, *C. gibba*, *L. nuda*, *T. matsutake* 945 v3.0, *T. saponaceum*, *T. sp.*, *T. terreum*, *T. flavovirens*, *T. bakamatsutake*, and *M. gigantea* were downloaded from JGI Genome Portal and National Center for Biotechnology Information (NCBI). In order to define the gene family clusters among the above species and *M. gigantea*, all-versus-all protein searches using BLASTP with the parameter of “*E* value =  $1e^{-5}$ ” were performed. Then, OrthoMCL (version 1.4, 17) was employed to handle the high-scoring segment pairs. The MCL package in OrthoMCL was then used to dig the final paralogous and orthologous genes with the “-abc -I = 1.5” parameter. The result was summarized and shown in the Venn diagram format via a web tool named *VENNY* 2.1 (<http://bioinfogp.cnb.csic.es/tools/venny/index.html>).

**2.5. Construct Preliminary Internal Transcribed Spacer Tree.** In our database, the sequences of Internal Transcribed Spacers (ITS) were acquired from GenBank following the fungal taxonomic tree, the Catalogue of Life, the Dictionary of Fungi, and its index. The ribosomal DNA, especially ITS1, ITS2, and 5.8S parts of rDNA, was obtained from NCBI and our assembly result. With reference to the classification results of JGI, we selected nearly 300 species of the *Agaricales* to be aligned on NCBI and finally obtained 2,127 of ITS sequences for preliminary classification of *M. gigantea* (Figure 1, Supplemental Table 3). The ITS sequence data were initially aligned by the release of Molecular Evolutionary Genetics Analysis version 5 (MEGA v5.05) with the default settings [17]. Then, the aligned results were manually adjusted. In addition, the Maximum Composite Likelihood analyses were also completed by MEGA with the General Time Reversible plus the Gamma distribution substitution model, alias as GTR+G. In order to assess the statistical support of clades, 1,000 fast-bootstrap (BS) replications were run. Besides, three species of *Agaricales* affiliated to three different families were selected as the outgroup taxa. The details can be found in Supplemental Table 8.

Because of the numerous insertions and deletions, all of the ITS sequences used in this study cannot be aligned unambiguously. However, in order to get a better and prior understanding of clade diversity within *Agaricus*, the ITS analyses for these sequences were conducted by making use of the Maximum Composite Likelihood (ML) model from various alignment methods [17]. This preliminary ML tree served as a map for sampling strategies, both for sequencing other genes and for the divergence time analysis. 342 samples representing species from each of the recognized sections and main lineages within each section were subsequently selected for generating ITS clade sequence data. Subsequently, the alignments were visually checked and corrected for the striking misaligned positions by MEGA5.05 to maximize primary sequence homology.

**2.6. Additional ITS Analysis with *M. gigantea*.** Our focus is to figure out which genus *M. gigantea* belongs to. To this end, we had performed an independent analysis of ITS sequences to identify the “proxy” specimens which can represent them in the multigene phylogeny (Supplemental Table 4). First, the ITS sequence data were aligned by MEGA with the default settings followed by manual adjustments [17]. Then, the maximum-likelihood analyses were performed with the GTR+G substitution model. For the purpose of assessing the statistical support of clades, we had run 1,000 fast-bootstrap (BS) replications under the General Time Reversible model. To get the best DNA models in MEGA5.05, the rates and patterns were filtered from gamma distributed with invariant sites (G+I) by running the program. The ITS sequences were also obtained from NCBI and our above assembly result. All the 553 ITS belonged to nearly 100 species. In fact, we performed BLAST on each species through NCBI and then selected the best 10 of the 50 results to represent the species. We selected the ITS sequences of all the species that can be found in the *Tricholomataceae* and used the same method for phylogenetic analysis. 94 species from *Tricholoma*, 3 species from *Macrocybe*, and *P. eryngii* and *C. cinerea* as outer groups were used in our tree (Supplemental Table 5 and Supplemental Figure2).

**2.7. Construct Phylogenetic Tree and Estimate Divergence Time.** In total, 157 single-copy orthologous genes from the aforementioned species were identified in the gene family cluster analysis. These genes were then imported to construct a phylogenetic tree. Here, for each gene, multiple sequence alignments were performed by employing the *MUSCLE* v.3.7 program with the default settings (<http://www.drive5.com/muscle>) [18]. For each species, four-fold degenerate sites were extracted from each gene and concatenated into a “supergene.” The *MrBayes* v3.1.2 program (<http://mrbayes.sourceforge.net>) [18] was utilized to reconstruct the phylogenetic trees among the species.

The *MCMCTREE* program of the *PAML* package [13] was applied here to evaluate the divergence time of *A. ostoyae* C18/9, *P. eryngii*, *C. cinerea*, *C. gibba*, *L. nuda*, *T. matsutake* 945 v3.0, *T. saponaceum*, *Tricholoma\_sp\_MG77*, *T. terreum*, *T. flavovirens*, *T. bakamatsutake*, and *M. gigantea*. The HKY85 model and the independent rate molecular clock

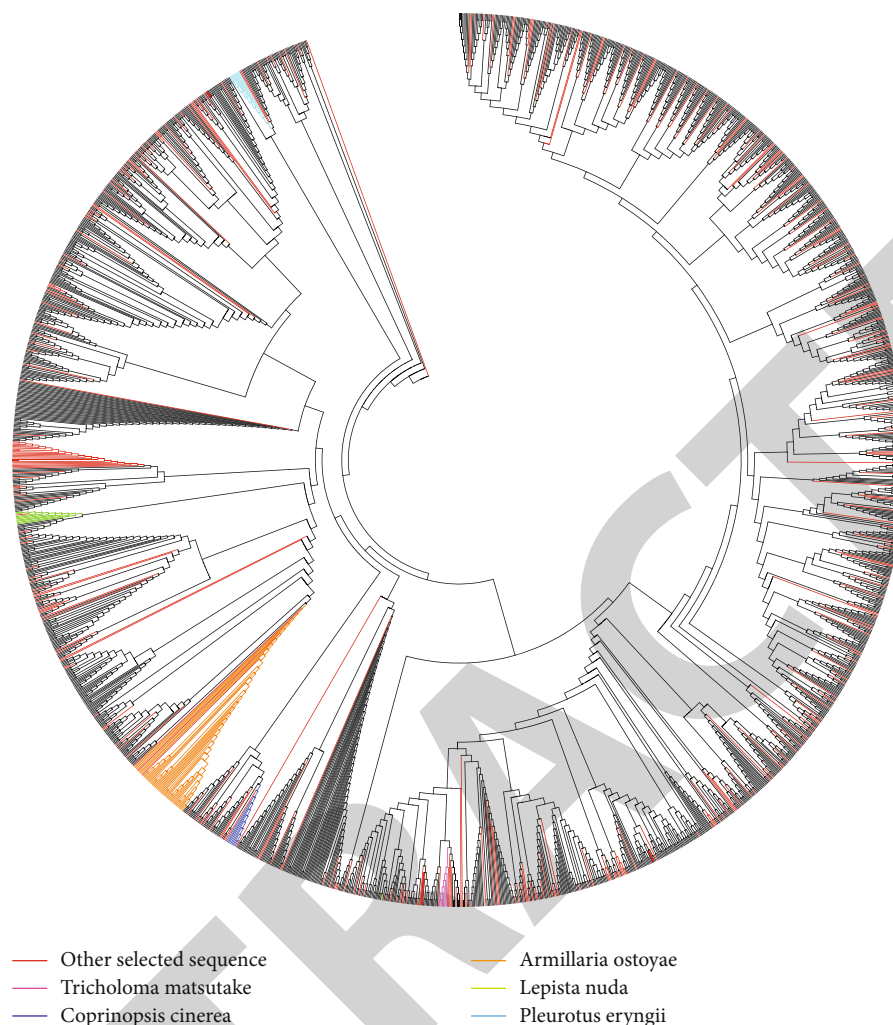


FIGURE 1: Evolutionary relationships of preliminary taxa. The evolutionary history was calculated by the neighbor-joining method. The figure shows an optimal tree with the sum of branch length = 33.54212249. The Maximum Composite Likelihood method was used to compute the evolutionary distances, which generated the units of the number of base substitutions per site. 2,127 nucleotide sequences were involved in this analysis. For each sequence pair, all ambiguous positions were removed.

were set to 4 and 2 for computation. The MCMC process in this program was executed 1,000,000 times within the samples, in one of which the frequency was set to 2 after a burn-in of 200,000.

**2.8. Identify Gene Families in Tricholomaceae.** We obtained *M. gigantea* sequences from the above assembly result. The BLAST program with the  $E$  value =  $e^{-5}$  parameter was locally performed with the Hidden Markov Model (HMM) profile in the Pfam database (<http://pfam.janelia.org/search/sequence>) to capture the candidate gene sequences. Candidate genes containing the known conserved domains were retained, and their presence was checked in the Pfam, SMART (<http://smart.embl-heidelberg.de/>), and NCBI Conserved Domain (<http://www.ncbi.nlm.nih.gov/Structure/cdd/wrpsb.cgi>) databases. The *A. ostoyae*, *P. eryngii*, *C. cinerea*, *C. gibba*, and *L. nuda* sequences were downloaded from the Department of Energy (DOE) in the Joint Genome Institute (JGI) located in America (<https://jgi.doe.gov>), and

the *Tricholomaceae* genome annotation results were downloaded from NCBI.

**2.9. Detect Contraction and Expansion of Gene Families.** *CAFÉ* v2.1 was employed to analyze the evolution of the gene family size according to the stochastic birth and death model [13, 19]. With the divergence time and the calculated phylogeny in hand, *CAFÉ* with the parameters “ $p$  value = 0.05, number of threads = 10, number of random = 1,000, and search for lambda” was used to define the gene families which had experienced the contraction and/or expansion in the aforementioned species.

**2.10. Detect Positively Selected Genes.** In order to screen out the genes under positive selection, we, respectively, blasted the CDS libraries of *C. gibba* and *A. ostoyae* C18/9 to the CDS library of *M. gigantea* with the BLASTn program. The best hits were carefully checked by the *Ka/KS Calculator* v.2.0 with the default parameters [19].

Moreover, another approach based upon syntenic comparison was also carried out to define the positively selected genes in *M. gigantea*. Briefly, protein sequences were aligned to themselves by using the BLASTp program. The five alignments at the top for each gene were retained. Then, the high-confidence collinear blocks with the  $E$  values less than  $e^{-10}$ , and the scores more than 300 were selected by *MCScanX* [20]. For the paired genes inferred from the syntenic alignment, we aligned the protein sequences by using the *CLUSTALW* program [21] and used the result to guide coding-sequence alignments by *PAL2NAL* [21]. In the yn00 program of the PAML package, the  $K_s$  and  $K_a$  values were calculated using the Yang–Nielsen method [13]. A Python script can be run to construct a pipeline including all the calculations. It is available at [http://github.com/tanghaibao/biopipeline/tree/master/synonymous\\_calculation](http://github.com/tanghaibao/biopipeline/tree/master/synonymous_calculation) for free download. Again, all programs above were executed with the default settings unless independent indications were given.

**2.11. Parse Gene Structure, Conserved Motif, and Promoter Cis-Acting Regulatory Element.** The motif-based sequence analysis tools (*MEME*) suite (<http://meme-suite.org/index.html>) and TBtools software [22] were used to define the conserved motifs with the following parameters: the number of repetitions is arbitrary, the optimal width of the motif is between 6 and 200 residues, and the maximum number of patterns is 20.

### 3. Results

**3.1. Genome Assembly of *M. gigantea*.** The *M. gigantea* genome was deeply sequenced with the PacBio RSII and PacBio Sequel platforms, which yielded ~8.75 Gb of raw data (213× coverage), totaling 1,135,758 reads (Supplemental Table 1). Ultimately, the sequencing data were assembled with CANU into 336 scaffolds (Table 1). The assembly size was 41.23 Mb, which was smaller than that of *Tricholoma matsutake* (189 Mb), *Tricholoma bakamatsutake* (140.67 Mb), and *Lepista nuda* (44.13 Mb; Supplemental Table 2). The final N50 size was 374,455 bp, and the N90 size was 38,255 bp. The completeness of the genome assembly was evaluated by the Benchmarking Universal Single-Copy Orthologs (BUSCO) analysis, and the result showed that 89.6% of complete BUSCO fungal set genes ( $n = 290$ ) and 6.9% of fragmented BUSCO genes could be found in the *M. gigantea* genome.

In the structural annotation procedure, the genome size of *M. gigantea* was computed as 41.23 Mb, and the number of annotated genes was 11,722. The number was less than the average number among the order *Agaricales*. For instance, *Tricholoma bakamatsutake*, *Coprinopsis cinerea*, and *Lepista nuda* genomes had 14,636, 13,393, and 14,880 predicted genes in their genomes, respectively [7, 23, 24].

In the next step, the OrthoMCL [25] software was used to construct the orthologous groups (OGs) with the best protein models from *Armillaria ostoyae* C18/9, *Pleurotus eryngii*, *C. cinerea*, *Clitocybe gibba*, *L. nuda*, *T. matsutake* 945 v3.0, *Tricholoma saponaceum*, *Tricholoma* sp. MG77, *Tricholoma terreum*, *Tricholoma flavovirens*, *T. bakamatsutake*, and *M.*

*gigantea* [7] with a scalable method. Each constructed OG was a set of proteins and across at least one species. Besides, all of the proteins exist in the 11 listed genomes which represent putative orthologs. The threshold value for all-versus-all BLASTP was set to  $10^{-8}$ .

Then, gene annotation was carried out based on the OG result. According to the bioinformatics initiative Gene Ontology, all of the 15,788 OGs were imported as a seed for the functional annotation process [26] (Table 1).

**3.2. Preliminary ITS Tree.** In order to understand the evolutionary relationship of *M. gigantea* within clades in *Agaricomycetes*, we performed neighbor-joining bootstrapping (NJ) analyses of the ITS sequence data [27, 28]. We first selected 342 taxa from a total of 2,127 *Agaricomycetes* samples for analyses based on this preliminary NJ tree, after excluding the ambiguous regions (Figure 1). After this, the best scoring ML trees with 342 sequences representing *Agaricomycetes* and bootstrap supported by GTR+G support were shown in Supplemental Figure 1 and Supplemental Table 3. In this tree, the genus *Tricholoma* and *Macrocybe* were clearly divided into two separate branches. The representatives of *Tricholoma*, *T. matsutake*, *T. bakamatsutake*, *T. terreum*, *T. saponaceum*, and *T. flavovirens* were grouped together, and the genus *Macrocybe* and *M. gigantea* were also grouped together. Evidently, *Tricholoma giganteum* was on the branch with the genus *Macrocybe*. In a previous research, Pegler et al. [1, 2, 29] took *T. giganteum* out of *Tricholoma* and grouped it into *Macrocybe*, and our phylogenetic tree supported this conclusion. Both *L. nuda* and *T. matsutake* belonged to the genus *Tricholoma* (<http://www.catalogueoflife.org>).

To further determine whether *M. gigantea* belonged to the genus *Tricholoma* or *Macrocybe*, we used the previous method (Supplemental Table 4) to select 553 sequences from the *Tricholoma* genus (a total of 369 species, 94 of which had sequence records) and *Macrocybe* genus (a total of 7 members, found that there are 3 members with sequence records) on the Catalogue of Life (Supplemental Table 5), while we also selected *C. cinerea*, *Agaricus parasubrutilescens*, and *P. eryngii* as representatives of another genus in *Tricholomataceae* and select *A. ostoyae* as the outgroup (Supplemental Figure 2). Finally, 90 sequences were selected from the above sequence (Figure 2(a), Supplemental Table 5, 6).

In this multigene tree (Figure 2(a)), three major clades were formed: *Macrocybe*, *Tricholoma*, and outgroup. The *Macrocybe* and *Tricholoma* clades were sister clades to each other, and all collections of *Macrocybe* showed a monophyletic relationship. Sections *Tricholoma* split into multiple clades (orange block). Section *Macrocybe* (light coral block), which contained the species *M. gigantea*, was not strongly supported as a monophyly with 1,000 Bootstrap Replications, but the topological structure of the classification of major species was supported in Zhao's article [28]. One striking exception, however, in this study is some species of the *Tricholoma* were split into another subgenus (e.g., MF034302.1 *Tricholoma sulphurescens*, LT0001741 *Tricholoma inamoenum*, AY462030.1 *Tricholoma bufonium*). We also found that the species named *Tricholoma giganteum* was also clustered on the branch *Macrocybe*, which is consistent with the



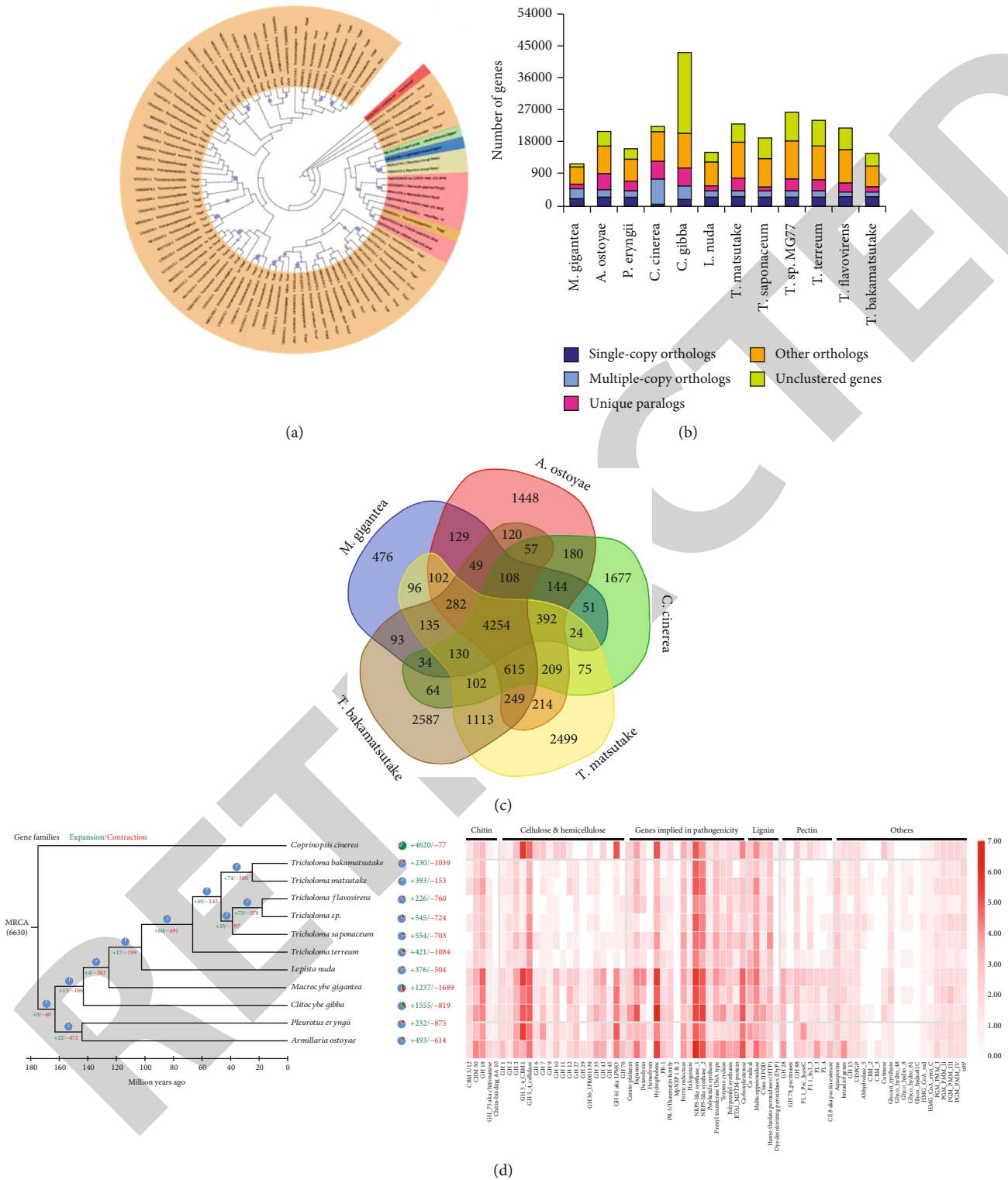


FIGURE 2: (a) Phylogeny of *Tricholomataceae* generated from Bayesian analysis of ITS sequences, rooted with *A. ostoyae*. Bootstrap support (BS) values > 50% are given at the internode bubbles (BS). We performed the maximum-likelihood (ML) analysis of ITS sequence data by Tamura 3-parameter model (T92)+Gamma Distributed (G) substitution model in MEGA5.05. The clade with a thick branch indicates the part we are interested in. Orange: *Tricholoma*; light coral: *Macrocybe*; cyan: *Agaricus*; khaki: *Pleurotus*; red: *Armillaria*. (b) Parameters of annotated *M. gigantea* genes in comparison with those of the *A. ostoyae*, *P. eryngii*, *C. cinerea*, *C. gibba*, *L. nuda*, *T. matsutake*, *T. saponaceum*, *T. sp.*, *T. terreum*, *T. flavovirens*, and *T. bakamatsutake*. (c) Gene family cluster analysis of *M. gigantea*, *A. ostoyae*, *C. cinerea*, *T. matsutake*, and *T. bakamatsutake*. (d) Left panel: Gene family expansion/contraction analysis of *C. cinerea*, *T. bakamatsutake*, *T. matsutake*, *T. flavovirens*, *T. sp.*, *T. saponaceum*, *T. terreum*, *L. nuda*, *C. gibba*, *P. eryngii*, *A. ostoyae*, and *M. gigantea*. Right panel: The right-bottom heat map illustrates the copy numbers of the gene coding plant cell wall degrading enzymes and pathogenicity-related gene families in the 12 species.

results of previous scholars [1]. We also obtained the same conclusion that *Tricholoma* and *Macrocybe* were not the same clade by constructing a phylogenetic tree using CDS sequences (Figure 2(d)) [30].

**3.3. Phylogenetic Analysis of *M. gigantea*.** The phylogenetic position of many species in the genus *Tricholoma* remains highly contentious [31, 32]. Since the time divergence can be served as a more objective and biologically informative criterion for the delimitation of taxonomic ranks [33], here, we presented a case study in which this criterion was applied for the systematics revision of a fungal genus. As a result, the taxonomic ranks were minimally disrupted as they were recognized in other studies. The uncertainties and limitations of the molecular divergence time estimation had been discussed in van Tuinen and Torres [34].

Phylogenomic analysis based on 1,976 concatenated conserved single-copy genes confirmed the position of *Macrocybe* in the *Tricholomaceae*, with *Pleurotus*, *Armillaria*, and *Coprinopsis* as their outgroup species (Figures 2(a) and 2(d)). We estimated the age of the most recent common ancestor (MRCA) of *Macrocybe* at 125 million years (Myr) and the divergence from *Clitocybe* at 143.5 Myr in the Early Cretaceous, which corresponded to the time when the Angiosperms evolved [35].

The genome-wide reconstruction of gene loss and duplication histories in 12 *Agaricales* species recovered an origin for most of the genes, the lineage-specific losses in genus-level groups, and in most of the gene families. 6,630 protein-coding genes were inferred for MRCA of *Agaricales* and 6,417 for the MRCA of *Tricholomaceae* (13 duplications, 186 losses) (Figures 2(b) and 2(c)). Further expansions happened in the 5,546 genes were inferred for the MRCA of *Tricholoma* (60 duplications, 491 losses). Further comparisons of all 12 species revealed 1,237 expanded gene families in the *M. gigantea* genome (Figure 2(c)). Remarkably, the products of many expanded genes even gene families are elements of the degrading enzymes in the plant cell wall (i.e., Cellulase Glyco\_hydro\_61, hydrophobins, carboxylesterase). The data strongly enhanced the annotated whole-genome sequence of *M. gigantea*.

Comparative analysis of *C. cinerea*, *A. ostoyae*, *T. matsutake*, *T. bakamatsutake*, and *M. gigantea* genes defined a total of 17,708 homologous gene families, of which 4,254 gene families were shared by all five species and 476 gene families were *M. gigantea* specific (Figure 2(c)). At the same time, we found that 129 genes were unique to the two species *M. gigantea* and *A. ostoyae*, which have huge fruiting bodies.

**3.4. Classify Energy Metabolism-Related Genes in *M. gigantea*.** The results of Sipos et al. and Peter et al. [36–38] indicated that the pathogenicity mechanisms and the evolution of the unique dispersal of *Armillaria* may have assorted a set of ancestral genetic tools for morphogenesis, complex multicellularity, and wood decay. Therefore, we compared the energy metabolism-related gene composition of *M. gigantea* species to the other *Tricholoma* with diverse lifestyles. Unsurprisingly, *M. gigantea* cause wood rotting like *A. ostoyae* in the saprotrophic phase of their lifecycle, which is reflected in their similar

heterotrophic method. The genome has the capability of encoding cellulose-, carboxylesterase-, and glycoside hydrolase, which implies the potential to degrade components of the plant cell wall (Figure 2(d), Supplemental Table 7). *M. gigantea* usually show similar gene counts as *A. ostoyae*, but not so obvious in *Tricholoma*. Besides, some pectinolytic families are overexpressed in *M. gigantea* and *Armillaria*. Pectin-degrading families consist of carbohydrate esterase 8 (CE8), polysaccharide lyase (PL)1, PL3 and PL4, GH28, GH88, and GH78. It is worth noting that compared to *Tricholoma*, GH28, PL3, and CE8 are significantly enriched in *M. gigantea*. The pectinolytic families of *M. gigantea* are unusual for wood-rotting fungi [39], and they might enable it to quickly gain energy in the wood to avoid competing with other microorganisms.

**3.5. Identification of the Pectinolytic Families in *M. gigantea*.** We focused on GH28 (Glyco\_hydro\_28) from the pectinolytic families. In sum, 65 candidate gene models related to the GH28 family of Pfam were initially captured. Some erroneously predicted GH28 gene models were manually removed (i.e., evm. model. tig00000709.146). Finally, according to the presence of apparently complete GH28 domains, a total of 54 gene models were gathered and annotated as *M. gigantea* GH28 genes.

The phylogenetic analysis (Figure 3, Supplemental Table 9) indicated that the *M. gigantea* GH28 domains can be separated into four big clades, namely clades I, II, III, and IV [40, 41]. Among these 10 GH28 proteins, 3 belong to group I, 3 to group II, 2 to group III, and 2 to group IV. The GH28 members from the phylogenetical species were closely clustered in the same clades. Take the clade IV as an example; it contained the members from *Tricholoma* (*T. matsutake*, *T. saponaceum*, *T. sp.*, *T. terreum*, *T. flavovirens*, *T. bakamatsutake*), which indicates they might be originated from a single ancestral gene or orthologues. Interestingly, three proteins from *M. gigantea* were clustered together with a series of *Armillaria* GH28 proteins (in clade I), suggesting that the different evolution patterns of GH28 in *M. gigantea* and *Armillaria* may occur after their divergence. We also employed the MEME [42] webserver to search the conserved motifs which were shared with the GH28 proteins. A total of 10 distinct conserved motifs were found. As illustrated in Figures 3 and 4, the 16 members from clade I contained two unique GH28 domains (Figure 4), indicating potential functional similarities among GH28 proteins, as only were the motif 5 and the adjacent-motif 7 coexisted in *M. gigantea*, *Armillaria*, and some outgroups GH28 proteins. The previous study says that the GH28 family played a major role in the initial stage of the development of fruit bodies [43]. The development of related fruiting bodies requires constant cell division and cell wall disintegration and reconstruction; the particular motifs might do contribution to the functional divergence of GH28 genes in a way.

## 4. Discussion and Conclusions

The genus *M. gigantea* evolved from saprotrophic ancestors in the *Agaricales*. By comparing the sequences in the



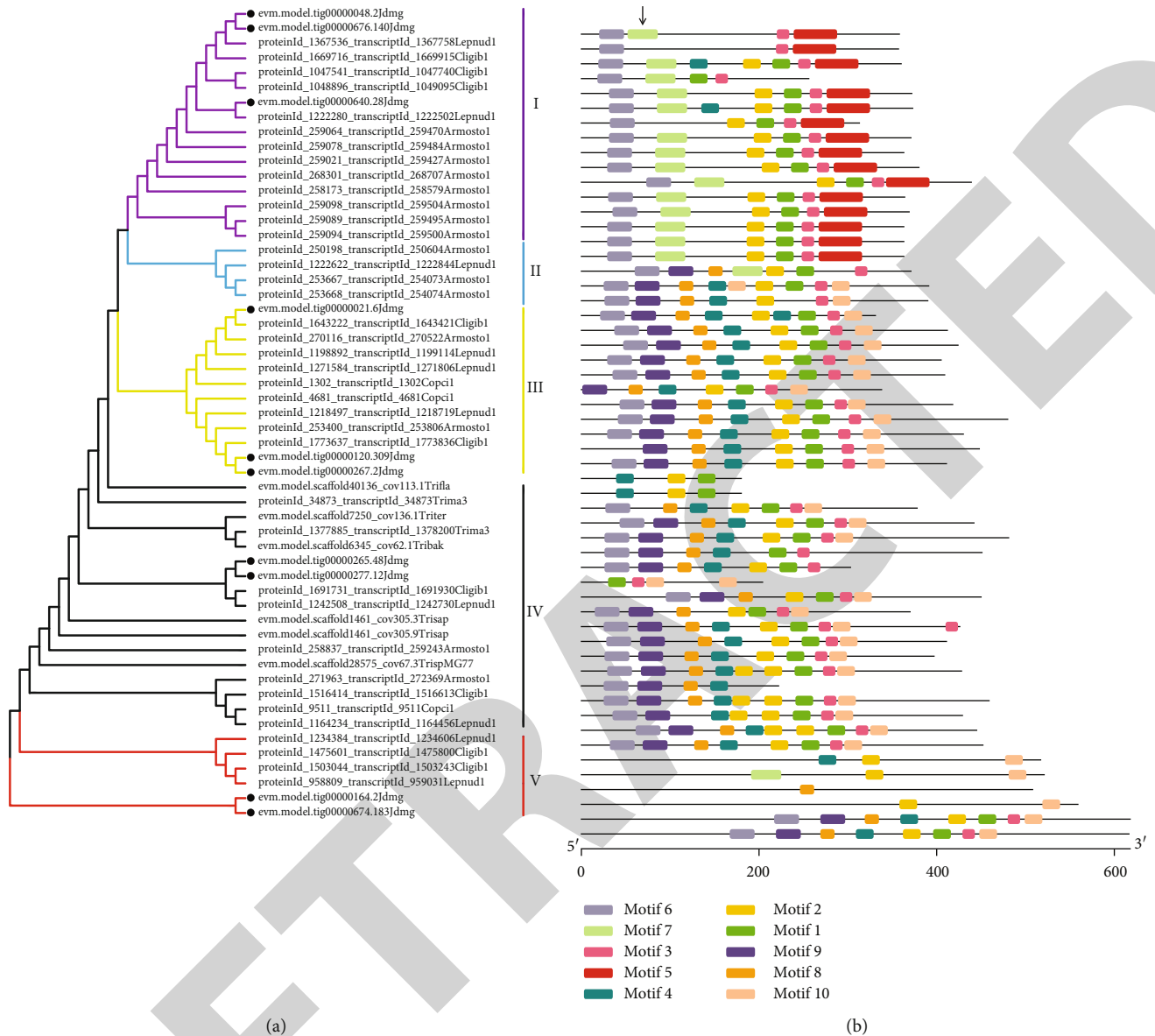


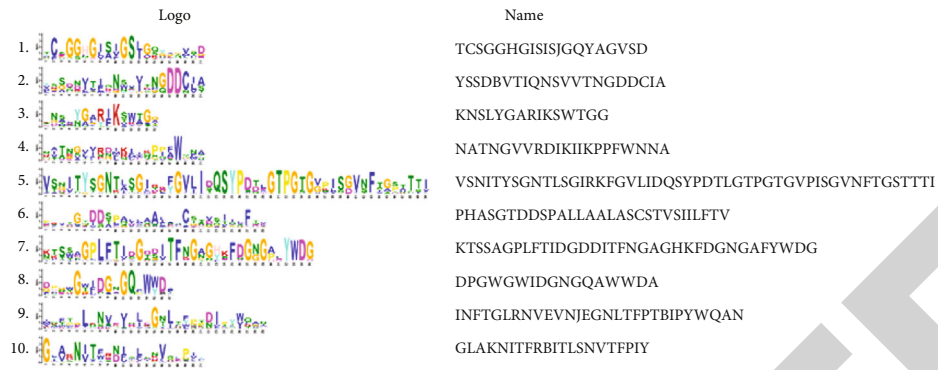
FIGURE 3: The motif compositions and phylogenetic relationships of *GH28* proteins from 11 different species. (a) An unrooted phylogenetic tree constructed by using the ML method of MEGA. The proteins are clustered into five main clades with a few subclades. The black solid circles indicate *GH28* proteins of *M. gigantea*. Subtree branch lines are colored which indicates different clades. (b) The distribution of conserved motifs in *GH28* proteins. The boxes with various colors stand for the different motifs and their positions in each *GH28* protein sequence.

genomes of *M. gigantea*, *C. cinerea*, and *A. ostoyae*, we found some specific gene profile similar to *A. ostoyae* in *M. gigantea*. Through the analysis of the genome sequence of *M. gigantea*, we found that *M. gigantea* encode a similar set of PCWDE genes like *A. ostoyae*, but obviously different from *Coprinopsis* and *Tricholoma*.

In previous studies, Singer et al. [44, 45] segregated the large-sized mushrooms of *Tricholoma* into a new sect. Later on, Pegler et al. [1] realized the need to separate this section into a new genus, *Macrocybe*. They also confirmed their hypothesis by molecular analysis using a large subunit (LSU) of rDNA [29, 44]. In the present work, the distinct lineage of *T. giganteum* was reevaluated using protein-coding

sequence on the genome [44, 46], and our studies also found that *T. giganteum*, *M. gigantea*, *Macrocybe crassa*, and *M. gigantea* are very close on the branches, they are even divided into the same branch; on the contrary, the branches containing *Tricholoma* and the branches of *Macrocybe* and *M. gigantea* belong to two different sister branches (Figure 2(d)). Mycologists are still hesitant to include their collections in *Macrocybe* [47]; maybe this is a good chance to change it.

In our phylogenetic analysis, *M. gigantea* was identified as a *Macrocybe* species and showed significant differences from *Tricholoma*. According to the work of Moncalvo et al. [44], *Macrocybe* is closer to *Entoloma* than *Tricholoma* or *Calocybe*. Perhaps, this is why *M. gigantea* was always



Motif 5	ID Name	Star	p-value	Site
	tig0000048.2	239	2.74e-47	---VINIT SGNIASICRLFQVLI DQS DTLITGSSVQVSGVNFITPTISI---
	tig00000676.140	238	2.74e-47	---VINIT SGNIASICRLFQVLI DQS DTLITGSSVQVSGVNFITPTISI---
	proID1367536_transID1367758	263	8.49e-47	---VINIT SGNATATIRQFQVLI DQS DTLITGSSVQVSGVNFVAFVSTI---
	proID1047541_transID1047740	276	4.20e-48	---VINIT SGNATIMRRFQVLI DQS DTLITGSSVQVSGVNFIAFPTISI---
	proID1048896_transID1049095	276	3.31e-44	---VSNVIT SGNATILRRFQVLI DQS DTLITGSSVQVSGVNFIAFVTTI---
	tig00000640.28	247	8.25e-38	---VSSVIT TNNKLSIITSFQVLI DQS DSTLITGSSVQVSGVNFITPTISI---
	proID1222280_transID1222502	275	4.77e-40	---VTGVT TGNKLSIITSFQVLI DQS DSTLITGSSVQVSGVNFITPTISI---
	proID259064_transID259470	267	1.23e-49	---VSDIT SGNITLSITKQVLI SQS DDAITGTTGPI SGVSEFOSAITV---
	proID259078_transID259484	284	1.23e-49	---VSDIT SGNITLSITKQVLI SQS DDAITGTTGPI SGVSEFOSAITV---
	proID259021_transID259427	343	1.11e-39	---SAKVSQITNITLSITKQVLI SQS DDAITGTTGPI SGVSEFOSAITV---
	proID268301_transID268707	268	3.73e-48	---VSGIT SGNKLSIEEFQVLI SQS DDDITGTTGPI SGVSEFOSAITV---
	proID258173_transID258579	273	3.51e-49	---VSGIT SGNITLSLDKQVLI TQS DDDITGTTGPI SGVSEFODAITI---
	proID259098_transID259504	267	3.18e-52	---VSGIT SGNITLSIDEVQVLI TQS DNEITGTTGPI SGVSEFOSAITI---
	proID259089_transID259495	267	6.63e-49	---VSGIT SGNITLSIDEVQVLI TQS SNEITGTTGPI SGVSEFOSAITI---
	proID259094_transID259500	267	2.99e-53	---VSGIT SGNITLSIDEVQVLI TQS DDEITGTTGPI SGVSEFOSAITI---
Motif 7	ID Name	Star	p-value	Site
	tig0000048.2	52	9.15e-26	---QALITLISQLRITITFNAG KFDGGPP WDG---
	proID1367536_transID1367758	73	1.11e-35	---NLSWGLFTVSGITITFNAG KFDGGPP WDG---
	proID1669716_transID1669915	72	5.82e-34	---NKSWSGLFTVSGITITFNAG KFDGGPP WDG---
	proID1047541_transID1047740	85	1.18e-36	---NKSWSGLFTVSGITITFNAG KFDGGPP WDG---
	proID1048896_transID1049095	85	1.25e-35	---NKSWSGLFTIISGITITFNAG KFDGGPP WDG---
	proID1222280_transID1222502	85	9.90e-28	---VRNWSGLMTITNDITFNAG NLVNDQ WDG---
	proID259064_transID259470	83	1.34e-36	---KITSSGLFTIDDSITEKAG KFNNGAS WDG---
	proID259078_transID259484	83	3.60e-35	---KITSSGLFTIDDSITEKAGV KFNNGAS WDG---
	proID259021_transID259427	127	3.39e-34	---KITSTAGLFTIDDNVTEKAG KFNNGAS WDG---
	proID268301_transID268707	84	1.75e-32	---KITSSGLFTIDDTITEKAGVFNNGAL WDG---
	proID258173_transID258579	89	3.69e-36	---QISTDGLFTIDDSITENAGV KFDNGAD WDG---
	proID259089_transID259495	83	4.70e-37	---KITSSDGLFTIDDDVITENAGV SFDNNGAE WDG---
	proID259094_transID259500	83	1.74e-36	---KITSSDGLFTIDDDVITENAGV SFDNNGAK WDG---

(a)



(b)

FIGURE 4: Continued.

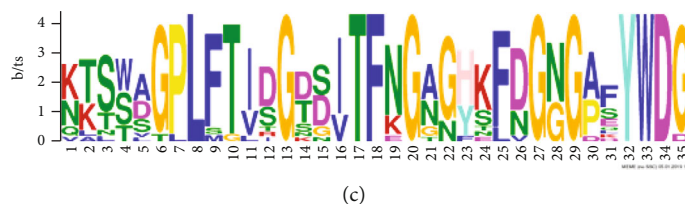


FIGURE 4: Alignment of multiple *GH28* and selected *GH28* domain amino acid sequences. (a) The basic sequence of all 10 selected motifs. (b), (c) The basic details of motif5 and motif 7.

assigned to a group far from *Tricholoma* in previous research. The *Tricholomataceae* are a large family of mushrooms within the *Agaricales*. The family is inclusive of any white red or yellow species in the *Agaricales* not already classified as belonging to, e.g., the *Amanitaceae*, *Entolomataceae*, *Hygrophoraceae*, or *Pluteaceae*. We also found similar phenomena when conducting evolutionary analysis, which was that always a few members of the *Tricholoma* genus that will gather into another independent clade. This study provides insights into the distinction between species by comparing differences between genes on the genome. It will further facilitate the understanding of the biology of the *Macrocybe*.

### Data Availability

The data sets supporting the results of this article are available in NCBI. The raw sequencing reads are available at SRR8617733, and the genome assembly data has been deposited at DDBJ/ENA/GenBank under the accession SJRY00000000. The version described in this paper is version SJRY01000000.

### Conflicts of Interest

The authors declare no conflict of interest.

### Authors' Contributions

Y.D., J.W., and J.S. contributed to the conceptualization. L.K. contributed to the methodology. Z.Z. and Y.W. is responsible for the software. X.D. is responsible for formal analysis. S.L. contributed to the investigation. Y.Z. contributed to the resources. Q.X. contributed to the data curation. L.K. and Z.Z. wrote the manuscript and is responsible for the original draft preparation. Y.D. wrote, reviewed, and edited the manuscript. Y.D. contributed to the supervision. Y.D. and L.K. are responsible for the project administration. J.S. is responsible for the funding acquisition. All authors have read and agreed to the published version of the manuscript.

### Acknowledgments

We thank all colleagues who assisted during fieldwork or provided plant material. Shufen Wang, Xuhai Zhu, Yunbing Pan, Wenqian Yu, Ling Yang, and Xianqin Fan provided valuable help with lab work. We also thank Zhengyu Zhang, Yun Gao, and Yuan Du for their assistance in genome analysis. Finally, we are particularly grateful to Dr. Chen for his valuable comments during the writing process. This research was funded by Yunnan Provincial Key Programs of Yunnan

Eco-friendly Food International Cooperation Research Center project, grant number 2019ZG00908, and Jiangsu University, grant number 20JJDG47.

### Supplementary Materials

*Supplementary 1.* Supplemental Figure 1. Molecular phylogenetic analysis by maximum likelihood method. The phylogeny tree shows the relationships among classes from the phylogenetic analysis of Agaricomycetes and allied phyla computed from the maximum likelihood analysis of ITS sequences data. Bootstrap support (BS) values > 50% are given at the internodes. The thickened branches imply the two types of species we are interested in. The tree with the highest log likelihood (-9,152.4805) is exhibited. The associated taxa were clustered together in the trees, and the percentages are shown close to the branches. Initial tree(s) for the heuristic search were automatically got as follows. When the number of common sites was <100 or less than one-fourth of the total number of sites, the maximum parsimony method was used; otherwise, the BIONJ method with MCL distance matrix was used. A discrete Gamma distribution was employed to model the evolutionary rate differences among sites (5 categories (+G, parameter = 0.2228)). The tree is drawn by a scale with the branch lengths measured in the number of substitutions per site. 342 nucleotide sequences were involved in this analysis.

*Supplementary 2.* Supplemental Figure 2. Molecular phylogenetic analysis by maximum likelihood method. The maximum likelihood method was used here to infer the evolutionary history based on the data-specific model. The tree with the highest log likelihood (-9,935.0324) is exhibited. The percentage of trees in which the associated taxa clustered together is shown next to the branches. Initial tree(s) for the heuristic search were obtained automatically as follows. When the number of common sites was <100 or less than one-fourth of the total number of sites, the maximum parsimony method was used; otherwise, BIONJ method with MCL distance matrix was used. A discrete Gamma distribution was used to model evolutionary rate differences among sites (5 categories (+G, parameter = 0.4200)). 553 nucleotide sequences were involved in this analysis.

*Supplementary 3.* Table S1. The library information and data statistics. This table is a summary of the library, sequence platform, and generated data information.

*Supplementary 4.* Table S2. The statistics of the fungal genomes used in this paper. WR: wood-rotting; ECM:

ectomycorrhizal; LD: litter decomposer; WD: wood decay; SN: saprotrophic nutrition; WR: wood rotting; ECM: ectomycorrhizal; LD: litter decomposer; WD: wood decay; SN: saprotrophic nutrition.

*Supplementary 5.* Supplemental Table 3. Maximum likelihood fits of 24 different nucleotide substitution models. Note. Models with the lowest BIC scores (Bayesian Information Criterion) are considered to describe the substitution pattern the best. For each model, the AICc value (Akaike Information Criterion, corrected), the maximum likelihood value (lnL), and the number of parameters (including branch lengths) are also presented [1]. Nonuniformity of evolutionary rates among sites may be modeled by using a discrete gamma distribution (+G) with 5 rate categories and by assuming that a certain fraction of sites is evolutionarily invariable (+I). Whenever applicable, estimates of the gamma shape parameter and/or the estimated fraction of invariant sites are shown. Assumed or estimated values of transition/transversion bias ( $R$ ) are shown for each model, as well. They are followed by nucleotide frequencies ( $f$ ) and rates of base substitutions ( $r$ ) for each nucleotide pair. Relative values of instantaneous  $r$  should be considered when evaluating them. For simplicity, the sum of the  $r$  values is made equal to 1 for each model. For estimating ML values, a tree topology was automatically computed. The analysis involved 342 nucleotide sequences. Codon positions included were 1st+2nd+3rd+noncoding. All positions with less than 95% site coverage were eliminated. That is, fewer than 5% alignment gaps, missing data, and ambiguous bases were allowed at any position. There were a total of 238 positions in the final dataset. Evolutionary analyses were conducted in MEGA5 [2]. Abbreviations: GTR: General Time Reversible; HKY: Hasegawa-Kishino-Yano; TN93: Tamura-Nei; T92: Tamura 3-parameter; K2: Kimura 2-parameter; JC: Jukes-Cantor. (1) Nei M. and Kumar S. (2000). *Molecular Evolution and Phylogenetics*. Oxford University Press, New York. (2) Tamura K., Peterson D., Peterson N., Stecher G., Nei M., and Kumar S. (2011). *MEGA5: Molecular Evolutionary Genetics Analysis using Maximum Likelihood, Evolutionary Distance, and Maximum Parsimony Methods*. *Molecular Biology and Evolution* (In Press). Disclaimer: Although utmost care has been taken to ensure the correctness of the caption, the caption text is provided “as is” without any warranty of any kind. The authors advise the user to carefully check the caption prior to its use for any purpose and report any errors or problems to the authors immediately (<http://www.megasoftware.net>). In no event shall the authors and their employers be liable for any damages, including but not limited to special, consequential, or other damages. The authors specifically disclaim all other warranties expressed or implied, including but not limited to the determination of the suitability of this caption text for a specific purpose, use, or application.

*Supplementary 6.* Supplemental Table 4. Maximum likelihood fits of 24 different nucleotide substitution models. NOTE. Models with the lowest BIC scores (Bayesian Information Criterion) are considered to describe the substitution pattern the best. For each model, the AICc value (Akaike

Information Criterion, corrected), the maximum likelihood value (lnL), and the number of parameters (including branch lengths) are also presented [1]. Nonuniformity of evolutionary rates among sites may be modeled by using a discrete gamma distribution (+G) with 5 rate categories and by assuming that a certain fraction of sites is evolutionarily invariable (+I). Whenever applicable, estimates of the gamma shape parameter and/or the estimated fraction of invariant sites are shown. Assumed or estimated values of transition/transversion bias ( $R$ ) are shown for each model, as well. They are followed by nucleotide frequencies ( $f$ ) and rates of base substitutions ( $r$ ) for each nucleotide pair. Relative values of instantaneous  $r$  should be considered when evaluating them. For simplicity, the sum of  $r$  values is made equal to 1 for each model. For estimating ML values, a tree topology was automatically computed. The analysis involved 553 nucleotide sequences. Codon positions included were 1st+2nd+3rd+noncoding. All positions with less than 95% site coverage were eliminated. That is, fewer than 5% alignment gaps, missing data, and ambiguous bases were allowed at any position. There were a total of 374 positions in the final dataset. Evolutionary analyses were conducted in MEGA5 [2]. Abbreviations: GTR: General Time Reversible; HKY: Hasegawa-Kishino-Yano; TN93: Tamura-Nei; T92: Tamura 3-parameter; K2: Kimura 2-parameter; JC: Jukes-Cantor. (1) Nei M. and Kumar S. (2000). *Molecular Evolution and Phylogenetics*. Oxford University Press, New York. (2) Tamura K., Peterson D., Peterson N., Stecher G., Nei M., and Kumar S. (2011). *MEGA5: Molecular Evolutionary Genetics Analysis using Maximum Likelihood, Evolutionary Distance, and Maximum Parsimony Methods*. *Molecular Biology and Evolution* (In Press). Disclaimer: Although utmost care has been taken to ensure the correctness of the caption, the caption text is provided “as is” without any warranty of any kind. The authors advise the user to carefully check the caption prior to its use for any purpose and report any errors or problems to the authors immediately (<http://www.megasoftware.net>). In no event shall the authors and their employers be liable for any damages, including but not limited to special, consequential, or other damages. The authors specifically disclaim all other warranties expressed or implied, including but not limited to the determination of the suitability of this caption text for a specific purpose, use, or application.

*Supplementary 7.* Supplemental Table 5. Species contained in *Tricholoma* and *Macrocybe* from the Catalogue of Life. This table lists 369 living species which belongs to *Tricholoma* and 6 living species which belongs to *Macrocybe*, respectively.

*Supplementary 8.* Supplemental Table 6. Maximum likelihood fits of 24 different nucleotide substitution models. NOTE. Models with the lowest BIC scores (Bayesian Information Criterion) are considered to describe the substitution pattern the best. For each model, the AICc value (Akaike Information Criterion, corrected), the maximum likelihood value (lnL), and the number of parameters (including branch lengths) are also presented [1]. Nonuniformity of evolutionary rates among sites may be modeled by using a discrete gamma distribution (+G) with 5 rate categories and by



assuming that a certain fraction of sites is evolutionarily invariable (+I). Whenever applicable, estimates of the gamma shape parameter and/or the estimated fraction of invariant sites are shown. Assumed or estimated values of transition/transversion bias ( $R$ ) are shown for each model, as well. They are followed by nucleotide frequencies ( $f$ ) and rates of base substitutions ( $r$ ) for each nucleotide pair. Relative values of instantaneous  $r$  should be considered when evaluating them. For simplicity, the sum of  $r$  values is made equal to 1 for each model. For estimating ML values, a tree topology was automatically computed. The analysis involved 90 nucleotide sequences. The codon positions included were 1st+2nd+3rd+noncoding. All positions with less than 95% site coverage were eliminated. That is, fewer than 5% alignment gaps, missing data, and ambiguous bases were allowed at any position. There were a total of 382 positions in the final dataset. Evolutionary analyses were conducted in MEGA5 [2]. Abbreviations: GTR: General Time Reversible; HKY: Hasegawa-Kishino-Yano; TN93: Tamura-Nei; T92: Tamura 3-parameter; K2: Kimura 2-parameter; JC: Jukes-Cantor. (1) Nei M. and Kumar S. (2000). *Molecular Evolution and Phylogenetics*. Oxford University Press, New York. (2) Tamura K., Peterson D., Peterson N., Stecher G., Nei M., and Kumar S. (2011). *MEGA5: Molecular Evolutionary Genetics Analysis using Maximum Likelihood, Evolutionary Distance, and Maximum Parsimony Methods*. *Molecular Biology and Evolution* (In Press). Disclaimer: Although utmost care has been taken to ensure the correctness of the caption, the caption text is provided "as is" without any warranty of any kind. The authors advise the user to carefully check the caption prior to its use for any purpose and report any errors or problems to the authors immediately (<http://www.megasoftware.net>). In no event shall the authors and their employers be liable for any damages, including but not limited to special, consequential, or other damages. The authors specifically disclaim all other warranties expressed or implied, including but not limited to the determination of the suitability of this caption text for a specific purpose, use, or application.

*Supplementary 9.* Supplemental Table 7. Species used in comparative genomic analyses. This table lists five main species (chitin, cellulose and hemicellulose, genes implied in pathogenicity, lignin, pectin) and others used in comparative genomic analyses.

*Supplementary 10.* Supplemental Table 8. Information used for the species originally screened. This table contained the main information which included accession on GenBank, genus, and species used for screening.

*Supplementary 11.* Supplemental Table 9. Maximum likelihood fits of 54 different amino acid substitution models. Note. Models with the lowest BIC scores (Bayesian Information Criterion) are considered to describe the substitution pattern the best. For each model, the AICc value (Akaike Information Criterion, corrected), the maximum likelihood value (lnL), and the number of parameters (including branch lengths) are also presented [1]. Nonuniformity of evolutionary rates among sites may be modeled by using a discrete gamma distribution (+G) with 5 rate categories and by assuming that a certain fraction of sites is evolutionarily

invariable (+I). Whenever applicable, estimates of the gamma shape parameter and/or the estimated fraction of invariant sites are shown. They are followed by amino acid frequencies ( $f$ ) and rates of amino acid substitutions ( $r$ ) for each amino acid pair. Relative values of instantaneous  $r$  should be considered when evaluating them. For simplicity, the sum of  $r$  values is made equal to 1 for each model. For estimating ML values, a user-specified topology was used. The analysis involved 54 amino acid sequences. All positions with less than 95% site coverage were eliminated. That is, fewer than 5% alignment gaps, missing data, and ambiguous bases were allowed at any position. There were a total of 56 positions in the final dataset. Evolutionary analyses were conducted in MEGA5 [2]. Abbreviations: GTR: General Time Reversible; JTT: Jones-Taylor-Thornton; rtREV: General Reverse Transcriptase; cpREV: General Reversible Chloroplast; mtREV24: General Reversible Mitochondrial. (1) Nei M. and Kumar S. (2000). *Molecular Evolution and Phylogenetics*. Oxford University Press, New York. (2) Tamura K., Peterson D., Peterson N., Stecher G., Nei M., and Kumar S. (2011). *MEGA5: Molecular Evolutionary Genetics Analysis using Maximum Likelihood, Evolutionary Distance, and Maximum Parsimony Methods*. *Molecular Biology and Evolution* (In Press). Disclaimer: Although utmost care has been taken to ensure the correctness of the caption, the caption text is provided "as is" without any warranty of any kind. The authors advise the user to carefully check the caption prior to its use for any purpose and report any errors or problems to the authors immediately (<http://www.megasoftware.net>). In no event shall the authors and their employers be liable for any damages, including but not limited to special, consequential, or other damages. The authors specifically disclaim all other warranties expressed or implied, including but not limited to the determination of the suitability of this caption text for a specific purpose, use, or application.

## References

- [1] D. N. Pegler, D. J. Lodge, and K. K. Nakasone, "The pantropical genus *Macrocybe* gen. nov.," *Mycologia*, vol. 90, no. 3, pp. 494–504, 2018.
- [2] A. Razaq, R. Nawaz, and A. N. Khalid, "An Asian edible mushroom, *Macrocybe gigantea*: its distribution and ITS-rDNA based phylogeny," *Mycosphere*, vol. 7, no. 4, pp. 525–530, 2016.
- [3] S. Khatua and K. Acharya, "Influence of extraction parameters on physico-chemical characters and antioxidant activity of water soluble polysaccharides from *Macrocybe gigantea* (Massee) Pegler & Lodge," *J Food Sci Technol*, vol. 53, no. 4, pp. 1878–1888, 2016.
- [4] A. R. Das, M. Borthakur, A. K. Saha, and S. R. Joshi, "Molecular characterization and antioxidant potential of three wild culinary-medicinal mushrooms from Tripura, Northeast India," *International Journal of Medicinal Mushrooms*, vol. 19, no. 1, pp. 55–63, 2017.
- [5] T. Gaur and P. B. Rao, "Analysis of antibacterial activity and bioactive compounds of the giant mushroom, *Macrocybe gigantea* (Agaricomycetes), from India," *International Journal of Medicinal Mushrooms*, vol. 19, no. 12, pp. 1083–1092, 2017.
- [6] S. D. S. Milhorini, F. R. Smiderle, S. M. P. Biscaia, F. R. Rosado, E. S. Trindade, and M. Iacomini, "Fucogalactan from the giant



- mushroom *Macrocybe titans* inhibits melanoma cells migration," *Carbohydrate Polymers*, vol. 190, pp. 50–56, 2018.
- [7] H. Li, S. Wu, X. Ma et al., "The Genome Sequences of 90 Mushrooms," *Scientific Reports*, vol. 8, no. 1, p. 9982, 2018.
- [8] O. H. Cisse and J. E. Stajich, "FGMP: assessing fungal genome completeness," *BMC Bioinformatics*, vol. 20, no. 1, p. 184, 2019.
- [9] I. V. Grigoriev, R. Nikitin, S. Haridas et al., "MycCosm portal: gearing up for 1000 fungal genomes," *Nucleic Acids Research*, vol. 42, no. D1, pp. D699–D704, 2013.
- [10] S. Koren, B. P. Walenz, K. Berlin, J. R. Miller, N. H. Bergman, and A. M. Phillippy, "Canu: scalable and accurate long-read assembly via adaptive k-mer weighting and repeat separation," *Genome Research*, vol. 27, no. 5, pp. 722–736, 2017.
- [11] G. Benson, "Tandem repeats finder a program to analyze DNA sequences," *Nucleic Acids Research*, vol. 27, no. 2, pp. 573–580, 1999.
- [12] M. Tarailo-Graovac and N. Chen, "Using RepeatMasker to identify repetitive elements in genomic sequences," *Current Protocols in Bioinformatics*, vol. 25, no. 1, 2009.
- [13] Z. Yang, "PAML 4: phylogenetic analysis by maximum likelihood," *Molecular Biology and Evolution*, vol. 24, no. 8, pp. 1586–1591, 2007.
- [14] E. Birney and R. Durbin, "Using GeneWise in the Drosophila annotation experiment," *Genome Research*, vol. 10, no. 4, pp. 547–548, 2000.
- [15] M. Stanke, O. Keller, I. Gunduz, A. Hayes, S. Waack, and B. Morgenstern, "AUGUSTUS: ab initio prediction of alternative transcripts," *Nucleic Acids Res*, vol. 34, no. Web Server issue, pp. W435–W439, 2006.
- [16] A. A. Hoffmann and Y. Willi, "Detecting genetic responses to environmental change," *Nature Reviews Genetics*, vol. 9, no. 6, pp. 421–432, 2008.
- [17] K. Tamura, D. Peterson, N. Peterson, G. Stecher, M. Nei, and S. Kumar, "MEGA5: molecular evolutionary genetics analysis using maximum likelihood, evolutionary distance, and maximum parsimony methods," *Molecular Biology and Evolution*, vol. 28, no. 10, pp. 2731–2739, 2011.
- [18] J. Geml, D. M. Geiser, and D. J. Royle, "Molecular evolution of *Agaricus* species based on ITS and LSU rDNA sequences," *Mycological Progress*, vol. 3, no. 2, pp. 157–176, 2004.
- [19] T. De Bie, N. Cristianini, J. P. Demuth, and M. W. Hahn, "CAFE: a computational tool for the study of gene family evolution," *Bioinformatics*, vol. 22, no. 10, pp. 1269–1271, 2006.
- [20] Y. Wang, H. Tang, J. D. DeBarry et al., "MCScanX: a toolkit for detection and evolutionary analysis of gene synteny and collinearity," *Nucleic Acids Research*, vol. 40, no. 7, article e49, 2012.
- [21] M. A. Larkin, G. Blackshields, N. P. Brown et al., "Clustal W and Clustal X version 2.0.," *Bioinformatics*, vol. 23, no. 21, pp. 2947–2948, 2007.
- [22] C.-J. Chen, H. Chen, Y. Zhang et al., "TBtools: An integrative toolkit developed for interactive analyses of big biological data," *Molecular Plant*, vol. 13, no. 8, pp. 1194–1202, 2020.
- [23] J. E. Stajich, S. K. Wilke, D. Ahren et al., "Insights into evolution of multicellular fungi from the assembled chromosomes of the mushroom *Coprinopsis cinerea* (*Coprinus cinereus*)," *Proceedings of the National Academy of Sciences*, vol. 107, no. 26, pp. 11889–11894, 2010.
- [24] C. Gostinčar, R. A. Ohm, T. Kogej et al., "Genome sequencing of four *Aureobasidium pullulans* varieties: biotechnological potential, stress tolerance, and description of new species," *BMC Genomics*, vol. 15, no. 1, p. 549, 2014.
- [25] L. Li, C. J. Stoeckert Jr., and D. S. Roos, "OrthoMCL: identification of ortholog groups for eukaryotic genomes," *Genome Research*, vol. 13, no. 9, pp. 2178–2189, 2003.
- [26] Consortium TGO, "Gene Ontology: tool for the unification of biology," *Nature Genetics*, vol. 25, pp. 25–29, 2000.
- [27] R.-L. Zhao, J.-L. Zhou, J. Chen et al., "Towards standardizing taxonomic ranks using divergence times – a case study for reconstruction of the *Agaricus* taxonomic system," *Fungal Diversity*, vol. 78, no. 1, pp. 239–292, 2016.
- [28] R.-L. Zhao, G.-J. Li, S. Sánchez-Ramírez et al., "A six-gene phylogenetic overview of *Basidiomycota* and allied phyla with estimated divergence times of higher taxa and a phyloproteomics perspective," *Fungal Diversity*, vol. 84, no. 1, pp. 43–74, 2017.
- [29] V. Hofstetter, H. Cléménçon, R. Vilgalys, and J.-M. Moncalvo, "Phylogenetic analyses of the *Lyophylleae* (*Agaricales*, *Basidiomycota*) based on nuclear and mitochondrial rDNA sequences," *Mycological Research*, vol. 106, no. 9, pp. 1043–1059, 2002.
- [30] R. Knight, A. Vrbanac, B. C. Taylor et al., "Best practices for analysing microbiomes," *Nature Reviews Microbiology*, vol. 16, no. 7, pp. 410–422, 2018.
- [31] Y.-Y. Cui, Q. Cai, L.-P. Tang, J.-W. Liu, and Z. L. Yang, "The family Amanitaceae: molecular phylogeny, higher-rank taxonomy and the species in China," *Fungal Diversity*, vol. 91, no. 1, pp. 5–230, 2018.
- [32] V. Motato-Vásquez, E. Grassi, A. M. Gugliotta, and G. L. Robledo, "Evolutionary relationships of *Bresadolia* (*Basidiomycota*, *Polyporales*) based on molecular and morphological evidence," *Mycological Progress*, vol. 17, no. 9, pp. 1031–1048, 2018.
- [33] J. C. Avise and G. C. Johns, "Proposal for a standardized temporal scheme of biological classification for extant species," *Proceedings of the National Academy of Sciences*, vol. 96, no. 13, pp. 7358–7363, 1999.
- [34] M. van Tuinen and C. R. Torres, "Potential for bias and low precision in molecular divergence time estimation of the Canopy of Life: an example from aquatic bird families," *Frontiers in Genetics*, vol. 6, p. 203, 2015.
- [35] C. R. Fitzpatrick, J. Copeland, P. W. Wang, D. S. Guttman, P. M. Kotanen, and M. T. J. Johnson, "Assembly and ecological function of the root microbiome across angiosperm plant species," *Proceedings of the National Academy of Sciences*, vol. 115, no. 6, pp. E1157–E1165, 2018.
- [36] F. Martin, A. Kohler, C. Murat, C. Veneault-Fourrey, and D. S. Hibbett, "Unearthing the roots of ectomycorrhizal symbioses," *Nature Reviews Microbiology*, vol. 14, no. 12, pp. 760–773, 2016.
- [37] M. Peter, A. Kohler, R. A. Ohm et al., "Ectomycorrhizal ecology is imprinted in the genome of the dominant symbiotic fungus *Cenococcum geophilum*," *Nature Communications*, vol. 7, no. 1, p. 12662, 2016.
- [38] G. Sipos, A. N. Prasanna, M. C. Walter et al., "Genome expansion and lineage-specific genetic innovations in the forest pathogenic fungi *Armillaria*," *Nature Ecology & Evolution*, vol. 1, no. 12, pp. 1931–1941, 2017.
- [39] J. Rytioja, K. Hilden, J. Yuzon, A. Hatakka, R. P. de Vries, and M. R. Makela, "Plant-polysaccharide-degrading enzymes from Basidiomycetes," *Microbiology and Molecular Biology Reviews*, vol. 78, no. 4, pp. 614–649, 2014.

## Research Article

# The Value of Combined Detection of D-dimer and CD62p in Judging the Severity of Acute Cerebral Infarction and Short-Term Prognosis

Min Xu <sup>1</sup>, Xiao-ying He <sup>2</sup>, and Pan Huang <sup>3</sup>

<sup>1</sup>Department of Neurology, The Second People's Hospital of Deyang City, No. 340 Minjiang West Road, Deyang, Sichuan 618000, China

<sup>2</sup>Department of Neurology, The Affiliated Hospital of Southwest Medical University, No. 25 Taiping Street, Luzhou, Sichuan 646000, China

<sup>3</sup>Department of Neurology, People's Hospital of Deyang City, No. 173 TaiShan North Road, Deyang, Sichuan 618000, China

Correspondence should be addressed to Pan Huang; 1032857970@qq.com

Received 23 December 2020; Revised 2 January 2021; Accepted 7 January 2021; Published 18 January 2021

Academic Editor: Yuzhen Xu

Copyright © 2021 Min Xu et al. This is an open access article distributed under the Creative Commons Attribution License, which permits unrestricted use, distribution, and reproduction in any medium, provided the original work is properly cited.

**Objective.** To explore the value of combined detection of peripheral blood P-selectin (CD62p) and D-dimer (D-dimer) in the judgment of acute cerebral infarction severity and short-term prognosis. **Methods.** 268 patients with acute cerebral infarction from February 2015 to February 2019 were selected as the observation group. According to the National Institute of Health stroke scale, there were 90 cases (SCI group), 88 cases (MOCI group), and 90 cases (MICI group) in the severe, moderate, and mild cerebral infarction groups, respectively. In the same period, 80 cases of healthy people served as the Normal group. Use flow cytometry to detect CD62p in peripheral blood and magnetic bead method to detect D-dimer level within 24 hours of onset. Logistic regression was used to analyze whether the two are factors affecting the short-term prognosis of acute cerebral infarction, and the ROC curve was drawn to evaluate the value of the combined detection of the two in the short-term prognosis of patients with acute cerebral infarction. **Results.** Peripheral blood D-dimer and CD62p levels ( $2.95 \pm 0.76$  ng/l,  $34.03 \pm 5.29$  ng/l) in the SCI group were higher than those in the MOCI group ( $2.30 \pm 0.51$  ng/l,  $27.58 \pm 5.56$  ng/l) and the MICI group ( $1.87 \pm 0.40$  ng/l,  $19.60 \pm 3.98$  ng/l); the difference between the groups was statistically significant ( $P < 0.05$ ). Logistic regression analysis showed that D-dimer and CD62p were independent risk factors affecting the poor prognosis of patients with acute cerebral infarction (OR values were 3.752 and 1.213, and 95% CI were 1.612-7.934 and 1.093-1.342, respectively, both  $P < 0.05$ ). The AUC of D-dimer combined with CD62p for predicting poor prognosis of acute cerebral infarction is 0.859, which is better than D-dimer and CD62p alone. **Conclusion.** Peripheral blood D-dimer combined with CD62p detection is helpful for the risk stratification and short-term prognosis assessment of patients with acute cerebral infarction. Clinical detection is of great significance for the prevention and monitoring of disease development.

## 1. Introduction

Acute cerebral infarction (ACI) is a common clinical disease and frequently occurring disease. Due to the nonrenewable nature of neurons, cerebral infarction has a very high disability rate and recurrence rate, which brings a serious burden to society and families. Therefore, it is very important to predict the early stage of high-risk patients with cerebral infarction and actively rescue the ischemic penumbra in the early stage

after cerebral infarction, restore the blood supply of brain cells to slow down the brain cell damage, and improve the clinical treatment rate of patients [1]. Studies have found that platelet activation, coagulation system, and fibrinolytic system imbalance are the main causes of cerebral thrombosis [2, 3]. P-selectin (CD62p), as a glycoprotein on the surface of platelets, can reflect the level of platelet activation, and D-dimer is a clear marker that reflects the high specificity of thrombosis and activation of the fibrinolytic system, which

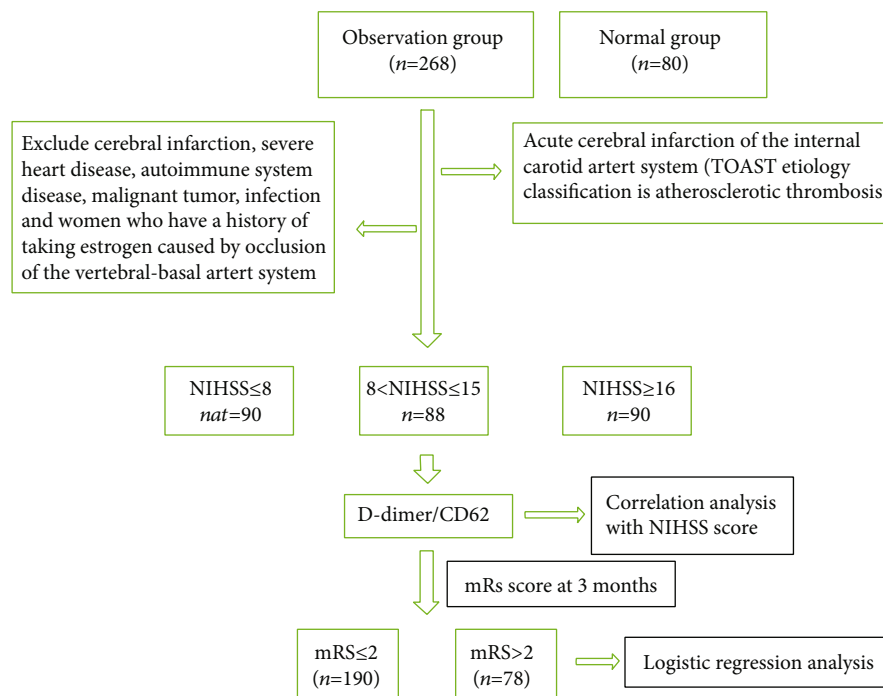


FIGURE 1: Flow chart.

helps thrombosis monitoring of formation and thrombolytic therapy. In order to clarify the application value of the two in the severity of acute cerebral infarction and short-term prognosis, this study performed D-dimer and CD62p detection on 268 patients with acute cerebral infarction admitted to our hospital. The report is as follows.

## 2. Materials and Methods

**2.1. Clinical Data.** 268 patients with acute cerebral infarction who were hospitalized in the Department of Neurology of our hospital from February 2015 to February 2019 were selected as the cerebral infarction group, including 148 males and 120 females, aged 45-82 ( $68.78 \pm 9.72$ ) years old. All selected cases meet the diagnostic criteria for acute ischemic stroke [4]. According to the diagnosis results of hematology, imaging, and cardiac examination, TOAST classification was carried out and confirmed by two researchers for consistency and acute cerebral infarction of the internal carotid artery system (TOAST etiology classification is atherosclerotic thrombosis). Also, exclude posterior circulation cerebral infarction, chronic obstructive pulmonary disease, ischemic heart disease, rheumatic heart disease, congenital heart disease, bacterial endocarditis and atrial fibrillation, autoimmune system disease, malignant tumor, infection, severe medical diseases (such as pulmonary embolism, venous sinus thrombosis, deep vein thrombosis), and women who have a history of taking estrogen. After the patients were admitted to the hospital, the cerebral infarction group was divided into 3 subgroups according to the National Institute of Health stroke scale: [5] MICI group 90 cases ( $\leq 8$  scores), MOCI group 88 cases (8-15 scores), and MICI group 90 cases ( $> 16$  scores). A total of 80 patients

were selected as the Normal group during the outpatient health examination in this hospital, including 42 males and 38 females, aged 46-81 ( $63.85 \pm 10.34$ ) years old. This study was approved by the Ethics Committee of Deyang People's Hospital, ethics approval number 2014-11-02. The test flow chart is shown in Figure 1.

**2.2. Specimen Collection and Measurement Methods.** All subjects were taken fasting anterior elbow venous blood before receiving treatment after admission 3 ml. Among them, the EDTA anticoagulant tube was used to separate and extract the plasma, and the anticoagulant tube was not added to separate and extract the serum and stored in the refrigerator at  $-20^{\circ}\text{C}$ . The CD62p level in serum was detected by flow cytometry (flow cytometer was American Applied Biosystems; the kit was Shanghai Xuanhao Technology Co., Ltd., operated according to the instructions). The content of D-dimer in plasma was detected by the magnetic bead method (normal value:  $0-1 \mu\text{g/ml}$ ).

**2.3. Prognosis Follow-Up.** After 3 months of onset, follow-up by telephone or outpatient service, evaluate the functional prognosis of the patients according to the mRS score, and group them according to the prognosis of the patients. mRS score  $\leq 2$  is a good prognosis group, and mRS score  $> 2$  is a poor prognosis group. Analyze the affected patient prognostic factors. The blind collection is used for data collection.

**2.4. Statistical Methods.** Using the SPSS17.0 statistical software, the measurement data is expressed as  $\bar{x} \pm s$ , the independent samplet-test is used for the comparison of the two groups, the ANOVA analysis is used for the comparison of

multiple groups, and the LSD-t method is used for the pairwise comparison. Logistic regression was used to analyze whether D-dimer and CD62p are factors affecting the prognosis of patients with acute cerebral infarction, and the ROC curve was drawn to calculate the area under the curve (AUC).  $P < 0.05$  indicates that the difference is statistically significant.

### 3. Result

**3.1. Comparison of Baseline Data between the Observation Group and Control Group.** There was no significant difference in the clinical data and laboratory examination between the observation group and the control group ( $P > 0.05$ ) (Table 1).

**3.2. The Levels of D-dimer and CD62p in the Peripheral Blood of the Observers Were Compared.** The results showed that the levels of D-dimer and CD62p in the cerebral infarction group were higher than those in the normal group, and the difference was statistically significant ( $P < 0.05$ ). The differences between the SCI group, MOCI group, and MICI group are also statistically significant (Table 2).

**3.3. Correlation Analysis of D-dimer, CD62p Levels, and NIHSS Scores in the Observation Group.** The results showed that D-dimer, CD62p, and NIHSS scores were all positively correlated ( $r = 0.455, 0.707$ ;  $P < 0.05$ ) (Table 3, Figures 2 and 3).

**3.4. Factors Affecting the Prognosis of Patients with Acute Cerebral Infarction.** With  $mRS \leq 2$  points in March as the good prognosis group (190 cases),  $mRS > 2$  points as the poor prognosis group (78 cases); D-dimer, CD62p, and general clinical data were used as independent variables for logistic regression analysis. It is shown that smoking history, D-dimer, and CD62p are all independent predictors of poor prognosis, as shown in Table 4.

**3.5. The Predictive Value of D-dimer and CD62p on the Poor Prognosis of Acute Cerebral Infarction.** The AUC of D-dimer and CD62p alone in predicting poor prognosis of acute cerebral infarction were 0.712 and 0.848 ( $P < 0.05$ ), respectively. The combined detection of the two to predict the poor prognosis of acute cerebral infarction AUC was 0.859 ( $P < 0.05$ ) (Table 5 and Figure 4).

### 4. Discussion

Acute cerebral infarction is a common clinical thromboembolic disease with an extremely high risk of disability, death, and recurrence. Therefore, it is of great significance to actively seek specific markers that can predict the severity and prognosis of the disease. Most of the TOAST etiological classification of cerebral infarction is atherosclerosis, and its pathological basis is platelets. Studies have found that platelet activation is closely related to the occurrence and development of thrombosis. Cerebral infarction is based on atherosclerotic plaques. Due to changes in hemodynamics or blood contents, platelet activation is intensified, forming

TABLE 1: Comparison of baseline data between observation group and control group.

Item	Observation group (n = 268)	Normal group (n = 80)	P
Age (years)	64.42 ± 8.72	63.97 ± 8.55	0.68
Sex (M/F)	136/132	38/32	0.85
Smoke (n, %)	145 (54.10%)	47 (58.75%)	0.76
Hypertension (n, %)	51 (19.02%)	15 (18.75%)	0.46
Diabetes (n, %)	41 (15.29%)	12 (15.00%)	0.09
SCr (μmol/l)	52.23 ± 6.46	51.89 ± 6.21	0.67
UA (μmol/l)	354.47 ± 37.15	361.12 ± 39.47	0.17
TC (mmol/l)	4.87 ± 0.42	4.91 ± 0.43	0.45
TG (mmol/l)	1.22 ± 0.24	1.27 ± 0.28	0.07
HDL-C (mmol/l)	0.93 ± 0.23	0.96 ± 0.24	0.61
LDL-C (mmol/l)	2.89 ± 0.43	2.83 ± 0.40	0.45
AST/ALT	0.75 ± 0.23	0.72 ± 0.22	0.65
BMI (kg/m <sup>2</sup> )	22.56 ± 1.23	22.74 ± 1.27	0.69
Drinker (n,%)	82 (30.59%)	22 (27.5%)	0.58

BMI: body mass index; TG: triglyceride; TC: total cholesterol; HDL-C: high-density lipoprotein-cholesterol; LDL-C: low high-density lipoprotein-cholesterol.

TABLE 2: Comparison of D-dimer and CD62p levels in peripheral blood of each group ( $x \pm s$ ).

Item	n	NIHSS scores	D-dimer (μg/ml)	CD62p (ng/l)
Normal	80	0	0.87 ± 0.23	16.20 ± 3.26
SCI	90	4.60 + 0.76	1.87 ± 0.40*	19.60 ± 3.98*
MOCI	88	12.40 + 2.56	2.30 ± 0.51 <sup>#</sup>	27.58 ± 5.56 <sup>#</sup>
MICI	90	18.79 + 2.98	2.95 ± 0.76* <sup>#</sup>	34.03 ± 5.29* <sup>#</sup>
P			0.00	0.00

\*The MICI group compares with the normal group  $P < 0.05$ ; <sup>#</sup>The MOCI group compares with the MICI group  $P < 0.05$ ; \*<sup>#</sup>The SCI group compares with the MICI group  $P < 0.05$ .

TABLE 3: Correlation analysis of D-dimer, CD62p, and NIHSS score.

	r	NIHSS score	P
D-Dimer	0.455		0.00
CD62p	0.707		0.00

platelet-vininogen thrombus, which blocks blood vessels and causes infarction [6–8].

Various reasons cause the damaged blood vessel wall to contract and change the local hemodynamic characteristics, which leads to the adhesion of platelets to the exposed subendothelial tissue under the action of plasma von Willebrand factor (VWF). The stimulation of collagen or thrombin released by endothelial cells undergoes morphological changes, and further release reaction and



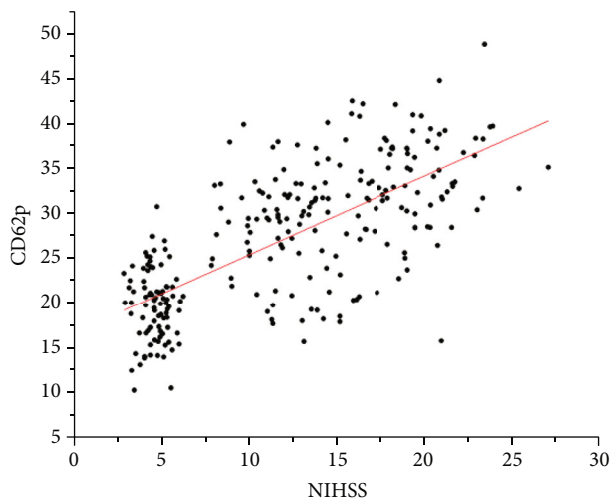


FIGURE 2: Correlation analysis between CD62p and NIHSS score.

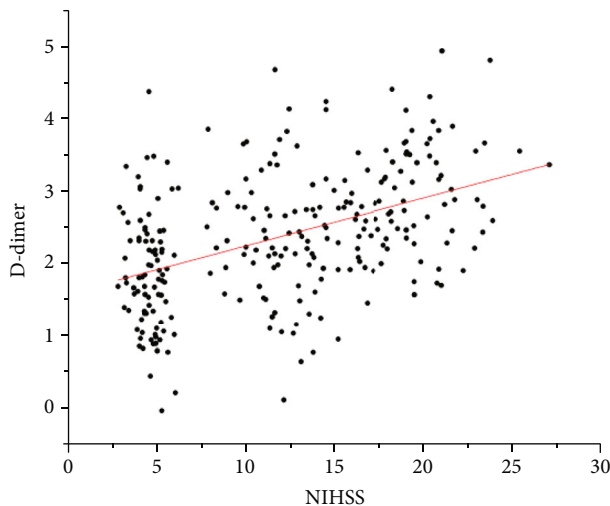


FIGURE 3: Correlation analysis between D-dimer and NIHSS score.

arachidonic acid metabolism occur. The ADP secreted by the release reaction and the metabolism of arachidonic acid to form thromboxane A2 can activate intracellular pathways to make Ca ion flow, which causes the bridging of platelets and fibrin to cause aggregation, and finally, plasma fibrinogen participates in the aggregation to form thrombus. The platelet adhesion-deformation-release-aggregation reaction in this process is the platelet activation reaction [9, 10]. It is precisely because platelet activation has such an important role; this study is based on this observation in order to find new ways to predict the severity and prognosis of the disease.

CD62p is a glycoprotein distributed on  $\alpha$  particles in stationary platelets. When platelets are activated,  $\alpha$  particles quickly fuse with the platelet membrane and release, so that CD62p is redistributed on the surface of platelets [11]. Studies have found that the concentration peak is reached 10 minutes after platelet activation, so it can be used as a specific marker for evaluating platelet activation

TABLE 4: Logistic regression analysis of factors affecting the prognosis of acute cerebral infarction.

Item	OR	95% CI	P
Age	1.052	0.883-1.256	0.556
Hypertension	7.281	0.458-113.230	0.152
Diabetes	4.352	0.426-44.684	0.214
Smoke	4.102	1.086-15.234	0.035
Drinke	0.715	0.064-8.231	0.724
SCr	0.269	0.023-3.487	0.312
BMI	1.213	0.115-12.485	0.885
D-Dimer	3.572	1.612-7.934	0.002
CD62p	1.213	1.093-1.342	0.003

TABLE 5: The predictive value of peripheral blood D-dimer and CD62p detection for end-point events.

Item	AUC	Standard error	95% CI	P
D-Dimer	0.712	0.033	0.647-0.777	0.026
CD62p	0.848	0.028	0.794-0.902	0.019
D-Dimer+CD62p	0.859	0.027	0.807-0.911	0.005

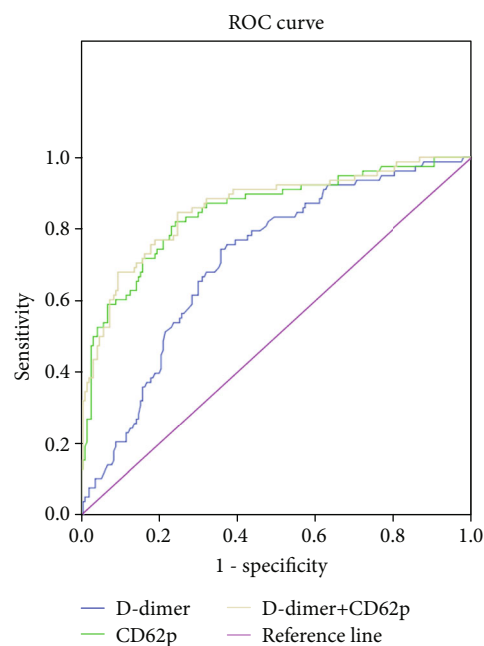


FIGURE 4: ROC curve.

status and thrombosis. Okada used mice and baboons to establish a model of cerebral ischemia and found that the expression of CD62p increased after 1 hour of cerebral ischemia, reaching a peak at 8 to 24 hours and lasting for 3 to 5 days [12]. The domestic scholar HUANG Tong dynamically detects CD62p in patients with acute cerebral infarction, and the results are basically consistent with OKada [13]. Cha observation of 45 patients with acute cerebral infarction showed that the upregulation of



CD62p is related to the clinical deterioration of patients with acute cerebral infarction [14]. In addition, acute cerebral infarction is often associated with dysfunction or disorder of the fibrinolytic system. D-dimer is a specific degradation product of cross-linked fibrin, the increase of peripheral blood D-dimer indicates the enhancement of in vivo fibrinolytic activity. Studies have found that D-dimer will only increase in plasma after thrombosis in the body, so it can be used as a specific molecular marker for the diagnosis of thrombosis. Studies have shown that D-dimer is related to the onset and recurrence of coronary heart disease and is also related to cerebral venous sinus thrombosis [15, 16].

This study shows that the levels of CD62p and D-dimer in patients with acute cerebral infarction are significantly higher than those in the normal control group, indicating that the two can be used as markers of acute cerebral infarction thrombosis, which is consistent with other relevant experimental conclusions [17–19]. The levels of D-dimer and CD62p can be dynamically monitored during clinical thrombolysis to evaluate whether thrombus fusion is possible. The levels of D-dimer and CD62p in the SCI group were higher than those in the MOCI group and the MICI group, and the differences were statistically significant ( $P < 0.05$ ), indicating that the higher the degree of platelet activation, the stronger the platelet adhesion and aggregation ability, and the easier to form arteries. Thrombus causes local brain tissue blood supply to be interrupted to form infarcts. Logistic regression analysis shows that D-dimer and CD62p are independent risk factors affecting the prognosis of patients with cerebral infarction. ROC curve analysis shows that peripheral blood D-dimer and CD62p levels have a higher predictive value for the poor prognosis of patients with acute cerebral infarction, which is consistent with the conclusions of other scholars [20, 21]. Therefore, the detection of peripheral blood D-dimer combined with CD62p in patients with acute cerebral infarction is timely, convenient, and economical and can early assess the risk stratification and prognosis of patients with acute cerebral infarction. However, the sample size of the cases collected in this study is small and cannot be monitored dynamically, which needs to be further improved.

## Data Availability

All data, models, and code generated or used during the study appear in the submitted article.

## Conflicts of Interest

The authors declare that they have no financial or other conflicts of interest in relation to this research and its publication.

## References

- [1] X. Yi, Z. Han, Q. Zhou, J. Lin, and P. Liu, “20-Hydroxyeicosatetraenoic acid as a predictor of neurological deterioration in acute minor ischemic stroke,” *Stroke*, vol. 47, pp. 3045–3047, 2016.
- [2] A. Mizuma, K. Iijima, S. Kohara et al., “Effect of atorvastatin co-treatment on inhibition of platelet activation by clopidogrel in patients with ischemic stroke,” *International Journal of Stroke*, vol. 10, pp. E90–E91, 2015.
- [3] H. Tohgi, S. Konno, S. Takahashi, D. Koizumi, R. Kondo, and H. Takahashi, “Activated coagulation/fibrinolysis system and platelet function in acute thrombotic stroke patients with increased C-reactive protein levels,” *Thrombosis research*, vol. 100, pp. 373–379, 2000.
- [4] Y. Pan, W. Chen, Y. Xu et al., “Genetic polymorphisms and clopidogrel efficacy for acute ischemic stroke or transient ischemic attack: a systematic review and meta-analysis,” *Circulation*, vol. 135, no. 1, pp. 21–33, 2017.
- [5] M. P. Thompson, Z. Luo, J. Gardiner, J. F. Burke, A. Nickles, and M. J. Reeves, “Quantifying selection bias in National Institute of Health Stroke Scale data documented in an acute stroke registry,” *Circulation: Cardiovascular Quality and Outcomes*, vol. 9, pp. 286–293, 2016.
- [6] S. Watanabe, F. Usui-Kawanishi, T. Komada et al., “ASC regulates platelet activation and contributes to thrombus formation independent of NLRP3 inflammasome,” *Biochemical and Biophysical Research Communications*, vol. 531, pp. 125–132, 2020.
- [7] L. J. Ren, Q. Li, T. You et al., “Humanin analogue, HNG, inhibits platelet activation and thrombus formation by stabilizing platelet microtubules,” *Journal of Cellular and Molecular Medicine*, vol. 24, no. 8, pp. 4773–4783, 2020.
- [8] D. Guo, Z. Zhu, C. Zhong et al., “Prognostic metrics associated with inflammation and atherosclerosis signaling evaluate the burden of adverse clinical outcomes in ischemic stroke patients,” *Clinical chemistry*, vol. 66, pp. 1434–1443, 2020.
- [9] A. Ruban, N. Daya, A. L. Schneider et al., “Liver enzymes and risk of stroke: the atherosclerosis risk in communities (ARIC) study,” *Journal of stroke*, vol. 22, pp. 357–368, 2020.
- [10] D. Sagris, G. Georgiopoulos, I. Leventis et al., “Antithrombotic treatment in patients with stroke and supracardiac atherosclerosis,” *Neurology*, vol. 95, pp. e499–e507, 2020.
- [11] X. Zhong, Z. Cao, J. Song, Y. Liu, and Q. Guo, “Relationship of platelet glycoprotein IIb/IIIa and CD62P with hypercoagulable state after oncologic surgery,” *Clinical and Applied Thrombosis/Hemostasis*, vol. 26, p. 1076029620977906, 2020.
- [12] Y. Okada and B. R. Copelancl, “P-selectin and intercellular adhesion molecules-1 expression after focal brain ischemia and reperfusion,” *Stroke*, vol. 25, no. 1, pp. 202–211, 1994.
- [13] X. S. Huang, Q. D. Yang, Y. H. Liu, and Z. J. Liu, “Changes of plasma CD 62 p levels in patients with acute cerebral infarction,” *Journal of Central South University. Medical sciences*, vol. 29, no. 4, pp. 445–447, 2004.
- [14] J. K. Cha, M. H. Jeong, E. K. Kim et al., “Surface expression of P-selectin on platelets is related with clinical worsening in acute ischemic stroke,” *Journal of Korean medical science*, vol. 17, no. 6, pp. 811–816, 2002.
- [15] E. Soyode, W. Pritchard, M. Hayman, A. Davenport, P. Sivasothy, and W. Thomas, “Validation of the age-adjusted D-dimer in an ambulatory deep vein thrombosis diagnostic service: beware of superficial thrombophlebitis,” *British Journal of Haematology*, vol. 191, pp. e94–e96, 2020.

- [16] R. Meng, X. Wang, M. Hussain et al., "Evaluation of plasma D-dimer plus fibrinogen in predicting acute CVST," *International Journal of Stroke*, vol. 9, no. 2, pp. 166–173, 2014.
- [17] H. Li, G. N. Bi, and C. M. Luo, "The expression of P-selectin and the change of myeloperoxidase activity in rats with cerebral ischemia-reperfusion," *Chinese Journal of Cerebrovascular Disease*, vol. 2, no. 10, pp. 454–458, 2005.
- [18] L. T. Zhang, X. J. Yang, and M. Pang, "The changes of serum soluble E-selectin and P-selectin levels in patients with ischemic stroke," *Chinese Journal of Cerebrovascular Diseases*, vol. 3, no. 2, pp. 69–70, 2006.
- [19] N. Li, C. H. Ren, F. Sun, and X. M. Ji, "Changes of plasma fibrinogen, D-dimer and antithrombin III levels in patients with acute cerebral infarction," *Chinese Journal of Cerebrovascular Diseases*, vol. 10, no. 5, pp. 268–272, 2013.
- [20] F. Lu and Z. H. Wang, "Role of CD62p in the diagnosis of acute brain infarction disease," *Journal of Capital Medical University*, vol. 36, no. 5, pp. 714–717, 2015.
- [21] T. Leng and Z. G. Xiong, "Treatment for ischemic stroke: from thrombolysis to thrombectomy and remaining challenges," *Brain circulation*, vol. 5, no. 1, p. 8, 2019.

## *Retraction*

# **Retracted: Safety and Efficacy of Early Carotid Endarterectomy in Patients with Symptomatic Carotid Artery Stenosis: A Meta-Analysis**

### **BioMed Research International**

Received 12 March 2024; Accepted 12 March 2024; Published 20 March 2024

Copyright © 2024 BioMed Research International. This is an open access article distributed under the Creative Commons Attribution License, which permits unrestricted use, distribution, and reproduction in any medium, provided the original work is properly cited.

This article has been retracted by Hindawi following an investigation undertaken by the publisher [1]. This investigation has uncovered evidence of one or more of the following indicators of systematic manipulation of the publication process:

- (1) Discrepancies in scope
- (2) Discrepancies in the description of the research reported
- (3) Discrepancies between the availability of data and the research described
- (4) Inappropriate citations
- (5) Incoherent, meaningless and/or irrelevant content included in the article
- (6) Manipulated or compromised peer review

The presence of these indicators undermines our confidence in the integrity of the article's content and we cannot, therefore, vouch for its reliability. Please note that this notice is intended solely to alert readers that the content of this article is unreliable. We have not investigated whether authors were aware of or involved in the systematic manipulation of the publication process.

Wiley and Hindawi regrets that the usual quality checks did not identify these issues before publication and have since put additional measures in place to safeguard research integrity.

We wish to credit our own Research Integrity and Research Publishing teams and anonymous and named external researchers and research integrity experts for contributing to this investigation.

The corresponding author, as the representative of all authors, has been given the opportunity to register their agreement or disagreement to this retraction. We have kept a record of any response received.

### **References**

- [1] X. Chen, J. Su, G. Wang et al., "Safety and Efficacy of Early Carotid Endarterectomy in Patients with Symptomatic Carotid Artery Stenosis: A Meta-Analysis," *BioMed Research International*, vol. 2021, Article ID 6623426, 8 pages, 2021.

## Review Article

# Safety and Efficacy of Early Carotid Endarterectomy in Patients with Symptomatic Carotid Artery Stenosis: A Meta-Analysis

Xiao Chen,<sup>1</sup> Jing Su,<sup>2</sup> Guojun Wang<sup>ID</sup>,<sup>2</sup> Han Zhao,<sup>2</sup> Shizhong Zhang,<sup>2</sup> Tao Liu,<sup>2</sup> Xindi Su,<sup>3</sup> and Ning Zhou<sup>4</sup>

<sup>1</sup>Shandong First Medical University (Shandong Academy of Medical Sciences), Jinan City, Shandong Province, China

<sup>2</sup>Shandong Taian City Central Hospital, Taian City, Shandong Province, China

<sup>3</sup>Jinzhou Medical University, Jinzhou City, Liaoning Province, China

<sup>4</sup>Shandong Taian City Central Hospital Branch, Taian City, Shandong Province, China

Correspondence should be addressed to Guojun Wang; [wguojun2002@163.com](mailto:wguojun2002@163.com)

Received 21 November 2020; Revised 9 December 2020; Accepted 24 December 2020; Published 9 January 2021

Academic Editor: Yuzhen Xu

Copyright © 2021 Xiao Chen et al. This is an open access article distributed under the Creative Commons Attribution License, which permits unrestricted use, distribution, and reproduction in any medium, provided the original work is properly cited.

**Background and Purpose.** This study is aimed at assessing the differences in postoperative stroke, myocardial infarction (MI), and mortality in patients with symptomatic carotid artery stenosis (sCAS) treated with early or late carotid endarterectomy (CEA) to determine and compare the safety of different operation timing. **Design.** A systematic document retrieval of studies published in the past 10 years reporting periprocedural stroke/mortality/MI after carotid endarterectomy (CEA) related to the time between CEA and qualifying neurological symptoms. The application database has “PubMed, EMBase and Cochrane databases.” RevMan5.3 software provided by the Cochrane collaboration was used for meta-analysis. **Results.** A systematic literature search was conducted in databases. A total of 10 articles were included in this study. They were divided into early CEA and delayed CEA with operation within 48 h, 1 w, or 2 w after onset of neurological symptoms. Incidence of the postoperative stroke in patients undergoing delayed CEA ( $\geq 48$  h) was significantly higher than patients with delayed CEA ( $< 48$  h) (OR = 2.14, 95% CI: 1.43-3.21,  $P = 0.0002$ ). The postoperative mortality of patients after delayed CEA ( $\geq 48$  h) was significantly higher than patients after early CEA ( $< 48$  h) (OR = 1.35, 95% CI: 1.06-1.71,  $P = 0.02$ ). The risk of postoperative mortality of patients treated with delayed CEA ( $\geq 7$  d) was significantly higher than patients after the early CEA group ( $< 7$  d) (OR = 1.69, 95% CI: 1.21-2.32,  $P = 0.001$ ). **Conclusion.** Early CEA is safe and effective for a part of patients with symptomatic carotid stenosis, but a comprehensive preoperative evaluation of patients with carotid stenosis must be performed.

## 1. Introduction

Stroke represents the fourth cause of death worldwide; carotid artery stenosis is one of the important causes of stroke [1]. Carotid endarterectomy (CEA) has been identified as the preferred treatment for carotid stenosis. In the past, it was believed that the risk of early recurrent TIA or stroke after the onset of neurological symptoms is not high, so CEA should be delayed for at least 6 weeks after an onset of neurological symptoms, and operating early on a recently symp-

tomatic “unstable” carotid plaque was associated with an increased risk of perioperative stroke [2]. In recent years, early surgical intervention within 1-2 weeks of symptom onset has been advocated for patients with symptomatic carotid artery stenosis [3]. Therefore, the timing of CEA surgery has been gradually attracted the attention of all, and studies on it have also increased gradually in recent years. The current recommendations about when to perform carotid endarterectomy to patients with sCAS rely on multiple uncertainties. The present study reviewed the studies

published in the past 10 years, and the risks of postoperative complications of early CEA or delayed CEA were summarized, and meta-analysis was made.

## 2. Methods

A systematic literature search was conducted in PubMed, MEDLINE, Embase, and Cochrane databases. The retrieval language is English. Various synonyms and related Medical Subject Headings (MeSH) for “carotid artery,” “operation timing,” “early endarterectomy,” “delayed endarterectomy,” “carotid stenosis,” “Endarterectomy, Carotid” to build the search syntax.

**2.1. Inclusion Criteria and Study Endpoints.** Inclusion criteria: (1) patients with symptomatic carotid stenosis; (2) the treatment was carotid endarterectomy; (3) patients were grouped according to symptom timing of surgery. Articles were excluded if they were (1) noncontrolled test, (2) did not study human subjects, and (3) not published in full text. If clinical studies were conducted by the same team, the articles with the most complete data, the largest sample size, or the most relevant results are selected.

The primary endpoints were stroke and mortality after CEA. The secondary end point was MI. They were divided into early CEA and delayed CEA with operation within 48 h, 1 w, or 2 w after onset of neurological symptoms.

**2.2. Study Selection and Data Extraction.** Three independent investigators comprehensively evaluated the included articles, carefully read the abstract of the articles, and evaluated the eligibility based on the full text, and judgement differences were resolved by communicating with each other. References of the included articles were carefully examined and searched for some references if necessary. Data of the included articles were recorded on a spreadsheet, including the basic characteristic of the paper (year of publication, author, research method, etc.), the year of recruitment of patients; baseline characteristic of preoperative patients, grouped base on CEA timing, postoperative complications, etc. If some studies do not report relevant data, corresponding authors were requested to provide these data. If the authors are still not provided, they will be excluded in some outcomes or subgroup group. Although we tried to contact the authors to refine the study, we did not obtain unpublished data.

**2.3. Assessment of Risk of Bias and Methodological Quality.** Assessment of risk of bias according to the Newcastle-Ottawa quality assessment scale. Evaluation standard: (1) Is the case definition adequate?; (2) Representativeness of the cases; (3) Selection of Controls; (4) Definition of Controls; (5) Comparability of cases and controls on the basis of the design or analysis; (6) Ascertainment of exposure; (7) Same method of ascertainment for cases and controls; (8) Nonresponse rate.

**2.4. Statistical Analysis.** If more than 1 study had available data, and it will be performed and analyzed, an  $I^2$  value was calculated to describe the percentage variance among studies attributable to heterogeneity. All meta-analyses were conducted using Review Manager (RevMan version 5.3). For

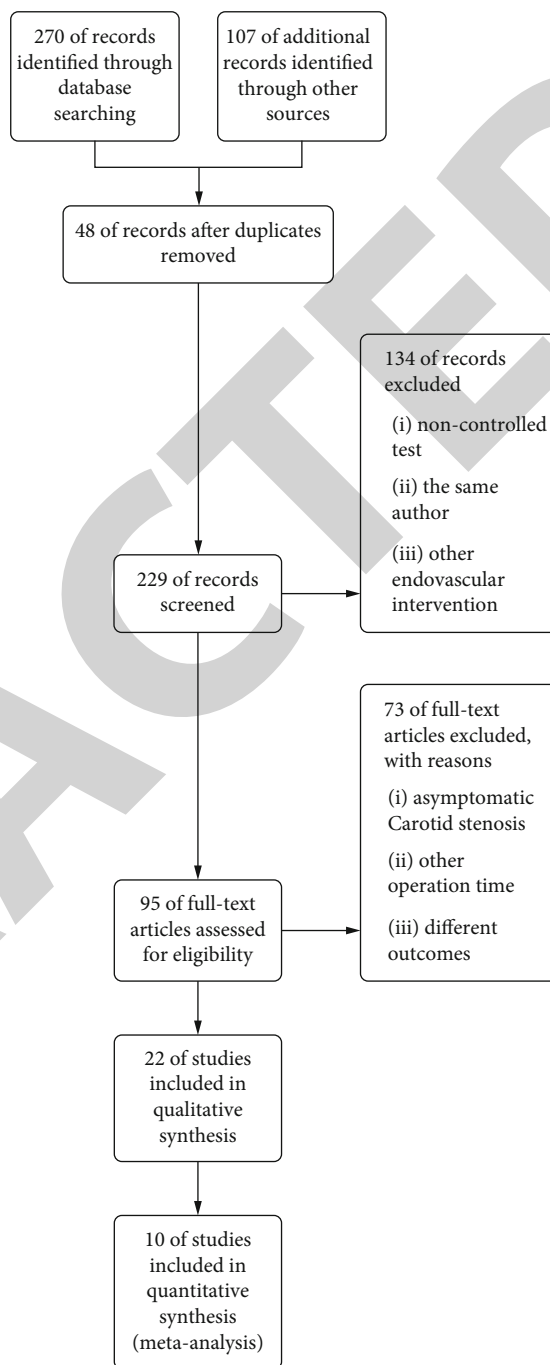


FIGURE 1: Flowchart showing the selection of articles for review.

each binary variable, an odds ratio (OR) and 95% confidence intervals (95% CI) were used to compare early CEA and delay CEA.  $I^2$  value was used to estimate the degree of heterogeneity,  $I^2$  values ranging from 0% to 100% (0-24%, low heterogeneity; 25-49%, moderate heterogeneity; 50%-74%, high heterogeneity; 75-100%, extreme heterogeneity). When there is low heterogeneity value ( $I^2 \leq 25\%$ ), Mantel-Haenszel fixed effect model was used for data synthesis. When there is high heterogeneity value ( $I^2 > 25\%$ ), the Mantel-Haenszel random effect model was selected as the endpoint, and sensitivity analysis was conducted to find the source of heterogeneity.



TABLE 1: Baseline characteristics of the included studies.

Trial	Year		Study size	Design	Operation timing	Outcome
	Publication	Recruitment				
Annambhotla et al. [4]	2012	1999-2010	312	Retrospective cohort study	0-7 d; 8-14 d; 15-21 d; 22-30 d; >30 d	Mortality/MI/stroke
Kjorstad et al. [5]	2017	2014-2015	371	Prospective	0-2 d; 3-7 d; 8-14 d; >14	Mortality/stroke
Rantner et al. [6]	2015	2004-2013	761	Retrospectively cohort study	0-2 d; 3-7 d; 8-14 d	MI/stroke
Stromberg et al. [7]	2011	2008-2011	2596	Prospectively	0-2 d; 3-7 d; 8-14 d; >14	Mortality/stroke
Salem et al. [8]	2012	2008-2010	109	Prospective	1-7 d; 8-14 d	Mortality/MI
Tsantilas et al. [9]	2017	2004-2014	401	Prospectively	0-2 d; 3-7 d; 8-14 d; >14	Mortality/stroke/MI
Ferrero et al. [10]	2010	2004-2007	285	Retrospective cohort study	<48 h; 48 h-2 weeks; 2-4 weeks; 4-8 weeks; 8-24 weeks.	Mortality/stroke/TIA
Villwock et al. [11]	2014	2002-2011	23729	Retrospective cohort study	Within 2weeks	Mortality/stroke
Nordanstig et al. [12]	2017	2010-2015	418	Prospectively	48 h; 48 h-2 w	Stroke/TIA
Sharpe et al. [13]	2013	2008-2013	475	Retrospective cohort study	2 d; 3-7 d; 8-14 d; >14 d	Stroke/TIA

*P* values were calculated for all subgroups. When  $P < 0.05$ , there was a statistical difference; otherwise, there was no statistical difference.

### 3. Results

**3.1. Search Results.** We used keywords to detect 377 related articles in each database and excluded 48 duplicates removed. A total of 95 articles were selected to check the full text by reading basic information and abstracts. The remaining 22 articles after excluding 73 articles according to asymptomatic patients, operation timing, and no reporting data were required. Finally, 10 articles were included for analysis (Figure 1).

**3.2. Quality Assessment.** The quality of the included studies was adequate, all of them have been published for nearly 10 years, and a total of 29,457 patients were included (Table 1). Quality evaluation was conducted according to the Newcastle-Ottawa quality assessment scale (Figure 2).

**3.3. Outcomes.** Stroke analysis of seven studies revealed that patients with delayed CEA (>48 h) had a higher incidence of postoperative stroke than those with early CEA ( $\leq 48$  h) (OR = 2.14, 95% CI: 1.43-3.21,  $P = 0.0002$ ); Analysis of seven studies revealed that there was no statistically significant difference in the incidence of postoperative stroke between delayed CEA (>1 w) and early CEA ( $\leq 1$  w) (OR = 1.37, 95% CI: 0.97-1.92,  $P = 0.07$ ); Analysis of eight studies revealed that there was no statistically significant difference in the incidence of postoperative stroke between delayed CEA (>2 w) and early CEA ( $\leq 2$  w) (OR = 1.07, 95% CI: 0.77-1.49,  $P = 0.69$ ).

Analysis of this group revealed the incidence of postoperative stroke in patients with delayed CEA was significantly

higher than that of patients with early CEA (OR = 1.37, 95% CI: 1.11-1.69,  $P = 0.003$ ) (Figure 3).

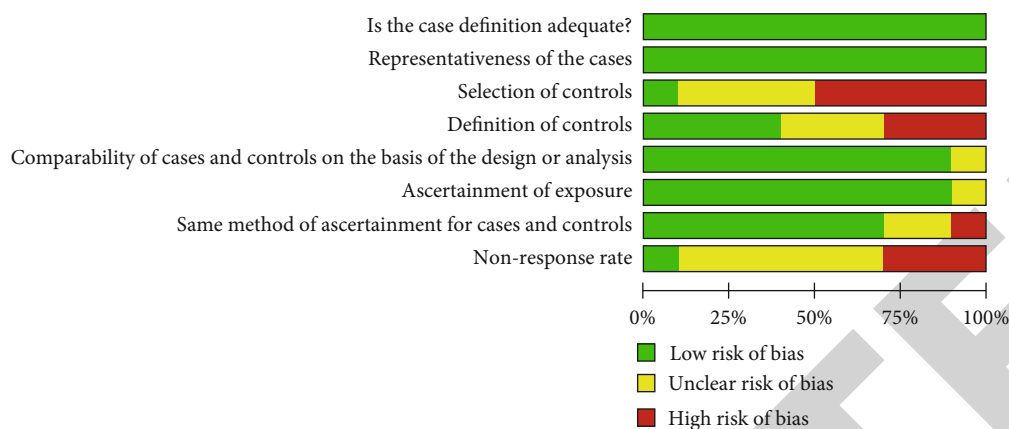
Mortality analysis of six studies revealed that patients with delayed CEA (>48 h) had a higher incidence of postoperative mortality than those with early CEA ( $\leq 48$  h) (OR = 1.35, 95% CI: 1.06-1.71,  $P = 0.02$ ). Analysis of five studies revealed that patients with delayed CEA (>1 w) had a higher incidence of postoperative mortality than those with early CEA ( $\leq 1$  w) (OR = 1.69, 95% CI: 1.24-2.32,  $P = 0.001$ ). Analysis of seven studies revealed that there was no statistically significant difference in the incidence of postoperative stroke between delayed CEA (>2 w) and early CEA ( $\leq 2$  w) (OR = 0.89, 95% CI: 0.51-1.55,  $P = 0.67$ ).

Analysis of this group revealed that the incidence of postoperative mortality in patients with delayed CEA was significantly higher than that of patients with early CEA (OR = 1.41, 95% CI: 1.17-1.68,  $P = 0.0002$ ) (Figure 4).

Myocardial infarction analysis of seven studies revealed that there was no statistically significant difference in the incidence of postoperative MI between delayed CEA and early CEA, whether it has 1 w (OR = 2.5, 95% CI: 0.38-16.50,  $P = 0.34$ ) or 2 w (OR = 1.33, 95% CI: 0.2-8.69,  $P = 0.76$ ) (Figure 5).

Analysis of this group revealed that there was no statistically significant difference in the incidence of postoperative MI between delayed CEA and early CEA (OR = 1.81, 95% CI: 0.48-6.8,  $P = 0.38$ ).

**3.4. Publication Bias.** It can be seen that the overall bias is acceptable by drawing the funnel plot (Figure 6). If the heterogeneity of the results is too high ( $I^2 > 25\%$ ), sensitivity analysis will be used to find the source of heterogeneity and remove it after it is identified.



	Is the case definition adequate?	Representativeness of the cases	Selection of controls	Definition of controls	Comparability of cases and controls on the basis of the design or analysis	Ascertainment of exposure	Same method of ascertainment for cases and controls	Non-response rate
Annambhotla 2012	+	+	-	+	+	+	+	-
Ferrero 2010	+	+	-	-	+	+	+	?
Kjorstad 2017	+	+	-	-	?	+	+	?
Nordanstig 2017	+	+	-	+	+	?	+	-
Rantner 2015	+	+	?	+	+	+	+	?
Salem 2011	+	+	?	?	+	+	?	+
Sharpe 2013	+	+	?	?	+	+	+	?
Stromberg 2012	+	+	+	+	+	+	?	-
Tsantilas 2017	+	+	?	-	+	+	+	?
Villwock 2014	+	+	-	?	+	+	-	?

FIGURE 2: Assessment of risk of bias and methodological quality.

#### 4. Discussion

CEA is an effective method to treat patients with symptomatic carotid artery stenosis. The choice of surgical timing is closely related to the patient’s postoperative recovery. The

views on the timing of CEA to treat patients with sCAS have been changed with the development of CEA and perioperative management techniques. The traditional view of carotid revascularization was the intervention is delayed by at least six weeks after an acute stroke. The studies published in the

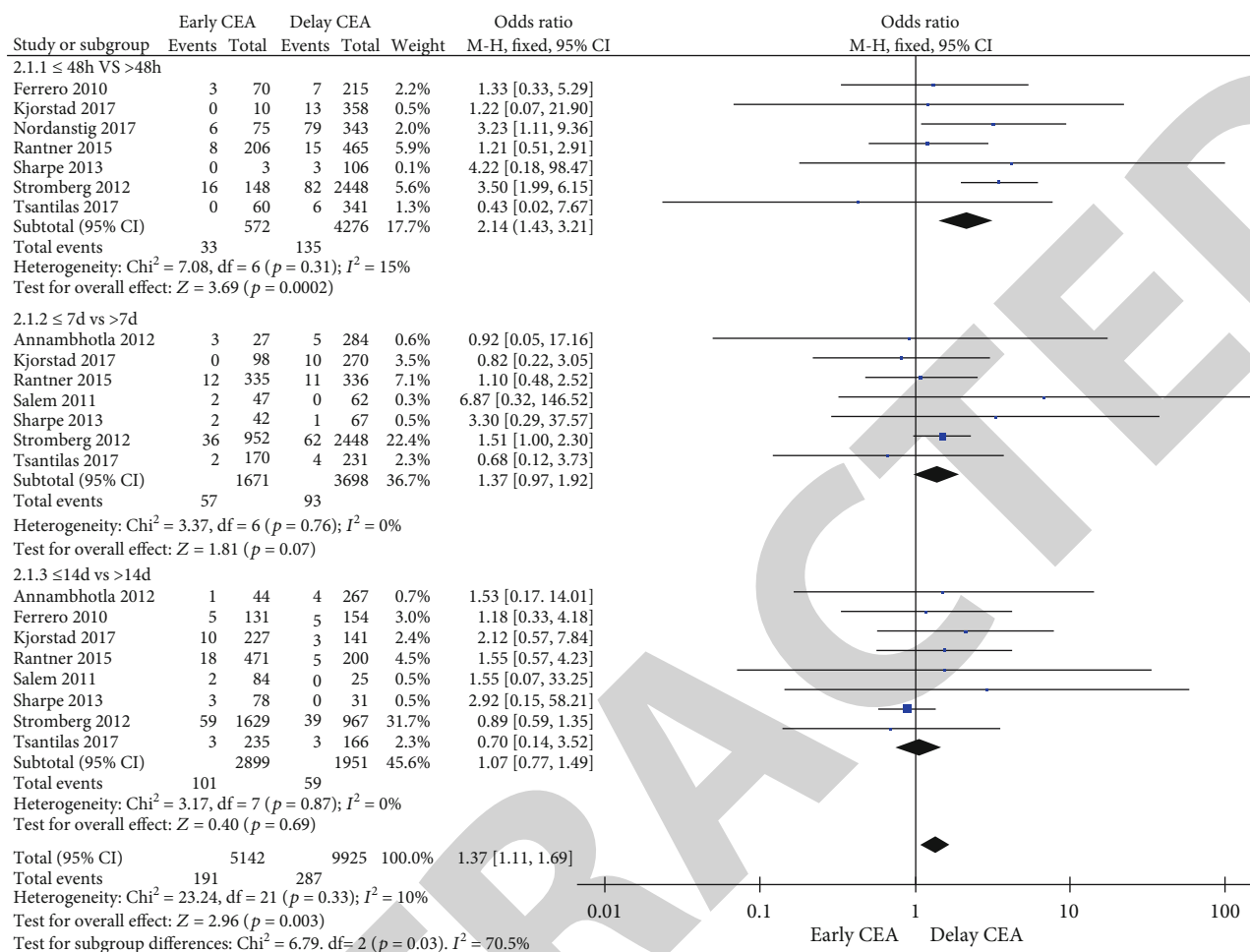


FIGURE 3: Differences in the incidence of post-CEA stroke between the early CEA groups and delayed CEA.

1960s and 1970s suggested that patients with ischemic stroke after early intervention have a higher risk of postoperative cerebral hemorrhage [14]. At that time, a retrospective study showed that the perioperative outcomes of patients with sCAS after early CEA were generally worse than delay CEA [15, 16].

However, a growing number of studies have found that early CEA may be associated with a slightly higher risk of perioperative complications in recent years, but it still is the best chance for symptomatic patients to avoid future strokes [17, 18]. The results of subgroup analysis of NASCET [19, 20] showed that the earlier CEA was performed after onset of neurological symptoms (TIA or minor stroke), the more significant of the prevention effect of secondary stroke in patients. A large number of evidences [17, 20, 21] revealed the safety of early CEA within 1-2 weeks after onset of a TIA or minor stroke. Dorigo et al. [21] indicate that CEA was performed within 15 days after onset of TIA or stroke, and risk of the perioperative stroke was <3.5%. The present study revealed that the incidence of postoperative stroke in patients with delay CEA was significantly higher than that of patients with early CEA (OR = 1.37, 95% CI: 1.11-1.69, P = 0.003); the incidence of postoperative mortality in patients with delay CEA was significantly higher than that of patients

with early CEA (OR = 1.41, 95% CI: 1.17-1.68.69, P = 0.0002 ). These outcomes may indicate that it is safe and effective of early CEA for a part of patients with sCAS. But it should be noted that the selection of early CEA or delay CEA for patients must be careful according to the current study. Ballotta et al. [22] categorize patients according to the Rankin assessment scale, Rankin 0/2 indicated minor or non disabling stroke, and Rankin 3/5 defined major or disabling stroke; the study showed early CEA after a non disabling ischemic stroke can be performed safely. Capoccia et al. [23] suggest that minimizing the time for intervention for patients National Institutes of Health Stroke Scale (NIHSS) ≥8 not only reduces the risk of recurrence but can also improve neurologic outcome. Therefore, the timing of the operation should be based on a comprehensive assessment of the patient.

The present study revealed that there was no statistically significant difference in the incidence of postoperative MI between delayed CEA and early CEA. Roussopoulou et al.'s [24] findings highlight that urgent CEA performed within two days from the index event is related to a nonsignificant increase in the risk of periprocedural MI, this is the same as the results of our study. Early CEA might not increase the risk of postoperative MI.

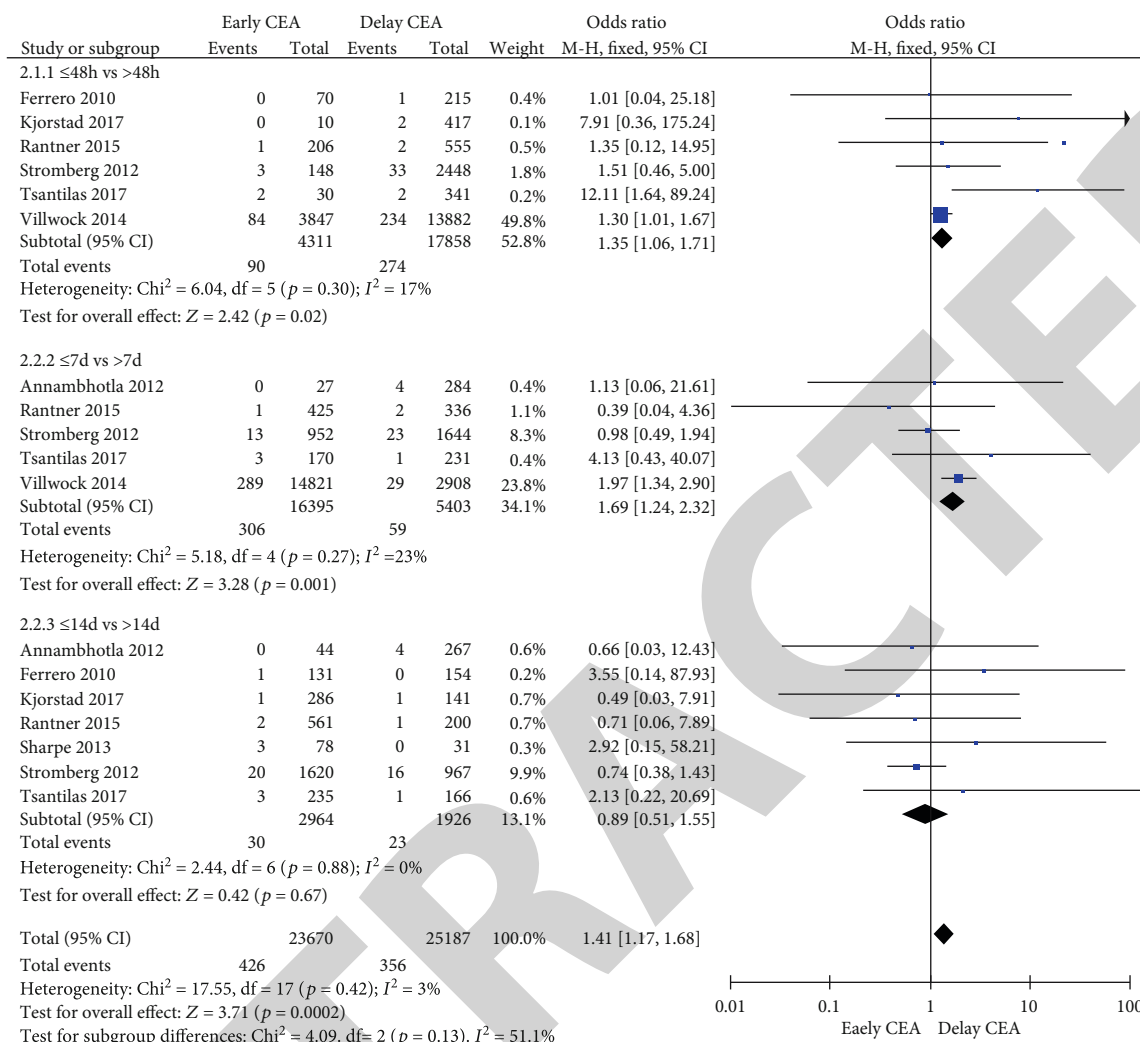


FIGURE 4: Differences in the incidence of post-CEA mortality between the early CEA groups and delayed CEA.

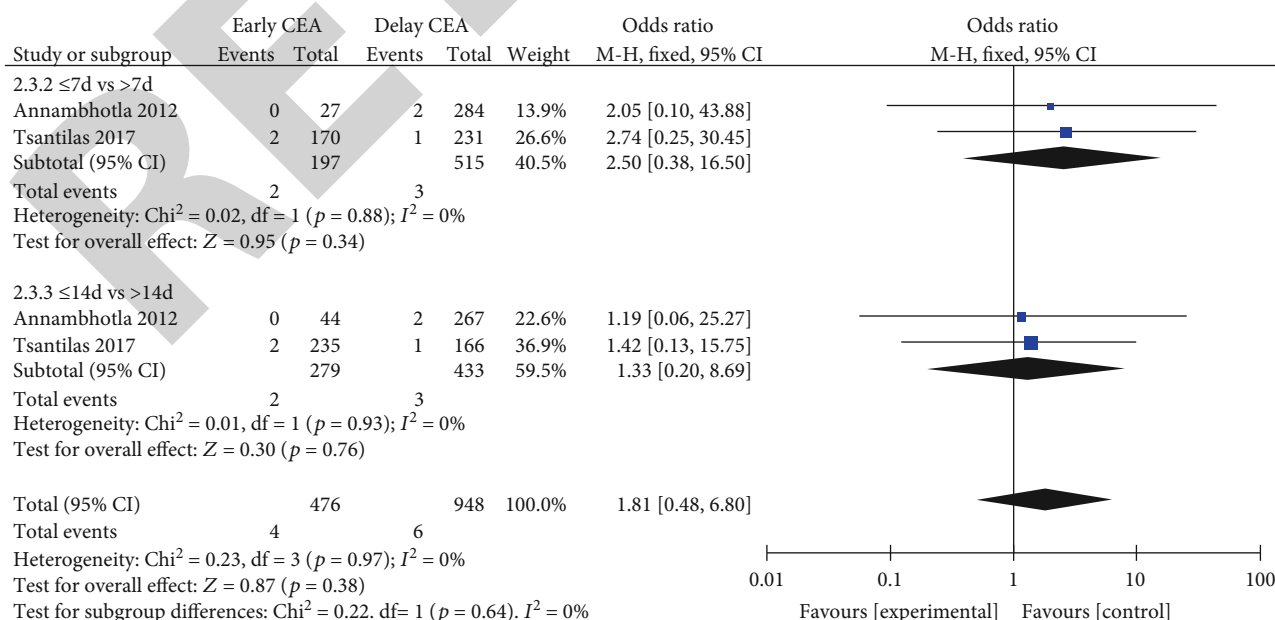


FIGURE 5: Differences in the incidence of post-CEA myocardial infarction between the early CEA groups and delayed CEA.

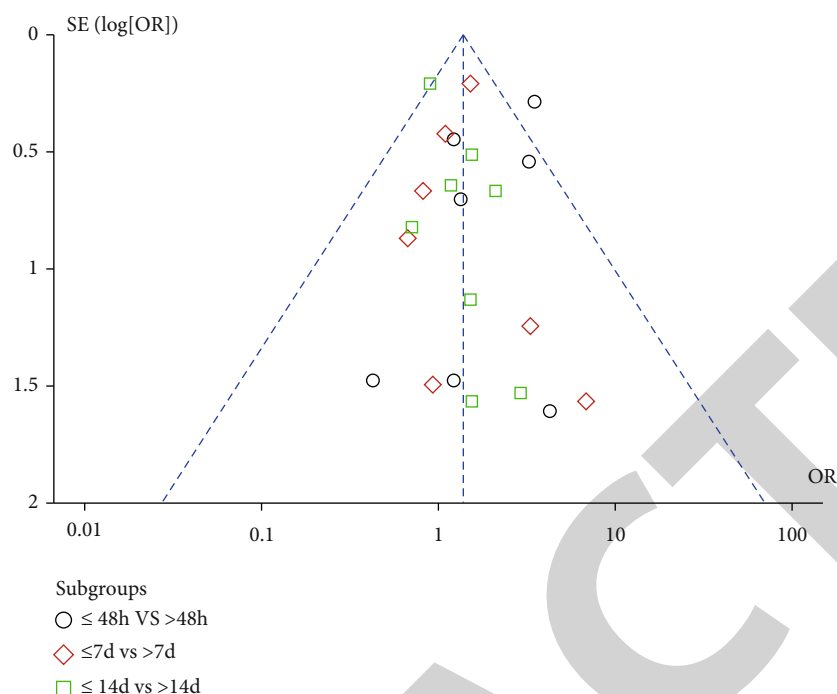


FIGURE 6; Funnel plot.

**4.1. Limitations.** CEA has been used for many years, and the perioperative management and operative style are generally uniform. Most of the articles are recorded, but some are not mentioned. It is not clear whether some patients are used technologies such as pCEA, etc. The follow-up time of the 10 articles that were included in the study was not the same; however, most of them could be followed up more than 30 days; the longest follow-up time could be up to 10 years. There is no clear data about the perioperative medication treatment of CEA. Symptomatic carotid artery is now not graded on admission. Patient with sCAS is not classified.

## 5. Conclusions

Early CEA is safe and effective for a part of patients with symptomatic carotid stenosis. Early CEA may be able to reduce postoperative complications of patients with sCAS, but a comprehensive preoperative evaluation of patients with sCAS must be performed. The safety of early CEA requires further evaluation in larger datasets.

## Data Availability

A systematic literature search was conducted in PubMed, MEDLINE, Embase, and Cochrane databases.

## Conflicts of Interest

The authors have no conflict of interest to declare.

## References

- [1] A. d. A. C. e. Silva, A. T. V. da Cruz Júnior, N. I. C. do Nascimento et al., "Positive balance recovery in ischemic post-stroke patients with delayed access to physical therapy," *BioMed Research International*, vol. 2020, Article ID 9153174, 8 pages, 2020.
- [2] K. I. Paraskevas and I. M. Loftus, "Safety of carotid revascularization within 48 hours of symptomatic presentation," *Journal of Cardiovascular Surgery*, vol. 58, no. 2, p. 139, 2016.
- [3] H. Liu, J. Chu, L. Zhang, C. Liu, Z. Yan, and S. Zhou, "Clinical comparison of outcomes of early versus delayed carotid artery stenting for symptomatic cerebral watershed infarction due to stenosis of the proximal internal carotid artery," *BioMed Research International*, vol. 2016, Article ID 6241546, 7 pages, 2016.
- [4] S. Annambhotla, M. S. Park, M. L. Keldahl et al., "Early versus delayed carotid endarterectomy in symptomatic patients," *Journal of Vascular Surgery*, vol. 56, no. 5, pp. 1296–1302, 2012.
- [5] K. E. Kjörstad, S. T. Baksaas, D. Bundgaard et al., "Editor's choice—The National Norwegian Carotid Study: time from symptom onset to surgery is too long, resulting in additional neurological events," *European Journal of Vascular & Endovascular Surgery*, vol. 54, pp. 415–422, 2017.
- [6] B. Rantner, C. Schmidauer, M. Knoflach, and G. Fraedrich, "Very urgent carotid endarterectomy does not increase the procedural risk," *European Journal of Vascular & Endovascular Surgery*, vol. 49, pp. 129–136, 2015.
- [7] S. Strömberg, J. Gelin, and T. Österberg, "Very urgent carotid endarterectomy confers increased procedural risk," *Stroke*, vol. 56, no. 3, pp. 877–877, 2012.
- [8] L. Jivegård, J. Gelin, S. Strömberg, and K. Österberg, "Comments regarding "rapid access carotid endarterectomy can be



## *Retraction*

# **Retracted: The Relationship between the Mean Platelet Volume and Carotid Atherosclerosis and Prognosis in Patients with Acute Cerebral Infarction**

### **BioMed Research International**

Received 12 March 2024; Accepted 12 March 2024; Published 20 March 2024

Copyright © 2024 BioMed Research International. This is an open access article distributed under the Creative Commons Attribution License, which permits unrestricted use, distribution, and reproduction in any medium, provided the original work is properly cited.

This article has been retracted by Hindawi following an investigation undertaken by the publisher [1]. This investigation has uncovered evidence of one or more of the following indicators of systematic manipulation of the publication process:

- (1) Discrepancies in scope
- (2) Discrepancies in the description of the research reported
- (3) Discrepancies between the availability of data and the research described
- (4) Inappropriate citations
- (5) Incoherent, meaningless and/or irrelevant content included in the article
- (6) Manipulated or compromised peer review

The presence of these indicators undermines our confidence in the integrity of the article's content and we cannot, therefore, vouch for its reliability. Please note that this notice is intended solely to alert readers that the content of this article is unreliable. We have not investigated whether authors were aware of or involved in the systematic manipulation of the publication process.

Wiley and Hindawi regrets that the usual quality checks did not identify these issues before publication and have since put additional measures in place to safeguard research integrity.

We wish to credit our own Research Integrity and Research Publishing teams and anonymous and named external researchers and research integrity experts for contributing to this investigation.

The corresponding author, as the representative of all authors, has been given the opportunity to register their agreement or disagreement to this retraction. We have kept a record of any response received.

### **References**

- [1] M. Xu, X.-y. He, and P. Huang, "The Relationship between the Mean Platelet Volume and Carotid Atherosclerosis and Prognosis in Patients with Acute Cerebral Infarction," *BioMed Research International*, vol. 2020, Article ID 6685740, 6 pages, 2020.

## Research Article

# The Relationship between the Mean Platelet Volume and Carotid Atherosclerosis and Prognosis in Patients with Acute Cerebral Infarction

Min Xu <sup>1</sup>, Xiao-ying He <sup>2</sup>, and Pan Huang <sup>3</sup>

<sup>1</sup>Department of Neurology, The Second People's Hospital of Deyang City, No. 340 Minjiang West Road, Deyang, Sichuan, China

<sup>2</sup>Department of Neurology, The Affiliated Hospital of Southwest Medical University, No. 25 Taiping Street, Luzhou, Sichuan, China

<sup>3</sup>Department of Neurology, People's Hospital of Deyang City, No. 173 TaiShan North Road, Deyang, Sichuan, China

Correspondence should be addressed to Pan Huang; 1032857970@qq.com

Received 25 November 2020; Revised 21 December 2020; Accepted 23 December 2020; Published 31 December 2020

Academic Editor: Yuzhen Xu

Copyright © 2020 Min Xu et al. This is an open access article distributed under the Creative Commons Attribution License, which permits unrestricted use, distribution, and reproduction in any medium, provided the original work is properly cited.

**Objective.** To investigate the relationship between mean platelet volume (MPV) level and carotid atherosclerosis and prognosis in patients with acute cerebral infarction. **Methods.** A retrospectively included 160 patients with acute cerebral infarction classified by TOAST classification as aortic atherosclerosis as the observation group. To analyze the relationship between MPV and carotid atherosclerosis, and use receiver operating characteristic (ROC) curves to analyze the role of MPV in predicting the prognosis of acute cerebral infarction in the observation group, grouping patients with different MPV by cut-off value, and analyze the differences in factors between the two groups of patients. **Results.** MPV has a positive correlation with carotid atherosclerosis in patients with acute cerebral infarction. Multivariate logistic regression analysis revealed that increased MPV was an independent predictor of poor functional outcome in patients with acute cerebral infarction (Odds Ratio (OR): 6.152, 95% CI: 2.385-13.625,  $P < 0.01$ ). ROC curve analysis showed that the area under the curve for MPV to predict poor prognosis was 0.868 (95% CI: 0.787-949,  $P < 0.01$ ). The cutoff value, sensitivity, and specificity were 12.65, 76.2%, and 87.6%. Compared with patients with  $MPV < 12.65$  at admission, patients with higher MPV levels ( $MPV \geq 12.65$ ) at admission have larger infarct size, more severe carotid artery stenosis, poor short-term prognosis, and higher mortality. **Conclusion.** MPV level is closely related to the degree of carotid atherosclerosis in patients with acute cerebral infarction, and it is also an independent predictor of poor prognosis in patients with acute cerebral infarction at 3 months.

## 1. Introduction

Acute cerebral infarction has a high risk of disability, death, and recurrence, which brings a serious burden to society and families [1]. Studies have shown that the important cause of acute cerebral infarction is carotid atherosclerosis. There are various screening methods for carotid atherosclerosis [2]. High-resolution CT angiography and digital subtraction angiography have high accuracy and specificity, but their price is more expensive; they are invasive examinations and have not yet been widely carried out. Doppler color ultra-

sound examination is convenient, fast, affordable, and suitable screening for large-scale carotid atherosclerosis. Platelets are the pathological basis of carotid atherosclerosis; mean platelet volume (MPV) is an important marker reflecting platelet activation and function [3, 4]. MPV is closely related to a variety of cardiovascular diseases or risk factors. It has been found that MPV may be related to the severity and prognosis of coronary artery disease [5, 6, 7]. At present, there are no obvious reports on the relationship between MPV and carotid atherosclerosis in patients with acute cerebral infarction and the prognostic value of patients.

Therefore, this study aimed to explore the relationship between peripheral blood MPV and carotid atherosclerosis in patients with acute cerebral infarction and its predictive value.

## 2. Objects and Methods

**2.1. Research Object.** 160 patients with acute cerebral infarction hospitalized from January 2013 to December 2019 in the Department of Neurology of our hospital were selected as the observation group, of which 80 were male. There were 80 females: age (44-89) years, average  $67.27 \pm 9.48$  years old, 104 patients with a history of hypertension, and 21 patients with a history of diabetes.

The following are the inclusion criteria: (1) all patients were confirmed to be patients with cerebral infarction by cranial CT/MRI [8], (2) were admitted to the hospital within 1 week of onset, and (3) were all first attacks. The following are the exclusion criteria: (1) patients with severe liver failure or acute or chronic renal insufficiency; (2) patients with abnormal thyroid function, (3) patients diagnosed with malignant tumors; (4) patients with a history of myocardial infarction or severe heart disease patients with disease; (5) are taking lipid-lowering drugs and vitamin preparations; (6) other chronic wasting diseases, recent history of infection, and history of surgical trauma; (7) patients who lost follow-up; and (8) patients with missing test results. The research protocol was reviewed and approved by the ethics committee of our hospital, and informed consent was obtained from patients and their families.

**2.2. Data Collection.** The collected general and clinical data of all patients include age, gender, history of hypertension, history of diabetes, follow-up methods, and follow-up results. Hypertension is defined as having been previously diagnosed with hypertension or taking antihypertensive drugs regularly or having systolic blood pressure  $\geq 140$  mmHg and/or diastolic blood pressure  $\geq 90$  mmHg measured at least twice on different days of admission. Diabetes is defined as having previously diagnosed diabetes or taking hypoglycemic drugs regularly, or random blood glucose  $> 11.1$  mmol/L, or rapid fasting blood glucose test  $> 7.0$  mmol/L at the time of admission.

**2.3. Carotid Artery Examination and Classification.** All subjects underwent a Doppler ultrasound examination within 3 days of admission. Sonographers in our hospital used the HDI-5000 color Doppler ultrasound system (probe frequency 7-10 MHz) produced by an American ATL company to perform the examination. Observe both sides of the carotid artery (common carotid artery, bifurcation and internal carotid artery), vascular shape, intima-media thickness, the presence or absence of atherosclerotic plaque in the blood vessel (if there is atherosclerotic plaque, observe and record its location and size and morphology), and whether there are stenosis and the degree of stenosis (for multisegment stenosis, take the most severe part of the stenosis). The average value of the bilateral carotid arteries reflects the degree of thickening of the carotid media. The definition of carotid

TABLE 1: MPV levels in patients with different degrees of carotid artery stenosis.

Group	N	MPV levels
IMT normal group	29	$10.31 \pm 1.06$
Mild stenosis group	89	$11.22 \pm 1.26$
Moderate to severe stenosis group	42	$12.90 \pm 1.20$
F	44.45	
P		$< 0.05$

IMT is the distance between the lumen intima interface and the media adventitia interface.

**2.4. MPV Determination.** For all the included subjects, 3 ml of fasting venous blood was collected before using antiplatelet drugs, placed in a precooled EDTA anticoagulant tube, and submitted for examination within 2 hours. The laboratory physician of our hospital will perform the test. The experiment is fully automated. The blood cell analyzer strictly follows the operating procedures of the instructions to detect the peripheral blood MPV level of patients with acute cerebral infarction.

**2.5. Determination of Cerebral Infarct Area.** Calculate the maximum slice diameter of the infarct on the head CT or MRI:  $< 1.5$  cm is a small-area cerebral infarction (lacunar infarction), 1.5-5.0 cm is a medium-area cerebral infarction, and  $> 5.0$  cm is a large-area cerebral infarction.

**2.6. Follow-Up and Grouping.** After 3 months of onset, follow-up by telephone or outpatient service, evaluate the functional prognosis of the patients according to the mRS score and group them according to the prognosis of the patients. mRS score  $\leq 2$  is the good prognosis group, and mRS score  $> 2$  is the poor prognosis group. Analysis of the impact on patient prognostic factors.

**2.7. Evaluation Standard.** Carotid artery IMT  $< 1.0$  mm is normal; IMT  $\geq 1.0$  mm or plaque formation is regarded as abnormal; the degree of carotid artery stenosis is divided into [9]: (1) mild stenosis: the stenosis rate is 1%-49%, and the grayscale image shows local plaque is formed, the tube diameter is relatively reduced, and the blood flow has no obvious change; (2) moderate stenosis: the stenosis rate is 50%-69%, the blood flow velocity in the stenosis section increases, and the pathological vortex is formed in the distal section of the stenosis; (3) severe stenosis: the stenosis rate is 70%-99%, the blood flow velocity in the stenosis segment is further increased, the velocity in the proximal segment of the stenosis is relatively reduced, and the blood flow signal of vortex and turbulence appears in the distal segment; and (4) vascular occlusion: the blood flow signal disappeared without blood flow.

**2.8. Statistical Methods.** Statistical analysis was performed using the SPSS 17.0 Chinese version statistical software. The measurement data are expressed as mean  $\pm$  standard deviation, independent sample *t*-test is used for comparison

TABLE 2: MPV of patients with different infarct areas was compared.

Group	N	MPV
Small area group	78	10.57 ± 0.93
Medium area group	42	11.14 ± 1.16
Large area group	41	12.79 ± 1.37
F	53.63	
P	<0.05	

between two groups, single-factor analysis of variance is used for multiple group comparison, and Pearson correlation analysis is used for correlation analysis. By constructing a receiver operating characteristic (ROC) curve and calculating the area under the curve (AUC) to evaluate the predictive ability of MPV for poor prognosis, at the same time, according to the cutoff value of MPV, all patients are divided; the difference in factors between patients with different MPV level groups was analyzed by univariate analysis for groups less than the cutoff level and greater than or equal to the cutoff level. The difference was statistically significant with  $P < 0.05$ .

### 3. Results

**3.1. Comparison of MPV Levels in Patients with Acute Cerebral Infarction with Different Degrees of Carotid Artery Stenosis.** The MPV levels of patients with acute cerebral infarction with different degrees of carotid artery stenosis were compared as shown in Table 1, in which the MPV levels of the mild and moderate to severe stenosis groups were compared with those of the IMT normal group, and the MPV levels of the moderate and severe stenosis group were compared with those of the mild and moderate stenosis group; the differences were statistically significant ( $P < 0.05$ ).

**3.2. Comparison of MPV Levels of Acute Cerebral Infarction in Different Areas.** The comparison of MPV levels of different carotid artery stenosis in patients with acute cerebral infarction is shown in Table 2. There were statistically significant differences in peripheral MPV among patients with different infarction areas ( $P < 0.05$ ).

**3.3. Correlation between Peripheral Blood MPV Level and the Degree and Areas of Carotid Artery Stenosis in Patients with Acute Cerebral Infarction.** Pearson correlation analysis showed that MPV was positively correlated with the degree of carotid artery stenosis ( $r = 0.531$ ,  $P < 0.05$ ), and MPV was positively correlated with cerebral infarct areas ( $r = 0.786$ ,  $P < 0.05$ ).

**3.4. Follow-Up Results.** At the 3-month follow-up, 137 patients (85.6%) had a good prognosis and were included in the good prognosis group; 23 patients (14.4%) had a poor prognosis and were included in the poor prognosis group.

**3.5. Univariate Analysis Results of General and Clinical Data of Patients in the Good Prognosis Group and Poor Prognosis Group.** The results of the univariate analysis showed that

the two groups of patients had statistically significant differences in age, admission infarct size classification, carotid artery stenosis, infarct location, red blood cell count at admission, hemoglobin, and red blood cell distribution width MPV (all  $P < 0.05$ ) Table 3.

**3.6. Multivariate Logistic Regression Analysis Results of Factors Affecting Poor Prognosis.** The results show that infarct size and MPV are independent factors affecting the prognosis of patients with acute cerebral infarction, and increased infarct size and MPV are risk factors for poor prognosis in patients with acute cerebral infarction Table 4.

**3.7. ROC Curve Analysis of MPV's Ability to Predict Poor Prognosis of Acute Cerebral Infarction.** The results showed that the AUC of MPV for predicting the poor prognosis of acute cerebral infarction was 0.868 (95% CI: 0.787-0.949,  $P < 0.01$ ), indicating that MPV has a better predictive ability for the prognosis of acute cerebral infarction. Calculate the cutoff value and select 12.65 as the critical value. When  $MPV \geq 12.65$ , the sensitivity of MPV to predict poor prognosis is 76.2%, and the specificity is 87.6% Figure 1.

**3.8. Comparison of Clinical Data of Patients in Different MPV Groups.** The results showed that patients with higher MPV ( $MPV \geq 12.65$ ) at admission had larger infarct size and more severe carotid artery stenosis (all  $P < 0.05$ , Table 5). There were statistically significant differences in the 3-month mRS scores and mortality between the two groups (all  $P < 0.05$ , Figure 2).

### 4. Discussion

Cerebral infarction is a group of syndromes that is caused by the sudden decrease or cessation of blood flow in the local blood supply arteries of the brain tissue, causing ischemia and hypoxia of the brain tissue in the blood supply area of the responsible blood vessel, leading to necrosis and softening of the brain tissue, and accompanied by corresponding neurological deficits. The carotid artery is the main blood supply artery of the brain. Once atherosclerosis causes stenosis, it can lead to cerebral infarction.

Platelets have been known as the pathological basis of atherosclerosis for a long time. It runs through atherosclerosis. It can be said that it is the promoter and inducer of atherosclerosis [10, 11, 12]. MPV stands for the average platelet size; a number of cardiovascular disease trials have confirmed that the MPV of the experimental group is significantly higher than that of the normal control. For example, MPV is positively correlated with the degree of coronary artery disease [13]. It also has predictive value for the prognosis of percutaneous coronary intervention [14], suggesting that MPV may become an important predictor of the occurrence and prognosis of cardiovascular and cerebrovascular diseases. The mechanism may be that the larger the MPV, the platelets bind to platelet activators such as adrenaline and ADP faster, produce more coagulants and vasoactive factors, and can also express more adhesion molecules, so that hemostasis time is shorter and more easily lead to embolic events [15]. Therefore, it can be said that MPV is a marker



TABLE 3: Univariate analysis results of the general and clinical data of patients in the good prognosis group and poor prognosis group.

	Good prognosis group (137)	Poor prognosis group (23)	P
Age (years)	65.32 ± 8.75	78.88 ± 9.32	<0.01
Male (n, %)	74 (54.1%)	15 (65.2%)	>0.05
High blood pressure (n,%)	94 (68.6%)	10 (43.4%)	>0.05
Diabetes (n, %)	18 (13.1%)	3 (12.3%)	>0.05
Infarct size (n, %)			<0.01
Small area	112 (81.7%)	7 (30.4%)	
Medium and large area	25 (18.3%)	16 (69.6%)	
Carotid artery stenosis degree (n,%)			<0.01
Normal ITM and mild stenosis	95 (69.3%)	4 (17.4%)	
Moderate and severe stenosis	42 (30.7%)	19 (82.6%)	
Infarct site (n, %)			<0.01
Front loop	108 (78.8%)	5 (23.8%)	
Post loop	29 (21.2%)	16 (76.2%)	
Red blood cell count (×10 <sup>9</sup> /l)	4.20 ± 0.52	3.78 ± 0.48	<0.01
Hemoglobin (g/l)	125.78 ± 34.28	116.41 ± 30.54	<0.01
MPV	11.03 ± 1.35	13.13 ± 1.34	<0.01

TABLE 4: Multivariate logistic regression analysis of factors influencing poor prognosis.

	OR (95% CI)	P
Age	1.042 (0.985-1.085)	0.126
Infarct size	14.849 (4.857-43.258)	<0.01
Red blood cell count	0.812 (0.142-4.1258)	0.589
Hemoglobin	0.998 (0.938-1.057)	0.899
MPV	6.152 (2.385-13.625)	<0.01
Infarct site	1.411 (0.415-4.802)	0.571

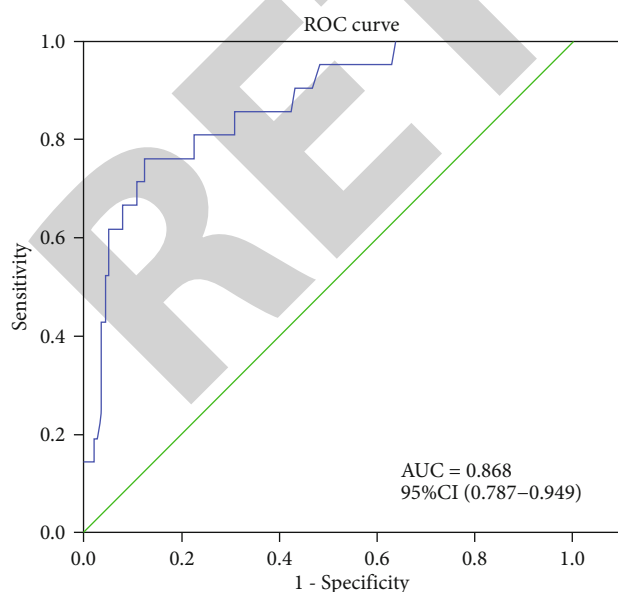


FIGURE 1: ROC curve.

of platelet activation and function. At present, there are not many domestic researchers engaged in this topic, and the authors conduct clinical trial observations based on this. This study shows that the MPV level in peripheral blood of patients with acute cerebral infarction is positively correlated with the degree of carotid atherosclerosis, indicating that high MPV is closely related to the occurrence and development of carotid atherosclerosis in patients with acute cerebral infarction. The possible reasons are as follows: (1) Platelets with larger MPV contain more thromboxane A<sub>2</sub>, express more glycoprotein receptors such as IIIa and IIb receptors, and have stronger chemotaxis, adhesion, and aggregation functions. In addition, the larger platelet volume can release more active factors, such as platelet factor-4 and P-selectin, which can aggravate vascular endothelial cell damage and inflammation, thereby promoting the progression of atherosclerosis and thrombosis [16]. (2) Patients with large MPV often have diseases such as hypertension, diabetes, and dyslipidemia. The synergistic effect of these factors causes vascular endothelial cell damage, causing increased secretion of interleukins and other cytokines, which in turn stimulates bone marrow hematopoietic cells to produce more platelets that become larger. The latter further promotes thrombosis and ischemic events [17]. Moreover, the ischemic tissue can also produce the above cytokines, which further promotes the bone marrow to produce more large-volume platelets [18]. (3) The larger the MPV, the platelets often exist in the form of nets, which can reduce the therapeutic effect of anti-platelet drugs and further increase the risk of thrombosis [19].

In addition, this study also showed that patients with acute cerebral infarction (MPV > 12.65) with a higher MPV level at admission had a poor short-term prognosis. Multivariate logistic regression analysis showed that patients with acute cerebral infarction at a high MPV level had a poor 3-month functional prognosis independent risk factors; the



TABLE 5: Comparison of general and clinical data of patients with acute cerebral infarction in different MPV groups.

	MPV < 12.65 (125)	MPV ≥ 12.65 (35)	P
Age (years)	66.98 ± 8.86	68.30 ± 9.35	>0.05
Male (n, %)	62 (49.6%)	17 (48.6%)	>0.05
High blood pressure (n, %)	87 (69.6%)	17 (48.6%)	>0.05
Diabetes (n, %)	16 (12.8%)	5 (14.3%)	>0.05
Infarct size (n, %)			<0.01
Small area	113 (90.4%)	6 (17.2%)	
Medium and large area	12 (9.6%)	29 (82.8%)	
Carotid artery stenosis degree (n, %)			<0.01
Normal ITM and mild stenosis	111 (88.8%)	7 (20.0%)	
Moderate and severe stenosis	14 (11.2%)	28 (80.0%)	
Infarct site (n, %)			>0.05
Front loop	75 (60.0%)	20 (57.2%)	
Post loop	50 (40.0%)	15 (42.8%)	
Red blood cell count (×10 <sup>9</sup> /l)	4.11 ± 0.48	4.24 ± 0.45	>0.05
Hemoglobin (g/l)	124.34 ± 32.64	124.76 ± 33.29	>0.05
mRS score			
≤2score	105 (84.0%)	7 (20.0%)	
>2score	17 (13.6%)	22 (62.8%)	
Death	3 (2.4%)	6 (17.2%)	<0.01

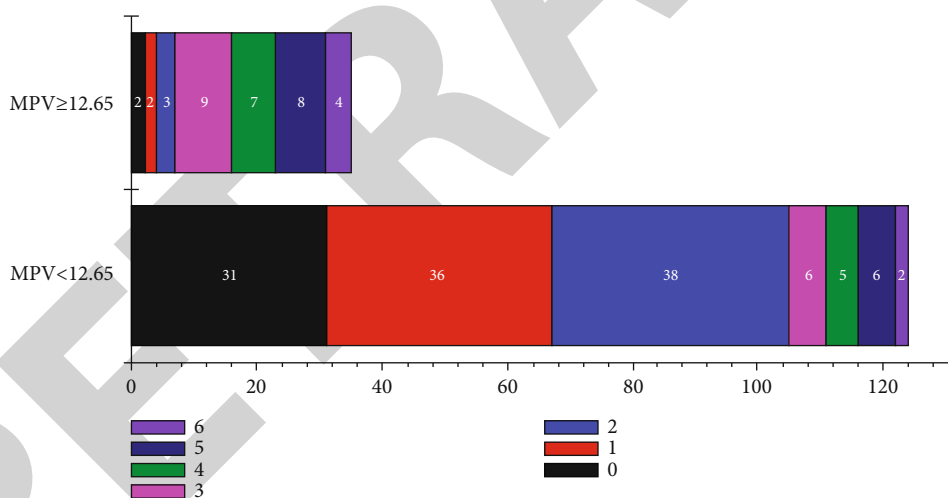


FIGURE 2: Comparison of the mRS score and fatality rate between the two groups of patients at 3 months.

ROC curve also shows that the area under the curve for MPV to predict the poor prognosis of patients with acute cerebral infarction is 0.868. The above results all indicate that the MPV level at admission can predict the short-term prognosis of patients with acute cerebral infarction. A number of previous studies have confirmed the significance of MPV in coronary atherosclerotic heart disease, sepsis, malignant tumors, chronic kidney disease, and other diseases, all showing the correlation between high MPV levels and adverse results. In this study, the possible mechanisms of high MPV leading to poor prognosis of acute cerebral infarction are as follows: (1) High MPV may lead to endothelial dysfunction and increased inflammation. An increase in MPV indicates that

the body is in a potentially proinflammatory state and further cascades. The amplified inflammatory response can lead to aggravated destruction of the blood-brain barrier, causing secondary brain damage [20, 21]. (2) The higher the risk of thrombosis in patients with high MPV levels, the greater the risk of thrombosis, which can cause repeated embolization of small blood vessels in the local brain tissue and aggravate nerves and functional impairment [22]. (3) High MPV levels are related to the balance of oxidative stress in the body, leading to the formation of high oxidative stress levels in the body, thereby weakening the deformability of red blood cells, increasing the adhesion of red blood cells and endothelial cells, and promoting thrombosis [23, 24]. The above specific

## *Retraction*

# **Retracted: Effects of Carotid Artery Stent and Carotid Endarterectomy on Cognitive Function in Patients with Carotid Stenosis**

### **BioMed Research International**

Received 12 March 2024; Accepted 12 March 2024; Published 20 March 2024

Copyright © 2024 BioMed Research International. This is an open access article distributed under the Creative Commons Attribution License, which permits unrestricted use, distribution, and reproduction in any medium, provided the original work is properly cited.

This article has been retracted by Hindawi following an investigation undertaken by the publisher [1]. This investigation has uncovered evidence of one or more of the following indicators of systematic manipulation of the publication process:

- (1) Discrepancies in scope
- (2) Discrepancies in the description of the research reported
- (3) Discrepancies between the availability of data and the research described
- (4) Inappropriate citations
- (5) Incoherent, meaningless and/or irrelevant content included in the article
- (6) Manipulated or compromised peer review

The presence of these indicators undermines our confidence in the integrity of the article's content and we cannot, therefore, vouch for its reliability. Please note that this notice is intended solely to alert readers that the content of this article is unreliable. We have not investigated whether authors were aware of or involved in the systematic manipulation of the publication process.

Wiley and Hindawi regrets that the usual quality checks did not identify these issues before publication and have since put additional measures in place to safeguard research integrity.

We wish to credit our own Research Integrity and Research Publishing teams and anonymous and named external researchers and research integrity experts for contributing to this investigation.

The corresponding author, as the representative of all authors, has been given the opportunity to register their agreement or disagreement to this retraction. We have kept a record of any response received.

### **References**

- [1] P. Huang, X.-y. He, and M. Xu, "Effects of Carotid Artery Stent and Carotid Endarterectomy on Cognitive Function in Patients with Carotid Stenosis," *BioMed Research International*, vol. 2020, Article ID 6634537, 7 pages, 2020.

## Review Article

# Effects of Carotid Artery Stent and Carotid Endarterectomy on Cognitive Function in Patients with Carotid Stenosis

Pan Huang <sup>1</sup>, Xiao-ying He <sup>2</sup>, and Min Xu <sup>3</sup>

<sup>1</sup>Department of Neurology, People's Hospital of Deyang City, No. 173 TaiShan North Road, DeYang, Sichuan 618000, China

<sup>2</sup>Department of Neurology, The Affiliated Hospital of Southwest Medical University, No. 25, Taiping Street, Jiangyang District, Luzhou City, Sichuan 646000, China

<sup>3</sup>Department of Neurology, The Second People's Hospital of Deyang City, No. 340 Minjiang West Road, DeYang, Sichuan 618000, China

Correspondence should be addressed to Min Xu; 782067723@qq.com

Received 16 November 2020; Revised 9 December 2020; Accepted 11 December 2020; Published 18 December 2020

Academic Editor: Yuzhen Xu

Copyright © 2020 Pan Huang et al. This is an open access article distributed under the Creative Commons Attribution License, which permits unrestricted use, distribution, and reproduction in any medium, provided the original work is properly cited.

**Background.** Carotid artery stenosis is closely related to cognitive dysfunction, in which decreased cerebral perfusion is one of the important factors. Both carotid artery stent implantation and carotid endarterectomy can relieve stenosis and increase cerebral perfusion. In this study, we aimed to compare the effects of carotid artery stent implantation and endarterectomy on cognitive function. **Methods.** A total of 98 patients with carotid artery stenosis hospitalized in our hospital from July 2015 to January 2017 were included. Among them, 50 cases underwent carotid artery stent implantation treatment as stent implantation group (CAS group), and 48 cases underwent carotid artery endarterectomy treatment as carotid endarterectomy group (CEA group). Using the Mini-Mental State Examination Scale (MMSE Scale) and the Montreal Cognitive Assessment Scale (MoCA Scale), the cognitive function scores of the two groups of patients before and after 3 and 6 months of operation were measured, and the patients were also measured before and after surgery, after the serum NSE, hs-CRP content. **Results.** The serum NSE, hs-CRP content, MMSE score, and MoCA score of the two groups before treatment were not statistically significant ( $P > 0.05$ ). The MMSE score and MoCA score of the two groups of patients before treatment were lower than the normal value, suggesting carotid artery stenosis combined with different degrees of cognitive dysfunction. Carotid artery stenosis is different, and patients' cognitive function is also different. The MMSE score and MoCA score of the two groups at 3 and 6 months after operation were higher than before treatment, and there was a statistically significant difference between 6 and 3 months after operation ( $P < 0.05$ ), but at each time There was no statistically significant difference between the two groups ( $P > 0.05$ ). The NSE content of the two groups of patients after operation decreased compared with that before treatment, and the decrease in 6 months after operation was more obvious than that in March ( $P < 0.05$ ). However, the difference between the two groups at each time point was not statistically significant ( $P > 0.05$ ). The content of hs-CRP in the two groups of patients was higher than that before the operation, and the CAS group was significantly higher than the CEA group; the difference was statistically significant ( $P < 0.05$ ). **Conclusion.** Carotid artery stent and carotid endarterectomy are effective in improving the cognitive function of patients with carotid stenosis, but there is no significant difference between the two.

## 1. Introduction

Carotid stenosis means that the inner diameter of the carotid artery becomes smaller or even occluded. Long-term stenosis can cause chronic cerebral ischemia and hypoxia, which can lead to changes in nerve function. It has been reported that severe carotid stenosis can cause cognitive dysfunction, and

its mechanisms include chronic hypoperfusion, leukoaraiosis of the brain, and the central nervous system function decline caused by chronic ischemia and hypoxia [1–3]. Since the decline in cerebral perfusion can cause cognitive dysfunction, however, CAS and CEA can relieve blood vessel stenosis and significantly improve cerebral blood flow perfusion [4–7]. So, can both improve cognitive dysfunction caused by stenosis?

Some researchers conducted a preoperative and postoperative cognitive function score on 48 patients with CAS and found that CAS can improve the cognitive function of patients [8]; other researchers followed up on 18 patients undergoing carotid endarterectomy and found that it could also improve patients' cognitive function [9]. In order to compare the differences in the efficacy of the two surgical methods for improving cognitive dysfunction, the authors designed this test, and the report is as follows.

## 2. Methods

**2.1. Study Population.** The patients who underwent carotid artery stenting or carotid endarterectomy due to carotid stenosis from July 2015 to 2017 were collected, and the subjects were screened according to the inclusion/exclusion criteria. Inclusion criteria are as follows: (1) carotid stenosis  $\geq 70\%$  confirmed by DSA, (2) transient cerebral ischemic attack or ischemic cerebral infarction occurred in the carotid artery blood supply area of the lesion side in the past six months, and (3) conform to carotid stenosis Indications for CAS or CEA. Exclusion criteria are as follows: (1) dementia caused by other reasons (such as Alzheimer's disease), (2) those with impaired consciousness or confusion in consciousness who cannot cooperate, (3) subarachnoid hemorrhage, cerebral hemorrhage, or intracranial history of tumor, (4) people with neuropsychiatric diseases, (5) history of drug poisoning such as CO poisoning, chronic alcohol moderate, (6) patients with normal intracranial pressure hydrocephalus, (7) specific and hereditary white matter disease patients, (8) history of MS and other white matter degeneration, (9) patients with visual and hearing impairments, (10) National Institutes of Health Stroke Scale (NIHSS) score  $\geq 21$  score after admission [10], and (11) severe infection and the estimated survival time is less than June.

Informed consent was obtained from all patients before the index procedure. Our local Ethics Committee approved the study protocol in accordance with the Declaration of Helsinki.

**2.2. Group.** 98 patients who met the test criteria were divided into the CAS group (50 cases) and the CEA group (48 cases) according to the type of surgery.

**2.3. Preoperative and Postoperative Routine Treatment.** Fasting for more than 6 h before surgery; stopping taking antihypertensive and lipid-lowering drugs 24 hours before surgery; 5 d before surgery, taking aspirin 100 mg/d, clopidogrel 75 mg/d, and oral stability sedative drugs. After the operation, follow the relevant surgical guidelines and the "Chinese Guidelines for Secondary Prevention of Ischemic Stroke and Transient Ischemic Attack 2010" for routine drug treatment [11].

**2.4. CAS Method.** The patients were locally anesthetized, and the stents were implanted under anesthesia. The femoral artery approach was used, and the surgical standards were in accordance with the guidelines of percutaneous carotid stent implantation by the Chinese Society of Cerebrovascular Diseases. The specific procedure is as follows: select the affected carotid artery under the guidance, and the catheter

stays in the relatively straight and smooth part of the blood vessel, 2-3 cm from the lower edge of the lesion. Preshape the protection device guide head according to the condition of the lesion, take the path map at the predetermined optimal projection angle of the lesion, gently send it through the lesion to the lower part of the rock bone, and release it. Perspectively confirm that the protective umbrella is well opened. Introduce the preselected balloon to the lower part of the lesion, observe the patient's blood pressure and heart rate, and instruct the nurse to prepare intravenous injection of atropine. Gently push the balloon to cover the whole process of the lesion and pressurize to "standard pressure." After fully inflated, release the pressure and release the ball. Capsule and angiography confirm the expansion effect. Introduce the stent and push it slowly into place; the stent must cover the entire lesion. Due to changes in the patient's posture or the traction of the blood vessel by the operating system, the relative position of the lesion may be changed. It is recommended to adjust the position of the stent to preselect the postural angiography that shows the entire course of the lesion and release the stent under the road state or under fluoroscopic monitoring. Then, review the contrast imaging evaluation and confirm that it is in a satisfactory state.

**2.5. CEA Method.** Take standard carotid endarterectomy (standardCEA, sCEA): the patient is placed in a supine position, with the head tilted to the opposite side, and a straight anterior incision of the sternocleidomastoid muscle is taken. If the lesion is located at a higher position, the upper edge of the incision should be turned back and up along the margin of the mandible to avoid damage to the marginal mandibular branch of the facial nerve; the skin, subcutaneous, and latissimus dorsi muscles were cut in sequence and separated longitudinally along the anterior margin of the sternocleidomastoid muscle. After the carotid sheath was exposed, the common carotid artery, internal carotid artery, and external carotid artery were freely exposed, and the superior thyroid artery, external carotid artery, internal carotid artery, and common carotid artery were blocked, respectively. Longitudinal incision of the walls of the common carotid artery and internal carotid artery, stripping the carotid artery intima and plaque, blocking the superior thyroid artery, external carotid artery, internal carotid artery, and common carotid artery, and traversing along the starting end of the internal carotid artery cut off the internal carotid artery, separate the plaque from the vessel wall along the circumference of the internal carotid artery, lift the internal carotid artery vessel wall, and peel off the carotid artery intima and plaque with a stripper. Then, like a sleeve, the internal carotid artery wall is separated upwards until the plaque and the normal intima transition section are sharply cut to remove the plaque. Finally, the end of the internal carotid artery is anastomosed to the original incision, and the incision is sutured.

**2.6. Laboratory Analysis.** Take the cubital venous blood of the selected patients on an empty stomach in the early morning, and determine the content of serum neuron-specific enolase (NSE) by enzyme-linked immunoassay (ELISA); determine the serum hypersensitivity by immunoturbidimetry C



reactive protein (hs-CRP) content. All operations are in accordance with the relevant instructions, of which hs-CRP  $>3 \text{ mg/l}$  is abnormal and NSE  $>16.3 \mu\text{g/l}$  is abnormal.

### 2.7. Variables of Interest

- (1) General data statistics of the two groups of patients
- (2) *Cognitive Function Assessment*. MMSE and MoCA scores were given to the two groups of patients before treatment, 3 months and 6 months after operation [12, 13]
- (3) Before and 3 months after treatment of the two groups of patients, June serum NSE, hs-CRP content

MMSE and MoCA scales were used to evaluate the cognitive function of the two groups. The MMSE scale includes 6 cognitive domains: orientation (time and place), timely memory, delayed memory, attention and computing power, language ability, and visual-spatial perception. The total scale of the scale is 0-30 score. 27-30 score are normal;  $<27$  is cognitive dysfunction; illiteracy  $<17$  score, elementary school  $<20$  score, secondary school, and above  $<24$  score are dementia [14].

The content of the MoCA scale test mainly includes cognitive space such as visual space/executive function, naming, attention, language, abstraction, delayed recall, and orientation. Among them, the visual space/executive function is 5 score, the name is 3 score, the attention is 6 score, the language is 3 score, the abstract is 2 score, the delayed recall is 5 score, the orientation is 6 score, and the total is 30 score, less than 12 years of total score plus 1 point, to correct the bias of education level. The lower the score, the worse the cognitive impairment. The higher the score, the better the cognitive function. 26 score or above is normal. The MMSE and MoCA scores are conducted by standardized doctors, and each MMSE and MoCA scale scores are completed within the specified time [15].

**2.8. Statistical Analysis.** Using the SPSS 17.0 statistical software, the normal distribution of measurement data is expressed by mean  $\pm$  standard ( $\bar{x} \pm s$ ), the comparison between the three groups is by single factor analysis of variance, and the comparison between two groups is by LSD method; the count data is expressed by frequency or rate, and the comparison between groups is by  $\chi^2$  test;  $P < 0.05$  indicates that the difference is statistically significant.

## 3. Results

The level of education is divided into 5 groups, namely none-educated (education time  $<1$  year), primary school (1-6 years), junior high school (7-9 years), high school (10-12 years), and college and higher education groups ( $>12$  years), respectively, called level 1, 2, 3, 4, and 5. The results show that the two groups of patients are not statistically significant in terms of baseline data ( $P > 0.05$ ) (Table 1).

The patients in the carotid stenosis group were divided into left, right, and bilateral carotid stenosis groups according

to the carotid stenosis, and the differences between MMSE and MoCA were compared. As shown in Table 2, the left carotid stenosis group, the MoCA and MoCA score items in the visual space, and executive ability scores were significantly lower than those in the right and bilateral carotid stenosis groups. The difference between the two groups was statistically significant ( $P < 0.05$ ). The naming score in the MoCA project of the right carotid stenosis group was significantly higher than that of the left and bilateral carotid stenosis groups, and the difference was statistically significant ( $P < 0.05$ ), the right carotid stenosis group and the bilateral carotid stenosis group. There was a statistically significant difference in the scores of MMSE, abstract power, and orientation power ( $P < 0.05$ ).

Table 3 shows that the MMSE scores and MoCA scores of the nodes before treatment and 3 months and 6 months after the treatment were not statistically significant ( $P > 0.05$ ). However, the comparison of MMSE score and MoCA score between the two groups of patients at 3 months after surgery and before treatment, at 6 months after surgery and at 3 months after surgery, was statistically significant ( $P < 0.05$ ).

Table 4 shows the comparison of NSE and hs-CRP content. There was no significant difference between the two groups before and after treatment at 3 and 6 months ( $P > 0.05$ ). However, the NSE content of the two groups of patients after operation decreased compared with that before treatment, and the difference in NSE content between 3 months and before treatment and between June and March was statistically significant ( $P < 0.05$ ). There was no significant difference between the two groups of patients before hs-CRP treatment ( $P > 0.05$ ). However, the content of hs-CRP after operation was higher than that before operation. There was a statistically significant difference between 3 months after operation and before treatment, 6 months after operation, and 3 months after operation, and the increase in the stent group was more obvious ( $P < 0.05$ ).

Table 5 shows the correlation analysis results of preoperative NSE and hs-CRP with MMSE and MoCA scores. The results show that preoperative NSE and hs-CRP are negatively correlated with MMSE and MoCA scores, and the difference is statistically significant ( $P < 0.05$ ).

## 4. Discussion

Cognition is the process by which the human brain receives external information and converts it into internal mental activity through processing to obtain knowledge or apply knowledge, including memory, language, visual space, execution, calculation, and understanding judgment. Cognitive dysfunction refers to the impairment of one or more of the abovementioned cognitive functions and affects the individual's daily or social abilities. Vascular cognitive dysfunction is a large category of syndromes from mild cognitive dysfunction to dementia caused by cerebrovascular disease risk factors or cerebrovascular disease [16, 17]. The Carotid artery is the main blood supply artery of the brain and has been confirmed to have carotid stenosis one of the risk factors for cerebrovascular disease [18], and carotid stenosis may be related to cognitive dysfunction [19]. As early as the early



TABLE 1: baseline data to compare two groups of patients before treatment.

Item	CAS group ( <i>n</i> = 50)	CEA group ( <i>n</i> = 48)	<i>t/x</i> <sup>2</sup>	<i>P</i>
Age (years)	52.48 ± 4.78	53.14 ± 4.82	0.68	0.49
M/F ( <i>n</i> )	26/24	23/25	0.16	0.68
Diabetes ( <i>n</i> )	15	12	0.02	0.87
Hypertension ( <i>n</i> )	22	19	0.31	0.57
Stroke ( <i>n</i> )	8	7	0.65	0.25
Smoke ( <i>n</i> )	28	30	0.81	0.36
Drinke ( <i>n</i> )	26	24	0.98	0.45
Education (level)	3.21 ± 0.51	3.34 ± 0.54	1.22	0.22
BMI (kg/m <sup>2</sup> )	1.24 ± 1.12	16.89 ± 1.04	1.60	0.11
Total cholesterol (mmol/l)	4.82 ± 0.64	5.01 ± 0.67	1.43	0.15
LDL-C (mmol/l)	2.89 ± 0.44	3.05 ± 0.49	1.70	0.09
HDL-C (mmol/L)	1.07 ± 0.20	1.02 ± 0.24	1.11	0.27
Hcy (μmol/l)	15.75 ± 3.23	16.15 ± 3.35	0.60	0.54
Glycated hemoglobin	6.08 ± 0.62	6.10 ± 0.78	0.14	0.89
Folic acid (mmol/L)	8.91 ± 1.98	9.33 ± 2.34	0.95	0.34
Vitamin B12 (pmol/L)	325.05 ± 98.76	331.77 ± 102.06	0.32	0.74

M/F: male/female; BMI: body mass index; HDL-C: high-density lipoprotein-cholesterol; LDL-C: low high-density lipoprotein-cholesterol.

TABLE 2: Comparison of cognitive function scores of patients with carotid stenosis in different sites.

(a)				
Item	<i>n</i>	MMSE	MoCA	Visual space and executive ability
Left	33	22.41 ± 1.16	21.73 ± 1.12	2.85 ± 0.85
Right	32	22.52 ± 1.13*	21.68 ± 1.18	3.65 ± 0.61 <sup>#</sup>
Bilateral	33	20.56 ± 1.08	20.12 ± 1.01	3.31 ± 0.87

(b)							
Item	<i>n</i>	Name	Attention	Language	Abstract ability	Delayed memory	Directional force
Left	33	2.56 ± 0.40	4.11 ± 0.72	2.23 ± 0.42	1.65 ± 0.40	3.28 ± 0.62	4.01 ± 0.68
Right	32	2.86 ± 0.51 <sup>#</sup>	4.41 ± 0.71	2.51 ± 0.43	1.41 ± 0.51 *	3.81 ± 0.71	4.78 ± 0.72*
Bilateral	33	2.61 ± 0.38	4.43 ± 0.73	2.55 ± 0.45	1.88 ± 0.58	4.27 ± 0.81	4.42 ± 0.69

MMSE: Mini-Mental State Examination, MoCA: Montreal Cognitive Assessment. Compared with the left carotid stenosis group, <sup>#</sup>*P* < 0.05; compared with the bilateral carotid stenosis group, \**P* < 0.05.

21st century, some studies included 4006 patients with carotid stenosis and found that severe left internal carotid stenosis was significantly associated with cognitive impairment [20], and more studies have shown that the performance of cognitive dysfunction caused by carotid stenosis is the same as the function of the lateral brain tissue is related. The left carotid stenosis often causes abnormal speech function, while the right side often causes abnormal visual space and executive function [21–23]. The possible mechanisms of carotid stenosis causing cognitive dysfunction are as follows: (1) decreased cerebral perfusion: studies have shown that carotid artery mild to moderate stenosis will not cause decreased cerebral perfusion, which is due to the auto-

nous regulation function of the brain. However, severe carotid stenosis can cause cerebral perfusion can be significantly reduced [24]. Hippocampus, frontotemporal lobe, and other neuronal tissues are very sensitive to ischemia and hypoxia. When chronic carotid stenosis causes a decrease in cerebral perfusion, neurons in these parts produce free radicals due to ischemia and hypoxia, which in turn stimulates brain tissue oxidative damage, which eventually causes cognitive dysfunction [25]. This mechanism is currently a more recognized mechanism. (2) Asymptomatic cerebral embolism: the carotid artery innervates the anterior 2/3 of the blood supply to the brain, including the frontal, temporal lobe, hippocampus, and limbic system. These parts

TABLE 3: two groups of patients with MMSE, MoCA score comparison.

Item	MMSE scores			MoCA scores		
	Before treatment	3 months	6 months	Before treatment	3 months	6 months
CAS group	22.78 ± 1.45	25.25 ± 1.68*	26.79 ± 1.73 <sup>#</sup>	21.34 ± 1.3	23.93 ± 1.57*	26.45 ± 1.72 <sup>#</sup>
CEA group	23.11 ± 1.48	24.75 ± 1.61*	26.36 ± 1.69 <sup>#</sup>	21.05 ± 1.31	23.84 ± 1.56*	26.37 ± 1.70 <sup>#</sup>
<i>t</i>	1.11	1.50	1.24	1.06	0.28	0.23
<i>P</i>	0.26	0.13	0.21	0.29	0.77	0.81

MMSE: Mini-Mental State Examination; MoCA: Montreal Cognitive Assessment; CEA: carotid endarterectomy; CAS: carotid artery stenting. Compared with before treatment, \**P* < 0.05; compared with 3 months after treatment, <sup>#</sup>*P* < 0.05.

TABLE 4: Patients with two groups of NSE, hs-cCRP levels.

Item	NSE			hs-CRP		
	Before treatment	3 months	6 months	Before treatment	3 months	6 months
CAS group	28.85 ± 1.91	24.34 ± 1.59*	18.12 ± 1.12 <sup>#</sup>	3.35 ± 0.52	4.11 ± 0.59*	4.87 ± 0.62 <sup>#</sup>
CEA group	29.12 ± 1.93	24.75 ± 1.61*	18.37 ± 1.14 <sup>#</sup>	3.42 ± 0.55	3.72 ± 0.57*	3.97 ± 0.58 <sup>#</sup>
<i>t</i>	0.48	1.26	1.09	0.64	3.32	7.41
<i>P</i>	0.69	0.21	0.27	0.51	<0.001	<0.001

CEA: carotid endarterectomy; CAS: carotid artery stenting. NSE: neuron-specific enolase; Hs-CRP: high-sensitive C reaction protein. Compared with before treatment, \**P* < 0.05; compared with 3 months after treatment, <sup>#</sup>*P* < 0.05.

TABLE 5: Correlation analysis of preoperative NSE, hs-CRP and MMSE, MoCA score.

	MMSE		MoCA	
	<i>r</i>	<i>P</i>	<i>r</i>	<i>P</i>
NSE	-0.783	<0.05	-0.832	<0.05
hs-CRP	-0.623	0.032	-0.652	<0.05

are closely related to cognitive function. Carotid plaque shedding may block the above parts. Microvasculature is a cognitive dysfunction that causes mild symptoms and cannot be detected in time [26]. (3) Brain white matter lesions: brain white matter lesions damage the neural network connection of the brain and cause cognitive dysfunction. Studies have shown that white matter lesions in patients with carotid stenosis are significantly increased and are associated with cognitive dysfunction [27, 28].

Due to the different functions of human left and right cerebral hemispheres, there are also obvious differences in the changes of cognitive function in patients with different carotid stenosis sites. This study showed that patients with left-sided carotid stenosis had significantly lower MoCA scores and visual space and executive ability scores than those with right-sided and bilateral carotid stenosis groups; the right-sided carotid stenosis group had significantly higher naming scores in MoCA. In the left and bilateral carotid stenosis groups, the right carotid stenosis group and the bilateral carotid stenosis group had significant differences in MMSE score, MoCA abstraction ability, and orientation ability score. A number of previous studies have found that the left and right patients with moderate or more internal carotid stenosis have significantly different MMSE scores, and repeated sets of neuropsychological state tests have

shown that patients with left or bilateral carotid stenosis have more significant cognitive impairment [29, 30]. The left cerebral hemisphere plays a major role in advanced language and memory function, and language, memory, and cognitive function are closely related, so some researchers found that patients with left carotid stenosis have impaired language function, while the right carotid stenosis have impaired visual space and visual structure [31]. For the results of this study, it is speculated that the cause may be related to the left hemisphere being the dominant hemisphere and the impairment of the language recapitulation caused by the damage of the language center. The cognitive dysfunction of the right carotid stenosis is mainly characterized by impaired visual space and delayed recall function, which is mainly related to the structural ability of the visual space and the right cerebral hemisphere [32].

Since carotid stenosis causes reduced cerebral perfusion and cognitive dysfunction. However, both CAS and CEA can significantly improve cerebral perfusion; can both of them improve patients' cognitive dysfunction? At present, there are indeed many research reports confirming that both have the effect of improving cognitive dysfunction, but there is no obvious report on the evaluation of the effect of the two surgical methods on improving cognitive function. In this study, there was no significant difference in baseline data, MMSE score, and MoCA score before treatment between the two groups of patients, suggesting that the groups were comparable and NSE and hs-CRP were negatively correlated with MMSE and MoCA scores. Neuron-specific enolase (NSE) is a marker that reflects neuronal damage [33], the MMSE score and MoCA score of the two groups of patients before treatment are less than the normal value, and the NSE is higher than the normal value, suggesting that patients with long-term carotid artery stenosis can indeed cause

neuronal damage. Postoperative MMSE score and MoCA score were higher than before treatment, but there was no statistically significant difference between the two groups, and the NSE value was lower than before surgery, suggesting that both procedures can improve patients with carotid stenosis; in cognitive function, its mechanism may be realized by expressing influence on NSE. In addition, hs-CRP was higher than normal before treatment in both groups of patients, suggesting that inflammation was related to carotid stenosis, while hs-CRP in the stent group was significantly higher than that in the exfoliation group. It is speculated that the possible reason is that the stent is a foreign body substance, and implantation into the blood vessel may cause local inflammation. However, current studies have shown that the improvement of vasomotor responsiveness after carotid artery intervention may be one of the main mechanisms of patients' cognitive improvement. The study believes that the reduction of vasomotor response on the same side of carotid artery stenosis can indicate that the cerebral blood vessels are in the blood vessel [34]. The expansion agent cannot fully expand under stimulation and reflects the damage of hemodynamic reserve. This change in vascular reactivity increases the risk of cerebral ischemia and is the cause of cognitive decline in the ipsilateral hemisphere [35]. The expansion of cerebral arterioles can offset the drop in cerebral perfusion pressure and keep blood flowing to the distal end of the carotid artery stenosis. In this study, although we did not carry out the influence of hemodynamic parameters on cognitive function changes, many studies have confirmed that inflammation is closely related to vasomotor and vasomotor, and inflammation can affect vasomotor function [36]. The more severe the inflammatory response, to a certain extent, it can cause vasoconstriction and further affect the perfusion of the brain, which leads to the decline of cognitive function. The level of hs-CRP decreased significantly after this study, suggesting that CAS or CEA can alleviate the inflammatory response, cause the expansion of the internal carotid artery branch arterioles, increase the hemodynamic parameters of the local brain tissue, increase cerebral perfusion, and further improve cognitive function.

This experiment has enriched the gaps in neural intervention to interfere with cognitive dysfunction. However, there are reports showing that carotid interventional surgery has no obvious effect on the improvement of cognitive function, which is not completely consistent with the results of this experiment. Speculation may be related to different research methods and interference factors. In addition, the sample size of this experiment is small, the follow-up time is short, and the mechanism of carotid artery interventional treatment for cognitive function is not clearly studied, and more clinical studies will be required in the future.

## Data Availability

The data supporting the findings of the article is available in the [http://datadryad.org] at [https://datadryad.org/stash/share/Lybuzaq0hftnYzXAwT4\_Yc4zZIHys7WeZ8PxazTkrww]”.

## Ethical Approval

All participants in this study were approved by the People's Hospital of Deyang City ethics committee and signed informed consent, Ethics approval number 2015-02-003.

## Disclosure

No potential conflict of interest was reported by the authors.

## Conflicts of Interest

The authors declare no potential conflicts of interest with respect to the authorship and/or publication of this article.

## References

- [1] H. Y. Jiang, “The relationship between carotid artery stenosis and cognitive dysfunction,” *Chinese Journal of Gerontology*, vol. 34, pp. 77–79, 2014.
- [2] X. Geng, Y. W. Wu, X. Chen, and G. Li, “Clinical study of cognitive dysfunction in patients with asymptomatic carotid stenosis,” *Chinese Journal of Geriatric Cardio-Cerebrovascular Disease*, vol. 16, pp. 465–467, 2014.
- [3] F. T. Feliziani, M. C. Polidori, P. De Rango et al., “Cognitive performance in elderly patients undergoing carotid endarterectomy or carotid artery stenting: a twelve-month follow-up study,” *Cerebrovascular Diseases*, vol. 30, no. 3, pp. 244–251, 2010.
- [4] H. D. Aridi, M. Arora, S. Locham et al., “IP101. Identification of predictors of high-grade restenosis after carotid endarterectomy in a multicenter national database,” *Journal of Vascular Surgery*, vol. 67, no. 6, pp. e114–e115, 2018.
- [5] X. G. Shi, B. Wu, Y. L. Zhang, Z. Q. Zhou, and H. Qian, “Observation of the therapeutic effect of carotid endarterectomy,” *Chinese Journal of Neurosurgery*, vol. 21, pp. 300–303, 2005.
- [6] A. Karpenko, V. Starodubtsev, P. Ignatenko et al., “Comparative analysis of carotid artery stenting and carotid endarterectomy in clinical practice,” *Journal of Stroke and Cerebrovascular Diseases*, vol. 29, no. 5, article 104751, 2020.
- [7] X. M. Yan, W. G. Li, and X. Y. Hong, “Comparison of carotid endarterectomy and carotid stent implantation in the treatment of carotid artery stenosis,” *Chinese Journal of Gerontology*, vol. 36, pp. 5602–5604, 2016.
- [8] J. Li, B. S. Han, Y. K. He, Z. S. Li, and T. X. Li, “Clinical study of cognitive function after stent implantation in severe carotid artery stenosis,” *Journal of Interventional Radiology*, vol. 24, pp. 943–945, 2015.
- [9] H. Z. Huo and D. L. Gan, “Changes of cognitive function after carotid endarterectomy in patients with carotid stenosis,” *Chinese Journal of Gerontology*, vol. 36, pp. 2880–2881, 2016.
- [10] M. Y. Gao, M. Yang, W. H. Kuang et al., “Screening validity evaluation of influencing factors and normal value of the summary mental status scale score,” *Journal of Peking University (Medical Edition)*, vol. 42, pp. 443–449, 2015.
- [11] Y. Yao, F. Yang, L. J. Wang et al., “Application of the Montreal Cognitive Assessment Scale in the diagnosis of mild cognitive dysfunction,” *Jilin University Journal (medical version)*, vol. 38, pp. 730–735, 2012.

## Retraction

# Retracted: Analysis of Age and Prevention Strategy on Outcome after Cerebral Venous Thrombosis

### BioMed Research International

Received 12 March 2024; Accepted 12 March 2024; Published 20 March 2024

Copyright © 2024 BioMed Research International. This is an open access article distributed under the Creative Commons Attribution License, which permits unrestricted use, distribution, and reproduction in any medium, provided the original work is properly cited.

This article has been retracted by Hindawi following an investigation undertaken by the publisher [1]. This investigation has uncovered evidence of one or more of the following indicators of systematic manipulation of the publication process:

- (1) Discrepancies in scope
- (2) Discrepancies in the description of the research reported
- (3) Discrepancies between the availability of data and the research described
- (4) Inappropriate citations
- (5) Incoherent, meaningless and/or irrelevant content included in the article
- (6) Manipulated or compromised peer review

The presence of these indicators undermines our confidence in the integrity of the article's content and we cannot, therefore, vouch for its reliability. Please note that this notice is intended solely to alert readers that the content of this article is unreliable. We have not investigated whether authors were aware of or involved in the systematic manipulation of the publication process.

Wiley and Hindawi regrets that the usual quality checks did not identify these issues before publication and have since put additional measures in place to safeguard research integrity.

We wish to credit our own Research Integrity and Research Publishing teams and anonymous and named external researchers and research integrity experts for contributing to this investigation.

The corresponding author, as the representative of all authors, has been given the opportunity to register their agreement or disagreement to this retraction. We have kept a record of any response received.

### References

- [1] X. Chu, J. Zhang, B. Zhang, and Y. Zhao, "Analysis of Age and Prevention Strategy on Outcome after Cerebral Venous Thrombosis," *BioMed Research International*, vol. 2020, Article ID 6637692, 6 pages, 2020.

## Research Article

# Analysis of Age and Prevention Strategy on Outcome after Cerebral Venous Thrombosis

Xiuli Chu,<sup>1</sup> Jianlin Zhang,<sup>2</sup> Bin Zhang<sup>1</sup> ,<sup>1</sup> and Yuwu Zhao<sup>1</sup> 

<sup>1</sup>Department of Neurology, Shanghai Jiao Tong University Affiliated Sixth People's Hospital, Shanghai, China 200233

<sup>2</sup>Department of Neurosurgery, Taian Central Hospital, Taian, Shandong Province, China 271000

Correspondence should be addressed to Bin Zhang; zhangbin1982zb@126.com and Yuwu Zhao; zhao\_yuwu2005@126.com

Received 23 November 2020; Revised 3 December 2020; Accepted 5 December 2020; Published 14 December 2020

Academic Editor: Yuzhen Xu

Copyright © 2020 Xiuli Chu et al. This is an open access article distributed under the Creative Commons Attribution License, which permits unrestricted use, distribution, and reproduction in any medium, provided the original work is properly cited.

**Object.** Cerebral venous sinus thrombosis (CVST) mainly affects middle-aged individuals. However, the association between age or prevention strategy with the functional outcome remains poorly investigated. **Method.** We identified adult CVST patients in our centers. Functional outcome and prevention strategy were extracted from medical records. Modified Rankin Scale (mRS)  $\leq 1$  is considered a good functional outcome. **Results.** A total of 113 patients were identified. The most common presenting symptoms were headache (86.72%) and nausea/vomiting (56.63%); the top two identified risk factors were local head/neck infection (27.43%) and pregnancy/puerperal period (19.47%). The medical encounter lag time was 0.04 d-120 d. Four enrolled patients were diagnosed as CVST again, and the interval time was 3-8 years from the first time. Thrombus was most frequently seen at superior sagittal sinus (53.10%) and sigmoid sinus (50.44%). 94 (83.19%) of the patients had good outcomes. In the acute phase, 91 (80.53%) patients received low molecular weight heparin, 29 (25.66%) took aspirin, 7 (6.19%) patients were put on low molecular weight heparin and aspirin together. During our follow up (6-24 m), there were 10 (8.85%) patients who suffered from thrombotic event recurrence. For the patients > 40 years old, they tended to suffer from neurological deficit (25.00%) and stupor/coma (16.67%) ( $p > 0.05$ ), with a higher rate of hemorrhage (20.83%) and death (4.16%) when compared with the younger patients (10.77% and 1.53%, separately) ( $p > 0.05$ ). **Conclusion.** Functional outcome after CVST appears good. For the patients over 40-year-old, neurological deficit and altered consciousness were more common, accompanied by a higher rate of hemorrhage and mortality. The recurrent rate of CVST was low, longer-term follow up needed. The prevention strategy after CVST was uncertain, further studies needed.

## 1. Introduction

Cerebral venous sinus thrombosis (CVST) is an uncommon cerebrovascular disease. Unlike the arterial stroke, it affects mainly middle-aged individuals and is more common among females [1]. CVST is generally accompanied with a good prognosis, the short-term mortality is <10%, and the majority of patients regain independence in daily living [2, 3]. In the International Study on Cerebral Vein and Dural Sinus Thrombosis (ISCVT) study, the death rate was 8%, 80% of patients recovered well (defined as a score of 0-1 on the modified Rankin Scale (mRS)), and the CVT recurrent rate was 1.5/100 patient per years [4]. Older age (>37 years), male sex, coma, seizure, deep CVST, brain hemorrhage, and concomitant diseases such as hematological pathologies,

systemic malignancy, and central nervous system infection were considered to be the risk factors [5]. Antithrombotic medication is the primary acute therapy for CVST, recommended by the American Heart Association and American Stroke Association [6]. However, treatment options remain controversial, and the clinical outcomes are uncertain. Most patients will accompany with a good prognosis, which may affect the patient's compliance with following preventive treatment. Relatively few small studies have investigated long-term outcomes (beyond 1-2 years) and prevention strategies after CVST [7-9].

The aims of this study were to investigate the association between age or prevention strategy with the functional outcome in a double-center patient population. We also explored their risk for recurrent venous thromboembolism



(VTE), antithrombotic medication use, and risk for bleeding events.

## 2. Methods

**2.1. Study Design.** This was a double-center retrospective cohort study. Patients were identified from January 2013 to June 2016 at the Shanghai Sixth People's Hospital affiliated to the Shanghai Jiao Tong University and Taian Central Hospital.

The inclusion criteria for this study are (1) CVST is made by clinical diagnosis with magnetic resonance imaging (MRI)/magnetic resonance venography (MRV); (2) age > 18 old years; (3) patient has at least one 6-month follow-up clinical visit after the index event.

We extracted the following information from medical records: demographic information, presenting symptoms (headache, vomiting, papilledema with/without visual loss, other neurological symptoms, or signs), NIHSS score, Glasgow Coma Scale (GCS) score, the imaging information, the location of the thrombus, comorbid medical history, and medication for CVT.

All patients were interviewed at 6 to 24 months by direct interview, or a telephone interview was done if the patient could not show up for an in-person visit. Follow-up data recorded were as follows: headaches, seizures, visual loss, functional outcomes measured by mRS, death, recurrent symptomatic sinus thrombosis (new clinical symptoms with new thrombus shown on MRV), VET or CVST events, pregnancy/abortion during the follow-up period, and antithrombotic treatment.

The primary outcome measures were the mRS. A favorable outcome was defined as mRS 0-1, indicating complete recovery or only mild residual symptoms not affecting everyday life.

**2.2. Statistical Analysis.** Baseline categorical variables will be listed as number (percentage). Baseline normally distributed continuous variables will be reported as mean  $\pm$  standard deviation (SD), while nonnormally distributed continuous variables will be reported in median (interquartile range [IQR]). Comparisons of continuous variables between the two groups were performed by the two-sample-testify normally distributed with equal variance between groups; otherwise, Wilcoxon rank-sum test would be used. Comparisons of categorical values between the two groups were performed by Chi-square test or Fisher's exact test. A two-sided difference is considered significant if the null hypothesis is rejected at the 0.05 probability level. Statistical analyses were performed using SPSS, version 24.0 (SPSS Inc., Chicago, IL, USA).

## 3. Results

**3.1. Baseline Patient Information, Presentation.** We identified 113 consecutive patients diagnosed as CVST. The median age of patients at diagnosis was 32.50 years (IQR rang 27-48.75): 63 (55.75%) of them were females. The median medical encounter lag time was 5.00 days (IQR range 2.00-10.00).

The most prevalent signs and symptoms were headache (86.72%), nausea/vomiting (56.63%), and motor or sensory deficit (22.12%). There were 28 (24.78%) patients who had a NIHSS score > 2. Of the 17 (30.36%) patients, headache was the only symptom they had. For the patients in the cohort, 36 (31.86%) patients were not identified with the specific reasons, 31 (27.43%) patients suffered from central nervous system infection, 22 (19.47%) patients under pregnancy/puerperal period, 14 (12.39%) had coagulation disorder, 8 (7.08%) had systemic prothrombotic disorder, 8 (7.08%) had anemia (all 8 were puerperal patients), 8 (7.08%) patients suffered from hemorrhoids surgery, 3 had malignancy (2.65%), 3 (2.65%) patients had the history of oral contraceptives, 2 (1.77%) had polycythemia, 1 (0.88%) had dural fistula confirmed by digital subtraction angiography (DSA), and 1 (0.88%) patient had dehydration for more than 12 hours (Table 1, Figure 1).

**3.2. Imaging Findings.** For the patients with neuroimaging at admission, combined with the CT/MRV/MRI exam, the results showed that there were 21 (18.58%) patients who showed infarct in CT/MRI, and 17 (15.04%) patients showed hemorrhage. Thrombus was most frequently localized at superior sagittal sinus (53.10%), sigmoid sinus (50.44%), transverse sinuses (48.67%), and straight sinus (7.08%). There were 41.59% patients who had one sinus that clotted, 35.40% patients had two sinuses that clotted, 23.01% patients had more than two sinus involved. Thirty-one patients had the risk factor of local infection, 19 (61.29%) patients localized at superior sagittal, 14 (45.16%) patients localized at transverse sinuses, 14 (45.16%) patients clotted at the sigmoid sinus, and 9 (29.03%) straight sinus. There were 5 (16.13%) patients who had more than two sinuses that clotted, 9 (29.03%) patients had two sinuses that clotted, 17 (54.83%) patients just had one sinus involved (Table 2, Figure 2).

**3.3. Antithrombotic and Prevention Strategy.** In the acute phase, 81 (71.68%) patients received low molecular weight heparin, 15 (25.00%) took aspirin, 10 (8.85%) patients were given warfarin, and 7 (6.19%) patients were put on low molecular weight heparin and aspirin together for combined with other diseases. Within the 113 patients, 5 patients were the recurrence of CVST and in charged into our hospital, the recurrent interval since the first diagnose was 2-8 years, and the recurrent syndrome was headache for all of them. One patient has taken aspirin for prevention, and recurrent 3 years later; two patients did not take medicine, and recurrent 2 and 3 years later, separately; 2 patients had taken warfarin, and recurrent 2 and 8 years later, separately. The median follow-up duration for the entire cohort was 10 (6-24) months. In the following period, 3 patients lost follow-up. By the end of the follow-up, 52 patients (46.02%) had taken warfarin for more than 6 months, 19 (16.81%) patients had taken aspirin instead for more than 6 months, 3 (2.65%) patients had a combination of medication, 8 (7.08%) patients had taken traditional medicine instead, and 28 (24.77%) patients declined to take any specific medication after discharge. Eleven (8.39%) patients experienced thrombotic

TABLE 1: Baseline characteristics of CVST patients.

	Total (113)	Age < 40 (65)	Age ≥ 40 (48)	p
Median age = 32.50 (IQR 27-48.75)				
Female, n (%)	63 (55.75%)	41 (63.07%)	22 (44.83%)	0.600
Follow-up period	10 m (6-24 months)			
Medical encounter lag time*	0.04 d-120 d (average 11.11)	12.48	9.26	
Median time (IQR)	5.00 (2.00-10.00)	4.50 (2.25-9.75)	5.00 (2.00-14.00)	<0.01
Symptoms and signs, n (%)				
Headache	98 (86.72%)	61 (93.84%)	37 (77.08%)	0.01
Visual loss	10 (8.85%)	8 (12.31%)	2 (4.17%)	0.18
Papilledema	17 (15.04%)	12 (18.46%)	5 (10.42%)	0.29
Nausea/vomiting	64 (56.63%)	39 (60.00%)	25 (52.08%)	0.44
Stupor or coma	12 (10.62%)	4 (6.15%)	8 (16.67%)	0.12
Motor or sensory deficit	25 (22.12%)	13 (20.00%)	12 (25.00%)	0.64
Seizure	20 (17.70%)	13 (20.00%)	7 (14.6%)	0.61
NIHSS score > 2	28 (24.78%)	16 (24.61%)	12 (25.0%)	1.00
Risk factors				
None identified	36 (31.86%)	7 (10.77%)	29 (60.42%)	<0.01
Malignancy	3 (2.65%)	2 (3.07%)	1 (2.08%)	1.00
Dural fistula	1 (0.88%)	0 (0.00%)	1 (2.08%)	0.42
Coagulation disorder	14 (12.39%)	8 (12.31%)	6 (12.50%)	1.00
Any systemic prothrombotic disorder	8 (7.08%)	6 (9.23%)	2 (4.17%)	0.46
Polycythemia	2 (1.77%)	1 (1.53%)	1 (2.08%)	1.00
Anemia	8 (7.08%)	8 (12.31%)	0 (0.00%)	0.02
Pregnancy/puerperium	22 (19.47%)	22 (33.84%)	0 (0.00%)	<0.01
Local infection	31 (27.43%)	19 (29.23%)	12 (25.00%)	0.67
Oral contraceptives	3 (2.65%)	3 (4.61%)	0 (0.00%)	0.26
Surgery	8 (7.08%)	8 (12.31%)	0 (0.00%)	0.02
Dehydration	1 (0.88%)	1 (1.53%)	0 (0.0%)	1.00
mRS < 2	94 (83.18%)	55 (84.61%)	39 (81.25%)	0.80
Death by 6 month	3 (2.65%)	1 (1.53%)	2 (4.16%)	0.57
CVST recurrent	10 (8.85%)	4 (6.15%)	6 (12.50%)	0.31

\*Medical encounter lag time (from symptom onset to first medical encounter).

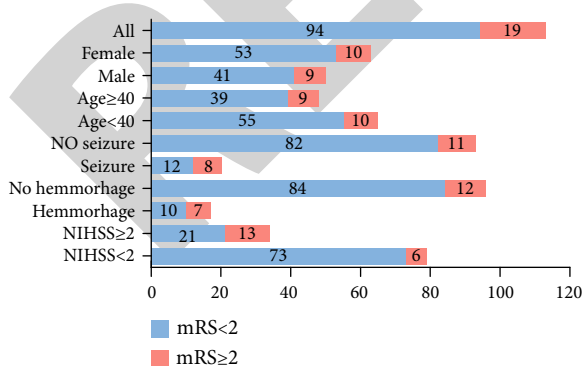


FIGURE 1: Modified Rankin Scale distribution by selected patient groups.

events recurrently during our follow-up period. Six patients had taken warfarin, 1 patient had taken aspirin, and 4 patients declined to take any medication.

3.4. Outcomes. Regardless of treatment strategy, 94 (83.18%) patients achieved a good clinical outcome (mRS 0-1). 4 (3.54%) patients had an intermittent headache, which affected their normal life. 10 pregnant patients all had smooth production. Intracranial hemorrhage (ICH) was the most cited complication, 9 (52.94%) of 17 patients suffered from hemorrhagic events requiring medical attention, which were potentially life-threatening (4 intracranial bleedings, 2 of which were traumatic), although none was fatal (Table 1).

Death was observed in 3 (2.65%) patients: 2 of them died from direct consequences of the indexed CVST in the hospital, the brain edema aggravated by coma, leading to death. 1 patient died from underlying malignancy in the following period.

3.5. Subgroup Analysis. Then, we divided the patients according to patients' age (≥40 vs. <40 years old). For the patients over the age of 40, they had shorter medical encounter lag time (median 5.00 days, IQR 2.00-14.00), compared to

TABLE 2: Imaging findings of CVST patients.

	Total (113)	Age < 40 (65)	Age > 40 (48)	<i>p</i>
Neuroimaging at admission				
CT/MRI showed infarct, <i>n</i> (%)	21 (18.58%)	10 (15.38%)	11 (22.92%)	0.33
CT/MRI showed hemorrhage, <i>n</i> (%)	17 (15.04%)	7 (10.77%)	10 (20.83%)	0.18
Occluded sinus/vein, <i>n</i> (%)				
Superior sagittal sinus	60 (53.10%)	31 (47.69%)	29 (60.42%)	0.18
Straight sinus	8 (7.08%)	3 (4.61%)	5 (10.42%)	0.28
Sigmoid sinus	57 (50.44%)	34 (52.31%)	23 (47.92%)	0.70
Transverse sinuses	55 (48.67%)	31 (47.69%)	24 (50.00%)	0.85
Number of affect sinus, <i>n</i> (%)				
One sinus	47 (41.59%)	26 (40.00%)	21 (43.75%)	0.70
Two sinuses	40 (35.40%)	24 (36.92%)	16 (33.33%)	0.84
More than two sinuses	26 (23.00%)	12 (18.46%)	14 (29.17%)	0.25

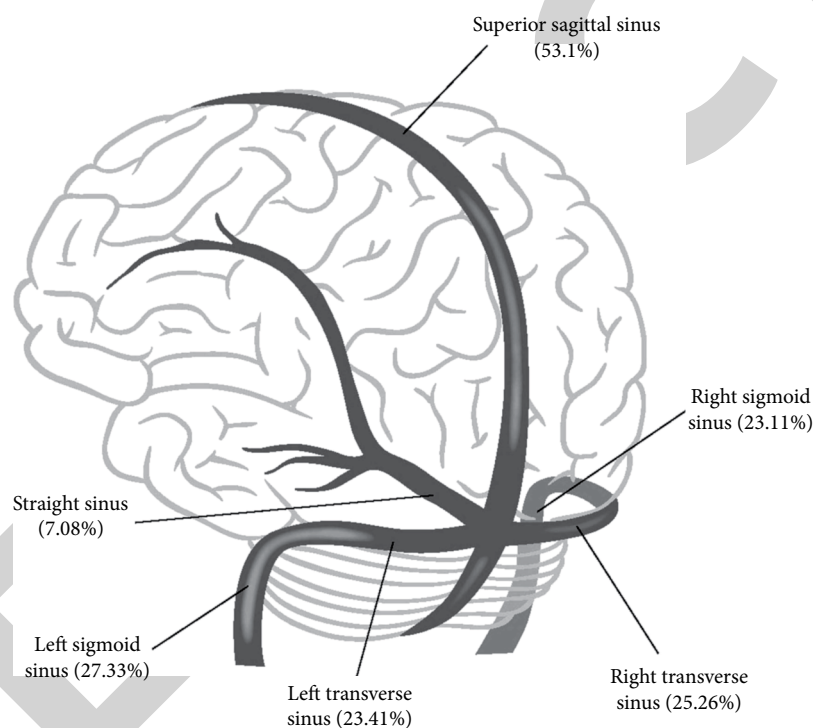


FIGURE 2: Schematic diagram of cerebral venous sinus thrombosis locations and distribution.

younger patients (median 4.50 days, IQR 2.25-9.75). They were more likely to suffer from motor or sensory deficit (25.00%) and stupor/coma (16.67%). To identify the risk factors, among the patients over 40-year-old, there were 60.42% of patients who could not find identical reasons ( $p < 0.01$ ). Among the patients under the age of 40, the risk factors were higher in anemia (12.31%,  $p < 0.05$ ), pregnancy/puerperium (33.84%,  $p < 0.05$ ), surgery (12.31%,  $p < 0.05$ ), central nervous system infection (29.23%,  $p > 0.05$ ), and oral contraceptives (4.61%,  $p > 0.05$ ). The patients over 40-year-old were more likely to suffer from hemorrhage (20.83%) and mortality rate (4.16%) compared to younger patients (10.77% and 1.53%, separately), but the results had no significant meanings ( $p > 0.05$ ) (Table 1, Figure 1).

#### 4. Discussion

Our study provided data on various aspects of outcomes in a double-center cohort of CVST patients. The recurrence risk for CVST was low. The majority of patients (83.18%) had a favorable outcome (mRS 0-1).

Our results were similar to the results of the ISCVT study (80.0%) [5] and the VENOST study (88.9%) [10], which were the two largest studies of CVST. CVST predominates in children and young and middle-aged adults and rarely happened in elder patients. Some of the risk factors, such as pregnancy, puerperium, and use of oral contraceptives, are no longer present in elderly patients, whereas others such as malignancy and dehydration may be more frequent [5], which

may cause the risk factors between each age groups are different and may impact the symptoms and outcome. The ISCVT found that older age (>37 years) was a predictor of poor outcome (mRS > 3) [5]. In our study, we divided the patients according to the age and carried a subgroup analysis. For the patients <40 y, the common risk factors were pregnancy/puerperium, central nervous system infection, anemia, and surgery; whereas for the patients over 40-year-old, there were 60.42% patients who could not find identical reasons, local infection rate were 25.00%, and the coagulation disorder rate reached 12.50%. The ages have influenced the outcome, for the patients  $\geq$  40 years old had a higher rate of hemorrhage (20.83%) and mortality (4.16%).

Headache is the most common presenting symptom of CVST patients (60%-90%) in many studies [5, 9, 10], and sometimes it may be the sole complaint in a large number of patients [10]. Of the 113 patients, 86.72% experienced headaches, and it was the only symptom in 29 (25.66%) patients. In our study, motor or sensory deficit and altered consciousness were more common in patients aged > 40 years old, whereas younger patients frequently presented with visual field deficit, headache symptoms, and seizure. And the older patients usually ignored the symptoms and unwilling to visit the doctor; unless the symptoms got worse (an unbearable headache), the medical encounter lag time of older patients (median time 5.00 days, IQR 2.00-14.00) was longer than the younger patients (median time 4.50 days, IQR 2.25-9.75). The clinical presentation of our cohort is almost identical to what has been reported in many previous studies.

The most frequently affected sinuses in our cohort were superior sagittal sinus (53.10%), sigmoid sinus (50.44%), and transverse sinuses (48.67%), possibly as a consequence of their morphological inferiority (often being hypoplastic) [11]. These results of the VENOST study showed 73.4% in transverse sinuses, 39.8% in sigmoid sinus, and 38.9% in sagittal sinus [10]. In the ICVST study, the superior sagittal sinus was the most commonly affected (62%), followed by the transverse sinuses (41.2%-44.7%). The association of transverse and sigmoid sinus thrombosis with local inflammation in the nasal, tonsillar, and middle ear area was commonly observed, which was similar to our research; the patients with local infection localized at superior sagittal most. With the increased use of antibiotic treatment, the global incidence of inflammatory phlebothrombosis was reduced, and the outcome became better [12]. In the developing countries, the reported proportion of a local infection in adults with CVST is only 15% [13], and the proportion has decreased to 6% to 12% in the developed world [14], compared with our study (17.86%).

Treatment options remain controversial. The American Heart Association and American Stroke Association have suggested anticoagulation should be started as long as there are no major contraindications, and the patients suggested to continue to receive oral anticoagulation for 3-12 months if the patient exhibits neurological improvement or remain stable [6]. However, until now, we just have limited data to suggest the anticoagulation treatment is safe [9, 15]; there were some studies that come to inconclusive results for the

clinical outcome with or without anticoagulation [16, 17]. In the ISCVT study, 83.3% of patients were given anticoagulation drugs, and 5.9% of patients received antiplatelet drugs [5]. In our study, in the acute phase, there were 80.53% of patients who received anticoagulation drugs, and 25.00% of patients received antiplatelet drugs. After the discharge from the hospital, the patients who had taken warfarin decreased to 46.02%, 16.81% patients chose to take aspirin, and 24.77% patients chose to observation without taking any medicine. By the end of follow-up, eleven (8.39%) patients experienced thrombotic events recurrently during our follow-up period. Six patients had taken warfarin, 1 patient had taken aspirin, and 4 patients declined to take any medication. No institutional guidelines are recommended for the use of aspirin, but doctors often prescribe aspirin to patients with no obvious or transient risk factors, or some patients chose to take aspirin for the lower rate of hemorrhage and the complex of regular monitoring of coagulation. Aspirin use may play a role in lowering the incidence of VTE, as aspirin reduces the risk of venous thrombosis by 42% [1, 18]. Further prospective studies are needed, as physicians might have been biased and treated severe clinical presentations more aggressively with anticoagulation, and the patients with other kinds of complications should be considered, for the higher rate of hemorrhage and recurrent rate.

Previous studies showed that the risk of recurrence of a thrombotic event seems to be the highest in the first year after diagnosis [4, 19]. Relatively few small studies have investigated long-term outcome (beyond 1-2 years) after CVST [1, 7]. In our cohort, 5 of the enrolled patients were CVST recurrence, the recurrent interval since the first diagnose was 2-8 years, and the recurrent syndrome was a headache for all of them. One patient has taken aspirin for prevention, and recurrent 3 years later; two patients did not take medicine, and recurrent 2 and 3 years later, separately; and 2 patients taken warfarin, and recurrent 2 and 8 years later, separately. Come to these conclusions, we considered that the recurrent rate may relate to the follow-up period, which may not be long enough; or may be due to insufficient sample size, further studies are needed, and subgroup analysis is necessary, to maximum benefit.

There are several limitations in our study. First, it is a retrospective study, not a randomized trial and, thus, more susceptible to bias. Second, some patients were evaluated only by phone at follow-up. Finally, the sample size was relatively small and potentially underpowered to assess for differences beyond that of the outcome for independence.

## 5. Conclusions

Our study reinforces the finding that outcomes after CVST are generally good, with the majority of patients achieving functional independence and a lower risk of recurrent events. For the patients over 40-year-old, motor or sensory deficit and altered consciousness were more common, and the hemorrhage rate and mortality rate were higher than the younger patients. A further dedicated study is needed.



## Research Article

# Association between Serum IL-37 and Spinal Cord Injury: A Prospective Observational Study

Yuanzhen Chen,<sup>1</sup> Dandan Wang,<sup>2</sup> Shengnan Cao,<sup>3</sup> Guangjian Hou,<sup>1</sup> Hong Ma ,<sup>4</sup> and Bin Shi <sup>1</sup>

<sup>1</sup>Neck-Shoulder and Lumbocrural Pain Hospital, Shandong First Medical University & Shandong Academy of Medical Sciences, Jinan, 250014 Shandong Province, China

<sup>2</sup>Shandong First Medical University, Jinan, 250014 Shandong Province, China

<sup>3</sup>School of Acupuncture-Tuina, Shandong University of Traditional Chinese Medicine, Jinan, 250355 Shandong Province, China

<sup>4</sup>Foshan Traditional Chinese Medicine Hospital, Foshan, 528000 Guangdong Province, China

Correspondence should be addressed to Hong Ma; fozhongyimahong@qq.com and Bin Shi; sdyky-shibin@163.com

Received 14 November 2020; Revised 28 November 2020; Accepted 30 November 2020; Published 11 December 2020

Academic Editor: Yuzhen Xu

Copyright © 2020 Yuanzhen Chen et al. This is an open access article distributed under the Creative Commons Attribution License, which permits unrestricted use, distribution, and reproduction in any medium, provided the original work is properly cited.

**Objective.** Interleukin-37 (IL-37) is a new cytokine that naturally inhibits inflammation. Inflammation plays an important role in acute spinal cord injury (SCI). The purpose of this study is to check whether serum IL-37 can be used as a clinical predictor of SCI. **Methods.** All subjects underwent venipuncture within 24 hours of enrollment to obtain peripheral blood and then centrifuged to obtain serum. The concentration of serum IL-37 was determined by enzyme-linked immunosorbent assay (ELISA). One month after the injury, the American Spinal Cord Injury Association (ASIA) impairment scale was used for neurological examination. **Results.** A total of 148 people were included in the study, including 52 normal controls (NC) and 96 patients with acute SCI within 24 hours of onset. The comparison of clinical baseline data (age, gender, BMI: body mass index, smoking, alcohol drinking, CHD: coronary heart disease, HBP: high blood pressure, and DM: diabetes mellitus) between the two groups was not statistically significant ( $p > 0.05$ ). However, the serum IL-37 concentration of SCI patients was significantly higher than that of the NC group, and the difference was statistically significant ( $p < 0.001$ ). And with the aggravation of SCI grade, the level of IL-37 increased significantly ( $p < 0.05$ ). Pearson correlation analysis further showed that serum IL-37 concentration is negatively correlated with AIS motor score ( $r = -0.327$ ,  $p < 0.05$ ). **Conclusion.** The serum IL-37 concentration of SCI patients is significantly increased, and it is closely related to the recovery of motor function. We proved for the first time that serum IL-37 has prognostic value in patients with SCI. In addition, serum IL-37 may be used as a prognostic biomarker for SCI.

## 1. Introduction

Spinal cord injury (SCI) refers to spinal cord injury that temporarily or permanently changes the function of the spinal cord [1]. Every year, about 200,000 people in the world have to face the consequences of SCI [2]. In particular, the impairment of motor function prevents the patients from being completely independent of function, which brings a heavy burden to the family and society [3]. In the United States, there are approximately 17,000 new cases of SCI recorded each year [4]. Therefore, it is necessary to find biomarkers of SCI in order to better understand the potential

molecular mechanisms of neurological damage after SCI and develop new treatment strategies.

Kumar et al. first discovered and identified the existence of interleukin-37 (IL-37) through computational sequence analysis in 2000 [5]. It was originally named IL-1H4 or IL-1F7. Later, Nold et al. found that it has the effect of suppressing the innate immune response and officially renamed it IL-37 [6]. Recently, IL-37 is considered to play an important regulatory role in the occurrence and development of various inflammatory diseases, autoimmune diseases, and vascular diseases [7–9]. However, the pathophysiological mechanism of IL-37 in the body has not yet been fully elucidated.



Animal experiments have suggested that IL-37 may be involved in the pathogenesis of SCI [10]. The purpose of our study is to check whether serum IL-37 can be used as a clinical predictor of SCI. If the relationship between IL-37 and SCI is confirmed, it will provide new possibilities for the prevention and treatment of SCI.

## 2. Methods

**2.1. Study Population.** Patients with acute SCI who attended Neck-Shoulder and Lumbocurral Pain Hospital, Shandong First Medical University & Shandong Academy of Medical Sciences from July 2017 to June 2020 were included in the study. The diagnosis of SCI is based on clinical manifestations and impact studies and is made by experienced clinicians [11]. The entry criteria of the SCI group: meet the diagnostic criteria of SCI; the onset is within 24 hours; the vital signs are stable. Exclusion criteria for the SCI group: accompanied by traumatic brain injury; severe infectious diseases; tumors; autoimmune diseases; take recent antibiotics or corticosteroids; multiple system dysfunction; failure to cooperate with examinations. In addition, volunteers matched with age and sex were selected as the normal control group (NC). A total of 148 subjects were included in this study, including 52 in the NC group and 96 in the SCI group. All subjects or guardians were informed of this study and signed a consent form. This study complied with the Declaration of Helsinki and was approved by the ethics committee of Neck-Shoulder and Lumbocurral Pain Hospital, Shandong First Medical University & Shandong Academy of Medical Sciences.

**2.2. Clinical Baseline Data.** The clinical baseline data were collected when the subjects were enrolled. The clinical baseline data is recorded by specialized clinicians. The recorded clinical baseline data include demographic data, living habits, and past medical history. Demographic data includes age, gender, and body mass index (BMI). Living habits include smoking and alcohol drinking. Past medical history includes coronary heart disease (CHD), hypertension (HBP), and diabetes (DM).

**2.3. Determination of Serum IL-37 Concentration.** Within 24 hours of admission, 5 ml of fasting blood from all subjects was collected into a test tube with a lid. After collecting the whole blood, the peripheral blood is allowed to coagulate at room temperature for 20 minutes. The peripheral blood was then centrifuged at  $2,000 \times g$  for 15 minutes in a refrigerated centrifuge. After centrifugation, immediately transfer the upper serum to a clean polypropylene tube. If the serum is not analyzed immediately, the serum should be divided into 0.5 ml aliquots and stored at  $-80^{\circ}\text{C}$ . The serum IL-37 concentration was determined using a sandwich enzyme-linked immunosorbent assay (ELISA). The ELISA experiment uses the commercialized Human IL-37 ELISA Kit (Abcam, Cambridge, MA, USA). The experimental procedures of ELISA are based on the reagent instructions and previous reports [12]. The experimental method is as follows: add  $100 \mu\text{L}$  standard or sample to appropriate wells incu-

bated at  $37^{\circ}\text{C}$  for 90 minutes; discard plate content and then add  $100 \mu\text{L}$  biotinylated antibody into all wells incubated at  $37^{\circ}\text{C}$  for 60 minutes. Wash each well three times with  $300 \mu\text{L}$  0.01 M PBS; add  $100 \mu\text{L}$  ABC working solution incubated at  $37^{\circ}\text{C}$  for 30 minutes; wash each well five times with  $300 \mu\text{L}$  0.01 M PBS and add  $90 \mu\text{L}$  of prepared TMB incubated at  $37^{\circ}\text{C}$  in dark for 30 minutes; add  $100 \mu\text{L}$  TMB Stop Solution and read OD at 450 nm within 30 minutes. Finally, the concentration of serum IL-37 was calculated by the standard curve.

**2.4. Cord Injury Association Impairment Scale Evaluation.** Cord Injury Association (ASIA) impairment scale evaluation is considered the international standard for neurological classification of spinal cord injury [13]. The ASIA impairment scale is used by ASIA as a general classification tool for spinal cord injuries, used to standardize sensory and motor functions, and is widely used in many countries around the world. According to the ASIA Impairment Scale, SCI can be divided into five levels: Grade A, complete injury. No motor or sensory function is preserved in the sacral segments S4 or S5; Grade B, sensory incomplete. Sensory but not motor function is preserved below the level of injury, including the sacral segments; Grade C, motor incomplete. Motor function is preserved below the level of injury, and more than half of muscles tested below the level of injury have a muscle grade less than 3; Grade D, motor incomplete. Motor function is preserved below the level of injury and at least half of the key muscles below the neurological level have a muscle grade of 3 or more; Grade E, normal. No motor or sensory deficits but deficits existed in the past. The total scores of motor function and sensory function evaluation were 100 and 224 points, respectively [14–16]. ASIA impairment scale evaluation is done by professionally trained physicians, and the physicians do not know the grouping and clinical baseline data of the subjects.

**2.5. Statistical Analysis.** All statistical calculations are performed using SPSS 20.0 (SPSS Inc., Chicago, IL, USA). Continuous variables are described by mean  $\pm$  standard deviation (SD), and categorical variables are described by numbers. Differences between groups were analyzed by one-way analysis of variance (ANOVA), and post hoc Newman-Keuls test was used for multiple groups. The correlation between variables is evaluated using the Pearson correlation coefficient. The statistical significance is set to 0.05.

## 3. Results

**3.1. Clinical Baseline Data.** The results of the clinical baseline data are shown in Table 1. The clinical baseline data of this study include age, gender, BMI, smoking, alcohol drinking, CHD, HBP, and DM. The results showed that there was no statistical difference between the clinical baseline data of the NC group and the SCI group ( $p > 0.05$ ).

**3.2. Serum Concentration of IL-37.** The concentration of serum IL-37 was determined by ELISA. The results of the serum concentration of IL-37 are shown in Figure 1 and Table 2. The results showed that the serum IL-37 concentrations of NC

TABLE 1: Clinical baseline data.

	NC ( <i>n</i> = 52)	SCI ( <i>n</i> = 96)	<i>p</i>
Age (years)	49.38 ± 5.21	50.17 ± 5.09	0.373
Gender (male/female)	31/21	60/36	0.731
BMI (kg/m <sup>2</sup> )	24.75 ± 1.43	24.81 ± 1.50	0.814
Smoking ( <i>n</i> )	31	54	0.693
Alcohol drinking ( <i>n</i> )	36	61	0.487
CHD ( <i>n</i> )	4	7	0.929
HBP ( <i>n</i> )	8	17	0.719
DM ( <i>n</i> )	7	11	0.722

Abbreviation: NC: normal controls; SCI: spinal cord injury; BMI: body mass index; CHD: coronary heart disease; HBP: high blood pressure; DM: diabetes mellitus.

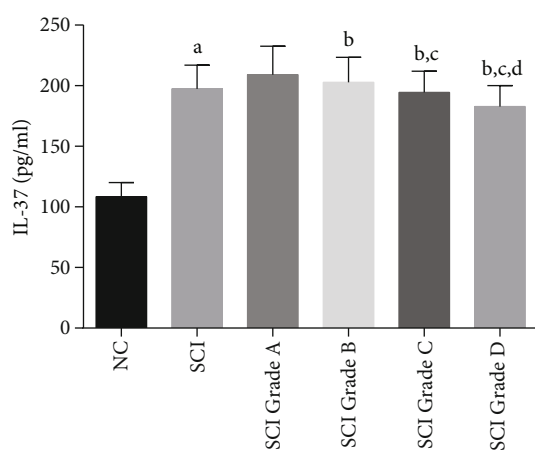


FIGURE 1: Serum concentration of IL-37. NC: normal controls; SCI: spinal cord injury. Compared with NC, <sup>a</sup> $p < 0.001$ ; compared with SCI Grade A, <sup>b</sup> $p < 0.05$ ; compared with SCI Grade B, <sup>c</sup> $p < 0.05$ ; compared with SCI Grade C, <sup>d</sup> $p < 0.05$ .

group and SCI group were (108.46 ± 11.74) pg/ml and (197.31 ± 19.68) pg/ml, respectively, and there was a statistical difference between the two ( $p < 0.05$ ). SCI patients are divided into four grades according to the AIS/A Impairment Scale, namely, Grade A, Grade B, Grade C, and Grade D. The serum IL-37 concentrations of patients with SCI Grade A, Grade B, Grade C, and Grade D were (209.16 ± 23.3) pg/ml, (202.75 ± 20.74) pg/ml, (194.52 ± 17.41) pg/ml, and (182.81 ± 17.22) pg/ml, and there are statistical differences among the four groups ( $p < 0.05$ ).

**3.3. Pearson Correlation Analysis.** The results of Pearson correlation analysis between IL-37 and ASIA motor score are shown in Figure 2. The results showed that in SCI patients, serum IL-37 concentration and ASIA motor score were negatively correlated ( $r = -0.327$ ,  $p < 0.05$ ).

## 4. Discussion

The main finding of this study is that the serum IL-37 concentration is elevated in SCI patients, and it is negatively correlated with ASIA motor scores. Further research found

that serum IL-37 can be used as a potential biomarker for the diagnosis of SCI. For the first time, we have confirmed the correlation between IL-37 and the prognosis of motor function in SCI patients.

The mechanism of SCI is complicated. In the early stages of SCI, mechanical damage causes local neurons and glial cells to die within minutes to hours. The subsequent delayed injury mainly manifested as neuronal and glial cell apoptosis and increased permeability of the blood-spinal cord barrier and neuroinflammatory response [17–19]. Neuroinflammation is an important mechanism of SCI, which can worsen the prognosis, so it is necessary to clarify the inflammatory mechanism of SCI.

IL-37 is a unique member of the IL-1 cytokine family, and its function is a natural inhibitor of inflammation and immune response [20]. Immune cells and nonimmune cells produce IL-37 precursors after proinflammatory stimulation, which is then activated and lysed by caspase-1 to transform into mature IL-37 and transfer to the nucleus, thereby inhibiting the transcription of proinflammatory genes [21, 22]. IL-37 is involved in the inflammatory process of a series of diseases, such as atherosclerosis, asthma, inflammatory bowel disease, psoriasis, rheumatoid arthritis, systemic lupus erythematosus, and ocular inflammatory diseases [7]. Interestingly, studies have pointed out that IL-37 is involved in the pathogenesis of multiple sclerosis, a neurological disease [23]. Iranian scholars found that the serum IL-37 concentration in patients with multiple sclerosis and optic neuromyelitis increased, suggesting that IL-37 is involved in its pathophysiological mechanism [24]. There are also animal experiments that show that the secretions of human periodontal ligament cells pretreated with hypoxia can have anti-inflammatory effects through IL-37 in multiple sclerosis experimental models [25]. The role of IL-37 in nerve injury-related diseases is gradually receiving attention from basic to clinical.

IL-37 may be one of the potential mechanisms involved in the pathogenesis of SCI. Marina Coll-Miró and his colleagues found that the SCI model made using IL-37 transgenic mice showed lower levels of proinflammatory factor secretion and less neurological damage. At the same time, exogenous administration of recombinant IL-37 can reduce the symptoms of SCI and further enhance IL-37's neuroprotective effect on SCI injury [10]. In order to further explore the neuroprotective mechanism of IL-37 on SCI, researchers from many countries have conducted a series of studies in a variety of genetically modified animals. Studies have proved that the translocation of IL-37 to the nucleus is not necessary for the neuroprotection of SCI, but the signal transduction of IL-37 outside the cell plays a decisive role [19]. However, we first confirmed the correlation between IL-37 and SCI in a clinical study.

Our research has some limitations. First, our sample size is small. Second, we are a single-center study, and its results may not be applicable to people from other regions or races. Third, we did not conduct dynamic monitoring of serum IL-37 nor did we conduct long-term follow-up of patients with SCI. Nevertheless, as far as we know, our study reported for the first time that IL-37 is involved in the pathogenesis of clinical SCI patients, which has important inspiration for the prevention and treatment of SCI.

TABLE 2: Serum concentration of IL-37.

	NC	Total	Grade A	SCI Grade B	Grade C	Grade D
IL-37 (pg/ml)	108.46 ± 11.74	197.31 ± 19.68 <sup>a</sup>	209.16 ± 23.35	202.75 ± 20.74 <sup>b</sup>	194.52 ± 17.41 <sup>b,c</sup>	182.81 ± 17.22 <sup>b,c,d</sup>

Abbreviation: NC: normal controls; SCI: spinal cord injury; IL-37: interleukin 37; ASIA: American Spinal Cord Injury Association; SCI: spinal cord injury; IL-37: interleukin 37. Compared with NC, <sup>a</sup> $p < 0.001$ ; compared with SCI Grade A, <sup>b</sup> $p < 0.05$ ; compared with SCI Grade B, <sup>c</sup> $p < 0.05$ ; compared with SCI Grade C, <sup>d</sup> $p < 0.05$ .

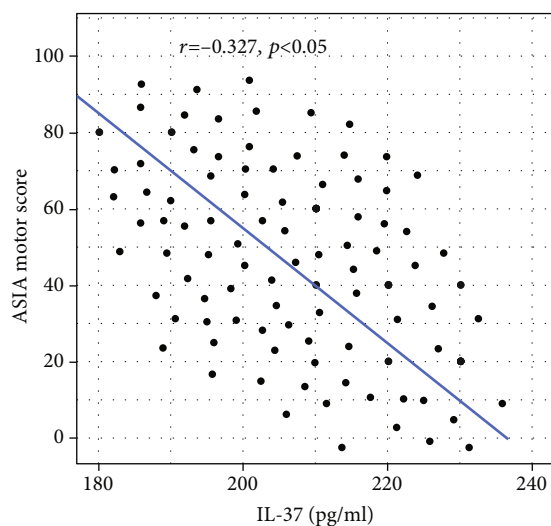


FIGURE 2: Pearson correlation analysis between IL-37 and ASIA motor score in SCI. ASIA: American Spinal Cord Injury Association; SCI: spinal cord injury.

## 5. Conclusions

Our research shows that the serum IL-37 of patients with SCI is significantly increased, and it is obviously related to the grades of SCI. That is, the more severe the SCI condition, the higher the serum SCI level. At the same time, serum IL-37 was significantly negatively correlated with the ASIA motor score of SCI, suggesting that IL-37 in the acute phase can predict the prognosis of SCI. Finally, serum IL-37 may be a potential biomarker for predicting SCI.

## Data Availability

The data used to support the findings of this study are available from the corresponding author upon request.

## Conflicts of Interest

All the authors declare no conflict of interests.

## Authors' Contributions

Yuanzhen Chen and Dandan Wang are co-first authors and they contributed equally to this work.

## Acknowledgments

All the authors are thankful to Neck-Shoulder and Lumbo-crural Pain Hospital, Shandong First Medical University & Shandong Academy of Medical Sciences, Jinan, China.

## References

- [1] L. D. Hachem, C. S. Ahuja, and M. G. Fehlings, "Assessment and management of acute spinal cord injury: from point of injury to rehabilitation," *The Journal of Spinal Cord Medicine*, vol. 40, no. 6, pp. 665–675, 2017.
- [2] T. A. Spoltore and A. M. O'Brien, "Rehabilitation of the spinal cord injured patient," *Orthopedic Nursing*, vol. 14, no. 3, pp. 7–14, 1995, quiz 15-6.
- [3] J. H. Badhiwala, J. R. Wilson, and M. G. Fehlings, "Global burden of traumatic brain and spinal cord injury," *The Lancet Neurology*, vol. 18, no. 1, pp. 24–25, 2019.
- [4] M. J. Eckert and M. J. Martin, "Trauma: spinal cord injury," *Surgical Clinics*, vol. 97, no. 5, pp. 1031–1045, 2017.
- [5] S. Kumar, P. C. McDonnell, R. Lehr et al., "Identification and initial characterization of four novel members of the interleukin-1 family," *Journal of Biological Chemistry*, vol. 275, no. 14, pp. 10308–10314, 2000.
- [6] M. F. Nold, C. A. Nold-Petry, J. A. Zepp, B. E. Palmer, P. Bufler, and C. A. Dinarello, "IL-37 is a fundamental inhibitor of innate immunity," *Nature Immunology*, vol. 11, no. 11, pp. 1014–1022, 2010.
- [7] J. Bai, Y. Li, M. Li, S. Tan, and D. Wu, "IL-37 as a potential biotherapeutics of inflammatory diseases," *Current Drug Targets*, vol. 21, no. 9, pp. 855–863, 2020.
- [8] W.-D. Xu, Y. Zhao, and Y. Liu, "Insights into IL-37, the role in autoimmune diseases," *Autoimmunity Reviews*, vol. 14, no. 12, pp. 1170–1175, 2015.
- [9] P. Conti, G. Lessiani, S. K. Kritas, G. Ronconi, A. Caraffa, and T. C. Theoharides, "Mast cells emerge as mediators of atherosclerosis: special emphasis on IL-37 inhibition," *Tissue and Cell*, vol. 49, no. 3, pp. 393–400, 2017.
- [10] M. Coll-Miró, I. Francos-Quijorna, E. Santos-Nogueira et al., "Beneficial effects of IL-37 after spinal cord injury in mice," *Proceedings of the National Academy of Sciences*, vol. 113, no. 5, pp. 1411–1416, 2016.
- [11] J. J. van Middendorp, B. Goss, S. Urquhart, S. Atresh, R. P. Williams, and M. Schuetz, "Diagnosis and prognosis of traumatic spinal cord injury," *Global Spine Journal*, vol. 1, no. 1, pp. 001–007, 2011.
- [12] J. Zhang, L. Tang, J. Hu, Y. Wang, and Y. Xu, "Uric acid is associated with cognitive impairment in the elderly patients receiving maintenance hemodialysis—a two-center study," *Brain and Behavior: A Cognitive Neuroscience Perspective*, vol. 10, no. 3, article e01542, 2020.

- [13] W. P. Waring III, F. Biering-Sorensen, S. Burns et al., “2009 review and revisions of the international standards for the neurological classification of spinal cord injury,” *The Journal of Spinal Cord Medicine*, vol. 33, no. 4, pp. 346–352, 2016.
- [14] B. Gündüz, “ASIA update-ASIA impairment scale: level determination, classification, and examples,” *Turkish Journal of Physical Medicine and Rehabilitation*, vol. 61, no. 1, pp. 25–531, 2015.
- [15] S. G. Pneumaticos, G. K. Triantafyllopoulos, and N. G. Lasanianos, “American spinal injury association-ASIA-impairment scale for neurological deficit,” in *Trauma and Orthopaedic Classifications*, pp. 227–228, Springer, 2015.
- [16] T. T. Roberts, G. R. Leonard, and D. J. Cepela, *Classifications in brief: American spinal injury association (ASIA) impairment scale*, Springer, 2017.
- [17] R. Rust and J. Kaiser, “Insights into the dual role of inflammation after spinal cord injury,” *Journal of Neuroscience*, vol. 37, no. 18, pp. 4658–4660, 2017.
- [18] J. Tremoleda, O. Thau-Zuchman, M. Davies et al., “In vivo PET imaging of the neuroinflammatory response in rat spinal cord injury using the TSPO tracer [18F]GE-180 and effect of docosahexaenoic acid,” *European Journal of Nuclear Medicine and Molecular Imaging*, vol. 43, no. 9, pp. 1710–1722, 2016.
- [19] J. Amo-Aparicio, A. Sanchez-Fernandez, S. Li et al., “Extracellular and nuclear roles of IL-37 after spinal cord injury,” *Brain, Behavior, and Immunity*, 2020.
- [20] H. Jia, J. Liu, and B. Han, “Reviews of interleukin-37: functions, receptors, and roles in diseases,” *BioMed Research International*, vol. 2018, 14 pages, 2018.
- [21] A.-M. Bulau, M. F. Nold, S. Li et al., “Role of caspase-1 in nuclear translocation of IL-37, release of the cytokine, and IL-37 inhibition of innate immune responses,” *Proceedings of the National Academy of Sciences*, vol. 111, no. 7, pp. 2650–2655, 2014.
- [22] C. A. Dinarello and P. Bufler, “Interleukin-37,” in *Seminars in immunology*, Elsevier, 2013.
- [23] X. Wang, K. Xu, S. Chen, Y. Li, and M. Li, “Role of interleukin-37 in inflammatory and autoimmune diseases,” *Iranian Journal of Immunology*, vol. 15, no. 3, pp. 165–174, 2018.
- [24] M. Farrokhi, A. Rezaei, A. Amani-Beni, M. Etemadifar, E. Kouchaki, and A. Zahedi, “Increased serum level of IL-37 in patients with multiple sclerosis and neuromyelitis optica,” *Acta Neurologica Belgica*, vol. 115, no. 4, pp. 609–614, 2015.
- [25] S. Giacoppo, S. R. Thangavelu, F. Diomedea et al., “Anti-inflammatory effects of hypoxia-preconditioned human periodontal ligament cell secretome in an experimental model of multiple sclerosis: a key role of IL-37,” *The FASEB Journal*, vol. 31, no. 12, pp. 5592–5608, 2017.



## Research Article

# Serum CCL21 as a Potential Biomarker for Cognitive Impairment in Spinal Cord Injury

Yuanzhen Chen,<sup>1</sup> Liangke Liang,<sup>2</sup> Shengnan Cao,<sup>3</sup> Guangjian Hou,<sup>1</sup> Qian Zhang,<sup>4</sup> Hong Ma ,<sup>2</sup> and Bin Shi <sup>1</sup>

<sup>1</sup>Neck-Shoulder and Lumbocrural Pain Hospital, Shandong First Medical University & Shandong Academy of Medical Sciences, Jinan, 250014 Shandong Province, China

<sup>2</sup>Foshan Traditional Chinese Medicine Hospital, Foshan, 528000 Guangdong Province, China

<sup>3</sup>School of Acupuncture-Tuina, Shandong University of Traditional Chinese Medicine, Jinan, 250355 Shandong Province, China

<sup>4</sup>Taian City Central Hospital, Taian, 271000 Shandong Province, China

Correspondence should be addressed to Hong Ma; fozhongyimahong@qq.com and Bin Shi; sdyky-shibin@163.com

Received 22 November 2020; Revised 30 November 2020; Accepted 2 December 2020; Published 10 December 2020

Academic Editor: Yuzhen Xu

Copyright © 2020 Yuanzhen Chen et al. This is an open access article distributed under the Creative Commons Attribution License, which permits unrestricted use, distribution, and reproduction in any medium, provided the original work is properly cited.

**Objective.** Cognitive impairment is considered to be an important complication of spinal cord injury (SCI), but its underlying mechanism remains unclear. The purpose of this study is to explore whether serum CCL21 can be used as a potential biomarker of cognitive impairment in SCI. **Methods.** In Neck-Shoulder and Lumbocrural Pain Hospital, Shandong First Medical University & Shandong Academy of Medical Sciences, hospitalized or treated acute SCI patients were included in the study as the SCI group (SCI). At the same time, a normal control group (NC) matching the age and sex of the SCI group was recruited in the outpatient clinic. Once the two groups were enrolled, their demographics and clinical characteristics were collected immediately. Enzyme-linked immunosorbent assay (ELISA) was used to detect serum CCL21 levels within 24 hours of admission. Three months later, the Montreal Cognitive Assessment (MoCA) was used to test the cognitive function of the population. **Results.** A total of 84 SCI patients and 49 NC populations were eligible for inclusion in the study. There was no significant statistical difference in the demographics and clinical characteristics (age, gender, BMI, TG, LDL-C, FBG, SBP, and DBP) between the two groups ( $p > 0.05$ ). Compared with the NC group, the SCI group had a higher serum CCL21 level ( $p < 0.001$ ) and a lower MoCA score ( $p < 0.001$ ). Serum CCL21 level in SCI was negatively correlated with MoCA score ( $p = 0.023$ ). Multivariable analyses showed that serum CCL21 level is an independent prognostic factor of cognitive impairment in SCI. **Conclusions.** MoCA score has a linear relationship with serum CCL21 quartile, and SCI cognitive function has a negative correlation with serum CCL21. Serum CCL21 is an independent risk factor for cognitive impairment after SCI.

## 1. Introduction

Spinal cord injury (SCI) can be defined as the injury caused by complete or incomplete damage to the motor function, sensory function, autonomic nerve, and reflex after the spinal cord is injured [1]. SCI is a common and highly destructive neurological disease, which has a profound impact on society from the perspectives of physiology, psychology, economy, family, and culture [2, 3]. The incidence of SCI is on the rise globally, with an estimated incidence of 10.4-83 per million per year. The incidence of SCI is 20.7-83.0 in North America, 8.0-130.6 in Europe, and 23.7-60.6 in China [4]. As there is

currently no effective treatment for SCI, patients with SCI have to bear a considerable economic burden in terms of treatment and rehabilitation [5]. Among the many complications of SCI, cognitive impairment has received more and more attention in recent years. According to reports, 40-60% of patients with SCI may have varying degrees of cognitive impairment [6]. However, the mechanism of cognitive impairment after SCI remains unclear.

Chemokines are chemotactic cytokines that coordinate the localization of cells including immune cells [7]. Chemokines play a key role in various processes, including the development and homeostasis of immune cells, the initiation of



innate and adaptive immune responses, and the recruitment of immune cells under pathological conditions [8]. CCL21 is an effective microglia-activating chemokine, which is synthesized by damaged neurons, transported by axons, and then released to activate microglia [9]. CCL21 is only expressed in injured neurons in the central nervous system and can quickly cause neuroinflammation in the injured local and remote sites [10]. CCL21 in vivo mainly plays a pathophysiological role through two receptors: CCR7 and CXCR3 [11]. However, the mechanism of CCL21 involved in nerve damage is still unclear, and it is a hotspot for future research.

The possible mechanism for the high risk of dementia in SCI patients is posttraumatic neuroinflammation and related neurodegeneration [12]. Chemotactic cytokines are important factors that initiate and participate in the inflammatory process [13]. The role of CCL21 in SCI has received considerable attention in recent years. The purpose of this study is to explore whether serum CCL21 can be used as a potential biomarker of cognitive impairment in SCI.

## 2. Methods

**2.1. Study Population.** Acute SCI patients who were treated at the Neck-Shoulder and Lumbocrural Pain Hospital, Shandong First Medical University & Shandong Academy of Medical Sciences, from March 2017 to February 2020 were included in this study. The diagnosis of SCI is based on the diagnostic criteria of the guidelines [14, 15]. Enrollment criteria are as follows: (1) SCI patients within 24 hours of onset; (2) 18-80 years old; and (3) able to complete relevant examinations. Exclusion criteria are as follows: (1) head injury; (2) unconsciousness or history of mental illness; (3) inflammatory disease or autoimmune disease; (4) suffering from cognitive dysfunction such as Alzheimer's disease (AD) and vascular dementia (VaD); (5) tumor; and (6) unable to complete related examinations. The study was approved by the local ethics committee. The research subjects were informed of the study, and informed consent was signed by them or their guardians.

**2.2. Demographics and Clinical Characteristics.** Once enrolled in the group, the demographics and clinical characteristics of the study population are registered. The demographics and clinical characteristics include age, gender, body mass index (BMI), triglycerides (TG), low-density lipoprotein cholesterol (LDL-C), fasting plasma glucose (FBG), systolic blood pressure (SBP), and diastolic blood pressure (DBP). Questionnaires are used to collect demographic data. The clinical characteristics are obtained by applying standard laboratory testing methods.

**2.3. Serum CCL21 Levels.** Collect 5 ml of fasting venous blood from all study populations within 24 hours of admission. The sample should be collected in a serum separation tube. After clot formation, centrifuge at  $2000 \times g$  for 10 minutes to collect serum. The sample is diluted into sample diluent NS and measured. Store the undiluted serum in aliquots at  $-20^{\circ}\text{C}$  or below for later use. Enzyme-linked immunosorbent assay (ELISA) was used to detect the level of serum CCL2.

TABLE 1: Demographics and clinical characteristics.

	NC ( $n = 49$ )	SCI ( $n = 84$ )	$p$
Age (years)	$46.62 \pm 4.98$	$47.31 \pm 5.03$	0.445
Gender (male/female)	35/14	56/28	0.569
BMI ( $\text{kg}/\text{m}^2$ )	$24.53 \pm 1.66$	$24.92 \pm 1.72$	0.204
TG ( $\text{mmol}/\text{L}$ )	$1.51 \pm 0.19$	$1.54 \pm 0.21$	0.412
LDL-C ( $\text{mmol}/\text{L}$ )	$2.43 \pm 0.25$	$2.49 \pm 0.28$	0.218
FBG ( $\text{mmol}/\text{L}$ )	$5.86 \pm 0.57$	$5.90 \pm 0.64$	0.718
SBP ( $\text{mmHg}$ )	$139.8 \pm 12.3$	$141.1 \pm 13.7$	0.585
DBP ( $\text{mmHg}$ )	$88.3 \pm 9.4$	$90.5 \pm 10.6$	0.231
CCL21 ( $\text{pg}/\text{ml}$ )	$41.3 \pm 5.2$	$119.7 \pm 13.5$	<0.001
MoCA (points)	$28.2 \pm 1.2$	$24.6 \pm 1.9$	<0.001

NC: normal controls; SCI: spinal cord injury; BMI: body mass index; TG: triglycerides; LDL-C: low-density lipoprotein cholesterol; FBG: fasting plasma glucose; SBP: systolic blood pressure; DBP: diastolic blood pressure; CCL21: chemokine (C-C motif) ligand 21; MoCA: Montreal Cognitive Assessment.

CCL2 antibody is a purchased commercial reagent (Abcam, MA, USA). The steps of ELISA refer to previous reports and reagent instructions [16]. Record the OD at 450 nm under a spectrophotometer.

**2.4. Cognitive Function Evaluation.** The evaluation of cognitive function uses the Montreal Cognitive Assessment (MoCA). MoCA is a widely used screening tool to detect cognitive impairment, which was created by Ziad Nasreddine in Montreal in 1996. MoCA has good sensitivity and specificity and is especially suitable for the detection of mild cognitive impairment. It has been widely used in many countries. The MoCA test is a test with a total score of 30 points and is completed in approximately 10 minutes. A score of 26 or more is considered normal [17]. The evaluation of MoCA is completed by professionally trained physicians, who are blind to the grouping and baseline data of the study population.

**2.5. Statistical Analysis.** The quantitative data of the normal distribution is expressed by the mean  $\pm$  standard deviation (SD), and the qualitative data is expressed by the rate. The comparison of quantitative data uses  $t$ -test, and the comparison of qualitative data uses nonparametric test. According to the quartile of serum CCL21, subjects were divided into four groups with the same sample size. Multivariable analyses were used to explore independent predictors of cognitive impairment after SCI. The SPSS version 20.0 (SPSS, Chicago, IL, USA) was used for statistical analysis, and  $p < 0.05$  was considered statistically significant.

## 3. Results

**3.1. Demographics and Clinical Characteristics.** A total of 133 subjects were recruited for this study, including 49 NC and 84 SCI patients. The demographics and clinical characteristics are shown in Table 1. In terms of age, gender, BMI, TG, LDL-C, FBG, SBP, and DBP, there was no significant

TABLE 2: Relationship between serum CCL21 and MoCA.

Variable	Serum CCL21 levels (pg/ml)				<i>p</i>
	Q1	Q2	Q3	Q4	
MoCA (point)	25.7 ± 1.2	24.9 ± 1.5	24.0 ± 1.7	22.6 ± 2.0	0.023

CCL21: chemokine (C-C motif) ligand 21; MoCA: Montreal Cognitive Assessment.

difference between the NC group and the SCI group ( $p > 0.05$ ). However, the CCL21 levels of the NC group and SCI group were  $41.3 \pm 5.2$  pg/ml and  $119.7 \pm 13.5$  pg/ml, respectively. The CCL21 level of the SCI group was significantly higher than that of the NC group, and there was a significant statistical difference between the two groups ( $p < 0.05$ ). In addition, the MoCA scores of the NC group and SCI group were  $28.2 \pm 1.2$  points and  $24.6 \pm 1.9$  points, respectively. The MoCA score of the SCI group was significantly lower than that of the NC group, and there was a significant statistical difference between the two groups ( $p < 0.05$ ).

**3.2. Relationship between Serum CCL21 and Cognitive Function in SCI.** According to the serum CCL21 quartile, the MoCA scores of SCI patients are shown in Table 2. The results showed that the MoCA score of SCI patients had a linear relationship with the quartile of serum CCL21; that is, the MoCA score of SCI patients decreased with the increase of serum CCL21 level ( $p = 0.023$ ).

**3.3. Independent Risk Factors for Cognitive Impairment with Multivariable Analyses in SCI.** The results of multivariable analyses are shown in Table 3. Multivariable analyses showed that serum CCL21 is an independent predictor of cognitive impairment after SCI ( $\beta = 0.328$ ,  $p = 0.027$ ). After adjusting for confounding factors such as age, gender, BMI, TG, LDL-C, FBG, SBP, and DBP, serum CCL21 still has a predictive effect on cognitive impairment after SCI.

## 4. Discussion

The main finding of the current study is that compared with the NC group, the serum CCL21 level in the SCI group was significantly increased, and the serum CCL21 level was negatively correlated with the MoCA score. Further research found that serum CCL21 can be used as a potential biomarker for the diagnosis of cognitive impairment after SCI. Our study confirmed for the first time the correlation between serum CCL21 and the prognosis of cognitive function in patients with SCI.

More and more evidences show that cognitive impairment is a complication of SCI. Zhang et al. observed mitochondrial swelling and vacuolation of the endoplasmic reticulum in the hippocampus in a pig thoracic spinal cord injury model, accompanied by a decline in learning and memory [18]. This is the first animal experiment to confirm the correlation between spinal cord injury and deterioration of brain cognitive function. In addition, in the rodent SCI model, we can not only observe long-term deficits in motor function but also gradually lose cognitive ability after 8 weeks of modeling [19, 20]. Not only in animal models but also in

TABLE 3: Multivariable analyses of risk factors with MoCA in SCI.

	Regression coefficient	<i>p</i>	95% CI
Age (years)	0.181	0.219	0.108-1.275
Male	0.346	0.393	0.298-1.201
BMI (kg/m <sup>2</sup> )	0.239	0.168	0.117-1.093
TG (mmol/L)	0.256	0.475	0.162-1.154
LDL-C (mmol/L)	0.266	0.311	0.143-1.138
FBG (mmol/L)	0.398	0.279	0.154-1.219
SBP (mmHg)	0.387	0.638	0.229-1.132
DBP (mmHg)	0.309	0.446	0.195-1.213
CCL21 (pg/ml)	0.328	0.027	0.202-0.807

MoCA: Montreal Cognitive Assessment; SCI: spinal cord injury; BMI: body mass index; TG: triglycerides; LDL-C: low-density lipoprotein cholesterol; FBG: fasting plasma glucose; SBP: systolic blood pressure; DBP: diastolic blood pressure; CCL21: chemokine (C-C motif) ligand 21.

human cognitive impairment after SCI has been reported in recent years. A US study of SCI patients in residential communities showed that after SCI, the risk of cognitive impairment is increased, mainly impairing patients' processing speed and executive function for specific tasks [21].

Although cognitive impairment after SCI has been widely reported, its underlying pathophysiological mechanism remains unclear [22]. SCI produces cell debris and releases intracellular proteins, which can induce a strong inflammatory response. In an inflammatory state, resident inflammatory cells, including astrocytes and microglia, are rapidly activated to release a variety of inflammatory mediators such as regulatory factors, cytokines, chemokines, and growth factors [23]. The release of chemokines and cytokines can recruit surrounding neutrophils and macrophages into the injured spinal cord. The first wave of infiltrating immune cells is neutrophils. Neutrophils have a bactericidal effect and are considered to be the first line of defense against invaders [24]. They are also considered to be the main contributor to SCI pathological damage. A Canadian study showed that the expression of IL-1 $\beta$ , an inflammatory factor in the central nervous system, can increase 15 minutes to 3 hours after SCI, and it can last for 24 hours. This inflammatory response was weakened in the IL-1 $\beta$  gene knockout mouse model of SCI, confirming that inflammation is involved in the acute injury of SCI [25]. A recent study showed that the expression of CD200 was downregulated after SCI, thereby attenuating the signal transduction of the CD200-CD200R1 axis and increasing neuroinflammation [26]. The above studies suggest that intervention of inflammation may be an important means to improve the prognosis of SCI.

CCL21 is an effective microglia-activating chemokine, and its role in SCI has recently been reported. Research by Honjoh and his colleagues showed that compared with

wild-type mice, the number of classically activated (M1 phenotype) microglia in mice with low expression of CCL21 gene mutations in the SCI model was significantly reduced [27]. This study suggests that CCL21 may be an important target for intervention in neuroinflammation after SCI. Research by Zhao et al. showed that after SCI, it can induce the upregulation of the neuroimmunomodulator CCL21 in the thalamus, thereby further enhancing the microglia-related inflammatory response associated with pain phenomena [28]. However, the specific mechanism of CCL21 involved in nerve damage after SCI is still unclear.

CCL21 has been reported in animal studies on cognitive impairment after SCI [20]. In different degrees of SCI mouse models, the upregulation of CCL21 and the activation of microglia can be seen, as well as neuron loss, hippocampal neurogenesis, and cognitive decline. The accumulation of CCL21 in the brain may be a potential target of cognitive impairment after SCI. However, our study confirmed the correlation between CCL21 and cognitive function in human SCI for the first time. This is the strength of our research. However, our research has limitations. First, this is a single-center study with a small sample; second, we did not monitor the dynamic changes of serum CCL21; and third, we did not collect information on the subjects' medications, which may interfere with our research results.

## 5. Conclusions

Serum CCL21 levels increased significantly after SCI. Moreover, serum CCL21 levels are significantly negatively correlated with cognitive function after SCI. After adjusting for confounding factors, the correlation between serum CCL21 and cognitive function after SCI still exists. These results suggest that serum CCL21 may be a potential biomarker for predicting cognitive impairment after SCI.

## Data Availability

The data used to support the findings of this study are available from the corresponding author upon request.

## Conflicts of Interest

All the authors declare no conflict of interests.

## Authors' Contributions

Yuanzhen Chen and Liangke Liang are co-first authors, and they contributed equally to this work.

## Acknowledgments

All the authors are thankful to Neck-Shoulder and Lumbar Pain Hospital, Shandong First Medical University & Shandong Academy of Medical Sciences, Jinan, China.

## References

- [1] Y. Kang, H. Ding, H. Zhou et al., "Epidemiology of worldwide spinal cord injury: a literature review," *Journal of Neurorestoration*, vol. 6, pp. 1–9, 2018.
- [2] R. Sweis and J. Biller, "Systemic complications of spinal cord injury," *Current Neurology and Neuroscience Reports*, vol. 17, pp. 1–8, 2017.
- [3] R. J. Dumont, D. O. Okonkwo, S. Verma et al., "Acute spinal cord injury, part I: pathophysiologic mechanisms," *Clinical Neuropharmacology*, vol. 24, no. 5, pp. 254–264, 2001.
- [4] S. Yuan, Z. Shi, F. Cao, J. Li, and S. Feng, "Epidemiological features of spinal cord injury in China: a systematic review," *Frontiers in Neurology*, vol. 9, p. 683, 2018.
- [5] H. Krueger, V. Noonan, L. Trenaman, P. Joshi, and C. Rivers, "The economic burden of traumatic spinal cord injury in Canada," *Chronic Diseases and Injuries in Canada*, vol. 33, no. 3, pp. 113–122, 2013.
- [6] Y. Li, T. Cao, R. M. Ritzel, J. He, A. I. Faden, and J. Wu, "Dementia, depression, and associated brain inflammatory mechanisms after spinal cord injury," *Cell*, vol. 9, 2020.
- [7] C. E. Hughes and R. J. Nibbs, "A guide to chemokines and their receptors," *The FEBS Journal*, vol. 285, no. 16, pp. 2944–2971, 2018.
- [8] K. Chen, Z. Bao, P. Tang, W. Gong, T. Yoshimura, and J. M. Wang, "Chemokines in homeostasis and diseases," *Cellular & Molecular Immunology*, vol. 15, no. 4, pp. 324–334, 2018.
- [9] K. Biber, M. Tsuda, H. Tozaki-Saitoh et al., "Neuronal CCL21 up-regulates microglia P2X4 expression and initiates neuropathic pain development," *The EMBO Journal*, vol. 30, no. 9, pp. 1864–1873, 2011.
- [10] P. Zhao, S. G. Waxman, and B. C. Hains, "Modulation of thalamic nociceptive processing after spinal cord injury through remote activation of thalamic microglia by cysteine–cysteine chemokine ligand 21," *Journal of Neuroscience*, vol. 27, no. 33, pp. 8893–8902, 2007.
- [11] M. A. Hauser and D. F. Legler, "Common and biased signaling pathways of the chemokine receptor CCR7 elicited by its ligands CCL19 and CCL21 in leukocytes," *Journal of Leukocyte Biology*, vol. 99, no. 6, pp. 869–882, 2016.
- [12] A. I. Faden, J. Wu, B. A. Stoica, and D. J. Loane, "Progressive inflammation-mediated neurodegeneration after traumatic brain or spinal cord injury," *British Journal of Pharmacology*, vol. 173, no. 4, pp. 681–691, 2016.
- [13] G. Ramesh, A. G. Mac Lean, and M. T. Philipp, "Cytokines and chemokines at the crossroads of neuroinflammation, neurodegeneration, and neuropathic pain," *Mediators of Inflammation*, vol. 2013, 20 pages, 2013.
- [14] J. J. van Middendorp, B. Goss, S. Urquhart, S. Atresh, R. P. Williams, and M. Schuetz, "Diagnosis and prognosis of traumatic spinal cord injury," *Global spine journal*, vol. 1, no. 1, pp. 001–007, 2011.
- [15] K. A. Martin Ginis, J. W. van der Scheer, A. E. Latimer-Cheung et al., "Evidence-based scientific exercise guidelines for adults with spinal cord injury: an update and a new guideline," *Spinal Cord*, vol. 56, no. 4, pp. 308–321, 2018.
- [16] J. Zhang, L. Tang, J. Hu, Y. Wang, and Y. Xu, "Uric acid is associated with cognitive impairment in the elderly patients receiving maintenance hemodialysis—a two-center study," *Brain and Behavior: A Cognitive Neuroscience Perspective*, vol. 10, article e01542, 2020.

- [17] Y. Xu, Q. Wang, Y. Liu, R. Cui, and Y. Zhao, "Is *Helicobacter pylori* infection a critical risk factor for vascular dementia?," *The International Journal of Neuroscience*, vol. 126, no. 10, pp. 899–903, 2016.
- [18] B. Zhang, Y. Huang, Z. Su et al., "Neurological, functional, and biomechanical characteristics after high-velocity behind armor blunt trauma of the spine," *The Journal of Trauma*, vol. 71, pp. 1680–1688, 2011.
- [19] J. Wu, B. A. Stoica, T. Luo et al., "Isolated spinal cord contusion in rats induces chronic brain neuroinflammation, neurodegeneration, and cognitive impairment: involvement of cell cycle activation," *Cell Cycle*, vol. 13, no. 15, pp. 2446–2458, 2014.
- [20] J. Wu, Z. Zhao, A. Kumar et al., "Endoplasmic reticulum stress and disrupted neurogenesis in the brain are associated with cognitive impairment and depressive-like behavior after spinal cord injury," *Journal of Neurotrauma*, vol. 33, no. 21, pp. 1919–1935, 2016.
- [21] M. L. Cohen, D. S. Tulskey, J. A. Holdnack et al., "Cognition among community-dwelling individuals with spinal cord injury," *Rehabilitation Psychology*, vol. 62, no. 4, pp. 425–434, 2017.
- [22] R. Sachdeva, F. Gao, C. C. Chan, and A. V. Krassioukov, "Cognitive function after spinal cord injury: a systematic review," *Neurology*, vol. 91, no. 13, pp. 611–621, 2018.
- [23] P. Gál, P. Kravčuková, M. Mokry, and D. Kluchová, "Chemokines as possible targets in modulation of the secondary damage after acute spinal cord injury: a review," *Cellular and Molecular Neurobiology*, vol. 29, no. 6-7, pp. 1025–1035, 2009.
- [24] V. Neirinckx, C. Coste, R. Franzen, A. Gothot, B. Rogister, and S. Wislet, "Neutrophil contribution to spinal cord injury and repair," *Journal of Neuroinflammation*, vol. 11, pp. 1–9, 2014.
- [25] T. Rice, J. Larsen, S. Rivest, and V. W. Yong, "Characterization of the early neuroinflammation after spinal cord injury in mice," *Journal of Neuropathology and Experimental Neurology*, vol. 66, no. 3, pp. 184–195, 2007.
- [26] N. Lago, B. Pannunzio, J. Amo-Aparicio, R. López-Vales, and H. Peluffo, "CD200 modulates spinal cord injury neuroinflammation and outcome through CD200R1," *Brain, Behavior, and Immunity*, vol. 73, pp. 416–426, 2018.
- [27] K. Honjoh, H. Nakajima, T. Hirai, S. Watanabe, and A. Matsumine, "Relationship of inflammatory cytokines from M1-type microglia/macrophages at the injured site and lumbar enlargement with neuropathic pain after spinal cord injury in the CCL21 knockout (plt) mouse," *Frontiers in Cellular Neuroscience*, vol. 13, p. 525, 2019.
- [28] P. Zhao, S. G. Waxman, and B. C. Hains, "Extracellular signal-regulated kinase-regulated microglia-neuron signaling by prostaglandin E2 contributes to pain after spinal cord injury," *The Journal of Neuroscience*, vol. 27, no. 9, pp. 2357–2368, 2007.



## Research Article

# The Role of miRNA-146a and Proinflammatory Cytokines in Carotid Atherosclerosis

Pan Huang <sup>1</sup>, Xiao-ying He <sup>2</sup>, and Min Xu <sup>3</sup>

<sup>1</sup>Department of Neurology, People's Hospital of Deyang City, 173 Taishan North Road, Deyang, Sichuan 618000, China

<sup>2</sup>Department of Neurology, The Affiliated Hospital of Southwest Medical University, No. 25, Taiping Street, Jiangyang District, Luzhou, Sichuan Province, Sichuan 646000, China

<sup>3</sup>Department of Neurology, The Second People's Hospital of Deyang City, 340 Minjiang West Road, Deyang, Sichuan 618000, China

Correspondence should be addressed to Min Xu; 782067723@qq.com

Received 31 October 2020; Revised 16 November 2020; Accepted 24 November 2020; Published 10 December 2020

Academic Editor: Yuzhen Xu

Copyright © 2020 Pan Huang et al. This is an open access article distributed under the Creative Commons Attribution License, which permits unrestricted use, distribution, and reproduction in any medium, provided the original work is properly cited.

The aim of this study was to investigate the expression and significance of miRNA-146a in peripheral blood of patients with carotid atherosclerosis (CAS). Patients with CAS were selected as the stenosis (CAS) group ( $n = 180$ ). According to the degree of stenosis, they were divided into the mild stenosis group (MS group,  $n = 64$ ), moderate stenosis group (M group,  $n = 62$  cases), and severe stenosis group (SS group,  $n = 54$ ). According to the plaque type, patients were divided into a stable plaque group (SP group,  $n = 96$ ) and a vulnerable plaque group (VP group,  $n = 84$ ). Patients without CAS represented the normal group ( $n = 90$ ). The expression levels of miRNA-146a as well as IL-6 and TNF- $\alpha$  in peripheral blood were detected by RT-PCR and ELISA, respectively. The expression levels of miRNA-146a, IL-6, and TNF- $\alpha$  in the CAS group were higher than those in the normal group and positively correlated with the degree of stenosis and plaque vulnerability. The expression levels of miRNA-146a, IL-6, and TNF- $\alpha$  in the stable plaque group were lower than those in the vulnerable plaque group. The area under the curve of miRNA-146a predicting the vulnerability of plaques was significant at 0.641. The expression level of miRNA-146a in the CAS group was positively correlated with IL-6 and TNF- $\alpha$  levels. Our results indicate that miRNA-146a may participate in the occurrence and development of CAS by regulating the expression of IL-6 and TNF- $\alpha$ , which may be potential biomarkers of CAS.

## 1. Introduction

Carotid atherosclerosis (CAS) is the leading cause of cerebral infarction. Studies have shown that the rate of carotid stenosis is 50–69%, 70–89%, and 90% of the following annual risks of stroke: 0.8%, 1.4%, and 1.9%, respectively [1]. The rupturing of vulnerable plaques in cerebral blood vessels is the main mechanism of cerebral infarction [2] [3]. Therefore, early assessment of the degree of stenosis, CAS, and plaque vulnerability is important for preventing and reducing cerebral infarction. DSA is currently the “gold standard” with high sensitivity for CAS diagnosis; however, its general development is more difficult, and carotid ultrasound and MRI are not good for predicting early CAS or plaques. Due to the shortcomings of imaging technology, researchers have turned their attention to circulating blood biomarkers. CAS has been widely recognized as an inflammatory reactive

disease [4], and active inflammatory responses also increase plaque vulnerability [5], suggesting that inflammatory cytokines may be potential biomarkers for predicting CAS. However, subsequent studies demonstrated that the sensitivity and specificity of inflammatory cytokines to CAS are not high [6].

With the development of genetic technology, microRNA (miRNA) has gradually gained attention [7]. miRNA can be stably expressed in peripheral blood and has become a biological marker of various diseases. miRNA-146a has been shown to regulate inflammatory responses, which are associated with the process of CAS [8]. Therefore, we postulated that there is a differential expression profile of miRNA-146a in CAS patients. Furthermore, we investigated whether miRNA-146a expression is related to the degree of CAS stenosis and plaque vulnerability and whether miRNA-146a participates in the regulation of inflammatory responses



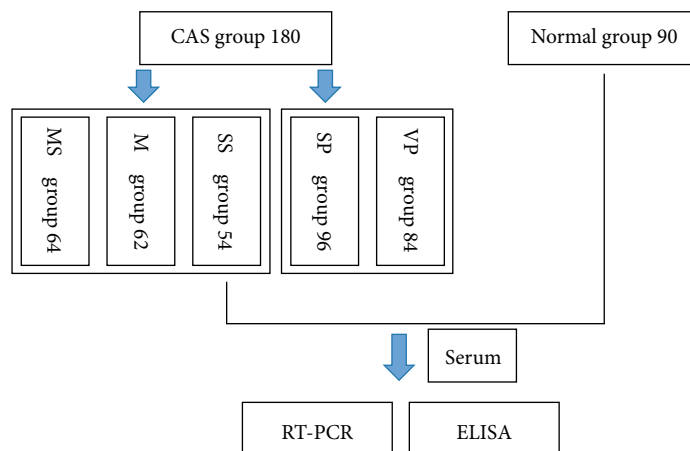


FIGURE 1: Flow chart of the inclusion process. MS: mild stenosis; M: moderate stenosis; SS: severe stenosis; SP: stable plaque; VP: vulnerable plaque.

and thus affects the occurrence of CAS and plaque vulnerability. To date, no study has addressed these mechanisms, and therefore, we investigated the expression of miRNA-146a in peripheral blood of CAS patients and its relationship with CAS stenosis, plaque vulnerability, and inflammatory cytokines. These findings may facilitate the discovery of biomarkers that could predict the degree of CAS stenosis and plaque vulnerability in the early stages of the disease.

## 2. Materials and Methods

**2.1. Study Type.** This study is a Nonrandomized Controlled Trial (nRCT).

**2.2. Research Subjects and Clinical Data.** In this study, 180 patients with CAS who were diagnosed by using carotid artery color Doppler in Deyang City People's Hospital were selected for the stenosis group. The inclusion criteria were as follows: there is compliance with color Doppler diagnosis for carotid intima-media thickening and atherosclerotic plaque formation, CT or MRI examination showed no cerebral infarction, cerebral hemorrhage, or other diseases, at least one risk factor was present (e.g., high blood pressure, diabetes, smoking, obesity, and hyperlipidemia), and patients are conscious and could cooperate until the test completion. The exclusion criteria were as follows: recent signs and symptoms of infection after relevant examinations, heart, liver, or kidney dysfunction, a history of combined immune system diseases and familial genetic diseases, malignant tumors or mobility problems, antibiotic use, and communication disorders that could prevent cooperation in the trial. According to the symptomatic classification of carotid stenosis in North America, the patients were divided into the following stenosis groups: mild stenosis group (MS group,  $n = 64$ ), moderate stenosis group (M group,  $n = 62$ ), and severe stenosis group (SS group,  $n = 54$ ). At the same time, all carotid ultrasounds were divided according to plaque characteristics, resulting in a stable plaque group (SP group,  $n = 96$ ) and a vulnerable plaque group (VP group,  $n = 84$ ). Patients without CAS ( $n = 90$ ) were selected for the control group (Figure 1).

In order to avoid bias, there was no statistically significant difference in age, gender, or risk factors between the stenosis and control groups ( $P > 0.05$ ).

**2.3. Specimen Collection and Serum Separation.** In the morning (after fasting), 5 ml samples of peripheral venous blood of the patient was taken and allowed to naturally coagulate for 10–20 min at room temperature. The coagulated blood sample was centrifuged for 30 min at 3000 rpm. One part of the supernatant was immediately used to detect routine clinical biochemical indicators (Beckman LX20 fully automated biochemical analyzer, USA), and the other part (peripheral blood mononuclear cell (PBMC)) was stored at  $-80^{\circ}\text{C}$  for total RNA extraction, RT-PCR, and ELISA.

**2.4. RT-PCR Detection of miRNA-146a Relative Expression.** After extracting total RNA according to the TRIzol kit (Invitrogen™, 15596-026), the value of  $O_{260}/O_{280}$  measured by the nucleic acid protein analyzer (Shanghai Qi Te, WXJ-9388) was regarded as quality RNA at 1.8–2.0, and then, M was used. The MLV reverse transcriptase kit for cDNA synthesis was used (Invitrogen™, C-28025). After first-strand cDNA synthesis, the RT-PCR reaction mixture was placed in 96 wells of a PCR machine (Hangzhou Bori Technology, TC-XP). The following were mixed in the reaction plate:  $5\ \mu\text{l}$  2x PCR Mix,  $1\ \mu\text{l}$  primer working solution ( $2.5\ \mu\text{M}$ ),  $1\ \mu\text{l}$  template,  $2.8\ \mu\text{l}$  ddH<sub>2</sub>O,  $0.2\ \mu\text{l}$  Rox, and  $10\ \mu\text{l}$  total volume, with three replicate wells per sample. The amplification cycle conditions were  $95^{\circ}\text{C}$  (1 min),  $95^{\circ}\text{C}$  (15 s),  $58^{\circ}\text{C}$  (20 s), and  $72^{\circ}\text{C}$  (45 s), for a total of 40 cycles. The miRNA-146a primer sequence was as follows: forward:  $5' - \text{CCTGAGAAGTGAAT TCCATGGG} - 3'$  and reverse:  $5' - \text{CTCAACTGGTGTCTGTG GAGTC} - 3'$ ; the internal reference gene U6 primer sequence was as follows: forward:  $5' - \text{CTCGCTTCGGCAGCACAT} - 3'$  and reverse:  $5' - \text{AACGCTTACGAATTTGCGT} - 3'$ . Since the Ct value in RT-PCR cannot be used as the original data for statistical analysis,  $2^{-\Delta\text{Ct}}$  was used to represent the relative expression level of miRNA.  $\Delta\text{Ct} = (\text{miRNA} - 146a\ \text{Ct value} - \text{U6 Ct value})$ .

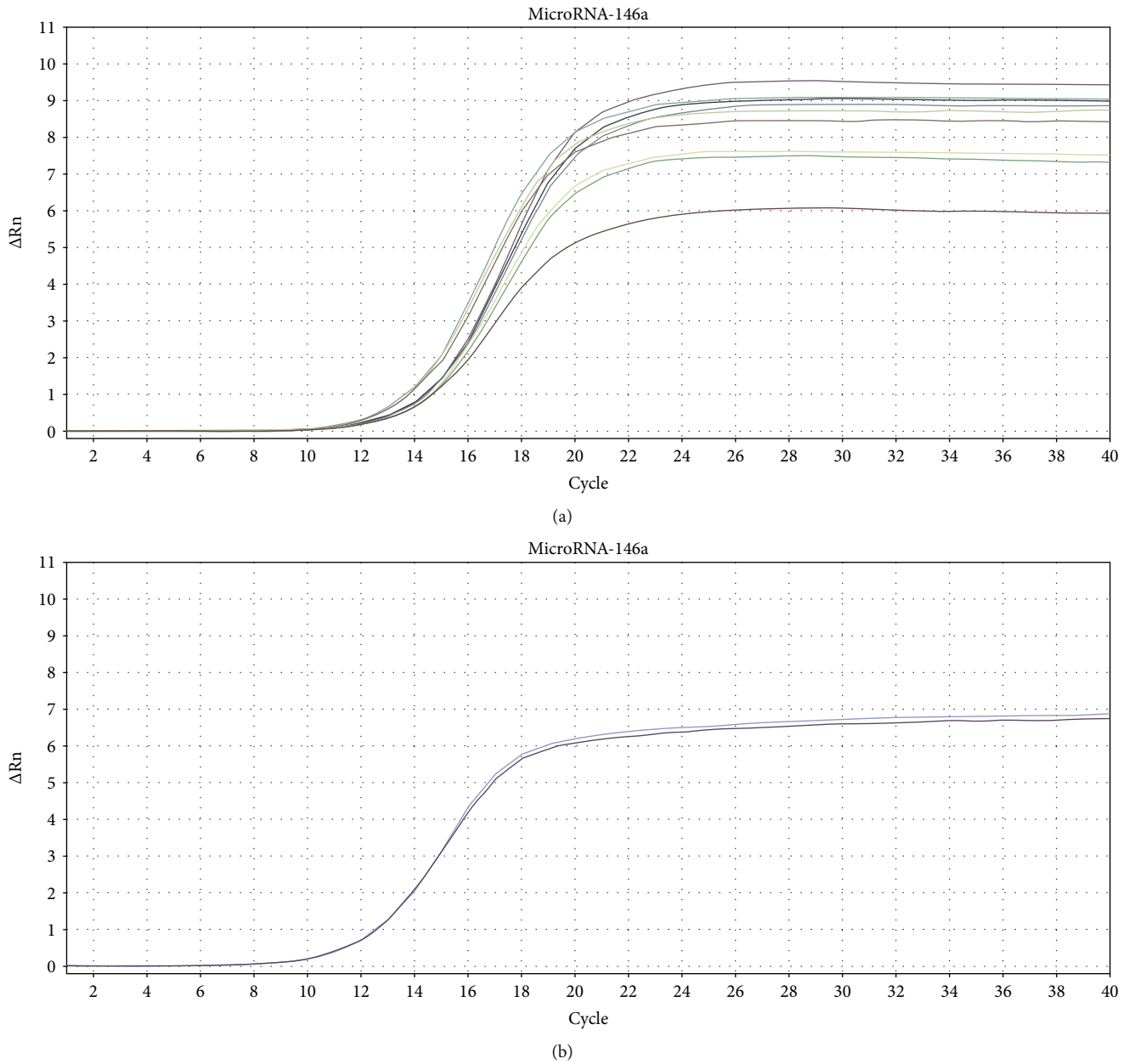


FIGURE 2: (a) MicroRNA-146a amplification curve in the CAS group. (b) MicroRNA-146a amplification curve in the normal group.

TABLE 1: Logistic analysis of CAS risk factors.

	$\beta$	$\sigma$	Wald	$P$	OR
Hypertension	1.534	0.335	21.027	$\leq 0.001$	4.638
LDL-C	1.087	0.402	7.326	0.007	2.965
HDL-C	-4.179	0.660	40.089	$\leq 0.001$	0.015

TABLE 2: The comparison of microRNA expression between the CAS group and normal group.

Item	CAS group	Normal group	$t$	$P$
MicroRNA-146a	$3.29 \pm 1.18$	$2.48 \pm 0.81$	2.15	0.032
IL-6 (ng/l)	$12.48 \pm 1.55$	$11.41 \pm 1.34$	4.84	$< 0.01$
TNF- $\alpha$ (pg/ml)	$292.27 \pm 33.58$	$261.28 \pm 36.59$	2.45	0.014

2.5. *miRNA-146a Stability Test.* In order to stably detect miRNA-146a in circulating blood, we performed RT-PCR pretests on three patients with CAS and three patients from the normal group. It was found that RT-PCR started to expand around the 14<sup>th</sup> cycle. After 28 cycles of amplification, the Ct value was meaningful, indicating that the selected

five miRNAs met the requirements and the experimental conditions were well controlled (Figures 2(a) and 2(b)).

2.6. *ELISA Detection of IL-6 and TNF- $\alpha$ .* ELISA was used to detect the expression level of IL-6 and TND- $\alpha$  in peripheral

TABLE 3: Comparison of microRNA-146a between different CAS groups.

Item	<i>n</i>	MicroRNA-146a	IL-6 (ng/l)	TNF- $\alpha$ (pg/ml)
Mild group	64	2.79 $\pm$ 0.97	11.68 $\pm$ 1.42	277.37 $\pm$ 35.85
Moderate group	62	3.17 $\pm$ 0.93 <sup>a</sup>	12.54 $\pm$ 1.05 <sup>a</sup>	295.34 $\pm$ 31.80 <sup>a</sup>
Severe stenosis group	54	4.02 $\pm$ 1.31b	13.35 $\pm$ 1.33 <sup>b</sup>	306.39 $\pm$ 25.19 <sup>b</sup>
<i>P</i>		$\leq 0.001$	$\leq 0.001$	$\leq 0.001$

Note: a indicates a statistically significant difference compared with the mild group ( $P < 0.05$ ); b indicates a statistically significant difference between the moderate group and the mild group ( $P < 0.05$ ).

blood of the CAS group and normal group (Wuhan Baiyier Biotechnology Co., Ltd., China).

**2.7. Statistical Analysis.** All data in this study were statistically analyzed with the SPSS 17.0 software. The measured data were expressed as mean  $\pm$  standard deviation ( $x \pm s$ ). The paired *t*-test was used to compare two groups. The comparison between groups was performed by the independent sample *t*-test. For one-way ANOVA, the variance was tested using the rank sum test. The count data was expressed as the composition ratio or rate (%), and the chi-square ( $\chi^2$ ) test was used to compare the count data. Data were compared using the Wilcoxon two-sample rank sum test comparison method. ROC curves were drawn to evaluate the value of miRNA prediction of CAS plaque vulnerability. Correlation analysis was performed using the Pearson analysis.  $P < 0.05$  was considered statistically significant.

### 3. Results

**3.1. Comparison of Baseline Data.** Comparison of baseline data showed that there was no significant difference in age, gender, or smoking between the CAS and normal groups ( $P > 0.05$ ).

**3.2. Analysis of CAS Risk Factors.** Multivariate logistic regression analysis was performed using the factors in the baseline data as independent variables and carotid stenosis as a dependent variable. It was found that hypertension and high LDL-C levels were risk factors for CAS, while high HDL-C levels were protective factors for CAS ( $P < 0.05$ ) (Table 1).

**3.3. Comparison of miRNA-146a, IL-6, and TNF- $\alpha$ .** The levels of miRNA-146a, IL-6, and TNF- $\alpha$  in the peripheral blood of the CAS group were higher than those in the normal group ( $P < 0.05$ ) (Table 2). Furthermore, the levels of miRNA-146a, IL-6, and TNF- $\alpha$  significantly increased with increasing degrees of CAS stenosis ( $P < 0.05$ ) (Table 3). Additionally, the levels of miRNA-146a, IL-6, and TNF- $\alpha$  of the stable plaque group were significantly lower than those of the vulnerable plaque group ( $P < 0.05$ ) (Table 4).

**3.4. Correlation Analysis between miRNA-146a and CAS Stenosis, IL-6, and TNF- $\alpha$ .** The results showed a statistically significant positive correlation between miRNA-146a and CAS stenosis ( $r = 0.839$ ,  $P \leq 0.001$ ) (Figure 3). Additionally, miRNA-146 was significantly positively correlated with IL-6 and TNF- $\alpha$  ( $r = 0.374$ ,  $0.327$ ,  $P < 0.05$ ) (Figure 4).

TABLE 4: The comparison of microRNA-146a/IL-6/TNF- $\alpha$  expression between the stable group and vulnerable plaque group.

Item	Stable group	Vulnerable plaque group	<i>t</i>	<i>P</i>
MicroRNA-146a	2.84 $\pm$ 0.86	3.31 $\pm$ 0.89	3.41	<0.001
IL-6 (ng/l)	11.88 $\pm$ 1.35	12.35 $\pm$ 0.85	2.43	0.015
TNF- $\alpha$ (pg/ml)	281.54 $\pm$ 37.97	293.33 $\pm$ 32.87	2.11	0.035

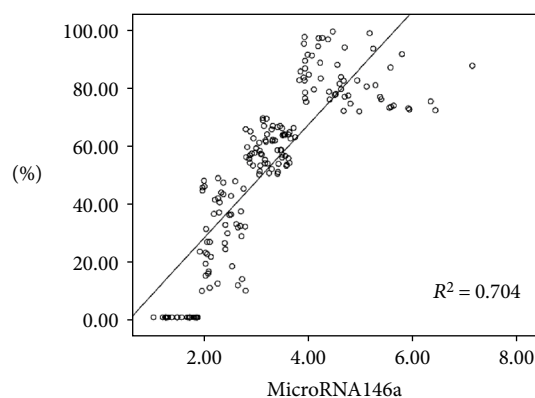


FIGURE 3: The correlation analysis between microRNA-146a and carotid stenosis.

**3.5. miRNA-146a Predicts Vulnerable Plaques.** To evaluate the predictive value of miRNA-146a for vulnerable plaques in CAS patients, we mapped the ROC curve where miRNA-146a was used as a test variable and plaque vulnerability was assigned as a state variable (1 for vulnerable plaques, 2 for stable plaques). miRNA-146a was found to have a predictive value for vulnerable plaques in CAS patients (AUC = 0.64, 95%CI = 0.613 – 0.769,  $\sigma = 0.040$ ,  $P < 0.05$ ) (Figure 5).

### 4. Discussion

**4.1. The Relationship between Inflammatory Cytokines and CAS.** The results of this study showed that the levels of IL-6 and TNF- $\alpha$  in peripheral blood of patients with CAS stenosis were higher than those in the normal group, which indicates that the inflammatory response plays an important role in

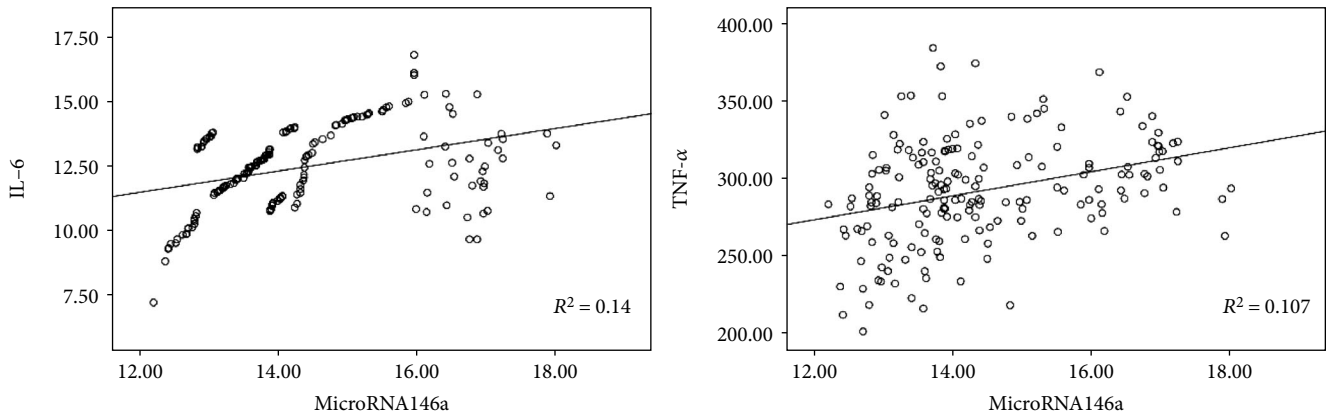


FIGURE 4: The correlation analysis between microRNA-14a and IL-6 and TNF- $\alpha$ .

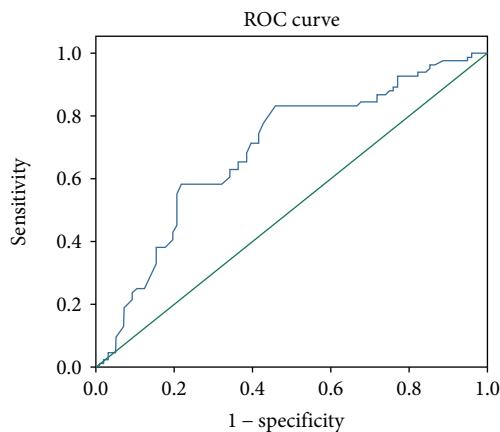


FIGURE 5: The ROC curve.

the occurrence of CAS. Pathological evidence has shown that CAS exhibits characteristics of inflammation, exudation, hyperplasia, and other inflammatory reactions and that inflammation-related cells are an important part of CAS plaques [9]. In 1999, Ross clearly stated that atherosclerosis is the formation of an intimal inflammatory response [10]. Since then, CAS has gradually become recognized as a chronic inflammatory disease. The inflammatory response not only causes endothelial cell dysfunction and an increase in the production of intercellular adhesion molecules [11] but also promotes the formation of CAS by promoting phagocytosis of macrophages and thus their transition into foam cells. In addition, the inflammatory response can also be passed. Activation of complement-related pathways promotes plaque enlargement [12]. In addition, this study also found that the levels of IL-6 and TNF- $\alpha$  gradually increased with increasing CAS stenosis, indicating that the inflammatory response plays an important role in the development of CAS. On the one hand, the inflammatory reaction can promote the rupture of foam cells after phagocytosis of lipids, releasing more lipid content that accelerates the increase in the atherosclerotic core volume; on the other hand, the inflammatory reaction can also cause carotid vascular remodeling, which leads to further narrowing of the vascular

lumen. Studies have shown that administration of tranilast in an animal model of vascular stenosis can reduce vascular remodeling and thus improve vascular stenosis [13].

The unstable rupture of plaques in the cerebral vasculature is the main mechanism of cerebral infarction. This study found that the levels of IL-6 and TNF- $\alpha$  in peripheral blood of patients with stable plaques were lower than those with vulnerable plaques. Correlation analysis demonstrated a positive correlation between IL-6 and TNF- $\alpha$  and plaque vulnerability, which indicates that the inflammatory response also has an impact on the vulnerability of plaques. Studies have shown that vascular smooth muscle cells and macrophages play an important role in plaque vulnerability: vascular smooth muscle cells can maintain the stability of atherosclerotic plaques by producing interstitial collagen, while macrophages can reduce plaque stability by producing a variety of hydrolyzed stroma collagen and extracellular matrix components of matrix metalloproteinase (MMP), such as MMP-9 and MMP-2. The inflammatory response can affect plaque vulnerability through the following mechanisms: the inflammatory response accelerates the oxidation of low-density lipoprotein to ox-LDL, causing more macrophages to phagocytose ox-LDL, which is then transferred to the mononuclear macrophage system. Foam cells change and rupture under the stimulation of the inflammatory reaction, and the released cell components and lipids are deposited locally in the blood vessel. This results in a gradual increase in the lipid core volume, thus a plaque with a larger lipid core volume and more easily broken [14]. Some inflammatory cytokines, such as IFN- $\gamma$ , can inhibit the proliferation and promote apoptosis of smooth muscle cells, which results in decreased extracellular matrix components, thinning of fibrous caps, and thus increased plaque vulnerability [15]. Inflammatory cytokines, such as IL-1 and TNF- $\alpha$ , can promote the ability of macrophages to secrete MMP, which results in decreased plaque fiber cap thickness and interstitial collagen composition and thus increased plaque vulnerability [16].

**4.2. The Relationship between miRNA-146a and CAS.** MicroRNA is a class of noncoding single-stranded RNAs of approximately 17–22 nucleotides in length encoded by an endogenous gene [17], which can be identical to the 3- or 5-terminal untranslated region of mRNA of the

corresponding target gene. Incomplete base complementary pairing is involved in the development of the disease, as it inhibits the translation or degradation of the corresponding mRNA. In recent years, miRNA-146a has been found to be differentially expressed in inflammatory diseases such as sepsis and COPD [18]. While CAS has been shown to be a chronic inflammatory disease, it is not known whether inflammation-related miRNAs are differentially expressed in CAS and can be used as biomarkers for CAS. The results of this study showed that miRNA-146a levels in the stenosis group were higher than those in the normal group and were positively correlated with the degree of CAS stenosis. The ROC curve also showed that miRNA-146a had a good predictive value for plaque vulnerability in CAS patients. Luo et al. also found that miRNA-146a was involved in the occurrence of atherosclerosis in ApoE<sup>-/-</sup> mice and was positively correlated with the severity of atherosclerosis [19], similar to the conclusion of this study. However, subject to the limitations of experimental conditions, this study only assessed the correlation and did not explore the specific regulatory mechanisms. Future studies should explore the specific underlying mechanisms of miRNA-146a.

**4.3. The Relationship between miRNA-146a and IL-6 and TNF- $\alpha$ .** This study revealed a positive correlation between miRNA-146a and IL-6 and TNF- $\alpha$ , suggesting that miRNA-146a may have a regulatory role in the inflammatory response in CAS. The miRNA-146a gene locus is located on the 5q33 chromosome, and its allele is involved in inflammatory signaling pathways such as TNF- $\alpha$  and CRP. The TLR4 (Toll-like receptor 4) signaling pathway is a common inflammatory signaling pathway in CAS [20]. When an exogenous inflammatory factor binds to the extracellular domain of TLR4, the signal is transduced into the cell via the TLR4 transcellular structure. Subsequently, TLR4 activates IRAK (IL-1 receptor-associated kinase) via the MyD88-dependent pathway, which further activates TRAF-6 (tumor necrosis factor receptor-associated factor 6). Activation of this signaling pathway may cause nuclear factor- $\kappa$ B (NF- $\kappa$ B) inhibitors to be degraded such that NF- $\kappa$ B is indirectly activated, followed by inflammatory cytokines such as IL-1. With the involvement of NF- $\kappa$ B, TNF- $\alpha$  is activated, and miRNA-146a can bind to the 3-terminal noncoding region of IRAK and TRAF-6 via base pair pairing, thereby negatively regulating the above inflammatory cytokines [21]. This indicates that miRNA-146a exerts an inhibitory effect on inflammation and should be inversely correlated with related inflammatory cytokines. This seems to contradict the results of this study, but careful observation found that the correlation coefficient of miRNA-146a and IL-6 and TNF- $\alpha$  was not high ( $r = 0.374, 0.327, P < 0.01$ ). There are more possible reasons for this. First, the subjects of the study were different; other studies investigated single cells, with singular influencing factors, whereas the research subject of our study was humans, and the human body is affected by many factors. Second, due to the small number of miRNAs and the large number of target genes, the related miRNAs can have various biological functions, and thus, there must be cross-regulation between different miRNAs. In addition to the negative

regulation of miRNA-146, the inflammatory cytokines of CAS patients in this study are also positively regulated by other miRNAs. We have not further controlled miRNA-146a or other positive regulatory miRNAs. The correlation analysis in this paper represents the specific effect of positive and negative regulation of miRNA synthesis. This study only performed correlation analysis, and the specific regulatory mechanisms of miRNA-146a on inflammatory cytokines in CAS remain to be further studied.

## Data Availability

All data, models, and codes generated or used during the study appear in the submitted article.

## Conflicts of Interest

The authors declare that they have no financial or other conflicts of interest in relation to this research and its publication.

## References

- [1] A. Nicolaides, M. Sabetai, S. K. Kakkos et al., "The Asymptomatic Carotid Stenosis and Risk of Stroke (ACSRS) study. Aims and results of quality control," *International Angiology A Journal of the International Union of Angiology*, vol. 22, no. 3, pp. 263–272, 2003.
- [2] C. M. Kramer and G. S. Treiman, "Vulnerable plaque in carotid arteries without "significant" stenosis," *Journal of the American College of Cardiology*, vol. 76, no. 19, pp. 2223–2225, 2020.
- [3] S. Shimoda, A. Kitamura, H. Imano et al., "Associations of carotid intima-media thickness and plaque heterogeneity with the risks of stroke subtypes and coronary artery disease in the Japanese general population: the Circulatory Risk in Communities Study," *Journal of the American Heart Association*, vol. 9, no. 19, p. e017020, 2020.
- [4] M. Wang, J. Li, J. Cai et al., "Overexpression of microRNA-16 alleviates atherosclerosis by inhibition of inflammatory pathways," *BioMed Research International*, vol. 2020, Article ID 8504238, 12 pages, 2020.
- [5] P. J. Kelly, P. Camps-Renom, N. Giannotti et al., "Carotid plaque inflammation imaged by 18F-fluorodeoxyglucose positron emission tomography and risk of early recurrent stroke," *Stroke*, vol. 50, no. 7, pp. 1766–1773, 2019.
- [6] M. B. Lobbes, M. E. Kooi, E. Lutgens et al., "Leukocyte counts, myeloperoxidase, and pregnancy-associated plasma protein a as biomarkers for cardiovascular disease: towards a multi-biomarker approach," *International Journal of Vascular Medicine*, vol. 2010, 9 pages, 2010.
- [7] E. N. Van Meter, A. Onyango Jackline, and A. Teske Kelly, "A review of currently identified small molecule modulators of microRNA function," *European Journal of Medicinal Chemistry*, vol. 188, no. 15, p. 112008, 2020.
- [8] Z. H. Xie, Y. Q. Yang, Y. Q. He et al., "In vivo assessment of inflammation in carotid atherosclerosis by noninvasive photoacoustic imaging," *Theranostics*, vol. 10, no. 10, pp. 4694–4704, 2020.
- [9] X. W. Tan, X. Zhang, L. Pan, X. Tian, and P. Dong, "Identification of key pathways and genes in advanced coronary



- atherosclerosis using bioinformatics analysis,” *BioMed Research International*, vol. 2017, Article ID 4323496, 12 pages, 2017.
- [10] J. S. Pober and W. C. Sessa, “Evolving functions of endothelial cells in inflammation,” *Nature Reviews. Immunology*, vol. 7, no. 10, pp. 803–815, 2007.
- [11] U. Ikeda, M. Takahashi, and K. Shimada, “C-reactive protein directly inhibits nitric oxide production by cytokine-stimulated vascular smooth muscle cells,” *Journal of Cardiovascular Pharmacology*, vol. 42, no. 5, pp. 607–611, 2003.
- [12] X. B. Cui, J. N. Luan, K. Dong et al., “RGC-32 (response gene to complement 32) deficiency protects endothelial cells from inflammation and attenuates atherosclerosis,” *Arteriosclerosis, Thrombosis, and Vascular Biology*, vol. 38, no. 4, pp. e36–e47, 2018.
- [13] S. W. Chen, Y. D. Wang, Y. M. Pan et al., “Novel role for tranilast in regulating NLRP3 ubiquitination, vascular inflammation, and atherosclerosis,” *Journal of the American Heart Association*, vol. 9, no. 12, p. e015513, 2020.
- [14] T. Ito, T. Ichihashi, H. Fujita, T. Sugiura, and N. Ohte, “Impact of malondialdehyde-modified low-density lipoprotein on coronary plaque vulnerability in patients not receiving lipid-lowering therapy: a whole coronary analysis with multislice-computed tomography,” *Heart Vessels*, vol. 33, no. 4, pp. 351–357, 2018.
- [15] S. D. Stojanović, M. Fuchs, M. Kunz et al., “Inflammatory drivers of cardiovascular disease: molecular characterization of senescent coronary vascular smooth muscle cells,” *Front Physiol*, vol. 11, no. 5, p. 520, 2020.
- [16] M. Gonzalez-Cotto, L. Guo, M. Karwan et al., “TREML4 promotes inflammatory programs in human and murine macrophages and alters atherosclerosis lesion composition in the apolipoprotein E deficient mouse,” *Front Immunol*, vol. 11, 2020.
- [17] T. Treiber, N. Treiber, and G. Meister, “Regulation of microRNA biogenesis and its crosstalk with other cellular pathways,” *Nature Reviews. Molecular Cell Biology*, vol. 20, no. 1, pp. 5–20, 2019.
- [18] H. H. Pua and K. M. Ansel, “MicroRNA regulation of allergic inflammation and asthma,” *Current Opinion in Immunology*, vol. 36, no. 1, pp. 101–108, 2015.
- [19] Y. Luo, W. Xiong, C. C. Chen, F. Liu, J. H. Li, and S. H. Dong, “Expression changes of microRNA-146a in atherosclerotic process in ApoE(-) mice,” *Journal of Clinical Cardiology*, vol. 33, no. 3, pp. 267–270, 2017.
- [20] N. Kuzmich, K. Sivak, V. Chubarev, Y. Porozov, T. Savateeva-Lyubimova, and F. Peri, “TLR4 signaling pathway modulators as potential therapeutics in inflammation and sepsis,” *Vaccine*, vol. 5, no. 4, p. 34, 2017.
- [21] K. D. Taganov, M. P. Boldin, K. J. Chang, and D. Baltimore, “NF-kappaB-dependent induction of microRNA miR-146, an inhibitor targeted to signaling proteins of innate immune responses,” *Proceedings of the National Academy of Sciences of the United States of America*, vol. 103, no. 33, pp. 12481–12486, 2006.

## Research Article

# Increased Levels of Serum Neuregulin 1 Associated with Cognitive Impairment in Vascular Dementia

Xiaoling Wang, Fengyu Zhang, Weibin Ma , Depeng Feng, Jingjing Zhang, and Jialei Xu 

Department of Neurology, Liaocheng People's Hospital, Liaocheng, Shandong, China 252000

Correspondence should be addressed to Weibin Ma; 13969560330@163.com

Received 27 October 2020; Revised 3 November 2020; Accepted 5 November 2020; Published 12 November 2020

Academic Editor: Yuzhen Xu

Copyright © 2020 Xiaoling Wang et al. This is an open access article distributed under the Creative Commons Attribution License, which permits unrestricted use, distribution, and reproduction in any medium, provided the original work is properly cited.

**Objective.** Neuregulin 1 (NRG 1) is a member of the epidermal growth factor (EGF) family and is believed to play an important role in neuroplasticity. However, the relationship between NRG 1 and vascular dementia (VaD) is poorly understood. The purpose of this study is to explore the correlation between neuregulin 1 and VaD. **Patients and Methods.** From October 2018 to September 2020, 93 VaD patients and 79 control populations who attended Liaocheng People's Hospital were included in the study. Baseline characteristics including age, gender, years of education, HDL, LDL, FBG, SBP, and DBP are collected. At the same time, peripheral blood was collected, and the concentration of serum NRG 1 was detected by enzyme-linked immunosorbent assay (ELISA). All research subjects received professional cognitive function assessment. **Results.** A total of 93 VaD patients and 79 controls were enrolled. There was no significant difference in age, gender, years of education, HDL, LDL, FBG, SBP, and DBP between the two groups ( $p > 0.05$ ). However, compared with the control group, VaD patients have lower MoCA and higher serum NRG 1 levels, and the difference is statistically significant ( $p < 0.001$ ). The correlation analysis of MoCA and baseline characteristics showed that the MoCA score in VaD was significantly negatively correlated with serum NRG 1 ( $r = -0.374$ ,  $p = 0.036$ ). The results of multivariate regression showed that the MoCA score of VaD patients was only associated with NRG 1 ( $\beta = 0.258$ ,  $p = 0.012$ ). **Conclusions.** The concentration of serum NRG 1 in VaD patients is significantly increased, which may be an independent risk factor for cognitive impairment in VaD patients.

## 1. Introduction

Vascular dementia (VaD) is one of the main causes of dementia syndrome and is defined as the impairment of cognitive function due to vascular disorders caused by impaired cerebral blood flow [1, 2]. There are currently 35.6 million dementia patients worldwide, and VaD is the subtype of dementia second only to Alzheimer's disease (AD) [3–5]. With the increase of life expectancy, neurovascular disorders are threatening human physical and mental health, and VaD is a public health issue that needs to be solved urgently [6]. There is currently no cure for VaD [7]. Therefore, finding low-invasive and high-efficiency biomarkers is a hot spot for clinical and scientific researchers.

Neuregulin 1 (NRG 1) is a trophic factor that contains an epidermal growth factor- (EGF-) like domain [8]. The gene encoding NRG 1 is 2.4 Mbp (chromosome 8) in mice and 2.6 Mbp in humans (chromosome 8) and rats (chromosome

16). NRG 1 encoded by the NRG 1 gene has at least 31 subtypes and 6 types of NRG 1 (I to VI), due to alternative splicing, and has been identified as a member of the active epithelial growth factor (EGF) family [9]. Most NRG 1 subtypes are synthesized as pro-NRG-1, which binds to the cell membrane and is contained in the extracellular EGF domain, which can be cleaved by three transmembrane NRG 1 proteolytic enzymes (ADAM17, BACE, and ADAM19) and then released into extracellular fluid as soluble NRG 1 [10]. These types or isomers perform a wide range of functions in the body and are considered to be key factors in neurodevelopment [11, 12]. The specific binding of NRG 1 to its receptor ErbB can activate a series of different pathophysiological processes, including maintaining myelin sheath stability, promoting neurite growth, and regulating cell proliferation, differentiation, and apoptosis [13].

More and more studies suggest that NRG 1 is involved in many neurological diseases, but its underlying mechanism is

still unclear. The purpose of our current research is to (1) explore the relationship between NRG 1 and VaD and (2) clarify whether NRG 1 can be used as a biomarker of VaD. These issues have not been reported in previous studies. The determination of the correlation between NRG 1 and vascular cognitive impairment will provide new possibilities for the treatment of VaD.

## 2. Patients and Methods

**2.1. Study Population.** 93 VaD patients and 79 normal controls who were treated in Liaocheng People's Hospital from October 2018 to September 2020 were used as the study population. The diagnostic criteria of VaD refer to the National Institute for Neurological Disorders and Stroke (NINDS-AIREN) and International Classification of Diseases, 11th revision (ICD-11) [14, 15]. All VaD diagnoses are made by an experienced neurologist. The exclusion criteria are as follows: (1) mixed dementia; (2) active neuroimmune disease, rheumatic system disease, or acute infection; (3) history of acute stroke and tumor; (4) mental diseases such as schizophrenia; and (5) the patient or family members do not cooperate with the examination. This study was authorized by the Ethics Committee of Liaocheng People's Hospital. The patients and their families knew the contents of the study and signed an informed consent form. Our research complies with the Declaration of Helsinki.

**2.2. Baseline Characteristics.** When the study population visited a doctor, their baseline data were collected and recorded in detail. The main baseline information includes the following aspects: age, gender, years of education, high-density lipoprotein (HDL), low-density lipoprotein (LDL), fasting blood glucose (FBG), systolic blood pressure (SBP), and diastolic blood pressure (DBP). Demographic information such as age, gender, and years of education is collected mainly by inquiries, and the subjects of inquiries are patients or guardians who are familiar with the patient's situation. The acquisition of clinical biochemical indicators such as HDL, LDL, FBG, SBP, and DBP adopts standardized laboratory testing methods.

**2.3. Serum NRG 1 Test.** The detection of serum NRG 1 uses a commercial ELISA reagent (NRG 1, Abcam, Cambridge, MA). All study populations were collected 5 ml of peripheral blood by nurses within 24 hours after visiting a doctor. The peripheral blood was allowed to stand at room temperature for half an hour and then centrifuged at 3000 rpm for 12 minutes in a cryogenic centrifuge. The serum was separated and kept in a refrigerator at  $-80^{\circ}\text{C}$  for later use. The operation process of ELISA refers to previous reports and product instructions [16, 17].

**2.4. Cognitive Function Test.** The Montreal Cognitive Assessment (MoCA) is a widely used screening assessment for detecting cognitive impairment established by Ziad Nasreddine in Montreal, Quebec, in 1996. Its reliability and validity have been confirmed and adopted by many countries. The MoCA test takes about 10 minutes and is a test with a total score of 30 points. MoCA can measure the following cogni-

tive domains: short-term memory recall task, visuospatial abilities, multiple aspects of executive functions, attention, concentration, and working memory, language, abstract reasoning, and orientation. A MoCA score of 26 and above is considered normal [18, 19]. The MoCA evaluation is carried out by an experienced neurologist who does not know the evaluation subject's baseline date.

**2.5. Statistical Analysis.** All data statistics in this study used SPSS 22.0 software (SPSS Inc., IL, USA). All data are expressed as  $n$  or mean  $\pm$  standard deviation (SD). This study is aimed at detecting significant changes between VaD patients and controls. The Shapiro-Wilk test is used to assess the normality of the data distribution. The statistics of categorical variables used  $\chi$  test, and the statistics of continuous variables used Student's  $t$  test. Spearman's rank correlation is used to assess the relationship of variables. A multiple regression model was established to screen independent risk factors for cognitive impairment in VaD patients. A two-tailed  $p$  value of 0.05 was considered statistically significant.

## 3. Results

**3.1. Baseline Characteristics.** Baseline data of 93 VaD patients and 79 control populations were collected, and the results are shown in Table 1. The results of statistical analysis showed that regarding baseline data (age, gender, years of education, HDL, LDL, FBG, SBP, and DBP), there was no significant difference between the control group and the VaD group ( $p > 0.05$ ). The MoCA scores of the control group and the VaD group were  $(27.8 \pm 1.1)$  and  $(20.9 \pm 1.8)$  points, respectively, and there were significant differences between the groups ( $p < 0.001$ ). The serum NRG 1 concentrations of the control group and the VaD group were  $(264.8 \pm 14.7)$  pg/ml and  $(396.8 \pm 19.9)$  pg/ml, respectively, and there were also significant differences between the groups ( $p < 0.001$ ).

**3.2. Spearman's Correlation Analysis.** In order to explore the related factors of cognitive impairment in VaD patients, we performed Spearman's correlation analysis of MoCA score and baseline data. The results of Spearman's correlation analysis are shown in Table 2. From the results of statistical analysis, we can see that the MoCA score of VaD patients is significantly negatively correlated with the serum NRG 1 concentration ( $r = -0.374$ ,  $p = 0.036$ ). However, there is no obvious correlation between MoCA score and age, gender, years of education, HDL, LDL, FBG, SBP, and DBP ( $p > 0.05$ ).

**3.3. Multivariate Regression Analysis.** To verify the independent risk factors for cognitive impairment in VaD patients, multivariate regression analysis was used. The statistical results of multivariate regression analysis are shown in Table 3. The results of regression analysis showed that after adjusting for age, gender, years of education, HDL, LDL, FBG, SBP, and DBP and other risk factors, serum NRG 1 concentration is still an independent predictor of cognitive impairment in VaD patients ( $\beta = 0.258$ ,  $p = 0.012$ ).

TABLE 1: Baseline characteristics of patients.

	Controls ( <i>n</i> = 79)	VaD ( <i>n</i> = 93)	<i>p</i>
Age (years)	63.4 ± 3.7	63.2 ± 3.9	0.732
Male ( <i>n</i> )	48	59	0.718
Education (years)	9.2 ± 1.6	9.5 ± 1.4	0.191
HDL (mmol/l)	1.3 ± 0.3	1.4 ± 0.4	0.069
LDL (mmol/l)	2.8 ± 0.4	2.9 ± 0.3	0.063
FBG (mmol/l)	6.3 ± 1.7	6.5 ± 2.0	0.485
SBP (mmHg)	137.2 ± 11.3	139.6 ± 12.1	0.183
DBP (mmHg)	82.5 ± 8.4	84.1 ± 8.6	0.221
NRG 1 (pg/ml)	264.8 ± 14.7	396.8 ± 19.9	<0.001
MoCA (points)	27.8 ± 1.1	20.9 ± 1.8	<0.001

Abbreviations: VaD: vascular dementia; HDL: high-density lipoprotein; LDL: low-density lipoprotein; FBG: fasting blood glucose; SBP: systolic blood pressure; DBP: diastolic blood pressure; NRG 1: neuregulin 1; MoCA: Montreal Cognitive Assessment.

TABLE 2: Correlation between MoCA and baseline characteristics in VaD.

	<i>r</i>	<i>p</i>
Age (years)	-0.323	0.284
Gender	-0.408	0.195
Education (years)	-0.667	0.317
HDL (mmol/l)	0.226	0.238
LDL (mmol/l)	-0.107	0.179
FBG (mmol/l)	-0.582	0.632
SBP (mmHg)	-0.465	0.503
DBP (mmHg)	-0.138	0.314
NRG 1 (pg/ml)	-0.374	0.036

Abbreviations: MoCA: Montreal Cognitive Assessment; VaD: vascular dementia; HDL: high-density lipoprotein; LDL: low-density lipoprotein; FBG: fasting blood glucose; SBP: systolic blood pressure; DBP: diastolic blood pressure; NRG 1: neuregulin 1.

TABLE 3: Multivariable analyses of MoCA and baseline characteristics in VaD.

	Regression coefficient	<i>p</i>	95% CI
Age (years)	0.199	0.132	0.118-1.007
Gender	0.246	0.284	0.221-1.098
Education (years)	0.433	0.249	0.163-1.106
HDL (mmol/l)	0.524	0.306	0.232-1.154
LDL (mmol/l)	0.317	0.108	0.186-1.113
FBG (mmol/l)	0.292	0.267	0.201-1.189
SBP (mmHg)	0.235	0.310	0.117-1.132
DBP (mmHg)	0.391	0.435	0.294-1.235
NRG 1 (pg/ml)	0.258	0.012	0.149-0.763

Abbreviations: MoCA: Montreal Cognitive Assessment; VaD: vascular dementia; HDL: high-density lipoprotein; LDL: low-density lipoprotein; FBG: fasting blood glucose; SBP: systolic blood pressure; DBP: diastolic blood pressure; NRG 1: neuregulin 1.

### 4. Discussion

The main purpose of the current study is to study the correlation between the cognitive function and serum NRG 1 levels in normal control groups and VaD patients. The results of the study showed that the serum NRG 1 level of VaD patients was significantly higher than that of the control population, while the MoCA score was significantly lower. Our further research also found that the MoCA score in VaD patients was significantly negatively correlated with serum NRG 1 concentration, and there was no interference with other clinical baseline data such as age, gender, years of education, HDL, LDL, FBG, SBP, and DBP. As far as we know, this is the first report to study serum NRG 1 as a biomarker for predicting cognitive impairment in VaD patients.

Neuregulin 1 is involved in the process of a series of neurological diseases [20]. A Shantou University study showed that spinal cord injury can induce pathophysiological changes in brain functional areas by regulating NRG 1 signals, thereby aggravating brain injury, indicating that exogenous NRG 1 may be a potential method for the treatment of spinal cord injury [21]. The same research team found that treatment of primary mouse neurons with recombinant NRG 1 can reduce oxidative stress caused by H<sub>2</sub>O<sub>2</sub> and inflammation caused by LPS [22]. Simmons et al. further confirmed the anti-inflammatory effect of NRG 1 in a cerebral ischemia model [23]. Interestingly, Spanish scholars also recently discovered the neuroprotective effect of NRG 1 in stroke models [24]. However, the signal pathway and neural network through which NRG 1 exerts neuroprotective effects are still unclear.

NRG 1 and ErbB4 are expressed in multiple regions of the adult brain, and NRG 1/ErbB4 plays an important role in neurodevelopment, neurotransmission, and synaptic plasticity. ErbB4 can colocalize and interact with the postsynaptic scaffold protein PSD95, which is essential for glutamatergic transmission and short-term plasticity. The regulation of GABA and ACh by NRG 1 is one of the important mechanisms for maintaining long-term plasticity [25]. A study showed that downregulation of NRG 1/ErbB4 signal is an important means to improve hippocampal learning and memory function [26]. Another study showed that the interaction of NRG 1 and ErbB4 can reduce the apoptosis of hippocampal neurons [27]. NRG 1 is involved in a number of pathophysiological processes, and the mechanism of its neuroprotective effect is far from elucidated.

Interestingly, the correlation between NRG 1 and AD has been widely reported in recent years. The study of Jiang et al. pointed out that NRG 1 has a preventive effect on AD, which provides a new perspective for the treatment of AD [28]. Xu team's research found that NRG 1 can improve cognitive impairment in AD [29]. The correlation between NRG 1 and AD has been reported in a number of studies [30–32]. These studies involve animal experiments and clinical studies, suggesting that NRG 1 can be used as a biomarker of AD, and exogenous NRG 1 can be used as a potential treatment for AD.

Our research has some limitations: first, our research is small sample research, and the correlation between NRG 1



and VaD still needs to be further confirmed; second, we have not obtained pathological samples of brain tissue, and the expression level of NRG 1 in the tissue is unknown; finally, we do not have longitudinal follow-up results for VaD patients. However, our study reported the correlation between NRG 1 and VaD for the first time, providing a new perspective on the prevention and treatment of VaD.

## 5. Conclusions

In summary, our study found that the serum NRG 1 level of VaD patients was significantly increased. We report for the first time that serum NRG 1 levels are involved in cognitive impairment in VaD patients. We hope that the relationship between the two will be further confirmed in the future. It is of great social significance to clarify the cognitive protective effect of NRG 1 on VaD.

## Data Availability

The data used to support the findings of this study are available from the corresponding author upon request.

## Conflicts of Interest

The authors declare that they have no any conflict of interests.

## Authors' Contributions

Xiaoling Wang and Fengyu Zhang are co-first authors, and they contributed equally to this work.

## Acknowledgments

All the authors are grateful to the Liaocheng People's Hospital.

## References

- [1] J. Li, S. Li, Y. Song et al., "Association of serum FAM19A5 with cognitive impairment in vascular dementia," *Disease Markers*, vol. 2020, Article ID 8895900, 5 pages, 2020.
- [2] Q. Wang, W. Yang, J. Zhang, Y. Zhao, and Y. Xu, "TREM2 overexpression attenuates cognitive deficits in experimental models of vascular dementia," *Neural Plasticity*, vol. 2020, Article ID 8834275, 10 pages, 2020.
- [3] Y. Xu, Q. Wang, Z. Qu, J. Yang, X. Zhang, and Y. Zhao, "Protective effect of hyperbaric oxygen therapy on cognitive function in patients with vascular dementia," *Cell Transplantation*, vol. 28, no. 8, pp. 1071–1075, 2019.
- [4] Q. Wang, Y. Xu, C. Qi, A. Liu, and Y. Zhao, "Association study of serum soluble TREM2 with vascular dementia in Chinese Han population," *The International Journal of Neuroscience*, vol. 130, no. 7, pp. 708–712, 2020.
- [5] K. Shao, S. Shan, W. Ru, and C. Ma, "Association between serum NPTX2 and cognitive function in patients with vascular dementia," *Brain and behavior*, vol. 10, article e01779, 2020.
- [6] Y. Xu, Q. Wang, R. Cui, K. Lu, Y. Liu, and Y. Zhao, "Uric acid is associated with vascular dementia in Chinese population," *Brain and behavior*, vol. 7, no. 2, article e00617, 2017.
- [7] Y. Xu, Q. Wang, Y. Liu, R. Cui, K. Lu, and Y. Zhao, "Association between Helicobacter pylori infection and carotid atherosclerosis in patients with vascular dementia," *Journal of the Neurological Sciences*, vol. 362, pp. 73–77, 2016.
- [8] M. Willem, "Proteolytic processing of neuregulin-1," *Brain Research Bulletin*, vol. 126, pp. 178–182, 2016.
- [9] X. Hu, Q. Fan, H. Hou, and R. Yan, "Neurological dysfunctions associated with altered BACE1-dependent neuregulin-1 signaling," *Journal of Neurochemistry*, vol. 136, no. 2, pp. 234–249, 2016.
- [10] G. Ronchi, B. E. Fornasari, A. Crosio et al., "Chitosan tubes enriched with fresh skeletal muscle fibers for primary nerve repair," *BioMed Research International*, vol. 2018, Article ID 9175248, 13 pages, 2018.
- [11] D. Fleck, M. Voss, B. Brankatschk et al., "Proteolytic processing of neuregulin 1 type III by three intramembrane-cleaving proteases," *The Journal of Biological Chemistry*, vol. 291, no. 1, pp. 318–333, 2016.
- [12] Y. Iwakura, R. Wang, N. Inamura et al., "Glutamate-dependent ectodomain shedding of neuregulin-1 type II precursors in rat forebrain neurons," *PLoS One*, vol. 12, no. 3, article e0174780, 2017.
- [13] H. Kataria, A. Alizadeh, and S. Karimi-Abdolrezaee, "Neuregulin-1/ErbB network: an emerging modulator of nervous system injury and repair," *Progress in Neurobiology*, vol. 180, p. 101643, 2019.
- [14] G. C. Román, T. K. Tatemichi, T. Erkinjuntti et al., "Vascular dementia: diagnostic criteria for research studies: report of the NINDS-AIREN International Workshop," *Neurology*, vol. 43, no. 2, pp. 250–260, 1993.
- [15] W. Gaebel, F. Jessen, and S. Kanba, "Neurocognitive disorders in ICD-11: the debate and its outcome," *World Psychiatry*, vol. 17, no. 2, pp. 229–230, 2018.
- [16] Y. Xu, Q. Wang, Z. Wu et al., "The effect of lithium chloride on the attenuation of cognitive impairment in experimental hypoglycemic rats," *Brain Research Bulletin*, vol. 149, pp. 168–174, 2019.
- [17] J. Zhang, L. Tang, J. Hu, Y. Wang, and Y. Xu, "Uric acid is associated with cognitive impairment in the elderly patients receiving maintenance hemodialysis—a two-center study," *Brain and behavior*, vol. 10, article e01542, 2020.
- [18] Y. Xu, Q. Wang, Y. Liu, R. Cui, and Y. Zhao, "Is helicobacter pylori infection a critical risk factor for vascular dementia?," *The International Journal of Neuroscience*, vol. 126, no. 10, pp. 899–903, 2016.
- [19] Z. Peng, H. Jiang, X. Wang et al., "The efficacy of cognitive training for elderly Chinese individuals with mild cognitive impairment," *BioMed Research International*, vol. 2019, Article ID 4347281, 10 pages, 2019.
- [20] L. Shi and C. M. Bergson, "Neuregulin 1: an intriguing therapeutic target for neurodevelopmental disorders," *Translational Psychiatry*, vol. 10, no. 1, p. 190, 2020.
- [21] W. K. Xue, W. J. Zhao, X. H. Meng, H. F. Shen, and P. Z. Huang, "Spinal cord injury induced neuregulin 1 signaling changes in mouse prefrontal cortex and hippocampus," *Brain Research Bulletin*, vol. 144, pp. 180–186, 2019.
- [22] J. Xu, C. Hu, S. Chen et al., "Neuregulin-1 protects mouse cerebellum against oxidative stress and neuroinflammation," *Brain Research*, vol. 1670, pp. 32–43, 2017.
- [23] L. J. Simmons, M. C. Surlles-Zeigler, Y. Li, G. D. Ford, G. D. Newman, and B. D. Ford, "Regulation of inflammatory



- responses by neuregulin-1 in brain ischemia and microglial cells in vitro involves the NF-kappa B pathway,” *Journal of Neuroinflammation*, vol. 13, no. 1, p. 237, 2016.
- [24] C. Navarro-González, A. Huerga-Gómez, and P. Fazzari, “Nrg1 intracellular signaling is neuroprotective upon stroke,” *Oxidative Medicine and Cellular Longevity*, vol. 2019, Article ID 3930186, 15 pages, 2019.
- [25] L. Mei and W. C. Xiong, “Neuregulin 1 in neural development, synaptic plasticity and schizophrenia,” *Nature reviews Neuroscience*, vol. 9, no. 6, pp. 437–452, 2008.
- [26] J. Tian, F. Geng, F. Gao et al., “Down-regulation of neuregulin1/ErbB4 signaling in the hippocampus is critical for learning and memory,” *Molecular Neurobiology*, vol. 54, no. 6, pp. 3976–3987, 2017.
- [27] Y. Hei, R. Chen, X. Mao, J. Wang, Q. Long, and W. Liu, “Neuregulin1 attenuates cognitive deficits and hippocampal CA1 neuronal apoptosis partly via ErbB4 receptor in a rat model of chronic cerebral hypoperfusion,” *Behavioural Brain Research*, vol. 365, pp. 141–149, 2019.
- [28] Q. Jiang, S. Chen, C. Hu, P. Huang, H. Shen, and W. Zhao, “Neuregulin-1 (Nrg1) signaling has a preventive role and is altered in the frontal cortex under the pathological conditions of Alzheimer’s disease,” *Molecular Medicine Reports*, vol. 14, no. 3, pp. 2614–2624, 2016.
- [29] J. Xu, F. de Winter, C. Farrokhi et al., “Neuregulin 1 improves cognitive deficits and neuropathology in an Alzheimer’s disease model,” *Scientific Reports*, vol. 6, no. 1, p. 31692, 2016.
- [30] J. Ryu, B. H. Hong, Y. J. Kim et al., “Neuregulin-1 attenuates cognitive function impairments in a transgenic mouse model of Alzheimer’s disease,” *Cell Death & Disease*, vol. 7, no. 2, article e2117, 2016.
- [31] K. A. Chang, K. Y. Shin, E. Nam et al., “Plasma soluble neuregulin-1 as a diagnostic biomarker for Alzheimer’s disease,” *Neurochemistry International*, vol. 97, pp. 1–7, 2016.
- [32] F. Mouton-Liger, J. Dumurgier, E. Cognat et al., “CSF levels of the BACE1 substrate NRG1 correlate with cognition in Alzheimer’s disease,” *Alzheimer’s Research & Therapy*, vol. 12, no. 1, p. 88, 2020.